Spin Dynamics

Basics of Nuclear Magnetic Resonance

Second edition

Malcolm H. Levitt

The University of Southampton, UK

John Wiley & Sons, Ltd

Spin Dynamics

Second Edition

Spin Dynamics

Basics of Nuclear Magnetic Resonance

Second edition

Malcolm H. Levitt
The University of Southampton, UK

John Wiley & Sons, Ltd

Copyright © 2008 John Wiley & Sons Ltd

The Atrium, Southern Gate
Chichester,
West Sussex PO19 8SQ, England
Telephone (+44) 1243 779777

Email (for orders and customer service enquiries): cs-books@wiley.co.uk
Visit our Home Page on www.wileyeurope.com or www.wiley.com

All Rights Reserved. No part of this publication may be reproduced, stored in a retrieval system or transmitted in any form or by any means, electronic, mechanical, photocopying, recording, scanning or otherwise, except under the terms of the Copyright, Designs and Patents Act 1988 or under the terms of a licence issued by the Copyright Licensing Agency Ltd, 90 Tottenham Court Road, London W1T 4LP, UK, without the permission in writing of the Publisher. Requests to the Publisher should be addressed to the Permissions Department, John Wiley & Sons Ltd, The Atrium, Southern Gate, Chichester, West Sussex PO19 8SQ, England, or emailed to permreq@wiley.co.uk, or faxed to (+44) 1243 770620.

Designations used by companies to distinguish their products are often claimed as trademarks. All brand names and product names used in this book are trade names, service marks, trademarks or registered trademarks of their respective owners. The Publisher is not associated with any product or vendor mentioned in this book.

This publication is designed to provide accurate and authoritative information in regard to the subject matter covered. It is sold on the understanding that the Publisher is not engaged in rendering professional services. If professional advice or other expert assistance is required, the services of a competent professional should be sought.

Other Wiley Editorial Offices

John Wiley & Sons Inc., 111 River Street, Hoboken, NJ 07030, USA

Jossey-Bass, 989 Market Street, San Francisco, CA 94103-1741, USA

Wiley-VCH Verlag GmbH, Boschstr. 12, D-69469 Weinheim, Germany

John Wiley & Sons Australia Ltd, 42 McDougall Street Milton, Queensland 4064, Australia

John Wiley & Sons (Asia) Pte Ltd, 2 Clementi Loop #02-01, Jin Xing Distripark, Singapore 129809

John Wiley & Sons Canada Ltd, 6045 Freemont Blvd, Mississauga, Ontario, L5R 4J3, Canada

Wiley also publishes its books in a variety of electronic formats. Some content that appears in print may not be available in electronic books.

Library of Congress Cataloging-in-Publication Data

Levitt, Malcolm H.
Spin dynamics : basics of nuclear magnetic resonance / Malcolm H. Levitt.
– 2nd ed.
p. cm.
Includes bibliographical references.
ISBN 978-0-470-51118-3 (hb : acid-free paper) – ISBN 978-0-470-51117-6
(pbk : acid-free paper)
1. Nuclear spin. 2. Nuclear magnetic resonance. I. Title.
QC793.3.S6L47 2007
538’.362–dc22
2007022146

British Library Cataloguing in Publication Data

A catalogue record for this book is available from the British Library
ISBN 9780470511183 HB
9780470511176 PB
Typeset in 9.5/11.5 Palatino Roman by Thomson Digital, Noida, India
Printed and bound in Great Britain by Antony Rowe Ltd, Chippenham, Wiltshire
This book is printed on acid-free paper responsibly manufactured from sustainable forestry in which
at least two trees are planted for each one used for paper production.

To my mother and father

Contents

Part 8 Appendices 597

Appendix A: Supplementary Material 599

Preface

In this second edition I have tried to address some of the deficiencies of the first edition, but without disturbing the structure of the text too much. I have now included an overview of the NMR of quadrupolar nuclei, given the important subject of pulsed field gradients more prominence, and addressed the subject of spin-1/2 pairs in solids more thoroughly. It is a complex task to revise a large book, and I am not sure whether I have been successful. Let's see what you think.

I am very grateful to all the people who pointed out errors in the first edition, which I hope to have corrected in this new version. These include Juan Alberdi, Bernard Ancian, Stefan Berger, Tom Bloemberg, Geoffrey Bodenhausen, Dave Bryce, Shidong Chu, André Dorsch, Nick Higham, Vladimir Hnizdo, Eric Johnson, Alan Kenwright, Karel Klika, Olivier Lafon, Linda Lai, Young Lee, Phil Lucht, Slobodan Macura, P. K. Madhu, Ian Malcolm, Arnold Maliniak, Emi Miyoshi, Gareth Morris, Norbert Müller, Juan Paniagua, Tanja Pietrass, Tatyana Polynova, E. J. Pone, Jan Rainey, Michael Roehrl, David Siminovitch, Chunpen Thomas, Bill Wallace, John Waugh, and Steven Wimperis. I also thank Zosia Beckles for help with the initial computer spadework.

As always, my research group and our research visitors have been a constant source of inspiration and enthusiasm. So I thank Giancarlo Antonioli, Jacco van Beek, Pauline Brouillaud, Darren Brouwer, Marina Carravetta, Maria Concistrè, André Dorsch, Axel Gansmüller, Natala Ivchenko, Ole Johannessen, Per-Eugen Kristiansen, Linda Lai, P. K. Madhu, Salvatore Mamone, Ildefonso Marín-Montesinos, Giulia Mollica, and Giuseppe Pileio for your input. Many of the new sections in this book have derived from our group discussions.

Special thanks to Geoffrey Bodenhausen and Angelika Sebald for giving detailed criticism on the text. Thanks to P. K. Madhu for the photograph from India.

Fiona Woods and Andy Slade at Wiley have been patient, encouraging and helpful during the preparation of this edition.

As usual, I take sole responsibility for any errors and omissions.

Finally, I thank my wife and daughter Latha and Leela again, for their renewed patience and support.

Technical Details

The book was written on Apple Macintosh© computers. The text was written in LaTeX©, using a large number of self-programmed macros. Most of the diagrams were drawn by the author using a combination of Mathematica© and Adobe Illustrator©. Errata and supplementary notes are available through the website www.mhl.soton.ac.uk

Preface to the First Edition

This book has a long prehistory. It began approximately 12 years ago, when I was persuaded by my friend (and squash court enemy) Jim Sudmeier, to give a short series of lectures on the basics of NMR at Tufts University in Boston, MA. The lectures were probably not a tremendous success, but I was inspired to write up the material as some sort of short book. I was naive enough to feel that I could probably cover the basics in perhaps 100 pages using a minimum of equations. I worked on this 'proto-book' for over a year in Cambridge, England, before I realised that I was only scratching the surface of the subject and that I was not yet prepared for the task.

The situation changed in Stockholm where I became involved in teaching an intensive course each year on NMR to third-year undergraduates. Over a period of around seven years I built up a large set of handwritten lecture notes. The experience of teaching made me realise how difficult it is to keep the subject accessible while still imparting something useful to those students wishing to continue into NMR research. Over many years I experimented with various permutations of the material until I ended up with a set of notes which form the basis of this book.

The bulk of the final writing was done in India where I enjoyed the hospitality of Professor Anil Kumar at the Indian Institute of Science in Bangalore for three months.

The book which emerged is still not precisely the one I wanted to write: I wanted to communicate the beauty and usefulness of NMR in a rather simple and non-mathematical way. In the end, I did not succeed at all in keeping down the number of equations. Teaching showed me that equations are simply the only way to present the subject clearly. Nevertheless, although some of the mathematics may look a little frightening to the uninitiated, I think none of it is truly difficult. Most workers in NMR, including myself, have somehow learnt to muddle through the mathematics without any formal training, and the mathematics given here is just a distillation of my own muddling.

The one thing more discouraging to students than anything else is bad terminology and notation, especially when its defects are not pointed out plainly. Faced with a confusing but accepted term, many students draw the conclusion that the problem lies in their own stupidity, rather in the true cause, which is often simple carelessness by its originators, amplified by uncritical perpetuation. This problem falls into a general pattern of teaching science as if everything is already understood and 'engraved in stone'. I care too much about NMR to accept such a static view of the subject and I have tried to combat the most offending eyesores in this book. Some of these suggestions may be controversial with established workers in the field. Nevertheless, I stand by these suggestions and hope that they will catch on in time. I point out the following items here: (i) I consistently distinguish between 'rate' (the change in something over a small time interval, divided by the duration of that interval) and 'rate constant' (a factor appearing in a rate equation); (ii) I consistently distinguish between 'time' (needs no explanation) and 'time constant' (inverse of a rate constant); (iii) I consistently distinguish between a 'time point' and an 'interval' (which is the separation between two time points); (iv) I use the notation t for a time point, and τ for an interval (with the single exception of the evolution interval in a two-dimensional experiment, for which I use the widespread notation t_1); (v) I consistently use the correct physical sign for the nuclear Larmor frequency, the correct physical sign for the spectral frequency axes, and the correct sign for all spin interactions; (vi) I change the sign of the cross-relaxation rate constant in the Solomon equations (Chapter 20), so as to bring it into line with a kinetic description; (vii) I avoid terminology such as 'emission peak', 'rotating-frame experiment', 'phase-sensitive 2D experiment', and 'time-reversal experiment' which are widely used in the field but which have no physical basis. I also avoid terminological fossils such as 'low field' and 'high field', whose original physical basis has been undermined by the development of NMR methodology, leaving them sadly marooned in a world in which they no longer make sense.

I have also not shied away from minor modifications of conventions for the sake of clarity. For example, I consistently use a deshielding convention for all elements of the chemical shift tensor, instead of using the deshielding convention for the isotropic chemical shift and the shielding convention for the chemical shift anisotropy, which seems to be the standard practice.

I have also introduced some novel notation, for example the 'box notation' for coherences in a weakly coupled system. I have personally used this notation for many years, and know that it is useful and that it works. However, I have only rarely used it in a scientific paper. Here, I am taking the opportunity of exposing it to a wider audience.

In one exceptional case I have allowed the convenience of the final equations, and consistency with most of the existing literature, to overrule the transparency of the physics: I have imposed mathematically positive rotations for r.f. pulses (the 'Ernst convention') by manipulating the definition of the rotating frame in a messy way.

Although I have tried to take care, I am sure that this book contains many remaining inconsistencies, and will be very grateful to be informed about them.

Another point of contention may be my presentation of quantum mechanics. In order to make NMR comprehensible I attack vigorously the widespread view that spin-1/2 particles only have two 'allowed orientations' (up and down). Quantum mechanics says no such thing but it is surprising how emotionally this view can be defended. Emotions may also be inflamed over my very 'physical' discussion of the dynamics of single spins. I have been told in all seriousness that quantum mechanics 'forbids' any such discussions. My view is that quantum mechanics is not understood in its completeness by anyone and that the field is wide open to any physical interpretation, as long as that interpretation is demonstrably useful in a particular situation. The interpretation presented in Chapter 9 and the following chapters is neither radical nor original, but is nevertheless very useful for understanding NMR. I am fully aware that this physical picture runs into trouble in certain situations (such as the observation of non-local entangled spin states, as in the Einstein–Rosen–Podolosky paradox). Nevertheless, the 'arrow' picture of a single spin is demonstrably useful over the limited domain of NMR, and I regularly use it myself in thinking about old experiments and developing new ones.

Since NMR is an enormous subject, I have had to select only a very few experiments for detailed discussion. Both my selection of topics and the very basic level at which many of these are treated will probably annoy the specialists. For this I can only apologize. I could simply manage no more material at this stage.

One point on which I am personally dissatisfied is how little I manage to say about solid-state NMR, which is my own main research interest. I had considered having a brief review of the field in a single chapter. However, I decided against that, since it became rapidly clear that I could not maintain a comparable depth of discussion without greatly increasing the size of the book. So I will have to defer the treatment of solid-state NMR to another time, maybe another book.

One remark on my literature referencing: I have been very sparse, and have generally tried to restrict myself to sources that I think will be useful to the reader. The references do not indicate the priority of some group in a particular area.

There are many people other than myself who have contributed to this book. As I mentioned above, the whole thing grew out of a series of lecture notes. Those notes would never have condensed into a useful form without the participation and probing questions of the students I have taught in Stockholm, including Kai Ulfstedt-Jäkel, Tomas Hirsch, Baltzar Stevensson and Clas Landersjö. There are many others: unfortunately I don't remember all of your names, but I do thank you if you read this. I did learn a lot from you all.

I do remember those students who went on to be my graduate students and co-workers, and I have relied over the years on your enthusiasm, support, and amazing hard work. Many of you have also made very specific and useful suggestions about this material. So thanks again to Zhiyan Song, Xiaolong Feng, Dick Sandström, Oleg Antzutkin, Mattias Edén, Torgny Karlsson, Andreas Brinkmann, Marina Carravetta, Xin Zhao, Lorens van Dam and Natala Ivchenko. I have also enjoyed the visits of many wonderful scientists, all of whom have contributed to this book in one way or another, at least in spirit. These include Young K. Lee, S. C. Shekar, K. D. Narayanan, Michael Helmle, Clemens Glaubitz, Angelika Sebald, Stefan Dusold, Peter Verdegem, Sapna Ravindranathan, Pratima Ramasubrahmanyan, Colan Hughes, Henrik Luthman, Jörn Schmedt auf der Günne and P. K. Madhu. I am extremely grateful to the critical reading and detailed suggestions of Gottfried Otting, Gareth Morris, Ole Johannessen, Arnold Maliniak, Dick Sandström, Maurice Goldman, Colan Hughes and Ad Bax. Thanks also to Melinda Duer for ploughing through the first (aborted) version of the book. I am also very grateful to Sapna Ravindranathan, Gottfried Otting, Warren Warren, Jianyun Lu and Ad Bax for supplying some of the figures. Special thanks to Anil Kumar for your hospitality in Bangalore and many delightful discussions. Very special thanks to Jozef Kowalewski for many years of invaluable support in Stockholm and for your constructive comments on the text.

Special thanks to Angelika Sebald for a very large number of insightful and constructive suggestions. Your knowledge and enthusiasm has been an inspiration.

In addition, I would like to thank Ray Freeman and Richard Ernst, from whom I learnt to think about NMR in two very different ways.

Although many people have commented on the text of this book, I take sole responsibility for any errors and omissions.

Finally, I thank my wonderful wife Latha and daughter Leela for your patience, understanding, advice, encouragement and help, as I climbed this personal mountain.

Introduction

> Commonplace as such experiments have become in our laboratories, I have not yet lost that sense of wonder, and delight, that this delicate motion should reside in all ordinary things around us, revealing itself only to him who looks for it.
>
> E. M. Purcell, Nobel Lecture, 1952

In December 1945, Purcell, Torrey and Pound detected weak radio-frequency signals generated by the nuclei of atoms in ordinary matter (in fact, about 1 kg of paraffin wax). Almost simultaneously, Bloch, Hansen and Packard independently performed a different experiment in which they observed radio signals from the atomic nuclei in water. These two experiments were the birth of the field we now know as nuclear magnetic resonance (NMR).

Before then, physicists knew a lot about atomic nuclei, but only through experiments on exotic states of matter, such as found in particle beams or through energetic collisions in accelerators. How amazing to detect atomic nuclei using nothing more sophisticated than a few army surplus electronic components, a rather strong magnet, and a block of wax!

In his Nobel Prize address, Purcell was moved to a poetic description of his feeling of wonder, cited above. He went on to describe how

> in the winter of our first experiments. . . looking on snow with new eyes. There the snow lay around my doorstep – great heaps of protons quietly precessing in the Earth's magnetic field. To see the world for a moment as something rich and strange is the private reward of many a discovery.

In the years since then, NMR has become an incredible physical tool for investigating matter. Its range is staggering, encompassing such diverse areas as brains, bones, cells, ceramics, inorganic chemistry, chocolate, liquid crystals, laser-polarized gases, protein folding, surfaces, superconductors, zeolites, blood flow, quantum geometric phases, drug development, polymers, natural products, electrophoresis, geology, colloids, catalysis, food processing, metals, gyroscopic navigation, cement, paint, wood, quantum exchange, phase transitions, ionic conductors, membranes, plants, micelles, grains, antiferromagnets, soil, quantum dots, explosives detection, coal, quantum computing, cement, rubber, glasses, oil wells and Antarctic ice.

Two brief examples may suffice here to show the range and power of NMR.

The first example is taken from *functional NMR imaging*. As explained in Section 12.6, it is possible to use the radio-frequency (r.f.) signals from the nuclei to build up a detailed picture of the three-dimensional structure of an object. The grey image given in Plate 1 shows this method applied to a human head, revealing the lobes of the brain inside the skull. The red and yellow flashes superimposed on the picture reveal *differences* in the NMR signals when the subject is performing some mental task, in this case processing the memory

---

Spin Dynamics: Basics of Nuclear Magnetic Resonance, Second Edition Malcolm H. Levitt

of a face that has just been removed from view. NMR can map out such mental processes because the brain activity changes slightly the local oxygenation and flow of the blood, which affects the precession of the protons in that region of the brain.

The second example illustrates the determination of biomolecular structures by NMR. Plate 2 shows the structure of a protein molecule in solution, determined by a combination of multidimensional NMR techniques, including the COSY and NOESY experiments described in Chapters 16 and 20. The structure is colour coded to reveal the mobility of different parts of the molecule, as determined by NMR relaxation experiments.

In this book, I want to provide the basic theoretical and conceptual equipment for understanding these amazing experiments. At the same time, I want to reinforce Purcell's beautiful vision: the heaps of snow, concealing innumerable nuclear magnets, in constant precessional motion. The years since 1945 have shown us that Purcell was right. *Matter really is like that*. My aim in this book is to communicate the rigorous theory of NMR, which is necessary for *really* understanding NMR experiments, but without losing sight of Purcell's heaps of precessing protons.

Part 1

Nuclear Magnetism

1 Matter

1.1 Atoms and Nuclei

Matter is made of *atoms*. Atoms are made up of electrons and *nuclei*. Each atomic nucleus has four important physical properties: *mass*, *electric charge*, *magnetism* and *spin*.

The *mass* of bulk matter is largely due to the mass of the nuclei. A large number of other physical properties, such as heat capacity and viscosity, are strongly dependent on the nuclear mass.

The *electric charge* of atomic nuclei is supremely important. Atoms and molecules are bound together by strong electrostatic interactions between the positively charged nuclei and the negatively charged electrons. The chemical properties of each element are determined by the electric charge on the atomic nuclei.

The other two properties, nuclear magnetism and nuclear spin, are much less evident. The magnetism of a nucleus implies that it interacts with magnetic fields, like a small bar magnet. However, nuclear magnetism is very weak and is of little consequence for atomic or molecular structure. The bulk magnetism of some materials, such as iron, is due to the electrons, not to the nuclei.

The *spin* of the nucleus is even less tangible. The spin of a nucleus indicates that, very loosely speaking, the atomic nucleus behaves as if it is spinning around, rotating in space like a tiny planet.

Nuclear magnetism and nuclear spin have almost no effect on the normal chemical and physical behaviour of substances. Nevertheless, these two properties provide scientists with a wonderful tool for spying on the microscopic and internal structure of objects without disturbing them.

Magnetic nuclei interact with magnetic fields. These magnetic fields may come from the molecular environment, e.g. the surrounding electrons, or from other nuclear spins in the same molecule. Magnetic fields may also originate from sources outside the sample, such as an external apparatus. This book tells a small part of a long, complicated, and rather unlikely story: How the extremely weak magnetic interactions of atomic nuclei with the molecular environment on one hand, and with the spectrometer apparatus on the other hand, give access to detailed molecular information which is inaccessible by any other current method.

1.2 Spin

The concept of spin is difficult. It was forced upon scientists by the experimental evidence.[1] Spin is a highly abstract concept, which may never be entirely 'grasped' beyond knowing how to manipulate the quantum mechanical equations.

Nevertheless, it is worth trying. NMR involves detailed manipulations of nuclear spins. The field has developed to a high level of sophistication, in part because of the possibility of thinking 'physically' and 'geometrically' about spins without being entirely wrong. Geometrical arguments can never tell the whole truth, because the human mind is probably incapable of grasping the entire content of quantum mechanics.

Spin Dynamics: Basics of Nuclear Magnetic Resonance, Second Edition Malcolm H. Levitt

Nevertheless, it is possible to acquire a feel for spin beyond a purely technical proficiency in the equations. In this book, I will try to communicate how I think one should think about nuclear spins, as well as presenting the technical mathematics.

1.2.1 Classical angular momentum

A rotating object possesses a quantity called *angular momentum*. This may be visualized as a vector pointing along the axis about which the object rotates; your right hand may be used to figure out which way the arrow points. If your thumb points along the rotation axis, then the right-hand fingers 'wrap around' in the direction of the rotation:

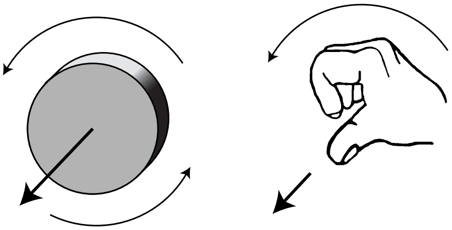

Figure 1.1
Macroscopic angular momentum.

1.2.2 Quantum angular momentum

In quantum mechanics, angular momentum is *quantized*. Consider, for example, a diatomic molecule:

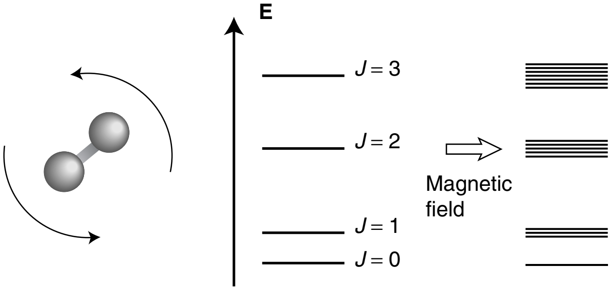

Figure 1.2
A rotating molecule, its energy levels, and the Zeeman effect.

As described in many texts (see *Further Reading*), and discussed further in Chapter 7, a rotating diatomic molecule possesses a set of stable rotational states, in which the total angular momentum L_{tot} has one of the values[2]

$$L_{\text{tot}} = [J(J+1)]^{1/2}\hbar \tag{1.1}$$

where J takes *integer* values $J = 0, 1, 2\ldots$ and $\hbar \cong 1.054 \times 10^{-34}$ J s is Planck's constant divided by 2π. This equation implies the *quantization of total angular momentum*.

The rotational energy of a molecule is proportional to the square of the total angular momentum, so the energy is also quantized. For a rigid molecule, the energies of the stable rotational states are

$$E_J = BJ(J+1) \tag{1.2}$$

where B is called the rotational constant for the molecule. B is small for a heavy molecule and is large for a light one.

The molecule may be in a stable state with zero total angular momentum, or with total angular momentum $\sqrt{2}\hbar$, or with total angular momentum $\sqrt{6}\hbar$, etc. The actual rotational state of a molecule depends on its history and its environment.

The total angular momentum of the molecule determines how fast it is rotating, but conveys no information on the axis of the rotation.

More detail about the rotation of the molecule is given by specifying a second quantum number, M_J. This quantum number M_J takes one of the $2J+1$ integer values $M_J = -J, -J+1 \ldots + J$, and says something about the direction of the rotation. The quantum number M_J is sometimes referred to as the *azimuthal quantum number*. The physical significance of M_J is examined more closely in Chapters 7 and 10.

In the absence of an external field, each of the $2J+1$ states with the same value of J but different values of M_J are *degenerate*, meaning that they have the same energy.

The application of a magnetic field breaks the degeneracy, causing each of the $(2J+1)$ sublevels to have a slightly different energy. This is called the *Zeeman effect*. The energy separation between the M_J sublevels in a magnetic field is called the *Zeeman splitting*.

The basic features of this phenomenon are displayed by any physical system that is able to rotate. Whatever the system is, there is always the same structure of $(2J+1)$-fold degenerate energy levels. The stable physical states of a rotating quantum system are always specified by a quantum number J for the total angular momentum and an azimuthal quantum number M_J that carries information on the direction of the rotation. The total angular momentum is always given by $[J(J+1)]^{1/2}\hbar$, and the azimuthal quantum number M_J always takes one of the values $M_J = -J, -J+1 \ldots + J$. The degeneracy of the M_J sublevels may be broken by applying an electric or magnetic field.

1.2.3 Spin angular momentum

Spin is also a form of angular momentum. However, it is not produced by a rotation of the particle, but is an *intrinsic* property of the particle itself.

The total angular momentum of particles with spin takes values of the form $[S(S+1)]^{1/2}\hbar$ (the symbol S is used instead of J to mark a distinction between spin angular momentum and rotational angular momentum). Particles with spin S have $(2S+1)$ sublevels, which are degenerate in the absence of external fields, but which may have a different energy if a magnetic or electric field is applied.

Each elementary particle has a particular value for the spin quantum number S. For some particles, S is given by an integer, i.e. one of 0, 1, 2 . . .. For other particles, S is given by a half integer, i.e. one of 1/2, 3/2, 5/2 . . ..

Particles with integer spin are called *bosons*. Particles with half-integer spin are called *fermions*.

The spin of an elementary particle, such as an electron, is *intrinsic* and is independent of its history. Elementary particles simply *have* spin; molecules *acquire* rotational angular momentum by energetic collisions. At the absolute zero of the temperature scale, all rotational motion ceases ($J = 0$). A particle such as an electron, on the other hand, always has spin, even at absolute zero.

Half-integer spin posed severe problems for the physicists of the 1920s and 1930s. It may be shown that half-integer spin cannot arise from 'something rotating', and, at that time, no other way of producing angular momentum could be imagined. The concept of half-integer spin was resisted until the pressure of experimental evidence became overwhelming. One of the greatest triumphs of theoretical physics was Dirac's derivation of electron spin-1/2 from relativistic quantum mechanics. Nowadays, spin is a central concept in our theoretical understanding of the world.

A particle like an electron may, therefore, have two kinds of angular momentum: (i) A 'conventional' angular momentum arising from its *motion*. For example, an electron in an atom may have *orbital angular momentum* due to its circulating motion around the nucleus. Such motion is associated with an *integer* angular momentum quantum number and behaves just like the angular momentum of a rotating molecule. (ii) ‘Intrinsic’ or *spin angular momentum*, which arises from nothing, being simply a feature of the electron’s ‘nature’, and which is always the same, namely spin $= 1/2$.

There is no such concept as the rotation of the electron around its own axis; there is only spin.

The concept of intrinsic angular momentum is very difficult to grasp. Why should this be so? Why is the intrinsic angular momentum of a particle more difficult to understand than intrinsic mass and intrinsic electric charge?

The level of difficulty of a concept tends to be inversely proportional to its familiarity in the macroscopic world. The concept of intrinsic mass is relatively easy to accept because mass has familiar everyday manifestations. This is because the mass of two particles is the sum of the masses of the individual particles. The mass of a book is therefore the sum of the masses of all the electrons, quarks, etc. of which the book is composed (minus a relativistic correction – but let’s forget about that!). So the concept of mass ‘makes it’ to the macroscopic world. We can ‘feel’ mass and can imagine that fundamental particles ‘have a mass’.

Electric charge is a little more difficult, because there are negative and positive charges, and in almost all cases they cancel out for macroscopic objects. However, by performing simple experiments, like rubbing a balloon on a woolly jumper, it is possible to separate some of the charges and achieve obvious macroscopic effects, such as sticking a balloon to the ceiling. Through such experiences it is possible to get a feel for charge, and become comfortable with the idea that fundamental particles ‘have a charge’.

Similarly, magnetism acquires familiarity through the existence of ferromagnetic objects that possess macroscopic magnetism.

Spin is more difficult, because there is no such thing as macroscopic spin. Matter is built up in such a way that the spins of the different particles cancel out in any large object. Spin doesn’t ‘make it’ to the macroscopic world.[2]

This is not to say that spin is unimportant. In fact electron spin has a very profound effect on the everyday world, because the stability of molecules and their chemical behaviour rely on it (as will be discussed shortly, in the context of the Pauli principle). However, this effect is not *obviously* a consequence of electron spin, and there are no large objects that have angular momentum ‘by themselves’, without rotating.[3]

Probably no-one really understands spin on a level above the technical mathematical rules. Fortunately it doesn’t matter so much. We know the rules for spin and that’s enough to be able to exploit the phenomenon.

1.2.4 Combining angular momenta

Consider a system with two parts, each one being a source of angular momentum, with quantum numbers J_1 and J_2. The angular momenta may be due to rotational motion or to spin. The total angular momentum of the entire system is given by $[J_3(J_3+1)]^{1/2}\hbar$, where J_3 takes one of the following possible values:

$$\boxed{J_3 = \begin{cases} |J_1 - J_2| \\ |J_1 - J_2| + 1 \\ \vdots \\ |J_1 + J_2| \end{cases}} \tag{1.3}$$

Expressed in words, this means that the complete system has a total angular momentum quantum number given either by the sum of the two individual angular momentum quantum numbers, or by the difference in the two individual angular moment quantum numbers, or any of the values in between, in integer steps.

In general, each of the possible total angular momentum states has a different energy. In many cases that state itself behaves like a new object with angular momentum quantum number J_3.

An important example of this combination rule involves two particles of spin-1/2, i.e. $S_1 = S_2 = 1/2$. In this case, we have $|S_1 - S_2| = 0$ and $|S_1 + S_2| = 1$. There are, therefore, only two possibilities for the total angular momentum quantum number, namely $S_3 = 0$ and $S_3 = 1$. In the state $S_3 = 0$, the spins of the two particles cancel each out. This idea is often expressed by saying that the spins are 'antiparallel' in the $S_3 = 0$ state:

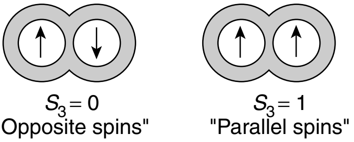

Figure 1.3
The combination of two spins-1/2 leads to a singlet state with spin $S = 0$ and a triplet state with spin $S = 1$.

In the 'parallel' spin state $S_3 = 1$, on the other hand, the spins of the two particles reinforce each other. In general, the $S_3 = 0$ and $S_3 = 1$ states have different energy. Note that it is not possible to make a general statement as to which state has the *lowest* energy; this depends on the details of the interactions in the system.

The $S_3 = 1$ energy level has three substates, with azimuthal quantum number $M_S = \{-1, 0, 1\}$. If the environment is isotropic (the same in all directions of space), the three substates have the same energy. States with total angular momentum $S_3 = 1$ are often called *triplet states*, to stress this threefold degeneracy. The degeneracy of the $S_3 = 1$ level may be broken by applying an external field (magnetic or electric).

The $S_3 = 0$ level, on the other hand, is not degenerate. The only state in this level has quantum number $M_S = 0$. States with total angular momentum $S_3 = 0$ are often called *singlet states*.

1.2.5 The Pauli Principle

The spin of particles has profound consequences. The *Pauli principle*[4] states

> two fermions may not have identical quantum states.

Since the electron is a fermion, this has major consequences for atomic and molecular structure. For example, the periodic system, the stability of the chemical bond, and the conductivity of metals may all be explained by allowing electrons to fill up available quantum states, at each stage pairing up electrons with opposite spin before proceeding to the next level. This is called the *Aufbau principle* of matter, and is explained in standard textbooks on atomic and molecular structure (see *Further Reading*).

The everyday fact that one's body does not collapse spontaneously into a black hole, therefore, depends on the spin-1/2 of the electron.

1.3 Nuclei

The next sections discuss briefly how the energy level structures of molecules, atoms, nuclei, and even the elementary particles within the nuclei, fit into the angular momentum hierarchy of nature, according to the rule given in Equation 1.3.

1.3.1 The fundamental particles

According to modern physics, everything in the universe is made up of three types of particle: *leptons*, *quarks* and *force particles*.

Leptons are low-mass particles. Six varieties of lepton have currently been identified, but only one is familiar to non-specialists. This is the *electron*, a lepton with electric charge $-e$ and spin-1/2. The unit of electric charge e is defined as *minus* the electron charge and is equal to 1.602×10^{-19} C.

Quarks are relatively heavy particles. At the time of writing (2007), it is believed that there are six 'flavours' of quarks in nature, all of which have spin-1/2. Three of the quarks have electric charge $+2e/3$. The other three quarks have electric charge $-e/3$. Apart from their charge, the quarks are distinguished by additional quantum numbers called 'strangeness', 'charm', 'top' and 'bottom', but there is no need to discuss these topics here. It is speculated that quarks are themselves built up of extended objects, which have received the dull name 'superstrings'.

Force particles are responsible for mediating the action of the different particles on each other. The most important force particle is the *photon*, which is the particle manifestation of the electromagnetic field. Light, which consists of electromagnetic waves, can be viewed as a stream of photons. The photon has no mass and no electric charge, and has spin $= 1$. There are also force particles called *gluons* and *vector bosons*. Gluons are manifestations of the so-called *strong nuclear force*, which holds the atomic nucleus and its constituent particles together. Vector bosons are manifestations of the *weak nuclear force*, which is responsible for radioactive β-decay.

1.3.2 Neutrons and protons

The *neutron* and the *proton* both consist of three quarks, stuck together by gluons.[4]

The *neutron* is composed of three quarks: two with charge $-e/3$ and one with charge $+2e/3$. Therefore, the total electric charge of the neutron is zero; hence its name. The neutron has spin-1/2. The neutron spin is due to combinations of quark spins.[5] For example, if two of the quark spins are antiparallel, we get an $S = 0$ state. Addition of the third quark spin gives a total neutron spin $S = 1/2$:

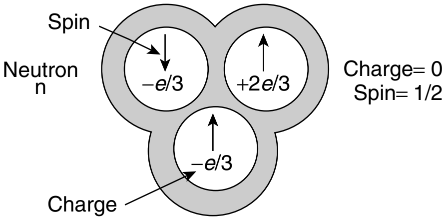

Figure 1.4
A neutron.

The *proton* is also composed of three quarks, but this time two of the quarks have charge $+2e/3$ and the other one has charge $-e/3$. Therefore, the total electric charge of the proton is $+e$. Just as for the neutron, an antiparallel spin configuration for two of the quarks gives rise to a net spin-1/2 state for the proton:[4]

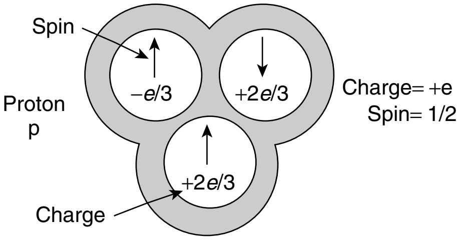

Figure 1.5
A proton.

What happens if the quark spins inside the neutron and proton have different configurations? For example, if the three quark spins were all parallel, the total spin would be 3/2. Such particles do in fact exist, but they are only known in high-energy physics experiments (for example, the spin-3/2 state of the proton is known as the Δ^+ particle). High-spin neutrons and protons have enormously higher energies than ordinary neutrons and protons. Under ordinary circumstances, these exotic states may be ignored. The

Table 1.1 Some properties of the most important elementary particles.

Particle	Rest mass/kg	Charge	Spin
e	9.109×10^{-31}	$-e$	1/2
n	1.675×10^{-26}	0	1/2
p	1.673×10^{-26}	$+e$	1/2
photon	0	0	1

neutron and proton may, therefore, be treated as distinct and independent particles, both with well-defined spin-1/2.

We also ignore the numerous other particles formed by combinations of different sets of quarks. From now on, the only particles to be considered are the electron, the neutron, the proton and the photon, whose relevant properties are summarized in Table 1.1.

1.3.3 Isotopes

The atomic nucleus consists of neutrons and protons.[6] Neutrons and protons are known collectively as *nucleons*.

An atomic nucleus is specified by three numbers: the *atomic number*, the *mass number*, and the *spin quantum number*.

The *atomic number* Z specifies the number of protons inside the nucleus. The electric charge of the nucleus is Ze. The electric charge of the nucleus determines the chemical properties of the atom of which the nucleus is a part. The atomic number is traditionally denoted by a chemical symbol, for example H for $Z = 1$, He for $Z = 2$, C for $Z = 6$, N for $Z = 7$, O for $Z = 8$, etc. The periodic table of the elements lists the atomic nuclei in order of increasing atomic number.

The *mass number* specifies the number of nucleons in the nucleus, i.e. the total number of protons and neutrons. Nuclei with the same atomic number but different mass numbers are called *isotopes*. Most isotopes in existence are *stable*, meaning that the nucleus in question has no measurable tendency to explode or disintegrate. Several isotopes are *unstable*, or *radioactive*, meaning that the nucleus tends to disintegrate spontaneously, ejecting energetic particles, which are often dangerous. NMR is mainly concerned with stable isotopes. Stable nuclei are usually formed from approximately equal numbers of protons and neutrons.

Some common examples of stable isotopes are:

$$\begin{array}{ll} {}^{1}\mathrm{H} = \mathrm{p} & {}^{12}\mathrm{C} = 6\mathrm{p} + 6\mathrm{n} \\ {}^{2}\mathrm{H} = \mathrm{p} + \mathrm{n} & {}^{13}\mathrm{C} = 6\mathrm{p} + 7\mathrm{n} \end{array}$$

and so on.

Some examples of unstable (radioactive) isotopes are:

$${}^{3}\mathrm{H} = \mathrm{p} + 2\mathrm{n}$$

$${}^{14}\mathrm{C} = 6\mathrm{p} + 8\mathrm{n}$$

Lighter atomic nuclei were formed by the primal condensation of nucleons as the heat of the big bang dissipated. Heavier nuclei (beyond and including iron) were synthesized later by nuclear fusion processes inside stars. These complex nuclear processes led to a mix of isotopes with varying *isotopic distributions*. These distributions are almost uniform over the surface of the Earth. For example, ~98.9% of carbon nuclei

Table 1.2 A selection of nuclear isotopes and their properties. A complete listing of nuclear spins, gyromagnetic ratios and Larmor frequencies (omitting the sign) may be found on the website `www.webelements.com`.

Isotope	Ground-state spin	Natural abundance/%	Gyromagnetic ratio $\gamma/10^6$ rad s^{-1} T^{-1}	NMR frequency at 11.74 T $(\omega^0/2\pi)$/ MHz
^{1}H	1/2	~100	267.522	−500.000
^{2}H	1	0.015	41.066	−76.753
^{3}H	1/2	0	285.349	−533.320
^{10}B	3	19.9	28.747	−53.718
^{11}B	3/2	80.1	85.847	−160.420
^{13}C	1/2	1.1	67.283	−125.725
^{14}N	1	99.6	19.338	−36.132
^{15}N	1/2	0.37	−27.126	+50.684
^{17}O	5/2	0.04	−36.281	+67.782
^{19}F	1/2	~100	251.815	−470.470
^{23}Na	3/2	~100	70.808	−132.259
^{27}Al	5/2	~100	69.763	−130.285
^{29}Si	1/2	4.7	−53.190	+99.336
^{31}P	1/2	~100	108.394	−202.606
^{35}Cl	3/2	75.77	10.610	−48.990
^{37}Cl	3/2	24.23	8.832	−40.779
^{63}Cu	3/2	69.17	71.118	−132.577
^{65}Cu	3/2	30.83	76.044	−142.018
^{107}Ag	1/2	51.84	−10.889	+20.239
^{109}Ag	1/2	48.16	−12.518	+23.268
^{129}Xe	1/2	24.4	−74.521	+139.045
^{207}Pb	1/2	22.1	55.805	−104.603
^{12}C	0	98.9		
^{16}O	0	~100		

have six neutrons (^{12}C), and ~1.1% have seven neutrons (^{13}C). The small local variations in nuclear isotopic distributions are useful for locating the origin and the age of objects. Some natural isotopic abundances are shown in Table 1.2.

1.4 Nuclear Spin

1.4.1 Nuclear spin states

Most atomic nuclei possess spin. The nuclear spin quantum number is conventionally denoted I.

The nucleus of the main isotope of hydrogen, ^{1}H, contains a single proton and has $I = 1/2$. The spins of other nuclei are formed by combining together the spins of the protons and the neutrons according to the usual rule (Equation 1.3).

Consider, for example, the ^{2}H nucleus, which contains one proton and one neutron. The proton and neutron spins may be combined in a parallel configuration, leading to a nuclear spin $I = 1$, or in an antiparallel configuration, leading to a nuclear spin $I = 0$:

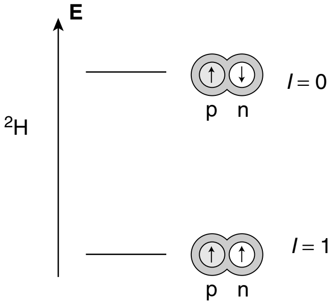

Figure 1.6
Energy levels of a ^{2}H nucleus.

These two nuclear spin states have a large energy difference of ~10^{11} kJ mol^{-1}. This greatly exceeds the energies available to ordinary chemical reactions or usual electromagnetic fields (for comparison, the available thermal energy at room temperature is around ~2.5 kJ mol^{-1}). The nuclear excited states may, therefore, be ignored, except in exotic circumstances.[7] The value of I in the lowest energy nuclear state is called the *ground state nuclear spin*. For deuterium (symbol D or ^{2}H), the ground state nuclear spin is $I = 1$.

For higher mass nuclei, the ground state is one of a large number of possible spin configurations of the protons and neutrons:

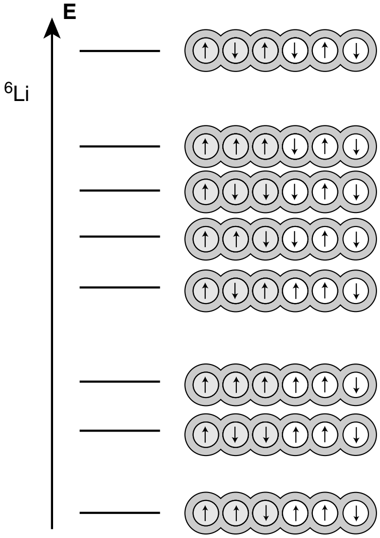

Figure 1.7
Energy levels of a ^{6}Li nucleus, showing the ground state spin $I = 1$.

In general, there are no simple rules for which of the many possible states is the ground state. For our purposes, the ground state nuclear spin is best regarded as an empirical property of each isotope.

Nevertheless, one property may be stated with certainty: from Equation 1.3, isotopes with even mass numbers have integer spin and isotopes with odd mass numbers have half-integer spin.

Two further guidelines apply to isotopes with even mass numbers:

1. If the numbers of protons and neutrons are both even, the ground state nuclear spin is given by $I = 0$. Some examples are: the nucleus ^{12}C, which contains six protons and six neutrons; the nucleus ^{16}O, which contains eight protons and eight neutrons; and the nucleus ^{56}Fe, which has 26 protons and 30 neutrons. All of these have a ground state spin $I = 0$.

2. If the numbers of protons and neutrons are both odd, the ground state nuclear spin is an integer larger than zero. Some examples are the nuclei ^{2}H (1p + 1n, ground state spin $I = 1$), ^{10}B (5p + 5n, ground state spin $I = 3$), ^{14}N (7p + 7n, ground state spin $I = 1$) and ^{40}K (19 p + 21n, ground state spin $I = 4$).

These rules may be understood using models of nuclear structure, a subject that will not be discussed further here.

From now on, the ground state nuclear spin is simply called the 'nuclear spin', for the sake of simplicity. Table 1.2 shows some of the nuclear isotopes of importance in NMR, together with their natural abundances. An overview of all nuclear spins is given in the inside cover as Plates A, B and C.

1.4.2 Nuclear Zeeman splitting

A nuclear state with spin I is $(2I + 1)$-fold degenerate. If a magnetic field is applied, the degeneracy is broken, just as in the case of ordinary angular momentum (see Figure 1.2). The splitting between the nuclear spin levels is called the *nuclear Zeeman splitting*. NMR is the spectroscopy of the nuclear Zeeman sublevels.

Figure 1.8 sketches the nuclear Zeeman levels of a ^{1}H nucleus, a ^{15}N nucleus, and a ^{27}Al nucleus as a function of the applied magnetic field. The ^{1}H and ^{15}N nuclei are both spin-1/2, and so the nuclear ground state splits into two sublevels in the applied magnetic field (since $2 \times (1/2) + 1 = 2$). The ^{27}Al nucleus is spin-5/2 and, hence, the nuclear ground state splits into six levels in the applied magnetic field (since $2 \times (5/2) + 1 = 6$).

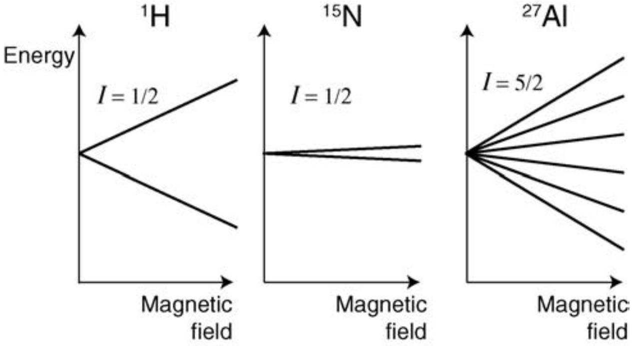

Figure 1.8
Nuclear Zeeman sublevels of the ^{1}H, ^{15}N and ^{27}Al nuclear ground states.

The Zeeman splitting of a proton nucleus is about 10 times larger than the Zeeman splitting of a ^{15}N nucleus, in the same magnetic field. This is because a proton is about 10 times more magnetic than a ^{15}N nucleus. This will be discussed in Chapter 2.

The Zeeman splitting *within* the nuclear ground state must not be confused with the enormously larger splitting between the nuclear ground state and the nuclear excited states. The Zeeman splittings are far smaller than thermal energies and are the subject of NMR spectroscopy. The splitting between the nuclear excited state and the nuclear ground state is so large that the nuclear excited states may be completely ignored in ordinary chemistry and spectroscopy.[6]

1.4.3 Zero-spin nuclei

A minority of nuclear isotopes have zero nuclear spin in the ground state and display no nuclear Zeeman effect. By a quirk of fate, organic substances contain many of these spinless isotopes. The most common isotopes of carbon, oxygen and sulfur, namely ^{12}C, ^{16}O and ^{32}S, all have zero nuclear spin and are NMR silent.

1.4.4 Spin-1/2 nuclei

Nuclei with spin $I = 1/2$ are of major importance in NMR. As discussed in Chapter 8, such nuclei are spherical in shape and have convenient magnetic properties. Plate A shows the distribution of spin-1/2 nuclei in the periodic table of the elements. They are mainly scattered around the right-hand side of the periodic table.

Most chemical elements have no spin-1/2 isotope. The alkali and alkaline earth metals possess no spin-1/2 isotopes at all. In contrast, spin-1/2 isotopes are well represented in organic materials. The most common isotopes of hydrogen and phosphorus have spin-1/2 (^{1}H and ^{31}P), and carbon and nitrogen possess the rare spin-1/2 isotopes ^{13}C and ^{15}N. The abundant fluorine isotope ^{19}F is also of importance.

Spin-1/2 isotopes are well represented in the precious and heavy metals, and the noble gases contain a possess two spin-1/2 isotopes, namely ^{3}He and ^{129}Xe.

1.4.5 Quadrupolar nuclei with integer spin

Nuclei with spin $I > 1/2$ are known as 'quadrupolar nuclei', for reasons discussed in Chapter 8. The NMR of such nuclei is a rich but relatively difficult field, which is increasing in popularity, especially in the context of solid-state NMR.

Quadrupolar nuclei with integer values of I are uncommon. Plate B shows their distribution in the periodic table. By far the most abundant nucleus of this type is ^{14}N, which occurs in almost 100% natural abundance. Deuterium (^{2}H) is of great importance despite its low natural abundance, since it is relatively easy to separate from ^{1}H by physical methods and to prepare ^{2}H-enriched substances.

The nuclear spins $I = 3, 4, 5, 6$ and 7 are represented by only one isotope each, some of which are obscure. There are no nuclei at all with ground state spin $I = 2$. The $I = 7$ isotope ^{176}Lu has the highest nuclear spin in the entire periodic table.

1.4.6 Quadrupolar nuclei with half-integer spin

Quadrupolar nuclei with $I = 3/2$, $5/2$, $7/2$ or $9/2$ are common (see Plate C). They are well represented throughout the entire periodic table, but are particularly prominent for the alkali metals, the boron-to-thallium group, and the halogens. There is a striking alternation across many parts of the periodic table, with every other element possessing an abundant isotope with a half-integer quadrupolar nucleus. I do not know the reason for this alternation, which must reflect some feature of nuclear structure and energetics.

The importance of the isotopes is not necessarily reflected by their abundance. For example, the isotope ^{17}O has a very low natural abundance but is, nevertheless, of great importance since it is the only stable oxygen isotope with nuclear spin.

1.5 Atomic and Molecular Structure

1.5.1 Atoms

The atomic nucleus has a positive electric charge $+Ze$. An *atom* is composed of a nucleus surrounded by Z electrons, each with charge $-e$. For example, an atom of ^{4}He consists of a nucleus, containing two neutrons and two protons, surrounded by a cloud of two electrons. The simplest atom is hydrogen, which contains a nucleus of one proton and a single orbiting electron.

An atom is electrically charged if the total charge on the nucleus does not balance out exactly the charge on the electron cloud. Such species are called *ions*. For example, a nucleus containing 11 protons and 12 neutrons, surrounded by a cloud of 10 electrons, is called a $^{23}\mathrm{Na}^{+}$ ion. A nucleus containing 17 protons and 18 neutrons, surrounded by a cloud of 18 electrons, is called a $^{35}\mathrm{Cl}^{-}$ ion.

Atomic structure does not really concern us here, but it is worth seeing how the angular momentum of the atom works out (see *Further Reading* for a more detailed discussion). There are three sources of angular momentum in a hydrogen atom: the electron spin, the proton spin, and the electron orbital angular momentum, which is associated with the motion of the electron around the nucleus. The orbital angular momentum of the electron is characterized by a quantum number, usually called l. Since this type of angular momentum is associated with motion, the quantum number l is an integer. Quantum states with zero electron orbital angular momentum are called *s-orbitals*. Quantum states with electron orbital angular momentum $l = 1$ are called *p-orbitals*, and so on. In addition, the energy levels of the H atom display *fine structure*, which is due to the coupling of the electron orbital angular momentum to the *electron spin*. Even closer observation of the energy levels reveals *hyperfine structure*, which is due to the participation of the *proton spin*.

Atoms containing more than one electron have many more possibilities, because each electron is a source of orbital angular momentum as well as spin angular momentum. In such systems, the *Pauli principle* comes into play. Electrons may only occupy identical orbital states if their spins are antiparallel. In practice this means that the lowest energy states in an atom usually have small values of total electron spin.

1.5.2 Molecules

An electron cloud containing more than one nucleus is called a *molecule*. For example, a molecule of water ($^{1}\mathrm{H}_2{}^{16}\mathrm{O}$) consists of a cloud of 10 electrons surrounding three nuclei: one with eight protons and eight neutrons (the oxygen nucleus), and two consisting of a single proton (the hydrogen nuclei).

In a molecule, the quantum mechanical motion of the electrons constrains the nuclei to a particular geometric configuration. In the case of the water molecule, the three nuclei are geometrically stable only when the three nuclei form a triangular configuration with an H—O—H angle of around 105°.

A typical molecule contains many potential sources of angular momentum: the motion of the electrons around the nuclei, the motion of the nuclear framework around the centre of mass of the molecule, in some cases the rotation of internal molecular groups, the electron spins, and the nuclear spins. However, because of the Pauli principle, and the quantum rules for chemical bonding, the electron orbital angular momenta and the electron spin angular momenta almost always cancel out in the lowest energy state of a chemically stable molecule (there are a few exceptions, such as O_2, which has total electron spin $S = 1$ in the ground state, and NO, which has finite orbital angular momentum in the ground state). In most cases, the only sources of angular momentum in the molecular ground state are the molecular rotation and the nuclear spins.

The motion of the nuclear framework can very often be treated 'classically': the molecule is treated as an ordinary object rotating in space. Inside this rotating molecule are trapped the nuclear spins. This ignores the quantum nature of the molecular motion. Nevertheless, it almost always gives reasonable answers, and we will use it from now on.

Molecules differing only in the mass numbers of the nuclei are called *isotopomers*. Isotopomers usually have almost identical chemical and physical properties, since these are determined almost completely by the charges on the nuclei and the number of surrounding electrons. All substances are mixtures of isotopomers, even when chemically pure. For example, pure water is composed mainly of the predominant isotopomer $^{1}\mathrm{H}_2{}^{16}\mathrm{O}$, but there are also small amounts of the minor isotopomers $^{1}\mathrm{H}^{2}\mathrm{H}^{17}\mathrm{O}$, $^{1}\mathrm{H}_2{}^{17}\mathrm{O}$, etc. The relative abundance of the isotopomers is governed by the natural statistical distributions of the various isotopes.

There are slight differences in the chemical and physical properties of isotopomers, due to the different nuclear masses. Molecules with different nuclear masses have different vibrational energy levels, altering slightly the rates of certain chemical reactions. Physical properties, such as diffusive mobilities, are also influenced by the molecular mass. This allows isotopomers to be separated by techniques such as gas chromatography. For example, it is possible to separate ^{13}CO molecules from the abundant ^{12}CO isotopomers by passing the gas through very long chromatographic columns. The ^{13}C-labelled carbon monoxide is used as a starting material for total organic synthesis of other ^{13}C-labelled substances. Many modern NMR experiments use isotopically enriched substances prepared in this way.

NMR is unusual in that different isotopomers behave completely differently. In many cases, one isotopomer gives a large signal while another isotopomer gives none, even though the substances are physically and chemically almost indistinguishable. NMR achieves this distinction because it is based upon the nuclear spin, rather than the nuclear mass.

The mass of a molecule is roughly equal to the sum of the nuclei in the molecule. In the biological sciences, it is popular to specify molecular masses in units of daltons (abbreviation Da). A ^{12}C atom has a mass of exactly 12 Da. A medium-sized protein molecule has a molecular mass of around 30×10^3 Da = 30 kDa (30 kilodaltons). Outside the biological sciences, molecular masses are usually specified in units of grams per mole (g mol^{-1}).

1.6 States of Matter

The states of matter are assembled from the basic building blocks of atoms, molecules and ions. We will now review the special features of the different material states, since the motions of the molecules in these states have a large effect on NMR experiments.

Traditionally, the material states are classified in terms of their bulk mechanical properties (i.e. hard or soft, rigid or flowing). These bulk mechanical properties often reflect the mobility of the constituent molecules or atoms.

1.6.1 Gases

Gases are defined as low-density material phases that fill the volume of any container to which they are confined, independent of its shape. Gases are characterized by very high mobility of the molecules or atoms. It is possible to perform NMR experiments on gases, although this is not done very often.[8]

1.6.2 Liquids

Liquids are relatively dense material phases characterized by their flow under shear forces. There is high molecular mobility in liquid phases. This molecular mobility has two aspects: translation mobility and rotational mobility (Figure 1.9). *Translation molecular mobility* means that the molecules or atoms slide past each other rather freely and wander over appreciable distances in a relatively short time. For example, a water molecule at room temperature typically wanders over a distance of ~7 μm over a time interval of 10 ms. *Rotational molecular mobility* means that the individual molecules rotate around their own centres of gravity in a more or less random fashion. For example, a medium-sized protein molecule in water solution typically rotates through an angle of around 1 rad after a time of around 10 ns. Both of these types of mobility are very important for NMR, because they tend to average out many of the nuclear spin interactions, simplifying the behaviour of the nuclear spins.

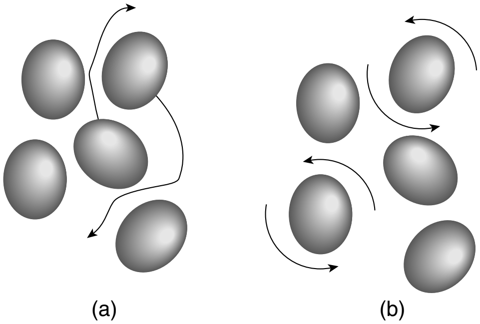

Figure 1.9
In a liquid, molecules have both translation mobility (a) and rotational mobility (b). If the liquid is isotropic, the mobilities are the same in all directions.

A further distinction must be made between *isotropic* and *anisotropic* liquid phases.

In isotropic liquids, the translation and rotational mobilities of the molecules are the same in all directions. This is true, for example, in ordinary water or for molecules dissolved at low concentration in common solvents. As discussed in Chapter 8, the molecular motion in an isotropic liquid effectively removes many of the nuclear spin interactions, leading to rather simple NMR spectra.

There are also *anisotropic liquids* (also called *liquid crystals*), in which the molecules adopt a non-isotropic spatial configuration. In some cases the molecules are arranged in layers, in other cases like coins stacked up on top of each other, and in still other cases the molecules adopt a sort of loose helical structure. Despite these loose spatial configurations, the molecules are still very mobile and the substance flows under shear forces, which distinguishes a liquid crystal from a solid. An everyday example of a liquid crystal is a soap film, in which the soap molecules are arranged in layers. As far as NMR is concerned, anisotropic liquids behave very differently from isotropic liquids because the translation and rotational mobilities of the molecules depend on the direction (Figure 1.10). Consider, for example, a case in which the molecules are shaped like long rods and all the rods are, on average, aligned along a particular direction in space (called the *director* in liquid-crystal science). It is easier for the molecules to spin around an axis that is parallel with the director than around an axis that is perpendicular to the director. In the former case they have a better chance of completing a full rotation without hitting a neighbouring molecule, as opposed to the latter case, where collisions are almost inevitable. This motional anisotropy leads to incomplete averaging of the nuclear spin interactions and, hence, more complicated NMR spectra. Nevertheless, the NMR spectra of liquid crystals, and of molecules dissolved in liquid crystals, can be very informative. One way in which anisotropic liquids are used to enhance the study of biological molecules is sketched in Section 16.4.

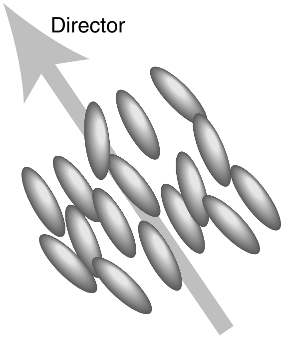

Figure 1.10
In an anisotropic liquid, the molecular mobilities depend on the direction in space.

1.6.3 Solids

Solids are high-density material phases that resist shear forces without flowing. Solid materials have an enormous variety of atomic structures. For example, there are *molecular solids*, which are composed of distinct molecules held together by rather weak intermolecular forces, and *non-molecular solids*, in which the atomic nuclei are gripped in an extended electron cloud network, which may extend to the boundaries of the material. There are *crystals*, in which the nuclei are arranged on a repeating lattice, as well as *glasses* and *amorphous solids*, in which long-range repeating patterns are difficult to identify.

The distinction between 'solid' and 'liquid' is not always unambiguous. The behaviour of matter under shear forces depends strongly on the time-scale involved. For example, an ordinary liquid resists deformations and appears as a hard solid on a time-scale of microseconds – as may be tested by diving stomach first into a swimming pool. On the other hand, hard solids, such as rocks, may behave as liquids under long time-scales.[9]

There is a great variety of electronic behaviour in solids. The majority of materials are *electrical insulators*, with very restricted electron mobility. However, in some cases the electron mobility is high, even though the atomic nuclei are more or less fixed in place. Such substances are *metals*. In special circumstances, the electrons may pair up to form bosons that form macroscopic coherent quantum waves. This happens in *superconductors*.

The motion of atoms and molecules is usually greatly restricted in solids. It is this feature that distinguishes solids from liquids on the molecular level. Nevertheless, there can be substantial local motion. For example, some molecular solids display considerable rotational motion of the molecules around their own lattice positions. This often happens for solids composed of near-spherical molecules, e.g. the football-like fullerene molecule C_{60}. At room temperature, the C_{60} 'footballs' rotate randomly and isotropically around their own centres in the solid:

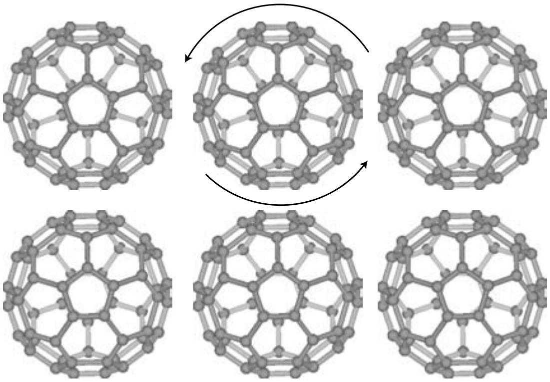

Figure 1.11
Rotation of C_{60} molecules in a solid.

Even in molecules that do not jump or rotate as entire units, there are often local groups which have considerable local mobility. For example, methyl groups $-CH_3$ usually rotate rapidly at room temperature, even in rigid solids. Often, solids display a variety of phases at different temperatures and pressures, with different modes of atomic or molecular mobility.

Generally speaking, the NMR spectra of solids are generally broader and more complex than in liquids. Nevertheless, there has been much recent technical progress in the NMR of solids. The development of experimental techniques has made it possible to obtain solid-state NMR spectra with a resolution approaching that obtained in isotropic liquids in many cases. This is very useful, because there are many substances which cannot, or should not, be dissolved or melted.

Notes

1. Electron spin was first postulated by the Dutch graduate students Uhlenbeck and Goudsmidt in 1925. Their supervisor stated that they could risk publication since they didn't yet have a reputation to destroy. The influential physicist Pauli initially poured scorn on the idea but later became one of its chief proponents.

2. Throughout this book, a box drawn around an equation indicates that it is important in its own right.

3. Some large objects do in fact 'have angular momentum "by themselves", without rotating', although the consequences are subtle and require fine experimental observations. For example, the *Einstein–de Haas effect* shows that the act of magnetizing a substance imparts angular momentum to it (for example, an object suspended by a fine thread starts rotating slowly as it is magnetized). A magnetized substance, like a lump of iron, does have angular momentum, without rotating! There is even a converse phenomenon called the Barnett effect: rotating an object magnetizes it! See E. T. Jaynes, *Rev. Mod. Phys. 34, 143 (1962).*

4. This is a simplified version of the Pauli principle. The full version is as follows:

   > The quantum mechanical state of a system containing two identical bosons is invariant under exchange of the two bosons. The quantum mechanical state of a system containing two identical fermions changes sign under exchange of the two fermions.

   The theorem that two fermions may not occupy the same state follows as a consequence of the full principle. As a matter of fact, the 'Pauli principle' was first given for fermions by Heisenberg, and for bosons by Bose. It is a little mysterious why the principle has become attached to the name of Pauli.

5. The discussion of neutron spin, proton spin, and nuclear spin given in this chapter is oversimplified. In fact, it is known that the orbital motions of the quarks and gluons also contribute to the spin of the proton and neutron (see, e.g., S. D. Bass, Science 315, 1672-1673 (2007)). I deliberately give a naive picture of neutron and proton spin here, because the details are not so important anyway for NMR and because it does make a good story.

6. The neutrons and protons are bound together by an interchange of particles known as mesons. Each meson is made up of two quarks.

7. In *Mössbauer spectroscopy*, transitions between the nuclear energy levels are excited using energetic γ-rays.

8. There are some interesting applications of NMR in gases, although the low density of matter in a gas leads to relatively weak NMR signals. For example, NMR of gaseous ^{129}Xe is used to make images of cavities inside hollow objects, including lungs. In this case, a special technique called *optical pumping* is used to prepare ^{129}Xe gas with a very high nuclear spin polarization, so as to enhance the NMR signals. See, for example, B. M. Goodson, *J. Magn. Reson.* **155**, 157–216 (2002). Some conventional gas-phase NMR spectra, obtained without the help of optical pumping, are shown in Figure 19.21.

9. The first edition of this book propagated the urban myth that old glass windows are thicker at the bottom because the glass creeps slowly under gravity. This is not true. The thickening at the bottom is simply due to the manufacturing process. Thanks to the copy editor for pointing this out.

Further Reading

- For the fundamentals of quantum mechanics and atomic structure, see J. J. Sakurai, *Modern Quantum Mechanics*, Addison-Wesley, 1994, and C. Cohen-Tannoudji, B. Diu, F. Laloë, *Quantum Mechanics* Wiley, London, 1977.
- For atomic structure and orbitals, see P. W. Atkins, *Molecular Quantum Mechanics*, Oxford University Press, Oxford, 1983.
- For the consituents of matter, see F. Close, 'The quark structure of matter' in *The New Physics*, P. Davies, (ed.), Cambridge University Press, Cambridge, 1989.

Exercises

1.1 Which of the following statements *must* be correct, which *might possibly* be correct, and which *cannot* be correct?

(i) The nucleus ^{89}Y (atomic number = 39) has a ground state spin $I = 1/2$.
(ii) The nucleus ^{90}Zr (atomic number = 40) has a ground state spin $I = 1$.
(iii) The nucleus ^{91}Zr (atomic number = 40) has a ground state spin $I = 1/2$.
(iv) The nucleus ^{92}Mo (atomic number = 42) has a ground state spin $I = 0$.
(v) The nucleus ^{138}La (atomic number = 57) has a ground state spin $I = 0$.

1.2 If a particle with spin $S = 5/2$ couples to a particle with spin $S = 3/2$, what are the possible values for the spin of the resulting particle?

2 Magnetism

2.1 The Electromagnetic Field

It is possible to use either a classical or a quantum description of the electromagnetic field.

In the quantum description, the field appears as a collection of photons. This description is accurate, but is difficult to use.

In the classical description, one associates two vectors, **E** and **B**, with every point of space. The field **E** is called the *electric field*, and interacts with *electric charges*. The field **B** is called the *magnetic field*, and interacts with *magnetic moments*[1].

In NMR, the discrepancy between the classical and quantum field descriptions is negligible, and the simpler classical formalism is preferable.

The magnitude of **B** is specified in units of tesla (symbol T). The older unit of gauss (symbol G) is also sometimes used. The conversion is as follows: $1\,\mathrm{G} = 10^{-4}\,\mathrm{T}$. The natural magnetic field at the surface of the Earth is $\sim 50\ \mu\mathrm{T}$. NMR spectrometers currently operate with magnetic fields between around 4 T and 20 T.

The behaviour of the fields **E** and **B** in time and space is governed by the *Maxwell equations*. As shown in standard texts (see *Further Reading*), these equations predict many effects, including the propagation of fields **E** and **B** in empty space. γ-rays, X-rays, light rays, infrared radiation, microwaves, and radio waves are all electromagnetic waves, distinguished only by frequency. A table of typical frequencies and free-space wavelengths for electromagnetic waves is given in Table 2.1.

Table 2.1 Typical frequencies and wavelengths of electromagnetic waves.

Type of Wave	Typical frequency/Hz	Typical wavelength
Radio	$\sim 10^8$	~ 3 m
Microwave	$\sim 10^{10}$	~ 3 cm
Infrared	$\sim 3 \times 10^{13}$	$\sim 10\ \mu$m
Ultraviolet	$\sim 3 \times 10^{16}$	~ 10 nm
X-ray	$\sim 3 \times 10^{18}$	~ 0.1 nm
γ ray	$\sim 3 \times 10^{20}$	~ 1 pm

2.2 Macroscopic Magnetism

All substances are *magnetic*, meaning that they have the capability of interacting with magnetic fields.

This interaction is usually expressed in terms of a magnetic moment $\boldsymbol{\mu}$. The magnetic energy of a small object depends on the interaction between its magnetic moment and the **B** field:

Spin Dynamics: Basics of Nuclear Magnetic Resonance, Second Edition Malcolm H. Levitt

$$E_{\text{mag}} = -\boldsymbol{\mu} \cdot \mathbf{B} \tag{2.1}$$

The dot product indicates that the magnetic energy depends on the relative direction of the vectors **B** and **μ**. The negative sign indicates that the magnetic energy is lowest if the magnetic moment **μ** is parallel to the **B** field:

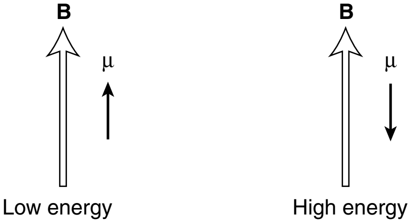

Figure 2.1
Magnetic energy.

In general, Equation 2.1 should be integrated over the volume of the object.

In some substances, the magnetic moment is *permanent*, as for a bar magnet or a compass needle. In the majority of substances, on the other hand, the magnetism is *induced*, meaning that the magnetic moment appears only when an external magnetic field is present.

An object that is free to move tends to align along an external magnetic field so as to minimize the magnetic energy. This is the principle of the compass needle, which has a permanent magnetic moment **μ**. The compass needle swings around to bring the magnetic moment **μ** parallel to the Earth's field **B**.

Most objects display *induced* magnetism and only possess a magnetic moment in the presence of an applied magnetic field. Such induced magnetic moments typically take some time to build up. The equilibrium value of the induced magnetic moment is often proportional to the applied magnetic field **B**, and has the same direction. In SI units, this relationship is written[2] as follows:

$$\mu_{\text{induced}} = \mu_0{}^{-1} V \chi \mathbf{B} \tag{2.2}$$

where $\mu_0 = 4\pi \times 10^{-7}\,\mathrm{H\,m^{-1}}$ is an awkward constant, called the *magnetic constant* or *vacuum permeability*. V is the volume of the object. The dimensionless number χ is called the *magnetic susceptibility* of the material. It expresses how readily the material develops a magnetic moment on exposure to an external magnetic field. χ may have either sign. Materials with a positive value of χ are called *paramagnetic*. Most materials have a negative value of χ, and are called *diamagnetic*. For example, pure water has a magnetic susceptibility $\chi = -9.05 \times 10^{-6}$.

The susceptibility of an object determines how an applied magnetic field is distorted. Objects with a positive susceptibility ($\chi > 0$) tend to pull the magnetic field into the material. Objects with negative susceptibility ($\chi < 0$) tend to push the magnetic field out of the material.

Paramagnetic susceptibilities tend to be larger in magnitude than diamagnetic susceptibilites (as hinted in Figure 2.2).

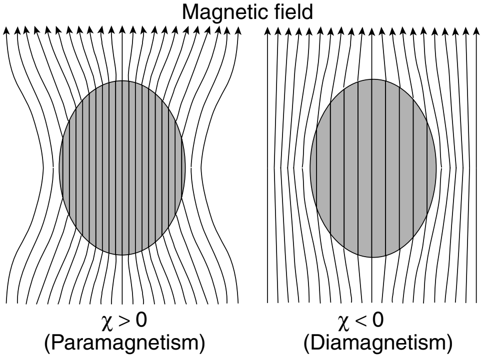

Figure 2.2
An object distorts the magnetic field according to its magnetic susceptibility. The effect is greatly exaggerated in the diagrams shown here.

2.3 Microscopic Magnetism

Where does magnetism come from?

There are three sources: (i) the circulation of electric currents, (ii) the magnetic moments of the electrons, and (iii) the magnetic moments of the atomic nuclei. The electronic contributions (i) and (ii) are almost always many orders of magnitude larger than the nuclear contribution (iii).

Generally speaking, the circulation of electric currents contributes a negative value to the susceptibility, whereas electron and nuclear magnetic moments contribute a positive value. In diamagnetic substances, contribution (i) is greater than contributions (ii) and (iii).

Effect (i) may be understood from elementary physics: If an electric current is made to flow in a loop, then a magnetic field is generated. In most materials, the circulating electric currents exist on a molecular distance scale and are confined to the atoms or molecules themselves. Consider, for example, a hydrogen atom. If the electron is in a *p*-orbital, it circulates around the proton, building a small 'current loop' that generates a magnetic field:

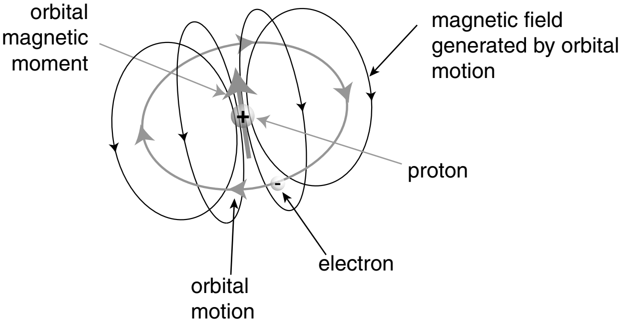

Figure 2.3
Orbital magnetism of the electron in a hydrogen atom.

Effects (ii) and (iii) are more difficult to understand. The electrons and nuclei both possess *intrinsic magnetism*, which is not due to a circulating current. The fundamental particles simply 'have' a magnetic moment, just like they simply 'have' spin angular momentum. Electrons and nuclei have a permanent magnetism.

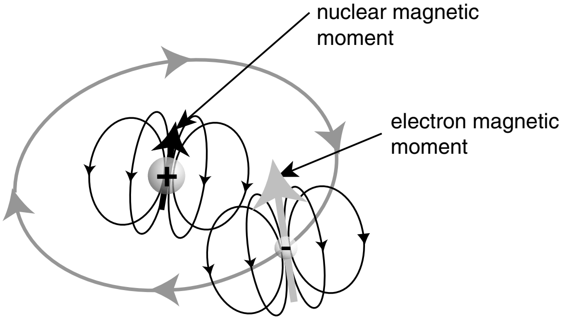

Figure 2.4
Electron and proton spin magnetism in a hydrogen atom.

Spin and magnetism are very closely linked. A very fundamental symmetry theorem[3] requires that the spin angular momentum and the magnetic moment are proportional to each other:

$$\hat{\boldsymbol{\mu}} = \gamma \hat{\mathbf{S}} \tag{2.3}$$

The 'hats' above these symbols indicate that they are quantum mechanical operators, as described in Chapter 7.

For atomic nuclei, the proportionality constant γ is called the *gyromagnetic ratio* (also called the *magnetogyric ratio*). The gyromagnetic ratio is normally specified in units of $\mathrm{rad\,s^{-1}\,T^{-1}}$, for reasons discussed in Section 2.4.

The gyromagnetic ratio may have either sign. For particles with a positive value of γ (including most atomic nuclei), the magnetic moment is parallel to the angular momentum. For particles with a negative value of γ (including the electron and a few atomic nuclei), the magnetic moment is opposite in direction to the angular momentum:

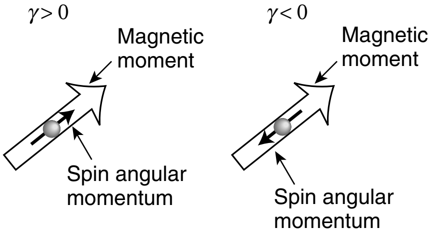

Figure 2.5
The gyromagnetic ratio γ.

The magnetic moment of the electron, like the spin of the electron, was derived by Dirac in his synthesis of quantum mechanics and relativity. The value for the electron's magnetic moment, predicted by quantum electrodynamical theory, is in agreement with the experimental result to the astonishing accuracy of 11 significant figures. The magnetic moments of the quarks, nucleons, and nuclei are not yet understood on this level of detail.

As discussed in Section 1.4.1, atomic nuclei have a ground state spin that derives from the spins and the orbital motions of the constituent particles. Similarly, the nuclear magnetic moment derives from the quark magnetic moments and the currents of charged particles inside the nucleus. The gyromagnetic ratios of some common atomic nuclei are shown in Table 1.2.

In diamagnetic materials, the pairing of the electron spins cancels out the electron magnetism, to a good approximation. The strong magnetism of paramagnetic and ferromagnetic materials is due to the presence of unpaired electron spins.

We return to the subject of macroscopic magnetism after considering the *dynamic* behaviour of nuclear spins in a magnetic field.

2.4 Spin Precession

The angular momentum of a rotating object is a vector. The direction of the vector indicates the axis of the rotational motion. The angular momentum vector may point in any possible direction in space.

The angular momentum of a particle with spin is also a vector, and may also point in any possible direction in space. In this book, the direction of the spin angular momentum is called the *spin polarization axis*. In general, particles with spin, such as proton nuclei, have spin polarization axes pointing in all possible directions:

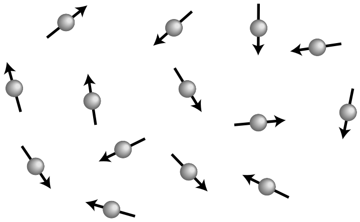

Figure 2.6
Randomly directed spin polarizations.

Elementary discussions of NMR often claim that, according to quantum mechanics, only certain directions of spin angular momentum are 'allowed'. For example, it is often stated that spin-1/2 particles may only be polarized either 'up' or 'down'. This is incorrect. In Chapter 10, I discuss what quantum mechanics *does* say about the behaviour of the spin angular momenta.

The magnetic moment of a nucleus points either in the same direction to the spin polarization (for nuclei with $\gamma > 0$), or in the opposite direction to the spin polarization (for nuclei with $\gamma < 0$). For a sample in equilibrium in the absence of a magnetic field, the distribution of magnetic moments is completely *isotropic*, i.e. all possible directions are equally represented.

Now suppose that a magnetic field is suddenly applied to the sample. What happens to the spin magnetic moments?

A compass needle rotates so as to bring the magnetic moment parallel to the field, minimizing the magnetic energy:

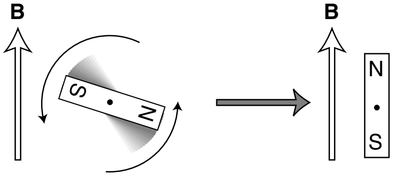

Figure 2.7
Motion of a compass in a magnetic field.

However, a nuclear spin is not a compass needle.[4] The actual response of the spin polarization is to move *around* the field. The magnetic moment of the spin moves on a cone, keeping a constant angle between the spin magnetic moment and the field. This motion is called *precession*.

Figure 2.8
Spin precession.

The spin polarization axis goes around and around on the same precession cone, always keeping the same angle between the spin axis and the field.

The angle of the cone depends only on the initial spin polarization. If the spin is initially polarized exactly along or against the field, then it simply stays there, corresponding to precession on a cone of zero angle. If the spin is initially polarized exactly perpendicular to the field, then the spin polarization moves on a flat disk. For the majority of spins, the angle is intermediate between these extremes:

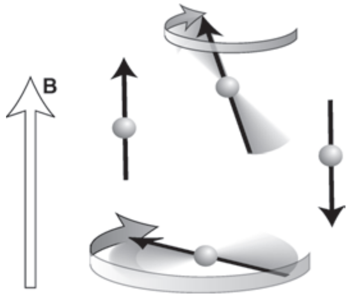

Figure 2.9
The angle of the precession cone depends on the initial direction of the spin.

Spins behave in this way because they possess *angular momentum* as well as a magnetic moment. The presence of angular momentum sharply changes the dynamical properties of the magnetic moment.

Spin precession has many parallels in classical physics. Consider for example, a child's spinning top:

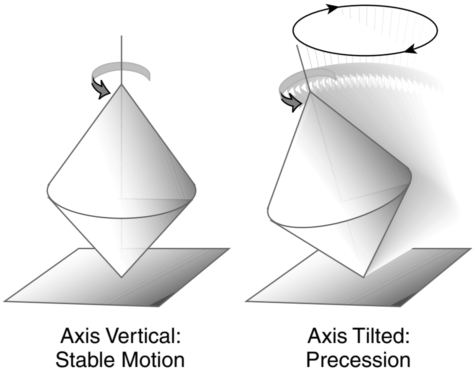

Figure 2.10
Precessional motion of a spinning top.

If the top is set spinning with its axis exactly vertical, it has a stable motion. However, if its axis is slightly skew, then the gravitational pull on the top plus the reaction of the ground on the top's tip combine to produce a torque that 'tries' to pull the top to the ground. Nevertheless, if the top is spinning fast enough, the top does not fall over immediately. Instead, the spinning axis executes a precessional motion, going around in a circle. The term 'precession' is used in classical physics to describe such phenomena.

A similar effect may be observed while riding a bicycle. By leaning slightly to one side, one produces a gravitational torque on the bicycle that might be expected to pull the bicycle immediately to the ground. However, since the wheels have angular momentum, the effect produced is instead to rotate the axis of the wheels so that the bicycle turns a corner. Motorcyclists exploit this effect by hanging off their vehicles on one side when rounding a corner at speed.

A full treatment of such classical examples is very complicated, since they also involve friction, internal degrees of freedom, and additional sources of angular momentum. It is possible to fall off a bicycle by leaning too far, and a skewed top eventually does fall over. For nuclear spins, on the other hand, there are essentially no complications. Precessing spins in a magnetic field offer extremely clean dynamics, free from complicating factors.

2.5 Larmor Frequency

A quantum description of spin precession is given in Chapter 10. This treatment shows that the frequency of precession ω^0 is equal to

$$\boxed{\omega^0 = -\gamma B^0 \qquad (2.4)}$$

where B^0 is the magnetic field at the site of the particle and γ is the gyromagnetic ratio. For nuclear spins, ω^0 is called the nuclear *Larmor frequency*. The Larmor frequency is proportional to the magnetic field.

There are two common ways of specifying the frequency of an oscillation. The most familiar way is to write a frequency in *cycles per second*, or hertz (which is the same thing). For example, a Larmor frequency of 200 MHz implies that the nuclear spin completes 200 million revolutions around its precession cone every second.

The second way of specifying a frequency is in units of radians per second. This is called an *angular frequency*, and is given by the frequency in hertz multiplied by a factor of 2π. A Larmor frequency of 200 MHz corresponds to an angular frequency of $400 \times 10^6\pi$ rad s^{-1}.

In general, the two frequency units may always be converted into each other through the relationships:

$$\boxed{\begin{aligned}\text{frequency in units of rad s}^{-1} &= 2\pi \times (\text{frequency in units of Hz})\\ \text{frequency in units of Hz} &= (\text{frequency in units of rad s}^{-1})/2\pi \qquad (2.5)\end{aligned}}$$

Although angular frequencies appear to be awkward, they make the equations simpler. In this book, the symbol ω always implies an angular frequency in units of radians per second. A frequency in hertz is usually written as $\omega/2\pi$, i.e. the angular frequency divided by 2π.

Equation 2.4 defines the Larmor frequency in radians per second. The Larmor frequency in hertz is given by $-\gamma B^0/2\pi$.

The Larmor frequency has a defined sign. The sign indicates the *sense* of the spin precession around the applied field.[5] Most nuclei have positive γ, in which case the Larmor frequency is *negative*. This means that the precession is in the *clockwise* direction, as seen when looking 'upstream' with respect to the direction of the magnetic field (i.e. standing at the top of Figure 2.11 and looking down):

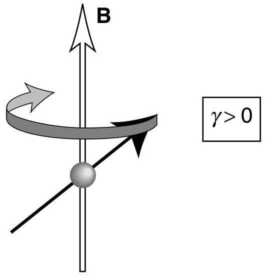

Figure 2.11
Negative precession for nuclei with positive gyromagnetic ratio.

A few nuclei, such as ^{15}N and ^{29}Si, and also the electron, have negative values of γ, in which case the Larmor frequency is *positive*. This indicates precession in the *anticlockwise* direction, as seen when looking 'upstream' with respect to the direction of the magnetic field:

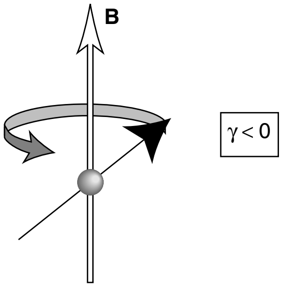

Figure 2.12
Positive precession for nuclei with negative gyromagnetic ratio.

The sense of positive and negative precessions may be obtained using one's right hand: if the thumb points along the magnetic field, the fingers wrap around in the direction of positive precession:

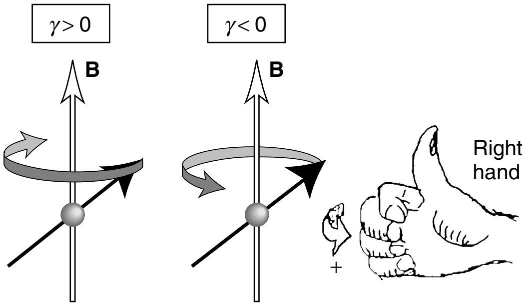

Figure 2.13
Using one's right hand to determine the sense of precession.

The Larmor frequencies of some common nuclear isotopes in a typical NMR field of $B^0 = 11.74\,\mathrm{T}$ are given in Table 1.2.

2.6 Spin–Lattice Relaxation: Nuclear Paramagnetism

Consider again the ^{1}H nuclei in a sample of water. In the absence of an external magnetic field, the spin polarizations are uniformly distributed, pointing in all possible directions in space. The *total* magnetic moment of the sample is very close to zero, since approximately the same number of spins point towards a given direction as against it.

If a magnetic field is suddenly turned on, all proton spins begin executing Larmor precession around the field. For the sake of concreteness, suppose that the external field is 11.74 T. The proton Larmor frequency is $\omega^0/2\pi \cong -500\,\mathrm{MHz}$. Each proton spin completes 500 million full cycles of precession every second, moving always in the negative sense (clockwise looking 'upstream' with respect to the magnetic field).

This precessional motion is essentially invisible. It does nothing to change the total magnetic moment of the sample. An *isotropic* distribution of spin polarizations makes no contribution to the magnetism of the material.

However, the proton spins are not alone: the water molecules, which carry the protons, undergo constant vigorous motion. The orientation of each molecule in space changes constantly, and the relative positions of the molecules interchange all the time. How does this affect the motion of the nuclear spins?

Remarkably, the answer is almost not at all. To a very good approximation, each nuclear spin is oblivious of its immediate environment. As the molecule rotates, the nuclear spin polarizations continue to point in the same direction in space. If a magnetic field is present, the spin polarization vectors steadily precess around the magnetic field, independent of the fact that they are transported in molecules undergoing violent rotations and collisions. One is reminded of a ship's gyroscopic compass, which keeps calm even in a rough sea.

However, on a closer look, one finds that the violent molecular surroundings do slightly influence the nuclear magnets. Each molecule is full of magnetic particles: the electrons and nuclei are all sources of magnetic fields. These fields are small, and they fluctuate rapidly because of the thermal motion of the environment. At any given moment, the spin precesses about a field that is the sum of the external field, which is static, and a very small microscopic field, which varies in time, and which may have any possible direction in space. The total magnetic field seen by each spin, therefore, has a slightly fluctuating magnitude, and also a slightly fluctuating *direction*. At any given time, the local magnetic field experienced by any one nuclear spin is slightly different, both in magnitude and direction, to that of its neighbour:

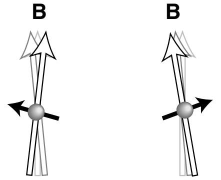

Figure 2.14
Microscopic fields.

These variations are very small: for protons in a sample of water in a 11.74 T field, the local magnetic field at the nuclei fluctuates in direction by only around 10^{-4} degrees. Nevertheless, these tiny fluctuations are very important, because in the long term they allow the isotropy of the nuclear spin polarization to be broken and, hence, a macroscopic nuclear magnetic moment to develop. Without the fluctuating molecular fields, nuclear magnetism would be unobservable.

What happens is quite complicated. The small fluctuating fields from the thermal environment cause a gradual breakdown of the constant-angle 'cone precession' of the nuclear spins. For each spin, the angle between the spin magnetic moment and the external field varies slightly. Over a long time, the magnetic moment of each nuclear spin wanders around, moving between different 'precession cones', and eventually sampling the entire range of possible orientations:

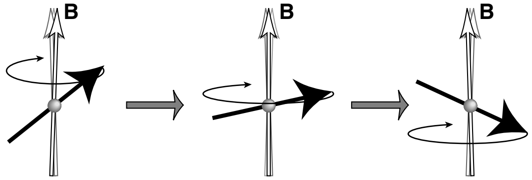

Figure 2.15
Precession in a fluctuating field.

The 'precessional' and 'wandering' motions have very different time-scales. For nuclear spins, the time-scale of the precessional motion is set by the inverse of the Larmor frequency, i.e. a few nanoseconds. The time-scale for the 'wandering motion' under the random molecular fields, on the other hand, is often as long as seconds. In typical cases, a nuclear spin executes many millions of precession circuits before deviating appreciably from its cone of constant angle with respect to the external field.

The important thing is that this wandering motion is *not* completely isotropic. Since the environment has a finite temperature, it is slightly more probable that the nuclear spin is driven towards an orientation with low magnetic energy than towards an orientation with high magnetic energy. The thermal wandering motion is therefore slightly biased towards spin orientations with magnetic moments parallel to the magnetic field.

The biased wandering motion leads eventually to a stable *anisotropic* distribution of nuclear spin polarizations, called *thermal equilibrium*. Although this thermal equilibrium distribution is *stable*, it is not *static* on a microscopic scale. The individual spin magnetic moments still execute continuously their precessing and wandering motion. However, the net *distribution* of spin orientations, with magnetic moments along the field slightly more probable than orientations with magnetic moments opposed to the field, is independent of time. The following figure greatly exaggerates the anisotropy, for the sake of clarity:

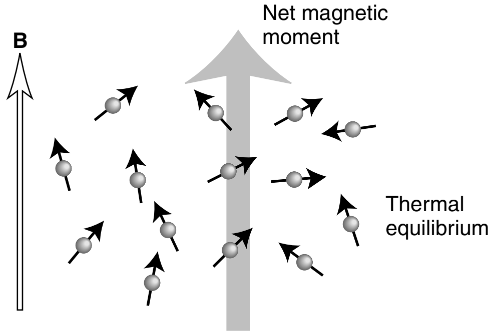

Figure 2.16
Thermal equilibrium.

At realistic field strengths, the anisotropy of the polarization distribution at thermal equilibrium is directly proportional to the ratio of the magnetic and thermal energies. The difference in magnetic energy between a single proton polarized along the field and one polarized opposite to the field is $\hbar\gamma B^0 = 3.3 \times 10^{-25}\,\text{J}$ in a field of $B^0 = 11.74\,\text{T}$. The available thermal energy at room temperature is $k_B T = 4.1 \times 10^{-21}\,\text{J}$, which is four orders of magnitude larger. For nuclear spins, there is only a very slight bias in the spin polarization distribution at thermal equilibrium.

The anisotropy of the magnetization distribution in thermal equilibrium means that the entire sample acquires a small net magnetic moment along the field, i.e. a *longitudinal* magnetic moment. This is the microscopic mechanism of *nuclear paramagnetism*. For protons in water, the nuclear contribution to the magnetic susceptibility may be calculated to be

$$\chi_{\text{nuc}} = \frac{\mu_0 \hbar^2 \gamma^2 c}{4 k_B T}$$

where c is the number of protons per unit volume. This evaluates to

$$\chi_{\text{nuc}} = +4.04 \times 10^{-9}$$

This is about three orders of magnitude smaller than the observed diamagnetism of water, which is due to the electrons rather than to the nuclei (see Section 2.2).

If the external magnetic field is suddenly turned on (or if the sample is rapidly brought into the field) the macroscopic nuclear magnetization is initially zero but gradually grows due to the biased wandering of the spin polarizations, as discussed above. The build-up curve is usually approximately exponential. Suppose that t_{on} is defined as the moment when the external magnetic field is applied, and the direction of the field is defined to be the z-axis. The build-up of longitudinal magnetization has the form

$$\boxed{M_z^{\text{nuc}}(t) = M_{\text{eq}}^{\text{nuc}} \left(1 - \exp\{-(t - t_{\text{on}})/T_1\}\right) \qquad (2.6)}$$

for times $t \geq t_{\text{on}}$:

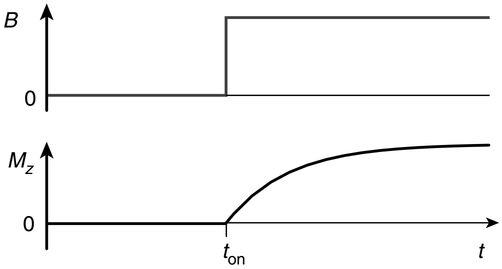

Figure 2.17
The build-up of longitudinal spin magnetization, after the magnetic field is turned on.

The exponential time constant for the process T_1 is known as either the *spin-lattice relaxation time constant* or the *longitudinal relaxation time constant*. The use of the term 'lattice' derives from the early days of NMR, when theoretical effort concentrated on the treatment of NMR in solids and when thermal equilibration was explained in terms of the interactions between the nuclear spins and the crystal lattice. By extension, the term is now used, misleadingly, even for NMR in liquids and gases, which lack a 'lattice'. The term 'longitudinal' simply indicates that the magnetization builds up in the same direction as the applied magnetic field.

The term 'relaxation' is widely used in the physical sciences to indicate the re-establishement of thermal equilibrium after some perturbation is applied. In the case under discussion, thermal equilibrium is first established in the absence of a field, so that all nuclear spin orientations are equally likely. When a magnetic field is applied, this situation no longer corresponds to equilibrium, and the system 'relaxes' to the new equilibrium state, in which the spin polarizations are distributed anisotropically. If the magnetic field is suddenly switched off at a later time t_{off} (where $t_{\text{on}} - t_{\text{off}} >> T_1$), the nuclear spin magnetization relaxes back to zero again, following the law

$$M_z^{\text{nuc}}(t) = M_{\text{eq}}^{\text{nuc}} \exp\{-(t - t_{\text{off}})/T_1\}$$

for times $t \geq t_{\text{off}}$:

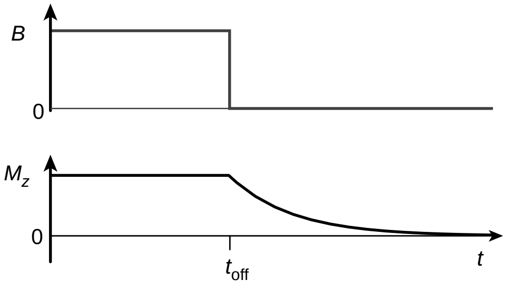

Figure 2.18
The decay of longitudinal spin magnetization, after the magnetic field is turned off.

The relaxation time constant T_1 depends on the nuclear isotope and the sample, including parameters such as temperature and viscosity, if the sample is a liquid. Typically, the value of T_1 is in the range milliseconds to seconds, although T_1 may be as long as days or even months in exceptional cases. The principles of nuclear spin relaxation are discussed in Chapter 20.

2.7 Transverse Magnetization and Transverse Relaxation

The longitudinal nuclear spin magnetization, described above, is almost undetectable. It is about four orders of magnitude less than the typical diamagnetism of the sample, associated with the electrons. Experimental study of the longitudinal nuclear magnetization is impractical.[6]

NMR spectroscopy takes a different approach. Instead of measuring the nuclear spin magnetization *along* the field, the magnetization *perpendicular* to the field is measured.

Suppose that the spin system is allowed to reach thermal equilibrium in a large magnetic field. The macroscopic nuclear magnetization has an equilibrium value $M_{\text{eq}}^{\text{nuc}}$ along the direction of the external field (the z-axis, by convention).

As described above, this equilibrium situation corresponds, on a microscopic level, to a large number of nuclear spin magnets, all precessing around the magnetic field at the same frequency ω^0. The overwhelming majority of nuclear magnets are polarized at an angle to the field and execute precessional motion on wide-angle cones. Nevertheless, there is no *net* magnetization perpendicular to the field, because, on average, the magnetization distribution in thermal equilibrium is cylindrically symmetrical around the z-axis.

Now suppose that the polarization of every single spin is suddenly rotated by $\pi/2$ radians around the x-axis, by some external agency. We will see in Chapter 10 that this is achieved by applying an *r.f. pulse* – an oscillating magnetic field, of appropriate frequency and duration. For the time being, however, we ignore the mechanism and discuss the consequences.

If a spin polarization is initially along the z-axis and is rotated by $\pi/2$ about the x-axis, then the result is a spin polarization along the $-y$-axis:

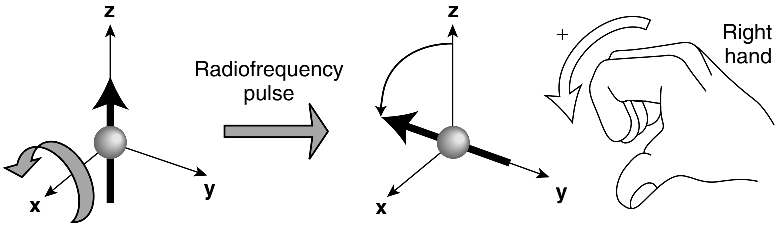

Figure 2.19
Rotation of a spin around the x-axis.

Since the pulse rotates the polarization of every single spin in the sample by the same angle, the pulse also rotates the entire nuclear magnetization distribution of the sample. The net spin polarization along the z-axis is therefore transferred into a net spin polarization along the $-y$-axis, i.e. along an axis perpendicular to the magnetic field. If we were to look 'down' the magnetic field, immediately after the pulse is switched off, we would see slightly more spins polarized along the $-y$-axis than along the y-axis:[7]

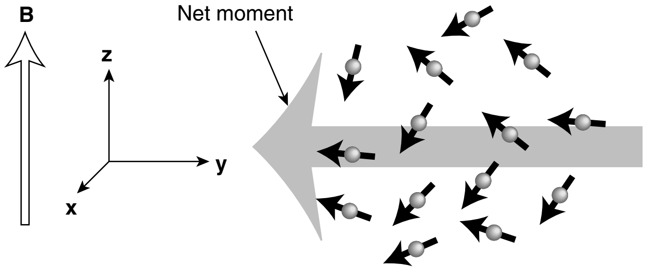

Figure 2.20
Polarization distribution after a pulse.

This net magnetic moment perpendicular to the magnetic field is called *transverse magnetization*.

Now suppose that the pulse is turned off and the spins resume their precessional motion. On a microscopic level, this is 'business as usual'. The individual spins precess on their individual cones. On a macroscopic scale, however, a new feature appears. The state immediately after the pulse corresponds to a net polarization *along the $-y$-axis*, perpendicular to the main field. Since every single spin precesses, the bulk magnetic moment also precesses. The macroscopic nuclear magnetization rotates in the xy-plane, perpendicular to the main magnetic field:

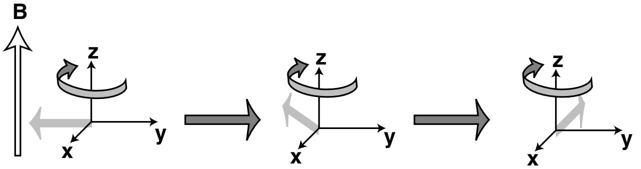

Figure 2.21
Precession of the transverse magnetization.

The precession frequency of the transverse magnetic moment is equal to the precession frequency of the individual spins, i.e. the nuclear Larmor frequency (Equation 2.4).

The macroscopic magnetization components at a time t after the pulse have the form

$$\boxed{\begin{aligned} M_y^{\text{nuc}} &= -M_{\text{eq}}^{\text{nuc}} \cos(\omega^0 t) \exp\{-t/T_2\} \\ M_x^{\text{nuc}} &= M_{\text{eq}}^{\text{nuc}} \sin(\omega^0 t) \exp\{-t/T_2\} \end{aligned} \qquad (2.7)}$$

The transverse magnetic moment precesses at the nuclear Larmor frequency ω^0, slowly decaying at the same time:

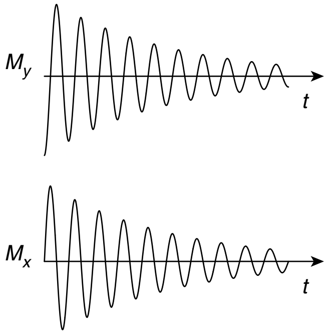

Figure 2.22
Decay and oscillation of the transverse magnetization.

The transverse magnetization decays slowly because it is impossible to maintain exact synchrony between the precessing nuclear magnets. Since the microscopic magnetic fields fluctuate slightly, the precessing nuclear magnets gradually get out of phase with each other. Imagine a large number of clocks, started at the same instant. For the first few hours or days, the clocks show exactly the same time. However, over a period of weeks, small fluctuations in the timing of the different clocks cause them to lose synchrony, and after a year or so the times shown will be completely random. The clocks will have lost coherence with each other.

This decay process is irreversible. Once the transverse magnetization is gone, it cannot be recovered. The clocks cannot be brought back into phase again without starting the whole experiment all over again. This type of process is called *homogeneous decay* in the jargon of NMR.

The time constant T_2 takes into account the homogeneous decay of the precessing macroscopic nuclear magnetization. This time constant has various names, the most common being *transverse relaxation time constant*, *coherence dephasing time constant*, *coherence decay time constant*, and *spin–spin relaxation time constant*. The last of these is misleading, as it seems to imply that the destruction of transverse magnetization requires interactions between the nuclear spins, which is not the case. All that is required is that different spins experience slightly different magnetic fields, so that they precess at slightly different frequencies. This will always be true in a real sample, independent of whether the spins interact with each other.

For the NMR of small molecules in liquids, T_2 is typically of the same order of magnitude as T_1, i.e. several seconds. This implies that the nuclear spins execute several tens of millions of Larmor precession cycles without losing synchrony, which is rather impressive. In other circumstances, such as for large molecules in liquids, or for solids, the transverse relaxation time constant T_2 may be as short as milliseconds.

This picture of transverse spin precession is greatly oversimplified because (i) it assumes that all spins in the sample experience exactly the same magnetic field on the average and (ii) the interactions *between* the nuclear spins are ignored. The true dynamics of nuclear spins are, in reality, considerably more complicated than this. Nevertheless, the conceptual sketch given above is a reasonable first approximation. In certain contexts, such as many NMR imaging experiments, this simple picture is quite adequate.

2.8 NMR Signal

The precessing transverse magnetization after an r.f. pulse is very small. Nevertheless, it is detectable, because it oscillates at a very well-defined frequency.

A rotating magnetic moment generates a rotating magnetic field. Through Maxwell's equations, a changing magnetic field is associated with an electric field.[8] If a wire coil is near the sample, then the electric field sets the electrons in the wire in motion, i.e. an oscillating electric current flows in the wire. It is possible to detect this small oscillating current by using a sensitive r.f. detector.

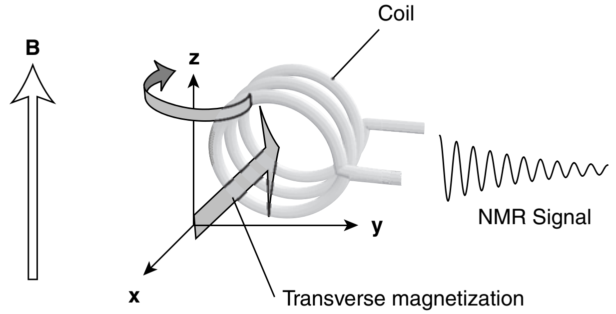

Figure 2.23
The induction of an NMR signal.

Note the geometry of this arrangement: the winding axis of the coil is *perpendicular* to the main magnetic field, in order to detect the precessing *transverse* magnetization.

Essentially the same principle is used in the *bicycle dynamo*, where a rotating magnet, driven by the wheels, generates an electric current that is used to power a lamp.[9]

The oscillating electric current induced by the precessing nuclear transverse magnetization is called the *NMR signal* or *free-induction decay* (FID).

The NMR spectrometer is basically a device capable of: (i) magnetizing the nuclear spins with a large applied magnetic field; (ii) rotating the spin polarizations by r.f. pulses to produce transverse nuclear magnetization; (iii) detecting the small oscillating electric currents induced by the precessing transverse spin magnetization. To some extent, everything else is details.

2.9 Electronic Magnetism

Since electronic magnetism is not the subject of this book, this summary is exceedingly brief. As far as NMR is concerned, the main points to note are as follows.

1. In most materials and molecules, the electronic *ground state* has no net electron spin and no net orbital angular momentum. This is a consequence of the Pauli principle, which requires electrons to pair up in stable molecules. Most molecules have an even number of electrons and, therefore, have no magnetic moment in the electronic ground state. However, there are exceptions. For example, molecular oxygen has a triplet ($S = 1$) ground state. Many transition metal compounds have finite electron spin in the ground state. Molecules with an odd number of electrons, such as free radicals, also have finite electron spin in the ground state.

2. The majority of substances have no magnetic moment in the electronic ground state and are weakly *diamagnetic* ($\chi < 0$). The weak diamagnetism of these substances arises from electron orbital currents induced by the applied magnetic field.

3. Substances with magnetic ground states are usually *paramagnetic* ($\chi > 0$). If the electron magnetic moments interact relatively weakly with each other, then it is possible to perform *electron paramagnetic resonance* (EPR) experiments which are closely analogous to NMR experiments (EPR is also called *electron magnetic resonance* (EMR) or *electron spin resonance* (ESR)). There are considerable technical differences between nuclear and electron magnetic resonance, connected with the much larger linewidths, higher frequencies, and shorter time-scales in the EPR case. We will not be concerned further with EPR here.

4. In many magnetic substances, the electron spins on neighbouring magnetic sites interact strongly. This can give rise to strong cooperative effects, such as *ferromagnetism* and *antiferromagnetism*. The direction of spin polarization on one molecular site strongly influences that of its neighbour, which in turn affects *its* neighbour, and so on. In the end, millions of spins may be aligned mutually by a small external perturbation, in a sort of molecular 'domino effect'. Cooperative electronic magnetism is often strong enough to be directly tangible. How long would it have taken for humanity to discover the magnetic field if naturally occuring pieces of ferromagnetic iron from meteorites did not exist?

For various reasons, NMR is relatively difficult in paramagnetic and ferromagnetic materials. This book is concerned with nuclear magnetism in diamagnetic materials, in which case the existence of electronic magnetism can be more or less ignored. This is not because it is small; on the contrary, electronic magnetism is typically many orders of magnitude larger than the nuclear magnetism, even in diamagnetic substances. Electronic diamagnetism is unimportant in NMR not because it is small, but because it is time independent. It simply leads to a small change of the bulk magnetic field inside the sample, which is easily taken into account by a rather trivial correction term.

The macroscopic aspects of electronic diamagnetism, therefore, are not very important in NMR. However, there is also a *microscopic* aspect to electronic magnetism that has more important consequences. The distribution of electrons in matter is very inhomogeneous when viewed on a molecular distance scale: most of the electrons are very close to the nuclei or are located in the chemical bonds between the nuclei. Nuclear spins at different sites within the same molecule, therefore, experience slightly different magnetic fields. This important effect is called the *chemical shift*, which is introduced in Chapter 3.

Notes

1. **B** is also called the *magnetic flux density field* or the *magnetic induction field*. The field **B** is often confused with a different field, conventionally notated **H**, which is introduced for mathematical convenience in certain calculations. **H** may be regarded as the field **B** corrected for the bulk magnetism of the material, and has no 'fundamental significance'. The **H** field is not used in this book.

2. The relationship shown by Equation 2.2 is not always valid. In anisotropic materials, such as solids and liquid crystals, the induced magnetic moment is not necessarily in the same direction as the applied field. The magnetic properties of anisotropic substances are described by a *susceptibility tensor*, which may be written as a 3×3 matrix.

3. The proportionality of the magnetic moment and the spin angular momentum may be deduced from the *Wigner–Eckart theorem* of quantum mechanics (see *Further Reading*).

4. Juan Paniagua has pointed out that the behaviour of a compass needle is not *fundamentally* different from that of a nuclear spin. The magnetism of a compass needle is derived from electron spins and is therefore also associated with an angular momentum. As a consequence, even a compass needle precesses around the magnetic field, at least in principle. The main difference is that the electron spins in a compass needle have very rapid spin–lattice relaxation. As a result, the magnetic energy is rapidly

converted into thermal energy before a significant amount of precession takes place. For a nucleus, on the other hand, the slow relaxation allows many millions of precession circuits to take place before relaxation leads to reorientation.

5. In many NMR experiments, it is not necessary to consider the sign of the precession frequency in order to perform the experiment. This is because one usually interacts with the nuclei with a *linearly polarized* r.f. field, rather than a *rotating* r.f. field (see Section 8.4.2). Despite this, I carefully include the sign of precession throughout this book, for the following reasons: (i) there are some NMR experiments, especially in NMR imaging, where a *rotating* r.f. field is used – in these cases, it is essential to get the sense of rotation correct in order to perform the experiment; (ii) careful consideration of signs is necessary in many experiments in order to interpret the data correctly; (iii) I'm just irrationally obsessed by the issue.

6. It is possible to detect longitudinal nuclear magnetism by using the very sensitive detector known as a superconducting quantum interference device (SQUID); see C. Connor, *Adv. Magn. Opt. Reson.* **15**, 201 (1990).

7. The axes mentioned here refer to the rotating reference frame, as explained in Chapter 10.

8. The relevant Maxwell equation is

$$\nabla \times \mathbf{E} = -\frac{\partial \mathbf{B}}{\partial t}$$

which links the time derivative of the magnetic field to a 'circulating' electric field. In NMR, the circulating electric field drives the electrons around the windings of the coil (see *Further Reading*).

9. In practice, a bicycle dynamo is usually constructed the other way round, with the coil rotating and the magnet fixed.

Further Reading

- For the relationship of the nuclear magnetic moment to the spin angular momentum, and the Wigner–Eckart theorem, see A. Abragam, *The Principles of Nuclear Magnetism*, Clarendon Press, Oxford, 1961, and E. Merzbacher, *Quantum Mechanics*, 3rd Edition, Wiley, New York, 1998.
- For texts on electromagnetism, see B. I. Bleaney and B. Bleaney, *Electricity and Magnetism*, Oxford University Press, Oxford, 1976, and J. D. Jackson, *Classical Electrodynamics*, Wiley, New York, 1975.

Exercises

2.1 A sample containing magnetic nuclei is left to reach thermal equilibrium in zero magnetic field. A magnetic field is switched on suddenly along the z-axis. After some time, the direction of the field is instantaneously switched to the x-axis. Predict the motion of the three components of the nuclear spin magnetization through this sequence of events, and describe the dynamics of the nuclear spins on a microscopic level.

3 NMR Spectroscopy

3.1 A Simple Pulse Sequence

The magnetic nuclear spins in a sample are detected through their *FID*. As discussed above, the FID is induced by (i) allowing them to reach thermal equilibrium in a large magnetic field; (ii) rotating the nuclear spin polarizations by an *r. f. pulse*; and (iii) detecting and amplifying the weak r. f. signal that is emitted as the spins resume their precessional motion in the magnetic field.

This basic NMR technique is often depicted by the following icon:

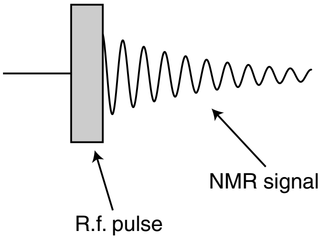

Figure 3.1
A simple pulse sequence.

showing the r. f. pulse and the induced NMR signal. We will see many such iconic pulse sequence representations in the following pages.

In the chapters below, we investigate the theory behind this process, and the instrumentation that is used to carry it out effectively. Before going into details, let us investigate, on a highly qualitative level, what the FID tells us about the nuclear spins and the sample in which they are located.

3.2 A Simple Spectrum

As discussed before, the transverse magnetization components after the r.f. pulse have the following form:

$$M_y^{\text{nuc}} = -M_{\text{eq}}^{\text{nuc}} \cos(\omega^0 t) \exp\{-t/T_2\}$$
$$M_x^{\text{nuc}} = M_{\text{eq}}^{\text{nuc}} \sin(\omega^0 t) \exp\{-t/T_2\} \qquad (3.1)$$

Both components oscillate at the nuclear Larmor frequency ω^0 and decay with the time constant T_2.

Suppose that these two oscillating magnetization components $M_y^{\text{nuc}}(t)$ and $M_x^{\text{nuc}}(t)$ are measured as a function of time, converted into digital form, and stored in a computer. In fact, the experiment cannot really

---

Spin Dynamics: Basics of Nuclear Magnetic Resonance, Second Edition Malcolm H. Levitt

be done this way, for technical reasons.[1] Nevertheless, let us persist with this 'thought experiment', for the sake of argument. Later on, the true operation of an NMR spectrometer is discussed.

The signals described in Equation 3.1 contain enough information to determine both the magnitude of the Larmor frequency ω^0 and the decay time constant T_2. The larger the Larmor frequency ω^0, the faster the magnetization oscillates; and the larger the decay time constant T_2, the more slowly the signals decay. The computer analyses the oscillations and presents the result as the following curve:

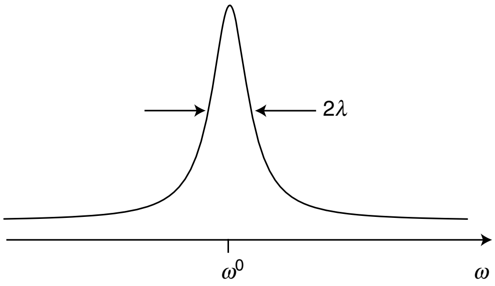

Figure 3.2
A simple spectrum.

The horizontal axis is an angular frequency axis, marked by the symbol ω. The centre of the peak is placed at the Larmor frequency of the spins, equal to ω^0.

In practice, this analysis is performed by a numerical operation called a *Fourier transform*, which is described fully in Chapter 5.

The above plot is a simple example of an *NMR spectrum*. The Fourier transform generates a function with the following mathematical form:

$$S(\omega) = \frac{\lambda}{\lambda^2 + (\omega - \omega^0)^2} \tag{3.2}$$

The value of S is at a maximum when the frequency coordinate ω is equal to the Larmor frequency ω^0, since $\omega - \omega^0$ vanishes in this case. The value of S is small when the frequency coordinate ω is far from the centre of the peak.

The parameter λ is called the *coherence decay rate constant*, and is equal to the inverse of the transverse relaxation time constant T_2:

$$\lambda = \frac{1}{T_2} \tag{3.3}$$

The function in Equation 3.2 is called an *absorption Lorentzian*. It is encountered very often in the theory of NMR.

The frequency axis in the NMR spectrum is labelled with the symbol ω. As mentioned in Section 2.5, this book uses the symbol ω to indicate an *angular frequency*, measured in units of radians per second. Angular frequency units are most convenient for NMR theory, since the equations have their simplest form in such units.

The Lorentzian peakshape has a finite width. As marked on the diagram, the *peakwidth at half-height*, measured in rad s^{-1}, is equal to $2/T_2 = 2\lambda$. This is defined in the following way: Determine the maximum peak height, and then draw a horizontal line at half this vertical value:

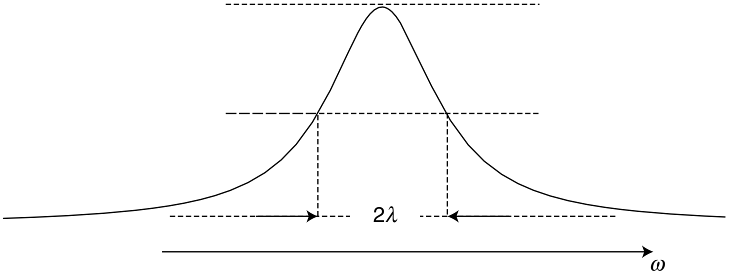

Figure 3.3
Full width at half-height.

The horizontal line intersects the Lorentzian peak at two points, which are separated by 2λ along the horizontal axis.

Since λ is equal to the inverse of the transverse relaxation time constant T_2, this implies that the peakwidth at half-height is equal to $2/T_2$, in units of radians per second.

The same NMR spectrum appears as follows when using a frequency scale of hertz:

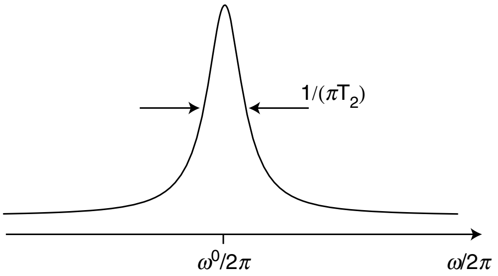

Figure 3.4
Frequency scale in hertz.

The peakwidth in units of hertz is given by $2\lambda/2\pi = \lambda/\pi = 1/(\pi T_2)$.

Note that a *rapid* decay of the transverse magnetization corresponds to a *broad* spectral peak. A *slow* decay of the transverse magnetization corresponds to a *narrow* spectral peak.

The two transverse magnetization components in Equation 3.1 contain enough information to determine the *sign* of the Larmor frequency ω^0, as well as its magnitude. Note the different appearance of the two oscillating components, for Larmor frequencies of the opposite sign:

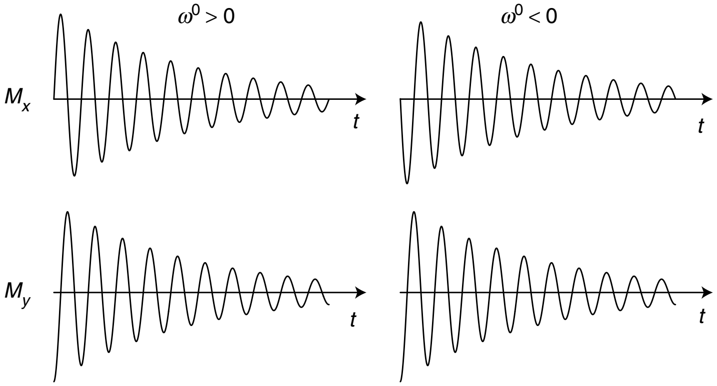

Figure 3.5
Transverse magnetization components for opposite signs of ω^0.

In this book, we will always be faithful to the sign of the Larmor frequency. As described in Section 2.4, the sign of the spin precession is a very real physical property of the nucleus, as real as the mass and the charge. Since the Larmor frequency is given by $\omega^0 = -\gamma B^0$, and the magnetic field B^0 is always positive, the sign of the Larmor frequency is opposite to the sign of the gyromagnetic ratio γ.

Most nuclear spins have positive γ and, therefore, have negative Larmor frequencies ω^0. In the 'NMR thought experiment' described above, the spectral peak for these nuclei would appear at negative frequencies:

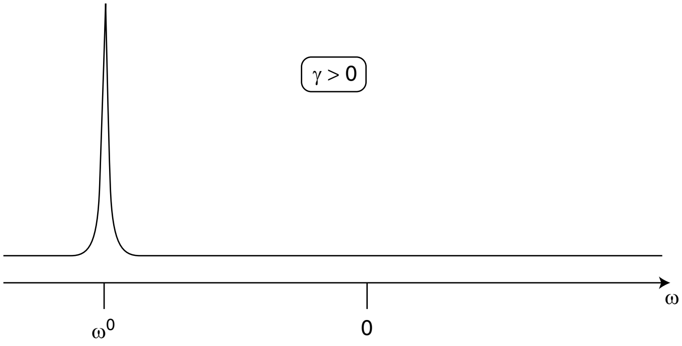

Figure 3.6 NMR spectrum for positive γ.

(The width of the peak is greatly exaggerated.)

Some nuclear spins have negative γ and, therefore, have positive Larmor frequencies ω^0. In the 'NMR thought experiment', the spectral peak would appear at positive frequencies:

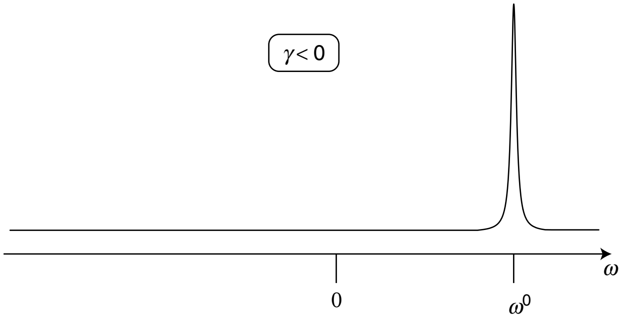

Figure 3.7 NMR spectrum for negative γ.

(The width of the peak is greatly exaggerated again.)

3.3 Isotopomeric Spectra

Now consider a real chemical compound and its NMR spectrum in the 'thought experiment'. Suppose that the sample is a tube containing pure liquid tetramethylsilane, $Si(CH_3)_4$ (TMS). The molecular structure of this compound is as follows:

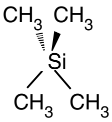

Figure 3.8 Tetramethylsilane (TMS).

This sample contains three chemical elements, Si and C, H, with the common isotopes shown in Table 3.1. It follows that the sample is a mixture of four major isotopomers (see Table 3.2).

Table 3.1 Common isotopes in TMS.

Isotope	Spin	Natural abundance/%	$\gamma/10^6$ rad s^{-1} T^{-1}
^{1}H	1/2	~ 100	267.5
^{12}C	0	~ 98.9	–
^{13}C	1/2	~ 1.1	67.3
^{28}Si	0	~ 92.2	–
^{29}Si	1/2	~ 4.7	−53.2
^{30}Si	0	~ 3.1	–

The abundances of the different isotopomers are easily calculated using simple statistical arguments. For example, the probability of a Si nucleus having mass number 28 is around 0.953, whereas the probability of a C nucleus having mass numbers 12 or 13 is around 0.989 and 0.011 respectively. The probability of a TMS molecule having one ^{28}Si nucleus, three ^{12}C nuclei, and one ^{13}C nucleus is therefore $\sim 4 \times 0.922 \times 0.989^3 \times 0.011 \cong 0.0392 = 3.92\%$ (the factor of 4 is needed because it doesn't matter which of the four carbon nuclei is ^{13}C, so there are four equivalent ways of getting the same isotopomer).

Each isotopomer emits a different NMR signal. Suppose that the magnetic field is 9.3950 T, so that the Larmor frequency of the proton spins is exactly $\omega^0/2\pi = -400.000$ MHz. In this magnetic field, the Larmor frequency of the ^{13}C spins is $\omega^0/2\pi = -100.577$ MHz, and the Larmor frequency of the ^{29}Si spins is $\omega^0/2\pi = +79.460$ MHz. The ^{12}C, ^{28}Si and ^{30}Si isotopes are 'silent', because these nuclei have no spin and are not magnetic.

In the 'thought experiment', we imagine that the complete NMR spectrum, generated by all nuclei at the same time, is detected. (To repeat, this is not actually possible, for technical reasons.) The individual NMR spectra from isotopomers I, II, III and IV would have the following appearance (the peak heights are not to scale):

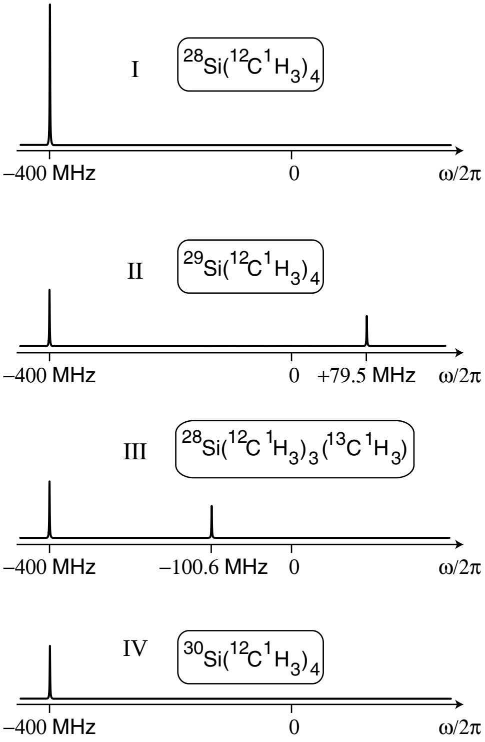

Figure 3.9
Subspectra of TMS isotopomers.

Table 3.2 Major isotopomers in TMS. Rare species containing ^{2}H nuclei, more than one ^{13}C nucleus, or a ^{13}C nucleus as well as a ^{29}Si nucleus are neglected.

Isotopomer	Isotopic composition	Natural abundance/%
I	$^{28}Si(^{12}C^{1}H_3)_4$	~ 88.2
II	$^{29}Si(^{12}C^{1}H_3)_4$	~ 4.5
III	$^{28}Si(^{12}C^{1}H_3)_3\,(^{13}C^{1}H_3)_1$	~ 3.9
IV	$^{30}Si(^{12}C^{1}H_3)_4$	~ 3.0

The *total* NMR spectrum from the TMS sample is sketched in Figure 3.10.

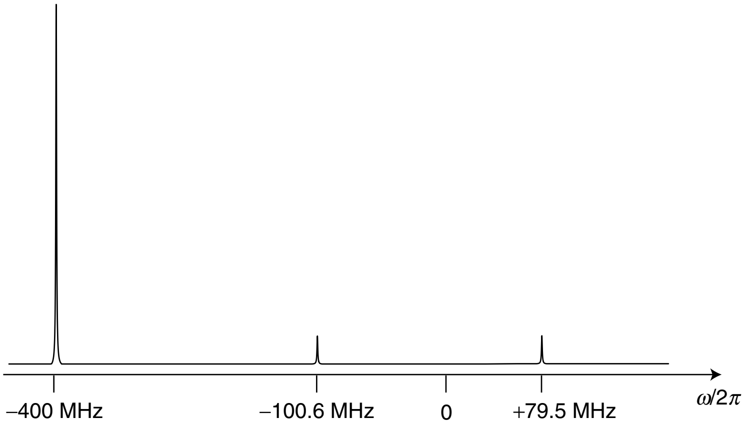

Figure 3.10
Total TMS spectrum.

These spectra use absolute frequency axes and neglect the spectral fine structure (see Sections 3.7 and 3.8).

Note carefully that the major spectral features are produced from different molecules. The proton peak at $\omega^0/2\pi = -400.00\,\text{MHz}$ comes mainly from isotopomers I and IV. The ^{29}Si peak at $\omega^0/2\pi = +79.460\,\text{MHz}$, on the other hand, comes mainly from isotopomer II. The ^{13}C peak at $\omega^0/2\pi = -100.577\,\text{MHz}$ comes mainly from isotopomer III.

The widths of the spectral peaks are greatly exaggerated in the spectra shown above. In reality, they are extremely narrow. The transverse relaxation time constant T_2 for protons in liquid TMS is around 5 s. This corresponds to a peakwidth-at-half-height of $1/(\pi T_2) \cong 50\,\text{mHz}$, which is about 10 orders of magnitude less than the Larmor frequencies themselves. If the spectra were drawn to scale, the width of the NMR peaks would be around the size of a single ink molecule!

3.4 Relative Spectral Frequencies: Case of Positive Gyromagnetic Ratio

In reality, it is not possible to examine the entire NMR spectrum at once. It is only possible to access a small number of narrow frequency 'bands' or 'windows'.

The NMR spectrometer has a set of independent frequency *channels*, each of which may be *tuned* so as to examine a single narrow frequency window. For example, a two-channel spectrometer may be used to examine narrow frequency windows around the ^{1}H and ^{13}C Larmor frequencies. For the TMS spectrum discussed above, the idea is as follows:

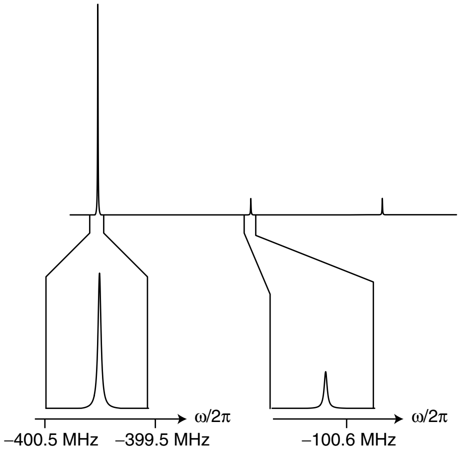

Figure 3.11
Regions of the TMS spectrum.

Only the ^{1}H and ^{13}C signals are visible with the spectrometer in this configuration.

In practice, the bandwidth of each 'window' is around 1 MHz or less, which is almost always smaller than the separation between nuclear Larmor frequencies of different isotopes. As a result, each spectrometer channel only detects the NMR signals from a single isotopic species, except in very rare cases. One therefore speaks of the '^{1}H channel', or the '^{13}C channel', and so on, when referring to the different frequency windows accessible to a given NMR instrument.

The centre frequency of each 'window' is under operator control. In this book, the centre frequency of a given channel is called the *reference frequency*, and denoted ω_{ref} (in units of radians per second). The sign of the reference frequency is the same as the sign of the nuclear Larmor frequency for the isotope detected in that channel. The reference frequency in units of hertz is written $\omega_{\text{ref}}/2\pi$.

The NMR spectrometer always determines *relative* frequencies, produced by subtracting the reference frequency ω_{ref} from the frequency coordinate. This may be thought of as a shift of the spectral window, to bring the reference frequency to the new zero position:

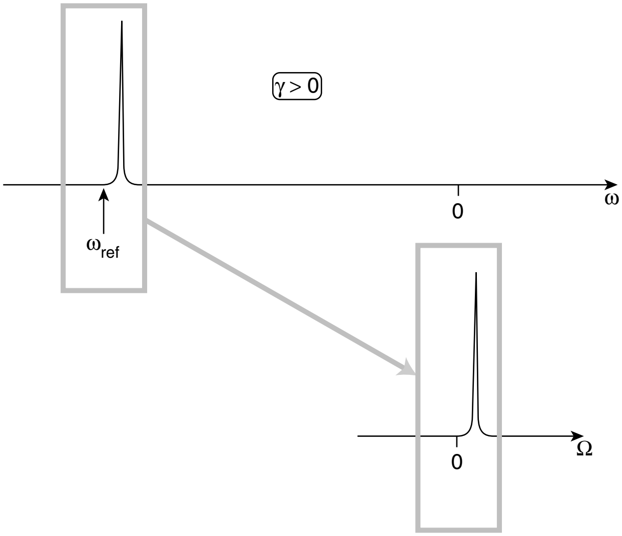

Figure 3.12
Constructing a spectrum using a relative frequency scale (case of positive γ).

In this book, relative frequencies are denoted by the symbol Ω:

$$\Omega = \omega - \omega_{\mathrm{ref}} \tag{3.4}$$

For example, the Larmor frequency ω^0, relative to the spectrometer reference frequency ω_{ref}, is defined as

$$\Omega^0 = \omega^0 - \omega_{\mathrm{ref}} \tag{3.5}$$

As usual, the symbol Ω indicates an angular frequency in units of radians per second. Frequencies in units of hertz are denoted $\Omega/2\pi$ and are obtained by dividing the angular frequency by 2π.

The relative Larmor frequency Ω^0 has a sign, indicating whether the absolute Larmor frequency ω^0 is more negative or more positive than the spectrometer reference frequency ω_{ref}. For example, suppose that the nuclear Larmor frequency for protons is exactly $\omega^0/2\pi = -400.000\,000$ MHz. If the reference frequency of the spectrometer 'window' is set to $\omega_{\mathrm{ref}}/2\pi = -399.999\,000$ MHz, then the centre of the NMR peak appears at $\Omega^0/2\pi = -1$ kHz. If the reference frequency of the spectrometer 'window' is set to $\omega_{\mathrm{ref}}/2\pi = -400.001\,000$ MHz, then the centre of the NMR peak appears at $\Omega^0/2\pi = +1$ kHz.

By convention the NMR spectra of spins with positive γ (the most common case) are plotted with the frequency axis Ω increasing from left to right. Signals with *negative* values of Ω^0 appear on the left-hand side of the spectrum; signals with *positive* values of Ω^0 appear on the right-hand side of the spectrum. For example, the case with reference frequency $\omega_{\mathrm{ref}}/2\pi = -399.999\,000$ MHz and Larmor frequency $\omega^0/2\pi = -400.000\,000$ MHz appears as follows:

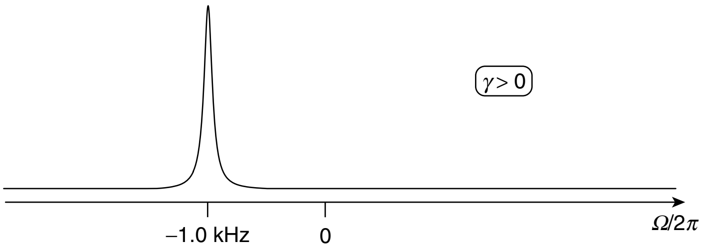

Figure 3.13
NMR spectrum using a relative frequency scale (case of positive γ).

The relative Larmor frequency Ω^0 is also known as the *resonance offset* or the *Larmor frequency in the rotating frame*. These names are explained in Chapter 10.

⚠ There is confusion about frequency axes in the NMR literature: very often the frequency axis is labelled *as if* positive relative frequencies appeared on the left, and negative relative frequencies appeared on the right.[2] Nevertheless, the sense in which the *spectrum* is plotted (but not necessarily the way the frequency axis is labelled!) *always* conforms to the conventions used in this book.

3.5 Relative Spectral Frequencies: Case of Negative Gyromagnetic Ratio

Unfortunately, the treatment of the NMR signals from spins with negative γ generates even more confusion.

Spins with negative γ have positive Larmor frequencies ω^0. The reference frequency ω_{ref} of the corresponding spectrometer channel is also positive. The spectrometer detects relative frequencies, defined according to

$$\Omega^0 = \omega^0 - \omega_{\mathrm{ref}}$$

One may imagine the spectral window to be shifted by $-\omega_{\text{ref}}$, so that it is centred around zero frequency:

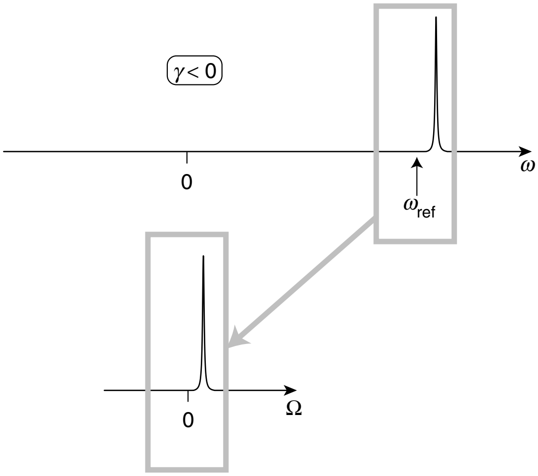

Figure 3.14
Constructing a spectrum using a relative frequency scale (case of negative γ).

For example, suppose that the nuclear Larmor frequency for ^{29}Si is exactly $\omega^0/2\pi = +79.460\,000$ MHz. If the reference frequency of the spectrometer 'window' is set to $\omega_{\text{ref}}/2\pi = +79.461\,000$ MHz, then the centre of the NMR peak appears at $\Omega^0/2\pi = -1$ kHz. If the reference frequency of the spectrometer 'window' is set to $\omega_{\text{ref}}/2\pi = +79.459\,000$ MHz, then the centre of the NMR peak appears at $\Omega^0/2\pi = +1$ kHz.

⚠Now here's a difficult thing: For technical reasons,[3] the spectra from spins with negative γ are always plotted with the frequency coordinate running 'backwards', i.e. with negative relative frequencies on the right and positive relative frequencies on the left! In other words, the spectrum is 'flipped over' before it is plotted:

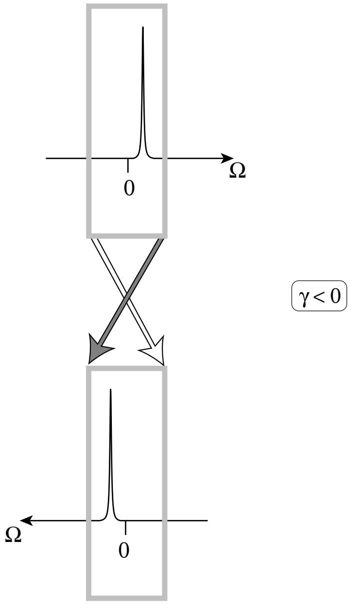

Figure 3.15
The conventional reversal of the frequency scale, in the case of negative γ.

For example, the case with reference frequency $\omega_{\text{ref}}/2\pi = +79.461\,000$ MHz and Larmor frequency $\omega^0/2\pi = +79.460\,000$ MHz is plotted as follows:

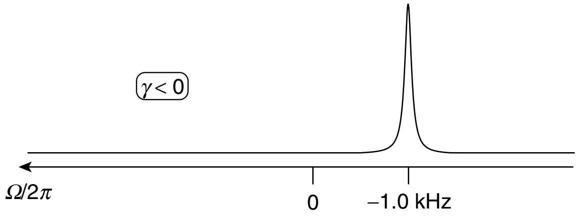

Figure 3.16
NMR spectrum using a relative frequency scale (case of negative γ).

As discussed in Section 3.7, this way of plotting spectra ensures that the chemical shift scale always increases from right to left, which is a universal convention in NMR.

The reader is again advised to ignore the frequency axis *labelling* of NMR spectra in the literature.[2] The way the *spectra themselves* are presented is always consistent with the usage in this book.

3.6 Inhomogeneous Broadening

So far, we have assumed that the magnetic field B^0 is the same in all parts of the sample, i.e. that the magnetic field is perfectly *homogeneous*. In practice, this may not be the case, since

- It is difficult to generate a perfectly homogeneous magnetic field, for technical reasons.
- The sample itself tends to distort the applied magnetic field, because of its magnetic susceptibility.
- In some NMR experiments, spatially dependent magnetic fields are *deliberately* applied, using specially designed additional field coils. This is the case in, for example, NMR imaging experiments.

An inhomogeneous magnetic field may be denoted $B^0(\mathbf{r})$, indicating that the value of the magnetic field depends on the position in space, denoted by the vector $\mathbf{r}$.

Suppose, for example, that the magnetic field B^0 is stronger at the 'top' of the sample than at the 'bottom'. This situation could be depicted as follows:

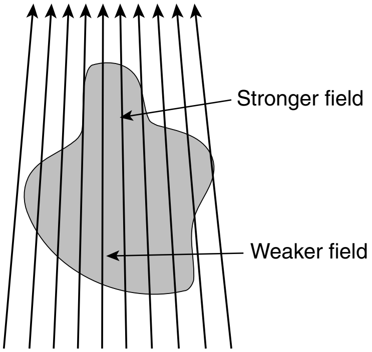

Figure 3.17
An inhomogeneous magnetic field

where closely spaced 'magnetic flux lines' indicate a stronger field, and more widely spaced 'magnetic flux lines' indicate a weaker field. This diagram is greatly exaggerated – in practice, the magnetic flux density differs only by about one part in a thousand even in NMR imaging experiments.

Suppose that the NMR spectrum is taken of nuclei with positive γ, such as protons. Since, the Larmor frequency ω^0 is proportional to the magnetic field, the nuclear Larmor frequency is spatially dependent:

$$\omega^0(\mathbf{r}) = -\gamma B^0(\mathbf{r})$$

With the magnetic field configuration indicated above, nuclear spins at the top of the sample have a *more negative* Larmor frequency, and appear on the *left-hand side* of the spectrum. Nuclear spins at the bottom of the sample have a *less negative* Larmor frequency, and appear on the *right-hand side* of the spectrum. The total proton NMR spectrum is a superposition of very many narrow peaks, each one coming from a different place in the sample:

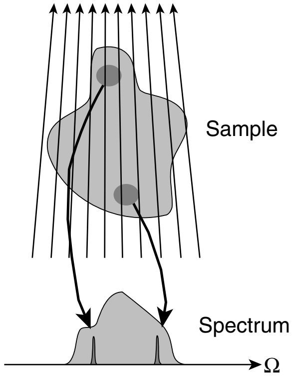

Figure 3.18
An inhomogeneously broadened spectrum.

This effect is called *inhomogeneous broadening*. Since the magnetic field is inhomogeneous, the width of the NMR peak may be much larger than would be predicted by the $1/(\pi T_2)$ formula.

For a long time, inhomogeneous broadening was assumed to be a nuisance, and great efforts were made in order to eliminate it. However, in 1972, Paul Lauterbur and Peter Mansfield realized independently that controlled inhomogeneous broadening can be enormously useful because it causes the NMR spectrum to depend on the *shape* of the sample and the distribution of magnetic spins within it. They received the Nobel Prize for this insight in 2003. The inhomogeneously broadened NMR spectrum is a way of examining the *spatial structure* of an object.

Consider, for example, the following bottle-shaped object, filled with a sample (such as water) containing magnetic nuclear spins (protons, in this case):

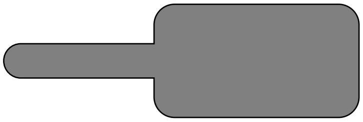

Figure 3.19
A bottle.

Suppose this sample is placed in a magnetic field that depends on position in the way described before. The top of the sample is in a stronger field than the bottom of the sample. If the magnetic field inhomogeneity is carefully controlled, so that the field varies linearly with respect to vertical position, then the NMR spectrum generated by the bottle-shaped sample has the following appearance:

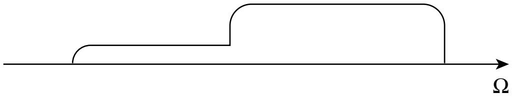

Figure 3.20
Spectrum of a bottle in a linear field gradient.

since the total amplitude of the NMR spectrum at a particular frequency depends on the number of spins with just that Larmor frequency. There are fewer spins in the 'neck' than in the 'body', so the height of the spectrum is less on the left than on the right. The 'bottle-shaped' profile of the sample is reproduced (lying down) along the frequency axis of the NMR spectrum.

If the sample had a ring shape:

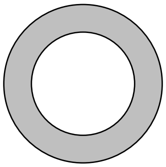

Figure 3.21
A ring.

and the magnetic field was unchanged, then the NMR spectrum would look as follows:

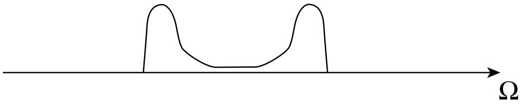

Figure 3.22
Spectrum of a ring in a linear field gradient.

The NMR spectra betray the *spin density distribution* in the sample, *projected* onto the vertical axis:

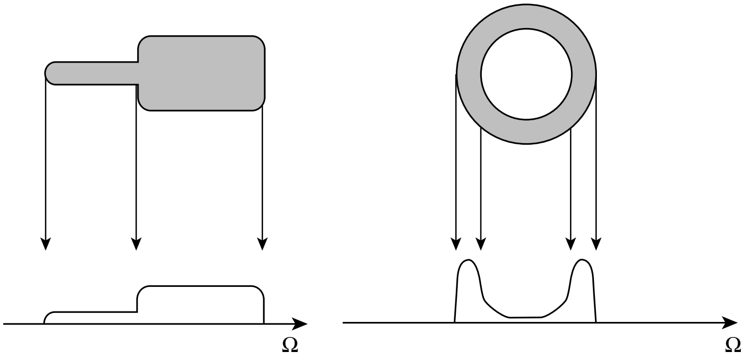

Figure 3.23
Spatial projections and NMR spectra in a field gradient.

An NMR spectrum taken in the presence of a magnetic field gradient is therefore a strange sort of image of the object, flattened onto one axis. Section 12.6 discusses how the method may be extended to remove this flattening effect, allowing one to build up two- or three-dimensional pictures.

This is *NMR imaging*, a method of immense medical value. NMR imaging allows doctors and surgeons to visualize the interior of the human body, without any invasive surgery or damaging high-energy radiation.

In order to avoid the term 'nuclear', which tends to cause anxiety, NMR imaging is generally known in the medical world as *magnetic resonance imaging* (MRI).

3.7 Chemical Shifts

Let us return to the situation in which the magnetic field is perfectly homogeneous, i.e. exactly the same over the entire volume of the sample. In this case, there is no inhomogeneous broadening, so the width of the NMR peaks is equal to the homogeneous peakwidth ($1/(\pi T_2)$ in units of hertz).

Since the magnetic field is homogeneous, it might be expected that each nuclear isotope would give a single narrow peak, reflecting its Larmor frequency in that magnetic field. For most substances, this turns out to be incorrect. Although the magnetic field may be made very uniform on a *macroscopic* scale, it always has small 'wrinkles' on a *microscopic* scale.

These microscopic magnetic wrinkles are caused by the fact that matter is made up of atoms. Although a sample of water appears to be very homogeneous on a macroscopic distance scale, it is not at all homogeneous when viewed on a molecular distance scale of a nanometre or less. The grainy microscopic environment creates a slight lumpiness in the magnetic field. The size of these small magnetic wrinkles is about the size of a single molecule:

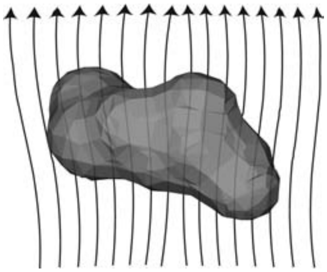

Figure 3.24
Microscopic field inhomogeneities.

Because of these microscopic wrinkles, the precise Larmor frequency of a given nucleus depends on the atomic environment.

There are two important microscopic effects that influence the Larmor frequency of a given nuclear spin:

- Since electrons are magnetic, the nuclear Larmor frequency depends on the local *electronic* environment. This effect is called the *chemical shift* in diamagnetic materials, the *Knight shift* in metals and superconductors, and the *paramagnetic shift* in paramagnetic substances.
- The Larmor frequency depends on the presence of *other magnetic nuclear spins* in the same molecule, and also the directions of their magnetic moments. This effect is called the *nuclear spin–spin coupling*.

These effects are very useful because they allow the atomic nuclei to behave as microscopic radio transmitters, sending out highly local molecular information encoded as radio waves. The nuclear magnetic signals reveal the electronic and nuclear environment of the observed spins.

Consider, for example, the chemical compound ethanol (CH_3CH_2OH), which is a liquid at room temperature. The molecular structure is as follows:

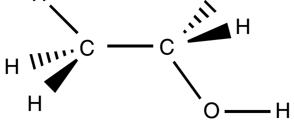

Figure 3.25
Ethanol.

The most common isotopomers are shown in Table 3.3.

Table 3.3 Major isotopomers in ethanol.

	Isotopomer	Natural abundance/%
I	$^{12}C^{1}H_3{}^{12}C^{1}H_2{}^{16}O^{1}H$	~ 97.8
II	$^{13}C^{1}H_3{}^{12}C^{1}H_2{}^{16}O^{1}H$	~ 1.1
III	$^{12}C^{1}H_3{}^{13}C^{1}H_2{}^{16}O^{1}H$	~ 1.1

The ^{13}C spectrum of ethanol is generated predominantly by isotopomers of type II and III. If the magnetic field is $B^0 = 4.70\,\mathrm{T}$, then the subspectrum from isotopomer II has the following form:

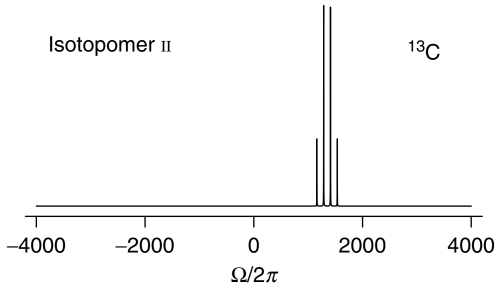

Figure 3.26
^{13}C spectrum of ethanol isotopomer II in a field of 4.7 T.

The subspectrum from isotopomer III has the form shown here:

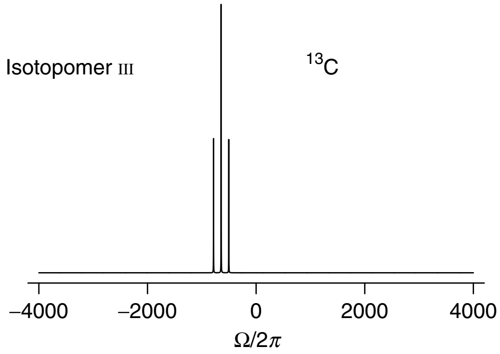

Figure 3.27
^{13}C spectrum of ethanol isotopomer III in a field of 4.7 T.

The total ^{13}C NMR spectrum is a superposition of these two subspectra, and appears as follows:

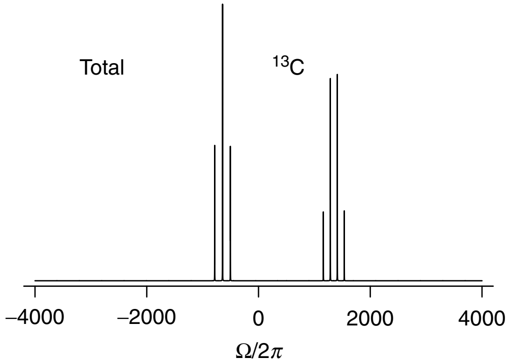

Figure 3.28
Total ^{13}C spectrum of ethanol in a field of 4.7 T.

The form of this spectrum is the result of two effects:

- Each ^{13}C peak is split into a *multiplet*, meaning a group of equally spaced peaks with a symmetrical intensity pattern.
- The multiplet from isotopomer II is shifted with respect to the multiplet from isotopomer III, by 1991 Hz in the positive direction.

We will consider the multiplet structure later. For the moment, consider the 1991 Hz frequency shift between the ^{13}C peaks of the two isotopomers.

This shift arises because the electrons in the outer atomic shells, and in the chemical bonds holding the ethanol molecule together, generate small magnetic fields that add to or subtract from the external magnetic field B^0. In some parts of the molecule the magnetic field is enhanced, in other places it is decreased, compared with the applied external magnetic field. The precession frequency of a given atomic nucleus is proportional to the local value of the magnetic field. As a result, the Larmor frequency depends on the location of the nucleus in the molecule and on details of the electronic structure.

This effect is called the *chemical shift* because the induced field is generated by the valence and bonding electrons, which are also heavily implicated in the chemical properties of the molecule.

The chemical shift (measured in frequency units) is *field dependent*. If the magnetic field is increased, then the chemical shift also increases. To a very good approximation, *the chemical shift, measured in frequency units, is linearly proportional to the applied magnetic field.*

If the external magnetic field is increased to $B^0 = 9.40\,\mathrm{T}$, then the ^{13}C NMR spectrum has the following appearance:

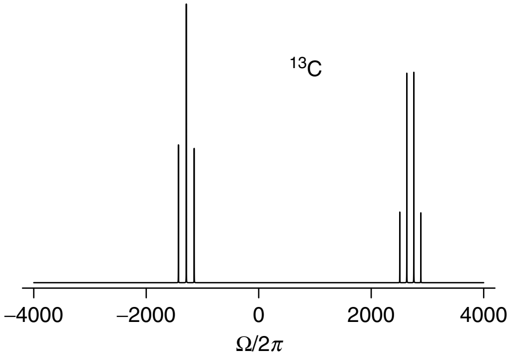

Figure 3.29
Total ^{13}C spectrum of ethanol in a field of 9.40 T.

The multiplet structure is the same, but the frequency difference between the isotopomer II and isotopomer III signals is doubled, and is given by 3983 Hz.

Since the nuclear Larmor frequency and the chemical shift are both proportional to the applied magnetic field, the ratio of these two quantities is fixed. In practical applications, it is convenient to specify chemical shifts in terms of this ratio, since it only depends on the sample, not on the instrument. The field-independent expression for the chemical shift is

$$\delta = \frac{\omega^0 - \omega^0_{\mathrm{TMS}}}{\omega^0_{\mathrm{TMS}}} \tag{3.6}$$

where ω^0 is the Larmor frequency of a particular nucleus, in the molecular site of interest, and ω^0_{TMS} is the Larmor frequency of the same isotope in a *reference compound* (TMS) exposed to the same applied field. If the applied field is increased, then both quantities ω^0 and ω^0_{TMS} increase in the same proportion, so the ratio δ remains constant.

The equation assumes that TMS is chosen as the reference compound, which is often the case. By definition, TMS spins have a chemical shift $\delta = 0$. TMS is particularly suitable as the chemical shift reference for the ^{1}H, ^{13}C, and ^{29}Si chemical shift scales. TMS is chemically rather inert, and gives a sharp strong NMR signal, which is usually at a frequency that is well displaced from other peaks. Often, a small amount of TMS is added to the sample in order to set the reference for the chemical shift δ scale.

Chemical shifts δ are small numbers. It is common to specify them in terms of parts per million (ppm), where the dimensionless symbol ppm has exactly the same meaning as 10^{-6}.

For ethanol, the CH_2 site has a ^{13}C chemical shift of 57.8 ppm, whereas the CH_3 site has a ^{13}C chemical shift of 18.2 ppm. The ethanol spectrum may be labelled with a δ scale as follows:

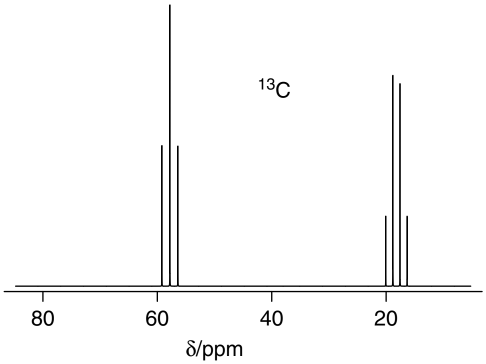

Figure 3.30
Total ^{13}C spectrum of ethanol in a field of 4.7 T (δ chemical shift scale).

⚠The chemical shift δ scale *always* increases from right to left in plotted spectra. This is a universal convention in NMR.

It is also convenient to associate the reference frequency of the spectrometer with a chemical shift value δ_{ref}, through the following equation:

$$\delta_{\mathrm{ref}} = \frac{\omega_{\mathrm{ref}} - \omega^0_{\mathrm{TMS}}}{\omega^0_{\mathrm{TMS}}} \tag{3.7}$$

The value of δ_{ref} corresponds to the exact centre of the NMR spectrum, on the ppm scale. The spectrum shown above assumes that the spectrometer reference frequency is placed at $\delta_{\mathrm{ref}} = 45.0$ ppm.

⚠The Larmor frequency of spins in the reference compound (denoted ω^0_{TMS}) should not be confused with the spectrometer reference frequency (denoted ω_{ref}). The frequency ω^0_{TMS} sets the origin of the chemical shift scale, whereas the frequency ω_{ref} determines the position of the centre of the NMR spectrum, and may be freely changed by the operator.

Equations 3.6 and 3.7 may be used to obtain the relative Larmor frequency of a spin with chemical shift δ, given the chemical shift at the centre of the spectrum δ_{ref}:

$$\Omega^0 = \omega^0 - \omega_{\mathrm{ref}} = (\delta - \delta_{\mathrm{ref}})\, \omega^0_{\mathrm{TMS}}$$

where ω^0_{TMS} is the Larmor frequency of spins in the reference compound.

In practice, the following slightly looser equation may safely be used:

$$\Omega^0 = \omega^0 - \omega_{\mathrm{ref}} \cong (\delta - \delta_{\mathrm{ref}})\, \omega^0 \tag{3.8}$$

which ignores the fine distinction between ω^0 and ω^0_{TMS}. The errors introduced are very small for chemical shifts of normal size.

For example, for ethanol, if the ^{13}C Larmor frequency is -50.288 MHz and the spectrometer reference frequency is placed at $\delta_{\mathrm{ref}} = 45.0$ ppm, then the relative ^{13}C Larmor frequency of the CH_2 site is

$$\Omega^0/2\pi = \left(57.8 \times 10^{-6} - 45.0 \times 10^{-6}\right) \times (-50.288 \times 10^6)\,\mathrm{Hz} = -643.6\,\mathrm{Hz}$$

and the relative ^{13}C Larmor frequency of the CH_3 site is

$$\Omega^0/2\pi = \left(18.2 \times 10^{-6} - 45.0 \times 10^{-6}\right) \times (-50.288 \times 10^6)\,\mathrm{Hz} = +1347.7\,\mathrm{Hz}$$

The chemical shift is an empirical tool of immense use in chemistry. Some typical chemical shifts for different nuclei are given in Figure 3.31. The molecular mechanism of the chemical shift is explored in Section 9.1.

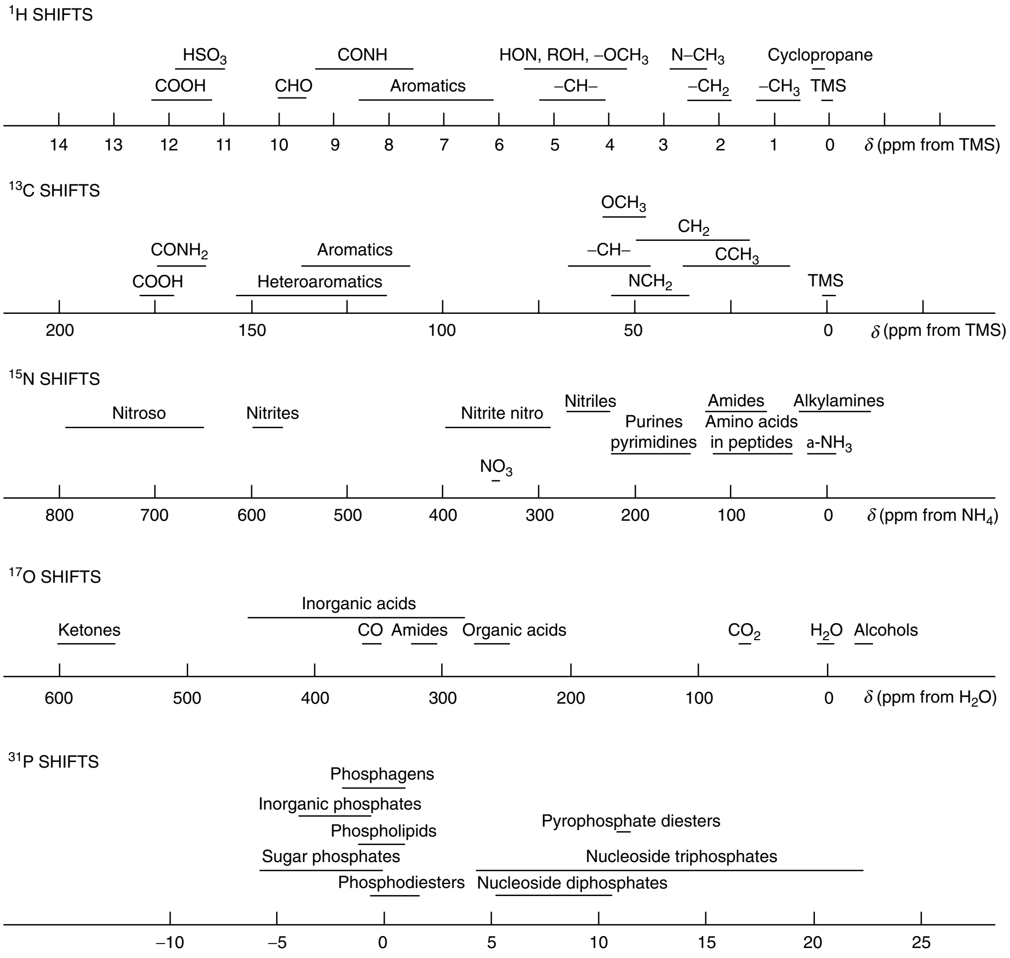

Figure 3.31 Typical chemical shift ranges for ^{1}H, ^{13}C, ^{15}N, ^{17}O and ^{31}P in organic compounds. After O. Jardetzky and G. C. K. Roberts, '*NMR in Molecular Biology*, Academic Press, New York, 1981, copyright Academic Press.

⚠The terms 'high-field' and 'low-field' are sometimes encountered. 'High-field' peaks correspond to small δ values, whereas 'low-field' peaks correspond to large δ values. These terms are of historical origin and are highly misleading.[5] I will avoid the high-field/low-field terminology in this book.

3.8 *J*-Coupling Multiplets

Now consider the multiplet structure of the ethanol ^{13}C spectrum.

The left-hand CH_2 peak, from isotopomer III, is split into a group of three equally spaced peaks, with relative intensities 1:2:1. A multiplet of this type is called a *triplet*. The right-hand CH_3 peak, from isotopomer II, is split into a group of four equally spaced peaks, with relative intensities 1:3:3:1. A multiplet of this type is called a *quartet*. The ^{13}C spectrum of liquid ethanol consists of a triplet on the left of the spectrum (which comes from isotopomer III) and a quartet on the right of the spectrum (which comes from isotopomer II).

Other compounds display different types of multiplet. A group of two peaks, with equal intensities, is called a *doublet*. A group of five equally spaced peaks, with relative intensities 1:4:6:4:1, is called a *quintet*. An isolated peak, which does not belong to a multiplet, is called a *singlet*.

These multiplets arise because the precessing ^{13}C spins are influenced by the magnetic ^{1}H nuclei in the same molecule. One says that the ^{13}C and ^{1}H spins are *coupled*.

As discussed in Chapter 8, there are two different mechanisms of spin–spin coupling. The strongest mechanism is called the *direct dipole–dipole coupling*. This involves the direct influence of each spin on its neighbour through the magnetic fields emanating through space. However, this mechanism is *not* responsible for the multiplet structure in isotropic liquids. As discussed in Section 9.3, the direct dipole–dipole coupling is effectively eliminated by the rapid molecular tumbling.

The mechanism responsible for the multiplet structure in isotropic liquids is called the *J-coupling*, or the *indirect dipole–dipole coupling*. The term 'indirect' indicates that the nuclear spins are coupled together with the help of the molecular electrons. Each proton weakly magnetizes the molecular electrons, which generate a magnetic field at the site of the ^{13}C spins. This transmitted field allows each ^{13}C spin to sense the presence of the neighbouring protons. The coupling also works the other way round: the ^{13}C spin also weakly magnetizes the electrons, which generate a field at the location of the ^{1}H spins. As discussed in Section 9.4, a part of this indirect dipole–dipole coupling survives in isotropic liquids, and generates the observed multiplet structure.

The J-coupling is always specified in hertz. For example, the J-coupling between the ^{13}C and ^{1}H spins in the CH_3 group of ethanol is $J_{CH} = 124.9\,\text{Hz}$. The J-coupling between the ^{13}C and ^{1}H spins in the CH_2 group is $J_{CH} = 140.4\,\text{Hz}$. These numbers correspond to the frequency separation between the multiplet peaks.

Sometimes a superscript prefix is used to specify the number of chemical bonds separating the nuclei involved in the J-coupling. The J-couplings specified above are written $^{1}J_{CH} = 124.9\,\text{Hz}$ and $^{1}J_{CH} = 140.4\,\text{Hz}$ to indicate that the participating atoms are separated by one chemical bond. There are also *long-range J-couplings* that involve atoms separated by two or more chemical bonds. For example, the J-coupling between a ^{13}C spin located on the CH_2 group and the three CH_3 protons of ethanol is $^{2}J_{CH} = -4.6\,\text{Hz}$.

The meaning of the sign of the J-coupling is discussed in Section 9.4.

The J-splitting phenomenon is explained in Chapters 15 and 17. For the moment, I mention the phenomenological rules for predicting the spectral structure, which work in many cases.

Consider first a simple case in which the molecules contain one ^{13}C spin and one ^{1}H, with a J-coupling equal to $J_{CH} = 100\,\text{Hz}$. The spectral peak generated by the ^{13}C spins is 'split' by the neighbouring proton, appearing as a doublet with one peak shifted to positive frequency by 50 Hz and one peak shifted to negative frequency by the same amount:

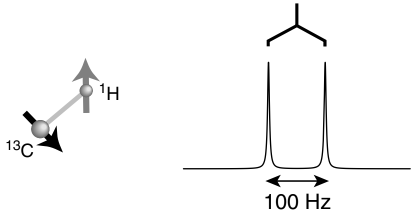

Figure 3.32
A ^{13}C doublet, caused by coupling to one proton.

If the ^{13}C spin is coupled to *two* protons, then the splitting occurs twice, one for each ^{13}C–^{1}H *J*-coupling. If both couplings are equal to $J_{\mathrm{CH}} = 100\,\mathrm{Hz}$, then a triplet pattern is generated:

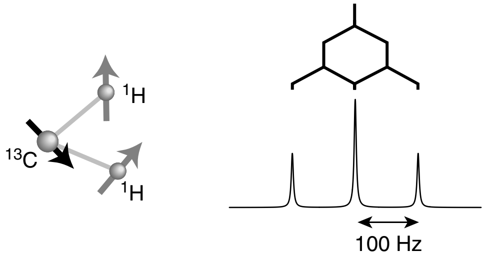

Figure 3.33
A ^{13}C triplet, caused by coupling to two protons.

The amplitude ratio of 1:2:1 occurs because there are two ways of generating the inner peaks and only one way of generating the outer ones.

If the ^{13}C spin is coupled to *three* protons, then the splitting occurs three times. If all three couplings are equal, then a quartet pattern is generated:

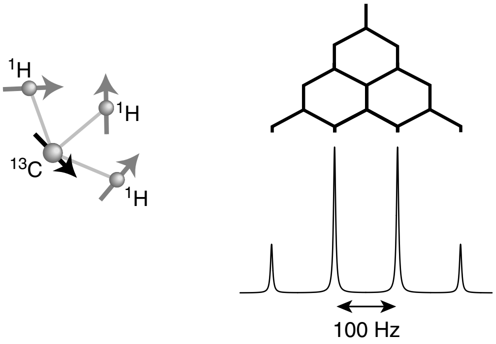

Figure 3.34
A ^{13}C quartet, caused by coupling to three protons.

The amplitude ratio of 1:3:3:1 occurs because there are three ways of generating the inner peaks and only one way of generating the outer ones.

In general, if a nuclear spin is coupled to n equivalent spins-1/2, its peak is split into an $(n+1)$-fold multiplet, where the peak intensities within the multiplet are proportional to the binomial coefficients ${}_nC_r$, where $r = 0, 1 \ldots n$. The binomial coefficients are given by

$${}_nC_r = \frac{n!}{(n-r)!r!}$$

For example, the NMR peak of a ^{13}C that is coupled to six equivalent protons is split into a 1:6:15:20:15:6:1 septet. The intensity ratios may be derived as follows:

$$
\begin{aligned}
{}_6C_0 &= \frac{6!}{6! \times 0!} = 1 \qquad & {}_6C_2 &= \frac{6!}{4! \times 2!} = 15 \\
{}_6C_1 &= \frac{6!}{5! \times 1!} = 6 \qquad & {}_6C_3 &= \frac{6!}{3! \times 3!} = 20
\end{aligned}
$$

and so on.

Now consider more closely the signals of ethanol isotopomer III, which are split into a triplet because of the one-bond coupling between the ^{13}C and ^{1}H spins in the CH$_2$ group. An experimental ^{13}C spectrum of the CH$_2$ region is shown below:

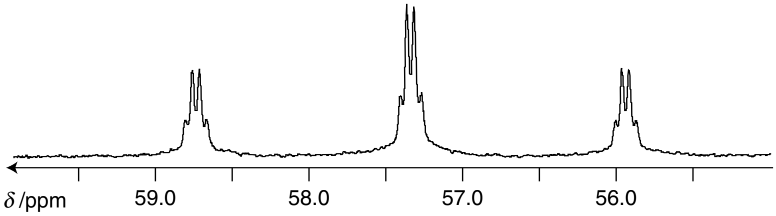

Figure 3.35
Experimental ^{13}C spectrum of the CH$_2$ region in ethanol.

This shows an additional quartet *fine structure*. This may be attributed to the two-bond coupling between the ^{13}C spin in the CH$_2$ group and the three ^{1}H spins in the CH$_3$ group.

In general, the spectral peaks are split again and again, according to the J-couplings of the corresponding spin with all the other spins in the molecule.

What about the *proton* spectrum of ethanol? This spectrum is generated mainly from the abundant isotopomer I, which does not contain a ^{13}C spin. At a field of $B^0 = 4.70\,\mathrm{T}$, and with a spectrometer reference frequency corresponding to $\delta_{\mathrm{ref}} = 2.4\,\mathrm{ppm}$, the spectrum of this isotopomer appears as follows:

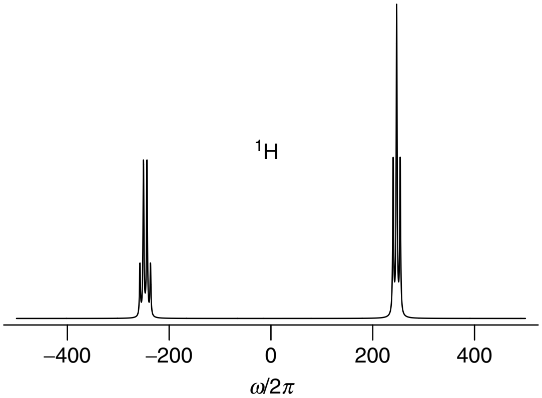

Figure 3.36
^{1}H spectrum of ethanol, in a field of 4.7 T.

The peak on the right is centred at $\delta_j = 1.19$ ppm, and arises from the three protons of the CH_3 group. This peak is split into a triplet because each of these protons has a ${}^3J_{HH} = 6.9$ Hz coupling with the two protons of the CH_2 group. The peak on the left is centred at $\delta_k = 3.66$ ppm, and arises from the two protons of the CH_2 group. This peak is split into a quartet by the ${}^3J_{HH} = 6.9$ Hz coupling with the three protons of the CH_3 group.

Note that the relative positions of the triplet and quartet are exchanged relative to the ${}^{13}C$ spectrum.

This spectrum illustrates two additional points.

First, the OH proton was ignored in the above discussion. Under most circumstances, this proton only gives broad signals, and does not split the signals of the other spins in the molecule. This is because of a *chemical exchange* process. The OH proton is labile and hops around rapidly between the ethanol molecules, unless the ethanol is exceptionally pure (the exchange process is catalysed by acid or base). In most circumstances, the chemical exchange is fast enough to remove the J-coupling to this proton completely. This phenomenon is discussed in Section 19.5.3.

Second, it is possible to predict the ${}^1H$ spectrum without considering the coupling of the two CH_2 protons *with each other*. In Chapter 17, it is shown that the coupling between the two CH_2 protons may be ignored because they are *magnetically equivalent*. This means that they have the same chemical shift, as well as the same J-couplings with other spins in the same molecule. The three CH_3 protons are also magnetically equivalent, so their mutual coupling may be ignored too. Magnetic equivalence and its consequences are discussed in Section 17.5.

3.9 Heteronuclear Decoupling

The J-coupling structure is very useful for providing qualitative molecular structural information. However, in some cases this splitting structure is undesirable, since

- The J-splittings distribute the signal intensity over many smaller peaks. This makes it more difficult to detect the NMR signals.
- In complex molecules, the J-splittings make the spectrum crowded and more difficult to interpret.

Fortunately, there is a very simple method for eliminating the ${}^{13}C - {}^1H$ splittings from ${}^{13}C$ spectra. One simply acquires the ${}^{13}C$ NMR signal at the same time as applying an r.f. field at the ${}^1H$ Larmor frequency. This is usually denoted as follows:

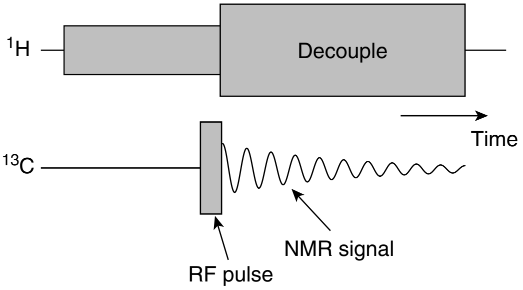

Figure 3.37
Heteronuclear pulse sequence involving ${}^1H$ decoupling.

If the ${}^1H$ r.f. field is sufficiently strong, and has a frequency sufficiently close to the Larmor frequency of the relevant protons, the ${}^{13}C$ spins behave *as if* the heteronuclear J-couplings does not exist. The ${}^{13}C$ spectrum is determined by the ${}^{13}C$ chemical shifts alone.

This method is called *heteronuclear decoupling*. In the case of ethanol, the proton-decoupled ${}^{13}C$ spectrum has the following appearance:

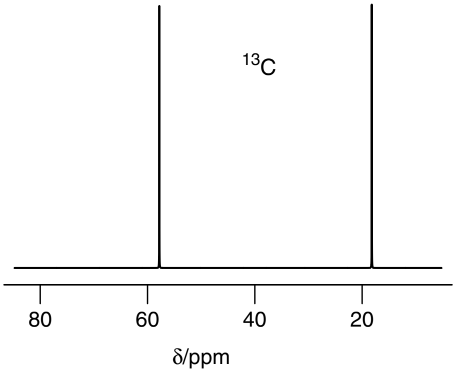

Figure 3.38
^{1}H-decoupled ^{13}C spectrum of ethanol.

The right-hand peak comes from isotopomer II; the left-hand peak comes from isotopomer III. Note the disappearance of the multiplet structure.

In practice, the ^{1}H decoupling field is usually subjected to a specialized modulation scheme, in order to make the decoupling more effective and to reduce the heating of the sample (see *Further Reading*).

The pulse sequence diagram given above also includes ^{1}H irradiation *before* the pulse is applied to the ^{13}C spins. The purpose of this irradiation is to enhance the ^{13}C magnetization through a phenomenon called the *nuclear Overhauser effect* (NOE), which is discussed in Section 20.5. The proton irradiation *before* the ^{13}C pulse has nothing to do with decoupling, but simply causes the ^{13}C signals to be stronger, in suitable cases.

Notes

1. The devices used to convert a varying voltage into digital form (analogue-to-digital converters) can only operate accurately enough at relatively low frequencies. In 2007, the maximum operation frequency of these devices is less than most common nuclear Larmor frequencies. However, the continuing advances in high-frequency electronics may soon change this situation.

2. The relative frequency axis used to label NMR spectra in much literature and on most commercial spectrometers corresponds to the coordinate $|\omega| - |\omega_{\text{ref}}|$. This is equal to $-\Omega$ in the case of positive γ, and is equal to $+\Omega$ in the case of negative γ.

3. NMR spectrometers do not actually process the data from nuclei with negative γ in a special way. The 'flipping' effect described in Section 3.5 is an unintentional consequence of ignoring the sign of precession during the excitation process and when the signal is detected. This issue is examined in detail in M. H. Levitt. *J. Magn. Reson.*,**126**, 164–182 (1997).

4. The symbols ppm and % do not represent *units* but *numbers*, i.e. $5\,\text{ppm} = 5 \times 10^{-6}$ and $5\% = 0.05$. Therefore, they behave differently from, for example, a unit such as the kilogram (an equation such as $1\,\text{kg} = 10^{-3}$ would be completely incorrect). This point is often misunderstood.

5. Before around 1966, most NMR spectra were acquired using a fixed r.f. frequency, while varying the external magnetic field in order to bring different spin sites into resonance. Traditionally, the applied magnetic field was plotted from left to right across the spectrum. Peaks appearing on the left-hand side of the spectrum were called 'low-field' peaks, and peaks appearing on the right-hand side were called 'high-field' peaks. Nowadays (2007), almost all NMR spectra are acquired in a completely different way,

using the pulse-Fourier transform approach at a fixed external magnetic field, which has rendered these terms obsolete and confusing. For example, a 'low-field' spin site actually has a high *local* magnetic field from the molecular environment, so that a relatively low *external* magnetic field is needed in order to bring this site into resonance in a variable-field NMR experiment.

Further Reading

- For the applications of chemical shifts and J-couplings in chemistry, see the many articles in the *Encyclopedia of Nuclear Magnetic Resonance*, D. M. Grant and R. K. Harris (eds), Wiley, 1996, as well as R. K. Harris, *Nuclear Magnetic Resonance Spectroscopy: A Physicochemical View*, Longman, 1986, and J. K. Sanders and B. K. Hunter, *Modern NMR Spectroscopy. A Guide for Chemists*, Oxford University Press, Oxford, 1993.
- For a review of modulation schemes for heteronuclear decoupling, and a summary of the theory, see A. J. Shaka and J. Keeler, *Prog. NMR Spectrosc.* **19**, 47(1987) and R. Freeman, *Spin Choreography. Basic Steps in High Resolution NMR*, Spektrum, Oxford, 1997.

Exercises

3.1 Describe the ^{1}H and ^{13}C spectra of the compound

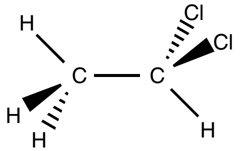

3.2 Assume isotopic abundances of 100% for ^{1}H and 1% for ^{13}C. Assume that the one-bond ^{13}C–^{1}H J-couplings are around 135 Hz and the three-bond ^{1}H–^{1}H J-couplings are 7 Hz. Ignore the couplings to the Cl nuclei. How would the ^{13}C spectrum change if strong r. f. irradiation were applied at the ^{1}H Larmor frequency?

3.3 A sample of acetone (propan-2-one, $(CH_3)_2CO$) is enriched in ^{13}C so that exactly 40% of the C atoms are ^{13}C and the other 60% are ^{12}C (spin $I = 0$). The ^{13}C atoms are randomly distributed. How many isotopomers are there, and what are their relative proportions? (Ignore the isotopes of hydrogen and oxygen.) Sketch the ^{1}H-decoupled ^{13}C spectrum of each isotopomer, assuming that one-bond ^{13}C–^{13}C couplings are 50 Hz. Sketch the ^{1}H-decoupled ^{13}C spectrum of the whole sample.

3.4 A compound has two different ^{13}C sites with chemical shifts equal to 30 ppm and 100 ppm.
(i) At what magnetic field is the chemical frequency difference equal to 10 kHz?
(ii) The relative Larmor frequency of peaks from the two ^{13}C sites are $\Omega_1^0/2\pi = +6.0$ kHz and $\Omega_2^0/2\pi = -4.0$ kHz. What is the ppm value δ_{ref} of the spectrometer reference frequency?

Part 2

The NMR Experiment

4 The NMR Spectrometer

The NMR experiment is technically difficult. First, the NMR signal is very weak. Second, the Larmor frequencies must be measured with extremely high accuracy (at least 1 part in 10^9). The twin challenges of *sensitivity* and *resolution* are the keynotes of NMR instrumentation.

The NMR signal is weak for two reasons. First, the individual nuclear magnetic moments are very small compared with those of electrons. Second, the distibution of nuclear magnetic moments is nearly isotropic. As described in Chapter 2, macroscopic nuclear magnetism depends on the very slight thermal imbalance of the distribution of magnetic moments. In ordinary circumstances, this imbalance represents only about 1 part in 10^5. Detection of the weak nuclear magnetism is a considerable instrumental challenge.

The problem of resolution has been mastered, and a great deal of progress has been made on the problem of sensitivity. Nevertheless, sensitivity remains a great limitation of the NMR technique, at least in its conventional form. Rather large amounts of sample are required, compared with other spectroscopies. Around 10^{14} nuclear spins are typically required to obtain a usable NMR signal.[1]

In the following sections, I outline the operation of a typical solution-state NMR spectrometer. Solid-state NMR spectrometers, and NMR imaging instruments, are based on similar principles, although with technical differences that are largely restricted to the probe and magnet.

4.1 The Magnet

Most NMR experiments require a magnetic field which is *homogeneous* (i.e. independent of position) within at least 1 part in 10^9. This extremely high magnetic field homogeneity must be maintained over the entire volume of the sample, i.e. around a cubic centimetre in solution NMR and many hundreds of cubic centimetres in NMR imaging experiments. The magnetic field must also be extremely stable with respect to time.

A perfectly uniform magnetic field avoids inhomogeneous broadening of the NMR signal (see Section 3.6) and allows the resolution of small differences in the nuclear Larmor frequency, due to chemical shifts, spin–spin couplings, or other molecular interactions.

Almost all NMR spectrometers employ *superconducting magnets*. Superconductors are capable of supporting large electric currents without any external source of power. Once charged with current, a superconducting magnet runs almost indefinitely, providing an extremely stable magnetic field with no outside interference.

At present (2007), superconducting materials must be cooled to around the boiling point of liquid He (4.18 K) in order to support large magnetic fields without electrical resistance.[2] The superconducting

---

Spin Dynamics: Basics of Nuclear Magnetic Resonance, Second Edition Malcolm H. Levitt

magnet windings are typically made from an alloy of Nb and Sn. The heart of an NMR magnet is a Nb–Sn coil immersed in a bath of liquid He. The liquid-He bath is itself insulated by a large reservoir of liquid N_2 (at a temperature of 77 K). The reservoirs are separated from each other, and from the outside environment, by evacuated barriers in order to reduce thermal leakage. The large insulated can of coolant is the visible portion of the magnet from outside:

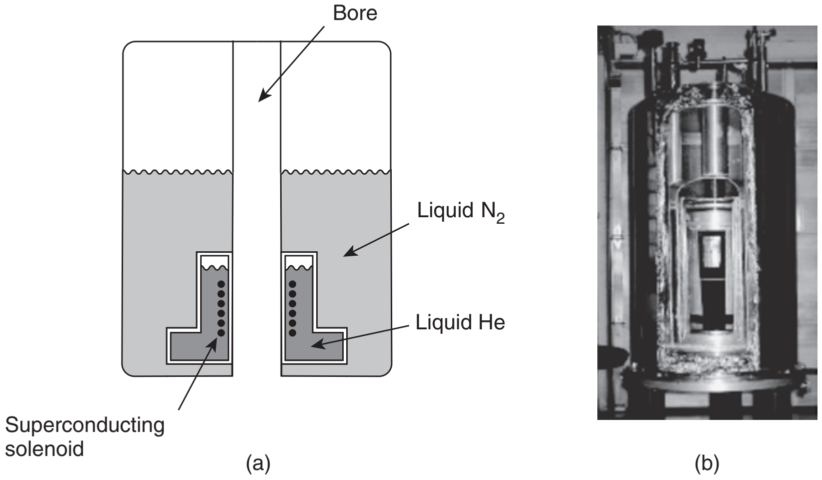

Figure 4.1
(a) Schematic picture of a superconducting NMR magnet. (b) A magnet that has been opened to reveal the superconducting shim coils and the solenoid around the bore (black tube). (Provided by JEOL, USA, Inc.)

Running through the centre of the cylindrical can, and through the centre of the superconducting coil, is a large hole called the *bore*. The sample is mounted in a cylindrical device called a *probe*, which is inserted into the bore so as to position the sample at the point of maximum field. The bore is separated from the superconducting coil by cooled evacuated barriers, allowing the probe and the sample to remain at room temperature.

Currently (2007), the largest commercially-available magnetic field for NMR use is around 22.3 T, corresponding to a proton Larmor frequency of $|\omega^0/2\pi| \cong 950\,\text{MHz}$.

The magnet is also provided with two sets of additional coils, called *shims*, for adjusting the homogeneity of the magnetic field.[3] One set of coils, called the *superconducting shims*, is wound from superconducting material and immersed in the liquid-He bath. This set of coils is charged when the magnet is installed so as to provide a primary correction for the inhomogeneity of the magnetic field. The second set of shims is supported on a tube that is inserted into the magnet bore. These are called the *room-temperature shims*. Whenever the sample or the probe is changed, the currents in the room-temperature shims are adjusted in order to optimize the field homogeneity (a process called 'shimming the magnet'). In modern instruments, the shimming process is conducted semi-automatically.

4.2 The Transmitter Section

NMR instruments require irradiation of the sample with r.f. waves at the nuclear Larmor frequency and detection of radio signals emitted by the nuclei. The following sections describe the instrumentation used for generating and detecting these radio signals.

The *transmitter section* is that part of the spectrometer which produces the r.f. irradiation. In general, there are several transmitter sections, each dedicated to producing r.f. signals at frequencies close to the Larmor frequencies of different isotopes. For simplicity, the operation of a *single-channel* instrument is described here.

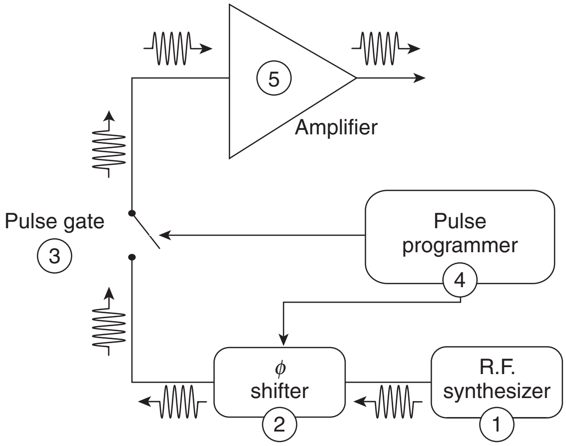

Figure 4.2
The transmitter section.

4.2.1 The synthesizer: radio-frequency phase shifts

The *r.f. synthesizer* ① produces an oscillating electrical signal with a very well-defined frequency. This electronic signal is usually subjected to a number of frequency conversion and electronic filtering steps, which we will not go into here. The result is an r.f. wave that oscillates at the *spectrometer reference frequency*,[4] denoted ω_{ref}.

As usual, the symbol ω specifies the frequency in units of radians per second. The reference frequency in hertz is therefore written $\omega_{\mathrm{ref}}/2\pi$. A reference frequency of 100 MHz corresponds to $\omega_{\mathrm{ref}}/2\pi = 100 \times 10^6$ Hz.

In general, the synthesizer output wave is given by

$$s_{\mathrm{synth}} \sim \cos(\omega_{\mathrm{ref}} t + \phi(t)) \tag{4.1}$$

where $\phi(t)$ is the r.f. phase and t is the time coordinate.

The *phase* of an oscillating wave indicates the position of the oscillation at the time origin $t = 0$:

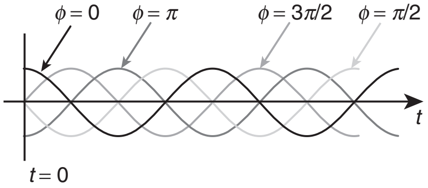

Figure 4.3
Four different phases of a wave.

In many NMR experiments, the r.f. phase $\phi(t)$ is jumped rapidly between different values. In the NMR spectrometer, these discontinuous phase jump events are controlled by a timing device called the *pulse programmer* (④ in Figure 4.2). The following figure shows the synthesizer output for a case in which the phase shift ϕ jumps from an initial value 0 to a value of $\pi/2$, and then back again to 0, after a certain interval:

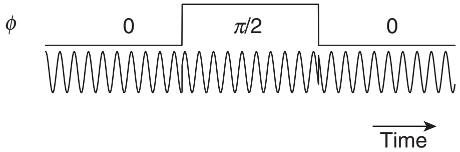

Figure 4.4
Changing the phase and changing it back.

Note the discontinuities in the synthesizer wave.

4.2.2 The pulse gate: radio-frequency pulses

The next item in the transmitter chain is the *pulse gate*, marked ③ in Figure 4.2. This is simply a fast switch that is opened at defined moments in order to allow the r.f. reference wave to pass through. The effect is to chop a 'time-slice' out of the r.f. waveform:

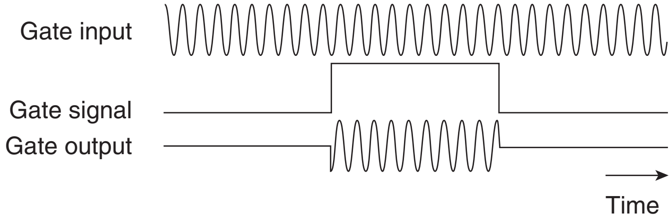

Figure 4.5
Constructing an r.f. pulse.

The duration of an r.f. pulse is sometimes referred to as the *pulse width*. In this book, the pulse duration (i.e. pulse width) is denoted by the symbol τ_p.

The gating events, just like the r.f. phase shifts, are controlled by the pulse programmer. By arranging appropriate timing of the phase shift and the gating events, it is possible to produce r.f. pulses of any desired phase ϕ. Normally, the phase shift is implemented a short time before the opening of the pulse gate and reset a short time after the pulse gate is closed, in order to generate clean transitions in the r.f. waveform:

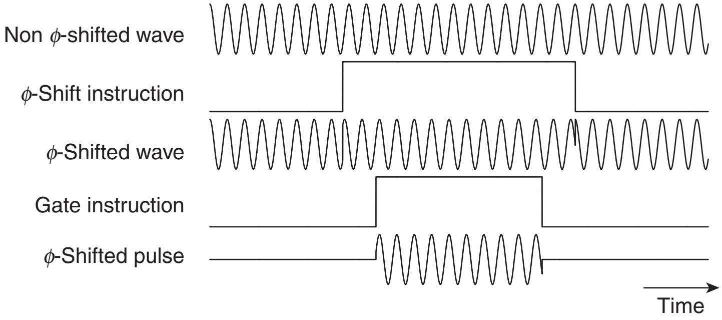

Figure 4.6
Detailed timing for an r.f. pulse.

⚠The phase of an r.f. pulse is governed by the underlying function $\cos(\omega_{\text{ref}}t + \phi)$ and not by the appearance of the waveform at the beginning of the pulse, which depends on the precise gating instant, a matter of little importance. The two pulses shown below both have phase 0, but look quite different:

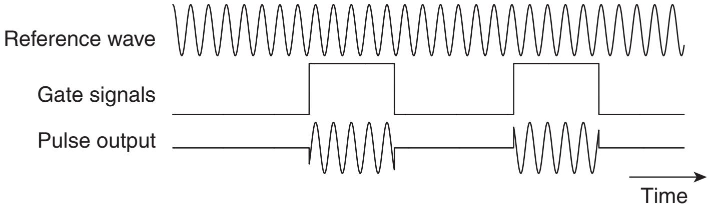

Figure 4.7
Two pulses with the same phase.

NMR spectroscopists often use a special jargon for the four phases that are multiples of $\pi/2$, summarized in Table 4.1. The symbols $\bar{x}$ and $\bar{y}$ are pronounced 'x-bar' and 'y-bar'. The reasons for this jargon are explained in Chapter 10.

The gating scheme described here generates a 'rectangular' r.f. pulse. Ideally, the waveform envelope rises infinitely fast at the beginning of the pulse, remains constant during the pulse, and falls off infinitely fast at

Table 4.1 Jargon used for r.f. phases.

R.f. phase	Jargon
$\phi = 0$	"x-pulse"
$\phi = \pi/2$	"y-pulse"
$\phi = \pi$	"$\bar{x}$-pulse" or "$-x$-pulse"
$\phi = 3\pi/2$	"$\bar{y}$-pulse" or "$-y$-pulse"

the end. There are many more complicated possibilities. Modern NMR experiments often use modulation schemes in which the amplitude, frequency, and phase of the r.f. pulses are varied smoothly.

4.2.3 Radio-frequency amplifier

The function of the r.f. amplifier ⑤ is to scale up the gated waveform so as to produce a large-amplitude r.f. pulse for transmission to the probe. Typical r.f. amplifiers for NMR applications have ratings between several watts and about 1 kW of peak output power.

4.3 The Duplexer

The amplified r.f. pulse travels down a cable into the *duplexer* ⑥. From the duplexer, two more cables emerge. One cable leads to the probe, which is mounted inside the magnet, and which contains the sample. The second cable leads to the receiver section, which is used to detect the weak r.f. signals generated by the nuclear spins.

The duplexer achieves an apparently impossible task: when a strong r.f. pulse arrives from the amplifier, the duplexer diverts it down the cable leading to the probe, not into the sensitive signal detection circuitry:

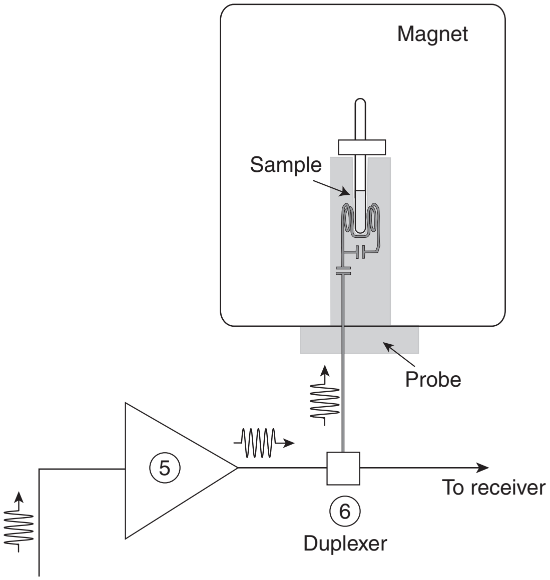

Figure 4.8
The duplexer in transmit mode.

When, on the other hand, the tiny NMR signal travels down the same cable in the opposite direction, i.e. from the probe to the duplexer, it is diverted into the signal detection path, not down the cable leading to the amplifier:

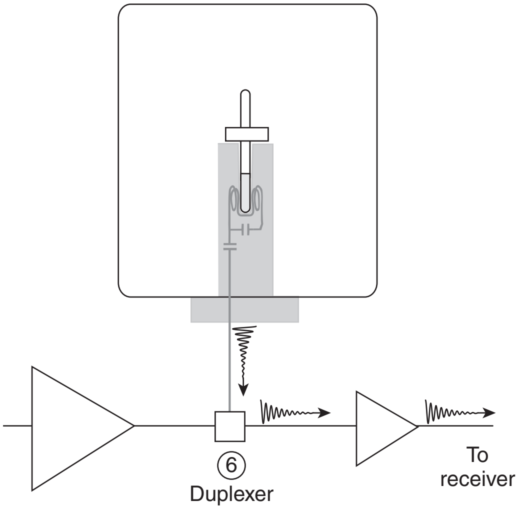

Figure 4.9
The duplexer in receive mode.

On some instruments, this demanding task is accomplished by a cunning arrangement of cables and diodes, without any external switching signals. In other instruments, the duplexer is switched rapidly between transmit and receive mode by a signal from the pulse programmer.

4.4 The Probe

The probe is a complex piece of apparatus that has several functions:

1. It locates the sample in the region of homogeneous magnetic field.
2. It includes r.f. electronic circuits for irradiating the sample with r.f. waves, and for detecting the subsequent r.f. emissions from the sample.
3. In some cases, the probe has a device for rotating the sample, in order to reduce the width of the NMR peaks.
4. In some cases, the probe has devices for stabilization of the temperature of the sample.
5. *Cryoprobes* employ cooling of the electronic circuits (not the sample!) to cryogenic temperatures (typically around 20 K) in order to improve the signal detection efficiency.
6. In some cases, the probe contains additional coils for creating magnetic fields with a controlled spatial inhomogeneity. These coils are used in NMR imaging experiments, and many other methods (see Section 4.7).

The probe is the most specialized part of the NMR spectrometer, and is often the only part that needs to be exchanged when switching between different NMR experiments, e.g. from liquid-state NMR experiments to solid-state NMR experiments.

No attempt is made here to survey the different types of NMR probe. For the present purposes, consider the following highly simplified representation of a liquid-state NMR probe:

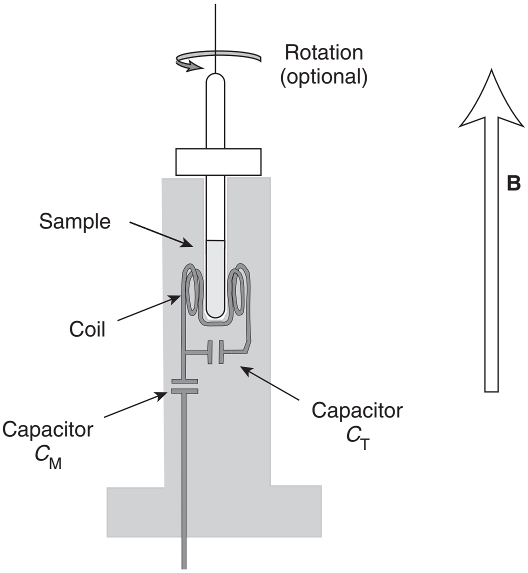

Figure 4.10
A single-channel solution NMR probe.

The sample is contained in a glass tube, which sits in a hole in the top of the probe so as to position the sample inside the r.f. coil. When the probe is mounted in the magnet bore, the sample is located in the region of homogeneous magnetic field.

For maximum resolution, NMR tubes are machined with high precision from very uniform glass, to avoid undesirable distortions of the magnetic field. All probe components in the vicinity of the sample are strictly non-magnetic. Even the electrical coil is usually made from a carefully chosen composite material with near-zero net magnetic susceptibility.

In liquid-state NMR, the sample tube is often rotated around its long axis at a frequency of around 10 Hz. This is a form of *motional averaging* of the nuclear spin interactions. The spatial inhomogeneities in the magnetic field are partially smoothed out by the sample motion, leading to enhanced resolution.

I now discuss the probe electronics. Figure 4.10 shows a highly simplified r.f. circuit consisting of a coil and two capacitors. The function of the coil is twofold. First, during the r.f. pulse, electrical currents in the coil generate an oscillating magnetic field at the sample. As shown later, this oscillating field rotates the nuclear spin polarizations and creates transverse magnetization. Second, when the r.f. pulse has terminated, the precessing nuclear magnetization generates electrical currents in the coil that give rise to a detectable signal travelling back down the cable again towards the duplexer. The duplexer diverts these weak NMR signals towards the receiver electronics.

The coil geometry is such that it generates an oscillating magnetic field that is predominantly *perpendicular* to the main magnetic field. This requires that the coil is *not* wound 'around' the sample tube, but perpendicular to it. The importance of this geometry will become apparent when we go into the theory.

The two capacitors in the probe circuit have the following functions. The one marked C_M is called the *matching capacitor*; this couples the external signals into the probe circuit with maximum efficiency. I will not discuss it further. The capacitor marked C_T is called the *tuning capacitor*; this is more important for our purposes. It is wired in parallel with the coil enclosing the sample.

The function of the tuning capacitor is to enhance the currents in the coil by electromagnetic resonance. According to elementary circuit theory, a parallel circuit of a capacitor of value C_T (in units of farads) and a coil of inductance L (in units of henrys) comprise an electromagnetic *oscillator*. The frequency of the oscillator, in radians per second is given approximately by

$$\boxed{\omega_{\text{osc}} = (LC_T)^{-1/2} \qquad (4.2)}$$

Energy in the circuit is stored alternately as an electric field between the plates of the tuning capacitor, and as a magnetic field enclosed by the windings of the coil.

The tuned oscillator acts as an *accumulator of energy* for electromagnetic fields with a frequency matching the oscillation frequency ω_{osc}. When the r.f. pulse arrives from the amplifier via the duplexer, it sets up oscillations in the tuned circuit. If the frequency of the pulse ω_{carrier} is close to the resonant frequency of the circuit ω_{osc}, the oscillations build up. The phenomenon is similar to a child's swing: by giving the swing small pushes at instants matching the natural resonant frequency, a large-amplitude motion is built up. The swing accumulates mechanical energy. Similarly, the tuned circuit accumulates electrical energy, building up a large oscillating magnetic field in the coil. This magnetic field is much larger than would be achieved in the absence of the tuning capacitor C_T.

The reciprocal phenomenon takes place when the NMR signal is detected. In this case, the oscillating magnetic field produced by Larmor precession of the spins drives resonant electrical oscillations in the tuned circuit. The oscillating electrical signal induced by the spin precession is much larger than would be achieved if the circuit were not tuned. The capacitor and coil act together to accumulate the energy of the weak NMR signal.

The electrical properties of the tuned circuit are affected by the nature of the sample. It is necessary, therefore, to adjust the values of the capacitors C_M and C_T every time the sample is changed. Normally, this is done by manual adjustments of the capacitors – a process called 'tuning the probe'.

Once a circuit is tuned, it may only be used for the observation of a single nuclear isotope. R.f. signals intended for different nuclear isotopes have too large a frequency difference to build up appreciable amplitude in the same tuned circuit. However, it is technically feasible to share the same coil between separate tuned circuits, each operating on a different frequency. This is called *multiple tuning*, and requires careful electronic construction to isolate each circuit from the others. A multiple-tuned coil is simultaneously involved in circuits resonating at a number of different frequencies. Each circuit may be tuned independently to resonate at the Larmor frequency of a particular nuclear isotope.

4.5 The Receiver Section

We now trace the fate of the r.f. NMR signal generated by the nuclear spins, using instrumentation typical for a relatively old-fashioned NMR instrument. Modern instruments employ a more sophisticated and integrated processing of the NMR signal, but the principles are basically the same.

The immediate fate of the NMR signal is as follows:

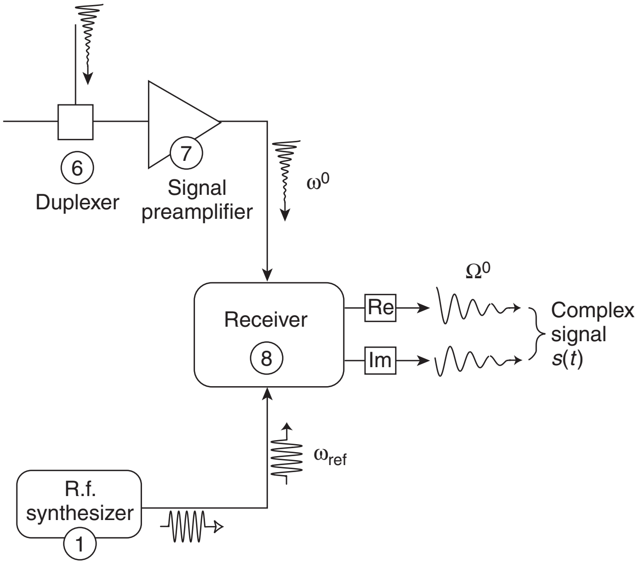

Figure 4.11
The receiver section.

4.5.1 Signal preamplifier

The NMR signal first arrives at the duplexer ⑥, which diverts it down the cable towards the *signal preamplifier* (often simply called the *preamplifier*) ⑦. This is a low-noise r.f. amplifier that scales up the tiny signal to a more convenient voltage level.

4.5.2 The quadrature receiver

The NMR signal must be fed into the computer for interpretation and presentation. Therefore, it is necessary to convert the NMR signal (an oscillating electrical current) into digital form (a sequence of 'ones' and 'zeros').

The process of converting a continuous current or voltage into digital form is called *analogue-to-digital conversion*. This task is accomplished by specialized electronic circuits called *analogue-to-digital converters* (ADCs).

One technical problem must first be faced. The 'raw' NMR signal oscillates at many hundreds of megahertz, which is too fast for current ADCs (as of 2007). Therefore, it is necessary to 'down-convert' the frequency of the NMR signals, so that they may be handled by the digital electronics at the next stage.

The *quadrature receiver* ⑧ accomplishes the signal frequency conversion by comparing it with a reference wave of frequency ω_{ref}, as supplied by the r.f. synthesizer (see Equation 4.1). The quadrature receiver combines the NMR signal, which oscillates at the Larmor frequency ω^0, with the reference signal, oscillating at the frequency ω_{ref}, to generate a new signal that oscillates at the *relative Larmor frequency*:

$$\Omega^0 = \omega^0 - \omega_{\mathrm{ref}}$$

This is the frequency conversion process encountered in Sections 3.4 and 3.5.

The offset frequency Ω^0 is usually of the order of 1 MHz or less. The signal emerging from the quadrature receiver varies slowly enough to be handled accurately by the digital electronics at the next stage.

A similar procedure takes place in an ordinary *radio receiver*. In that case, the modulated r.f. waves, travelling through space, are detected and down-converted to the audible frequency range, where they are transformed into mechanical oscillations to generate sound.

Usually, *two* output signals emerge from the receiver. The use of two outputs, rather than one, will now be motivated.

Consider the r.f. signal from nuclear spins with Larmor frequency ω^0 (for simplicity, suppose that there is only one peak in the NMR spectrum). The NMR signal (FID) s_{FID} has the form

$$s_{\text{FID}}(t) \sim \cos\left(\omega^0 t\right) \exp\{-\lambda t\}$$

including a damping factor with the rate constant $\lambda = T_2{}^{-1}$.

Now consider the output of the receiver. The simplest form of frequency down-conversion would substitute ω^0 by Ω^0, leading to

$$\cos\left(\Omega^0 t\right) \exp\{-\lambda t\} \tag{4.3}$$

However, there is a problem. Equation 4.3 does not distinguish between signals generated by spins whose precession frequencies ω^0 are *larger* than ω_{ref} from those whose precession frequencies ω^0 are *smaller* than ω_{ref}. For example, suppose that protons are observed and that the proton Larmor frequency is close to -500 MHz. Suppose that the spectrometer reference frequency is set to exactly $\omega_{\text{ref}}/2\pi = -500.000\,000$ MHz. The precise precession frequency of the nuclei depends on the molecular environment. Nuclear spins in environments with slightly stronger magnetic fields precess slightly faster, e.g. $\omega^0/2\pi = -500.001\,000$ MHz; nuclear spins in environments with slightly smaller magnetic fields precess slightly slower, e.g. $\omega^0/2\pi = -499.999\,000$ MHz. The difference frequency for spins of the first type is $\Omega^0/2\pi = -1.000$ kHz, whereas the difference frequency for spins of the second type is $\Omega^0/2\pi = +1.000$ kHz. Equation 4.3 does not distinguish the signals from these physically distinct situations.

To resolve this ambiguity, the receiver supplies *two* output signals, of the form

$$s_{\text{A}}(t) \sim \cos\left(\Omega^0 t\right) \exp\{-\lambda t\}$$
$$s_{\text{B}}(t) \sim \sin\left(\Omega^0 t\right) \exp\{-\lambda t\}$$

These two signals may be interpreted as the real and imaginary components of a single complex signal $s(t)$, i.e.

$$s_{\text{A}}(t) = \text{Re}\{s(t)\} \quad s_{\text{B}}(t) = \text{Im}\{s(t)\}$$

where

$$\boxed{s(t) = s_{\text{A}}(t) + \text{i}s_{\text{B}}(t) \sim \exp\{(\text{i}\Omega^0 - \lambda)t\}} \tag{4.4}$$

This complex NMR signal distinguishes between positive and negative values of Ω^0 and retains full information as to the magnitude of the Larmor frequency relative to that of the reference wave.

This two-output scheme is called *quadrature detection*. The electronic configuration and operation of a typical quadrature detector is discussed in Appendix A.5.

The representation of an NMR signal as *complex*, with both a real and an imaginary part, is mathematically very convenient. NMR signals with a *decaying complex exponential* form, as in Equation 4.4, will be encountered a lot from now on.

4.5.3 Analogue–digital conversion

Each of the two outputs of the quadrature receiver ⑧ are connected to their own ADC ⑨:

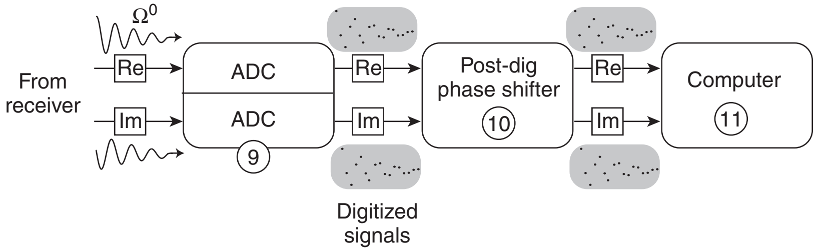

Figure 4.12
The digitizer and phase shifter chain.

An ADC is an electronic circuit that rapidly measures the voltage level of an input signal and presents the information as a string of 'ones' and 'zeros'. The NMR signal is converted to digital form by repeating the measurement at a set of consecutive time points and storing the information in the computer as an ordered set of values. This is called *digitization*:

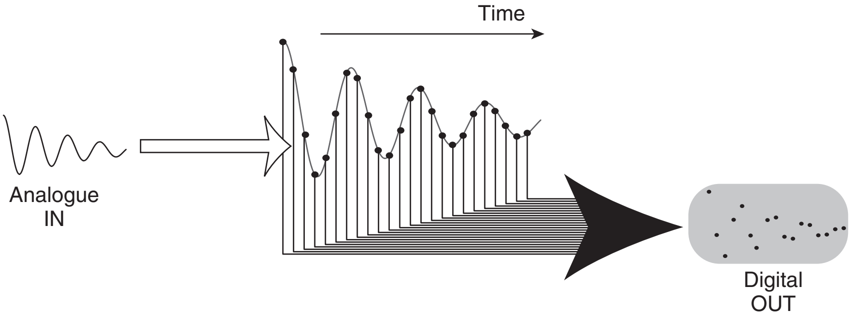

Figure 4.13
Digitization.

The time separation between the sampling points of the ADCs is called the *sampling interval*, or the *dwell time* in older literature (symbol τ_{sample}). The inverse of the sampling interval is the *sampling bandwidth*, often referred to (somewhat misleadingly) as the *spectral width*. The sampling bandwidth sets the maximum range of signal frequencies that is represented accurately by the sampling process (see *Further Reading*). NMR signals with a wide range of frequencies (common in solid-state NMR) require more rapid sampling than signals that span a narrow frequency range (common in liquid-state NMR). Typical sampling bandwidths are around 4 MHz in solid-state NMR and around 250 kHz for liquid-state NMR. This corresponds to sampling intervals τ_{sample} of 250 ns and 4 μs respectively.

For technical reasons, the number of sampled points n_{sample} is usually an integer power of 2. There is a special jargon for the larger powers, as summarized in Table 4.2. For example, $n_{\text{sample}} = 2^{10} = 1024$ is referred to as '1k', etc.

Table 4.2 Jargon used for the number of digital sampling points.

Number of points	Power of 2	Jargon
1 024	10	1k
2 048	11	2k
4 096	12	4k
8 192	13	8k
16 384	14	16k
32 768	15	32k

The total duration over which the signal is sampled is called the *acquisition time* and is given by

$$\tau_{\mathrm{acq}} = n_{\mathrm{sample}} \tau_{\mathrm{sample}} \tag{4.5}$$

For reasons of sensitivity and resolution, it is usually desirable to sample the NMR signal until it has died out completely. The digitization of 32k points, at 20 μs per point, covers a time-span of about 0.65 s, which is adequate in most circumstances (see *Further Reading*).

4.5.4 Signal phase shifting

In many experiments, the phases of the r.f. pulses, and that of the NMR signal, are changed in a dynamic way as the experiment proceeds. As discussed later, this allows NMR signals to be distinguished from experimental artefacts, and also allows different types of NMR signal to be distinguished from each other.

The phases of r.f. pulses are changed as described in Section 4.2.2. The phase of the NMR signal may also be changed as it passes through the receiver/digitizer chain. There are two ways to give the signal a controllable phase shift. Both are in common use.

1. *Receiver reference phase.* As described above, the quadrature receiver compares the NMR signal with a reference wave from the synthesizer. If the phase of the synthesizer reference wave is changed during the entire period of signal detection, then this phase shift is transferred to the signal emerging from the receiver.

2. *Post-digitization phase.* The second method for changing the signal phase operates on the *digitized* signal emerging from the ADCs. The digitized complex signal is passed into a device called a *post-digitization phase shifter* ⑩, which multiplies the signal by a complex phase factor before it is passed to the computer ⑪.

In modern instruments, both types of phase shifting are essentially equivalent and I will not distinguish between them.[5] The overall phase shift imparted to the NMR signal as it passes through the receiver–digitizer chain is called the *receiver phase* and is denoted ϕ_{rec}.

Mathematically, the application of a receiver phase ϕ_{rec} multiplies the complex NMR signal by the factor $\exp\{-\mathrm{i}\phi_{\mathrm{rec}}\}$. This property will be used later on, when we analyse some actual NMR experiments.

4.6 Overview of the Radio-Frequency Section

Figure 4.14 gives an overview of the r.f. generation and data processing pathway of a single-channel NMR spectrometer.

The different electronic circuits are orchestrated by the pulse programmer, which receives its directions from the computer. The computer is, in turn, controlled by the spectrometer operator.

The digitized NMR signal is returned to the computer, where it may be processed and displayed, as described in Chapter 5.

A block diagram of a multiple-channel spectrometer, capable of excitation and detection at the Larmor frequency of several isotopes simultaneously, may be derived from this one by duplicating the r.f. network ①–②–③–⑤–⑥–⑦–⑧ shown in Figure 4.14. The probe is the only r.f. component that is not duplicated: as described in Section 4.4, a multiple-channel probe accomodates many r.f. channels at the same time. Sometimes, the receiver is not duplicated either, but assigned to one of the r.f. channels before the experiment starts.

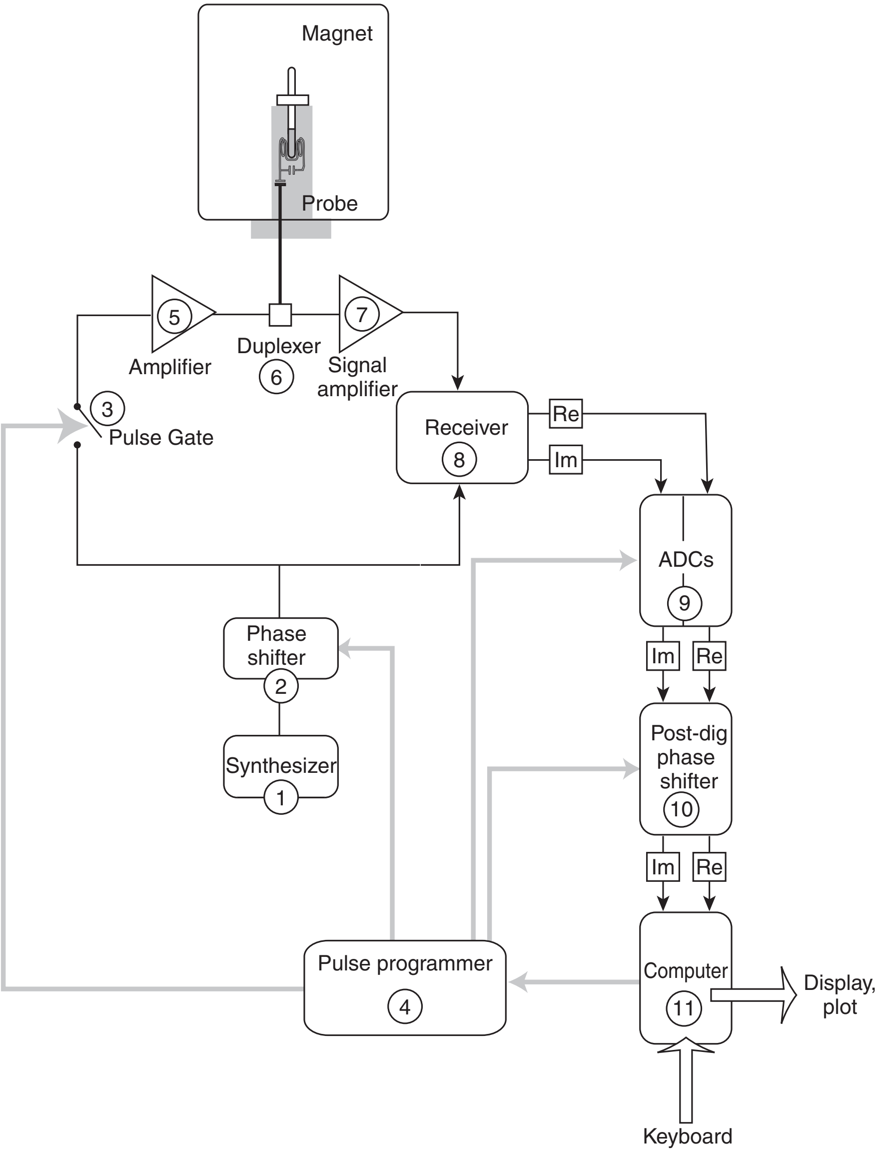

Figure 4.14
Schematic overview of a single-channel spectrometer, without pulsed field gradient equipment.

4.7 Pulsed Field Gradients

Many NMR experiments require the application of pulsed static magnetic fields, as well as r.f. fields. As described in Section 3.6, NMR spectra taken in the presence of a magnetic field gradient contains information on the spatial distribution of nuclei; in Section 12.6, we will see how the switching of field gradients along different axes may be used to construct full three-dimensional images. Switched magnetic field gradients are also used for the study of flow and diffusion by NMR (see Chapter 19), and for selecting certain classes of NMR signals while suppressing others (see Appendix A.12). Pulsed magnetic field gradients may also be used to perform many different NMR experiments at the same time in different parts of the sample tube.[6]

4.7.1 Magnetic field gradients

In the absence of a magnetic field gradient, the magnetic field is homogeneous. It has the same magnitude, and same direction, at all points in space. If the strength of the magnetic field is B^0, and its direction is defined as the z-axis, the magnetic field at point $\mathbf{r}$ is

$$\mathbf{B}(\mathbf{r}) = B^0\mathbf{e}_z$$

where $\mathbf{e}_z$ is a unit vector along the z-axis.

In the presence of a field gradient, on the other hand, the magnitude of the field varies in a controlled fashion along the gradient direction. Consider, for example, a field gradient of magnitude G_x applied along the x-axis, i.e. perpendicular to the main magnetic field. The magnetic field at point $\mathbf{r}$ in the presence of this gradient is

$$\mathbf{B}(\mathbf{r}) = B^0\mathbf{e}_z + G_x x\mathbf{e}_z \tag{4.6}$$

where x is the coordinate along the x-axis, i.e.

$$x = \mathbf{r} \cdot \mathbf{e}_x$$

Note carefully that Equation 4.6 describes a magnetic field that still points along the z-axis, but whose *magnitude* varies as a function of x. The magnetic field in the presence of G_x may be visualized as follows:

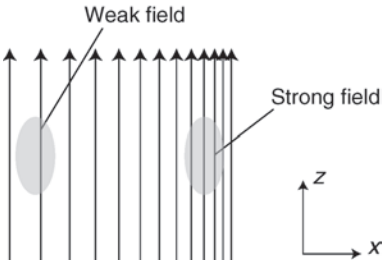

Figure 4.15
Magnetic flux lines in the presence of a strong magnetic field along the z-axis and a field gradient along the x-axis.

The magnitude of the field is proportional to the density of field lines. Note the variation in the strength of the field, but not its direction, along the x-axis.

For clarity, the sketch in Figure 4.15 greatly exaggerates the gradient. In practice, the variation of the magnetic field across the sample is many orders of magnitude less than the size of the main magnetic field.

Similarly, the magnetic field in the presence of a gradient G_z along the z-axis is described by

$$\mathbf{B}(\mathbf{r}) = B^0\mathbf{e}_z + G_z z\mathbf{e}_z \tag{4.7}$$

where $z = \mathbf{r} \cdot \mathbf{e}_z$. The magnetic field lines in the presence of G_z are visualized in Figure 4.16. This time, the magnitude of the magnetic field varies along the z-axis, while its direction remains almost unchanged.[7] Once again, the magnitude of the gradient is greatly exaggerated in this sketch.

Figure 4.16
Magnetic flux lines in the presence of a strong magnetic field along the *z*-axis and a field gradient along the *z*-axis.

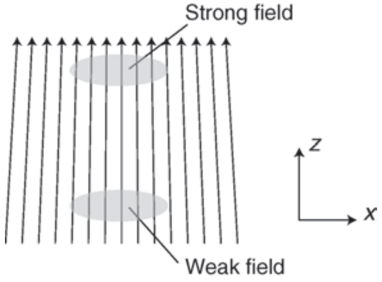

A field gradient G_y along the y-axis is described by the equation

$$\mathbf{B}(\mathbf{r}) = B^0\mathbf{e}_z + G_y y\mathbf{e}_z \tag{4.8}$$

where $y = \mathbf{r} \cdot \mathbf{e}_y$. It may be visualized by constructing a picture as in Figure 4.15, but where the field lines get closer as one 'goes into the paper'.

4.7.2 Field gradient coils

Magnetic field gradients are imposed in NMR experiments by passing electrical currents through carefully designed coils near the sample. In some cases, these gradient coils are incorporated into the NMR probe itself; in other cases, they are part of the magnet and shim assembly.

For example, a gradient G_z may be generated by passing currents through opposed coils above and below the sample:

Figure 4.17
Coil and current configuration used to generate a magnetic field gradient along the *z*-axis. The flux lines shown in the sample region assume that a strong homogeneous magnetic field is applied at the same time along the *z*-axis.

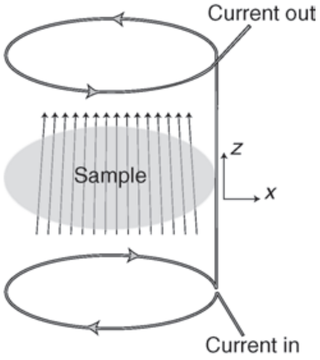

The field generated by the upper coil enhances the magnetic field in the sample, while the field generated by the lower coil opposes it. Careful design of the geometry and current paths can lead to an accurate linear field gradient G_z across the sample volume.

Similarly, a gradient G_x may be generated by the coil configuration sketched in Figure 4.18. The currents running down each arm of the coils generate a field that enhances the magnetic field on the right-hand side of the sample, but which opposes it on the left-hand side.

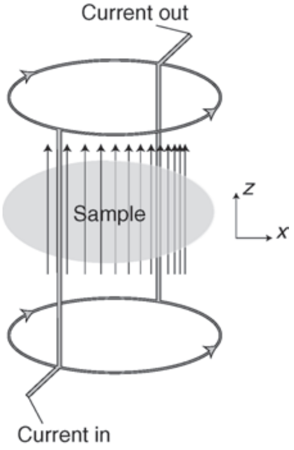

Figure 4.18
Coil and current configuration used to generate a magnetic field gradient along the *x*-axis. The flux lines shown in the sample region assume that a strong homogeneous magnetic field is applied at the same time along the *z*-axis.

A gradient along the *y*-axis is generated by rotating the coil arrangement in Figure 4.18 by 90° around the *z*-axis.

Field gradient coils are usually carefully shielded, in order to minimize the magnetic fields they generate in regions remote from the sample. This is because pulsed magnetic fields induce transient electric 'eddy currents' in metal parts of the probe and magnet assembly. Such eddy currents take some time to dissipate and themselves generate magnetic fields that can interfere with the NMR experiment.

Typical field gradient strengths in human-scale NMR imaging applications are around ~10 mT m^{-1}. For diffusion studies, and microimaging applications, gradients of up to ~1000 mT m^{-1} are used.

4.7.3 Field gradient control

In most spectrometers, each magnetic field gradient is controlled by a separate channel, which resembles that used in the r.f. section. Each gradient channel consists of a *digital-to-analogue converter* (DAC) and a *gradient driver*. The DAC converts timed digital instructions from the pulse programmer into an analogue voltage level. It therefore performs the inverse function of the ADCs used in the receiver circuit. The gradient driver is a powerful amplifier that converts the analogue input voltage into a strong, well-controlled current. This electric current is driven through the gradient coils, generating the desired magnetic field gradient pulse (see Figure 4.19). These circuits allow each gradient pulse to be shaped accurately as a function of time.

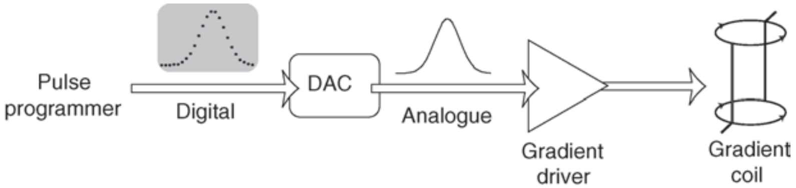

Figure 4.19
The circuits involved in driving a gradient coil.

An overview of a spectrometer with a single r.f. channel and one pulsed field gradient channel is given in Figure 4.20. The pulsed field gradient channels are duplicated if the probe or magnet assembly contains more than one pulsed field gradient coil, and the r.f. channels are duplicated if the probe allows irradiation and/or detection at the Larmor frequency of more than one nuclear isotope.

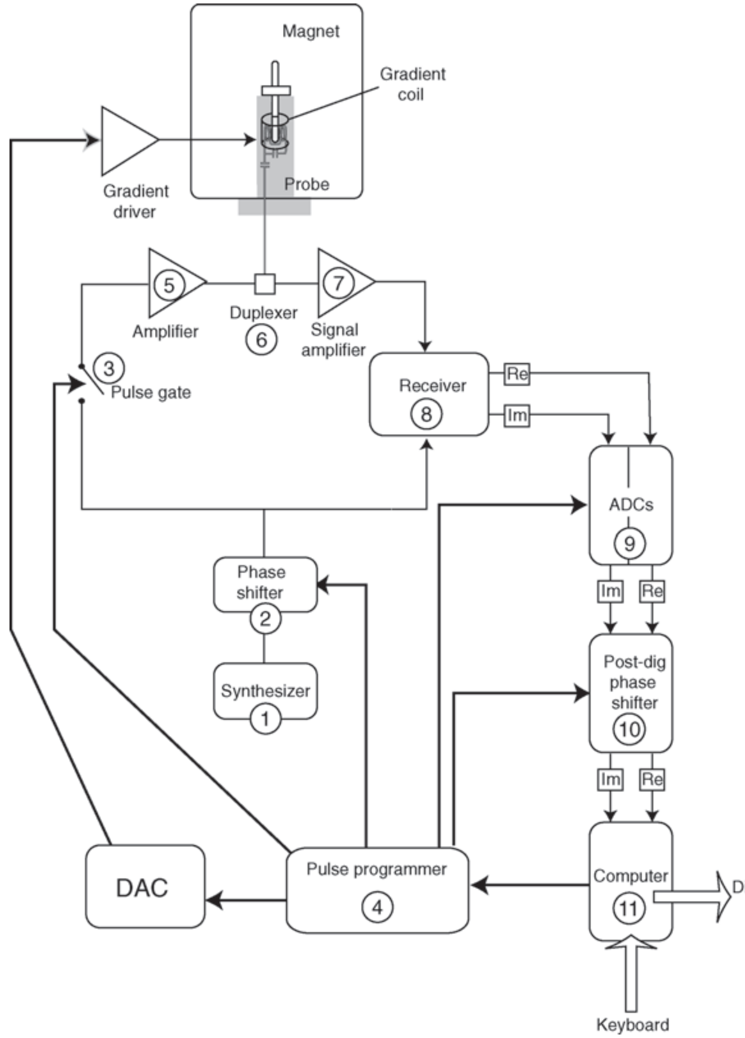

Figure 4.20
Schematic overview of a single-channel spectrometer, incorporating one pulsed field gradient channel.

Notes

1. Various methods are available for transcending the sensitivity limitations of conventional NMR. These schemes are aimed either at enhancing the net polarization of the nuclei or at improving the detection strategy, or both. In *dynamic nuclear polarization* (DNP), the nuclear spin polarization of paramagnetically doped materials is greatly enhanced by using microwave irradiation (e.g. see D. A. Hall *et al., Science,* **276**, 930 (1997) and J. H. Ardenkjaer-Larsen *et al., Proc. Nat. Acad. Sci. USA,* **100,** 10 158–10 163 (2003). Other polarization enhancement techniques include optical pumping of noble gas nuclei (e.g. see B. M. Goodson, *J. Magn. Reson.* **155**, 157–216 (2002)), chemical reactions of parahydrogen (e.g. see S. B. Duckett, C. J. Sleigh, *Prog. NMR Spectrosc.*, **34**, 71 (1999)), and photoinduced radical-pair creation (M. G. Zysmilich, A. E. McDermott, *Proc. Natl. Acad. Sci. USA,* **93**, 6857(1996)). Alternative detection methods have been proposed, such as superconducting quantum

interference devices (SQUIDs) (see C. Connor, *Adv. Magn. Opt. Reson.*, **15**, 201 (1990)) and the rotation of polarized light by the bulk nuclear magnetization (see I. M. Savukov *et al.*, *Nature* **442**, 1021–1024 (2006)). Mechanical oscillators are already sensitive enough to detect single *electron* spins (see D. Rugar *et al.*, *Nature*, **430**, 329–*332* (2004)), and have been used to detect small numbers of nuclear spins (see D. Rugar *et al.*, *Nature*, **360**, 563 (1992)). The magnetic properties of individual nuclear spins have been probed by optical techniques (see J. Kohler *et al.*, *Science*, **268**, 1457 (1995), J. Wrachtrup *et al.*, *Nature*, **363**, 244 (1993), and F. Jelezko *et al.*, *Phys. Rev. Lett.*, **93**, 130501 (2004). None of these methods has proven generally applicable, although many are very promising in specialized circumstances.

2. At the moment (year 2007) the materials known as high-T_c superconductors have not proven to be suitable for the main coils of NMR magnets.

3. The English word *shim* means a small piece of metal. The field adjustment coils are called shim coils because the original method for adjusting the field inhomogeneity involved moving small metal pieces around. Apart from the shims, there is another coil that is used for compensating any small undesired changes in the magnitude of the magnetic field, due to fluctuations in air pressure and temperature, slight imperfections in the superconducting material, or other magnetic disturbances. A feedback circuit continuously monitors the magnetic field in the sample and compensates any changes by increasing or decreasing the current in the extra coil. In order for this to work, this compensation circuit must obtain accurate, up-to-date, information as to the actual magnetic flux density in the sample. Such information can only be provided with sufficient accuracy by one method, namely NMR itself. Commercial spectrometers often run a separate NMR experiment on ^{2}H spins, deliberately introduced into the sample, in order to monitor the magnetic field. This feedback system is called the *field-frequency lock*. It normally runs ‘in the background’, without intervention from the operator.

4. There are some subtle issues concerning the signs of the frequencies and phase shifts used in the spectrometer. For the sake of simplicity, I have ignored these complications. A complete treatment may be found in M. H. Levitt, *J. Magn. Reson.*, **126,** 164 (1997) and M. H. Levitt, O. G. Johannessen, *J. Magn. Reson.*, **142,** 190–194 (2000).

5. Until recently, it was advisable to distinguish between the receiver reference phase and the post-digitization phase, since they have slightly different characteristics: (i) the post-digitization phase shift occurs *after* the quadrature detection of the NMR signal and is therefore immune to instrumental imperfections such as misbalance of the two sections of the quadrature detector; (ii) in older instruments, the choice of post-digitization phase shifts was frequently limited to multiples of $\pi/2$; (iii) in some NMR instruments, the hardware does not permit a receiver reference phase shift, whereas any value of the receiver reference phase is permitted in others. In order to cater for the variety of spectrometer configurations, the first edition of this book distinguished sharply between these two types of signal phase shift. Fortunately, advances in receiver technology, such as oversampling and digital signal post-processing, have largely erased these distinctions in modern instruments.

6. For example, see L. Frydman, T. Scherf, A. Lupulescu, *Proc. Natl. Acad. Sci. USA*, **99,** 15 858–15 862, (2002).

7. Because of the geometrical properties of magnetic fields, it is strictly impossible to construct field gradients that involve a pure variation of only one component of the magnetic field in only one direction, while keeping the direction of the magnetic field constant. Figure 4.16 illustrates this difficulty: the direction of the field is not strictly constant, as its magnitude is varied along the z-axis. Fortunately, the errors caused by these inevitable field distortions are negligible in ordinary high-field NMR and NMR imaging applications.

Further Reading

- For more on the practical aspects of the spectrometer, see E. Fukushima, S. B. W. Roeder, *Experimental Pulse NMR. A Nuts and Bolts Approach*, Perseus Press, Cambridge, MA, USA, 1986.
- For discussion of the appropriate choice of sampling bandwidth and the total acquisition duration, see A. E. Derome, *Modern NMR Techniques in Chemistry Research*, Pergamon Press, Oxford, 1990.

5 Fourier Transform NMR

In this chapter, I describe how the different components of the spectrometer are coordinated so as to produce an NMR signal. The fate of the NMR signal is followed as it is processed and converted into an NMR spectrum by the computer.

5.1 A Single-Pulse Experiment

Consider a simple NMR experiment consisting of a single r.f. pulse on a single r.f. channel, followed by signal detection. The sequence of events is as follows:

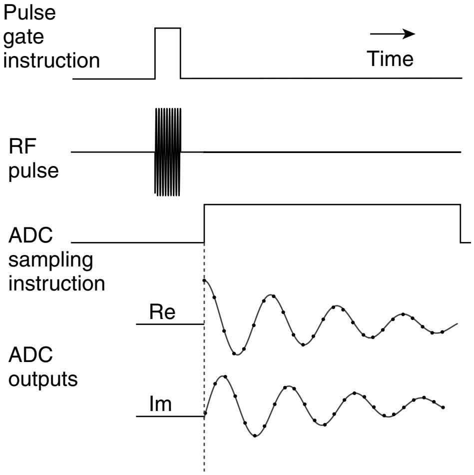

Figure 5.1
Timing sequence for a simple one-pulse experiment.

1. *Initialization.* Before the experiment starts, the computer downloads instructions to the pulse programmer and to other pieces of hardware, such as the synthesizer and the ADCs, setting up the carrier frequency, the sampling frequency and the number of sampled points, etc.

2. *Excitation.* On initiation, the pulse programmer executes a timed sequence of instructions to set the phase of the r.f. synthesizer and open the pulse gate. An r.f. pulse travels into the probe from the amplifier, via the duplexer. This r.f. pulse sets up resonant oscillations in the tuned circuit of the probe, irradiating the sample with an r.f. field close to the Larmor frequency of the chosen nuclear isotope. As decribed

---

Spin Dynamics: Basics of Nuclear Magnetic Resonance, Second Edition Malcolm H. Levitt

in Section 2.7, this r.f. pulse disturbs the equilibrium of the nuclear spin system and creates transverse nuclear magnetization.

3. *Detection.* The pulse is switched off. After some microseconds, the pulse energy in the tuned circuit dissipates and the system is ready to detect the NMR signal. The precession of the nuclear spin magnetization sets up oscillations in the tuned circuit, which give rise to an r.f. NMR signal (the FID), travelling back down the cable from the probe to the duplexer. This signal is amplified by the signal preamplifier and converted down in frequency by the quadrature receiver. The pulse programmer issues an instruction to the ADCs, which proceed to digitize the two quadrature receiver outputs. The digitized complex signal $s(t)$ is stored in the computer memory.

4. *Processing and display.* The digital complex signal is subjected to various mathematical operations, including the numerical calculation called *Fourier transformation* (FT), discussed in Section 5.8.1. FT converts the NMR signal, which is a function of time, into an NMR *spectrum*, which is a function of frequency. The NMR spectrum may be displayed on the computer screen, printed or plotted on a sheet of paper, or subjected to any of the chicanery of digital communications or processing.

In practice, there are additional timing signals for blanking the r.f. amplifiers, and switching off the receiver during the r.f. pulses, so as to avoid undesirable electronic interference. These complications are ignored here.

In pulse sequence diagrams, the above timing steps are often condensed to the following iconic form:

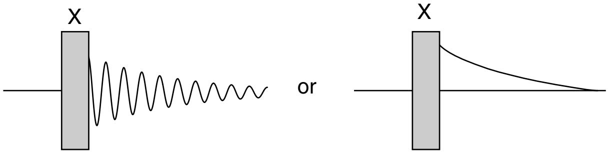

Figure 5.2
Icons representing a one-pulse sequence.

The symbol 'x' over the pulse indicates that the phase of the synthesizer is set to zero during the pulse (see Table 4.1).

Pulse sequence timing diagrams are rarely drawn to scale along the time axis. In reality, each r.f. pulse usually lasts only a few microseconds, whereas the signal acquisition interval may last several seconds.

5.2 Signal Averaging

The NMR signal is very weak. The signal emerging from the probe also contains uncontrolled random signals called *noise*. The battle against noise is a persistent feature of NMR spectroscopy.

The complex signal $s(t)$ at the output of the digitizer is given by

$$s(t) = s_{\mathrm{NMR}}(t) + s_{\mathrm{noise}}(t) \tag{5.1}$$

where s_{NMR} is the NMR signal and s_{noise} is the noise contribution. Typically, r.f. noise looks as follows:

Figure 5.3
Typical appearance of r.f. noise.

Noise is analogous to the 'hiss' in an old-fashioned transistor radio.

In a well-designed spectrometer, the main origins of r.f. noise are as follows: (i) thermal motion of charged particles in the sample, such as dissolved ions; (ii) thermal motions of electrons in the receiver coil. In most cases, the latter is the dominant noise source.[1]

The NMR spectrocopist has three ways of tackling the problem of noise. It is possible to exploit: (1) the narrow frequency spectrum of the NMR signals, compared with the noise; (2) the different time-profiles of the NMR signal and the noise – whereas the NMR signal tends to damp out as a function of time, the noise remains time independent, on the average; and (3) the different statistical properties of the NMR signal and the noise.

Property (1) may be exploited by good design of the r.f. hardware. It is not discussed further here. Property (2) may be exploited by manipulating the data in the computer, after the NMR experiment is finished.[2] See *Further Reading* for some practical recommendations in this respect.

In this section, we will consider how to exploit property (3). The NMR signals are reproducible (to a good approximation), whereas noise signals are random. If the same experiment is repeated, then the NMR signal is identical (assuming that the sample is unchanged, the spins are in similar states at the beginning of each experiment, and all the experimental parameters are well controlled). The noise, on the other hand, varies in an irreproducible way if the experiment is repeated, since it comes from sources other than nuclear spins. This property may be used to enhance the NMR signal at the expense of the noise. All that is needed is to repeat the same experiment many times and to add the signals together. This procedure is called *signal averaging*. (This term is not used very strictly. Often, the signal is 'summed' rather than 'averaged'. Nevertheless, I will continue to use the more familiar term.)

To see how signal averaging works, consider two independent, identical, NMR experiments. The true NMR signal $s_{\mathrm{NMR}}(1)$ from the first experiment is the same as the NMR signal $s_{\mathrm{NMR}}(2)$ from the second experiment. The sum of the two NMR signals, denoted $s_{\mathrm{NMR}}(1+2)$, is simply twice the signal from any individual experiment:

$$s_{\mathrm{NMR}}(1+2) = s_{\mathrm{NMR}}(1) + s_{\mathrm{NMR}}(2) = 2\,s_{\mathrm{NMR}}(1)$$

This simple relationship does not apply to the noise contributions, which are random. A suitable definition of the noise amplitude in a single experiment is provided by the *root-mean-square* (RMS) *noise*, defined as follows:

$$\sigma_{\mathrm{noise}}(1) = \left\langle s_{\mathrm{noise}}(1)^2 \right\rangle^{1/2}$$

where the angled bracket indicates the average over all the sampling points. Note that the simpler expression $\langle s_{\mathrm{noise}} \rangle$ would not do to quantify the noise, since the average of the noise points is approximately zero (the noise is just as likely to be positive as to be negative).

This RMS noise statistic is the same for the two experiments, to a good approximation, assuming that the noise is *stationary* (i.e. the amount of noise does not change from time to time):

$$\sigma_{\mathrm{noise}}(1) \cong \sigma_{\mathrm{noise}}(2)$$

However, this does not imply that the sum of the noise signals from two experiments has twice the RMS value. The RMS value of the summed noise is

$$\begin{aligned}
\sigma_{\mathrm{noise}}(1+2) &= \left\langle (s_{\mathrm{noise}}(1) + s_{\mathrm{noise}}(2))^2 \right\rangle^{1/2} \\
&= \left\langle s_{\mathrm{noise}}(1)^2 + 2 s_{\mathrm{noise}}(1) s_{\mathrm{noise}}(2) + s_{\mathrm{noise}}(2)^2 \right\rangle^{1/2} \\
&= \left\{ \left\langle s_{\mathrm{noise}}(1)^2 \right\rangle + \left\langle 2 s_{\mathrm{noise}}(1) s_{\mathrm{noise}}(2) \right\rangle + \left\langle s_{\mathrm{noise}}(2)^2 \right\rangle \right\}^{1/2}
\end{aligned}$$

Now, since the noise is *uncorrelated* between the two experiments, the 'cross-term' $\left\langle s_{\mathrm{noise}}(1) s_{\mathrm{noise}}(2) \right\rangle$ vanishes. The summed noise over two experiments, therefore, has the RMS value

$$\sigma_{\mathrm{noise}}(1+2) \cong \sqrt{2}\,\sigma_{\mathrm{noise}}(1)$$

It is larger than the noise over a single experiment, but only by the approximate factor $\sqrt{2}$. The *signal-to-noise ratio* for the sum of the two experimental signals is $\sqrt{2}$ larger than that for one experiment:

$$\frac{s_{\mathrm{NMR}}(1+2)}{\sigma_{\mathrm{noise}}(1+2)} \cong \frac{2s_{\mathrm{NMR}}(1)}{\sqrt{2}\sigma_{\mathrm{noise}}(1)} = \sqrt{2}\frac{s_{\mathrm{NMR}}(1)}{\sigma_{\mathrm{noise}}(1)}$$

The arguments above are easily extended to show that the signal-to-noise ratio accumulated by adding together $\mathfrak{N}$ transients is a factor $\sqrt{\mathfrak{N}}$ larger than the signal-to-noise ratio for a single transient:

$$\frac{s_{\mathrm{NMR}}(1+2+\ldots\mathfrak{N})}{\sigma_{\mathrm{noise}}(1+2+\ldots\mathfrak{N})} \cong \sqrt{\mathfrak{N}}\frac{s_{\mathrm{NMR}}(1)}{\sigma_{\mathrm{noise}}(1)} \tag{5.2}$$

The signal-to-noise ratio is approximately proportional to the square root of the number of summed transients.

It follows that repetition of experiments, and summation of signals, gradually distinguishes the NMR signals from the noise. The NMR signals and the noise both increase on signal averaging, but the NMR signals increase faster:

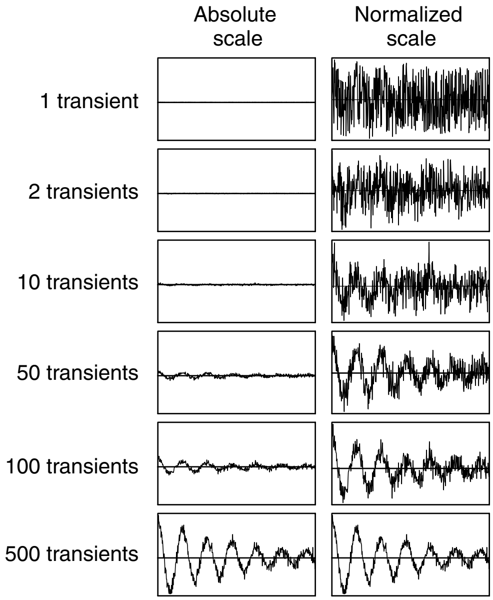

Figure 5.4
Adding together transients causes the NMR signals to build up faster than the noise.

The plots in the left column employ a uniform vertical scale, whereas the plots in the right column are rescaled so that the highest peak fills the box.

In NMR jargon, the separate experiments that compose a signal averaging scheme are called *transients*. The terms 'shots' and 'scans' are also used.

In principle, signal averaging always allows the NMR signals to be 'pulled out' of the noise. However, signal averaging is very time consuming. In order to repeat an experiment precisely, it is necessary to wait for the spin system to attain thermal equilibrium again. The different NMR experiments must be separated by an interval that is longer than the spin–lattice relaxation time constant T_1, several seconds in most cases. The available instrumental time and the limitations on the long-term stability of the instrument or the sample restrict the possibilities for distinguishing NMR signals from noise. For example, suppose that the signal-to-noise ratio in the spectrum obtained from a single transient is $1/10$ (meaning that the signal is completely buried in the noise). The signal-to-noise ratio may be transformed into 10:1 (which is usable), by averaging the results of 10 000 transients. If each transient takes 1 s, then collecting the whole set requires about 3 h of instrument time, which is acceptable. If, on the other hand, the signal-to-noise ratio in the spectrum obtained from a single transient is only 1/100, then 300 h of instrument time would be required to obtain an acceptable result. In many cases, this is not feasible.

5.3 Multiple-Pulse Experiments: Phase Cycling

Most NMR experiments employ more than one r.f. pulse. Consider, for example, the following pulse sequence:

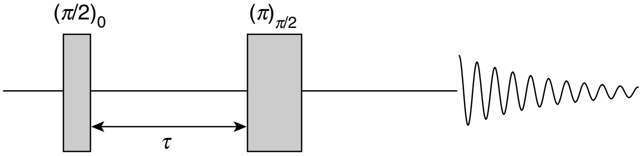

Figure 5.5
A two-pulse sequence.

This consists of two r.f. pulses, with the second pulse twice as long as the first. The time interval between the pulses, marked by a *double-headed arrow*, is denoted τ.

This pulse sequence is used to observe a phenomenon called a *spin echo*, discussed in Section 12.2. At the moment, I am not going to explain this pulse sequence, but merely discuss the notation.

The two pulses are annotated in the form β_ϕ. For the first pulse, β has the value $\pi/2$; for the second pulse, $\beta = \pi$. The value of β is called the *flip angle* of the r.f. pulse. The flip angle is a specialized notation for the *time duration* of the pulse, as described in Section 10.8.2. The fact that β for the second pulse is twice as large as for the first pulse conveys the same information as the timing diagram, where the second pulse is drawn twice as thick along the time axis as the first. As usual, the time axis is not realistic: the interval between the pulses is usually several orders of magnitude larger than the pulse durations.

The value of ϕ in the notation β_ϕ describes the *phase* of the pulse, as described in Section 4.2.1.

In the scheme above, the first pulse has phase $\phi = 0$, and the second pulse has phase $\phi = \pi/2$. This explicit notation implies that the pulse phases are fixed. If the experiment is repeated for the purposes of signal averaging, then the same phases are used on each transient.

The following pulse sequence diagram means the same thing:

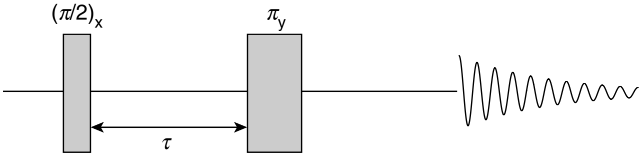

Figure 5.6
The same two-pulse sequence.

The subscripts 'x' and 'y' indicate r.f. phases according to Table 4.1.

Consider now the following pulse sequence diagram:

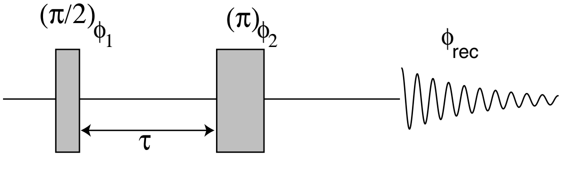

Figure 5.7
Two-pulse sequence with symbolic phases.

Table 5.1 A four-step phase cycle ($\mathfrak{n} = 4$) appropriate for a spin echo experiment.

Cycle counter $\mathfrak{m}$	ϕ_1	ϕ_2	ϕ_{rec}
0	0	0	0
1	0	$\pi/2$	π
2	0	π	0
3	0	$3\pi/2$	π

Here, the two pulse phases have *symbolic* values ϕ_1 and ϕ_2. In addition, the signal acquisition is labelled with the receiver phase ϕ_{rec}. The use of symbolic phases, rather than explicit phases, usually indicates the execution of a *phase cycle*. This means that, when the experiment is repeated, the phases of the pulses are not constant, but run through a set of values, often summarized in a table. For example, a suitable phase table for the spin echo experiment is given in Table 5.1.

This phase table should be understood as follows. Suppose each transient is specified by the value of a *transient counter* $\mathfrak{M}$, which starts at the value 0 and increases to the value $\mathfrak{N} - 1$, where $\mathfrak{N}$ is the total number of co-added transients. The phases to be used depend on the value of the *cycle counter* $\mathfrak{m}$, which is calculated as

$$\mathfrak{m} = \text{mod}(\mathfrak{M}, \mathfrak{n})$$

Here, $\mathfrak{n}$ is the number of steps in the phase cycle, equal to four in the example shown. The modulo function calculates the remainder when $\mathfrak{M}$ is divided by $\mathfrak{n}$. In the example, as $\mathfrak{M}$ increases 0, 1, 2, 3, 4, 5, 6, 7, 8, 9 . . ., the counter $\mathfrak{m}$ takes the values 0, 1, 2, 3, 0, 1, 2, 3, 0, 1 . . .. The phases $\{\phi_1, \phi_2, \phi_{\text{rec}}\}$ for a given transient $\mathfrak{M}$ may be read from the table by calculating $\mathfrak{m}$ and taking the appropriate row. The phase table should, therefore, be read from top to bottom, and then from top to bottom again, etc. until the number of transients $\mathfrak{N}$ is completed. The number of averaged transients $\mathfrak{N}$ should be an integer multiple of the number of steps in the phase cycle $\mathfrak{n}$.

In the example shown, the phase ϕ_1 is always zero. In more complicated cases, any combination of phases is cycled.

Phase cycles are used for two main purposes. First, they are used to *select* NMR signals that have certain properties of interest, while removing other types of NMR signal. For example, Section 16.2 describes a technique in which phase cycling is used to select signals from nuclear spins that have J-couplings to other nuclear spins, while suppressing signals from spins with no coupling partners. Second, phase cycles are used to suppress spurious signals generated by imperfections in the spectrometer hardware. I concentrate on the first use of phase cycling in this book.

5.4 Heteronuclear Experiments

Most NMR experiments are conducted with r.f. irradiation of more than a single isotope, using a multiple-channel spectrometer and a multiply-tuned probe. A simple example, already encountered in Section 3.9, is shown below:

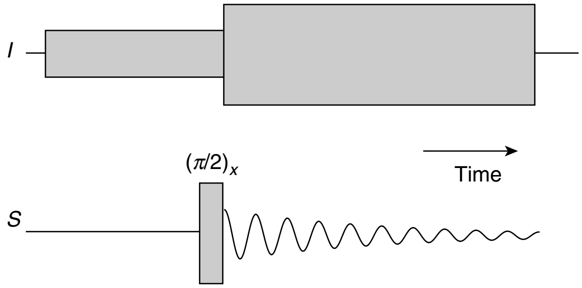

Figure 5.8
A heteronuclear pulse sequence.

The synchronized r.f. sequences on the two channels are shown one above the other and are to be read in parallel, like a musical score.

In the example shown, one-pulse excitation and detection is performed at the Larmor frequency of a nuclear isotope S. Before the application of the S-spin pulse, continuous r.f. irradiation is applied at the Larmor frequency of a different nuclear isotope I. After the S-spin pulse is applied, the I-spin irradiation continues, with increased amplitude, while the S-spin signal is detected.

As mentioned already in Section 3.9, the purpose of the I-spin irradiation *before* the S-spin pulse is to enhance the S-spin magnetization through the NOE. The purpose of the I-spin irradiation *during* the S-spin observation is to *decouple* the two spin species, simplifying the spectrum of the observed species.

This is only one example of a large class of techniques that involves synchronized r.f. irradiation at the Larmor frequencies of more than one nuclear isotope. Another important class of methods involves *heteronuclear polarization transfer*. In this case, magnetization is transferred from one set of nuclear spins to another, in order to enhance the NMR signals or to trace out the network of magnetic spin–spin interactions. Some examples of this method are treated in Sections 16.3 and 18.12.

5.5 Pulsed Field Gradient Sequences

Many NMR experiments involve magnetic field gradient pulses as well as r.f. pulses, arranged in a strict time sequence. An example is shown below:

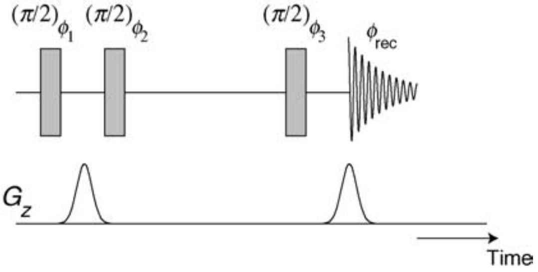

Figure 5.9
A pulse sequence involving two field gradient pulses and three r.f. pulses.

This is a *stimulated echo* pulse sequence, used for the study of molecular diffusion and flow (see Section 19.8). In the case shown, the field gradient pulses have identical shape and length, and both implement a field gradient along the z-axis (see Section 4.7). In general, the pulses may have any shape in time (including a change in sign), depending on the capabilities of the probe and spectrometer.

NMR imaging experiments often involve pulses on all three gradient channels (G_x, G_y and G_z). Some simple examples will be encountered in Section 12.6.

5.6 Arrayed Experiments

So far, we have assumed that the acquired NMR signals are simply added together, in order to enhance the signal-to-noise ratio. We now encounter some more sophisticated data acquisition motifs.

The pulse sequence shown below is used in *two-dimensional correlation spectroscopy*, described in Section 16.1:

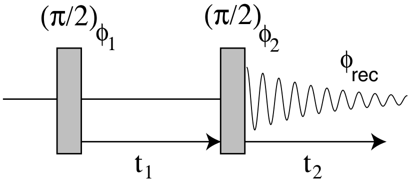

Figure 5.10
A two-dimensional pulse sequence.

The sequence consists of two r.f. pulses with equal durations (both have flip angles $\beta = \pi/2$), and with phases ϕ_1 and ϕ_2. Signal acquisition is conducted using a receiver phase ϕ_{rec}. As above, the use of these symbolic phase values indicates the use of a phase cycle. A number of different transients are added together, varying the pulse phases between consecutive pulse sequences, according to a phase table.

In Figure 5.10, the interval between the pulses is labelled with a *single-headed arrow*, marked t_1. By convention, the single-headed arrow indicates that a series of separate experiments is conducted, with the interval t_1 taking a set of different values. The digitized FIDs generated by pulse sequences with different values of t_1 are not added together, but stored in separate locations in the computer.

The data acquisition is marked with another single-headed arrow, labelled t_2. The symbol t_1 indicates the variable interval between the two pulses, and the symbol t_2 indicates the time coordinate of the digitized signal.

The variation of both time variables, with separate data storage for each value of t_1, leads to the compilation of a *data matrix*. This may be regarded as the compilation of a two-dimensional signal surface $s(t_1, t_2)$, one row at a time:

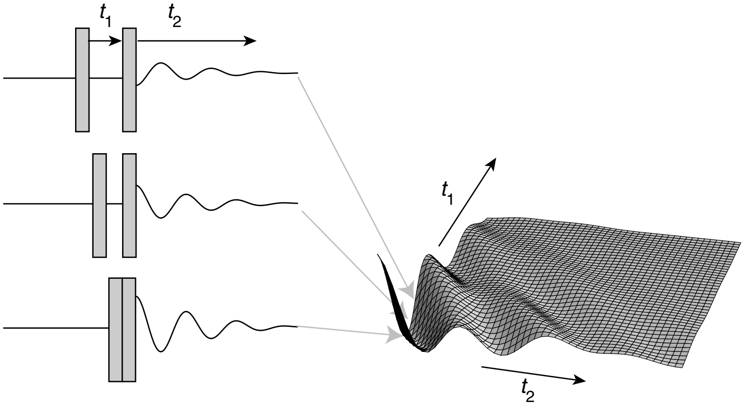

Figure 5.11
Compilation of a two-dimensional signal surface by arrayed data acquisition.

Each row of the data matrix is the result of a complete set of phase cycled experiments, all with the same value of t_1, but with cycling of the phases ϕ_1, ϕ_2 and ϕ_{rec} according to the phase table. When acquisition of one row is completed, the variable delay t_1 is changed, and the acquisition procedure is repeated. The iconic pulse sequence diagrams imply a timing hierarchy, with time interval incrementation enclosing an inner level of phase cycling.

Arrayed signal acquisition is the basis of most forms of *two-dimensional spectroscopy*.[3]

Arraying may be extended to three dimensions by introduction of an additional variable parameter. For example, a three-dimensional experiment may involve two variable delays, t_1 and t_2, in addition to the ordinary time coordinate for the data acquisition (usually renamed t_3 in this type of experiment). For each value of t_1 and t_2, a complete phase cycle is performed, compiling a single line through a 'data cube' $s(t_1, t_2, t_3)$. This entire procedure is repeated, keeping t_1 constant, but incrementing t_2, building up a sampled 'plane' of data. Repetition for all values of t_1 constructs the entire three-dimensional data set, plane by plane. The experimental hierarchy reads as follows: an upper level of t_2 incrementation; inside this a level of t_1

incrementation; and the innermost loop, a phase cycle for each set of averaged transients. The hierarchical experimental structure often means that a single data set is compiled by performing thousands of separate NMR pulse sequences, none of them identical.

The arraying concept may be extended to any number of dimensions. High-dimensional experiments of this type are frequently performed in biomolecular solution NMR.

The degree of complexity attained by some modern NMR pulse sequences is illustrated in the example shown in Figure 5.12, which is a fairly typical excerpt from the *Journal of Magnetic Resonance*. The increase in the number of spectrometer channels has led to an elongation of pulse sequence diagrams in the vertical direction, with a growing resemblance to orchestral musical scores.

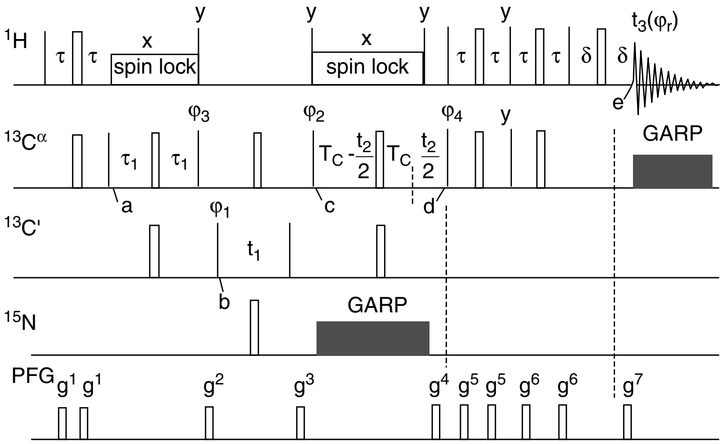

Figure 5.12
A typical example of a complicated r.f. pulse sequence. Note the pulsed field gradient pulses on the lowest line. From Y. Xia *et al.*, *J. Magn. Reson.* **143**, 407 (2000). (Reproduced by permission of Academic Press.)

5.7 NMR Signal

In Section 4.5.2, I introduced the following expression for the quadrature-detected NMR signal:

$$s(t) \sim \exp\{(i\Omega^0 - \lambda)t\}$$

This expression corresponds to a spectrum with just one peak. A more generally applicable equation is

$$s(t) = \sum_{\ell} s_\ell(t) \qquad (5.3)$$

where

$$s_\ell(t) = a_\ell \exp\{(i\Omega_\ell - \lambda_\ell)\,t\} \qquad (5.4)$$

This describes a superposition of many different signal components s_ℓ. In general, each component s_ℓ has a different frequency Ω_ℓ, a different damping rate constant λ_ℓ, and a different amplitude a_ℓ.

Equations 5.3 and 5.4 apply to the NMR signal generated by *any* pulse sequence. The peak frequencies Ω_ℓ and damping constants λ_ℓ depend only on what happens to the spins *when* the signal is detected. The peak amplitudes a_ℓ depend only on what happens to the spins *before* the signal is detected[4] (see Figure 5.13):

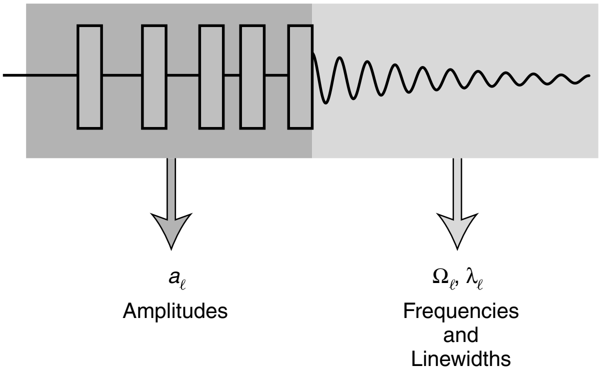

Figure 5.13
The relationship between the pulse sequence, the amplitudes, the frequencies, and the linewidths.

Most of the rest of this book is concerned with how to calculate a_ℓ, Ω_ℓ and λ_ℓ in specific cases.

The amplitudes a_ℓ are complex numbers in general. Each *complex amplitude* may be written as follows:

$$a_\ell = |a_\ell| \exp\{i\phi_\ell\} \tag{5.5}$$

The magnitude $|a_\ell|$ is called the *intensity* of the signal component. The factor ϕ_ℓ is the *phase* of the signal component.

The real and imaginary parts of the signal s are shown below for four different cases, all of which have only one signal component. The corresponding values of the complex amplitude, the frequency, and the damping rate constant are shown next to each plot:

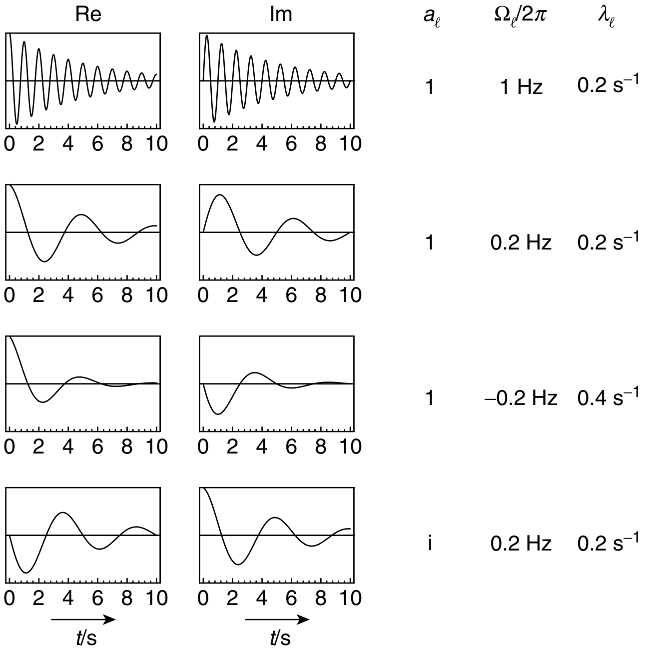

Figure 5.14
Four time-domain NMR signals, each with a single component.

The second case has a much lower frequency than the first case. The second and third cases differ in the sign of the frequency Ω_ℓ, which is reflected in the sign of the imaginary component. In addition, the third case has a larger value of λ_ℓ, which gives rise to a steeper decay as a function of time. The fourth case has an imaginary complex amplitude a_ℓ. This interchanges the types of modulation seen in the real and imaginary parts of the signal.

A signal with two components:

$$s(t) = 0.5\exp\{(2\pi\mathrm{i} - 0.2)\,t\} + 0.5\exp\{(0.4\pi\mathrm{i} - 0.2)\,t\} \tag{5.6}$$

has the following appearance:

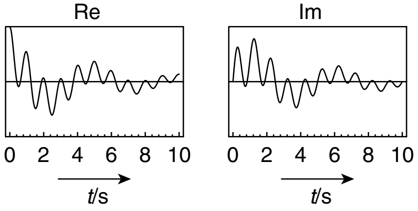

Figure 5.15
A complex NMR signal with two components.

which is much more difficult to interpret by eye.

In the last example, there are four signal components:

$$\begin{aligned} s(t) = {} & 0.25\exp\{(2\pi\mathrm{i} - 0.2)\,t\} + 0.25\exp\{(0.4\pi\mathrm{i} - 0.2)\,t\} \\ & + 0.25\exp\{(-0.4\pi\mathrm{i} - 0.4)\,t\} + 0.25\mathrm{i}\exp\{(-3.6\pi\mathrm{i} - 0.2)\,t\} \end{aligned}$$

leading to a very complicated appearance:

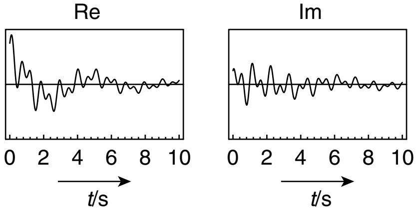

Figure 5.16
A complex NMR signal with four components.

The experimental FID from the proton spins in a solution of a protein is shown in Figure 5.17a. In this case, there are hundreds of signal components.

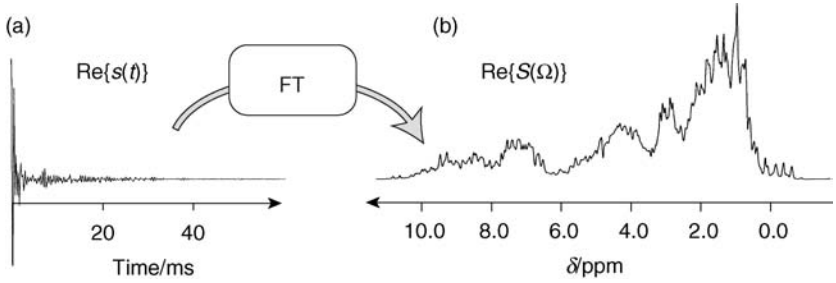

Figure 5.17 Proton NMR signal $s(t)$ for a solution of a protein (a) and its Fourier transform (b). Only the real parts of the signal and the spectrum are shown – in fact, the imaginary part of the signal $s(t)$ is also required for the Fourier transform. Thanks to Jianyun Lu for supplying these data.

5.8 NMR Spectrum

We now investigate the fate of the NMR signal after it has been stored in the computer.

5.8.1 Fourier transformation

Fourier transformation (FT) is a mathematical technique that converts a function of time into a function of frequency. The effect of FT is to make visible the individual components of the signal and plot their frequencies in a visually accessible form. FT does not enhance the theoretical information content, but makes the information in the signal more accessible to the human eye.

The mathematical definition of FT^5 is

$$\boxed{S(\Omega) = \int_0^{\infty} s(t) \exp\{-\mathrm{i}\Omega t\}\, \mathrm{d}t \qquad (5.7)}$$

The 'input' s is a function of time t; the 'output' S is a function of a frequency variable Ω, and is called the *spectrum*.

Both the time-domain signal $s(t)$ and the spectrum $S(\Omega)$ are complex functions. The functional relationship between the real and imaginary parts of $s(t)$ and $S(\Omega)$ may be depicted as follows:

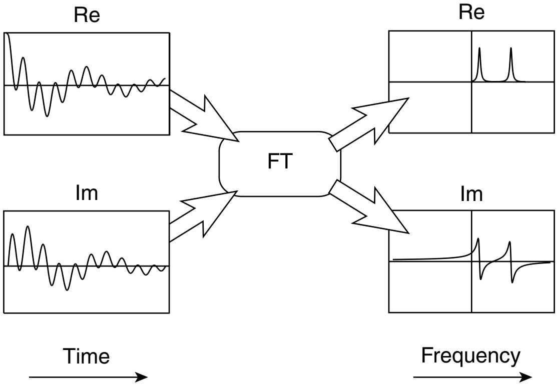

Figure 5.18 The relationship between the real and imaginary parts of $s(t)$ and $S(\Omega)$.

Note that the real and imaginary parts of the spectrum are each derived from *both* the real part and the imaginary part of the signal.

Figure 5.18 shows what happens when the signal has two components, as in Equation 5.6. Fourier transformation renders the two components clearly visible as two spectral peaks.

5.8.2 Lorentzians

FT may be understood either on a purely mathematical level or by using physical arguments. I first give a mathematical interpretation, and return later to the 'physical explanation'.

If Equation 5.7 is applied to Equation 5.3, we obtain

$$S(\Omega) = \sum_{\ell} S_{\ell}(\Omega) \qquad (5.8)$$

where each spectral component $S_\ell(\Omega)$ is the Fourier transform of the corresponding signal component:

$$S_\ell(\Omega) = \int_0^\infty s_\ell(t)\,\exp\{-\mathrm{i}\Omega t\}\,\mathrm{d}t$$

From Equation 5.4, this may be written as

$$S_\ell(\Omega) = a_\ell \int_0^\infty \exp\{-\,(\mathrm{i}(\Omega - \Omega_\ell) + \lambda_\ell)\,t\}\,\mathrm{d}t$$

Direct integration gives

$$S_\ell(\Omega) = -\frac{a_\ell}{\lambda_\ell + \mathrm{i}(\Omega - \Omega_\ell)}\Big[\exp\{-\,(\mathrm{i}(\Omega - \Omega_\ell) + \lambda_\ell)\,t\}\Big]_{t=0}^{t\to\infty} \tag{5.9}$$

Evaluation of the lower limit ($t = 0$) is easy, since $e^0 = 1$, but it is less obvious how to handle the upper limit ($t \to \infty$). The way forward is to use the following identity:

$$\exp\{(\mathrm{i}\omega - \lambda)t\} = (\cos\omega t + \mathrm{i}\sin\omega t)\,\exp\{-\lambda t\} \tag{5.10}$$

Since the decay rate constant λ is positive by definition, the factor $\exp\{-\lambda t\}$ goes to zero at $t \to \infty$. Furthermore, the cosine and sine functions are bounded by -1 and $+1$. Hence, the complete expression in Equation 5.10 must vanish at $t \to \infty$. The upper limit of Equation 5.9, therefore, evaluates to zero, and we get

$$S_\ell(\Omega) = -\frac{a_\ell}{\lambda_\ell + \mathrm{i}(\Omega - \Omega_\ell)} \times (0 - 1) = a_\ell \times \left(\frac{1}{\lambda_\ell + \mathrm{i}(\Omega - \Omega_\ell)}\right) \tag{5.11}$$

The bracketed function is very important in the theory of NMR, and is called the *complex Lorentzian*. It is defined as

$$\boxed{\mathcal{L}(\Omega; \Omega_\ell, \lambda) = \frac{1}{\lambda + \mathrm{i}(\Omega - \Omega_\ell)}} \tag{5.12}$$

In the notation $\mathcal{L}(\Omega; \Omega_\ell, \lambda)$, the 'argument' of the function is the frequency coordinate Ω, and Ω_ℓ and λ are 'parameters'. The parameter Ω_ℓ indicates the centre frequency of the peak and λ is a peakwidth parameter.

The spectral component in Equation 5.11 may be written in terms of the complex Lorentzian as follows:

$$S_\ell(\Omega) = a_\ell\,\mathcal{L}(\Omega; \Omega_\ell, \lambda_\ell) \tag{5.13}$$

Just as the time-domain signal is a superposition of oscillating components s_ℓ, the spectrum is a superposition of Lorentzian spectral components S_ℓ.

The *real part* of the complex Lorentzian is called the *absorption Lorentzian*:

$$\boxed{\mathcal{A}(\Omega; \Omega_\ell, \lambda) = \mathrm{Re}\{\mathcal{L}(\Omega; \Omega_\ell, \lambda)\} = \frac{\lambda}{\lambda^2 + (\Omega - \Omega_\ell)^2}} \tag{5.14}$$

The *imaginary part* of the complex Lorentzian is called the *dispersion Lorentzian*:[6]

$$\boxed{\mathcal{D}(\Omega; \Omega_\ell, \lambda) = \mathrm{Im}\{\mathcal{L}(\Omega; \Omega_\ell, \lambda)\} = -\frac{\Omega - \Omega_\ell}{\lambda^2 + (\Omega - \Omega_\ell)^2}} \tag{5.15}$$

The three peakshapes are related through the following equation:

$$\boxed{\mathcal{L} = \mathcal{A} + i\mathcal{D} \qquad (5.16)}$$

Whereas $\mathcal{L}$ is a complex function, $\mathcal{A}$ and $\mathcal{D}$ are both real functions.

The absorption and dispersion Lorentzian peakshapes are sketched below:[7]

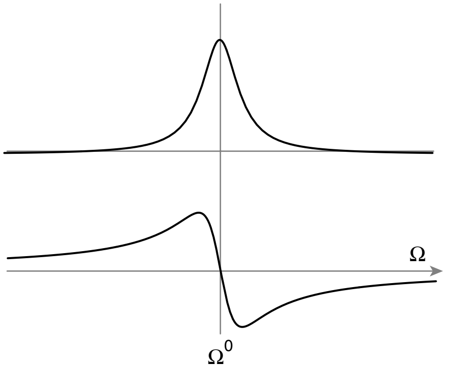

Figure 5.19
Absorption and dispersion Lorentzians.

The absorption Lorentzian has an integral of π and a maximum height equal to λ^{-1}. The *full-width-at-half-height* (FWHH) of the absorption Lorentzian is given by 2λ in units of radians per second. This is easily seen from

$$\mathcal{A}(\Omega; \Omega_\ell, \lambda) = \frac{1}{2}\lambda^{-1}$$

which has solutions at

$$\Omega = \Omega_\ell \pm \lambda$$

The FWHH of the absorption Lorentzian in units of hertz is $2\lambda/2\pi = \lambda/\pi$.

The dispersion Lorentzian has zero integral. The function passes through zero at the frequency coordinate Ω_ℓ. The frequency separation between the maximum and minimum points is 2λ in units of radians per second, which is the same as the FWHH of the absorption Lorentzian.

The absorption Lorentzian is proportional to $(\Omega - \Omega_\ell)^{-2}$ at large offsets $\Omega - \Omega_\ell$ from the centre frequency. This inverse square dependence causes the absorption Lorentzian to die off rather quickly away from the peak centre. The dispersion Lorentzian, on the other hand, has a $(\Omega - \Omega_\ell)^{-1}$ dependence at large offsets and dies away much more slowly. As a result, dispersion Lorentzians have broader wings than absorption Lorentzians. This fact is important in crowded spectra, since the wings from one peak may distort a neighbouring, partially overlapping, peak.

Equation 5.8 indicates that the spectrum $S(\Omega)$ is a superposition of complex Lorentzian peakshapes, each deriving from a single oscillating time-domain component $s_\ell(t)$. The effect of the Fourier transform is therefore to make visible the frequency components contained in the complicated time-domain signal $s(t)$. Each frequency component is marked by a Lorentzian peak.

The plots shown in Figure 5.20 present the real and imaginary parts of the spectrum for four different cases, each of which has only one spectral component.

Note how the parameters a_ℓ, Ω_ℓ and λ_ℓ affect the appearance of the real and imaginary parts of the spectrum. In the first three cases, the amplitudes a_ℓ are real, so the real part of the spectrum contains an absorption signal and the imaginary part of the spectrum contains a dispersion signal. In the last case, the amplitude a_ℓ is imaginary, so the positions of the absorption and dispersion signals are interchanged. The third case has a larger value of λ_ℓ, which gives rise to a broader peak.

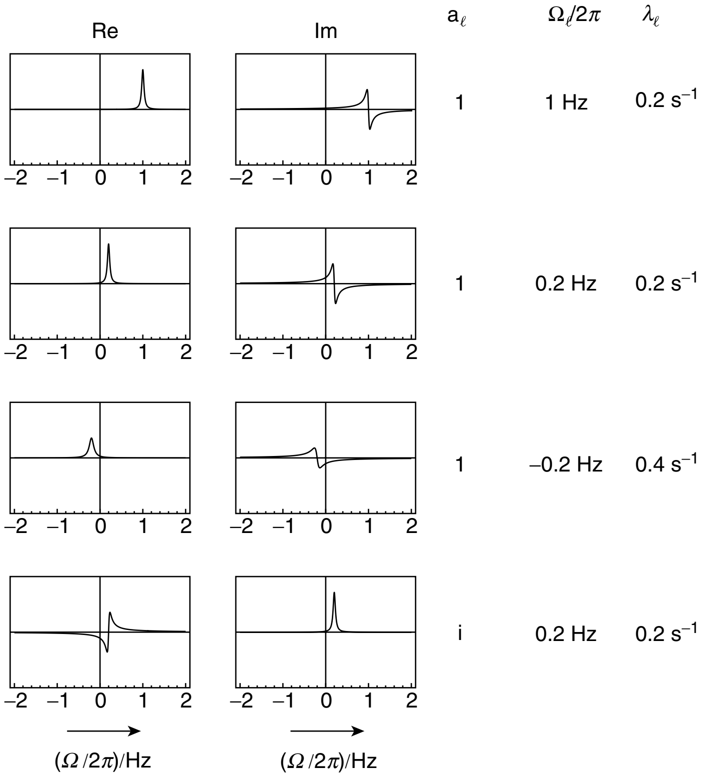

Figure 5.20
Four NMR spectra, each with a single component. These are the Fourier transforms of the signals in Figure 5.14.

This is an example of an important general principle:

$$\boxed{\begin{aligned}\text{Fast signal decay} &\Longleftrightarrow \text{Broad peak}\\ \text{Slow signal decay} &\Longleftrightarrow \text{Narrow peak}\end{aligned}} \tag{5.17}$$

A spectrum with two components:

$$S(\omega) = 0.5\mathcal{L}(\Omega; 2\pi, 0.2) + 0.5\mathcal{L}(\Omega; 0.4\pi, 0.2) \tag{5.18}$$

has the following appearance:

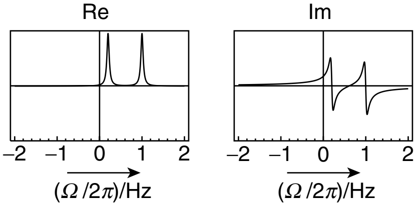

Figure 5.21
Four NMR spectra, each with two components. These are the Fourier transforms of the signals in Figure 5.15.

which is easy to interpret. Note how the position of each peak in the spectrum corresponds to the value of the parameter Ω_ℓ in the Lorentzian function $\mathcal{L}(\Omega; \Omega_\ell, \lambda)$.

Interpretation is still easy for a case with four signal components:

$$\begin{aligned}S(\Omega) = {} & 0.25\mathcal{L}(\Omega; 2\pi, 0.2) + 0.25\mathcal{L}(\Omega; 0.4\pi, 0.2) \\ & +0.25\mathcal{L}(\Omega; -0.4\pi, 0.4) + 0.25\mathrm{i}\mathcal{L}(\Omega; -3.6\pi, 0.2)\end{aligned}$$

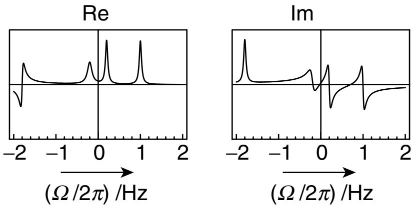

Figure 5.22
Four NMR spectra, each with four components. These are the Fourier transforms of the signals in Figure 5.16.

Note the appearance of the peak on the far left of the spectrum, which has an imaginary complex amplitude, and that one of the peaks is broader than the other three.

The Fourier transform of the experimental NMR signal shown in Figure 5.17a is shown in Figure 5.17b. Compared with the FID, the NMR spectrum is readily interpretable in terms of signals from protons in different types of molecular environment.

5.8.3 Explanation of fourier transformation

How does FT actually 'work'?

The following explanation considers only the real parts of signals, for the sake of simplicity:

1. Suppose that I have a signal $s(t)$ that looks like this:

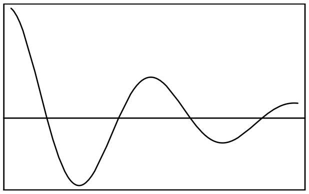

Figure 5.23
An oscillating signal.

I want to know its frequency.

2. First guess a frequency Ω_{guess}. Create a signal function s_{guess} that oscillates at this frequency:

$$s_{\text{guess}} = \exp\{\mathrm{i}\Omega_{\text{guess}}t\}$$

The real part of this function might look like this:

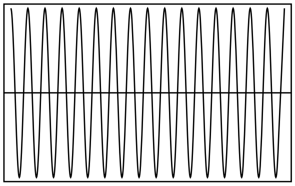

Figure 5.24
An oscillating function based on the first guess at the frequency.

In this case the guess was wrong. The guessed frequency is too high.

3. Multiply $s(t)$ by $s_{\text{guess}}(t)^*$. The real part of the result looks like this:

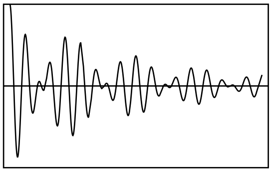

Figure 5.25
The product of the signal and the first oscillating function.

4. Integrate over time. In this case, the guess was not very good. The functions $s(t)$ and $s_{\text{guess}}(t)$ do not match, so the product $s(t)s_{\text{guess}}(t)^*$ has as many positive as negative excursions, and the integral is close to zero. The low value of this integral corresponds to the low value of the spectral function $S(\Omega)$ when Ω is well away from the centre of the peak.

5. Try again with a frequency Ω'_{guess}. The appropriate signal function is

$$s'_{\text{guess}} = \exp\{i\Omega'_{\text{guess}}t\}$$

Suppose it looks like this:

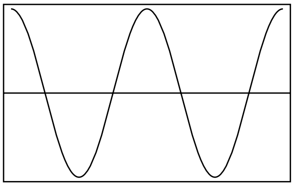

Figure 5.26
An oscillating function based on the second guess at the frequency.

This time the guess is good. The guessed function s'_{guess} matches the oscillations of the signal $s(t)$ rather well.

6. This is seen by multiplying $s(t)$ by $s_{\text{guess}}(t)^*$:

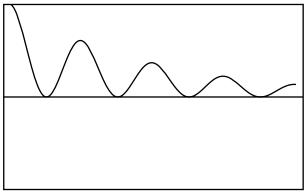

Figure 5.27
The product of the signal and the second oscillating function.

This time the positions of the positive and negative excursions match in $s(t)$ and $s'_{\text{guess}}(t)$. When $s(t)$ is positive, so is $s'_{\text{guess}}(t)$, and the product of the two is positive. When $s(t)$ is negative, so is $s'_{\text{guess}}(t)$, and the product of the two is again positive. As a result, the integral of $s(t)s'_{\text{guess}}(t)^*$ is large. The high value of this integral corresponds to the large value of the spectral function $S(\Omega)$ when Ω is close to the centre of the peak.

7. One can visualize the Fourier transform as an automation of this procedure, stepping through all possible values of Ω_{guess}. When Ω_{guess} hits the true frequency of a signal component, the integral goes up. When Ω_{guess} is far away from any of the frequency components in the signal, the integral goes down:

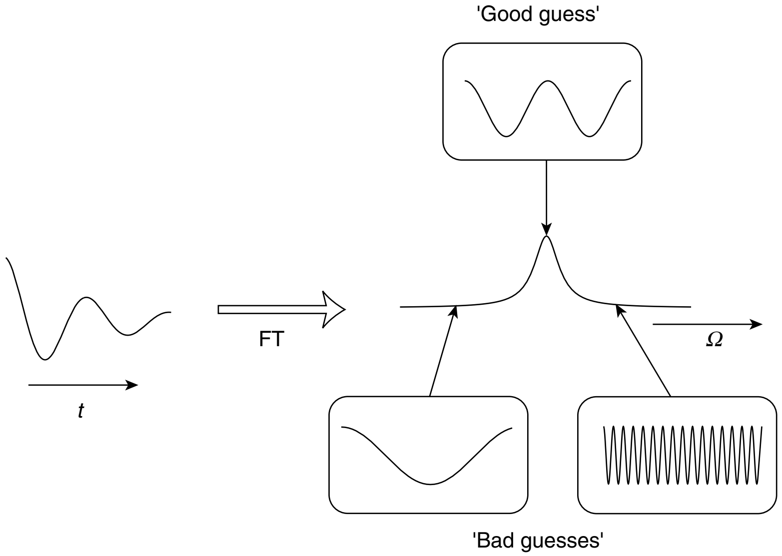

Figure 5.28
How FT works.

In this way, the Fourier transform 'detects' the presence of oscillating components in the time-domain signal and presents their frequencies in a visually accessible form.

Fourier transforms are not actually computed this way. In reality, a special numerical algorithm called the *fast Fourier transform* (FFT) is used.[8] This algorithm is very fast, but has the restriction that the number of Fourier-transformed points must be an integer power of 2. This is the reason for the peculiar numbers given in Table 4.2.

FT is not the only method for extracting the frequency components of a data set. There are other schemes in common use, such as the *maximum entropy method*, *linear prediction*, etc. None of these methods is as robust as the Fourier transform, although they may have advantages in certain cases, such as when the signal-to-noise ratio is good but when there are only a few sampling points available. See *Further Reading*.

5.8.4 Spectral phase shifts

If the amplitudes a_ℓ of the individual signal components are all real numbers, then the real part of the spectrum $\mathrm{Re}\{S(\Omega)\}$ consists of absorption Lorentzians and the imaginary part of the spectrum $\mathrm{Im}\{S(\Omega)\}$ consists of dispersion Lorentzians. Since absorption Lorentzians have better resolution than dispersion Lorentzians, only the real part of the spectrum is usually displayed.

In general, the amplitudes a_ℓ of the spectral components S_ℓ are complex. The real and imaginary components of the spectrum are then mixtures of absorption and dispersion Lorentzians. This is seen by applying the following identities:

$$\begin{aligned}\mathrm{Re}\{ab\} &= \mathrm{Re}\{a\}\,\mathrm{Re}\{b\} - \mathrm{Im}\{a\}\,\mathrm{Im}\{b\}\\ \mathrm{Im}\{ab\} &= \mathrm{Re}\{a\}\,\mathrm{Im}\{b\} + \mathrm{Im}\{a\}\,\mathrm{Re}\{b\}\end{aligned}$$

The result for one spectral component is

$$\begin{aligned}\mathrm{Re}\{a_\ell \mathcal{L}(\Omega;\Omega_\ell,\lambda_\ell)\} &= \mathrm{Re}\{a_\ell\}\mathcal{A}(\Omega;\Omega_\ell,\lambda_\ell) - \mathrm{Im}\{a_\ell\}\mathcal{D}(\Omega;\Omega_\ell,\lambda_\ell)\\ \mathrm{Im}\{a_\ell \mathcal{L}(\Omega;\Omega_\ell,\lambda_\ell)\} &= \mathrm{Re}\{a_\ell\}\mathcal{D}(\Omega;\Omega_\ell,\lambda_\ell) + \mathrm{Im}\{a_\ell\}\mathcal{A}(\Omega;\Omega_\ell,\lambda_\ell)\end{aligned}$$

or in terms of the phase ϕ_ℓ of the complex amplitude (Equation 5.5):[9]

$$\begin{aligned}\mathrm{Re}\{a_\ell \mathcal{L}(\Omega;\Omega_\ell,\lambda_\ell)\} &= |a_\ell|\mathcal{A}(\Omega;\Omega_\ell,\lambda_\ell)\cos\phi_\ell - |a_\ell|\mathcal{D}(\Omega;\Omega_\ell,\lambda_\ell)\sin\phi_\ell \\ \mathrm{Im}\{a_\ell \mathcal{L}(\Omega;\Omega_\ell,\lambda_\ell)\} &= |a_\ell|\mathcal{D}(\Omega;\Omega_\ell,\lambda_\ell)\cos\phi_\ell + |a_\ell|\mathcal{A}(\Omega;\Omega_\ell,\lambda_\ell)\sin\phi_\ell\end{aligned}$$

The mixture of absorption and dispersion modes gives a 'skewed' appearance to the peakshapes: the spectrum is said to be 'out of phase'. The spectral appearance for different values of ϕ_ℓ is shown in Figure 5.29.

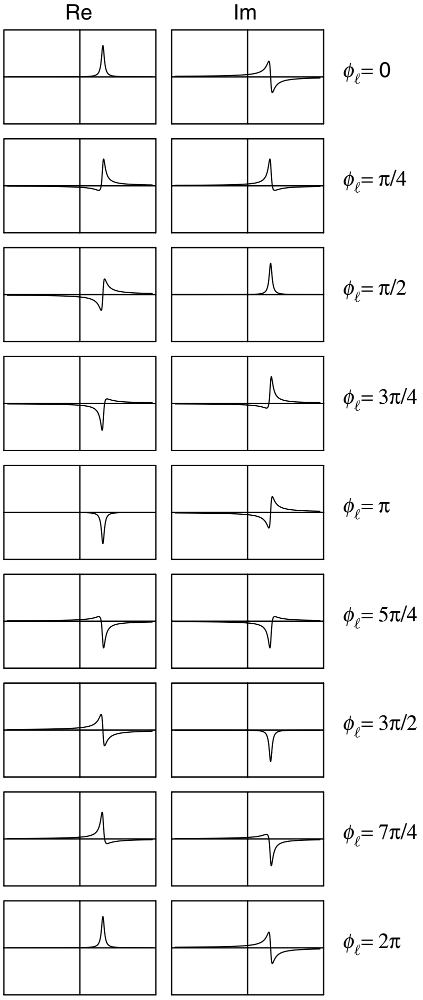

Figure 5.29
The phase of the complex amplitude and the real and imaginary parts of the spectrum.

5.8.5 Frequency-dependent phase correction

In general, the amplitudes a_ℓ of the different spectral components depend on the details of the pulse sequence before the acquisition interval and may have any possible phase. However, in some common situations, the phases of the peaks depend in a simple, linear, fashion on the centre frequency of the spectral component:

$$\phi_\ell \cong \phi^{(0)} + \phi^{(1)}\Omega_\ell \tag{5.19}$$

where the terms $\phi^{(0)}$ and $\phi^{(1)}$ are the same for all peaks in the spectrum.

A simple, one-pulse, experiment often leads to peak phases of this form. The spectrometer electronics give rise to unavoidable $\phi^{(0)}$ and $\phi^{(1)}$ terms. In addition, $\phi^{(1)}$ is associated with experimental time delays, such as the delay that must be left after the r.f. pulse before the NMR signal can be sampled, in order to allow the pulse energy to dissipate. These phase shifts are often sample dependent and cannot be eliminated in a universal way by spectrometer adjustments.

A four-peak spectrum showing a linear frequency-dependent phase shift is shown in Figure 5.30a.

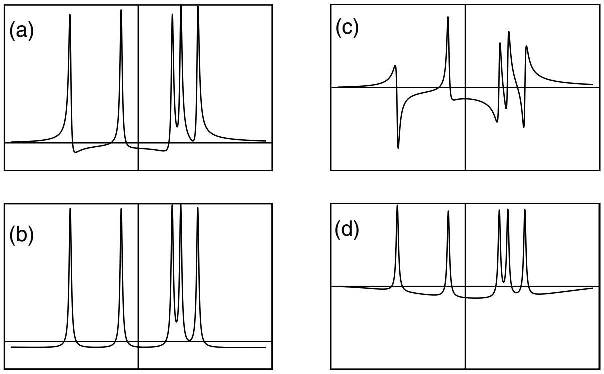

Figure 5.30 (a) A spectrum showing a mild frequency-dependent phase shift. (b) Phase-correction of the spectrum shown in (a). (c) A spectrum showing a strong frequency-dependent phase shift. (d) Phase-correction of the spectrum shown in (c), displaying a rolling baseline.

If $\phi^{(1)}$ is not too large, then the phase of the spectrum may be corrected after the FT, to a good approximation. Instead of displaying the real part of the spectrum $S(\Omega)$, one displays the real part of the *phase-corrected spectrum* $S_{\text{corr}}(\Omega)$:

$$S_{\text{corr}}(\Omega) = S(\Omega)\exp\{-\mathrm{i}\left(\phi^{(0)}_{\text{corr}} + \phi^{(1)}_{\text{corr}}\Omega\right)\} \tag{5.20}$$

In practice, the parameters $\phi^{(0)}_{\text{corr}}$ and $\phi^{(1)}_{\text{corr}}$ are varied manually in an interactive fashion, until the spectrum 'comes into phase'. The spectrum achieves its best appearance when $\phi^{(0)}_{\text{corr}} = \phi^{(0)}$ and $\phi^{(1)}_{\text{corr}} = \phi^{(1)}$. The result of phase-correcting Figure 5.30a is shown in Figure 5.30b.

Spectral phase correction is not a mathematically exact procedure for eliminating dispersion-mode contributions from the spectrum. This is because Equation 5.19 indicates the *centre frequency* Ω_ℓ of the peaks, whereas Equation 5.20 employs the *spectral frequency coordinate* Ω. As a result, frequency-dependent spectral phase correction does not work precisely in the wings of the peaks or in regions where peaks overlap. The distortions can be serious when the linear term $\phi^{(1)}$ is large, as illustrated in Figure 5.30c and d. Experimental NMR spectra often display such 'rolling baselines', which are frequently removed by a further stage of data correction (not dealt with here).

To summarize, a linear frequency dependence of the phase of the spectral peaks is expected in many simple experiments. If the frequency dependence is small, then the spectrum may be corrected, to a good approximation. In the case of an arbitrary excitation sequence, on the other hand, there is no simple relationship between the phases of the peaks and their centre frequencies. No general correction of the spectrum is possible in this case.

5.9 Two-Dimensional Spectroscopy

5.9.1 Two-dimensional signal surface

Suppose that an *arrayed* experiment is conducted, as described in Section 5.6. The result is a two-dimensional data matrix as a function of two time variables, which can be visualized as a three-dimensional surface:

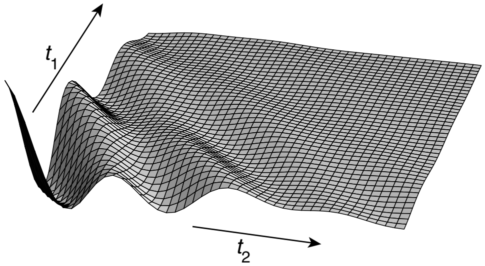

Figure 5.31
A two-dimensional signal surface.

As this book progresses, we will see that in many important cases the signal surface has the following general form:

$$s(t_1, t_2) = \sum_{\ell} s_\ell(t_1, t_2) \tag{5.21}$$

where

$$s_\ell(t_1, t_2) = a_\ell \exp\left\{\left(\mathrm{i}\Omega_\ell^{(1)} - \lambda_\ell^{(1)}\right) t_1 + \left(\mathrm{i}\Omega_\ell^{(2)} - \lambda_\ell^{(2)}\right) t_2\right\}$$

This is a straightforward extension of Equation 5.3: the two-dimensional signal is a sum of individual contributions ℓ; each contribution has a complex amplitude a_ℓ, with frequency $\Omega_\ell^{(1)}$ in the t_1 dimension and frequency $\Omega_\ell^{(2)}$ in the t_2 dimension, and peakwidth parameters $\lambda_\ell^{(1)}$ and $\lambda_\ell^{(2)}$ in the two dimensions.

Many examples of two-dimensional signal surfaces with the form of Equation 5.21 are given in later chapters, where the origin of the signal $s(t_1, t_2)$ is described in detail for several cases.

The two-dimensional signal surface expressed by Equation 5.21 is complex; it has a real and an imaginary part, just as the ordinary one-dimensional signal $s(t)$ has a real and an imaginary part.

5.9.2 Two-dimensional fourier transformation

The two-dimensional signal surface may be subjected to two-dimensional FT, which is defined through the double integral

$$S(\Omega_1, \Omega_2) = \int_0^\infty \mathrm{d}t_1 \int_0^\infty \mathrm{d}t_2 \; s(t_1, t_2) \exp\{-\mathrm{i}\,(\Omega_1 t_1 + \Omega_2 t_2)\} \tag{5.22}$$

in direct analogy to Equation 5.7. The function $S(\Omega_1, \Omega_2)$ is called the *two-dimensional spectrum*. It is a function of two frequency variables and may also be visualized as a surface:

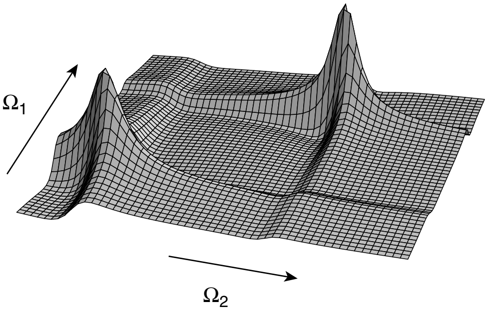

Figure 5.32
A two-dimensional spectrum.

The two-dimensional spectrum has peaks at the coordinates $(\Omega_\ell^{(1)}, \Omega_\ell^{(2)})$, corresponding to the frequencies of the underlying oscillating signal contributions s_ℓ.

Just as in the one-dimensional case, the real and imaginary parts of the two-dimensional spectrum are both derived from the real and imaginary parts of the time-domain signal:

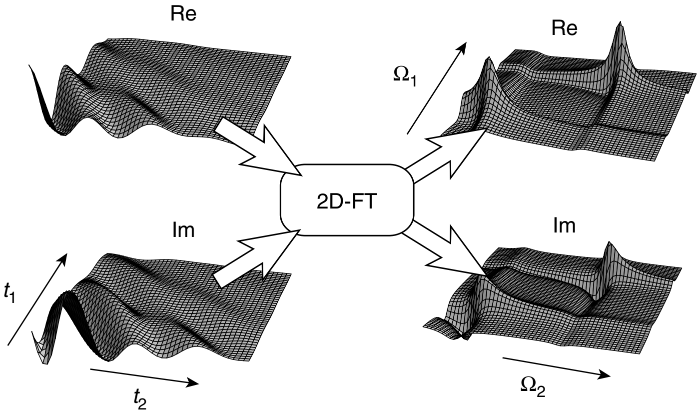

Figure 5.33
The relationship between the real and imaginary parts of $s(t_1, t_2)$ and $S(\Omega_1, \Omega_2)$.

Two-dimensional spectra may be depicted either as surface plots (as in the above figures) or as contour plots (as in a topographic map). The same two-dimensional NMR spectrum is shown in both representations in Figure 5.34.

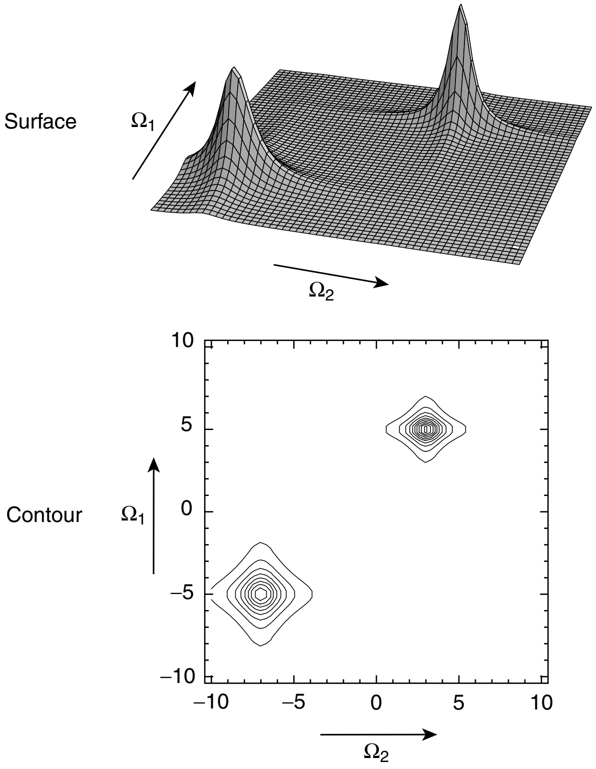

Figure 5.34
Two different representations of a two-dimensional spectrum.

5.9.3 Phase twist peaks

Evaluation of Equation 5.22 for the signal in Equation 5.21 gives the following form of the two-dimensional spectrum:

$$S(\Omega_1, \Omega_2) = \sum_{\ell} S_\ell(\Omega_1, \Omega_2) \tag{5.23}$$

where

$$S_\ell(\Omega_1, \Omega_2) = a_\ell \, \mathcal{L}(\Omega_1, \Omega_2; \Omega_\ell^{(1)}, \lambda_\ell^{(1)}, \Omega_\ell^{(2)}, \lambda_\ell^{(2)})$$

The function $\mathcal{L}(\Omega_1, \Omega_2; \Omega_\ell^{(1)}, \lambda_\ell^{(1)}, \Omega_\ell^{(2)}, \lambda_\ell^{(2)})$ is called the *two-dimensional complex Lorentzian*. It is equal to a product of two one-dimensional complex Lorentzians:

$$\boxed{\mathcal{L}(\Omega_1, \Omega_2; \Omega_\ell^{(1)}, \lambda_\ell^{(1)}, \Omega_\ell^{(2)}, \lambda_\ell^{(2)}) = \mathcal{L}(\Omega_1; \Omega_\ell^{(1)}, \lambda_\ell^{(1)}) \mathcal{L}(\Omega_2; \Omega_\ell^{(2)}, \lambda_\ell^{(2)}) \qquad (5.24)}$$

The one-dimensional complex Lorentzian peakshape is specified in Equation 5.12.

How does the complex Lorentzian look? The *real* part of the two-dimensional complex Lorentzian may be evaluated as follows:

$$\mathrm{Re}\{\mathcal{L}_1\mathcal{L}_2\} = \mathrm{Re}\{\mathcal{L}_1\}\,\mathrm{Re}\{\mathcal{L}_2\} - \mathrm{Im}\{\mathcal{L}_1\}\,\mathrm{Im}\{\mathcal{L}_2\}$$

using obvious abbreviations. This leads to

$$\begin{aligned} &\mathrm{Re}\{\mathcal{L}(\Omega_1, \Omega_2; \Omega_\ell^{(1)}, \lambda_\ell^{(1)}, \Omega_\ell^{(2)}, \lambda_\ell^{(2)})\} = \\ &\mathcal{A}(\Omega_1; \Omega_\ell^{(1)}, \lambda_\ell^{(1)}) \mathcal{A}(\Omega_2; \Omega_\ell^{(2)}, \lambda_\ell^{(2)}) - \mathcal{D}(\Omega_1; \Omega_\ell^{(1)}, \lambda_\ell^{(1)}) \mathcal{D}(\Omega_2; \Omega_\ell^{(2)}, \lambda_\ell^{(2)}) \end{aligned} \tag{5.25}$$

This two-dimensional function is shown below:

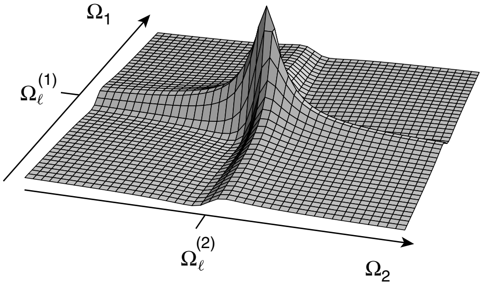

Figure 5.35
The real part of a complex two-dimensional Lorentzian.

As can be seen, it is a peculiar mixture of absorption and dispersion-mode one-dimensional Lorentzians. Near the centre of the peak, slices appear as absorption Lorentzians, but slices appear as dispersion Lorentzians far from the centre.

The *imaginary* part of the two-dimensional complex Lorentzian may be evaluated through the following:

$$\mathrm{Im}\{\mathcal{L}_1\mathcal{L}_2\} = \mathrm{Re}\{\mathcal{L}_1\}\,\mathrm{Im}\{\mathcal{L}_2\} + \mathrm{Im}\{\mathcal{L}_1\}\,\mathrm{Re}\{\mathcal{L}_2\}$$

leading to

$$\begin{aligned}&\mathrm{Im}\{\mathcal{L}(\Omega_1, \Omega_2; \Omega_\ell^{(1)}, \lambda_\ell^{(1)}, \Omega_\ell^{(2)}, \lambda_\ell^{(2)})\} =\\ &\mathcal{A}(\Omega_1; \Omega_\ell^{(1)}, \lambda_\ell^{(1)})\mathcal{D}(\Omega_2; \Omega_\ell^{(2)}, \lambda_\ell^{(2)}) + \mathcal{D}(\Omega_1; \Omega_\ell^{(1)}, \lambda_\ell^{(1)})\mathcal{A}(\Omega_2; \Omega_\ell^{(2)}, \lambda_\ell^{(2)})\end{aligned}$$

This function is plotted below:

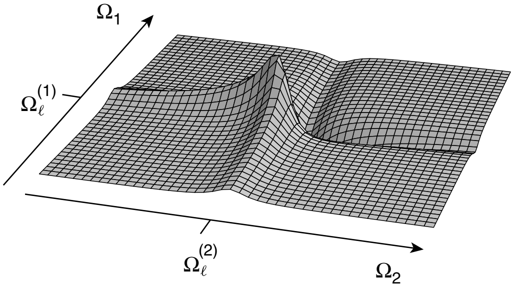

Figure 5.36
The imaginary part of a complex two-dimensional Lorentzian.

This is also a peculiar mixture of absorption and dispersion-mode one-dimensional Lorentzians, but this time with dispersion in the middle and absorption at the edges.

The strange appearance of these functions has led to the name *phase twist peaks*. Just as the absorption and dispersion Lorentzians are the ‘fundamental’ peakshapes in one-dimensional spectroscopy, so these weird phase twists are the ‘fundamental’ peakshapes in two-dimensional spectroscopy.

These phase twist peakshapes are undesirable because of their long dispersion tails. In contrast to one-dimensional FT NMR, the dispersion components in two-dimensional spectra may *not* be removed by phase correction of the spectrum, at least not in any simple way. As shown in Equation 5.35, the real part of the two-dimensional complex Lorentzian contains both absorption and dispersion mode shapes, inextricably entangled.

5.9.4 Pure absorption two-dimensional spectra

In *some* forms of two-dimensional spectroscopy, it is possible to suppress dispersion mode contributions to the two-dimensional spectrum, by combining together *two* different data sets in a careful way. The result is a spectrum containing *two-dimensional absorption Lorentzian* peaks, of the following form:

$$\boxed{\mathcal{A}(\Omega_1, \Omega_2; \Omega_\ell^{(1)}, \lambda_\ell^{(1)}, \Omega_\ell^{(2)}, \lambda_\ell^{(2)}) = \mathcal{A}(\Omega_1; \Omega_\ell^{(1)}, \lambda_\ell^{(1)})\mathcal{A}(\Omega_2; \Omega_\ell^{(2)}, \lambda_\ell^{(2)}) \qquad (5.26)}$$

This has a much more attractive appearance, as shown in Figure 5.37.

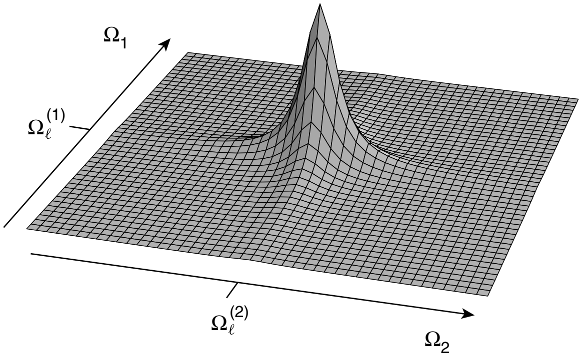

Figure 5.37
A pure absorption two-dimensional peak.

The removal of the dispersion contributions greatly improves the spectral resolution.

The engineering of absorption mode peakshapes in multidimensional spectra is a very important component of modern NMR technology. I now discuss the so-called *States method* for accomplishing this task[10] ('States' is the surname of one of the inventors of the technique).

The key to the States method is the concept of *amplitude modulation*. Consider the general form of the two-dimensional signal matrix, given in Equation 5.21:

$$s(t_1, t_2) = \sum_\ell a_\ell \exp\left\{\left(i\Omega_\ell^{(1)} - \lambda_\ell^{(1)}\right) t_1 + \left(i\Omega_\ell^{(2)} - \lambda_\ell^{(2)}\right) t_2\right\}$$

This represents a superposition of two-dimensional signals, with different complex amplitudes a_ℓ, frequencies $(\Omega_\ell^{(1)}, \Omega_\ell^{(2)})$, and decay rate constants $(\lambda_\ell^{(1)}, \lambda_\ell^{(2)})$. In general, there is no particular relationship between the amplitudes, frequencies, and decay rate constants of the different peaks.

However, in some special cases, the two-dimensional signal fulfils the following conditions:

1. The amplitudes a_ℓ are all *real numbers* ($a_\ell = a_\ell{}^*$).
2. For every component with frequency coordinates $(\Omega_\ell^{(1)}, \Omega_\ell^{(2)})$, there is a 'mirror image' component with identical amplitude a_ℓ and decay parameters $(\lambda_\ell^{(1)}, \lambda_\ell^{(2)})$, but with frequency coordinates $(-\Omega_\ell^{(1)}, \Omega_\ell^{(2)})$.

This means that the two-dimensional spectrum contains peaks that are arranged symmetrically about the $\Omega_1 = 0$ axis, as shown schematically below:

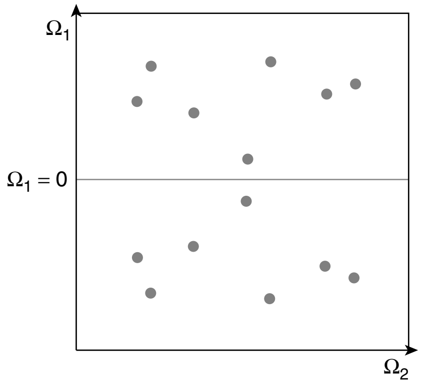

Figure 5.38
A two-dimensional spectrum with symmetry about the $\Omega_1 = 0$ axis.

In the time domain, this implies that the two-dimensional signal may be written as

$$s^{\cos}(t_1, t_2) = \sum_{\ell} a_\ell \cos(\Omega_\ell^{(1)} t_1)\ \exp\{-\lambda_\ell^{(1)} t_1\} \exp\{\left(\mathrm{i}\Omega_\ell^{(2)} - \lambda_\ell^{(2)}\right) t_2\} \tag{5.27}$$

This equation means that the NMR signal is *amplitude modulated* with respect to the evolution interval t_1. As t_1 increases, the amplitude of the NMR signal oscillates up and down, but its phase never changes. The form of the modulation is a cosine wave, hence the superscript 'cos' in Equation 5.27.

The effect of amplitude modulation is seen most clearly if a one-dimensional Fourier transform is calculated with respect to the time variable t_2, according to

$$S(t_1, \Omega_2) = \int_0^\infty \mathrm{d}t_2\ s(t_1, t_2) \exp\{-\mathrm{i}\Omega_2 t_2\}$$

Applied to the cosine-modulated signal, we get

$$S^{\cos}(t_1, \Omega_2) = \sum_{\ell} a_\ell \cos(\Omega_\ell^{(1)} t_1) \exp\{-\lambda_\ell^{(1)} t_1\}\, \mathcal{L}(\Omega_2; \Omega_\ell^{(2)}, \lambda_\ell^{(2)}) \tag{5.28}$$

The real part of $S^{\cos}(t_1, \Omega_2)$ for a typical cosine-modulated signal is shown below:

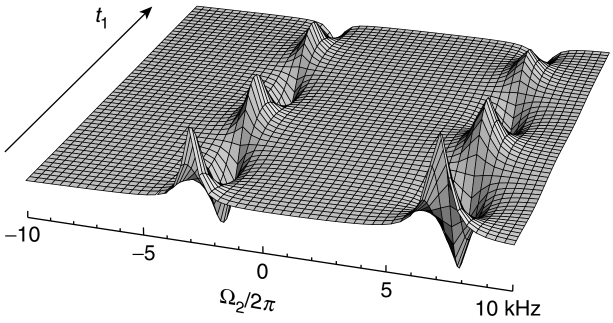

Figure 5.39
The real part of the cosine-modulated signal $S^{\cos}(t_1, \Omega_2)$.

In this example, the two-dimensional signal contains two signal components, with parameters $\{\Omega_\ell^{(1)}/2\pi, \Omega_\ell^{(2)}/2\pi\} = \{5\,\text{kHz}, -3\,\text{kHz}\}$ (on the left) and $\{-5\,\text{kHz}, +7\,\text{kHz}\}$ (on the right), as well as their mirror images at $\{\Omega_\ell^{(1)}/2\pi, \Omega_\ell^{(2)}/2\pi\} = \{-5\,\text{kHz}, -3\,\text{kHz}\}$ and $\{+5\,\text{kHz}, +7\,\text{kHz}\}$. Notice how the peak amplitudes are at a maximum for $t_1 = 0$, and oscillate as t_1 is increased, whereas the peak phases remain constant.

Now suppose that a *second* two-dimensional experiment is performed that generates an amplitude modulated two-dimensional signal, where the modulation function is a *sine wave*:

$$s^{\sin}(t_1, t_2) = \sum_\ell a_\ell \sin(\Omega_\ell^{(1)} t_1)\ \exp\{-\lambda_\ell^{(1)} t_1\} \exp\left\{\left(\mathrm{i}\Omega_\ell^{(2)} - \lambda_\ell^{(2)}\right) t_2\right\} \tag{5.29}$$

FT with respect to t_2 provides a signal of the form.

$$S^{\sin}(t_1, \Omega_2) = \sum_\ell a_\ell \sin(\Omega_\ell^{(1)} t_1) \exp\{-\lambda_\ell^{(1)} t_1\}\, \mathcal{L}(\Omega_2; \Omega_\ell^{(2)}, \lambda_\ell^{(2)}) \tag{5.30}$$

The real part of $S^{\sin}(t_1, \Omega_2)$ is shown below:

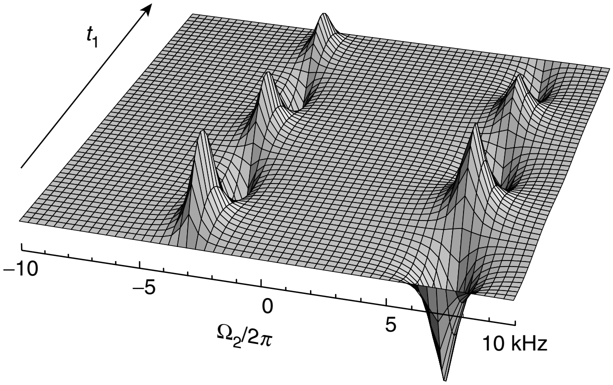

Figure 5.40
The real part of the sine-modulated signal $S^{\sin}(t_1, \Omega_2)$.

Note that the signal amplitude is zero for $t_1 = 0$. As t_1 is increased, the signal amplitude increases in the positive sense for the component with $\{\Omega_\ell^{(1)}/2\pi, \Omega_\ell^{(2)}/2\pi\} = \{5\,\text{kHz}, -3\,\text{kHz}\}$ (since $\Omega_\ell^{(1)}$ is positive), and it increases in the negative sense for the component with $\{\Omega_\ell^{(1)}/2\pi, \Omega_\ell^{(2)}/2\pi\} = \{-5\,\text{kHz}, +7\,\text{kHz}\}$ (since $\Omega_\ell^{(1)}$ is negative in this case).

Typically, the pulse sequences for generating $s^{\cos}$ and $s^{\sin}$ are related by changing the phase of one or more r.f. pulses. Some concrete examples are given in Sections 16.1, 19.7 and 20.6.

If two-dimensional Fourier transforms of the signals $s^{\cos}$ and $s^{\sin}$ are taken in the usual way, then one obtains an unattractive mess of overlapping phase twist peaks. The plots below show the real parts of the two-dimensional spectra $S^{\cos}(\Omega_1, \Omega_2)$ and $S^{\sin}(\Omega_1, \Omega_2)$, generated by two-dimensional FT of $s^{\cos}(t_1, t_2)$ and $s^{\sin}(t_1, t_2)$:

Cosine modulated

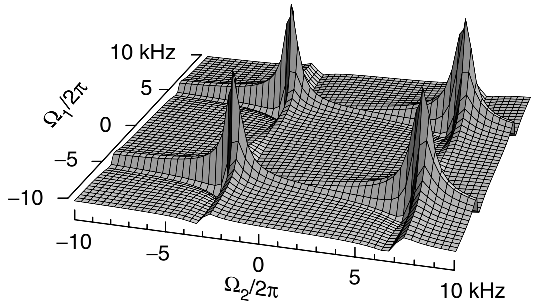

Sine modulated

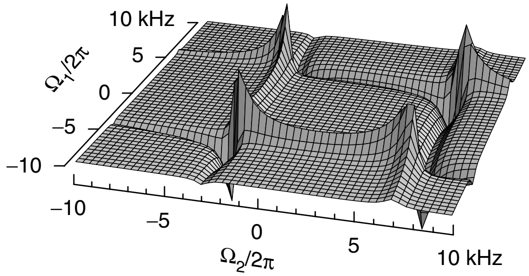

Figure 5.41
Two-dimensional spectra of the cosine- and sine-modulated signals.

These spectra are full of dispersion modes and spectral overlap and would not be of much use.

In the States method, the results of the two different two-dimensional experiments are combined in a special way. The real parts of the data matrices $S^{\cos}(t_1, \Omega_2)$ and $S^{\sin}(t_1, \Omega_2)$ are put together to make a new complex signal,[11] called here $S_{\text{States}}(t_1, \Omega_2)$:

$$S_{\text{States}}(t_1, \Omega_2) = \operatorname{Re}\{S^{\cos}(t_1, \Omega_2)\} + \mathrm{i}\operatorname{Re}\{S^{\sin}(t_1, \Omega_2)\} \tag{5.31}$$

This 'hybrid' signal has the following mathematical form:

$$S_{\text{States}}(t_1, \Omega_2) = \sum_{\ell} a_\ell \exp\{(\mathrm{i}\Omega_\ell^{(1)} - \lambda_\ell^{(1)})t_1\}\, \mathcal{A}(\Omega_2; \Omega_\ell^{(2)}, \lambda_\ell^{(2)}) \tag{5.32}$$

FT of the States signal with respect to t_1 gives a two-dimensional spectrum:

$$\begin{aligned} S_{\text{States}}(\Omega_1, \Omega_2) &= \int_0^\infty \mathrm{d}t_1 \; S_{\text{States}}(t_1, \Omega_2) \exp\{-\mathrm{i}\Omega_1 t_1\} \\ &= \sum_{\ell} a_\ell \mathcal{L}(\Omega_1; \Omega_\ell^{(1)}, \lambda_\ell^{(1)}) \mathcal{A}(\Omega_2; \Omega_\ell^{(2)}, \lambda_\ell^{(2)}) \end{aligned} \tag{5.33}$$

The real part of this spectrum is in pure absorption:

$$\operatorname{Re}\{S_{\text{States}}(\Omega_1, \Omega_2)\} = \sum_{\ell} a_\ell \mathcal{A}(\Omega_1; \Omega_\ell^{(1)}, \lambda_\ell^{(1)}) \mathcal{A}(\Omega_2; \Omega_\ell^{(2)}, \lambda_\ell^{(2)})$$

as shown below:

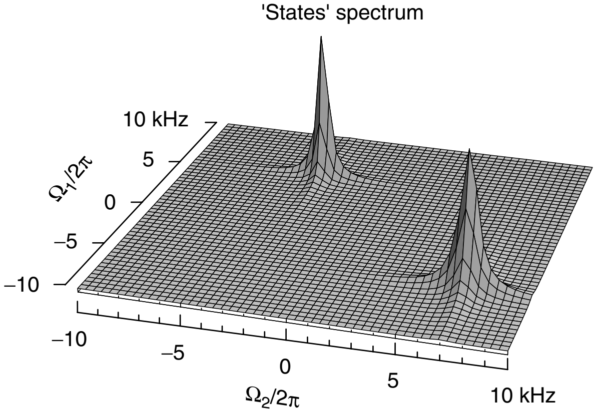

Figure 5.42
The real part of the States two-dimensional spectrum.

The 'image' peaks are eliminated and the peaks are in pure absorption. Note that the signs of the Ω_1 coordinates appear correctly for the two spectral components $\{\Omega_\ell^{(1)}/2\pi, \Omega_\ell^{(2)}/2\pi\} = \{5\,\mathrm{kHz}, -3\,\mathrm{kHz}\}$ and $\{-5\,\mathrm{kHz}, +7\,\mathrm{kHz}\}$.

To summarize, the States data acquisition/data processing scheme involves the following steps:

1. Design the two-dimensional NMR experiment so as to provide a cosine-modulated two-dimensional signal, of the form given in Equation 5.27.
2. Perform this experiment so as to acquire a data matrix $s^{\cos}(t_1, t_2)$.
3. Compute the Fourier transform with respect to t_2 to obtain the data matrix $S^{\cos}(t_1, \Omega_2)$ (Equation 5.28).
4. Construct a different two-dimensional NMR experiment so as to provide a sine-modulated two-dimensional signal, of the form given in Equation 5.29.
5. Perform this second experiment so as to acquire a data matrix $s^{\sin}(t_1, t_2)$.
6. Compute the Fourier transform with respect to t_2 to obtain the data matrix $S^{\sin}(t_1, \Omega_2)$ (Equation 5.30).
7. Combine the real parts of $S^{\cos}(t_1, \Omega_2)$ and $S^{\sin}(t_1, \Omega_2)$ as a complex pair, in order to obtain the data matrix $S_{\mathrm{States}}(t_1, \Omega_2)$ (Equation 5.31).
8. Compute the Fourier transform with respect to t_1 to obtain the two-dimensional spectrum $S_{\mathrm{States}}(\Omega_1, \Omega_2)$ (Equation 5.33).
9. The real part of this two-dimensional spectrum is in pure absorption mode.

A flow chart for the States procedure is shown in Figure 5.43.

Not all two-dimensional experiments are amenable to States data acquisition and processing. The conditions for cosine and sine modulation are quite stringent and are not satsified in all two-dimensional experiments. However, the practical advantages of pure absorption two-dimensional spectra are so great that essentially all *popular* two-dimensional experiments employ the States method (or an equivalent procedure; see Note 10).

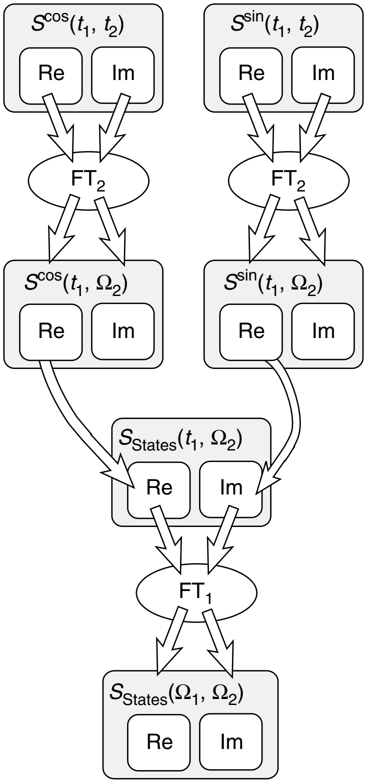

Figure 5.43
A flow chart for the 'States' procedure (see Note 10).

The schemes described in this section are known under a variety of names: *quadrature detection in the second dimension*, *pure phase two-dimensional spectroscopy*, and *phase-sensitive two-dimensional spectroscopy*. Some of these terms do not seem to be too meaningful (why 'phase sensitive' for instance?), but they are used prolifically and more or less interchangeably in the NMR literature.

5.10 Three-Dimensional Spectroscopy

A three-dimensional 'data cube' $s(t_1, t_2, t_3)$ may be acquired by incrementing the values of two pulse sequence delays t_1 and t_2 independently, while acquiring the signal as a function of t_3. The three-dimensional spectrum $S(\Omega_1, \Omega_2, \Omega_3)$ is computed by applying a three-dimensional Fourier transform to the signal $s(t_1, t_2, t_3)$:

$$\boxed{S(\Omega_1, \Omega_2, \Omega_3) = \int_0^\infty \mathrm{d}t_1 \int_0^\infty \mathrm{d}t_2 \int_0^\infty \mathrm{d}t_3 \; s(t_1, t_2, t_3) \exp\{-\mathrm{i}\,(\Omega_1 t_1 + \Omega_2 t_2 + \Omega_3 t_3)\} \qquad (5.34)}$$

The three-dimensional spectrum may be visualized as a cube, with peaks suspended at particular frequency coordinates. An experimental example is shown in Figure 5.44.

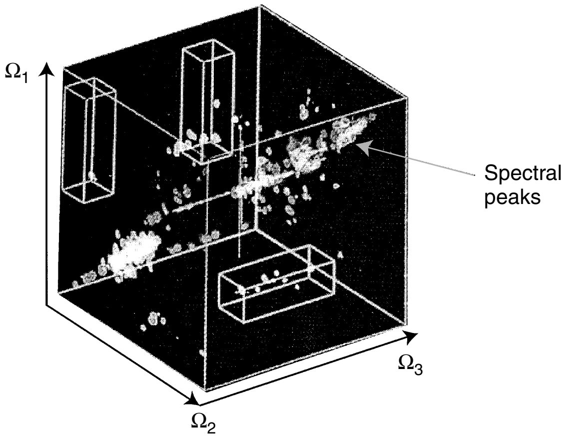

Figure 5.44
A three-dimensional spectrum. Adapted from C. Griesinger *et al.*, *J. Magn. Reson.* **84**, 14 (1989). (Copyright, Academic Press.)

In practice, such fully three-dimensional displays are rather difficult to use. It is more common to examine a set of sections of the three-dimensional spectrum, each of which is a two-dimensional spectrum.

Three- and higher-dimensional spectroscopies are an important feature of modern biomolecular NMR. However, I will not treat them further in this book.

Notes

1. Since the main source of r.f. noise is often the motion of electrons in the coil, the signal-to-noise ratio of NMR spectrometers may be considerably increased by cooling the coil and associated electronics to cryogenic temperatures (usually in the vicinity of 20 K). Probes equipped with such devices are called *cryoprobes*.

2. The most common procedure is to multiply the NMR signal by a *matched weighting function* before applying the Fourier transform. To obtain the optimal signal-to-noise ratio in the final spectrum, the weighting function should match the envelope of the NMR signal exactly: where the NMR signal is large, the weighting function should also be large, and where the NMR signal is small, the weighting function should also be small. Matched weighting accentuates the NMR signal at those times when it has the best chance of dominating the noise, and it reduces the noise at those times when the signal is weak. However, the gain in signal-to-noise does not come for free: it is always accompanied by a loss in spectral resolution. See *Further Reading*.

3. 'Ultrafast' forms of two-dimensional spectroscopy have been invented that do not require arrayed signal acquisition: instead of performing a set of consecutive experiments with different timings, the 'ultrafast' experiments use pulsed magnetic field gradients to perform many experiments in parallel in different parts of the sample tube. See for example L. Frydman *et al.*, *Proc. Natl. Acad. Sci. USA* **99**, 15 858–15 862 (2002) and M. Gal *et al.*, *J. Am. Chem. Soc.* **128**, 951–956 (2006).

4. There are a number of subtle effects that cause the peak frequencies and damping constants to depend on what happens *before* the signal is detected. All of these effects involve some form of feedback from the macroscopic nuclear spin magnetization to the magnetic fields acting on the spins themselves. The effects called *radiation damping* and the *nuclear demagnetizing field* fall into this category. For a review of this subject, see M. H. Levitt, *Concepts in Magn. Reson.* **8,** 77 (1996) and references therein. I ignore these effects in this book.

5. In practice, the FT is computed from the set of complex points sampled by the two ADCs. This numerical computation differs from Equation 5.7 in a number of respects. First, the value of the signal is available only up to a maximum time τ_{acq}, not to infinity. Second, the signal is available as a set of discrete samples, evenly spaced along the time axis, rather than as a continuous mathematical function. The discrepancy between the 'discrete FT' performed by the computer and the 'continuous FT' indicated by Equation 5.7 leads to certain spectral effects, such as *truncation distortions* and the *folding* of peaks. Fortunately, most of the dangerous effects of the discrete FT may be avoided by simple experimental precautions. See *Further Reading* for a discussion of these technical issues.

6. A common definition of the dispersion Lorentzian has the opposite sign.

7. The terms 'absorption' and 'dispersion' are purely historical in origin and have no physical significance in the ordinary NMR context. They are *not* related to the absorption of energy or the dispersion of electromagnetic waves. The term 'emission', which is sometimes used to indicate a negative absorption peak, is not recommended.

8. The FFT algorithm was invented by Cooley and Tukey in the 1950s, and has had a crucial influence on the development of NMR. Tukey made a further memorable contribution: He invented the term 'software'!

9. The word 'phase' has a number of different uses in NMR:
   - The term *phase of matter* indicates whether the substance is a solid, isotropic liquid, anisotropic liquid, or a gas.
   - The *phase of an r.f. signal* indicates the time origin of the oscillation; this is the meaning of phase in, for example, Section 4.2.1.
   - The *phase of a complex number* indicates the value of ϕ in expressions of the form $a = |a| \exp\{i\phi\}$.
   - The *phase of a spectral peak* indicates the proportions of absorption and dispersion peakshape contributions, as discussed in Section 5.8.4.

   The last three meanings are closely related, as explained in this book.

10. The States method was originally described in D. J. States, R. A. Haberkorn, D. J. Ruben *J. Magn. Reson.* **48,** 286(1982). There is a slightly different data acquisition/processing scheme called *time-proportional phase incrementation* (TPPI) that also suppresses image peaks and leads to pure absorption two-dimensional spectra (D. Marion, K. Wüthrich, *Biochem. Biophys. Res. Commun.* **113,** 967 (1983)). These methods are not totally equivalent, and in some circumstances the TPPI method is slightly superior. As described in the text, the States method combines two data sets that differ only in the phase of the excited coherences. The evolution frequency of the excited coherences is unchanged. In the TPPI method, on the other hand, the phase of the excited coherences is linked to incrementation of the evolution interval, generating an effective frequency change of the coherences. This turns out to be useful. For example, consider the case where longitudinal magnetization is present during the evolution interval t_1. This magnetization does not evolve (neglecting relaxation), and so generates 'axial peaks' on the $\Omega_1 = 0$ axis. In the States method, these axial peaks sit in the middle of the single-quantum spectrum and must usually be removed by a further stage of phase cycling (see Appendix A.11). In the TPPI method, on the other hand, the effective frequency shift of the coherences displaces the interesting two-dimensional peaks from the vicinity of the $\Omega_1 = 0$ axis to the edges of the two-dimensional spectrum, so that, in many circumstances, a further level of phase cycling is unnecessary. In such cases, the TPPI method is more economical of instrument time than the States method. Despite this subtle advantage of TPPI, I have chosen to emphasize the States method in this book, since it is somewhat easier to explain.

11. For historical reasons, most current practical implementations of the States method generate two data sets, one of which is cosine modulated and the second of which is sine modulated, but *with an inverted sign*. This requires that the sign of the imaginary part must also be inverted when combining the data

sets according to Equation 5.31. In this book, I have imposed a more natural phase convention for the States procedure. All the phase cycles given in this book are compatible with Equation 5.31, as written.

Further Reading

- For a discussion of post-processing of the NMR data to optimize sensitivity or resolution, see J. Keeler, *Understanding NMR Spectroscopy*, Wiley, Chichester, 2005, and A. E. Derome, *Modern NMR Techniques in Chemistry Research*, Pergamon Press, Oxford, 1990.
- For a discussion of the equivalence between the States method and TPPI, and a more thorough treatment of two-dimensional data processing, see R. R. Ernst, G. Bodenhausen and A. Wokaun, *Principles of Nuclear Magnetic Resonance in One and Two Dimensions*, Clarendon Press, Oxford, 1987.
- For more information on FT and some other data processing methods, see: A. G. Marshall and F. R. Verdun, *Fourier Transforms in NMR, Optical, and Mass Spectrometry*, Elsevier, Amsterdam, 1990 ; R. N. Bracewell, *The Fourier Transform and its Applications*, McGraw-Hill, New York, 1986; E. O. Brigham, *The Fast Fourier Transform and its Applications*, Prentice Hall, Upper Saddle River, NJ, USA, 1988.
- For the mathematical principles underlying the FFT computer algorithm, see G. Strang, *Linear Algebra and its Applications*, 3rd edition, Harcourt Brace Jovanovich, San Diego, CA, USA, 1988.
- For a review of fast data acquisition and processing schemes, see R. Freeman and E. Kupče, *Concepts Magn. Reson.* **23**, 63–75 (2004).

Exercises

5.1 Sketch roughly the Fourier transforms of the following time-domain functions (the horizontal axes show time in units of seconds):

(i)

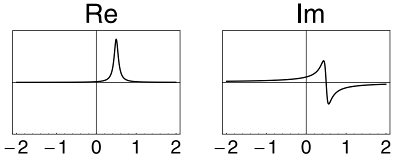

(iv)

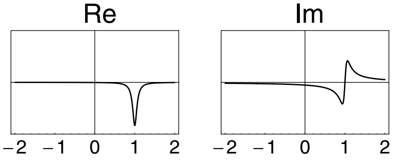

(ii)

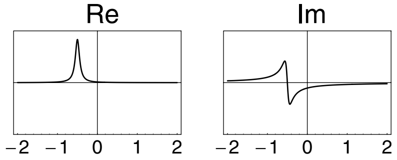

(v)

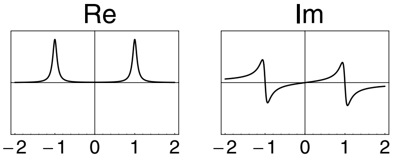

(iii)

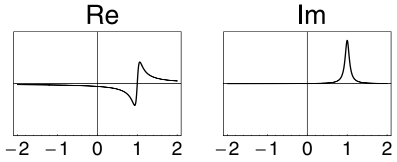

(vi)

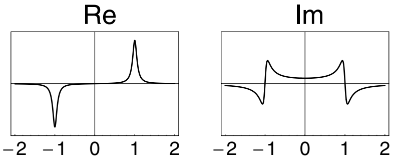

5.2 The T_1 of a certain sample decreases with increasing temperature. At 20 °C it is necessary to leave 10 s between transients, whereas at 40 °C only 5 s is required. Suppose that 3 h of NMR spectrometer time is available and that the instrument is already set up for operation at 20 °C. It takes 1 h to warm the sample to 40 °C and to stabilize the temperature. Assume that the NMR signals are identical at the two temperatures. What is the best strategy for acquiring the signals: running for 3 h at 20 °C, or warming the sample and running for 2 h at 40 °C?

Part 3

Quantum Mechanics

6 Mathematical Techniques

This chapter, and the following one, contain a brief review of mathematical techniques and the basic results of quantum mechanics. Other texts should be consulted for a fuller discussion (see *Further Reading*). A more 'physical' presentation is given in the following chapters.

It is impossible to provide the necessary background without employing some rather technical mathematics, which some readers may find difficult. It should be possible to skip these chapters on a first reading.

6.1 Functions

6.1.1 Continuous functions

Spinless quantum mechanics makes extensive use of *continuous functions*. An example of a continuous function of the coordinate x is the sine function $\sin(x)$. The term 'continuous' indicates that the function never makes a sudden jump when x changes by small amounts.

The discussion below uses the following set of continuous functions:

$$\psi_n(x) = \begin{cases} 0 & \text{if } x < 0 \\ 2^{1/2}\sin(\pi n x) & \text{if } 0 \leq x \leq 1 \\ 0 & \text{if } 1 < x \end{cases} \tag{6.1}$$

If n is an integer, each function $\psi_n(x)$ is continuous, since there are no sudden jumps at the points $x = 0$ and $x = 1$:

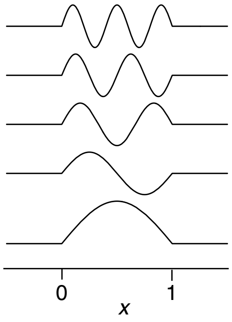

Figure 6.1 Some continuous functions.

The function $\psi_n(x)$ is *localized* to the interval $0 \leq x \leq 1$.

Spin Dynamics: Basics of Nuclear Magnetic Resonance, Second Edition Malcolm H. Levitt

Functions of importance to quantum mechanics are often complex. The complex conjugate is denoted by an asterisk:

$$\begin{aligned} f(x) &= \mathrm{Re}\{f(x)\} + \mathrm{i}\,\mathrm{Im}\{f(x)\} \\ f(x)^* &= \mathrm{Re}\{f(x)\} - \mathrm{i}\,\mathrm{Im}\{f(x)\} \end{aligned}$$

6.1.2 Normalization

A function $f(x)$ of one variable x is said to be *normalized* if the following condition holds:

$$\boxed{\int_{-\infty}^{\infty} \mathrm{d}x\; f(x)^* f(x) = 1 \qquad \text{(normalization)} \qquad (6.2)}$$

Functions may be normalized by multiplication with a suitable scaling factor, chosen to satisfy Equation 6.2.

6.1.3 Orthogonal and orthonormal functions

Two functions $f(x)$ and $g(x)$ are said to be *orthogonal* if the following condition holds:

$$\boxed{\int_{-\infty}^{\infty} \mathrm{d}x\; f(x)^* g(x) = 0 \qquad \text{(orthogonality)} \qquad (6.3)}$$

The set of functions $\psi_n(x)$, with $n = 1, 2, 3\ldots$ are all orthogonal to each other:

$$\int_{-\infty}^{\infty} \mathrm{d}x\; \psi_m(x)^* \psi_n(x) = \delta_{mn} \tag{6.4}$$

In this expression, the *Kronecker delta function* δ_{mn} is used. This symbol has the following meaning:

$$\boxed{\delta_{mn} = \begin{cases} 1 & \text{if } m = n \\ 0 & \text{otherwise} \end{cases} \qquad (6.5)}$$

A set of orthogonal, normalized functions are said to be *orthonormal*.

6.1.4 Dirac notation

The functions $\psi_n(x)$ are distinguished by the value of the integer n. Dirac introduced the following elegant notation for orthonormal functions, indexed by the integer n:

$$\psi_n(x) \equiv |n\rangle \qquad \psi_n(x)^* \equiv \langle n|$$

The symbol $|n\rangle$ is pronounced 'ket-n'. The symbol $\langle n|$ is pronounced 'bra-n'.

The 'bra-ket' $\langle m|n\rangle$ implies integration, as follows:

$$\langle m|n\rangle = \int_{-\infty}^{\infty} \mathrm{d}x\; \psi_m(x)^* \psi_n(x)$$

The orthonormalization condition (Equation 6.4) may therefore be written very concisely:

$$\boxed{\langle m|n\rangle = \delta_{mn} \qquad \text{(orthonormality)} \qquad (6.6)}$$

In general, the Dirac 'bra' and the 'ket' are related to each other by an operation known as the *adjoint*, denoted by a dagger (†):

$$\langle n| = \{|n\rangle\}^\dagger \qquad |n\rangle = \{\langle n|\}^\dagger$$

For functions, the adjoint is equivalent to taking the complex conjugate. A more general definition of the adjoint, which applies to operators as well as to functions, is given in Section 6.2.6.

6.1.5 Vector representation of functions

Suppose that a function $f(x)$ is expressed as a sum of the orthonormal functions $|n\rangle$, multiplied by numbers, called *coefficients*:

$$f(x) = f_1\psi_1(x) + f_2\psi_2(x) + f_3\psi_3(x) + \dots$$

In the above example, this is possible only if the function $f(x)$ vanishes in the regions $x < 0$ and $x > 1$, since all of the functions $\psi_n(x)$ also vanish there.

Using the Dirac notation, the above expression reads

$$|f\rangle = f_1|1\rangle + f_2|2\rangle + f_3|3\rangle + \dots$$

(The Dirac notation $|f\rangle$ for the function $f(x)$ is a little loose, but is convenient.)

By multiplying both sides from the left by $\langle n|$, and using orthonormality, we get

$$\langle n|f\rangle = f_n$$

which shows that the coefficents in the expansion may be evaluated from the integral

$$f_n = \int_{-\infty}^{\infty} \mathrm{d}x\ \psi_n(x)^* f(x)$$

For example, consider the following normalized function:

$$f(x) = \begin{cases} 0 & \text{if } x < 0 \\ \frac{16}{3\sqrt{7}}\sin^5(\pi x) & \text{if } 0 \le x \le 1 \\ 0 & \text{if } 1 < x \end{cases} \qquad (6.7)$$

which has the following appearance:

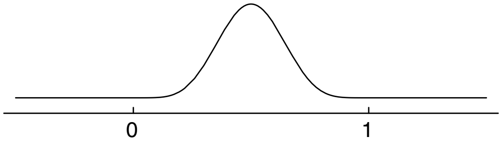

Figure 6.2
The function given in Equation 6.7.

The expansion coefficients in terms of the basis functions in Equation 6.1 may be evaluated as follows:

$$\begin{aligned}
f_1 &= \frac{5}{3}\sqrt{\frac{2}{7}} & f_2 &= 0 \\
f_3 &= -\frac{5}{3\sqrt{14}} & f_4 &= 0 \\
f_5 &= \frac{1}{3\sqrt{14}} \\
&\vdots
\end{aligned} \tag{6.8}$$

All higher terms $f_6, f_7 \ldots$ are equal to zero in this case.

It is convenient to list the coefficients $f_1, f_2 \ldots$ as a *column vector*, which is conveniently written as $|f\rangle$:

$$|f\rangle = \begin{pmatrix} f_1 \\ f_2 \\ f_3 \\ f_4 \\ \vdots \end{pmatrix}$$

This is called the *vector representation* of the function $f(x)$ in the *basis* $\{\psi_1(x), \psi_2(x), \ldots\}$.

For example, the function in Equation 6.7 could be written as

$$|f\rangle = \begin{pmatrix} \frac{5}{3}\sqrt{\frac{2}{7}} \\ 0 \\ -\frac{5}{3\sqrt{14}} \\ 0 \\ \frac{1}{3\sqrt{14}} \\ 0 \\ 0 \\ \vdots \end{pmatrix}$$

The 'bra' representation of f is a *row vector*, generated by exchanging rows and columns, and taking the complex conjugate:

$$\langle f| = \{|f\rangle\}^\dagger = \begin{pmatrix} f_1{}^*, & f_2{}^*, & f_3{}^*, & f_4{}^*, & f_5{}^* & \cdots \end{pmatrix}$$

(Note that the adjoint turns a column vector into a row vector, as well as taking the complex conjugate.) For example, the bra vector for the function given above is

$$\langle f| = \{|f\rangle\}^\dagger = \left(\tfrac{5}{3}\sqrt{\tfrac{2}{7}},\ 0,\ -\tfrac{5}{3\sqrt{14}},\ 0,\ \tfrac{1}{3\sqrt{14}}\ 0,\ 0\cdots \right)$$

(The complex conjugate does not do anything in this case, since the coefficients are real.)

By definition, the vector representation of a basis ket contains only zeros, except in one place, where the number one appears, for example:

$$|2\rangle = \begin{pmatrix} 0 \\ 1 \\ 0 \\ 0 \\ \vdots \end{pmatrix}$$

and

$$\langle 2| = (0,\quad 1,\quad 0,\quad 0,\quad \ldots)$$

Using this representation, the orthonormality of the basis states appears as a straightforward application of matrix multiplication; for example:

$$\langle 1|2\rangle = (1,\quad 0,\quad 0,\quad 0,\quad \ldots)\begin{pmatrix} 0 \\ 1 \\ 0 \\ 0 \\ \vdots \end{pmatrix} = 0$$

6.2 Operators

Quantum mechanics makes extensive use of *operators*, denoted in this book by a hat (ˆ). Two examples are the first and second derivative operators $\widehat{D}_x$ and $\widehat{D}_x^2$, which have the following effect on operand functions $f(x)$:

$$\widehat{D}_x f(x) = \frac{\mathrm{d}f(x)}{\mathrm{d}x}$$

$$\widehat{D}_x^2 f(x) = \widehat{D}_x\left\{\widehat{D}_x f(x)\right\} = \frac{\mathrm{d}^2 f(x)}{\mathrm{d}x^2}$$

Another example is the operator $\hat{x}$, which has the effect of multiplying the operand by the coordinate value:

$$\hat{x} f(x) = x f(x)$$

For example, the operator $\widehat{D}_x$ applied to the function $\psi_n(x)$ yields

$$\widehat{D}_x \psi_n(x) = \sqrt{2}\, n\pi \cos(n\pi x)$$

in the range $0 < x < 1$.

A trivial example of an operator is the *unity operator* $\widehat{1}$, which simply leaves any operand unchanged:

$$\widehat{1}f(x) = f(x)$$

Another trivial example is the *null operator* $\widehat{0}$, which always generates the result zero, whatever the operand:

$$\widehat{0}f(x) = 0$$

6.2.1 Commutation

In everyday life, the effect of consecutive operations depends on their order. For example, the effect of driving straight for 100 m, then turning left, and driving straight for 50 m, is different from the effect of driving straight for 50 m, turning left, and driving straight for 100 m.

The effect of mathematical operators is also dependent on their order. The effect of applying an operator $\widehat{A}$ and then applying the operator $\widehat{B}$ is notated $\widehat{B}\widehat{A}$, which implies

$$\widehat{B}\widehat{A}f(x) = \widehat{B}\left\{\widehat{A}f(x)\right\}$$

Similarly, the effect of applying an operator $\widehat{B}$ and then applying the operator $\widehat{A}$ is notated $\widehat{A}\widehat{B}$. Note that operators are written in order from *right to left*.

The *commutator* of two operators is defined thus:

$$\boxed{\left[\widehat{A}, \widehat{B}\right] = \widehat{A}\widehat{B} - \widehat{B}\widehat{A} \qquad (6.9)}$$

For example, the commutator of the operators $\hat{x}$ and $\widehat{D}_x$ is given by

$$\left[\hat{x}, \widehat{D}_x\right] = -\widehat{1}$$

which may be seen by applying the operators to a function $f(x)$:

$$\begin{aligned}
\left[\hat{x}, \widehat{D}_x\right] f(x) &= \hat{x}\left\{\widehat{D}_x f(x)\right\} - \widehat{D}_x\left\{\hat{x}f(x)\right\} \\
&= \hat{x}\left\{\frac{\mathrm{d}f(x)}{\mathrm{d}x}\right\} - \frac{\mathrm{d}}{\mathrm{d}x}\left\{xf(x)\right\} \\
&= x\frac{\mathrm{d}f(x)}{\mathrm{d}x} - \left\{x\frac{\mathrm{d}f(x)}{\mathrm{d}x} + f(x)\frac{\mathrm{d}x}{\mathrm{d}x}\right\} \\
&= -f(x) \qquad (6.10)
\end{aligned}$$

Two operators are said to *commute* if their commutator is zero. The result of applying two commuting operators does not depend on the order in which they are applied. For example, the unity operator $\widehat{1}$ commutes with all other operators.

Any operator commutes with any number. The symbols $a\widehat{A}$ and $\widehat{A}a$ have the same meaning.

6.2.2 Matrix representations

The *matrix element* of an operator $\widehat{Q}$ is defined as follows:

$$\boxed{\langle m|\widehat{Q}|n\rangle = \int_{-\infty}^{\infty} \mathrm{d}x \; \psi_m{}^* \widehat{Q} \psi_n \qquad (6.11)}$$

The matrix element depends on the basis states.

Here are some examples of matrix elements, using the operators discussed above and the basis set defined in Equation 6.1:

$$\begin{aligned}
\langle 1|\widehat{D}_x|3\rangle &= 0 & \langle 1|\hat{x}|4\rangle &= -\frac{32}{225\pi^2} \\
\langle 1|\widehat{D}_x^2|1\rangle &= -\pi^2 & \langle 1|\hat{x}\widehat{D}_x|3\rangle &= \frac{3}{4} \\
\langle 2|\widehat{D}_x^2|2\rangle &= -4\pi^2 & \langle 1|\widehat{D}_x\hat{x}|3\rangle &= \frac{3}{4} \\
\langle 1|\hat{x}|2\rangle &= -\frac{16}{9\pi^2} & \langle 1|\hat{x}\widehat{D}_x|1\rangle &= -\frac{1}{2} \\
\langle 1|\hat{x}|3\rangle &= 0 & \langle 1|\widehat{D}_x\hat{x}|1\rangle &= \frac{1}{2}
\end{aligned} \qquad (6.12)$$

The *matrix representation* of an operator is an array of all possible matrix elements:

$$\widehat{Q} = \begin{pmatrix} \langle 1|\widehat{Q}|1\rangle & \langle 1|\widehat{Q}|2\rangle & \dots \\ \langle 2|\widehat{Q}|1\rangle & \langle 2|\widehat{Q}|2\rangle & \dots \\ \vdots & \vdots & \ddots \end{pmatrix} \qquad (6.13)$$

The matrix representation of an operator depends on the choice of basis.

For example, the operator $\hat{x}$ has the following matrix representation in the basis set of Equation 6.1:

$$\hat{x} = \begin{pmatrix} \frac{1}{2} & -\frac{16}{9\pi^2} & 0 & -\frac{32}{225\pi^2} & \dots \\ -\frac{16}{9\pi^2} & \frac{1}{2} & -\frac{48}{25\pi^2} & 0 & \dots \\ 0 & -\frac{48}{25\pi^2} & \frac{1}{2} & -\frac{96}{49\pi^2} & \dots \\ -\frac{32}{225\pi^2} & 0 & -\frac{96}{49\pi^2} & \frac{1}{2} & \dots \\ \vdots & \vdots & \vdots & \vdots & \ddots \end{pmatrix} \qquad (6.14)$$

The operators $\widehat{0}$ and $\widehat{1}$ have the following matrix representations:

$$\widehat{0} = \begin{pmatrix} 0 & 0 & 0 & 0 & \dots \\ 0 & 0 & 0 & 0 & \dots \\ 0 & 0 & 0 & 0 & \dots \\ 0 & 0 & 0 & 0 & \dots \\ \vdots & \vdots & \vdots & \vdots & \ddots \end{pmatrix}$$

$$\widehat{1} = \begin{pmatrix} 1 & 0 & 0 & 0 & \cdots \\ 0 & 1 & 0 & 0 & \cdots \\ 0 & 0 & 1 & 0 & \cdots \\ 0 & 0 & 0 & 1 & \cdots \\ \vdots & \vdots & \vdots & \vdots & \ddots \end{pmatrix} \tag{6.15}$$

In this book, I use the same symbol for an operator and its matrix representation. There are occasional pitfalls in this practice, which will be pointed out when they occur.

The *matrix representation of the product of two operators* is given by the usual law for matrix multiplication, i.e.

$$\boxed{\langle m|\widehat{B}\widehat{A}|n\rangle = \sum_{p} \langle m|\widehat{B}|p\rangle\langle p|\widehat{A}|n\rangle} \tag{6.16}$$

where the sum runs over all basis states $|p\rangle$.

For example, the matrix representations of $\hat{x}\widehat{D}_x$ and $\widehat{D}_x\hat{x}$ in the basis set of Equation 6.1 are given by

$$\begin{aligned} \hat{x}\widehat{D}_x &= \begin{pmatrix} -\frac{1}{2} & -\frac{4}{3} & \frac{3}{4} & -\frac{8}{15} & \cdots \\ \frac{4}{3} & -\frac{1}{2} & -\frac{12}{5} & \frac{4}{3} & \cdots \\ -\frac{3}{4} & \frac{12}{5} & -\frac{1}{2} & -\frac{24}{7} & \cdots \\ \frac{8}{15} & -\frac{4}{3} & \frac{24}{7} & -\frac{1}{2} & \cdots \\ \vdots & \vdots & \vdots & \vdots & \ddots \end{pmatrix} \\ \widehat{D}_x\hat{x} &= \begin{pmatrix} \frac{1}{2} & -\frac{4}{3} & \frac{3}{4} & -\frac{8}{15} & \cdots \\ \frac{4}{3} & \frac{1}{2} & -\frac{12}{5} & \frac{4}{3} & \cdots \\ -\frac{3}{4} & \frac{12}{5} & \frac{1}{2} & -\frac{24}{7} & \cdots \\ \frac{8}{15} & -\frac{4}{3} & \frac{24}{7} & \frac{1}{2} & \cdots \\ \vdots & \vdots & \vdots & \vdots & \ddots \end{pmatrix} \end{aligned} \tag{6.17}$$

Note that the matrix representations of $\hat{x}\widehat{D}_x$ and $\widehat{D}_x\hat{x}$ are different, since the operators $\hat{x}$ and $\widehat{D}_x$ do not commute. The matrix representations obey the equation $\left[\hat{x}, \widehat{D}_x\right] = \hat{x}\widehat{D}_x - \widehat{D}_x\hat{x} = -\widehat{1}$, as they should according to Equation 6.10.

6.2.3 Diagonal matrices

The matrix representation of an operator is said to be *diagonal* if it has the following type of structure:

$$\begin{pmatrix}
\bullet & 0 & 0 & 0 & 0 & 0 & 0 & 0 & 0 & 0 & 0 & \cdots \\
0 & \bullet & 0 & 0 & 0 & 0 & 0 & 0 & 0 & 0 & 0 & \cdots \\
0 & 0 & \bullet & 0 & 0 & 0 & 0 & 0 & 0 & 0 & 0 & \cdots \\
0 & 0 & 0 & \bullet & 0 & 0 & 0 & 0 & 0 & 0 & 0 & \cdots \\
0 & 0 & 0 & 0 & \bullet & 0 & 0 & 0 & 0 & 0 & 0 & \cdots \\
0 & 0 & 0 & 0 & 0 & \bullet & 0 & 0 & 0 & 0 & 0 & \cdots \\
0 & 0 & 0 & 0 & 0 & 0 & \bullet & 0 & 0 & 0 & 0 & \cdots \\
0 & 0 & 0 & 0 & 0 & 0 & 0 & \bullet & 0 & 0 & 0 & \cdots \\
0 & 0 & 0 & 0 & 0 & 0 & 0 & 0 & \bullet & 0 & 0 & \cdots \\
0 & 0 & 0 & 0 & 0 & 0 & 0 & 0 & 0 & \bullet & 0 & \cdots \\
0 & 0 & 0 & 0 & 0 & 0 & 0 & 0 & 0 & 0 & \bullet & \cdots \\
\vdots & \vdots & \vdots & \vdots & \vdots & \vdots & \vdots & \vdots & \vdots & \vdots & \vdots & \ddots
\end{pmatrix} \tag{6.18}$$

where the symbol $\bullet$ represents any number. The matrix representation of $\widehat{1}$, given in Equation 6.15, is diagonal.

6.2.4 Block diagonal matrices

A matrix representation is said to be *block-diagonal* if it has the following type of structure:

$$\begin{pmatrix}
\bullet & 0 & 0 & 0 & 0 & 0 & 0 & 0 & 0 & 0 & 0 & \cdots \\
0 & \bullet & \bullet & 0 & 0 & 0 & 0 & 0 & 0 & 0 & 0 & \cdots \\
0 & \bullet & \bullet & 0 & 0 & 0 & 0 & 0 & 0 & 0 & 0 & \cdots \\
0 & 0 & 0 & \bullet & 0 & 0 & 0 & 0 & 0 & 0 & 0 & \cdots \\
0 & 0 & 0 & 0 & \bullet & \bullet & \bullet & 0 & 0 & 0 & 0 & \cdots \\
0 & 0 & 0 & 0 & \bullet & \bullet & \bullet & 0 & 0 & 0 & 0 & \cdots \\
0 & 0 & 0 & 0 & \bullet & \bullet & \bullet & 0 & 0 & 0 & 0 & \cdots \\
0 & 0 & 0 & 0 & 0 & 0 & 0 & \bullet & \bullet & \bullet & \bullet & \cdots \\
0 & 0 & 0 & 0 & 0 & 0 & 0 & \bullet & \bullet & \bullet & \bullet & \cdots \\
0 & 0 & 0 & 0 & 0 & 0 & 0 & \bullet & \bullet & \bullet & \bullet & \cdots \\
0 & 0 & 0 & 0 & 0 & 0 & 0 & \bullet & \bullet & \bullet & \bullet & \cdots \\
\vdots & \vdots & \vdots & \vdots & \vdots & \vdots & \vdots & \vdots & \vdots & \vdots & \vdots & \ddots
\end{pmatrix} \tag{6.19}$$

where the symbol $\bullet$ represents any number.

6.2.5 Inverse

If two operators $\widehat{A}$ and $\widehat{B}$ satisfy the two relationships

$$\widehat{B}\widehat{A} = \widehat{A}\widehat{B} = \widehat{1}$$

then the operators are said to be *inverses* of each other. This relationship may be written

$$\widehat{A} = \widehat{B}^{-1}$$
$$\widehat{B} = \widehat{A}^{-1}$$

The inverse of a product of two operators is equal to the product of the inverses, taken in opposite order, i.e.

$$\left\{\widehat{D}\widehat{C}\right\}^{-1} = \widehat{C}^{-1}\widehat{D}^{-1}$$

6.2.6 Adjoint

Two operators $\widehat{A}$ and $\widehat{B}$ are said to be *adjoints* of each other if their matrix elements are related as follows:

$$\langle m|\widehat{A}|n\rangle = \langle n|\widehat{B}|m\rangle^*$$

for all (m, n). The adjoint relationship between these operators is written

$$\widehat{A} = \widehat{B}^\dagger$$
$$\widehat{B} = \widehat{A}^\dagger$$

The matrix representations of adjoint operators are related by (i) taking the *complex conjugate* of all elements and (ii) *exchanging rows and columns* (equal to transposing the matrix). For example, the adjoint of the operator $\hat{x}\widehat{D}_x$ has the following matrix representation in the basis set of Equation 6.1:

$$\left(\hat{x}\widehat{D}_x\right)^\dagger = \begin{pmatrix} -\frac{1}{2} & \frac{4}{3} & -\frac{3}{4} & \frac{8}{15} & \cdots \\ -\frac{4}{3} & -\frac{1}{2} & \frac{12}{5} & -\frac{4}{3} & \cdots \\ \frac{3}{4} & -\frac{12}{5} & -\frac{1}{2} & \frac{24}{7} & \cdots \\ -\frac{8}{15} & \frac{4}{3} & -\frac{24}{7} & -\frac{1}{2} & \cdots \\ \vdots & \vdots & \vdots & \vdots & \ddots \end{pmatrix} \tag{6.20}$$

The adjoint of a product of two operators is equal to the product of the adjoints, taken in opposite order, i.e.

$$\left\{\widehat{D}\widehat{C}\right\}^\dagger = \widehat{C}^\dagger\widehat{D}^\dagger$$

The adjoint of an operator multiplied by a number is given by the adjoint of the operator, multiplied by the complex conjugate of the number, as follows:

$$\left\{a\widehat{C}\right\}^\dagger = a^*\widehat{C}^\dagger$$

6.2.7 Hermitian operators

An operator that is equal to its own adjoint is said to be *hermitian*:

$$\widehat{A} = \widehat{A}^\dagger \qquad \text{(hermitian)} \tag{6.21}$$

The operators $\hat{x}$ and $\widehat{D}_x^2$ are hermitian (the proofs are left as an exercise). The operator $\hat{x}\widehat{D}_x$, on the other hand, is not hermitian, as may be seen by comparing Equations 6.17 and 6.20.

In quantum mechanics, all experimental observations are associated with hermitian operators.

6.2.8 Unitary operators

If the adjoint of an operator is equal to the inverse, then the operator is said to be *unitary*:

$$\widehat{A}^{-1} = \widehat{A}^\dagger \qquad \text{(unitary)} \tag{6.22}$$

6.3 Eigenfunctions, Eigenvalues and Eigenvectors

6.3.1 Eigenequations

When an operator $\widehat{Q}$ is applied to a function $f(x)$, the result is in general a completely new function. For example, the application of $\widehat{D}_x$ to $\sin(x)$ leads to the function $\cos(x)$. However, in some cases, the result is simply proportional to the original function. An example of this is when the double derivative operator $\widehat{D}_x^2$ is applied to the function $\sin(x)$:

$$\widehat{D}_x^2 \sin(x) = \widehat{D}_x \cos(x) = -\sin(x)$$

The original function $\sin(x)$ is regenerated, but with a negative sign. This is an example of an *eigenequation*.[1] The function $\sin(x)$ is said to be an *eigenfunction* of the operator $\widehat{D}_x^2$, with *eigenvalue* -1.

In general, an eigenequation has the form

$$\widehat{Q}|f\rangle = q|f\rangle \tag{6.23}$$

where $|f\rangle$ is an *eigenfunction* of $\widehat{Q}$, and q is a number (possibly complex), called the *eigenvalue*.

An operator may have many possible eigenfunctions, each with its own eigenvalue. For example, the functions $|n\rangle = \psi_n(x)$, defined in Equation 6.1, are all eigenfunctions of $\widehat{D}_x^2$, with eigenvalues $-\pi^2 n^2$:

$$\widehat{D}_x^2|n\rangle = -\pi^2 n^2 |n\rangle$$

6.3.2 Degeneracy

In some cases, several eigenvalues of an operator are identical, even though the corresponding eigenfunctions are different. This is called *degeneracy*, and the identical eigenvalues are said to be *degenerate*. If all the eigenvalues of an operator are different, then that operator is said to be *non-degenerate*.

6.3.3 Eigenfunctions and eigenvalues of hermitian operators

The eigenfunctions and eigenvalues of *hermitian operators* have some useful properties: (i) the eigenvalues are real and (ii) the eigenfunctions associated with non-degenerate eigenvalues are orthogonal. It is always possible to choose the normalized eigenfunctions of a hermitian operator so as to form an orthonormal basis set, called the *eigenbasis* of that operator. For example, the set of functions $\psi_n(x)$ defined in Equation 6.1 is an eigenbasis of the hermitian operator $\widehat{D}_x^2$.

By definition, the matrix representation of a hermitian operator is *diagonal* in its own eigenbasis. For example, the matrix representation of $\widehat{D}_x^2$, in its own eigenbasis, is given by the following:

$$\widehat{D}_x^2 = \begin{pmatrix} -\pi^2 & 0 & 0 & 0 & \dots \\ 0 & -4\pi^2 & 0 & 0 & \dots \\ 0 & 0 & -9\pi^2 & 0 & \dots \\ 0 & 0 & 0 & -16\pi^2 & \dots \\ \vdots & \vdots & \vdots & \vdots & \ddots \end{pmatrix} \tag{6.24}$$

6.3.4 Eigenfunctions of commuting operators: non-degenerate case

Suppose that two operators $\widehat{A}$ and $\widehat{B}$ commute and that all the eigenvalues of the operator $\widehat{A}$ are different. Then *the eigenbasis of $\widehat{A}$ is also the eigenbasis of $\widehat{B}$*.

This property may be stated a little more narrowly: if $\widehat{A}$ has an eigenfunction $|f\rangle$ with a non-degenerate eigenvalue a:

$$\widehat{A}|f\rangle = a|f\rangle$$

then $|f\rangle$ must also be an eigenfunction of $\widehat{B}$:

$$\widehat{B}|f\rangle = b|f\rangle$$

The same property may be stated using the matrix representations of operators: *if $\widehat{A}$ has non-degenerate eigenvalues and if $\widehat{A}$ commutes with $\widehat{B}$, then the matrix representation of an operator $\widehat{B}$ in the eigenbasis of $\widehat{A}$ is diagonal*.

6.3.5 Eigenfunctions of commuting operators: degenerate case

What happens if $\widehat{A}$ does have degenerate eigenvalues? Suppose, for example, that the matrix representation of $\widehat{A}$ in its own eigenbasis has the following form:

$$\begin{pmatrix}
a_1 & 0 & 0 & 0 & 0 & 0 & 0 & 0 & 0 & 0 & 0 & \cdots \\
0 & a_2 & 0 & 0 & 0 & 0 & 0 & 0 & 0 & 0 & 0 & \cdots \\
0 & 0 & a_2 & 0 & 0 & 0 & 0 & 0 & 0 & 0 & 0 & \cdots \\
0 & 0 & 0 & a_3 & 0 & 0 & 0 & 0 & 0 & 0 & 0 & \cdots \\
0 & 0 & 0 & 0 & a_4 & 0 & 0 & 0 & 0 & 0 & 0 & \cdots \\
0 & 0 & 0 & 0 & 0 & a_4 & 0 & 0 & 0 & 0 & 0 & \cdots \\
0 & 0 & 0 & 0 & 0 & 0 & a_4 & 0 & 0 & 0 & 0 & \cdots \\
0 & 0 & 0 & 0 & 0 & 0 & 0 & a_5 & 0 & 0 & 0 & \cdots \\
0 & 0 & 0 & 0 & 0 & 0 & 0 & 0 & a_5 & 0 & 0 & \cdots \\
0 & 0 & 0 & 0 & 0 & 0 & 0 & 0 & 0 & a_5 & 0 & \cdots \\
0 & 0 & 0 & 0 & 0 & 0 & 0 & 0 & 0 & 0 & a_5 & \cdots \\
\vdots & \vdots & \vdots & \vdots & \vdots & \vdots & \vdots & \vdots & \vdots & \vdots & \vdots & \ddots
\end{pmatrix}$$

where $a_1, a_2 \ldots$ are all different, but the second and third eigenfunctions are degenerate, as are the fifth, sixth and seventh. If $\widehat{A}$ and $\widehat{B}$ commute, then the matrix representation of $\widehat{B}$ is block diagonal in the eigenbasis of $\widehat{A}$:

$$\widehat{B} = \begin{pmatrix}
\bullet & 0 & 0 & 0 & 0 & 0 & 0 & 0 & 0 & 0 & 0 & \cdots \\
0 & \bullet & \bullet & 0 & 0 & 0 & 0 & 0 & 0 & 0 & 0 & \cdots \\
0 & \bullet & \bullet & 0 & 0 & 0 & 0 & 0 & 0 & 0 & 0 & \cdots \\
0 & 0 & 0 & \bullet & 0 & 0 & 0 & 0 & 0 & 0 & 0 & \cdots \\
0 & 0 & 0 & 0 & \bullet & \bullet & \bullet & 0 & 0 & 0 & 0 & \cdots \\
0 & 0 & 0 & 0 & \bullet & \bullet & \bullet & 0 & 0 & 0 & 0 & \cdots \\
0 & 0 & 0 & 0 & \bullet & \bullet & \bullet & 0 & 0 & 0 & 0 & \cdots \\
0 & 0 & 0 & 0 & 0 & 0 & 0 & \bullet & \bullet & \bullet & \bullet & \cdots \\
0 & 0 & 0 & 0 & 0 & 0 & 0 & \bullet & \bullet & \bullet & \bullet & \cdots \\
0 & 0 & 0 & 0 & 0 & 0 & 0 & \bullet & \bullet & \bullet & \bullet & \cdots \\
0 & 0 & 0 & 0 & 0 & 0 & 0 & \bullet & \bullet & \bullet & \bullet & \cdots \\
\vdots & \vdots & \vdots & \vdots & \vdots & \vdots & \vdots & \vdots & \vdots & \vdots & \vdots & \ddots
\end{pmatrix}$$

Note how the blocks follow the pattern of degeneracy in the eigenvalues of $\widehat{A}$.

6.3.6 Eigenfunctions of commuting operators: summary

The interplay of degeneracy and the form of matrix representations is therefore quite tricky. The key results, for two commuting operators $\widehat{A}$ and $\widehat{B}$, are as follows:

1. If the eigenvalues of $\widehat{A}$ are all different, then the matrix represention of $\widehat{B}$ in the eigenbasis of $\widehat{A}$ is always *diagonal*.

2. If some of the eigenvalues of $\widehat{A}$ are degenerate, then the matrix represention of $\widehat{B}$ in the eigenbasis of $\widehat{A}$ is *block diagonal*, but not necessarily diagonal.

3. In *all* cases, a basis may be *found* in which the matrix representations of two commuting operators $\widehat{A}$ and $\widehat{B}$ are *both* diagonal. However, one may have to look for such a basis.

6.3.7 Eigenvectors

The vector representation of an operator eigenfunction is called an *eigenvector*. The eigenvectors of a matrix are the vector representations of the eigenfunctions of the corresponding operator.

For example, suppose that an operator $\widehat{A}$ has the following eigenequation:

$$\widehat{A}|f\rangle = a|f\rangle$$

where a is the eigenvalue and $|f\rangle$ is the eigenfunction.

The following matrix-vector equation then applies:

$$\mathbf{Af} = a\mathbf{f}$$

where $\mathbf{A}$ is the matrix representation of the operator $\widehat{A}$ and $\mathbf{f}$ is the vector representation of the function $|f\rangle$. This equation implies that when the vector $\mathbf{f}$ is multiplied from the left by the matrix $\mathbf{A}$, the result is the same as the starting vector $\mathbf{f}$, but multiplied by a number a.

Eigenfunctions and eigenvectors are so closely related that the terms are often used interchangeably.

6.4 Diagonalization

A square matrix $\mathbf{A}$ may always be written in the following form:

$$\boxed{\mathbf{A} = \mathbf{XDX}^{-1} \qquad (6.25)}$$

where the matrix $\mathbf{D}$ is diagonal. The expression Equation 6.25 is called the *diagonal form* of $\mathbf{A}$, and the procedure for finding the matrices $\mathbf{X}$ and $\mathbf{D}$ is called the *diagonalization* of $\mathbf{A}$.

Diagonalization is closely related to finding the eigenvalues and eigenvectors of a matrix:

1. The elements of the diagonal matrix $\mathbf{D}$ are the *eigenvalues* of $\mathbf{A}$.

2. The *columns* of the matrix $\mathbf{X}$ are *eigenvectors* of $\mathbf{A}$.

Suppose, for example, that a matrix $\mathbf{A}$ has a set of eigenvalues $\{a_1, a_2 \ldots\}$, each with a corresponding eigenvector $\{\mathbf{f}_1, \mathbf{f}_2 \ldots\}$:

$$\mathbf{Af}_1 = a_1\mathbf{f}_1$$

$$\mathbf{Af}_2 = a_2\mathbf{f}_2$$

The diagonal elements of $\mathbf{D}$ are the eigenvalues of $\mathbf{A}$:

$$\mathbf{D} = \begin{pmatrix} a_1 & 0 & 0 & \ldots \\ 0 & a_2 & 0 & \ldots \\ 0 & 0 & a_3 & \ldots \\ \vdots & \vdots & \vdots & \ddots \end{pmatrix}$$

The columns of the matrix **X** are the eigenvectors of **A**:

$$\mathbf{X} = \begin{pmatrix} \vdots & \vdots & \vdots & \\ \mathbf{f}_1\ , & \mathbf{f}_2\ , & \mathbf{f}_3\ , & \dots \\ \vdots & \vdots & \vdots & \end{pmatrix}$$

6.4.1 Diagonalization of hermitian or unitary matrices

In general, the matrix $\mathbf{X}^{-1}$ must be determined by a full matrix inversion of **X**. However, in the common case that **A** is *hermitian* or *unitary*, a shortcut is available. Suppose that the eigenvectors are *normalized*, so that

$$\mathbf{f}_1{}^{\dagger} \cdot \mathbf{f}_1 = 1$$
$$\mathbf{f}_2{}^{\dagger} \cdot \mathbf{f}_2 = 1$$

and so on, where the adjoint (†) implies transforming a column vector into a row vector, followed by taking the complex conjugate. If the eigenvectors are normalized, then the matrix $\mathbf{X}^{-1}$ is simply the adjoint of **X**:

$$\mathbf{X}^{-1} = \mathbf{X}^{\dagger}$$

In this case, the diagonalization Equation 6.25 reads

$$\mathbf{A} = \mathbf{X}\mathbf{D}\mathbf{X}^{\dagger} \tag{6.26}$$

The adjoint is much easier to calculate than the inverse, so this form is very useful.

⚠Equation 6.26 may only be used if **A** is hermitian or unitary, and the eigenvectors are *normalized*.

6.5 Exponential Operators

6.5.1 Powers of operators

The symbol $\widehat{A}^N$, where N is an integer, should be understood in the following way:

$$\begin{aligned} \widehat{A}^0 &= \widehat{1} \\ \widehat{A}^1 &= \widehat{A} \\ \widehat{A}^2 &= \widehat{A}\widehat{A} \\ \widehat{A}^3 &= \widehat{A}\widehat{A}\widehat{A} \end{aligned} \tag{6.27}$$

and so on.

All powers of an operator commute with each other, which implies that they have the same eigenfunctions; i.e. if

$$\widehat{Q}|f\rangle = q|f\rangle$$

then

$$\widehat{Q}^N|f\rangle = q^N|f\rangle \qquad (6.28)$$

The powers of the null and unity operators are given by

$$\begin{aligned}\widehat{0}^N &= \widehat{0}\\ \widehat{1}^N &= \widehat{1}\end{aligned} \qquad (6.29)$$

6.5.2 Exponentials of operators

The exponential of an ordinary number q is given by the following series:

$$\exp\{q\} = 1 + q + \frac{1}{2!}q^2 + \frac{1}{3!}q^3 + \ldots$$

Similarly, the exponential of an operator has the following meaning:

$$\exp\{\widehat{Q}\} = \widehat{1} + \widehat{Q} + \frac{1}{2!}\widehat{Q}^2 + \frac{1}{3!}\widehat{Q}^3 + \ldots \qquad (6.30)$$

The exponential of an operator commutes with the original operator and, therefore, has the same eigenfunctions. The eigenvalues of $\exp\{\widehat{Q}\}$ are given by the exponentials of the eigenvalues of $\widehat{Q}$, i.e.

$$e^{\widehat{Q}}|f\rangle = e^q|f\rangle \qquad (6.31)$$

The matrix representation of an exponential operator $\exp\{\widehat{Q}\}$ is diagonal in the eigenbase of $\widehat{Q}$. For example, the matrix representation of the operator $\exp\{\widehat{D}_x^2\}$, in the eigenbasis $|n\rangle$, is given from Equation 6.24 by

$$\exp\{\widehat{D}_x^2\} = \begin{pmatrix} e^{-\pi^2} & 0 & 0 & 0 & \ldots \\ 0 & e^{-4\pi^2} & 0 & 0 & \ldots \\ 0 & 0 & e^{-9\pi^2} & 0 & \ldots \\ 0 & 0 & 0 & e^{-16\pi^2} & \ldots \\ \vdots & \vdots & \vdots & \vdots & \ddots \end{pmatrix}$$

6.5.3 Exponentials of unity and null operators

From Equations 6.29 and 6.30, the exponential of the unity operator is given by

$$\exp\{\widehat{1}\} = e \times \widehat{1}$$

and the exponential of the null operator is equal to the unity operator:

$$\exp\{\widehat{0}\} = \widehat{1}$$

6.5.4 Products of exponential operators

In the mathematics of ordinary numbers, the following equation is always valid: $\exp\{a+b\} = \exp\{a\}\exp\{b\} = \exp\{b\}\exp\{a\}$. The analogous property is true for *commuting operators*:

$$\boxed{\exp\{\widehat{A}+\widehat{B}\} = \exp\{\widehat{A}\}\exp\{\widehat{B}\} = \exp\{\widehat{B}\}\exp\{\widehat{A}\} \qquad \text{if} \quad \left[\widehat{A},\widehat{B}\right] = 0} \tag{6.32}$$

If the operators $\widehat{A}$ and $\widehat{B}$ do not commute, then there is no general result for $\exp\{\widehat{A}+\widehat{B}\}$. However, if the non-commuting operators are both *small*, then an *approximate* formula for the exponential of their sum does exist (see Equation 6.35).

6.5.5 Inverses of exponential operators

The inverse of an exponential operator is produced simply by changing the sign of the exponent:

$$\exp\{\widehat{A}\}^{-1} = \exp\{-\widehat{A}\}$$

This is easily proved by using Equation 6.32 and the fact that any operator commutes with itself:

$$\exp\{\widehat{A}\}\exp\{-\widehat{A}\} = \exp\{\widehat{A}-\widehat{A}\} = \exp\{\widehat{0}\} = \widehat{1}$$

6.5.6 Complex exponentials of operators

The *complex exponential* of an operator has a straightforward meaning:

$$\boxed{\exp\{\mathrm{i}\widehat{Q}\} = \widehat{1} + \mathrm{i}\widehat{Q} + \frac{\mathrm{i}^2}{2!}\widehat{Q}^2 + \frac{\mathrm{i}^3}{3!}\widehat{Q}^3 + \ldots} \tag{6.33}$$

The complex exponential of a hermitian operator is unitary:

$$\exp\{\mathrm{i}\widehat{Q}\}^\dagger = \exp\{(\mathrm{i}\widehat{Q})^\dagger\} = \exp\{(\mathrm{i}^*)(\widehat{Q}^\dagger)\} = \exp\{(-\mathrm{i})\widehat{Q}\} = \exp\{\mathrm{i}\widehat{Q}\}^{-1}$$

6.5.7 Exponentials of small operators

If an operator $\widehat{A}$ is *small*,[2] then the exponential may be approximated thus:

$$\exp\{\widehat{A}\} \cong \widehat{1} + \widehat{A} \tag{6.34}$$

It follows that the product of exponentials of two *small* operators may be written as

$$\boxed{\exp\{\widehat{A}\}\exp\{\widehat{B}\} \cong \exp\{\widehat{B}\}\exp\{\widehat{A}\} \cong \exp\{\widehat{B}+\widehat{A}\}} \tag{6.35}$$

Note that this property only applies to *general* operators if the operators commute (see Section 6.5.4).

6.5.8 Matrix representations of exponential operators

Suppose that an operator $\widehat{A}$ has a matrix representation $\mathbf{A}$. What is the matrix representation of $\exp\{\widehat{A}\}$?

If $\mathbf{A}$ is diagonal, then the result is very simple. The matrix representation of $\widehat{A}$ is also diagonal and the diagonal elements are simply the exponentials of the original matrix elements. For example, if

$$\mathbf{A} = \begin{pmatrix} a_1 & 0 & 0 & \ldots \\ 0 & a_2 & 0 & \ldots \\ 0 & 0 & a_3 & \ldots \\ \vdots & \vdots & \vdots & \ddots \end{pmatrix}$$

then

$$\exp\{\mathbf{A}\} = \begin{pmatrix} \exp\{a_1\} & 0 & 0 & \ldots \\ 0 & \exp\{a_2\} & 0 & \ldots \\ 0 & 0 & \exp\{a_3\} & \ldots \\ \vdots & \vdots & \vdots & \ddots \end{pmatrix} \tag{6.36}$$

⚠ Note that one cannot derive $\exp\{\mathbf{A}\}$ from $\mathbf{A}$ by taking the exponentials of *each* element (remember that $\exp\{0\} = 1$!).

If $\mathbf{A}$ is *not* diagonal, then the route to the matrix $\exp\{\mathbf{A}\}$ leads through *diagonalization* (see Section 6.4): suppose that matrix $\mathbf{A}$ is diagonalized, so that the matrices $\mathbf{X}$ and $\mathbf{D}$ solving the following equation are known:

$$\mathbf{A} = \mathbf{X}\mathbf{D}\mathbf{X}^{-1}$$

The matrix representation of the exponential operator may be calculated through the following equation:

$$\boxed{\exp\{\mathbf{A}\} = \mathbf{X}\exp\{\mathbf{D}\}\mathbf{X}^{-1} \qquad (6.37)}$$

Since $\mathbf{D}$ is diagonal, the matrix $\exp\{\mathbf{D}\}$ is readily calculated through Equation 6.36.

6.6 Cyclic Commutation

6.6.1 Definition of cyclic commutation

Consider the three operators $\widehat{A}$, $\widehat{B}$ and $\widehat{C}$, which obey the following three commutation relationships:

$$\begin{aligned} \left[\widehat{A}, \widehat{B}\right] &= \mathrm{i}\widehat{C} \\ \left[\widehat{C}, \widehat{A}\right] &= \mathrm{i}\widehat{B} \\ \left[\widehat{B}, \widehat{C}\right] &= \mathrm{i}\widehat{A} \end{aligned} \tag{6.38}$$

This is called a *cyclic commutation* relationship, since the three relationships may be generated from each other by permuting the operators in a cyclic fashion, i.e.

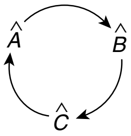

Figure 6.3
Cyclic permutation of three operators.

Cyclic commutation is very important in the theory of NMR, and a special symbol ↻ is now introduced for it. The following single expression implies *all three* relationships in Equation 6.38:

$$\left[\widehat{A}, \widehat{B}\right] = \mathrm{i}\widehat{C} \qquad \circlearrowright \tag{6.39}$$

6.6.2 Sandwich formula

If the three operators $\widehat{A}$, $\widehat{B}$ and $\widehat{C}$ cyclically commute, then the following *sandwich formula* applies:

$$\exp\{-\mathrm{i}\theta\widehat{A}\}\widehat{B}\exp\{+\mathrm{i}\theta\widehat{A}\} = \widehat{B}\cos\theta + \widehat{C}\sin\theta \qquad \circlearrowright \tag{6.40}$$

Geometrically, this result may be depicted as the ‘rotation’ of an operator $\widehat{B}$ ‘by’ an operator $\widehat{A}$, through an angle θ:

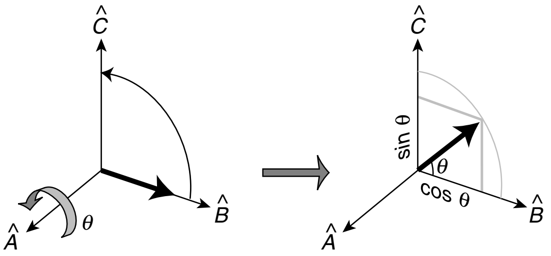

Figure 6.4
Geometrical representation of the sandwich formula (Equation 6.40).

This relationship provides a fundamental link between cyclic commutation and the geometry of rotations. It is of fundamental importance to the geometrical description of nuclear spin dynamics. A proof is given in Appendix A.2.

The symbol ↻ in Equation 6.40 indicates that the operators may be cyclically permuted $\widehat{A} \to \widehat{B} \to \widehat{C} \to \widehat{A} \ldots$. By doing this one gets two more relationships:

$$\exp\{-\mathrm{i}\theta\widehat{B}\}\widehat{C}\exp\{+\mathrm{i}\theta\widehat{B}\} = \widehat{C}\cos\theta + \widehat{A}\sin\theta \tag{6.41}$$

and

$$\exp\{-\mathrm{i}\theta\widehat{C}\}\widehat{A}\exp\{+\mathrm{i}\theta\widehat{C}\} = \widehat{A}\cos\theta + \widehat{B}\sin\theta \tag{6.42}$$

which have the following geometrical interpretation:

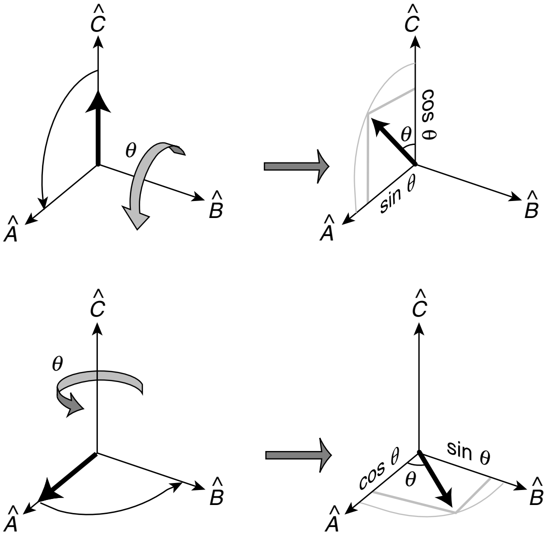

Figure 6.5
Geometrical representation of Equations 6.41 and 6.42.

What happens if the operator $\widehat{A}$ is rotated by $\widehat{B}$? One can figure this out by rearranging the cyclic commutation relationship as follows:

$$\begin{aligned}\left[\widehat{A}, \widehat{B}\right] &= \mathrm{i}\widehat{C} \qquad \circlearrowleft \\ -\left[\widehat{B}, \widehat{A}\right] &= \mathrm{i}\widehat{C} \qquad \circlearrowleft \\ \left[(-\widehat{B}), \widehat{A}\right] &= \mathrm{i}\widehat{C} \qquad \circlearrowleft \end{aligned} \tag{6.43}$$

This implies that

$$\begin{aligned}\exp\{-\mathrm{i}\theta\widehat{B}\}\widehat{A}\exp\{+\mathrm{i}\theta\widehat{B}\} &= \exp\{-\mathrm{i}(-\theta)(-\widehat{B})\}\widehat{A}\exp\{+\mathrm{i}(-\theta)(-\widehat{B})\} \\ &= \widehat{A}\cos(-\theta) + \widehat{C}\sin(-\theta) \\ &= \widehat{A}\cos\theta - \widehat{C}\sin\theta \qquad \circlearrowleft \end{aligned} \tag{6.44}$$

which has the following geometric interpretation:

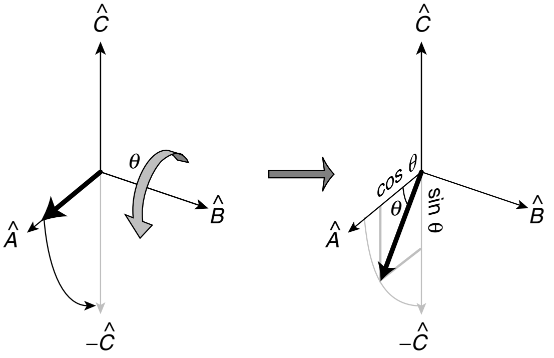

Figure 6.6
Geometrical representation of Equation 6.44.

Note that the rotation goes towards the negative axis this time.

By cyclically permuting Equation 6.44, one gets two more sandwich relationships:

$$\exp\{-\mathrm{i}\theta\widehat{C}\}\widehat{B}\exp\{+\mathrm{i}\theta\widehat{C}\} = \widehat{B}\cos\theta - \widehat{A}\sin\theta$$

$$\exp\{-\mathrm{i}\theta\widehat{A}\}\widehat{C}\exp\{+\mathrm{i}\theta\widehat{A}\} = \widehat{C}\cos\theta - \widehat{B}\sin\theta$$

Notes

1. The term 'eigen' is a German word meaning 'own' or 'characteristic'.

2. An operator is 'small' if the largest and the smallest eigenvalues differ by much less than 1.

Further Reading

- For a good introduction to the mathematics of complex numbers and matrices, see E. Steiner, *The Chemistry Maths Book*, Oxford University Press, Oxford, 1996.
- For a good textbook on matrices and linear algebra, see G. Strang, *Linear Algebra and its Applications*, 3rd edition, Harcourt Brace Jovanovich, San Diego, 1988.

Exercises

6.1 (i) Prove that the functions $\psi_n(x)$ in Equation 6.1 are normalized.
(ii) Prove that the function $f(x)$ in Equation 6.7 is normalized.
(iii) What value of N normalizes the following function?

$$g(x) = \begin{cases} 0 & \text{if } x < 0 \\ N\sin^3(\pi x) & \text{if } 0 \le x \le 1 \\ 0 & \text{if } 1 < x \end{cases}$$

6.2 Prove that the functions $\psi_n(x)$ in Equation 6.1 are orthogonal.

6.3 Evaluate the commutator $\left[\hat{x}, \widehat{D}_x^2\right]$, by using the same technique as in Equation 6.10.

6.4 Derive the matrix elements listed in Equation 6.12.

6.5 Derive the first row of the matrix representation in Equation 6.14.

6.6 (i) Prove that the eigenvalues of Hermitian operators are real.
(ii) Prove that non-degenerate eigenvectors of Hermitian operators are orthogonal.

7 Review of Quantum Mechanics

Quantum mechanics provides three major theoretical tools: (1) a mathematical tool for describing the *state* of the particle, at any moment of time; (2) a mathematical tool for predicting how the state of the particle changes in time and space (the *equation of motion*); (3) a set of rules for predicting the results of experimental *observations*.

These rules are essentially postulates that are justified by comparing predictions with experimental results. In 2007, there were no verified discrepancies between quantum theory and experimental results.

7.1 Spinless Quantum Mechanics

Consider a single quantum particle, able to move in one spatial direction, specified by the coordinate x. For now, we assume that the particle has no spin.

7.1.1 The state of the particle

In spinless quantum mechanics, the state of the particle is described by a continuous function of space, denoted $\psi(x, t)$ in the case of a single spatial coordinate x. This *wavefunction* (or *state function*) is, in general, complex, i.e. $\psi(x, t) \neq \psi(x, t)^*$.

The wavefunction is indexed with the parameter t to emphasize the fact that the wavefunction is, in general, time dependent. The wavefunction may be visualized as a wave, moving through time and space:

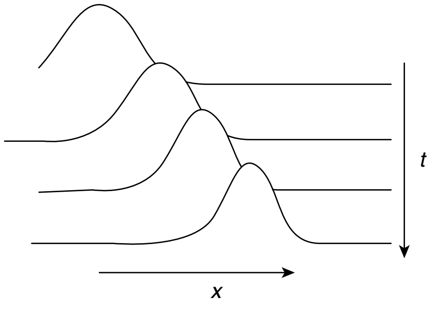

Figure 7.1
A moving wavefunction.

The wavefunction of the particle is *normalized*:

$$\int_{-\infty}^{\infty} \mathrm{d}x\, \psi(x, t)^* \psi(x, t) = 1 \qquad \text{(normalization)} \tag{7.1}$$

Spin Dynamics: Basics of Nuclear Magnetic Resonance, Second Edition Malcolm H. Levitt

7.1.2 The equation of motion

The equation of motion of the wavefunction is given by the following:

$$\frac{\mathrm{d}}{\mathrm{d}t}\psi(x,t) = -\mathrm{i}\hbar^{-1}\widehat{\mathrm{H}}\psi(x,t) \tag{7.2}$$

which is known as the *time-dependent Schrödinger equation*. The constant $\hbar$ (pronounced "h-bar") is given by

$$\hbar = \frac{h}{2\pi} \tag{7.3}$$

where h is Planck's constant. The numerical value is $\hbar = 1.054 \times 10^{-34}\,\mathrm{J\,s}$.

The symbol $\widehat{\mathrm{H}}$ signifies a special operator, known as the *Hamiltonian*. The Hamiltonian is a hermitian operator, given by

$$\widehat{\mathrm{H}} = \widehat{\mathrm{V}} + \widehat{\mathrm{K}} \tag{7.4}$$

where $\widehat{\mathrm{V}}$ is the *potential energy operator* and $\widehat{\mathrm{K}}$ is the *kinetic energy operator*.

The potential energy operator $\widehat{\mathrm{V}}$ depends on the forces acting on the particle. For the case of a particle confined to an infinitely deep square 'potential well', with edges at $x = 0$ and $x = 1$, the potential energy operator is given by

$$\widehat{\mathrm{V}} = \begin{cases} \infty & \text{if } x < 0 \\ 0 & \text{if } 0 \leq x \leq 1 \\ \infty & \text{if } 1 < x \end{cases}$$

The infinite potential energy outside the box has the effect of confining the particle completely to the interior of the box. Situations involving more realistic potential energy operators are treated in many texts (see *Further Reading*) and are not discussed further here.

In one-dimensional quantum mechanics, the kinetic energy operator is proportional to the second derivative operator, divided by the mass of the particle m:

$$\widehat{\mathrm{K}} = -(\hbar^2/2m)\widehat{D}_x^2 \tag{7.5}$$

In the case of the one-dimensional square well, there is no potential energy inside the box, so the Hamiltonian $\widehat{\mathrm{H}}$ is equal to the kinetic energy operator.

Knowledge of the Hamiltonian allows one to specify the equation of motion (Equation 7.2). In principle, this equation of motion may be solved to predict all future quantum states of the particle, if the initial state is known.

7.1.3 Experimental observations

Quantum mechanics provides a procedure for predicting the results of experimental observations – or, more precisely, for predicting the *probabilities* of obtaining particular results. This distinction is important. Quantum mechanics states that, in some circumstances, it is *fundamentally impossible* to predict the result of even highly controlled experiments. Only the *probabilities* may be predicted. This is one of the most counter-intuitive and controversial aspects of quantum mechanics, which is nevertheless in full agreement with all known experimental results.

In quantum mechanics, each experimental observation is associated with a hermitian operator. For example, the measurement of the position of a particle along the x-axis is associated with the operator $\hat{x}$.

According to quantum mechanics, there are several *possible* results of any experimental observation, which correspond to the *eigenvalues of the observable operator*. For example, an observation of the position of a particle can only lead to a result that is an eigenvalue of the observable $\hat{x}$. In general, there are many such eigenvalues and, hence, many possible results of a given observation.

Can one specify the answer more precisely? Which of the many possible eigenvalues is actually chosen when an observation is made? Remarkably, quantum mechanics does not make any definite commitment about this. It only gives a formula for the *probability* of getting a particular eigenvalue. If the quantum state is $|\psi\rangle$ and the observable operator is $\widehat{Q}$, then the probability of obtaining the result q_n is given by

$$\boxed{\mathtt{P}(q_n) = |\langle n|\psi\rangle|^2 \qquad (7.6)}$$

where $|n\rangle$ is the eigenstate of $\widehat{Q}$ with eigenvalue q_n, i.e.

$$\widehat{Q}|n\rangle = q_n|n\rangle$$

The probability of getting a particular result q_n is equal to 1 only if the system is in the corresponding eigenstate, i.e. $|\psi\rangle = |n\rangle$. In this case, the result is certain: the same experiment always gives the same result, namely q_n. In all other cases, the results of observations only follow statistical laws and the result of an individual experiment is fundamentally unpredictable.

Although quantum mechanics is non-committal about the result of *single* observations, it does give a definite formula for the *average* result of *very many* observations. This is called the *expectation value*, equal to the matrix element

$$\boxed{\langle\widehat{Q}\rangle = \langle\psi|\widehat{Q}|\psi\rangle \qquad (7.7)}$$

where $\widehat{Q}$ is the observable operator. The implications for nuclear spins are explored in Chapter 10.

7.2 Energy Levels

Since the Hamiltonian is hermitian, its eigenstates are orthogonal and its eigenvalues are real. The Hamiltonian eigenstates and eigenvalues play a very important role in the behaviour of quantum systems and have special names. The Hamiltonian eigenvalues are called the *energy levels* of the quantum system, and the Hamiltonian eigenstates are called the *stationary states* of the system or, equivalently, the *energy eigenstates*.

It is customary to draw an energy level diagram of the system, in which the Hamiltonian eigenvalues are represented by horizontal lines. For example, a 'particle in a one-dimensional box' has a set of Hamiltonian eigenstates that are equal to the functions $|n\rangle = \psi_n(x)$ defined in Equation 6.1:

$$\boxed{\widehat{\mathrm{H}}|n\rangle = E_n|n\rangle \qquad (7.8)}$$

Here, E_n is the energy of the state $|n\rangle$, given by

$$E_n = \frac{\pi^2 n^2 \hbar^2}{2mL^2}$$

where L is the length of the box ($L = 1$ in the current case).

Equation 7.8 is known as the *time-independent Schrödinger equation*. The diagram below shows the first few energy levels E_n, and the corresponding stationary wavefunctions $|n\rangle$, for the particle in a box:

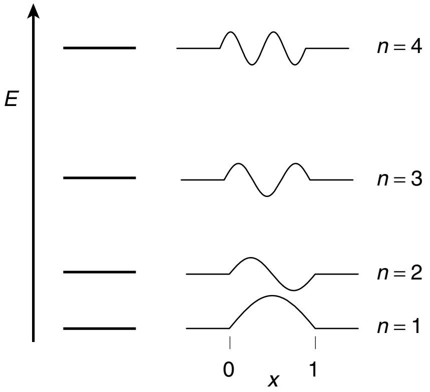

Figure 7.2
Energy levels for a particle in a box and the corresponding wavefunctions.

7.3 Natural Units

The factor $\hbar^{-1}$ in Equation 7.2 is inconvenient. It may be removed by defining a 'Hamiltonian in natural units' $\widehat{\mathcal{H}}$ as follows:

$$\widehat{\mathcal{H}} = \hbar^{-1}\widehat{\mathrm{H}} \tag{7.9}$$

The Schrödinger equation then reads

$$\boxed{\frac{\mathrm{d}}{\mathrm{d}t}\psi(x,t) = -\mathrm{i}\widehat{\mathcal{H}}\psi(x,t)} \tag{7.10}$$

which proves to be more convenient to handle.

The Hamiltonians $\widehat{\mathcal{H}}$ and $\widehat{\mathrm{H}}$ have the same eigenfunctions:

$$\widehat{\mathcal{H}}|n\rangle = \omega_n|n\rangle$$

The eigenvalues of $\widehat{\mathcal{H}}$ are denoted ω_n, and are given by

$$\omega_n = \hbar^{-1}E_n$$

The eigenvalues ω_n, therefore, are the energies of the states $|n\rangle$, in units of $\hbar$. For the particle in a one-dimensional box, the energies ω_n are given by

$$\omega_n = \frac{\pi^2 n^2 \hbar}{2m}$$

From now on, natural units are used consistently. Energies in natural units are denoted by the symbol ω, to emphasize that they have the dimensions of frequency (s^{-1}). The energies may be converted into SI units (joules) by multiplication with the factor $\hbar$.

7.4 Superposition States and Stationary States

It is sometimes stated that the only 'allowed' states of a quantum system are the energy eigenstates, and that the system moves between these allowed states by discontinuous transitions ('quantum jumps'). These statements are incorrect. In fact, *any* state of the form

$$|f\rangle = f_1|1\rangle + f_2|2\rangle + f_3|3\rangle + \ldots$$

is a valid quantum state, providing that all of $\{|1\rangle, |2\rangle \ldots\}$ are energy eigenstates and that the total state $|f\rangle$ is normalized (Equation 6.2).

Superposition states are of fundamental importance in the theory of NMR, and they are discussed at length in the following chapters.

What is the significance of the energy eigenstates $|n\rangle$, given that they are not the only 'allowed' states?

The answer is that the energy eigenstates are the only states that are *stationary*. This means that if the system is prepared in an energy eigenstate, then it remains in that eigenstate and does not change into some other state, as long as the Hamiltonian does not change.

This may be seen as follows. Suppose that the state of the system is described at some time t by the state vector $|\psi\rangle(t)$. The Schrödinger equation for the system is

$$\frac{\mathrm{d}}{\mathrm{d}t}|\psi\rangle(t) = -\mathrm{i}\widehat{\mathcal{H}}|\psi\rangle(t)$$

If the Hamiltonian $\widehat{\mathcal{H}}$ is time independent, then this is a first-order differential equation and is easily solved. The solution is

$$|\psi\rangle(t) = \exp\{-\mathrm{i}\widehat{\mathcal{H}}t\}|\psi\rangle(0) \tag{7.11}$$

where the exponential operator should be interpreted as in Section 6.5 and where $|\psi\rangle(0)$ is the state of the system at time $t = 0$. Now suppose that the system is in an energy eigenstate at time $t = 0$:

$$|\psi\rangle(0) = |n\rangle$$

From Section 6.5, this state is an eigenstate of the exponential operator $\exp\{-\mathrm{i}\widehat{\mathcal{H}}t\}$:

$$\exp\{-\mathrm{i}\widehat{\mathcal{H}}t\}|n\rangle = \exp\{-\mathrm{i}\omega_n t\}|n\rangle$$

It follows that the state of the system at time t is given by

$$|\psi\rangle(t) = \exp\{-\mathrm{i}\omega_n t\}|\psi\rangle(0)$$

The system, therefore, remains in the same state, multiplied by a complex time-dependent number, called a *phase factor*. As discussed in Chapter 10, this phase factor may often be ignored, for most purposes. The important thing is that the state $|n\rangle$ does not evolve into a mixture of states with different quantum numbers.

This simple relationship between the initial and final states only applies if the system is initially in an energy eigenstate. For this reason, the energy eigenstates are said to be *stationary*. As time goes on, each stationary state $|n\rangle$ acquires a complex phase factor $\exp\{-\mathrm{i}\omega_n t\}$, but does not mix with the other states.

The stationary states of a quantum system have a clear relationship with the 'normal modes' of a vibrating molecule, or the 'standing wave patterns' in a guitar string or an organ pipe. They represent conserved patterns of motion, which persist over a substantial length of time.

7.5 Conservation Laws

The following general theorem is important:

> If an operator $\widehat{Q}$ commutes with the Hamiltonian $\widehat{\mathcal{H}}$, and the Hamiltonian is independent of time, then the expectation value of $\widehat{Q}$ is also independent of time. The expectation value $\langle\widehat{Q}\rangle$ is said to be *conserved*.

This theorem is easily proved from the formula for the expectation value:

$$\langle\widehat{Q}\rangle(t) = \langle\psi|(t)\ \widehat{Q}\ |\psi\rangle(t)$$

The wavefunction evolves in time as given in Equation 7.11:

$$|\psi\rangle(t) = \exp\{-\mathrm{i}\widehat{\mathcal{H}}t\}|\psi\rangle(0)$$

The adjoint of this equation may be taken as follows:

$$\begin{aligned}\langle\psi|(t) &= \left\{|\psi\rangle(t)\right\}^{\dagger} = \left\{\exp\{-\mathrm{i}\widehat{\mathcal{H}}t\}|\psi\rangle(0)\right\}^{\dagger} = \langle\psi|(0)\left\{\exp\{-\mathrm{i}\widehat{\mathcal{H}}t\}\right\}^{\dagger}\\ &= \langle\psi|(0)\exp\{+\mathrm{i}\widehat{\mathcal{H}}^{\dagger}t\} = \langle\psi|(0)\exp\{+\mathrm{i}\widehat{\mathcal{H}}t\}\end{aligned}$$

Note that the adjoint involves taking complex conjugates as well as reversing the order of multiplication. The last identity exploits the fact that the Hamiltonian is hermitian.

The expectation value is therefore given by

$$\langle\widehat{Q}\rangle(t) = \langle\psi|(0)\exp\{+\mathrm{i}\widehat{\mathcal{H}}t\}\widehat{Q}\exp\{-\mathrm{i}\widehat{\mathcal{H}}t\}|\psi\rangle(0)$$

If $\widehat{\mathcal{H}}$ and $\widehat{Q}$ commute, then $\widehat{\mathcal{H}}\widehat{Q} = \widehat{Q}\widehat{\mathcal{H}}$, and it is easily shown that

$$\exp\{+\mathrm{i}\widehat{\mathcal{H}}t\}\widehat{Q}\exp\{-\mathrm{i}\widehat{\mathcal{H}}t\} = \widehat{Q}$$

and hence

$$\langle\widehat{Q}\rangle(t) = \langle\psi|(0)\ \widehat{Q}\ |\psi\rangle(0) = \langle\widehat{Q}\rangle(0)$$

It follows that the expectation value of $\widehat{Q}$ is *conserved*.

A trivial example of this theorem is when the operator $\widehat{Q}$ is equal to the Hamiltonian $\widehat{\mathcal{H}}$. Since the expectation value of $\widehat{\mathcal{H}}$ is the energy of the system, the above theorem states that the energy of the system is conserved (first law of thermodynamics).

7.6 Angular Momentum

Consider now the quantum mechanics of systems that are free to *rotate* in three-dimensional space, e.g. a molecule floating freely in a vacuum, or an electron circling around a positive central charge, as in the hydrogen atom:

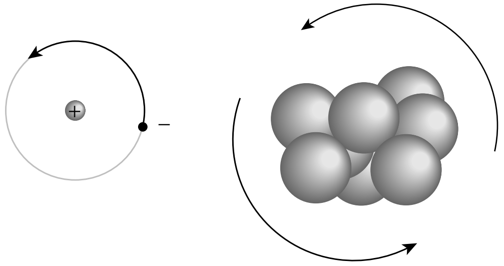

Figure 7.3
Two rotating objects.

The quantum state of a particle moving in three-dimensional space is a function of all three spatial coordinates, as well as the time coordinate, i.e. $\psi = \psi(x, y, z, t)$.

7.6.1 Angular momentum operators

Quantum mechanical theory attaches great importance to the *angular momentum operators* of a rotating object. There are three such operators, representing the angular momentum components along the three Cartesian axes, as follows:

$$\begin{aligned}
\hat{l}_x &= -\mathrm{i}(\hat{y}\hat{D}_z - \hat{z}\hat{D}_y)\\
\hat{l}_y &= -\mathrm{i}(\hat{z}\widehat{D}_x - \hat{x}\hat{D}_z)\\
\hat{l}_z &= -\mathrm{i}(\hat{x}\hat{D}_y - \hat{y}\widehat{D}_x)
\end{aligned} \tag{7.12}$$

The operators $\hat{x}$, $\hat{y}$ and $\hat{z}$ multiply the operand by the spatial coordinate, e.g.

$$\hat{x}\psi(x, y, z, t) = x\psi(x, y, z, t)$$

The operators $\widehat{D}_x$, $\hat{D}_y$ and $\hat{D}_z$ take the partial derivative with respect to one of the spatial coordinates, keeping the other coordinates fixed; for example:

$$\widehat{D}_x\psi(x, y, z, t) = \frac{\partial}{\partial x}\psi(x, y, z, t)$$

The definitions in Equation 7.12 provide the angular momentum operators in 'natural units' of $\hbar$: the right-hand sides should be multiplied by $\hbar$ to obtain the expressions in SI units.

The angular momentum operators are hermitian.

It may be shown (see *Further Reading*) that the three angular momentum operators obey the cyclic commutation relationships, defined in Equation 6.38:

$$\boxed{\left[\hat{l}_x, \hat{l}_y\right] = \mathrm{i}\hat{l}_z \qquad \circlearrowleft} \tag{7.13}$$

7.6.2 Rotation operators

The complex exponentials of angular momentum operators are called *rotation operators*. The rotation operators around the three Cartesian axes are denoted as follows:

$$
\begin{aligned}
\widehat{R}_x(\beta) &= \exp\{-\mathrm{i}\beta\hat{I}_x\} \\
\widehat{R}_y(\beta) &= \exp\{-\mathrm{i}\beta\hat{I}_y\} \\
\widehat{R}_z(\beta) &= \exp\{-\mathrm{i}\beta\hat{I}_z\}
\end{aligned}
\tag{7.14}
$$

Here, β denotes the rotation angle. For example, the operator $\widehat{R}_x(\pi/2)$ performs a rotation through the angle $\pi/2$ about the x-axis:

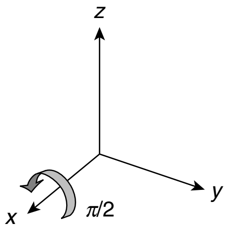

Figure 7.4
A rotation by $\pi/2$ about the x-axis.

The operator $\widehat{R}_y(\pi)$ performs a rotation through the angle π about the y-axis:

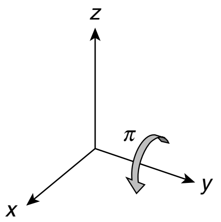

Figure 7.5
A rotation by π about the y-axis.

Note that the formulae for the rotation operators in Equation 7.14 involve a negative sign. The operator for a *positive* rotation about the x-axis through the angle β is equal to $\exp\{-\mathrm{i}\beta\hat{I}_x\}$.

The inverse of a rotation through the angle β is a rotation through the angle $-\beta$, about the same axis; for example:

$$\widehat{R}_x(\beta)\widehat{R}_x(-\beta) = \widehat{R}_x(-\beta)\widehat{R}_x(\beta) = \widehat{1}$$

Since the angular momentum operators are hermitian, the rotation operators are *unitary*:

$$\widehat{R}_x(\beta)^\dagger = \widehat{R}_x(\beta)^{-1} = \widehat{R}_x(-\beta)$$

A rotation operator commutes with the angular momentum operator about the same axis; for example:

$$\widehat{R}_x(\beta)\hat{I}_x = \hat{I}_x\widehat{R}_x(\beta)$$

This implies the following sandwich relationship:

$$\widehat{R}_x(\beta)\hat{I}_x\widehat{R}_x(-\beta) = \hat{I}_x$$

Geometrically, this corresponds to the fact that a rotation of a vector about its own axis does nothing:

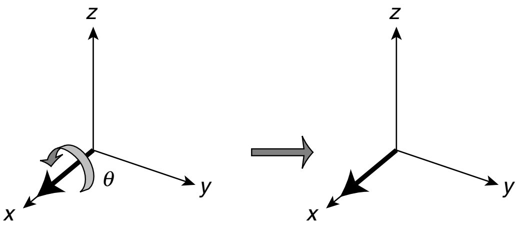

Figure 7.6
Rotation of a vector along the *x*-axis about the *x*-axis.

When a rotation operator is applied to the angular momentum about a different axis, the sandwich relationship reads

$$\widehat{R}_x(\beta)\hat{I}_y\widehat{R}_x(-\beta) = \hat{I}_y \cos\beta + \hat{I}_z \sin\beta$$

which follows from the cyclic commutation of the angular momentum operators. The equation above has the following geometric interpretation:

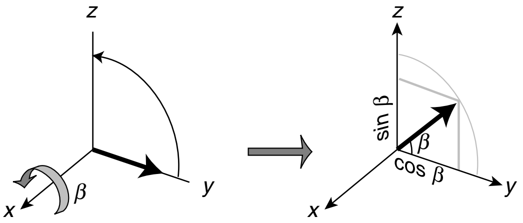

Figure 7.7
Rotation of a vector along the *y*-axis about the *x*-axis.

7.6.3 Rotation sandwiches

As shown in Appendix A.3, the sandwich relationship for angular momentum operators

$$\widehat{R}_x(\theta)\hat{I}_y\widehat{R}_x(-\theta) = \hat{I}_y \cos\theta + \hat{I}_z \sin\theta \qquad \circlearrowleft$$

implies a corresponding sandwich relationship for rotation operators:

$$\boxed{\widehat{R}_x(\theta)\widehat{R}_y(\beta)\widehat{R}_x(-\theta) = \exp\{-\mathrm{i}\beta(\hat{I}_y \cos\theta + \hat{I}_z \sin\theta)\} \qquad \circlearrowleft \qquad (7.15)}$$

where the operator on the right-hand side implies a rotation through the angle β about the axis $\mathbf{e}_y \cos\theta + \mathbf{e}_z \sin\theta$, i.e. an axis in the *yz*-plane, subtending an angle θ with respect to the *y*-axis:

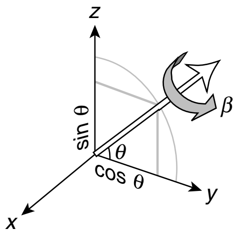

Figure 7.8
Rotation around an axis in the *yz*-plane.

A specific example of Equation 7.15 is as follows:

$$\widehat{R}_x(\pi/2)\widehat{R}_y(\beta)\widehat{R}_x(-\pi/2) = \widehat{R}_z(\beta)$$

This states that a $-\pi/2$ rotation about the x-axis, followed by a rotation through β about the y-axis, followed by a $+\pi/2$ rotation about the x-axis is the same as a rotation through β about the z-axis (Note carefully that the order of the rotations should be read from right to left.) This may be seen physically by rotating any three-dimensional shape through the sequence of rotations given on the left-hand side of the equation:

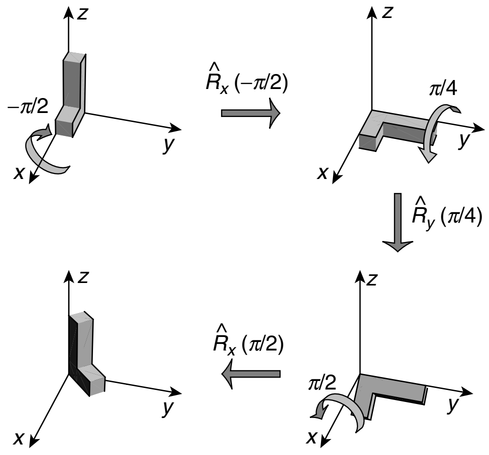

Figure 7.9
An L-shaped object undergoes a sequence of three rotations.

(This is shown for the case $\beta = \pi/4$.) The result is the same as a single rotation by $\pi/4$ around the z-axis:

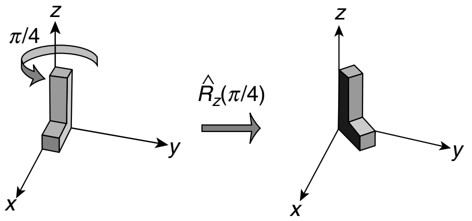

Figure 7.10
The same result is obtained by a single rotation.

Some further examples are

$$\widehat{R}_x(\pi)\widehat{R}_y(\beta)\widehat{R}_x(-\pi) = \widehat{R}_y(-\beta)$$
$$\widehat{R}_z(\pi/2)\widehat{R}_x(\beta)\widehat{R}_z(-\pi/2) = \widehat{R}_y(\beta)$$

These equations all have the form of two equal and opposite rotations bracketing another rotation about a different axis. This common motif is called a *rotation sandwich*.

7.6.4 Angular momentum eigenstates and eigenvalues

Consider now the eigenstates and eigenvalues of one of the angular momentum operators. The traditional choice is $\hat{l}_z$, although, in principle, any one of the three operators could be considered. In many textbooks (see *Further Reading*) it is shown that the eigenstates of $\hat{l}_z$ may be specified by two quantum numbers, called here ℓ and m, which take the following values:

$$\begin{aligned} \ell &= 0, 1, 2, \ldots \\ m &= -\ell,\ -\ell+1,\ -\ell+2\ \ldots\ +\ell \end{aligned} \tag{7.16}$$

The eigenstates of $\hat{l}_z$ may, therefore, be written $|\ell, m\rangle$ and obey the following eigenequation:

$$\hat{l}_z|\ell, m\rangle = m|\ell, m\rangle \tag{7.17}$$

The eigenvalue of angular momentum along the z-axis is therefore given by an integer m called the *azimuthal quantum number* or *projection quantum number*.

The permitted values of m depend on the quantum number ℓ. If $\ell = 0$, then only the value $m = 0$ is allowed. If $\ell = 1$, then there are three possible values: $m = -1$, 0 or 1. If $\ell = 2$, then there are five possible values: $m = -2, -1, 0, 1$ or 2, and so on.

The quantum number ℓ does not appear in Equation 7.17. The role of ℓ is revealed if an operator $\hat{l}^2$ is defined as follows:

$$\hat{l}^2 = \hat{l}_x^2 + \hat{l}_y^2 + \hat{l}_z^2 \tag{7.18}$$

This is called the *total square angular momentum operator*. It is shown in standard texts (see *Further Reading*) that $\hat{l}^2$ commutes with $\hat{l}_z$, and that the eigenequation for $\hat{l}^2$ is

$$\hat{l}^2|\ell, m\rangle = \ell(\ell+1)|\ell, m\rangle \tag{7.19}$$

The quantum number ℓ defines the total square angular momentum, and the quantum number m defines the angular momentum along the z-axis.

Since the operators $\hat{l}_z$ and $\hat{l}^2$ are hermitian, the set of eigenfunctions $|\ell, m\rangle$ is orthogonal. The set of functions $|\ell, m\rangle$ may, therefore, be used as a basis for matrix representations, and is called here the *Zeeman eigenbasis*.

If the eigenstates are arranged in the order $|\ell, m\rangle = |0, 0\rangle, |1, 1\rangle, |1, 0\rangle, |1, -1\rangle, |2, 2\rangle, |2, 1\rangle, |2, 0\rangle, |2, -1\rangle, |2, -2\rangle \ldots$, then the matrix representations of $\hat{l}_z$ and $\hat{l}^2$ in the Zeeman eigenbasis are

$$\hat{l}_z = \begin{pmatrix} 0 & 0 & 0 & 0 & 0 & 0 & 0 & 0 & 0 & \ldots \\ 0 & 1 & 0 & 0 & 0 & 0 & 0 & 0 & 0 & \ldots \\ 0 & 0 & 0 & 0 & 0 & 0 & 0 & 0 & 0 & \ldots \\ 0 & 0 & 0 & -1 & 0 & 0 & 0 & 0 & 0 & \ldots \\ 0 & 0 & 0 & 0 & 2 & 0 & 0 & 0 & 0 & \ldots \\ 0 & 0 & 0 & 0 & 0 & 1 & 0 & 0 & 0 & \ldots \\ 0 & 0 & 0 & 0 & 0 & 0 & 0 & 0 & 0 & \ldots \\ 0 & 0 & 0 & 0 & 0 & 0 & 0 & -1 & 0 & \ldots \\ 0 & 0 & 0 & 0 & 0 & 0 & 0 & 0 & -2 & \ldots \\ \vdots & \vdots & \vdots & \vdots & \vdots & \vdots & \vdots & \vdots & \vdots & \ddots \end{pmatrix}$$

and

$$\hat{l}^2 = \begin{pmatrix} 0 & 0 & 0 & 0 & 0 & 0 & 0 & 0 & 0 & \dots \\ 0 & 2 & 0 & 0 & 0 & 0 & 0 & 0 & 0 & \dots \\ 0 & 0 & 2 & 0 & 0 & 0 & 0 & 0 & 0 & \dots \\ 0 & 0 & 0 & 2 & 0 & 0 & 0 & 0 & 0 & \dots \\ 0 & 0 & 0 & 0 & 6 & 0 & 0 & 0 & 0 & \dots \\ 0 & 0 & 0 & 0 & 0 & 6 & 0 & 0 & 0 & \dots \\ 0 & 0 & 0 & 0 & 0 & 0 & 6 & 0 & 0 & \dots \\ 0 & 0 & 0 & 0 & 0 & 0 & 0 & 6 & 0 & \dots \\ 0 & 0 & 0 & 0 & 0 & 0 & 0 & 0 & 6 & \dots \\ \vdots & \vdots & \vdots & \vdots & \vdots & \vdots & \vdots & \vdots & \vdots & \ddots \end{pmatrix}$$

Note that both of these matrices are diagonal and that the diagonal elements reflect the eigenequations in Equations 7.17 and 7.19.

7.6.5 The angular momentum eigenstates

The eigenstates $|\ell, m\rangle$ are functions of space, called *spherical harmonics*. They may be familiar to the reader as the angular parts of the hydrogen atom orbitals. The function $|0, 0\rangle$ has a spherical symmetry and resembles the s-orbital of a hydrogen atom. The three functions $|1, 1\rangle$, $|1, 0\rangle$ and $|1, -1\rangle$ have the symmetry of the three p-orbitals. The five functions $|2, 2\rangle$, $|2, 1\rangle$, $|2, 0\rangle$, $|2, -1\rangle$ and $|2, -2\rangle$ have the symmetry of the five d-orbitals, and so on. Figure 7.11 shows a physical representation of these functions:[1]

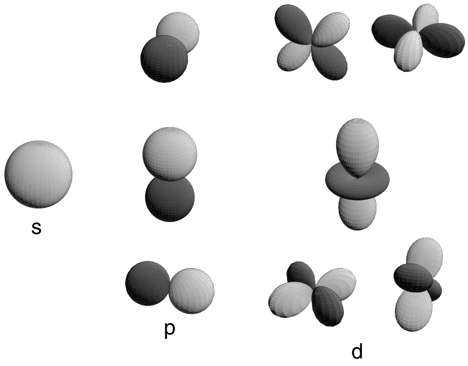

Figure 7.11
The spatial form of the angular momentum eigenfunctions. In some cases, linear combinations of the eigenfunctions have been taken, in order to remove imaginary factors (see Note 1). A negative sign is indicated by a darker colour.

The explicit forms of the angular momentum eigenfunctions are given in many quantum mechanics texts (see *Further Reading*).

7.6.6 Shift operators

The angular momentum operators $\hat{l}_x$ and $\hat{l}_y$ do not commute with $\hat{l}_z$, so their matrix representations are not diagonal in the $\hat{l}_z$ eigenbasis. In order to investigate the matrix representations of $\hat{l}_x$ and $\hat{l}_y$, it is convenient to define the *shift operators* $\hat{l}^+$ and $\hat{l}^-$ as follows:

$$\begin{aligned}\hat{l}^{+} &= \hat{l}_x + \mathrm{i}\hat{l}_y \\ \hat{l}^{-} &= \hat{l}_x - \mathrm{i}\hat{l}_y\end{aligned} \tag{7.20}$$

The shift operators have the following effect on the eigenstates of $\hat{l}_z$:

$$\begin{aligned}\hat{l}^{+}|\ell, m\rangle &= \left\{\ell(\ell+1) - m(m+1)\right\}^{1/2}|\ell, m+1\rangle \\ \hat{l}^{-}|\ell, m\rangle &= \left\{\ell(\ell+1) - m(m-1)\right\}^{1/2}|\ell, m-1\rangle\end{aligned} \tag{7.21}$$

The shift operator $\hat{l}^{+}$ increases the quantum number m by one, while leaving ℓ unchanged; the shift operator $\hat{l}^{-}$ decreases the quantum number m by one, while leaving ℓ unchanged. In both cases, the shift in quantum number m is accompanied by scaling of the quantum state by one of the fearsome-looking factors given in Equation 7.21. These factors are called *shift operator matrix elements*.

The matrix representations of the shift operators in the Zeeman eigenbasis are therefore

$$\hat{l}^{+} = \begin{pmatrix} 0 & 0 & 0 & 0 & 0 & 0 & 0 & 0 & 0 & \dots \\ 0 & 0 & \sqrt{2} & 0 & 0 & 0 & 0 & 0 & 0 & \dots \\ 0 & 0 & 0 & \sqrt{2} & 0 & 0 & 0 & 0 & 0 & \dots \\ 0 & 0 & 0 & 0 & 0 & 0 & 0 & 0 & 0 & \dots \\ 0 & 0 & 0 & 0 & 0 & 2 & 0 & 0 & 0 & \dots \\ 0 & 0 & 0 & 0 & 0 & 0 & \sqrt{6} & 0 & 0 & \dots \\ 0 & 0 & 0 & 0 & 0 & 0 & 0 & \sqrt{6} & 0 & \dots \\ 0 & 0 & 0 & 0 & 0 & 0 & 0 & 0 & 2 & \dots \\ 0 & 0 & 0 & 0 & 0 & 0 & 0 & 0 & 0 & \dots \\ \vdots & \vdots & \vdots & \vdots & \vdots & \vdots & \vdots & \vdots & \vdots & \ddots \end{pmatrix}$$

and

$$\hat{l}^{-} = \begin{pmatrix} 0 & 0 & 0 & 0 & 0 & 0 & 0 & 0 & 0 & \dots \\ 0 & 0 & 0 & 0 & 0 & 0 & 0 & 0 & 0 & \dots \\ 0 & \sqrt{2} & 0 & 0 & 0 & 0 & 0 & 0 & 0 & \dots \\ 0 & 0 & \sqrt{2} & 0 & 0 & 0 & 0 & 0 & 0 & \dots \\ 0 & 0 & 0 & 0 & 0 & 0 & 0 & 0 & 0 & \dots \\ 0 & 0 & 0 & 0 & 2 & 0 & 0 & 0 & 0 & \dots \\ 0 & 0 & 0 & 0 & 0 & \sqrt{6} & 0 & 0 & 0 & \dots \\ 0 & 0 & 0 & 0 & 0 & 0 & \sqrt{6} & 0 & 0 & \dots \\ 0 & 0 & 0 & 0 & 0 & 0 & 0 & 2 & 0 & \dots \\ \vdots & \vdots & \vdots & \vdots & \vdots & \vdots & \vdots & \vdots & \vdots & \ddots \end{pmatrix}$$

The shift operators are not hermitian. Note that the matrix elements are zero except on a line next to the diagonal.

7.6.7 Matrix representations of the angular momentum operators

The operators $\hat{l}_x$ and $\hat{l}_y$ are related to the shift operators as follows:

$$\boxed{\begin{aligned}\hat{l}_x &= \frac{1}{2}(\hat{l}^+ + \hat{l}^-) \\ \hat{l}_y &= \frac{1}{2\mathrm{i}}(\hat{l}^+ - \hat{l}^-)\end{aligned} \qquad (7.22)}$$

The matrix representations of the angular momentum operators along the x and y-axes, in the Zeeman eigenbasis, are as follows:

$$\hat{l}_x = \frac{1}{2}\begin{pmatrix} 0 & 0 & 0 & 0 & 0 & 0 & 0 & 0 & 0 & \dots \\ 0 & 0 & \sqrt{2} & 0 & 0 & 0 & 0 & 0 & 0 & \dots \\ 0 & \sqrt{2} & 0 & \sqrt{2} & 0 & 0 & 0 & 0 & 0 & \dots \\ 0 & 0 & \sqrt{2} & 0 & 0 & 0 & 0 & 0 & 0 & \dots \\ 0 & 0 & 0 & 0 & 0 & 2 & 0 & 0 & 0 & \dots \\ 0 & 0 & 0 & 0 & 2 & 0 & \sqrt{6} & 0 & 0 & \dots \\ 0 & 0 & 0 & 0 & 0 & \sqrt{6} & 0 & \sqrt{6} & 0 & \dots \\ 0 & 0 & 0 & 0 & 0 & 0 & \sqrt{6} & 0 & 2 & \dots \\ 0 & 0 & 0 & 0 & 0 & 0 & 0 & 2 & 0 & \dots \\ \vdots & \vdots & \vdots & \vdots & \vdots & \vdots & \vdots & \vdots & \vdots & \ddots \end{pmatrix} \qquad (7.23)$$

and

$$\hat{l}_y = \frac{1}{2\mathrm{i}}\begin{pmatrix} 0 & 0 & 0 & 0 & 0 & 0 & 0 & 0 & 0 & \dots \\ 0 & 0 & \sqrt{2} & 0 & 0 & 0 & 0 & 0 & 0 & \dots \\ 0 & -\sqrt{2} & 0 & \sqrt{2} & 0 & 0 & 0 & 0 & 0 & \dots \\ 0 & 0 & -\sqrt{2} & 0 & 0 & 0 & 0 & 0 & 0 & \dots \\ 0 & 0 & 0 & 0 & 0 & 2 & 0 & 0 & 0 & \dots \\ 0 & 0 & 0 & 0 & -2 & 0 & \sqrt{6} & 0 & 0 & \dots \\ 0 & 0 & 0 & 0 & 0 & -\sqrt{6} & 0 & \sqrt{6} & 0 & \dots \\ 0 & 0 & 0 & 0 & 0 & 0 & -\sqrt{6} & 0 & 2 & \dots \\ 0 & 0 & 0 & 0 & 0 & 0 & 0 & -2 & 0 & \dots \\ \vdots & \vdots & \vdots & \vdots & \vdots & \vdots & \vdots & \vdots & \vdots & \ddots \end{pmatrix} \qquad (7.24)$$

Since $\hat{l}^2$ has degenerate eigenvalues and commutes with both $\hat{l}_x$ and $\hat{l}_y$, the matrix representations given in Equations 7.23 and 7.24 are *block diagonal*, as described in Section 6.3.6. The matrix representations of $\hat{l}_x$ and $\hat{l}_y$ contain only zeros except for within the one-dimensional, three-dimensional, and five-dimensional blocks corresponding to the quantum numbers $\ell = 0, 1, 2 \ldots$:

$$\begin{pmatrix} \boxed{\bullet} & 0 & 0 & \cdots \\ 0 & \boxed{\begin{matrix} \bullet & \bullet & \bullet \\ \bullet & \bullet & \bullet \\ \bullet & \bullet & \bullet \end{matrix}} & 0 & \cdots \\ 0 & 0 & \boxed{\begin{matrix} \bullet & \bullet & \bullet & \bullet & \bullet \\ \bullet & \bullet & \bullet & \bullet & \bullet \\ \bullet & \bullet & \bullet & \bullet & \bullet \\ \bullet & \bullet & \bullet & \bullet & \bullet \\ \bullet & \bullet & \bullet & \bullet & \bullet \end{matrix}} & \cdots \\ \vdots & \vdots & \vdots & \ddots \end{pmatrix} \tag{7.25}$$

7.7 Spin

Long before the experimental demonstration of particles with spin, mathematicians had noticed the *abstract* possibility of ℓ taking *half-integer* values $1/2, 3/2 \ldots$, as well as the integer values $0, 1, 2 \ldots$ that arise from angular momentum physics, as discussed above.

For example, if ℓ is equal to $3/2$, then Equation 7.16 shows that m may take the values $m = +3/2, +1/2, -1/2$ and $-3/2$. The four states $|\ell, m\rangle = |3/2, +3/2\rangle$, $|3/2, +1/2\rangle$, $|3/2, -1/2\rangle$ and $|3/2, -3/2\rangle$ define a four-dimensional 'block', in the sense of Equation 7.25. The same cyclic commutation relationships apply as before, and the shift operators have matrix elements that conform to the standard equation, Equation 7.21.

However, there is a catch. Although half-integer spin is a fully consistent 'mathematical' possibility, it long appeared to have absolutely no relationship with the real world.[2] The 'physical' angular momentum operators defined in Equation 7.12 can *never* generate half-integer values of ℓ.

Nevertheless, there is a wealth of experimental evidence for the *existence*, and even the *prevalence*, of half-integer spin in the world of fundamental particles. The existence of half-integer spin has been forced upon scientists by the weight of experimental evidence, although it is now understood on a deeper level using relativistic quantum mechanics.

Spin is now interpreted as *intrinsic* angular momentum of the particle, completely distinct from the rotational motion described by the angular momentum operators given in Equation 7.12. Remarkably, the mathematics of spin has taken on a life of its own, released from any 'physical' framework. As long as the mathematics is consistent, there is no need to ask 'where does the angular momentum come from'.

Most of this book concerns the spin of atomic nuclei. The symbol I is used for the nuclear spin angular momentum.

7.7.1 Spin angular momentum operators

The operators for the three components of the spin angular momentum are denoted $\hat{I}_x$, $\hat{I}_y$ and $\hat{I}_z$, and have the cyclic commutation relationships

$$\boxed{\left[\hat{I}_x, \hat{I}_y\right] = \mathrm{i}\hat{I}_z \qquad \circlearrowleft} \tag{7.26}$$

If the nuclear spin quantum number is I, then the operator $\hat{I}_z$ has $2I+1$ eigenstates $|M\rangle$:

$$\hat{I}_z|I, M\rangle = M|I, M\rangle \tag{7.27}$$

The azimuthal quantum number M takes one of the $2I+1$ values:

$$M = -I,\ -I+1,\ -I+2\ \ldots\ +I \tag{7.28}$$

The shift operators $\hat{I}^+$ and $\hat{I}^-$ are defined as

$$\begin{aligned}\hat{I}^+ &= \hat{I}_x + \mathrm{i}\hat{I}_y\\ \hat{I}^- &= \hat{I}_x - \mathrm{i}\hat{I}_y\end{aligned} \tag{7.29}$$

and have the following effect on the spin states:

$$\begin{aligned}\hat{I}^+|I, M\rangle &= \left\{I(I+1) - M(M+1)\right\}^{1/2}|I, M+1\rangle\\ \hat{I}^-|I, M\rangle &= \left\{I(I+1) - M(M-1)\right\}^{1/2}|I, M-1\rangle\end{aligned} \tag{7.30}$$

7.7.2 Spin rotation operators

The spin rotation operators are given by

$$\begin{aligned}\widehat{R}_x(\beta) &= \exp\{-\mathrm{i}\beta\hat{I}_x\}\\ \widehat{R}_y(\beta) &= \exp\{-\mathrm{i}\beta\hat{I}_y\}\\ \widehat{R}_z(\beta) &= \exp\{-\mathrm{i}\beta\hat{I}_z\}\end{aligned} \tag{7.31}$$

just as in Equation 7.14.

The same sandwich relationships apply as for 'ordinary' angular momentum; for example:

$$\widehat{R}_x(\beta)\hat{I}_y\widehat{R}_x(-\beta) = \hat{I}_y\cos\beta + \hat{I}_z\sin\beta$$

and

$$\widehat{R}_x(\pi/2)\widehat{R}_y(\beta)\widehat{R}_x(-\pi/2) = \widehat{R}_z(\beta)$$

7.7.3 Spin Zeeman basis

Any spin state of a nucleus with quantum number I may be represented as a superposition of the $2I+1$ Zeeman eigenstates $|M\rangle$. One says that the Zeeman eigenstates $|M\rangle$ form a *finite basis* for the representation of the spin operators, with *dimension* $2I+1$.

The spin operators of a nucleus with quantum number I may, therefore, be represented as matrices with dimension $(2I+1)\times(2I+1)$. For example, the matrix representation of the operator $\hat{I}_x$ for a spin-3/2 nucleus, in the Zeeman eigenbasis $\{|3/2, +3/2\rangle, |3/2, +1/2\rangle, |3/2, -1/2\rangle, |3/2, -3/2\rangle\}$ is given by

$$\hat{I}_x = \frac{1}{2}\begin{pmatrix} 0 & \sqrt{3} & 0 & 0 \\ \sqrt{3} & 0 & 2 & 0 \\ 0 & 2 & 0 & \sqrt{3} \\ 0 & 0 & \sqrt{3} & 0 \end{pmatrix} \tag{7.32}$$

For 'conventional' angular momentum, it is possible to visualize the angular momentum eigenstates as spherical harmonics, spreading out in a symmetrical way in three-dimensional space. No such construction is possible for spin. The question 'apart from the mathematics, what *is* the spin state $|3/2, +1/2\rangle$?' appears to have no meaningful answer. Certainly, the spin state $|3/2, +1/2\rangle$ does not correspond to any function of spatial coordinates $\{x, y, z\}$. Remarkably, it appears to be possible to exploit and manipulate these spin states, without ever acquiring a deeper understanding of what these states 'actually are'. Maybe the spin states *are* their mathematical properties – nothing more, and nothing less.

7.7.4 Trace

The sum of diagonal matrix elements is called the *trace* of an operator:

$$\mathrm{Tr}\{\widehat{A}\} = \sum_m \langle m|\widehat{A}|m\rangle \tag{7.33}$$

The trace of an operator may only be defined for a *finite* basis.

For example, the trace of the operator $\hat{I}_x$ is equal to zero, since all diagonal elements in Equation 7.32 are equal to zero. An operator with zero trace is said to be *traceless*.

The traces of spin operators have several important properties, which will be used extensively in later sections:

1. The trace of an operator is independent of the basis, as long as the basis is orthonormal.
2. The trace of the product of two operators is independent of the order of the operators:[3]

$$\mathrm{Tr}\{\widehat{A}\widehat{B}\} = \sum_{m,n} \langle m|\widehat{A}|n\rangle\langle n|\widehat{B}|m\rangle = \sum_{m,n} \langle n|\widehat{B}|m\rangle\langle m|\widehat{A}|n\rangle = \mathrm{Tr}\{\widehat{B}\widehat{A}\}$$

3. The trace of a product of three or more operators is unchanged by a cyclic permutation of the operators:

$$\mathrm{Tr}\{\widehat{A}\widehat{B}\widehat{C}\} = \mathrm{Tr}\{\widehat{C}\widehat{A}\widehat{B}\} = \mathrm{Tr}\{\widehat{B}\widehat{C}\widehat{A}\}$$

A further useful property of the trace is as follows:

$$\mathrm{Tr}\{\widehat{A}|r\rangle\langle s|\} = \langle s|\widehat{A}|r\rangle \tag{7.34}$$

This may be seen from

$$\mathrm{Tr}\{\widehat{A}|r\rangle\langle s|\} = \sum_m \langle m|\widehat{A}|r\rangle\langle s|m\rangle = \sum_m \langle m|\widehat{A}|r\rangle\delta_{sm} = \langle s|\widehat{A}|r\rangle$$

in which δ_{sm} is the Kronecker delta (see Section 6.1.3) and $|r\rangle$, $|s\rangle$ and $|m\rangle$ are orthonormal basis functions.

7.8 Spin-1/2

Nuclei with $I = 1/2$ are particularly important in NMR, and some special notation has been developed for the eigenstates and spin operators of these nuclei.

7.8.1 Zeeman eigenstates

Spin-1/2 nuclei have two Zeeman eigenstates, for which the following special symbols are used:

$$\begin{aligned} |\alpha\rangle &= |\tfrac{1}{2},+\tfrac{1}{2}\rangle \\ |\beta\rangle &= |\tfrac{1}{2},-\tfrac{1}{2}\rangle \end{aligned} \tag{7.35}$$

The symbol β is used here to denote a spin state. Sometimes, β is used to denote an angle instead. The meaning should be clear from the context.

The result of applying the spin operators to these states is as follows:

$$\begin{aligned} \hat{I}_z|\alpha\rangle &= +\tfrac{1}{2}|\alpha\rangle & \hat{I}_z|\beta\rangle &= -\tfrac{1}{2}|\beta\rangle \\ \hat{I}^+|\alpha\rangle &= 0 & \hat{I}^+|\beta\rangle &= |\alpha\rangle \\ \hat{I}^-|\alpha\rangle &= |\beta\rangle & \hat{I}^-|\beta\rangle &= 0 \end{aligned}$$

7.8.2 Angular momentum operators

The matrix representations of the three angular momentum operators in the Zeeman eigenbasis $\{|\alpha\rangle, |\beta\rangle\}$ are

$$\hat{I}_x = \frac{1}{2}\begin{pmatrix} 0 & 1 \\ 1 & 0 \end{pmatrix} \quad \hat{I}_y = \frac{1}{2\mathrm{i}}\begin{pmatrix} 0 & 1 \\ -1 & 0 \end{pmatrix} \quad \hat{I}_z = \frac{1}{2}\begin{pmatrix} 1 & 0 \\ 0 & -1 \end{pmatrix} \tag{7.36}$$

The reader should verify the cyclic commutation relationships for these matrices (Equation 6.38).

7.8.3 Spin-1/2 rotation operators

As shown in Appendix A.4, the spin-1/2 matrix representations of the rotation operators are

$$\begin{aligned} \widehat{R}_x(\beta) &= \begin{pmatrix} \cos\frac{1}{2}\beta & -\mathrm{i}\sin\frac{1}{2}\beta \\ -\mathrm{i}\sin\frac{1}{2}\beta & \cos\frac{1}{2}\beta \end{pmatrix} \\ \widehat{R}_y(\beta) &= \begin{pmatrix} \cos\frac{1}{2}\beta & -\sin\frac{1}{2}\beta \\ \sin\frac{1}{2}\beta & \cos\frac{1}{2}\beta \end{pmatrix} \\ \widehat{R}_z(\beta) &= \begin{pmatrix} \exp\{-\mathrm{i}\frac{1}{2}\beta\} & 0 \\ 0 & \exp\{+\mathrm{i}\frac{1}{2}\beta\} \end{pmatrix} \end{aligned} \tag{7.37}$$

One should verify that these matrices obey the relevant sandwich relationships; for example:

$$\widehat{R}_x(\beta)\hat{I}_y\widehat{R}_x(-\beta) = \hat{I}_y \cos\beta + \hat{I}_z \sin\beta$$

and

$$\widehat{R}_x(\pi/2)\widehat{R}_y(\beta)\widehat{R}_x(-\pi/2) = \widehat{R}_z(\beta)$$

7.8.4 Unity operator

The unity operator for spin-1/2 has the following matrix representation:

$$\widehat{1} = \begin{pmatrix} 1 & 0 \\ 0 & 1 \end{pmatrix}$$

It is convenient to multiply the unity operator by a factor 1/2 in order to give it the same 'size' as the three angular momentum operators:

$$\frac{1}{2}\widehat{1} = \frac{1}{2}\begin{pmatrix} 1 & 0 \\ 0 & 1 \end{pmatrix} \tag{7.38}$$

7.8.5 Shift operators

The matrix representations of the shift operators have a very simple form for spins-1/2. Consider, for example, the following matrix element:

$$\langle\alpha|\hat{I}^+|\beta\rangle = \langle\frac{1}{2}, +\frac{1}{2}|\hat{I}^+|\frac{1}{2}, -\frac{1}{2}\rangle$$

Direct application of Equation 7.30 leads to a simple result:

$$\left\{\frac{1}{2}\left(\frac{1}{2}+1\right) - \left(-\frac{1}{2}\right)\left(-\frac{1}{2}+1\right)\right\}^{1/2} = \left\{\frac{3}{4}+\frac{1}{4}\right\}^{1/2} = 1$$

Repetition for all elements provides the following matrix representations of the shift operators:

$$\hat{I}^+ = \begin{pmatrix} 0 & 1 \\ 0 & 0 \end{pmatrix} \quad \hat{I}^- = \begin{pmatrix} 0 & 0 \\ 1 & 0 \end{pmatrix} \tag{7.39}$$

In the case of spins-1/2, all of the matrix elements are either 0 or 1.

7.8.6 Projection operators

The unity operator may be combined with $\hat{I}_z$ to give two new operators, denoted $\hat{I}^\alpha$ and $\hat{I}^\beta$:

$$\begin{aligned} \hat{I}^\alpha &= \frac{1}{2}\widehat{1} + \hat{I}_z \\ \hat{I}^\beta &= \frac{1}{2}\widehat{1} - \hat{I}_z \end{aligned} \tag{7.40}$$

These operators have the properties

$$\begin{aligned} \hat{I}^{\alpha}|\alpha\rangle &= |\alpha\rangle \quad \hat{I}^{\beta}|\alpha\rangle = 0 \\ \hat{I}^{\alpha}|\beta\rangle &= 0 \quad \hat{I}^{\beta}|\beta\rangle = |\beta\rangle \end{aligned}$$

Their matrix representations are as follows:

$$\hat{I}^{\alpha} = \begin{pmatrix} 1 & 0 \\ 0 & 0 \end{pmatrix} \quad \hat{I}^{\beta} = \begin{pmatrix} 0 & 0 \\ 0 & 1 \end{pmatrix} \tag{7.41}$$

The operators $\hat{I}^{\alpha}$ and $\hat{I}^{\beta}$ are called *projection operators* in this book.[4] The term *polarization operator* is also used.[5] The polarization operator matrices (Equation 7.41) and shift operator matrices (Equation 7.39) complement each other nicely.

7.8.7 Ket-bra notation

Sometimes it is convenient to notate the operators in terms of 'ket-bra' products. For spin-1/2, the shift and projection operators may be written as follows:

$$\begin{aligned} \hat{I}^{\alpha} &= |\alpha\rangle\langle\alpha| \qquad \hat{I}^{+} = |\alpha\rangle\langle\beta| \\ \hat{I}^{\beta} &= |\beta\rangle\langle\beta| \qquad \hat{I}^{-} = |\beta\rangle\langle\alpha| \end{aligned} \tag{7.42}$$

One can see how this works by applying an operator to a particular state and using the orthonormality of the states (Equation 6.6). For example, we have

$$\hat{I}^{+}|\beta\rangle = |\alpha\rangle\langle\beta|\beta\rangle = |\alpha\rangle \times 1 = |\alpha\rangle$$

and similarly for the other states and other operators.

The 'ket-bra' product $|\alpha\rangle\langle\beta|$ must be distinguished from the 'bra-ket' product $\langle\alpha|\beta\rangle$, which evaluates to zero in this case.

Using this notation, the three angular momentum operators and the half-unity operator may be written as follows:

$$\begin{aligned} \hat{I}_x &= \tfrac{1}{2}(\hat{I}^{+} + \hat{I}^{-}) = \tfrac{1}{2}(|\alpha\rangle\langle\beta| + |\beta\rangle\langle\alpha|) \\ \hat{I}_y &= \tfrac{1}{2\mathrm{i}}(\hat{I}^{+} - \hat{I}^{-}) = \tfrac{1}{2\mathrm{i}}(|\alpha\rangle\langle\beta| - |\beta\rangle\langle\alpha|) \\ \hat{I}_z &= \tfrac{1}{2}(\hat{I}^{\alpha} - \hat{I}^{\beta}) = \tfrac{1}{2}(|\alpha\rangle\langle\alpha| - |\beta\rangle\langle\beta|) \\ \tfrac{1}{2}\hat{1} &= \tfrac{1}{2}(\hat{I}^{\alpha} + \hat{I}^{\beta}) = \tfrac{1}{2}(|\alpha\rangle\langle\alpha| + |\beta\rangle\langle\beta|) \end{aligned} \tag{7.43}$$

7.9 Higher Spin

The matrix representations of the angular momentum and rotation operators for spin > 1/2 may be calculated using the general equations in Sections 7.7.1 and 7.7.2. These matrices are now given explicitly for a few important cases.

7.9.1 Spin $I = 1$

In the case of spin $I = 1$, the matrix elements of the shift operators are either 0 or $\sqrt{2}$. For example, consider the matrix element $\langle 1, +1|\hat{I}^+|1, 0\rangle$, which may be evaluated by using Equation 7.30 as follows:

$$\langle 1, +1|\hat{I}^+|1, 0\rangle = \left\{1 \times (1+1) - 0 \times (0+1)\right\}^{1/2} = 2^{1/2}$$

Repetition for all relevant elements leads to the following matrices for angular momentum along the *x*- and *y*-axes:

$$\hat{I}_x = \frac{1}{2}\begin{pmatrix} 0 & \sqrt{2} & 0 \\ \sqrt{2} & 0 & \sqrt{2} \\ 0 & \sqrt{2} & 0 \end{pmatrix} \quad \text{for } I = 1 \tag{7.44}$$

and

$$\hat{I}_y = \frac{1}{2\mathrm{i}}\begin{pmatrix} 0 & \sqrt{2} & 0 \\ -\sqrt{2} & 0 & \sqrt{2} \\ 0 & -\sqrt{2} & 0 \end{pmatrix} \quad \text{for } I = 1 \tag{7.45}$$

As usual, the matrix representation of the operator $\hat{I}_z$ is diagonal in the Zeeman basis, with the quantum numbers $M = \{1, 0, -1\}$ on the diagonal:

$$\hat{I}_z = \begin{pmatrix} +1 & 0 & 0 \\ 0 & 0 & 0 \\ 0 & 0 & -1 \end{pmatrix} \quad \text{for } I = 1 \tag{7.46}$$

The reader should verify the cyclic commutation relationships in Equation 6.38 by calculating the matrix products.

The spin-1 matrix representations for the rotation operators may be derived by using the techniques described in Section 6.5.8. The results are

$$\widehat{R}_x(\beta) = \exp\{-\mathrm{i}\beta\hat{I}_x\} = \begin{pmatrix} \cos^2(\beta/2) & -\mathrm{i}2^{-1/2}\sin\beta & -\sin^2(\beta/2) \\ -\mathrm{i}2^{-1/2}\sin\beta & \cos\beta & -\mathrm{i}2^{-1/2}\sin\beta \\ -\sin^2(\beta/2) & -\mathrm{i}2^{-1/2}\sin\beta & \cos^2(\beta/2) \end{pmatrix} \quad \text{for } I = 1 \tag{7.47}$$

$$\widehat{R}_y(\beta) = \exp\{-\mathrm{i}\beta\hat{I}_y\} = \begin{pmatrix} \cos^2(\beta/2) & -2^{-1/2}\sin\beta & \sin^2(\beta/2) \\ 2^{-1/2}\sin\beta & \cos\beta & -2^{-1/2}\sin\beta \\ \sin^2(\beta/2) & 2^{-1/2}\sin\beta & \cos^2(\beta/2) \end{pmatrix} \quad \text{for } I = 1 \tag{7.48}$$

$$\widehat{R}_z(\phi) = \exp\{-\mathrm{i}\phi\hat{I}_z\} = \begin{pmatrix} \exp\{-\mathrm{i}\phi\} & 0 & 0 \\ 0 & 1 & 0 \\ 0 & 0 & \exp\{+\mathrm{i}\phi\} \end{pmatrix} \quad \text{for } I = 1 \tag{7.49}$$

7.9.2 Spin $I = 3/2$

In the case $I = 3/2$, the non-zero matrix elements of the shift operators are equal to either 2 or $\sqrt{3}$; for example:

$$\langle 3/2, +3/2|\hat{I}^{+}|3/2, +1/2\rangle = \left\{\frac{3}{2} \times \left(\frac{3}{2}+1\right) - \frac{1}{2} \times \left(\frac{1}{2}+1\right)\right\}^{1/2} = \sqrt{3}$$

$$\langle 3/2, +1/2|\hat{I}^{+}|3/2, -1/2\rangle = \left\{\frac{3}{2} \times \left(\frac{3}{2}+1\right) - \left(-\frac{1}{2}\right) \times \left(-\frac{1}{2}+1\right)\right\}^{1/2} = 2$$

The transverse angular momentum matrices are therefore given by

$$\hat{I}_x = \frac{1}{2}\begin{pmatrix} 0 & \sqrt{3} & 0 & 0 \\ \sqrt{3} & 0 & 2 & 0 \\ 0 & 2 & 0 & \sqrt{3} \\ 0 & 0 & \sqrt{3} & 0 \end{pmatrix} \quad \text{for } I = 3/2 \tag{7.50}$$

and

$$\hat{I}_y = \frac{1}{2\mathrm{i}}\begin{pmatrix} 0 & \sqrt{3} & 0 & 0 \\ -\sqrt{3} & 0 & 2 & 0 \\ 0 & -2 & 0 & \sqrt{3} \\ 0 & 0 & -\sqrt{3} & 0 \end{pmatrix} \quad \text{for } I = 3/2 \tag{7.51}$$

The longitudinal angular momentum matrix has the eigenvalues $\{+3/2, +1/2, -1/2, -3/2\}$ along the diagonal:

$$\hat{I}_z = \frac{1}{2}\begin{pmatrix} +3 & 0 & 0 & 0 \\ 0 & +1 & 0 & 0 \\ 0 & 0 & -1 & 0 \\ 0 & 0 & 0 & -3 \end{pmatrix} \quad \text{for } I = 3/2 \tag{7.52}$$

The expressions for the spin-3/2 rotation matrices are complicated and are not given here.

7.9.3 Higher spins

The angular momentum matrices for higher spins are readily derived using the same formalism. For example, the matrix $\hat{I}_x$ for spin-5/2 is given by

$$\hat{I}_x = \frac{1}{2}\begin{pmatrix} 0 & \sqrt{5} & 0 & 0 & 0 & 0 \\ \sqrt{5} & 0 & 2\sqrt{2} & 0 & 0 & 0 \\ 0 & 2\sqrt{2} & 0 & 3 & 0 & 0 \\ 0 & 0 & 3 & 0 & 2\sqrt{2} & 0 \\ 0 & 0 & 0 & 2\sqrt{2} & 0 & \sqrt{5} \\ 0 & 0 & 0 & 0 & \sqrt{5} & 0 \end{pmatrix} \quad \text{for } I = 5/2 \tag{7.53}$$

This concludes our brief review of quantum mechanics. Further theoretical results will be introduced as they are needed.

Notes

1. The ‘balloon’ pictures in Figure 7.11 are used in many texts to represent the angular momentum eigenfunctions, and hence the angular parts of the atomic orbitals. However, it should be noted that, although they are angular momentum eigenfunctions, they do not all represent eigenfunctions of the *same* angular momentum operator. For example, the angular part of the p_z orbital (second column, centre row in Figure 7.11) is an eigenfunction of the $\hat{l}_z$ operator, with eigenvalue 0, and is the same as the ket $|1, 0\rangle$. The angular part of the p_x orbital (second column, top row in Figure 7.11), on the other hand, is an eigenfunction of the $\hat{l}_x$ operator, also with eigenvalue 0. It is a superposition of two eigenfunctions of the $\hat{l}_z$ operator, namely $|1, +1\rangle$ and $|1, -1\rangle$. The angular part of the p_y orbital (second column, lowest row in Figure 7.11) is an eigenfunction of the $\hat{l}_y$ operator, with eigenvalue 0, and is also a superposition of the $|1, +1\rangle$ and $|1, -1\rangle$ functions. The three p-orbitals sketched in Figure 7.11, therefore, are all eigenfunctions of *different* angular momentum operators. It would be difficult to draw the $\hat{l}_z$ eigenfunctions $|1, +1\rangle$ and $|1, -1\rangle$ directly, since they are complex. Similar considerations apply to the d-orbitals.

2. One of the more bizarre mathematical properties of half-integer spins is called *spinor* behaviour. Spinors have the property that they do not return to their initial state after a full 2π rotation, but instead change sign. They only return to their initial state after a 4π rotation, i.e. *two* full revolutions.

3. The matrix representations of $\hat{x}\widehat{D}_x$ and $\widehat{D}_x\hat{x}$ given in Equation 6.17 appear to contradict this. In the former case, all the diagonal elements are $-\frac{1}{2}$, whereas in the latter case all the diagonal elements are $+\frac{1}{2}$. So how can the sum of the diagonal elements be the same in both cases? This paradox may be resolved by noting that the trace is only defined for a *finite* basis. The matrix representations in Equation 6.17 are *infinite*, and do not allow a definition of the trace.

4. The justification for the term *projection operator* is as follows. Consider a spin-1/2 in an arbitrary superposition state, of the form

$$|\psi\rangle = c_\alpha|\alpha\rangle + c_\beta|\beta\rangle$$

where c_α and c_β are complex numbers. This spin state may be written as a two-dimensional vector:

$$|\psi\rangle = \begin{pmatrix} c_\alpha \\ c_\beta \end{pmatrix}$$

Application of the operator $\hat{I}^\alpha$ to this state has the following effect:

$$\hat{I}^\alpha|\psi\rangle = \begin{pmatrix} 1 & 0 \\ 0 & 0 \end{pmatrix}\begin{pmatrix} c_\alpha \\ c_\beta \end{pmatrix} = c_\alpha \begin{pmatrix} 1 \\ 0 \end{pmatrix} = c_\alpha|\alpha\rangle$$

The operator $\hat{I}^\alpha$ removes the '$|\beta\rangle$ part' of the state $|\psi\rangle$, and leaves only the '$|\alpha\rangle$ part'. Mathematically, this corresponds to a *projection* of the state $|\psi\rangle$ onto the state $|\alpha\rangle$.

5. The operators $\hat{I}^\alpha$ and $\hat{I}^\beta$ are often referred to as *polarization operators*, but this is rather misleading. The polarization of the spin along a particular axis is associated with the *angular momentum operator* along that axis, not with the $\hat{I}^\alpha$ or $\hat{I}^\beta$ operators.

Further Reading

- Some recommended quantum mechanics textbooks include the following: J. J. Sakurai, *Modern Quantum Mechanics*, Addison-Wesley, 1994; P. W. Atkins, *Molecular Quantum Mechanics*, Oxford University Press, Oxford, 1983; C. Cohen-Tannoudji, B. Diu and F. Laloë, *Quantum Mechanics*, Wiley, London, 1977; E. Merzbacher, *Quantum Mechanics*, 3rd edition, Wiley, New York, 1998.
- For the quantum theory of angular momentum, see the textbooks above and also W. J. Thompson, *Angular Momentum*, Wiley, New York, 1994.
- For an accessible article describing the origin of spin-1/2, see N. Zumbulyadis, *Concepts Magn. Reson.* **3**, 89 (1991).
- The following book is recommended to the more advanced reader as a useful compilation of formulae relating to the quantum mechanics of angular momentum: D. A. Varshalovich, A. N. Moskalev and V. K. Kheronskii, *Quantum Theory of Angular Momentum*, World Scientific, Singapore, 1988.

Exercises

7.1 The following three operators have a cyclic commutation relationship (in the case of spins-1/2):

$$\left[2\hat{I}_{1x}\hat{I}_{2y}, 2\hat{I}_{1x}\hat{I}_{2z}\right] = \mathrm{i}\hat{I}_{2x} \qquad \circlearrowleft \tag{7.54}$$

(i) Write down explicitly the three commutation relationships implied by Equation 7.54.
(ii) Evaluate the following expression:

$$\exp\{-\mathrm{i}\theta 2\hat{I}_{1x}\hat{I}_{2y}\}2\hat{I}_{1x}\hat{I}_{2z}\exp\{+\mathrm{i}\theta 2\hat{I}_{1x}\hat{I}_{2y}\}$$

(iii) Evaluate the following expression:

$$\exp\{-\mathrm{i}\theta 2\hat{I}_{1x}\hat{I}_{2y}\}\hat{I}_{2x}\exp\{+\mathrm{i}\theta 2\hat{I}_{1x}\hat{I}_{2y}\}$$

7.2 Suppose that a particle is confined to a one-dimensional box between $x = 0$ and $x = 1$ and has a quantum wave function given by Equation 6.7. An observation is performed that is associated with the operator $\widehat{Q} = \widehat{D}_x^2$.

(i) What is the probability of obtaining the result $-\pi^2$?
(ii) What is the probability of obtaining the result $-9\pi^2$?
(iii) What is the probability of obtaining the result 2?
(iv) Suppose that a large number of measurements are made, on particles all in the same state given by Equation 6.7. The results of all the measurements are averaged. To what value does the average tend, as the number of measurements becomes very large?

7.3 Prove that the result of three consecutive rotations $\widehat{R}_x(\pi/2)\widehat{R}_y(\pi)\widehat{R}_x(\pi/2)$ is the same as that given by a single rotation $\widehat{R}_y(\pi)$. Verify the identity by rotating your shoe.

7.4 Write down the matrix representations of $\hat{I}^+$, $\hat{I}^-$, $\hat{I}_y$ and $\hat{I}_z$ for a spin-5/2 particle.

Part 4

Nuclear Spin Interactions

8 Nuclear Spin Hamiltonian

It is a goal of this book to explain the *dynamics* of nuclear spins. To do this we need to solve the time-dependent Schrödinger equation for the nuclei. The first step is to write down the Hamiltonian operator.

The next two chapters give the form of the nuclear spin Hamiltonian in diamagnetic materials and attempt to explain physically why it looks as it does.

8.1 Spin Hamiltonian Hypothesis

The nuclear spins are not alone. Any real sample contains an astronomical number of electrons as well as nuclei. In principle, the Schrödinger equation involves the motions of all the nuclei and all the electrons, and the Hamiltonian operator involves the interactions between all of these particles.

In principle, the quantum state of the entire sample is fully described by a wave function $|\psi_{\mathrm{full}}\rangle$, which contains information as to the positions, velocities, and spin states of all the electrons and nuclei. This wavefunction obeys the time-dependent Schrödinger equation:

$$\frac{\mathrm{d}}{\mathrm{d}t}|\psi_{\mathrm{full}}(t)\rangle = -\mathrm{i}\widehat{\mathcal{H}}_{\mathrm{full}}|\psi_{\mathrm{full}}(t)\rangle$$

where the Hamiltonian $\widehat{\mathcal{H}}_{\mathrm{full}}$ contains all interactions in the system.

This equation is complete, but useless. It cannot be solved in any realistic situation. For the purposes of NMR, one works with a much simpler equation, in which only the nuclear spin states appear:

$$\boxed{\frac{\mathrm{d}}{\mathrm{d}t}|\psi_{\mathrm{spin}}(t)\rangle \cong -\mathrm{i}\widehat{\mathcal{H}}_{\mathrm{spin}}|\psi_{\mathrm{spin}}(t)\rangle \qquad (8.1)}$$

Here, $|\psi_{\mathrm{spin}}\rangle$ is the spin state of the nuclei and $\widehat{\mathcal{H}}_{\mathrm{spin}}$ is the *nuclear spin Hamiltonian*. The nuclear spin Hamiltonian contains only terms that depend on the directions of the nuclear spin polarizations. This assumes the magnetic and electrical influences of the rapidly moving electrons are blurred out, so that only their average is seen. These 'blurred-out' electronic influences are contained in the spin Hamiltonian $\widehat{\mathcal{H}}_{\mathrm{spin}}$.

This massive simplification is called the *spin Hamiltonian hypothesis*. It rests on a separation of time-scales for nuclear and electronic motions. The electronic motions are so rapid that the nuclear spins only sense a time average of the fields they generate. Furthermore, the nuclear spin energies are assumed to be too small to affect the motions of the electrons within the molecules, or the motions of the molecules themselves. In practice, the nuclear spin Hamiltonian is a secure concept for almost all systems at ordinary temperatures.[1]

Spin Dynamics: Basics of Nuclear Magnetic Resonance, Second Edition Malcolm H. Levitt

From now on, the operator $\widehat{\mathcal{H}}$ is taken to imply the nuclear spin Hamiltonian, and the quantum states $|\psi\rangle$ are taken to imply the nuclear spin states.

8.2 Electromagnetic Interactions

First consider a single atomic nucleus. The nucleus interacts with its environment because (i) it has an electric charge, which interacts with electric fields, and (ii) it may have a magnetic moment, which interacts with magnetic fields.

In order to understand many NMR phenomena, it is important to realize that many nuclei are not spherical. In general, the atomic nucleus should be visualized as a small lumpy magnet, with (i) a magnetic moment and (ii) a non-uniform distribution of positive electric charge:

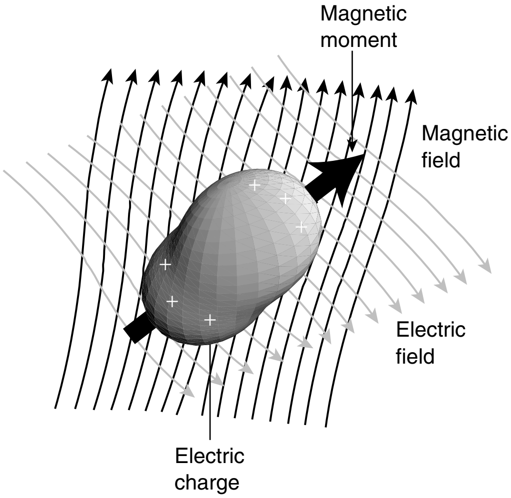

Figure 8.1
Interaction of the nucleus with electric and magnetic fields.

The nucleus interacts with the surrounding fields in two ways: it may move bodily in space, or it may rotate.

The motion of the nucleus in space, and the motion of the surrounding electrons, is the subject of molecular structure and spectroscopy. It is a very important subject, but is not of direct consequence for NMR.

NMR is concerned with the *rotational* motion of nuclei. If the nucleus rotates, then the nuclear magnetic moment and nuclear electric charges rotate with it. This changes the energy of the nucleus, because the nuclear electric charges and the nuclear magnetic moment both adopt a different orientation with respect to the surrounding fields:

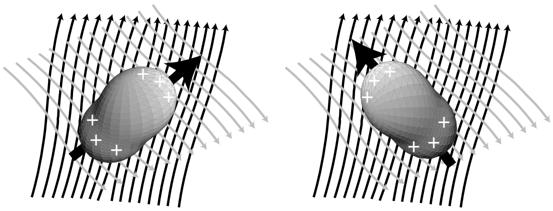

Figure 8.2
The energy of the nucleus depends on its orientation with respect to the fields.

The nuclear spin Hamiltonian contains terms that describe this *orientation dependence* of the nuclear energy. In general, there are two terms: an *electric spin Hamiltonian*, which describes the way the nuclear *electric energy* changes as the nucleus rotates, and a *magnetic spin Hamiltonian*, which describes the way the nuclear *magnetic energy* changes as the nucleus rotates. The spin Hamiltonian operator for nucleus I_j may therefore be written as

$$\boxed{\widehat{\mathcal{H}}_j = \widehat{\mathcal{H}}_j^{\text{elec}} + \widehat{\mathcal{H}}_j^{\text{mag}} \qquad (8.2)}$$

8.2.1 Electric spin Hamiltonian

The distribution of electric charge in the nucleus is denoted by the symbol $\mathbb{C}(\mathbf{r})$.

It is very convenient to represent this 'lumpy' charge distribution as a superposition of *electric multipoles*:

$$\mathbb{C}(\mathbf{r}) = \mathbb{C}^{(0)}(\mathbf{r}) + \mathbb{C}^{(1)}(\mathbf{r}) + \mathbb{C}^{(2)}(\mathbf{r}) + \ldots \qquad (8.3)$$

Here, $\mathbb{C}^{(0)}$ represents a *spherical* charge distribution, $\mathbb{C}^{(1)}$ represents a *dipolar* electric charge distribution, $\mathbb{C}^{(2)}$ represents a *quadrupolar* electric charge distribution, and so on. Mathematically, these functions are proportional to the spherical harmonics, and have exactly the same form as the s-, p- and d-orbitals in a hydrogen atom:

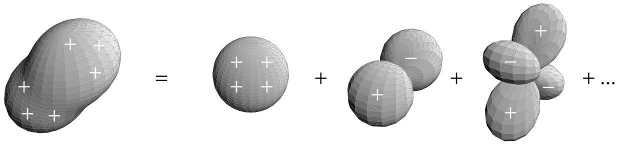

Figure 8.3
Decomposition of the electric charge distribution into multipole components.

The magnitude of the $\mathbb{C}^{(0)}$ term is the *total electric charge* of the nucleus, the magnitude of the $\mathbb{C}^{(1)}$ term is called the *electric dipole moment* of the nucleus, the magnitude of the $\mathbb{C}^{(2)}$ term is called the *electric quadrupolar moment* of the nucleus, and so on.

Now suppose that the nucleus is immersed in an electric environment, which may be represented by an *electric potential field* $V(\mathbf{r})$, which depends on position:

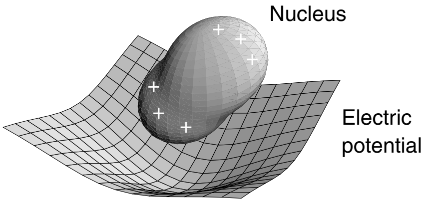

Figure 8.4
Interaction of the nucleus with an electric potential field.

In a real molecule, the centre of the nucleus adopts a stable position at a minimum of the electric potential. Note, however, that the electric potential may still vary from one side of the nucleus to the other, which influences its rotational motion.

The electric potential field may be represented as a superposition of terms:

$$V(\mathbf{r}) = V^{(0)}(\mathbf{r}) + V^{(1)}(\mathbf{r}) + V^{(2)}(\mathbf{r}) + \ldots$$

Here, $V^{(0)}$ is the electric potential at the centre of the nucleus, $V^{(1)}$ is the potential *gradient* at the centre of the nucleus (proportional to the difference in the potential from one side of the nucleus to the other), $V^{(2)}$

is the *gradient of the gradient* (i.e. how much the *slope* of the potential changes from one side of the nucleus to the other), and so on. (For explicit expressions, see the text by Slichter in *Further Reading*.)

The electric interaction energy of the nucleus and the field may be written as follows:

$$E_{\text{elec}} = E^{(0)}_{\text{elec}} + E^{(1)}_{\text{elec}} + E^{(2)}_{\text{elec}} + E^{(3)}_{\text{elec}} + \ldots$$

where each term comes from the interaction of a single multipole component of the charge distribution with a different aspect of the potential:

$$\begin{aligned} E^{(0)}_{\text{elec}} &= \int d\mathbf{r}\, \mathbb{C}^{(0)} V^{(0)}(\mathbf{r}) \\ E^{(1)}_{\text{elec}} &= \int d\mathbf{r}\, \mathbb{C}^{(1)} V^{(1)}(\mathbf{r}) \\ E^{(2)}_{\text{elec}} &= \int d\mathbf{r}\, \mathbb{C}^{(2)} V^{(2)}(\mathbf{r}) \end{aligned} \tag{8.4}$$

and so on.

The first term $E^{(0)}_{\text{elec}}$ corresponds to the point charge approximation for the atomic nucleus. This term is decisive for atomic and molecular structure, since it represents the electrostatic forces between the nuclei and the electrons. However, it is of no *direct* importance in NMR. It is only responsible for holding the nuclei in place at their appropriate molecular sites.

The term $E^{(1)}_{\text{elec}}$ represents the interaction of the nuclear electric dipole moment with the gradient of the electric potential, i.e. the electric field. Since the electric fields inside a molecule are enormous, this term might be expected to be huge. However, a very special circumstance intervenes. Nuclear physicists have shown that, within experimental error, there is *no nuclear electric dipole moment*.[2] The electric terms $E^{(1)}_{\text{elec}}, E^{(3)}_{\text{elec}}, E^{(5)}_{\text{elec}} \ldots$ all vanish.

In addition, there is another symmetry property, which links the *shape* of the nucleus to the *value of the nuclear spin*:[3]

$$\boxed{\mathbb{C}^{(n)} = 0 \qquad \text{for } n > 2I} \tag{8.5}$$

This means that the series in Equation 8.3 does not go on for ever, but cuts off at $2I$.

This has consequences. Let us examine the situation for nuclei with $I = 1/2$, and then proceed to nuclei of higher spin.

Spin-1/2 *nuclei.* For spin-1/2 nuclei, all electric multipole moments vanish except $\mathbb{C}^{(0)}$ (but see Note 4). The only interaction between the nuclear spin and the electric potential is via the $E^{(0)}_{\text{elec}}$ term. This means that, for spins-1/2, *there are no electric energy terms that depend on the orientation or internal structure of the nucleus*. This is quite extraordinary. It means, for example, that the 47 protons and 62 neutrons in a nucleus of ^{109}Ag behave *exactly* like a single point charge at the nuclear centre, as far as electrical effects are concerned. The same holds for any spin-1/2 nucleus. Whatever the electrical environment, the nuclear electric energy is totally independent of the orientation of the nucleus in space. A spin-1/2 nucleus is not 'lumpy', but behaves as a perfectly smooth, magnetic, billiard ball:

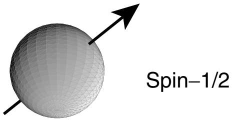

Figure 8.5
A spin-1/2 nucleus is spherical.

For spin-1/2 nuclei, the electric interactions vanish:

$$\hat{\mathcal{H}}_j^{\text{elec}} = 0 \qquad (\text{for spin } I = 1/2) \tag{8.6}$$

It is quite fantastic that this result may be derived purely on the grounds of symmetry and without any detailed calculations.

For spins-1/2, the magnetic effects are left with a completely free hand. These nuclei really behave like perfect magnetic gyroscopes mounted on absolutely frictionless bearings.

Spins $I > 1/2$. For higher spin nuclei, the electric charge distribution is not spherically symmetrical. The electric energy of the nucleus depends on its orientation with respect to the rest of the molecule. The most important term is usually $E_{\text{elec}}^{(2)}$, which represents the interaction of the quadrupole charge distribution of the nucleus with the $V^{(2)}$ term, which we called above the gradient of the gradient of the electric potential. Since the gradient of the potential is the same as the electric field, the gradient of the gradient of the potential is the same as the gradient of the electric field. The main orientation-dependent electric term is therefore the interaction of the *electric quadrupole moment* of the nucleus with the *electric field gradient* in the surrounding space:[5]

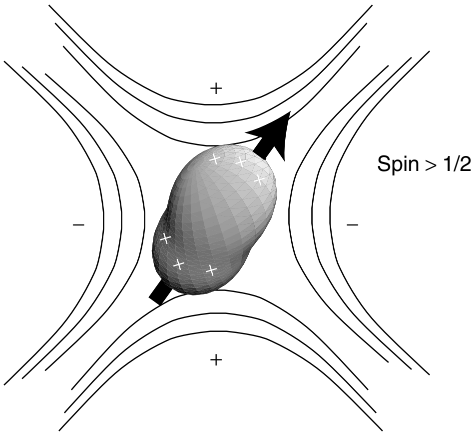

Figure 8.6
Interaction of a spin > 1/2 nucleus with the electric field gradient.

The electric part of the spin Hamiltonian is therefore called the electric quadrupole interaction:

$$\hat{\mathcal{H}}_j^{\text{elec}} = \hat{\mathcal{H}}_{\text{j}}^{\text{Q}} \qquad (\text{for spin } I \geq 1) \tag{8.7}$$

The full form of the quadrupolar spin Hamiltonian is given in Appendix A.5. The quadrupole interaction depends on a property of the nucleus (the nuclear quadrupole moment) as well as a property of the molecular environment (the electric field gradient). For many nuclei of spin $I > 1/2$, the quadrupole coupling is often as large as many megahertz, and in some cases hundreds of megahertz.

The term *quadrupolar nucleus* means 'nucleus of spin $I > 1/2$'. The NMR of quadrupolar nuclei is a more complicated and richer field than that of spins-1/2, because there are electric as well as magnetic influences on the reorientation of the nuclei. Generally speaking, the NMR of quadrupolar nuclei is technically more difficult than the NMR of spin-1/2 nuclei. There are some exceptions: for example, ^{2}H is a relatively 'friendly' quadrupolar nucleus, since its electric quadrupolar moment is rather small. The NMR of quadrupolar nuclei is an important and expanding field (see *Further Reading*).

8.2.2 Magnetic spin interactions

The nuclear magnetic dipole moment interacts with the surrounding magnetic field. Suppose that the magnetic field at the site of the nucleus is described by a three-dimensional vector **B**:

$$\mathbf{B} = B_x \mathbf{e}_x + B_y \mathbf{e}_y + B_z \mathbf{e}_z \tag{8.8}$$

where $\mathbf{e}_x$, $\mathbf{e}_y$ and $\mathbf{e}_z$ are unit vectors along three orthogonal directions in space:

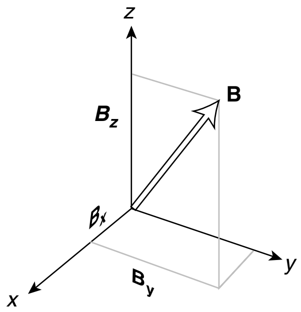

Figure 8.7
The magnetic field vector.

The nuclear magnetic moment is equal to the spin angular momentum multiplied by the gyromagnetic ratio γ_j. The relationship between the magnetic moment and angular momentum operators is

$$\boxed{\hat{\boldsymbol{\mu}}_\mathrm{j} = \gamma_j \hat{\mathbf{I}}_j} \tag{8.9}$$

or, more, explicitly:

$$\hat{\boldsymbol{\mu}}_\mathrm{j} = \gamma_j (\hat{I}_{jx} \mathbf{e}_x + \hat{I}_{jy} \mathbf{e}_y + \hat{I}_{jz} \mathbf{e}_z)$$

The nuclear magnetic energy for spin I_j depends on *minus the dot product* of the magnetic moment and the field:

$$\boxed{\widehat{\mathcal{H}}_j^{\mathrm{mag}} = -\hat{\boldsymbol{\mu}}_\mathrm{j} \cdot \mathbf{B}} \tag{8.10}$$

The magnetic energy is at a minimum when the magnetic moment is parallel to the field, and is at a maximum when the magnetic moment is aligned in the opposite direction to the field (just like a compass needle, which minimizes its magnetic energy by aligning with the field):

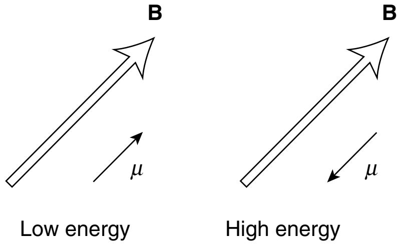

Figure 8.8
Magnetic energy.

Equations 8.8 and 8.9 may be combined to give

$$\widehat{\mathcal{H}}_j^{\mathrm{mag}} = -\gamma_j \left(B_x \hat{I}_{jx} + B_y \hat{I}_{jy} + B_z \hat{I}_{jz} \right) \tag{8.11}$$

8.3 External and Internal Spin Interactions

The electric and magnetic fields experienced by a nuclear spin may originate from the external apparatus or from the sample itself. In the first case, one speaks of *external spin interactions*. In the second case, the term *internal spin interactions* is used.

External spin interactions are purely magnetic, except in exotic circumstances.[6] In almost all cases, one uses applied magnetic fields of various types to manipulate the nuclear spins.

Internal spin interactions are purely magnetic for spins-1/2. In the case of spins > 1/2, the electric quadrupolar interaction is also involved.

It is a remarkable feature of NMR that the external interactions are usually much larger than the internal interactions. In other words, the nuclear spins are *more strongly coupled to the external apparatus than to their own molecular environment*.

It is hard to emphasize enough how unusual this situation is. In most forms of spectroscopy, the behaviour of the system is set by the molecular structure itself and information is gained by relatively weak external perturbations. The inverted situation in NMR leads to extraordinary possibilities, because it means that, in a sense, the 'system under study' includes the apparatus itself, whereas the 'weak probing' is done, in a sense, by the molecules. It is instructive to consider the extraordinary pulse sequences used in NMR as artificial 'spectroscopic systems' that are probed, non-destructively, by a weak 'molecular observer!' No other spectroscopy offers such a bizarre inversion of roles.

8.3.1 Spin interactions: summary

The following diagram summarizes the overall organization of the spin interactions:

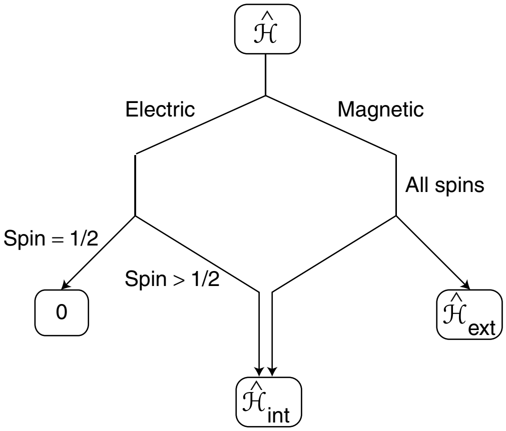

Figure 8.9
Organization of the spin interaction terms.

8.4 External Magnetic Fields

The NMR spectrometer usually supplies up to three kinds of external magnetic field.

1. The main superconducting solenoid provides a very strong, very homogeneous, static magnetic field, called here $\mathbf{B}^0$ (see Section 4.1).

2. The r.f. coil in the probe generates an r.f. oscillating field, denoted here $\mathbf{B}_{\mathrm{RF}}(t)$ (see Section 4.4). In normal circumstances, this field is as spatially homogeneous as possible.

3. Suitably equipped spectrometers may also provide a magnetic field gradient field, called here $\mathbf{B}_{\mathrm{grad}}(\mathbf{r}, t)$. This field is much weaker than $\mathbf{B}^0$, is dependent on the position coordinate $\mathbf{r}$, and may have a controlled time dependence. This field is provided by the gradient coils (see Section 4.7).

The physical configuration of the first two applied magnetic fields is shown below:

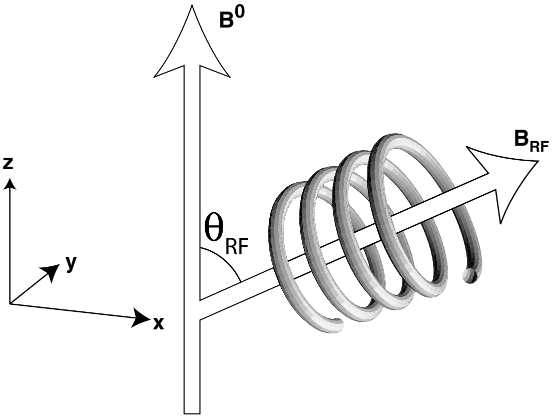

Figure 8.10
The laboratory frame, the r.f. coil, and the applied fields $\mathbf{B}^0$ and $\mathbf{B}_{\mathrm{RF}}$. The gradient fields are parallel to $\mathbf{B}^0$ and are not shown.

Ideally, the r.f. field $\mathbf{B}_{\mathrm{RF}}$ is perpendicular to the static field B^0. However, in some cases, physical constraints make it necessary to tilt the r.f. coil away from the perpendicular (this is true, for example, in magic-angle-spinning NMR experiments; see Section 19.6). The tilt angle between the r.f. field and the static field is denoted here θ_{RF}.

The external part of the spin Hamiltonian is therefore given to a good approximation by:

$$\widehat{\mathcal{H}}_{\mathrm{ext}}(t) = \widehat{\mathcal{H}}_{\mathrm{static}} + \widehat{\mathcal{H}}_{\mathrm{grad}}(\mathbf{r}, t) + \widehat{\mathcal{H}}_{\mathrm{RF}}(t) \tag{8.12}$$

where

$$\begin{aligned}\widehat{\mathcal{H}}_{\mathrm{static}} &= \sum_j \widehat{\mathcal{H}}_j^{\mathrm{static}} \\ \widehat{\mathcal{H}}_{\mathrm{grad}}(\mathbf{r}, t) &= \sum_j \widehat{\mathcal{H}}_j^{\mathrm{grad}}(\mathbf{r}, t) \\ \widehat{\mathcal{H}}_{\mathrm{RF}}(t) &= \sum_j \widehat{\mathcal{H}}_j^{\mathrm{RF}}(t)\end{aligned} \tag{8.13}$$

and the sums are taken over all spins in the sample. Here, $\widehat{\mathcal{H}}_j^{\mathrm{static}}$ is the interaction of each spin I_j with the longitudinal static field $\mathbf{B}^0$, $\widehat{\mathcal{H}}_j^{\mathrm{grad}}$ is the interaction of each spin I_j with the gradient field $\mathbf{B}_{\mathrm{grad}}$, and $\widehat{\mathcal{H}}_j^{\mathrm{RF}}$ is the interaction of each spin with the r.f. field $\mathbf{B}_{\mathrm{RF}}$ generated by the r.f. coil.

It is usual to choose an axis system in which the static field is along the z-axis, while the oscillating field is in the xz-plane. This is called the *laboratory reference frame*.

8.4.1 Static field

The static field is written in the laboratory frame:

$$\mathbf{B}^0 = B^0\,\mathbf{e}_z$$

(lightface symbols are used for the *magnitudes* of vectors).

The spin Hamiltonian for the interaction of each spin with the static longitudinal field B^0 is given by

$$\boxed{\widehat{\mathcal{H}}_j^{\text{static}} = -\gamma_j B^0 \hat{I}_{jz}} \qquad (8.14)$$

This is called the *nuclear Zeeman interaction*.

The term $-\gamma_j B^0$ may be identified as the Larmor frequency of spin I_j. This is discussed in Section 9.1, after including the chemical shift, which slightly changes the Larmor frequency.

8.4.2 Radio-frequency field

The r.f. coil generates a field $\mathbf{B}_{\text{RF}}$ along the tilted axis shown in Figure 8.10. During an r.f. pulse on a single spectrometer channel, the magnitude of this field oscillates at the spectrometer reference frequency ω_{ref}. Between pulses, the r.f. field is equal to zero. If the pulse is perfectly rectangular, then the r.f. field has the form:

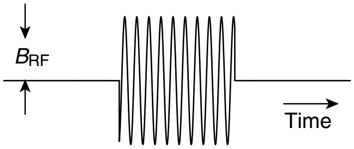

Figure 8.11
The oscillating r.f. field.

This corresponds to

$$\mathbf{B}_{\text{RF}}(t) = \begin{cases} B_{\text{RF}}(\mathbf{e}_z \cos\theta_{\text{RF}} + \mathbf{e}_x \sin\theta_{\text{RF}})\cos(\omega_{\text{ref}}t + \phi_{\text{p}}) & \text{during an r.f. pulse} \\ 0 & \text{otherwise} \end{cases} \qquad (8.15)$$

where the *maximum* r.f. amplitude during the pulse is denoted B_{RF}.

The r.f. field consists of a longitudinal component proportional to $\cos\theta_{\text{RF}}$ plus a transverse component proportional to $\sin\theta_{\text{RF}}$. It turns out to be useful to imagine that the transverse oscillating field is actually a sum of two *rotating* components. Both components rotate in the xy-plane, at the same frequency, but in opposite directions:

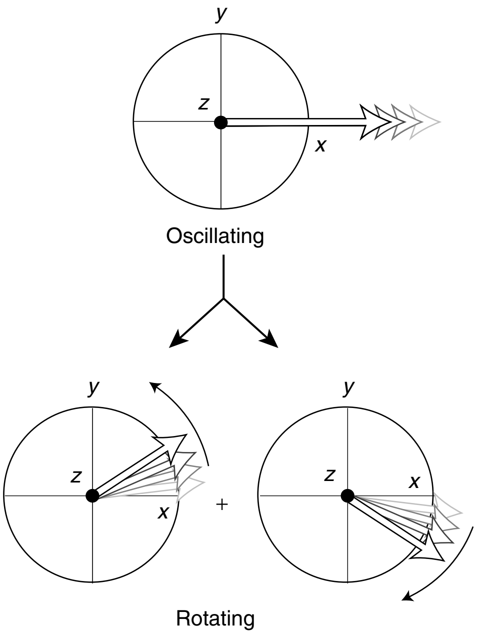

Figure 8.12
The oscillating r.f. field may be represented as the sum of two rotating fields.

(This shows the view from above.) The transverse component rotating in the same sense as the spin precession (negative for spins with $\gamma > 0$, positive sense for spins with $\gamma < 0$) is called the *resonant component* of the r.f. field. The transverse component rotating in the opposite sense to the Larmor frequency (positive for spins with $\gamma > 0$, and negative sense for spins with $\gamma < 0$) is called the *non-resonant* r.f. field component.

Mathematically, the oscillating r.f. field is expressed as

$$\mathbf{B}_{\mathrm{RF}}(t) = \mathbf{B}^{\mathrm{RF}}_{\mathrm{res}}(t) + \mathbf{B}^{\mathrm{RF}}_{\text{non-res}}(t) + \mathbf{B}^{\mathrm{RF}}_{\mathrm{long}}(t)$$

where the two transverse components are as follows:

$$\mathbf{B}^{\mathrm{RF}}_{\mathrm{res}}(t) = \begin{cases} \frac{1}{2} B_{\mathrm{RF}} \sin\theta_{\mathrm{RF}} \left\{\cos\left(\omega_{\mathrm{ref}} t + \phi_{\mathrm{p}}\right)\mathbf{e}_x + \sin\left(\omega_{\mathrm{ref}} t + \phi_{\mathrm{p}}\right)\mathbf{e}_y\right\} & \text{during an r.f. pulse} \\ 0 & \text{otherwise} \end{cases}$$

$$\mathbf{B}^{\mathrm{RF}}_{\text{non-res}}(t) = \begin{cases} \frac{1}{2} B_{\mathrm{RF}} \sin\theta_{\mathrm{RF}} \left\{\cos\left(\omega_{\mathrm{ref}} t + \phi_{\mathrm{p}}\right)\mathbf{e}_x - \sin\left(\omega_{\mathrm{ref}} t + \phi_{\mathrm{p}}\right)\mathbf{e}_y\right\} & \text{during an r.f. pulse} \\ 0 & \text{otherwise} \end{cases}$$

and the longitudinal r.f. field is given by

$$\mathbf{B}^{\mathrm{RF}}_{\mathrm{long}}(t) = \begin{cases} B_{\mathrm{RF}} \cos\theta_{\mathrm{RF}} \cos\left(\omega_{\mathrm{ref}} t + \phi_{\mathrm{p}}\right)\mathbf{e}_z & \text{during an r.f. pulse} \\ 0 & \text{otherwise} \end{cases}$$

For spins with positive γ, the frequency ω_{ref} is negative; for spins with negative γ, the frequency ω_{ref} is positive.

It may be shown that, under ordinary circumstances, the longitudinal and non-resonant components of the r.f. field have almost no influence on the motion of the spins. They may safely be neglected.[7] The transverse part of the spin Hamiltonian may therefore be approximated as

$$\widehat{\mathcal{H}}_j^{\mathrm{RF}}(t) \cong \begin{cases} -\omega_{\mathrm{nut}}^j \left\{\cos\left(\omega_{\mathrm{ref}}t + \phi_{\mathrm{p}}\right) \hat{I}_{jx} + \sin\left(\omega_{\mathrm{ref}}t + \phi_{\mathrm{p}}\right) \hat{I}_{jy}\right\} & \text{during an r.f. pulse} \\ 0 & \text{otherwise} \end{cases} \tag{8.16}$$

where the *nutation frequency* ω_{nut}^j is defined as

$$\boxed{\omega_{\mathrm{nut}}^j = \left|\tfrac{1}{2}\gamma_j B_{\mathrm{RF}} \sin\theta_{\mathrm{RF}}\right| \qquad (8.17)}$$

When we come to the quantum theory, we will see that Equation 8.16 is much easier to handle than Equation 8.15, even though it appears to be more complicated.

The nutation frequency ω_{nut}^j is a measure of the resonant r.f. field strength, experienced by spin I_j, expressed in angular frequency units. The meaning of the term 'nutation' is discussed in Section 10.8. Typically, the nutation frequency $\omega_{\mathrm{nut}}^j/2\pi$ is in the range $1 - 200$ kHz. Therefore, it is three to four orders of magnitude smaller than the Larmor frequency, even under the strongest r.f. pulses.

The factor 1/2 in Equation 8.17 arises because one-half of the r.f. field amplitude is 'wasted' on the non-resonant rotating component.[8] The factor $\sin\theta_{\mathrm{RF}}$ takes into account the tilt angle of the r.f. coil. In the optimal case, the axis of the r.f. coil is perpendicular to the main field $\theta_{\mathrm{RF}} = \pi/2$, so this factor is equal to 1. A coil that is tilted away from the perpendicular is less efficient in generating a resonant r.f. field.

The above equations apply for pulses on a single spectometer channel. Equation 8.16 is readily generalized to the multiple-channel case by adding together several similar-looking terms, with different frequencies.

8.4.3 Gradient field

The interactions of a spin I_j, located in a molecule at a spatial position $\mathbf{r} = (x, y, z)$, with field gradients along the three laboratory frame axes, are given by

$$\begin{aligned} \widehat{\mathcal{H}}_j^{\mathrm{grad}}(\mathbf{r}, t) &= -\gamma_j G_x(t) x \hat{I}_{jz} && \text{for gradient } G_x \text{ along } x\text{-axis} \\ \widehat{\mathcal{H}}_j^{\mathrm{grad}}(\mathbf{r}, t) &= -\gamma_j G_y(t) y \hat{I}_{jz} && \text{for gradient } G_y \text{ along } y\text{-axis} \\ \widehat{\mathcal{H}}_j^{\mathrm{grad}}(\mathbf{r}, t) &= -\gamma_j G_z(t) z \hat{I}_{jz} && \text{for gradient } G_z \text{ along } z\text{-axis} \end{aligned} \tag{8.18}$$

Note that in all cases the relevant spin operator is always $\hat{I}_{jz}$, whatever the direction of the gradient. This is because the transverse components of the gradient fields are usually far weaker than the static field, and may be ignored (see Section 8.5.2 and Chapter 4, Note 7).

8.4.4 External spin interactions: summary

The following diagram summarizes the form of the external spin interactions:

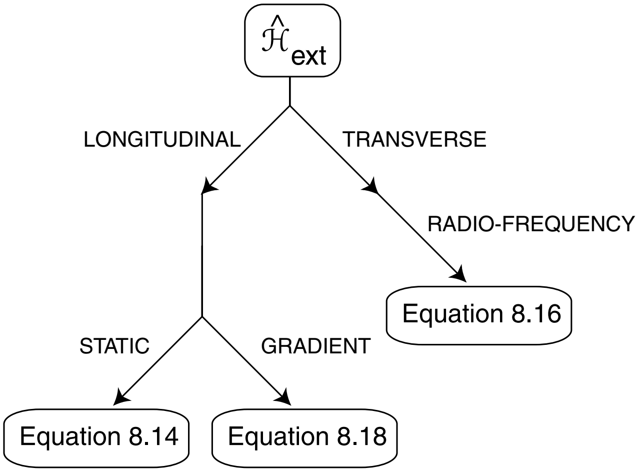

Figure 8.13
Organization of the external spin interactions.

8.5 Internal Spin Hamiltonian

The nuclei experience magnetic and electric fields originating from the sample itself. These interactions are included in the internal spin Hamiltonian $\widehat{\mathcal{H}}_{\text{int}}$.

The following discussion concentrates on nuclear spin interactions in diamagnetic substances, which lack unpaired electron spins. See *Further Reading* for details of the nuclear spin interactions in paramagnetic materials and metals.

8.5.1 The internal spin interactions

The internal spin Hamiltonian in diamagnetic substances contains the following terms:

1. *Chemical shift terms*. These terms represent the indirect magnetic interaction of the external magnetic field and the nuclear spins, through the involvement of the electrons:

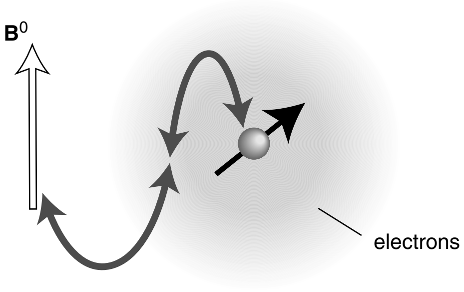

Figure 8.14
The chemical shift interaction. The electrons are depicted by a grey cloud.

These terms are discussed in Section 9.1.

2. *Quadrupolar couplings*. These represent the electric interactions of spin $> 1/2$ nuclei with the surrounding electric fields:

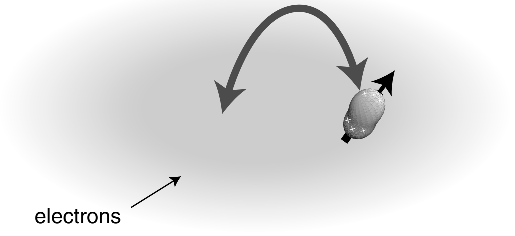

Figure 8.15
The quadrupole coupling interaction.

These terms are discussed in Section 9.2.

3. *Direct dipole–dipole couplings*. These represent the direct magnetic interactions of nuclear spins with each other:

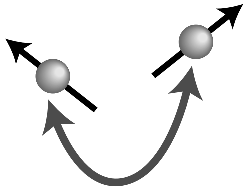

Figure 8.16
The direct dipole–dipole coupling.

These terms are discussed in Section 9.3.

4. *J-couplings*. These represent the indirect magnetic interactions of nuclear spins with each other, through the involvement of the electrons:

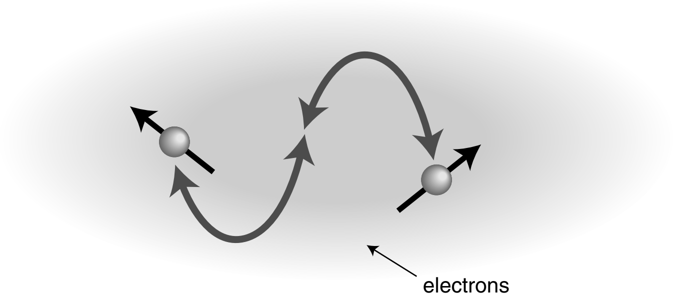

Figure 8.17
The indirect dipole–dipole coupling (J-coupling).

These terms are discussed in Section 9.4.

5. *Spin–rotation interactions*. These represent the interactions of the nuclear spins with magnetic fields generated by rotational motion of the molecules:

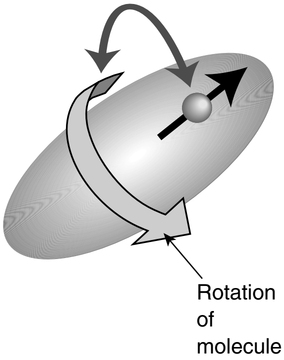

Figure 8.18
The spin–rotation interaction.

These terms are discussed in Section 9.5.

The following diagram summarizes the organization and rough magnitude of the internal spin interactions terms:

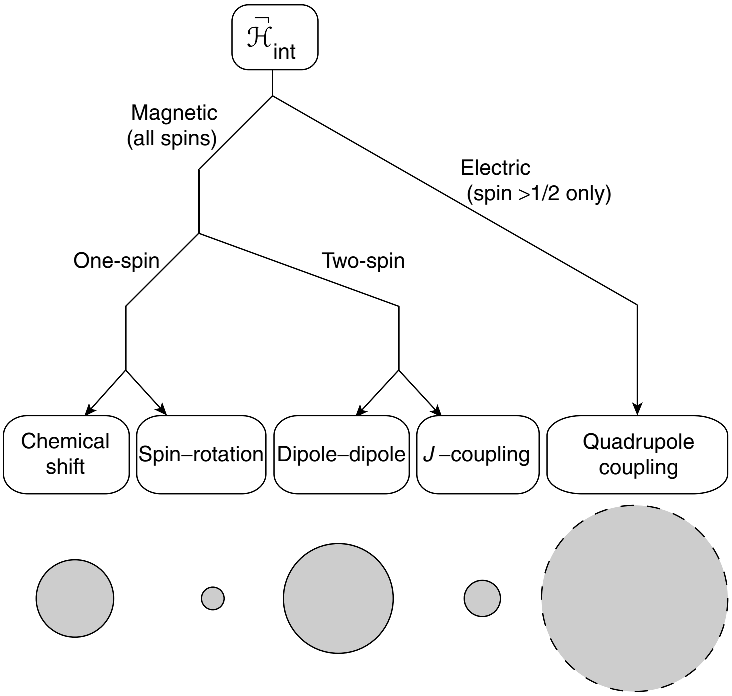

Figure 8.19
Organization of the internal spin interaction terms, and their rough relative magnitudes. The quadrupolar coupling vanishes for spins-1/2.

The circles display the typical relative size of these terms, in the absence of molecular motion. For spins $> 1/2$, the quadrupole coupling is usually the largest term. However, this term vanishes for spins-1/2.

The direct dipole–dipole couplings and chemical shift terms are usually the next largest, followed by the J-couplings and the spin–rotation interactions.

8.5.2 Simplification of the internal Hamiltonian

The mathematical forms of the nuclear spin interactions are quite complicated. Fortunately, it is usually possible to use a simplified form of the internal Hamiltonian. This is because of (i) the very strong external magnetic field and (ii) the rapid molecular motion in liquids and gases, and in some solids.

The very strong external magnetic field leads to the *secular approximation*. The rapid molecular motion leads to *motional averaging*.

As will be discussed in Section 19.3, these phenomena have a rather complicated interplay, depending on the time-scales involved. Here, I overlook these complications and summarize the situation by the following diagram:

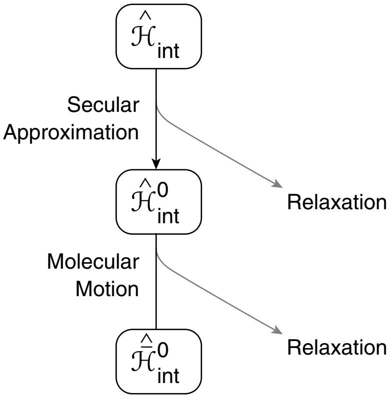

Figure 8.20
Simplification of the internal spin Hamiltonian.

1. The *secular approximation* of the internal spin Hamiltonian terms is discussed in Appendix A.6. It arises because the spin dynamics are dominated by the large interaction with the external magnetic field, which tends to mask some components of the internal spin interactions. The secular approximation allows each term $\widehat{\mathcal{H}}_{\text{int}}$ to be replaced by a simplified form, called here $\widehat{\mathcal{H}}^0_{\text{int}}$. It is usually a very good approximation, except for the case of quadrupolar spins, where a more complete treatment is often necessary.

2. *Motional averaging*. If the molecules undergo rapid molecular motion, then the interaction terms fluctuate in time. If the molecular motion is sufficiently fast, then the fluctuating interaction $\widehat{\mathcal{H}}^0_{\text{int}}$ may be replaced by its *motionally averaged value*, denoted $\overline{\widehat{\mathcal{H}}}^0_{\text{int}}$. The parts of $\widehat{\mathcal{H}}_{\text{int}}$ that have a zero time-average are discarded. Use of the motionally averaged spin Hamiltonian is usually a good approximation in gases and liquids, unless the molecular motion is slow.

The discarded parts of the internal spin Hamiltonian terms are responsible for the *relaxation* of the nuclear spin system, as sketched in Sections 2.6 and 2.7 and discussed more thoroughly in Chapter 20. For the time being we will consider the motionally averaged secular terms, which determine the form of the NMR spectrum.[9]

8.6 Motional Averaging

The form of the motionally averaged Hamiltonian depends very strongly on the type and the time-scale of molecular motion, and hence on the phase of matter.

8.6.1 Modes of molecular motion

There are three relevant modes of molecular motion, namely *internal molecular motions*, *molecular translation* and *molecular rotations*.

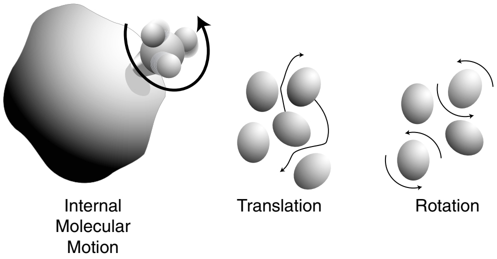

Figure 8.21
Types of molecular motion.

Internal molecular motions involve vibrations of the molecule, rotations of some internal molecular groups, and chemical isomerizations. For most of this book, I disregard the internal molecular motions and consider only the rotations or translations of the molecules as a whole. The important subject of internal molecular motion is encountered briefly in Chapter 19.

8.6.2 Molecular rotations

Molecular rotation involves a change in the *orientation* of each molecule in space.

In general, one needs *three* angles to specify the orientation of a molecule in three-dimensional space (see Appendix A.1). In this book, I will use the symbol Θ to denote the molecular orientation. Each secular Hamiltonian term depends on the molecular orientation and may be written as $\widehat{\mathcal{H}}^0_{\text{int}}(\Theta)$.

In liquids and gases, and some solids, the molecular orientation depends on time. Each secular Hamiltonian term may therefore be written $\widehat{\mathcal{H}}^0_{\text{int}}(\Theta(t))$. The effect of motional averaging is to replace the secular Hamiltonian by its time average, according to

$$\overline{\widehat{\mathcal{H}}}{}^0_{\text{int}} = \tau^{-1} \int_0^{\tau} \mathrm{d}t \; \widehat{\mathcal{H}}^0_{\text{int}}(\Theta(t))$$

where τ is large. In most cases, it is possible to invoke the *ergodic hypothesis*, meaning that an average over time is equivalent to an average over molecular orientation. The basic idea is that, over a sufficiently long time, the molecules sample all possible orientations, so that a time average may be replaced by an orientational average. The motionally averaged secular Hamiltonian is given by

$$\overline{\widehat{\mathcal{H}}}{}^0_{\text{int}} = \int \mathrm{d}\Theta \; \mathrm{p}(\Theta)\widehat{\mathcal{H}}^0_{\text{int}}(\Theta) \tag{8.19}$$

where $p(\Theta)$ is the *probability density* of the molecule having a certain orientation Θ, and the integral is taken over all orientations Θ. This probability function depends on the molecular structure, the phase of matter, and other physical variables, such as temperature and pressure.

1. In *gases* and *isotropic liquids*, all orientations are equally likely, so the probability density $p(\Theta)$ is the same for all orientations. In this case, the orientational average of a secular interaction $\widehat{\mathcal{H}}^{0}_{\text{int}}$ is given by

   $$\boxed{\widehat{\mathcal{H}}^{\text{iso}}_{\text{int}} = N^{-1} \int d\Theta \, \widehat{\mathcal{H}}^{0}_{\text{int}}(\Theta) \qquad (8.20)}$$

   where N is a normalization constant, chosen so that the total probability is one:

   $$N = \int d\Theta$$

   The expression given in Equation 8.20 is called the *isotropic average* of $\widehat{\mathcal{H}}^{0}_{\text{int}}$.

2. In an *anisotropic liquid*, there is considerable molecular motion, but all orientations are not equally probable. In many cases, the liquid crystal is oriented along an external axis, called the *director*. Usually, molecular orientations close to the director axis are more probable than orientations far from the director:

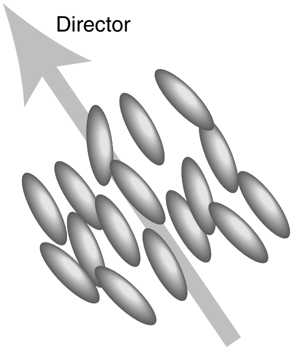

Figure 8.22
In an anisotropic liquid, the molecules orient along the director.

   In many liquid crystals, the magnetic field itself acts as the director. However, more complex situations are possible, as discussed in Section 16.4.

   In an anisotropic liquid, the motionally averaged spin interactions are not the same as their isotropic values: they depend on the orientation of the liquid crystal director with respect to the magnetic field.

3. In a *solid*, the atomic motion is usually heavily restricted. Each internal spin Hamiltonian term is different from its isotropic value and depends strongly on the orientation of the solid with respect to the magnetic field.

8.6.3 Molecular translations

There are two types of molecular translational motion: *diffusion*, in which the motion of neighbouring molecules is random, and *flow*, in which the molecular motion is biased in some particular direction by an external pressure gradient.

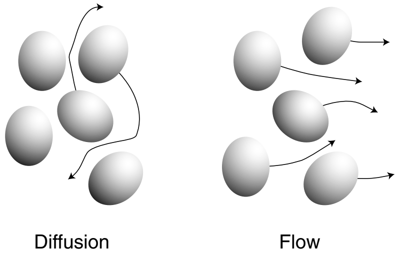

Figure 8.23
Diffusion and flow.

In most cases, significant molecular diffusion only occurs in liquids and gases. Here, it proves to be important to consider the *distance range* of molecular diffusion, on the time-scale of the NMR experiment (typically, around 0.5 s).

1. In *gases*, diffusion is extremely fast and easily extends to the physical boundaries of the sample on the time-scale of an NMR experiment. We may assume, therefore, that the positions of all molecules in a gas are exchanged during an NMR pulse sequence:

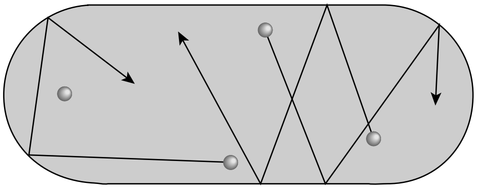

Figure 8.24
Diffusion in a gas proceeds over the entire volume of the sample.

2. In *liquids*, diffusion is much slower, depending on the molecular size and on the viscosity. It is possible to imagine a *diffusion sphere* in a liquid, within which the molecules are interchanged on the time-scale of an NMR experiment. In most liquids, such a sphere has a radius of only around 10 μm:

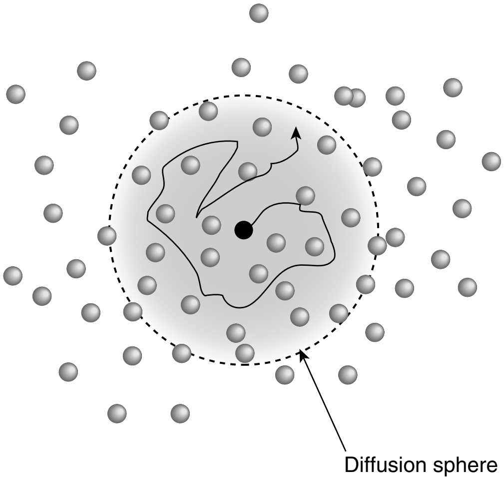

Figure 8.25
Diffusion in a liquid is restricted to a spherical volume of a few tens of micrometres in diameter, on the time-scale of an NMR experiment.

The picture above is not realistic: In practice, the diffusion sphere contains $\sim 10^{10}$ molecules, which are all in close contact.
The precise boundary of a diffusion sphere is vague, but this proves not to be too important.

3. In *solids*, the diffusional motion of the molecules is usually insignificant on the NMR time-scale.

8.6.4 Intramolecular and intermolecular spin interactions

The effect of diffusion on spin interaction terms depends on whether these interactions are *intra*molecular (involving particles on the same molecule) or *inter*molecular (involving particles on different molecules). The diagram below shows intramolecular and intermolecular couplings between nuclear spins:

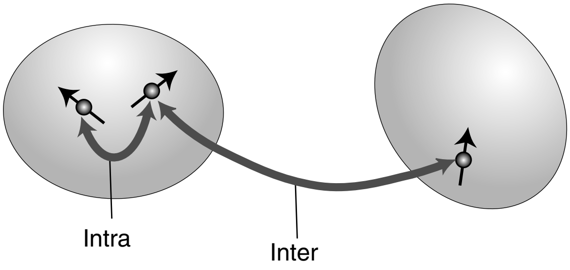

Figure 8.26
Intramolecular and intermolecular dipole–dipole couplings.

Most internal spin interactions have both intramolecular and intermolecular components. The rough relative magnitudes of these components are indicated by the following diagram:

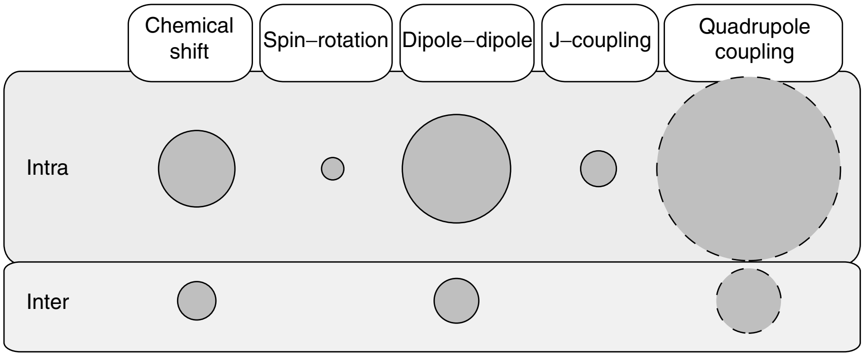

Figure 8.27
Rough relative magnitudes of the intramolecular and intermolecular components of the internal spin interactions.

To a good approximation, the J-coupling and spin–rotation interactions are purely intramolecular (see Sections 9.4 and 9.5).

In a liquid, one must also distinguish *long-range* and *short-range* intermolecular interactions. Short-range interactions involve molecules that share the same diffusion sphere. Long-range intermolecular interactions involve molecules that do not share the same diffusion sphere: The long-range interactions are far smaller than the short-range interactions, but they still lead to significant effects in some circumstances (see *Further Reading*).

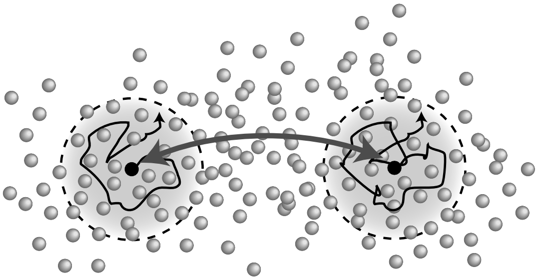

Long-range intermolecular interaction

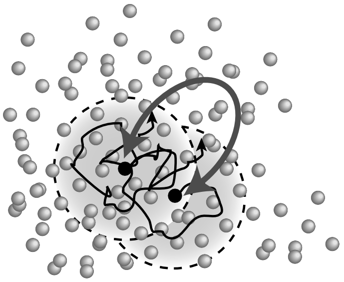

Short-range intermolecular interaction

Figure 8.28
The distinction between short-range and long-range intermolecular interactions in a liquid.

8.6.5 Summary of motional averaging

The effect of motional averaging in different phases of matter may now be summarized:

1. In a *gas*, the rapid and complete rotational and translational motion averages all *intra*molecular spin interactions to their isotropic values, as given in Equation 8.20, and averages all *inter*molecular interactions to a very small value, essentially zero.[10] The following flow chart summarizes the effect of motional averaging in gases:

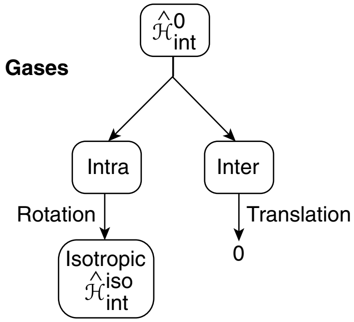

Figure 8.29
Averaging of the spin interactions in gases.

2. In an *isotropic liquid*, the rotational motion of the molecules averages all *intramolecular* spin interactions to their isotropic values, as given in Equation 8.20.

   The diffusional motion of the molecules in an isotropic liquid averages the *short-range intermolecular* interactions to zero. However, the diffusional motion in a liquid is not able to average out the *long-range intermolecular interactions*.

The following flow chart summarizes the effect of motional averaging in isotropic liquids:

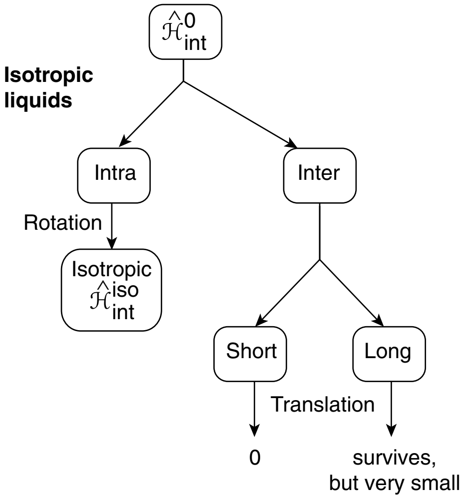

Figure 8.30
Averaging of the spin interactions in isotropic liquids.

3. In an *anisotropic liquid*, the rotational motion of the molecules averages all *intramolecular* spin interactions to values that are different from their isotropic values.

   The diffusional motion of the molecules in an anisotropic liquid averages the *short-range intermolecular* interactions to zero, whereas the *long-range intermolecular interactions* survive, just as for an isotropic liquid.

   The following flow chart summarizes the effect of motional averaging in anisotropic liquids:

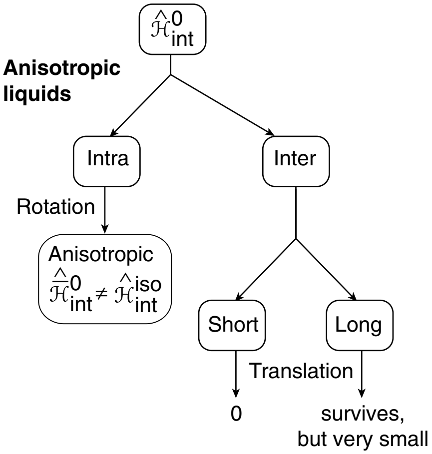

Figure 8.31
Averaging of the spin interactions in anisotropic liquids.

4. In most *solids*, the atomic motion is highly restricted and there is little averaging of the internal spin interactions, except by the restricted motions of some molecular groups. Both intramolecular and inter-

molecular spin interactions survive, and the internal spin Hamiltonian terms depend on the orientation of the sample with respect to the magnetic field:

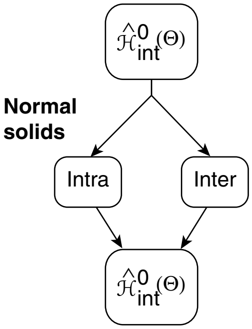

Figure 8.32
The spin interactions of a normal solid.

5. In certain molecular solids, called *plastic crystals*, an unusual situation arises. In these systems, the centres of gravity of the molecules are fixed with respect to the crystal lattice, but the molecules themselves rotate rapidly about their lattice sites, in many cases isotropically. One example is the C_{60} solid depicted in Section 1.6; another common example is provided by the hydrocarbon *adamantane*, which has the following molecular structure:

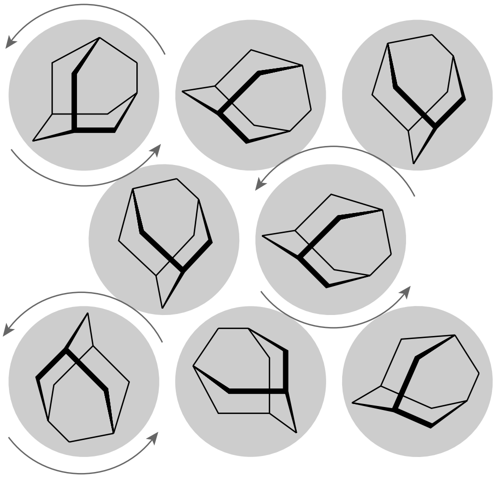

Figure 8.33
Molecular structure of adamantane.

In these special systems, the rapid molecular rotation averages out the *intra*molecular interactions to their isotropic values, whereas the averaging of the *inter*molecular interactions is incomplete, since the molecular diffusion is slow. Figure 8.34 shows a flow chart for plastic crystals.

The plastic crystal adamantane is commonly encountered as a test substance in solid-state NMR.

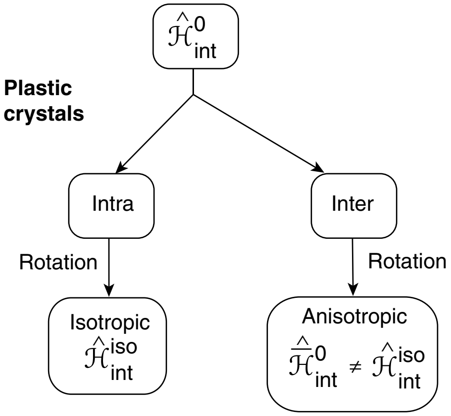

Figure 8.34
The spin interactions in a plastic crystal (assuming isotropic molecular rotation).

Notes

1. The phenomenon of *longitudinal spin relaxation* presents difficulties for the spin Hamiltonian hypothesis. As discussed in Section 2.6, the nuclear spin system relaxes towards an anisotropic equilibrium state, in which there are more spins with magnetic moments along the field than in the opposite direction to the field. This asymmetric equilibrium state would be impossible if the nuclear spin states did not have a small influence on the motion of the molecules. It follows that Equation 8.1 cannot be exactly valid and, furthermore, that NMR would be impossible if it were! See Section 20.3.6 for more on this tricky issue.

2. This property is connected with a symmetry property associated with the "standard model" of nuclear physics called *parity conservation*. Although parity conservation holds to a very good approximation, there is experimental evidence that parity-breaking leads to unconventional electric moments for heavy nuclei (see, for example C. S. Wood *et al. Science* **275**, 1759-1763 (1997)).

3. This profound and non-intuitive result may be derived from the Wigner–Eckart theorem of quantum mechanics. See the text by Slichter in *Further Reading*.

4. Nuclear physicists distinguish between the *intrinsic quadrupolar moment* of a nucleus, usually denoted Q_0, and the *spectroscopic quadrupolar moment*, usually denoted Q. Roughly speaking, Q_0 may be regarded as the 'true' quadrupolar moment and Q is the result of averaging the intrinsic quadrupole moment over the angular momentum of the nucleus. Q_0 may be finite for nuclei with spin < 1, whereas Q vanishes for such nuclei. The relevant quantity in NMR is the spectroscopic quadrupole moment Q. See e.g. P. Pyykkö, *Mol. Phys.* **99**, 1617–1629 (2001).

5. Some attempts have been made to detect the interaction of higher-order nuclear electric moments with the surrounding electric fields, e.g. see M.-Y. Liao and G. S. Harbison, *J. Chem. Phys.* **100**, 1895 (1994).

6. An exotic NMR experiment using applied electric fields to interact with the nuclear spins is described in M. Lukac and E. L. Hahn, *Adv. Magn. Reson.* **14**, 75 (1990).

7. The non-resonant and longitudinal components of the r.f. field can be important in NMR experiments in very low field, and for NMR experiments in the presence of very large internal spin interactions, such as quadrupolar couplings. For example, *overtone* NMR experiments sometimes exploit the longitudinal r.f. field. See R. Tycko and S. J. Opella, *J. Chem. Phys.* **86**, 1761 (1986).

8. It is technically possible to create an r.f. field that rotates, rather than oscillates (this is sometimes done in NMR imaging instruments). This requires that the r.f. field rotates in the correct sense with respect to the static field (see Section 2.5). In the case of a rotating r.f. field, the factor 1/2 may be omitted in Equation 8.16.

9. The non-secular terms may cause shifts in the peak positions, called *dynamic frequency shifts*. These shifts are usually very small, except for the case of quadrupolar interactions. Dynamic frequency shifts are ignored in this book.

10. In rare cases, the chemical shift anisotropy (CSA) in gases does not average completely to zero. The residual interaction is determined by the collisions of the noble gas atoms with the walls of the container, which leads to NMR spectra that depend on the shape of the vessel. This phenomenon has been observed for gas-phase ^{129}Xe NMR; see B. M. Goodson, *J. Magn. Reson.* **155**, 157–216 (2002).

Further Reading

- For a treatment of the nuclear quadrupolar interaction, see C. P. Slichter, *Principles of Magnetic Resonance, 3rd edition*, Springer, Berlin, 1989.
- For a review of some effects involving long-range intermolecular dipolar interactions in liquids, see M. H. Levitt, *Concepts Magn. Reson.*, **8**, 77 (1996).
- For applications of long–range dipole–dipole couplings, see S. Vathyam, S. Lee and W. S. Warren, *Science*, **272**, 92 (1996) and references therein.

Exercises

8.1 An r.f. coil is tuned to oscillate at a frequency of $\omega_{\text{osc}}/2\pi = 50.0\,\text{MHz}$. The peak value of the oscillating magnetic field in the coil is $B_{\text{RF}} = 1\,\text{mT}$.
- (i) What value of the static field B^0 brings ^{1}H spins into resonance with the coil?
- (ii) What is the nutation frequency ω_{nut} of ^{1}H spins in the coil if the static field is set to the value calculated in (i) and the coil is oriented perpendicular to the field ($\theta_{\text{RF}} = \pi/2$)?
- (iii) What is the nutation frequency ω_{nut} of ^{1}H spins in the coil if the static field is set to the value calculated in (i) and the coil is at the magic angle to the field ($\theta_{\text{RF}} = \arctan\sqrt{2}$)?
- (iv) What value of the static field B^0 brings ^{15}N spins into resonance with the coil?
- (v) What is the nutation frequency ω_{nut} of ^{15}N spins in the coil if the static field is set to the value calculated in (iv) and the coil is oriented perpendicular to the field ($\theta_{\text{RF}} = \pi/2$)?
- (vi) What is the nutation frequency ω_{nut} of ^{15}N spins in the coil if the static field is set to the value calculated in (iv) and the coil is at the magic angle to the field ($\theta_{\text{RF}} = \arctan\sqrt{2}$)?

9 Internal Spin Interactions

In this chapter, the internal spin interaction terms are examined in more detail.

9.1 Chemical Shift

The electrons in the molecules cause the local magnetic fields to vary on a *submolecular* distance scale. The magnetic fields experienced by nuclei at two sites in the same molecule are different if the electronic environments are different. For example, protons located in the $-CH_3$ groups of ethanol molecules experience slightly different magnetic fields than protons located in the $-CH_2$ groups. This effect is called the *chemical shift*. It is of major importance to the chemical applications of NMR.

The chemical shift is predominantly an intramolecular interaction, but it does have a significant intermolecular component as well. For example, chemical shifts are slightly different in different solvents, and are slightly different for the same molecular system in solids and in liquids. Chemical shifts may even be different for formally identical molecules in the same crystal if the asymmetric unit of the crystal structure contains more than one molecule, as is often the case.

The mechanism of the chemical shift is a two-step process. (i) The external magnetic field $\mathbf{B}^0$ induces *currents* in the electron clouds in the molecule. (ii) The circulating molecular currents in turn generate a magnetic field (called the *induced field* $\mathbf{B}_j^{\text{induced}}$):

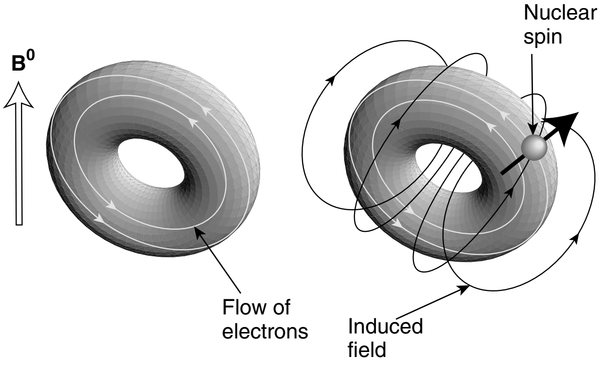

Figure 9.1 Mechanism of the chemical shift.

The nuclear spins sense the sum of the applied external field and the induced field generated by the molecular electrons:

Spin Dynamics: Basics of Nuclear Magnetic Resonance, Second Edition Malcolm H. Levitt

$$\boxed{\mathbf{B}_j^{\mathrm{loc}} = \mathbf{B}^0 + \mathbf{B}_j^{\mathrm{induced}} \qquad (9.1)}$$

Typically, the induced field is only around 10^{-4} of the external field B^0. This is small, but large enough to give rise to measurable shifts in the spin precession frequencies.

The strength of the induced currents, and hence the induced field, is directly proportional to the applied field B^0.

The induced currents themselves may be explained by the quantum-mechanical behaviour of the electrons. Two contributions to the induced currents have been identified: (1) field-induced circulation of electrons in the ground electronic state (diamagnetic term)[1] and (2) electron circulation through participation of excited electronic states (paramagnetic term). These terms have similar magnitudes but opposite signs, which makes the calculation of accurate chemical shifts a challenging task (see *Further Reading*).

9.1.1 Chemical shift tensor

The induced field is, to a very good approximation, linearly dependent on the applied field, and may be written[2]

$$\boxed{\mathbf{B}_j^{\mathrm{induced}} = \boldsymbol{\delta}^j \cdot \mathbf{B}^0 \qquad (9.2)}$$

The symbol $\boldsymbol{\delta}^j$ represents a 3×3 matrix of real numbers, called the *chemical shift tensor* of site I_j. In matrix-vector form, the equation reads

$$\begin{pmatrix} B_{j,x}^{\mathrm{induced}} \\ B_{j,y}^{\mathrm{induced}} \\ B_{j,z}^{\mathrm{induced}} \end{pmatrix} = \begin{pmatrix} \delta_{xx}^j & \delta_{xy}^j & \delta_{xz}^j \\ \delta_{yx}^j & \delta_{yy}^j & \delta_{yz}^j \\ \delta_{zx}^j & \delta_{zy}^j & \delta_{zz}^j \end{pmatrix} \cdot \begin{pmatrix} 0 \\ 0 \\ B^0 \end{pmatrix} \qquad (9.3)$$

which evaluates to

$$\begin{pmatrix} B_{j,x}^{\mathrm{induced}} \\ B_{j,y}^{\mathrm{induced}} \\ B_{j,z}^{\mathrm{induced}} \end{pmatrix} = \begin{pmatrix} \delta_{xz}^j B^0 \\ \delta_{yz}^j B^0 \\ \delta_{zz}^j B^0 \end{pmatrix}$$

assuming that the applied static field B^0 is along the z-axis of the laboratory frame. The use of the matrix δ^j takes into account the fact that the induced field is usually in a different direction to the applied field. For example, $\delta_{xz}^j B^0$ signifies the component of the induced field in the x-direction when the external field is applied in the z-direction. It may usually be assumed that δ^j is symmetric, i.e. $\delta_{xy}^j = \delta_{yx}^j$, and so on.[3]

Why is the induced field not always parallel to the applied field? The basic idea is simple: since the induced field lines form closed loops, they must change direction as they go around the molecule. In addition, molecules have a definite three-dimensional shape, and the electrons may find it easier to circulate around certain axes. For example, electrons run readily around the doughnut-shaped orbitals in a benzene ring. If the ring is at some skewed orientation with respect to the field, one can easily imagine that the induced field runs through the hole in the doughnut and out round the sides (illustrated in Figure 9.1). The magnitude and direction of the induced field at a given nuclear site, therefore, depends on the orientation of the molecule with respect to the external field, and also on the location of the nuclear spin within the molecule.

9.1.2 Principal axes

For each nuclear site, there are three *special* directions of the external magnetic field for which the induced field *is* parallel to the external field. These special directions are always perpendicular to each other, and are called the *principal axes of the chemical shift tensor*. The principal axes are indicated by the capital letters X, Y and Z. Their directions often correlate with local molecular structural features. For example, consider a ^{13}C nucleus at the carbon site of a carboxylate group. In most cases, one of the principal axes of the chemical shift tensor is approximately perpendicular to the carboxylate plane. The other two principal axes are close to the CO_2 plane, with their orientation within the plane being sensitive to the local electronic environment:

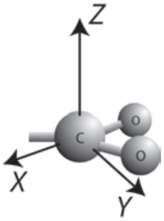

Figure 9.2
The Z-principal axis of the ^{13}C chemical shift tensor of a carboxylate group is approximately perpendicular to the CO_2 plane.

The induced field is parallel to the applied field whenever the applied field is in one of these special directions:

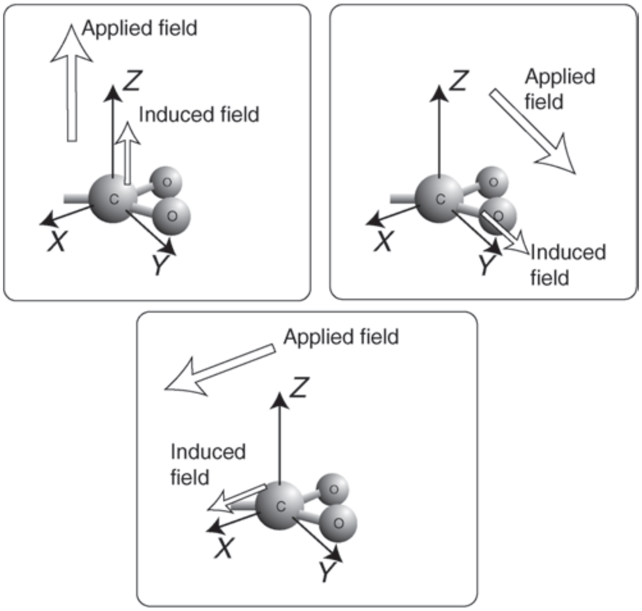

Figure 9.3
If the static magnetic field is applied along a principal axis direction, the induced field is parallel to the static field.

It is important to realize that every nuclear site in a molecule has, in general, a chemical shift tensor with a *different* principal axis system.

9.1.3 Principal values

If the external magnetic field $\mathbf{B}^0$ is applied along a principal axis of the chemical shift tensor of a site j, the induced field at the same site is in the same direction and is given by the following equations:

$$\begin{aligned}\mathbf{B}_j^{\text{induced}} &= \delta_{XX}^j \mathbf{B}^0 \quad (\text{if } \mathbf{B}^0 \text{ is along the } X \text{ principal axis})\\ \mathbf{B}_j^{\text{induced}} &= \delta_{YY}^j \mathbf{B}^0 \quad (\text{if } \mathbf{B}^0 \text{ is along the } Y \text{ principal axis})\\ \mathbf{B}_j^{\text{induced}} &= \delta_{ZZ}^j \mathbf{B}^0 \quad (\text{if } \mathbf{B}^0 \text{ is along the } Z \text{ principal axis})\end{aligned}$$

The numbers δ_{XX}^j, δ_{YY}^j and δ_{ZZ}^j are called the *principal values* of the chemical shift tensor for site j. In general, the three principal values are all different. Capital subscripts XX, YY and ZZ are used to denote the principal values.

By definition, 'off-diagonal' shift tensor elements, such as δ_{XZ}^j, δ_{YZ}^j, etc., are all equal to zero in the principal axis system.

9.1.4 Isotropic chemical shift

The mean of the three principal values is called the *isotropic chemical shift*:

$$\boxed{\delta_j^{\text{iso}} = \frac{1}{3}\left(\delta_{XX}^j + \delta_{YY}^j + \delta_{ZZ}^j\right) \qquad (9.4)}$$

As discussed below, the isotropic chemical shift determines the positions of peaks in isotropic liquids. In many cases, when the term 'chemical shift' is used, it is the isotropic chemical shift that is meant.

9.1.5 Chemical shift anisotropy (CSA)

If all three principal values are equal, then the chemical shift tensor is said to be *isotropic*. If two or more principal values of the chemical shift tensor are different, then the chemical shift tensor is said to be *anisotropic*. The *CSA* quantifies the deviation from isotropy.

The most widespread convention[4] for assigning the CSA principal values and principal axes is as follows:

1. Assign the Z principal axis to the principal value that is *furthest* from the isotropic chemical shift.
2. Assign the Y principal axis to the principal value that is *closest* to the isotropic chemical shift.
3. Assign the X principal axis to the *other* principal value. This procedure leads to the following ordering:

$$|\delta^j_{ZZ} - \delta^{\text{iso}}_j| \geq |\delta^j_{XX} - \delta^{\text{iso}}_j| \geq |\delta^j_{YY} - \delta^{\text{iso}}_j| \tag{9.5}$$

The *CSA* is defined as the *largest deviation in chemical shift from the isotropic value* (including the sign):

$$\delta^{\text{aniso}}_j = \delta^j_{ZZ} - \delta^{\text{iso}}_j \tag{9.6}$$

The difference between the other two principal values is quantified by a parameter which is denoted η_j, and which is known by a variety of names.[5] In this book I use the term *biaxiality*. It is defined as follows:

$$\eta_j = \frac{\delta^j_{YY} - \delta^j_{XX}}{\delta^{\text{aniso}}_j} \tag{9.7}$$

With this set of definitions, the biaxiality η_j takes values in the range 0 to 1.

If two principal values are equal, then the biaxiality η_j is equal to zero. The chemical shift tensor is then said to be *uniaxial*.[6]

⚠The conventional assignment of chemical shift principal values, given in Equation 9.5, does *not* generally correspond to an ascending sequence $\delta^j_{XX} \leq \delta^j_{YY} \leq \delta^j_{ZZ}$. This is commonly misunderstood.[4]

The chemical shift tensor of a particular molecular site is often represented by an ellipsoid. The principal axes of the ellipsoid coincide with the chemical shift principal values. An isotropic CSA tensor is represented by a sphere, whereas a uniaxial CSA tensor is represented by a cigar shape, and a biaxial CSA tensor is represented by a flattened ellipsoid with different dimensions in all three directions:

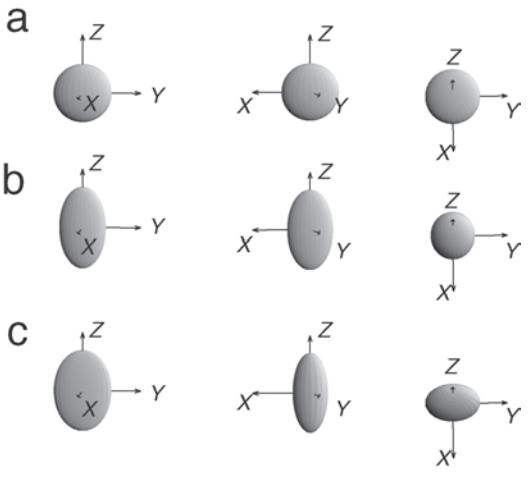

Figure 9.4
Ellipsoids representing CSA tensors, shown from three different viewpoints: (a) an isotropic CSA tensor ($\delta^{\text{aniso}}_j = 0$); (b) a uniaxial CSA tensor ($\delta^{\text{aniso}}_j \neq 0$, $\eta_j = 0$); (c) a biaxial CSA tensor ($\delta^{\text{aniso}}_j \neq 0$, $\eta_j \neq 0$).

In a complex molecular structure, the CSA tensors of the individual nuclear sites may be visualized by drawing a molecular structure with ellipsoids centred at the relevant molecular position. The orientation, size, and biaxiality of the ellipsoids allows one to visualize the principal values and principal axis orientations of the individual chemical shift tensors. Figure 9.5 depicts peptide planes in a protein, with typical CSA tensors attached to the ^{13}C, ^{1}H and ^{15}N sites.

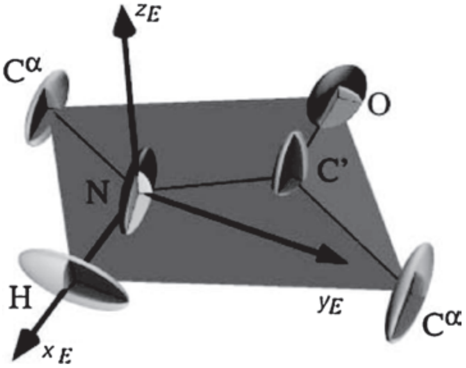

Figure 9.5 A peptide bond (–NH—CO–) joins adjacent amino acids in a protein. In most cases, the four atoms of the peptide bond lie close to the same plane, shown by the shaded region. The ellipsoids represent typical CSA tensors for the chemical shielding of ^{13}C, ^{15}N and ^{1}H nuclei at the C, N and H sites, and a typical electric field gradient tensor for the quadrupolar interaction of a ^{17}O nucleus at the carbonyl oxygen site. The arrows show an orthogonal local axis system attached to the peptide plane. Adapted from M. Bak, R. Schultz, Y. Vosegaard and N. C. Nielsen, *J. Magn. Reson.* **154**, 28–45 (2002), copyright Elsevier.

9.1.6 Chemical shift for an arbitrary molecular orientation

Suppose, now, that the direction of the magnetic field does not coincide with a principal axis direction. In this case, the observed chemical shift is not equal to one of the three principal values.

The general case may be handled by writing the CSA tensor as follows:

$$\boldsymbol{\delta}^j = \mathcal{R}^j(\Theta)\cdot\begin{pmatrix}\delta^j_{XX} & 0 & 0\\ 0 & \delta^j_{YY} & 0\\ 0 & 0 & \delta^j_{ZZ}\end{pmatrix}\cdot\mathcal{R}^j(\Theta)^{-1} \tag{9.8}$$

where the orientation of the molecule is denoted Θ and $\mathcal{R}^j(\Theta)$ is a 3×3 *rotation matrix* that describes the relative orientation of the CSA principal axis and the external magnetic field:

$$\mathcal{R}^j(\Theta) = \begin{pmatrix}R^j_{xX}(\Theta) & R^j_{xY}(\Theta) & R^j_{xZ}(\Theta)\\ R^j_{yX}(\Theta) & R^j_{yY}(\Theta) & R^j_{yZ}(\Theta)\\ R^j_{zX}(\Theta) & R^j_{zY}(\Theta) & R^j_{zZ}(\Theta)\end{pmatrix} \tag{9.9}$$

and

$$\mathcal{R}^j(\Theta)^{-1} = \begin{pmatrix}R^j_{Xx}(\Theta) & R^j_{Yx}(\Theta) & R^j_{Zx}(\Theta)\\ R^j_{Xy}(\Theta) & R^j_{Yy}(\Theta) & R^j_{Zy}(\Theta)\\ R^j_{Xz}(\Theta) & R^j_{Yz}(\Theta) & R^j_{Zz}(\Theta)\end{pmatrix} \tag{9.10}$$

Expressions for the elements of $\mathcal{R}^j(\Theta)$ and $\mathcal{R}^j(\Theta)^{-1}$ are given in Appendix A.1.

The nuclear spin interacts with the induced field according to the recipe in Section 8.2.2. The full form of the chemical shift interaction of spin I_j is therefore

$$\begin{aligned}\widehat{\mathcal{H}}_j^{\text{CS,full}} &= -\hat{\boldsymbol{\mu}}_j \cdot \mathbf{B}_j^{\text{induced}} \\ &= -\gamma_j \delta_{xz}^j(\Theta) B^0 \hat{I}_{jx} - \gamma_j \delta_{yz}^j(\Theta) B^0 \hat{I}_{jy} - \gamma_j \delta_{zz}^j(\Theta) B^0 \hat{I}_{jz} \end{aligned} \tag{9.11}$$

where

$$\delta_{zz}^j(\Theta) = R_{zX}^j(\Theta)\delta_{XX}^j R_{Xz}^j(\Theta) + R_{zY}^j(\Theta)\delta_{YY}^j R_{Yz}^j(\Theta) + R_{zZ}^j(\Theta)\delta_{ZZ}^j R_{Zz}^j(\Theta) \tag{9.12}$$

and similarly for the elements $\delta_{xx}^j(\Theta)$ and $\delta_{yy}^j(\Theta)$.

9.1.7 Chemical shift frequency

As shown in Appendix A.6, only the last term in Equation 9.11 is retained in the secular approximation. The secular chemical shift Hamiltonian, after motional averaging, is therefore

$$\widehat{\mathcal{H}}_j^{\text{CS}} \cong -\gamma_j \overline{\delta_{zz}^j(\Theta)} B^0 \hat{I}_{jz} \tag{9.13}$$

where the term δ_{zz}^j depends on the molecular orientation Θ and the chemical shift principal values according to Equation 9.12.

It is convenient to combine the external interaction in Equation 8.14 and the chemical shift interaction in Equation 9.13:

$$\widehat{\mathcal{H}}_j^0 = \widehat{\mathcal{H}}_j^{\text{static}} + \widehat{\mathcal{H}}_j^{\text{CS}} = \omega_j^0 \hat{I}_{jz} \tag{9.14}$$

where ω_j^0 is called the *chemically shifted Larmor frequency*.

In general, the chemically shifted Larmor frequency ω_j^0 depends on the motionally averaged chemical shift according to

$$\omega_j^0 = -\gamma_j B^0 \left(1 + \overline{\delta_{zz}^j(\Theta)}\right) \tag{9.15}$$

This formula neglects susceptibility effects and the chemical shift of the reference compound used to set the origin of the $\delta = 0$ scale (usually TMS).

As usual, the sign of the chemically shifted Larmor frequency ω_j^0 depends on the sign of γ_j, i.e. negative for spins with positive γ_j and positive for spins with negative γ_j.

9.1.8 Chemical shift interaction in isotropic liquids

In an isotropic liquid, the molecules tumble rapidly through every conceivable molecular orientation, with equal probability for each orientation. The observed chemical shift is therefore the *isotropic average* of the term $\delta_{zz}^j(\Theta)$:

$$\overline{\delta_{zz}^j(\Theta)} = \mathrm{N}^{-1} \int \mathrm{d}\Theta\ \delta_{zz}^j(\Theta) \qquad \text{(in isotropic liquids)}$$

where N is a normalization constant, chosen so that the sum probability of all orientations is unity.

The isotropic average of $\delta^j_{zz}(\Theta)$ is simply the isotropic chemical shift, as defined in Equation 9.4:

$$\overline{\delta^j_{zz}(\Theta)} = \delta^{\mathrm{iso}}_j \qquad \text{(in isotropic liquids)}$$

The motionally averaged chemical shift Hamiltonian in isotropic liquids is therefore given by Equation 9.14, where the *isotropic chemical shift frequency* is defined through:

$$\boxed{\omega^0_j = -\gamma_j B^0 \left(1 + \delta^{\mathrm{iso}}_j\right) \qquad \text{(in isotropic liquids)} \qquad (9.16)}$$

In an isotropic liquid, the chemical shift is equal to the isotropic chemical shift and does not depend on the orientation of the sample with respect to the magnetic field.

The isotropic chemical shift is of central importance in chemistry as a diagnostic tool for molecular structure and dynamics. The literature on the subject is enormous (see *Further Reading*). Here, I simply note the following qualitative observations:

- The major contribution to the chemical shift usually comes from the influence of low-lying electronic excited states. Heavier atoms tend to have more low-lying excited states than lighter atoms, leading to a larger chemical shift range for heavy isotopes. For example, the chemical shift range for ^{1}H is normally only around 10 ppm, whereas for ^{13}C it is around 200 ppm. Heavy nuclei, such as ^{209}Pb, often have chemical shifts of many thousands of parts per million.

- The chemical shift δ correlates well with electronegativity: electronegative atoms, like O, Cl, F, etc, tend to withdraw electron density from neighbouring groups, increasing the local fields at the nuclei of neighbouring atoms, which leads to increased δ values.

- In rigid molecules with a well-defined three-dimensional structure, the chemical shift is influenced by neighbouring molecular units with a strong magnetic susceptibility, even if there is no direct chemical link. For example, a benzene ring readily supports induced electron currents and tends to decrease the local fields of nuclei situated close to the local symmetry axis (decreasing δ) and increase the local fields of nuclei close to the plane of the ring (increasing δ):

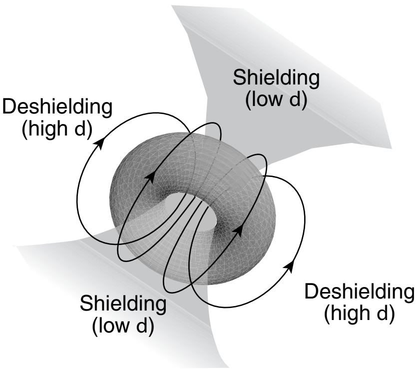

Figure 9.6
The ring current shift.

This is called the *ring-current shift*. It is sometimes used to provide clues about the secondary molecular structure.

- The isotropic chemical shift is an average over rapid molecular motions. In cases with significant dynamics, this can be quite misleading. Consider, for example, the case where a molecule may exist in two different chemical forms, each of which has a different chemical shift. The NMR spectrum normally contains two peaks for each nuclear site, corresponding to the two molecular forms. However, if a rapid chemical exchange process occurs, which causes the molecules to jump frequently from one state to the other, the NMR spectrum contains only one peak for each nuclear site, at the average chemical shift of the two species (see Section 19.5). This average chemical shift must be interpreted with care. At no time does any chemical species exist that actually has this average chemical shift.

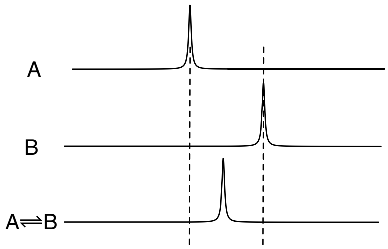

Figure 9.7
Averaging of the chemical shift over a chemical exchange process.

- The chemical shift of a spin in a particular nuclear site depends slightly on the nuclear isotopes in neighbouring nuclear sites. For example, the methyl proton chemical shifts in isotopomers of ethanol, such as $^{12}CH_3{}^{12}CH_2OH$, $^{13}CH_3{}^{12}CH_2OH$, etc., are slightly different. This small effect is called the *secondary isotope shift* (not to be confused with the *isotropic* chemical shift).[7]

- Chemical shifts are subject to fairly remote influences, such as those due to neighbouring molecules. For this reason, isotropic chemical shifts in the solid state may differ slightly from isotropic chemical shifts in solution. Similarly, chemically identical molecules in the same crystal may have slightly different chemical shifts, if they are not related by a crystal symmetry operation. This is the case when the asymmetric unit of a crystal contains more than one molecule.[8]

Typical chemical shift ranges for a number of different isotopes are given in Figure 3.31.

9.1.9 Chemical shift interaction in anisotropic liquids

In an anisotropic liquid (liquid crystal), the motional average of the chemical shift tensor element δ^j_{zz} is given by

$$\overline{\delta^j_{zz}(\Theta)} = \int \mathrm{d}\Theta \; \delta^j_{zz}(\Theta)\, \mathrm{p}(\Theta)$$

and $\mathrm{p}(\Theta)\mathrm{d}\Theta$ is the probability of the molecule having an orientation in the range Θ to $\Theta + \mathrm{d}\Theta$. In general, this is not equal to the isotropic chemical shift δ^{iso}_j.

As a result, the NMR peak frequencies change suddenly if the system undergoes a phase transition from a liquid crystalline phase to an isotropic liquid phase:

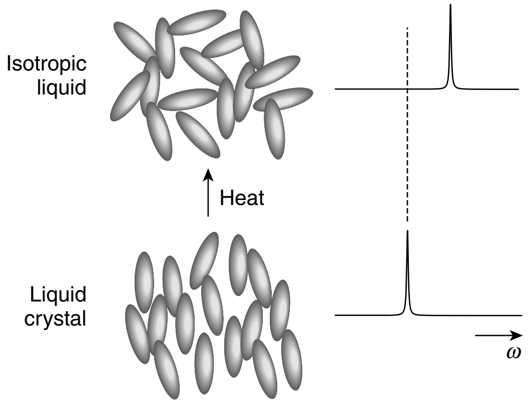

Figure 9.8
The chemical shift changes upon a phase transition.

This phenomenon makes NMR a useful spectroscopic method for studying phase transitions in liquid crystals.

9.1.10 Chemical shift interaction in solids

The chemical shift Hamiltonian in Equation 9.13 depends on the tensor component δ^j_{zz}. This chemical shift tensor element depends on the orientation Θ of the atomic framework with respect to the magnetic field. In solids, the chemical shift frequency is given by

$$\boxed{\omega^0_j(\Theta) = -\gamma_j B^0 \left(1 + \delta^j_{zz}(\Theta)\right) \qquad (9.17)}$$

which depends on the molecular orientation, as well as the principal values and axes of the chemical shift tensor through Equation 9.12.

Consider, for example, a single crystal of a molecular solid. In this case, the molecules are lined up on a rigid lattice, and in the simplest case, all molecules have the same orientation.[9] As a result, the chemical shift is the same for all molecules and depends on the orientation of the crystal with respect to the magnetic field. It is possible to change the chemical shift by rotating the crystal:

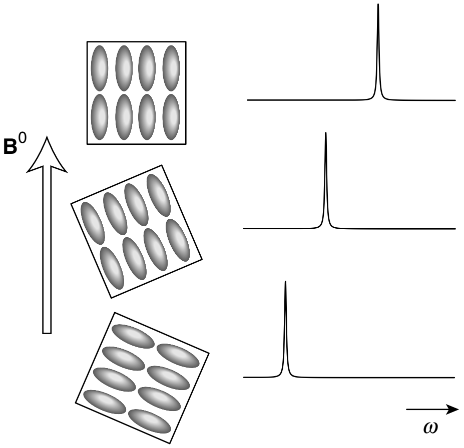

Figure 9.9
In a crystal, the chemical shift depends on the orientation of the solid with respect to the magnetic field.

A *powder*, on the other hand, the molecules have all possible orientations. The NMR spectrum of a powder is often very broad, because the chemical shift of each crystallite is different. The solid-state NMR spectrum of a powder has a typical broad shape with sharp corners, called a *powder pattern*:

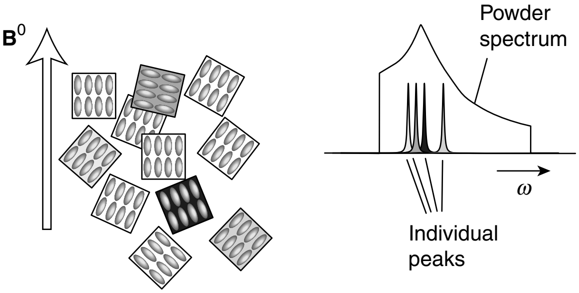

Figure 9.10
Formation of a powder pattern.

The broad pattern comes from the superposition of many sharp peaks with different frequencies, each one coming from a crystallite with a different orientation. The broadening of powder NMR spectra due to CSA is an example of *inhomogeneous broadening*.

The sharp features of a chemical shift powder pattern coincide with the principal values of the chemical shift tensor $\{\delta^j_{XX}, \delta^j_{YY}, \delta^j_{ZZ}\}$. The shape of the static powder pattern generated by nuclei in a single molecular site depends on the CSA (including the sign) and the biaxiality of the chemical shift tensor. Some typical spectral shapes for single molecular sites in a powder sample are shown in Figure 9.11. An experimental example is shown in Figure 9.12.

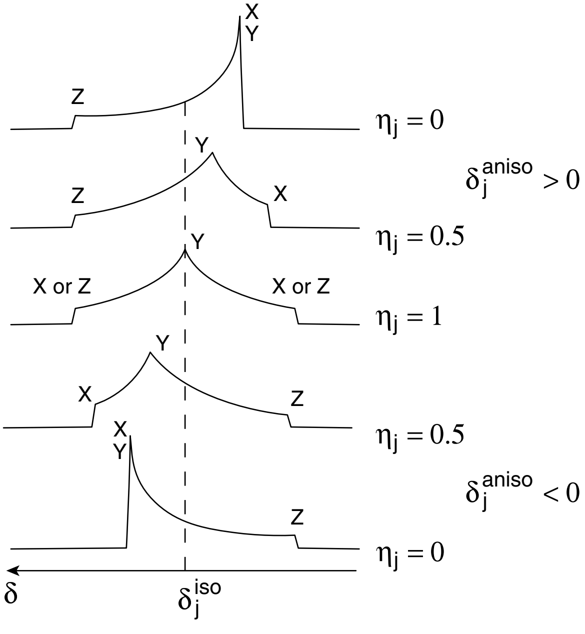

Figure 9.11
Powder pattern lineshapes for a single molecular site with CSA. All patterns belong to sites with the same magnitude of CSA $|\delta_j^{\text{aniso}}|$. The CSA is positive for the upper two patterns, and negative for the lower two. The sign of the CSA may be chosen arbitrarily in the case of maximum biaxiality ($\eta_j = 1$). The dashed line shows the position of the isotropic chemical shift δ_j^{iso}.

The orientation dependence of the chemical shift in a solid may be reduced greatly if there is significant molecular motion. In the extreme case of *plastic crystals* (see Section 8.6), the rapid isotropic motion of the molecules almost completely removes the CSA.

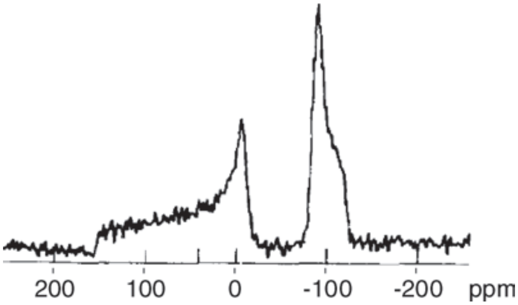

Figure 9.12 Experimental ^{1}H-decoupled ^{13}C spectrum for frozen acetic anhydride. The spectrum displays a powder pattern for each of the two chemically distinct ^{13}C sites. Both CSA tensors are almost uniaxial $\eta_j \cong 0$, but the sign and magnitude of the CSA are different. Reused from A. Pines, M. G. Gibby and J. S. Waugh, *J. Chem. Phys.* **59**, 569–590 (1973). Copyright 1973, American Institute of Physics.

9.1.11 Chemical shift interaction: summary

The following diagram summarizes the form of the chemical shift interaction in liquids and solids:

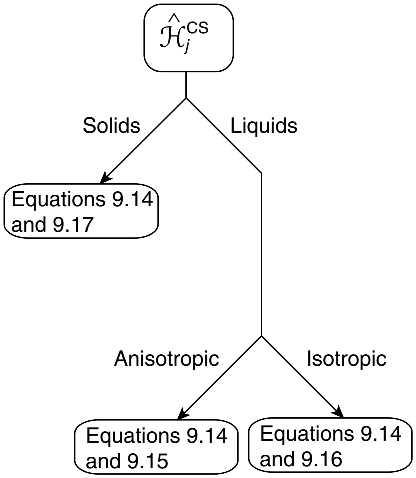

Figure 9.13
Flow diagram for the chemical shift interaction.

9.2 Electric Quadrupole Coupling

If the nuclear spin is greater than 1/2, the electric quadrupole moment of the nucleus interacts strongly with the electric field gradients generated by the surrounding electron clouds.^{10} The quadrupolar coupling is predominantly, but not exclusively, an intramolecular interaction.

Table 9.1 Quadrupole moments of selected nuclear isotopes with $I > 1/2$. A complete listing of nuclear quadrupole moments may be found on the website `www.webelements.com`.

Isotope	Ground-state spin	Natural abundance/%	Electric quadrupole moment/ 10^{-28}m^2
^{2}H	1	0.012	0.2860
^{6}Li	1	7.59	−0.0808
^{7}Li	3/2	92.41	−4.01
^{11}B	3/2	80.1	4.059
^{14}N	1	99.6	2.044
^{17}O	5/2	0.038	−2.558
^{23}Na	3/2	100	10.4
^{27}Al	5/2	100	14.66
^{45}Sc	7/2	100	−22
^{51}V	7/2	99.8	−5.2
^{55}Mn	5/2	100	0.33
^{59}Co	7/2	100	0.42
^{63}Cu	3/2	69.2	−0.22
^{65}Cu	3/2	30.8	−0.204
^{87}Rb	3/2	27.8	0.132
^{93}Nb	9/2	100	−0.32

Electric quadrupole moments for several nuclear isotopes are listed in Table 9.1.

The quadrupolar coupling involves both a *nuclear* property (the quadrupole moment of the nucleus) and a *molecular* property (the electric field gradient created by the electrons at the site of the nucleus).[11] As a result, the nuclear quadrupole *moments* listed in Table 9.1 do not accurately reflect the typical magnitudes of the electric quadrupole *interaction*. For example, nuclei with large quadrupole moments may still have small quadrupole couplings, if the nuclear environment is so symmetric that the local electric field gradients are small. This is often the case for metal nuclei such as ^{7}Li ($I = 3/2$), ^{23}Na ($I = 3/2$) and ^{27}Al ($I = 5/2$), which are often found in symmetrical ionic environments. The opposite phenomenon occurs for ^{14}N ($I = 1$), which has a much smaller electric quadrupole moment than that of ^{23}Na and ^{27}Al, but which is usually found in covalently bonded sites with large local field gradients. As a result, the electric quadrupole coupling of ^{14}N is usually large, except in exceptional cases of high symmetry, such as NH_4^+ and other quaternary ions.

In order to simplify the notation, the spin index j is dropped for the rest of this section.

9.2.1 Electric field gradient tensor

The electric field gradient at the nuclear site is a tensor, similar in properties to the CSA tensor. The electric field gradient tensor at the site of a nucleus I has principal values,[12] denoted V_{XX}, V_{YY} and V_{ZZ}, that sum to zero:

$$V_{XX} + V_{YY} + V_{ZZ} = 0$$

These three principal values are associated with three principal axes, which are often close to local molecular symmetry axes. For example, Figure 9.5 shows an ellipsoid at the oxygen site, representing the local electric field gradient tensor as experienced by a ^{17}O nucleus.

The electric field gradient at the site of a nucleus I is usually specified by using two parameters, called eq and η_Q. The parameter eq is the largest principal value of the electric field gradient tensor:[12]

$$eq = V_{ZZ} \tag{9.18}$$

The parameter η_Q is the biaxiality of the electric field gradient tensor,[12] at the site of nucleus I:

$$\eta_Q = (V_{XX} - V_{YY})/V_{ZZ} \tag{9.19}$$

The biaxiality is a number between 0 and 1.

The electric field gradient tensor for an arbitrary molecular orientation Θ may be written as a 3×3 matrix as follows:

$$\mathbf{V}(\Theta) = \mathcal{R}_Q(\Theta) \cdot \begin{pmatrix} V_{XX} & 0 & 0 \\ 0 & V_{YY} & 0 \\ 0 & 0 & V_{ZZ} \end{pmatrix} \cdot \mathcal{R}_Q(\Theta)^{-1}$$

where the 3×3 rotation matrix $\mathcal{R}_Q(\Theta)$ describes the relative orientation of the electric field gradient principal axis system and the static magnetic field, and Θ is the molecular orientation. Explicit expressions for $\mathcal{R}_Q(\Theta)$ are given in Appendix A.7. Note the similarity between this equation and Equation 9.8 for the CSA.

9.2.2 Nuclear quadrupole Hamiltonian

The full form of the nuclear quadrupole Hamiltonian, for an arbitrary molecular orientation, is given by the following equation:

$$\widehat{\mathcal{H}}_Q^{\text{full}}(\Theta) = \frac{eQ}{2I(2I-1)\hbar}\, \hat{\mathbf{I}} \cdot \mathbf{V}(\Theta) \cdot \hat{\mathbf{I}} \tag{9.20}$$

where Q is the nuclear quadrupole moment, I is the nuclear spin quantum number, and the dot product has the following meaning:

$$\hat{\mathbf{I}} \cdot \mathbf{V}(\Theta) \cdot \hat{\mathbf{I}} = \hat{I}_x V_{xx}(\Theta)\hat{I}_x + \hat{I}_x V_{xy}(\Theta)\hat{I}_y + \hat{I}_x V_{xz}(\Theta)\hat{I}_z + \hat{I}_y V_{yx}(\Theta)\hat{I}_x + \ldots$$

If the quadrupolar interaction is much smaller than the Zeeman interaction, then the secular approximation may be used to discard many of the terms, just as for the chemical shift. However, the large size of the quadrupolar interaction often makes it necessary to include more than one term in the series:

$$\widehat{\mathcal{H}}_Q^{\text{full}} = \widehat{\mathcal{H}}_Q^{(1)} + \widehat{\mathcal{H}}_Q^{(2)} + \ldots \tag{9.21}$$

where $\widehat{\mathcal{H}}_Q^{(1)}$ is the *first-order quadrupolar Hamiltonian* and $\widehat{\mathcal{H}}_Q^{(2)}$ is the *second-order quadrupolar Hamiltonian*. The inclusion of $\widehat{\mathcal{H}}_Q^{(1)}$ alone is equivalent to the secular approximation, and is sufficient when the quadrupolar interaction is small. The second-order term $\widehat{\mathcal{H}}_Q^{(2)}$ must be included when the quadrupolar interaction is large.[13] Third-order terms are sometimes also necessary.

The *first-order quadrupolar Hamiltonian* may be written as follows:[14]

$$\hat{\mathcal{H}}_{\mathrm{Q}}^{(1)} = \omega_{\mathrm{Q}}^{(1)} \frac{1}{6}\left(3\hat{I}_z^2 - I(I+1)\hat{1}\right) \tag{9.22}$$

where $\omega_{\mathrm{Q}}^{(1)}$ is the *first-order quadrupolar coupling*.

In general, the first-order quadrupolar coupling is given by

$$\omega_{\mathrm{Q}}^{(1)} = \frac{3eQ\overline{V}_{zz}}{2I(2I-1)\hbar} \tag{9.23}$$

where $\overline{V}_{zz}$ denotes the average of the secular electric field gradient component $V_{zz}(\Theta)$ over molecular motion. For a fixed molecular orientation Θ, this secular component is given by

$$V_{zz}(\Theta) = R_{zX}^{\mathrm{Q}}(\Theta)V_{XX}R_{Xz}^{\mathrm{Q}}(\Theta) + R_{zY}^{\mathrm{Q}}(\Theta)V_{YY}R_{Yz}^{\mathrm{Q}}(\Theta) + R_{zZ}^{\mathrm{Q}}(\Theta)V_{ZZ}R_{Zz}^{\mathrm{Q}}(\Theta) \tag{9.24}$$

where $R_{zX}^{\mathrm{Q}}\ldots$ are the elements of the rotation matrix defining the orientation of the electric field gradient principal axis system with respect to the magnetic field. This equation is similar to Equation 9.12 and leads to a complicated dependence of the quadrupolar interaction on the molecular orientation.

The second-order quadrupolar Hamiltonian is a more complex term (see *Further Reading*). The *second-order quadrupole coupling* is of the order of the square of the first-order quadrupole coupling divided by the Larmor frequency:

$$\omega_{\mathrm{Q}}^{(2)} \sim \left|\frac{\left\{\omega_{\mathrm{Q}}^{(1)}\right\}^2}{\omega^0}\right| \tag{9.25}$$

The second-order quadrupolar coupling is therefore *inversely* proportional to the external magnetic field.

9.2.3 Isotropic liquids

In an *isotropic liquid*, the first-order quadrupolar coupling $\omega_{\mathrm{Q}}^{(1)}$ averages to zero. As a result, the motional average of the first-order quadrupolar Hamiltonian vanishes:

$$\hat{\mathcal{H}}_{Q}^{(1)} = 0 \qquad \text{(in isotropic liquids)} \tag{9.26}$$

The first-order quadrupolar interaction does not influence the position of peaks in the NMR spectra of isotropic liquids, to a first approximation.[15] The quadrupolar interaction does, on the other hand, strongly influence the *relaxation* of nuclear spins > 1/2 in isotropic liquids.

9.2.4 Anisotropic liquids

In an *anisotropic liquid* (liquid crystal), the electric field gradient term $V_{zz}(\Theta)$ does not average to zero. The first-order quadrupolar Hamiltonian in anisotropic liquids is given by Equations 9.22 and 9.23, where the electric field gradient component is averaged over molecular orientations, weighted by their probability in the liquid crystalline phase:

$$\overline{V_{zz}(\Theta)} = \int \mathrm{d}\Theta \; V_{zz}(\Theta)\, \mathrm{p}(\Theta) \tag{9.27}$$

The motionally averaged quadrupolar interaction of spins $> 1/2$ jumps from zero to some finite value if the system makes a phase transition from an isotropic liquid phase to a liquid crystalline phase.

The NMR of quadrupolar nuclei such as ^{2}H is a very powerful method for studying the ordering and dynamics of liquid crystals.

9.2.5 Solids

In a rigid solid, the first-order quadrupolar Hamiltonian is given by Equation 9.22, where the electric field gradient element V_{zz} depends on the electric field gradient principal values and the molecular orientation in a complicated way, as described by Equation 9.24. In general, the quadrupolar Hamiltonian depends on the orientation as well as the parameters eq and η_Q defining the magnitude and biaxiality of the electric field gradient tensor.

In the NMR of solids, it is common to specify the *quadrupole coupling constant* C_Q and the biaxiality parameter η_Q (Equation 9.19). The quadrupole coupling constant of a nucleus I is defined as follows:

$$C_Q = \frac{e^2 q Q}{h} \tag{9.28}$$

The coupling constant C_Q has units of hertz. Typical values of the quadrupole coupling constant range from a few kilohertz to tens or even hundreds of megahertz.[16]

The first-order quadrupolar interaction in a solid is written as follows:

$$\hat{\mathcal{H}}_Q^{(1)}(\Theta) = \omega_Q^{(1)}(\Theta) \times \frac{1}{6}\left(3\hat{I}_z^2 - I(I+1)\hat{1}\right) \quad \text{(in solids)} \tag{9.29}$$

where Θ is the molecular orientation. In the case of a uniaxial electric field gradient tensor ($\eta_Q = 0$), the first-order quadrupolar coupling $\omega_Q^{(1)}$ is given in terms of C_Q by the following expression:

$$\omega_Q^{(1)}(\Theta) = \frac{3\pi C_Q}{I(2I-1)} \times \frac{1}{2}(3\cos^2\theta_Q - 1) \quad (\text{for } \eta_Q = 0) \tag{9.30}$$

where θ_Q is the angle between the principal Z-axis of the electric field gradient tensor and the static magnetic field.

9.2.6 Quadrupole interaction: summary

The following diagram summarizes the form of the first-order quadrupolar coupling interaction in liquids and solids:

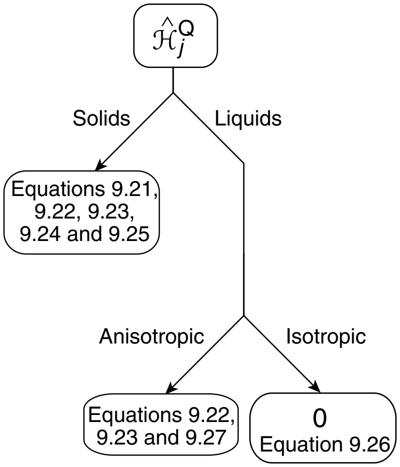

Figure 9.14
Flow diagram for the first-order quadrupole interaction.

9.3 Direct Dipole–Dipole Coupling

The direct dipole–dipole coupling between spins is easy to visualize. Since each nuclear spin is magnetic, it generates a magnetic field, looping around in the surrounding space, according to the direction of the spin magnetic moment. A second nuclear spin interacts with this magnetic field:

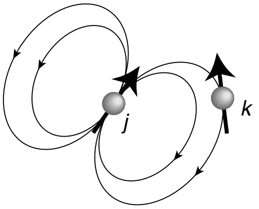

Figure 9.15
Magnetic field generated by spin j at the site of spin k.

The interaction between the spins is mutual. The first nuclear spin also experiences the field generated by the second nuclear spin:

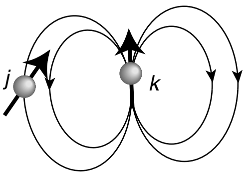

Figure 9.16
The dipole–dipole interaction is mutual.

This interaction is called the *through-space dipole–dipole coupling*, or *direct dipole–dipole coupling*, because the fields between the nuclear spins propagate through the intervening space, without involving the electron clouds. The more concise terms *dipole–dipole coupling* or *DD-coupling* are often used (somewhat loosely) as implying the through-space mechanism.

The dipole–dipole coupling may be either intramolecular or intermolecular.

The full form of the direct dipole–dipole interaction between spins I_j and I_k is represented in the spin Hamiltonian by the following term:

$$\widehat{\mathcal{H}}_{jk}^{\mathrm{DD,full}} = b_{jk}\left(3(\hat{\mathbf{I}}_j \cdot \mathbf{e}_{jk})(\hat{\mathbf{I}}_k \cdot \mathbf{e}_{jk}) - \hat{\mathbf{I}}_j \cdot \hat{\mathbf{I}}_k\right) \tag{9.31}$$

where $\mathbf{e}_{jk}$ is a unit vector parallel to the line joining the centres of the two nuclei:

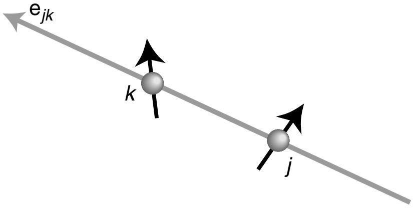

Figure 9.17
The unit vector $\mathbf{e}_{jk}$ is parallel to the line passing through both spins.

Note that the magnitude of the vector $\mathbf{e}_{jk}$ is defined to be $\mathbf{e}_{jk} \cdot \mathbf{e}_{jk} = 1$.

The magnitude of the through-space interaction is given by the *dipole–dipole coupling constant*, usually denoted b_{jk}, and given by

$$b_{jk} = -\frac{\mu_0}{4\pi}\frac{\gamma_j\gamma_k\hbar}{r_{jk}^3} \tag{9.32}$$

where γ_j and γ_k are the gyromagnetic ratios of the two spins (units of radians per second) and r_{jk} is the spin–spin distance between the two spins (units of metres). The clumsy magnetic constant $\mu_0 = 4\pi \times 10^{-7}\,\mathrm{H\,m^{-1}}$ is required in SI units.

Equation 9.32 provides the through-space coupling in units of radians per second. For example, two ^{1}H spins separated by a distance of 0.2 nm experience an interaction $b_{jk}/2\pi = -15.012$ kHz. The interaction goes down according to the inverse cube of the internuclear distance, and scales linearly with the gyromagnetic ratio of each interacting spin. Note that the dipole–dipole coupling b_{jk} is a *constant* and does not depend on molecular orientation. The dipole–dipole spin *Hamiltonian* in Equation 9.31, on the other hand, is orientation dependent, since the vector $\mathbf{e}_{jk}$ changes direction as the molecule rotates.

The negative sign in Equation 9.32 indicates that the coupling energy of the pair of interacting spins is minimized when both are pointing in the same direction along the internuclear vector, like two bar magnets arranged in a line, head to tail:

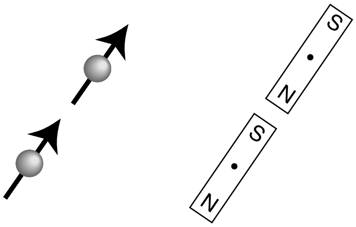

Figure 9.18
Magnetic spins are like bar magnets. Head to tail is the lowest energy configuration.

The direct dipole–dipole coupling is very useful for molecular structural studies, since it depends only on known physical constants and the inverse cube of the internuclear distance r_{jk}^{-3}. Estimation of this coupling provides a direct spectroscopic route to the distances between nuclei, and hence the geometrical form of the molecule. Measuring the through-space couplings of many spin pairs in a molecule can tie down the molecular structure and conformation unambiguously:

The NOESY and ROESY experiments (see Sections 20.6 and 20.7) make use of this principle.

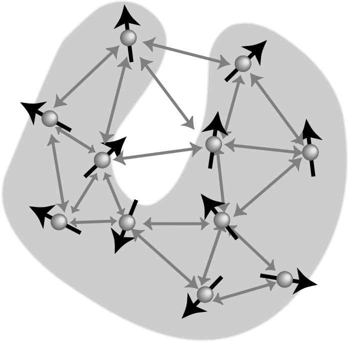

Figure 9.19
The magnitudes of many dipole-dipole couplings may be used to determine the molecular structure.

9.3.1 Secular dipole–dipole coupling

Consider now a sample containing many spins. Each pair of spins has a direct dipole–dipole coupling, described by Equation 9.31. The dipole–dipole coupling spin Hamiltonian of the whole sample is given by

$$\widehat{\mathcal{H}}^{\mathrm{DD,full}} = \sum_{k} \sum_{j}^{k-1} \widehat{\mathcal{H}}_{jk}^{\mathrm{DD,full}}$$

The double summation takes in all *pairs* of spins in the sample. This summation over pairs may also be written:

$$\widehat{\mathcal{H}}^{\mathrm{DD,full}} = \sum_{j<k} \widehat{\mathcal{H}}_{jk}^{\mathrm{DD,full}}$$

In high magnetic field, the non-secular part of the dipole–dipole coupling terms may be discarded. The form of the secular dipole–dipole coupling depends on whether the spins I_j and I_k are of the same isotopic species or not. As described in Appendix A.6, the secular approximation is based on the energy level differences between energy eigenstates, and these energy level differences depend strongly on whether the spin system is homonuclear or heteronuclear.

If the spins are of the same isotopic species (*homonuclear case*), then the secular part of the dipole–dipole spin Hamiltonian is given by

$$\boxed{\widehat{\mathcal{H}}_{jk}^{\mathrm{DD}}(\Theta_{jk}) = d_{jk}\ \left(3\hat{I}_{jz}\hat{I}_{kz} - \hat{\mathbf{I}}_j \cdot \hat{\mathbf{I}}_k\right) \qquad \text{(homonuclear case)} \qquad (9.33)}$$

where d_{jk} is the *secular dipole–dipole coupling*, given by

$$\boxed{d_{jk} = b_{jk}\,\frac{1}{2}\left(3\cos^2\Theta_{jk} - 1\right) \qquad (9.34)}$$

and Θ_{jk} is the angle between the vector joining the spins and the external magnetic field, i.e.

$$\cos\Theta_{jk} = \mathbf{e}_{jk}\cdot\mathbf{e}_z$$

as shown below:

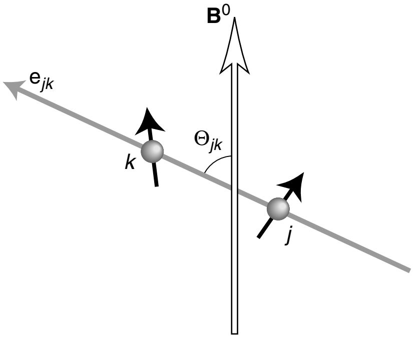

Figure 9.20
The angle Θ_{jk} is used in the calculation of the secular dipole–dipole coupling.

Note carefully the difference between the dipole–dipole coupling constant b_{jk} and the secular dipole–dipole coupling d_{jk}. The coupling constant b_{jk} depends on the distance between the spins, but does not depend on the orientation of the spin pair with respect to the magnetic field. The secular dipole–dipole coupling d_{jk} depends on the orientation and the distance.

If the spins are of different isotopic species (*heteronuclear case*), then the secular part of the direct dipole–dipole Hamiltonian is given by

$$\boxed{\widehat{\mathcal{H}}_{jk}^{\mathrm{DD}}(\Theta_{jk}) = d_{jk}\,2\hat{I}_{jz}\hat{I}_{kz} \qquad \text{(heteronuclear case)} \qquad (9.35)}$$

where d_{jk} is given by Equation 9.34. In both cases, the direct dipole–dipole coupling depends on the molecular orientation, through the angle Θ_{jk}.

The secular dipole–dipole coupling has opposite sign for spin pairs aligned along the field ($\Theta_{jk} = 0$) compared with spin pairs oriented perpendicular to the field ($\Theta_{jk} = \pi/2$). The secular dipole-dipole coupling d_{jk} is equal to zero when the angle Θ_{jk} between the internuclear vector and the static field satisfies the equation

$$3\cos^2\Theta_{jk} - 1 = 0 \qquad (9.36)$$

The solution of this equation is called the *magic angle*:

$$\boxed{\Theta_{\mathrm{magic}} = \arctan\sqrt{2} \cong 54.74^\circ \qquad (9.37)}$$

There is also a solution of Equation 9.36 at $\Theta_{jk} = \pi - \Theta_{\mathrm{magic}} \sim 125.26^\circ$.

9.3.2 Dipole–dipole coupling in isotropic liquids

In an *isotropic liquid*, the secular parts of the intramolecular dipole–dipole couplings average to zero. This is easily seen by evaluating the following integral:

$$\int_0^\pi \mathrm{d}\Theta_{jk} \sin\Theta_{jk} \left(3\cos^2\Theta_{jk} - 1\right) = 0 \tag{9.38}$$

The factor $\sin\Theta_{jk}$ is necessary in order to give all orientations equal probability. The area element on the surface of a sphere is proportional to $\sin\Theta_{jk}$:

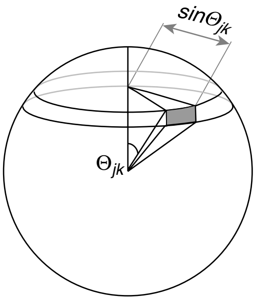

Figure 9.21
Area elements on the surface of a sphere.

The basic idea is that there are only two ways to orient a spin–spin vector along the magnetic field (up or down), whereas there are many ways of orienting a vector perpendicular to the magnetic field:

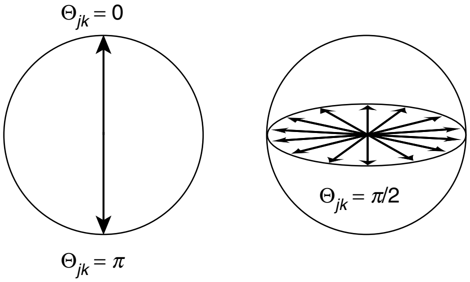

Figure 9.22
Relative probabilities for parallel and perpendicular orientations.

Similarly, the *short-range intermolecular* dipole–dipole couplings average to zero because of the translational motion of the molecules. The long-range dipole–dipole couplings do not average to zero in isotropic liquids, but these couplings are very small, and in most circumstances they may be ignored.

To a good approximation, therefore, we may write

$$\boxed{\widehat{\mathcal{H}}_{jk}^{\mathrm{DD}} \cong 0 \qquad \text{(in isotropic liquids)} \qquad (9.39)}$$

Although the secular dipole–dipole couplings essentially vanish in isotropic liquids, it is still possible to exploit the non-secular dipole–dipole couplings through their effect on the relaxation of the spin system, as discussed in Chapter 20.

9.3.3 Dipole–dipole coupling in liquid crystals

In an *anisotropic* liquid (liquid crystal), there is a preferential molecular orientation, as well as considerable translational motion of the molecules.

The *intra*molecular dipole–dipole couplings do not average out completely in an anisotropic liquid. The dipole–dipole Hamiltonian terms in an anisotropic liquid are given by Equation 9.33 in the homonuclear case and by Equation 9.35 in the heteronuclear case, where the secular dipole–dipole couplings are equal to

$$\boxed{d_{jk} = b_{jk}\,\overline{\frac{1}{2}\left(3\cos^2\Theta_{jk} - 1\right)} \qquad \text{(anisotropic liquids)} \qquad (9.40)}$$

The overbar indicates an average over all the orientations sampled by the molecules in the liquid crystalline phase, weighted by their probabilities.

The rapid diffusional motion in an anisotropic liquid averages out the *short-range intermolecular* dipole–dipole couplings, to a good approximation. The long-range intermolecular couplings survive the motional averaging, but are very small and may usually be ignored.

The form of the dipole–dipole coupling Hamiltonian in a liquid crystal is illustrated by the following diagram:

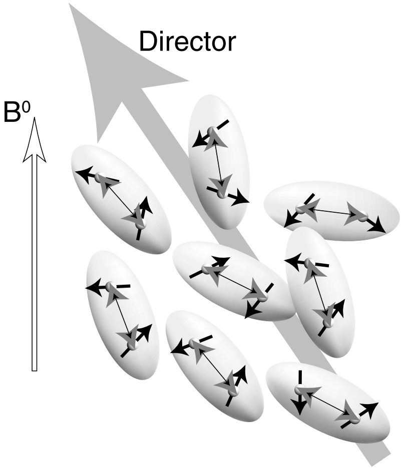

Figure 9.23
Dipole-dipole couplings in a liquid crystal.

Note the survival of intramolecular couplings and the absence of intermolecular couplings.

Intramolecular dipole–dipole couplings in an anisotropic liquid are encountered again in Section 16.4.

9.3.4 Dipole–dipole coupling in solids

In normal solids, every spin is coupled to every other spin. The dipole–dipole part of the spin Hamiltonian in solids is given by a sum of secular terms $\widehat{\mathcal{H}}_{jk}^{\mathrm{DD}}$ for every spin pair in the sample:

$$\widehat{\mathcal{H}}^{\mathrm{DD}} = \sum_{j<k} \widehat{\mathcal{H}}_{jk}^{\mathrm{DD}} \qquad \text{(in solids)}$$

The terms $\widehat{\mathcal{H}}_{jk}^{\mathrm{DD}}$ are given by Equation 9.33 if the spins I_j and I_k are of the same isotopic type (homonuclear case), and by Equation 9.35 if the spins I_j and I_k are of different isotopic types (heteronuclear case).

Both inter- and intra-molecular dipole–dipole couplings are important in a normal molecular solid:

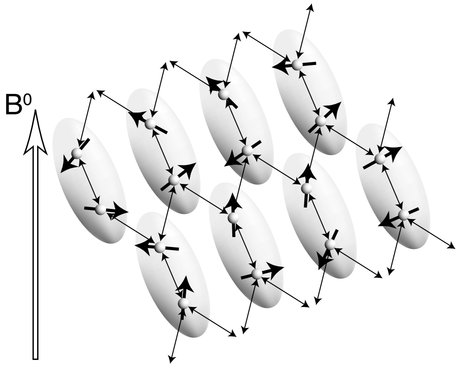

Figure 9.24
Dipole–dipole couplings in a normal molecular solid. For simplicity, only short range couplings are shown.

The situation is slightly different in plastic crystals such as adamantane (Section 8.6), since the rapid isotropic molecular rotations remove all the *intra*molecular interactions, leaving only the *inter*molecular interactions intact:

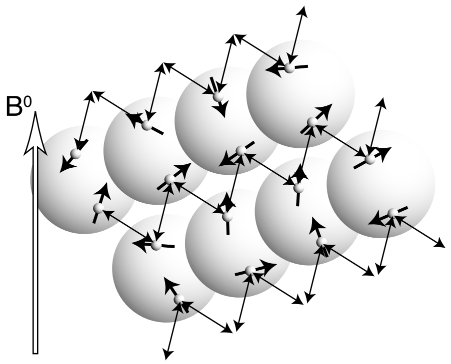

Figure 9.25
Dipole–dipole couplings in a plastic crystal.

As a result, the dipole–dipole couplings in a plastic crystal such as adamantane are much weaker than in a normal solid.

9.3.5 Dipole–dipole interaction: summary

The following diagram summarizes the form of the dipole–dipole coupling interaction in liquids and solids:

9.4 *J*-Coupling

Since the direct dipole–dipole coupling between nuclear spins has a zero average in isotropic liquids, it came as a great surprise to the spectoscopists of the 1950s when liquid-state NMR spectra were produced that showed clear signs of spin–spin coupling. Eventually, it was accepted that nuclear spins are coupled

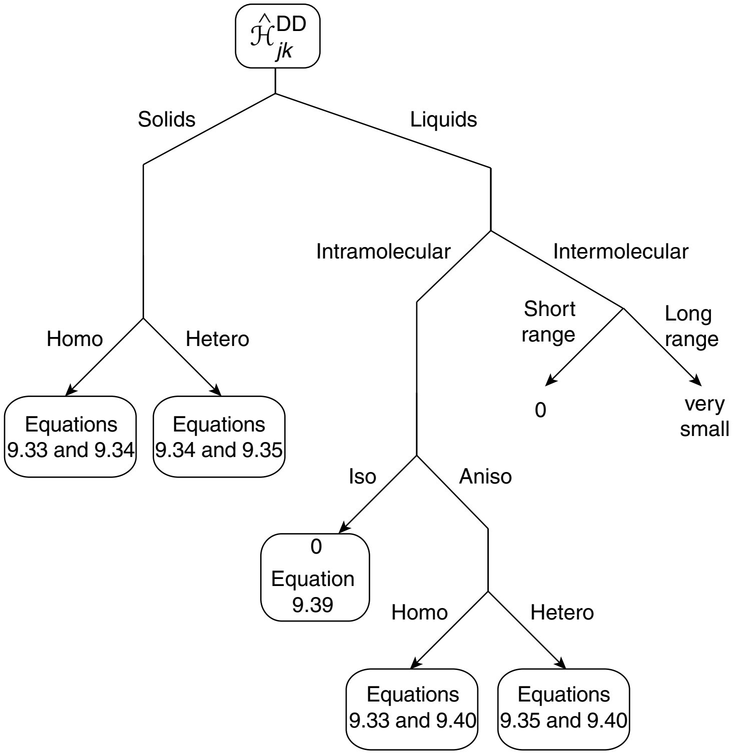

Figure 9.26
Flow diagram for the dipole-dipole interaction.

together even in completely isotropic liquids, because of the influence of the bonding electrons on the magnetic fields running between the nuclear spins. This type of nucleus–nucleus coupling is called *indirect*, to indicate the assistance of the bonding electrons in the coupling mechanism.

The participation of the electrons changes the orientation dependence of the interaction, thus generating an isotropic part that survives motional averaging in an isotropic liquid. The indirect coupling is usually represented by the symbol J. The terms *indirect spin–spin coupling*, *J-coupling*, and *indirect dipole–dipole coupling* are all synonyms.[17]

The J-coupling represents the second great link between NMR and chemistry. The chemical shift indicates the local electronic environment and the J-coupling provides a direct spectral manifestation of the *chemical bond*. Two spins have a measurable J-coupling only if they are linked together through a small number of chemical bonds, including hydrogen bonds. The J-coupling is exclusively intramolecular.

The full form of the intramolecular J-coupling interaction between spins I_j and I_k on the same molecule is

$$\boxed{\hat{\mathcal{H}}_{jk}^{\mathrm{J,full}} = 2\pi\, \hat{\mathbf{I}}_j \cdot \mathbf{J}_{jk} \cdot \hat{\mathbf{I}}_k \qquad (9.41)}$$

where $\mathbf{J}_{jk}$ is the *J-coupling tensor*, a 3×3 real matrix. The factor of 2π appears because the J-coupling is invariably quoted in units of hertz, whereas all equations in this book use radians per second. In matrix-vector form, the equation reads as follows:

$$\widehat{\mathcal{H}}_{jk}^{\mathrm{J,full}} = 2\pi \begin{pmatrix} \hat{I}_{jx}, & \hat{I}_{jy}, & \hat{I}_{jz} \end{pmatrix} \cdot \begin{pmatrix} J_{xx}^{jk} & J_{xy}^{jk} & J_{xz}^{jk} \\ J_{yx}^{jk} & J_{yy}^{jk} & J_{yz}^{jk} \\ J_{zx}^{jk} & J_{zy}^{jk} & J_{zz}^{jk} \end{pmatrix} \cdot \begin{pmatrix} \hat{I}_{kx} \\ \hat{I}_{ky} \\ \hat{I}_{kz} \end{pmatrix}$$

or more explicitly

$$\widehat{\mathcal{H}}_{jk}^{\mathrm{J,full}} = 2\pi J_{xx}^{jk} \hat{I}_{jx} \hat{I}_{kx} + 2\pi J_{yx}^{jk} \hat{I}_{jy} \hat{I}_{kx} + \ldots$$

9.4.1 Isotropic *J*-coupling

The *J*-coupling tensor $\mathbf{J}_{jk}$ depends on molecular orientation. In an isotropic liquid, this tensor is averaged out by the rapid molecular tumbling. The isotropic form of the *J*-coupling Hamiltonian is given by

$$\widehat{\mathcal{H}}_{jk}^{\mathrm{iso}} = 2\pi J_{jk}\, \hat{\mathbf{I}}_j \cdot \hat{\mathbf{I}}_k \tag{9.42}$$

or explicitly:

$$\widehat{\mathcal{H}}_{jk}^{\mathrm{iso}} = 2\pi J_{jk} \left(\hat{I}_{jx} \hat{I}_{kx} + \hat{I}_{jy} \hat{I}_{ky} + \hat{I}_{jz} \hat{I}_{kz} \right)$$

The term J_{jk} is called the *isotropic J-coupling*, or the *scalar coupling*. It is equal to the average of the diagonal elements of the *J*-coupling tensor:

$$J_{jk} = \frac{1}{3}(J_{xx}^{jk} + J_{yy}^{jk} + J_{zz}^{jk}) \tag{9.43}$$

The term 'scalar' indicates that $\widehat{\mathcal{H}}_{jk}^{\mathrm{iso}}$ is independent of molecular orientation.

Equation 9.43 resembles the definition of the isotropic chemical shift (Equation 9.4). The physical arguments used to justify the form of the isotropic chemical shift may also be used to justify the step from Equation 9.41 to Equation 9.42.

The secular forms of the *J*-coupling Hamiltonian depend on whether the two spins are of the same isotopic type (homonuclear case) or of different isotopic type (heteronuclear case).

In the *homonuclear* case, the secular *J*-coupling is the same as in Equation 9.42:

$$\widehat{\mathcal{H}}_{jk}^{\mathrm{J}} = 2\pi J_{jk}\, \hat{\mathbf{I}}_j \cdot \hat{\mathbf{I}}_k \qquad \text{(homonuclear case, isotropic liquids)} \tag{9.44}$$

In the *heteronuclear* case, the secular form of the interaction is different:

$$\widehat{\mathcal{H}}_{jk}^{\mathrm{J}} = 2\pi J_{jk}\, \hat{I}_{jz} \hat{I}_{kz} \qquad \text{(heteronuclear case, isotropic liquids)} \tag{9.45}$$

Unlike the chemical shift, the J-coupling is independent of the applied magnetic field.

The J-coupling has a sign. A positive value of J_{jk} indicates that the spin–spin coupling makes a positive contribution to the energy when the spin polarizations are parallel and a negative contribution when the spin polarizations are opposite. In the case of negative J_{jk}, the energy changes are in the opposite direction:

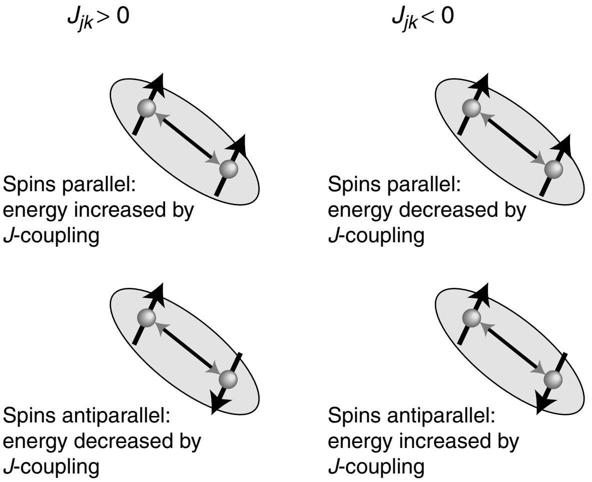

Figure 9.27
The physical meaning of the sign of J.

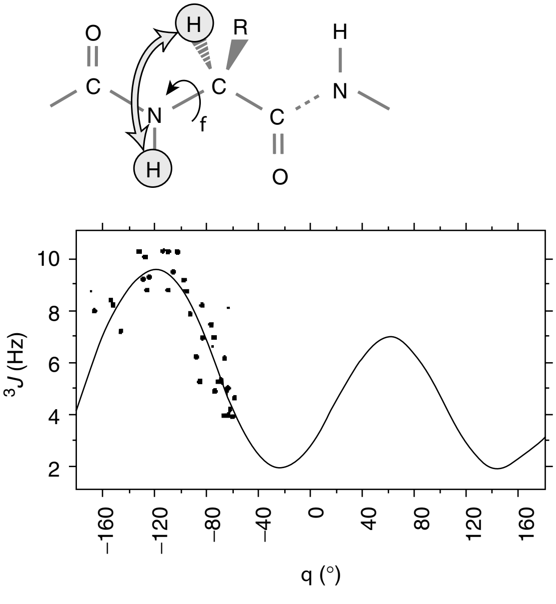

Figure 9.28 The three-bond J-couplings between H^N protons and H^α protons in a protein have a well-defined dependence on the molecular torsional angle ϕ. Each filled circle represents a single amino acid residue in a protein. The x-coordinate is the torsional angle as determined by X-ray crystallography; the y-coordinate is the J-coupling as measured by solution NMR. The solid line is a semi-empirical curve called the Karplus equation, which has the form $^3J = (6.4\cos^2\theta - 1.4\cos\theta + 1.9)$ Hz, where θ is the H–N–C–H torsional angle, given in terms of the backbone torsional angle ϕ by $\theta = \phi - \pi/3$. Adapted from A. Pardi, M. Billeter and K. Wüthrich, *J. Mol. Biol.*, **180**, 741–751 (1984). (Copyright Academic Press).

J_{jk} is *positive* for spins with the *same* sign of gyromagnetic ratio, connected by one chemical bond. J_{jk} is *negative* for spins with *opposite* signs of gyromagnetic ratio, connected by one chemical bond. The signs of longer-range J-couplings are variable and depend on the molecular geometry and many other factors. For protons in organic materials, three-bond J-couplings (denoted ^3J) are typically around 7 Hz when averaged over all rotamers. One-bond J-couplings between ^{1}H and ^{13}C are typically around 135 Hz, whereas one-bond J-couplings between directly bonded ^{13}C spins are usually around 50 Hz. These figures may vary considerably, depending on the local molecular structure.

In some cases, the values of J-couplings depend in a simple way on molecular structural parameters, such as bond angles and torsional angles. For example, consider the two-bond J-coupling $^2J_{XX}$ in molecules containing the fragment X–Y–X (where X and Y are arbitrary isotopes). In general, molecules in which the X–Y–X bond angle is large have a larger value of $^2J_{XX}$ than molecules in which the X–Y–X bond angle is small. Such relationships are particularly useful for molecular structural investigations in inorganic chemistry.

Another important relationship of this kind applies to three-bond ^{1}H–^{1}H J-couplings in rigid organic molecules. The important parameter is the *torsional angle* around the central bond transmitting the coupling. Figure 9.28 shows the measured values of ^3J between amide NH protons and C$^\alpha$ protons in a small protein. There is a sinusoidal dependence of ^3J on the torsional angle around the N–C$^\alpha$ bonds of the peptide links between the amino acid units. These *Karplus relationships* are used by protein NMR spectroscopists to provide information on the secondary protein structure.

9.4.2 Liquid crystals and solids

In anisotropic liquids and solids, the anisotropic part of the J-coupling survives. This *J-anisotropy* is usually small and is often ignored. In any case, it is very difficult to distinguish it from the direct dipole–dipole coupling, which is usually much larger and has the same form.[18] I will say no more about it in this book.

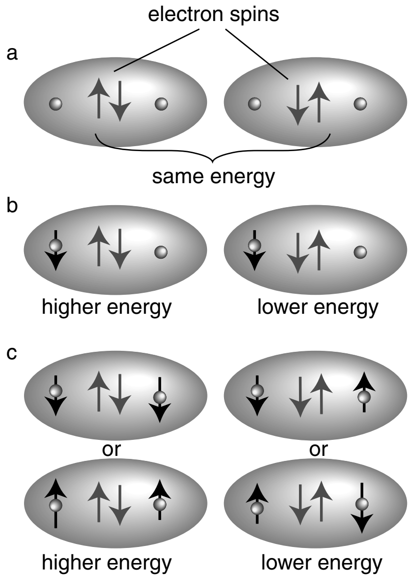

Figure 9.29
Mechanism of J-coupling through a single chemical bond. The arrows denote the direction of the spin angular momenta, and both nuclei are assumed to have positive values of γ.

9.4.3 Mechanism of the J-coupling

I now briefly outline the mechanism of the indirect spin–spin coupling.[17] The reader is directed to the text by Slichter for more details (see *Further Reading*). The basic idea is illustrated in Figure 9.29, which shows a simplified situation with two nuclear spins and a bonding orbital containing two paired electron spins. Because of the Pauli principle, the electron spins are paired; and in the absence of the nuclei, the electron wavefunctions consist of an equal admixture of an 'up–down' state and 'down–up' state, these two states being exactly degenerate (Figure 9.29a).The introduction of a nuclear spin on one side changes matters, because the nuclear spin has a negative magnetic hyperfine interaction with the electron. The energy of the state shown in the right-hand side of Figure 9.29b, in which the electron spin close to the nucleus has the same direction as the nuclear spin polarization, is slightly reduced since the magnetic moments are opposite. The electron spin distribution is therefore slightly shifted by the presence of the nuclear spin: there is a slight tendency for electrons near the nucleus to be polarized in the same sense as the nucleus. When a second nucleus is introduced, the energy of the system now depends on whether the two nuclei have the same or opposite polarizations. The state in which the two nuclei have opposite polarizations is relatively low in energy, because in this state both nuclei couple to electrons with favourable spin orientations, while keeping the electron spin polarizations opposite: The state where the two nuclei have the same polarization is relatively high in energy, because it is not possible to achieve consistently favourable spin orientations (see Figure 9.29c). This mechanism, therefore, predicts a positive value of the J-coupling, as found experimentally for one-bond couplings between spins with the same sign of γ.

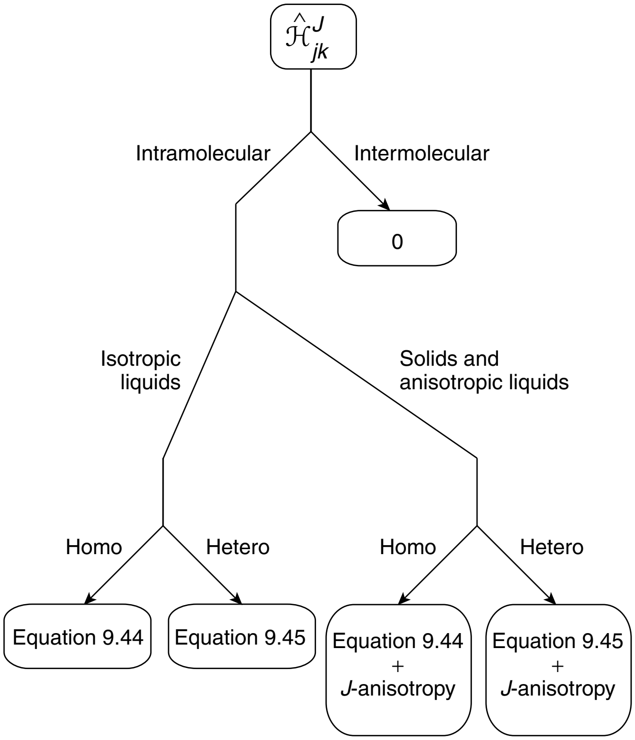

Figure 9.30
Flow diagram for the J-coupling interaction.

9.4.4 *J*-coupling: summary

Figure 9.30 summarizes the form of the *J*-coupling interaction in liquids and solids.

9.5 Spin–Rotation Interaction

A molecule consists of positive electric charges (nuclei) and negative electric charges (electrons). If a molecule rotates, then the charges circulate, which corresponds to an electric current. The rotation of a molecule, therefore, generates local magnetic fields, which may interact with the magnetic moments of the nuclei.

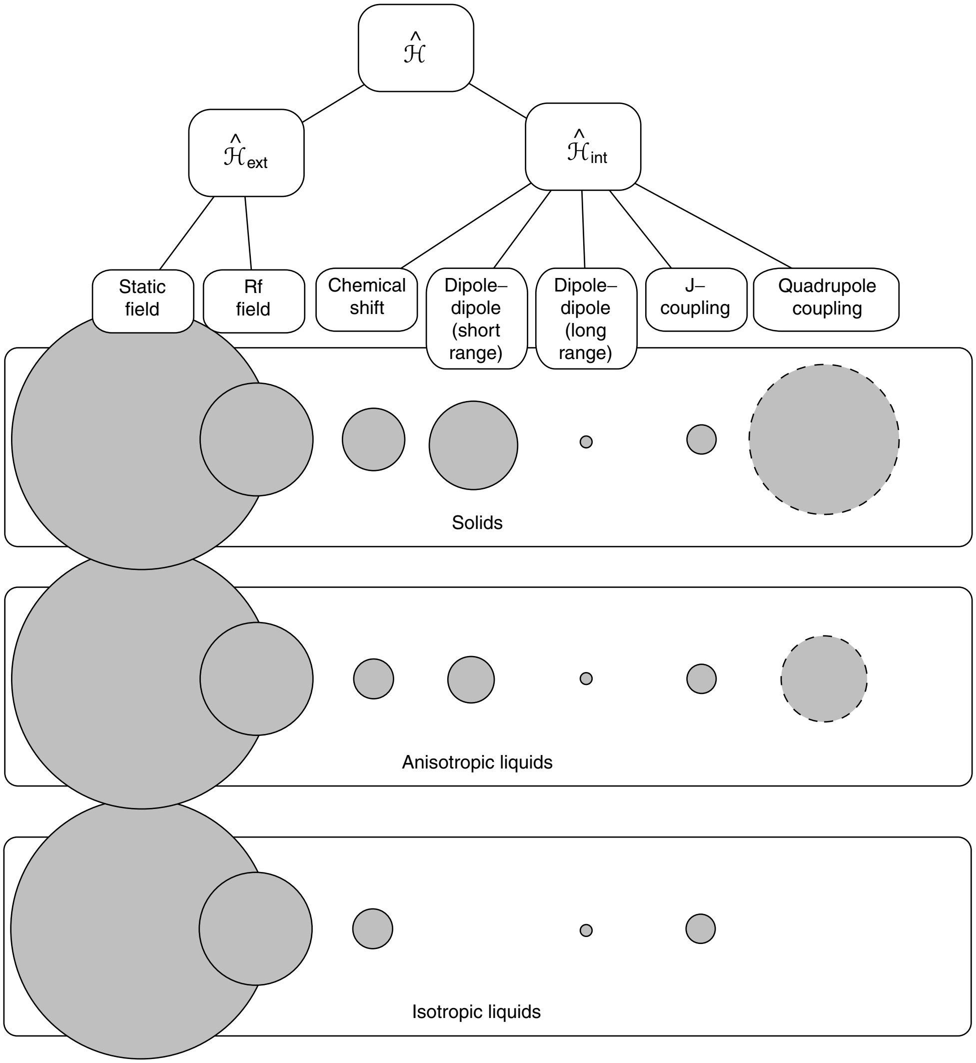

Figure 9.31 Summary of the motionally averaged spin Hamiltonian terms and their rough relative magnitudes, in different phases of matter. The quadrupolar coupling vanishes for spins-1/2.

The *spin–rotation interaction* takes into account the direct interaction between the magnetic fields generated by rapid molecular rotation and the nuclear spins.

The nuclear spin–rotation interaction is important in the microwave spectroscopy of gases, but is of only marginal importance in NMR. The secular part of the spin–rotation interaction averages to zero in isotropic liquids. However, the non-secular part of the spin–rotation interaction occasionally causes relaxation in liquids and is often a dominant relaxation mechanism in gases (see Section 20.2).

The spin–rotation interaction is also unimportant in solid-state NMR, because the molecular rotation is restricted.[19]

9.6 Summary of the Spin Hamiltonian Terms

Figure 9.31 gives the form and the rough relative magnitude of the motionally averaged spin Hamiltonian terms, in different phases of matter. Note that the case of isotropic liquids is very special, since all the largest internal terms average to zero. In addition, remember that the quadrupolar coupling vanishes for spins-1/2.

Notes

1. The diamagnetic contribution to the chemical shift consists of field-induced electron currents in the electronic ground states. At first sight, the existence of such currents is surprising, because in most cases the electronic ground states have an orbital angular momentum quantum number equal to $l = 0$, which sounds as if the electrons cannot circulate (circulation of the electrons implying finite orbital angular momentum). This paradox is resolved by noting that most elementary discussions of quantum mechanics are conducted in the absence of a magnetic field, and are misleading. In fact, if the Schrödinger equation is solved in the presence of a magnetic field, one finds that electrons in $l = 0$ electronic states *do* have electronic angular momentum in a magnetic field. Electron currents in $l = 0$ electronic states are responsible for a number of effects, including the bulk diamagnetism of many materials.

2. Unfortunately, the field of chemical shifts is plagued by contradictory conventions. In this book, I always use the *deshielding* convention for both isotropic and anisotropic chemical shifts, which are denoted by the symbol δ. This conforms to standard practice for isotropic shifts in solution-state NMR (δ increases from right to left in the spectrum). In solid-state NMR, on the other hand, it is quite common to use a *shielding* convention, which is usually indicated by the symbol σ. The shielding and deshielding chemical shifts have the same magnitude but opposite signs. Unfortunately, many research articles do not state which convention they use, and do not use the symbols consistently either.

3. In the most general case, the chemical shift tensor is not exactly symmetric about the diagonal (for example, $\delta^j_{xy} \neq \delta^j_{yx}$). Normally, this lack of symmetry may be ignored, since it has no direct effects on NMR lineshapes, and only a weak influence on relaxation. In this book, the *antisymmetric part of the chemical shift tensor* is ignored, and all chemical shift tensors are assumed to have symmetric matrix representations. Do not confuse the (very obscure) *antisymmetric* part of the chemical shift tensor with the common and important case of a *biaxial* chemical shift tensor ($\eta_j \neq 0$). The potential for confusion is not reduced by the common practice of calling the biaxiality η_j the 'asymmetry parameter' (see Note 5).

4. *Numerical* subscripts are used to indicate sequential ordering of the chemical shift principal values: $\delta^j_{11} > \delta^j_{22} > \delta^j_{33}$. When the *shielding* notation is used (see Note 2), the ordering is as follows: $\sigma^j_{11} < \sigma^j_{22} < \sigma^j_{33}$. The correspondence between $\{\delta^j_{XX}, \delta^j_{YY}, \delta^j_{ZZ}\}$ and $\{\delta^j_{11}, \delta^j_{22}, \delta^j_{33}\}$ depends on the sign of δ^{aniso}_j (see Figure 9.11). If δ^{aniso}_j is positive, then the correspondence is as follows: $\delta^j_{XX} = \delta^j_{33}$, $\delta^j_{YY} = \delta^j_{22}$,

and $\delta^j_{ZZ} = \delta^j_{11}$. If δ^{aniso}_j is negative, then the correspondence is instead: $\delta^j_{XX} = \delta^j_{11}$, $\delta^j_{YY} = \delta^j_{22}$, and $\delta^j_{ZZ} = \delta^j_{33}$. The convention above is due to Ulrich Haeberlen.

5. The term η_j is commonly known as the *asymmetry parameter* or the *rhombicity* of the chemical shift tensor. I find the term 'asymmetry' uninformative and confusing: the matrix representation of the *relevant* part of the CSA tensor is *always* symmetric about the diagonal, irrespective of the value of η_j (although see Note 3). I favour the term *biaxiality*, which represents analogous phenomena in liquid crystal science and in optics. The term *rhombicity* is used in similar circumstances in electron spin resonance and also has its merits.

6. The term *symmetric tensor* is sometimes used to indicate the case with $\eta_j = 0$. This is poor terminology, since the matrix representation of the relevant part of the CSA tensors is *always* symmetric about the diagonal, irrespective of the value of η_j (see Note 5). I favour the term *uniaxial* to indicate the situation with $\eta_j = 0$.

7. A *primary* isotope shift concerns, for example, the difference in chemical shifts for ^{1}H nuclei in $CHCl_3$ and for ^{2}H nuclei in $CDCl_3$.

8. The *asymmetric unit* of a crystal is the smallest unit from which the entire crystal may be constructed by applying symmetry operations (rotations, reflections, etc.). In general, several asymmetric units combine to form a *unit cell*, from which the entire structure may be derived by translations alone.

9. Many molecular crystal structures contain more than one molecule in the *asymmetric unit*. In a single crystal at an arbitrary orientation, the number of peaks generated by one chemical site is given by the number of molecules in the asymmetric unit.

10. The conventions used for the quadrupolar interaction follow those in A. Jerschow, *Prog. NMR Spectrosc.* **46**, 63–78 (2005).

11. It is now possible to calculate chemical shift tensors and electric field gradient tensors with high accuracy and reliability in a wide variety of molecular systems, using quantum-mechanical calculations of the electronic structure. See *Further Reading*.

12. The accepted convention for assigning the principal values of the electric field gradient tensor is as follows:

$$|V_{ZZ}| \geq |V_{YY}| \geq |V_{XX}|$$

This is slightly different than that used for the chemical shift tensor (Equation 9.5).

13. The second-order quadrupolar term takes into account the second-order changes in the Hamiltonian *eigenvalues*, but does not take into account the perturbation of the spin *eigenstates* by the quadrupole coupling. There are some effects, such as *overtone transitions*, that require a more subtle treatment (see Chapter 13, Note 4).

14. The unity operator $\widehat{1}$ is often implied, rather than being written explicitly.

15. In liquids, the motionally averaged second-order quadrupole interaction gives rise to a shift in the nuclear Larmor frequency, called the *dynamic frequency shift*.

16. The conventional definition of the quadrupole coupling constant C_Q can be misleading, since the Hamiltonian contains a factor of $2I(2I-1)$ in the denominator (see Equation 9.30). For high spin

quantum numbers, this factor can reduce the effect of the quadrupole coupling by more than an order of magnitude. For example, the factor $2I(2I-1)$ is equal to 72 for the spin-9/2 case.

17. In certain circumstances, the J-coupling has a contribution from the *nuclear exchange interaction* as well as the indirect spin–spin coupling. The nuclear exchange coupling involves a spatial overlap of the quantum wavefunctions of the two nuclei. It is analogous to the very important *electron exchange interaction* that is of central importance in a wide range of phenomena such as chemical bonding and macroscopic magnetism. The nuclear exchange coupling is usually negligible, but it can be significant for light atoms, such as hydrogen, in compounds with a low potential barrier for nuclear exchange. For example, the nuclear exchange coupling give rises to large temperature-dependent J-couplings in certain metal hydride complexes (e.g. see K. W. Zilm and J. M. Millar, *Adv. Magn. Opt. Reson.* **15**, 163 (1990)). In special cases, the exchange coupling can be extremely large. For example, in the dihydrogen molecule (H_2), the exchange coupling between the two protons is more than 10 orders of magnitude larger than the "ordinary" J-coupling! The enormous nuclear exchange coupling between the protons in H_2 forms the basis of *parahydrogen-enhanced NMR*; e.g. see J. Natterer and J. Bargon, *Prog. NMR Spectrosc.* **31**, 293–315 (1997).

18. J-couplings involving heavy nuclei are sometimes large. In these cases, the J-anisotropy may be comparable to or even exceed the direct dipole–dipole coupling.

19. Solid samples are sometimes rapidly rotated at frequencies up to 70 kHz in order to improve the spectral resolution (see Section 19.6). It is conceivable that the rapid bulk rotation of the sample could lead to measurable spin–rotation effects at such frequencies.

Further Reading

- Other books that summarize the nuclear spin interactions are:
  A. Abragam, *The Principles of Nuclear Magnetism*, Clarendon Press, Oxford, 1961; C. P. Slichter*Principles of Magnetic Resonance*, 3rd edition, Springer, Berlin, 1989; M. Mehring, *High Resolution NMR in Solids*, 2nd edition, Springer, Berlin, 1982. Slichter is particularly recommended for nuclear spin interactions in metallic and paramagnetic systems, and for the mechanism of the chemical shift and J-coupling.
- For a review of influences on isotropic chemical shifts, see H. Günther, "NMR Spectroscopy", 2nd Edition, (Wiley, Chichester, 1995).
- For the calculation of spin interaction parameters using quantum chemistry techniques, see M. Kaupp, M. Bühl and V. G. Malkin, *Calculation of NMR and EPR Parameters. Theory and Applications*, Wiley–VCH, 2004.
- For a review of chemical shift anisotropies in biomolecules, including calculation techniques, see D. Sitkoff and D. A. Case, *Prog. NMR Spectrosc.* **32**, 165–190 (1998).
- For a review of spin–spin coupling tensors, including quantum calculation methods, see J. Vaara, J. Jokisaari, R. E. Wasylishen and D. L. Bryce, *Prog. NMR Spectrosc.* **41**, 187–232 (2002).

Exercises

9.1 (i) A molecule contains three protons I_1, I_2 and I_3 arranged on the corners of an equilateral triangle with sides of length r. The magnetic field B^0 is in the plane of the triangle, subtending an angle θ with the line joining protons I_1 and I_2:

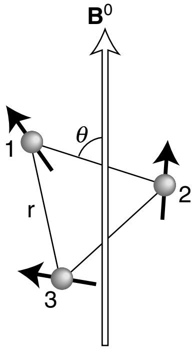

(ii) Calculate the dipole–dipole coupling constant b_{12} between spins I_1 and I_2 in the case that $r = 0.2\,\text{nm}$ and $\theta = \pi/2$.
(iii) Calculate the dipole–dipole coupling constant b_{13} between spins I_1 and I_3 in the case that $r = 0.2\,\text{nm}$ and $\theta = \pi/2$.
(iv) Calculate the secular dipole–dipole coupling d_{12} between spins I_1 and I_2 in the case that $r = 0.2\,\text{nm}$ and $\theta = \pi/2$.
(v) Calculate the secular dipole–dipole coupling d_{13} between spins I_1 and I_3 in the case that $r = 0.2\,\text{nm}$ and $\theta = \pi/2$.
(vi) Calculate all three secular dipole–dipole couplings in the case that $r = 0.2\,\text{nm}$ and $\theta = \pi/4$.

9.2 Suppose that the probability density of the angle Θ_{jk} between two spins I_j and I_k in an anisotropic liquid is given by

$$\mathrm{p}(\Theta_{jk}) = \frac{3}{124}(21 + \cos 2\Theta_{jk})$$

9.3 This probability density function implies that molecular orientations with the vector $\mathbf{e}_{jk}$ nearly parallel to the field are slightly favoured in the anisotropic liquid.
(i) Verify that $\mathrm{p}(\Theta_{jk})$ is normalized, i.e.

$$\int_0^{\pi} \mathrm{d}\Theta_{jk}\, \mathrm{p}(\Theta_{jk}) \sin \Theta_{jk} = 1$$

(ii) Calculate the secular dipole–dipole coupling d_{jk} in the anisotropic liquid if the distance between the spins is $r = 0.3\,\text{nm}$.

Part 5

Uncoupled Spins

10 Single Spin-1/2

The next four chapters concern the dynamics of one-spin systems, i.e. isolated nuclei that are assumed not to interact with each other, to a good approximation. Many very important NMR experiments, such as NMR imaging, may be treated well within this approximation.

We start by considering the simplest possible case: systems of isolated spins-1/2.

10.1 Zeeman Eigenstates

According to the quantum theory of angular momentum (Chapter 7), a single spin-1/2 has two eigenstates of angular momentum along the z-axis, denoted $|\alpha\rangle$ and $|\beta\rangle$. These states are defined:

$$\boxed{\begin{aligned} |\alpha\rangle &= |\tfrac{1}{2}, +\tfrac{1}{2}\rangle \\ |\beta\rangle &= |\tfrac{1}{2}, -\tfrac{1}{2}\rangle \end{aligned} \qquad (10.1)}$$

using the notation $|I, M\rangle$, as given in Section 7.7. The states $|\alpha\rangle$ and $|\beta\rangle$ are called the *Zeeman eigenstates* of the single spin-1/2 and obey the following eigenequations:

$$\boxed{\begin{aligned} \hat{I}_z|\alpha\rangle &= +\frac{1}{2}|\alpha\rangle \\ \hat{I}_z|\beta\rangle &= -\frac{1}{2}|\beta\rangle \end{aligned} \qquad (10.2)}$$

Equation 10.2 indicates that the state $|\alpha\rangle$ is an eigenstate of angular momentum along the z-axis, with eigenvalue $+1/2$. A spin that is in the state $|\alpha\rangle$ is said to be *polarized along the z-axis*. Similarly, the state $|\beta\rangle$ is an eigenstate of angular momentum along the z-axis, with eigenvalue $-1/2$. A spin that is in the state $|\beta\rangle$ is said to be *polarized along the $-z$-axis*.

In diagrams, the spin states $|\alpha\rangle$ and $|\beta\rangle$ are represented by arrows pointing along the positive or negative z-axis:

Spin Dynamics: Basics of Nuclear Magnetic Resonance, Second Edition Malcolm H. Levitt

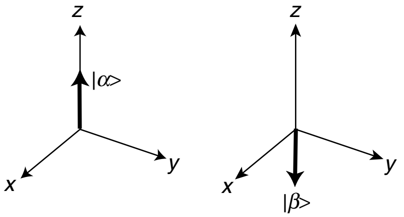

Figure 10.1
The two Zeeman eigenstates of a single spin-1/2.

The state $|\alpha\rangle$ is sometimes called the 'spin-up' state; the state $|\beta\rangle$ is sometimes said to be 'spin-down'.

10.2 Measurement of Angular Momentum: Quantum Indeterminacy

Suppose a spin is in a certain quantum state and the z-component of angular momentum is measured. I leave aside the technical issue as to how this is actually done; suffice it to say that such observations are possible.[1]

Consider first the situation in which the spin is in state $|\alpha\rangle$ when the z-component of angular momentum is measured. The state $|\alpha\rangle$ is an eigenstate of the operator $\hat{I}_z$, with eigenvalue $+1/2$. According to the postulates of quantum mechanics (Section 7.1.3), the observation of z-angular momentum on a spin in state $|\alpha\rangle$ always gives the same result, namely the eigenvalue $+1/2$ (in units of $\hbar$, as usual). The z-angular momentum of state $|\alpha\rangle$ is said to be *sharp*, or *well defined*.

Similarly, the observation of z-angular momentum on a spin in the state $|\beta\rangle$ always gives the same result, namely $-1/2$.

What happens if the spin is in state $|\alpha\rangle$, but the x-component of angular momentum is observed instead of the z-component? Since the state $|\alpha\rangle$ is *not* an eigenstate of the operator $\hat{I}_x$, the result is *fundamentally unpredictable*. The result is always either $+1/2$ or $-1/2$, but it is *impossible* to predict which of the two answers will be given. The diagram below shows the results of many identical observations, all on spins prepared in identical physical states $|\alpha\rangle$:

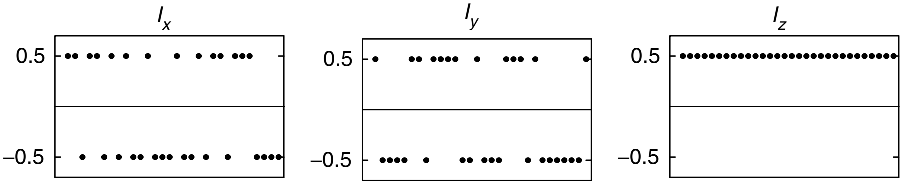

Figure 10.2
Observations of spins in state $|\alpha\rangle$.

Similarly, if the spins are prepared in identical states $|\beta\rangle$, the measurement of z-angular momentum gives the reproducible value $-1/2$, and measurements of the x- or y-components give results that are equally and randomly distributed between the values $\pm 1/2$:

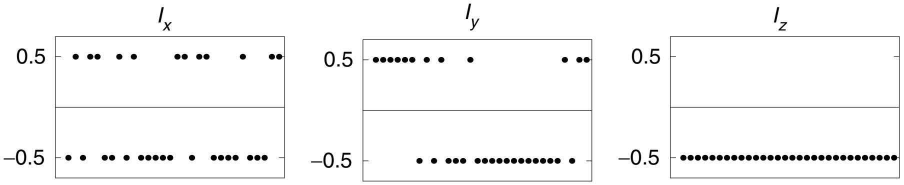

Figure 10.3
Observations of spins in state $|\beta\rangle$.

The irreproducibility of these results is not due to instrumental imperfections. Nor is it due to something 'inside' the spin that decides whether the result is going to be $+1/2$ or $-1/2$. This possibility has been ruled out by more subtle experimental observations (see *Further Reading*).

The random outcome of certain observations is now broadly accepted as a *feature or reality itself*. Even though the quantum state is a complete description of the physical system, it is *not sufficient* to give unambiguous results for all observations. In plain language, sometimes *even the spin* does not 'know' what the answer is going to be! Colloquially speaking, if the spin is in state $|\alpha\rangle$ and the z-component of angular momentum is measured, then the spin 'knows the answer'. It says '$+1/2$'. But if the x-component of angular momentum is measured, the spin says: 'I don't know. I'll choose $+1/2$ or $-1/2$ at random'.

This feature of quantum mechanics is a very deep mystery. Probably it is beyond human understanding. Many scientists, such as Einstein, could never reconcile themselves to it ('God does not play dice'). Nevertheless, it is supported by massive experimental evidence and is now broadly accepted (see *Further Reading*).

No pictorial representation of a spin state is completely satisfactory. The diagrams in Figure 10.1 use an arrow to indicate the spin polarization, i.e. the direction along which the angular momentum is well-defined. The state $|\alpha\rangle$ is represented by an arrow along the z-axis, and the state $|\beta\rangle$ is represented by an arrow pointing along the $-z$-axis. These 'spin arrows' must not be overinterpreted. An arrow along the z-axis does *not* imply that the angular momentum along the x-axis is zero. In fact, the angular momentum along the x-axis is *undefined*: measurements give the result ±1/2, with equal probability. It is impossible to accomodate this feature in a pictorial representation.

Some books try to depict the quantum indeterminacy by drawing the spin state as a sort of cone. Such diagrams are always incorrect on closer examination and are best avoided.

⚠ These 'spin polarization arrows' do *not* behave like ordinary vectors. For example, the arrow diagrams do *not* imply that $|\alpha\rangle$ and $|\beta\rangle$ are related by a sign change:

$$|\alpha\rangle = -|\beta\rangle \qquad \text{⚠WRONG!} \tag{10.3}$$

The 'arrow' is a pictorial device for depicting the direction of well-defined spin angular momentum, and nothing else.

10.3 Energy Levels

If the magnetic field is along the z-axis and has magnitude B^0, the spin Hamiltonian is proportional to $\hat{I}_z$:

$$\boxed{\hat{\mathcal{H}}^0 = \omega^0 \hat{I}_z} \tag{10.4}$$

where the (chemically shifted) Larmor frequency is given by $\omega^0 = -\gamma B^0(1+\delta)$. The states $|\alpha\rangle$ and $|\beta\rangle$ are eigenstates of the spin Hamiltonian, obeying the eigenequations

$$\hat{\mathcal{H}}^0|\alpha\rangle = +\frac{1}{2}\omega^0|\alpha\rangle$$

$$\hat{\mathcal{H}}^0|\beta\rangle = -\frac{1}{2}\omega^0|\beta\rangle$$

The eigenvalues $\pm\frac{1}{2}\omega^0$ are the *energies* of the states. The two states $|\alpha\rangle$ and $|\beta\rangle$ have well-defined (sharp) energies. An energy level diagram may be constructed, in which each 'energy level' belongs to a different state. The energy level splitting of the spin in the magnetic field is known as the *Zeeman splitting* and is equal to the Larmor frequency ω^0 (as usual, in units of $\hbar$):

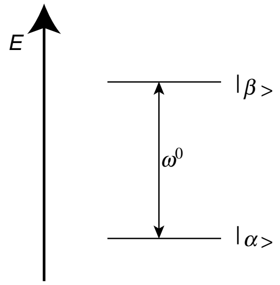

Figure 10.4
Energy levels for a spin-1/2 in a magnetic field.

This diagram is appropriate for a spin of positive gyromagnetic ratio γ, and hence negative Larmor frequency ω^0. Note that the state $|\alpha\rangle$ has lower energy than the state $|\beta\rangle$ in this case.

10.4 Superposition States

10.4.1 General spin states

A spin-1/2 particle is not restricted to the $|\alpha\rangle$ or $|\beta\rangle$ state, but may be in a *superposition* of the two energy eigenstates:

$$\boxed{|\psi\rangle = c_\alpha|\alpha\rangle + c_\beta|\beta\rangle \qquad (10.5)}$$

where c_α and c_β are complex numbers, called *superposition coefficients*. The only restriction on the values of the superposition coefficients is that the state must be *normalized*:

$$\boxed{|c_\alpha|^2 + |c_\beta|^2 = 1 \qquad (10.6)}$$

10.4.2 Vector notation

The state $|\psi\rangle = c_\alpha|\alpha\rangle + c_\beta|\beta\rangle$ is conveniently written as a two-dimensional column vector with complex components:

$$|\psi\rangle = \begin{pmatrix} c_\alpha \\ c_\beta \end{pmatrix}$$

In this notation, the Zeeman eigenstates are written

$$|\alpha\rangle = \begin{pmatrix} 1 \\ 0 \end{pmatrix} \qquad |\beta\rangle = \begin{pmatrix} 0 \\ 1 \end{pmatrix}$$

The bra state $\langle\psi|$ is written as a *row vector*, with elements given by the complex conjugates of the corresponding ket column vector:

$$\langle\psi| = |\psi\rangle^\dagger = (\, c_\alpha{}^* \,, \quad c_\beta{}^* \,)$$

Note that the adjoint operation corresponds to taking the transpose (which turns a row vector into a column vector), followed by taking the complex conjugate.

The normalization condition corresponds to the usual multiplication rule for row and column vectors:

$$\langle\psi|\psi\rangle = (\, c_\alpha{}^*, \quad c_\beta{}^*\,) \begin{pmatrix} c_\alpha \\ c_\beta \end{pmatrix} = c_\alpha{}^* c_\alpha + c_\beta{}^* c_\beta = |c_\alpha|^2 + |c_\beta|^2 = 1$$

10.4.3 Some particular states

Consider the following superposition state:

$$|{+x}\rangle = \frac{1}{\sqrt{2}}|\alpha\rangle + \frac{1}{\sqrt{2}}|\beta\rangle$$

or in vector notation:

$$|{+x}\rangle = \frac{1}{\sqrt{2}} \begin{pmatrix} 1 \\ 1 \end{pmatrix}$$

This state is called $|{+x}\rangle$ because it is an eigenstate of the operator $\hat{I}_x$ with eigenvalue $+1/2$:

$$\hat{I}_x|{+x}\rangle = \frac{1}{2}\begin{pmatrix} 0 & 1 \\ 1 & 0 \end{pmatrix} \frac{1}{\sqrt{2}} \begin{pmatrix} 1 \\ 1 \end{pmatrix} = \frac{1}{2\sqrt{2}} \begin{pmatrix} 1 \\ 1 \end{pmatrix} = \frac{1}{2} \cdot \frac{1}{\sqrt{2}} \begin{pmatrix} 1 \\ 1 \end{pmatrix} = \frac{1}{2}|{+x}\rangle$$

For this state, the x-component of spin angular momentum is 'sharp', whereas the y- and z-components are not:

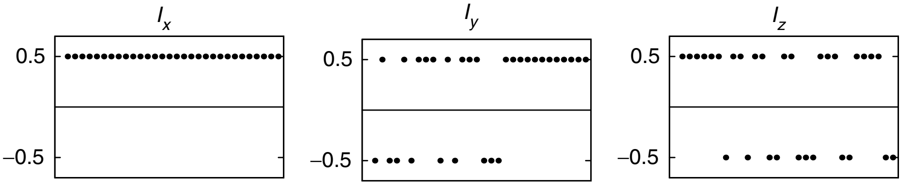

Figure 10.5
Observations of spins in state $|{+x}\rangle$.

This state, therefore, can be depicted as an arrow along the $+x$-axis:

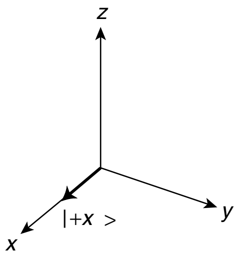

Figure 10.6
Pictorial representation of the state $|{+x}\rangle$.

Similarly, consider the state $|-y\rangle$, defined as

$$|-y\rangle = \frac{1}{2}(1+\mathrm{i})|\alpha\rangle + \frac{1}{2}(1-\mathrm{i})|\beta\rangle = \frac{1}{2}\begin{pmatrix} 1+\mathrm{i} \\ 1-\mathrm{i} \end{pmatrix}$$

This is an eigenstate of the operator $\hat{I}_y$ with eigenvalue $-1/2$:

$$\hat{I}_y|-y\rangle = \frac{1}{2\mathrm{i}}\begin{pmatrix} 0 & 1 \\ -1 & 0 \end{pmatrix}\frac{1}{2}\begin{pmatrix} 1+\mathrm{i} \\ 1-\mathrm{i} \end{pmatrix} = -\frac{1}{2}\cdot\frac{1}{2}\begin{pmatrix} 1+\mathrm{i} \\ 1-\mathrm{i} \end{pmatrix} = -\frac{1}{2}|-y\rangle$$

The y-component of spin angular momentum is 'sharp', whereas the x- and z-components are not:

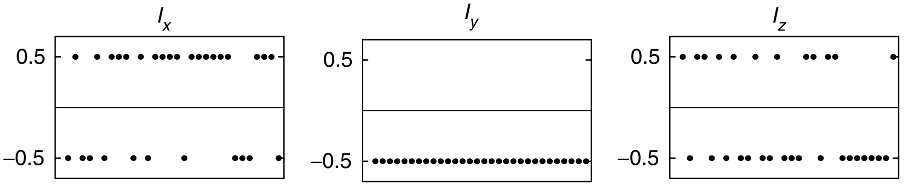

Figure 10.7
Observations of spins in state $|-y\rangle$.

This state, therefore, can be depicted as a arrow along the $-y$-axis:

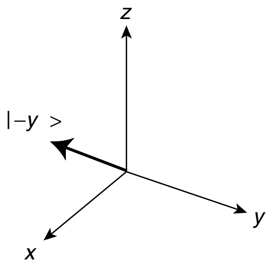

Figure 10.8
Pictorial representation of the state $|-y\rangle$.

If the magnetic field is along the z-axis, then superposition states such as $|+x\rangle$ and $|-y\rangle$ do not have sharp energies. Therefore, it is not possible to attach these states to energy level diagrams. The spin is 'in between' the energy levels. Nevertheless, the superposition states have just as much physical reality as the Zeeman eigenstates, and they play a very important role in NMR.

A variety of spin-1/2 quantum states, and ways of depicting these states, is shown below:

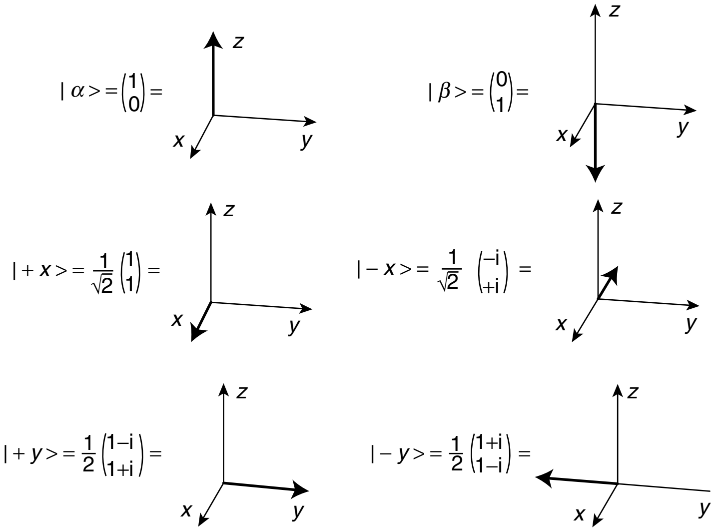

Figure 10.9
A selection of spin states.

It is possible to construct quantum states with well-defined angular momentum in *any* spatial direction, not just along the *x*-, *y*- or *z*-axes. For example, the state

$$|\theta, \phi\rangle = \begin{pmatrix} \cos\frac{1}{2}\theta\, e^{-i\frac{1}{2}\phi} \\ \sin\frac{1}{2}\theta\, e^{+i\frac{1}{2}\phi} \end{pmatrix}$$

obeys the following eigenequation:

$$\left(\hat{I}_z \cos\theta + \hat{I}_x \sin\theta\cos\phi + \hat{I}_y \sin\theta\sin\phi\right)|\theta, \phi\rangle = +\frac{1}{2}|\theta, \phi\rangle$$

and has the following geometric representation:

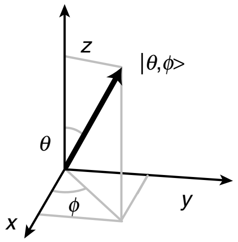

Figure 10.10
Pictorial representation of the state $|\theta, \phi\rangle$.

10.4.4 Phase factors

Two states $|\psi\rangle$ and $|\psi\rangle'$ differ by a *phase factor* if they can be expressed as follows:

$$|\psi\rangle' = e^{i\phi}|\psi\rangle$$

For example, the state

$$|-y\rangle' = \frac{1}{\sqrt{2}}\begin{pmatrix} i \\ 1 \end{pmatrix}$$

is related to the state

$$|-y\rangle = \frac{1}{2}\begin{pmatrix} 1+\mathrm{i} \\ 1-\mathrm{i} \end{pmatrix}$$

by the phase factor $\exp\{\mathrm{i}\pi/4\}$.

States related by a phase factor obey the same eigenequation and give the same results for most observations (within the limits of quantum indeterminacy, as described above). Nevertheless, there are certain situations in which the phase factors are relevant, so it is best to retain them.

It is not convenient to show the phase of the state on 'arrow diagrams'. The states $|-y\rangle$ and $|-y\rangle'$, given above, both have sharp y angular momentum of $-1/2$, and must both be depicted as arrows pointing along the negative y-axis. The arrow diagrams are always incomplete in this sense.

⚠ Changing the sign of a spin state is equivalent to multiplying it by the phase factor $\exp\{\mathrm{i}\pi\} = -1$. As just mentioned, this does *not* change the direction of the spin polarization 'arrow'. The 'arrow' for $-|\alpha\rangle$ is the same as the arrow for $|\alpha\rangle$; both point along the z-axis. Multiplying $|\alpha\rangle$ by -1 does *not* change it into the state $|\beta\rangle$ (see Equation 10.3).

10.5 Spin Precession

In general, the spin state $|\psi\rangle$ depends on time – the spin precesses.

Suppose that one knows the spin state $|\psi\rangle(t_\mathrm{a})$ at an initial time point t_a, and wishes to predict the spin state at a later time point t_b. The interval between the time points is given by $\tau = t_\mathrm{b} - t_\mathrm{a}$:

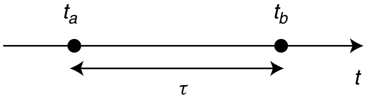

Figure 10.11
Two time points.

The law of motion of the spin is the time-dependent Schrödinger equation:

$$\boxed{\frac{\mathrm{d}}{\mathrm{d}t}|\psi\rangle(t) = -\mathrm{i}\widehat{\mathcal{H}}|\psi\rangle(t) \qquad (10.7)}$$

If there is no r.f. field, the spin Hamiltonian is

$$\widehat{\mathcal{H}} = \widehat{\mathcal{H}}^0 = \omega^0 \hat{I}_z$$

The equation of motion of the spin, in the absence of an r.f. field, is therefore:

$$\frac{\mathrm{d}}{\mathrm{d}t}|\psi\rangle(t) = -\mathrm{i}\omega^0 \hat{I}_z|\psi\rangle(t)$$

This is a simple first-order differential equation. The solution is

$$|\psi\rangle(t_\mathrm{b}) = \exp\{-\mathrm{i}\omega^0\tau\hat{I}_z\}|\psi\rangle(t_\mathrm{a}) \qquad (10.8)$$

The exponential operator was already encountered in Section 7.8. It is equal to a *rotation operator* for the spin around the z-axis:

$$\widehat{R}_z(\phi) = \exp\{-\mathrm{i}\phi\hat{I}_z\} \qquad (10.9)$$

The solution of the Schrödinger equation, in the absence of r.f. fields, is therefore:

$$|\psi\rangle(t_\mathrm{b}) = \widehat{R}_z\left(\omega^0\tau\right)|\psi\rangle(t_\mathrm{a}) \tag{10.10}$$

In the absence of r.f. fields, the Schrödinger equation says that *the spin rotates around the z-axis, through the angle* $\omega^0\tau$. We will examine the physical meaning of this in a moment.

As described in Section 7.8, the matrix representation of the rotation operator is:

$$\widehat{R}_z(\phi) = \exp\{-\mathrm{i}\phi\hat{I}_z\} = \begin{pmatrix} \exp\{-\mathrm{i}\frac{1}{2}\phi\} & 0 \\ 0 & \exp\{+\mathrm{i}\frac{1}{2}\phi\} \end{pmatrix} \tag{10.11}$$

This matrix is now used to do some explicit calculations.

10.5.1 Dynamics of the eigenstates

The motion of these states depends on the value of $\omega^0\tau$, where τ is the elapsed interval between times t_a and t_b. For simplicity, consider a special case. Suppose that the elapsed interval τ is given by

$$\tau = \left|\frac{\pi}{2\omega^0}\right|$$

The absolute value is necessary because a time interval τ is always positive, whatever the sign of the Larmor frequency. If the gyromagnetic ratio γ is positive, then the Larmor frequency $\omega^0 = -\gamma B^0$ is negative, so the (positive) interval τ is given by

$$\tau = -\frac{\pi}{2\omega^0}$$

In this case, the relevant angle is

$$\omega^0\tau = -\pi/2$$

The relationship between states at times t_a and t_b is therefore

$$|\psi\rangle(t_\mathrm{b}) = \widehat{R}_z(-\pi/2)|\psi\rangle(t_\mathrm{a})$$

where the rotation operator has a matrix representation:

$$\widehat{R}_z(-\pi/2) = \begin{pmatrix} \exp\{+\mathrm{i}\pi/4\} & 0 \\ 0 & \exp\{-\mathrm{i}\pi/4\} \end{pmatrix} = \frac{1}{\sqrt{2}}\begin{pmatrix} 1+\mathrm{i} & 0 \\ 0 & 1-\mathrm{i} \end{pmatrix}$$

Suppose that the spin is in an eigenstate $|\psi\rangle(t_\mathrm{a}) = |\alpha\rangle$ at time t_a. At time t_b, it is in the state

$$|\psi\rangle(t_\mathrm{b}) = \widehat{R}_z(-\pi/2)|\psi\rangle(t_\mathrm{a}) = \frac{1}{\sqrt{2}}\begin{pmatrix} 1+\mathrm{i} & 0 \\ 0 & 1-\mathrm{i} \end{pmatrix}\begin{pmatrix} 1 \\ 0 \end{pmatrix} = \frac{1}{\sqrt{2}}(1+\mathrm{i})\begin{pmatrix} 1 \\ 0 \end{pmatrix} = \exp\{+\mathrm{i}\pi/4\}|\alpha\rangle$$

The new state $|\psi\rangle(t_\mathrm{b})$ is still an eigenstate of $\hat{I}_z$, with eigenvalue $+1/2$. Apart from the phase factor $\exp\{+\mathrm{i}\pi/4\}$, the spin ‘didn't move’. The eigenstate $|\alpha\rangle$ is *stationary*:

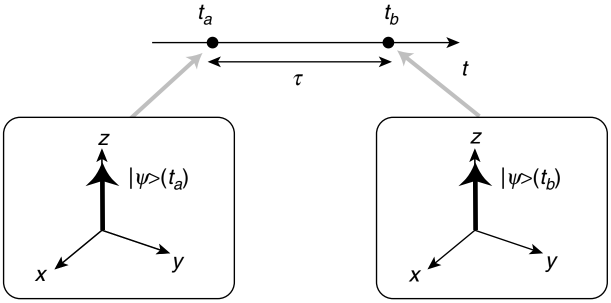

Figure 10.12
The state $|\alpha\rangle$ is stationary under free evolution.

(The phase factor is not shown.)

This result is general. If the spin is in an eigenstate of the Hamiltonian, it remains in that eigenstate, only accumulating a phase factor, for as long as the Hamiltonian remains constant.

10.5.2 Dynamics of the superposition states

If the spin is initially in the superposition state

$$|\psi\rangle(t_\mathrm{a}) = |+x\rangle = \frac{1}{\sqrt{2}}\begin{pmatrix}1\\1\end{pmatrix}$$

it evolves over the interval τ according to

$$\begin{aligned}|\psi\rangle(t_\mathrm{b}) &= \widehat{R}_z(-\pi/2)|\psi\rangle(t_\mathrm{a}) = \widehat{R}_z(-\pi/2)|+x\rangle \\ &= \frac{1}{\sqrt{2}}\begin{pmatrix}1+\mathrm{i} & 0\\ 0 & 1-\mathrm{i}\end{pmatrix}\frac{1}{\sqrt{2}}\begin{pmatrix}1\\1\end{pmatrix} = \frac{1}{2}\begin{pmatrix}1+\mathrm{i}\\1-\mathrm{i}\end{pmatrix} = |-y\rangle\end{aligned}$$

The initial state $|+x\rangle$ evolves into the state $|-y\rangle$ over the time τ. This can be depicted pictorially as a rotation of the spin polarization around the z-axis:

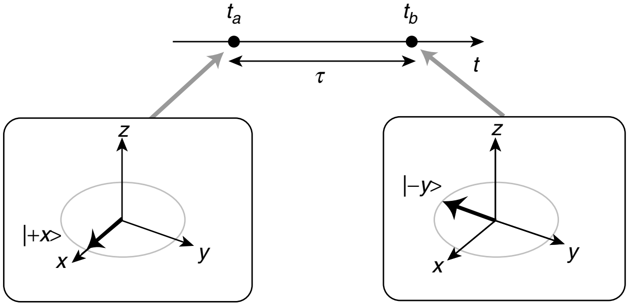

Figure 10.13
Precession transforms the state $|+x\rangle$ into the state $|-y\rangle$.

If the evolution is continued for a further three intervals τ, the pattern of the motion is more obvious:

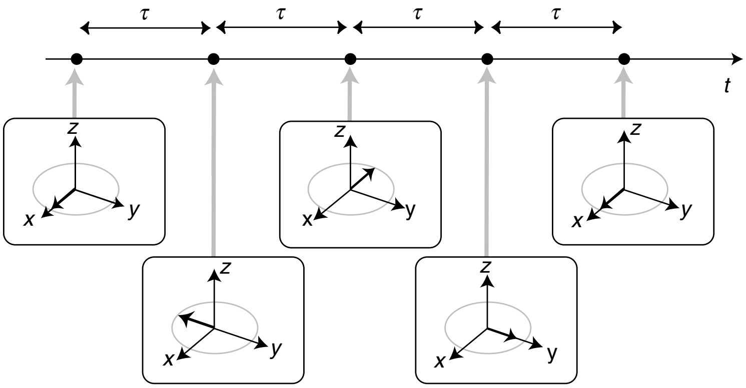

Figure 10.14
Precession of superposition states.

(The reader should verify this by calculation.)

This *precession* of the spin angular momentum axis was described in Section 2.4. Note the negative sense of the precession. The precession frequency is equal to the Larmor frequency ω^0, which is a negative number for positive-γ spins.

The free precession of the spin starting in state $|{+x}\rangle$ may therefore be written as

$$\begin{aligned}
|{-y}\rangle &= \widehat{R}_z(-\pi/2)|{+x}\rangle & \quad |-x\rangle &= \widehat{R}_z(-\pi/2)|{-y}\rangle \\
|{+y}\rangle &= \widehat{R}_z(-\pi/2)|-x\rangle & \quad |{+x}\rangle &= \widehat{R}_z(-\pi/2)|{+y}\rangle
\end{aligned}$$

and so on. If γ is positive, each interval τ leads to spin precession through the angle $-\pi/2$ about the z-axis.

The precessional motion of the spin angular momentum is a consequence of quantum mechanics. Nevertheless, it resembles many everyday classical phenomena, as mentioned in Chapter 2 (bicycle riding, precession of a child's top, etc.).

To summarize: if the spin is initially in an energy eigenstate ($|\alpha\rangle$ or $|\beta\rangle$), then it remains in that state, only accumulating a complex phase factor. If the spin is in a superposition state, then it precesses around the z-axis at the Larmor frequency.

10.6 Rotating Frame

The equation of motion is more complicated in the presence of r.f. pulses, since the spin Hamiltonian is time dependent in that case. In order to solve the spin dynamics in the presence of an r.f. field, a special trick is needed. This mathematical trick is equivalent to viewing the nuclear spins from a reference frame revolving around the z-axis. Under suitable approximations, the spin Hamiltonian *appears* to be time independent in the rotating frame.

The rotating frame is useful because the resonant part of the r.f. field is rotating (see Section 8.4.2). By viewing the spins from a frame that rotates 'with the field', it is possible to make the r.f. field look as if it is static:

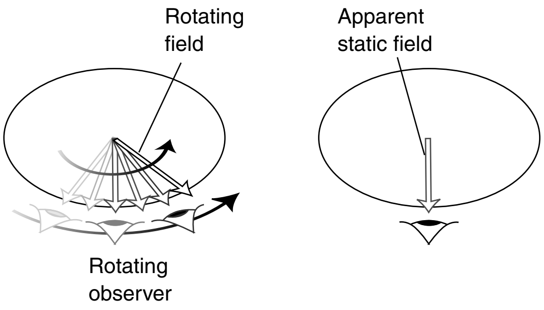

Figure 10.15
The rotating reference frame.

In this way, a difficult time-dependent problem is reduced to a simpler form.

The use of the rotating frame is a necessary evil, and requires some notational complexity. The reader may prefer to skip to the main results (Equations 10.15 and 10.16).

Consider two reference frames, i.e. a fixed reference frame, with axes $\mathbf{e}_x$, $\mathbf{e}_y$, $\mathbf{e}_z$, and a rotating reference frame, with axes denoted $\mathbf{e}'_x$, $\mathbf{e}'_y$, $\mathbf{e}'_z$:

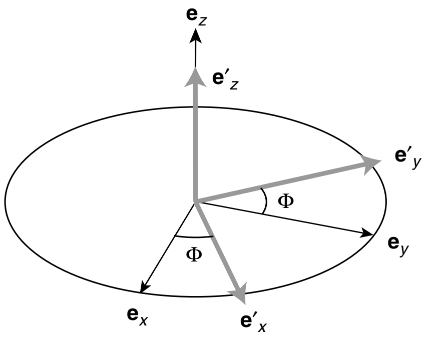

Figure 10.16
The rotating frame axes $\mathbf{e}'_x$, $\mathbf{e}'_y$ and $\mathbf{e}'_z$.

The frame axes are related as

$$\begin{aligned}\mathbf{e}'_x &= \mathbf{e}_x \cos\Phi(t) + \mathbf{e}_y \sin\Phi(t)\\ \mathbf{e}'_y &= \mathbf{e}_y \cos\Phi(t) - \mathbf{e}_z \sin\Phi(t)\\ \mathbf{e}'_z &= \mathbf{e}_z\end{aligned}$$

where $\Phi(t)$ is a time-dependent angle. We consider the case where the frame rotates with a constant frequency ω_{ref} around the z-axis:

$$\Phi(t) = \omega_{\text{ref}} t + \phi_{\text{ref}} \tag{10.12}$$

The appropriate choice of frame phase ϕ_{ref} is discussed below.

For brevity, the symbol (t) indicating time dependence is now dropped.

Consider a spin with a Larmor frequency exactly equal to the reference frequency ω_{ref}. If this spin were prepared in a state $|+x\rangle$, then it would precess at the frequency ω_{ref}, keeping its polarization arrow always along the rotating axis $\mathbf{e}'_x$. By the arguments of the previous section, this spin state must have the form

$$|+x'\rangle = \widehat{R}_z(\Phi)|+x\rangle$$

in which the angle Φ increases in time, as given in Equation 10.12.

Now imagine that one were viewing the spin *from the rotating frame*. Clearly, the spin would appear to be static, and identical to the state $|+x\rangle$. This statement can be formalized by writing

$$\widetilde{|+x'\rangle} = |+x\rangle$$

where the $\tilde{}$ symbol ('tilde') is taken to mean 'as viewed from the rotating frame'. It follows that the spin state 'as viewed from the rotating frame' must be related to the spin state 'as viewed from the laboratory frame' through

$$\widetilde{|+x'\rangle} = \widehat{R}_z(-\Phi)|+x'\rangle$$

This relationship may be generalized: Any spin state 'viewed from the rotating frame' is related to the spin state 'viewed from the fixed frame' through

$$\boxed{|\widetilde{\psi}\rangle = \widehat{R}_z(-\Phi)|\psi\rangle \qquad (10.13)}$$

This equation may now be used to derive the equation of motion of the spin states 'as seen from the rotating frame', $|\widetilde{\psi}\rangle$.

I will now use the term *rotating-frame spin states* to mean 'spin states as seen from the rotating frame'.

Consider the time derivative of the rotating-frame state $|\widetilde{\psi}\rangle$. By the usual chain rule for differentiation, it is given by

$$\frac{\mathrm{d}}{\mathrm{d}t}|\widetilde{\psi}\rangle = \frac{\mathrm{d}}{\mathrm{d}t}\left\{\widehat{R}_z(-\Phi)|\psi\rangle\right\} = \left\{\frac{\mathrm{d}}{\mathrm{d}t}\widehat{R}_z(-\Phi)\right\}|\psi\rangle + \widehat{R}_z(-\Phi)\left\{\frac{\mathrm{d}}{\mathrm{d}t}|\psi\rangle\right\} \qquad (10.14)$$

From Equation 10.9, the time derivative of the rotation operator is

$$\frac{\mathrm{d}}{\mathrm{d}t}\widehat{R}_z(-\Phi) = \frac{\mathrm{d}}{\mathrm{d}t}\exp\{+\mathrm{i}\Phi\hat{I}_z\} = \mathrm{i}\hat{I}_z\left\{\frac{\mathrm{d}}{\mathrm{d}t}\Phi\right\}\exp\{+\mathrm{i}\Phi\hat{I}_z\} = \mathrm{i}\omega_{\mathrm{ref}}\hat{I}_z\widehat{R}_z(-\Phi)$$

The first term on the right-hand-side of Equation 10.14 is therefore

$$\left\{\frac{\mathrm{d}}{\mathrm{d}t}\widehat{R}_z(-\Phi)\right\}|\psi\rangle = \mathrm{i}\omega_{\mathrm{ref}}\hat{I}_z\widehat{R}_z(-\Phi)|\psi\rangle = \mathrm{i}\omega_{\mathrm{ref}}\hat{I}_z|\widetilde{\psi}\rangle$$

The second term on the right-hand side may be calculated by the time-dependent Schrödinger equation:

$$\widehat{R}_z(-\Phi)\left\{\frac{\mathrm{d}}{\mathrm{d}t}|\psi\rangle\right\} = -\mathrm{i}\widehat{R}_z(-\Phi)\widehat{\mathcal{H}}|\psi\rangle = -\mathrm{i}\widehat{R}_z(-\Phi)\widehat{\mathcal{H}}\widehat{R}_z(\Phi)|\widetilde{\psi}\rangle$$

where the last line uses the inverse of the relationship in Equation 10.13. All of these equations may be combined to give the *rotating-frame Schrödinger equation*:

$$\boxed{\frac{\mathrm{d}}{\mathrm{d}t}|\widetilde{\psi}\rangle = -\mathrm{i}\hat{\widetilde{\mathcal{H}}}|\widetilde{\psi}\rangle \qquad (10.15)}$$

where the operator $\tilde{\hat{\mathcal{H}}}$ is given by

$$\tilde{\hat{\mathcal{H}}} = \widehat{R}_z(-\Phi)\widehat{\mathcal{H}}\widehat{R}_z(\Phi) - \omega_{\mathrm{ref}}\hat{I}_z \tag{10.16}$$

Equation 10.15 is identical to the time-dependent Schrödinger equation (Equation 10.7), except for the substitution of the rotating-frame state $|\tilde{\psi}\rangle$ for the fixed-frame state $|\psi\rangle$, and the substitution of the operator $\tilde{\hat{\mathcal{H}}}$ for the spin Hamiltonian $\widehat{\mathcal{H}}$. Therefore, it is natural to call the operator $\tilde{\hat{\mathcal{H}}}$ the *rotating-frame spin Hamiltonian*. It plays the same role in the rotating frame as the ordinary Hamiltonian does in the fixed frame.

Equation 10.15 and Equation 10.16 are the main results of this section. They give a recipe for deriving the dynamics of the spin states 'as viewed from the rotating frame'. One simply uses the ordinary time-dependent Schrödinger equation, but substitutes the rotating-frame spin Hamiltonian $\tilde{\hat{\mathcal{H}}}$ for the ordinary spin Hamiltonian.

What is the physical significance of the two terms in Equation 10.16? The first term may be interpreted as the usual Hamiltonian, rotated about the z-axis through the angle Φ. This rotation arises because the system is viewed from a frame which is itself rotating. Any static spin operators appear to be rotating backwards when viewed from this frame. The second term in Equation 10.16 is more subtle. It produces an additional correction to the spin dynamics, over and above the transformations of the spin operators. This correction arises because the frame is not executing a linear motion, but is rotating and, therefore, accelerating in the technical sense.

An analogy with the everyday world may help. We all live on a rotating frame, because the Earth is rotating about the north–south axis. In everyday life, we find it convenient to use our own planetary rotating frame, rather than a frame that is fixed with respect to the stars. For example, when we say 'go west' or 'go east', we are using implicitly the rotating reference frame (otherwise we would have to use different directions every few minutes, as the Earth rotates). This procedure corresponds to using only the first term in Equation 10.16. One simply forgets that the Earth is rotating, because we are rotating with it. However, just occasionally, the second term makes its presence felt, often in a rather non-intuitive way. For example, the circulation of the winds and the ocean currents are manifestations of planetary rotation. Sometimes fictitious forces, called 'Coriolis forces', are invented to account for such effects, but the real cause is simply the rotation of the planet. For nuclear spins, described in the rotating frame, the second term in Equation 10.16 takes into account the ficititious 'Coriolis forces'.

So far, the equations were developed for the rotating frame in a rather general way. We must now be more specific in our choice of frame. As discussed in Section 8.4.2, the frame frequency ω_{ref} is equal to the frequency of the resonant component of the r.f. pulse (i.e. the component that rotates in the same sense as the spin precession). If γ is positive, then the Larmor frequency $\omega^0 = -\gamma B^0$ is negative, so ω_{ref} is also negative. On the other hand, if γ is negative, then the Larmor frequency and ω_{ref} are both positive. In addition, one has to choose the phase of the rotating frame at time $t = 0$ (ϕ_{ref} in Equation 10.12). There are a number of different conventions for this initial phase.

The convention followed in this book is as follows:

$$\begin{aligned} \phi_{\mathrm{ref}} &= \pi \qquad (\text{for } \gamma > 0) \\ \phi_{\mathrm{ref}} &= 0 \qquad (\text{for } \gamma < 0) \end{aligned} \tag{10.17}$$

The convention for ϕ_{ref} has no practical consequences, but makes some calculations more convenient, as will be seen.

10.7 Precession in the Rotating Frame

We now examine the precessional motion of the spin in the presence of the static magnetic field, as seen from the rotating reference frame.

The spin Hamiltonian in the static field is

$$\hat{\mathcal{H}}^0 = \omega^0 \hat{I}_z$$

so that the rotating-frame Hamiltonian is

$$\hat{\tilde{\mathcal{H}}}^0 = \omega^0 \widehat{R}_z(-\Phi)\hat{I}_z\widehat{R}_z(\Phi) - \omega_{\mathrm{ref}}\hat{I}_z = (\omega^0 - \omega_{\mathrm{ref}})\hat{I}_z$$

The last equation follows because the rotation operator $\widehat{R}_z(\Phi)$ commutes with the angular momentum operator $\hat{I}_z$ (see Section 7.7.2).

The frequency $\omega^0 - \omega_{\mathrm{ref}}$ is the difference between the Larmor frequency and that of the frame. It is called the *relative Larmor frequency*, *offset frequency*, or *resonance offset*, and is denoted Ω^0:

$$\boxed{\Omega^0 = \omega^0 - \omega_{\mathrm{ref}}} \qquad (10.18)$$

The rotating-frame spin Hamiltonian, in the presence of the static field, is therefore

$$\boxed{\hat{\tilde{\mathcal{H}}}^0 = \Omega^0 \hat{I}_z} \qquad (10.19)$$

This has just the same form as the laboratory-frame spin Hamiltonian, except that the offset frequency Ω^0 is involved instead of the Larmor frequency ω^0. The previous discussion may therefore be used without modification. The rotating-frame spin states $|\tilde{\psi}\rangle$ precess around the z-axis at the offset frequency Ω^0. Over a time interval τ, the spin precesses through the angle $\Omega^0\tau$ in the rotating frame:

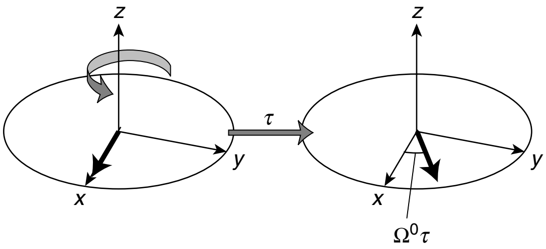

Figure 10.17
Precession in the rotating frame.

The offset frequency Ω^0, unlike the Larmor frequency ω^0, is under experimental control at fixed magnetic field. Adjustment of the spectrometer reference frequency changes the offset Ω^0. For example, if the spectrometer reference frequency is set exactly equal to the Larmor frequency ($\omega^0 = \omega_{\mathrm{ref}}$), then the resonance offset is zero. This is called the case of *exact resonance*.

The offset frequency Ω^0 is related to the chemical shift of the spin and the setting for the reference frequency. Suppose that the spectrometer reference frequency corresponds to the chemical shift δ_{ref}, i.e.

$$\omega_{\mathrm{ref}} = -\gamma B^0(1 + \delta_{\mathrm{ref}}) \tag{10.20}$$

In this case, the offset frequency is given by

$$\Omega^0 = -\gamma B^0(\delta - \delta_{\mathrm{ref}}) \tag{10.21}$$

where $-\gamma B^0$ is the Larmor frequency, including the sign.

Sections 3.4 and 3.5 examined the relationship between the offset frequency Ω^0 and the chemical shift scale. For spins of positive γ, peaks on the left-hand side of the spectrum (high δ) correspond to spins precessing in the negative sense in the rotating frame, whereas peaks on the right-hand side of the spectrum (low δ) correspond to spins precessing in the positive sense in the rotating frame. Spins with chemical shifts equal to δ_{ref} have an offset frequency $\Omega^0 = 0$:

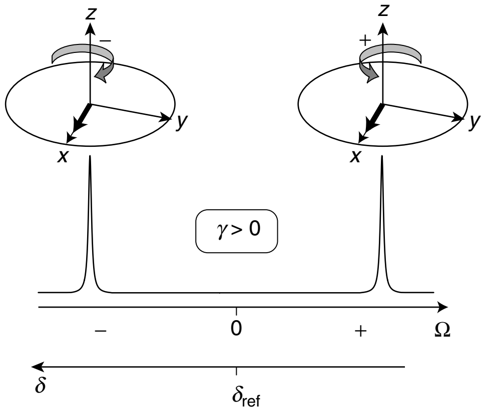

Figure 10.18
Rotating frame precession and the frequency axis for $\gamma > 0$.

For spins with negative γ, the offset frequency axis runs in the opposite direction:

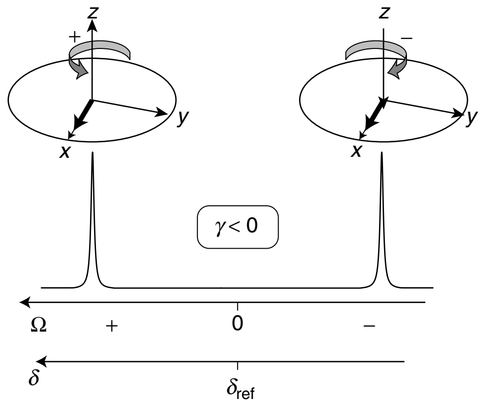

Figure 10.19
Rotating frame precession and the frequency axis for $\gamma < 0$.

10.8 Radio-Frequency Pulse

When an r.f. pulse is applied, the spin experiences two magnetic fields: a static field generated by the magnet and an oscillating field from the excitation coil. The static field is many orders of magnitude larger than the oscillating field.

Why does the weak r.f. field produce a large effect on the nuclear spin, in the presence of the much larger static field?

The key point is that the r.f. field is *resonant* with the precession of the spin. As the spin precesses, the rotating r.f. field 'keeps up' with it. This allows the effect of the weak r.f. field to accumulate as time goes on. If the pulse is applied for long enough, then the weak r.f. field can give rise to a large change in the spin state.

In practice, a significant change in the spin polarization is induced after several microseconds of r.f. irradiation. This corresponds to hundreds of Larmor precession cycles.

The effect is analogous to a child's swing. Each small push on the swing only produces a small effect, but if the pushes are applied at a frequency that corresponds to the natural oscillation frequency of the swing, the accumulated effect after many pushes can be large.

In this section, we examine the mathematics of this process. The use of the rotating frame makes the calculation easier. Nevertheless, the following derivation displays some mathematical complexity and some readers may want to skip to the main result (Equation 10.26).

10.8.1 Rotating-frame Hamiltonian

Consider an r.f. pulse of phase ϕ_p applied along the x-axis of the fixed reference system. As described in Section 8.4.2, the r.f. field oscillates in amplitude at the spectrometer reference frequency ω_ref. This oscillation may be described as two components rotating in opposite senses. The *resonant* field component rotates in the same sense as the nuclear spin precession. The *non-resonant* field component rotates in the opposite sense. Under normal circumstances, it is possible to neglect the non-resonant component, and this is what we will do now.[2]

With this approximation, the spin Hamiltonian during an r.f. pulse is given by

$$\widehat{\mathcal{H}}(t) = \omega^0 \hat{I}_z + \widehat{\mathcal{H}}_\mathrm{RF}(t)$$

where

$$\widehat{\mathcal{H}}_\mathrm{RF}(t) \cong -\frac{1}{2}\gamma B_\mathrm{RF} \sin\theta_\mathrm{RF} \left\{\cos\left(\omega_\mathrm{ref}t + \phi_\mathrm{p}\right)\hat{I}_x + \sin\left(\omega_\mathrm{ref}t + \phi_\mathrm{p}\right)\hat{I}_y\right\} \tag{10.22}$$

and B_RF is the peak value of the oscillating r.f. field, in units of tesla (see Section 8.4.2).

It is convenient to write the r.f. part of the spin Hamiltonian in a different form. We can use the sandwich relationship in Section 6.6.2 to write Equation 10.22 as

$$\widehat{\mathcal{H}}_\mathrm{RF}(t) \cong -\frac{1}{2}\gamma B_\mathrm{RF} \sin\theta_\mathrm{RF}\ \widehat{R}_z\left(\Phi_p\right)\hat{I}_x\widehat{R}_z\left(-\Phi_p\right)$$

where the time-dependent angle Φ_p is given by

$$\Phi_p(t) = \omega_\mathrm{ref}t + \phi_\mathrm{p}$$

In the rotating frame, the appropriate spin Hamiltonian is given by applying Equation 10.16. The result is

$$\hat{\hat{\mathcal{H}}} = -\frac{1}{2}\gamma B_{\mathrm{RF}} \sin\theta_{\mathrm{RF}} \widehat{R}_z\left(-\Phi + \Phi_p\right) \hat{I}_x \widehat{R}_z\left(\Phi - \Phi_p\right) + (\omega^0 - \omega_{\mathrm{ref}})\hat{I}_z$$

where Φ is specified in Equation 10.12.

If all the terms are gathered up, and substitutions are made, we get

$$\hat{\hat{\mathcal{H}}} \cong -\frac{1}{2}\gamma B_{\mathrm{RF}} \sin\theta_{\mathrm{RF}} \widehat{R}_z\left(-\phi_{\mathrm{ref}} + \phi_{\mathrm{p}}\right) \hat{I}_x \widehat{R}_z\left(\phi_{\mathrm{ref}} - \phi_{\mathrm{p}}\right) + \Omega^0 \hat{I}_z \qquad (10.23)$$

where Ω^0 is the resonance offset.

Note that the time dependence has vanished from this expression.[2] This is the point of the rotating frame: it transforms a time-dependent quantum-mechanical problem into a time-independent one.

As a final simplification, we can substitute in the value of ϕ_{ref}, as specified in Equation 10.17. For positive γ spins, ϕ_{ref} is equal to π, which has the effect of changing the sign of the first term in the equation. Equation 10.23 becomes

$$\hat{\hat{\mathcal{H}}} \cong \omega_{\mathrm{nut}} \widehat{R}_z\left(\phi_{\mathrm{p}}\right) \hat{I}_x \widehat{R}_z\left(-\phi_{\mathrm{p}}\right) + \Omega^0 \hat{I}_z \qquad (10.24)$$

where the nutation frequency is defined as

$$\boxed{\omega_{\mathrm{nut}} = \left|\tfrac{1}{2}\gamma B_{\mathrm{RF}} \sin\theta_{\mathrm{RF}}\right| \qquad (10.25)}$$

The nutation frequency is a measure of the r.f. field amplitude and is always positive, which proves to be convenient.[3]

For negative γ spins, ϕ_{ref} is equal to zero, so exactly the same equations apply.

The sandwich property may be used again to write Equation 10.24 as

$$\boxed{\hat{\hat{\mathcal{H}}} \cong \Omega^0 \hat{I}_z + \omega_{\mathrm{nut}}\left(\hat{I}_x \cos\phi_{\mathrm{p}} + \hat{I}_y \sin\phi_{\mathrm{p}}\right) \qquad (10.26)}$$

The final form of the rotating-frame Hamiltonian during the pulse, Equation 10.26, is very simple, and should be memorized.

10.8.2 *x*-pulse

Consider a strong pulse of frequency ω_{ref}, duration τ_{p} and phase $\phi_{\mathrm{p}} = 0$ (an '*x*-pulse', in the usual NMR jargon). The amplitude of the pulse is specified through the nutation frequency ω_{nut}:

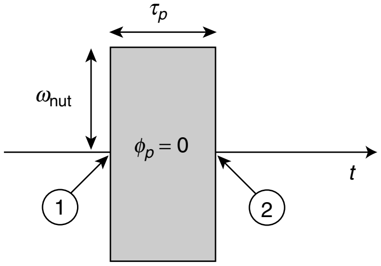

Figure 10.20
A pulse of phase $\phi_{\mathrm{p}} = 0$ and duration τ_{p}.

Consider the case in which the pulse is applied exactly on resonance ($\Omega^0 = 0$). This is ensured by setting the reference frequency to the exact Larmor frequency ($\omega_{\mathrm{ref}} = \omega^0$).

The time points ① and ② indicate the start and end of the pulse, which is assumed to be perfectly rectangular.

The rotating-frame spin Hamiltonian during the pulse is

$$\hat{\tilde{\mathcal{H}}} = \omega_{\text{nut}} \hat{I}_x$$

The motion of the spin states may be calculated through the rotating-frame Schrödinger equation (Equation 10.15). Suppose that the spin state before the pulse is given by $|\tilde{\psi}\rangle_{①}$, and the spin state after the pulse is given by $|\tilde{\psi}\rangle_{②}$. By direct integration of the Schrödinger equation, these states are related by

$$\boxed{|\tilde{\psi}\rangle_{②} = \widehat{R}_x(\beta_{\text{p}})|\tilde{\psi}\rangle_{①}} \tag{10.27}$$

where the *pulse propagator* $\widehat{R}_x(\beta_{\text{p}})$ is defined as

$$\boxed{\widehat{R}_x(\beta_{\text{p}}) = \exp\{-\text{i}\beta_{\text{p}}\hat{I}_x\}} \tag{10.28}$$

and the angle β_{p} is given by

$$\boxed{\beta_{\text{p}} = \omega_{\text{nut}}\tau_{\text{p}}} \tag{10.29}$$

The angle β_{p} is called the *flip angle* of the pulse, and is by definition always positive. It is proportional to the amplitude of the pulse, through the factor ω_{nut}, and is also proportional to the duration of the pulse τ_{p}.

In order to discover what the pulse does, we can use the matrix representation of the rotation operator $\widehat{R}_x(\beta_{\text{p}})$. This is derived in Appendix A.4, and is equal to

$$\boxed{\widehat{R}_x(\beta) = \begin{pmatrix} \cos\frac{1}{2}\beta & -\text{i}\sin\frac{1}{2}\beta \\ -\text{i}\sin\frac{1}{2}\beta & \cos\frac{1}{2}\beta \end{pmatrix}} \tag{10.30}$$

This matrix representation may be used to calculate what the pulse does to spins prepared in various states.

1. *A $(\pi/2)_x$ pulse applied to a spin in state $|\alpha\rangle$.* The notation $(\pi/2)_x$ implies that the flip angle is $\beta_{\text{p}} = \pi/2$ and the phase is $\phi_{\text{p}} = 0$. The transformation of the state may be calculated as follows:

$$\widehat{R}_x(\pi/2)|\alpha\rangle = \frac{1}{\sqrt{2}}\begin{pmatrix} 1 & -\text{i} \\ -\text{i} & 1 \end{pmatrix}\begin{pmatrix} 1 \\ 0 \end{pmatrix} = \frac{1}{\sqrt{2}}\begin{pmatrix} 1 \\ -\text{i} \end{pmatrix} = \text{e}^{-\text{i}\pi/4}\frac{1}{2}\begin{pmatrix} 1+\text{i} \\ 1-\text{i} \end{pmatrix} = \text{e}^{-\text{i}\pi/4}|-y\rangle$$

   Apart from the unimportant phase factor, the pulse transforms the state $|\alpha\rangle$ into the state $|-y\rangle$, i.e. rotates the polarization of the spin by $\pi/2$ around the x-axis:

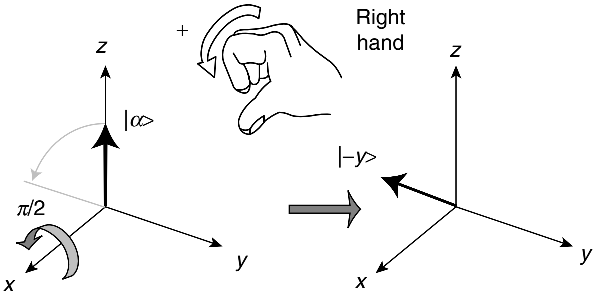

Figure 10.21
The state $|\alpha\rangle$ is transformed into the state $|-y\rangle$ by a $(\pi/2)_x$ pulse.

Note the sense of the *positive* rotation: *anticlockwise* looking down the rotation axis towards the origin.

2. *A π_x pulse applied to a spin in state $|\alpha\rangle$*. This time the flip angle is $\beta_\mathrm{p} = \pi$ and the phase is $\phi_\mathrm{p} = 0$. The transformation of the state is

$$\widehat{R}_x(\pi)|\alpha\rangle = \begin{pmatrix} 0 & -\mathrm{i} \\ -\mathrm{i} & 0 \end{pmatrix} \begin{pmatrix} 1 \\ 0 \end{pmatrix} = -\mathrm{i} \begin{pmatrix} 0 \\ 1 \end{pmatrix} = -\mathrm{i}|\beta\rangle$$

Apart from the phase factor, the pulse transforms the state $|\alpha\rangle$ into the state $|\beta\rangle$:

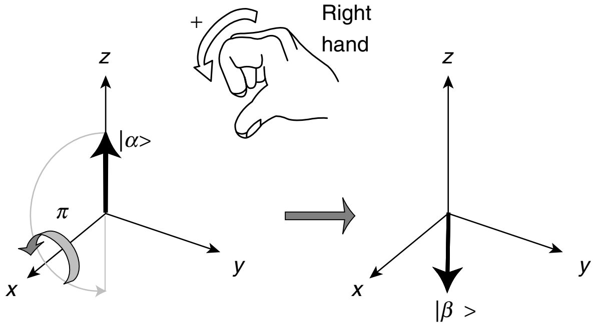

Figure 10.22
The state $|\alpha\rangle$ is transformed into the state $|\beta\rangle$ by a π_x pulse.

3. *A $(\pi)_x$ pulse applied to a spin in state $|+x\rangle$*. The transformation this time is:

$$\widehat{R}_x(\pi)|+x\rangle = \begin{pmatrix} 0 & -\mathrm{i} \\ -\mathrm{i} & 0 \end{pmatrix} \frac{1}{\sqrt{2}} \begin{pmatrix} 1 \\ 1 \end{pmatrix} = -\mathrm{i}\frac{1}{\sqrt{2}} \begin{pmatrix} 1 \\ 1 \end{pmatrix} = -\mathrm{i}|+x\rangle$$

Apart from the phase factor, the pulse leaves the state $|+x\rangle$ unchanged:

Do you get the idea? Whatever the intial state of the spin in the rotating frame, the action of the pulse can always be calculated geometrically, just by rotating the angular momentum around the x-axis through an angle equal to the flip angle of the pulse. Only the phase factors are left out, and these are usually unimportant.

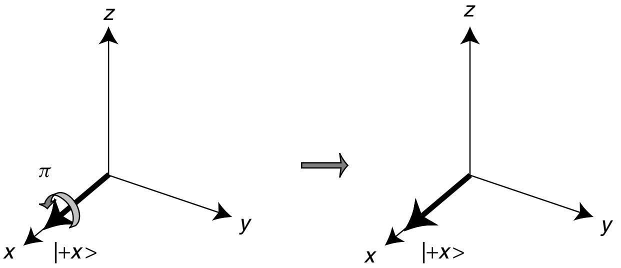

Figure 10.23
A π_x pulse applied to $|{+x}\rangle$ has no effect.

10.8.3 Nutation

The above calculations concern the rotating-frame spin states $|\widetilde{\psi}\rangle$. In order to examine the motion of the spin states in the fixed reference frame, we have to transform back again. From

$$|\widetilde{\psi}\rangle_{②} = \widehat{R}_x(\beta_{\mathrm{p}})|\widetilde{\psi}\rangle_{①}$$

and the relationship in Equation 10.13 between the fixed-frame and the rotating-frame states, we get

$$|\psi\rangle_{②} = \widehat{R}_z\left(\Phi(t_{②})\right)\widehat{R}_x(\beta_{\mathrm{p}})\widehat{R}_z\left(-\Phi(t_{①})\right)|\psi\rangle_{①}$$

where $t_{①}$ and $t_{②}$ are the time coordinates at the beginning and end of the pulse ($t_{②} = t_{①} + \tau_{\mathrm{p}}$). This relationship is *much* more complicated. The rotation of the spin polarization around the *x*-axis, induced by the pulse, occurs simultaneously with the rapid rotation around the *z*-axis, due to the motion of the frame. These two simultaneous rotations generate a sort of spiralling motion. This motion may be visualized by imagining that the tip of the spin polarization arrow leaves a track behind. The track has the following form:

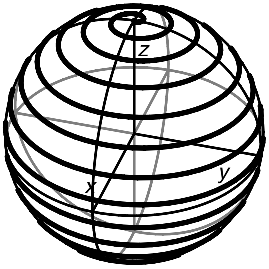

Figure 10.24
The track left behind by the tip of the spin polarization arrow under an r.f. pulse, in the fixed frame.

The diagram uses unrealistic parameters to bring out the nature of the motion more clearly. In practice, there are many thousands of revolutions around the *z*-axis for every revolution around the *x*-axis.

This complicated double rotational motion is called *nutation* in classical mechanics. This is the origin of the term *nutation frequency* for the quantity ω_{nut}.

Since the motion of the spin states during the pulse is so much more complicated in the static frame, it is customary to analyse the entire NMR experiment in the rotating frame.

10.8.4 Pulse of general phase

Now consider a pulse that is exactly on resonance ($\Omega^0 = 0$), but which has a general r.f. phase ϕ_p. The rotating-frame spin Hamiltonian during the pulse is

$$\hat{\hat{\mathcal{H}}} = \omega_\mathrm{nut} \left(\hat{I}_x \cos\phi_\mathrm{p} + \hat{I}_y \sin\phi_\mathrm{p}\right) \tag{10.31}$$

From the form of this operator, one can see that the effect of the phase shift is to change the axis about which the spin polarizations rotate. The rotation axis is still in the *xy*-plane, but subtends an angle ϕ_p with the *x*-axis:

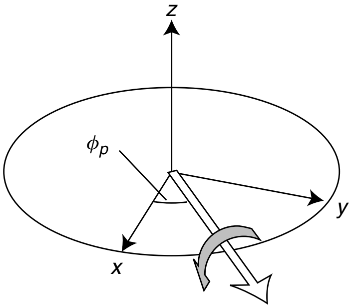

Figure 10.25
Rotation axis for a pulse of general phase.

For example, a pulse of phase $\phi_\mathrm{p} = \pi/2$ rotates the spin polarization around the *y*-axis, a pulse of phase $\phi_\mathrm{p} = \pi$ rotates the spin polarization around the $-x$-axis, and so on. This property is the origin of the jargon for pulse phases summarized in Table 4.1.

The *propagator for an on-resonance pulse of general phase* is given by

$$\begin{aligned}\widehat{R}_{\phi_p}\left(\beta_\mathrm{p}\right) &= \exp\{-\mathrm{i}\omega_\mathrm{nut}\tau_\mathrm{p}\left(\hat{I}_x\cos\phi_\mathrm{p} + \hat{I}_y \sin\phi_\mathrm{p}\right)\}\\ &= \exp\{-\mathrm{i}\beta_\mathrm{p}\left(\hat{I}_x\cos\phi_\mathrm{p} + \hat{I}_y \sin\phi_\mathrm{p}\right)\}\end{aligned}$$

The results of Section 7.6.3 may be used to set this in the form

$$\boxed{\widehat{R}_{\phi_p}\left(\beta_\mathrm{p}\right) = \widehat{R}_z\left(\phi_\mathrm{p}\right)\widehat{R}_x\left(\beta_\mathrm{p}\right)\widehat{R}_z\left(-\phi_\mathrm{p}\right)} \tag{10.32}$$

This is a product of three rotation operators: two about the *z*-axis and one about the *x*-axis.

The matrix representation of the operator $\widehat{R}_{\phi_p}\left(\beta_\mathrm{p}\right)$ is easily derived by multiplying together these three matrices. The result is

$$\boxed{\widehat{R}_{\phi_p}\left(\beta_\mathrm{p}\right) = \begin{pmatrix} \cos\frac{1}{2}\beta_\mathrm{p} & -\mathrm{i}\sin\frac{1}{2}\beta_\mathrm{p}\mathrm{e}^{-\mathrm{i}\phi_\mathrm{p}} \\ -\mathrm{i}\sin\frac{1}{2}\beta_\mathrm{p}\mathrm{e}^{+\mathrm{i}\phi_\mathrm{p}} & \cos\frac{1}{2}\beta_\mathrm{p} \end{pmatrix}} \tag{10.33}$$

The reader should be able to verify the properties:

$$\widehat{R}_y(\pi/2)|\alpha\rangle = \text{phase factor} \times |{+x}\rangle$$

$$\widehat{R}_{\bar{x}}(\pi/2)|{+y}\rangle = \text{phase factor} \times |\beta\rangle$$

which have the following geometrical representation:

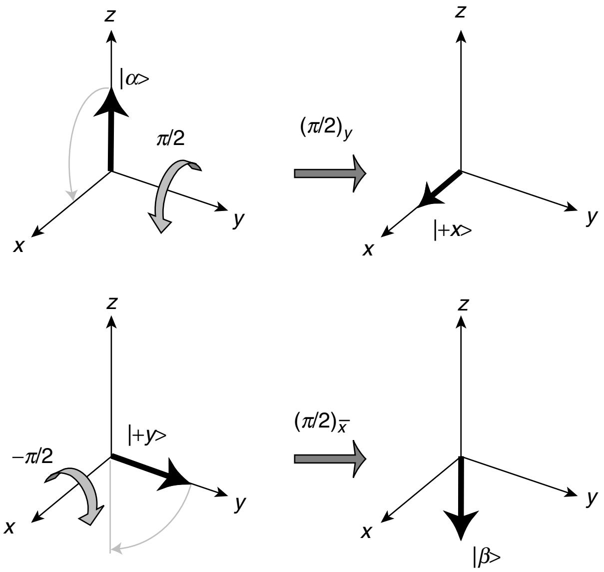

Figure 10.26
More examples of pulses acting on spins.

The notation 'y' implies a phase $\phi_\mathrm{p} = \pi/2$; the notation '$\overline{x}$' implies a phase $\phi_\mathrm{p} = \pi$, and so on. Note carefully the *negative* rotation in the last example (point the thumb of your right hand along the *negative* x-axis, and see which way your fingers curl).

10.8.5 Off-resonance effects

Up to now, we have assumed that the r.f. pulse was exactly on resonance, $\Omega^0 = 0$. In general, it is not possible to ensure exact resonance for all spins at the same time, so this condition cannot always be satisfied. We must consider the case $\Omega^0 \neq 0$, i.e. the problem of *off-resonance* effects.

I will not consider this case very thoroughly, but simply emphasize the results and their experimental significance.

The spin Hamiltonian during a general rectangular pulse is given by

$$\hat{\hat{\mathcal{H}}} = \Omega^0 \hat{I}_z + \omega_\mathrm{nut} \left(\hat{I}_x \cos \phi_\mathrm{p} + \hat{I}_y \sin \phi_\mathrm{p} \right)$$

By analogy with the previous discussion, one can guess what happens. The rotation axis of the spin polarization now has a z-component as well as an x- and a y-component. The axis is therefore 'tilted' out of the xy-plane. The sense of the 'tilt' depends on the sign of Ω^0. If Ω^0 is positive, the axis is tilted in the positive x-direction, i.e. 'above' the plane. If Ω^0 is negative, then the axis is tilted in the negative x-direction, i.e. 'below' the plane:

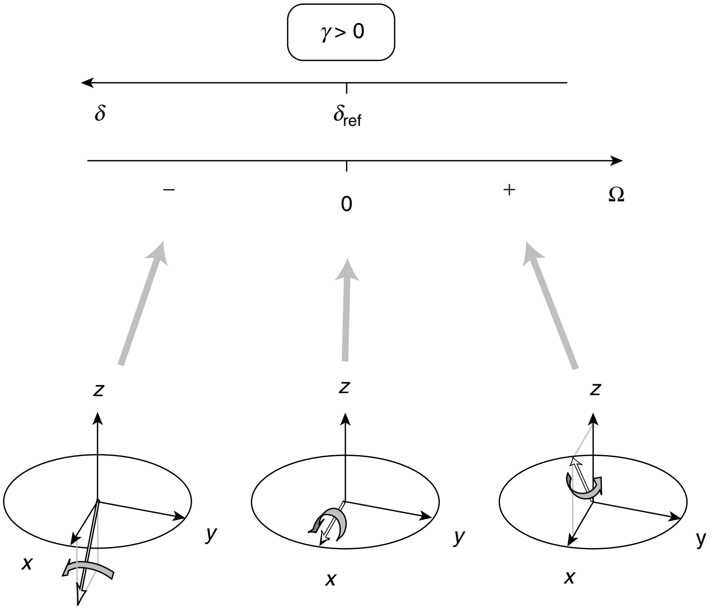

Figure 10.27
Rotation axes for off-resonance pulses.

(These diagrams apply to the case $\gamma > 0$.)

I will not derive the propagator in this case explicitly. The following results are stated without proof, although they may easily be verified from the matrix representations. The rotating-frame spin Hamiltonian for an off-resonant pulse may be written

$$\hat{\tilde{\mathcal{H}}} = \boldsymbol{\omega}_{\text{eff}} \cdot \hat{\mathbf{I}}$$

where $\boldsymbol{\omega}_{\text{eff}}$ is the *effective rotation axis*, given by

$$\boxed{\boldsymbol{\omega}_{\text{eff}} = \omega_{\text{eff}} \left\{ \mathbf{e}'_x \sin\theta_{\text{p}} \cos\phi_{\text{p}} + \mathbf{e}'_y \sin\theta_{\text{p}} \sin\phi_{\text{p}} + \mathbf{e}'_z \cos\theta_{\text{p}} \right\} \qquad (10.34)}$$

and $\{\mathbf{e}'_x, \mathbf{e}'_y, \mathbf{e}'_z\}$ are the axes of the rotating reference frame. The vector operator $\hat{\mathbf{I}}$ is defined as

$$\hat{\mathbf{I}} = \mathbf{e}'_x \hat{I}_x + \mathbf{e}'_y \hat{I}_y + \mathbf{e}'_z \hat{I}_z$$

The *tilt* of the rotation axis away from the z-axis is given by

$$\boxed{\theta_{\text{p}} = \arctan\left(\frac{\omega_{\text{nut}}}{\Omega^0}\right) \qquad (10.35)}$$

The *magnitude* of the rotation frequency around the tilted axis is given by

$$\boxed{\omega_{\text{eff}} = \left\{ (\omega_{\text{nut}})^2 + (\Omega^0)^2 \right\}^{1/2} \qquad (10.36)}$$

The tilt θ_{p} is defined such that $\theta_{\text{p}} = \pi/2$ in the exact on-resonance case ($\Omega^0 = 0$).

Using these parameters, the rotating-frame spin Hamiltonian may be written as

$$\hat{\tilde{\mathcal{H}}} = \omega_{\text{eff}} \widehat{R}_z(\phi_{\text{p}}) \widehat{R}_y(\theta_{\text{p}}) \hat{I}_z \widehat{R}_y(-\theta_{\text{p}}) \widehat{R}_z(-\phi_{\text{p}})$$

The rotating-frame spin states before and after the pulse are related through

$$|\widetilde{\psi}\rangle_{②} = \widehat{R}_{\mathrm{off}}|\widetilde{\psi}\rangle_{①}$$

where $\widehat{R}_{\mathrm{off}}$ is the off-resonance pulse propagator, given by

$$\boxed{\widehat{R}_{\mathrm{off}} = \widehat{R}_z(\phi_{\mathrm{p}})\widehat{R}_y(\theta_{\mathrm{p}})\widehat{R}_z(\omega_{\mathrm{eff}}\tau_{\mathrm{p}})\widehat{R}_y(-\theta_{\mathrm{p}})\widehat{R}_z(-\phi_{\mathrm{p}})} \qquad (10.37)$$

The off-resonance pulse propagator, therefore, may be written as a product of *five* rotations about orthogonal axes. The frequency of the rotation is no longer equal to the nutation frequency ω_{nut}, but is given by the square root of the sum of the squares of the nutation frequency and the offset Ω^0. Therefore, the rotation frequency for a pulse applied off-resonance is always *larger* than the nutation frequency, so that the rotation angle is always larger than the nominal flip angle $\beta_{\mathrm{p}} = |\omega_{\mathrm{nut}}\tau_{\mathrm{p}}|$. However, the rotation occurs about a tilted axis, which makes it less effective.

Rather than delving into the mathematics of these transformations, I show below what happens to the polarization of a spin in state $|\alpha\rangle$ exposed to a $\pi/2$ pulse with different resonance offsets Ω^0. For clarity, the track of the *tip* of the polarization arrow is drawn during the pulse, but not the polarization arrow itself. The diagrams depict the motion of the spin polarization around the rotation axis, which is shown as an 'open' arrow. All pictures are shown in the rotating frame, and the value of $\Omega^0/\omega_{\mathrm{nut}}$ is given above each diagram:

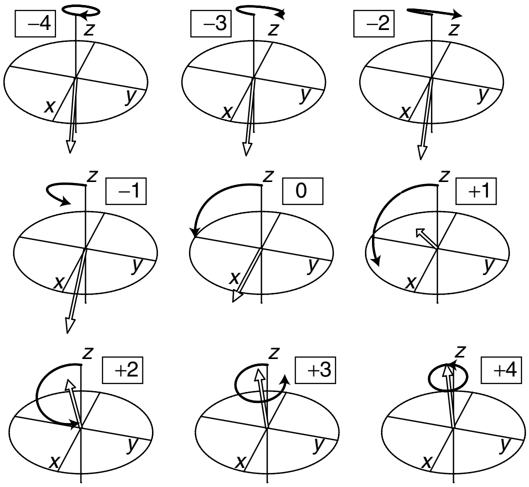

Figure 10.28
Off-resonance pulses acting on spins initially in the state $|\alpha\rangle$. The white arrow indicates the rotation axis. The black arrow indicates the trace left by the tip of the spin polarization arrow. The labels show the value of $\Omega^0/\omega_{\mathrm{nut}}$. The pulse has an on-resonance flip angle $\omega_{\mathrm{nut}}\tau_{\mathrm{p}} = \pi/2$.

When the pulse is far off resonance, nothing much happens. The tilt angle ϕ_{p} is small, and the spin polarization simply wobbles a number of times about an axis which is close to the z-axis. As the frequency of the pulse approaches resonance, the excursions of the polarization arrow become larger until, at exact resonance, the pulse transforms the state $|\alpha\rangle$ exactly into the state $|-y\rangle$, as calculated before. When the frequency of the pulse is changed further, the axis tilts in the opposite sense, and for large offsets there is only a minor disturbance of the spin.

Another way to think about this is in terms of the *transition probability* for the spin states. The quantity

$$\mathtt{P}_{\alpha\to\beta} = |\langle\beta|\widehat{R}_{\mathrm{off}}(\Omega^0)|\alpha\rangle|^2$$

corresponds to the probability that a spin in state $|\alpha\rangle$ before the pulse is found in the state $|\beta\rangle$ after the pulse. Figure 10.29 shows the transition probability $\mathtt{P}_{\alpha\to\beta}$ as a function of resonance offset Ω^0, in the case of a π pulse:

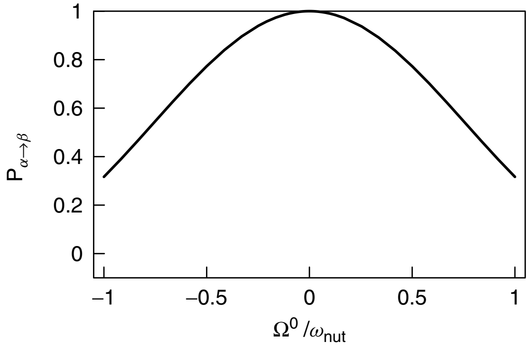

Figure 10.29
Transition probability for the process $|\alpha\rangle \to |\beta\rangle$ as a function of resonance offset, in the case of a π pulse.

Exactly on resonance, the transition probability is unity because the pulse transforms the state $|\alpha\rangle$ into the state $|\beta\rangle$. Off resonance, the transition probability declines, since the pulse becomes less effective.

Figure 10.30 explores the behaviour of the transition probability $P_{\alpha\to\beta}$ for larger resonance offsets or, equivalently, for weaker r.f. fields:

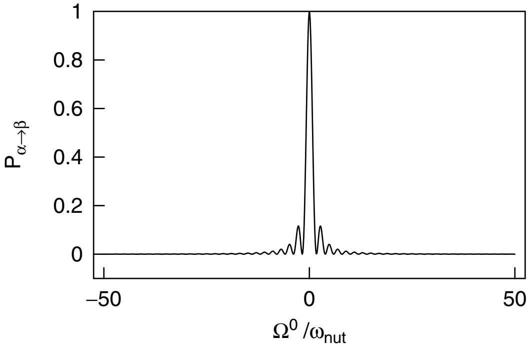

Figure 10.30
Transition probability for the process $|\alpha\rangle \to |\beta\rangle$ as a function of resonance offset, in the case of a π pulse.

This shows clearly that a realistic r.f. pulse is frequency selective. Only spins that precess at a frequency close to that of the r.f. irradiation are significantly affected by the pulse. In terms of the ‘swing’ analogy, this corresponds to the everyday experience that small pushes must be timed very well to get a swing going.

The *bandwidth* of the pulse is proportional to the nutation frequency, and hence to the peak r.f. amplitude.[4] If the pulse is *strong* (large peak r.f. amplitude), then the pulse is less frequency selective. If the pulse is *weak* (small peak r.f. amplitude), then the pulse is more frequency selective.

These results have a large effect on the methodology of NMR. Generally speaking, it is desirable to use r.f. fields that are as large as possible, so as to ‘cover’ all spins in the practical chemical shift range. Strong pulses allow a reasonably uniform manipulation of all spins in the spectrum, irrespective of their chemical shifts. In terms of the swing analogy, this corresponds to the use of brute force to correct for deficiencies in one’s timing.

The nutation frequency is limited by technical considerations. The largest achievable nutation frequency is usually around 200 kHz, which is smaller than the difference in Larmor frequency between different isotopes. An r.f. field applied near the Larmor frequency of one isotope generally has an insignificant influence on the spins of a different isotope. This fact accounts for the design of multinuclear magnetic resonance spectrometers, which employ multiple transmitter circuits and multiply tuned probes, in order to irradiate the sample with a set of r.f. fields, each close to resonance for a different spin isotope.

In the rest of this book, I assume that r.f. pulses are strong, and use the form of the pulse propagator given in Equation 10.33.

Some NMR experiments employ a *weak* r.f. pulse (small value of ω_{nut}), in order to influence only those spins whose Larmor frequency falls in a narrow defined range. This is called a *frequency-selective pulse*.

The above calculations considered a *rectangular r.f. pulse of constant phase*, defined as one for which the r.f. amplitude climbs infinitely fast at the start of the pulse, falls infinitely fast to zero at the end of the pulse, and in which the phase and amplitude are constant during the pulse. It may be shown that a rectangular r.f. pulse does not have optimal frequency selectivity. Much effort has gone into the development of *shaped* r.f. pulses, whose waveforms are smoother and more complicated than a rectangular pulse, but which can achieve a cleaner frequency selection. Such methods are widely used in NMR imaging.

Notes

1. Atoms may be sorted according to their spin angular momentum by allowing them to float through a region of inhomogeneous magnetic field (*Stern–Gerlach* experiments). See the text by Cohen-Tannoudji *et al.* in *Further Reading*.

2. The treatment given here neglects the effect of the non-resonant rotating component of the r.f. field. This approximation is very good as long as the r.f. field is weak compared with the static field, which is almost always the case.

3. The choice of rotating frame phase ϕ_{ref} (Equation 10.17) leads to a consistently positive nutation frequency ω_{nut} (Equation 10.25). With this convention, all pulses execute positive right-handed rotations around the rotating-frame axes. The NMR community is evenly split between those who use positive right-handed rotations for pulses (as in this book), and those who prefer negative right-handed rotations (so that, for example, a rotation by $\pi/2$ around the x-axis transforms a vector along the z-axis into a vector along the positive y-axis). All conventions lead, of course, to equivalent results, providing that they are used consistently.

4. The relationship between the pulse bandwidth (the width of the frequency response) and the r.f. nutation frequency ω_{nut} is not straightforward. There are essentially two main regimes, determined by the value of the flip angle $\beta_{\mathrm{p}} = \omega_{\mathrm{nut}}\tau_{\mathrm{p}}$, where τ_{p} is the pulse duration. If the flip angle is smaller than around $\pi/2$ (the *linear regime*), then the pulse bandwidth is determined by the inverse of the pulse duration, rather than the nutation frequency – i.e. the shorter the pulse, the wider its bandwidth. However, most r.f. pulses operate in the *non-linear regime*, in which the flip angles are large ($\beta_{\mathrm{p}} \geq \pi/2$). In the non-linear regime, it is the nutation frequency ω_{nut} that determines the bandwidth of the frequency response, not the pulse duration.

Further Reading

- For more on the quantum mechanics of a single spin-1/2, see C. Cohen-Tannoudji, B. Diu and F. Laloë, *Quantum Mechanics*, Wiley, London, 1977.
- For a review of current thinking about the observation process in quantum mechanics, see A. Whitaker, *Einstein, Bohr and the Quantum Dilemma*, Cambridge University Press, 1996.
- For more discussion of the rotating frame, and a treatment of selective pulses and shaped pulses, see R. Freeman, *Spin Choreography. Basic Steps in High Resolution NMR*, Spektrum, Oxford, 1997.
- For a review of shaped pulses, see R. Freeman, *Prog. NMR Spectrosc.* **32**, 59–106 (1998).

Exercises

10.1 In the following calculation, the spin-1/2 state $|\theta\rangle$ is defined as

$$|\theta\rangle = \cos\tfrac{1}{2}\theta|\alpha\rangle + \mathrm{i}\sin\tfrac{1}{2}\theta|\beta\rangle$$

(i) Show that the spin-1/2 state $|\theta\rangle$ is an eigenstate of $\hat{I}_z\cos\theta + \hat{I}_y\sin\theta$ and give the eigenvalue.
(ii) Give a pictorial representation of the state $|\theta\rangle$.
(iii) What pulse transforms the state $|\theta\rangle$ into the state $|\pi/2\rangle$? Derive the result geometrically and then verify it mathematically.

10.2 A sample containing protons is exposed to an r.f. magnetic field with peak amplitude $B_{\mathrm{RF}} = 469.8\,\mu\mathrm{T}$. The frequency of the r.f. field is exactly resonant with the proton Larmor precession.
(i) What is the nutation frequency of the protons in units of hertz?
(ii) How long should the r.f. field be applied in order to generate a pulse with a flip angle of $\pi/2$?
(iii) What is the flip angle of the protons if the pulse duration is kept as in (ii) but the peak r.f. field is increased to $B_{\mathrm{RF}} = 939.6\,\mu\mathrm{T}$?

10.3 A single spin-1/2 in state $|\alpha\rangle$ is exposed to a three-pulse sequence $(\pi/2)_x\pi_y(\pi/2)_x$.
(i) Calculate the spin state after the three-pulse sequence.
(ii) Show that the final spin state is an eigenstate of $\hat{I}_z$. What is the eigenvalue?
(iii) Interpret the trajectory of the spin geometrically.

10.4 A single spin-1/2 in state $|\alpha\rangle$ is exposed to a $\pi/2$ pulse of phase $\pi/2$, followed by a π pulse of phase $5\pi/4$.
(i) Calculate the spin state after the two-pulse sequence.
(ii) Show that the final spin state is an eigenstate of $\hat{I}_y$. What is the eigenvalue?
(iii) Interpret the trajectory of the spin geometrically.

10.5 A pulse with nutation frequency $\omega_{\mathrm{nut}}/2\pi = 10\,\mathrm{kHz}$ is applied to a single spin-1/2 in state $|\alpha\rangle$. The resonance offset of the pulse is exactly $\Omega^0/2\pi = 10\,\mathrm{kHz}$. If the spin has a 50% probability of making a transition to the state $|\beta\rangle$, what is the pulse duration?

11 Ensemble of Spins-1/2

11.1 Spin Density Operator

Consider a sample containing only magnetically equivalent spins-1/2, such as the protons in a tube of pure water (neglecting rare isotopes). To a good approximation, the $\sim 10^{22}$ spins do not influence each other. The spin magnetic moments precess and nutate, independently of each other.[1]

A collection of independent, identical systems is called an *ensemble*. The proton spins in a tube of water behave, to a very good approximation, as an *ensemble of isolated spins*-1/2.

At any particular moment, each of the protons has a different polarization state. A few are very close to the state $|\alpha\rangle$ and a few are very close to the state $|\beta\rangle$ but the vast majority are in superposition states that are intermediate between $|\alpha\rangle$ and $|\beta\rangle$. The proton spin polarization vectors are distributed almost uniformly, pointing in all possible directions of space:

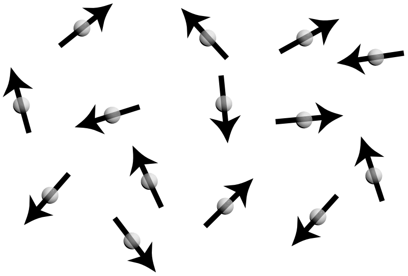

Figure 11.1
Ensemble of isolated spins-1/2.

Each proton spin behaves as described in Chapter 10. The total nuclear magnetization is the sum of innumerable small contributions from the individual spins. To calculate a macroscopic quantity, such as the magnetization, it is possible, at least in principle, to treat each spin individually and then to add the results together.

This calculation is impractical because there are so many spins. Fortunately, there is an elegant alternative, called the method of the *density operator*. The density operator describes the quantum state of the entire ensemble, without referring to the individual spin states. It is a tool of central importance in the theory of NMR.

Spin Dynamics: Basics of Nuclear Magnetic Resonance, Second Edition Malcolm H. Levitt

The density operator method is based on the properties of the expectation value of an observable (see Section 7.1.3). Consider a single spin in a general superposition state:

$$|\psi\rangle = \begin{pmatrix} c_\alpha \\ c_\beta \end{pmatrix} \tag{11.1}$$

The expectation value of an operator $\widehat{Q}$ is given by

$$\begin{aligned}\langle\widehat{Q}\rangle &= \langle\psi|\widehat{Q}|\psi\rangle \\ &= (\, c_\alpha{}^*\,, \quad c_\beta{}^*\,) \begin{pmatrix} Q_{\alpha\alpha} & Q_{\alpha\beta} \\ Q_{\beta\alpha} & Q_{\beta\beta} \end{pmatrix} \begin{pmatrix} c_\alpha \\ c_\beta \end{pmatrix} \\ &= c_\alpha c_\alpha{}^* Q_{\alpha\alpha} + c_\alpha c_\beta{}^* Q_{\alpha\beta} + c_\beta c_\alpha{}^* Q_{\beta\alpha} + c_\beta c_\beta{}^* Q_{\beta\beta}\end{aligned} \tag{11.2}$$

The expression involves *quadratic products* of the superposition coefficients c_α and c_β. This suggests a way of representing the state of the spin by these quadratic products, rather than the coefficients themselves. A suitable construction is a matrix formed by multiplying the column vector $|\psi\rangle$ and the row vector $\langle\psi|$:

$$|\psi\rangle\langle\psi| = \begin{pmatrix} c_\alpha \\ c_\beta \end{pmatrix} (\, c_\alpha{}^*\,, \quad c_\beta{}^*\,) = \begin{pmatrix} c_\alpha c_\alpha{}^* & c_\alpha c_\beta{}^* \\ c_\beta c_\alpha{}^* & c_\beta c_\beta{}^* \end{pmatrix} \tag{11.3}$$

Note the order in which the bra and the ket are multiplied. If they were multiplied the other way round ($\langle\psi|\psi\rangle$), the result would be unity.

The expectation value of the operator $\widehat{Q}$ may be extracted from the object $|\psi\rangle\langle\psi|$ as follows:

$$\langle\widehat{Q}\rangle = \mathrm{Tr}\{|\psi\rangle\langle\psi|\,\widehat{Q}\} \tag{11.4}$$

where the trace operation is described in Section 7.7.4. It may easily be verified that the expressions shown in Equations 11.2 and 11.4 are equivalent.

So far, this does not seem particularly helpful, since the state of the spin is represented in the matrix of Equation 11.3 by four complex numbers, instead of the two complex numbers required in the column vector of Equation 11.1.

However, now suppose there are two independent spins involved. Suppose the first spin has state $|\psi_1\rangle$ and the second spin has state $|\psi_2\rangle$. The result of measuring Q is still uncertain in general, because of quantum indeterminacy. However, the most likely outcome is the sum of the two expectation values:

$$Q_{\mathrm{obs}}(\text{most likely}) = \langle\psi_1|\widehat{Q}|\psi_1\rangle + \langle\psi_2|\widehat{Q}|\psi_2\rangle$$

which may be rewritten

$$Q_{\mathrm{obs}}(\text{most likely}) = \mathrm{Tr}\{(|\psi_1\rangle\langle\psi_1| + |\psi_2\rangle\langle\psi_2|)\,\widehat{Q}\}$$

If there are a large number of spins involved, then repetition of this derivation gives

$$Q_{\mathrm{obs}}(\text{most likely}) = \mathrm{Tr}\{(|\psi_1\rangle\langle\psi_1| + |\psi_2\rangle\langle\psi_2| + \ldots)\,\widehat{Q}\}$$

where the sum is taken over all spins in the ensemble.

Now suppose that an operator $\hat{\rho}$ is defined:

$$\hat{\rho} = \mathbb{N}^{-1}\,(|\psi_1\rangle\langle\psi_1| + |\psi_2\rangle\langle\psi_2| + \ldots)$$

where $\mathbb{N}$ is the number of members of the ensemble. For brevity, this expression may be written as

$$\boxed{\hat{\rho} = \overline{|\psi\rangle\langle\psi|}} \tag{11.5}$$

where the overbar indicates the *average* over all members of the ensemble. The *macroscopic* observation of Q for the entire ensemble of spins yields the result

$$Q_{\text{macro}} \cong \mathbb{N}\,\text{Tr}\{\hat{\rho}\widehat{Q}\}$$

which suddenly looks rather simple.

For the large numbers of spins involved in NMR, it may be shown that this equation is exact to within about $\mathbb{N}^{-1/2}$, which is smaller than 10^{-7} in the cases encountered in NMR.

If both sides are divided by $\mathbb{N}$, the equation becomes

$$\mathbb{N}^{-1} Q_{\text{macro}} = \text{Tr}\{\hat{\rho}\widehat{Q}\}$$

Normally this equation is written (rather loosely) as

$$\boxed{\langle Q\rangle = \text{Tr}\{\hat{\rho}\widehat{Q}\} \qquad (11.6)}$$

Strictly, the left-hand side is not really the expectation value for a single system, but the average contribution of each ensemble member to the final macroscopic result, which is a slightly different thing. Nevertheless, I will not be pedantic and continue with the usual notation (Equation 11.6).

For historical reasons, the operator $\hat{\rho}$, defined in Equation 11.5, is known as the *spin density operator*.[2,3] The term is unfortunate. The operator $\hat{\rho}$ has no relationship with the physical density of the sample.

One should be aware of the very remarkable nature of this result. Equation 11.6 says that the result of *any* macroscopic observation may be deduced from two spin operators, with one representing the observable that is being measured and the other representing the state of *the entire spin ensemble*, independent of the number of spins it contains. This is an amazing simplification of the problem; instead of specifying the individual microscopic states of $\sim 10^{22}$ spins, one gets away with specifying the value of a single operator, i.e. the spin density operator $\hat{\rho}$.

11.2 Populations and Coherences

11.2.1 Density matrix

The matrix representation of the density operator, for an ensemble of non-interacting spins-1/2, is given by

$$\boxed{\hat{\rho} = \begin{pmatrix} \rho_{\alpha\alpha} & \rho_{\alpha\beta} \\ \rho_{\beta\alpha} & \rho_{\beta\beta} \end{pmatrix} = \begin{pmatrix} \overline{c_\alpha c_\alpha{}^*} & \overline{c_\alpha c_\beta{}^*} \\ \overline{c_\beta c_\alpha{}^*} & \overline{c_\beta c_\beta{}^*} \end{pmatrix} \qquad (11.7)}$$

The overbars indicate an average over the ensemble. The right-hand-side in this equation is called the *density matrix*.

The *diagonal* elements of the spin density operator $\rho_{\alpha\alpha}$ and $\rho_{\beta\beta}$ are called the *populations*[4] of states $|\alpha\rangle$ and $|\beta\rangle$. The *off-diagonal* elements $\rho_{\alpha\beta}$ and $\rho_{\beta\alpha}$ are called the *coherences* between states $|\alpha\rangle$ and $|\beta\rangle$.

11.2.2 Box notation

In this book, I use a special *box notation* for the populations and coherences. The population of state $|\alpha\rangle$ is denoted $\rho_{\boxed{\alpha}}$, and is given by

$$\rho_{\boxed{\alpha}} = \langle\alpha|\hat{\rho}|\alpha\rangle = \overline{c_\alpha c_\alpha{}^*} \tag{11.8}$$

Similarly, the population of state $|\beta\rangle$ is denoted $\rho_{\boxed{\beta}}$, and is given by

$$\rho_{\boxed{\beta}} = \langle\beta|\hat{\rho}|\beta\rangle = \overline{c_\beta c_\beta{}^*} \tag{11.9}$$

The two coherences are denoted $\rho_{\boxed{+}}$ and $\rho_{\boxed{-}}$, and are given by

$$\begin{aligned} \rho_{\boxed{+}} &= \langle\alpha|\hat{\rho}|\beta\rangle = \overline{c_\alpha c_\beta{}^*} \\ \rho_{\boxed{-}} &= \langle\beta|\hat{\rho}|\alpha\rangle = \overline{c_\beta c_\alpha{}^*} \end{aligned} \tag{11.10}$$

Using this notation, the density matrix is

$$\hat{\rho} = \begin{pmatrix} \rho_{\boxed{\alpha}} & \rho_{\boxed{+}} \\ \rho_{\boxed{-}} & \rho_{\boxed{\beta}} \end{pmatrix}$$

The density operator may also be written as

$$\hat{\rho} = \rho_{\boxed{\alpha}} \hat{I}^\alpha + \rho_{\boxed{\beta}} \hat{I}^\beta + \rho_{\boxed{+}} \hat{I}^+ + \rho_{\boxed{-}} \hat{I}^-$$

using the shift operators $\hat{I}^+$ and $\hat{I}^-$, and the projection operators $\hat{I}^\alpha$ and $\hat{I}^\beta$. This can be seen from the matrix elements given in Sections 7.8.5 and 7.8.6.

The box notation is particularly useful for systems of many coupled spins, as will be seen later.

11.2.3 Balls and arrows

The state of the spin-1/2 ensemble is specified by the values of the populations $\rho_{\boxed{\alpha}}$ and $\rho_{\boxed{\beta}}$ and the coherences $\rho_{\boxed{+}}$ and $\rho_{\boxed{-}}$, which may be depicted by a diagram. The populations are drawn as 'little balls' sitting on the appropriate energy level, and the coherences are drawn as arrows 'connecting' the energy levels:

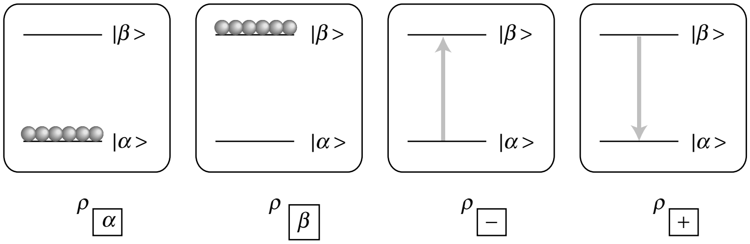

Figure 11.2
Pictorial representation of populations and coherences.

⚠The 'arrow' representation of coherences should not be misinterpreted: in particular, there is no 'flow' or 'transition' going on between the connected states. The arrow indicates only that there is a *coherence* between the states, defined mathematically in Equation 11.10. I will discuss in a moment what this means on a microscopic level.

11.2.4 Orders of coherence

It proves useful to classify the spin coherences on the basis of a quantum number called the *coherence order*.

Consider a coherence ρ_{rs} between two energy eigenstates $|r\rangle$ and $|s\rangle$, defined as

$$\rho_{rs} = \langle r|\hat{\rho}|s\rangle = \overline{\langle r|\psi\rangle\langle\psi|s\rangle}$$

In high magnetic field, the two energy eigenstates have well-defined values of the angular momentum in the magnetic field direction, by convention the z-axis:

$$\hat{I}_z|r\rangle = M_r|r\rangle$$

$$\hat{I}_z|s\rangle = M_s|s\rangle$$

The *order* p_{rs} of the coherence ρ_{rs} is defined as

$$\boxed{p_{rs} = M_r - M_s \qquad (11.11)}$$

i.e. the difference in the z-angular momentum of the connected states.

For an ensemble of non-interacting spins-1/2, there are only two states, with z-angular momentum quantum numbers $\pm 1/2$. The two coherences, therefore, have order $+1$ and -1.

For the coherence $\rho_{\boxed{+}}$, the state $|r\rangle$ is equal to $|\alpha\rangle$, and the state $|s\rangle$ is equal to $|\beta\rangle$. The order of the coherence $\rho_{\boxed{+}}$ is

$$p_{\boxed{+}} = (+\tfrac{1}{2}) - (-\tfrac{1}{2}) = +1$$

The coherence $\rho_{\boxed{+}}$ is known as a (+1)-*quantum coherence*.

For the coherence $\rho_{\boxed{-}}$, the state $|r\rangle$ is equal to $|\beta\rangle$, and the state $|s\rangle$ is equal to $|\alpha\rangle$. The order of the coherence $\rho_{\boxed{-}}$ is

$$p_{\boxed{-}} = (-\tfrac{1}{2}) - (+\tfrac{1}{2}) = -1$$

The coherence $\rho_{\boxed{-}}$ is known as a (−1)-*quantum coherence*.

Since populations are diagonal elements, their coherence order is zero.

For non-interacting spins-1/2, there are three possible values for the coherence order: −1, 0 and +1.

⚠The relationship between coherence order and the 'arrow diagrams' requires care. The coherence order corresponds to the z-angular momentum of the state at the arrow *head*, minus the z-angular momentum of the state at the arrow *tail*. For spins of positive γ, energy is proportional to negative z-angular momentum, so the arrows for (+1)-quantum coherences point *down*, whereas the arrows for (−1)-quantum coherence point *up*.

11.2.5 Relationships between populations and coherences

Coherences are *complex numbers*.

The (±1)-quantum coherences are complex conjugates of each other:

$$\boxed{\rho_{\boxed{+}} = \overline{c_\alpha c_\beta{}^*} = \left\{\overline{c_\beta c_\alpha{}^*}\right\}^* = \rho_{\boxed{-}}{}^* \qquad (11.12)}$$

It is impossible, therefore, to have a (+1)-quantum coherence without a (−1)-quantum coherence. *Coherences come in conjugate pairs.*

The populations are also interdependent. The state of each spin is normalized:

$$c_\alpha c_\alpha{}^* + c_\beta c_\beta{}^* = 1$$

Since this applies to all spins in the ensemble, it also applies to the ensemble average. The sum of the populations is therefore unity:

$$\boxed{\rho_{\boxed{\alpha}} + \rho_{\boxed{\beta}} = 1 \qquad (11.13)}$$

In addition, the populations are by definition real and positive:

$$\rho_{\boxed{\alpha}}{}^{*} = \rho_{\boxed{\alpha}}; \qquad \rho_{\boxed{\beta}}{}^{*} = \rho_{\boxed{\beta}}$$

The population of any state lies between 0 and 1.

11.2.6 Physical interpretation of the populations

What is the physical interpretation of the components of the density operator, in terms of the microscopic states of the individual spins?

We start with the populations. Since the sum of the populations is always equal to one, only the *difference* in populations between the two states has any physical significance. The difference in spin state populations indicates net *longitudinal* spin polarization, i.e. magnetization of the sample in the direction of the field.

A state in which the population of state $|\alpha\rangle$ is *larger* than that of $|\beta\rangle$ indicates that there is a net polarization of the spins *along* the external field direction:

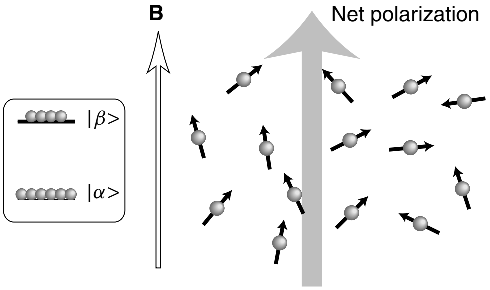

Figure 11.3
Net spin polarization along the field.

Similarly, a state in which the population of state $|\alpha\rangle$ is *less* than that of $|\beta\rangle$ indicates that there is a net polarization of the spins *against* the external field:

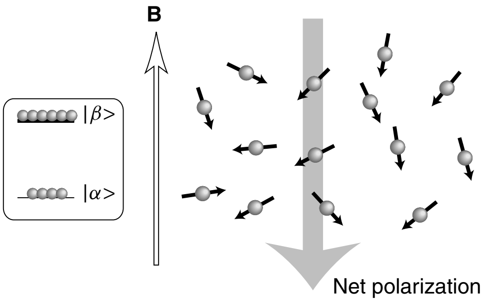

Figure 11.4
Net spin polarization against the field.

If the populations of the two states are equal ($\rho_{\boxed{\alpha}} = \rho_{\boxed{\beta}} = 1/2$), then there is no net polarization in the direction of the field. The number of spins pointing ‘up’ is equal, on the average, to the number of spins pointing ‘down’.

⚠The population of a state does *not* indicate the fraction of spins that are ‘in’ that state. In the drawings given above, there are no *individual* spins that are polarized exactly along or against the external field and, therefore, no spins which are exactly in the states $|\alpha\rangle$ and $|\beta\rangle$. Under ordinary circumstances, the majority of spins are always in superpositions of the two energy eigenstates, and point in an arbitrary direction.[5]

⚠In the diagrams above, the degree of spin polarization is greatly exaggerated, for the sake of clarity. In reality, the net spin polarization in any particular direction is usually extremely small.

11.2.7 Physical interpretation of the coherences

The presence of coherences $\rho_{\boxed{+}}$ and $\rho_{\boxed{-}}$ indicates transverse spin magnetization, i.e. a net spin polarization *perpendicular* to the external field.

Suppose, for example, that the spin density operator has the following form:

$$\rho_{\boxed{\alpha}} = \rho_{\boxed{\beta}} = 1/2$$

$$\rho_{\boxed{-}} = \rho_{\boxed{+}}{}^{*} \quad \neq 0$$

This state has the following physical interpretation:

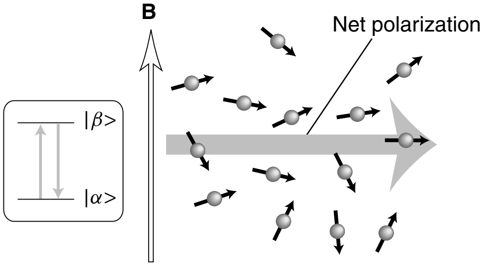

Figure 11.5
Net spin polarization perpendicular to the field.

The spins are equally likely to point either along or against the magnetic field. Nevertheless, there is net spin polarization *perpendicular* to the magnetic field.

Coherence, therefore, requires the existence of spins that have *transverse* polarization vectors, i.e. spins which are in superposition states. However, this is not sufficient. For coherence to exist, the transverse polarizations must also be partially aligned. Polarization vectors that are uniformly distributed in the *xy*-plane provide no coherence.[6] This idea is expressed in the following pictures of the *xy*-plane, perpendicular to the magnetic field:

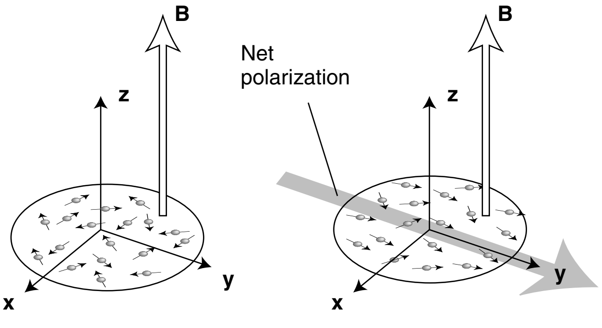

No coherence

Coherence

Figure 11.6
Partial alignment of spins in the transverse plane.

(The degree of alignment of the spins is greatly exaggerated.)

The coherences $\rho_{\boxed{+}}$ and $\rho_{\boxed{-}}$ are complex numbers. They have a phase and an amplitude. What is the physical significance of the phase of these complex numbers?

The phase of the coherences indicates the *direction* of the transverse spin polarization in the xy-plane. The phase of the (-1)-quantum coherence $\rho_{\boxed{-}}$ in the complex plane is the same as the angle of the transverse magnetization with respect to the x-axis:

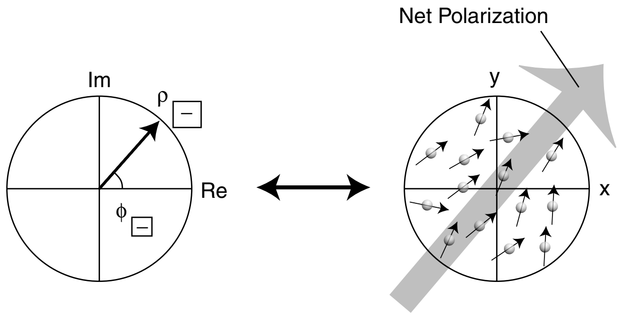

Figure 11.7
Phase of the (-1)-quantum coherence and the direction of the transverse polarization.

(The magnetic field points up, out of the paper.) If the (-1)-quantum coherence is written

$$\rho_{\boxed{-}} = |\rho_{\boxed{-}}| \exp\{i\phi_{\boxed{-}}\}$$

then the preferential polarization axis of the spins is

$$\mathbf{e}'_x \cos\phi_{\boxed{-}} + \mathbf{e}'_y \sin\phi_{\boxed{-}}$$

where $\mathbf{e}'_x$ and $\mathbf{e}'_y$ are the rotating frame axes (see Section 10.6). For example, when $\phi_{\boxed{-}} = 0$, the spins are preferentially polarized along the rotating-frame x-axis; when $\phi_{\boxed{-}} = \pi/2$, the spins are preferentially polarized along the rotating-frame y-axis, and so on.

What about the $(+1)$-quantum coherence?

This turns out to have no useful physical interpretation at all. It is simply a mirror image of the (-1)-quantum coherence. The $(+1)$-quantum coherence always accompanies the (-1)-quantum coherence, but carries no extra information. It is best to forget about it and concentrate on the (-1)-quantum coherence.[7]

11.3 Thermal Equilibrium

The density operator allows the state of the entire spin-1/2 ensemble to be specified using four numbers – an extraordinary simplification. Nevertheless, the method would not be very useful if there was no way of knowing what these numbers are.

If the state of the spin ensemble is known at one point in time, then it is possible to predict it at later times by applying the Schrödinger equation to each individual spin.

But how can one know the spin density operator at one point in time? The answer is that one can't know for certain, but it is possible to make a good guess. A spin system that has been left undisturbed for a long time, in contact with the molecular surroundings, is expected to reach a state of *thermal equilibrium* with those surroundings. Statistical arguments allow one to guess the values of the populations and the coherences in the thermal equilibrium state. For the numbers of spins involved in NMR, this guess is essentially foolproof.

Consider a general spin system with a set of energy eigenstates $|r\rangle$ with corresponding energies ω_r:

$$\widehat{\mathcal{H}}|r\rangle = \omega_r|r\rangle$$

Quantum statistical mechanics states that in thermal equilibrium at temperature T, the following properties hold:

1. The coherences between the states are all zero:

$$\rho_{rs}^{\mathrm{eq}} = 0 \qquad (\text{for } r \neq s) \tag{11.14}$$

2. The populations of the energy states obey the *Boltzmann distribution*:

$$\rho_{rr}^{\mathrm{eq}} = \frac{\exp\{-\hbar\omega_r/k_{\mathrm{B}}T\}}{\sum_s \exp\{-\hbar\omega_s/k_{\mathrm{B}}T\}} \tag{11.15}$$

where $k_{\mathrm{B}} = 1.38066 \times 10^{-23}\,\mathrm{J\,K^{-1}}$ is the *Boltzmann constant*, and the sum is over all eigenstates.

The Boltzmann distribution causes the lower energy eigenstates to be more populated than the higher energy eigenstates:

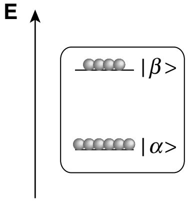

Figure 11.8
Boltzmann distribution of populations for spins with positive γ.

The difference in the population of two states at thermal equilibrium depends on their energy difference, compared with the available thermal energy at the temperature of the sample. At room temperature, the available thermal energy is $k_{\mathrm{B}}T \cong 4.1 \times 10^{-21}\,\mathrm{J}$.

For the case of the spin-1/2 ensemble, the energies of the states are

$$\omega_{\boxed{\alpha}} = \frac{1}{2}\omega^0 \qquad \omega_{\boxed{\beta}} = -\frac{1}{2}\omega^0$$

where $\omega^0 = -\gamma B^0$. The energy difference between the Zeeman states, for the case of protons in a field of 11.74 T, is $|\hbar\omega^0| \cong 3.3 \times 10^{-25}\,\mathrm{J}$.

Since the difference in energy between the Zeeman eigenstates is four orders of magnitude smaller than the available thermal energy, the thermal equilibrium population difference between the states is very small. It is possible to simplify Equation 11.15 by using some approximations.

Define the *Boltzmann factor* $\mathbb{B}$ through the following:

$$\mathbb{B} = \frac{\hbar\gamma B^0}{k_{\mathrm{B}}T} \tag{11.16}$$

The exponential factors in Equation 11.15 may be written as follows:

$$\exp\{-\frac{\hbar\omega_{\boxed{\alpha}}}{k_{\mathrm{B}}T}\} = \exp\{\frac{1}{2}\mathbb{B}\} \qquad \exp\{-\frac{\hbar\omega_{\boxed{\beta}}}{k_{\mathrm{B}}T}\} = \exp\{-\frac{1}{2}\mathbb{B}\}$$

In practice, $\mathbb{B}$ is a very small number. Therefore, it is possible to expand the exponentials as a power series and take only the first term:

$$\exp\{-\frac{\hbar\omega_{\boxed{\alpha}}}{k_{\rm B}T}\} \cong 1+\frac{1}{2}\mathbb{B} \qquad \exp\{-\frac{\hbar\omega_{\boxed{\beta}}}{k_{\rm B}T}\} \cong 1-\frac{1}{2}\mathbb{B}$$

The denominator of Equation 11.15 is given by

$$\exp\{-\hbar\omega_{\boxed{\alpha}}/k_BT\} + \exp\{-\hbar\omega_{\boxed{\beta}}/k_BT\} \cong 2$$

The thermal equilibrium populations of the two states are therefore:

$$\begin{aligned}\rho^{\rm eq}_{\boxed{\alpha}} &\cong \frac{1}{2}(1+\frac{1}{2}\mathbb{B}) = \frac{1}{2}+\frac{1}{4}\mathbb{B}\\ \rho^{\rm eq}_{\boxed{\beta}} &\cong \frac{1}{2}(1-\frac{1}{2}\mathbb{B}) = \frac{1}{2}-\frac{1}{4}\mathbb{B}\end{aligned}$$

The above approximation is called the *high-temperature approximation*. This is a bit misleading, because it applies very well for any temperature warmer than a fraction of a degree kelvin.

For positive γ, the low-energy $|\alpha\rangle$ state is populated slightly more than the high-energy $|\beta\rangle$ state. The population difference is exceedingly small at ordinary temperatures and fields, only about 1 part in 10^5.

Physically, this means that, in thermal equilibrium, there is only a very slight polarization of the spin angular momentum vectors along the direction of the external magnetic field.

The *thermal equilibrium density matrix* for isolated spins-1/2 is therefore approximately given by

$$\hat{\rho}^{\rm eq} = \begin{pmatrix} \frac{1}{2}+\frac{1}{4}\mathbb{B} & 0 \\ 0 & \frac{1}{2}-\frac{1}{4}\mathbb{B}\end{pmatrix} \tag{11.17}$$

In terms of angular momentum operators, this corresponds to:

$$\hat{\rho}^{\rm eq} = \frac{1}{2}\widehat{1} + \frac{1}{2}\mathbb{B}\hat{I}_z \tag{11.18}$$

This *thermal equilibrium density operator* forms the starting point for subsequent calculations.

11.4 Rotating-Frame Density Operator

We need the response of the spin ensemble to r.f. pulses. As discussed in Section 10.6, the calculation is best done by using the rotating frame. It is necessary, therefore, to transform the spin density operator into the rotating frame.

As shown in Section 10.6, the rotating-frame spin states are related to the fixed-frame states through the transformation

$$|\widetilde{\psi}\rangle = \widehat{R}_z(-\Phi(t))|\psi\rangle \tag{11.19}$$

where

$$\Phi(t) = \omega_{\rm ref}t + \phi_{\rm ref}$$

and $\omega_{\rm ref}$ is the reference frequency of the spectrometer, equal to the frequency of the rotating frame. The operator $\widehat{R}_z(-\Phi)$ generates a rotation around the z-axis, through the angle $-\Phi$.

The *rotating-frame spin density operator* is defined through

$$\boxed{\hat{\tilde{\rho}} = \overline{|\tilde{\psi}\rangle\langle\tilde{\psi}|} \qquad (11.20)}$$

and is related to the fixed-frame density operator by:

$$\hat{\tilde{\rho}} = \widehat{R}_z(-\Phi(t))\hat{\rho}\widehat{R}_z(+\Phi(t))$$

The matrix representations of the rotation operators (Appendix A.4) may be used to make the following correspondences between the rotating-frame and fixed-frame populations and coherences:

$$\begin{aligned} \tilde{\rho}_{\boxed{\alpha}} &= \rho_{\boxed{\alpha}} & \tilde{\rho}_{\boxed{\beta}} &= \rho_{\boxed{\beta}} \\ \tilde{\rho}_{\boxed{-}} &= \rho_{\boxed{-}} \exp\{-\mathrm{i}\Phi(t)\} & \tilde{\rho}_{\boxed{+}} &= \rho_{\boxed{+}} \exp\{+\mathrm{i}\Phi(t)\} \end{aligned} \qquad (11.21)$$

The rotating-frame and fixed-frame populations are equal, and the rotating-frame and fixed-frame coherences are related by a time-dependent phase factor.

The thermal equilibrium density operator contains only populations, and is the same in both frames:

$$\hat{\tilde{\rho}}^{\mathrm{eq}} = \hat{\rho}^{\mathrm{eq}}$$

From Equation 11.18, the thermal equilibrium density operator in the rotating frame is given by

$$\boxed{\hat{\tilde{\rho}}^{\mathrm{eq}} = \frac{1}{2}\widehat{1} + \frac{1}{2}\mathbb{B}\hat{I}_z \qquad (11.22)}$$

Since the description of r.f. pulses is much easier in the rotating frame, we will use the rotating frame consistently from now on.[8] *The tilde symbol is dropped*.

11.5 Magnetization Vector

In Chapter 10, the state of a single spin-1/2 was represented by an arrow, indicating the direction of well-defined spin angular momentum. The response of the spin to magnetic fields could be depicted by rotating this arrow around different axes in three-dimensional space.

A similar construction is possible for the *ensemble* of isolated spins-1/2. The spin density operator may be represented as a *magnetization vector* **M**, indicating the magnitude and direction of the net magnetization:

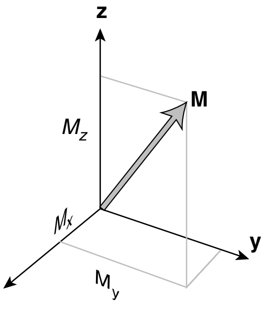

Figure 11.9
The magnetization vector.

The dynamics of the spin-1/2 ensemble correspond to the motion of the magnetization vector in three-dimensional space.

The magnetization vector has three Cartesian components:

$$\mathbf{M} = M_x \mathbf{e}'_x + M_y \mathbf{e}'_y + M_z \mathbf{e}'_z$$

The longitudinal component M_z is related to the *population difference* between the states:

$$\boxed{M_z = 2\mathbb{B}^{-1}(\rho_{\boxed{\alpha}} - \rho_{\boxed{\beta}}) \qquad (11.23)}$$

The transverse components M_x and M_y are related to the (-1)-quantum coherence between the states:

$$\begin{aligned} M_x &= 4\mathbb{B}^{-1}\,\mathrm{Re}\{\rho_{\boxed{-}}\} \\ M_y &= 4\mathbb{B}^{-1}\,\mathrm{Im}\{\rho_{\boxed{-}}\} \end{aligned} \tag{11.24}$$

The numerical factors in Equations 11.23 and 11.24 are chosen so that the thermal equilibrium magnetization vector is equal to a unit vector along the z-axis:

$$\boxed{\mathbf{M}^{\mathrm{eq}} = \mathbf{e}'_z \qquad (11.25)}$$

With these definitions, the spin density operator may always be written as

$$\begin{aligned} \hat{\rho} &= \frac{1}{2}\widehat{1} + \frac{1}{2}\mathbb{B}\mathbf{M}\cdot\hat{\mathbf{I}} \\ &= \frac{1}{2}\widehat{1} + \frac{1}{2}\mathbb{B}\left(M_x\hat{I}_x + M_y\hat{I}_y + M_z\hat{I}_z\right) \end{aligned} \tag{11.26}$$

The populations and coherences may be derived from the magnetization vector by using the definitions in Equations 11.23 and 11.24:

$$\begin{aligned} \rho_{\boxed{\alpha}} &= \frac{1}{2} + \frac{1}{4}\mathbb{B}M_z & \rho_{\boxed{\beta}} &= \frac{1}{2} - \frac{1}{4}\mathbb{B}M_z \\ \rho_{\boxed{+}} &= \frac{1}{4}\mathbb{B}(M_x - \mathrm{i}M_y) & \rho_{\boxed{-}} &= \frac{1}{4}\mathbb{B}(M_x + \mathrm{i}M_y) \end{aligned}$$

Note the direct relationship between the phase of the (-1)-quantum coherence and the transverse magnetization, as described in Section 11.2.7.

11.6 Strong Radio-Frequency Pulse

We are now ready to calculate the effect of a strong r.f. pulse on the spin-1/2 ensemble.

Consider a strong rectangular r.f. pulse of general phase ϕ_{p} and flip angle β_{p}, as described in Section 10.8:

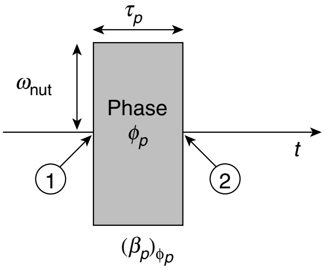

Figure 11.10
An r.f. pulse.

The flip angle of the pulse β_{p} is given by $\beta_{\text{p}} = \omega_{\text{nut}}\tau_{\text{p}}$, where the nutation frequency ω_{nut} is a measure of the amplitude of the r.f. field and τ_{p} is the pulse duration. The time points ① and ② define the start and end of the pulse. The pulse is assumed to be strong enough that the off-resonance effects described in Section 10.8.5 may be ignored.[9]

For each spin in the ensemble, the rotating-frame state after the pulse is related to the rotating-frame state before the pulse through the following:

$$|\psi\rangle_{②} = \widehat{R}_{\phi_{\text{p}}}(\beta_{\text{p}})|\psi\rangle_{①}$$

The corresponding equation for the 'bra' states is

$$\langle\psi|_{②} = \langle\psi|_{①}\widehat{R}_{\phi_{\text{p}}}(\beta_{\text{p}})^{\dagger}$$

where the dagger symbol denotes the adjoint. Note that the adjoint reverses the order, as described in Section 6.2.6.

Since the rotation operators are unitary (see Section 7.6.2), this may be written as

$$\langle\psi|_{②} = \langle\psi|_{①}\widehat{R}_{\phi_{\text{p}}}(-\beta_{\text{p}})$$

The spin density operator after the pulse is therefore given by

$$\hat{\rho}_{②} = \overline{|\psi\rangle_{②}\langle\psi|_{②}} = \overline{\widehat{R}_{\phi_{\text{p}}}(\beta_{\text{p}})|\psi\rangle_{①}\langle\psi|_{①}\widehat{R}_{\phi_{\text{p}}}(-\beta_{\text{p}})}$$

The overbar in this equation means an average over all spins in the ensemble.

Now assume that all spins in the ensemble experience the same magnetic field. The ensemble average may be restricted to the central part of this expression, giving

$$\hat{\rho}_{②} = \widehat{R}_{\phi_{\text{p}}}(\beta_{\text{p}})\overline{|\psi\rangle_{①}\langle\psi|_{①}}\widehat{R}_{\phi_{\text{p}}}(-\beta_{\text{p}})$$

which is equal to

$$\boxed{\hat{\rho}_{②} = \widehat{R}_{\phi_{\text{p}}}(\beta_{\text{p}})\hat{\rho}_{①}\widehat{R}_{\phi_{\text{p}}}(-\beta_{\text{p}}) \qquad (11.27)}$$

The pulse 'sandwiches' the density operator with two opposite rotation operators.

11.6.1 Excitation of coherence

We now use the sandwich equation to calculate the effect of a strong $(\pi/2)_x$ pulse on an ensemble of non-interacting spins-1/2 in a state of thermal equilibrium.

Before the pulse, the spin density operator is

$$\hat{\rho}_{①} = \hat{\rho}^{\text{eq}} = \frac{1}{2}\widehat{1} + \frac{1}{2}\mathbb{B}\hat{I}_z$$

There are no coherences, and the populations are governed by the Boltzmann distribution, in the high-temperature limit.

After the pulse, the spin density operator is

$$\begin{aligned}\hat{\rho}_{\textcircled{2}} &= \widehat{R}_x(\pi/2)\hat{\rho}_{\textcircled{1}}\,\widehat{R}_x(-\pi/2) = \frac{1}{2}\widehat{R}_x(\pi/2)\widehat{1}\widehat{R}_x(-\pi/2) + \frac{1}{2}\mathbb{B}\,\widehat{R}_x(\pi/2)\hat{I}_z\widehat{R}_x(-\pi/2)\\ &= \frac{1}{2}\widehat{1} + \frac{1}{2}\mathbb{B}\,\widehat{R}_x(\pi/2)\hat{I}_z\widehat{R}_x(-\pi/2)\end{aligned}$$

since the unity operator $\widehat{1}$ commutes with all other operators.

The last term on the right-hand side may be calculated using the sandwich relationships given in Section 6.6.2:

$$\widehat{R}_x(\pi/2)\hat{I}_z\widehat{R}_x(-\pi/2) = -\hat{I}_y$$

The result is

$$\hat{\rho}_{\textcircled{2}} = \frac{1}{2}\widehat{1} - \frac{1}{2}\mathbb{B}\hat{I}_y$$

If written in terms of the magnetization vector, this transformation is very simple:

$$\begin{tikzcd}\mathbf{M}_{\textcircled{1}} = \mathbf{e}_z \arrow[d, "(\pi/2)_x"] \\ \mathbf{M}_{\textcircled{2}} = -\mathbf{e}_y\end{tikzcd}$$

The $(\pi/2)_x$ pulse rotates the magnetization vector from the z-axis to the $-y$-axis:

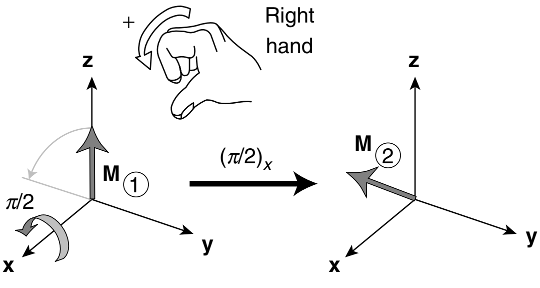

Figure 11.11
A $(\pi/2)_x$ pulse acting on a magnetization vector along the z-axis.

What happens to the populations and the coherences? In terms of the matrix representations, the action of the pulse is as follows:

$$\hat{\rho}_{\textcircled{1}} = \begin{pmatrix}\frac{1}{2}+\frac{1}{4}\mathbb{B} & 0\\ 0 & \frac{1}{2}-\frac{1}{4}\mathbb{B}\end{pmatrix} \xrightarrow{(\pi/2)_x} \hat{\rho}_{\textcircled{2}} = \begin{pmatrix}\frac{1}{2} & -\frac{1}{4\mathrm{i}}\mathbb{B}\\ \frac{1}{4\mathrm{i}}\mathbb{B} & \frac{1}{2}\end{pmatrix}$$

The pulse, therefore, accomplishes two tasks:

1. The pulse *equalizes the populations* of the two states.
2. The pulse converts the *population difference* into *coherences*.

This process may be depicted as follows:

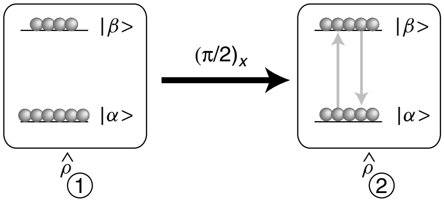

Figure 11.12
Excitation of coherence by a $(\pi/2)_x$ pulse.

11.6.2 Population inversion

Now calculate the action of a π_x pulse on the thermal equilibrium state. The calculation goes as follows:

$$\begin{aligned}\hat{\rho}_{②} &= \widehat{R}_x(\pi)\hat{\rho}_{①}\,\widehat{R}_x(-\pi) = \frac{1}{2}\widehat{1} + \frac{1}{2}\mathbb{B}\widehat{R}_x(\pi)\hat{I}_z\widehat{R}_x(-\pi) \\ &= \frac{1}{2}\widehat{1} - \frac{1}{2}\mathbb{B}\hat{I}_z\end{aligned}$$

In terms of the magnetization vector, this transformation may be written as

$$\begin{tikzcd} \mathbf{M}_{①} = \mathbf{e}_z \arrow[d, "\pi_x"] \\ \mathbf{M}_{②} = -\mathbf{e}_z \end{tikzcd}$$

The π_x pulse accomplishes an *inversion* of the magnetization vector:

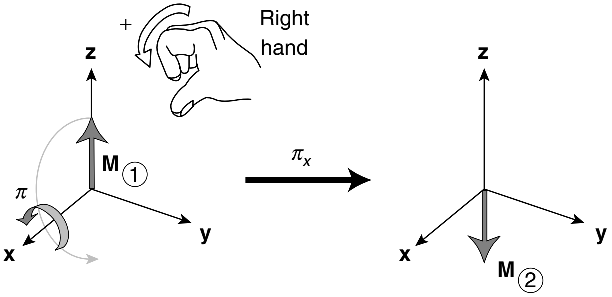

Figure 11.13
A π_x pulse acting on a magnetization vector along the z-axis.

In terms of the populations and coherences, the transformation reads as follows:

$$\hat{\rho}_{①} = \begin{pmatrix} \frac{1}{2} + \frac{1}{4}\mathbb{B} & 0 \\ 0 & \frac{1}{2} - \frac{1}{4}\mathbb{B} \end{pmatrix} \xrightarrow{\pi_x} \hat{\rho}_{②} = \begin{pmatrix} \frac{1}{2} - \frac{1}{4}\mathbb{B} & 0 \\ 0 & \frac{1}{2} + \frac{1}{4}\mathbb{B} \end{pmatrix}$$

The π_x pulse exchanges the populations of the two states, generating an *inverted population distribution*, in which the higher-energy state is more populated than the lower-energy state:

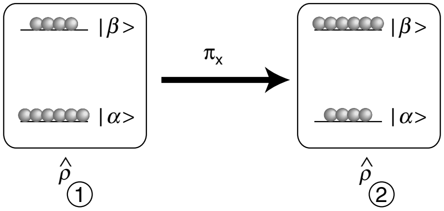

Figure 11.14
Population inversion by a π_x pulse.

11.6.3 Cycle of states

A π_x pulse is the same as two consecutive $(\pi/2)_x$ pulses. The calculations given above are readily continued for any number of consecutive $(\pi/2)_x$ pulses. Each $\pi/2$ pulse steps the spin system through the following cycle:

$$\begin{tikzcd}
\frac{1}{2}\hat{1} + \frac{1}{2}\mathbb{B}\hat{I}_z \arrow[r, "(\pi/2)_x"] & \frac{1}{2}\hat{1} - \frac{1}{2}\mathbb{B}\hat{I}_y \arrow[d, "(\pi/2)_x"] \\
\frac{1}{2}\hat{1} + \frac{1}{2}\mathbb{B}\hat{I}_y \arrow[u, "(\pi/2)_x"] & \frac{1}{2}\hat{1} - \frac{1}{2}\mathbb{B}\hat{I}_z \arrow[l, "(\pi/2)_x"']
\end{tikzcd}$$

In terms of the magnetization vector **M**, the cycle of states reads:

$$\begin{tikzcd}
+\mathbf{e}_z \arrow[r, "(\pi/2)_x"] & -\mathbf{e}_y \arrow[d, "(\pi/2)_x"] \\
+\mathbf{e}_y \arrow[u, "(\pi/2)_x"] & -\mathbf{e}_z \arrow[l, "(\pi/2)_x"']
\end{tikzcd}$$

Figure 11.15 shows the cycle of states using icons to represent the populations and coherences.

The first pulse equalizes the populations and generates coherences. The second pulse converts the coherences back into populations, generating an inverted population distribution. The third pulse equalizes the populations again and generates coherences once more (the 'icon' for the fourth state looks the same as that for the second state, but this is misleading, since the coherence *phases* are not shown). The fourth pulse destroys the coherences again and returns the system to equilibrium. The cycle may be continued with a fifth $(\pi/2)_x$ pulse, generating coherences again, and so on.

In principle, this cycle may be continued indefinitely. In practice, instrumental imperfections and relaxation cause losses. The spin system is not completely restored to equilibrium after every fourth $(\pi/2)_x$ pulse. Nevertheless, fairly accurate completion of four or five cycles is usually feasible in practice.

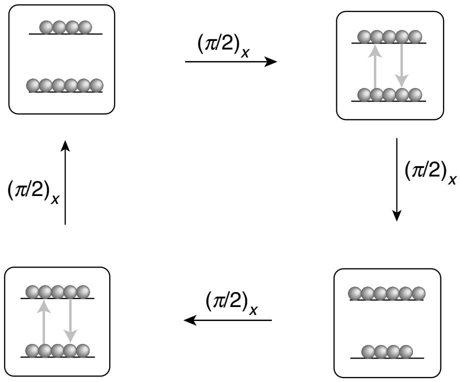

Figure 11.15
Cycle of states.

11.6.4 Stimulated absorption and emission

It is interesting to reflect on the excursions of the *energy* of the spin system during this cycle. In the initial state of thermal equilibrium, the energy of the spin system is low, since the low-energy state is more populated than the high-energy state. The first $(\pi/2)_x$ pulse raises the energy of the spin system, since the populations are equalized. The second $(\pi/2)_x$ pulse raises the energy still more, generating an inverted population distribution. The effect of the first two $(\pi/2)_x$ pulses is therefore to *raise* the energy of the spin system. The energy contained in the r.f. pulses is *absorbed* by the nuclear spins. This process corresponds to the *stimulated absorption* process in optical spectroscopy:

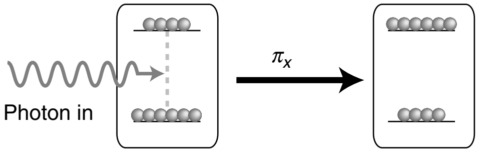

Figure 11.16
Stimulated absorption.

The behaviour of the energy during the next two $\pi/2$ pulses is more surprising. The third $\pi/2$ pulse equalizes the populations again, thereby *decreasing* the energy of the spin system. The fourth $\pi/2$ pulse decreases the energy of the spin system still more, thus regenerating the low-energy initial state.

At first sight, it is puzzling that the energetic r.f. pulses *decrease* the energy of the spin system. In fact, this phenomenon corresponds to *stimulated emission* in optical spectroscopy. If a system is not in equilibrium, then arrival of a photon may stimulate the emisson of a second photon by the spin system. The net effect is a release of energy by the molecular system back into the electromagnetic field:

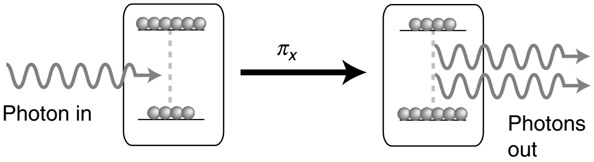

Figure 11.17
Stimulated emission.

Stimulated emission is the basis of the *laser*.

11.7 Free Precession Without Relaxation

Now consider the evolution of the density operator in the intervals between r.f. pulses. For example, suppose that, at the end of the pulse (time point $t_{\textcircled{2}}$), the r.f. field is turned off and an interval τ is allowed to elapse:

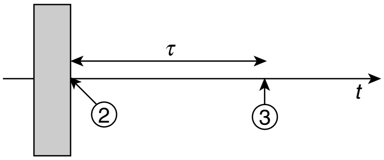

Figure 11.18 R.f. pulse and subsequent interval.

What is the spin density operator at time point $t_{\textcircled{3}} = t_{\textcircled{2}} + \tau$?

For the moment, ignore relaxation during the interval τ.

As described in Section 10.7, the rotating-frame state of a single spin evolves in the absence of r.f. fields according to

$$|\psi\rangle_{\textcircled{3}} = \widehat{R}_z(\Omega^0\tau)|\psi\rangle_{\textcircled{2}}$$

where Ω^0 is the resonance offset. The arguments given above may be repeated to obtain the following equation for the evolution of the spin density operator over an interval of free precession τ:

$$\boxed{\hat{\rho}_{\textcircled{3}} = \widehat{R}_z(\Omega^0\tau)\,\hat{\rho}_{\textcircled{2}}\,\widehat{R}_z(-\Omega^0\tau) \qquad \text{(ignoring relaxation)} \qquad (11.28)}$$

This shows that the spin density operator gets sandwiched by two rotation operators around the z-axis, under an interval of free precession.

What does this mean for the populations and coherences?

If the matrix representations are multiplied out, we get the following equations for the populations:

$$\boxed{\begin{aligned} \rho_{\boxed{\alpha}}\textcircled{3} &= \rho_{\boxed{\alpha}}\textcircled{2} \\ \rho_{\boxed{\beta}}\textcircled{3} &= \rho_{\boxed{\beta}}\textcircled{2} \qquad \text{(ignoring relaxation)} \qquad (11.29) \end{aligned}}$$

If relaxation is neglected, then *the populations of the states are constant during the intervals between r.f. pulses.*

For the (−1)-quantum coherence, we get

$$\boxed{\rho_{\boxed{-}}\textcircled{3} = \exp\{+\mathrm{i}\Omega^0\tau\}\rho_{\boxed{-}}\textcircled{2} \qquad \text{(ignoring relaxation)} \qquad (11.30)}$$

Between the pulses, the (−1)-quantum coherence revolves in the complex plane at the resonance offset frequency Ω^0:

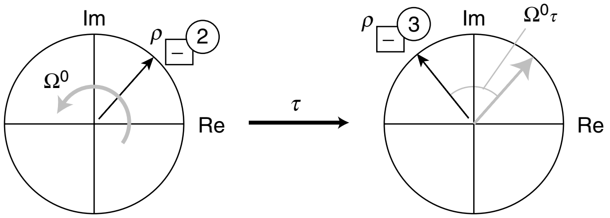

Figure 11.19
Precession of (−1)-quantum coherence.

The corresponding equation for the (+1)-quantum coherence is

$$\rho_{\boxed{+}}\text{③} = \exp\{-\mathrm{i}\Omega^0\tau\}\rho_{\boxed{+}}\text{②} \qquad \text{(ignoring relaxation)}$$

which shows that the (+1)-quantum coherence rotates in the opposite sense at the same frequency.

The free precession equations may also be written in terms of the magnetization vector. The magnetization vectors at the two time points are related by

$$\boxed{\begin{aligned} M_x\text{③} &= M_x\text{②}\cos\Omega^0 t - M_y\text{②}\sin\Omega^0 t \\ M_y\text{③} &= M_x\text{②}\sin\Omega^0 t + M_y\text{②}\cos\Omega^0 t \\ M_z\text{③} &= M_z\text{②} \\ &\qquad\qquad \text{(ignoring relaxation)} \qquad\qquad (11.31) \end{aligned}}$$

which represents a rotation of the magnetization vector around the z-axis at the frequency Ω^0:

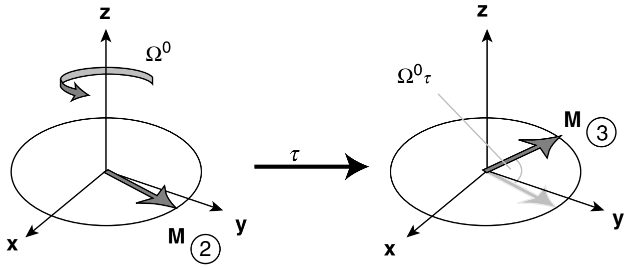

Figure 11.20
Precession of the magnetization vector.

For example, consider a $(\pi/2)_x$ pulse applied to a spin ensemble in thermal equilibrium, followed by an interval τ of free precession:

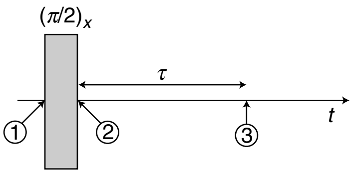

Figure 11.21
$(\pi/2)_x$ pulse, followed by a free precession interval.

The transformations of the spin density operator may be written as follows:

$$\begin{tikzcd}
\hat{\rho}_{\text{①}} = \hat{\rho}^{\mathrm{eq}} = \tfrac{1}{2}\hat{1} + \tfrac{1}{2}\mathbb{B}\hat{I}_z \arrow[d, "(\pi/2)_x"] \\
\hat{\rho}_{\text{②}} = \tfrac{1}{2}\hat{1} - \tfrac{1}{2}\mathbb{B}\hat{I}_y \arrow[d, "\tau"] \\
\hat{\rho}_{\text{③}} = \tfrac{1}{2}\hat{1} + \tfrac{1}{2}\mathbb{B}\left(-\hat{I}_y \cos\Omega^0\tau + \hat{I}_x \sin\Omega^0\tau\right)
\end{tikzcd} \tag{11.32}$$

For the magnetization vector, this reads as

$$\begin{tikzcd}
\mathbf{M}_{\text{①}} = \mathbf{e}_z \arrow[d, "(\pi/2)_x"] \\
\mathbf{M}_{\text{②}} = -\mathbf{e}_y \arrow[d, "\tau"] \\
\mathbf{M}_{\text{③}} = \left(-\mathbf{e}_y \cos\Omega^0\tau + \mathbf{e}_x \sin\Omega^0\tau\right)
\end{tikzcd}$$

which may be depicted graphically as follows:

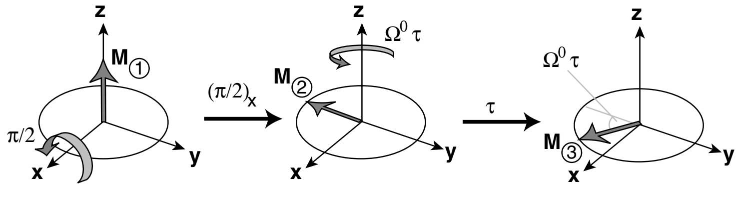

Figure 11.22
Motion of the magnetization vector during a pulse and the following interval.

If the equations in Equation 11.32 are compared, one may say loosely that the operator $\hat{I}_z$ is 'transformed' into $-\hat{I}_y$ by the $(\pi/2)_x$ pulse, and that the operator $-\hat{I}_y$ is 'transformed' into $-\hat{I}_y \cos\Omega^0\tau + \hat{I}_x \sin\Omega^0\tau$ by the interval of free precession. This is a convenient way of speaking, but should not be taken too literally. The operators themselves are not changed, of course. It is the state of the spin ensemble that changes – and this motion corresponds to the *substitution* of one angular momentum operator by another.

11.8 Operator Transformations

For convenience, the 'transformations' of the angular momentum operators under commonly-encountered pulses and precession intervals are now summarized. To calculate the effect of a pulse, or a precession interval, the angular momentum operators are substituted according to the rules given below.

11.8.1 Pulse of phase $\phi_\mathrm{p} = 0$

The effect of a pulse $\left(\beta_\mathrm{p}\right)_x$ with flip angle β_p and phase $\phi_\mathrm{p} = 0$ may be calculated by the following operator substitutions:

pulse phase
$\phi_\mathrm{p} = 0$
'x-pulse'

$$\begin{cases} \hat{I}_x \rightarrow \hat{I}_x \\ \hat{I}_y \rightarrow \hat{I}_y \cos\beta_\mathrm{p} + \hat{I}_z \sin\beta_\mathrm{p} \\ \hat{I}_z \rightarrow \hat{I}_z \cos\beta_\mathrm{p} - \hat{I}_y \sin\beta_\mathrm{p} \end{cases} \tag{11.33}$$

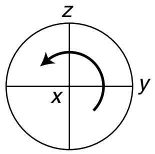

11.8.2 Pulse of phase $\phi_\mathrm{p} = \pi/2$

The effect of a pulse $\left(\beta_\mathrm{p}\right)_y$ with flip angle β_p and phase $\phi_\mathrm{p} = \pi/2$ may be calculated by the following operator substitutions:

pulse phase
$\phi_\mathrm{p} = \pi/2$
'y-pulse'

$$\begin{cases} \hat{I}_x \rightarrow \hat{I}_x \cos\beta_\mathrm{p} - \hat{I}_z \sin\beta_\mathrm{p} \\ \hat{I}_y \rightarrow \hat{I}_y \\ \hat{I}_z \rightarrow \hat{I}_z \cos\beta_\mathrm{p} + \hat{I}_x \sin\beta_\mathrm{p} \end{cases} \tag{11.34}$$

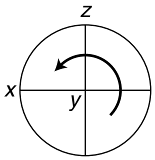

11.8.3 Pulse of phase $\phi_\mathrm{p} = \pi$

The effect of a pulse $\left(\beta_\mathrm{p}\right)_{\bar{x}}$ with flip angle β_p and phase $\phi_\mathrm{p} = \pi$ may be calculated by the following substitutions:

pulse phase
$\phi_\mathrm{p} = \pi$
'$\bar{x}$-pulse'

$$\begin{cases} \hat{I}_x \rightarrow \hat{I}_x \\ \hat{I}_y \rightarrow \hat{I}_y \cos\beta_\mathrm{p} - \hat{I}_z \sin\beta_\mathrm{p} \\ \hat{I}_z \rightarrow \hat{I}_z \cos\beta_\mathrm{p} + \hat{I}_x \sin\beta_\mathrm{p} \end{cases} \tag{11.35}$$

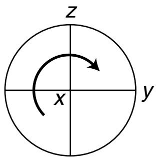

11.8.4 Pulse of phase $\phi_\mathrm{p} = 3\pi/2$

The effect of a pulse $\left(\beta_p\right)_{\bar{y}}$ with flip angle β_p and phase $\phi_\mathrm{p} = 3\pi/2$ may be calculated by the following substitutions:

pulse phase
$\phi_\mathrm{p} = 3\pi/2$
"$\bar{y}$-pulse"

$$\begin{cases} \hat{I}_x \rightarrow \hat{I}_x \cos\beta_\mathrm{p} + \hat{I}_z \sin\beta_\mathrm{p} \\ \hat{I}_y \rightarrow \hat{I}_y \\ \hat{I}_z \rightarrow \hat{I}_z \cos\beta_\mathrm{p} - \hat{I}_x \sin\beta_\mathrm{p} \end{cases} \tag{11.36}$$

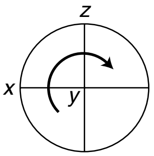

11.8.5 Pulse of general phase ϕ_p

From Equation 10.32, the effect of a pulse $\left(\beta_p\right)_{\phi_p}$ with flip angle β_p and general phase ϕ_p may be deduced by executing the following sequence of *three* transformations:

$$\xrightarrow{\widehat{R}_z(-\phi_\mathrm{p})} \quad \xrightarrow{\widehat{R}_x(\beta_\mathrm{p})} \quad \xrightarrow{\widehat{R}_z(\phi_\mathrm{p})}$$

where the z-rotations transform the spin operators as follows:

z-rotation
through
the angle ϕ_p

$$\begin{cases} \hat{I}_x \rightarrow \hat{I}_x \cos\phi_\mathrm{p} + \hat{I}_y \sin\phi_\mathrm{p} \\ \hat{I}_y \rightarrow \hat{I}_y \cos\phi_\mathrm{p} - \hat{I}_x \sin\phi_\mathrm{p} \\ \hat{I}_z \rightarrow \hat{I}_z \end{cases} \tag{11.37}$$

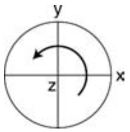

The effect of the central $\widehat{R}_x(\beta_\mathrm{p})$ rotation is given in Equation 11.33.

11.8.6 Free precession for an interval τ

The effect of free precession for an interval τ may be calculated as follows:

free precession
(no relaxation)

$$\begin{cases} \hat{I}_x \rightarrow \hat{I}_x \cos\Omega^0\tau + \hat{I}_y \sin\Omega^0\tau \\ \hat{I}_y \rightarrow \hat{I}_y \cos\Omega^0\tau - \hat{I}_x \sin\Omega^0\tau \\ \hat{I}_z \rightarrow \hat{I}_z \end{cases} \tag{11.38}$$

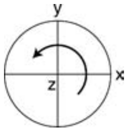

This neglects relaxation during the interval τ.

In all cases, the populations and coherences after a particular transformation may be calculated by writing the spin density operator as a matrix and identifying the appropriate matrix elements. Another method is to convert the angular momentum operators and the unity operator into shift and projection operators using the following relationships:

$$\frac{1}{2}\hat{1} = \frac{1}{2}\hat{I}^\alpha + \frac{1}{2}\hat{I}^\beta \qquad \hat{I}_z = \frac{1}{2}\hat{I}^\alpha - \frac{1}{2}\hat{I}^\beta$$

$$\hat{I}_x = \frac{1}{2}\hat{I}^+ + \frac{1}{2}\hat{I}^- \qquad \hat{I}_y = \frac{1}{2\mathrm{i}}\hat{I}^+ - \frac{1}{2\mathrm{i}}\hat{I}^-$$

The populations and coherences may be identified as the coefficients of the shift and projection operators in the expression for the density operator:

$$\hat{\rho} = \rho_{\boxed{\alpha}}\hat{I}^\alpha + \rho_{\boxed{\beta}}\hat{I}^\beta + \rho_{\boxed{+}}\hat{I}^+ + \rho_{\boxed{-}}\hat{I}^-$$

11.9 Free Evolution with Relaxation

The above equations predict that, in the absence of an r.f. field, the populations do not change, and the coherences oscillate indefinitely at the frequency Ω^0 in the rotating frame.

Experimentally, one observes deviations from this ideal behaviour:

1. The populations are not time independent, but gradually drift towards their thermal equilibrium values.

2. The coherences do not last for ever, but gradually decay to zero.

These deviations are due to *relaxation*. The r.f. pulse causes the state of the spin system to depart from thermal equilibrium. Over a sufficiently long time, the fluctuating molecular surroundings cause the thermal equilibrium state to be gradually re-established.

This process corresponds to the 'wandering' motion of the precessing nuclear spins, introduced in Section 2.6. The fluctuations in the direction of the local magnetic fields, mentioned in that section, are due to the non-secular spin interactions discussed in Section 8.5.2.

In this section, I approach relaxation from a 'phenomenological' point of view, which is a polite way of saying that the equation of motion is simply faked so as to conform to the experimentally observed facts. The theory of relaxation is discussed more fully in Chapter 20.

In the phenomenological approach of Bloch, two relaxation time constants are introduced. The time constant T_1 (the *longitudinal relaxation time constant*, or *spin–lattice relaxation constant*) takes into account the drift of the populations towards their thermal equilibrium values. The time constant T_2 (the *transverse relaxation time constant*, or *spin–spin relaxation constant*) takes into account the decay of the coherences.[10]

11.9.1 Transverse relaxation

In practice, the coherences do not last for ever, but decay to zero. This behaviour is ensured in the equations by introducing an exponential decay term. The phenomenological equation for the rotating-frame coherences between time points ② and ③ is

$$\begin{aligned} \rho_{\boxed{-}}\text{③} &= \rho_{\boxed{-}}\text{②}\ \exp\{\left(\mathrm{i}\Omega^0 - \lambda\right)\tau\} \\ \rho_{\boxed{+}}\text{③} &= \rho_{\boxed{+}}\text{②}\ \exp\{\left(-\mathrm{i}\Omega^0 - \lambda\right)\tau\} \end{aligned} \tag{11.39}$$

where τ is the time interval between the two time points (compare this with Equation 11.30). The damping rate constant λ is given by the inverse of the *transverse relaxation time constant* T_2:

$$\lambda = T_2{}^{-1} \tag{11.40}$$

These equations for the coherences correspond to the following substitution rules for the transverse spin angular momentum operators:

free precession (with relaxation)

$$\begin{cases} \hat{I}_x \rightarrow \left(\hat{I}_x \cos\Omega^0\tau + \hat{I}_y \sin\Omega^0\tau\right) \mathrm{e}^{-\lambda\tau} \\ \hat{I}_y \rightarrow \left(\hat{I}_y \cos\Omega^0\tau - \hat{I}_x \sin\Omega^0\tau\right) \mathrm{e}^{-\lambda\tau} \end{cases} \tag{11.41}$$

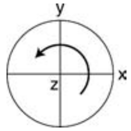

This is an 'improved' version of Equation 11.38.

For the transverse components of the magnetization vector, the appropriate equations are

$$
\begin{aligned}
M_x③ &= \left(M_x② \cos \Omega^0 t - M_y② \sin \Omega^0 t\right) \mathrm{e}^{-\lambda\tau} \\
M_y③ &= \left(M_x② \sin \Omega^0 t + M_y② \cos \Omega^0 t\right) \mathrm{e}^{-\lambda\tau}
\end{aligned}
$$

which improves on Equation 11.31. The basic idea is that the transverse components of the magnetization vector *decay* at the same time as they precess:

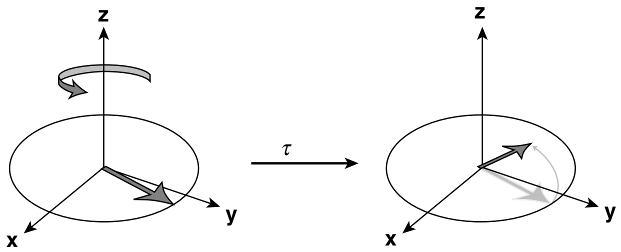

Figure 11.23 Precession of the magnetization vector, accompanied by T_2 decay.

(Note the shrinkage in the magnetization vector.)

Physically, it is easy to see why the coherences decay. Coherence requires a consistent polarization direction of the spin ensemble. Each spin precesses around the *z*-axis according to the strength of the local magnetic field. On the average, all spins experience the same field in a liquid, because of motional averaging, which creates identical conditions for all the spins, *on the average*. However, at any particular instant in time, the fields are slightly different on different spins, which causes a gradual loss of synchronization, like clocks in a clock shop, all started at the same time.

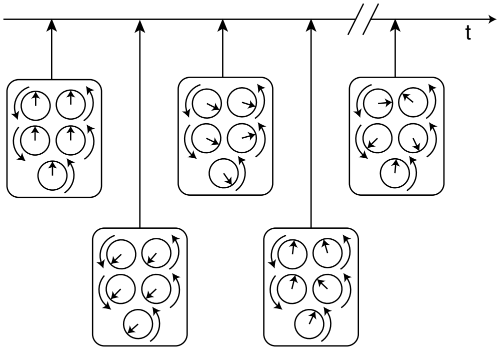

Figure 11.24 Microscopic mechanism of coherence decay.

For nuclear spins, the loss of synchronization can be remarkably slow. In many cases, the spins execute hundreds of millions of precession circuits before losing synchronization.

The decay of coherence does not necessarily involve any exchange of *energy* with the surroundings.[11] Coherence decay does, however, increase the *entropy* of the spin ensemble. The decay of coherence is therefore an *irreversible* process.

11.9.2 Longitudinal relaxation

The equation of motion for the populations is more complicated than for the coherences, in the presence of relaxation. The populations drift back to their thermal equilibrium values, while the coherences decay to zero.

The phenomological equation for the populations is

$$\boxed{\begin{aligned}\rho_{\boxed{\alpha}}\text{③} &= (\rho_{\boxed{\alpha}}\text{②} - \rho_{\boxed{\alpha}}^{\text{eq}})e^{-\tau/T_1} + \rho_{\boxed{\alpha}}^{\text{eq}}\\ \rho_{\boxed{\beta}}\text{③} &= \left(\rho_{\boxed{\beta}}\text{②} - \rho_{\boxed{\beta}}^{\text{eq}}\right)e^{-\tau/T_1} + \rho_{\boxed{\beta}}^{\text{eq}}\end{aligned} \qquad (11.42)}$$

where the thermal equilibrium populations are

$$\rho_{\boxed{\alpha}}^{\text{eq}} = \frac{1}{2} + \frac{1}{4}\mathbb{B} \qquad \rho_{\boxed{\beta}}^{\text{eq}} = \frac{1}{2} - \frac{1}{4}\mathbb{B}$$

The time-constant T_1 is the *longitudinal* or *spin–lattice relaxation time*, and is typically in the range 100 ms–100 s. In exceptional cases, T_1 may be as long as hours or even months.

When the interval τ is equal to zero, Equation 11.42 gives the result $\rho_{\boxed{\alpha}}\text{③} = \rho_{\boxed{\alpha}}\text{②}$, as it should. If τ is large, on the other hand, the population becomes equal to its thermal equilibrium value, $\rho_{\boxed{\alpha}}\text{③} = \rho_{\boxed{\alpha}}^{\text{eq}}$. A similar property holds for the population of the $|\beta\rangle$ state.

For example, consider the motion of the populations after a π_x pulse, applied to a spin ensemble in thermal equilibrium. The populations immediately after the pulse are given by

$$\rho_{\boxed{\alpha}}\text{②} = \frac{1}{2} - \frac{1}{4}\mathbb{B} \qquad \rho_{\boxed{\beta}}\text{②} = \frac{1}{2} + \frac{1}{4}\mathbb{B}$$

as described in Section 11.6.2. The equation of motion of the populations after the pulse, as given by Equation 11.42, is therefore

$$\begin{aligned}\rho_{\boxed{\alpha}}\text{③} &= \frac{1}{2} + \frac{1}{4}\mathbb{B}\left(1 - 2e^{-\tau/T_1}\right)\\ \rho_{\boxed{\beta}}\text{③} &= \frac{1}{2} - \frac{1}{4}\mathbb{B}\left(1 - 2e^{-\tau/T_1}\right)\end{aligned}$$

The motion of the populations during and after the pulse is as follows:

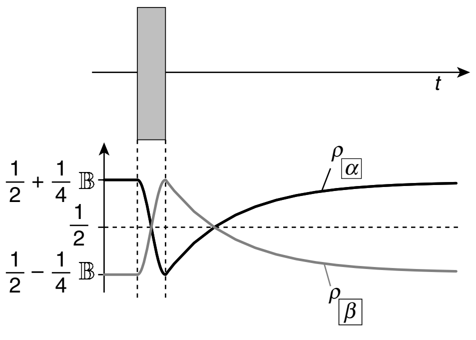

Figure 11.25
Motion of the populations during and after a π_x pulse.

The populations are inverted by the pulse and then slowly relax back to their equilibrium values. (The duration of the pulse is exaggerated for clarity; in practice, the duration of the pulse is around five orders of magnitude shorter than the time constant T_1.)

As a second example, consider a $(\pi/2)_x$ pulse. In this case, the populations are equalized by the pulse

$$\rho_{\boxed{\alpha}}\textcircled{2} = \frac{1}{2} \qquad \rho_{\boxed{\beta}}\textcircled{2} = \frac{1}{2}$$

The equation of motion of the populations after the pulse is as follows:

$$\begin{aligned} \rho_{\boxed{\alpha}}\textcircled{3} &= \frac{1}{2} + \frac{1}{4}\mathbb{B}\left(1 - \mathrm{e}^{-\tau/T_1}\right) \\ \rho_{\boxed{\beta}}\textcircled{3} &= \frac{1}{2} - \frac{1}{4}\mathbb{B}\left(1 - \mathrm{e}^{-\tau/T_1}\right) \end{aligned}$$

which corresponds to the following motion:

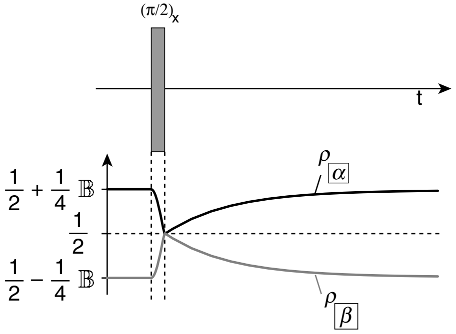

Figure 11.26
Motion of the populations during and after a $(\pi/2)_x$ pulse.

The populations are equalized by the pulse and then drift back to their different equilibrium values.

Longitudinal relaxation involves an exchange of energy between the spin system and the molecular surroundings. The energy transport in a pulse experiment may be depicted as follows:

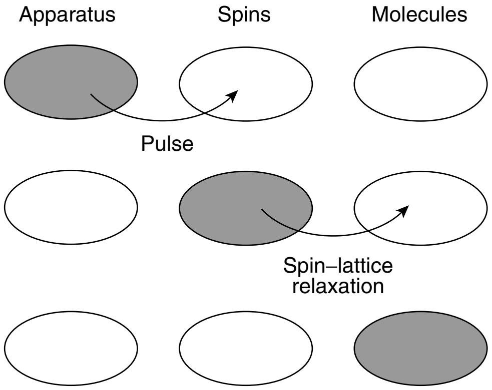

Figure 11.27
Energy transport in a pulsed NMR experiment.

The value of T_1 sets a theoretical upper limit on the possible value of T_2. This is because the fluctuating molecular fields cannot rotate the individual spin polarizations towards the z-axis while maintaining coherence of the transverse spin polarizations in the xy-plane. The following relationship holds absolutely:[12]

$$\boxed{T_2 \leq 2T_1 \qquad \text{(theoretical limit)} \qquad (11.43)}$$

In most cases, however, it is usually found that T_2 is less than, or equal to, T_1:

$$T_2 \leq T_1 \qquad \text{(usual practical limit)} \tag{11.44}$$

The case $2T_1 > T_2 > T_1$ is possible, but is rarely encountered.[13]

It is also possible to visualize longitudinal relaxation in terms of the z-component of the magnetization vector. From Equations 11.23 and 11.42, the motion of the longitudinal component of the magnetization vector is

$$M_z③ = (M_z② - 1)\,\mathrm{e}^{-\tau/T_1} + 1 \tag{11.45}$$

where thermal equilibrium is represented by a unit magnetization vector along the z-axis.

Consider again a π_x pulse. The trajectory of the z-component of the magnetization vector looks as follows:

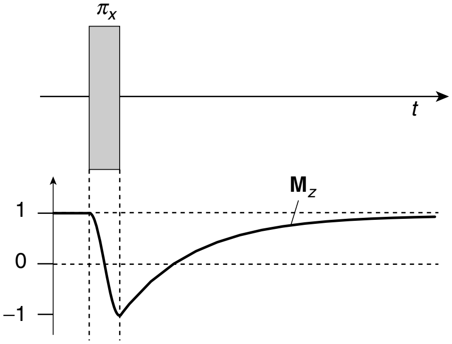

Figure 11.28 Motion of the z-component of the magnetization vector during and after a π_x pulse.

The magnetization vector is inverted and then relaxes back to its initial position.

In the case of a $(\pi/2)_x$ pulse, the z-component of the magnetization vector is destroyed by the pulse and then recovers:

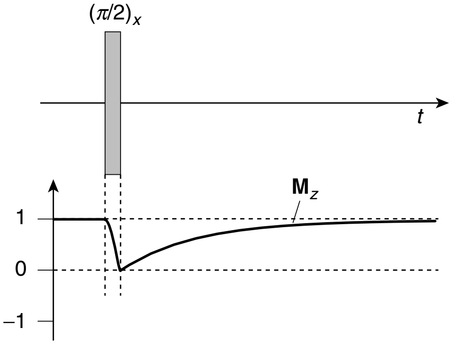

Figure 11.29 Motion of the z-component of the magnetization vector during and after a $(\pi/2)_x$ pulse.

11.10 Magnetization Vector Trajectories

In general, the populations and coherences change at the same time. The magnetization vector tracks out a trajectory in three-dimensional space.

For example, consider a single $(\pi/2)_x$ pulse, applied to a thermal equilibrium system:

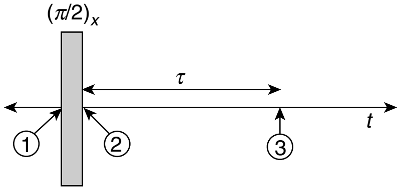

Figure 11.30
A $(\pi/2)_x$ pulse, followed by a free precession interval.

If the results in the previous sections are combined, we get the following evolution of the spin density operator:

$$\hat{\rho}_{①} = \hat{\rho}^{\text{eq}} = \tfrac{1}{2}\widehat{1} + \tfrac{1}{2}\mathbb{B}\hat{I}_z$$

$$\Big\downarrow (\pi/2)_x$$

$$\hat{\rho}_{②} = \tfrac{1}{2}\widehat{1} - \tfrac{1}{2}\mathbb{B}\hat{I}_y$$

$$\Big\downarrow \tau$$

$$\hat{\rho}_{③} = \tfrac{1}{2}\widehat{1} + \tfrac{1}{2}\mathbb{B}\left(1 - \mathrm{e}^{-\tau/T_1}\right)\hat{I}_z + \tfrac{1}{2}\mathbb{B}\left(-\hat{I}_y\cos\Omega^0\tau + \hat{I}_x\sin\Omega^0\tau\right)\mathrm{e}^{-\tau/T_2}$$

This corresponds to the following motion of the magnetization vector in the interval after the pulse:

$$\begin{aligned} M_x(\tau) &= \sin\Omega^0\tau\ \mathrm{e}^{-\tau/T_2} \\ M_y(\tau) &= -\cos\Omega^0\tau\ \mathrm{e}^{-\tau/T_2} \\ M_z(\tau) &= 1 - \mathrm{e}^{-\tau/T_1} \end{aligned}$$

In order to visualize this motion, it is useful to follow the track left by the *tip* of the magnetization vector. The following plots show the track traced out by the tip of the magnetization vector after a $\pi/2$ pulse, for various parameters:

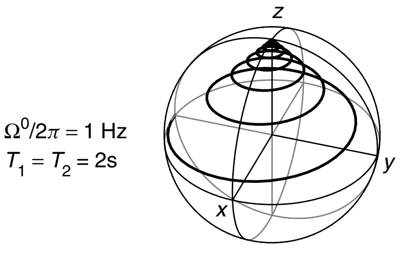

Figure 11.31
The trajectory taken by the tip of the magnetization vector, after a $(\pi/2)_x$ pulse (case 1).

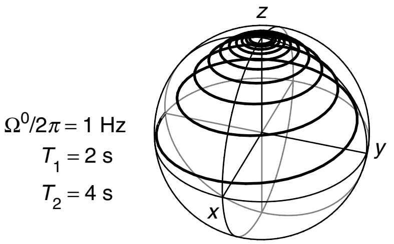

Figure 11.32
The trajectory taken by the tip of the magnetization vector, after a $(\pi/2)_x$ pulse (case 2).

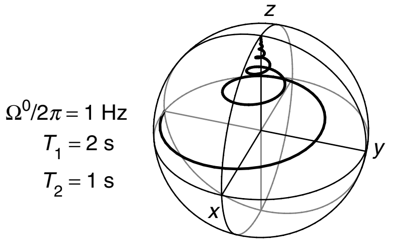

Figure 11.33
The trajectory taken by the tip of the magnetization vector, after a $(\pi/2)_x$ pulse (case 3).

Figure 11.32 corresponds to the rare case[13] in which T_2 is equal to $2T_1$.

Note how the transverse magnetization oscillates and dies out, at the same time as the longitudinal magnetization relaxes back towards the *z*-axis.

11.11 NMR Signal and NMR Spectrum

The precessing transverse nuclear magnetization induces an electric current in the coil surrounding the sample.[11] As discussed in Chapter 4, the current is amplified and subjected to quadrature detection. The two outputs of the quadrature detector are digitized and stored in the computer as a set of complex numbers. The NMR signal is Fourier transformed to obtain the NMR spectrum.

In Appendix A.5, it is shown that the complex NMR signal has the following relationship with the rotating-frame (−1)-quantum coherence:

$$\boxed{s(t) \sim 2\mathrm{i}\rho_{\boxed{-}}(t)\exp\{-\mathrm{i}\phi_{\mathrm{rec}}\} \qquad (11.46)}$$

where ϕ_{rec} is the receiver phase shift, as discussed in Section 4.5.4.

Equation 11.46 states that only the rotating-frame (−1)-quantum coherence is detected in the quadrature receiver.[14] The populations and the (+1)-quantum coherence are both invisible. Only the (−1)-quantum coherence gives rise to an NMR signal, and hence to the peak in the NMR spectrum:

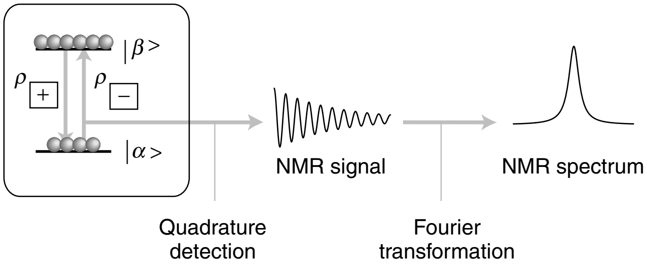

Figure 11.34
The relationship between the (−1)-quantum coherence and the spectral peak.

Let's get more quantitative. Suppose that the r.f. pulse sequence generates a (−1)-quantum coherence with amplitude $\rho_{\boxed{-}}(0)$ at the time point $t = 0$, which is defined as the start of signal acquisition.[15] From Equation 11.39, the amplitude of the coherence at a later time $t \geq 0$ is given by

$$\rho_{\boxed{-}}(t) = \rho_{\boxed{-}}(0)\exp\{\big(\mathrm{i}\Omega^0 - \lambda)t\big)\}$$

where $\lambda = T_2{}^{-1}$. These equations may be put together to obtain

$$s(t) = 2\mathrm{i}\rho_{\boxed{-}}(0)\exp\{-\mathrm{i}\phi_{\mathrm{rec}} + (\mathrm{i}\Omega^0 - \lambda)t\}$$

which may be written as

$$s(t) = a\ \exp\{\big(\mathrm{i}\Omega^0 - \lambda)t\big)\} \tag{11.47}$$

The *signal amplitude a* is given by

$$a = 2\mathrm{i}\rho_{\boxed{-}}(0)\exp\{-\mathrm{i}\phi_{\mathrm{rec}}\} \tag{11.48}$$

The amplitude of the NMR signal is therefore equal to the value of the (−1)-quantum coherence at the beginning of signal detection multiplied by some phase factors.

The expression for the NMR signal in Equation 11.47 has the same form as that assumed in Section 5.7.

The discussion in Section 5.8.1 may now be followed to obtain the NMR *spectrum* after Fourier transformation. The result is as follows:

$$S(\Omega) = a\mathcal{L}(\Omega; \Omega^0, \lambda) \tag{11.49}$$

where $\mathcal{L}$ is the complex Lorentzian function defined in Equation 5.12. For an ensemble of isolated spins-1/2, the NMR spectrum consists of a single Lorentzian peak at the resonance offset Ω^0. The width at half-height of the absorption peak is given in units of radians per second by 2λ, where λ is the coherence decay constant $\lambda = T_2{}^{-1}$. In units of hertz, the width at half-height is equal to $2\lambda/2\pi = 1/(\pi T_2)$. The complex amplitude of the peak is given by Equation 11.48, and is proportional to the (−1)-quantum coherence at the time point $t = 0$, i.e. the start of the signal acquisition.

To summarize, for a system of isolated spins-1/2, the NMR spectrum for a sequence of pulses may be calculated through the following steps:

1. Determine the resonance offset Ω^0, based on the known chemical shift of the spins and the position of the spectrometer reference frequency (Equation 10.21).

2. Set the spin density operator to the thermal equilibrium value (Equation 11.18).

3. Transform the spin density operator by the r.f. pulses according to Equations 11.33–11.36. For free precession, use Equations 11.29 and 11.38 if the intervals are short, so that relaxation may be neglected. For long intervals, use Equations 11.41 and 11.42.

4. Stop the calculation at the beginning of signal acquisition, time point $t = 0$. Determine the (−1)-quantum coherence $\rho_{\boxed{-}}$ at this point.

5. The spectrum is given by Equation 11.49. This describes a Lorentzian peak centred at frequency Ω^0, and with width at half-height 2λ, where λ is the inverse of T_2.

6. The complex amplitude of the peak is given by Equation 11.48, which involves the (-1)-quantum coherence at time point $t = 0$, as well as the signal phase shift parameters.

7. Normally only the real part of the spectrum is plotted. Consult Section 5.8.4 to determine the appearance of the spectrum in the case that the amplitude a is a complex number.

11.12 Single-Pulse Spectra

These results are now applied to some simple situations.

1. *Single* $(\pi/2)_x$ *pulse.* Suppose that a strong $(\pi/2)_x$ pulse is used for excitation and that the receiver phase ϕ_{rec} is set to zero during the acquisition of the NMR signal. The signal acquisition is started immediately after the pulse.

The density operator at the end of the pulse is calculated in the usual way starting from the thermal equilibrium state:

$$\begin{tikzcd}
\hat{\rho}^{\text{eq}} = \tfrac{1}{2}\hat{1} + \tfrac{1}{2}\mathbb{B}\hat{I}_z \arrow[d, "(\pi/2)_x"] \\
\hat{\rho}(0) = \tfrac{1}{2}\hat{1} - \tfrac{1}{2}\mathbb{B}\hat{I}_y
\end{tikzcd}$$

The result may be written in terms of the shift and projection operators:

$$\hat{\rho}(0) = \frac{1}{2}\hat{I}^{\alpha} + \frac{1}{2}\hat{I}^{\beta} - \frac{1}{4\mathrm{i}}\mathbb{B}\hat{I}^{+} + \frac{1}{4\mathrm{i}}\mathbb{B}\hat{I}^{-}$$

The (-1)-quantum coherence is equal to the coefficient of the $\hat{I}^{-}$ operator:

$$\rho_{\boxed{-}}(0) = \frac{1}{4\mathrm{i}}\mathbb{B}$$

The signal amplitude a is therefore

$$a = 2\mathrm{i}\frac{1}{4\mathrm{i}}\mathbb{B} = \frac{1}{2}\mathbb{B}$$

assuming that there is no receiver phase shift ($\phi_{\text{rec}} = 0$).

The amplitude a is a real positive number, indicating that the real part of the NMR spectrum is an absorption Lorentzian and that the imaginary part of the spectrum is a dispersion Lorentzian:

$$\begin{aligned}
\mathrm{Re}\{S(\Omega)\} &= \frac{1}{2}\mathbb{B}\mathcal{A}(\Omega; \Omega^0, \lambda) \\
\mathrm{Im}\{S(\Omega)\} &= \frac{1}{2}\mathbb{B}\mathcal{D}(\Omega; \Omega^0, \lambda)
\end{aligned}$$

as shown below:

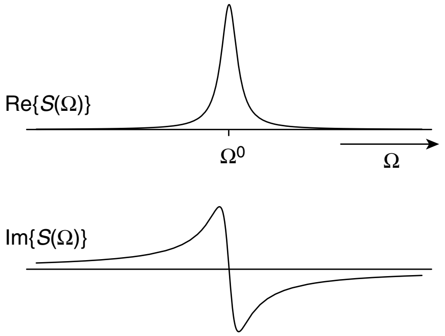

Figure 11.35
Real and imaginary parts of the spectrum generated by a $(\pi/2)_x$ pulse with $\phi_{\text{rec}} = 0$.

2. *Single* $(\pi/2)_y$ *pulse.* If a strong $(\pi/2)_y$ pulse is used instead, the calculation of the spin density operator runs as follows:

$$\hat{\rho}^{\text{eq}} = \tfrac{1}{2}\widehat{1} + \tfrac{1}{2}\mathbb{B}\hat{I}_z$$

$$\Big\downarrow (\pi/2)_y$$

$$\begin{aligned}\hat{\rho}(0) &= \tfrac{1}{2}\widehat{1} + \tfrac{1}{2}\mathbb{B}\hat{I}_x \\ &= \tfrac{1}{2}\hat{I}^{\alpha} + \tfrac{1}{2}\hat{I}^{\beta} + \tfrac{1}{4}\mathbb{B}\hat{I}^{+} + \tfrac{1}{4}\mathbb{B}\hat{I}^{-}\end{aligned}$$

The amplitude of the (-1)-quantum coherence at the start of the detection is

$$\rho_{\boxed{-}}(0) = \frac{1}{4}\mathbb{B}$$

The signal amplitude a is therefore

$$a = 2\mathrm{i}\frac{1}{4}\mathbb{B} = \mathrm{i}\frac{1}{2}\mathbb{B} \tag{11.50}$$

assuming no receiver phase shift ($\phi_{\text{rec}} = 0$).

In this case, the amplitude a is imaginary. The real part of the NMR spectrum is a negative dispersion Lorentzian and the imaginary part of the spectrum is in absorption:

$$\text{Re}\{S(\Omega)\} = -\frac{1}{2}\mathbb{B}\mathcal{D}(\Omega; \Omega^0, \lambda) \qquad \text{Im}\{S(\Omega)\} = \frac{1}{2}\mathbb{B}\mathcal{A}(\Omega; \Omega^0, \lambda)$$

as shown below:

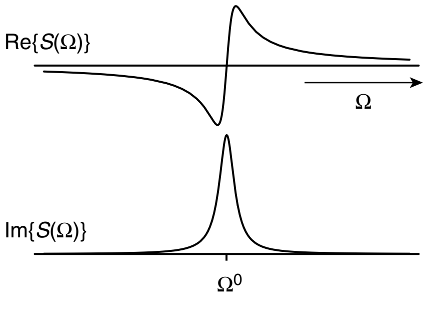

Figure 11.36
Real and imaginary parts of the spectrum generated by a $(\pi/2)_y$ pulse with $\phi_{\text{rec}} = 0$.

Similar calculations may be performed for pulses of any desired phase. It is easy to verify that the real part of the spectrum is in negative absorption for a $(\pi/2)_{\bar{x}}$ pulse, and that the real part of the spectrum is in negative dispersion for a $(\pi/2)_{\bar{y}}$ pulse.

Normally, these calculations are not performed in such detail. With experience, the form of the spectrum is determined simply *by inspection* of the density operator at the beginning of the detection period. The simple rules in the case $\phi_{\text{rec}} = 0$ are:

1. If the spin density operator $\hat{\rho}(0)$ contains a term proportional to $-\hat{I}_y$ (and no $\hat{I}_x$ terms), then the real part of the spectrum is in *positive absorption*.
2. If the spin density operator $\hat{\rho}(0)$ contains a term proportional to $\hat{I}_x$ (and no $\hat{I}_y$ terms), then the real part of the spectrum is in *negative dispersion*.
3. If the spin density operator $\hat{\rho}(0)$ contains a term proportional to $+\hat{I}_y$ (and no $\hat{I}_x$ terms), then the real part of the spectrum is in *negative absorption*.
4. If the spin density operator $\hat{\rho}(0)$ contains a term proportional to $-\hat{I}_x$ (and no $\hat{I}_y$ terms), then the real part of the spectrum is in *positive dispersion*.

Even more concisely:

$$\begin{aligned}
\hat{\rho}(0) &\sim -\hat{I}_y \xrightarrow{\phi_{\text{rec}}=0} \text{positive absorption}\\
\hat{\rho}(0) &\sim +\hat{I}_x \xrightarrow{\hspace{2em}} \text{negative dispersion}\\
\hat{\rho}(0) &\sim +\hat{I}_y \xrightarrow{\hspace{2em}} \text{negative absorption}\\
\hat{\rho}(0) &\sim -\hat{I}_x \xrightarrow{\hspace{2em}} \text{positive dispersion}
\end{aligned} \tag{11.51}$$

If the receiver phase is shifted, then the correspondences between the spin density operator and the spectrum are different. For example, the rules for the case $\phi_{\text{rec}} = \pi/2$ are as follows:

$$\begin{aligned}
\hat{\rho}(0) &\sim -\hat{I}_y \xrightarrow{\phi_{\text{rec}}=\pi/2} \text{positive dispersion}\\
\hat{\rho}(0) &\sim +\hat{I}_x \xrightarrow{\hspace{2em}} \text{positive absorption}\\
\hat{\rho}(0) &\sim +\hat{I}_y \xrightarrow{\hspace{2em}} \text{negative dispersion}\\
\hat{\rho}(0) &\sim -\hat{I}_x \xrightarrow{\hspace{2em}} \text{negative absorption}
\end{aligned}$$

Notes

1. The protons in water behave independently of each other if one ignores (i) the *intra*molecular coupling between the protons in each water molecule and also (ii) the *inter*molecular couplings between protons on different water molecules. As shown in Chapter 14, the *intra*molecular coupling may be neglected (except for relaxation effects) if the two chemical shifts are the same and the sample is an isotropic liquid. Both conditions are satisfied for the protons in water. The *inter*molecular couplings in water are purely long range (see Section 8.6.4) and may also be neglected, in most circumstances (see *Further Reading* to Chapter 8).

2. The much better term *statistical operator* is sometimes encountered.

3. The symbol $\hat{\sigma}$ is sometimes used in the NMR literature instead of $\hat{\rho}$.

4. The sum of the diagonal elements is equal to one, so they are best understood as the *fractional populations* of the states. However, the term *population* has become standard.

5. The density operator does not specify a *unique* microscopic situation. The density operator only provides sufficient information for predicting the results of macroscopic observations, which are ensemble averages. For example, a hypothetical situation in which half the spins really are precisely in the state $|\alpha\rangle$ and half are precisely in the state $|\beta\rangle$ would have a density operator with equal populations $\rho_{\boxed{\alpha}} = \rho_{\boxed{\beta}} = \frac{1}{2}$. This state would give the same value for all macroscopic observables as a more general state, in which the spins are in superposition states and point in all possible directions. However, the situation in which most of the spins are in superposition states is much more *likely* to be correct.

6. In systems of spins $I > 1/2$, and coupled spin systems, there may arise additional types of coherence that cannot be represented as the alignment of spin polarizations with an external axis. This subject is explored in Chapters 13 and 15.

7. The (+1)-quantum coherence may make its presence felt if the quadrature receiver is not correctly adjusted, in which case it gives rise to *quadrature image peaks* at the frequency $-\Omega^0$ (see Appendix A.5). Such image peaks have been rendered negligible by advances in receiver technology.

8. Although almost all NMR calculations are performed in the rotating frame, there is one important exception. The estimation of the thermal equilibrium state through the Boltzmann distribution (Equation 11.15) must be performed using the fixed-frame Hamiltonian. For example, it is incorrect to use the eigenvalues of the rotating-frame Hamiltonian $\hat{\hat{\mathcal{H}}}$ in the Boltzmann distribution.

9. The treatment of r.f. pulses in Section 11.8 ignores off-resonance effects and relaxation during the pulses. A more complete treatment is given by the *Bloch equations*, which are discussed in Appendix A.13.

10. In practice, the relaxation behaviour of spin systems is often quite complicated and cannot be described by single exponential functions. One example is analysed more fully in Chapter 20.

11. The coupling of the spins to the receiver coil withdraws a small amount of energy from the spin system, and acts in some respects like an additional relaxation mechanism. The generation of the NMR signal itself tends to pull the magnetization vector towards its thermal equilibrium value. This effect is called *radiation damping* or *coil reaction*. The real situation is complicated because of the 'feedback' between the nuclear spin system and the tuned circuit in the probe: the nuclear spins induce an NMR signal in the coil, which is amplified by electromagnetic resonance in the tuned circuit, which generates a magnetic field in the sample, which acts back on the spins again, and so on. The evolution of the signal can get quite complicated, with marked deviations from the simple form of Equation 11.47. It is even possible for the signal to *grow*, rather than decay! See A. Vlassenbroek, J. Jeener and P. Broekaert, *J. Chem. Phys.*, **103**, 5886 (1995). Such feedback effects are only dramatic in special circumstances, and I ignore them in this book.

12. The relationship between T_1 and T_2 given in Equation 11.43 may be understood using relaxation theory, as sketched in Chapter 20. In that chapter, it is shown that, for isolated spins-1/2, the longitudinal relaxation rate constant ${T_1}^{-1}$ is equal to $2W$, where W is the transition probability per unit time between the states. In general, the transverse relaxation rate constant has two contributions, i.e. an *adiabatic* contribution, which is due to the fluctuations of the energy levels, and a *non-adiabatic* contribution due

to the limited lifetime of the energy eigenstates, as a result of transitions. The transverse relaxation rate constant ${T_2}^{-1}$ cannot be smaller than the non-adiabatic contribution, which is equal to the transition probability per unit time, W. Hence, we have ${T_2}^{-1} \geq W$ and ${T_1}^{-1} = 2W$, which leads to Equation 11.43. In most common cases, there is also an adiabatic contribution to the transverse relaxation rate constant, so that ${T_2}^{-1}$ is either approximately the same as or larger than the longitudinal relaxation rate constant ${T_1}^{-1}$.

13. The case where $T_2 > T_1$ is encountered when the spin relaxation is caused by fluctuating microscopic fields that are predominantly transverse rather than longitudinal. One mechanism which gives rise to fields of this form involves the *antisymmetric component of the chemical shift tensor* (not to be confused with the CSA). In the notation of Section 9.1, this mechanism involves differences in non-secular chemical shift tensor components of the form $\delta^j_{xz} - \delta^j_{zx}$ and $\delta^j_{yz} - \delta^j_{zy}$. Molecular systems in which this mechanism is dominant are exceedingly rare (see F. A. L. Anet, D. J. O'Leary, C. G. Wade and R. D. Johnson, *Chem. Phys. Lett.*, **171**, 401 (1990)).

14. The fact that only the (-1)-quantum coherence is observable often causes confusion. As shown in Appendix A.5, this is not a fundamental property of the detection process, but rather derives from the particular representation of the quadrature receiver outputs as the two components of a complex signal.

15. The choice of time origin $t = 0$ as the start of signal acquisition is consistent with the definition of Fourier transformation, given in Section 5.8.1. Much NMR literature defines $t = 0$ to be the starting point of the pulse sequence, but this is strictly incorrect. The distinction becomes important for experiments on rotating samples, as is common in solid-state NMR.

Further Reading

- For further pedagogical discussion on the meaning of the spin density operator, see J. C. Paniagua, *Concepts Magn. Reson. A* **28**, 384–409 (2006).
- For a more thorough introduction to the spin density operator, see M. Goldman, *Quantum Description of High-Resolution NMR in Liquids*, Clarendon Press, Oxford, 1988 and R. R. Ernst, G. Bodenhausen and A. Wokaun, *Principles of Nuclear Magnetic Resonance in One and Two Dimensions*, Clarendon Press, Oxford, 1987.
- For the connection between NMR and coherent optics, see E. Lippert and J. D. Macomber, *Dynamics During Spectroscopic Transitions*, Springer, Berlin, 1995, and D. Suter, *The Physics of Laser–Atom Interactions*, Cambridge University Press, Cambridge, 1997.

Exercises

11.1 An ensemble of isolated protons is in thermal equilibrium at a temperature of 300 K.

(i) At what magnetic field is the population difference between the $|\alpha\rangle$ and $|\beta\rangle$ spin states equal to 5×10^{-5}?

(ii) What is the proton Larmor frequency in this field?

(iii) What is the thermal equilibrium population difference between the $|\alpha\rangle$ and $|\beta\rangle$ states of ^{13}C spins at the same temperature and in the same field?

11.2 In real experiments, the r.f. field created by the coil is not precisely uniform over the volume of the sample. This imperfection is called *r.f. inhomogeneity*. This exercise examines one strategy for rendering experiments less sensitive to r.f. inhomogeneity.

(i) An NMR experiment is performed on isolated proton spins. Suppose that the peak r.f. field in the *centre* of the sample is $B_{\mathrm{RF}} = 4.697\,\mathrm{mT}$, and that a pulse of duration $\tau_{\mathrm{p}} = 5\,\mu\mathrm{s}$ and phase $\phi_{\mathrm{p}} = 0$ is applied. What is the flip angle of the pulse in the centre of the sample? If the magnetization vector before the pulse is $\mathbf{M} = \mathbf{e}_z$, what is the magnetization vector after the pulse? Ignore off-resonance effects.

(ii) At the *edge* of the sample, the peak r.f. field is only $B_{\mathrm{RF}} = 4.228\,\mathrm{mT}$. If the magnetization vector at the edge of the sample before the pulse is $\mathbf{M} = \mathbf{e}_z$, what is the magnetization vector at the edge of the sample after the pulse? What is the angle between the magnetization vectors at the edge of the sample and at the centre of the sample, after the pulse?

(iii) Now suppose that the single r.f. pulse is replaced by a sequence of three pulses of durations $2.5\,\mu\mathrm{s}$, $5.0\,\mu\mathrm{s}$ and $2.5\,\mu\mathrm{s}$, with phases 0, $\pi/2$ and 0, respectively. This three-pulse sequence is an example of a *composite pulse*. If the magnetization vector before the pulse is $\mathbf{M} = \mathbf{e}_z$, what is the magnetization vector at the *centre* of the sample after the pulse?

(iv) Calculate the magnetization vector at the *edge* of the sample after the composite pulse. What is the angle between the magnetization vector at the edge of the sample and the magnetization vector at the centre of the sample, after the pulse?

(v) Explain the operation of the composite pulse geometrically.

12 Experiments on Non-Interacting Spins-1/2

In this chapter I discuss some common NMR experiments that may be understood using the density operator theory.

12.1 Inversion Recovery: Measurement of T_1

The first experiment is a method for measuring the longitudinal relaxation time constant of the spins, T_1. The value of T_1 provides valuable information as to the motion and dynamics of the molecules (see Chapter 20). Here, we are only concerned with the measurement procedure itself.

The usual technique for measuring T_1 is called *inversion recovery*. The pulse sequence is given by:

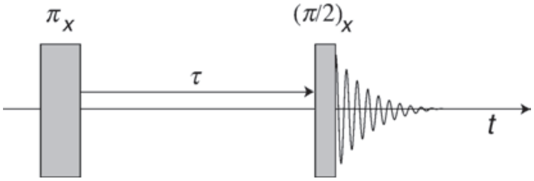

Figure 12.1
Inversion-recovery pulse sequence.

and consists of two r.f. pulses separated by an interval τ. The use of a single-headed arrow indicates that the experiment is performed in an *arrayed* fashion, as described in Section 5.6. This means that the pulse sequence is repeated, with different values of the interval τ, and the results compiled in a two-dimensional data matrix. If the time variable during the signal acquisition interval is denoted t, then the two-dimensional data matrix may be denoted $s(\tau, t)$.

The iconic pulse sequence given above conceals a number of details. First, for each value of τ, the pulse sequence and data acquisition are normally repeated many times, adding the signals together in order to enhance the signal at the expense of the noise, as described in Section 5.2. Second, each repetition of the pulse sequence is separated by a long interval τ_{wait}, during which the spins return to a reproducible thermal equilibrium state. For this to be satisfied, the waiting interval τ_{wait}, plus the signal acquisition period τ_{acq}, must be several times the relaxation time constant T_1 (which implies that one should already have a good guess as to the value of T_1 before determining it this way). Third, a phase cycle of the pulses is normally

---

Spin Dynamics: Basics of Nuclear Magnetic Resonance, Second Edition Malcolm H. Levitt

performed to reduce the sensitivity of the experiment to imperfections. In the following discussion, I ignore the phase cycle and assume that the r.f. pulses are perfect.

The first pulse in the sequence is a π_x pulse and generates an inverted population distribution. The populations relax back towards thermal equilibrium during the interval τ: their progress is monitored by the second pulse, which converts the population difference into coherences, including the observable (-1)-quantum coherence, which induces an NMR signal:

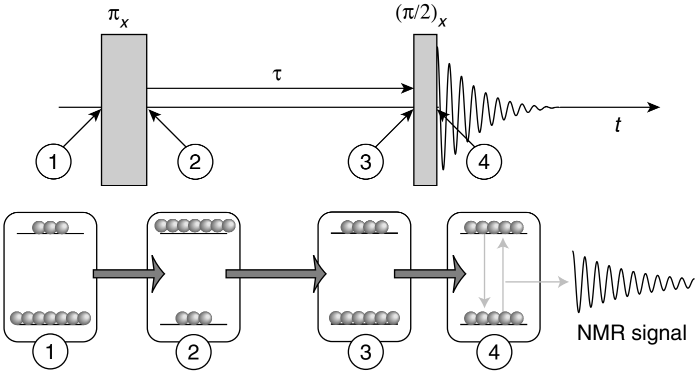

Figure 12.2
Populations and coherences during the inversion-recovery pulse sequence.

The spin density operator goes through the following transformations:

$$\hat{\rho}_{①} = \hat{\rho}^{\mathrm{eq}} = \tfrac{1}{2}\hat{1} + \tfrac{1}{2}\mathbb{B}\hat{I}_z$$

$$\Big\downarrow \; \pi_x$$

$$\hat{\rho}_{②} = \widehat{R}_x(\pi)\hat{\rho}_{①}\,\widehat{R}_x(-\pi) = \tfrac{1}{2}\hat{1} - \tfrac{1}{2}\mathbb{B}\hat{I}_z$$

$$\Big\downarrow \; \tau$$

$$\hat{\rho}_{③} = \tfrac{1}{2}\hat{1} + \tfrac{1}{2}\mathbb{B}\left(1 - 2\mathrm{e}^{-\tau/T_1}\right)\hat{I}_z$$

$$\Big\downarrow \; (\pi/2)_x$$

$$\hat{\rho}_{④} = \widehat{R}_x(\pi/2)\hat{\rho}_{③}\,\widehat{R}_x(-\pi/2) = \tfrac{1}{2}\hat{1} - \tfrac{1}{2}\mathbb{B}\left(1 - 2\mathrm{e}^{-\tau/T_1}\right)\hat{I}_y$$

The observable spin coherence is therefore a function of the interval between the pulses τ and the time t after the last pulse. If the resonance offset of the spins is Ω^0, then the NMR signal is

$$s(\tau, t) = a(\tau)\exp\{\left(\mathrm{i}\Omega^0 - \lambda\right)t\}$$

where the amplitude $a(\tau)$ reflects the history of the longitudinal magnetization:

$$a(\tau) = \frac{1}{2}\mathbb{B}\left(1 - 2\mathrm{e}^{-\tau/T_1}\right)$$

The spectral peak amplitude is negative for small values of τ, but goes through zero and becomes positive for large values of τ:

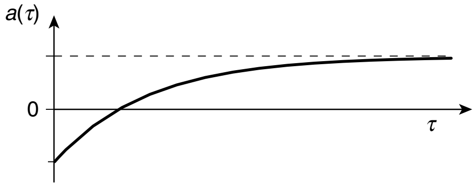

Figure 12.3
Trajectory of the peak amplitude a as a function of τ in the inversion-recovery experiment.

Now suppose that there are several different spin ensembles in the sample. Each different spin ensemble might belong to a different chemical compound, or to different isotopomers of the same compound. Different regions of the sample may also constitute individual ensembles, if, for example, the magnetic field is different at different points of space. In all cases, the total signal is simply a superposition of contributions from each ensemble:

$$s(\tau, t) = \sum_j a_j(\tau) \exp\{\left(\mathrm{i}\Omega_j^0 - \lambda_j\right) t\}$$

Here, Ω_j^0 is the resonance offset of spins in ensemble j and λ_j is a peakwidth parameter for ensemble j. The amplitude a_j of each signal component reflects the spin–lattice relaxation history of spins in each ensemble:

$$a_j(\tau) = \frac{1}{2}\mathbb{B}\left(1 - 2\mathrm{e}^{-\tau/T_1^j}\right)$$

where T_1^j is the spin–lattice relaxation time constant of spins belonging to ensemble j.

The data matrix $s(\tau, t)$ is Fourier transformed with respect to t according to

$$S(\tau, \Omega) = \int_0^\infty s(\tau, t) \exp\{-\mathrm{i}\Omega t\}\, \mathrm{d}t$$

The result is

$$S(\tau, \Omega) = \sum_j a_j(\tau) \mathcal{L}\left(\Omega; \Omega_j^0, \lambda_j\right)$$

We get a superposition of Lorentzian peaks, one for spins in each ensemble. Each peak amplitude depends on τ according to the spin–lattice relaxation time constant for the corresponding ensemble j:

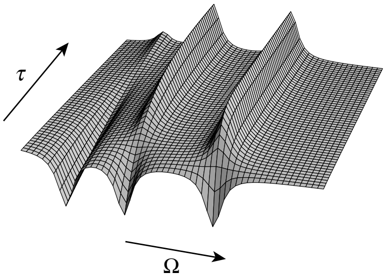

Figure 12.4
Real part of a signal data matrix $s(\tau, t)$ obtained from an inversion-recovery experiment.

In the surface above, note that the three peaks relax back to equilibrium at different rates. The value of T_1^j for each ensemble may be deduced by tracking the individual amplitudes $a_j(\tau)$.

An experimental data matrix $S(\tau, \Omega)$ for a sample with four different chemical sites is shown in Figure 12.5. In this case, each peak in the spectrum comes from a different isotopomer.

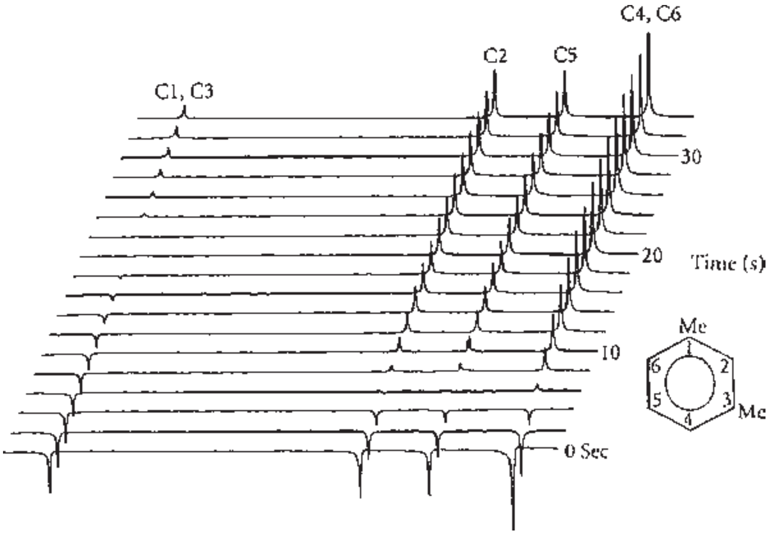

Figure 12.5
Set of experimental inversion-recovery spectra. From R. Freeman, *Spin Choreography*, Spektrum, Oxford, 1997, p. 47. (Copyright Spektrum Academic Publishers).

The value of T_1 may be extracted from the experimental peak amplitudes $a(\tau)$ by standard methods. For example, the values $\log(a(\infty) - a(\tau))$ may be plotted against τ and fitted to a straight line. The slope of the best-fit line is the estimated value of $-T_1{}^{-1}$.

12.2 Spin Echoes: Measurement of T_2

12.2.1 Homogenous and inhomogenenous broadening

The relaxation time constant T_2 conveys information about the dynamics of the molecules (see Chapters 19 and 20).

According to the theory given in Chapter 11, the width-at-half-height of the spectral peak (in hertz) is given by $1/(\pi T_2)$, where T_2 is the transverse relaxation time constant. This suggests that T_2 may be estimated simply by measuring the width of the spectral peak.

Unfortunately, this rarely gives a reliable estimate of T_2. The width of the NMR peaks tends to be larger than $1/(\pi T_2)$, because of *inhomogeneous broadening*, as discussed in Section 3.6. The magnetic field varies from place to place in the sample, which spreads the peaks out, thus giving a larger overall linewidth.

Therefore, there are (at least) two mechanisms of peak broadening in NMR spectra:

1. *Homogeneous broadening*. This is due to fluctuating *microscopic* magnetic fields, and is quantified by the transverse relaxation time constant T_2.

2. *Inhomogeneous broadening*. This is due to the variation of the *macroscopic* magnetic field over the volume of the sample, due to instrumental imperfections, or susceptibility effects.

The full peakwidth in the spectrum is a superposition of these two effects.[1]

The *spin echo method* allows the homogeneous decay to be distinguished from the inhomogeneous decay, so that T_2 may be measured even when the magnetic field is inhomogeneous.

12.2.2 Inhomogenenous broadening in the time domain

The mechanism of inhomogeneous broadening may be visualized in the frequency domain, as was done in Section 3.6. The magnetic field causes the Larmor frequency to vary from place to place in the sample. The spectrum consists of many overlapping peaks at slightly different positions, which gives rise to additional line broadening.

It is also instructive to view the effect of inhomogeneous broadening in the time domain. The FID from the whole sample is a superposition of many FID components, each with a slightly different frequency, and decaying with the natural decay time constant T_2. The many different frequency components get out of phase with each other and destructively interfere at long times, giving rise to an artificially rapid decay of the total signal:[1]

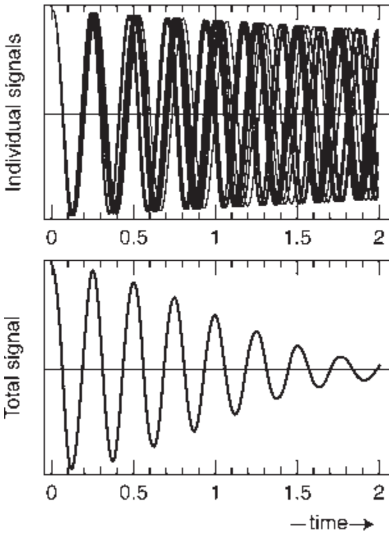

Figure 12.6
Inhomogeneous broadening gives rise to a superposition of signals with different frequencies. These interfere to give an enhanced signal decay.

Since the total signal decays faster, FT gives a spectrum with an increased peakwidth.

In the *spin echo* experiment, the *inhomogeneous* part of the signal decay is reversed by the application of a second r.f. pulse. This allows the *homogeneous* decay constant T_2 to be measured even in a non-uniform magnetic field.

12.2.3 Spin echo pulse sequence

The spin echo pulse sequence is as follows:

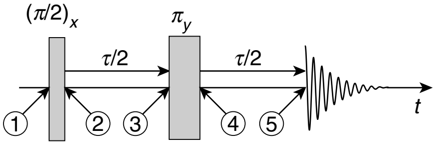

Figure 12.7
Spin echo pulse sequence.

The interval between the first pulse and the second pulse is equal to $\frac{1}{2}\tau$. The same interval is left after the second pulse before signal acquisition starts. As denoted by the single-headed arrows, an arrayed experiment is performed in which the experiment is repeated with different values of τ (the two delays marked $\frac{1}{2}\tau$ are always kept the same as each other). The data matrix $s(\tau, t)$ is Fourier transformed with respect to t to give a spectrum $S(\tau, \Omega)$, containing peaks whose amplitudes varies as a function of τ:

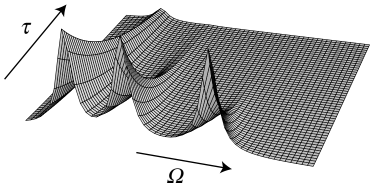

Figure 12.8
Spectral data matrix $S(\tau, \Omega)$ from the spin echo experiment.

The τ-dependence of each peak amplitude may be analysed to obtain the value of T_2 for each spin ensemble, independent of the inhomogeneous broadening.

I first give a mathematical description of the experiment, returning afterwards to a more 'physical' explanation.

For simplicity, consider first the case of just one spin ensemble. The transformation of the spin density operator by the first pulse should be familiar by now:

$$\begin{tikzcd}[row sep=large] \hat{\rho}_{\textcircled{1}} = \hat{\rho}^{\mathrm{eq}} = \frac{1}{2}\widehat{1} + \frac{1}{2}\mathbb{B}\hat{I}_z \arrow[d, "(\pi/2)_x"] \\ \hat{\rho}_{\textcircled{2}} = \frac{1}{2}\widehat{1} - \frac{1}{2}\mathbb{B}\hat{I}_y \end{tikzcd}$$

From now on, the 'population parts' of the density operator (terms proportional to $\widehat{1}$ and $\hat{I}_z$) will be dropped. The subsequent evolution, including the second r.f. pulse, does not convert them into coherences, so they do not contribute to the final NMR signal.

The evolution during the first $\frac{1}{2}\tau$ period runs as follows:

$$\begin{tikzcd}[row sep=large] \hat{\rho}_{\textcircled{2}} = -\frac{1}{2}\mathbb{B}\hat{I}_y + \ldots \arrow[d, "\frac{1}{2}\tau"] \\ \hat{\rho}_{\textcircled{3}} = \frac{1}{2}\mathbb{B}\left(-\hat{I}_y \cos \Omega^0 \frac{1}{2}\tau + \hat{I}_x \sin \Omega^0 \frac{1}{2}\tau\right) \mathrm{e}^{-\lambda \frac{1}{2}\tau} + \ldots \end{tikzcd}$$

This describes a rotation of the magnetization vector around the z-axis at the offset frequency Ω^0:

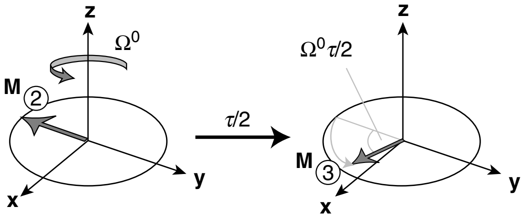

Figure 12.9
Precession of the magnetization during the first $\frac{1}{2}\tau$ interval.

The homogeneous decay of the transverse magnetization is taken into account by the $\exp\{-\lambda\frac{1}{2}\tau\}$ term (note the 'shrinkage' of the magnetization vector in the diagram above).

The second π_y pulse has the effect of reversing the $\hat{I}_x$ component, leaving the $\hat{I}_y$ component unchanged:

$$\begin{aligned}\hat{\rho}_{③} &= \tfrac{1}{2}\mathbb{B}\left(-\hat{I}_y\cos\Omega^0\tfrac{1}{2}\tau + \hat{I}_x\sin\Omega^0\tfrac{1}{2}\tau\right)\mathrm{e}^{-\lambda\frac{1}{2}\tau} + \ldots \\ &\Big\downarrow \pi_y \\ \hat{\rho}_{④} &= \tfrac{1}{2}\mathbb{B}\left(-\hat{I}_y\cos\Omega^0\tfrac{1}{2}\tau - \hat{I}_x\sin\Omega^0\tfrac{1}{2}\tau\right)\mathrm{e}^{-\lambda\frac{1}{2}\tau} + \ldots\end{aligned}$$

This is shown below:

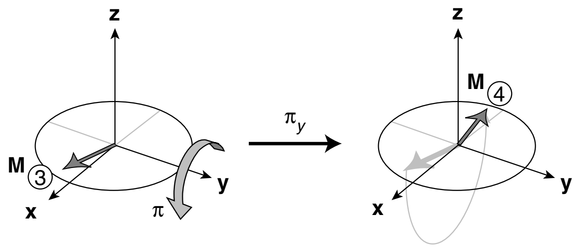

Figure 12.10
Rotation of the magnetization by the $(\pi/2)_y$ pulse.

There now follows another $\frac{1}{2}\tau$ interval, before the signal is detected. During this period, the magnetization vector rotates through an angle $\Omega^0\frac{1}{2}\tau$ again. This rotation exactly compensates the precession between the two pulses, leading to a magnetization vector exactly along the negative y-axis at time $t = 0$:

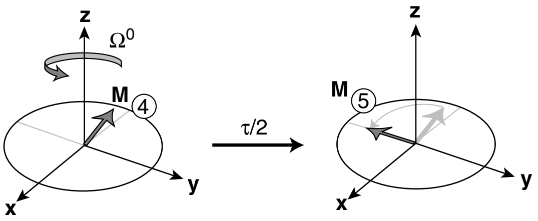

Figure 12.11
Precession of the magnetization during the second $\frac{1}{2}\tau$ interval.

It may be verified from the explicit transformation rules in Section 11.8, or from simple geometrical arguments, that the result is

$$\hat{\rho}_{⑤} = -\frac{1}{2}\mathbb{B}\hat{I}_y\mathrm{e}^{-\lambda\tau} + \ldots \tag{12.1}$$

The peak amplitudes in the NMR spectra $S(\tau, \Omega)$ are therefore given by

$$a(\tau) = \frac{1}{2}\mathbb{B}\mathrm{e}^{-\tau/T_2}$$

The exponential decay may readily be analysed to obtain an estimate for the value of T_2.

The key point here is that the final density operator $\hat{\rho}_{⑤}$, as given in Equation 12.1, is independent of the value of the resonant offset Ω^0. This implies that the signal at this time point is independent of the value of the magnetic field. By analysing the peak heights as a function of τ, an estimate of T_2 is obtained, independent of the inhomogeneous broadening.

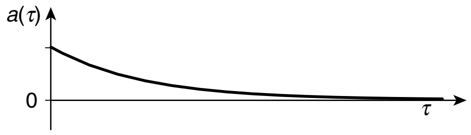

Figure 12.12
Trajectory of the peak amplitude a as a function of τ in the spin echo experiment.

12.2.4 Refocusing

Physically, the evolution under the second half of the pulse sequence corresponds to a reversal of the inhomogeneous part of the signal decay. The π_y pulse causes the magnetization vectors to be set up in such a way that the signal grows bigger rather than smaller:

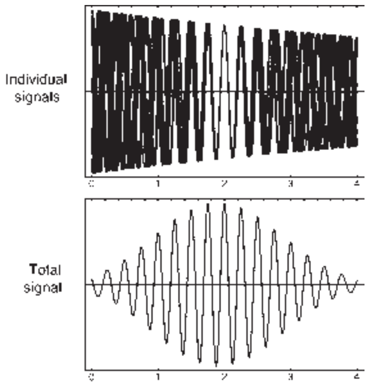

Figure 12.13
Constructive interference of the inhomogeneous signal components produces a spin echo.

The effect can be dramatic. It is quite feasible for the NMR signal to die out completely at the end of the first $\frac{1}{2}\tau$ interval, only to be resurrected, seemingly from nowhere, at the end of the second $\frac{1}{2}\tau$ interval. The term 'spin echo' is descriptive of this mysterious appearance of the signal from a state of silence.

The discovery of the spin echo by Erwin Hahn in 1950 may be regarded as the birth of modern pulsed NMR.[2]

The geometrical mechanism of the spin echo is seen clearly by associating a magnetization vector with many small sample regions, located at different points in space. If the field is inhomogeneous, then the precession frequencies of the magnetization vectors are all different. The pictures below show the trajectories of many magnetization vectors, with darker shading for those belonging to sample regions in relatively strong magnetic fields.

The magnetization vectors from different spatial regions fan out after the first pulse, as shown by the following snapshots during the first $\tau/2$ interval:

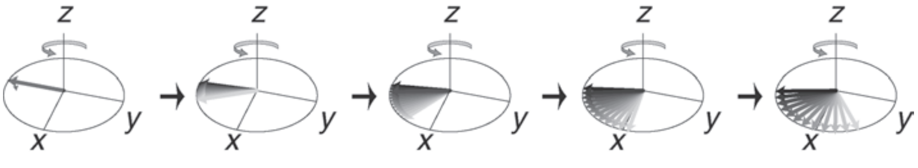

Figure 12.14
Spreading of magnetization vectors during the first $\tau/2$ interval.

This is called *dephasing*, and leads to a loss in the total signal during the first $\tau/2$ interval.

The second pulse rotates all vectors by π around the y-axis. Figure 12.15 shows the trajectories traced out by the tips of the magnetization vectors as they are rotated by their pulse, and their final positions after the π rotation:

Figure 12.15
Rotation of magnetization vectors during the π_y pulse.

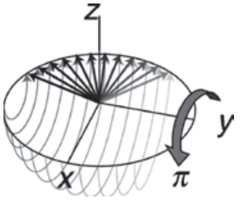

After the pulse, each vector rotates around the z-axis, at the frequency corresponding to its local magnetic field. Since the π pulse inverts the relative positions of the magnetization vectors belonging to strong and weak magnetic fields, they all *refocus* simultaneously at the $-y$-axis after the second $\tau/2$ interval, forming the echo:

Figure 12.16
Refocusing of magnetization vectors during the second $\tau/2$ interval.

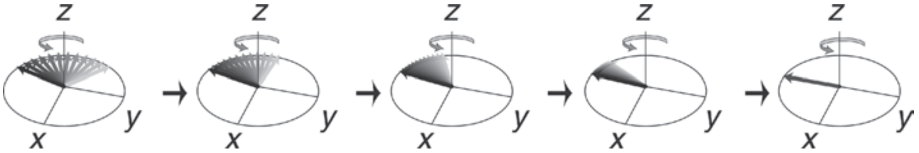

An experimental spin echo signal is shown in Figure 12.17.

Perfect refocusing requires that the inhomogeneous magnetic fields do not change while the pulse sequence is going on, so that the precession angle during the second $\tau/2$ interval is exactly the same as the precession angle during the first $\tau/2$ interval. The echo formation is disturbed if there is any sort of motion of the spins into different field regions, or if the fields themselves vary in time. If the fields change, or if the spins move into a region with a different magnetic field, then the precession after the π_y pulse no longer cancels exactly the precession before the pulse, thus leading to a reduction in signal at the echo maximum. This property can be very useful, because it allows the spin echo to detect *molecular motion*. Spin echo experiments are often used to quantify *diffusion* and *flow* processes (see Exercise 12.2 and Section 19.8).

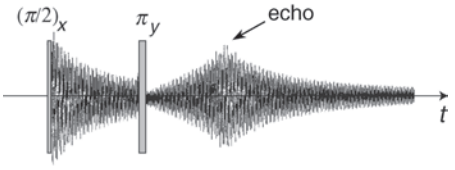

Figure 12.17 Experimental echo signal. Adapted from A. E. Derome, *Modern NMR Techniques for Chemistry Research*, Pergamon Press, Oxford, 1987, p. 91. Copyright, Elsevier Science.

12.2.5 Coherence interpretation

An equivalent interpretation of spin echo formation follows the histories of individual spin *coherences* during the echo sequence, rather than the magnetization vector trajectories. The coherence interpretation is more abstract than the magnetization vector interpretation, but proves to be easier to generalize to higher spin quantum numbers and coupled spin systems.

As discussed in Section 11.11, the quadrature-detected NMR signal is generated by (-1)-quantum coherences existing during the detection interval. However, the π pulse *inverts* the coherence order, as one can see from the following transformation properties:

$$\begin{aligned}\widehat{R}_y(\pi)\hat{I}^+\widehat{R}_y(\pi)^\dagger &= -\hat{I}^- \\ \widehat{R}_y(\pi)\hat{I}^-\widehat{R}_y(\pi)^\dagger &= -\hat{I}^+ \end{aligned} \tag{12.2}$$

It follows that the echo signal derives from (+1)-quantum coherences existing *before* the π pulse (time point ③), which are transformed by the pulse into observable (−1)-quantum coherences.

The following coherence transfer processes, therefore, give rise to the echo signal:

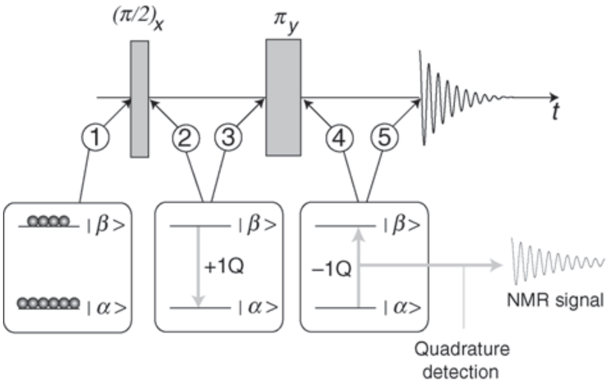

Figure 12.18
Coherence transfer processes leading to the spin echo signal.

The thermal equilibrium population difference is transformed by the $\pi/2$ pulse into a (+1)-quantum coherences, which evolves during the first $\tau/2$ interval (a (−1)-quantum coherence is also generated, but this does not give rise to a final NMR signal, and may therefore be ignored). The (+1)-quantum coherence is transformed by the π_y pulse into a (−1)-quantum coherence, which, after evolving for a further interval $\tau/2$, generates the quadrature NMR signal.

In the coherence interpretation, it is the *sign inversion of coherence order* induced by the π pulse that gives rise to the spin echo formation. As discussed in Section 11.7, the (+1)-quantum coherences evolve in the complex plane at the *negative* resonance offset under free precession, and hence

$$\rho_{\boxed{+}}\text{③} = \rho_{\boxed{+}}\text{②}\ \exp\{(-\mathrm{i}\Omega-\lambda)\tau/2\} \tag{12.3}$$

As shown in Equation 12.2, the π_y pulse converts the (+1)-quantum coherence into a (−1)-quantum coherence:

$$\rho_{\boxed{-}}\text{④} = -\rho_{\boxed{+}}\text{③} \tag{12.4}$$

The (−1)-quantum coherence evolves in the complex plane at the *positive* resonance offset under free precession, and hence

$$\rho_{\boxed{-}}\text{⑤} = \rho_{\boxed{-}}\text{④}\ \exp\{(+\mathrm{i}\Omega-\lambda)\tau/2\} \tag{12.5}$$

These equations may be combined to get

$$\begin{aligned}\rho_{\boxed{-}}\text{⑤} &= -\rho_{\boxed{+}}\text{②}\ \exp\{(-\mathrm{i}\Omega-\lambda)\tau/2\}\exp\{(+\mathrm{i}\Omega-\lambda)\tau/2\} \\ &= -\rho_{\boxed{+}}\text{②}\ \exp\{-\lambda\tau\}\end{aligned} \tag{12.6}$$

The observable (−1)-quantum coherence at the peak of the echo is therefore independent of the resonance offset, and hence of the local magnetic field strength.

This is an example of an important principle: whenever the sign of the coherence order is inverted by a pulse and the magnetic field is inhomogeneous, a spin echo may be formed.

12.2.6 Coherence transfer pathway

The sequence of coherence transfer events leading to a spin echo may be summarized by drawing a *coherence transfer pathway diagram*. The history of coherence orders leading to the observable signal is denoted as follows:

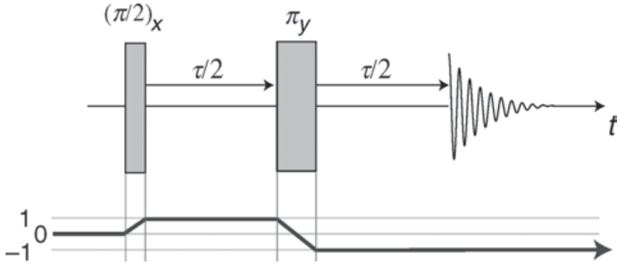

Figure 12.19 Coherence transfer pathway diagram for a spin echo.

In the lower part of the diagram, the accessible coherence orders are depicted as horizontal lines. For an ensemble of isolated spins-1/2, the only accessible orders are -1, 0 and $+1$. The coherence transfer pathway leading to the observable signal is represented by the bold line with an arrowhead. The initial thermal equilibrium state has order 0, since the corresponding density operator contains only populations. The first $\pi/2$ pulse converts the population difference into (± 1)-quantum coherence. Only the $(+1)$-quantum coherence is shown on the coherence transfer pathway diagram, since only this coherence gives rise to the observable signal at the end of the pulse sequence. The sign of the coherence order is inverted by the π pulse; as discussed above, it is this sign change that gives rise to a spin echo in an inhomogeneous magnetic field. The coherence transfer pathway terminates with order -1, since only (-1)-quantum coherences are observable under quadrature detection of the NMR signal. Note that the pathway diagram always shows horizontal lines during the intervals of free precession, to indicate that no changes in coherence order take place in the absence of r.f. pulses.

Coherence transfer pathway diagrams are very useful tools for portraying the essential features of complex NMR experiments, without going into details. They are particularly useful for constructing phase cycles (see Appendix A.11).

12.3 Spin Locking: Measurement of $T_{1\rho}$

In the Carr–Purcell echo, transverse magnetization is allowed to precess freely before reversing its evolution using a π pulse. In contrast, the *spin-locking* method employs a resonant r.f. field to *suppress* the free evolution of transverse magnetization, locking it to a particular direction in the rotating frame.

A typical spin-locking pulse sequence is as follows:

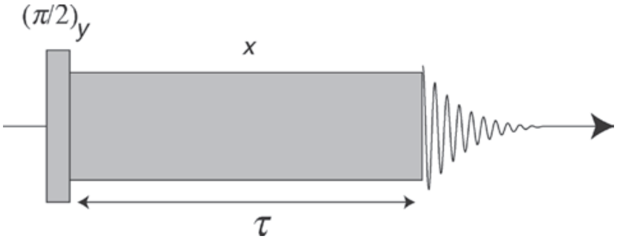

Figure 12.20 Pulse sequence for a spin-locking experiment.

The operation of this pulse sequence is as follows:

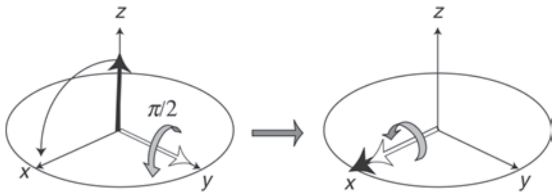

Figure 12.21 Spin magnetization (black arrow) is rotated from the z-axis to the x-axis by a $(\pi/2)_y$ pulse, where it is locked by an r.f. field along the x-axis (white arrow).

The initial $(\pi/2)_y$ pulse converts the initial longitudinal magnetization into transverse magnetization along the rotating-frame x-axis. The phase of the r.f. field is then suddenly changed to $\phi = 0$, so that the rotating-frame r.f. field is also along the x-axis, i.e. in the same direction as the transverse magnetization. If the r.f. field is large enough, then the transverse magnetization is unable to precess away from the x-axis – it is said to be *spin locked*. After a time τ, the locking field is turned off, releasing the transverse magnetization and allowing it to generate an NMR signal.

In most cases, the spin-locked magnetization decays roughly exponentially to zero.[3] The decay process may be followed by conducting a series of experiments with several values of the locking time τ. The time constant of the exponential decay is usually denoted $T_{1\rho}$, and is usually called the *spin–lattice relaxation time constant in the rotating frame*.[4]

The study of the time constant $T_{1\rho}$ can reveal details of slow molecular dynamics. The procedure is often used for the study of motions in polymers.

12.4 Gradient Echoes

R.f. pulses are not the only way to induce spin echoes. A different type of spin echo arises when an applied field gradient (see Section 4.7) is reversed in sign. This is called a *gradient echo*. Consider the following pulse sequence:

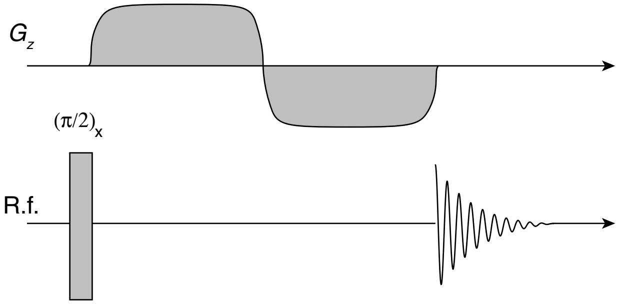

Figure 12.22 Pulse sequence for inducing a gradient echo.

After transverse magnetization is excited by the first $\pi/2$ pulse, a magnetic field gradient is switched on along the z-axis. After a certain time interval the gradient is reversed in sign for the same interval. The gradient echo forms when the integral of the field gradient over time is equal to zero.

The gradient echo may be visualized by imagining the transverse magnetization vectors of a series of small volume elements displaced along the direction of the field gradient, i.e. along the z-axis in the case of a G_z gradient. In the presence of the gradient, spins at different positions z experience different local magnetic fields, so that the transverse magnetization components precess at different frequencies. As the evolution proceeds in the presence of the gradient, a *magnetization helix* is wound around the z-axis:

Figure 12.23
The evolution of transverse magnetization vectors at different points along the z-axis, in the presence of a field gradient G_z.

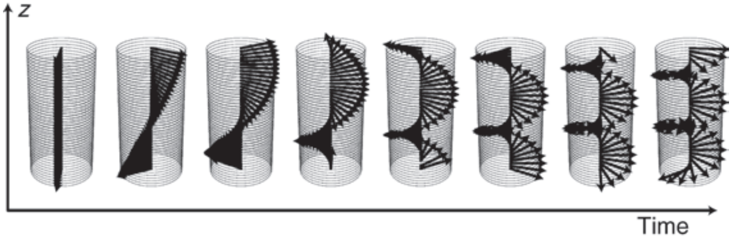

The pitch of the helix is inversely proportional to the magnitude of the gradient, and the time for which it is applied. Large gradients applied for long times lead to a short pitch. When the gradient is applied for a long enough time, the pitch of the helix becomes much smaller than the sample dimensions and the signal vanishes, since the individual magnetization components cancel out.

The magnetization helix is unwound by reversing the sign of the gradient:

Figure 12.24
Reversal of the sign of G_z causes the magnetization helix to unwind, forming a field gradient echo.

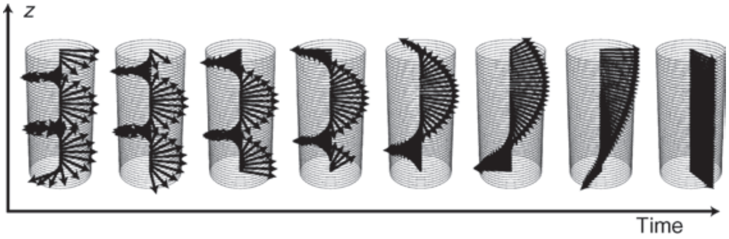

The right-hand frame in Figure 12.24 represents the gradient echo: all transverse magnetization components are restored with the same phase, so the bulk transverse magnetization reappears.

Note that the phase of the gradient echo (right-hand frame in Figure 12.24) is different from that of the initial state after the $\pi/2$ pulse (left-hand frame in Figure 12.23).This is due to the chemical shift evolution during the gradient periods. Chemical shift precession occurs in parallel with the evolution under the field gradient, and is not influenced by the sign of the gradient. Unlike pulsed spin echoes, gradient echoes do not refocus the evolution due to chemical shifts or other local field deviations.

Gradient echoes are a common motif in NMR imaging experiments. They are also used to measure the physical diffusion of molecules along the gradient axis (see Section 19.8).

12.5 Slice Selection

If a weak r.f. pulse is applied at the same time as a field gradient, NMR signals are selected from a set of volume elements that lie in a plane, perpendicular to the gradient axis. This is called *slice selection*.

Consider, for example, the following pulse sequence:

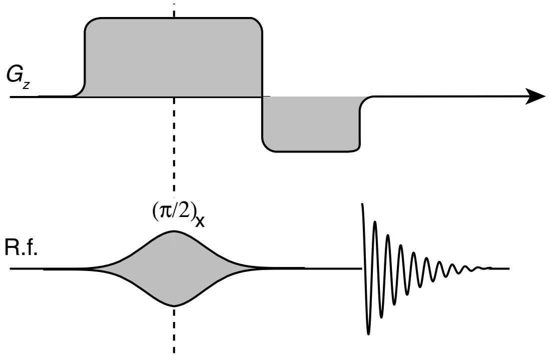

Figure 12.25
Pulse sequence for selecting NMR signals from a plane perpendicular to the z-axis.

The pulse sequence is similar to the gradient echo sequence in Figure 12.22, but there are three differences. First, the field gradient G_z is turned on *before* the r.f. pulse is applied, so that the centre of the r.f. pulse coincides with the centre of the positive gradient pulse (dashed line). Second, the r.f. pulse is not rectangular, but has a smooth amplitude profile. Third, the negative gradient pulse is only half the duration of the positive gradient pulse.

When the field gradient G_z is applied, the Larmor frequencies of the nuclei become dispersed along the z-axis. As a result, the r.f. pulse is only exactly resonant with nuclei at one position along the z-axis. At this position, the r.f. frequency is the same as the gradient-shifted Larmor frequency. For nuclei located at this value of z, the on-resonance $(\pi/2)_x$ pulse excites transverse magnetization along the rotating-frame $-y$-axis.

Now consider nuclei a short distance δz above the position of exact resonance. Spins at this point experience a resonance offset in the presence of the field gradient, given by

$$\Omega^0(\delta z) = -\gamma G_z \delta z$$

The effect of an off-resonance pulse is discussed in Section 10.8.5. Transverse magnetization will still be excited by the pulse, providing that the resonance offset is not too large compared with the nutation frequency ω_{nut}, which depends on the strength of the r.f. field. The width of the excited slice is therefore approximately equal to $2|\omega_{\text{nut}}/\gamma G_z|$. Strong r.f. fields and weak gradients excite a thick slice. Weak r.f. fields and strong gradients excite a thin slice. The smooth shaping of the r.f. pulse profile in Figure 12.25 optimizes the selectivity, giving rise to insignificant excitation of transverse magnetization outside the selected slice.

We must also consider the phase of the excited transverse magnetization. For nuclei that are exactly on-resonance with the pulse, the transverse magnetization is generated along the rotating frame $-y$-axis, as usual. But for nuclei that are slightly above or below the plane of exact resonance, the transverse magnetization is generated with a phase shift, as discussed in Section 10.8.5. This phase shift depends on the resonance offset, and hence on position along the z-axis. It may be shown that the phase shift is the same as that which would have arisen if the transverse magnetization had been generated instantaneously at the exact centre of the pulse (dashed line in Figure 12.25), and then allowed to precess in the presence of the field gradient. In order to obtain a significant NMR signal, the phase shift across the selected slice must be refocused by reversing the sign of the gradient. The gradient echo forms when the integral of the positive gradient, *measured from the centre of the pulse onwards*, is equal to the integral of the negative gradient. This is the configuration shown in Figure 12.25.

Figure 12.26 shows the evolution of the magnetization helix during the interval when a negative field gradient is applied. Note that the final transverse magnetization components come into phase at the end of the negative gradient pulse, and that the excited transverse magnetization originates in a region with a narrow range of z-coordinates.

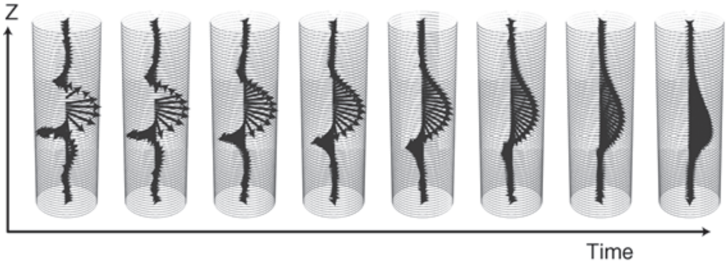

Figure 12.26
Formation of a gradient echo in the second half of a slice selection sequence.

12.6 NMR Imaging

NMR imaging is certainly the most visible form of NMR to the general public. Generally known as *magnetic resonance imaging* (MRI), it has reached most regions of the planet:

Figure 12.27
NMR imaging has become routine (a scene from southern India).

MRI is particularly useful in medicine, where it has become a routine diagnostic tool, especially for conditions of the brain, nervous system, and soft tissues of the body. Peter Mansfield and Paul Lauterbur were awarded the Nobel Prize in 2003 for their role in the early development of NMR imaging.

NMR imaging is based on a very simple insight: in the presence of a field gradient, the NMR spectrum maps the density of nuclear spins along the gradient axis. To see what this means, suppose that the sample is a long thin rod, oriented along the x-axis, perpendicular to the main magnetic field. Suppose also that the rod is made of some material that absorbs water, but that the distribution of water in the material is not uniform. The water is concentrated in two regions:

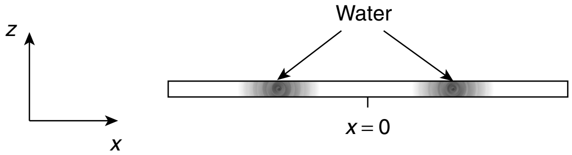

Figure 12.28
A thin rod containing two regions of high water density.

The density of the water may be described by a function $d(x)$, which in the case above has the following form:

Figure 12.29
The water density in the rod.

The centre of the rod is assumed to be the point $x = 0$.

Suppose now that a field gradient G_x is applied along the x-axis, using the coils and drivers described in Section 4.7. In the presence of the gradient, nuclear spins in the rod experience a total field that is given by the sum of the main magnetic field and the gradient field:

$$\mathbf{B} = (B^0 + G_x x)\,\mathbf{e}_z$$

(ignoring chemical shifts). Note that the gradient field and the main field are *both* along the z-axis. As described in Section 4.7, a gradient G_x does not describe a field along the x-axis, but instead a field along the z-axis that depends on the x-coordinate.[5]

In the presence of the gradient, the Larmor frequency of a spin is dependent on its position in space x, and is given by

$$\omega^0(x) = -\gamma(B^0 + G_x x) = \omega^0(0) - \gamma G_x x$$

where $\omega^0(0)$ is the Larmor frequency in the exact centre of the rod.

Suppose now that an NMR experiment is performed using a spectrometer reference frequency ω_{ref} equal to the Larmor frequency at the centre of the rod $\omega^0(0)$. The offset frequency of the spins is spatially dependent:

$$\Omega^0(x) = \omega^0(x) - \omega_{\text{ref}} = -\gamma G_x x$$

The important point is that the Larmor frequency depends in a very simple way on spatial position. Each part of the sample gives an NMR peak at a frequency that is directly proportional to the spatial coordinate of the precessing spins:

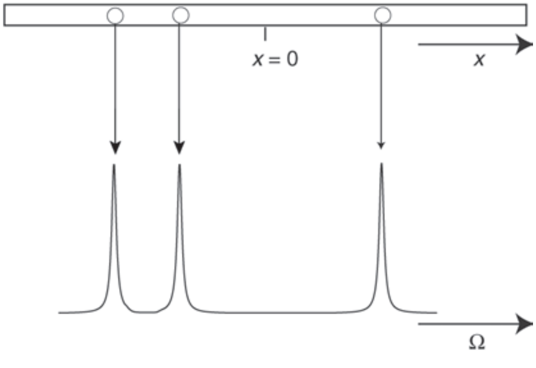

Figure 12.30
Mapping of spatial position on to spectral coordinate, for a field gradient along the x-axis.

(This is drawn for a negative gradient.)

This simple relationship between the frequency of a peak and the position in space works the other way round as well. If one obtains a peak at a frequency Ω, then this signal must originate from a point in space x_Ω, given by

$$\Omega = -\gamma G_x x_\Omega$$

and hence

$$x_\Omega = -\frac{\Omega}{\gamma G_x} \tag{12.7}$$

If the field gradient G_x is known, then one can work out from which part of the sample a given NMR signal comes from.

Now consider the NMR spectrum from the entire sample. All the peaks add up, and the more spins there are in a particular place, the more peaks add up at a particular point in the spectrum. As a result, the *total* spectral amplitude at a particular spectral coordinate Ω is directly proportional to the total spin density at the corresponding spatial coordinate x:

$$S(\Omega) \sim d(x_\Omega)$$

Here $d(x)$ is the spin density function, and x_Ω is the spatial coordinate corresponding to the offset frequency Ω, in the presence of the field gradient G_x.

The NMR spectrum is therefore a *map* of the spin density function $d(x)$:

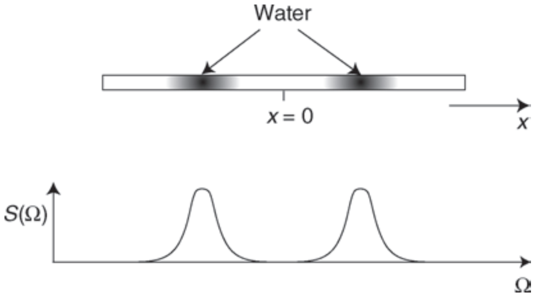

Figure 12.31
Mapping of spin density onto the NMR spectrum, for a field gradient along the x-axis.

The NMR spectrum in the presence of the gradient reveals directly the distribution of water in the rod.

In practice, most samples are not long thin rods. The above technique does not work very well for a sample of general shape, because there are many positions in the sample that have the same x-coordinate, and which give NMR peaks at the same place in the spectrum. The one-dimensional spectrum of the form gives the *projection* of the spin density along the x-axis, as illustrated below:

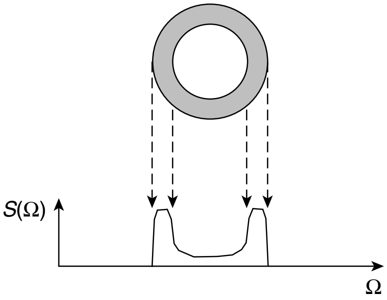

Figure 12.32
Projection of spin density on to the x-axis, for a ring-shaped sample.

The projection gives some clues about the spatial distribution of nuclear spins, but not the whole answer. Two objects may have very different spatial spin distributions, but still give the same projection along the *x*-axis:

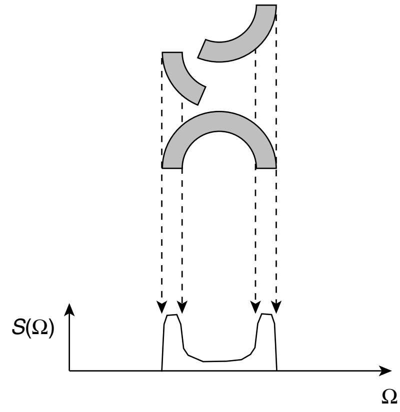

Figure 12.33
A different sample geometry that gives the same projection onto the *x*-axis.

To get more spatial information, the method has to be extended further, using the concept of two-dimensional spectroscopy (Section 5.9). Suppose that the sample is a flat pancake, oriented in the *xy*-plane:

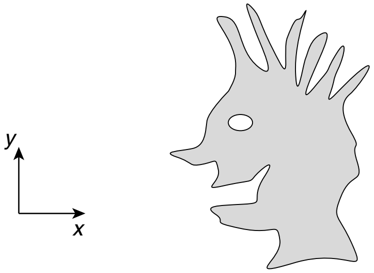

Figure 12.34
A pancake-shaped object in the *xy*-plane.

We wish to make an image of this flat object by NMR.
Consider the following pulse sequence:

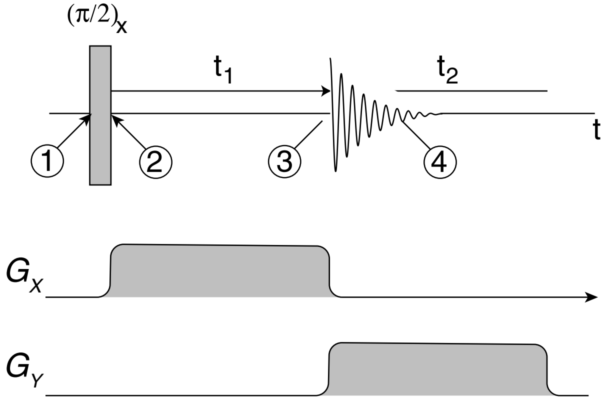

Figure 12.35
A two-dimensional NMR imaging pulse sequence.

After the initial $\pi/2$ pulse for exciting the spin coherences, there follows a variable evolution interval t_1 during which the gradient G_x is applied, and the magnetic field has the following form:

$$\mathbf{B} = (B^0 + G_x x)\,\mathbf{e}_z \qquad \text{(during } t_1\text{)}$$

At time point ③, the magnetic field gradient G_x is turned off, and the gradient G_y is turned on. The magnetic field has the following form during the signal acquisition interval t_2:

$$\mathbf{B} = (B^0 + G_y y)\,\mathbf{e}_z \qquad \text{(during } t_2\text{)}$$

The experiment is conducted in an arrayed fashion, with the interval t_1 taking a large set of values, so that a data matrix $s(t_1, t_2)$ is built up, in the fashion described in Section 5.6.

Consider first the NMR signal from just one point in the sample, with spatial coordinate (x, y):

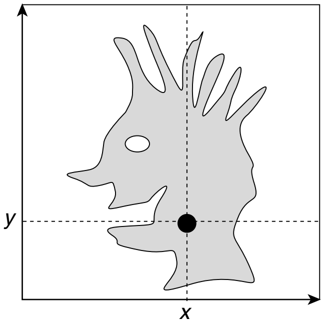

Figure 12.36
One point in the pancake-shaped object, with coordinates x and y.

The Larmor frequency of the spins is different in the two parts of the pulse sequence, because the external magnetic field is different. During the t_1 interval, the magnetic field gradient is along the x-axis, so the offset frequency during t_1 is given by

$$\Omega^0(1) = -\gamma G_x x \tag{12.8}$$

During the t_2 interval, the magnetic field gradient is along the z-axis, so the offset frequency during t_2 is given instead by

$$\Omega^0(2) = -\gamma G_y y \tag{12.9}$$

After the first $\pi/2$ pulse, the spin density operator at the point (x, y) is given as usual by

$$\hat{\rho}_{\textcircled{2}} = \frac{1}{2}\hat{1} - \frac{1}{2}\mathbb{B}\hat{I}_y$$

The observable (-1)-quantum coherence at this point is therefore

$$\rho_{\boxed{-}\textcircled{2}} = \frac{1}{4\mathrm{i}}\mathbb{B}$$

During the subsequent t_1 period, this coherence precesses at the frequency $\Omega^0(1)$, so that at time point ③ the coherence amplitude is

$$\rho_{\boxed{-}\textcircled{3}} = \frac{1}{4\mathrm{i}}\mathbb{B}\exp\{\left(\mathrm{i}\Omega^0(1) - \lambda\right) t_1\}$$

where λ is the inverse of T_2. The precession continues during the t_2 period, so that at time point ④ the coherence amplitude is

$$\rho_{\boxed{-}\textcircled{4}} = \frac{1}{4\mathrm{i}}\mathbb{B}\exp\{\left(\mathrm{i}\Omega^0(1) - \lambda\right) t_1 + \left(\mathrm{i}\Omega^0(2) - \lambda\right) t_2\}$$

The NMR signal is proportional to the amplitude of the (−1)-quantum coherence. The component of the two-dimensional NMR signal originating from a volume element at point (x, y) is therefore

$$s(t_1, t_2; x, y) \sim \exp\{\left(\mathrm{i}\Omega^0(1) - \lambda\right) t_1 + \left(\mathrm{i}\Omega^0(2) - \lambda\right) t_2\} \tag{12.10}$$

Now suppose that a two-dimensional FT is performed, as described in Section 5.9. The two-dimensional spectrum contains a peak at the frequency coordinates $(\Omega^0(1), \Omega^0(2))$:

$$S(\Omega_1, \Omega_2; x, y) \sim \mathcal{L}\,(\Omega_1, \Omega_2; \Omega^0(1), \lambda, \Omega^0(2), \lambda)$$

using the two-dimensional complex Lorentzian function defined in Equation 5.20.

Now from Equations 12.8 and 12.9, the frequency coordinates $\Omega^0(1)$ and $\Omega^0(2)$ are directly proportional to the spatial coordinates x and y. The position of the peak in the two-dimensional spectrum, therefore, maps directly onto the position of the spins in the spatial (x, y) plane:

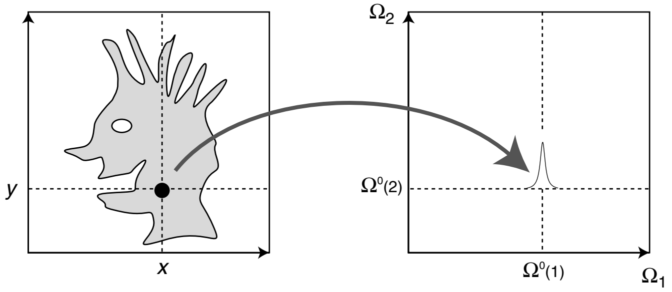

Figure 12.37
A point in the object gives a peak at the corresponding position in the two-dimensional spectrum.

A different point in the object generates a peak at a different position in the two-dimensional spectrum:

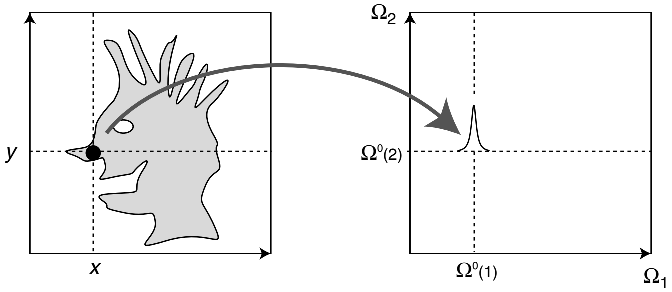

Figure 12.38
A different point in the object gives a peak at a different position in the two-dimensional spectrum.

(These sketches are for negative gradients G_x and G_y.)

In practice, all regions in the sample contribute simultaneously. The two-dimensional spectrum is a superposition of many two-dimensional peaks. The *total* amplitude at a certain point in the two-dimensional spectrum depends on how many spins are found at the corresponding point in real space, according to

$$S(\Omega_1, \Omega_2) \sim d(x_{\Omega_1}, y_{\Omega_2})$$

where $d(x, y)$ is the density of spins at point (x, y), and the coordinates x_{Ω_1} and y_{Ω_2} are given by

$$x_{\Omega_1} = -\frac{\Omega_1}{\gamma G_x} \qquad y_{\Omega_2} = -\frac{\Omega_2}{\gamma G_y}$$

by analogy to Equation 12.7.

The two-dimensional spectrum is therefore an *image* of the two-dimensional spin density:

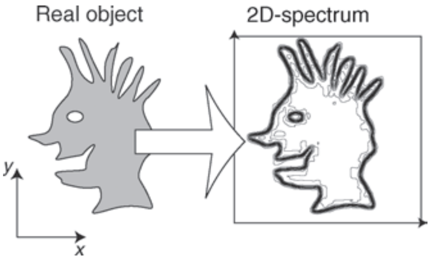

Figure 12.39
Mapping of a two-dimensional object onto a two-dimensional NMR spectrum (shown as a contour plot).

An image of a three-dimensional object may be constructed by performing a three-dimensional NMR experiment, using gradients along all three axes, followed by three-dimensional FT of the data matrix, as described in Section 5.10. Alternatively, a two-dimensional image of a slice through the object may be generated by the following pulse sequence:

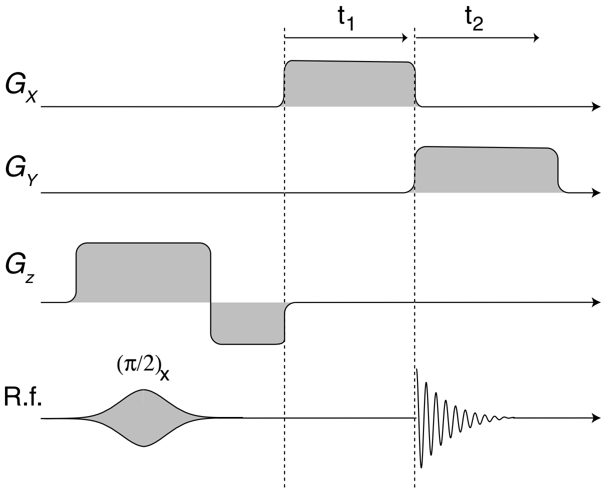

Figure 12.40
Pulse sequence for NMR imaging of a slice through a three-dimensional object, perpendicular to the z-axis.

This combines the two-dimensional pulse sequence of Figure 12.35 with the slice selection technique of Figure 12.25. The position and thickness of the slice along the z-axis is set by adjusting the r.f. pulse frequency and the amplitude of the G_z gradient.

Whereas an ordinary photograph (or an X-ray image) counts *photons*, an NMR image counts *protons*.

This discussion only scratches the surface of a very rich subject. The simple pulse sequences described above give relatively poor resolution and are susceptible to various instrumental imperfections. In practice, a whole array of more sophisticated procedures is available that gives better, faster, and more reliable performance (see *Further Reading*). Contrast is often enhanced by using pulse sequences that are sensitive to T_1 or T_2, as well as the spin density. It is also possible to produce images that contain signals only from spins in a *flowing* liquid, such as blood. One may also combine imaging with the other techniques described in this book to produce NMR spectra at certain points in the body, and hence follow the concentration of metabolites.

Three-dimensional NMR images are shown in Plate 3 and Plate 4.

An even more remarkable development is *functional NMR imaging* (fMRI), in which small differences in the brain NMR image are detected when mental processes are underway (see *Further Reading*). An example of fMRI is given in Plate 1. The mechanism of functional contrast in NMR imaging is believed to involve changes in blood flow, and the different magnetic susceptibilities of oxygenated and deoxygenated blood.

Notes

1. The effects of T_2 decay and inhomogeneous broadening are sometimes combined by using an 'effective T_2' parameter, usually denoted $T_2{}^*$, where $T_2{}^* \leq T_2$ (the asterisk does not indicate the complex conjugate in this case). The inhomogeneously broadened linewidth is given by $1/(\pi T_2{}^*)$ in units of hertz. Unlike T_2, the effective time constant $T_2{}^*$ has no fundamental significance and depends on the magnetic field homogeneity. Only the inhomogeneous contribution to $T_2{}^*$ is refocused by using a spin echo.

2. The spin echoes originally described by Hahn involved two $\pi/2$ pulses (see E. L. Hahn, *Phys. Rev.,* **80,** 580(1950)). However, this type of spin echo is relatively weak and difficult to use. The 'modern' type of spin echo, induced by a π pulse, was developed by Carr and Purcell (see H. Y. Carr, E. M. Purcell, *Phys. Rev.* **94,** 630(1954)). Despite this, π-pulse echoes are commonly called 'Hahn echoes'.

3. One occasionally finds a statement that the spin-locked magnetization does not decay to zero, but to a position of thermal equilibrium state along the spin-locking field, i.e. a value proportional to $\gamma B^{\mathrm{RF}}/k_B T$, where B^{RF} is the locking field and T is the temperature. This is not correct. The final state of the spin system is unrelated to thermal equilibrium, since the spin Hamiltonian is time dependent. The correct final value of the transverse magnetization is zero, assuming that the nutation frequency is large compared with the relaxation time constants.

4. The notation $T_{1\rho}$, and the term 'spin-lattice relaxation in the rotating frame' are unfortunate for the following reasons. First, exchange of energy with the lattice is *not* required for the $T_{1\rho}$ process. Second, the decay of spin-locked transverse magnetization is more closely related to T_2 than to T_1. Third, the use of a rotating reference frame is obviously irrelevant to a physical phenomenon such as the decay of magnetization. A more accurate term would be 'decay time constant for transverse magnetization in the presence of an r.f. field', with the suggested notation $T_2{}^{\mathrm{RF}}$.

5. The fields created by the gradient coils also have components in the x- and y-directions. These transverse field components are unimportant in practice, because of the dominating effect of the main magnetic field (compare Section 9.1.7).

Further Reading

- For more on spin echoes, see R. Freeman, *Spin Choreography. Basic Steps in High Resolution NMR*, Spektrum, Oxford, 1997, and J. Keeler, *Understanding NMR Spectroscopy*, Wiley, Chichester, 2005.
- For the theory of $T_{1\rho}$, see T. E. Bull, *Prog. NMR Spectrosc.* **24**, 377–410 (1992).
- NMR imaging is an enormous field. For an early review, see P. Mansfield and P. G. Morris, 'NMR imaging in biomedicine', *Adv. Magn. Reson. Suppl. 2*, (1982).
  For later material, see the many entries in D. M. Grant and R. K. Harris (eds), *Encyclopedia of Nuclear Magnetic Resonance*, Wiley, 1996.
- For the applications of imaging to small objects, see P. T. Callaghan, *Principles of Nuclear Magnetic Resonance Microscopy*, Clarendon Press, Oxford, 1991.
- For a theoretical treatment of selected imaging methodologies, see the appropriate chapter of R. R. Ernst, G. Bodenhausen, A. Wokaun, *Principles of Nuclear Magnetic Resonance in One and Two Dimensions*, Clarendon Press, Oxford, 1987.
- For the mechanism and examples of functional NMR imaging, see S. A. Huettel, A. W. Song and G. McCarthy, *Functional Magnetic Resonance Imaging*, Sinauer, Sunderland, USA, 2004.

Exercises

12.1 The amplitudes of two peaks in an inversion-recovery experiment depend on the interval τ as shown in the following table:

τ/s	Amplitude of peak 1	Amplitude of peak 2
0	−0.96	−0.96
1	−0.18	−0.67
2	0.30	−0.37
3	0.60	−0.11
4	0.69	0.10
5	0.84	0.27
6	0.88	0.41
7	0.92	0.55
8	1.00	0.61
9	1.00	0.72
10	0.98	0.78

Estimate the value of T_1 for each peak.

12.2 This exercise illustrates the measurement of *flow* by NMR. An NMR probe is equipped with special field coils, which slightly enhance the magnetic field along the z-axis for spatial positions $x < 0$, and which slightly decrease the magnetic field along the z-axis for spatial positions $x > 0$. A pipe containing a flowing liquid is mounted in the probe, with the liquid flowing along the x-axis:

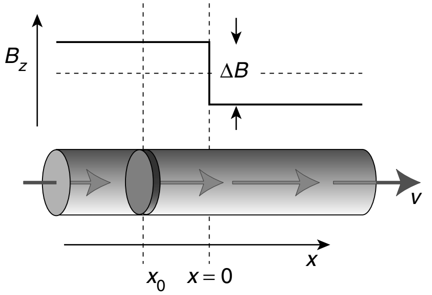

The flow velocity is $v\,\mathrm{m\,s^{-1}}$. We follow the proton NMR signals from a plug of liquid, positioned initially at x_0. One may imagine that only the plug of liquid contains protons, the rest of the fluid being non-protonated. Suppose that the difference in magnetic field for positive and negative values of x is equal to ΔB.

A spin echo sequence $(\pi/2)_x - \tau/2 - \pi_y - \tau/2 -$ (acquire signal) is applied to the flowing sample. The plug of liquid has position x_0 at the beginning of the pulse sequence (the diagram shows a negative value of x_0).

Calculate the *phase* of the NMR signals at the end of the pulse sequence in the following cases:

(i) x_0 is positive, so that the plug of liquid does not cross the line $x = 0$ during the pulse sequence.
(ii) x_0 satisfies $-v\tau/2 < x_0 < 0$, so that the plug crosses the line $x = 0$ before the π pulse arrives.
(iii) x_0 satisfies $-v\tau < x_0 < -v\tau/2$, so that the plug crosses the line $x = 0$ after the π pulse arrives.
(iv) x_0 satisfies $x_0 < -v\tau$, so that the plug of liquid does not cross the line $x = 0$ before signal acquisition.

13 Quadrupolar Nuclei

Nuclei with spin $I > 1/2$ have an electric quadrupole moment. Quadrupolar nuclear isotopes are widely distributed throughout the periodic table, and include many important elements that lack spin-1/2 isotopes, such as the alkali metals. The NMR of quadrupolar nuclei offers many theoretical and practical challenges, due to the strong interactions between the nuclear electric quadrupole moments and the local electric field gradients that are present in many substances. This chapter only scratches the surface of a very rich subject.

13.1 Spin $I = 1$

The only natural spin $I = 1$ nuclei are ^{2}H, ^{14}N and ^{6}Li (see Plate B).

Although nitrogen is a very important element, and ^{14}N is 99.6% abundant, NMR experiments on ^{14}N nuclei are seldom performed. This is because ^{14}N often experiences considerable electric field gradients, giving rise to coupling constants C_Q of many megahertz. The large quadrupolar interactions and relatively low gyromagnetic ratio makes ^{14}N a difficult NMR nucleus in most circumstances.[1]

Deuterium (^{2}H), in contrast, has a very low natural abundance (0.012%), but a low electric quadrupolar moment. Since it is often relatively easy and inexpensive to enrich materials in ^{2}H, and the low value of Q leads to rather small nuclear quadrupolar interactions, deuterium NMR is very popular, especially in the NMR of solids and liquid crystals.

The quadrupolar coupling constant C_Q for ^{2}H depends strongly on the local electronic environment and on internal molecular motion. For ^{2}H nuclei in CD groups, attached to rigid parts of the molecule, the quadrupolar coupling constant is typically around $C_Q = 130\,\text{kHz}$. The quadrupole coupling can be considerably reduced in the presence of internal molecular motions. For example, ^{2}H nuclei in rapidly rotating ND_3^+ groups have a typical quadrupolar coupling constant of around 50 kHz. The quadrupole coupling tensor may become strongly biaxial ($\eta_Q \neq 0$) if the local molecular motion lacks symmetry. The sensitivity of ^{2}H spectra to the symmetry and time-scale of molecular motion is one of the informative and useful features of solid-state ^{2}H NMR.

NMR experiments on ^{6}Li are uncommon, since the spin-3/2 isotope ^{7}Li is more abundant and has a larger gyromagnetic ratio.

13.1.1 Spin-1 states

A spin-1 nucleus I has three eigenstates of angular momentum along the z-axis, denoted by the kets $|1, M\rangle$ where the quantum number M is equal to $+1$, 0, or -1. These Zeeman eigenstates have the properties given in Section 7.9:

$$\begin{aligned} \hat{I}_z|1, M\rangle &= M|1, M\rangle \\ \hat{I}^2|1, M\rangle &= I(I+1)|1, M\rangle = 2|1, M\rangle \end{aligned} \tag{13.1}$$

Spin Dynamics: Basics of Nuclear Magnetic Resonance, Second Edition Malcolm H. Levitt

where $\hat{I}^2 = \hat{I}_x^2 + \hat{I}_y^2 + \hat{I}_z^2$.

In general, the quantum state of a spin-1 nucleus is a *superposition* of all three Zeeman eigenstates, as follows:

$$|\psi\rangle = c_1|1, +1\rangle + c_0|1, 0\rangle + c_{-1}|1, -1\rangle$$

where the coefficients $\{c_1, c_0, c_{-1}\}$ are complex numbers.[2] The same state may be written in column vector form:

$$|\psi\rangle = \begin{pmatrix} c_1 \\ c_0 \\ c_{-1} \end{pmatrix}$$

The 'bra' state is the adjoint of the 'ket' state:

$$\langle\psi| = (c_1{}^*, \quad c_0{}^*, \quad c_{-1}{}^*)$$

The normalization condition is as follows:

$$\langle\psi|\psi\rangle = |c_1|^2 + |c_0|^2 + |c_{-1}|^2 = 1$$

13.1.2 Spin-1 energy levels

In the presence of a strong external magnetic field B^0 along the z-axis, a spin-1 nucleus experiences a Zeeman Hamiltonian of the usual form:

$$\boxed{\widehat{\mathcal{H}}^0 = \omega^0 \hat{I}_z \qquad (13.2)}$$

where the nuclear Larmor frequency is given by

$$\omega^0 = -\gamma B^0(1 + \delta)$$

and δ is the chemical shift. The states $|1, M\rangle$ are energy eigenstates in the presence of the field B^0:

$$\widehat{\mathcal{H}}^0|1, M\rangle = M\omega^0|1, M\rangle$$

The energy-level diagram for a spin-1 nucleus I, therefore, has three energy levels, spaced evenly by ω^0 in natural units, if the quadrupole interaction is ignored:

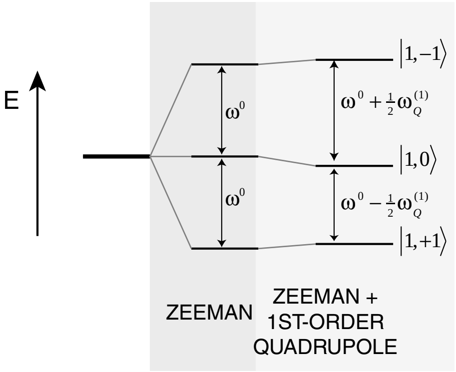

Figure 13.1
Energy levels of a spin-1 nucleus.

If the nuclear environment is anisotropic after motional averaging, the spin Hamiltonian is equal to the sum of the Zeeman and quadrupole coupling terms:

$$\widehat{\mathcal{H}} = \widehat{\mathcal{H}}^0 + \widehat{\mathcal{H}}_Q^{(1)} + \widehat{\mathcal{H}}_Q^{(2)} + \ldots \tag{13.3}$$

where the first-order quadrupolar Hamiltonian is given by

$$\boxed{\begin{aligned}\widehat{\mathcal{H}}_Q^{(1)} &= \omega_Q^{(1)} \times \frac{1}{6}\left(3\hat{I}_z^2 - I(I+1)\widehat{1}\right)\\ &= \omega_Q^{(1)} \times \frac{1}{6}\left(3\hat{I}_z^2 - 2 \times \widehat{1}\right) \qquad \text{(for spin } I = 1\text{)}\end{aligned}} \tag{13.4}$$

and the first-order quadrupolar coupling $\omega_Q^{(1)}$ is given in the general case by Equation 9.23. The first-order quadrupolar coupling $\omega_Q^{(1)}$ depends on the nuclear quadrupole moment, the electronic environment of the nucleus, the phase of matter, and the molecular orientation, as described in Section 9.2.

The series in Equation 13.3 may be truncated after the first term, if the quadrupolar coupling constant $C_Q = e^2qQ/h$ is much smaller in magnitude than the Larmor frequency ω^0. This is usually a good approximation for ^{2}H.

In solids, the first-order quadrupolar coupling is given in terms of the quadrupolar coupling constant C_Q by

$$\boxed{\begin{aligned}\omega_Q^{(1)}(\theta_Q) &= \frac{3\pi C_Q}{2I(2I-1)} \times \left(3\cos^2\theta_Q - 1\right)\\ &= 3\pi C_Q \times \frac{1}{2}\left(3\cos^2\theta_Q - 1\right) \qquad \text{(for spin } I = 1\text{)}\end{aligned}} \tag{13.5}$$

assuming a uniaxial electric field gradient tensor ($\eta_Q = 0$). Here, θ_Q is the angle between the major principal axis of the electric field gradient tensor and the magnetic field.

The Zeeman eigenstates are eigenstates of the first-order quadrupolar Hamiltonian:

$$\begin{aligned}\widehat{\mathcal{H}}_Q^{(1)}|1, +1\rangle &= +\frac{1}{6}\omega_Q^{(1)}|1, +1\rangle\\ \widehat{\mathcal{H}}_Q^{(1)}|1, 0\rangle &= -\frac{1}{3}\omega_Q^{(1)}|1, 0\rangle\\ \widehat{\mathcal{H}}_Q^{(1)}|1, -1\rangle &= +\frac{1}{6}\omega_Q^{(1)}|1, -1\rangle\end{aligned}$$

A positive quadrupolar coupling $\omega_Q^{(1)}$ shifts the states $|1, \pm 1\rangle$ up in energy, whereas the central state $|1, 0\rangle$ shifts down in energy by twice as much. All shifts are in the opposite direction if $\omega_Q^{(1)}$ is negative.

13.1.3 Spin-1 density matrix

Suppose now that the sample contains an ensemble of isolated spins-1. The *density operator* technique introduced in Chapter 11 may be used to describe the quantum state of the entire spin-1 ensemble. The density operator contains enough information to calculate the expectation values of all spin observables.

The density operator of the spin-1 ensemble may be written as follows:

$$\hat{\rho} = \overline{|\psi\rangle\langle\psi|}$$

where the overbar denotes an ensemble average. For a spin-1 ensemble, the matrix representation of the density operator (the *density matrix*) is a 3 × 3 complex matrix of the following form:

$$\hat{\rho} = \begin{pmatrix} \overline{c_1{}^* c_1} & \overline{c_1{}^* c_0} & \overline{c_1{}^* c_{-1}} \\ \overline{c_0{}^* c_1} & \overline{c_0{}^* c_0} & \overline{c_0{}^* c_{-1}} \\ \overline{c_{-1}{}^* c_1} & \overline{c_{-1}{}^* c_0} & \overline{c_{-1}{}^* c_{-1}} \end{pmatrix}$$

Each element of the density matrix is given by a product of superposition coefficients for a pair of spin states, averaged over the ensemble.

Populations appear on the diagonal of the density operator, and are denoted in this book by the following symbols:

$$\begin{aligned} \rho_{|+1\rangle} &= \overline{c_1{}^* c_1} \\ \rho_{|0\rangle} &= \overline{c_0{}^* c_0} \\ \rho_{|-1\rangle} &= \overline{c_{-1}{}^* c_{-1}} \end{aligned}$$

The populations are often represented by 'little balls' sitting on the energy levels:

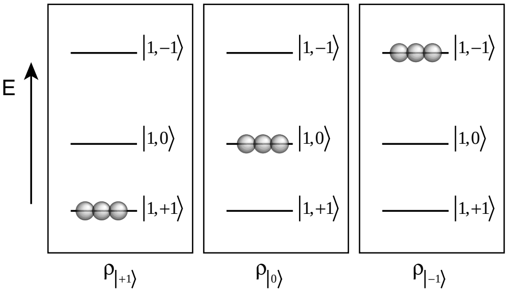

Figure 13.2
State populations for an ensemble of spins-1.

The three populations $\rho_{|+1\rangle}$, $\rho_{|0\rangle}$ and $\rho_{|-1\rangle}$ of the spin-1 ensemble are analogous to the two populations $\rho_{\boxed{\alpha}}$ and $\rho_{\boxed{\beta}}$ of the spin-1/2 ensemble. The three spin-1 populations sum to unity:

$$\rho_{|+1\rangle} + \rho_{|0\rangle} + \rho_{|-1\rangle} = 1$$

The off-diagonal density matrix elements are called *coherences*. The spin-1 ensemble supports six coherences, instead of two for the spin-1/2 ensemble. The coherences are represented by arrows linking a pair of energy levels:

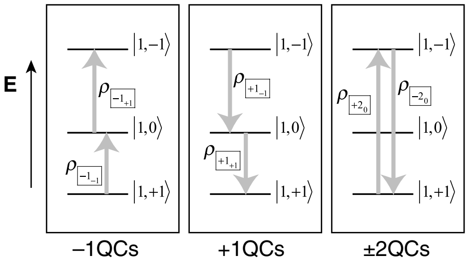

Figure 13.3
Coherences for an ensemble of spins-1.

In this book, the coherences of quadrupolar nuclei are denoted as follows:

$$\langle I, M_r|\hat{\rho}|I, M_s\rangle = \rho_{\boxed{{p_{rs}}_{q_{rs}}}} \tag{13.6}$$

The subscript p_{rs} denotes the *coherence order*, which is equal to the *difference* in Zeeman quantum numbers M for the connected states (see Section 11.2.4). The sub-subscript q_{rs} is called the *satellite order*, and is equal to the difference in the *squares* of the Zeeman quantum numbers M for the connected states:[3]

$$\begin{aligned} p_{rs} &= M_r - M_s \\ q_{rs} &= M_r^2 - M_s^2 \end{aligned} \tag{13.7}$$

The spin-1 ensemble supports two (-1)-quantum coherences, which connect states differing in angular momentum by -1 unit:

$$\begin{aligned} \rho_{\boxed{-1_{-1}}} &= \overline{c_0{}^*c_1} \\ \rho_{\boxed{-1_{+1}}} &= \overline{c_{-1}{}^*c_0} \end{aligned} \tag{13.8}$$

These are analogous to the (-1)-quantum coherence $\rho_{\boxed{-}}$ of the spin-1/2 ensemble.

Similarly, there are two $(+1)$-quantum coherences, which connect states differing in angular momentum by $+1$ unit:

$$\begin{aligned} \rho_{\boxed{+1_{+1}}} &= \overline{c_1{}^*c_0} \\ \rho_{\boxed{+1_{-1}}} &= \overline{c_0{}^*c_{-1}} \end{aligned} \tag{13.9}$$

These are analogous to the $(+1)$-quantum coherence $\rho_{\boxed{+}}$ of the spin-1/2 ensemble.

The spin-1 density matrix may also contain *double-quantum coherences*, which have quantum order $p = \pm 2$ and satellite order $q = 0$:

$$\begin{aligned} \rho_{\boxed{-2_0}} &= \overline{c_{-1}{}^*c_1} \\ \rho_{\boxed{+2_0}} &= \overline{c_1{}^*c_{-1}} \end{aligned} \tag{13.10}$$

These double-quantum coherences have no direct analogy in the ensemble of isolated spins-1/2.

The density matrix may be written, using the notation above:

$$\hat{\rho} = \begin{pmatrix} \rho_{|+1\rangle} & \rho_{\boxed{+1_{+1}}} & \rho_{\boxed{+2_0}} \\ \rho_{\boxed{-1_{-1}}} & \rho_{|0\rangle} & \rho_{\boxed{+1_{-1}}} \\ \rho_{\boxed{-2_0}} & \rho_{\boxed{-1_{+1}}} & \rho_{|-1\rangle} \end{pmatrix}$$

13.1.4 Coherence evolution

Suppose that a particular spin-1 density operator exists at a time point t_a. We wish to predict the spin density operator at a later time $t_b = t_a + \tau$, where the two time points are separated by an interval τ of free evolution, in the absence of applied r.f. fields:

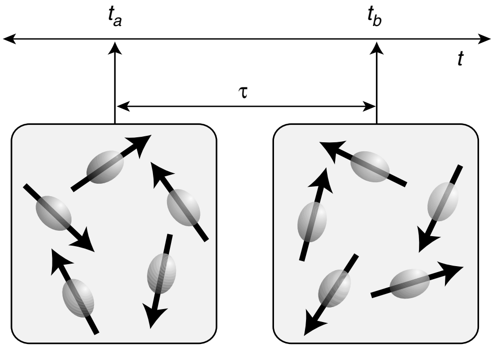

Figure 13.4 Free evolution of a spin-1 ensemble over an interval τ.

If spin–lattice relaxation is ignored, and no r.f. field is applied, then the populations do not change:

$$\begin{aligned} \rho_{|+1\rangle}(t_\mathrm{b}) &\cong \rho_{|+1\rangle}(t_\mathrm{a}) \\ \rho_{|0\rangle}(t_\mathrm{b}) &\cong \rho_{|0\rangle}(t_\mathrm{a}) \\ \rho_{|-1\rangle}(t_\mathrm{b}) &\cong \rho_{|-1\rangle}(t_\mathrm{a}) \end{aligned}$$

The coherences, on the other hand, oscillate at the energy level differences of the connected states, as described in Section 11.7. The rotating-frame frequencies of all six coherences in the spin-1 ensemble are as follows:

$$\boxed{\begin{aligned} \Omega_{\boxed{-1_{-1}}} &= \Omega^0 + \frac{1}{2}\omega_\mathrm{Q}^{(1)} \\ \Omega_{\boxed{-1_{+1}}} &= \Omega^0 - \frac{1}{2}\omega_\mathrm{Q}^{(1)} \\ \Omega_{\boxed{+1_{+1}}} &= -\Omega^0 - \frac{1}{2}\omega_\mathrm{Q}^{(1)} \\ \Omega_{\boxed{+1_{-1}}} &= -\Omega^0 + \frac{1}{2}\omega_\mathrm{Q}^{(1)} \\ \Omega_{\boxed{-2_{0}}} &= 2\Omega^0 \\ \Omega_{\boxed{+2_{0}}} &= -2\Omega^0 \end{aligned}} \tag{13.11}$$

where the chemical shift offset frequency is given by

$$\boxed{\Omega^0 = -\gamma B^0(\delta - \delta_\mathrm{ref})} \tag{13.12}$$

as in the spin-1/2 case. Here, δ is the chemical shift and δ_ref is the chemical shift corresponding to the spectrometer reference frequency.

For example, the (−1)-quantum coherences evolve as follows:

$$\begin{aligned} \rho_{\boxed{-1_{-1}}}(t_\mathrm{b}) &= \rho_{\boxed{-1_{-1}}}(t_\mathrm{a}) \exp\{(\mathrm{i}\Omega_{\boxed{-1_{-1}}} - \lambda)\tau\} \\ \rho_{\boxed{-1_{+1}}}(t_\mathrm{b}) &= \rho_{\boxed{-1_{+1}}}(t_\mathrm{a}) \exp\{(\mathrm{i}\Omega_{\boxed{-1_{+1}}} - \lambda)\tau\} \end{aligned}$$

where the decay constant $\lambda = T_2{}^{-1}$ takes into account the homogeneous decay. From Equation 13.11, the evolution frequencies of the two (-1)-quantum coherences differ by the first-order quadrupolar interaction $\omega_Q^{(1)}$.

Note that the double-quantum frequencies $\rho_{\boxed{-2_0}}$ and $\rho_{\boxed{+2_0}}$ are independent of the first-order quadrupolar interaction. This is because the first-order quadrupolar interaction shifts the energies of the $|1, \pm 1\rangle$ states by the same amount in the same direction (see Figure 13.1).

13.1.5 Observable coherences and NMR spectrum

As described in Appendix A.5, quadrature detection provides a complex NMR signal given by

$$s(t) \sim 2\mathrm{i}\langle \hat{I}^+ \rangle \exp\{-\mathrm{i}\phi_{\mathrm{rec}}\} \tag{13.13}$$

where ϕ_{rec} is the receiver phase. The spin-1 matrix representation of the shift operator $\hat{I}^+$ is given in Section 7.9, as follows:

$$\hat{I}^+ = \begin{pmatrix} 0 & \sqrt{2} & 0 \\ 0 & 0 & \sqrt{2} \\ 0 & 0 & 0 \end{pmatrix}$$

The NMR signal may be evaluated in terms of the coherence amplitudes by using $\langle \hat{I}^+ \rangle = \mathrm{Tr}\{\hat{I}^+ \hat{\rho}\}$. This gives the following expression:

$$s(t) \sim 2\mathrm{i}\sqrt{2} \exp\{-\mathrm{i}\phi_{\mathrm{rec}}\} \left(\rho_{\boxed{-1_{-1}}}(t) + \rho_{\boxed{-1_{+1}}}(t) \right) \qquad \text{(for spin } I = 1) \tag{13.14}$$

From this we see that the two (-1)-quantum coherences contribute equally to the spin-1 NMR signal, providing that they have the same amplitude.

The populations, the $(+1)$-quantum coherences, and the (± 2)-quantum coherences do not give rise to detectable NMR signals.[4] This does not imply, of course, that these density matrix elements are unimportant. They may give rise to NMR signals later on, if they are transformed into detectable (-1)-quantum coherences by subsequent pulses.

If the NMR signal from a spin-1 ensemble is collected as a function of time variable t, and Fourier transformed, the result is an NMR spectrum containing two Lorentzian peaks:

$$\begin{aligned} S(\Omega) &= a_{\boxed{-1_{-1}}} \mathcal{L}(\Omega; \Omega_{\boxed{-1_{-1}}}, \lambda) + a_{\boxed{-1_{+1}}} \mathcal{L}(\Omega; \Omega_{\boxed{-1_{+1}}}, \lambda) \\ &= a_{\boxed{-1_{-1}}} \mathcal{L}(\Omega; \Omega^0 + \frac{1}{2}\omega_Q^{(1)}, \lambda) + a_{\boxed{-1_{+1}}} \mathcal{L}(\Omega; \Omega^0 - \frac{1}{2}\omega_Q^{(1)}, \lambda) \end{aligned} \tag{13.15}$$

where the Lorentzian functions are defined in Equation 5.12. The peak amplitudes are proportional to the (-1)-quantum coherences existing at the beginning of the detection interval:

$$\begin{aligned} a_{\boxed{-1_{-1}}} &= 2\mathrm{i}\sqrt{2} \exp\{-\mathrm{i}\phi_{\mathrm{rec}}\} \rho_{\boxed{-1_{-1}}}(0) \\ a_{\boxed{-1_{+1}}} &= 2\mathrm{i}\sqrt{2} \exp\{-\mathrm{i}\phi_{\mathrm{rec}}\} \rho_{\boxed{-1_{+1}}}(0) \end{aligned} \tag{13.16}$$

The NMR spectrum generated by a spin-1 ensemble is therefore a *doublet* with a splitting of $\omega_Q^{(1)}$, with each peak corresponding to one of the (-1)-quantum coherences. If the amplitudes $a_{\boxed{-1_{\pm 1}}}$ are real numbers, then the two peaks are in the absorption phase, as illustrated below:

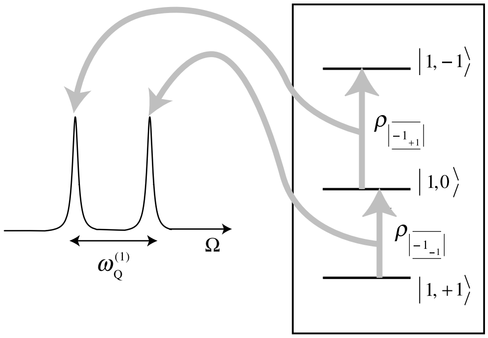

Figure 13.5
Each (−1)-quantum coherence in a spin-1 ensemble gives rise to a spectral peak.

13.1.6 Thermal equilibrium

In thermal equilibrium, the density matrix contains populations given by the Boltzmann distribution, and no coherences. If the temperature is high compared with the Zeeman splitting and the Zeeman splitting is much larger than the quadrupolar interaction, then the thermal equilibrium populations may be calculated according to the technique in Section 11.3. This leads to the following equilibrium spin-1 populations:

$$\rho_{|+1\rangle} \cong \frac{1}{3}(1+\mathbb{B}) \qquad \rho_{|0\rangle} \cong \frac{1}{3} \qquad \rho_{|-1\rangle} \cong \frac{1}{3}(1-\mathbb{B})$$

where the Boltzmann factor $\mathbb{B}$ is given in Equation 11.16. Since $\mathbb{B}$ is very small, this represents a tiny excess of population in the lower $|1,+1\rangle$ state and a tiny deficit of population in the upper $|1,-1\rangle$ state:

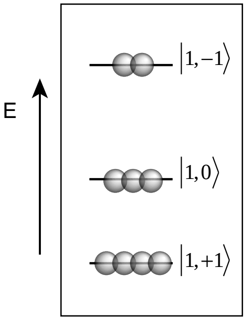

Figure 13.6
Thermal equilibrium state for an ensemble of spins-1 (the population differences are greatly exaggerated).

The thermal equilibrium spin density operator is therefore given by

$$\hat{\rho}^{\mathrm{eq}} = \frac{1}{3}\hat{1} + \frac{1}{3}\mathbb{B}\hat{I}_z \tag{13.17}$$

13.1.7 Strong radio-frequency pulse

Suppose that a strong r.f. pulse of phase ϕ_p and duration τ_p is applied to an ensemble of spins-1. We wish to calculate the spin density operator at time point ② after the pulse, if it is known at time point ① before the pulse:

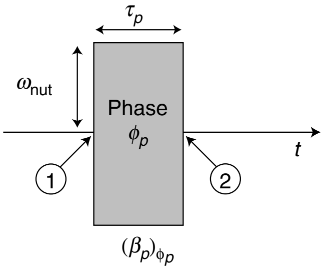

Figure 13.7
R.f. pulse applied to a spin-1 ensemble.

The rotating-frame spin Hamiltonian during the pulse is given by

$$\widehat{\mathcal{H}}_{\text{p}} = \widehat{\mathcal{H}}_{\text{int}} + \omega_{\text{nut}}(\hat{I}_x \cos\phi_{\text{p}} + \hat{I}_y \sin\phi_{\text{p}}) \tag{13.18}$$

where the nutation frequency ω_{nut} is proportional to the strength of the resonant r.f. field component, as in Equation 10.25:

$$\boxed{\omega_{\text{nut}} = |\tfrac{1}{2}\gamma B^{\text{RF}} \sin\theta_{\text{RF}}| \tag{13.19}}$$

$\widehat{\mathcal{H}}_{\text{int}}$ is the internal spin Hamiltonian in the rotating reference frame:

$$\widehat{\mathcal{H}}_{\text{int}} = \Omega^0 \hat{I}_z + \widehat{\mathcal{H}}_{\text{Q}}$$

It can be difficult to treat the evolution of the spin system under the Hamiltonian in Equation 13.18, since the internal and external parts of the Hamiltonian may have similar magnitudes and do not commute with each other. However, the problem becomes much simpler to handle in the *strong pulse limit*. This requires that the interaction with the r.f. field is much stronger than the chemical shifts and the first-order quadrupolar interaction:

$$\boxed{|\omega_{\text{nut}}| >> |\Omega^0|, |\omega_{\text{Q}}^{(1)}| \tag{13.20}}$$

The 'strong pulse' condition in Equation 13.20 requires either a small quadrupolar interaction, or a very strong r.f. field.

The strong pulse condition is usually difficult to satisfy for ^{14}N, due to the very large quadrupole interaction. The rest of this section, therefore, mainly concerns ^{2}H NMR, where the strong pulse condition is often satisfied to a good approximation.

In the strong pulse limit, the internal spin Hamiltonian may be ignored during the r.f. pulse, so the rotating-frame spin Hamiltonian during the pulse is given by

$$\widehat{\mathcal{H}}_{\text{p}} \cong \omega_{\text{nut}}(\hat{I}_x \cos\phi_{\text{p}} + \hat{I}_y \sin\phi_{\text{p}})$$

The nuclear spin states, therefore, are transformed by the pulse as follows:

$$|\psi\rangle_{②} = \widehat{R}_{\phi_{\text{p}}}(\beta_{\text{p}})|\psi\rangle_{①}$$

where $|\psi\rangle_{①}$ is the spin state before the pulse, $|\psi\rangle_{②}$ is the spin state after the pulse, and the *flip angle* is given by

$$\boxed{\beta_{\text{p}} = \omega_{\text{nut}}\tau_{\text{p}} \tag{13.21}}$$

where τ_{p} is the pulse duration, and $\widehat{R}_{\phi_{\text{p}}}(\beta_{\text{p}})$ is a rotation operator, as described in Section 10.8.

The spin density operator, which describes the state of the entire spin-1 ensemble, is transformed according to the sandwich equation (see Section 11.6).

$$\hat{\rho}_{\textcircled{2}} = \widehat{R}_{\phi_\mathrm{p}}(\beta_\mathrm{p})\,\hat{\rho}_{\textcircled{1}}\,\widehat{R}_{\phi_\mathrm{p}}(\beta_\mathrm{p})^\dagger$$

Here, $\hat{\rho}_{\textcircled{1}}$ is the density operator before the pulse and $\hat{\rho}_{\textcircled{2}}$ is the density operator after the pulse. The action of a sufficiently strong r.f. pulse on a spin-1 ensemble has exactly the same mathematical form as for spins-1/2.

13.1.8 Excitation of coherence

We can now calculate what happens if a pulse with flip angle $\beta_\mathrm{p} = \pi/2$ and phase $\phi_\mathrm{p} = 0$ is applied to a spin-1 ensemble in thermal equilibrium. From Equation 13.17, the density operator after the pulse is given by

$$\hat{\rho}_{\textcircled{2}} = \frac{1}{3}\hat{1} + \frac{1}{3}\mathbb{B}\widehat{R}_x(\pi/2)\hat{I}_z\widehat{R}_x(\pi/2)^\dagger = \frac{1}{3}\hat{1} - \frac{1}{3}\mathbb{B}\hat{I}_y$$

The operator matrix representations in Section 7.9 may be used to write this in the following form:

$$\hat{\rho}_{\textcircled{2}} = \frac{1}{3}\begin{pmatrix} 1 & \mathrm{i}\frac{1}{\sqrt{2}}\mathbb{B} & 0 \\ -\mathrm{i}\frac{1}{\sqrt{2}}\mathbb{B} & 1 & \mathrm{i}\frac{1}{\sqrt{2}}\mathbb{B} \\ 0 & -\mathrm{i}\frac{1}{\sqrt{2}}\mathbb{B} & 1 \end{pmatrix} \tag{13.22}$$

This shows that the $\pi/2$ pulse transforms the thermal population difference between the Zeeman states into (±1)-quantum coherences:

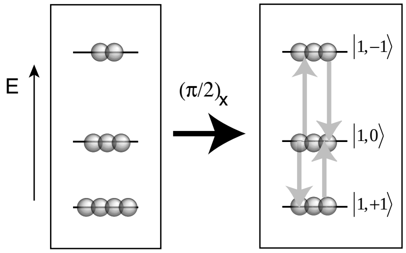

Figure 13.8
Excitation of (±1)-quantum coherences in a spin-1 ensemble by a $\pi/2$ pulse applied to a thermal equilibrium state.

Spins-1 behave in much the same way as spins-1/2. The main difference is that *two* pairs of (±1)-quantum coherences are excited by the pulse, instead of one in the spin-1/2 case. The amplitudes of the two (-1)-quantum coherences at the end of the pulse are given by

$$\rho_{\boxed{-1_{-1}}}\textcircled{2} = \rho_{\boxed{-1_{+1}}}\textcircled{2} = -\mathrm{i}\frac{1}{3\sqrt{2}}\mathbb{B} \tag{13.23}$$

Note that only (±1)-quantum coherences are excited by the strong pulse applied to a thermal equilibrium spin-1 ensemble. Double-quantum coherences are not excited:

$$\rho_{\boxed{-2_0}}\textcircled{2} = \rho_{\boxed{+2_0}}\textcircled{2} = 0$$

13.1.9 NMR spectrum

Suppose that the NMR signal is acquired immediately after the pulse, using receiver phase $\phi_\mathrm{rec} = 0$.

FT of the NMR signal provides the NMR spectrum, which consists of two Lorentzian peaks, at frequencies $\Omega^0 \pm \frac{1}{2}\omega_Q^{(1)}$, as described in Equation 13.15. The amplitudes of the peaks may be calculated by combining Equations 13.16 and 13.23, in the case $\phi_{\text{rec}} = 0$:

$$a_{\boxed{-1_{-1}}} = a_{\boxed{-1_{+1}}} = 2\mathrm{i}\sqrt{2} \times \{-\mathrm{i}\frac{1}{3\sqrt{2}}\mathbb{B}\} = \frac{2}{3}\mathbb{B}$$

Since the amplitudes are real, the real part of the NMR spectrum consists of two absorption-mode Lorentzian peaks, with equal amplitudes (see Section 11.11):

$$S(\Omega) = \frac{2}{3}\mathbb{B}\left(\boldsymbol{\mathcal{A}}(\Omega; \Omega^0 + \frac{1}{2}\omega_Q^{(1)}, \lambda) + \boldsymbol{\mathcal{A}}(\Omega; \Omega^0 - \frac{1}{2}\omega_Q^{(1)}, \lambda)\right)$$

The form of the NMR spectrum depends strongly on the phase of matter, since this determines the size of the motionally averaged first-order quadrupolar coupling $\omega_Q^{(1)}$:

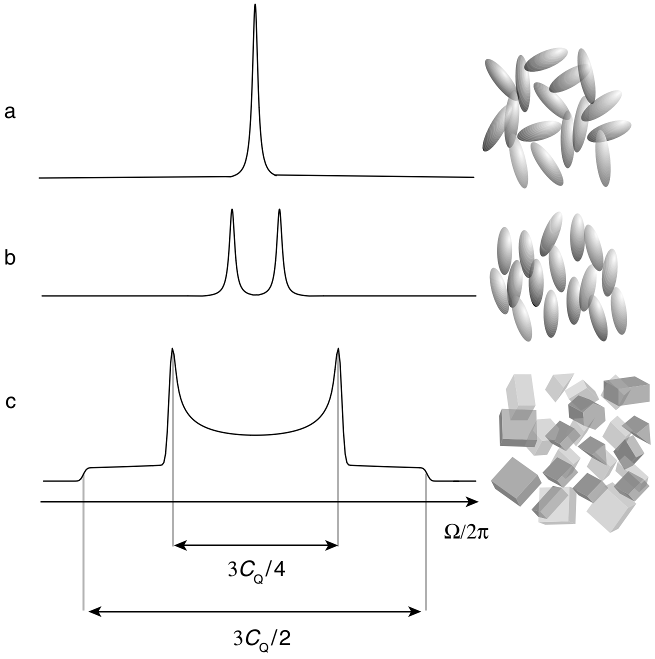

Figure 13.9
Typical appearance of spin-1 spectra for: (a) an isotropic liquid; (b) a nematic liquid crystal oriented along the magnetic field; (c) a solid powder.

Isotropic liquids. The first-order quadrupole coupling $\omega_Q^{(1)}$ vanishes in isotropic liquids, so the two peaks coincide. There is no quadrupolar splitting for spins-1 in isotropic liquids (see Figure 13.9a).[5]

Liquid crystals. A quadrupolar splitting $\omega_Q^{(1)}$ is observed in anisotropic liquids (see Figure 13.9b). The quadrupolar splitting is proportional to the nuclear quadrupole moment, and the motional average of the electric field gradient at the site of the nucleus (see Equation 9.23). The appearance of a ^{2}H quadrupolar splitting is a clear signature of a liquid crystal phase.[6]

Solid powders. In solids, the quadrupolar splitting $\omega_Q^{(1)}$ depends on the orientation of the electric field gradient tensor with respect to the external magnetic field (see Equation 13.5). In a powder, the molecules take a variety of orientations with respect to the magnetic field. This leads to a distribution of first-order splittings $\omega_Q^{(1)}$, and hence a broad spectrum with a characteristic shape. In the common case of a uniaxial electric field gradient tensor ($\eta_Q = 0$), the spectrum has a characteristic symmetric shape, called a *Pake doublet*[7] (see Figure 13.9c).

For a uniaxial electric field gradient tensor, the splitting between the two outermost shoulders of the spin-1 Pake doublet is equal to $3C_Q/2$, in units of hertz, where the quadrupole coupling constant is $C_Q = e^2qQ/h$. The splitting between the strong inner peaks is $3C_Q/4$, in units of hertz.

The strong inner peaks of the Pake doublet are generated by molecules for which the unique principal axis of the electric field gradient tensor is *perpendicular* to the magnetic field. The weaker outer shoulders of the Pake doublet correspond to molecules for which the unique principal axis of the electric field gradient tensor is *parallel* to the magnetic field:

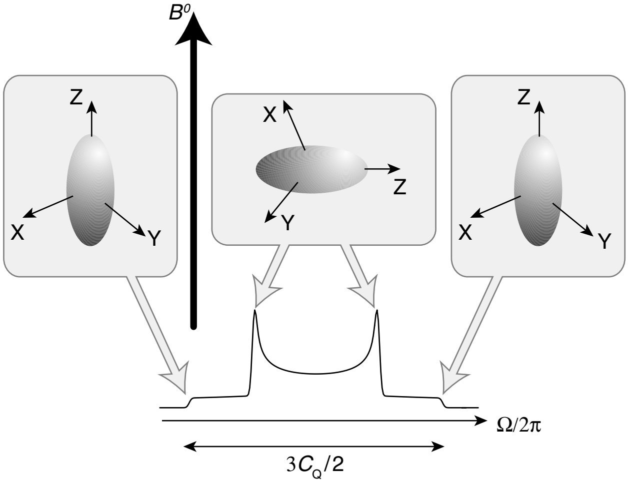

Figure 13.10
The main features of the spin-1 Pake pattern, and the corresponding orientations of the electric field gradient tensor.

The shoulders are weaker than the main peaks because it is much more likely that the unique electric field gradient principal axis is almost perpendicular to the field, rather than almost parallel to it.[8]

The symmetrical Pake doublet[9] is actually a superposition of two asymmetric spectral components, each generated by a different (−1)-quantum coherence. The underlying spectral components are made clearer in the following diagram:

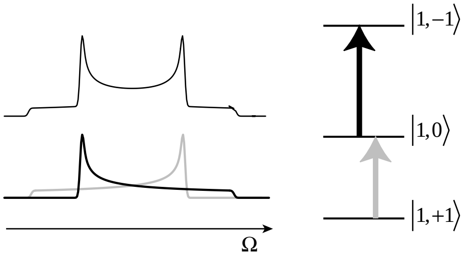

Figure 13.11
A Pake doublet has two components, one from each of the (−1)-quantum coherences.

The lineshape generated by each coherence has the same form as the powder pattern for a uniaxial CSA tensor (see Section 9.1).

A biaxial electric field gradient tensor ($\eta_Q \neq 0$) can arise if the local molecular motion does not have a high degree of symmetry. In that case the spectral lineshapes do not have the Pake form.

13.1.10 Quadrupolar echo

For rigid sites in deuterated organic solids, the full width of the ^{2}H spectrum is over 200 kHz. Such a broad spectrum corresponds to an FID with components that decay rapidly to almost zero within around 5 μs of the end of the pulse.[10]

In practice, the capture of a rapidly decaying NMR signal is exceedingly difficult, since the weak NMR signal coincides with the release of accumulated electrical energy from the tuned circuit in the probe at the end of the pulse. Electrical interference makes it essentially impossible to detect the weak NMR signal until around 5 μs after a pulse has finished, which is too late to detect most of the powder ^{2}H NMR signal.

This problem may be avoided by generating a spin echo, in order to displace the NMR signal to a region in time that is well separated from the end of the pulse. In the case of a spin-1 ensemble, a suitable spin echo is generated by a sequence of two strong $\pi/2$ pulses, with a relative phase shift of $\pi/2$:

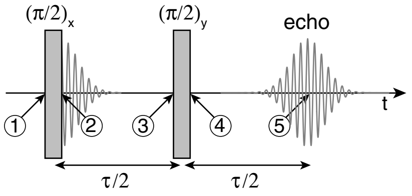

Figure 13.12
Spin-1 quadrupolar echo pulse sequence.

The interval between the two $\pi/2$ pulses is denoted $\tau/2$. The echo forms at a time $\tau/2$ after the end of the second pulse.

This type of spin echo is called a *quadrupolar echo*. In contrast to those described in Sections 12.2 and 12.4, the quadrupolar echo involves the refocusing of spin evolution under a *distribution of first-order quadrupolar interactions*, rather than a distribution in local magnetic fields or chemical shifts.

The two-pulse sequence in Figure 13.12 only generates a quadrupolar echo in the case of spin-1 systems. It does not work for higher spin quantum numbers.

To see how the quadrupolar echo works, consider the density operator at time point ③, which is at a time interval $\tau/2$ after the end of the first pulse. If relaxation is ignored, the (± 1)-quantum coherences at this time point are given as follows:

$$\begin{aligned}
\rho_{\boxed{-1_{-1}}}\text{③} &= \rho_{\boxed{-1_{-1}}}\text{②}\exp\{\mathrm{i}\Omega_{\boxed{-1_{-1}}}\tau/2\} = -\mathrm{i}\frac{1}{3\sqrt{2}}\mathbb{B}\exp\{\mathrm{i}\Omega_{\boxed{-1_{-1}}}\tau/2\} \\
\rho_{\boxed{-1_{+1}}}\text{③} &= \rho_{\boxed{-1_{+1}}}\text{②}\exp\{\mathrm{i}\Omega_{\boxed{-1_{+1}}}\tau/2\} = -\mathrm{i}\frac{1}{3\sqrt{2}}\mathbb{B}\exp\{\mathrm{i}\Omega_{\boxed{-1_{+1}}}\tau/2\} \\
\rho_{\boxed{+1_{-1}}}\text{③} &= \rho_{\boxed{+1_{-1}}}\text{②}\exp\{\mathrm{i}\Omega_{\boxed{+1_{-1}}}\tau/2\} = +\mathrm{i}\frac{1}{3\sqrt{2}}\mathbb{B}\exp\{\mathrm{i}\Omega_{\boxed{+1_{-1}}}\tau/2\} \\
\rho_{\boxed{+1_{+1}}}\text{③} &= \rho_{\boxed{+1_{+1}}}\text{②}\exp\{\mathrm{i}\Omega_{\boxed{+1_{+1}}}\tau/2\} = +\mathrm{i}\frac{1}{3\sqrt{2}}\mathbb{B}\exp\{\mathrm{i}\Omega_{\boxed{+1_{+1}}}\tau/2\} \qquad (13.24)
\end{aligned}$$

The coherence frequencies are given by Equation 13.11. If the chemical shift offset frequency Ω^0 is neglected,[11] Equation 13.24 may be simplified as follows:

$$
\begin{aligned}
\rho_{\boxed{-1_{-1}}}\textcircled{3} &= -\mathrm{i}\frac{1}{3\sqrt{2}}\mathbb{B}\exp\{\mathrm{i}\frac{1}{4}\omega_{\mathrm{Q}}^{(1)}\tau\} &\qquad \rho_{\boxed{-1_{+1}}}\textcircled{3} &= -\mathrm{i}\frac{1}{3\sqrt{2}}\mathbb{B}\exp\{-\mathrm{i}\frac{1}{4}\omega_{\mathrm{Q}}^{(1)}\tau\} \\
\rho_{\boxed{+1_{-1}}}\textcircled{3} &= +\mathrm{i}\frac{1}{3\sqrt{2}}\mathbb{B}\exp\{\mathrm{i}\frac{1}{4}\omega_{\mathrm{Q}}^{(1)}\tau\} &\qquad \rho_{\boxed{+1_{+1}}}\textcircled{3} &= +\mathrm{i}\frac{1}{3\sqrt{2}}\mathbb{B}\exp\{-\mathrm{i}\frac{1}{4}\omega_{\mathrm{Q}}^{(1)}\tau\}
\end{aligned}
\tag{13.25}
$$

Since the first-order quadrupolar coupling $\omega_{\mathrm{Q}}^{(1)}$ depends on molecular orientation, all coherences dephase in the complex plane during the first interval $\tau/2$. Note that the complex phase factors in Equation 13.25 depend on the satellite order of the coherences (lower subscript). The (-1)-quantum coherence $\rho_{\boxed{-1_{-1}}}$ has the same complex phase factor as the $(+1)$-quantum coherence $\rho_{\boxed{+1_{-1}}}$, and similarly for $\rho_{\boxed{-1_{+1}}}$ and $\rho_{\boxed{+1_{+1}}}$.

For this reason, it is convenient to group coherences according to the satellite order. The (±1)-quantum part of the density matrix at time point ③ may be written in the following way:

$$
\hat{\rho}_{\textcircled{3}} = -\mathrm{i}\frac{1}{3\sqrt{2}}\mathbb{B}\exp\{\mathrm{i}\frac{1}{4}\omega_{\mathrm{Q}}^{(1)}\tau\}\begin{pmatrix} 0 & 0 & 0 \\ 1 & 0 & -1 \\ 0 & 0 & 0 \end{pmatrix} - \mathrm{i}\frac{1}{3\sqrt{2}}\mathbb{B}\exp\{-\mathrm{i}\frac{1}{4}\omega_{\mathrm{Q}}^{(1)}\tau\}\begin{pmatrix} 0 & -1 & 0 \\ 0 & 0 & 0 \\ 0 & 1 & 0 \end{pmatrix}
\tag{13.26}
$$

The first term in the right-hand side of Equation 13.26 includes coherences with satellite order $q = -1$ and the second term includes coherences with satellite order $q = +1$.

Now consider the second $(\pi/2)_y$ pulse, which is also assumed to be strong. This pulse transforms the density operator as follows:

$$
\hat{\rho}_{\textcircled{4}} = \widehat{R}_y(\pi/2)\hat{\rho}_{\textcircled{3}}\widehat{R}_y(\pi/2)^{\dagger}
$$

where the spin-1 matrix representation of the rotation operator is given in Section 7.9.1:

$$
\widehat{R}_y(\pi/2) = \frac{1}{2}\begin{pmatrix} 1 & -\sqrt{2} & 1 \\ \sqrt{2} & 0 & -\sqrt{2} \\ 1 & \sqrt{2} & 1 \end{pmatrix}
$$

Straightforward matrix multiplication leads to the following properties:

$$
\begin{aligned}
\widehat{R}_y(\pi/2)\begin{pmatrix} 0 & 0 & 0 \\ 1 & 0 & -1 \\ 0 & 0 & 0 \end{pmatrix}\widehat{R}_y(\pi/2)^{\dagger} &= \begin{pmatrix} 0 & -1 & 0 \\ 0 & 0 & 0 \\ 0 & 1 & 0 \end{pmatrix} \\
\widehat{R}_y(\pi/2)\begin{pmatrix} 0 & -1 & 0 \\ 0 & 0 & 0 \\ 0 & 1 & 0 \end{pmatrix}\widehat{R}_y(\pi/2)^{\dagger} &= \begin{pmatrix} 0 & 0 & 0 \\ 1 & 0 & -1 \\ 0 & 0 & 0 \end{pmatrix}
\end{aligned}
\tag{13.27}
$$

These are the central results leading to the spin-1 quadrupolar echo: the set of coherences with satellite order $q = +1$ is exchanged with the set of coherences with satellite order $q = -1$. These *coherence transfer processes* are depicted in Figure 13.13.

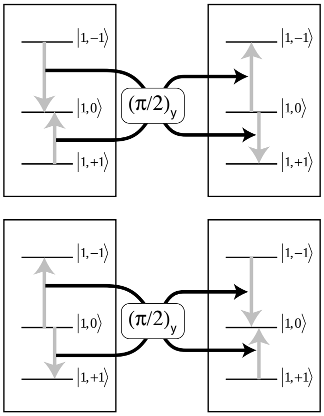

Figure 13.13
Coherence exchange processes induced by the second pulse in a quadrupolar spin echo.

Equations 13.26 and 13.27 may be combined to obtain the spin density operator after the second pulse:

$$\hat{\rho}_{\text{④}} = -\mathrm{i}\frac{1}{3\sqrt{2}}\mathbb{B}\exp\{-\mathrm{i}\frac{1}{4}\omega_Q^{(1)}\tau\}\begin{pmatrix}0 & 0 & 0\\ 1 & 0 & -1\\ 0 & 0 & 0\end{pmatrix} - \mathrm{i}\frac{1}{3\sqrt{2}}\mathbb{B}\exp\{\mathrm{i}\frac{1}{4}\omega_Q^{(1)}\tau\}\begin{pmatrix}0 & -1 & 0\\ 0 & 0 & 0\\ 0 & 1 & 0\end{pmatrix} \tag{13.28}$$

The (-1)-quantum coherences after the second pulse are therefore given by

$$\rho_{\boxed{-1_{-1}}}\text{④} = -\mathrm{i}\frac{1}{3\sqrt{2}}\mathbb{B}\exp\{-\mathrm{i}\frac{1}{4}\omega_Q^{(1)}\tau\}$$
$$\rho_{\boxed{-1_{+1}}}\text{④} = -\mathrm{i}\frac{1}{3\sqrt{2}}\mathbb{B}\exp\{\mathrm{i}\frac{1}{4}\omega_Q^{(1)}\tau\}$$

Further evolution for the interval $\tau/2$ refocuses the dispersion of phases, leading to:

$$\rho_{\boxed{-1_{-1}}}\text{⑤} = \rho_{\boxed{-1_{-1}}}\text{④}\exp\{+\mathrm{i}\frac{1}{4}\omega_Q^{(1)}\tau\} = -\mathrm{i}\frac{1}{3\sqrt{2}}\mathbb{B}$$
$$\rho_{\boxed{-1_{+1}}}\text{⑤} = \rho_{\boxed{-1_{+1}}}\text{④}\exp\{-\mathrm{i}\frac{1}{4}\omega_Q^{(1)}\tau\} = -\mathrm{i}\frac{1}{3\sqrt{2}}\mathbb{B}$$

The two (-1)-quantum coherences come into phase at the time point ⑤, leading to a spin density operator that is independent of the first-order quadrupole coupling $\omega_Q^{(1)}$. This is the quadrupolar echo. Acquisition of the decaying NMR signal after the quadrupolar echo, followed by FT, generates a spin-1 NMR spectrum, undisturbed by interference from the r.f. pulses. An experimental example of a spectrum obtained this way is shown in Figure 13.14.

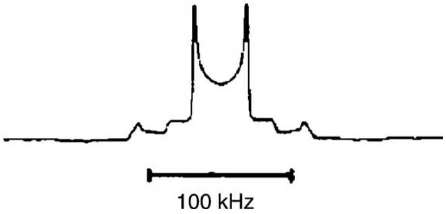

Figure 13.14 Experimental ^{2}H spectrum of deuterated poly(methylmethacrylate), showing two superimposed Pake patterns with different values of the quadrupole coupling constant C_Q. Adapted from M. H. Levitt, D. Suter and R. R. Ernst, *J. Chem. Phys.* **80**, 3064 (1984). Copyright 1984, American Institute of Physics.

A coherence transfer pathway diagram for the quadrupolar echo pulse sequence is shown below.

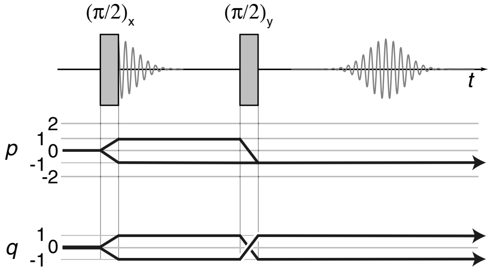

Figure 13.15 Coherence transfer pathway diagram for a quadrupolar spin echo.

The two staves depict the histories of coherence orders p and satellite orders q leading to the final NMR signal. The upper stave spans all orders p between -2 and $+2$, since the spin-1 density matrix may contain double-quantum coherences as well as populations and single-quantum coherences.

The upper stave shows that the pathway leading to the NMR signal starts with order 0, corresponding to thermal equilibrium populations, and terminates with order -1, corresponding to the quadrature-detected NMR signal. Double-quantum coherences are not involved. Note that the coherence transfer pathway for the quadrupolar echo involves both orders $p = \pm 1$ between the two pulses, unlike the Hahn echo (see Section 12.2.6), for which only the $(+1)$-quantum pathway forms an echo.

The lower stave shows the sign change of satellite order induced by the second $\pi/2$ pulse. It is this change in satellite order q that leads to the quadrupolar echo. The final NMR signal is induced by both (-1)-quantum coherences, with satellite orders $q = \pm 1$.

13.2 Spin $I = 3/2$

There is a large number of spins-3/2 isotopes in the periodic table (see Plate C). The alkali metals are especially well represented: ^{7}Li, ^{23}Na, ^{39}K and ^{87}Rb. There are also several halogen isotopes with spin-3/2: ^{35}Cl, ^{37}Cl, ^{79}Br and ^{81}Br. The semi-metal nuclides ^{69}Ga, ^{71}Ga and ^{75}As are particularly useful for the study of semiconductors. Other important spin-3/2 nuclides include the two copper isotopes ^{63}Cu and ^{65}Cu, the boron isotope ^{11}B, the gold isotope ^{197}Au, the iridium isotopes ^{191}Ir and ^{193}Ir, and the noble gas nuclides ^{21}Ne and ^{131}Xe.

13.2.1 Spin-3/2 energy levels

The quantum mechanics of a spin-3/2 nucleus may be developed on the same lines as for spin-1. In the case of spin-3/2, there are four eigenstates of angular momentum along the z-axis, denoted $|\frac{3}{2}, M\rangle$ where the quantum number M is equal to +3/2, +1/2, −1/2 or −3/2, and the Zeeman eigenstates have the following properties:

$$\begin{aligned} \hat{I}_z|\frac{3}{2}, M\rangle &= M|\frac{3}{2}, M\rangle \\ \hat{I}^2|\frac{3}{2}, M\rangle &= I(I+1)|\frac{3}{2}, M\rangle = \frac{15}{4}|\frac{3}{2}, M\rangle \end{aligned} \tag{13.29}$$

For a spin-3/2, the first-order quadrupolar Hamiltonian is given by

$$\begin{aligned} \widehat{\mathcal{H}}_Q^{(1)} &= \omega_Q^{(1)} \times \frac{1}{6}\left(3\hat{I}_z^2 - I(I+1)\hat{1}\right) \\ &= \omega_Q^{(1)} \times \frac{1}{6}\left(3\hat{I}_z^2 - \frac{15}{4}\hat{1}\right) \qquad \text{(for spin } I = 3/2) \end{aligned} \tag{13.30}$$

where the first-order quadrupolar coupling $\omega_Q^{(1)}$ is given by Equation 9.23.

In the case of a solid, the first-order quadrupolar coupling is given by

$$\begin{aligned} \omega_Q^{(1)}(\theta_Q) &= \frac{3\pi C_Q}{2I(2I-1)}\left(3\cos^2\theta_Q - 1\right) \\ &= \pi C_Q \times \frac{1}{2}\left(3\cos^2\theta_Q - 1\right) \qquad \text{(for spin } I = 3/2) \end{aligned} \tag{13.31}$$

assuming a uniaxial electric field gradient tensor ($\eta_Q = 0$). Here, θ_Q is the angle between the major principal axis of the electric field gradient tensor and the magnetic field. Note that the first-order quadrupolar coupling for spin-3/2 is three times smaller that for spin-1, given the same quadrupole coupling constant C_Q (compare Equation 13.5 and 13.31).

The four Zeeman eigenstates $|\frac{3}{2}, M\rangle$ are eigenstates of the first-order quadrupolar Hamiltonian:

$$\widehat{\mathcal{H}}_Q^{(1)}|\frac{3}{2}, M\rangle = +\frac{1}{2}\left(M^2 - \frac{5}{4}\right)\omega_Q^{(1)}|\frac{3}{2}, M\rangle$$

leading to the following eigenequations:

$$\widehat{\mathcal{H}}_Q^{(1)}|\frac{3}{2}, \pm\frac{3}{2}\rangle = +\frac{1}{2}\omega_Q^{(1)}|\frac{3}{2}, \pm\frac{3}{2}\rangle \qquad \widehat{\mathcal{H}}_Q^{(1)}|\frac{3}{2}, \pm\frac{1}{2}\rangle = -\frac{1}{2}\omega_Q^{(1)}|\frac{3}{2}, \pm\frac{1}{2}\rangle$$

If the quadrupolar coupling $\omega_Q^{(1)}$ is positive, then the energies of the outer states $|\frac{3}{2}, \pm\frac{3}{2}\rangle$ are shifted upwards in energy by $\omega_Q^{(1)}/2$, while the energies of the inner states $|\frac{3}{2}, \pm\frac{1}{2}\rangle$ are shifted down in energy by the same amount (see Figure 13.16).

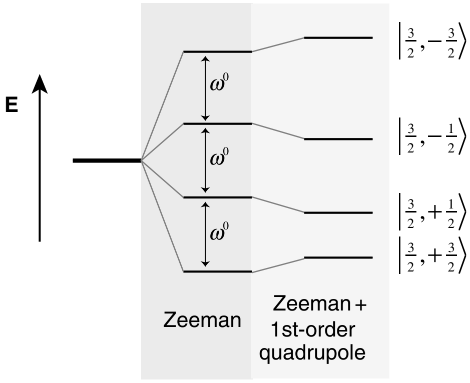

Figure 13.16
Energy levels of a spin-3/2 nucleus, in the case of positive gyromagnetic ratio.

13.2.2 Populations and coherences

The quantum state of a spin-3/2 ensemble may be written as a 4 × 4 density matrix, as follows:

$$\hat{\rho} = \overline{|\psi\rangle\langle\psi|} = \begin{pmatrix} \rho_{|+3/2\rangle} & \rho_{\boxed{+1_{+2}}} & \rho_{\boxed{+2_{+2}}} & \rho_{\boxed{+3_0}} \\ \rho_{\boxed{-1_{-2}}} & \rho_{|+1/2\rangle} & \rho_{\boxed{+1_0}} & \rho_{\boxed{+2_{-2}}} \\ \rho_{\boxed{-2_{-2}}} & \rho_{\boxed{-1_0}} & \rho_{|-1/2\rangle} & \rho_{\boxed{+1_{-2}}} \\ \rho_{\boxed{-3_0}} & \rho_{\boxed{-2_{+2}}} & \rho_{\boxed{-1_{+2}}} & \rho_{|-3/2\rangle} \end{pmatrix} \tag{13.32}$$

The populations of the four Zeeman states are denoted $\rho_{|+3/2\rangle}$, $\rho_{|+1/2\rangle}$, $\rho_{|-1/2\rangle}$ and $\rho_{|-3/2\rangle}$, and may be represented diagramatically as 'little balls' sitting on the corresponding energy level:

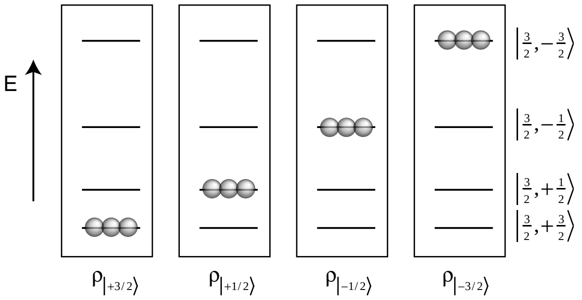

Figure 13.17
State populations for an ensemble of spins-3/2.

The 12 coherences of the spin-3/2 ensemble are labelled using the coherence order and satellite order, as defined in Equation 13.7. For example, the coherence $\rho_{\boxed{+1_{+2}}}$ is given by the following density matrix element:

$$\rho_{\boxed{+1_{+2}}} = \langle 3/2, +3/2|\, \hat{\rho}\, |3/2, +1/2\rangle$$

The two subscript labels of this coherence are derived as follows:

$$p = \left(\frac{3}{2}\right) - \left(\frac{1}{2}\right) = +1 \quad q = \left(\frac{3}{2}\right)^2 - \left(\frac{1}{2}\right)^2 = +2$$

The other labels in Equation 13.32 are derived in a similar way.

The spin-1 ensemble supports three (−1)-quantum coherences, denoted $\rho_{\boxed{-1_{-2}}}$, $\rho_{\boxed{-1_0}}$ and $\rho_{\boxed{-1_{+2}}}$:

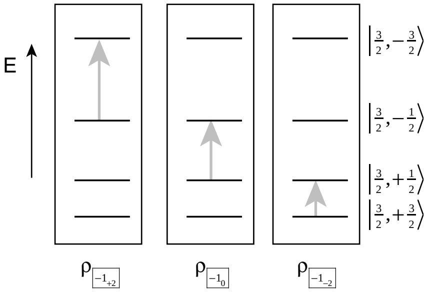

Figure 13.18
The (−1)-quantum coherences for an ensemble of spins-3/2.

The coherence $\rho_{\boxed{-1_0}}$ involves the two innermost eigenstates $|3/2, \pm 1/2\rangle$, and is particularly important, as discussed below. It is associated with the *central transition* of the spin-3/2 system.

The (+1)-quantum coherences $\rho_{\boxed{+1_{-2}}}$, $\rho_{\boxed{+1_0}}$ and $\rho_{\boxed{+1_{+2}}}$ may be represented by arrows running in the opposite direction to the (−1)-quantum coherences:

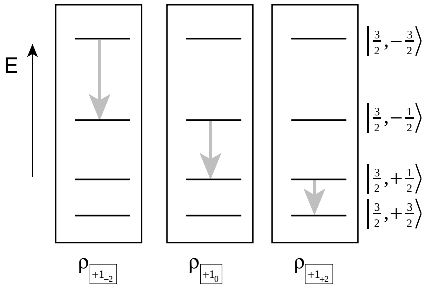

Figure 13.19
The (+1)-quantum coherences for an ensemble of spins-3/2.

The spin-3/2 ensemble may also support *double-quantum coherences* (with order $p = \pm 2$) and a pair of *triple-quantum coherences* (with order $p = \pm 3$). These may be depicted as follows:

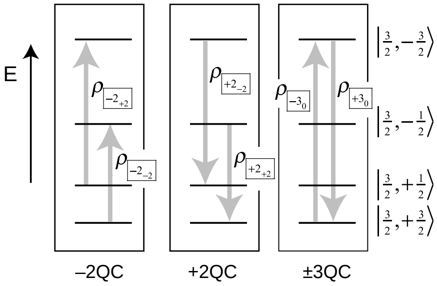

Figure 13.20
The (±2)-quantum coherences and (±3)-quantum coherences for an ensemble of spins-3/2.

These double- and triple-quantum coherences have no counterpart for spins-1/2.

The evolution frequencies of the spin-3/2 coherences are as follows:

$$\begin{aligned}
\Omega_{\boxed{-3_0}} &= 3\Omega^0 & \Omega_{\boxed{+1_{+2}}} &= -\Omega^0 - \omega_Q^{(1)} \\
\Omega_{\boxed{-2_{+2}}} &= 2\Omega^0 - \omega_Q^{(1)} & \Omega_{\boxed{+1_0}} &= -\Omega^0 \\
\Omega_{\boxed{-2_{-2}}} &= 2\Omega^0 + \omega_Q^{(1)} & \Omega_{\boxed{+1_{-2}}} &= -\Omega^0 + \omega_Q^{(1)} \\
\Omega_{\boxed{-1_{+2}}} &= \Omega^0 - \omega_Q^{(1)} & \Omega_{\boxed{+2_{+2}}} &= -2\Omega^0 - \omega_Q^{(1)} \\
\Omega_{\boxed{-1_0}} &= \Omega^0 & \Omega_{\boxed{+2_{-2}}} &= -2\Omega^0 + \omega_Q^{(1)} \\
\Omega_{\boxed{-1_{-2}}} &= \Omega^0 + \omega_Q^{(1)} & \Omega_{\boxed{+3_0}} &= -3\Omega^0
\end{aligned} \tag{13.33}$$

where Ω^0 is the chemically shifted resonance offset (see Equation 13.12). Note that the contribution from the quadrupolar coupling $\omega_Q^{(1)}$ is proportional to the satellite order of the coherence. The coherences $\rho_{\boxed{\pm1_0}}$ and $\rho_{\boxed{\pm3_0}}$ are not influenced by the first-order quadrupole interaction.

13.2.3 NMR signal

An expression for the NMR signal is derived by combining Equation 13.13 with the spin-3/2 matrix representation of the shift operator, as given in Section 7.9:

$$\hat{I}^+ = \begin{pmatrix} 0 & \sqrt{3} & 0 & 0 \\ 0 & 0 & 2 & 0 \\ 0 & 0 & 0 & \sqrt{3} \\ 0 & 0 & 0 & 0 \end{pmatrix} \tag{13.34}$$

Using $\langle \hat{I}^+ \rangle = \text{Tr}\{\hat{I}^+ \hat{\rho}\}$ leads to the following expression for the spin-3/2 NMR signal:

$$s(t) \sim 2\text{i} \exp\{-\text{i}\phi_{\text{rec}}\} \left(\sqrt{3}\rho_{\boxed{-1_{-2}}}(t) + 2\rho_{\boxed{-1_0}}(t) + \sqrt{3}\rho_{\boxed{-1_{+2}}}(t) \right)$$

$$(\text{for spin } I = 3/2) \tag{13.35}$$

Each (−1)-quantum coherence gives rise to an NMR signal, but the three coherences do not contribute equally. The central coherence $\rho_{\boxed{-1_0}}$ provides a more intense signal than the outer coherences $\rho_{\boxed{-1_{\pm2}}}$.

Fourier transformation of $s(t)$ provides an NMR spectrum $S(\Omega)$ containing three Lorentzian peaks:

$$\begin{aligned}
S(\Omega) &= a_{\boxed{-1_{-2}}} \mathcal{L}(\Omega; \Omega_{\boxed{-1_{-2}}}, \lambda) + a_{\boxed{-1_0}} \mathcal{L}(\Omega; \Omega_{\boxed{-1_0}}, \lambda) + a_{\boxed{-1_{+2}}} \mathcal{L}(\Omega; \Omega_{\boxed{-1_{+2}}}, \lambda) \\
&= a_{\boxed{-1_{-2}}} \mathcal{L}(\Omega; \Omega^0 + \omega_Q^{(1)}, \lambda) + a_{\boxed{-1_0}} \mathcal{L}(\Omega; \Omega^0, \lambda) + a_{\boxed{-1_{+2}}} \mathcal{L}(\Omega; \Omega^0 - \omega_Q^{(1)}, \lambda)
\end{aligned} \tag{13.36}$$

The peak intensities are proportional to the (−1)-quantum coherence amplitudes at the beginning of the detection interval:

$$\begin{aligned}
a_{\boxed{-1_{-2}}} &= 2\text{i}\sqrt{3} \exp\{-\text{i}\phi_{\text{rec}}\}\rho_{\boxed{-1_{-2}}}(0) \\
a_{\boxed{-1_0}} &= 4\text{i} \exp\{-\text{i}\phi_{\text{rec}}\}\rho_{\boxed{-1_0}}(0) \\
a_{\boxed{-1_{+2}}} &= 2\text{i}\sqrt{3} \exp\{-\text{i}\phi_{\text{rec}}\}\rho_{\boxed{-1_{+2}}}(0)
\end{aligned} \tag{13.37}$$

The NMR spectrum generated by a spin-3/2 ensemble is therefore a *triplet* with a splitting of $\omega_Q^{(1)}$ between each of the components.

13.2.4 Single pulse spectrum

Consider a single-pulse experiment in which a strong $(\pi/2)_x$ pulse is applied to an ensemble of spins-3/2. The discussion below uses the timing diagram in Figure 13.7.

The thermal equilibrium density matrix contains populations satisfying the Boltzmann distribution, and no coherences. Within the high-temperature approximation, the thermal equilibrium populations are given by

$$\begin{aligned} \rho_{|+3/2\rangle} &\cong \frac{1}{4}(1 + 3\mathbb{B}/2) & \qquad \rho_{|-1/2\rangle} &\cong \frac{1}{4}(1 - \mathbb{B}/2) \\ \rho_{|+1/2\rangle} &\cong \frac{1}{4}(1 + \mathbb{B}/2) & \qquad \rho_{|-3/2\rangle} &\cong \frac{1}{4}(1 - 3\mathbb{B}/2) \end{aligned}$$

The thermal equilibrium spin density operator at time point ① (before the pulse) is therefore given by

$$\boxed{\hat{\rho}_{①} = \frac{1}{4}\hat{1} + \frac{1}{4}\mathbb{B}\hat{I}_z \qquad (13.38)}$$

Suppose that the r.f. field is strong enough to satisfy the strong-pulse condition:

$$|\omega_{\text{nut}}| >> |\omega_Q^{(1)}| \tag{13.39}$$

In this case, the density operator after the pulse is given by

$$\hat{\rho}_{②} = \widehat{R}_x(\pi/2)\hat{\rho}_{①}\,\widehat{R}_x(\pi/2)^\dagger = \frac{1}{4}\hat{1} - \frac{1}{4}\mathbb{B}\hat{I}_y \tag{13.40}$$

The case of a weak r.f. pulse is considered in Section 13.2.7.

The density matrix corresponding to Equation 13.40 may be derived using the spin-3/2 matrix representation of $\hat{I}_y$ given in Section 7.9. The result is as follows:

$$\hat{\rho}_{②} = \frac{1}{4}\begin{pmatrix} 1 & \mathrm{i}\mathbb{B}\frac{1}{2}\sqrt{3} & 0 & 0 \\ -\mathrm{i}\mathbb{B}\frac{1}{2}\sqrt{3} & 1 & \mathrm{i}\mathbb{B} & 0 \\ 0 & -\mathrm{i}\mathbb{B} & 1 & \mathrm{i}\mathbb{B}\frac{1}{2}\sqrt{3} \\ 0 & 0 & -\mathrm{i}\mathbb{B}\frac{1}{2}\sqrt{3} & 1 \end{pmatrix}$$

This shows that the double- and triple-quantum coherences are not excited by the pulse, and that the excited (-1)-quantum coherences are given by

$$\begin{aligned} \rho_{\boxed{-1_{+2}}}② &= -\mathrm{i}\frac{1}{8}\sqrt{3}\,\mathbb{B} \\ \rho_{\boxed{-1_0}}② &= -\mathrm{i}\frac{1}{4}\mathbb{B} \\ \rho_{\boxed{-1_{-2}}}② &= -\mathrm{i}\frac{1}{8}\sqrt{3}\,\mathbb{B} \end{aligned} \tag{13.41}$$

Note that the central coherence has a larger amplitude than the satellite coherences.

The effect of the strong pulse on the populations and coherences is as follows:

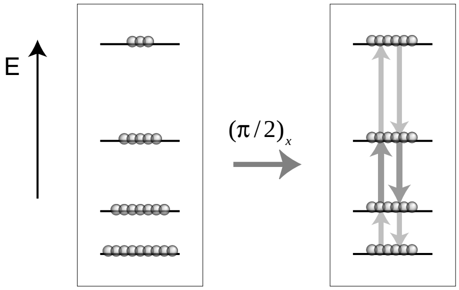

Figure 13.21
A strong $\pi/2$ pulse eliminates population differences and creates (±1)-quantum coherences.

All populations are equalized, and (±1)-quantum coherences are created. The stronger amplitudes of the central coherences are represented by the heavier arrows.

Equation 13.41 may be combined with Equations 13.36 and 13.37 to derive the NMR spectrum obtained by Fourier transforming the quadrature-detected NMR signal. If the receiver phase is zero ($\phi_{\text{rec}} = 0$), the result is

$$S(\Omega) = \frac{3}{4}\mathbb{B}\mathcal{L}(\Omega; \Omega^0 + \omega_Q^{(1)}, \lambda) + \mathbb{B}\mathcal{L}(\Omega; \Omega^0, \lambda) + \frac{3}{4}\mathbb{B}\mathcal{L}(\Omega; \Omega^0 - \omega_Q^{(1)}, \lambda)$$

The NMR spectrum of a single spin-3/2 ensemble, excited by a strong $\pi/2$ pulse, is a 3:4:3 triplet, with a splitting of $\omega_Q^{(1)}$ between adjacent peaks:

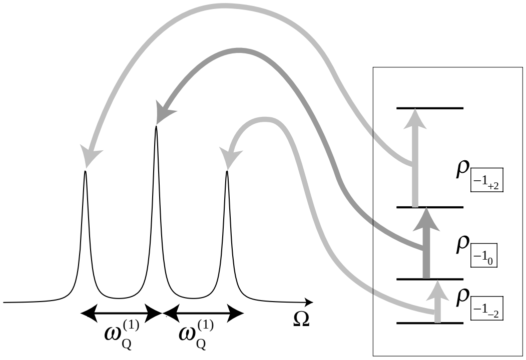

Figure 13.22
The spectrum of a spin-3/2 ensemble and the corresponding (-1)-quantum coherences.

The unequal peak intensities arise because (i) the satellite (-1)-quantum coherences have a smaller amplitude than the central (-1)-quantum coherence and (ii) the satellite (-1)-quantum coherences are less efficient in inducing an NMR signal than the central (-1)-quantum coherence. The peak intensity ratio $3:4:3$ corresponds to the *squares* of the $\hat{I}^+$ matrix elements, which are given by $\{\sqrt{3}, 2, \sqrt{3}\}$ (see Equation 13.34).

The central peak of the spin-3/2 triplet is of particular importance and is called the *central transition*. The outer peaks are called *satellite transitions*.[12]

13.2.5 Spin-3/2 spectra for small quadrupole couplings

The first-order quadrupolar coupling $\omega_Q^{(1)}$ depends strongly on the phase of matter. This determines the nature of the spin-3/2 NMR spectrum.

Isotropic liquids. As in the spin-1 case, there is no quadrupolar splitting for spins-3/2 in isotropic liquids, since the three triplet components coincide:

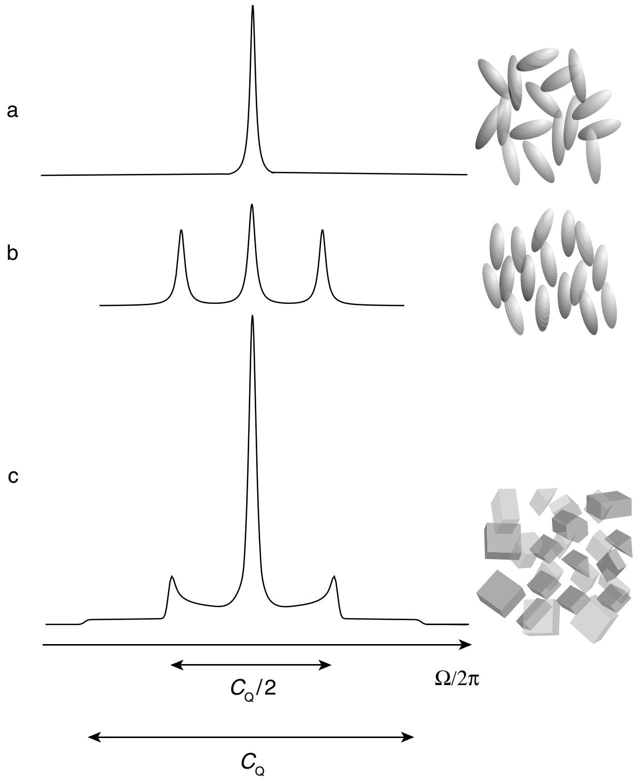

Figure 13.23 Typical appearance of spin-3/2 spectra for: (a) an isotropic liquid; (b) a nematic liquid crystal oriented along the magnetic field; (c) a solid powder for the case of a small quadrupole coupling constant C_Q.

Anisotropic liquids. The spectrum of spins-3/2 has the form of a 3:4:3 triplet in a nematic liquid crystal[6] (see Figure 13.23b). An experimental ^{23}Na spectrum showing the triplet structure is shown in Figure 13.24a.

Solid powders. In solids, the two satellites generate a broad Pake pattern, assuming a uniaxial electric field gradient tensor ($\eta_Q = 0$). The splitting between the 'parallel' shoulders is C_Q, in units of hertz, and the splitting between the 'perpendicular' peaks in the Pake pattern is $C_Q/2$. The quadrupole coupling constant is defined as usual by $C_Q = e^2qQ/h$. The central transition is not affected by the first-order quadrupolar coupling and gives rise to a strong narrow peak at the centre of the Pake pattern (see Figure 13.23c).

In practice, the satellite Pake pattern can be very difficult to observe, since it is so broad compared with the central transition. In many cases, only the central transition of spins-3/2 is observed in a solid, unless the quadrupole coupling constant C_Q is exceptionally small.

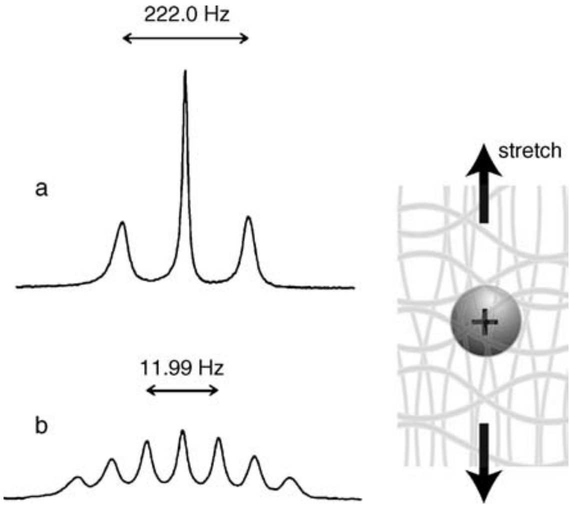

Figure 13.24 NMR spectra of alkali metal ions in a stretched gelatine gel. The mechanical stretching of the gel creates a slight anisotropy in the ionic environments, leading to a small quadrupole coupling C_Q. (a) ^{23}Na (spin $I = 3/2$) and (b) ^{133}Cs (spin $I = 7/2$). Adapted from P. W. Kuchel, B. E. Chapman, N. Müller, W. A. Bubb, D. J. Philp and A. M. Torres, *J. Magn. Reson.* **180**, 256–265 (2006), copyright Elsevier.

13.2.6 Second-order quadrupole couplings

If C_Q is large, the satellite transitions are too broad to be observed, and are also excited very inefficiently. In this case, only the central transition peak is observed. This peak is relatively narrow, since the central transition frequency $\Omega_{\boxed{-1_0}}$ is independent of the first-order quadrupolar interaction $\omega_Q^{(1)}$.

In the case of large C_Q, *second-order quadrupolar interactions* become important. The second-order quadrupolar coupling is proportional to the square of the first-order quadrupole coupling divided by the Larmor frequency (see Equation 9.25). Since the second-order quadrupolar coupling depends on molecular orientation, the central transitions of spins-3/2 display complicated broad lineshapes in powdered solids.

These second-order effects can be very considerable. It is not uncommon for second-order central-transition lineshapes to be hundreds of kilohertz wide.

The second-order quadrupolar broadening is usually undesirable, since it makes the spectra very complicated and obscures chemical shifts. Since the second-order coupling is inversely proportional to the static magnetic field (see Equation 9.25), it may be reduced in magnitude by increasing the static field. In general, the solid-state NMR spectroscopy of spins-3/2 (and half-integer spins in general) benefits greatly from using the highest possible magnetic field strengths.

Although the second-order quadrupolar broadening may be reduced by increasing the static magnetic field, it may not be eliminated completely in this way. A range of experimental methods are available for completely eliminating the second-order quadrupolar broadening,[13] greatly improving the chemical site resolution of half-integer quadrupolar NMR. One set of methods involves rotating the sample rapidly about two different axes, either simultaneously (*double rotation*, or *DOR*) or sequentially (*dynamic angle spinning*, or *DAS*). Another set of methods involves combining rapid sample rotation with pulse-induced coherence transfers. One variant is called multiple-quantum NMR (*multiple-quantum magic-angle-spinning* or *MQ-MAS*). Another method involves satellite coherences instead of multiple-quantum coherences, and is called *satellite transition magic-angle-spinning* or *ST-MAS*. See *Further Reading* for a description of these techniques.

13.2.7 Central transition excitation

If the quadrupole coupling constant C_{Q} is very large, then practical r.f. field strengths are too weak to impose the strong-pulse condition of Equation 13.39, at least for the vast majority of molecular orientations. The analysis in Section 13.2.4 is therefore invalid in the case of strong quadrupolar coupling.

Consider the spin Hamiltonian during an r.f. pulse of phase $\phi_{\mathrm{p}} = 0$. If the second-order quadrupolar coupling and chemical shifts are ignored, the total rotating-frame spin Hamiltonian is given by

$$\widehat{\mathcal{H}}_{\mathrm{p}} = \widehat{\mathcal{H}}_{\mathrm{Q}}^{(1)} + \omega_{\mathrm{nut}} \hat{I}_x = \omega_{\mathrm{Q}}^{(1)} \left(\hat{I}_z^2 - \frac{5}{4}\widehat{1} \right) + \omega_{\mathrm{nut}} \hat{I}_x$$

The spin-3/2 matrix representation of this Hamiltonian is as follows:

$$\widehat{\mathcal{H}}_{\mathrm{p}} = \begin{pmatrix} \frac{1}{2}\omega_{\mathrm{Q}}^{(1)} & \frac{1}{2}\sqrt{3}\omega_{\mathrm{nut}} & 0 & 0 \\ \frac{1}{2}\sqrt{3}\omega_{\mathrm{nut}} & -\frac{1}{2}\omega_{\mathrm{Q}}^{(1)} & \omega_{\mathrm{nut}} & 0 \\ 0 & \omega_{\mathrm{nut}} & -\frac{1}{2}\omega_{\mathrm{Q}}^{(1)} & \frac{1}{2}\sqrt{3}\omega_{\mathrm{nut}} \\ 0 & 0 & \frac{1}{2}\sqrt{3}\omega_{\mathrm{nut}} & \frac{1}{2}\omega_{\mathrm{Q}}^{(1)} \end{pmatrix} \tag{13.42}$$

Now suppose that the nutation frequency under the r.f. field is *weak* compared with the first-order quadrupolar coupling:

$$|\omega_{\mathrm{nut}}| << |\omega_{\mathrm{Q}}^{(1)}|$$

This is the opposite limit to that discussed in Section 13.2.4.

In the weak-pulse limit, the secular approximation may be applied to Equation 13.42. Off-diagonal matrix elements that connect large differences in diagonal elements are ignored (see Appendix A.6). This leads to the following approximate expression for the Hamiltonian during the pulse:

$$\widehat{\mathcal{H}}_{\mathrm{p}} \cong \begin{pmatrix} \frac{1}{2}\omega_{\mathrm{Q}}^{(1)} & 0 & 0 & 0 \\ 0 & -\frac{1}{2}\omega_{\mathrm{Q}}^{(1)} & \omega_{\mathrm{nut}} & 0 \\ 0 & \omega_{\mathrm{nut}} & -\frac{1}{2}\omega_{\mathrm{Q}}^{(1)} & 0 \\ 0 & 0 & 0 & \frac{1}{2}\omega_{\mathrm{Q}}^{(1)} \end{pmatrix} \tag{13.43}$$

Suppose now that the pulse is applied to a thermal equilibrium spin density operator of the form

$$\hat{\rho}_{①} = \frac{1}{4}\widehat{1} + \frac{1}{4}\mathbb{B}\hat{I}_z$$

where the matrix representation of $\hat{I}_z$ is given by

$$\hat{I}_z = \begin{pmatrix} \frac{3}{2} & 0 & 0 & 0 \\ 0 & \frac{1}{2} & 0 & 0 \\ 0 & 0 & -\frac{1}{2} & 0 \\ 0 & 0 & 0 & -\frac{3}{2} \end{pmatrix} \tag{13.44}$$

Since Equations 13.43 and 13.44 are block diagonal, it is easy to show that the density operator after the pulse is given by

$$\begin{aligned} \hat{\rho} &= \frac{1}{4}\widehat{1} + \frac{1}{4}\mathbb{B}\exp\{-\mathrm{i}\widehat{\mathcal{H}}_{\mathrm{p}}\tau_{\mathrm{p}}\}\hat{I}_z\exp\{+\mathrm{i}\widehat{\mathcal{H}}_{\mathrm{p}}\tau_{\mathrm{p}}\} \\ &= \frac{1}{4}\widehat{1} + \frac{1}{4}\mathbb{B}\begin{pmatrix} \frac{3}{2} & 0 & 0 & 0 \\ 0 & \frac{1}{2}\cos(\beta_{\mathrm{p}}^{\mathrm{C}}) & +\mathrm{i}\frac{1}{2}\sin(\beta_{\mathrm{p}}^{\mathrm{C}}) & 0 \\ 0 & -\mathrm{i}\frac{1}{2}\sin(\beta_{\mathrm{p}}^{\mathrm{C}}) & -\frac{1}{2}\cos(\beta_{\mathrm{p}}^{\mathrm{C}}) & 0 \\ 0 & 0 & 0 & -\frac{3}{2} \end{pmatrix} \end{aligned} \tag{13.45}$$

where $\beta_{\mathrm{p}}^{\mathrm{C}}$ is the *central-transition flip angle*, given by

$$\boxed{\beta_{\mathrm{p}}^{\mathrm{C}} = \omega_{\mathrm{nut}}^{\mathrm{C}}\tau_{\mathrm{p}}} \tag{13.46}$$

and $\omega_{\mathrm{nut}}^{\mathrm{C}}$ is the *nutation frequency on the central transition*, given by

$$\boxed{\omega_{\mathrm{nut}}^{\mathrm{C}} = 2\omega_{\mathrm{nut}} \qquad \text{(for spins } I = 3/2\text{)}} \tag{13.47}$$

The excitation of the central-transition coherence is maximized for the central-transition flip angle $\beta_{\mathrm{p}}^{\mathrm{C}} = \pi/2$. This corresponds to a *selective $\pi/2$ rotation on the central transition of the spin-3/2 system*. Under these conditions, the population difference across the central transition is completely converted into central-transition (±1)-quantum coherences:

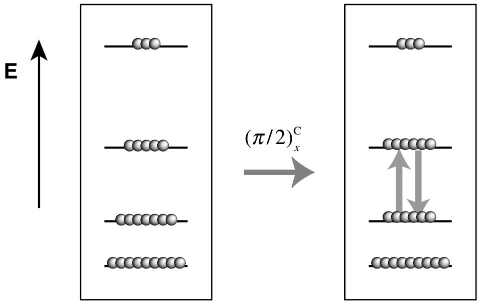

Figure 13.25
A selective $\pi/2$ pulse on the central transition converts the central transition population difference into central transition coherences.

Note that the populations of the outer levels are not perturbed by the selective pulse on the central transition.[14]

One curious feature should be noted carefully. Equation 13.47 shows that the central-transition nutation frequency in the selective pulse regime is *twice* that which would be expected for a strong pulse using the same r.f. field. This counter-intuitive effect may be rationalized by imagining that a strong, non-selective, pulse 'wastes' some of the r.f. power on exciting the satellite transitions. The pulse becomes twice as efficient when the r.f. field is concentrated on the central transition alone.

This effect often catches out inexperienced spectroscopists. For example, suppose that the ^{23}Na nutation frequency is calibrated by observing the pulse response in a solution of NaCl. In this case, the quadrupole coupling is zero, so the pulse operates in the 'strong-pulse' regime, and the nuclei respond according to the non-selective nutation frequency ω_{nut}. The NMR signal is maximized by choosing a pulse duration τ_{p} such that $\beta_{\mathrm{p}} = \omega_{\mathrm{nut}}\tau_{\mathrm{p}} = \pi/2$. However, if the same pulse is used on a solid sample containing ^{23}Na ions in a high-C_{Q} environment, the ^{23}Na NMR signal vanishes! This is because the r.f. field is now selective on the central transition, with a central transition nutation frequency $\omega_{\mathrm{nut}}^{\mathrm{C}} = 2\omega_{\mathrm{nut}}$. The central transition flip angle for the same pulse duration τ_{p} is $\beta_{\mathrm{p}}^{\mathrm{C}} = \omega_{\mathrm{nut}}^{\mathrm{C}}\tau_{\mathrm{p}} = \pi$, which leads to a failure of central transition coherence excitation. The correct procedure is to *halve* the pulse duration on changing from the low-C_{Q} to the high-C_{Q} sample.

13.2.8 Central transition echo

The shifts caused by the second-order quadrupolar interaction lead to an inhomogeneous broadening of the central transition peak. This corresponds to a rapid decay of the NMR signal after the central-transition excitation pulse. The inhomogeneous decay may be refocused by applying a π pulse to the central transition, in order to generate a spin echo. In this respect, the second-order quadrupolar broadening for the central transition of spins $I = 3/2$ behaves in the same way as CSA broadening of spins $I = 1/2$ in powdered solids. In both cases, a π pulse leads to a spin echo.

⚠The pulse duration must take into account the fact that the nutation frequency on the $I = 3/2$ central transition is twice the non-selective nutation frequency for the same r.f. field strength, as described above. A central-transition echo is induced by a pulse with a duration τ_{p} satisfying the condition $\omega_{\mathrm{nut}}^{\mathrm{C}}\tau_{\mathrm{p}} = 2\omega_{\mathrm{nut}}\tau_{\mathrm{p}} = \pi$.

⚠Do not confuse the central-transition spin echo for $I = 3/2$ with the non-selective spin echo for $I = 1$. Although the quadrupolar interaction is involved in both cases, the pulse sequences are completely different. The $I = 1$ echo involves two $\pi/2$ pulses, with a phase shift of $\pi/2$ (a '90–90 echo'), whereas the second pulse in the $I = 3/2$ sequence has a central-transition flip angle of π (a '90–180 echo').

13.3 Spin $I = 5/2$

The most important nuclides with spin $I = 5/2$ are ^{17}O, ^{25}Mg, ^{27}Al, ^{55}Mn, ^{121}Sb, ^{127}I and the two rhenium isotopes ^{185}Re and ^{187}Re.

^{17}O is the only stable oxygen isotope that is NMR active. It is, therefore, of great importance, despite its very low natural abundance and large quadrupole moment. It is feasible, although expensive, to enrich materials with ^{17}O so that NMR may be used to probe the local environments of the oxygen atoms in a molecule or mineral.

^{27}Al NMR is of great importance in inorganic chemistry. It is a relatively 'easy' spin-5/2 isotope, since it has a high natural abundance and a reasonably large gyromagnetic ratio.

The quantum mechanics of spins-5/2 may be developed in the same way as for spins-3/2. There are six Zeeman eigenstates, with the following properties:

$$\hat{I}_z|\frac{5}{2}, M\rangle = M|\frac{5}{2}, M\rangle$$
$$\hat{I}^2|\frac{5}{2}, M\rangle = I(I+1)|\frac{5}{2}, M\rangle = \frac{35}{4}|\frac{5}{2}, M\rangle$$

where $M = \{5/2, 3/2 \ldots -5/2\}$. The first-order quadrupolar Hamiltonian is given by

$$\begin{aligned}\widehat{\mathcal{H}}_Q^{(1)} &= \omega_Q^{(1)} \times \frac{1}{6}\left(3\hat{I}_z^2 - I(I+1)\widehat{1}\right) \\ &= \omega_Q^{(1)} \times \frac{1}{2}\left(\hat{I}_z^2 - \frac{7}{4}\widehat{1}\right) \qquad \text{(for spin } I = 5/2\text{)}\end{aligned} \tag{13.48}$$

The first-order quadrupolar coupling is given by

$$\omega_Q^{(1)}(\theta_Q) = \frac{\pi C_Q}{10} \times \frac{1}{2}\left(3\cos^2\theta_Q - 1\right) \qquad \text{(for spin } I = 5/2\text{)} \tag{13.49}$$

assuming a uniaxial electric field gradient tensor ($\eta_Q = 0$). Note the factor of 10 in the denominator of the right-hand side of Equation 13.49. The effect of the quadrupole coupling constant C_Q is scaled down strongly for spin-5/2.

The Zeeman eigenstates are also eigenstates of the first-order quadrupolar Hamiltonian, as follows:

$$\widehat{\mathcal{H}}_Q^{(1)}|\frac{5}{2}, \pm\frac{5}{2}\rangle = +\frac{5}{3}\omega_Q^{(1)}|\frac{5}{2}, \pm\frac{5}{2}\rangle$$
$$\widehat{\mathcal{H}}_Q^{(1)}|\frac{5}{2}, \pm\frac{3}{2}\rangle = -\frac{1}{3}\omega_Q^{(1)}|\frac{5}{2}, \pm\frac{3}{2}\rangle$$
$$\widehat{\mathcal{H}}_Q^{(1)}|\frac{5}{2}, \pm\frac{1}{2}\rangle = -\frac{4}{3}\omega_Q^{(1)}|\frac{5}{2}, \pm\frac{1}{2}\rangle$$

For spins-5/2, a positive first-order coupling $\omega_Q^{(1)}$ increases the energy of the outer pair of states, while decreasing the energy of the inner four states (see Figure 13.26). This figure is appropriate for the ^{27}Al case, which has a positive gyromagnetic ratio. The arrangement of energy levels is inverted in the case of ^{17}O, which has a negative gyromagnetic ratio.

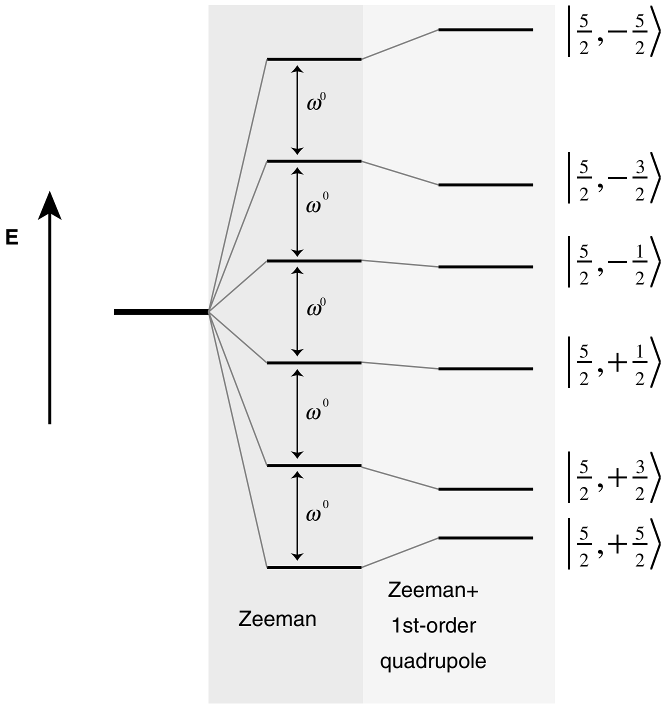

Figure 13.26
Energy levels of a spin-5/2 nucleus, for a positive gyromagnetic ratio.

The quantum state of a spin-5/2 ensemble may be represented by a 6 × 6 density matrix, comprising six populations on the diagonal, five (−1)-quantum coherences, five (+1)-quantum coherences, four (−2)-quantum coherences, four (+2)-quantum coherences, three (−3)-quantum coherences, three (+3)-quantum coherences, two (−4)-quantum coherences, two (+2)-quantum coherences, and a pair of coherences with order ±5. The complete density matrix, including the satellite order indices, is as follows:

$$\hat{\rho} = \begin{pmatrix}
\rho_{|+5/2\rangle} & \rho_{\boxed{+1_{+4}}} & \rho_{\boxed{+2_{+6}}} & \rho_{\boxed{+3_{+6}}} & \rho_{\boxed{+4_{+4}}} & \rho_{\boxed{+5_{0}}} \\
\rho_{\boxed{-1_{-4}}} & \rho_{|+3/2\rangle} & \rho_{\boxed{+1_{+2}}} & \rho_{\boxed{+2_{+2}}} & \rho_{\boxed{+3_{0}}} & \rho_{\boxed{+4_{-4}}} \\
\rho_{\boxed{-2_{-6}}} & \rho_{\boxed{-1_{-2}}} & \rho_{|+1/2\rangle} & \rho_{\boxed{+1_{0}}} & \rho_{\boxed{+2_{-2}}} & \rho_{\boxed{+3_{-6}}} \\
\rho_{\boxed{-3_{-6}}} & \rho_{\boxed{-2_{-2}}} & \rho_{\boxed{-1_{0}}} & \rho_{|-1/2\rangle} & \rho_{\boxed{+1_{-2}}} & \rho_{\boxed{+2_{-6}}} \\
\rho_{\boxed{-4_{-4}}} & \rho_{\boxed{-3_{0}}} & \rho_{\boxed{-2_{+2}}} & \rho_{\boxed{-1_{+2}}} & \rho_{|-3/2\rangle} & \rho_{\boxed{+1_{-4}}} \\
\rho_{\boxed{-5_{0}}} & \rho_{\boxed{-4_{+4}}} & \rho_{\boxed{-3_{+6}}} & \rho_{\boxed{-2_{+6}}} & \rho_{\boxed{-1_{+4}}} & \rho_{|-5/2\rangle}
\end{pmatrix}$$

As usual, the observable (−1)-quantum coherences are the most important. Excitation with a $\pi/2$ pulse in the strong-pulse regime ($|\omega_{\text{nut}}| >> |\omega_Q^{(1)}|$) provides a five-peak spectrum, with intensities in the ratio 5:8:9:8:5, as shown below:

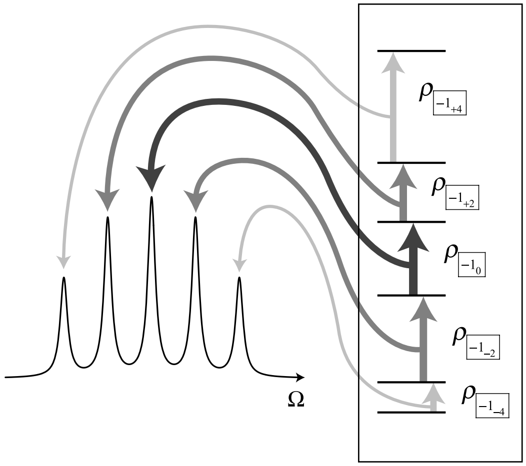

Figure 13.27
The spectrum of a spin-5/2 ensemble and the corresponding (−1)-quantum coherences.

The splitting between adjacent peaks is $\omega_Q^{(1)}$, as for spins-1 and spins-3/2. The peak intensities correspond to the squares of the matrix elements of $\hat{I}^+$:

$$\hat{I}^+ = \begin{pmatrix} 0 & \sqrt{5} & 0 & 0 & 0 & 0 \\ 0 & 0 & 2\sqrt{2} & 0 & 0 & 0 \\ 0 & 0 & 0 & 3 & 0 & 0 \\ 0 & 0 & 0 & 0 & 2\sqrt{2} & 0 \\ 0 & 0 & 0 & 0 & 0 & \sqrt{5} \\ 0 & 0 & 0 & 0 & 0 & 0 \end{pmatrix}$$

In isotropic liquids, the first-order quadrupolar coupling vanishes, so all five spectral peaks are coincident. For example, the NMR spectrum of ^{17}O-labelled water is a single line (the J-couplings to the protons are unresolved).

In anisotropic liquids, the five-peak multiplet of Figure 13.27 becomes visible.

In powdered solids, the satellite peaks from the $\rho_{\boxed{-1_{\pm2}}}$ and $\rho_{\boxed{-1_{\pm4}}}$ coherences are generally too broad to observe. The spectra are dominated by the central-transition peak from the coherence $\rho_{\boxed{-1_{0}}}$, for which the frequency is independent of the first-order quadrupole coupling $\omega_Q^{(1)}$. Nevertheless, the central-transition peaks are broadened by the second-order quadrupole coupling $\omega_Q^{(2)}$, which may be as large as hundreds of kilohertz, in the case of ^{17}O. An experimental example is shown in Figure 13.28.

As in the spin-3/2 case, the second-order quadrupole broadening may be reduced by using a strong static magnetic field, and may be eliminated entirely using methods such as DAS, DOR, MQ-MAS, or ST-MAS (see *Further Reading*).

When C_Q is large, r.f. pulses act selectively on the central transition, as described in Section 13.2.7. The central-transition nutation frequency is given by

$$\boxed{\omega_{\text{nut}}^{\text{C}} = 3\omega_{\text{nut}} \qquad (\text{for spins } I = 5/2) \qquad (13.50)}$$

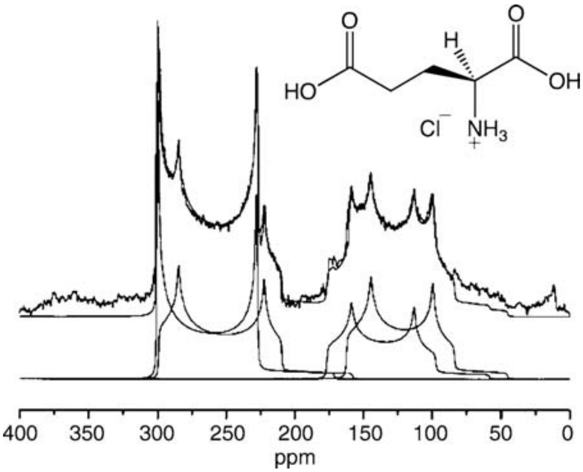

Figure 13.28 Solid-state magic-angle-spinning ^{17}O NMR spectra of ^{17}O-labelled L-glutamic acid hydrochloride obtained at a magnetic field of 14.1 T. All spectral features are generated by the ^{17}O central transition coherences; the satellite signals are too broad to be detected. The spectrum contains contributions from four different ^{17}O sites, with different quadrupole and chemical shift parameters. Each spectral contribution has a complicated shape due to second-order quadrupolar broadening. Simulations of the lineshape components are shown below the experimental data. Adapted from V. Lemaître, K. J. Pike, A. Watts, T. Anupõld, A. Samoson, M. E. Smith and R. Dupree, *Chem. Phys. Lett.* **371**, 91–97 (2003), copyright Elsevier.

For spins-5/2, the r.f. pulse is *three times* as effective when acting selectively on the central transition, compared with the non-selective regime.

13.4 Spins $I = 7/2$

Nuclear isotopes with spin $I = 7/2$ include ^{45}Sc, ^{51}V, ^{59}Co, ^{133}Cs, ^{139}La and ^{165}Ho.

Spin-7/2 nuclei have eight Zeeman energy levels, so the NMR spectrum contains contributions from seven (-1)-quantum coherences. In an isotropic environment, all seven peaks are superimposed, but a seven-peak multiplet is observed if the environment is anisotropic. Excitation in the strong-pulse regime provides a seven-peak multiplet with intensities in the ratio 7:12:15:16:15:12:7. These numbers are the squares of the $\hat{I}^{+}$ matrix elements. An experimental ^{133}Cs spectrum displaying a seven-peak multiplet is shown in Figure 13.24b.

In powdered solids, only the central transition is usually observed, if C_Q is large. In this regime, an r.f. pulse acts selectively on the central transition. The central-transition nutation frequency is

$$\boxed{\omega_{\text{nut}}^{\text{C}} = 4\omega_{\text{nut}} \qquad \text{(for spins } I = 7/2) \qquad (13.51)}$$

Note the large enhancement factor for the central-transition nutation frequency.

13.5 Spins $I = 9/2$

Spin $I = 9/2$ isotopes include ^{83}Kr, ^{93}Nb, ^{115}In, and ^{209}Bi.

The $I = 9/2$ isotope ^{93}Nb is the most magnetic nuclide in the periodic table. The magnitude of the nuclear magnetic moment is given by

$$\langle \mu \rangle = \langle \hat{\boldsymbol{\mu}}^2 \rangle^{1/2} = \gamma\hbar\{I(I+1)\}^{1/2}$$

Although the gyromagnetic ratio of ^{93}Nb is only 24% that of ^{1}H, the high nuclear spin of ^{93}Nb leads to a nuclear magnetic moment $\langle \mu \rangle$ that is about 50% greater than that of ^{1}H.

Notes

1. ^{14}N NMR is relatively straightforward if the nitrogen is in a sufficiently symmetrical environment (e.g. in the case of NH_4^+ ions), or if the molecular site has a high degree of mobility, so that the electric field gradient is averaged to a small value.

2. A general quantum state of a spin-1/2 nucleus may be depicted by drawing a polarization arrow pointing in the direction of defined $+\frac{1}{2}$ angular momentum. By extension, the general quantum state of a spin-1 nucleus may be depicted using *two* arrows, and the general quantum state of a spin-3/2 nucleus may be depicted using *three* arrows, and so on. This technique is sketched in R. Penrose, '*The Emperor's New Mind*', Oxford University Press, 1989, p. 353.

3. The use of the satellite order index was developed by S. Antonijevic and G. Bodenhausen, *J. Magn. Reson.* **180**, 297–304 (2006), following the early analysis of I. Solomon, *Phys. Rev.* **110**, 61 (1958).

4. The (±2)-quantum coherences of spins $I = 1$ give rise to weak NMR signals at *twice* the Larmor frequency, in the case of large quadrupolar couplings. These peaks are called *overtones* and result from the breakdown of the secular approximation. The (±2)-quantum overtone frequencies are insensitive to the first-order quadrupole coupling (see Equation 13.11). Overtone ^{14}N spectroscopy may be used to study peptide conformations (e.g. see R. Tycko and S. J. Opella, *J. Am. Chem. Soc.* **108**, 3531 (1986)).

5. The absence of a quadrupolar splitting for ^{2}H nuclei in isotropic liquids allows the ^{2}H resonance to be used for stabilizing the magnetic field in solution NMR experiments. See Chapter 4 Note 3.

6. There is a rich variety of liquid crystal phases, and not all of them give rise to the simple multiplets depicted in Figures 13.9 and 13.23. In general, more complex spectra are observed, which depend on the orientational distribution of the liquid crystal director axes with respect to the magnetic field.

7. The lineshape is named after its discoverer, George E. Pake (*J. Chem. Phys.* **16**, 327 (1948)).

8. The greater probability of perpendicular orientations compared with parallel orientations is discussed in Section 9.3.2.

9. This discussion of quadrupolar lineshapes neglects the influence of CSA. In the presence of CSA interactions, the contributions from the two (−1)-quantum coherences are different, giving rise to asymmetrical powder lineshapes.

10. The effective time origin of the ^{2}H NMR signal is actually at the *centre* of the r.f. pulse, so a reduction in the 'dead time' to zero would still not be good enough to detect an accurate powder NMR signal.

11. The description of the spin-1 quadrupolar echo is significantly more complicated if chemical shifts cannot be neglected. In that case, coherences must be followed individually, instead of grouping them together as in Equation 13.26. A full analysis distinguishes between coherence transfers that change both the coherence order and the satellite order (such as $\rho_{\boxed{+1_{+1}}} \Rightarrow \rho_{\boxed{-1_{-1}}}$) and coherence transfers that only change the satellite order (such as $\rho_{\boxed{-1_{+1}}} \Rightarrow \rho_{\boxed{-1_{-1}}}$). In the former case, a Zeeman echo is formed at the same time as the quadrupolar echo. This means that the chemical shift evolution refocuses at the same time as the first-order quadrupole evolution. In the second case, only a quadrupolar echo is formed. This means that the first-order quadrupole evolution refocuses, but the chemical shift evolution does not. The echo signal is a superposition of these different components.

12. Strictly speaking, the spectral peaks do not arise from *transitions*, but from *coherences*. Nevertheless, I retain the common terms *central transition* and *satellite transition*, for the sake of consistency with the literature.

13. Although techniques such as DOR and MQ-MAS remove second-order quadrupolar *broadening*, they do not remove *all* effects of the second-order quadrupolar interaction. There is also a *second-order quadrupolar shift*, which is analogous to a chemical shift, and which is not removed by DOR, MQ-MAS, and similar methods. This second-order shift is also observed in isotropic liquids where it is given the name 'dynamic frequency shift'.

14. Figure 13.25 suggests that the population difference across the central transition is enhanced if the populations are first equalized across each of the two satellite transitions. Saturation of the two satellite transitions by using a suitably modulated r.f. field may, therefore, be used to enhance the central-transition signal generated by a subsequent selective $(\pi/2)_x^{\mathrm{C}}$ pulse. A number of experimental methods exploit this trick. One example is described in H. T. Kwak, S. Prasad, T. Clark and P. J. Grandinetti, *Solid State Nucl. Magn. Reson.* **24**, 71–77 (2003). See Exercise 13.1.

Further Reading

- A good introduction to the solid-state NMR of quadrupolar nuclei is given in M. J. Duer, *Introduction to Solid-State NMR Spectroscopy*, Blackwell Science, 2004.
- The following article is recommended as a good introduction to solid-state NMR in general, including a concise overview of quadrupolar NMR techniques: D. D. Laws, H.-M. L. Bitter and A. Jerschow, *Angew. Chem. Int. Ed.* **41**, 3096–3129 (2002).
- It needs a steady head to navigate the formal theory of quadrupolar NMR in solids. A reliable guide is provided by A. Jerschow, *Prog. NMR Spectrosc.* **46**, 63–78 (2005).
- A review of ^{23}Na NMR in anisotropic environments is given in R. Kemp-Harper, S. P. Brown, C. E. Hughes, S. Peter and S. Wimperis, *Prog. NMR Spectrosc.* **30**, 157–181 (1997).
- Techniques for the NMR of quadrupolar nuclei in solids are reviewed by M. E. Smith and E. R. H. van Eck, *Prog. NMR Spectrosc.* **34**, 159–201 (1999), and S. E. Ashbrook and M. J. Duer, *Concepts Magn. Reson. A* **28**, 183–248 (2006).
- An excellent review of satellite-transition magic-angle-spinning experiments is given in S. E. Ashbrook and S. Wimperis, *Prog. NMR Spectrosc.* **45**, 53–108 (2004).
- The following classic paper on quadrupolar echoes in solids is still instructive: I. Solomon, *Phys. Rev.* **110**, 61 (1958).

Exercises

13.1 Consider an ensemble of spin-I nuclei, where I is a half-integer greater than 1 (i.e. $I = 3/2$, or $5/2$, or $7/2$, etc.) The spin system is left to reach thermal equilibrium, and then all the satellite transitions are completely saturated by a suitably modulated r.f. field. What is the enhancement factor for the population difference across the central transition?

13.2 In Section 13.2.7, it is shown that the nutation frequency of the spin $I = 3/2$ central transition is enhanced by a factor 2 when the transition is excited selectively, compared with the non-selective case. What is the enhancement factor for general I (assuming that I is a half-integer greater than 1)?

13.3 The quadrupolar echo pulse sequence in Figure 13.12 uses two $\pi/2$ pulses with a relative phase shift of $\pi/2$. Show that the same sequence generates double-quantum coherence if the two pulses have the same phase.

13.4 How many peaks are observed for an ensemble of spin-9/2 nuclei in a slightly anisotropic environment? What are the relative intensities of the multiplet components for ideal strong-pulse excitation?

Part 6

Coupled Spins

14 Spin-1/2 Pairs

In all real samples, the nuclear spins interact with each other. In the previous chapters, these spin–spin interactions were either completely ignored or absorbed into phenomenological relaxation parameters, which describe the damping of the coherences or the drift of the populations towards their thermal equilibrium values.

Most samples consist of more complex molecules which contain more than one spin. In general, the spin–spin couplings cannot be ignored. In this chapter, I discuss the simplest possible situation: a large number of identical molecules, each containing only two spins-1/2. In this case, the set of nuclear spins comprises an *ensemble of spin*-1/2 *pairs*:

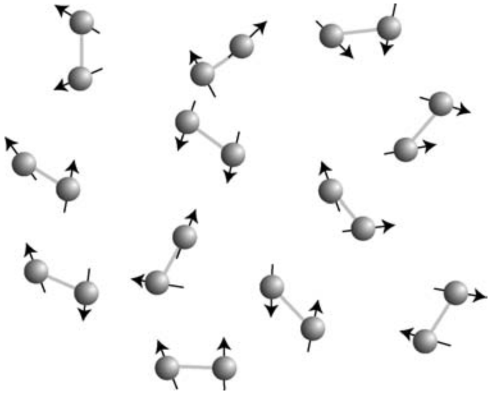

Figure 14.1
Ensemble of spin-1/2 pairs.

If the members of the pair are of the same isotopic type, then the spin system consists of a *homonuclear spin pair*. If the members of the pair are of different isotopic types, then the term *heteronuclear spin pair* is used.

I now examine the behaviour of spin-1/2 pairs in the presence of dipole–dipole couplings as well as J-couplings, allowing the treatment of spin-1/2 pairs in isotropic liquids, liquid crystals, and solids. The pairs are assumed to be *homonuclear* for most of this chapter.

14.1 Coupling Regimes

The behaviour of homonuclear spin-1/2 pairs depends strongly on the difference in chemical shifts between the spins, as compared to the spin-spin coupling.

Spin Dynamics: Basics of Nuclear Magnetic Resonance, Second Edition Malcolm H. Levitt

Weakly coupled pairs. If the *difference* in chemical shift frequencies is much larger than the spin–spin coupling, then the spin pair is said to be weakly coupled. A weakly coupled spin pair is denoted by the symbol AX (this 'alphabet notation' is discussed in more detail in Chapter 17).

Strongly coupled pairs. If the chemical shift frequency difference has roughly the same magnitude as the spin–spin coupling, then the spin system is said to be *strongly coupled*. The spin pair is denoted AB in this case.

Identical chemical shifts. If the chemical shifts of the two spins are the same,[1] then the two spins are said to be *magnetically equivalent*. The spin system in each molecule is denoted by the symbol A_2. An example is given by the protons in water.

The behaviour of strongly coupled spin systems is examined in Appendix A.8. The following discussion concentrates on the magnetically equivalent and weakly coupled cases.

14.2 Zeeman Product States and Superposition States

The pair of coupled spins-1/2 form a single quantum system. The state of the spin pair is described by a single ket, which has the following general form:

$$\boxed{|\psi\rangle = c_{\alpha\alpha}|\alpha\alpha\rangle + c_{\alpha\beta}|\alpha\beta\rangle + c_{\beta\alpha}|\beta\alpha\rangle + c_{\beta\beta}|\beta\beta\rangle \qquad (14.1)}$$

The states $|\alpha\alpha\rangle$, $|\alpha\beta\rangle$ ... are called *Zeeman product states* of the two spin-1/2 particles. In the notation $|\alpha\beta\rangle$, the α symbol indicates that the z-angular momentum of spin I_1 has the definite value $+1/2$, and the β symbol indicates that the z-angular momentum of spin I_2 has the definite value $-1/2$. The four Zeeman product states of the spin-1/2 pair obey the following eigenequations:

$$\begin{aligned}
\hat{I}_{1z}|\alpha\alpha\rangle &= +\tfrac{1}{2}|\alpha\alpha\rangle & \hat{I}_{2z}|\alpha\alpha\rangle &= +\tfrac{1}{2}|\alpha\alpha\rangle \\
\hat{I}_{1z}|\alpha\beta\rangle &= +\tfrac{1}{2}|\alpha\beta\rangle & \hat{I}_{2z}|\alpha\beta\rangle &= -\tfrac{1}{2}|\alpha\beta\rangle \\
\hat{I}_{1z}|\beta\alpha\rangle &= -\tfrac{1}{2}|\beta\alpha\rangle & \hat{I}_{2z}|\beta\alpha\rangle &= +\tfrac{1}{2}|\beta\alpha\rangle \\
\hat{I}_{1z}|\beta\beta\rangle &= -\tfrac{1}{2}|\beta\beta\rangle & \hat{I}_{2z}|\beta\beta\rangle &= -\tfrac{1}{2}|\beta\beta\rangle
\end{aligned}$$

⚠The use of the Zeeman product states $|\alpha\alpha\rangle$, $|\beta\alpha\rangle$ ... does *not* imply that the spin pair may *only* adopt such states, any more than the use of $|\alpha\rangle$ and $|\beta\rangle$ for a single spin-1/2 implies that the spin polarization may only be 'up' or 'down'. The single spin-1/2 may be, and usually is, in a superposition of the 'up' or 'down' states, and the spin-1/2 pair may be, and usually is, in a superposition of the four Zeeman product states.

Physically, the state in Equation 14.1 describes a spin pair with both polarizations pointing in some arbitrary direction:

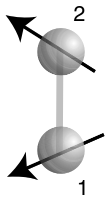

Figure 14.2
A pair of coupled spins.

The coefficients $c_{\alpha\alpha}$, $c_{\beta\alpha}$ ... are complex numbers. As usual, they must be normalized:

$$|c_{\alpha\alpha}|^2 + |c_{\alpha\beta}|^2 + |c_{\beta\alpha}|^2 + |c_{\beta\beta}|^2 = 1$$

The superposition state in Equation 14.1 is conveniently written as a column vector:

$$|\psi\rangle = \begin{pmatrix} c_{\alpha\alpha} \\ c_{\alpha\beta} \\ c_{\beta\alpha} \\ c_{\beta\beta} \end{pmatrix}$$

The normalization condition may then be written as

$$\langle\psi|\psi\rangle = (\, c_{\alpha\alpha}{}^{*}, \quad c_{\alpha\beta}{}^{*}, \quad c_{\beta\alpha}{}^{*}, \quad c_{\beta\beta}{}^{*}\,) \cdot \begin{pmatrix} c_{\alpha\alpha} \\ c_{\alpha\beta} \\ c_{\beta\alpha} \\ c_{\beta\beta} \end{pmatrix} = 1$$

Once again, note the use of the complex conjugate when transforming the 'ket' column vector to the 'bra' row vector.

14.3 Spin-Pair Hamiltonian

The behaviour of an individual spin pair is treated by constructing the Hamiltonian and solving the Schrödinger equation.

Start with the most general case. Each of the spins I_1 and I_2 has a different chemical shift δ_1 and δ_2, leading to chemically shifted Larmor frequencies given by

$$\begin{aligned} \omega_1^0 &= -\gamma B^0(1+\delta_1) \\ \omega_2^0 &= -\gamma B^0(1+\delta_2) \end{aligned} \tag{14.2}$$

The spins have a mutual J-coupling J_{12}, and also a secular dipole–dipole coupling d_{12}, as described in Sections 9.3 and 9.4.

The secular spin Hamiltonian is equal to

$$\widehat{\mathcal{H}}^0 = \omega_1^0 \hat{I}_{1z} + \omega_2^0 \hat{I}_{2z} + 2\pi J_{12} \hat{\mathbf{I}}_1 \cdot \hat{\mathbf{I}}_2 + d_{12}(3\hat{I}_{1z}\hat{I}_{2z} - \hat{\mathbf{I}}_1 \cdot \hat{\mathbf{I}}_2) \tag{14.3}$$

Our first task is to form the matrix representation of this Hamiltonian in the basis of Zeeman product states $\{|\alpha\alpha\rangle, |\alpha\beta\rangle, |\beta\alpha\rangle, |\beta\beta\rangle\}$. To do this, first expand the scalar product $\hat{\mathbf{I}}_1 \cdot \hat{\mathbf{I}}_2$ into the explicit angular momentum operators:

$$\hat{\mathbf{I}}_1 \cdot \hat{\mathbf{I}}_2 = \hat{I}_{1x}\hat{I}_{2x} + \hat{I}_{1y}\hat{I}_{2y} + \hat{I}_{1z}\hat{I}_{2z}$$

The products of the x- and y-operators may be expanded into shift operators (see Section 7.8.5), as follows:

$$\hat{I}_{1x}\hat{I}_{2x} + \hat{I}_{1y}\hat{I}_{2y} = \frac{1}{2}\left(\hat{I}_1^+\hat{I}_2^- + \hat{I}_1^-\hat{I}_2^+\right)$$

The spin Hamiltonian in Equation 14.3 may be split into two terms:

$$\widehat{\mathcal{H}}^0 = \widehat{\mathcal{H}}^0_{\mathrm{A}} + \widehat{\mathcal{H}}^0_{\mathrm{B}} \tag{14.4}$$

where the two parts are

$$\begin{aligned}\widehat{\mathcal{H}}^0_{\mathrm{A}} &= \omega_1^0 \hat{I}_{1z} + \omega_2^0 \hat{I}_{2z} + \omega_{12}^{\mathrm{A}} 2\hat{I}_{1z}\hat{I}_{2z}\\ \widehat{\mathcal{H}}^0_{\mathrm{B}} &= \omega_{12}^{\mathrm{B}} \frac{1}{2}\left(\hat{I}_1^+ \hat{I}_2^- + \hat{I}_1^- \hat{I}_2^+\right)\end{aligned} \tag{14.5}$$

The spin–spin coupling terms are defined as follows:

$$\begin{aligned}\omega_{12}^{\mathrm{A}} &= \pi J_{12} + d_{12}\\ \omega_{12}^{\mathrm{B}} &= 2\pi J_{12} - d_{12}\end{aligned} \tag{14.6}$$

The term $\widehat{\mathcal{H}}^0_{\mathrm{A}}$ is called the *diagonal part* of the spin Hamiltonian. The term $\widehat{\mathcal{H}}^0_{\mathrm{B}}$ is called the *off-diagonal part* of the spin Hamiltonian, or sometimes the *flip-flop term*. Equation 14.6 shows that the J-coupling and the dipole–dipole coupling contribute to both terms, but with different pre-factors and different signs.

The matrix representations of the two parts of the Hamiltonian in the Zeeman product basis $\{|\alpha\alpha\rangle, |\alpha\beta\rangle, |\beta\alpha\rangle, |\beta\beta\rangle\}$ are given by

$$\widehat{\mathcal{H}}^0_{\mathrm{A}} = \frac{1}{2}\begin{pmatrix} \omega_1^0 + \omega_2^0 + \omega_{12}^{\mathrm{A}} & 0 & 0 & 0\\ 0 & \omega_1^0 - \omega_2^0 - \omega_{12}^{\mathrm{A}} & 0 & 0\\ 0 & 0 & -\omega_1^0 + \omega_2^0 - \omega_{12}^{\mathrm{A}} & 0\\ 0 & 0 & 0 & -\omega_1^0 - \omega_2^0 + \omega_{12}^{\mathrm{A}} \end{pmatrix} \tag{14.7}$$

and

$$\widehat{\mathcal{H}}^0_{\mathrm{B}} = \frac{1}{2}\begin{pmatrix} 0 & 0 & 0 & 0\\ 0 & 0 & \omega_{12}^{\mathrm{B}} & 0\\ 0 & \omega_{12}^{\mathrm{B}} & 0 & 0\\ 0 & 0 & 0 & 0 \end{pmatrix} \tag{14.8}$$

For example, the element in the second row and third column of the matrix representation of $\widehat{\mathcal{H}}^0_{\mathrm{B}}$ may be calculated as follows:

$$\begin{aligned}\langle\alpha\beta|\widehat{\mathcal{H}}^0_{\mathrm{B}}|\beta\alpha\rangle &= \frac{1}{2}\omega_{12}^{\mathrm{B}}\, \langle\alpha\beta|\left(\hat{I}_1^+ \hat{I}_2^- + \hat{I}_1^- \hat{I}_2^+\right)|\beta\alpha\rangle\\ &= \frac{1}{2}\omega_{12}^{\mathrm{B}}\left(\langle\alpha\beta|\hat{I}_1^+ \hat{I}_2^-|\beta\alpha\rangle + \langle\alpha\beta|\hat{I}_1^- \hat{I}_2^+|\beta\alpha\rangle\right)\\ &= \frac{1}{2}\omega_{12}^{\mathrm{B}}\left(\langle\alpha\beta|\alpha\beta\rangle + 0\right)\\ &= \frac{1}{2}\omega_{12}^{\mathrm{B}}\end{aligned}$$

I now consider the cases of magnetic equivalence and weak coupling separately.

14.4 Pairs of Magnetically Equivalent Spins

14.4.1 Singlets and triplets

If the two chemical shifts are the same $\omega_1^0 = \omega_2^0 = \omega^0$, the spins are magnetically equivalent. The matrix representation of the spin Hamiltonian is given by

$$\widehat{\mathcal{H}}^0 = \frac{1}{2}\begin{pmatrix} 2\omega^0 + \omega_{12}^{\mathrm{A}} & 0 & 0 & 0 \\ 0 & -\omega_{12}^{\mathrm{A}} & \omega_{12}^{\mathrm{B}} & 0 \\ 0 & \omega_{12}^{\mathrm{B}} & -\omega_{12}^{\mathrm{A}} & 0 \\ 0 & 0 & 0 & -2\omega^0 + \omega_{12}^{\mathrm{A}} \end{pmatrix} \qquad \text{(in the Zeeman product basis)} \tag{14.9}$$

This matrix is not diagonal, which indicates that the Zeeman product states $\{|\alpha\alpha\rangle, |\alpha\beta\rangle, |\beta\alpha\rangle, |\beta\beta\rangle\}$ are not all eigenstates of the Hamiltonian.

The Hamiltonian matrix may be *diagonalized* by choosing a different set of four basis states, called the *singlet–triplet basis*. Choose three *triplet states*, defined as follows:

$$\begin{aligned} |T_{+1}\rangle &= |\alpha\alpha\rangle \\ |T_0\rangle &= \frac{1}{\sqrt{2}}\left(|\alpha\beta\rangle + |\beta\alpha\rangle\right) \\ |T_{-1}\rangle &= |\beta\beta\rangle \end{aligned} \tag{14.10}$$

and one *singlet state*, defined as follows:

$$|S_0\rangle = \frac{1}{\sqrt{2}}\left(|\alpha\beta\rangle - |\beta\alpha\rangle\right) \tag{14.11}$$

The triplet states $|T_{+1}\rangle$ and $|T_{-1}\rangle$ are the same as the Zeeman product states $|\alpha\alpha\rangle$ and $|\beta\beta\rangle$ respectively. The states $|T_0\rangle$ and $|S_0\rangle$ are normalized superpositions of the states $|\alpha\beta\rangle$ and $|\beta\alpha\rangle$, but with opposite signs.

The matrix elements of the Hamiltonian in the singlet–triplet basis may be derived according to the following example:

$$\begin{aligned} \langle S_0|\widehat{\mathcal{H}}^0|T_0\rangle &= \frac{1}{2}\left(\langle\alpha\beta| - \langle\beta\alpha|\right)\widehat{\mathcal{H}}^0\left(|\alpha\beta\rangle + |\beta\alpha\rangle\right) \\ &= \frac{1}{2}\Big(\langle\alpha\beta|\widehat{\mathcal{H}}^0|\alpha\beta\rangle - \langle\beta\alpha|\widehat{\mathcal{H}}^0|\alpha\beta\rangle + \langle\alpha\beta|\widehat{\mathcal{H}}^0|\beta\alpha\rangle - \langle\beta\alpha|\widehat{\mathcal{H}}^0|\beta\alpha\rangle\Big) \\ &= \frac{1}{4}\Big(-\omega_{12}^{\mathrm{A}} - \omega_{12}^{\mathrm{B}} + \omega_{12}^{\mathrm{B}} - (-\omega_{12}^{\mathrm{A}})\Big) = 0 \end{aligned}$$

Repetition for all elements generates the following matrix representation in the singlet–triplet basis:

$$\widehat{\mathcal{H}}^0 = \frac{1}{2}\begin{pmatrix} \omega^0 + \frac{1}{2}\pi J_{12} + \frac{1}{2}d_{12} & 0 & 0 & 0 \\ 0 & -d_{12} + \frac{1}{2}\pi J_{12} & 0 & 0 \\ 0 & 0 & -\omega^0 + \frac{1}{2}\pi J_{12} + \frac{1}{2}d_{12} & 0 \\ 0 & 0 & 0 & -\frac{3}{2}\pi J_{12} \end{pmatrix}$$

$$\text{(in the singlet–triplet basis)} \tag{14.12}$$

Since this matrix is diagonal, the singlet–triplet basis states $\{|T_{+1}\rangle, |T_0\rangle, |T_{-1}\rangle, |S_0\rangle\}$ are the energy eigenstates of the magnetically equivalent spin pair.

The three triplet states of the spin-1/2 pair behave in a similar way to the three states of a *single* nuclear spin with $I = 1$. The analogy may be emphasized by constructing *total* angular momentum operators by adding together the angular momentum operators of the two spins:

$$\boxed{\begin{aligned}\hat{I}_x &= \hat{I}_{1x} + \hat{I}_{2x}\\ \hat{I}_y &= \hat{I}_{1y} + \hat{I}_{2y}\\ \hat{I}_z &= \hat{I}_{1z} + \hat{I}_{2z}\end{aligned}} \tag{14.13}$$

The *total square angular momentum* operator may be constructed as follows:

$$\boxed{\hat{I}^2 = \hat{I}_x^2 + \hat{I}_y^2 + \hat{I}_z^2} \tag{14.14}$$

The three triplet states obey the following eigenequations:

$$\begin{aligned}\hat{I}_z|T_M\rangle &= M|T_M\rangle\\ \hat{I}^2|T_M\rangle &= 2|T_M\rangle\end{aligned} \tag{14.15}$$

where M is equal to $+1$, 0, or -1. Equation 14.15 is exactly the same as the eigenequations for the three states $|1, M\rangle$ of a spin-1 nucleus (see Equation 13.1).

Similarly, the singlet state $|S_0\rangle$ behaves in the same way as the state of a spin $I = 0$ nucleus:

$$\begin{aligned}\hat{I}_z|S_0\rangle &= 0\\ \hat{I}^2|S_0\rangle &= 0\end{aligned} \tag{14.16}$$

The magnetically equivalent pairs of spins-1/2 behave like a set of independent spin-0 and spin-1 nuclei.[2]

14.4.2 Energy levels

The energy levels are equal to the diagonal elements of Equation 14.12. The corresponding eigenequations are as follows:

$$\begin{aligned}\widehat{\mathcal{H}}^0|T_{+1}\rangle &= (\omega^0 + \frac{1}{2}\pi J_{12} + \frac{1}{2}d_{12})\,|T_{+1}\rangle\\ \widehat{\mathcal{H}}^0|T_0\rangle &= (\frac{1}{2}\pi J_{12} - d_{12})\,|T_0\rangle\\ \widehat{\mathcal{H}}^0|T_{-1}\rangle &= (-\omega^0 + \frac{1}{2}\pi J_{12} + \frac{1}{2}d_{12})\,|T_{-1}\rangle\\ \widehat{\mathcal{H}}^0|S_0\rangle &= (-\frac{3}{2}\pi J_{12})\,|S_0\rangle\end{aligned}$$

The energy contributions of the different terms are sketched in Figure 14.3. The Zeeman interaction of one spin with the magnetic field creates a splitting ω^0. Each level is split again by the Zeeman interaction of the second spin with the field. This leads to a three-level structure, with the central level being doubly degenerate. The J-coupling breaks the degeneracy by shifting three levels in one direction, with one of the central levels being shifted by three times as much in the opposite direction. Finally, the dipole–dipole coupling shifts two of the levels up and one level down. Note that the energy of the singlet state (shown in grey) is not affected by the dipole–dipole coupling.

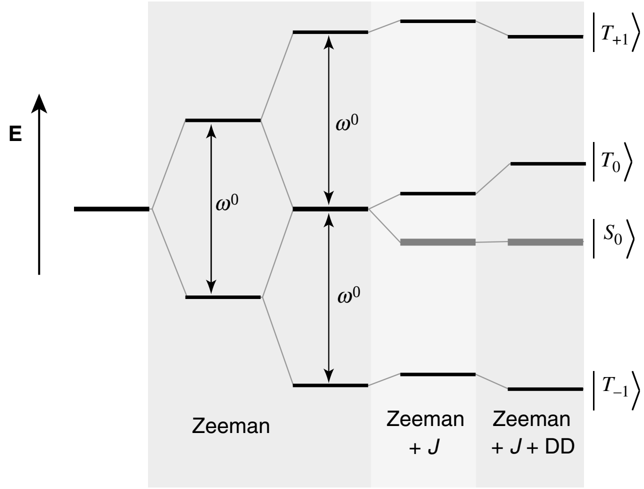

Figure 14.3 Energy levels for a pair of magnetically equivalent spins-1/2. The singlet state is shown in grey. The energy level shifts due to the spin–spin couplings are greatly exaggerated. The J-coupling and dipole–dipole (DD) coupling are assumed to have opposite signs.

If the energy levels of the singlet and triplet states are separated, then we get the picture shown in Figure 14.4. The energy level differences between adjacent triplet states are $\omega^0 \pm \frac{3}{2}d_{12}$. The J-coupling shifts the energy of the singlet state relative to the triplet states, but does not influence the triplet splittings.

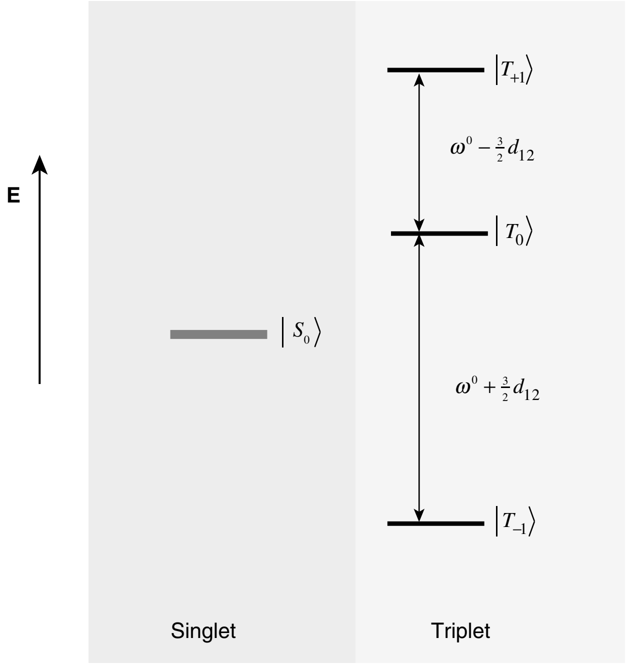

Figure 14.4 Singlet and triplet energy levels for a pair of magnetically equivalent spins-1/2.

The energy levels of the triplet states, therefore, are the same as for a spin-1 nucleus (see Figure 13.1), but with the first-order quadrupolar coupling $\omega_Q^{(1)}$ replaced by three times the dipole–dipole coupling d_{12}.

14.4.3 NMR spectra

A pair of magnetically equivalent spins-1/2 has four energy eigenstates: three triplet states and one singlet state. The singlet state has total spin $I = 0$ and is non-magnetic. It may usually be completely ignored in the context of NMR experiments.[2] All NMR signals are associated with the three triplet states, which behave in exactly the same way as the three Zeeman states of a spin-1 nucleus, except that the first-order quadrupolar interaction is substituted by three times the dipole–dipole coupling. The treatment of spin-1 dynamics given in Section 13.1 may therefore be recycled, with only minor changes.

Since there are two (-1)-quantum coherences within the triplet manifold, the spectrum consists of a doublet, in the general case:

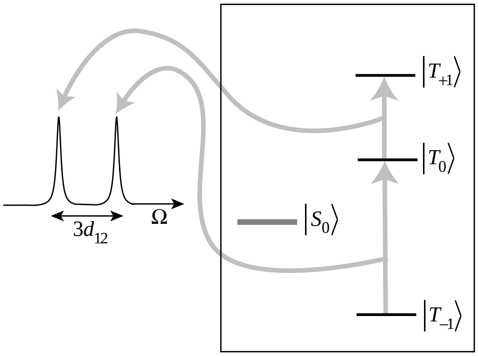

Figure 14.5 Doublet NMR spectrum generated by magnetically equivalent spin-1/2 pairs.

The splitting is given by $3d_{12}$, where d_{12} is the secular part of the dipole–dipole coupling. Compare with the spin-1 case depicted in Figure 13.5, in which the splitting is equal to the first-order quadrupolar coupling $\omega_Q^{(1)}$.

Pairs of magnetically equivalent spins-1/2 generate the following types of NMR spectra in the different phases of matter.

Isotropic liquids. Since the secular dipole–dipole coupling d_{12} vanishes in isotropic liquids, the two peaks coincide. This is why the NMR spectrum of liquid water is a singlet (see Figure 14.6a).

Liquid crystals. A dipolar splitting $3d_{12}$ is observed in anisotropic liquids[3] (see Figure 14.6b). The magnitude of this splitting depends on the secular dipole–dipole coupling, averaged over the anisotropic molecular motion (see Equation 9.40).

Powders. In solids, the dipolar splitting $3d_{12}$ depends on the orientation of the internuclear vector with respect to the external magnetic field (see Equation 9.40). As in the spin-1 case, this orientation dependence leads to a Pake doublet spectrum for pairs of magnetically equivalent spins-1/2 in a solid powder (see Figure 14.6c).

The splitting between the prominent peaks of the Pake doublet is equal to $3b_{12}$, in units of radians per second. Here, b_{12} is the dipole–dipole coupling constant in radians per second (see Equation 9.32), which is inversely proportional to the distance r_{12} between the nuclei I_1 and I_2:

$$\boxed{b_{12} = -\frac{\mu_0}{4\pi}\frac{\gamma^2\hbar}{r_{12}^3} \qquad (14.17)}$$

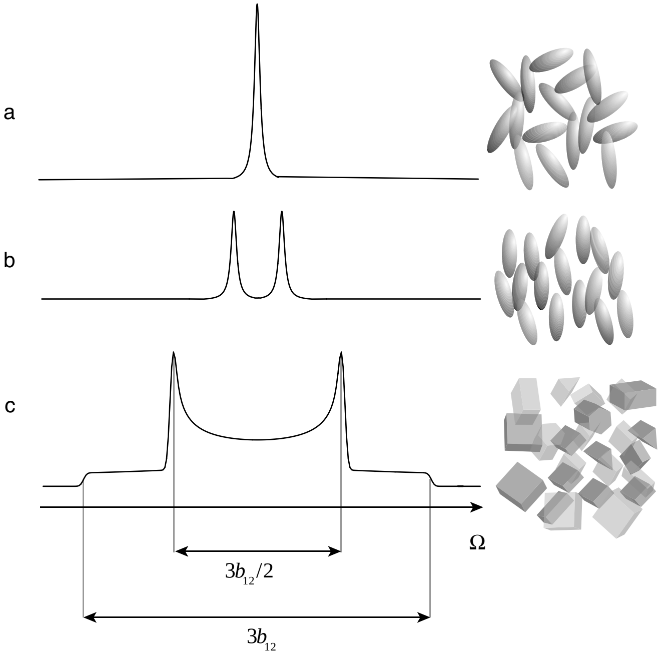

Figure 14.6
Typical spectra of magnetically equivalent spin-1/2 pairs in. (a) isotropic liquids; (b) nematic liquid crystals; (c) solid powders.

The powder NMR spectra of spin-1/2 pairs may, therefore, be used to estimate the distance between the nuclei (see Exercise 14.1).

14.4.4 Dipolar echo

Since the triplet manifold of equivalent spin-1/2 pairs behaves exactly like a spin-1, except with the dipole–dipole coupling replacing the quadrupole coupling, the two-pulse echo technique described in Section 13.1.10 also works in the spin-pair case. In this context, the echo involves the refocusing of homonuclear dipole–dipole interactions and is called a *dipolar echo*.[4]

14.5 Weakly Coupled Spin Pairs

14.5.1 Weak coupling

The spin-pair system is said to be weakly coupled if the following general condition is satisfied:[5]

$$\boxed{\frac{1}{2}|\omega_{12}^{\mathrm{B}}| << |\omega_1^0 - \omega_2^0| \qquad (14.18)}$$

where the flip-flop coupling term is $\omega_{12}^{\mathrm{B}} = 2\pi J_{12} - d_{12}$.

In the case of isotropic liquids, the secular dipole–dipole coupling vanishes. The weak-coupling condition in isotropic phase is therefore

$$|\pi J_{12}| << |\omega_1^0 - \omega_2^0|$$

or equivalently

$$\left|\frac{1}{2}J_{12}\right| << \left|(\delta_1 - \delta_2)\frac{\omega^0}{2\pi}\right| \qquad \text{(in isotropic liquids)} \qquad (14.19)$$

This is the most commonly used version of the weak-coupling condition. Half the J-coupling (in hertz) must be much less than the chemical shift frequency difference (also in hertz).

⚠Equation 14.19 is the weak-coupling condition in the *isotropic phase*. In solids or liquid crystals, the more general form of Equation 14.18 must be used.

14.5.2 AX spin systems

Actual compounds containing homonuclear AX spin systems are rather uncommon. An example of a ^{1}H AX system is dichloroacetaldehyde in isotropic solution:

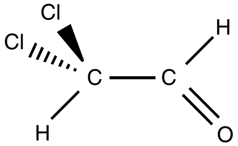

Figure 14.7
Dichloroacetaldehyde.

The isotopomers of this molecule potentially contain five types of magnetic spin: ^{1}H, ^{35}Cl, ^{37}Cl, ^{13}C and ^{2}H. The abundant ^{35}Cl and ^{37}Cl nuclei have a large electric quadrupole moment and relax rapidly. As discussed in Section 17.3, these quadrupolar spins may be ignored. The isotopes ^{13}C and ^{2}H occur in low natural abundance. By far the most common isotopomer of dichloroacetaldehyde contains only two magnetic nuclei, both protons. The two protons have very different chemical shifts due to the strong electronegativity of the Cl atoms. The chemical shift difference between the two protons is $\delta_1 - \delta_2 = 3.28\,\text{ppm}$ and their isotropic J-coupling is $J_{12} = 2.9\,\text{Hz}$.

The weak-coupling condition (Equation 14.19) is satisfied at all reasonable magnetic fields. For example, if the proton Larmor frequency is $|\omega^0/2\pi| = 500\,\text{MHz}$, then the chemical shift frequency difference is $3.28\,\text{ppm} \times 500\,\text{MHz} = 1.64\,\text{kHz}$, which is three orders of magnitude larger than $\frac{1}{2}J_{12} = 1.45\,\text{Hz}$.

A liquid sample of dichloroacetaldehyde, therefore, may be considered, to a good approximation, to consist of an ensemble of identical ^{1}H AX spin systems. The minor isotopomers containing ^{13}C or ^{2}H spins give rise to small additional spectral peaks, which are ignored here.[6]

14.5.3 Energy levels

If the general form of the weak-coupling condition (Equation 14.18) is satisfied, then the *secular approximation* (see Appendix A.6) may be used to discard the flip-flop Hamiltonian term $\widehat{\mathcal{H}}^0_{\mathrm{B}}$. The spin Hamiltonian may be approximated by the $\widehat{\mathcal{H}}^0_{\mathrm{A}}$ part alone:

$$\widehat{\mathcal{H}}^0_{\mathrm{A}} = \omega^0_1 \hat{I}_{1z} + \omega^0_2 \hat{I}_{2z} + \omega^{\mathrm{A}}_{12} 2\hat{I}_{1z}\hat{I}_{2z} \qquad (14.20)$$

where $\omega^{\mathrm{A}}_{12} = \pi J_{12} + d_{12}$. An immediate consequence of weak coupling is that the Zeeman product states $\{|\alpha\alpha\rangle, |\alpha\beta\rangle, |\beta\alpha\rangle, |\beta\beta\rangle\}$ are also eigenstates of the spin Hamiltonian. The matrix representation of the weak-coupling Hamiltonian is given in Equation 14.7. The corresponding eigenequations are

$$\widehat{\mathcal{H}}_A^0|\alpha\alpha\rangle = \omega_{\alpha\alpha}|\alpha\alpha\rangle \quad \widehat{\mathcal{H}}_A^0|\alpha\beta\rangle = \omega_{\alpha\beta}|\alpha\beta\rangle$$
$$\widehat{\mathcal{H}}_A^0|\beta\alpha\rangle = \omega_{\beta\alpha}|\beta\alpha\rangle \quad \widehat{\mathcal{H}}_A^0|\beta\beta\rangle = \omega_{\beta\beta}|\beta\beta\rangle$$

where the energies of the states are given by

$$\begin{aligned}
\omega_{\alpha\alpha} &= +\frac{1}{2}\omega_1^0 + \frac{1}{2}\omega_2^0 + \frac{1}{2}\omega_{12}^A \\
\omega_{\alpha\beta} &= +\frac{1}{2}\omega_1^0 - \frac{1}{2}\omega_2^0 - \frac{1}{2}\omega_{12}^A \\
\omega_{\beta\alpha} &= -\frac{1}{2}\omega_1^0 + \frac{1}{2}\omega_2^0 - \frac{1}{2}\omega_{12}^A \\
\omega_{\beta\beta} &= -\frac{1}{2}\omega_1^0 - \frac{1}{2}\omega_2^0 + \frac{1}{2}\omega_{12}^A
\end{aligned} \tag{14.21}$$

The contributions to the energy levels of the weakly coupled spin pair are sketched in Figure 14.8. The Zeeman interactions of the two spins with the magnetic field create a three-level structure, with the central level being doubly degenerate. The different chemical shifts of the two spins, followed by the J-coupling and the dipole–dipole coupling, break the degeneracy. In contrast to the magnetically equivalent case, the J-coupling and the dipole–dipole coupling work in exactly the same way, and either reinforce each other or partially cancel, depending on the relative signs.

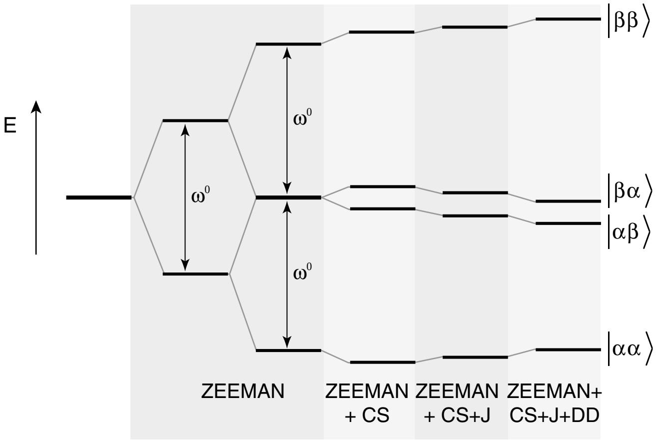

Figure 14.8
Energy levels for a weakly coupled spin-1/2 pair.

The figure above is not to scale; in reality, the splitting between the two central levels is far smaller than the Zeeman splitting.

14.5.4 AX spectrum

The NMR spectrum of an AX system contains four peaks, corresponding to the four different (−1)-quantum coherences in the AX spin ensemble, as shown in Figure 14.9. In general, the splitting between the components of each doublet is $2\omega_{12}^A = 2\pi J_{12} + 2d_{12}$. The splitting, therefore, contains a contribution from both the J-coupling and the secular dipole–dipole coupling.

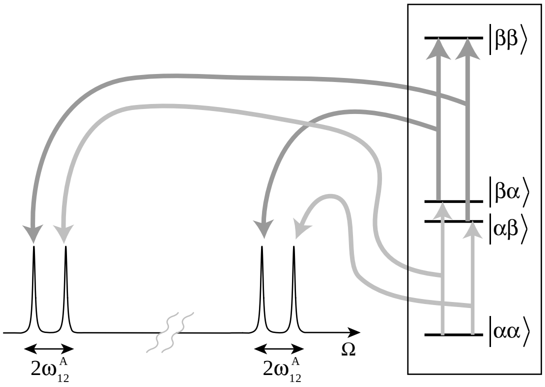

Figure 14.9
NMR spectrum containing two doublets, generated by weakly coupled spin-1/2 pairs.

In isotropic liquids, the secular dipole–dipole coupling vanishes. The splitting in this case is equal to $2\pi J_{12}$ in radians per second. When written in hertz, the splitting is simply J_{12}. This is the origin of the doublet multiplet structure introduced in Section 3.8.

The proton spectrum of dichloroacetaldehyde in solution is shown below. Note the splitting of 2.9 Hz in each doublet:

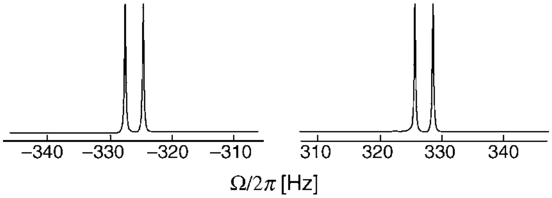

Figure 14.10
Proton spectrum of dichloroacetaldehyde, in a field of 4.7 T.

14.5.5 Heteronuclear spin pairs

Heteronuclear spin pairs contain two nuclei of different isotopic types, e.g. a ^{13}C nucleus coupled to a ^{1}H nucleus. Since the Larmor frequency difference between different isotopes is very large, heteronuclear spin pairs are always weakly coupled.

Notes

1. In general, two spins with the same chemical shift are only magnetically equivalent if the couplings to *other* spins fulfil additional symmetry requirements. This subject is discussed in detail in Section 17.5. The current chapter considers isolated pairs of spins, and neglects couplings to spins outside the pair. In this context, spins with the same chemical shift are also magnetically equivalent.

2. Since the singlet states of spin-1/2 pairs behave as if they are spin-0 nuclei, they are non-magnetic and have some unusual properties. In particular, these states are immune to many of the common relaxation mechanisms and have very long lifetimes in some circumstances. Rather surprisingly, the long lifetimes of singlet states may be exploited even if the spins are not magnetically equivalent. For example, see M. Carravetta, O. G. Johannessen and M. H. Levitt, *Phys. Rev. Lett.* **92**, 153003 (2004) and M. Carravetta and M. H. Levitt, *J. Am. Chem. Soc.* **126**, 6228–6229 (2004).

3. See Chapter 13 Note 6.

4. The dipolar echo induced by a two-pulse sequence is sometimes called a *solid echo*. The terms *dipolar echo* and *solid echo* are both rather misleading, since the echo formation is specific to well-separated pairs of magnetically equivalent spins-1/2.

5. Equation 14.19 does not ensure the validity of neglecting $\widehat{\mathcal{H}}_B^0$ under *all* experimental situations (see Section 18.14).

6. Small additional peaks due to minor isotopomers are sometimes termed *satellites*. The same term has a completely different meaning in the context of quadrupolar nuclei (see Chapter 13).

Exercises

14.1 In the original paper by G. E. Pake (*J. Chem. Phys.* **16**, 327 (1948)), the distance between the protons in water was estimated by measuring the ^{1}H powder spectrum of gypsum (calcium sulfate dihydrate). The splitting between the strong peaks in the Pake doublet was found to be 10.8 G (1.08 mT), in an old-fashioned swept-field experiment.

(i) Show that the Pake splitting corresponds to 45.98 kHz in a modern NMR protocol.

(ii) Use this number to estimate the distance between the two protons in a water molecule.

15 Homonuclear AX System

I now examine the dynamics of a homonuclear AX system in more detail.

Each molecule contains two spins-1/2, I_1 and I_2, which are of the same isotopic type but with different chemical shifts. The sketches below use different symbols to denote the inequivalence of the sites:

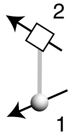

Figure 15.1
A pair of coupled spins with different chemical shifts.

In the following discussion, the spins are assumed to have a positive gyromagnetic ratio γ. The chemical shifts of the two sites are arranged in the order $\delta_1 < \delta_2$. This implies that the resonances of spin I_1 appear to the right of those of spins I_2, in a conventionally presented spectrum. The chemically shifted Larmor frequencies ω_1^0 and ω_2^0 are defined in Equation 14.2, and are both negative, with $\omega_1^0 > \omega_2^0$.

For simplicity, an isotropic liquid phase is assumed. The diagonal part of the coupling term is therefore given by $\omega_{12}^{\mathrm{A}} = \pi J_{12}$ (see Equation 14.6).

The spin system is assumed to satisfy Equation 14.19 and is therefore weakly coupled. The off-diagonal coupling term $\widehat{\mathcal{H}}_{\mathrm{B}}^0$ is neglected, as described in Section 14.5.

15.1 Eigenstates and Energy Levels

The weakly coupled spin Hamiltonian for a spin-1/2 pair in isotropic liquids is given by

$$\boxed{\widehat{\mathcal{H}}^0 \cong \omega_1^0 \hat{I}_{1z} + \omega_2^0 \hat{I}_{2z} + 2\pi J_{12} \hat{I}_{1z} \hat{I}_{2z} \qquad (15.1)}$$

The Zeeman product states $\{|\alpha\alpha\rangle, |\alpha\beta\rangle, |\beta\alpha\rangle, |\beta\beta\rangle\}$ are eigenstates of the weakly coupled spin Hamiltonian, as follows:

$$\widehat{\mathcal{H}}^0 |\alpha\alpha\rangle = \omega_{\alpha\alpha} |\alpha\alpha\rangle \qquad \widehat{\mathcal{H}}^0 |\alpha\beta\rangle = \omega_{\alpha\beta} |\alpha\beta\rangle$$
$$\widehat{\mathcal{H}}^0 |\beta\alpha\rangle = \omega_{\beta\alpha} |\beta\alpha\rangle \qquad \widehat{\mathcal{H}}^0 |\beta\beta\rangle = \omega_{\beta\beta} |\beta\beta\rangle$$

where the energies of the states are given in isotropic phase by

---

Spin Dynamics: Basics of Nuclear Magnetic Resonance, Second Edition Malcolm H. Levitt

$$
\begin{aligned}
\omega_{\alpha\alpha} &= +\frac{1}{2}\omega_1^0 + \frac{1}{2}\omega_2^0 + \frac{1}{2}\pi J_{12} \\
\omega_{\alpha\beta} &= +\frac{1}{2}\omega_1^0 - \frac{1}{2}\omega_2^0 - \frac{1}{2}\pi J_{12} \\
\omega_{\beta\alpha} &= -\frac{1}{2}\omega_1^0 + \frac{1}{2}\omega_2^0 - \frac{1}{2}\pi J_{12} \\
\omega_{\beta\beta} &= -\frac{1}{2}\omega_1^0 - \frac{1}{2}\omega_2^0 + \frac{1}{2}\pi J_{12}
\end{aligned}
\tag{15.2}
$$

The energy level structure is sketched in Figure 14.8.

The four Zeeman product states are eigenstates of the total z-angular momentum operator $\hat{I}_z$, with eigenvalues denoted M. The corresponding eigenequations are

$$
\begin{aligned}
\hat{I}_z|\alpha\alpha\rangle &= |\alpha\alpha\rangle \quad (M_{\alpha\alpha} = +1) \\
\hat{I}_z|\alpha\beta\rangle &= 0 \quad (M_{\alpha\beta} = 0) \\
\hat{I}_z|\beta\alpha\rangle &= 0 \quad (M_{\beta\alpha} = 0) \\
\hat{I}_z|\beta\beta\rangle &= -|\beta\beta\rangle \quad (M_{\beta\beta} = -1)
\end{aligned}
$$

The two central energy levels have total z-angular momentum $M = 0$, and the two extreme energy levels have $M = \pm 1$.

15.2 Density Operator

In a real sample, such as dichloroacetaldehyde, there is a very large number of independent spin-pair systems. The collection of independent, non-interacting spin pairs forms an *ensemble of AX spin systems*:

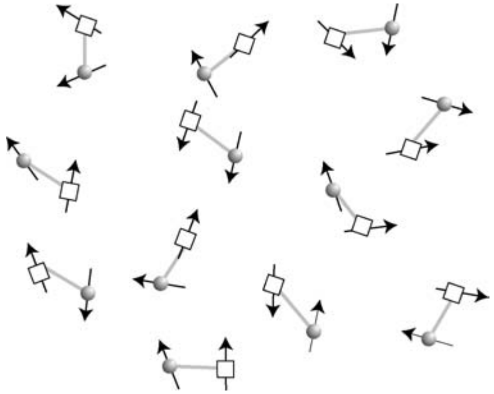

Figure 15.2
Ensemble of AX spin systems.

The quantum state of a spin-pair ensemble is constructed in just the same way as for non-interacting spins. The density operator $\hat{\rho}$ is defined as

$$
\boxed{\hat{\rho} = \overline{|\psi\rangle\langle\psi|}} \tag{15.3}
$$

where the overbar denotes an average over all ensemble members.

The density matrix for the spin-pair ensemble may be constructed by multiplying the column and row vectors in the usual way:

$$\hat{\rho} = \overline{\begin{pmatrix} c_{\alpha\alpha} \\ c_{\alpha\beta} \\ c_{\beta\alpha} \\ c_{\beta\beta} \end{pmatrix} \left(c_{\alpha\alpha}{}^*, \quad c_{\alpha\beta}{}^*, \quad c_{\beta\alpha}{}^*, \quad c_{\beta\beta}{}^* \right)} = \begin{pmatrix} \overline{c_{\alpha\alpha}c_{\alpha\alpha}{}^*} & \overline{c_{\alpha\alpha}c_{\alpha\beta}{}^*} & \overline{c_{\alpha\alpha}c_{\beta\alpha}{}^*} & \overline{c_{\alpha\alpha}c_{\beta\beta}{}^*} \\ \overline{c_{\alpha\beta}c_{\alpha\alpha}{}^*} & \overline{c_{\alpha\beta}c_{\alpha\beta}{}^*} & \overline{c_{\alpha\beta}c_{\beta\alpha}{}^*} & \overline{c_{\alpha\beta}c_{\beta\beta}{}^*} \\ \overline{c_{\beta\alpha}c_{\alpha\alpha}{}^*} & \overline{c_{\beta\alpha}c_{\alpha\beta}{}^*} & \overline{c_{\beta\alpha}c_{\beta\alpha}{}^*} & \overline{c_{\beta\alpha}c_{\beta\beta}{}^*} \\ \overline{c_{\beta\beta}c_{\alpha\alpha}{}^*} & \overline{c_{\beta\beta}c_{\alpha\beta}{}^*} & \overline{c_{\beta\beta}c_{\beta\alpha}{}^*} & \overline{c_{\beta\beta}c_{\beta\beta}{}^*} \end{pmatrix}$$

As for non-interacting spins, I now introduce the 'box notation', and write the density matrix as follows:

$$\hat{\rho} = \begin{pmatrix} \rho_{\boxed{\alpha\alpha}} & \rho_{\boxed{\alpha+}} & \rho_{\boxed{+\alpha}} & \rho_{\boxed{++}} \\ \rho_{\boxed{\alpha-}} & \rho_{\boxed{\alpha\beta}} & \rho_{\boxed{+-}} & \rho_{\boxed{+\beta}} \\ \rho_{\boxed{-\alpha}} & \rho_{\boxed{-+}} & \rho_{\boxed{\beta\alpha}} & \rho_{\boxed{\beta+}} \\ \rho_{\boxed{--}} & \rho_{\boxed{-\beta}} & \rho_{\boxed{\beta-}} & \rho_{\boxed{\beta\beta}} \end{pmatrix} \tag{15.4}$$

The four elements on the diagonal represent the populations of the four energy eigenstates. The 12 off-diagonal elements represent coherences between pairs of states.

Although there are 16 elements in the density operator, they are not all independent of each other. The four populations sum to unity, since the state of each spin pair is normalized:

$$\rho_{\boxed{\alpha\alpha}} + \rho_{\boxed{\beta\alpha}} + \rho_{\boxed{\alpha\beta}} + \rho_{\boxed{\beta\beta}} = 1$$

The coherences appear in complex conjugate pairs:

$$\rho_{\boxed{\beta-}} = \rho_{\boxed{\beta+}}{}^* \qquad \rho_{\boxed{+-}} = \rho_{\boxed{-+}}{}^*$$

and so on. There are nine independent quantities in the density operator of the ensemble of spin-1/2 pairs.

The coherences are classified according to the difference in the quantum number M for the connected states.

Coherences connecting states whose total z-angular momentum quantum numbers differ by one are called (±1)-quantum coherences, or *single-quantum coherences*. Such coherences also arise for isolated spins-1/2, as discussed in Chapter 11.

Coherences connecting states whose total z-angular momentum quantum numbers differ by two are called (±2)-quantum coherences, or *double-quantum coherences*. Such coherences cannot arise for isolated spins-1/2, but may exist for nuclei with $I \geq 1$ (see Chapter 13).

Coherences connecting states whose total z-angular momentum quantum numbers are the same are called *zero-quantum coherences*. These coherences are a feature of coupled spin systems, and cannot arise for isolated nuclei.

The term *multiple-quantum coherence* is used for coherences with orders not equal to ±1. Zero-quantum coherences are also classed as multiple-quantum coherences.

The 'box notation' allows the coherence order to be determined by inspection. The order is the sum of contributions from each symbol in the box, a '$-$' contributing -1, a '$+$' contributing $+1$, and 'α' and 'β' both contribute zero. For example, populations such as $\rho_{\boxed{\alpha\alpha}}$ have order zero, whereas $\rho_{\boxed{++}}$ is a (+2)-quantum coherence.

It is sometimes convenient to use a pictorial representation of the populations and coherences. For example, the term $\rho_{\boxed{\alpha\alpha}}$ is defined as

$$\rho_{\boxed{\alpha\alpha}} = \overline{c_{\alpha\alpha}c_{\alpha\alpha}{}^*}$$

and represents the (fractional) population of state $|\alpha\alpha\rangle$. It may be depicted by 'little balls' sitting on the $|\alpha\alpha\rangle$ energy level:

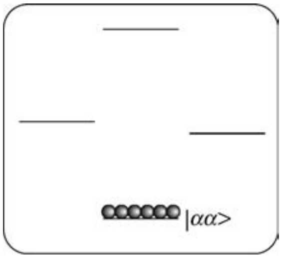

Figure 15.3
The population of state $|\alpha\alpha\rangle$.

The (−1)-quantum coherence $\rho_{\boxed{-\alpha}}$ is defined as

$$\rho_{\boxed{-\alpha}} = \overline{c_{\beta\alpha} c_{\alpha\alpha}{}^*} \tag{15.5}$$

It represents the coherent superposition of states $|\alpha\alpha\rangle$ and $|\beta\alpha\rangle$. It may be represented on a diagram as an arrow leading from state $|\alpha\alpha\rangle$ to state $|\beta\alpha\rangle$:

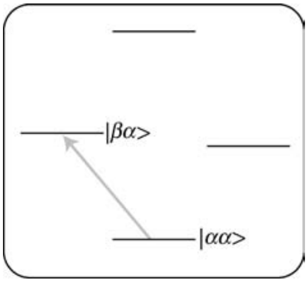

Figure 15.4
The coherence $\rho_{\boxed{-\alpha}}$.

The arrow for a (−1)-quantum coherence points *up* for spins of positive γ.

⚠To understand the correspondence between the two sides of Equation 15.5, read the product $\overline{c_{\beta\alpha} c_{\alpha\alpha}{}^*}$ from *right to left*. The quantum number for the first spin changes in the negative direction on going from right to left (from +1/2 to −1/2), hence the '−' label. The quantum number for the second spin remains unchanged at +1/2, hence the 'α' label. This is the significance of the box notation $\rho_{\boxed{-\alpha}}$. Similar arguments apply to the box notation for the other populations and coherences.

Loosely speaking, the coherence $\rho_{\boxed{-\alpha}}$ may be referred to as a '(−1)-quantum coherence of spin I_1, with spin I_2 in the state $|\alpha\rangle$'. This language is misleading, since almost all spins in the ensemble are in superposition states under ordinary circumstances. Nevertheless, the above terminology is a useful shorthand.

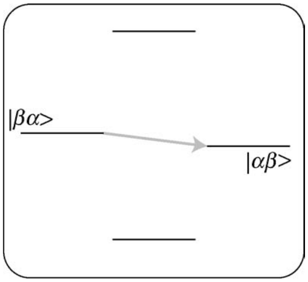

Figure 15.5
The coherence $\rho_{\boxed{+-}}$.

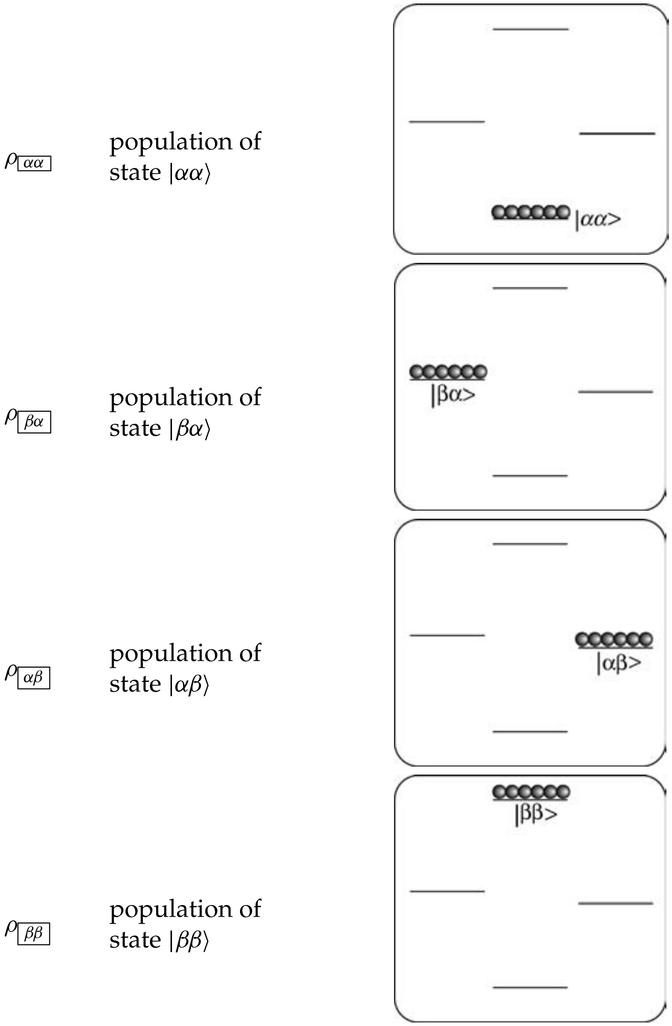

Figure 15.6 Representations of populations in an AX spin ensemble.

To continue: the zero-quantum coherence $\rho_{\boxed{+-}}$ is defined as

$$\rho_{\boxed{+-}} = \overline{c_{\alpha\beta}c_{\beta\alpha}{}^{*}}$$

It represents a coherent superposition of states $|\beta\alpha\rangle$ and $|\alpha\beta\rangle$. Its diagrammatic representation is shown in Figure 15.5. Diagrammatic representations of all populations and coherences are shown in Figures 15.6 and 15.7.

$$\left.\begin{matrix}\rho_{\boxed{-\alpha}}\\ \rho_{\boxed{-\beta}}\end{matrix}\right\}$$ (−1)-quantum coherences of spin I_1

$$\left.\begin{matrix}\rho_{\boxed{\alpha-}}\\ \rho_{\boxed{\beta-}}\end{matrix}\right\}$$ (−1)-quantum coherences of spin I_2

$$\left.\begin{matrix}\rho_{\boxed{+\alpha}}\\ \rho_{\boxed{+\beta}}\end{matrix}\right\}$$ (+1)-quantum coherences of spin I_1

$$\left.\begin{matrix}\rho_{\boxed{\alpha+}}\\ \rho_{\boxed{\beta+}}\end{matrix}\right\}$$ (+1)-quantum coherences of spin I_2

$$\left.\begin{matrix}\rho_{\boxed{-+}}\\ \rho_{\boxed{+-}}\end{matrix}\right\}$$ zero-quantum coherences

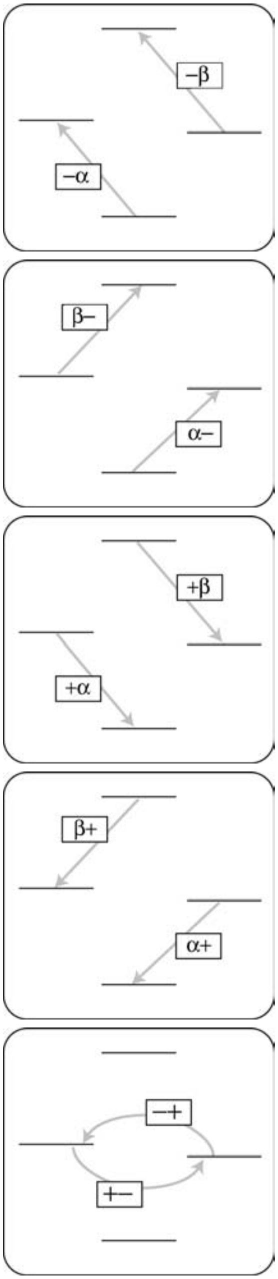

Figure 15.7 Representations of coherences in an AX spin ensemble.

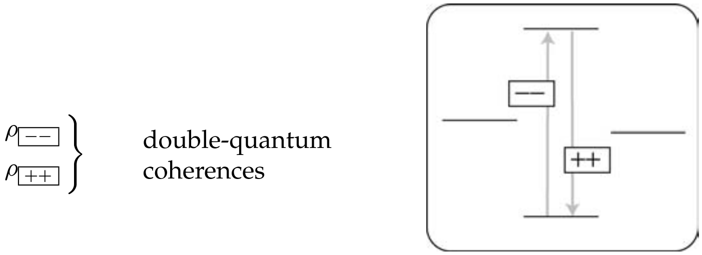

Figure 15.7 (*Continued*).

15.3 Rotating Frame

The behaviour of the spin-pair system is analysed most conveniently in a rotating reference frame, in which the action of the r.f. fields appears as simple as possible. The theory of the rotating frame may be developed by extending the arguments given in Section 10.6 for non-interacting spins.

A rotating-frame spin density operator is defined as follows:

$$\hat{\hat{\rho}} = \widehat{R}_z(-\Phi(t))\hat{\rho}\widehat{R}_z(+\Phi(t))$$

where the rotating-frame transformation operator is

$$\widehat{R}_z(\Phi) = \exp\{-\mathrm{i}\Phi\hat{I}_z\} = \exp\{-\mathrm{i}\Phi(\hat{I}_{1z} + \hat{I}_{2z})\}$$

The rotation angle of the frame is given, as before, by

$$\Phi(t) = \omega_{\mathrm{ref}}t + \phi_{\mathrm{ref}}$$

where the appropriate choices for ω_{ref} and ϕ_{ref} are discussed in Section 10.6.

The spin density operator evolves under the rotating-frame Hamiltonian $\hat{\hat{\mathcal{H}}}$, given by

$$\hat{\hat{\mathcal{H}}} = \widehat{R}_z(-\Phi)\widehat{\mathcal{H}}\widehat{R}_z(\Phi) - \omega_{\mathrm{ref}}\hat{I}_z \tag{15.6}$$

In the absence of an r.f. pulse, the rotating-frame spin Hamiltonian for the weakly coupled spin pair is

$$\hat{\hat{\mathcal{H}}}^0 = \widehat{R}_z(-\Phi)\widehat{\mathcal{H}}^0\widehat{R}_z(\Phi) - \omega_{\mathrm{ref}}\hat{I}_z$$

This evaluates to

$$\boxed{\hat{\hat{\mathcal{H}}}^0 = \Omega_1^0\hat{I}_{1z} + \Omega_2^0\hat{I}_{2z} + 2\pi J_{12}\hat{I}_{1z}\hat{I}_{2z} \tag{15.7}}$$

where the offset frequencies Ω_1^0 and Ω_2^0 represent differences between the chemically shifted Larmor frequencies and the spectrometer reference frequency:

$$\begin{aligned}\Omega_1^0 &= \omega_1^0 - \omega_{\mathrm{ref}} = -\gamma B^0(\delta_1 - \delta_{\mathrm{ref}})\\ \Omega_2^0 &= \omega_2^0 - \omega_{\mathrm{ref}} = -\gamma B^0(\delta_2 - \delta_{\mathrm{ref}})\end{aligned}$$

As usual, δ_{ref} is the chemical shift corresponding to the spectrometer reference frequency, i.e. the exact centre of the spectrum.

The rotating-frame Hamiltonian $\hat{\tilde{\mathcal{H}}}^0$ is exactly the same as the fixed-frame Hamiltonian, except with the offset frequencies Ω_1^0 and Ω_2^0 replacing the absolute Larmor frequencies ω_1^0 and ω_2^0. The eigenvalues of the rotating-frame spin Hamiltonian are given by

$$\begin{aligned} \Omega_{\alpha\alpha} &= +\frac{1}{2}\Omega_1^0 + \frac{1}{2}\Omega_2^0 + \frac{1}{2}\pi J_{12} \qquad & \Omega_{\beta\alpha} &= -\frac{1}{2}\Omega_1^0 + \frac{1}{2}\Omega_2^0 - \frac{1}{2}\pi J_{12} \\ \Omega_{\alpha\beta} &= +\frac{1}{2}\Omega_1^0 - \frac{1}{2}\Omega_2^0 - \frac{1}{2}\pi J_{12} \qquad & \Omega_{\beta\beta} &= -\frac{1}{2}\Omega_1^0 - \frac{1}{2}\Omega_2^0 + \frac{1}{2}\pi J_{12} \end{aligned} \tag{15.8}$$

The matrix representation of the weakly coupled spin Hamiltonian, in the absence of an r.f. field, is

$$\hat{\tilde{\mathcal{H}}}^0 = \begin{pmatrix} \Omega_{\alpha\alpha} & & & \\ & \Omega_{\alpha\beta} & & \\ & & \Omega_{\beta\alpha} & \\ & & & \Omega_{\beta\beta} \end{pmatrix}$$

The rotating frame is assumed for the rest of this chapter. The tilde symbols are dropped.

15.4 Free Evolution

Suppose that the spin-pair ensemble has a certain state at time point ②. The system is allowed to evolve freely over an interval τ, up to time point ③. We now investigate the relationship between the spin density operators at these two time points.

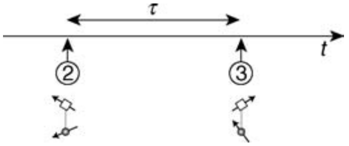

Figure 15.8
Free precession of a spin pair.

In the following discussion, I ignore relaxation.

15.4.1 Evolution of a spin pair

Consider a single spin pair, with a state $|\psi\rangle_{②}$ at the beginning of the free evolution interval. In general, the spin pair is in a superposition of the four energy eigenstates:

$$|\psi\rangle_{②} = \begin{pmatrix} c_{\alpha\alpha}② \\ c_{\alpha\beta}② \\ c_{\beta\alpha}② \\ c_{\beta\beta}② \end{pmatrix}$$

where the superposition coefficients $c_{\alpha\alpha}② \ldots$, etc., are complex numbers.

The Schrödinger equation for the spin pair is

$$\frac{\mathrm{d}}{\mathrm{d}t}|\psi\rangle = -\mathrm{i}\widehat{\mathcal{H}}^{0}|\psi\rangle$$

where the rotating-frame Hamiltonian $\widehat{\mathcal{H}}^{0}$ is given by Equation 15.7.

The Schrödinger equation has the solution

$$|\psi\rangle_{\textcircled{3}} = \widehat{U}(\tau)|\psi\rangle_{\textcircled{2}}$$

where the operator $\widehat{U}(\tau)$ is called the *free evolution propagator*, and is defined by

$$\widehat{U}(\tau) = \exp\{-\mathrm{i}\widehat{\mathcal{H}}^{0}\tau\}$$

The free evolution propagator has the following matrix representation:

$$\widehat{U}(\tau) = \exp\{-\mathrm{i}\widehat{\mathcal{H}}^{0}\tau\} = \begin{pmatrix} \exp\{-\mathrm{i}\Omega_{\alpha\alpha}\tau\} & & & \\ & \exp\{-\mathrm{i}\Omega_{\alpha\beta}\tau\} & & \\ & & \exp\{-\mathrm{i}\Omega_{\beta\alpha}\tau\} & \\ & & & \exp\{-\mathrm{i}\Omega_{\beta\beta}\tau\} \end{pmatrix}$$

Each superposition coefficient oscillates with a frequency equal to the energy of the corresponding eigenstate:

$$\begin{aligned} c_{\alpha\alpha}\textcircled{3} &= c_{\alpha\alpha}\textcircled{2}\exp\{-\mathrm{i}\Omega_{\alpha\alpha}\tau\} \\ c_{\alpha\beta}\textcircled{3} &= c_{\alpha\beta}\textcircled{2}\exp\{-\mathrm{i}\Omega_{\alpha\beta}\tau\} \\ &\vdots \end{aligned}$$

15.4.2 Evolution of the coherences

Now consider the ensemble of very many spin pairs.

The evolution of the populations and coherences may be treated by reproducing the discussion in Section 11.7. In the absence of relaxation, the populations of the spin system remain unchanged over the interval τ. The coherences rotate in the complex plane, according to the energy difference between the participating states. In general, the following equation of motion applies:

$$\boxed{\rho_{rs}\textcircled{3} \cong \rho_{rs}\textcircled{2}\exp\{-\mathrm{i}(\Omega_r - \Omega_s)\tau\} \qquad (15.9)}$$

where Ω_r and Ω_s are the eigenvalues of $\widehat{\mathcal{H}}^{0}$.

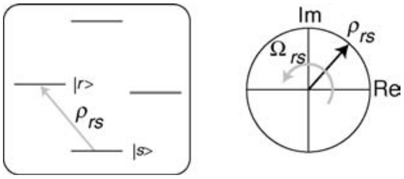

Figure 15.9
Free evolution of a coherence.

For example, the coherence $\rho_{\boxed{-\beta}}$ involves the states $|r\rangle = |\beta\beta\rangle$ and $|s\rangle = |\alpha\beta\rangle$. The coherence, therefore, evolves according to

$$\rho_{\boxed{-\beta}}\textcircled{3} = \rho_{\boxed{-\beta}}\textcircled{2}\ \exp\{\mathrm{i}\Omega_{\boxed{-\beta}}\tau\}$$

where the characteristic frequency $\Omega_{\boxed{-\beta}}$ is

$$\Omega_{\boxed{-\beta}} = -(\Omega_{\beta\beta} - \Omega_{\alpha\beta}) = \Omega_1^0 - \pi J_{12}$$

Similar equations apply for the other coherences. For completeness, the characteristic frequencies of all coherences are listed here:

$$\begin{aligned}
\Omega_{\boxed{--}} &= -(\Omega_{\beta\beta} - \Omega_{\alpha\alpha}) = \Omega_1^0 + \Omega_2^0 \\
\Omega_{\boxed{-\beta}} &= -(\Omega_{\beta\beta} - \Omega_{\alpha\beta}) = \Omega_1^0 - \pi J_{12} \\
\Omega_{\boxed{-\alpha}} &= -(\Omega_{\beta\alpha} - \Omega_{\alpha\alpha}) = \Omega_1^0 + \pi J_{12} \\
\Omega_{\boxed{\beta-}} &= -(\Omega_{\beta\beta} - \Omega_{\beta\alpha}) = \Omega_2^0 - \pi J_{12} \\
\Omega_{\boxed{\alpha-}} &= -(\Omega_{\alpha\beta} - \Omega_{\alpha\alpha}) = \Omega_2^0 + \pi J_{12} \\
\Omega_{\boxed{-+}} &= -(\Omega_{\beta\alpha} - \Omega_{\alpha\beta}) = \Omega_1^0 - \Omega_2^0 \\
\Omega_{\boxed{+-}} &= -(\Omega_{\alpha\beta} - \Omega_{\beta\alpha}) = -\Omega_1^0 + \Omega_2^0 \\
\Omega_{\boxed{+\beta}} &= -(\Omega_{\alpha\beta} - \Omega_{\beta\beta}) = -\Omega_1^0 + \pi J_{12} \\
\Omega_{\boxed{+\alpha}} &= -(\Omega_{\alpha\alpha} - \Omega_{\beta\alpha}) = -\Omega_1^0 - \pi J_{12} \\
\Omega_{\boxed{\beta+}} &= -(\Omega_{\beta\alpha} - \Omega_{\beta\beta}) = -\Omega_2^0 + \pi J_{12} \\
\Omega_{\boxed{\alpha+}} &= -(\Omega_{\alpha\alpha} - \Omega_{\alpha\beta}) = -\Omega_2^0 - \pi J_{12} \\
\Omega_{\boxed{++}} &= -(\Omega_{\alpha\alpha} - \Omega_{\beta\beta}) = -\Omega_1^0 - \Omega_2^0
\end{aligned} \tag{15.10}$$

Relaxation may be included in the evolution equations in a phenomenological way by adding a damping term. The evolution of a (-1)-quantum coherence is written as

$$\rho_{\boxed{-\beta}}\textcircled{3} = \rho_{\boxed{-\beta}}\textcircled{2}\ \exp\{(\mathrm{i}\Omega_{\boxed{-\beta}} - \lambda)\tau\}$$

where λ is the damping rate constant (inverse of T_2 for that particular coherence). In general, each of the six independent coherences in the spin-pair ensemble has a different damping rate constant. For simplicity, I assume here that all the damping rate constants are the same.[1]

The relaxation of the *populations* in a spin-pair ensemble is an important but complicated subject, which is tackled in Chapter 20.

15.5 Spectrum of the AX System: Spin–Spin Splitting

Assume that an r.f. pulse sequence is applied to the spin-pair ensemble, and the NMR signal detected afterwards. As always, the time point $t = 0$ is defined as the start of signal detection, i.e. just after the end of the pulse sequence. The pulse sequence leads to a spin density operator $\hat{\rho}(0)$, which then evolves freely over the subsequent time interval. The complex NMR signal emerging from the quadrature receiver is collected and digitized. In this section, I consider the form of the NMR signal generated by the spin-pair ensemble, and its relationship with the coherences existing at time $t = 0$.

By repeating the arguments given in Appendix A.5, one gets the following relationship between the quadrature NMR signal and the (−1)-quantum coherences of the spin system:

$$s(t) = 2\mathrm{i}(\rho_{\boxed{-\beta}}(t) + \rho_{\boxed{-\alpha}}(t) + \rho_{\boxed{\beta-}}(t) + \rho_{\boxed{\alpha-}}(t)) \exp\{-\mathrm{i}\phi_{\mathrm{rec}}\} \tag{15.11}$$

Here, ϕ_{rec} is the overall signal phase shift in the receiver and digitizer, as discussed in Section 4.5.4.

For an ensemble of spin-1/2 pairs, there are four (−1)-quantum coherences, and hence four independent contributions to the NMR signal.

The four (−1)-quantum coherences evolve in the rotating frame according to the following equations:

$$\begin{aligned}
\rho_{\boxed{-\beta}}(t) &= \rho_{\boxed{-\beta}}(0) \exp\{(\mathrm{i}\Omega_{\boxed{-\beta}} - \lambda)t\} \\
\rho_{\boxed{-\alpha}}(t) &= \rho_{\boxed{-\alpha}}(0) \exp\{(\mathrm{i}\Omega_{\boxed{-\alpha}} - \lambda)t\} \\
\rho_{\boxed{\beta-}}(t) &= \rho_{\boxed{\beta-}}(0) \exp\{(\mathrm{i}\Omega_{\boxed{\beta-}} - \lambda)t\} \\
\rho_{\boxed{\alpha-}}(t) &= \rho_{\boxed{\alpha-}}(0) \exp\{(\mathrm{i}\Omega_{\boxed{\alpha-}} - \lambda)t\}
\end{aligned}$$

where $\Omega_{\boxed{-\beta}} \ldots$ are the characteristic frequencies, given in Equation 15.10.

After FT, the NMR spectrum from the spin-pair ensemble contains *four* peaks:

$$\begin{aligned}
S(\Omega) = {} & a_{\boxed{-\beta}}\mathcal{L}(\Omega; \Omega_{\boxed{-\beta}}, \lambda) + a_{\boxed{\beta-}}\mathcal{L}(\Omega; \Omega_{\boxed{\beta-}}, \lambda) + \\
& a_{\boxed{-\alpha}}\mathcal{L}(\Omega; \Omega_{\boxed{-\alpha}}, \lambda) + a_{\boxed{\alpha-}}\mathcal{L}(\Omega; \Omega_{\boxed{\alpha-}}, \lambda)
\end{aligned}$$

where the complex amplitude of each peak depends on the amplitude of the corresponding coherence at the beginning of the detection period:

$$\begin{aligned}
a_{\boxed{-\beta}} &= 2\mathrm{i}\rho_{\boxed{-\beta}}(0) \exp\{-\mathrm{i}\phi_{\mathrm{rec}}\} & a_{\boxed{\beta-}} &= 2\mathrm{i}\rho_{\boxed{\beta-}}(0) \exp\{-\mathrm{i}\phi_{\mathrm{rec}}\} \\
a_{\boxed{-\alpha}} &= 2\mathrm{i}\rho_{\boxed{-\alpha}}(0) \exp\{-\mathrm{i}\phi_{\mathrm{rec}}\} & a_{\boxed{\alpha-}} &= 2\mathrm{i}\rho_{\boxed{\alpha-}}(0) \exp\{-\mathrm{i}\phi_{\mathrm{rec}}\}
\end{aligned} \tag{15.12}$$

Just as for the spin-1/2 case, the appearance of the spectral peaks depends on the phase of the complex amplitudes. For example, if $a_{\boxed{-\beta}}$ is real and positive, then the real part of $S(\Omega)$ contains a positive absorption Lorentzian centred at $\Omega = \Omega_{\boxed{-\beta}}$, and so on.

The peak frequencies correspond to the precession frequencies of the (−1)-quantum coherences in the rotating frame, given by Equation 15.10. These frequencies may be deduced by inspection from the 'box notation'. The spin with a '−' symbol contributes the chemical shift offset frequency, and the spin with an 'α' or 'β' symbol contributes plus or minus one-half of the J-coupling. For example, the coherence $\rho_{\boxed{-\beta}}$ generates a peak at the frequency $\Omega_{\boxed{-\beta}} = \Omega_1^0 - \pi J_{12}$, whereas the coherence $\rho_{\boxed{\alpha-}}$ generates a peak at the frequency $\Omega_{\boxed{\alpha-}} = \Omega_2^0 + \pi J_{12}$.

The spectrum, therefore, contains four peaks, two of which are near the chemical shift frequency Ω_1^0 and two of which are near the chemical shift frequency Ω_2^0, with a 'splitting' given by the J-coupling $2\pi J_{12}$.

The assignment of the peaks to particular coherences depends on the sign of the gyromagnetic ratio and the sign of the J-coupling. In Figures 15.10 and 15.11, it is assumed that the gyromagnetic ratio γ is positive, so that the frequency axis increases from left to right.

In the case $J_{12} > 0$, the peak assignments are as follows:

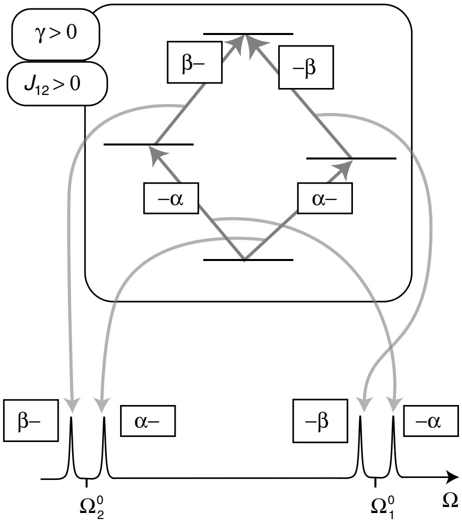

Figure 15.10
Relationship between the coherences and the spectrum for $\gamma > 0$ and $J_{12} > 0$.

The α-components are displaced towards positive frequency if the J-coupling is positive.

For $J_{12} < 0$, the peaks are assigned as follows:

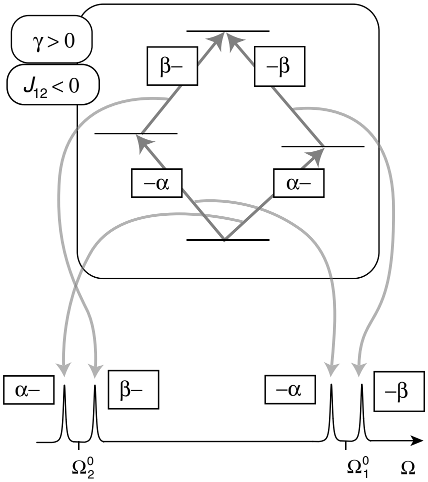

Figure 15.11
Relationship between the coherences and the spectrum for $\gamma > 0$ and $J_{12} < 0$.

The α-components are displaced towards negative frequency if the J-coupling is negative.

If the gyromagnetic ratio γ is negative, then the frequency axis increases from right to left (see Section 3.5). The peak assignments are as follows:

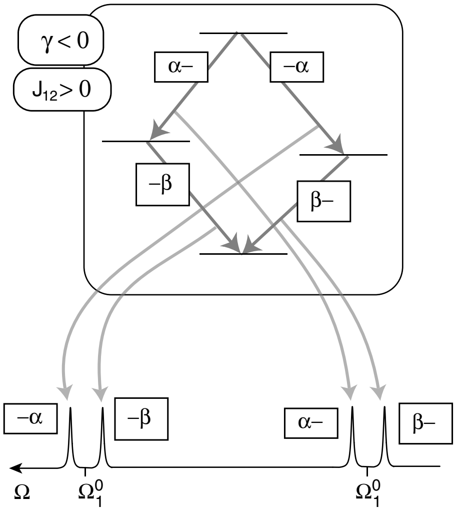

Figure 15.12
Relationship between the coherences and the spectrum for $\gamma > 0$ and $J_{12} < 0$.

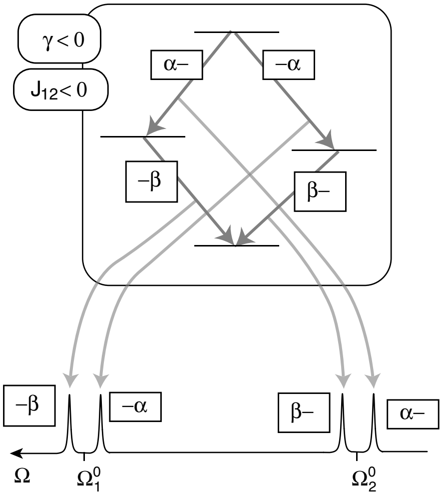

Figure 15.13
Relationship between the coherences and the spectrum for $\gamma < 0$ and $J_{12} < 0$.

As before, the α-components are displaced towards positive frequency if the J-coupling is positive, but are displaced towards negative frequency if the J-coupling is negative.

This is the origin of the spectral splittings by J-couplings, described in Section 3.8.[2]

15.6 Product Operators

We now calculate the evolution of the spin-pair density operator through some r.f. pulse sequences.

Recall the treatment of non-interacting spins-1/2. In that case, spin dynamical calculations are performed most conveniently by rotating the angular momentum operators $\hat{I}_x$, $\hat{I}_y$ and $\hat{I}_z$ in three-dimensional space, as summarized in Section 11.8. During strong r.f. pulses, the spin angular momentum is rotated about axes in the xy-plane of the rotating frame, according to the flip angles and phases of the pulses. During intervals of free precession, the spin angular momentum is rotated about the z-axis, at the chemical shift frequency in the rotating frame.

For coupled spin systems, this technique is extended. Instead of rotating single angular momentum operators, one must rotate *products* of angular momentum operators. The effect of spin–spin couplings must be considered alongside the action of strong r.f. pulses and chemical shifts.

The *product operator formalism* is a calculation method for weakly coupled spin systems. It is most useful for pulse sequences consisting of only two sorts of elements, i.e. very short r.f. pulses and free precession intervals in which the r.f. field is turned completely off. In such cases, the product operator method often allows the dynamics of coupled spin systems to be calculated by simple geometrical arguments and employing minimal mathematics.

In this section, the product operator method is applied to the homonuclear AX system.

15.6.1 Construction of product operators

The subject of product operators may be introduced through their matrix representations.

For an isolated spin-1/2, the four operators $\frac{1}{2}\widehat{1}$, $\hat{I}_x$, $\hat{I}_y$ and $\hat{I}_z$ have the following matrix representations in the basis $\{|\alpha\rangle, |\beta\rangle\}$:

$$\tfrac{1}{2}\widehat{1} = \frac{1}{2}\begin{pmatrix} 1 & 0 \\ 0 & 1 \end{pmatrix} \qquad \hat{I}_z = \frac{1}{2}\begin{pmatrix} 1 & 0 \\ 0 & -1 \end{pmatrix}$$

$$\hat{I}_x = \frac{1}{2}\begin{pmatrix} 0 & 1 \\ 1 & 0 \end{pmatrix} \qquad \hat{I}_y = \frac{1}{2\mathrm{i}}\begin{pmatrix} 0 & 1 \\ -1 & 0 \end{pmatrix}$$

For the two-spin system, 16 product operators may be constructed through the following recipe:

$$\boxed{\text{product operator}} = 2 \times \boxed{\begin{array}{l}\text{operator for}\\ \text{spin } I_1\\ \text{(4 choices)}\end{array}} \times \boxed{\begin{array}{l}\text{operator for}\\ \text{spin } I_2\\ \text{(4 choices)}\end{array}}$$

Examples of valid product operators for the two-spin system are $2\hat{I}_{1z}\hat{I}_{2x}$ and $2\hat{I}_{1x}\hat{I}_{2x}$.

When $\frac{1}{2}\widehat{1}$ operators are involved, the product operator may be abbreviated; for example:

$$2\,\frac{1}{2}\widehat{1}_1\,\frac{1}{2}\widehat{1}_2 = \frac{1}{2}\widehat{1}$$

$$2\,\frac{1}{2}\,\hat{I}_{1z}\widehat{1}_2 = \hat{I}_{1z}$$

The operators $\widehat{1}_1$, $\widehat{1}_2$ and $\widehat{1}$ are entirely equivalent:

$$\widehat{1}_1 = \widehat{1}_2 = \widehat{1}$$

The subscripts 1 and 2 are useful for bookkeeping, but have no other significance in this context. Note carefully that the implied summation

$$\widehat{1} = \widehat{1}_1 + \widehat{1}_2 \qquad \text{(incorrect!)}$$

does *not* hold for the unity operators.

It is advisable to retain the factors of two in product operators such as $2\hat{I}_{1z}\hat{I}_{2z}$, $2\hat{I}_{1x}\hat{I}_{2y}$. Do not group the factors of two with any other numerical factors. Always use a consistent order for indices 1 and 2.

The matrix representations of the product operators may be constructed by taking the *direct product* of the matrix representations of the individual operators:

Example 1

$$
\begin{aligned}
2\hat{I}_{1x}\hat{I}_{2z} &= 2\,\frac{1}{2}\begin{pmatrix} 0 & 1 \\ 1 & 0 \end{pmatrix} \otimes \frac{1}{2}\begin{pmatrix} 1 & 0 \\ 0 & -1 \end{pmatrix} = \frac{1}{2}\begin{pmatrix} 0 & 1 \\ 1 & 0 \end{pmatrix} \otimes \begin{pmatrix} 1 & 0 \\ 0 & -1 \end{pmatrix} \\
&= \frac{1}{2}\begin{pmatrix} 0\begin{pmatrix} 1 & 0 \\ 0 & -1 \end{pmatrix} & 1\begin{pmatrix} 1 & 0 \\ 0 & -1 \end{pmatrix} \\ 1\begin{pmatrix} 1 & 0 \\ 0 & -1 \end{pmatrix} & 0\begin{pmatrix} 1 & 0 \\ 0 & -1 \end{pmatrix} \end{pmatrix} \\
&= \frac{1}{2}\begin{pmatrix} 0 & 0 & 1 & 0 \\ 0 & 0 & 0 & -1 \\ 1 & 0 & 0 & 0 \\ 0 & -1 & 0 & 0 \end{pmatrix}
\end{aligned}
$$

Example 2

$$
\begin{aligned}
\hat{I}_{2y} = 2\,\frac{1}{2}\widehat{1}_1\hat{I}_{2y} &= \frac{1}{2\mathrm{i}}\begin{pmatrix} 1 & 0 \\ 0 & 1 \end{pmatrix} \otimes \begin{pmatrix} 0 & 1 \\ -1 & 0 \end{pmatrix} \\
&= \frac{1}{2\mathrm{i}}\begin{pmatrix} 1\begin{pmatrix} 0 & 1 \\ -1 & 0 \end{pmatrix} & 0\begin{pmatrix} 0 & 1 \\ -1 & 0 \end{pmatrix} \\ 0\begin{pmatrix} 0 & 1 \\ -1 & 0 \end{pmatrix} & 1\begin{pmatrix} 0 & 1 \\ -1 & 0 \end{pmatrix} \end{pmatrix} \\
&= \frac{1}{2\mathrm{i}}\begin{pmatrix} 0 & 1 & 0 & 0 \\ -1 & 0 & 0 & 0 \\ 0 & 0 & 0 & 1 \\ 0 & 0 & -1 & 0 \end{pmatrix}
\end{aligned}
$$

The construction of the direct product should be self-explanatory from these examples: copies of the *second* matrix are multiplied by the elements of the *first* matrix, and assembled into a larger matrix.

15.6.2 Populations and coherences

In general, the spin density operator may be expressed as a sum of product operator terms, i.e.

$$\hat{\rho} = a\widehat{1} + b\hat{I}_{1z} + c2\hat{I}_{1x}\hat{I}_{2y} + \ldots \tag{15.13}$$

where a, b, c, etc. are real numbers. The presence of a particular product operator term in the density operator implies a certain configuration of the populations and the coherences.

Example 1. The operator $\hat{I}_{1z}$ has a matrix representation of

$$\hat{I}_{1z} = \frac{1}{2}\begin{pmatrix} 1 & & & \\ & 1 & & \\ & & -1 & \\ & & & -1 \end{pmatrix}$$

(omitting zero elements). If $\hat{\rho}$ contains a (positive) term $\hat{I}_{1z}$, then the populations of states $|\beta\alpha\rangle$ and $|\beta\beta\rangle$ are *depleted* with respect to the populations of states $|\alpha\beta\rangle$ and $|\alpha\alpha\rangle$. The product operator $\hat{I}_{1z}$ indicates a *population differential* across the single-quantum transitions of spin I_1:

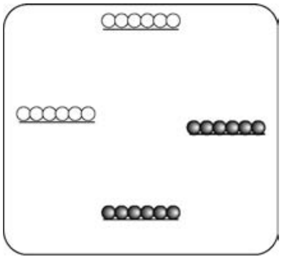

Figure 15.14
Population distribution corresponding to a density operator term $\hat{I}_{1z}$.

In this diagram, 'hollow balls' represent 'negative populations', and 'filled balls' represent 'positive populations'. The concept of a negative population is possible because we are only considering the contribution of a single term to the density operator; when all terms are taken into account, the *total* population of each state is always positive.

Example 2. The operator $2\hat{I}_{1z}\hat{I}_{2z}$ has a matrix representation of

$$2\hat{I}_{1z}\hat{I}_{2z} = \frac{1}{2}\begin{pmatrix} 1 & & & \\ & -1 & & \\ & & -1 & \\ & & & 1 \end{pmatrix}$$

If $\hat{\rho}$ contains a (positive) term $2\hat{I}_{1z}\hat{I}_{2z}$, then the two central states $|\alpha\beta\rangle$ and $|\beta\alpha\rangle$ are depleted in population with respect to the outer states $|\alpha\alpha\rangle$ and $|\beta\beta\rangle$:

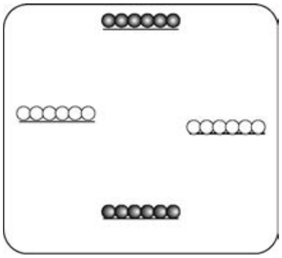

Figure 15.15
Population distribution corresponding to a density operator term $2\hat{I}_{1z}\hat{I}_{2z}$.

This population pattern is called *two-spin Zeeman order*.

Example 3. The operator $-\hat{I}_{1y}$ has a matrix representation of

$$-\hat{I}_{1y} = \frac{1}{2\mathrm{i}} \begin{pmatrix} 0 & 0 & -1 & 0 \\ 0 & 0 & 0 & -1 \\ 1 & 0 & 0 & 0 \\ 0 & 1 & 0 & 0 \end{pmatrix}$$

If $\hat{\rho}$ contains a term $-\hat{I}_{1y}$, then the spin ensemble contains single-quantum coherences belonging to spin I_1:

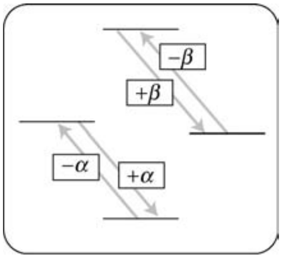

Figure 15.16
Coherences corresponding to a density operator term $-\hat{I}_{1y}$.

Single-quantum coherences are capable of inducing an NMR signal, so the presence of a term $-\hat{I}_{1y}$ in the density operator $\hat{\rho}(0)$ is associated with observable spectral peaks. For example, suppose that the receiver phase shift ϕ_{rec} is zero. If the density operator at the start of signal detection $\hat{\rho}(0)$ contains a component proportional to $-\hat{I}_{1y}$, then the (-1)-quantum coherences $\rho_{\boxed{-\beta}}(0)$ and $\rho_{\boxed{-\alpha}}(0)$ are proportional to (1/2i). From Equation 15.12, FT of the signal generates a spectrum with two absorption peaks near the chemical shift of spin I_1:

Figure 15.17
In-phase spectral multiplet corresponding to a density operator term $-\hat{I}_{1y}$.

(This sketch is shown for the case of positive γ and positive J_{12}.) This spectral configuration is called an *in-phase multiplet* of spin I_1.

Example 4. The operator $-2\hat{I}_{1y}\hat{I}_{2z}$ has a matrix representation of

$$-2\hat{I}_{1y}\hat{I}_{2z} = \frac{1}{2\mathrm{i}} \begin{pmatrix} 0 & 0 & -1 & 0 \\ 0 & 0 & 0 & 1 \\ 1 & 0 & 0 & 0 \\ 0 & -1 & 0 & 0 \end{pmatrix}$$

If $\hat{\rho}$ contains a term $-2\hat{I}_{1y}\hat{I}_{2z}$, then the (-1)-quantum coherences $\rho_{\boxed{-\beta}}$ and $\rho_{\boxed{-\alpha}}$ have opposite sign. The spectrum obtained by Fourier transforming the signal displays two absorption peaks near the chemical shift of spin I_1, with the $\rho_{\boxed{-\beta}}$ peak inverted in sign with respect to the $\rho_{\boxed{-\alpha}}$ peak:

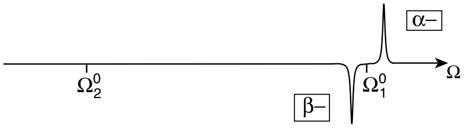

Figure 15.18 Antiphase spectral multiplet corresponding to a density operator term $-2\hat{I}_{1y}\hat{I}_{2z}$.

This spectral configuration is called an *antiphase multiplet* of spin I_1.

An antiphase multiplet of spin I_2 is produced by a density operator term $-2\hat{I}_{1z}\hat{I}_{2y}$.

Example 5. The operator $2\hat{I}_{1x}\hat{I}_{2y}$ has a matrix representation of

$$2\hat{I}_{1x}\hat{I}_{2y} = \frac{1}{2\mathrm{i}}\begin{pmatrix} & & & 1 \\ & & -1 & \\ & 1 & & \\ -1 & & & \end{pmatrix}$$

The presence of this operator as a component of $\hat{\rho}$ indicates that the spin ensemble contains zero- and double-quantum coherences:

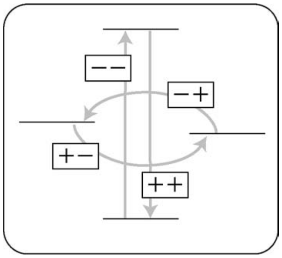

Figure 15.19 Coherences corresponding to a density operator term $2\hat{I}_{1x}\hat{I}_{2y}$.

Unlike single-quantum coherences, zero- and double-quantum coherences do not induce NMR signals, and hence cannot be associated with a particular configuration of peaks in the spectrum. These coherences are important, nevertheless because they may be converted by r.f. pulses into single-quantum coherences, which *do* induce signals.

It is also possible to use shift and projection operators to determine the configuration of populations and coherences in a product operator term, without writing out the matrices. For example, suppose that the density operator is

$$\hat{\rho} = \ldots + r\, 2\hat{I}_{1y}\hat{I}_{2x} + \ldots$$

where r is a real number. The amplitude of the zero-quantum coherence $\rho_{\boxed{-+}}$ may be calculated as follows:

$$\begin{aligned}\hat{\rho} &= \ldots + r\, 2\frac{1}{2\mathrm{i}}\left(\hat{I}_1^+ - \hat{I}_1^-\right)\frac{1}{2}\left(\hat{I}_2^+ + \hat{I}_2^-\right) + \ldots \\ &= \ldots - \frac{r}{2\mathrm{i}}\hat{I}_1^-\hat{I}_2^+ + \ldots\end{aligned}$$

The coherence $\rho_{\boxed{-+}}$ is the coefficient of $\hat{I}_1^-\hat{I}_2^+$ in the density operator, and is equal to $-r/(2\mathrm{i})$ in this case.

Similar calculations may be made for any other population or coherence.

15.6.3 Spin orientations

What do the product operator terms mean physically?

In this section, I draw schematic pictures of microscopic spin orientations for a few different members of the ensemble. I distinguish between the two sets of spins by using a 'ball' for spins 1 and a 'square' for spins 2. To bring out the features of each product operator, I have greatly exaggerated the preference of the spins for particular configurations, which is sometimes misleading. In practice, the statistical tendencies are exceedingly small (around 10^{-5}), and would be invisible if drawn realistically.

Example 1. The operator $\hat{I}_{1z}$. If the spin density operator contains a term $\hat{I}_{1z}$, there is a net polarization of spins I_1 along the magnetic field direction (z-axis). The polarizations of spins I_2 are isotropically distributed:

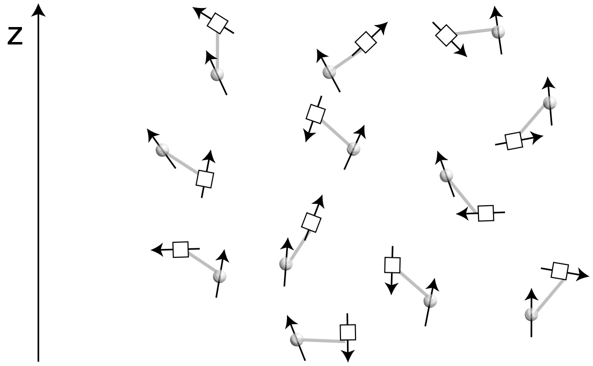

Figure 15.20 Microscopic spin polarizations corresponding to a density operator term $\hat{I}_{1z}$. Spins I_1 are shown as spheres; spins I_2 are shown as squares.

Example 2. The operator $\hat{I}_{2z}$. The presence of a term $\hat{I}_{2z}$ in the density operator implies that there is a net polarization of spins I_2 along the magnetic field, and the polarizations of spins I_1 are isotropically distributed:

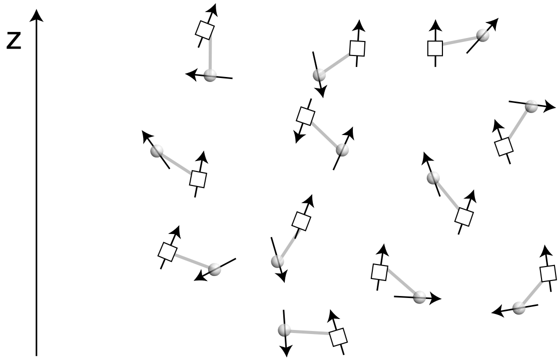

Figure 15.21 Microscopic spin polarizations corresponding to a density operator term $\hat{I}_{2z}$.

Example 3. The operator $\hat{I}_{1x}$. The presence of a term $\hat{I}_{1x}$ in the density operator implies that the polarization vectors of spins I_1 tend to be aligned along the x-axis. The polarization vectors of spins I_2 have no preferential orientation (see Figure 15.22).

The following examples introduce the new concept of *correlations* between the polarizations of the two spins.

Example 4. The operator $2\hat{I}_{1z}\hat{I}_{2z}$. The presence of the two-spin Zeeman order term $2\hat{I}_{1z}\hat{I}_{2z}$ in the density operator implies that there is *no* net tendency for either of the spin species to be polarized along the z-axis. Nevertheless, there is a *correlation* between the spin polarizations. Although the polarization direction for a given spin I_1 is unpredictable, its neighbour I_2 is likely to have the *same* direction of polarization along the magnetic field, as shown in Figure 15.23. Note that the correlation only applies to the z-components of the spin polarization vectors.

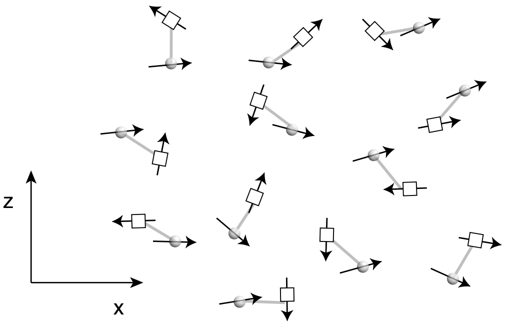

Figure 15.22
Microscopic spin polarizations corresponding to a density operator term $\hat{I}_{1x}$.

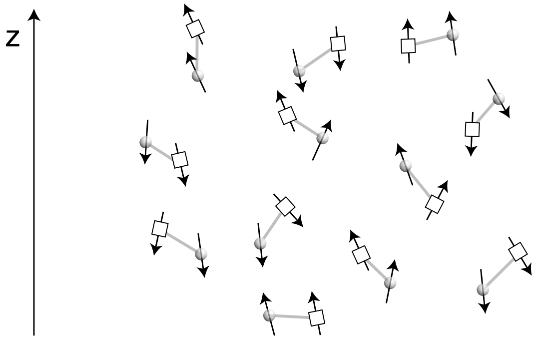

Figure 15.23
Microscopic spin polarizations corresponding to a density operator term $2\hat{I}_{1z}\hat{I}_{2z}$.

The concept of correlation is subtle but important. The following analogy might help. Choose at random a large number of married couples. Now pick blindly one married pair from this 'ensemble'. There is no way of predicting in advance whether the man is shorter or taller than the average. The same goes for the woman. However, one may state with some confidence that if the man is shorter than the average, then so is the woman. Similarly, if the chosen man is taller than the average, then the woman also tends to be taller. This is because height is strongly *correlated* within married couples.

Something analogous is going on for a spin-pair ensemble in a density operator state containing the term $2\hat{I}_{1z}\hat{I}_{2z}$. The z-components of the polarizations are randomly distributed, but correlated within each spin pair.

Example 5. The operator $2\hat{I}_{1x}\hat{I}_{2x}$. The presence of the product operator term $2\hat{I}_{1x}\hat{I}_{2x}$ implies a correlation in the x-components of the spin polarizations:

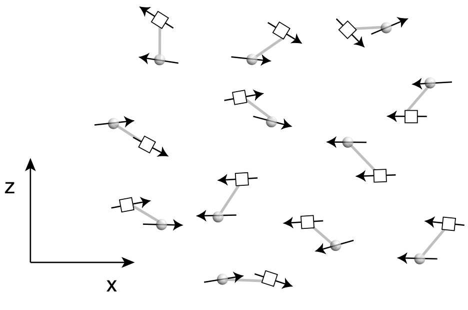

Figure 15.24
Microscopic spin polarizations corresponding to a density operator term $2\hat{I}_{1x}\hat{I}_{2x}$.

There is no *individual* tendency for either set of spins to be polarized in a particular direction. However, if a given spin is polarized along $+x$, then its neighbour tends also to be polarized along $+x$. Similarly, if a given spin is polarized along $-x$, then its neighbour tends also to be polarized along $-x$.

There are also more complicated possibilites. For example, the presence of a term $2\hat{I}_{1z}\hat{I}_{2x}$ implies a correlation of the z-components of the polarizations of spins I_1 with the x-components of the polarizations of spins I_2, i.e. if a spin I_1 is polarized along the z-axis, then its neighbour tends to be polarized along the x-axis, and so on. It is difficult to convey these properties accurately in a simple diagram, and I will not attempt it.

The presence of a *negative* term $-2\hat{I}_{1z}\hat{I}_{2z}$ in the spin density operator implies *anticorrelation*. The two members of a spin pair tend to have *opposite* spin polarizations along the z-axis.

The above diagrams shed light on the physical significance of zero- and double-quantum coherences. It is sometimes stated that multiple-quantum coherences are intrinsically quantum mechanical. This conclusion is false. Zero- and double-quantum coherences are contained in product operator terms like $2\hat{I}_{1x}\hat{I}_{2x}$, which merely indicate certain modes of correlation of the transverse spin polarizations. Correlation is by no means a quantum-mechanical concept, as illustrated by the married couple analogy given above.

In general, the spin density operator contains a sum of product operator terms, as in Equation 15.13. The statistical distribution of the microscopic spin polarizations is therefore a superposition of the elemental distributions described above. This is quite difficult to visualize, and an analogy may help again. A random selection of people from a crowd includes single people as well as married couples. The married couples display a correlation of characteristics, such as height (the two-spin terms, such as $2\hat{I}_{1x}\hat{I}_{2y}$); the single people are, for the moment, uncorrelated with anyone else (the one-spin terms, such as $\hat{I}_{1z}$). A statistical measurement of the entire population, without knowledge of marital status, displays a superposition of the statistical properties of these two independent segments of the population. As time goes by, the interactions between single people lead to the development of new correlated states, and also their destruction. These phenomena also have their analogy in the world of the spins (see below).

15.7 Thermal Equilibrium

When the spin ensemble is left undisturbed for a sufficient amount of time, it adopts a state of thermal equilibrium with respect to the molecular environment. The thermal equilibrium spin density operator may be estimated by making use of the same assumptions as in Section 11.3, namely: (1) no coherences; (2) populations determined by the Boltzmann distribution at the temperature of the molecular environment.

For example, the population of state $|\alpha\alpha\rangle$ in thermal equilibrium at temperature T is given by

$$\rho^{\mathrm{eq}}_{\boxed{\alpha\alpha}} = \frac{\exp\{-\hbar\omega_{\alpha\alpha}/k_{\mathrm{B}}T\}}{\sum_s \exp\{-\hbar\omega_s/k_{\mathrm{B}}T\}}$$

where k_{B} is the Boltzmann constant and the sum is over all four eigenstates. Employing the high-temperature appoximation ($k_{\mathrm{B}}T$ much greater than 1Q spin energy differences), the exponentials in this expression may be written as

$$\exp\{-\hbar\omega_{\alpha\alpha}/k_{\mathrm{B}}T\} \cong 1 - \frac{\hbar\omega_{\alpha\alpha}}{k_{\mathrm{B}}T}$$

Since the sum of the fixed-frame energies is zero (see Equation 15.2):

$$\omega_{\alpha\alpha} + \omega_{\beta\alpha} + \omega_{\alpha\beta} + \omega_{\beta\beta} = 0$$

the sum in the denominator reduces to

$$\sum_s \exp\{-\hbar\omega_s/k_{\mathrm{B}}T\} \cong 4$$

within the same level of approximation. The population of state $|\alpha\alpha\rangle$ is therefore given by

$$\rho^{\text{eq}}_{\boxed{\alpha\alpha}} \cong \frac{1}{4}\left(1 - \frac{\hbar\omega_{\alpha\alpha}}{k_{\text{B}}T}\right)$$

Now, from Equation 15.2, the energy of state $|\alpha\alpha\rangle$ is

$$\begin{aligned}\omega_{\alpha\alpha} &= \frac{1}{2}\omega_1^0 + \frac{1}{2}\omega_2^0 + \frac{1}{2}\pi J_{12}\\ &= -\gamma B^0 + \left\{-\frac{1}{2}\gamma B^0(\delta_1 + \delta_2) + \frac{1}{2}\pi J_{12}\right\}\end{aligned}$$

Under ordinary circumstances, the second term is around five orders of magnitude smaller than the first, and may be ignored for the purposes of estimating the thermal equilibrium populations. This is called the *high-field approximation*. Within the twin approximations of high field and high temperature, the thermal equilibrium population of state $|\alpha\alpha\rangle$ may be expressed as

$$\rho^{\text{eq}}_{\boxed{\alpha\alpha}} \cong \frac{1}{4} + \frac{1}{4}\mathbb{B}$$

where the Boltzmann factor is defined as

$$\boxed{\mathbb{B} = \frac{\hbar\gamma B^0}{k_{\text{B}}T}} \qquad (15.14)$$

as before.

Repetition of these arguments gives the following values for the thermal equilibrium populations:

$$\begin{aligned}\rho^{\text{eq}}_{\boxed{\alpha\alpha}} &\cong \frac{1}{4} + \frac{1}{4}\mathbb{B} & \rho^{\text{eq}}_{\boxed{\beta\alpha}} &\cong \frac{1}{4}\\ \rho^{\text{eq}}_{\boxed{\alpha\beta}} &\cong \frac{1}{4} & \rho^{\text{eq}}_{\boxed{\beta\beta}} &\cong \frac{1}{4} - \frac{1}{4}\mathbb{B}\end{aligned}$$

which has the following form:

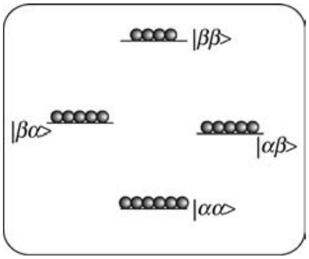

Figure 15.25
Thermal equilibrium populations in the AX spin ensemble.

The lowest energy state $|\alpha\alpha\rangle$ is the most populated; the highest energy state $|\beta\beta\rangle$ is the least populated. The two central energy states $|\alpha\beta\rangle$ and $|\beta\alpha\rangle$ are approximately degenerate and have the same populations in thermal equilibrium.

The thermal equilibrium density matrix, for an ensemble of spin-1/2 pairs, is therefore

$$\hat{\rho}^{\mathrm{eq}} \cong \frac{1}{4}\begin{pmatrix} 1+\mathbb{B} & & & \\ & 1 & & \\ & & 1 & \\ & & & 1-\mathbb{B} \end{pmatrix}$$

or in operator form:

$$\begin{aligned} \hat{\rho}^{\mathrm{eq}} &\cong \frac{1}{4}\hat{1} + \frac{1}{4}\mathbb{B}\hat{I}_z \\ &= \frac{1}{4}\hat{1} + \frac{1}{4}\mathbb{B}\hat{I}_{1z} + \frac{1}{4}\mathbb{B}\hat{I}_{2z} \end{aligned} \tag{15.15}$$

This density operator may now be used as a starting point for product operator calculations of the spin dynamics.

15.8 Radio-Frequency Pulses

Suppose that a strong, short, r.f. pulse is applied to the spin-pair ensemble:

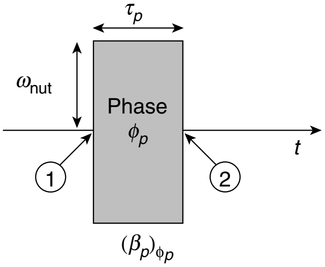

Figure 15.26
An r.f. pulse.

The flip angle of the pulse is $\beta_{\mathrm{p}} = \omega_{\mathrm{nut}}\tau_{\mathrm{p}}$, where the nutation frequency ω_{nut} is the amplitude of the r.f. field, measured in frequency units, and τ_{p} is the duration of the pulse.

The pulse duration τ_{p} is assumed to be short enough that the resonance offsets and J-coupling cause negligible evolution during the pulse.

If these conditions are satisfied, then only the effect of the r.f. field during the pulse is important. The r.f. field affects the two spins equally. For a pair of spins-1/2, the rotating-frame spin Hamiltonian during the pulse is

$$\widehat{\mathcal{H}}_{\mathrm{p}} \cong \omega_{\mathrm{nut}}\left(\hat{I}_x \cos\phi_{\mathrm{p}} + \hat{I}_y \sin\phi_{\mathrm{p}}\right)$$

where

$$\begin{aligned} \hat{I}_x &= \hat{I}_{1x} + \hat{I}_{2x} \\ \hat{I}_y &= \hat{I}_{1y} + \hat{I}_{2y} \end{aligned}$$

I first consider the effect of the pulse on a single spin pair, and then on an ensemble of spin pairs.

15.8.1 Rotations of a single spin pair

Consider a single spin pair in a rotating-frame state $|\psi\rangle_{①}$ before the pulse. During the pulse, the spin state evolves according to the time-dependent Schrödinger equation:

$$\frac{\mathrm{d}}{\mathrm{d}t}|\psi\rangle(t) = -\mathrm{i}\widehat{\mathcal{H}}_{\mathrm{p}}|\psi\rangle(t)$$

with the solution

$$|\psi\rangle_{②} = \widehat{R}_{\phi_{\mathrm{p}}}\left(\beta_{\mathrm{p}}\right)|\psi\rangle_{①}$$

where the rotation operator is

$$\widehat{R}_{\phi_{\mathrm{p}}}\left(\beta_{\mathrm{p}}\right) = \exp\{-\mathrm{i}\widehat{\mathcal{H}}_{\mathrm{p}}\tau_{\mathrm{p}}\}$$

Since all operators of spin I_1 commute with the operators of spin I_2, the spin-pair rotation operator may be factorized:

$$\widehat{R}_{\phi_{\mathrm{p}}}\left(\beta_{\mathrm{p}}\right) = \widehat{R}_{1,\phi_{\mathrm{p}}}(\beta_{\mathrm{p}})\widehat{R}_{2,\phi_{\mathrm{p}}}(\beta_{\mathrm{p}})$$

where the rotation operators for the individual spins are

$$\begin{aligned}\widehat{R}_{1,\phi_{\mathrm{p}}}(\beta_{\mathrm{p}}) &= \exp\{-\mathrm{i}\beta_{\mathrm{p}}\left(\hat{I}_{1x}\cos\phi_{\mathrm{p}} + \hat{I}_{1y}\sin\phi_{\mathrm{p}}\right)\}\\ \widehat{R}_{2,\phi_{\mathrm{p}}}(\beta_{\mathrm{p}}) &= \exp\{-\mathrm{i}\beta_{\mathrm{p}}\left(\hat{I}_{2x}\cos\phi_{\mathrm{p}} + \hat{I}_{2y}\sin\phi_{\mathrm{p}}\right)\}\end{aligned}$$

Repeating the discussion in Section 10.8, these rotation operators may be written as

$$\widehat{R}_{1,\phi_{\mathrm{p}}}(\beta_{\mathrm{p}}) = \widehat{R}_{1z}\left(\phi_{\mathrm{p}}\right)\widehat{R}_{1x}\left(\beta_{\mathrm{p}}\right)\widehat{R}_{1z}\left(-\phi_{\mathrm{p}}\right)$$

where

$$\begin{aligned}\widehat{R}_{1z}\left(\phi_{\mathrm{p}}\right) &= \exp\{-\mathrm{i}\phi_{\mathrm{p}}\hat{I}_{1z}\}\\ \widehat{R}_{1x}\left(\beta_{\mathrm{p}}\right) &= \exp\{-\mathrm{i}\beta_{\mathrm{p}}\hat{I}_{1x}\}\end{aligned}$$

and similarly for the operators of spin I_2.

It is possible to examine the effect of the pulse on an individual spin pair by using the matrix representations of the rotation operators. The matrix representation of $\widehat{R}_{\phi_{\mathrm{p}}}\left(\beta_{\mathrm{p}}\right)$ is given by the direct product of the individual rotation operators:

$$\begin{aligned}\widehat{R}_{\phi_{\mathrm{p}}}\left(\beta_{\mathrm{p}}\right) = \widehat{R}_{1,\phi_{\mathrm{p}}}(\beta_{\mathrm{p}})\widehat{R}_{2,\phi_{\mathrm{p}}}(\beta_{\mathrm{p}}) &= \begin{pmatrix} c & -\mathrm{i}se_{-} \\ -\mathrm{i}se_{+} & c \end{pmatrix} \otimes \begin{pmatrix} c & -\mathrm{i}se_{-} \\ -\mathrm{i}se_{+} & c \end{pmatrix}\\ &= \begin{pmatrix} c^2 & -\mathrm{i}sce_{-} & -\mathrm{i}sce_{-} & -s^2e_{-}^2 \\ -\mathrm{i}sce_{+} & c^2 & -s^2 & -\mathrm{i}sce_{-} \\ -\mathrm{i}sce_{+} & -s^2 & c^2 & -\mathrm{i}sce_{-} \\ -s^2e_{-}^2 & -\mathrm{i}sce_{+} & -\mathrm{i}sce_{+} & c^2 \end{pmatrix}\end{aligned}$$

using the abbreviations

$$\begin{aligned}c &= \cos\tfrac{1}{2}\beta_{\mathrm{p}}\\ s &= \sin\tfrac{1}{2}\beta_{\mathrm{p}}\\ e_{\pm} &= \exp\{\pm\mathrm{i}\phi_{\mathrm{p}}\}\end{aligned}$$

For example, suppose that the spin pair is in the state $|\alpha\alpha\rangle$ and a pulse $(\pi/2)_x$ is applied. The spin state after the pulse may be calculated as follows:

$$|\psi\rangle_{\textcircled{2}} = \frac{1}{2}\begin{pmatrix} 1 & -i & -i & -1 \\ -i & 1 & -1 & -i \\ -i & -1 & 1 & -i \\ -1 & -i & -i & 1 \end{pmatrix}\begin{pmatrix} 1 \\ 0 \\ 0 \\ 0 \end{pmatrix} = \frac{1}{2}\begin{pmatrix} 1 \\ -i \\ -i \\ -1 \end{pmatrix}$$

The pulse transforms the stationary state $|\alpha\alpha\rangle$ into a superposition of all four stationary states:

$$|\psi\rangle_{\textcircled{2}} = \frac{1}{2}\{|\alpha\alpha\rangle - i|\alpha\beta\rangle - i|\beta\alpha\rangle - |\beta\beta\rangle\}$$

15.8.2 Rotations of the spin density operator

The transformation of the spin density operator by the r.f. pulse is easily calculated by the 'sandwich equation':

$$\hat{\rho}_{\textcircled{2}} = \widehat{R}_{\phi_p}(\beta_p)\hat{\rho}_{\textcircled{1}}\widehat{R}_{\phi_p}(-\beta_p)$$

Consider, for example, the case where the spin density operator is initially in thermal equilibrium:

$$\hat{\rho}_{\textcircled{1}} = \frac{1}{4}\widehat{1} + \frac{1}{4}\mathbb{B}\left(\hat{I}_{1z} + \hat{I}_{2z}\right)$$

If a strong $(\pi/2)_x$ pulse is applied, then the state after the pulse may be calculated from the matrix representations:

$$\begin{aligned}\hat{\rho}_{\textcircled{2}} &= \widehat{R}_x(\beta_p)\hat{\rho}_{\textcircled{1}}\widehat{R}_x(-\beta_p) \\ &= \frac{1}{2}\begin{pmatrix} 1 & -i & -i & -1 \\ -i & 1 & -1 & -i \\ -i & -1 & 1 & -i \\ -1 & -i & -i & 1 \end{pmatrix} \times \frac{1}{4}\begin{pmatrix} 1+\mathbb{B} & & & \\ & 1 & & \\ & & 1 & \\ & & & 1-\mathbb{B} \end{pmatrix} \times \frac{1}{2}\begin{pmatrix} 1 & i & i & -1 \\ i & 1 & -1 & i \\ i & -1 & 1 & i \\ -1 & i & i & 1 \end{pmatrix} \\ &= \frac{1}{4}\begin{pmatrix} 1 & \frac{1}{2}i\mathbb{B} & \frac{1}{2}i\mathbb{B} & 0 \\ -\frac{1}{2}i\mathbb{B} & 1 & 0 & \frac{1}{2}i\mathbb{B} \\ -\frac{1}{2}i\mathbb{B} & 0 & 1 & \frac{1}{2}i\mathbb{B} \\ 0 & \frac{1}{2}i\mathbb{B} & \frac{1}{2}i\mathbb{B} & 1 \end{pmatrix}\end{aligned}$$

This may be identified as a representation of the operator:

$$\hat{\rho}_{\textcircled{2}} = \frac{1}{4}\widehat{1} - \frac{1}{4}\mathbb{B}\left(\hat{I}_{1y} + \hat{I}_{2y}\right)$$

The pulse rotates both z-operators by $\pi/2$ around the x-axis, transforming them into $-y$-operators:

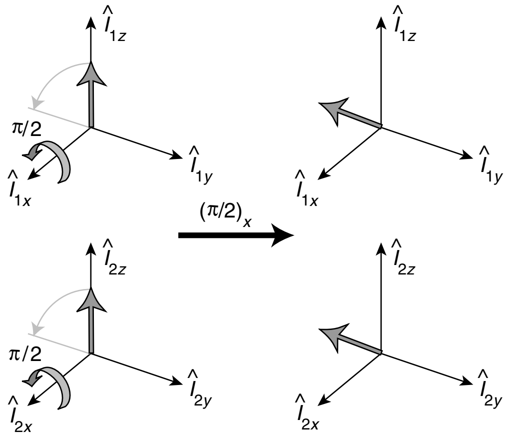

Figure 15.27
A $(\pi/2)_x$ pulse transforms the thermal equilibrium AX density operator.

In a second example, consider an initial density operator of the form

$$\hat{\rho}_{①} = \ldots + r 2\hat{I}_{1x}\hat{I}_{2y} + \ldots$$

where r is a real number. The matrix representation of $2\hat{I}_{1x}\hat{I}_{2y}$ may be found in the usual way:

$$2\hat{I}_{1x}\hat{I}_{2y} = 2\,\frac{1}{2}\begin{pmatrix} 0 & 1 \\ 1 & 0 \end{pmatrix} \otimes \frac{1}{2\mathrm{i}}\begin{pmatrix} 0 & 1 \\ -1 & 0 \end{pmatrix} = \frac{1}{2\mathrm{i}}\begin{pmatrix} 0 & 0 & 0 & 1 \\ 0 & 0 & -1 & 0 \\ 0 & 1 & 0 & 0 \\ -1 & 0 & 0 & 0 \end{pmatrix}$$

The density operator contains zero- and double-quantum coherences.

The action of the pulse on the multiple-quantum coherences may be calculated as follows:

$$\widehat{R}_x(\pi/2) 2\hat{I}_{1x}\hat{I}_{2y}\widehat{R}_x(-\pi/2) =$$

$$\frac{1}{8\mathrm{i}}\begin{pmatrix} 1 & -\mathrm{i} & -\mathrm{i} & -1 \\ -\mathrm{i} & 1 & -1 & -\mathrm{i} \\ -\mathrm{i} & -1 & 1 & -\mathrm{i} \\ -1 & -\mathrm{i} & -\mathrm{i} & 1 \end{pmatrix} \times \begin{pmatrix} 0 & 0 & 0 & 1 \\ 0 & 0 & -1 & 0 \\ 0 & 1 & 0 & 0 \\ -1 & 0 & 0 & 0 \end{pmatrix} \times \begin{pmatrix} 1 & \mathrm{i} & \mathrm{i} & -1 \\ \mathrm{i} & 1 & -1 & \mathrm{i} \\ \mathrm{i} & -1 & 1 & \mathrm{i} \\ -1 & \mathrm{i} & \mathrm{i} & 1 \end{pmatrix}$$

$$= \frac{1}{2}\begin{pmatrix} 0 & 0 & 1 & 0 \\ 0 & 0 & 0 & -1 \\ 1 & 0 & 0 & 0 \\ 0 & -1 & 0 & 0 \end{pmatrix} = 2\,\frac{1}{2}\begin{pmatrix} 0 & 1 \\ 1 & 0 \end{pmatrix} \otimes \frac{1}{2}\begin{pmatrix} 1 & 0 \\ 0 & -1 \end{pmatrix} = 2\hat{I}_{1x}\hat{I}_{2z}$$

The multiple-quantum coherences are transformed by the pulse into antiphase single-quantum coherences. A ‘rotation picture’ again clarifies this transformation:

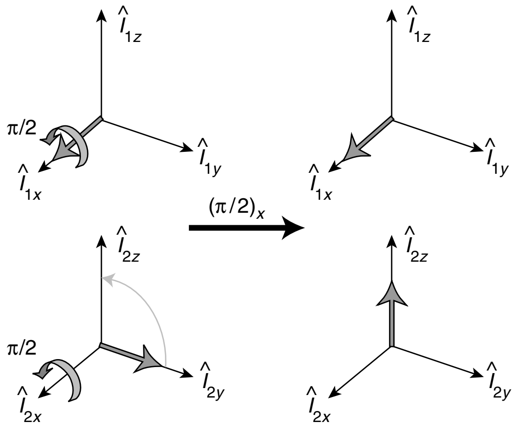

Figure 15.28
A $(\pi/2)_x$ pulse transforms the density operator term $2\hat{I}_{1x}\hat{I}_{2y}$.

15.8.3 Operator transformations

The matrix multiplication scheme described above is straightforward, but clumsy. Much work is saved by using the *commutation relationships* of the operators, rather than their matrix representations.

Consider, for example, the transformation of multiple-quantum coherences, as analysed above. The same relationship may also be deduced in the following way:

$$\begin{aligned}\widehat{R}_x(\pi/2)2\hat{I}_{1x}\hat{I}_{2y}\widehat{R}_x(-\pi/2) &= \widehat{R}_{1x}(\pi/2)\widehat{R}_{2x}(\pi/2)\cdot 2\hat{I}_{1x}\hat{I}_{2y}\cdot \widehat{R}_{1x}(-\pi/2)\widehat{R}_{2x}(-\pi/2)\\ &= 2\,\widehat{R}_{1x}(\pi/2)\hat{I}_{1x}\widehat{R}_{1x}(-\pi/2)\cdot \widehat{R}_{2x}(\pi/2)\hat{I}_{2y}\widehat{R}_{2x}(-\pi/2)\end{aligned}$$

The last step follows because all operators that act on spins I_1 commute with all operators acting on spins I_2.

The first term in the product is given by

$$\widehat{R}_{1x}(\pi/2)\hat{I}_{1x}\widehat{R}_{1x}(-\pi/2) = \hat{I}_{1x}$$

since the operator for a rotation around the x-axis commutes with $\hat{I}_{1x}$.

The second term $\widehat{R}_{2x}(\pi/2)\hat{I}_{2y}\widehat{R}_{2x}(-\pi/2)$ may be analysed using the *cyclic commutation relationships* of the angular momentum operators for spin I_2:

$$\left[\hat{I}_{2x}, \hat{I}_{2y}\right] = \mathrm{i}\hat{I}_{2z} \qquad \circlearrowleft$$

As shown in Section 6.6.2, cyclic commutation leads to the following property:

$$\widehat{R}_{2x}\left(\beta_\mathrm{p}\right)\hat{I}_{2y}\widehat{R}_{2x}\left(-\beta_\mathrm{p}\right) = \hat{I}_{2y}\cos\beta_\mathrm{p} + \hat{I}_{2z}\sin\beta_\mathrm{p}$$

The transformation

$$2\hat{I}_{1x}\hat{I}_{2y} \xrightarrow{(\pi/2)_x} 2\hat{I}_{1x}\hat{I}_{2z}$$

follows easily.

The transformation rules for a pulse with phase $\phi_\mathrm{p} = 0$ ('x-pulse') may be depicted as

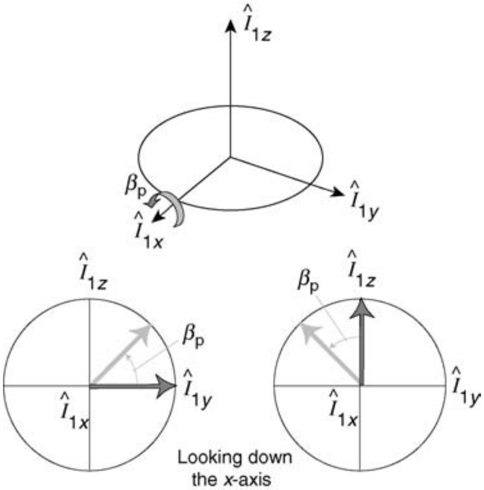

Figure 15.29 Transformation rules for a pulse with phase $\phi_p = 0$.

and summarized as follows:

$$\begin{aligned}
\tfrac{1}{2}\hat{1}_1 &\rightarrow \tfrac{1}{2}\hat{1}_1 \\
\hat{I}_{1x} &\rightarrow \hat{I}_{1x} \\
\hat{I}_{1y} &\rightarrow \hat{I}_{1y}\cos\beta_p + \hat{I}_{1z}\sin\beta_p \\
\hat{I}_{1z} &\rightarrow \hat{I}_{1z}\cos\beta_p - \hat{I}_{1y}\sin\beta_p
\end{aligned} \tag{15.16}$$

and similarly for spin I_2.

The transformation rules for a pulse with phase $\phi_p = \pi/2$ ('*y*-pulse') may be depicted as:

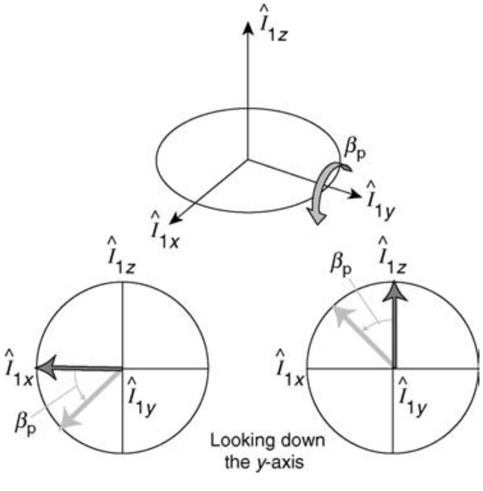

Figure 15.30 Transformation rules for a pulse with phase $\phi_p = \pi/2$.

and summarized as follows:

$$\begin{aligned}
\tfrac{1}{2}\hat{1}_1 &\rightarrow \tfrac{1}{2}\hat{1}_1 \\
\hat{I}_{1x} &\rightarrow \hat{I}_{1x}\cos\beta_\text{p} - \hat{I}_{1z}\sin\beta_\text{p} \\
\hat{I}_{1y} &\rightarrow \hat{I}_{1y} \\
\hat{I}_{1z} &\rightarrow \hat{I}_{1z}\cos\beta_\text{p} + \hat{I}_x\sin\beta_\text{p}
\end{aligned} \tag{15.17}$$

and similarly for spin I_2.

These transformations have a straightforward physical interpretation in terms of the microscopic polarization states of the spins. For example, a density operator term proportional to $\hat{I}_{1z}$ indicates a preferential polarization of spins I_1 along the z-axis, uncorrelated with the states of spins I_2. A $(\pi/2)_y$ pulse rotates all spin polarizations around the y-axis through an angle of $\pi/2$, so that spins I_1 become preferentially polarized along the x-axis after the pulse, but are still uncorrelated with spins I_2.

The transformation properties of the individual spin operators, for pulses of any phase, are summarized in Section 11.8.

15.9 Free Evolution of the Product Operators

Now consider the free evolution of the spin density operator between the pulses. It is possible to perform this calculation using the individual populations and coherences, as discussed in Section 15.4. However, in many cases, the calculations are made more comfortable by using the cyclic commutation properties of the product operators.

Assume that the spin density operator $\hat{\rho}_{\textcircled{2}}$ is known at a time point ②, and that we want to calculate it at a later time ③. The two time points are separated by an interval τ of free evolution in the absence of applied r.f. fields.

If relaxation is ignored, the evolution may be calculated by the 'sandwich equation':

$$\hat{\rho}_{\textcircled{3}} = \widehat{U}(\tau)\hat{\rho}_{\textcircled{1}}\,\widehat{U}(\tau)^{-1}$$

where

$$\widehat{U} = \exp\{-\text{i}\widehat{\mathcal{H}}^0\tau\}$$

and $\widehat{\mathcal{H}}^0$ is the weakly coupled spin Hamiltonian in the rotating frame (Equation 15.7).

The spin Hamiltonian is the sum of three terms, all of which commute with each other:

$$\widehat{\mathcal{H}}^0 = \widehat{\mathcal{H}}^0_1 + \widehat{\mathcal{H}}^0_2 + \widehat{\mathcal{H}}^0_{12}$$

where

$$\begin{aligned}
\widehat{\mathcal{H}}^0_1 &= \Omega^0_1\hat{I}_{1z} \\
\widehat{\mathcal{H}}^0_2 &= \Omega^0_2\hat{I}_{2z} \\
\widehat{\mathcal{H}}^0_{12} &= \pi J_{12}\, 2\hat{I}_{1z}\hat{I}_{2z}
\end{aligned}$$

and

$$\left[\widehat{\mathcal{H}}^0_1, \widehat{\mathcal{H}}^0_2\right] = \left[\widehat{\mathcal{H}}^0_1, \widehat{\mathcal{H}}^0_{12}\right] = \left[\widehat{\mathcal{H}}^0_2, \widehat{\mathcal{H}}^0_{12}\right] = 0$$

From Equation 6.32, the evolution operator may be factorized into three commuting terms:

$$\boxed{\widehat{U}(\tau) = \widehat{U}_1(\tau)\widehat{U}_2(\tau)\widehat{U}_{12}(\tau) \qquad (15.18)}$$

where

$$\left[\widehat{U}_1, \widehat{U}_2\right] = \left[\widehat{U}_1, \widehat{U}_{12}\right] = \left[\widehat{U}_2, \widehat{U}_{12}\right] = 0$$

The mutual commutation of these terms implies that the product in Equation 15.18 may be written in any order.

The term $\widehat{U}_1$ is the *chemical shift propagator for spins* I_1:

$$\boxed{\widehat{U}_1 = \exp\{-\mathrm{i}\Omega_1^0\tau\, \hat{I}_{1z}\} = \widehat{R}_{1z}\left(\Omega_1^0\tau\right) \qquad (15.19)}$$

The term $\widehat{U}_2$ is the *chemical shift propagator for spins* I_2:

$$\boxed{\widehat{U}_2 = \exp\{-\mathrm{i}\Omega_2^0\tau\, \hat{I}_{2z}\} = \widehat{R}_{2z}\left(\Omega_2^0\tau\right) \qquad (15.20)}$$

The term $\widehat{U}_{12}$ is the *J-coupling propagator*:

$$\boxed{\widehat{U}_{12} = \exp\{-\mathrm{i}\pi J_{12}\tau\, 2\hat{I}_{1z}\hat{I}_{2z}\} \qquad (15.21)}$$

The spin density operator at time point ③ may be calculated using any order for the three operations:

$$\hat{\rho}_{③} = \underbrace{\widehat{U}_{12}(\tau)\,\underbrace{\widehat{U}_2(\tau)\,\underbrace{\widehat{U}_1(\tau)\hat{\rho}_{②}\,\widehat{U}_1(\tau)^{-1}}_{\substack{\text{chemical shift}\\ \text{of spin } I_1}}\,\widehat{U}_2(\tau)^{-1}}_{\text{chemical shift of spin } I_2}\,\widehat{U}_{12}(\tau)^{-1}}_{\text{spin–spin coupling}}$$

or

$$\hat{\rho}_{③} = \underbrace{\widehat{U}_{12}(\tau)\,\underbrace{\widehat{U}_1(\tau)\,\underbrace{\widehat{U}_2(\tau)\hat{\rho}_{②}\,\widehat{U}_2(\tau)^{-1}}_{\substack{\text{chemical shift of}\\ \text{spin } I_2}}\,\widehat{U}_1(\tau)^{-1}}_{\text{chemical shift of spin } I_1}\,\widehat{U}_{12}(\tau)^{-1}}_{\text{spin–spin coupling}}$$

or

$$\hat{\rho}_{③} = \underbrace{\widehat{U}_2(\tau)\quad \underbrace{\widehat{U}_1(\tau)\,\underbrace{\widehat{U}_{12}(\tau)\hat{\rho}_{②}\,\widehat{U}_{12}(\tau)^{-1}}_{\text{spin–spin coupling}}\,\widehat{U}_1(\tau)^{-1}}_{\text{chemical shift of spin } I_1}\quad \widehat{U}_2(\tau)^{-1}}_{\text{chemical shift of spin } I_2}$$

and so on. The order of the operations may be chosen according to the circumstances of the calculation.

Using an obvious notation, these calculation methods may be denoted as follows:

$$\hat{\rho}_{②} \xrightarrow{\Omega_1^0\tau} \xrightarrow{\Omega_2^0\tau} \xrightarrow{\pi J_{12}\tau} \hat{\rho}_{③}$$

or alternatively:

$$\hat{\rho}_{②} \xrightarrow{\Omega_2^0\tau} \xrightarrow{\Omega_1^0\tau} \xrightarrow{\pi J_{12}\tau} \hat{\rho}_{③}$$

and so on.

15.9.1 Chemical shift evolution

The transformation of the density operator under the terms $\widehat{U}_1$ and $\widehat{U}_2$ is very similar to their transformations under r.f. pulses. The only differences are: (1) the rotations occur around the z-axis, rather than around axes in the xy-plane; (2) the rotation angles are different for the two spins.

The transformation rules may be summarized as

$$\boxed{\begin{array}{lcl} \frac{1}{2}\widehat{1}_1 & \xrightarrow{\Omega_1^0\tau} & \frac{1}{2}\widehat{1}_1 \\ \hat{I}_{1x} & \longrightarrow & \hat{I}_{1x}\cos\Omega_1^0\tau + \hat{I}_{1y}\sin\Omega_1^0\tau \\ \hat{I}_{1y} & \longrightarrow & \hat{I}_{1y}\cos\Omega_1^0\tau - \hat{I}_{1x}\sin\Omega_1^0\tau \\ \hat{I}_{1z} & \longrightarrow & \hat{I}_{1z} \end{array} \qquad (15.22)}$$

and depicted as follows:

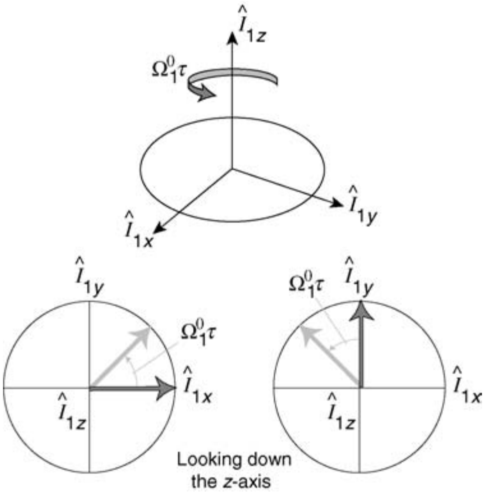

Figure 15.31
Transformation rules for the chemical shift evolution of spins I_1.

Similar relationships apply for spin I_2.

For example, the chemical shift evolution of a density operator term $\hat{I}_{1x}$ may be calculated as follows:

$$\begin{tikzcd} \hat{I}_{1x} \arrow[d, "\Omega_2^0\tau"] \\ \hat{I}_{1x} \arrow[d, "\Omega_1^0\tau"] \\ \hat{I}_{1x}\cos\Omega_1^0\tau + \hat{I}_{1y}\sin\Omega_1^0\tau \end{tikzcd}$$

or written more formally:

$$\widehat{U}_1(\tau)\widehat{U}_2(\tau)\hat{I}_{1x}\widehat{U}_2(\tau)^{-1}\widehat{U}_1(\tau)^{-1} = \hat{I}_{1x}\cos\Omega_1^0\tau + \hat{I}_{1y}\sin\Omega_1^0\tau$$

The result is the same if the operations are taken the other way round.

Similarly, the chemical shift evolution of the product operator term $2\hat{I}_{1x}\hat{I}_{2y}$ may be calculated as follows:

$$\begin{tikzcd} 2\hat{I}_{1x}\hat{I}_{2y} \arrow[d, "\Omega_1^0\tau"] \\ 2\left(\hat{I}_{1x}\cos\Omega_1^0\tau + \hat{I}_{1y}\sin\Omega_1^0\tau\right)\hat{I}_{2y} \arrow[d, "\Omega_2^0\tau"] \\ \begin{array}{c} 2\hat{I}_{1x}\left(\hat{I}_{2y}\cos\Omega_2^0\tau - \hat{I}_{2x}\sin\Omega_2^0\tau\right)\cos\Omega_1^0\tau \\ +2\hat{I}_{1y}\left(\hat{I}_{2y}\cos\Omega_2^0\tau - \hat{I}_{2x}\sin\Omega_2^0\tau\right)\sin\Omega_1^0\tau \end{array} \end{tikzcd}$$

or more formally:

$$\begin{aligned} \widehat{U}_1(\tau)\widehat{U}_2(\tau)2\hat{I}_{1x}\hat{I}_{2y}\widehat{U}_2(\tau)^{-1}\widehat{U}_1(\tau)^{-1} &= 2\hat{I}_{1x}\hat{I}_{2y}\cos\Omega_1^0\tau\ \cos\Omega_2^0\tau - 2\hat{I}_{1x}\hat{I}_{2x}\cos\Omega_1^0\tau\ \sin\Omega_2^0\tau \\ &\quad +2\hat{I}_{1y}\hat{I}_{2y}\sin\Omega_1^0\tau\ \cos\Omega_2^0\tau - 2\hat{I}_{1y}\hat{I}_{2x}\sin\Omega_1^0\tau\ \sin\Omega_2^0\tau \end{aligned}$$

Remember that the action of the J-coupling is not yet included.

These transformations correspond to the independent precession of the spins around the z-axis at their individual chemical shift offset frequencies.

15.9.2 *J*-coupling evolution

The action of the J-coupling introduces some new features. Density operator terms proportional to single-spin operators such as $\hat{I}_{1x}$ are converted into two-spin terms such as $2\hat{I}_{1y}\hat{I}_{2z}$, and vice versa. This indicates *the creation, and destruction, of correlations between the spin polarizations, under the influence of the spin–spin couplings.*

The transformations of the product operator terms may be calculated from the following cyclic commutation relationships, which apply to the spin-1/2 matrix representations:

$$\boxed{\begin{aligned}\left[2\hat{I}_{1z}\hat{I}_{2z}, \hat{I}_{1x}\right] &= \mathrm{i}2\hat{I}_{1y}\hat{I}_{2z} \circlearrowleft\\ \left[2\hat{I}_{1z}\hat{I}_{2z}, \hat{I}_{2x}\right] &= \mathrm{i}2\hat{I}_{1z}\hat{I}_{2y} \circlearrowleft\\ \left[2\hat{I}_{1x}\hat{I}_{2z}, \hat{I}_{1y}\right] &= \mathrm{i}2\hat{I}_{1z}\hat{I}_{2z} \circlearrowleft\\ \left[2\hat{I}_{1z}\hat{I}_{2x}, \hat{I}_{2y}\right] &= \mathrm{i}2\hat{I}_{1z}\hat{I}_{2z} \circlearrowleft\end{aligned} \qquad (15.23)}$$

The cyclic commutation relationships may be depicted geometrically:

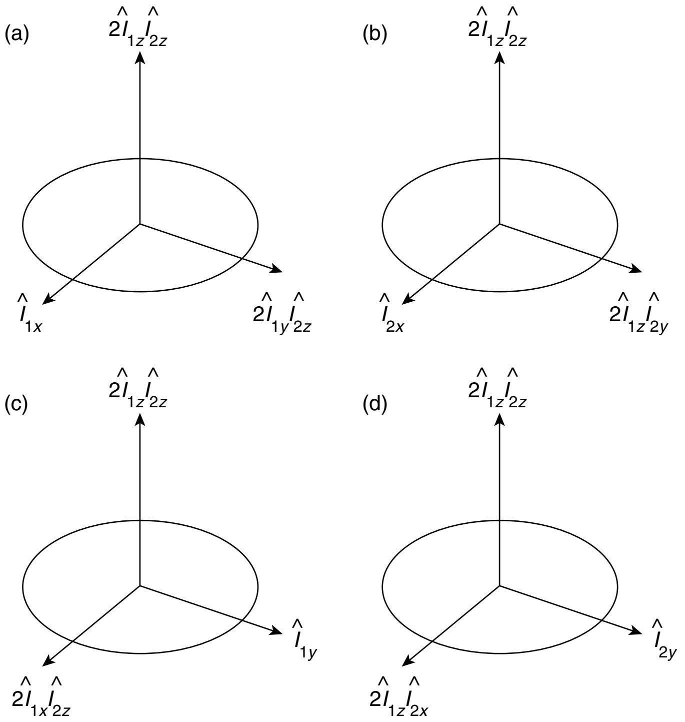

Figure 15.32
Cyclic commutation relationships of product operators.

Note the common pattern. In the right-handed axis system, with a z-operator along the vertical axis, an x-operator is always placed on the left and a y-operator on the right. If the x-operator occurs in a product with a z-operator on the left, then the z-operator is missing on the right. If the z-operator is missing on the left, then the y-operator occurs in a product with a z-operator on the right. Note also that the operators are always written with the indices 1 and 2 in the same order. This is not essential, but it simplifies the bookkeeping.

Each of the diagrams above implies a geometrical representation of the product operator transformations. For example, Figures 15.32a indicates the following transformations:

$$\widehat{U}_{12}(\tau)\hat{I}_{1x}\widehat{U}_{12}(\tau)^{-1} = \hat{I}_{1x}\cos\pi J_{12}\tau + 2\hat{I}_{1y}\hat{I}_{2z}\sin\pi J_{12}\tau$$

$$\widehat{U}_{12}(\tau)2\hat{I}_{1y}\hat{I}_{2z}\widehat{U}_{12}(\tau)^{-1} = 2\hat{I}_{1y}\hat{I}_{2z}\cos\pi J_{12}\tau - \hat{I}_{1x}\sin\pi J_{12}\tau$$

which are conveniently notated as

$$\begin{array}{rcl} \hat{I}_{1x} & \xrightarrow{\pi J_{12}\tau} & \hat{I}_{1x}\cos\pi J_{12}\tau + 2\hat{I}_{1y}\hat{I}_{2z}\sin\pi J_{12}\tau \\ 2\hat{I}_{1y}\hat{I}_{2z} & \xrightarrow{\phantom{\pi J_{12}\tau}} & 2\hat{I}_{1y}\hat{I}_{2z}\cos\pi J_{12}\tau - \hat{I}_{1x}\sin\pi J_{12}\tau \end{array}$$

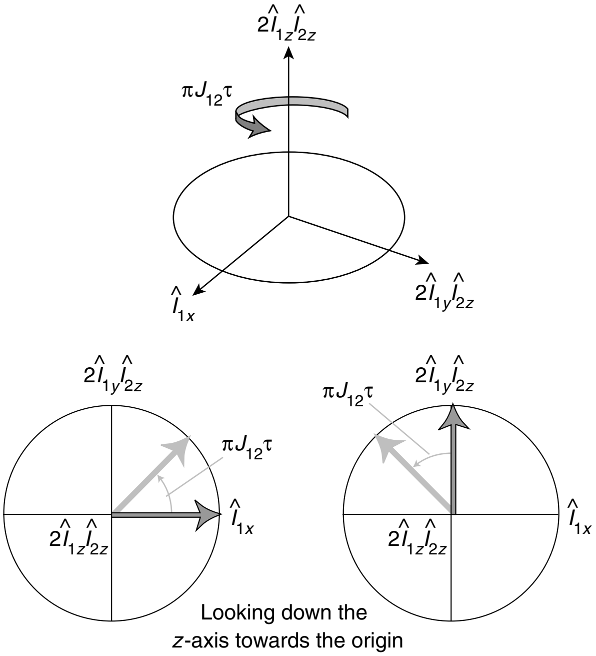

Figure 15.33
Transformation rules for the *J*-coupling (part 1).

Similarly, Figure 15.32c indicates the following transformations:

$$\begin{array}{rcl} 2\hat{I}_{1x}\hat{I}_{2z} & \xrightarrow{\pi J_{12}\tau} & 2\hat{I}_{1x}\hat{I}_{2z}\cos\pi J_{12}\tau + \hat{I}_{1y}\sin\pi J_{12}\tau \\ \hat{I}_{1y} & \xrightarrow{\phantom{\pi J_{12}\tau}} & \hat{I}_{1y}\cos\pi J_{12}\tau - 2\hat{I}_{1x}\hat{I}_{2z}\sin\pi J_{12}\tau \end{array}$$

These diagrams are shown for the case of positive J_{12}; if J_{12} is negative, the rotation is in the opposite sense.

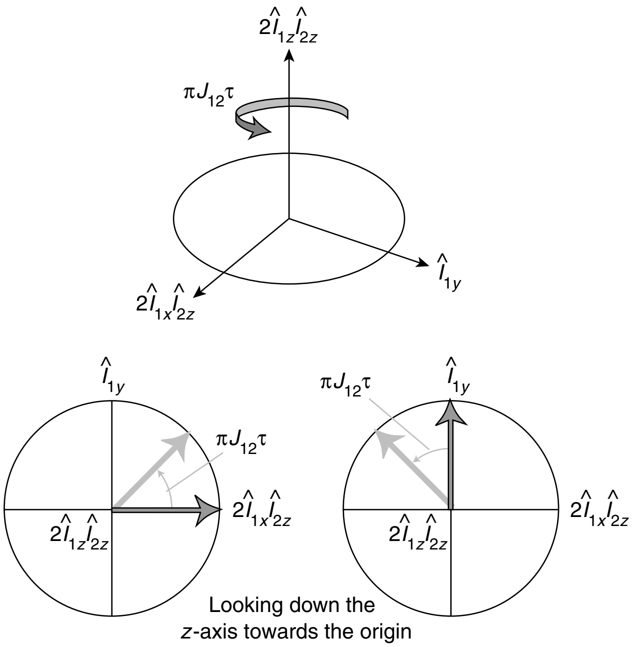

Figure 15.34
Transformation rules for the J-coupling (part 2).

These relationships indicate the creation and destruction of spin correlations by evolution in the presence of the couplings. This works as follows on the microscopic level. In the presence of couplings, the magnetic fields at the sites of spins I_1 depend on the instantaneous polarizations of the spins I_2. The angle through which spins I_1 precess over a certain interval depends, therefore, on the states of spins I_2. Over a period of time, the *transverse* polarizations of spins I_1 develop a correlation with the *longitudinal* polarizations of spins I_2. The correlated spin state that develops corresponds to the presence of a density operator term $2\hat{I}_{1y}\hat{I}_{2z}$. The same correlation may also be destroyed by a continuation of the same mechanism.

To complete the picture of evolution under the J-coupling, one also needs the following commutation relationships:[3]

$$\boxed{\begin{aligned}\left[2\hat{I}_{1z}\hat{I}_{2z}, \hat{I}_{1z}\right] &= \left[2\hat{I}_{1z}\hat{I}_{2z}, \hat{I}_{2z}\right] = 0\\ \left[2\hat{I}_{1z}\hat{I}_{2z}, 2\hat{I}_{1z}\hat{I}_{2z}\right] &= \left[2\hat{I}_{1z}\hat{I}_{2z}, \widehat{1}\right] = 0\\ \left[2\hat{I}_{1z}\hat{I}_{2z}, 2\hat{I}_{1x}\hat{I}_{2x}\right] &= \left[2\hat{I}_{1z}\hat{I}_{2z}, 2\hat{I}_{1x}\hat{I}_{2y}\right] = 0\\ \left[2\hat{I}_{1z}\hat{I}_{2z}, 2\hat{I}_{1y}\hat{I}_{2x}\right] &= \left[2\hat{I}_{1y}\hat{I}_{2z}, 2\hat{I}_{1x}\hat{I}_{2y}\right] = 0\end{aligned}} \tag{15.24}$$

This implies that the J-coupling does not cause any evolution of density operator terms such as $2\hat{I}_{1y}\hat{I}_{2x}$:

$$\begin{aligned} 2\hat{I}_{1y}\hat{I}_{2x} &\xrightarrow{\pi J_{12}\tau} 2\hat{I}_{1y}\hat{I}_{2x}\\ 2\hat{I}_{1x}\hat{I}_{2x} &\xrightarrow{\phantom{\pi J_{12}\tau}} 2\hat{I}_{1x}\hat{I}_{2x}\end{aligned}$$

Double- and zero-quantum coherences do not evolve under the coupling between the two involved spins.

We are now ready to complete the calculation of the free evolution of the density operator term $\hat{I}_{1x}$:

$$\begin{tikzcd}
\hat{I}_{1x} \arrow[d, "\Omega_2^0\tau"] \\
\hat{I}_{1x} \arrow[d, "\Omega_1^0\tau"] \\
\hat{I}_{1x}\cos\Omega_1^0\tau + \hat{I}_{1y}\sin\Omega_1^0\tau \arrow[d, "\pi J_{12}\tau"] \\
\begin{array}{c} \hat{I}_{1x}\cos\Omega_1^0\tau\ \cos\pi J_{12}\tau + \hat{I}_{1y}\sin\Omega_1^0\tau\ \cos\pi J_{12}\tau \\ +2\hat{I}_{1y}\hat{I}_{2z}\cos\Omega_1^0\tau\ \sin\pi J_{12}\tau - 2\hat{I}_{1x}\hat{I}_{2z}\sin\Omega_1^0\tau\ \sin\pi J_{12}\tau \end{array}
\end{tikzcd}$$

If the initial term is instead $2\hat{I}_{1x}\hat{I}_{2y}$, the free evolution transformations are instead:

$$\begin{tikzcd}
2\hat{I}_{1x}\hat{I}_{2y} \arrow[d, "\pi J_{12}\tau"] \\
2\hat{I}_{1x}\hat{I}_{2y} \arrow[d, "\Omega_1^0\tau"] \\
2\hat{I}_{1x}\hat{I}_{2y}\cos\Omega_1^0\tau + 2\hat{I}_{1y}\hat{I}_{2y}\sin\Omega_1^0\tau \arrow[d, "\Omega_2^0\tau"] \\
\begin{array}{c} 2\hat{I}_{1x}\hat{I}_{2y}\cos\Omega_1^0\tau\ \cos\Omega_2^0\tau + 2\hat{I}_{1y}\hat{I}_{2y}\sin\Omega_1^0\tau\ \cos\Omega_2^0\tau \\ -2\hat{I}_{1x}\hat{I}_{2x}\cos\Omega_1^0\tau\ \sin\Omega_2^0\tau - 2\hat{I}_{1y}\hat{I}_{2x}\sin\Omega_1^0\tau\ \sin\Omega_2^0\tau \end{array}
\end{tikzcd}$$

Note that the term $2\hat{I}_{1x}\hat{I}_{2y}$ is unchanged by the spin–spin coupling. This follows from the commutation properties in Equation 15.24.

15.9.3 Relaxation

The free evolution of the product operators also involves relaxation.

The relaxation of product operators that involve *populations*, such as $\hat{I}_{1z}$ and $2\hat{I}_{1z}\hat{I}_{2z}$, is rather complicated in a coupled spin system. This subject is discussed further in Chapter 20.

The relaxation of product operators involving *coherences* is very simple if one assumes that all coherences in the product operator relax with the same rate constant. One simply multiplies each product operator by a decay factor of the form $\exp\{-\lambda\tau\}$.

The simple assumption of identical coherence decay rate constants breaks down in some circumstances. For example, this happens if the relaxation mechanisms are *cross-correlated*, as described in Section 20.8. A more sophisticated treatment of the product operator evolution is necessary in that case.

In this book, I generally neglect the relaxation of the product operators in the intervals between pulses.

15.10 Spin Echo Sandwich

As indicated above, free evolution of product operators usually leads to an increase in complexity. Each term splits up into many other terms. In addition, the final state is often strongly dependent on the chemical shift values.

These features are often undesirable, but may be avoided by building pulse sequences around the following element:

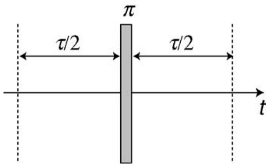

Figure 15.35
A spin echo sandwich of duration τ.

i.e. two intervals of free evolution, both of duration $\tau/2$, 'sandwiching' a strong, short, pulse of flip angle π (in practice, the pulse is many orders of magnitude shorter than the precession intervals). This pulse sequence element is called a *spin echo sandwich* (SES).

To a good approximation,[4] the state of the spins after the spin echo sandwich is the same as that produced by the following fictitious sequence:

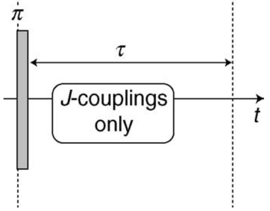

Figure 15.36
A short-cut for calculating the evolution under a spin-echo sandwich.

i.e. a π pulse, followed by a full interval τ of evolution *under the J-couplings only*.

Mathematically, this implies that the spin echo sandwich propagator, given by

$$\widehat{U}_{\text{SES}} = \widehat{U}(\tau/2)\widehat{R}_x(\pi)\widehat{U}(\tau/2)$$

may be written as

$$\boxed{\widehat{U}_{\text{SES}} \cong \widehat{U}_{12}(\tau)\widehat{R}_x(\pi) \qquad (15.25)}$$

This property is proved in Appendix A.10.

By basing a pulse sequence upon spin echo sandwich elements, it is possible to make use of the J-couplings without worrying about the precise values of the chemical shifts. The calculation of the spin dynamics is easier, and the pulse sequences are more effective.

A further simplification may often be made. In many cases, the values of the J-couplings are rather well known beforehand. For example, three-bond ^{1}H–^{1}H J-couplings are often around ~7.5 Hz in conformationally mobile systems, and one-bond ^{1}H–^{13}C J-couplings are around ~135 Hz. Suppose that the total duration of the spin echo sandwich τ is set equal to the value

$$\tau = |(2J_{12})^{-1}|$$

(The magnitude symbol is necessary, because J_{12} may be negative, while τ is always positive.) This implies that τ should be set close to the value 67 ms in the case of three-bond ^{1}H–^{1}H J-couplings, and close to the value 3.7 ms in the case of one-bond ^{1}H–^{13}C J-couplings.

If τ is set to the value $|(2J_{12})^{-1}|$ and J_{12} is positive, then $\pi J_{12}\tau$ is equal to $+\pi/2$, and the transformations of product operators by the J-coupling part of the propagator become simple:

$$\left.\begin{array}{rcr}
\hat{I}_{1x} & \xrightarrow{\pi J_{12}\tau} & 2\hat{I}_{1y}\hat{I}_{2z} \\
2\hat{I}_{1y}\hat{I}_{2z} & \xrightarrow{\pi J_{12}\tau} & -\hat{I}_{1x} \\
\hat{I}_{2x} & \xrightarrow{\pi J_{12}\tau} & 2\hat{I}_{1z}\hat{I}_{2y} \\
2\hat{I}_{1z}\hat{I}_{2y} & \xrightarrow{\pi J_{12}\tau} & -\hat{I}_{2x} \\
2\hat{I}_{1x}\hat{I}_{2z} & \xrightarrow{\pi J_{12}\tau} & \hat{I}_{1y} \\
\hat{I}_{1y} & \xrightarrow{\pi J_{12}\tau} & -2\hat{I}_{1x}\hat{I}_{2z} \\
2\hat{I}_{1z}\hat{I}_{2x} & \xrightarrow{\pi J_{12}\tau} & \hat{I}_{2y} \\
\hat{I}_{2y} & \xrightarrow{\pi J_{12}\tau} & -2\hat{I}_{1z}\hat{I}_{2x}
\end{array}\right\}\text{for } J_{12} > 0$$

All other product operators are unchanged. To calculate the full effect of the spin echo sandwich, the π pulse should be taken into account as well. If the π pulse has phase $\phi_{\text{p}} = 0$, we get

$$\left.\begin{array}{rcrcr}
\hat{I}_{1x} & \xrightarrow{\pi_x} & \hat{I}_{1x} & \xrightarrow{\pi J_{12}\tau} & 2\hat{I}_{1y}\hat{I}_{2z} \\
2\hat{I}_{1y}\hat{I}_{2z} & \xrightarrow{\pi_x} & 2\hat{I}_{1y}\hat{I}_{2z} & \xrightarrow{\pi J_{12}\tau} & -\hat{I}_{1x} \\
\hat{I}_{2x} & \xrightarrow{\pi_x} & \hat{I}_{2x} & \xrightarrow{\pi J_{12}\tau} & 2\hat{I}_{1z}\hat{I}_{2y} \\
2\hat{I}_{1z}\hat{I}_{2y} & \xrightarrow{\pi_x} & 2\hat{I}_{1z}\hat{I}_{2y} & \xrightarrow{\pi J_{12}\tau} & -\hat{I}_{2x} \\
2\hat{I}_{1x}\hat{I}_{2z} & \xrightarrow{\pi_x} & -2\hat{I}_{1x}\hat{I}_{2z} & \xrightarrow{\pi J_{12}\tau} & -\hat{I}_{1y} \\
\hat{I}_{1y} & \xrightarrow{\pi_x} & -\hat{I}_{1y} & \xrightarrow{\pi J_{12}\tau} & 2\hat{I}_{1x}\hat{I}_{2z} \\
2\hat{I}_{1z}\hat{I}_{2x} & \xrightarrow{\pi_x} & -2\hat{I}_{1z}\hat{I}_{2x} & \xrightarrow{\pi J_{12}\tau} & -\hat{I}_{2y} \\
\hat{I}_{2y} & \xrightarrow{\pi_x} & -\hat{I}_{2y} & \xrightarrow{\pi J_{12}\tau} & 2\hat{I}_{1z}\hat{I}_{2x}
\end{array}\right\} \text{for } J_{12} > 0$$

A spin echo sandwich with an appropriately chosen duration may, therefore, be used for the *complete conversion of uncorrelated spin states into correlated spin states*, and vice versa. Spin echo sandwiches are ubiquitous in liquid-state NMR. Some examples are given in Chapter 16.

If $\tau = |(2J_{12})^{-1}|$ and J_{12} is negative, then $\pi J_{12}\tau$ is equal to $-\pi/2$, and the transformations by the spin echo sandwich have the opposite sign; for example:

$$\left.\begin{array}{rcrcr}
\hat{I}_{1x} & \xrightarrow{\pi_x} & \hat{I}_{1x} & \xrightarrow{\pi J_{12}\tau} & -2\hat{I}_{1y}\hat{I}_{2z} \\
2\hat{I}_{1y}\hat{I}_{2z} & \xrightarrow{\pi_x} & 2\hat{I}_{1y}\hat{I}_{2z} & \xrightarrow{\pi J_{12}\tau} & +\hat{I}_{1x}
\end{array}\right\} \quad \text{for } J_{12} < 0$$

Notes

1. Cross-correlation effects (see Section 20.8) may cause coherences such as $\rho_{\boxed{-\alpha}}$ and $\rho_{\boxed{-\beta}}$ to relax with different rate constants.

2. It is tempting to make the following 'physical interpretation' of the splitting associated with the J-coupling: the peak at frequency $\Omega_{\boxed{-\alpha}} = \Omega_1^0 + \pi J_{12}$ is associated with the precession of spins I_1, with spins I_2 in the $|\alpha\rangle$ state, whereas the peak at frequency $\Omega_{\boxed{-\beta}} = \Omega_1^0 - \pi J_{12}$ is associated with the precession of spins I_1, with spins I_2 being in the $|\beta\rangle$ state. Spins in the $|\alpha\rangle$ state shift the magnetic field experienced by their neighbours in one direction, and spins in the $|\beta\rangle$ state shift the magnetic field of their neighbours in the opposite direction.

   Although this argument is tempting, it must be wrong, since most of the spin pairs in the ensemble are actually in superposition states, with spin polarization vectors pointing in arbitrary directions. The discussion given in this chapter explains the appearance of the spectral splittings from the Schrödinger equation while avoiding the unrealistic assumption that the spins are only in states $|\alpha\rangle$ or $|\beta\rangle$.

3. The last two cyclic commutation relationships in Equation 15.24 only apply to spins-1/2 and may be derived by multiplying out the matrix representations.

4. See Appendix A.10 for a general treatment of spin echo sandwiches.

Further Reading

- For more product operator theory, see: R. R. Ernst, G. Bodenhausen and A. Wokaun, *Principles of Nuclear Magnetic Resonance in One and Two Dimensions*, Clarendon Press, Oxford, 1987; M. Goldman, *Quantum Description of High-Resolution NMR in Liquids*, Clarendon Press, Oxford, 1988; J. Cavanagh, W. J. Fairbrother, A. G. Palmer and N. J. Skelton, *Protein NMR Spectroscopy. Principles and Practice*, Academic, New York, 1996; and J. Keeler, *Understanding NMR Spectroscopy*, Wiley, Chichester, 2005.

Exercises

15.1 This exercise concerns the transformation of a single population $\rho_{\boxed{\alpha\alpha}}$ in an AX spin system. Suppose that the spin ensemble is only populated in the single state $|\alpha\alpha\rangle$, i.e.

$$\hat{\rho} = \begin{pmatrix} 1 & 0 & 0 & 0 \\ 0 & 0 & 0 & 0 \\ 0 & 0 & 0 & 0 \\ 0 & 0 & 0 & 0 \end{pmatrix}$$

(i) What is the density operator after a strong $(\pi/2)_y$ pulse?

(ii) What is the density operator after a pulse with phase $\pi/2$ and an arbitrary flip angle β?

(iii) Suppose that the flip angle β is very small, and ignore all terms that have a power of 3 or higher in β after the pulse. Which coherences are excited by the pulse to *first order* in β? Which coherences are excited by the pulse to *second order* in β? Suggest a pattern for these observations.

16 Experiments on AX Systems

This chapter discusses some practical NMR experiments on coupled spins in isotropic liquids. For simplicity, I assume that the experiments are conducted on weakly coupled AX systems.

16.1 COSY

16.1.1 The assignment problem

Suppose that the sample contains a mixture of two different compounds, each with a different AX spin system, but with identical J-couplings. The NMR spectrum would have the following appearance:

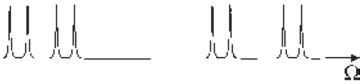

Figure 16.1
An ambiguous one-dimensional spectrum.

Clearly, this spectrum has a number of different interpretations. The peaks might belong to the different spin systems as follows:

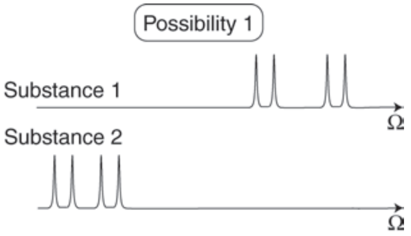

Figure 16.2
One interpretation.

or

Spin Dynamics: Basics of Nuclear Magnetic Resonance, Second Edition Malcolm H. Levitt

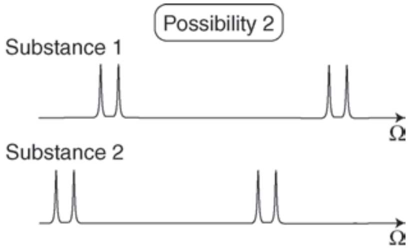

Figure 16.3
A second interpretation.

or perhaps:

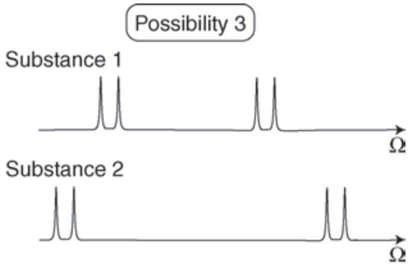

Figure 16.4
A third interpretation.

It is not possible to distinguish between these interpretations by examining the one-dimensional NMR spectrum alone.

If the compounds are known, then chemical shift values may provide some clues. However, in many cases, chemical shifts do not provide an unambiguous answer.

The above example illustrates the *assignment problem*. The one-dimensional NMR spectrum provides no indication as to which NMR peaks originate in the same spin system, and which originate in different spin systems.

Ideally, one would like a 'correlation map', indicating pictorially which peaks 'belong together'. The 'correlation maps' for the three possible peak assignments all look different:

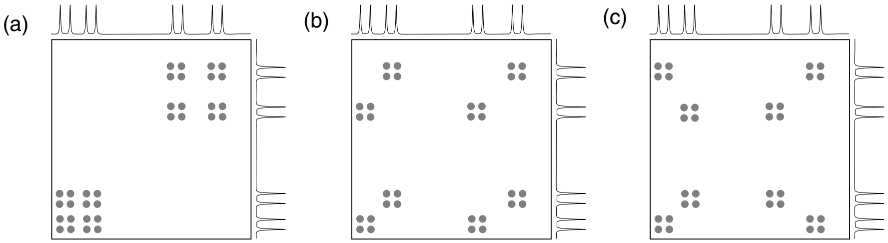

Figure 16.5 Correlation maps for (a) the first interpretation, (b) the second interpretation and (c) the third interpretation.

In this section, we investigate a simple two-dimensional NMR technique, called *correlation spectroscopy* (COSY), that provides such experimental correlation maps, indicating the correct assignment of peaks. COSY is now an essential tool in the NMR of complex molecules.

16.1.2 COSY pulse sequence

COSY was the first two-dimensional NMR experiment, described by the Belgian scientist Jean Jeener in 1971, but never published in a scientific journal. Fortunately, a graduate student of R. R. Ernst took detailed notes of Jeener's sketchy conference report. Ernst's group took up the idea and developed multidimensional spectroscopy into an immensely powerful and versatile range of methods (while giving full credit to Jeener!). Ernst was awarded the Nobel Prize in 1991.

The pulse sequence for COSY is very simple. It contains just two $\pi/2$ pulses, separated by a variable delay t_1. The experiment is conducted in the usual arrayed fashion:

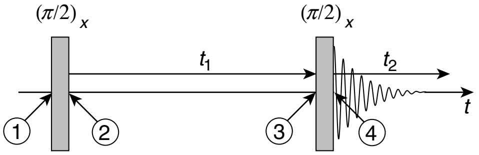

Figure 16.6
COSY pulse sequence: 'cosine' version.

This two-dimensional pulse sequence provides the 'cosine' two-dimensional data matrix $s^{\cos}(t_1, t_2)$ in the States procedure (see Section 5.9.4). The 'sine' data matrix is obtained by using the same pulse sequence, but with a $-\pi/2$ phase shift of the first pulse:[1]

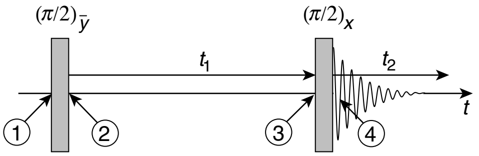

Figure 16.7
COSY pulse sequence: 'sine' version.

The two data matrices are combined and Fourier transformed as in Section 5.9.4 to obtain the two-dimensional spectrum $S(\Omega_1, \Omega_2)$.

16.1.3 Theory of COSY: coherence interpretation

Consider an ensemble of AX spin systems, subjected to the 'cosine' pulse sequence, in which the phases of the pulses are both zero.

The density operator is transformed by the first $\pi/2$ pulse as follows:

$$\begin{aligned} \hat{\rho}_{①} &= \hat{\rho}^{\mathrm{eq}} = \hat{I}_{1z} + \hat{I}_{2z} \\ &\Big\downarrow (\pi/2)_x \\ \hat{\rho}_{②} &= -\hat{I}_{1y} - \hat{I}_{2y} \end{aligned}$$

omitting the unity operator and unnecessary constants.

The density operator after the first pulse $\hat{\rho}_{②}$ may be written in terms of shift and projection operators as follows:

$$\hat{\rho}_{②} = \frac{1}{2\mathrm{i}} \hat{I}_1^- \hat{I}_2^\alpha + \frac{1}{2\mathrm{i}} \hat{I}_1^- \hat{I}_2^\beta + \ldots$$

The (-1)-quantum coherences immediately after the first pulse are therefore given by:

$$\rho_{\boxed{-\alpha}}\textcircled{2} = \frac{1}{2\mathrm{i}} \qquad \rho_{\boxed{\alpha-}}\textcircled{2} = \frac{1}{2\mathrm{i}}$$
$$\rho_{\boxed{-\beta}}\textcircled{2} = \frac{1}{2\mathrm{i}} \qquad \rho_{\boxed{\beta-}}\textcircled{2} = \frac{1}{2\mathrm{i}}$$

The first pulse may be thought of as generating a branching 'tree' of (±1)-quantum coherences:

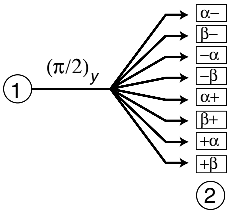

Figure 16.8
Generation of coherences by the first pulse in COSY.

During the interval t_1, the coherences evolve at their characteristic frequencies. At time point ③, just before the second $\pi/2$ pulse, the (-1)-quantum coherences have the following amplitudes:

$$\rho_{\boxed{-\alpha}}\textcircled{3} = \frac{1}{2\mathrm{i}}\exp\{\left(\mathrm{i}\Omega_{\boxed{-\alpha}} - \lambda\right)t_1\} \qquad \rho_{\boxed{\alpha-}}\textcircled{3} = \frac{1}{2\mathrm{i}}\exp\{\left(\mathrm{i}\Omega_{\boxed{\alpha-}} - \lambda\right)t_1\}$$
$$\rho_{\boxed{-\beta}}\textcircled{3} = \frac{1}{2\mathrm{i}}\exp\{(\mathrm{i}\Omega_{\boxed{-\beta}} - \lambda)t_1\} \qquad \rho_{\boxed{\beta-}}\textcircled{3} = \frac{1}{2\mathrm{i}}\exp\{(\mathrm{i}\Omega_{\boxed{\beta-}} - \lambda)t_1\}$$

where the characteristic frequencies of the coherences are given in Equation 15.10. I have assumed that all the decay constants λ are the same, for the sake of simplicity.

The spin density operator at time point ③ is therefore given by

$$\hat{\rho}_{\textcircled{3}} = \frac{1}{2\mathrm{i}}\exp\{\left(\mathrm{i}\Omega_{\boxed{-\alpha}} - \lambda\right)t_1\}\hat{I}_1^-\hat{I}_2^\alpha + \frac{1}{2\mathrm{i}}\exp\{(\mathrm{i}\Omega_{\boxed{-\beta}} - \lambda)t_1\}\hat{I}_1^-\hat{I}_2^\beta + \ldots$$

i.e. one term for each of the excited coherences. In the 'tree' picture, the t_1 evolution causes each branch to 'grow', without branching any further:

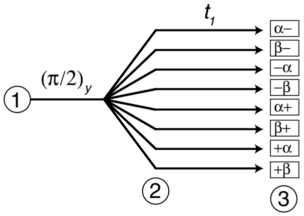

Figure 16.9
Evolution of coherences during t_1.

Let us take just one of these branches and examine how it gives rise to an NMR signal in the period after the second $\pi/2$ pulse.

The fate of the coherence $\rho_{\boxed{-\alpha}}\textcircled{3}$ may be examined by evaluating the following transformation:

$$\widehat{R}_x(\pi/2)\hat{I}_1^-\hat{I}_2^\alpha\widehat{R}_x(-\pi/2)$$

This is conveniently evaluated by using the matrix representations. The matrix representation of the rotation operator $\widehat{R}_x(\pi/2)$ is

$$\widehat{R}_x(\pi/2) = \frac{1}{\sqrt{2}}\begin{pmatrix} 1 & -\mathrm{i} \\ -\mathrm{i} & 1 \end{pmatrix} \otimes \frac{1}{\sqrt{2}}\begin{pmatrix} 1 & -\mathrm{i} \\ -\mathrm{i} & 1 \end{pmatrix} = \frac{1}{2}\begin{pmatrix} 1 & -\mathrm{i} & -\mathrm{i} & -1 \\ -\mathrm{i} & 1 & -1 & -\mathrm{i} \\ -\mathrm{i} & -1 & 1 & -\mathrm{i} \\ -1 & -\mathrm{i} & -\mathrm{i} & 1 \end{pmatrix}$$

The transformation of the coherence $\rho_{\boxed{-\alpha}}$ by the second $\pi/2$ pulse is therefore

$$\widehat{R}_x(\pi/2)\hat{I}_1^-\hat{I}_2^\alpha\widehat{R}_x(-\pi/2) = \frac{1}{2}\begin{pmatrix} 1 & -\mathrm{i} & -\mathrm{i} & -1 \\ -\mathrm{i} & 1 & -1 & -\mathrm{i} \\ -\mathrm{i} & -1 & 1 & -\mathrm{i} \\ -1 & -\mathrm{i} & -\mathrm{i} & 1 \end{pmatrix}\begin{pmatrix} 0 & 0 & 0 & 0 \\ 0 & 0 & 0 & 0 \\ 1 & 0 & 0 & 0 \\ 0 & 0 & 0 & 0 \end{pmatrix}$$

$$\times\frac{1}{2}\begin{pmatrix} 1 & \mathrm{i} & \mathrm{i} & -1 \\ \mathrm{i} & 1 & -1 & \mathrm{i} \\ \mathrm{i} & -1 & 1 & \mathrm{i} \\ -1 & \mathrm{i} & \mathrm{i} & 1 \end{pmatrix} = \frac{1}{4}\begin{pmatrix} -\mathrm{i} & 1 & 1 & \mathrm{i} \\ -1 & -\mathrm{i} & -\mathrm{i} & 1 \\ 1 & \mathrm{i} & \mathrm{i} & -1 \\ -\mathrm{i} & 1 & 1 & \mathrm{i} \end{pmatrix}$$

This indicates that the pulse transforms the single coherence $\rho_{\boxed{-\alpha}}$ into *every other* population and coherence in the spin system:

$$\rho_{\boxed{-\alpha}} \xrightarrow{(\pi/2)_x} \frac{1}{4}\rho_{\boxed{-\alpha}} + \frac{1}{4}\rho_{\boxed{-\beta}} - \frac{1}{4}\rho_{\boxed{\alpha-}} + \frac{1}{4}\rho_{\boxed{\beta-}} + \ldots$$

Each 'branch' of the 'tree' forks again into many different 'twigs':

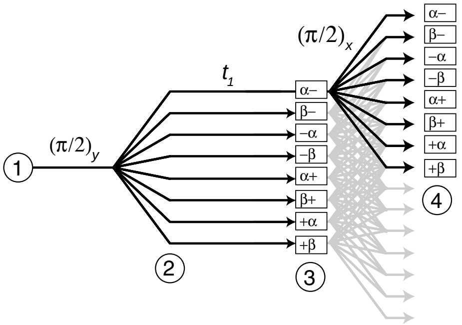

Figure 16.10
Branching of coherences induced by the second pulse in COSY.

The process by which a single coherence is converted by an r.f. pulse into one or more different coherences is called *coherence transfer*.

Let us concentrate for the moment on a single 'twig' of the 'tree', corresponding to the following coherence transfer history:

$$\hat{\rho}^{\mathrm{eq}} \xrightarrow{(\pi/2)_y} \rho_{\boxed{-\alpha}} \xrightarrow{(\pi/2)_x} \rho_{\boxed{\alpha-}}$$

The NMR signal component from this single 'twig' will be denoted

$$s_{\boxed{-\alpha}\rightarrow\boxed{\alpha-}}(t_1, t_2)$$

The signal generated by this single *coherence transfer pathway* is proportional to (1) the efficiency with which the coherence $\rho_{\boxed{-\alpha}}$ is excited by the first r.f. pulse, (2) the amplitude factor accumulated by the coherence $\rho_{\boxed{-\alpha}}$ during its evolution in the t_1 period, (3) the amplitude for conversion of the coherence $\rho_{\boxed{-\alpha}}$ into $\rho_{\boxed{\alpha-}}$ by the second $\pi/2$ pulse, (4) the amplitude factor accumulated by the coherence $\rho_{\boxed{\alpha-}}$ during its evolution in the t_2 period, and (5) a factor 2i coming from the quadrature detection process.[2] By combining all these factors we get the following result:

$$s_{\boxed{-\alpha}\rightarrow\boxed{\alpha-}}(t_1, t_2) = \left(\frac{1}{2\mathrm{i}}\right) \times \exp\{\left(\mathrm{i}\Omega_{\boxed{-\alpha}} - \lambda\right) t_1\} \times \left(-\frac{1}{4}\right) \times \exp\{\left(\mathrm{i}\Omega_{\boxed{\alpha-}} - \lambda\right) t_2\} \times (2\mathrm{i})$$

giving

$$s_{\boxed{-\alpha}\rightarrow\boxed{\alpha-}}(t_1, t_2) = -\frac{1}{4} \exp\{\left(\mathrm{i}\Omega_{\boxed{-\alpha}} - \lambda\right) t_1 + \left(\mathrm{i}\Omega_{\boxed{\alpha-}} - \lambda\right) t_2\}$$

We have seen this type of two-dimensional signal in Section 5.9. After two-dimensional FT, we get a two-dimensional spectrum with a peak at the frequency coordinates $(\Omega_1, \Omega_2) = (\Omega_{\boxed{-\alpha}}, \Omega_{\boxed{\alpha-}})$. Since the frequency of coherence $\rho_{\boxed{-\alpha}}$ is $\Omega_{\boxed{-\alpha}} = \Omega_1^0 + \pi J_{12}$, and the frequency of coherence $\rho_{\boxed{\alpha-}}$ is $\Omega_{\boxed{\alpha-}} = \Omega_2^0 + \pi J_{12}$, this contribution to the two-dimensional spectrum has the following appearance:

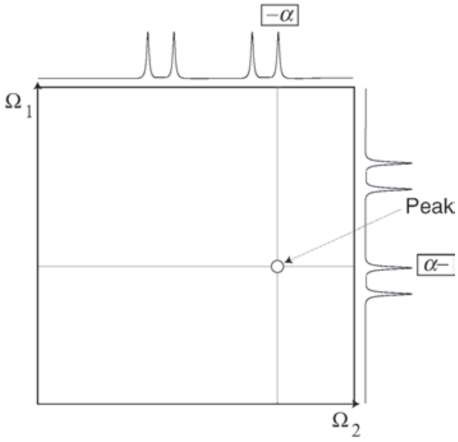

Figure 16.11
A single peak in a COSY spectrum.

This is only one 'twig' of the 'tree'. In fact, every coherence in the spin system is converted into every other coherence by the second $\pi/2$ pulse. When the signal is summed over all 'twigs', we get a two-dimensional spectrum with a peak in every possible place, as shown in Figure 16.12.

Peaks with the same frequency in the two dimensions are called *diagonal peaks* (they lie on the dashed line in the plot above). Peaks with different frequency in the two dimensions are called *cross-peaks*. In general, diagonal peaks are not particularly informative, whereas cross-peaks carry useful information.

The phases of the COSY peaks (indicated by the shading) are discussed below.

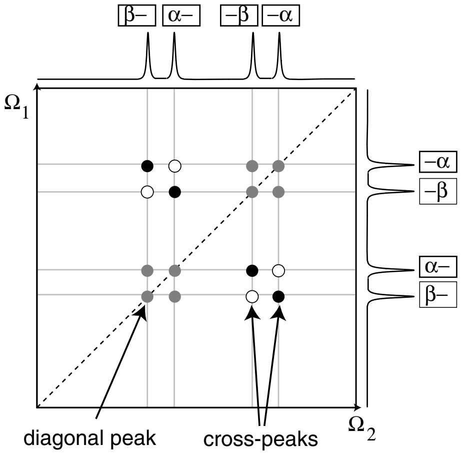

Figure 16.12
All peaks in the COSY spectrum of an AX ensemble.

Now consider the situation in which there are two different types of AX system in the sample. Each type of AX system generates its own 'tree' and its own two-dimensional correlation map. But since coherences are not transferred between different molecules, it is not possible to generate two-dimensional peaks connecting signals belonging to different spin systems. If 'possibility 1' is the correct assignment, as in Figure 16.2, then the two-dimensional COSY spectrum of a mixture of two AX spin systems has the following form:

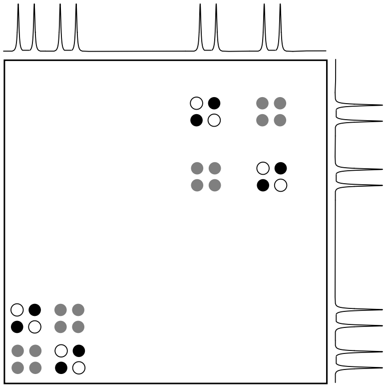

Figure 16.13
The form of the COSY spectrum for two AX systems.

This is precisely the sort of two-dimensional correlation map that I tried to motivate at the beginning of this section.

16.1.4 Product operator interpretation

It is possible to calculate the details of the COSY spectrum by repeating the calculation above for every coherence in the system. However, a more economical interpretation of COSY is obtained using product operators. Consider again the 'cosine' pulse sequence (Figure 16.6). The spin density operator after the first pulse is given by

$$\hat{\rho}^{\cos}_{②} = -\hat{I}_{1y} - \hat{I}_{2y}$$

omitting the unity operator and the numerical factors. The product operator evolution rules in Section 15.9 may be used to write down the density operator at the end of the t_1 interval, time point ③:

$$\begin{aligned}
\hat{\rho}_{\textcircled{3}}^{\cos} &= -\hat{I}_{1y}\cos(\Omega_1^0 t_1)\cos(\pi J_{12} t_1) + 2\hat{I}_{1x}\hat{I}_{2z}\cos(\Omega_1^0 t_1)\sin(\pi J_{12} t_1) \\
&\quad + \hat{I}_{1x}\sin(\Omega_1^0 t_1)\cos(\pi J_{12} t_1) + 2\hat{I}_{1y}\hat{I}_{2z}\sin(\Omega_1^0 t_1)\sin(\pi J_{12} t_1) \\
&\quad - \hat{I}_{2y}\cos(\Omega_2^0 t_1)\cos(\pi J_{12} t_1) + 2\hat{I}_{1z}\hat{I}_{2x}\cos(\Omega_2^0 t_1)\sin(\pi J_{12} t_1) \\
&\quad + \hat{I}_{2x}\sin(\Omega_2^0 t_1)\cos(\pi J_{12} t_1) + 2\hat{I}_{1z}\hat{I}_{2y}\sin(\Omega_2^0 t_1)\sin(\pi J_{12} t_1) \qquad (16.1)
\end{aligned}$$

This is a superposition of in-phase single-quantum terms ($\hat{I}_{1x}$, $\hat{I}_{1y}$, $\hat{I}_{2x}$ and $\hat{I}_{2y}$) and antiphase single-quantum terms ($2\hat{I}_{1y}\hat{I}_{2z}$, $2\hat{I}_{1x}\hat{I}_{2z}$, $2\hat{I}_{1z}\hat{I}_{2y}$ and $2\hat{I}_{1z}\hat{I}_{2x}$).

This density operator is transformed by the $(\pi/2)_x$ pulse according to the rules given in Section 15.8:

$$\begin{aligned}
\hat{\rho}_{\textcircled{4}}^{\cos} &= -\hat{I}_{1z}\cos(\Omega_1^0 t_1)\cos(\pi J_{12} t_1) - 2\hat{I}_{1x}\hat{I}_{2y}\cos(\Omega_1^0 t_1)\sin(\pi J_{12} t_1) \\
&\quad + \hat{I}_{1x}\sin(\Omega_1^0 t_1)\cos(\pi J_{12} t_1) - 2\hat{I}_{1z}\hat{I}_{2y}\sin(\Omega_1^0 t_1)\sin(\pi J_{12} t_1) \\
&\quad - \hat{I}_{2z}\cos(\Omega_2^0 t_1)\cos(\pi J_{12} t_1) - 2\hat{I}_{1y}\hat{I}_{2x}\cos(\Omega_2^0 t_1)\sin(\pi J_{12} t_1) \\
&\quad + \hat{I}_{2x}\sin(\Omega_2^0 t_1)\cos(\pi J_{12} t_1) - 2\hat{I}_{1y}\hat{I}_{2z}\sin(\Omega_2^0 t_1)\sin(\pi J_{12} t_1)
\end{aligned}$$

In order to analyse the NMR signal, we need only consider the single-quantum terms:

$$\begin{aligned}
\hat{\rho}_{\textcircled{4}}^{\cos} &= +\hat{I}_{1x}\sin(\Omega_1^0 t_1)\cos(\pi J_{12} t_1) - 2\hat{I}_{1z}\hat{I}_{2y}\sin(\Omega_1^0 t_1)\sin(\pi J_{12} t_1) \\
&\quad + \hat{I}_{2x}\sin(\Omega_2^0 t_1)\cos(\pi J_{12} t_1) - 2\hat{I}_{1y}\hat{I}_{2z}\sin(\Omega_2^0 t_1)\sin(\pi J_{12} t_1) + \ldots \qquad (16.2)
\end{aligned}$$

If we repeat the calculation for the 'sine' pulse sequence (Figure 16.7), we get

$$\begin{aligned}
\hat{\rho}_{\textcircled{4}}^{\sin} &= -\hat{I}_{1x}\cos(\Omega_1^0 t_1)\cos(\pi J_{12} t_1) + 2\hat{I}_{1z}\hat{I}_{2y}\cos(\Omega_1^0 t_1)\sin(\pi J_{12} t_1) \\
&\quad - \hat{I}_{2x}\cos(\Omega_2^0 t_1)\cos(\pi J_{12} t_1) + 2\hat{I}_{1y}\hat{I}_{2z}\cos(\Omega_2^0 t_1)\sin(\pi J_{12} t_1) + \ldots \qquad (16.3)
\end{aligned}$$

Examine in detail the second terms in Equations 16.2 and 16.3:

$$\begin{aligned}
\hat{\rho}_{\textcircled{4}}^{\cos} &= -2\hat{I}_{1z}\hat{I}_{2y}\sin(\Omega_1^0 t_1)\sin(\pi J_{12} t_1) + \ldots \\
\hat{\rho}_{\textcircled{4}}^{\sin} &= +2\hat{I}_{1z}\hat{I}_{2y}\cos(\Omega_1^0 t_1)\sin(\pi J_{12} t_1) + \ldots
\end{aligned}$$

Standard trigonometric identities may be used to write these terms as follows:

$$\begin{aligned}
\hat{\rho}_{\textcircled{4}}^{\cos} &= -2\hat{I}_{1z}\hat{I}_{2y} \times \frac{1}{2}\left\{\cos\left((\Omega_1^0 - \pi J_{12})t_1\right) - \cos\left((\Omega_1^0 + \pi J_{12})t_1\right)\right\} + \ldots \\
\hat{\rho}_{\textcircled{4}}^{\sin} &= -2\hat{I}_{1z}\hat{I}_{2y} \times \frac{1}{2}\left\{\sin\left((\Omega_1^0 - \pi J_{12})t_1\right) - \sin\left((\Omega_1^0 + \pi J_{12})t_1\right)\right\} + \ldots \qquad (16.4)
\end{aligned}$$

These terms display the appropriate cosine and sine amplitude modulations for the two pulse sequences, as required in the States procedure (Section 5.9.4). The frequency of these modulations is $\Omega_1^0 \pm \pi J_{12}$, with the two components having opposite sign. In addition, the density operator term $-2\hat{I}_{1z}\hat{I}_{2y}$ implies an antiphase absorption peak, centred around frequency Ω_2^0 in the Ω_2 dimension. Equation 16.4, therefore, signifies a *doubly antiphase cross-peak*, in which each component has pure absorption phase, after States data processing. An expansion of the cross-peak is shown on the following page:

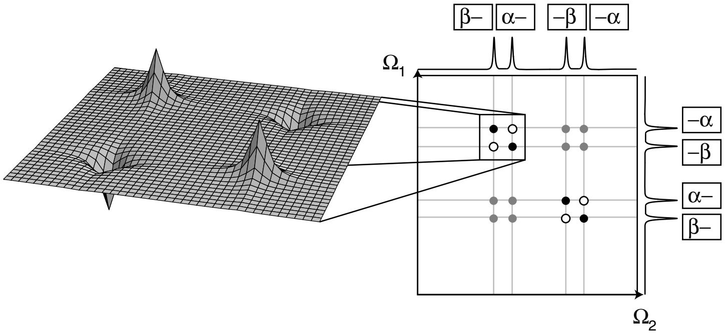

Figure 16.14
The form of a COSY cross-peak multiplet.

If one examines the fourth terms in Equations 16.2 and 16.3, one finds another doubly antiphase pure absorption cross-peak, but this time centred at frequency coordinates $(\Omega_1, \Omega_2) = (\Omega_2^0, \Omega_1^0)$.

The first and third terms in Equations 16.2 and 16.3 do not work out so comfortably. These terms describe diagonal and near-diagonal peaks, and are given by

$$\begin{aligned}\hat{\rho}_{\textcircled{4}}^{\cos} &= \hat{I}_{1x}\sin(\Omega_1^0 t_1)\cos(\pi J_{12} t_1) + \ldots\\ \hat{\rho}_{\textcircled{4}}^{\sin} &= -\hat{I}_{1x}\cos(\Omega_1^0 t_1)\cos(\pi J_{12} t_1) + \ldots\end{aligned}$$

Trigonometric identities give

$$\begin{aligned}\hat{\rho}_{\textcircled{4}}^{\cos} &= \hat{I}_{1x} \times \frac{1}{2}\left\{\sin((\Omega_1^0 + \pi J_{12})t_1) + \sin((\Omega_1^0 - \pi J_{12})t_1)\right\} + \ldots\\ \hat{\rho}_{\textcircled{4}}^{\sin} &= \hat{I}_{2x} \times \frac{1}{2}\left\{-\cos((\Omega_1^0 + \pi J_{12})t_1) - \cos((\Omega_1^0 - \pi J_{12})t_1)\right\} + \ldots \qquad (16.5)\end{aligned}$$

Everything is wrong here. We have sine modulations with respect to t_1 in the 'cosine' data set, and we have cosine modulations with respect to t_1 in the 'sine' data set. Furthermore, the $\hat{I}_{1x}$ terms in the density operator indicate dispersion peaks in the Ω_2 dimension, instead of absorption peaks. As a result, the States procedure does not work at all for these peaks. States data processing, as described in Section 5.9.4, gives the following shape for the diagonal peak:

$$\begin{aligned}\mathrm{Re}\{S_{\mathrm{States}}(\Omega_1, \Omega_2)\} = &\frac{1}{2}\mathcal{D}(\Omega_1; \Omega_1^0 - \pi J_{12}, \lambda)\mathcal{D}(\Omega_2; \Omega_1^0 - \pi J_{12}, \lambda)\\ &+\frac{1}{2}\mathcal{D}(\Omega_1; \Omega_1^0 + \pi J_{12}, \lambda)\mathcal{D}(\Omega_2; \Omega_1^0 - \pi J_{12}, \lambda)\\ &+\frac{1}{2}\mathcal{D}(\Omega_1; \Omega_1^0 - \pi J_{12}, \lambda)\mathcal{D}(\Omega_2; \Omega_1^0 + \pi J_{12}, \lambda)\\ &+\frac{1}{2}\mathcal{D}(\Omega_1; \Omega_1^0 + \pi J_{12}, \lambda)\mathcal{D}(\Omega_2; \Omega_1^0 + \pi J_{12}, \lambda)\end{aligned}$$

which appears as follows:

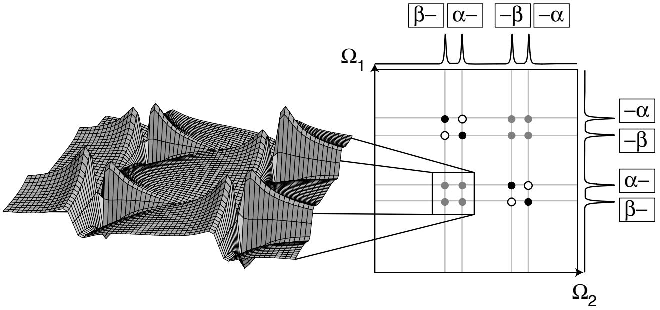

Figure 16.15
The form of a COSY diagonal-peak multiplet.

The ugly double-dispersion appearance of the diagonal peaks is a drawback of the original COSY pulse sequence. The long dispersion tails of the diagonal peaks tend to obscure any nearby cross-peaks.

A variant called *double-quantum-filtered COSY* provides absorption lineshapes for both the diagonal peaks and the cross-peaks, and is usually used in practice (see Exercise 16.2).

16.1.5 Experimental examples

Figure 16.16 shows an experimental COSY spectrum of an organic molecule in solution. It would be an exceedingly difficult task to assign all of the NMR peaks in such a complex spectrum without the aid of two-dimensional spectra.

Apart from being more informative, two-dimensional spectra have the advantage of being much *less crowded* than one-dimensional spectra. There is much more room in a two-dimensional spectral plane compared with the one-dimensional frequency axis of a one-dimensional NMR spectrum. The chance of peaks landing on top of each other is greatly reduced in two dimensions. Figure 16.17 shows the ^{1}H double-quantum-filtered COSY spectrum of a medium-sized protein molecule in aqueous solution (the huge water resonance is visible as an ugly vertical stripe). The protein contains approximately 1000 non-equivalent proton sites.

Although the use of two-dimensional spectroscopy greatly reduces the problems caused by overlapping peaks, the spectra of biological molecules are still often too crowded. Figure 16.17 displays several spectral regions in which the peaks assignments remain problematic. In the NMR of large molecules, it is fairly usual to record three- or higher-dimensional NMR spectra in order to reduce the spectral crowding further.

16.2 INADEQUATE

The pulse sequence INADEQUATE was designed by Ad Bax and co-workers in 1980. The ironical acronym stands for ‘Incredible Natural Abundance Double Quantum Technique’. The aim of this pulse sequence is to suppress signals from isolated ^{13}C spins, allowing the selective detection of NMR signals from very rare molecules containing natural pairs of ^{13}C atoms.

16.2.1 ^{13}C isotopomers

As background to this method, consider a sample of ordinary ethanol (CH_3CH_2OH). There are two C sites in each molecule, which are occupied by either ^{13}C or ^{12}C nuclei, according to their natural abundances. The natural abundance of ^{12}C (spin = 0) is ∼98.9%; the natural abundance of ^{13}C (spin-1/2) is ∼1.1%. An ethanol molecule has four carbon isotopomers:

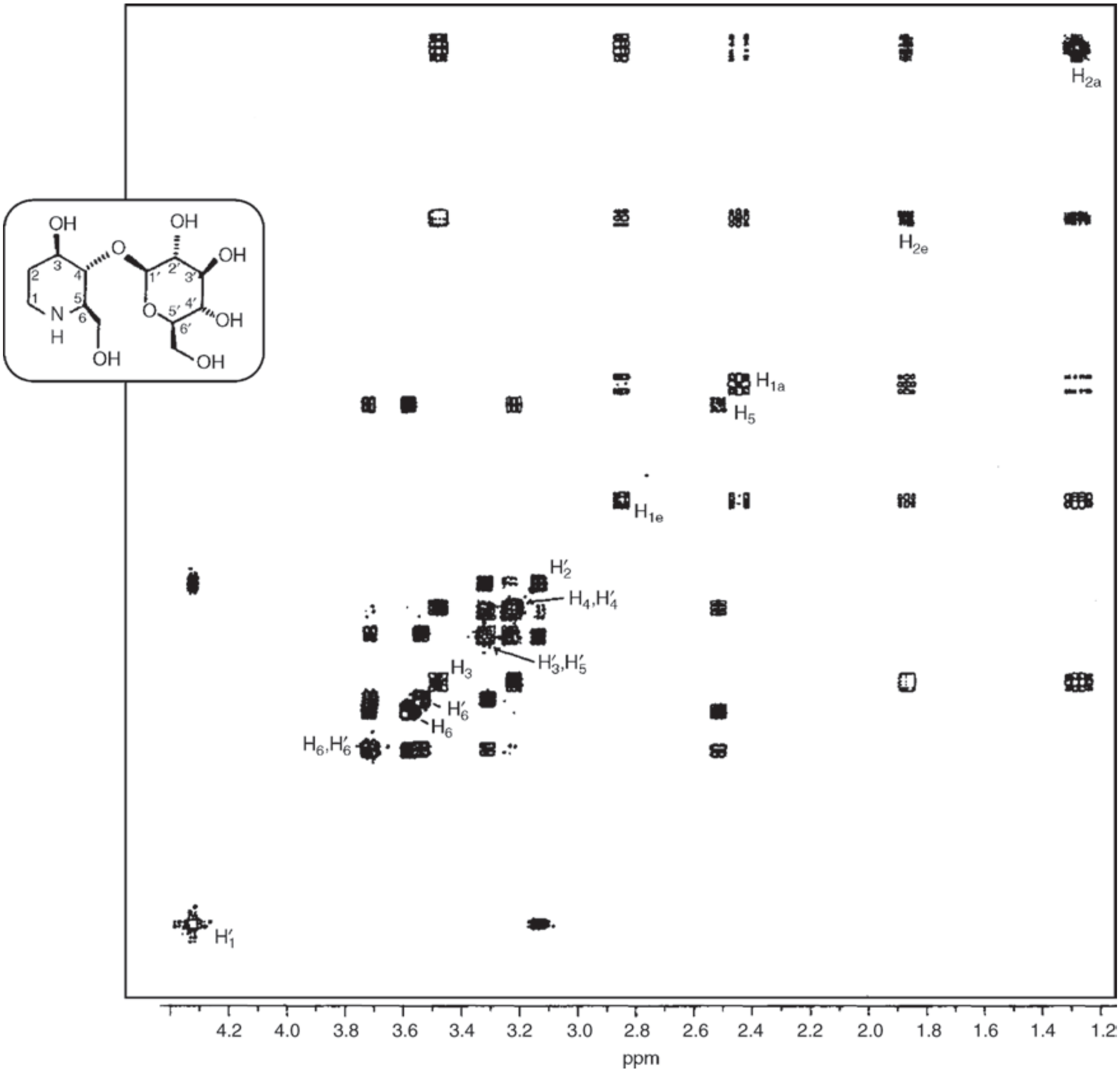

Figure 16.16 Experimental ^{1}H COSY spectrum of an organic molecule in solution. Adapted from A. E. Derome, *Modern NMR Techniques in Chemistry Research*, Pergamon Press, Oxford, 1990, p. 192. Copyright 1990, Elsevier Science.

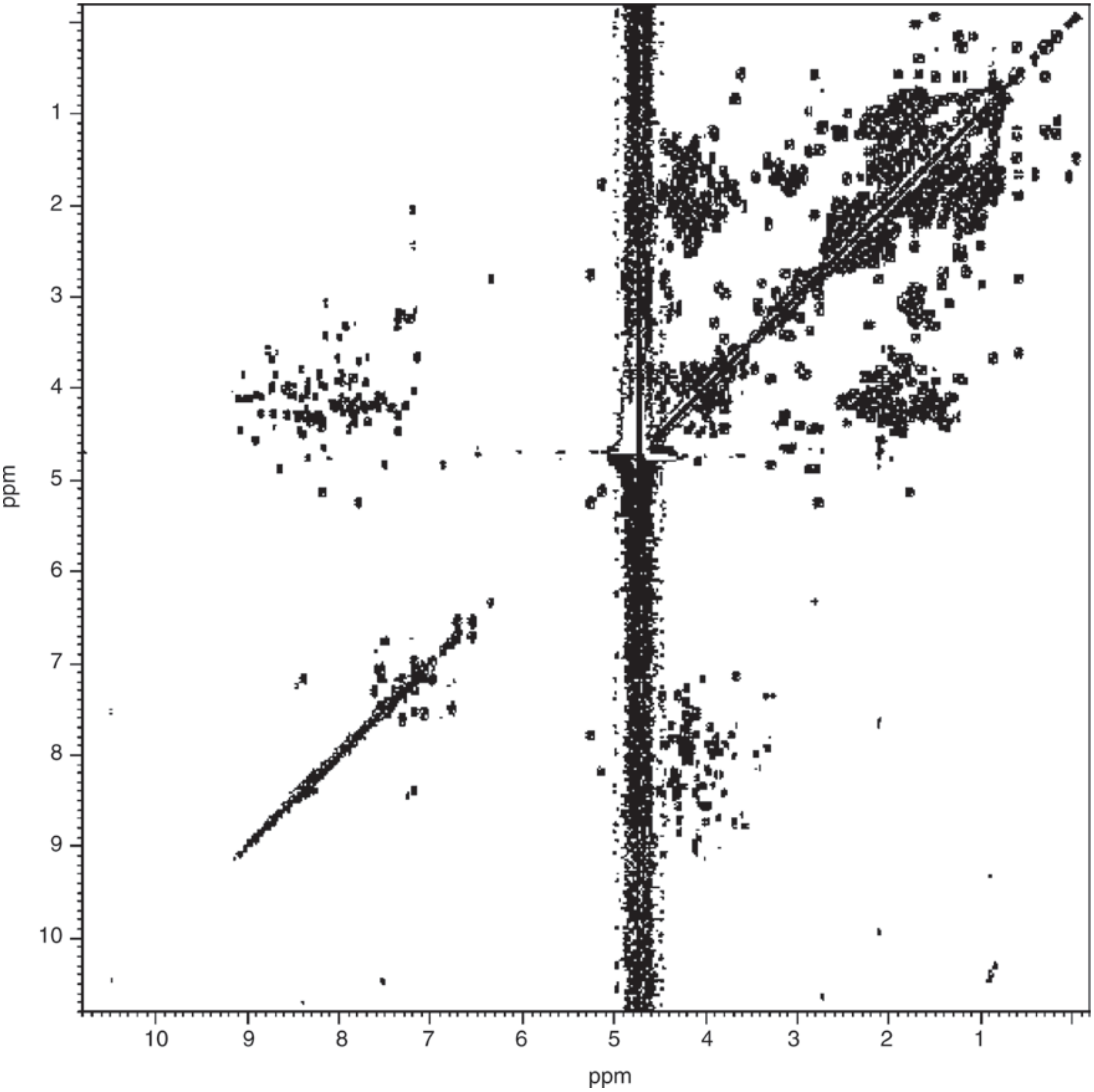

Figure 16.17 Experimental ^{1}H COSY spectrum of a medium-sized biomolecule in solution (the C-terminal domain of rat ERp29 protein). The protein contains 120 amino acid residues. A long interval of weak r.f. irradiation at the water proton Larmor frequency ('presaturation') was applied before the start of the pulse sequence to suppress the water proton signals. The residual water signal is visible as a strong vertical band in the centre of the spectrum. Thanks to E. Liepinsh and G. Otting for supplying this spectrum.

- *Species I.* $^{12}CH_3{}^{12}CH_2OH$; both C sites are occupied by ^{12}C nuclei.
- *Species II.* $^{13}CH_3{}^{12}CH_2OH$; the CH_3 site is occupied by ^{13}C and the CH_2 site is occupied by ^{12}C.
- *Species III.* $^{12}CH_3{}^{13}CH_2OH$; the CH_3 site is occupied by ^{12}C and the CH_2 site is occupied by ^{13}C.
- *Species IV*. $^{13}CH_3{}^{13}CH_2OH$; both C sites are occupied by ^{13}C nuclei.

The relative abundances of these isotopomers may be calculated as follows. Suppose that the fractional abundance of ^{13}C is x, and that of ^{12}C is $1-x$. The fractional abundance of species I is equal to the probability that the CH_3 site is occupied by ^{12}C, multiplied by the probability that the CH_2 site is *also* occupied by ^{12}C. This probability is

$$p_{\mathrm{I}} = (1-x)(1-x) \cong 97.81\%$$

using the value $x \cong 1.1\%$.

Similarly, the fractional abundance of species II is equal to the probability that the CH_3 site is occupied by ^{13}C, multiplied by the probability that the CH_2 site is occupied by ^{12}C:

$$p_{\mathrm{II}} = (1-x)x \cong 1.09\%$$

and likewise for the fractional abundance of species III:

$$p_{\mathrm{III}} = x(1-x) \cong 1.09\%$$

The fractional abundance of the $^{13}C_2$ species IV is equal to:

$$p_{\mathrm{IV}} = x^2 \cong 0.012\%$$

This means that only around 1 out of every 10 000 ethanol molecules contains two ^{13}C spins.

Since the dominant isotopomer I contains no ^{13}C spins, the ^{13}C spectrum of ethanol is dominated by signals from the isotopomers II and III. If the ^1H spins are decoupled by an r.f. field at the proton Larmor frequency, each of these isotopomers contributes a single spectral peak, at the chemical shift of the ^{13}C site. Isotopomer II gives a peak at the chemical shift of spins in the ethanol CH_3 site, and isotopomer III gives a peak at the chemical shift of spins in the ethanol CH_2 site:

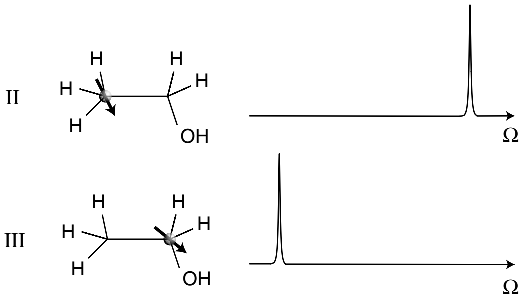

Figure 16.18
Ethanol isotopomers II and III and their ^1H-decoupled ^{13}C spectra.

The rare isotopomer IV contains two ^{13}C spins, which form a homonuclear AX system in the presence of proton decoupling. The J-coupling between the ^{13}C spins is around 50 Hz. This isotopomer contributes a four-line spectral pattern:

IV

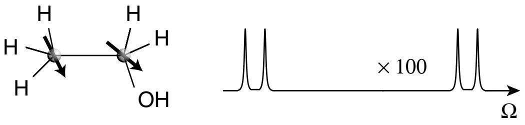

Figure 16.19 Ethanol isotopomer IV and its ^{1}H-decoupled ^{13}C spectrum.

(The spectrum is shown at 100 times magnification). The total spectrum therefore consists of two large peaks from the relatively common isotopomers II and III, and four very small *satellite* peaks generated by the rare isotopomer IV:

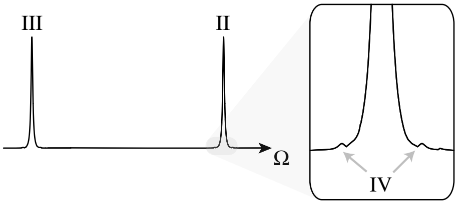

Figure 16.20 Total ^{1}H-decoupled ^{13}C spectrum of ethanol.

In practice, the satellite peaks are extremely difficult to observe, since the main peaks are ~200 times larger. (A factor of 100 comes from the relative abundances of the isotopomers, and a further factor of 2 comes from the fact that the ^{13}C$_2$ peaks are split by the J-coupling.)

INADEQUATE is a method that supresses the main peaks, which come from non-interacting spins-1/2. Only 'satellite' signals from the rare spin-1/2 pairs appear in the final spectrum.

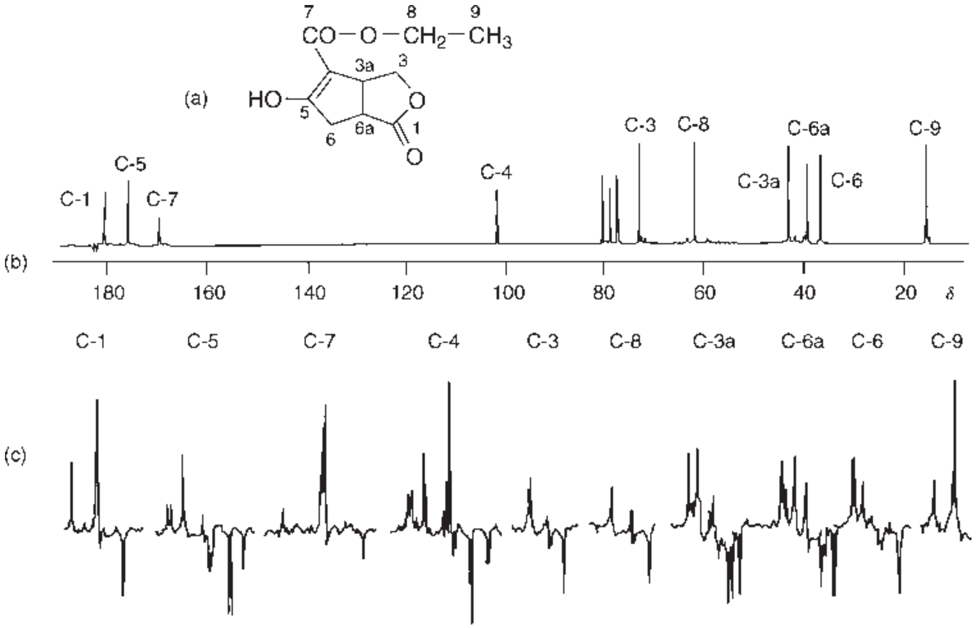

Figure 16.21 ^{13}C spectra of the compound shown in (a) (a small amount of a paramagnetic relaxation agent was added to the solution in order to decrease the waiting interval between transients). (b) Proton-decoupled ^{13}C spectrum. (c) Expanded sections of the ^{13}C INADEQUATE spectrum, showing the antiphase ^{13}C$_2$ satellites. The data were taken over 16 h on 1.2 g of material in a field of 9.4 T. Adapted from J. Buddrus and H. Bauer, *Angew. Chem. Int. Ed. Engl.* **26**, 625 (1987). (Reproduced by permission of Wiley–VCH.)

An experimental example is given in Figure 16.21, which shows the INADEQUATE spectrum of a sample in which each molecule has 10 inequivalent carbon sites. In this case, there are 45 possible $^{13}C_2$ isotopomers ($_{10}C_2 = 10!/(2!\,8!) = 45$), each giving four satellite signals. The experimental INADEQUATE spectrum at the top of the figure displays many such $^{13}C_2$ signals. The satellite signals are invisible in the conventional ^{13}C spectrum in Figure 16.21b.

The satellite peaks produced by INADEQUATE have a characteristic antiphase configuration. We will see why soon.

Why is the observation of satellite signals useful? First, the observation of $^{13}C_2$ satellites allows the measurement of ^{13}C–^{13}C J-couplings. These couplings, especially longer-range couplings, often provide useful information as to the geometry of the molecules. Second, the examination of $^{13}C_2$ satellite spectra assists greatly in the *assignment* of the ^{13}C spectrum: molecules with many carbon sites provide a spectrum with many ^{13}C peaks, and it is not always possible to decide which peak belongs to which site. By observing the ^{13}C–^{13}C couplings, one may figure out which carbon site is a neighbour to which other site.

16.2.2 Pulse sequence

The INADEQUATE pulse sequence is as follows:

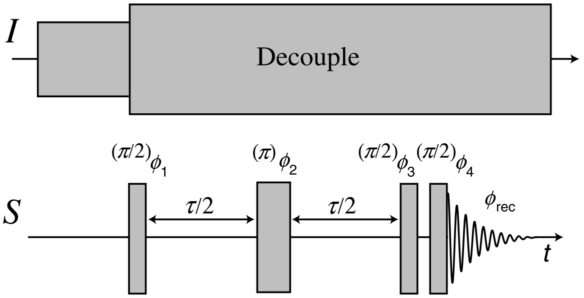

Figure 16.22
INADEQUATE pulse sequence.

The ^1H r.f. fields are denoted I, and the ^{13}C r.f. fields are denoted S.

The pulse sequence on the ^{13}C spins consists of three pulses of flip angle $\pi/2$ and one pulse of flip angle π. The last two $\pi/2$ pulses follow each other almost immediately; it is only necessary to wait a few microseconds for the r.f. phase shift to be implemented.

The first part of the pulse sequence involves a spin echo sandwich with duration τ. The interval τ is chosen to match the ^{13}C–^{13}C coupling constant, according to

$$\tau = |(2J_{12})^{-1}|$$

One-bond ^{13}C–^{13}C couplings are often around +50 Hz, so the value of τ is approximately 10 ms. The pulse sequence intervals, therefore, are $\tau/2 \cong 5$ ms. However, one should be aware that the values of one-bond ^{13}C–^{13}C coupling constants vary considerably from compound to compound, so that the figure of 5 ms is only a rough estimate.

Irradiation is applied at the ^1H Larmor frequency throughout the sequence and the observation interval, in order to decouple the ^{13}C spins from the protons. In addition, one normally applies low-level ^1H irradiation for several seconds before the start of the ^{13}C pulse sequence. This enhances the ^{13}C magnetization through the *NOE*, as discussed in Section 20.5.

As usual, the pulse sequence is not drawn to scale along the time axis. In practice, the durations of the pulses are much smaller than the intervals between the pulses, and the ^1H irradiation before the sequence lasts much longer than anything else.

Table 16.1 A four-step phase cycle ($\mathfrak{n} = 4$) appropriate for the INADEQUATE experiment.

Cycle counter $\mathfrak{m}$	ϕ_1	ϕ_2	ϕ_3	ϕ_4	ϕ_{rec}
0	0	0	0	$\pi/2$	0
1	0	0	0	π	$3\pi/2$
2	0	0	0	$3\pi/2$	π
3	0	0	0	0	$\pi/2$

The phases of the ^{13}C pulses are denoted ϕ_1, ϕ_2, ϕ_3 and ϕ_4. The signal is detected using a receiver phase shift ϕ_{rec}. These phases are subject to a phase cycle, as described in Section 5.3. A series of independent experiments is performed, with different values for the pulse phases $\phi_1 \ldots \phi_4$ and receiver phase ϕ_{rec}. The signals from these different experiments are added together.

A simple phase cycle suitable for the INADEQUATE experiment is shown in Table 16.1. The symbol $\mathfrak{n}$ is used for the number of steps in the phase cycle ($\mathfrak{n} = 4$ in this case) and the symbol $\mathfrak{m}$ is used for the phase cycle counter. This may be calculated from the transient counter $\mathfrak{M} = 0, 1, 2, 3, 4, 5 \ldots$ through the following formula:

$$\mathfrak{m} = \text{mod}(\mathfrak{M}, 4)$$

The phase cycle counter, therefore, runs $\mathfrak{m} = 0, 1, 2, 3, 0, 1, 2 \ldots$, implying that the phase cycle is to be read from top-to-bottom, top-to-bottom, etc., until a complete number of phase cycle steps is completed. The number of acquired transients must be a multiple of 4.

In the cycle shown, only the phase ϕ_4 of the last pulse and the receiver phase ϕ_{rec} change during the phase cycle. Some longer and more sophisticated phase cycles are presented in Appendix A.11.

16.2.3 Theory of INADEQUATE

We now calculate the spectral peak amplitudes generated by the INADEQUATE pulse sequence. For simplicity, the effects of relaxation are ignored.

As described in Section 15.10, the operation of the pulse sequence may be analysed using the simplified form shown in Figure 16.23, which uses phases given in the first row of Table 16.1. Conceptually, the π pulse in the centre of the spin echo sandwich is shifted to the beginning of that period, where it merges with the first $\pi/2$ pulse to form one pulse of flip angle $3\pi/2$, followed by an interval τ, in which only the J-couplings are active.

The calculation is conducted in two parts: First for isolated spin signals and then for two-spin signals. We wish to demonstrate that isolated spin signals are destroyed, whereas the signals from spin pairs build up.

1. *Isolated spin signals.* Consider, first, the signals from the one-spin systems (the dominant ^{13}C$_1$ isotopomers). The initial density operator is given by

$$\hat{\rho}_{①} = \frac{1}{2}\widehat{1} + \epsilon_{\text{NOE}}\frac{1}{2}\mathbb{B}\hat{I}_z$$

where ϵ_{NOE} is the nuclear Overhauser enhancement factor brought about by ^{1}H irradiation before the start of each experiment (see Section 20.5). Typically, $\epsilon_{\text{NOE}} \sim 2$.

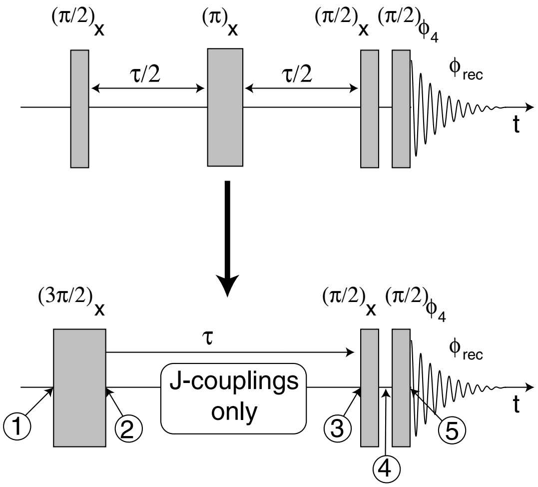

Figure 16.23
Conceptual simplification of the INADEQUATE pulse sequence.

The density operator may be written in a simplified form, leaving out the unity operator and numerical factors:

$$\hat{\rho}_{①} \sim \hat{I}_z$$

This notation is loose but convenient.

The evolution of the density operator up to time point ⑤ runs as follows:

$$\hat{\rho}_{①} = \hat{\rho}^{\mathrm{eq}} = \hat{I}_z$$

$$\Big\downarrow (3\pi/2)_x$$

$$\hat{\rho}_{②} = +\hat{I}_y$$

$$\tau \Big\downarrow \text{(chemical shifts suppressed)}$$

$$\hat{\rho}_{③} = +\hat{I}_y$$

$$\Big\downarrow (\pi/2)_x$$

$$\hat{\rho}_{④} = \hat{I}_z$$

The τ interval has no effect for isolated spins-1/2, since there are no J-couplings.

The phase of the next pulse depends on the step in the phase cycle. Let $\hat{\rho}_{\textcircled{5}}^{[\mathfrak{m}]}$ denote the density operator at time point ⑤, for phase cycle step $\mathfrak{m}$.

For $\mathfrak{m} = 0$, the phase of the last pulse is $\phi_4 = \pi/2$, leading to

$$\hat{\rho}_{\textcircled{4}} = \hat{I}_z \quad \xrightarrow{(\pi/2)_y} \quad \hat{\rho}_{\textcircled{5}}^{[0]} = \hat{I}_x$$

For the other phase cycle steps, we get different final states:

$$\begin{aligned}
\hat{\rho}_{\textcircled{4}} \quad &\xrightarrow{(\pi/2)_{\bar{x}}} \quad \hat{\rho}_{\textcircled{5}}^{[1]} = \hat{I}_y \\
\hat{\rho}_{\textcircled{4}} \quad &\xrightarrow{(\pi/2)_{\bar{y}}} \quad \hat{\rho}_{\textcircled{5}}^{[2]} = -\hat{I}_x \\
\hat{\rho}_{\textcircled{4}} \quad &\xrightarrow{(\pi/2)_{x}} \quad \hat{\rho}_{\textcircled{5}}^{[3]} = -\hat{I}_y
\end{aligned}$$

Time point ⑤ is the start of signal detection, defined as usual $t = 0$. The amplitudes of the (-1)-quantum coherence at this time are deduced from the density operator in the usual way:

$$\begin{aligned}
\rho^{[0]}_{\boxed{-}}\textcircled{5} &= \frac{1}{2} & \rho^{[2]}_{\boxed{-}}\textcircled{5} &= -\frac{1}{2} \\
\rho^{[1]}_{\boxed{-}}\textcircled{5} &= -\frac{1}{2\mathrm{i}} & \rho^{[3]}_{\boxed{-}}\textcircled{5} &= +\frac{1}{2\mathrm{i}}
\end{aligned}$$

The amplitude of the spectral peak is given by the equation:

$$a = 2\mathrm{i}\rho_{\boxed{-}}\textcircled{5}\ \exp\{-\mathrm{i}\phi_{\mathrm{rec}}\}$$

The receiver phase ϕ_{rec} depends on the step in the phase cycle, according to Table 16.1. The peak amplitude for each step in the phase cycle must be worked out individually. For example, for the phase cycle step $\mathfrak{m} = 1$, the signal amplitude works out as

$$a^{[1]} = 2\mathrm{i}\rho^{[1]}_{\boxed{-}}\textcircled{5}\ \exp\{-\mathrm{i}3\pi/2\} = -\mathrm{i}$$

The results for all the phase cycle steps are

$$\begin{aligned}
a^{[0]} &= \mathrm{i} & a^{[2]} &= \mathrm{i} \\
a^{[1]} &= -\mathrm{i} & a^{[3]} &= -\mathrm{i}
\end{aligned}$$

The average phase-cycled peak amplitude is therefore identically zero:

$$a^{\mathrm{av}} = \frac{1}{4}\sum_{\mathfrak{m}=0}^{3} a^{[\mathfrak{m}]} = 0$$

This is the expected result. *The signals from isolated spins cancel out.*

2. *Two-spin signals.* Turning now to the calculation of the two-spin signals, the initial density operator may be written strictly as

$$\hat{\rho}_{\text{①}} = \frac{1}{4}\hat{1} + \epsilon_{\mathrm{NOE}}\frac{1}{4}\mathbb{B}\left(\hat{I}_{1z} + \hat{I}_{2z}\right)$$

where ϵ_{NOE} is the nuclear Overhauser enhancement factor. For simplicity, use the loose form:

$$\hat{\rho}_{\text{①}} \sim \hat{I}_{1z} + \hat{I}_{2z}$$

The propagation of the spin-pair density operator up to time point ④ runs as follows:

$$\begin{tikzcd}
\hat{\rho}_{\text{①}} = \hat{\rho}^{\mathrm{eq}} = \hat{I}_{1z} + \hat{I}_{2z} \arrow[d, "(3\pi/2)_x"] \\
\hat{\rho}_{\text{②}} = \hat{I}_{1y} + \hat{I}_{2y} \arrow[d, "\pi J_{12}\tau"] \\
\hat{\rho}_{\text{③}} = -2\hat{I}_{1x}\hat{I}_{2z} - 2\hat{I}_{1z}\hat{I}_{2x} \arrow[d, "(\pi/2)_x"] \\
\hat{\rho}_{\text{④}} = 2\hat{I}_{1x}\hat{I}_{2y} + 2\hat{I}_{1y}\hat{I}_{2x}
\end{tikzcd}$$

This assumes that the interval τ is exactly matched to the J-coupling, $\tau = |(2J_{12})^{-1}|$, and $J_{12} > 0$.

For the spin-pair system, the density operator at time point ④ corresponds to a state of correlated spin polarizations. If the last two terms are expanded in terms of shift operators, we get

$$2\hat{I}_{1x}\hat{I}_{2y} + 2\hat{I}_{1y}\hat{I}_{2x} = -\mathrm{i}\hat{I}_1^+\hat{I}_2^+ + \mathrm{i}\hat{I}_1^-\hat{I}_2^- \tag{16.6}$$

This indicates the presence of double-quantum coherences at time point ④:

$$\begin{aligned}
\rho_{\boxed{++}\text{④}} &= -\mathrm{i} \\
\rho_{\boxed{--}\text{④}} &= \mathrm{i}
\end{aligned}$$

The presence of double-quantum coherences at the junction of the last two pulses is crucial for the operation of the pulse sequence.

For the moment, we proceed by calculating the individual result of each step in the phase cycle.

The state of the spin-pair ensemble after the last pulse, for each of the phase cycle steps, is

$$\begin{aligned}
\hat{\rho}_{\text{④}} &\xrightarrow{(\pi/2)_y} \hat{\rho}^{[0]}_{\text{⑤}} = -2\hat{I}_{1z}\hat{I}_{2y} - 2\hat{I}_{1y}\hat{I}_{2z} \\
\hat{\rho}_{\text{④}} &\xrightarrow{(\pi/2)_{\bar{x}}} \hat{\rho}^{[1]}_{\text{⑤}} = -2\hat{I}_{1x}\hat{I}_{2z} - 2\hat{I}_{1z}\hat{I}_{2x} \\
\hat{\rho}_{\text{④}} &\xrightarrow{(\pi/2)_{\bar{y}}} \hat{\rho}^{[2]}_{\text{⑤}} = 2\hat{I}_{1z}\hat{I}_{2y} + 2\hat{I}_{1y}\hat{I}_{2z} \\
\hat{\rho}_{\text{④}} &\xrightarrow{(\pi/2)_x} \hat{\rho}^{[3]}_{\text{⑤}} = 2\hat{I}_{1x}\hat{I}_{2z} + 2\hat{I}_{1z}\hat{I}_{2x}
\end{aligned} \tag{16.7}$$

All of these density operators correspond to states of antiphase transverse magnetization, as discussed in Section 15.6.

Each spin-pair ensemble has four (−1)-quantum coherences and generates four spectral peaks. Consider for the moment the peak associated with the coherence $\rho_{\boxed{-\beta}}$. The amplitude of this coherence at the end of the pulse sequence, for each of the four steps of the phase cycle, is given by

$$\begin{aligned}
\rho^{[0]}_{\boxed{-\beta}}\text{⑤} &= \frac{1}{2}\mathrm{i} & \rho^{[2]}_{\boxed{-\beta}}\text{⑤} &= -\frac{1}{2}\mathrm{i} \\
\rho^{[1]}_{\boxed{-\beta}}\text{⑤} &= \frac{1}{2} & \rho^{[3]}_{\boxed{-\beta}}\text{⑤} &= -\frac{1}{2}
\end{aligned} \tag{16.8}$$

The amplitude of this peak, in the successive experiments, is given by

$$a^{[0]}_{\boxed{-\beta}} = a^{[1]}_{\boxed{-\beta}} = a^{[2]}_{\boxed{-\beta}} = a^{[3]}_{\boxed{-\beta}} = -1 \tag{16.9}$$

taking into account the changing values of ϕ_{rec} on the different steps of the cycle.

This peak has the same amplitude for the four different experiments, despite the fact that the phases of the pulses and the receiver are different. The average phase-cycled amplitude is therefore:

$$a^{\text{av}}_{\boxed{-\beta}} = \frac{1}{4}\sum_{\mathfrak{m}=0}^{3} a^{[\mathfrak{m}]}_{\boxed{-\beta}} = -1 \tag{16.10}$$

The arguments may be repeated for the other three coherences, which have phase-cycled amplitudes:

$$\begin{aligned}
a^{\text{av}}_{\boxed{-\alpha}} &= +1 \\
a^{\text{av}}_{\boxed{\beta-}} &= -1 \\
a^{\text{av}}_{\boxed{\alpha-}} &= +1
\end{aligned} \tag{16.11}$$

The INADEQUATE spectrum from the two-spin systems, therefore, has a characteristic antiphase appearance:

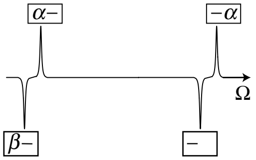

Figure 16.24
Appearance of the INADEQUATE spectrum of a two-spin system.

These antiphase doublets are very visible in experimental spectra, such as that shown in Figure 16.21.

16.2.4 Coherence transfer pathways and phase cycling

The participation of double-quantum coherences at time point ④ is very important for the operation of INADEQUATE. The history of coherence orders during the pulse sequence may be emphasized by drawing a *coherence transfer pathway diagram*, as introduced in Section 12.2.6. For INADEQUATE, this diagram appears as follows:

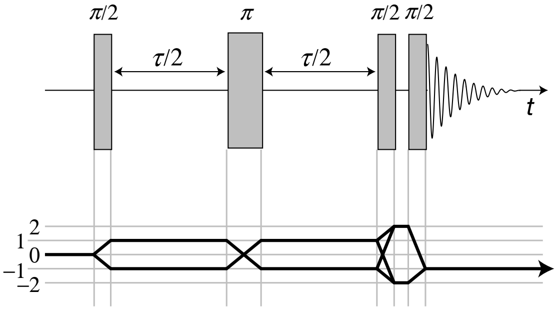

Figure 16.25
Coherence transfer pathway diagram for INADEQUATE.

The pathway starts at order 0, corresponding to thermal equilibrium. The first $\pi/2$ pulse excites (± 1)-quantum coherences, which evolve in the first $\tau/2$ interval. The π pulse inverts the coherence orders, as may be seen through properties such as

$$\widehat{R}_x(\pi)\hat{I}_1^-\hat{I}_2^\alpha\widehat{R}_x(-\pi) = \hat{I}_1^+\hat{I}_2^\beta$$

The second $\pi/2$ pulse converts the single-quantum coherences into double-quantum coherences. The branching of the pathway indicates that both (± 2)-quantum coherences are generated, and that each of the (± 1)-quantum coherences contributes to each of the double-quantum orders. The double-quantum coherences are immediately converted back into single-quantum coherences by the last $\pi/2$ pulse. All pathways terminate at level -1, to indicate quadrature detection of the NMR signal.

As proved in Appendix A.11, the *only* signals that survive the phase cycle given in Table 16.1 pass through (± 2)-quantum coherence during the short interval between the last two $\pi/2$ pulses. This allows the theory of the experiment to be greatly abbreviated, since one only needs to calculate the first step in the phase cycle. The theory in Appendix A.11 proves that (i) the signals from the other phase cycle steps are the same, providing that the density operator elements correspond to (±2)-quantum coherences at time point ④, and (ii) signals passing through all other density operator components at time point ④ vanish.

Using this point of view, the calculation up to time point ④ may be repeated for the spin-pair signals:

$$\begin{tikzcd}
\hat{\rho}_{\textcircled{1}} = \hat{\rho}^{\mathrm{eq}} = \hat{I}_{1z} + \hat{I}_{2z} \arrow[d, "(3\pi/2)_x"] \\
\hat{\rho}_{\textcircled{2}} = \hat{I}_{1y} + \hat{I}_{2y} \arrow[d, "\pi J_{12}\tau"] \\
\hat{\rho}_{\textcircled{3}} = -2\hat{I}_{1x}\hat{I}_{2z} - 2\hat{I}_{1z}\hat{I}_{2x} \arrow[d, "(\pi/2)_x"] \\
\hat{\rho}_{\textcircled{4}} = 2\hat{I}_{1x}\hat{I}_{2y} + 2\hat{I}_{1y}\hat{I}_{2x} \arrow[d, "\text{allow only}"', "(\pm 2)\text{-quantum coherences}"] \\
\hat{\rho}_{\textcircled{4}} = 2\hat{I}_{1x}\hat{I}_{2y} + 2\hat{I}_{1y}\hat{I}_{2x}
\end{tikzcd} \tag{16.12}$$

The density operator term $2\hat{I}_{1x}\hat{I}_{2y} + 2\hat{I}_{1y}\hat{I}_{2x}$ passes through the final step unscathed, since it contains only (±2)-quantum coherences (Equation 16.6).

The first step of the phase cycle may be used to continue the calculation:

$$\begin{tikzcd}
\hat{\rho}_{\textcircled{4}} = 2\hat{I}_{1x}\hat{I}_{2y} + 2\hat{I}_{1y}\hat{I}_{2x} \arrow[d, "(\pi/2)_y"] \\
\hat{\rho}_{\textcircled{5}} = -2\hat{I}_{1z}\hat{I}_{2y} - 2\hat{I}_{1y}\hat{I}_{2z}
\end{tikzcd}$$

As described in Section 15.6, these terms represent antiphase absorption peaks for both spins. The form of the INADEQUATE spectrum may, therefore, be deduced without the laborious step-by-step calculations of Equations 16.7–16.11.

This approach is even more powerful for the single-spin signals. Since isolated spins-1/2 cannot support double-quantum coherences, those signals are completely destroyed by the phase cycle. Formally, we get

$$\begin{tikzcd}
\hat{\rho}_{\textcircled{1}} = \hat{\rho}^{\mathrm{eq}} = \hat{I}_z \arrow[d, "(3\pi/2)_x"] \\
\hat{\rho}_{\textcircled{2}} = \hat{I}_y \arrow[d, "\tau"', "\text{(chemical shifts suppressed)}"] \\
\hat{\rho}_{\textcircled{3}} = \hat{I}_y \arrow[d, "(\pi/2)_x"] \\
\hat{\rho}_{\textcircled{4}} = \hat{I}_z \arrow[d, "\text{allow only}"', "(\pm 2)\text{-quantum coherences}"] \\
0
\end{tikzcd}$$

This conclusion remains valid even if the r.f. pulses are imperfect or if there is relaxation in the intervals between pulses.

16.2.5 Two-dimensional INADEQUATE

The INADEQUATE experiment is easily extended to a very useful two-dimensional form by inserting a variable evolution interval t_1 between the last two $\pi/2$ pulses. In spin-pair systems, the double-quantum coherences evolve during this interval, before being converted into observable (-1)-quantum coherences by the last $\pi/2$ pulse:

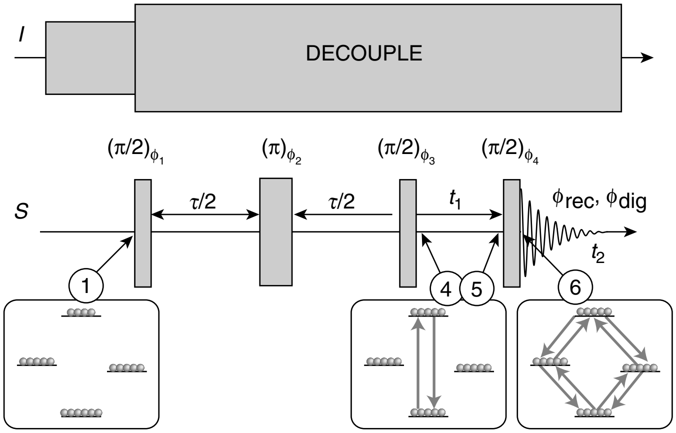

Figure 16.26
Two-dimensional INADEQUATE pulse sequence and the transformations of populations and coherences.

A phase cycle suitable for the two-dimensional INADEQUATE experiment is given in Table 16.2. It is the same as in the one-dimensional experiment, except for an additional phase shift of the first three pulses, which is used in the States procedure for obtaining pure absorption two-dimensional lineshapes (see Section 5.9.4).

The operation of the first part of the 'cosine' pulse sequence is as follows:

$$\hat{\rho}_{①} = \hat{\rho}^{\mathrm{eq}} = \hat{I}_{1z} + \hat{I}_{2z}$$

$$\Big\downarrow (3\pi/2)_x$$

$$\Big\downarrow \pi J_{12}\tau$$

$$\Big\downarrow (\pi/2)_x$$

$$\hat{\rho}_{④}^{\cos} = 2\hat{I}_{1x}\hat{I}_{2y} + 2\hat{I}_{1y}\hat{I}_{2x}$$

where the superscript 'cos' refers to the 'cosine' pulse sequence ($\Psi = 0$ in Table 16.2).

The phase cycling selects only (±2)-quantum coherences at this point, which leaves this particular density operator unscathed. All signals from isolated spins-1/2 are suppressed.

Table 16.2 A four-step phase cycle ($\mathfrak{n} = 4$) appropriate for the two-dimensional INADEQUATE experiment. The phase Ψ is equal to zero for the 'cosine' data set in the States procedure, whereas $\Psi = -\pi/4$ for the 'sine' data set in the States procedure.[1]

Cycle counter $\mathfrak{m}$	ϕ_1	ϕ_2	ϕ_3	ϕ_4	ϕ_{rec}
0	Ψ	Ψ	Ψ	$\pi/2$	0
1	Ψ	Ψ	Ψ	π	$3\pi/2$
2	Ψ	Ψ	Ψ	$3\pi/2$	π
3	Ψ	Ψ	Ψ	0	$\pi/2$

The evolution during the t_1 interval may be calculated according to the principles in Section 15.9:

$$\begin{tikzcd}
\hat{\rho}^{\cos}_{\textcircled{4}} = 2\hat{I}_{1x}\hat{I}_{2y} + 2\hat{I}_{1y}\hat{I}_{2x} \arrow[d, "t_1"] \\
\begin{aligned} \hat{\rho}^{\cos}_{\textcircled{5}} &= \left(2\hat{I}_{1x}\hat{I}_{2y} + 2\hat{I}_{1y}\hat{I}_{2x}\right)\cos\left((\Omega^0_1 + \Omega^0_2)t_1\right) \\ &\quad - \left(2\hat{I}_{1x}\hat{I}_{2x} - 2\hat{I}_{1y}\hat{I}_{2y}\right)\sin\left((\Omega^0_1 + \Omega^0_2)t_1\right) \end{aligned}
\end{tikzcd}$$

Note that the double-quantum evolution proceeds as the sum of the two chemical shift frequencies and is independent of the J-coupling.

The final $\pi/2$ pulse transforms the spin-pair density operator as follows:

$$\begin{tikzcd}
\begin{aligned} \hat{\rho}^{\cos}_{\textcircled{5}} &= \left(2\hat{I}_{1x}\hat{I}_{2y} + 2\hat{I}_{1y}\hat{I}_{2x}\right)\cos\left((\Omega^0_1 + \Omega^0_2)t_1\right) \\ &\quad - \left(2\hat{I}_{1x}\hat{I}_{2x} - 2\hat{I}_{1y}\hat{I}_{2y}\right)\sin\left((\Omega^0_1 + \Omega^0_2)t_1\right) \end{aligned} \arrow[d, "(\pi/2)_y"] \\
\begin{aligned} \hat{\rho}^{\cos}_{\textcircled{6}} &= -\left(2\hat{I}_{1z}\hat{I}_{2y} + 2\hat{I}_{1y}\hat{I}_{2z}\right)\cos\left((\Omega^0_1 + \Omega^0_2)t_1\right) \\ &\quad - \left(2\hat{I}_{1z}\hat{I}_{2z} - 2\hat{I}_{1y}\hat{I}_{2y}\right)\sin\left((\Omega^0_1 + \Omega^0_2)t_1\right) \end{aligned}
\end{tikzcd}$$

Only the first term in $\hat{\rho}^{\cos}_{\textcircled{6}}$ contains observable single-quantum coherences. For the purpose of the final NMR signal, the density operator may therefore be simplified as follows:

$$\hat{\rho}^{\cos}_{\textcircled{6}} = -\left(2\hat{I}_{1z}\hat{I}_{2y} + 2\hat{I}_{1y}\hat{I}_{2z}\right)\cos\left((\Omega^0_1 + \Omega^0_2)t_1\right) + \ldots \tag{16.13}$$

The observable operators generate antiphase multiplets, as in the one-dimensional experiment. Note the cosine modulation of the signal with respect to the evolution interval t_1.

If the calculation is repeated for the 'sine' pulse sequence in the States procedure[1] ($\Psi = -\pi/4$ in Table 16.2), we get

$$\hat{\rho}^{\text{sin}}_{⑥} = -\left(2\hat{I}_{1z}\hat{I}_{2y} + 2\hat{I}_{1y}\hat{I}_{2z}\right)\sin\left((\Omega_1^0 + \Omega_2^0)t_1\right) + \ldots \tag{16.14}$$

In this case, the signal has a sine modulation with respect to the evolution interval t_1.

For a single AX system, States data processing (Section 5.9.4) of the cosine and sine two-dimensional data sets gives a two-dimensional spectrum of the following form:

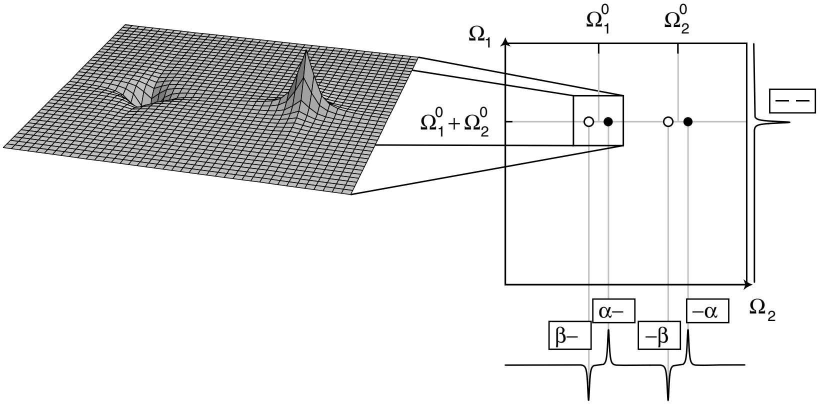

Figure 16.27
Two-dimensional INADEQUATE spectrum of a single AX spin ensemble.

The peaks are in positive and negative pure absorption, and appear at the double-quantum frequency $\Omega_1^0 + \Omega_2^0$ in the Ω_1-dimension.

Note that the double-quantum coherences are not *directly* observable, but are observed *indirectly* in the two-dimensional experiment by transforming them into observable (−1)-quantum coherences using a $\pi/2$ pulse. The modulations of the observable signals reveal the existence of the 'hidden' (±2)-quantum coherences during the t_1 interval.

If the two-dimensional INADEQUATE experiment is performed on a sample containing many AX systems (e.g. the natural ^{13}C–^{13}C isotopomers of an organic compound containing more than two carbon sites), then the two-dimensional spectrum has the following appearance:
The two-dimensional peaks are symmetrically disposed about the 'double-quantum diagonal' (the dashed line $\Omega_1 = 2\Omega_2$ in Figure 16.28). A practical example of a two-dimensional ^{13}C INADEQUATE spectrum of an organic compound is given in Figure 16.29. Such two-dimensional INADEQUATE spectra are extremely useful for assigning ^{13}C spectra and deducing the molecular structure.

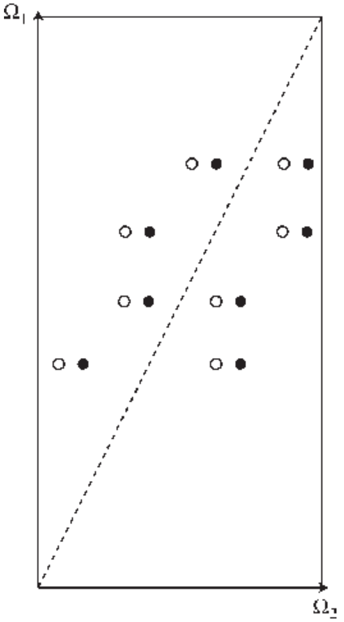

Figure 16.28
Form of the two-dimensional INADEQUATE spectrum for many $^{13}C_2$ pairs.

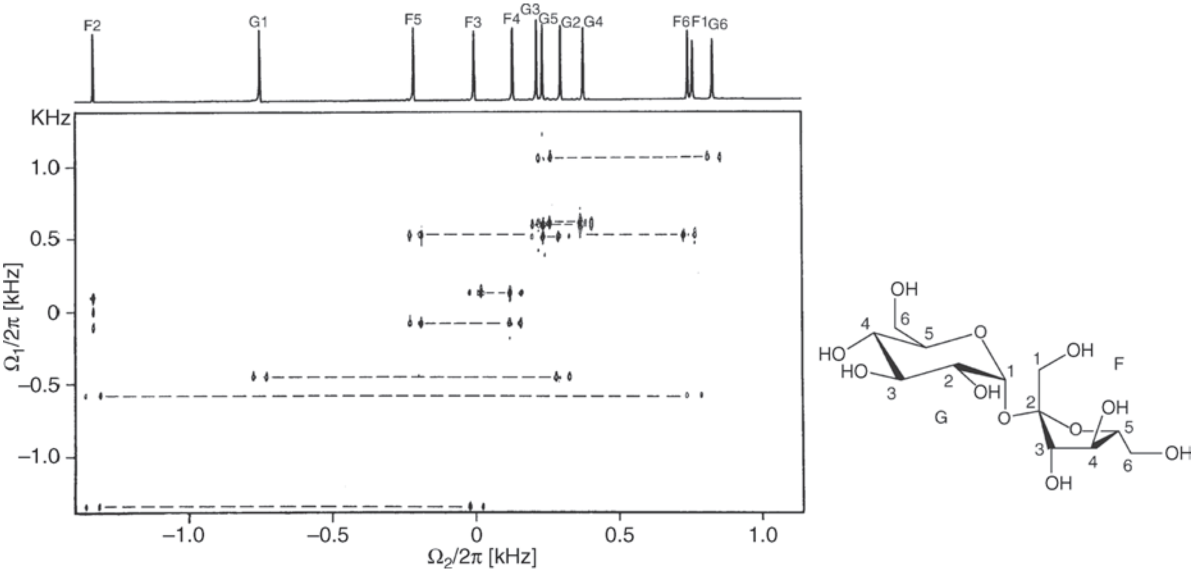

Figure 16.29 Two-dimensional INADEQUATE ^{13}C spectrum of a sucrose solution. The conventional ^{13}C spectrum at the top of the plot was assigned by noting which resonances are linked in the double-quantum ^{13}C spectrum. Adapted from A. Bax, R. Freeman, T. A. Frenkiel and M. H. Levitt, *J. Magn. Reson.* **43**, 478 (1981). Copyright, Academic Press.

The main drawback of the INADEQUATE experiment, as applied to ^{13}C in natural abundance, is its very low sensitivity, due to the extreme rarity of the natural $^{13}C_2$ isotopomers. In most cases, the experiment requires large quantities of material in order to obtain sufficient signal.

16.3 INEPT

16.3.1 The sensitivity of nuclear isotopes

In general, nuclear isotopes with high gyromagnetic ratio γ are easier to observe than those with small γ values. There are several reasons for this:

1. The nuclear magnetic moment is proportional to γ. A large value of γ implies strongly magnetic spins, a large macroscopic magnetic moment, and a strong NMR signal.

2. The magnitude of the nuclear Larmor frequency is proportional to γ. The induced current in the coil is proportional to the *rate of change* of the magnetic moment, so the strength of the NMR signal is proportional to the Larmor frequency (see Appendix A.5).

3. At thermal equilibrium, the Boltzmann polarization of the spins in the magnetic field is proportional to the Zeeman energy level splitting, which is also proportional to γ.

4. Strongly magnetic spins couple strongly to the molecular environment, and tend to have shorter values of T_1. This allows experiments to be repeated more quickly, in order to enhance the signal-to-noise ratio (see Section 5.2).[3]

One factor that works in the *opposite sense* is:

5. Empirically, the noise generated by electrons in the coil is approximately proportional to the square root of the frequency.

Overall, these factors lead to the following rough dependence of signal-to-noise ratio on γ and field B^0 (see Note 4):

$$\text{signal/noise} \propto |\gamma|^{5/2}(B^0)^{3/2} \tag{16.15}$$

For example, a certain number of ^1H nuclei provide a signal-to-noise ratio that is about 300 times larger than an equal number of ^{15}N nuclei, at the same magnetic field. This implies that one needs about 100 000 times longer to acquire a ^{15}N spectrum with the same signal-to-noise ratio as a ^1H spectrum, even if the number of spins is the same in the two cases.

In this section, I discuss a method for transferring polarization from the strongly magnetic proton spins to the weakly magnetic ^{15}N nuclei, using the J-couplings between the spins. This gets around factors 3 and 4 in the list above. After polarization transfer, the magnetization of the ^{15}N nuclei depends not on the ^{15}N γ-value but on that of the bonded protons. For ^{15}N, polarization transfer from neighbouring ^1H nuclei enhances the NMR signal by a factor of up to $|\gamma(^1H)/\gamma(^{15}N)| \cong 10$. In addition, experiments may be repeated at a rate set by the T_1 values of the protons, rather than those of the ^{15}N spins, which are usually longer.

This corresponds to more than a 100-fold decrease in the experimental time required to obtain the same signal-to-noise ratio.

One of the most popular pulse sequences for achieving this signal enhancement is called INEPT (Insensitive Nuclei Enhanced by Polarization Transfer).[5]

16.3.2 INEPT pulse sequence

The basic INEPT pulse sequence is as follows:

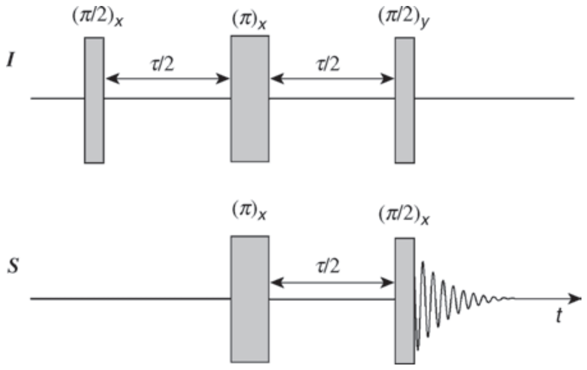

Figure 16.30
Pulse sequence for INEPT.

This is a heteronuclear pulse sequence involving synchronized r.f. irradiation on two spectrometer channels. We use the convention that I denotes the high-γ species and S denotes the low γ-species. In the case of ^{1}H and ^{15}N, the I-spins are protons and the S-spins are ^{15}N nuclei.

Several of the pulses are shown as simultaneous on the two channels. In practice, it does not matter if the pulses are really simultaneous or if one pulse slightly precedes the other (in any order).

The first part of the pulse sequence is a spin echo sandwich. The sandwich looks a little different here, because it is applied to a heteronuclear system. Nevertheless, as shown in Appendix A.10.4, it is possible to apply the conclusions of Section 15.10, as long as the π pulses are applied to *both* channels. The INEPT pulse sequence may, therefore, be analysed by using the following simplified form:

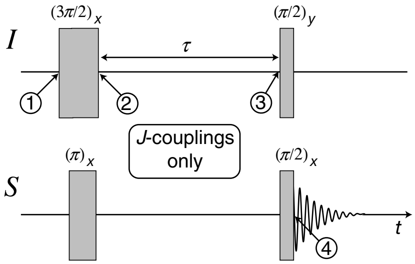

Figure 16.31
Equivalent pulse sequence for INEPT.

The interval τ is chosen to be equal to

$$\tau = |(2J_{IS})^{-1}|$$

where J_{IS} is the J-coupling (in hertz) between the two spins. In the case of directly bonded ^{1}H and ^{15}N spins in biomolecules, the J-coupling is usually around $J_{IS} \cong -93\,\text{Hz}$, so the pulse sequence intervals $\tau/2$ should be set to a value around 2.7 ms.

The spin density operator at time point ① corresponds to thermal equilibrium. For a heteronuclear two-spin system, this is given by

$$\hat{\rho}_{\textcircled{1}} = \frac{1}{4}\hat{1} + \frac{1}{4}\mathbb{B}_I\hat{I}_z + \frac{1}{4}\mathbb{B}_S\hat{S}_z \tag{16.16}$$

where $\mathbb{B}_I$ and $\mathbb{B}_S$ are the Boltzmann factors of the two spin species:

$$\mathbb{B}_I = \frac{\gamma_I B^0}{k_B T} \qquad \mathbb{B}_S = \frac{\gamma_S B^0}{k_B T} \tag{16.17}$$

and γ_I and γ_S are the gyromagnetic ratios. In the case of $I = {}^1\text{H}$ and $S = {}^{15}\text{N}$, the Boltzmann factors are related by $\mathbb{B}_I \cong -10\mathbb{B}_S$.

The density operator may be propagated through the pulse sequence, using the fact that pulses on the I-channel only rotate the polarizations of the I-spins, and similarly for the pulses on the S-channel. For example, the effect of the first two pulses is as follows:

$$\begin{tikzcd}
\hat{\rho}_{\textcircled{1}} = \frac{1}{4}\hat{1} + \frac{1}{4}\mathbb{B}_I\hat{I}_z + \frac{1}{4}\mathbb{B}_S\hat{S}_z \arrow[d, "(3\pi/2)^I_x"] \\
\hat{\rho}_{\textcircled{2}} = \frac{1}{4}\hat{1} + \frac{1}{4}\mathbb{B}_I\hat{I}_y + \frac{1}{4}\mathbb{B}_S\hat{S}_z \arrow[d, "\pi^S_x"] \\
\hat{\rho}_{\textcircled{2}} = \frac{1}{4}\hat{1} + \frac{1}{4}\mathbb{B}_I\hat{I}_y - \frac{1}{4}\mathbb{B}_S\hat{S}_z
\end{tikzcd}$$

The effect of the spin echo sandwich may be calculated using the results of Section 15.10. If J_{IS} is negative (the usual situation for ^{1}H and ^{15}N spins) and the delay τ is set to the value $|2J_{IS}|^{-1}$, then the angle πJ_{IS} is equal to $-\pi/2$. The calculation continues as follows:

$$\begin{tikzcd}
\hat{\rho}_{\textcircled{2}} = \frac{1}{4}\hat{1} + \frac{1}{4}\mathbb{B}_I\hat{I}_y - \frac{1}{4}\mathbb{B}_S\hat{S}_z \arrow[d, "\pi J_{IS}\tau\ (J\text{-couplings only})"] \\
\hat{\rho}_{\textcircled{3}} = \frac{1}{4}\hat{1} + \frac{1}{4}\mathbb{B}_I 2\hat{I}_x\hat{S}_z - \frac{1}{4}\mathbb{B}_S\hat{S}_z
\end{tikzcd}$$

The last two $\pi/2$ pulses rotate the spin species about different axes. The result is

$$\hat{\rho}_{\textcircled{3}} = \frac{1}{4}\widehat{1} + \frac{1}{4}\mathbb{B}_I 2\hat{I}_x\hat{S}_z - \frac{1}{4}\mathbb{B}_S\hat{S}_z$$

$$\Big\downarrow (\pi/2)^I_y$$

$$\frac{1}{4}\widehat{1} - \frac{1}{4}\mathbb{B}_I 2\hat{I}_z\hat{S}_z - \frac{1}{4}\mathbb{B}_S\hat{S}_z$$

$$\Big\downarrow (\pi/2)^S_x$$

$$\hat{\rho}_{\textcircled{4}} = \frac{1}{4}\widehat{1} + \underbrace{\frac{1}{4}\mathbb{B}_I 2\hat{I}_z\hat{S}_y}_{\text{transferred}} + \underbrace{\frac{1}{4}\mathbb{B}_S\hat{S}_y}_{\text{non-transferred}} \tag{16.18}$$

The 'transferred' term corresponds to antiphase *S*-spin magnetization, and is proportional to the Boltzmann factor of spin *I*. The 'non-transferred' term corresponds to negative in-phase *S*-spin magnetization, and is proportional to the Boltzmann factor of spin *S*. The resulting ^{15}N spectrum is a superposition of both of these components, and appears as follows for the directly bonded ^{1}H–^{15}N case (see Note 6):

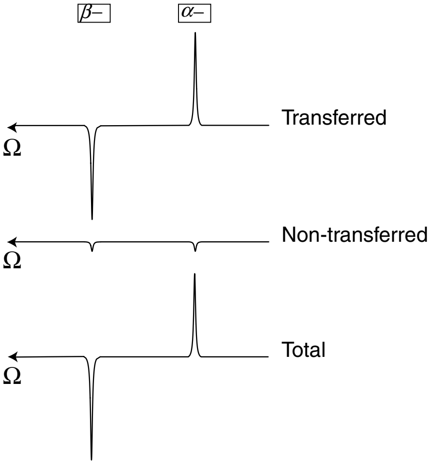

Figure 16.32
Components of the INEPT spectrum for the case of a ^{1}H–^{15}N system.

Note that the transferred signal is much larger than the non-transferred signal, and is in antiphase. Figure 16.33 shows some experimental INEPT spectra, which display the expected enhancement.

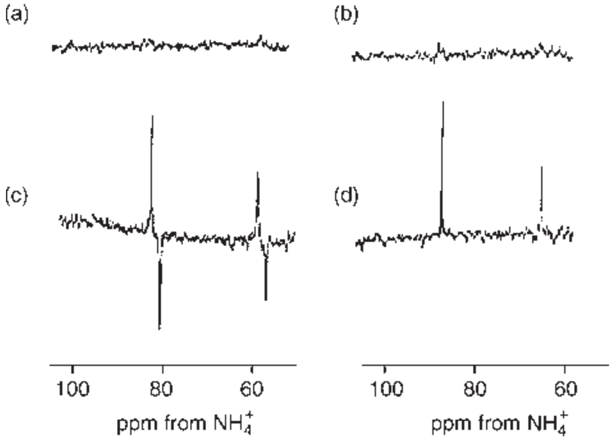

Figure 16.33 Experimental natural-abundance ^{15}N spectra of a small peptide in solution; the same instrument time was used for each spectrum. (a) The ^{15}N signals were excited using a single $\pi/2$ pulse and observed without a proton decoupling field. (b) The ^{15}N signals were excited using a single $\pi/2$ pulse and observed with a proton decoupling field. In both cases, the ^{15}N signals are almost invisible. (c) The INEPT pulse sequence was used to enhance the ^{15}N magnetization by polarization transfer from the J-coupled protons. (d) The refocused INEPT pulse sequence was used and the signals were observed with ^{1}H decoupling. Adapted from G. A. Morris, *J. Am. Chem. Soc.* **102**, 428 (1980), copyright, the American Chemical Society.

16.3.3 Refocused INEPT

In many cases, it is desirable to observe the S-spin signal in the presence of decoupling irradiation of the I-spins. As described in Section 3.9, this simplifies the spectrum and further enhances the signal, by collapsing split signal components into a single resonance.

It is not possible to decouple the INEPT-enhanced signal simply by applying an I-spin decoupling field under the acquisition interval, starting at time point ④. The decoupling field would simply collapse the J-splitting and cause the enhanced antiphase signals to cancel out. The only part of the spectrum that survives the decoupling is the in-phase non-transferred component:

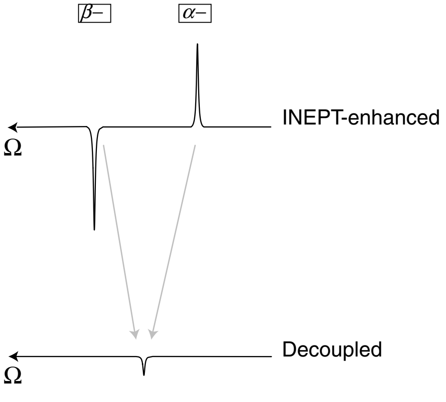

Figure 16.34
^{1}H decoupling of an INEPT spectrum destroys the transferred antiphase component.

In order to allow decoupling, it is necessary to *refocus* the enhanced antiphase components, so that they are brought back into phase again. This may be done by adding another spin echo sandwich to the pulse sequence. The *refocused INEPT* pulse sequence is as follows:

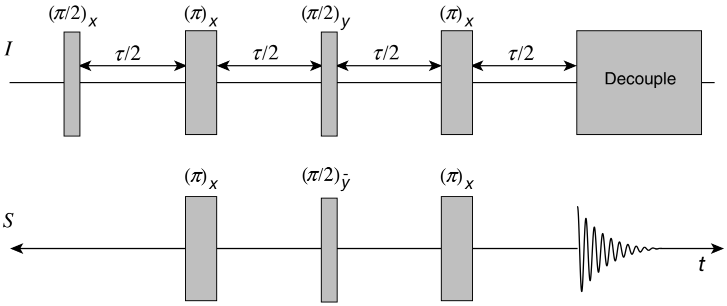

Figure 16.35
Refocused INEPT pulse sequence.

Apart from the additional spin echo sandwich, the phase of one of the *S*-spin pulses has been changed. This modification allows one to produce enhanced spectra in absorption phase.

The pulse sequence may be analysed by using the standard simplifications for the spin echo sandwiches:

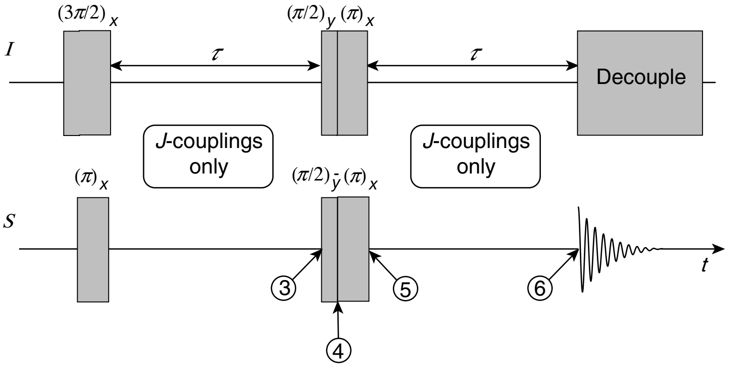

Figure 16.36
Equivalent refocused INEPT pulse sequence.

The propagation of the density operator through the last part of the pulse sequence is as follows:

$$\hat{\rho}_{\textcircled{3}} = \frac{1}{4}\hat{1} + \frac{1}{4}\mathbb{B}_I 2\hat{I}_x\hat{S}_z - \frac{1}{4}\mathbb{B}_S\hat{S}_z$$

$$\Big\downarrow \ (\pi/2)^I_y,\ (\pi/2)^S_{\bar{y}}$$

$$\hat{\rho}_{\textcircled{4}} = \frac{1}{4}\hat{1} + \frac{1}{4}\mathbb{B}_I 2\hat{I}_z\hat{S}_x + \frac{1}{4}\mathbb{B}_S\hat{S}_x$$

$$\Big\downarrow \ \pi^I_x,\ \pi^S_x$$

$$\hat{\rho}_{\textcircled{5}} = \frac{1}{4}\hat{1} - \frac{1}{4}\mathbb{B}_I 2\hat{I}_z\hat{S}_x + \frac{1}{4}\mathbb{B}_S\hat{S}_x$$

$$\Big\downarrow \ \pi J_{IS}\tau \ (J\text{-couplings only})$$

$$\hat{\rho}_{⑥} = \frac{1}{4}\hat{1} + \underbrace{\frac{1}{4}\mathbb{B}_I \hat{S}_y}_{\text{transferred}} - \underbrace{\frac{1}{4}\mathbb{B}_S 2\hat{I}_z \hat{S}_y}_{\text{non-transferred}}$$

The ‘transferred’ term corresponds to in-phase S-spin magnetization and is proportional to the Boltzmann factor of spin I. It gives rise to a positive in-phase signal (see Note 6). The ‘non-transferred’ term corresponds to antiphase S-spin magnetization. Upon decoupling, the non-transferred term cancels out, leaving only a greatly enhanced signal from the in-phase transferred term (see Figure 16.37). An experimental spectrum obtained with refocused-INEPT is shown in Figure 16.38.

The behaviour of INEPT in systems with more than two spins is discussed in Section 18.12.

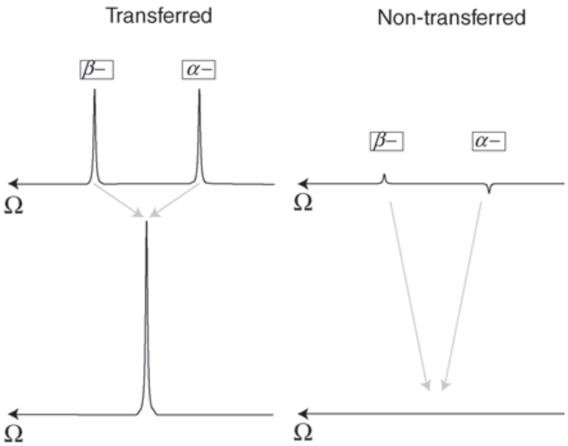

Figure 16.37 Subspectral components for refocused INEPT.

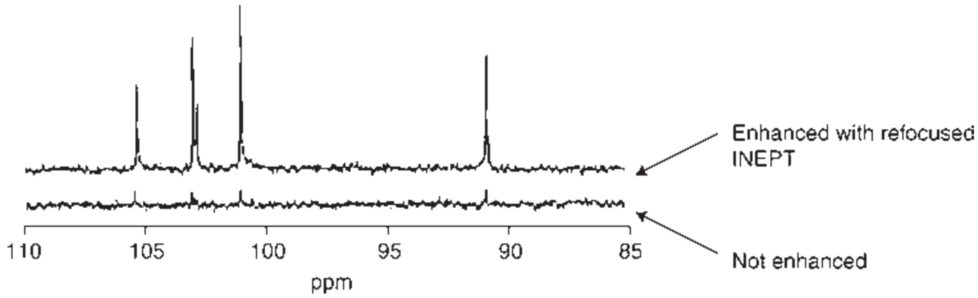

Figure 16.38 Experimental ^{15}N spectra of gramicidin in aqueous solution, using a single $\pi/2$ pulse to excite the ^{15}N spectrum (bottom) and using refocused INEPT (top). Adapted from *Encyclopedia of Nuclear Magnetic Resonance*, Vol. 4, D. M. Grant and R. K. Harris (eds), Wiley, Chichester, p. 2533 (Reproduced by permission of Wiley & Sons, Inc.)

16.4 Residual Dipolar Couplings

So far, all the experiments in this chapter have dealt with spin systems in an isotropic liquid phase, in which the molecular orientations are uniformly distributed. In this section, I discuss the use of *weakly oriented liquids* in biomolecular NMR. In these phases, the molecules tumble freely, but there is a very slight preference for some particular orientation, or set of orientations (see Section 1.6).

For simplicity, I will discuss these effects in the context of an ensemble of heteronuclear two-spin systems, such as ^{13}C–^{1}H or ^{15}N–^{1}H pairs in an isotopically labelled biomolecule. However, experiments of this type are also applicable to the NMR of inorganic substances.

16.4.1 Angular information

Consider a ^{13}C–^{1}H pair in a weakly oriented biomolecule. For simplicity, suppose that the molecule is shaped like an ellipsoid, and denote the angle between the ^{13}C–^{1}H vector and the molecular long axis by the symbol θ_{IS}:

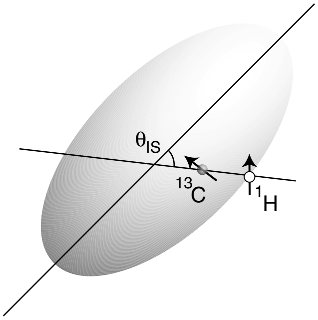

Figure 16.39
The angle θ_{IS} between the internuclear vector and the molecular long axis.

By dissolving the biomolecules in an anisotropic liquid phase, it becomes possible to estimate the angle θ_{IS}, which determines which way the ^{13}C–^{1}H vector ‘points’ with respect to the rest of the molecule. This important angular information complements nicely the internuclear distance information revealed by the NOESY or ROESY experiments (see Sections 20.6 and 20.7). By measuring the angles θ_{IS} for many different heteronuclear spin pairs, and combining this information with internuclear distances from NOESY or ROESY, it is possible to build up a very detailed picture of the molecular structure (see *Further Reading*).

16.4.2 Spin Hamiltonian

Denote the angle between the long axis of the molecule and the magnetic field as Θ. In a liquid, Θ fluctuates rapidly as the molecules tumble. The distribution of molecular orientations is not uniform, if the liquid is anisotropic. Denote the angle between the ^{13}C–^{1}H vector and the *field* by the symbol Θ_{IS} (see Figure 16.40). The angle Θ_{IS} depends in a complicated way on the molecular orientation and the angle θ_{IS}, and fluctuates strongly in a liquid.

From Equations 9.40 and 14.20the spin Hamiltonian for the pair is

$$\widehat{\mathcal{H}} = \omega_I^0 \hat{I}_z + \omega_S^0 \hat{S}_z + \omega_{IS} 2\hat{I}_z\hat{S}_z \tag{16.19}$$

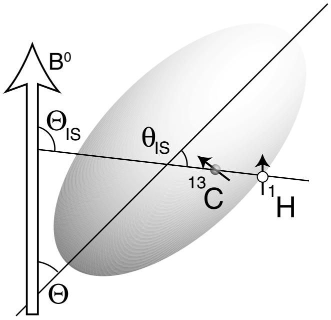

Figure 16.40
The angle Θ between the molecular long axis and the field, and the angle Θ_{IS} between the internuclear vector and the field.

where the ^{1}H nucleus is denoted I and the ^{13}C nucleus is denoted S, and the Larmor frequencies in the anisotropic phase are

$$\omega_I^0 = -\gamma_I B^0 \left(1 + \overline{\delta_{zz}^I(\Theta)}\right)$$

$$\omega_S^0 = -\gamma_S B^0 \left(1 + \overline{\delta_{zz}^S(\Theta)}\right)$$

The spin–spin coupling in the anisotropic phase is

$$\omega_{IS} = d_{IS} + \pi J_{IS} \tag{16.20}$$

where the secular part of the dipole–dipole coupling is

$$\boxed{d_{IS} = b_{IS}\,\frac{1}{2}\overline{(3\cos^2\Theta_{IS} - 1)} \qquad (16.21)}$$

The overbars denote averages over all molecular orientations Θ, weighted by their probability, and b_{IS} is the dipole–dipole coupling constant:

$$b_{IS} = -\frac{\mu_0}{4\pi}\frac{\gamma_I \gamma_S \hbar}{r_{IS}^3}$$

where r_{IS} is the distance between the spins. The symbols $\delta_{zz}^I(\Theta)$ and $\delta_{zz}^S(\Theta)$ denote the secular parts of the chemical shift tensors for the ^{1}H and ^{13}C sites respectively (see Section 9.1.9).

In general, the angles Θ, Θ_{IS} and θ_{IS} are linked with each other in rather a complicated way. As the molecule tumbles, Θ changes, and this changes in turn the value of Θ_{IS}, in a way that depends on the angle θ_{IS}.

The term d_{IS} in Equation 16.19 is called the *residual dipolar coupling*. In a fully isotropic liquid, d_{IS} vanishes. In a weakly anisotropic liquid, on the other hand, d_{IS} is small but finite. Measurement of d_{IS} allows one to estimate the angle θ_{IS}, which describes the orientation of the heteronuclear vector with respect to the molecular long axis.

16.4.3 Orienting media

There are many different physical media that generate weakly oriented liquid solvents. These include suspensions of virus particles, suspensions of cell membrane fragments, polyacrylamide gels that have been slightly squeezed in one direction, and *bicelles*, which are aggregates of *lipid* molecules. The area is under intense current development (see *Further Reading*). In this section, I discuss the specific case of bicelles, which were one of the first media to be used for this purpose.[7]

Lipids are amphiphilic organic molecules, with a polar headgroup attached to hydrophobic aliphatic chains. In water, the lipid molecules tend to aggregate spontaneously into *bilayers*, in which the hydrophobic tails are in contact and shielded from the water by the hydrophilic headgroups. For certain mixtures of lipids, the bilayers form disk-shaped aggregates called bicelles, which swim around freely in the aqueous solution.[7] Often, the bicelles are circular in profile, and, under suitable conditions, the bicelle disks orient spontaneously in a strong external magnetic field, because they have an anisotropic magnetic susceptibility (see Section 2.2). In many cases, the disks tend to orient so that the external magnetic field is approximately in the plane of each disk:

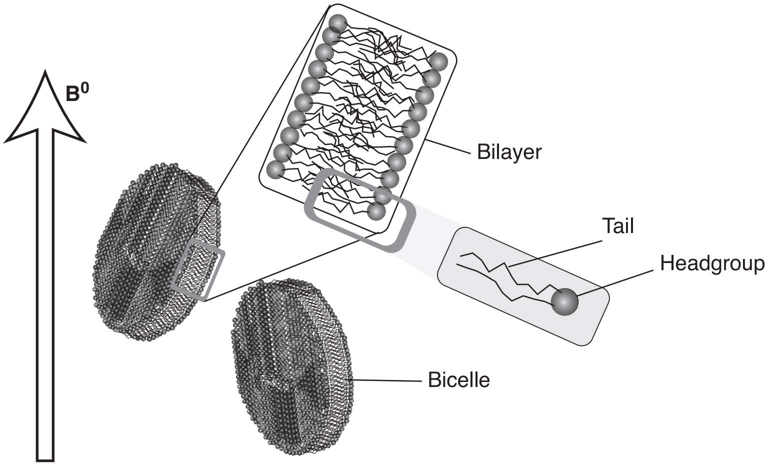

Figure 16.41
A bicelle is composed of a lipid bilayer.

In addition, steric interference between the bicelle disks causes them to stack up like coins. The bicelle disks, therefore, are oriented with respect to each other as well as with respect to the magnetic field. Locally, the director for the bicelle phase is *perpendicular* to the magnetic field:

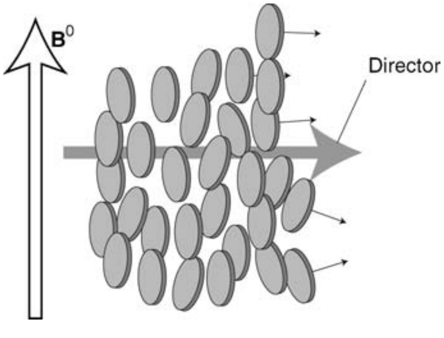

Figure 16.42
The bicelle director is perpendicular to the field. The normals to the bicelle planes (indicated by arrows) are aligned with the director.

If biomolecules are dissolved in the liquid between the bicelles, then the orientation of the bicelles is transferred weakly to the orientation of the biomolecules. One simple mechanism for this *orientation transfer* process is sketched here. In practice, the process may be complex and involves a superposition of several different mechanisms.

Biomolecules in solution acquire a partial orientation by collisions with the bicelle disks. The usual tendency is for the long axes of the molecules to become slightly oriented *parallel* to the bicelle planes – one can imagine the molecules being squeezed between the bicelles, and there is more room for the molecules if they are oriented this way:

In reality, the tendency for orientation is very small (only around 10^{-3}), but this is enough to lead to useful effects on the NMR spectrum.

Note carefully that the long axes of the molecules are not oriented *along* the magnetic field. The long axes of the molecules are uniformly distributed around the director, which is itself perpendicular to the magnetic field. Any orientation of the molecular long axis that is perpendicular to the director is equally likely.

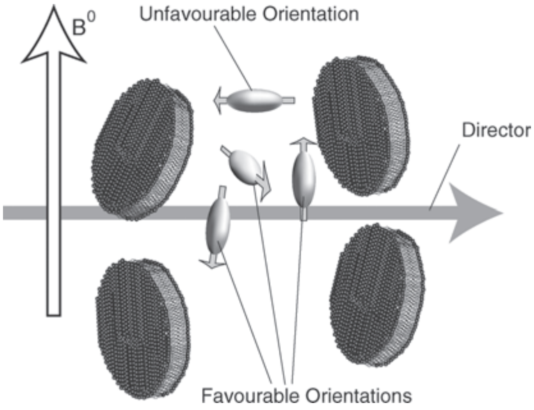

Figure 16.43
Molecules in solution tend to be oriented so that their long axes are in the plane of the bicelles, i.e. perpendicular to the director.

16.4.4 Doublet splittings

The spin Hamiltonian for the weakly oriented heteronuclear spin pair, Equation 16.19, is identical to that in an isotropic phase, except that (i) the chemical shift terms are different and (ii) that the J-coupling term πJ_{IS} is replaced by a term ω_{IS} including both the J-coupling and the residual dipolar coupling (see Equation 16.19).

The ^{13}C spectrum, therefore, consists of a doublet with splitting $2\omega_{IS} = 2\pi J_{IS} + 2d_{IS}$ in units of radians per second, or $J_{IS} + d_{IS}/\pi$ in units of hertz. The doublet splitting is either slightly larger than the J-coupling or slightly smaller, depending on the orientation of the ^{13}C–^{1}H vector with respect to the molecule.

If the ^{13}C–^{1}H vector is *parallel* to the long axis of the molecule, then the doublet splitting is slightly *smaller*. This may be seen as follows. Suppose, for simplicity, that the orientation of the molecules by the bicelles is extreme, so that all molecular long axes are forced to be parallel to the bicelle planes. View the system along the bicelle director, so that the bicelle planes appear to be in the plane of the paper:

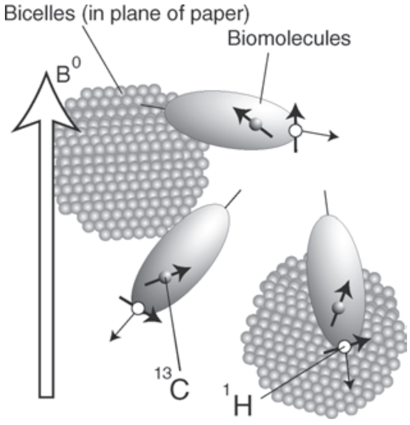

Figure 16.44
Case where the ^{13}C–^{1}H vectors are along the long axis of the molecules, and the molecular long axes are parallel to the bicelle planes.

In this case, the angle Θ_{IS} between the ^{13}C–^{1}H vector and the field takes all possible angles with equal probability, even though the molecules are partially ordered. The relevant orientational average is therefore

$$\frac{1}{2}\overline{(3\cos^2\Theta_{IS}-1)} = (2\pi)^{-1}\int_0^{2\pi} \mathrm{d}\Theta_{IS}\,\frac{1}{2}\left(3\cos^2\Theta_{IS}-1\right) = \frac{1}{4}$$

(Note the subtle difference between this *planar* average and the *spherical* average calculated in Equation 9.38.) It follows that, in this extreme situation of perfect orientation by the bicelles, with the ^{13}C–^{1}H vectors along the long axes of the molecules, the doublet splitting is given in units of radians per second by

$$2\omega_{IS} = 2\pi J_{IS} + \frac{1}{2}b_{IS} \tag{16.22}$$

In practice, the degree of orientation by the bicelles is very small, so the relevant factor is much less than 1/2. Nevertheless, the residual dipolar coupling retains the same sign as in the idealized calculation. Since the dipolar coupling constant b_{IS} is *negative* for ^{13}C–^{1}H interactions, whereas the one-bond J-coupling is *positive*, the effect of the orientation by the bicelles is to *reduce* the doublet splitting slightly, compared with its value in isotropic liquids:

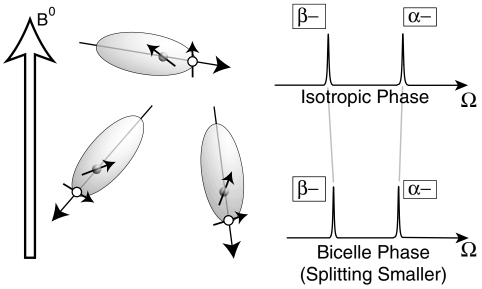

Figure 16.45
If the ^{13}C-^{1}H vectors are parallel to the molecular long axes, then the ^{13}C–^{1}H splitting is slightly smaller in the oriented bicelle phase.

The calculation for ^{13}C–^{1}H vectors which are perpendicular to the molecular long axis is more complicated, since there are two degrees of freedom in this case. The molecules may tumble around their own long axes, and the long axes may themselves rotate in the plane of the bicelles. A detailed calculation (not reproduced here) gives the following result:

$$\frac{1}{2}\overline{(3\cos^2\Theta_{IS}-1)} = -\frac{1}{8}$$

The doublet splitting, in the case that the ^{13}C–^{1}H vectors are perpendicular to the molecular long axes, is given in this extreme case by

$$2\omega_{IS} = 2\pi J_{IS} - \frac{1}{4}b_{IS} \tag{16.23}$$

Since b_{IS} is negative, the doublet splitting in the oriented phase is slightly larger than its value in isotropic phase:

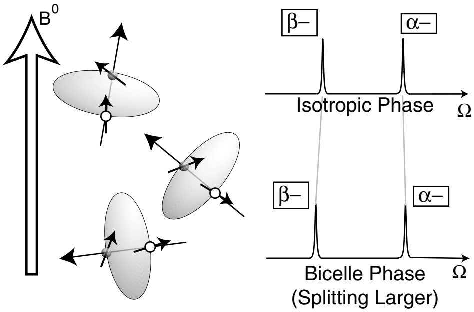

Figure 16.46
If the ^{13}C-^{1}H vectors are perpendicular to the molecular long axes, the ^{13}C–^{1}H splitting is slightly larger in the oriented bicelle phase.

By studying the small changes in the doublet splittings, when a biomolecule is dissolved in a bicelle solution, it is possible to deduce the orientations of the ^{13}C–^{1}H vectors with respect to the molecular long axes. An experimental example is shown in Figure 16.47.

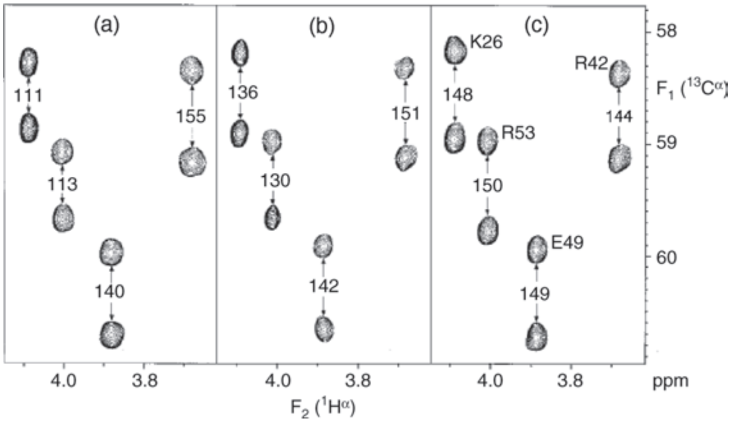

Figure 16.47 Experimental measurements of residual dipolar couplings in a weakly oriented liquid. The plots show extracts from the C^{α}–H^{α} regions of two-dimensional ^{1}H–^{13}C correlation spectra, for solutions of the small protein called bovine pancreatic trypsin inhibitor (BPTI). The ^{13}C resonances are split into doublets through the coupling to the directly bonded proton. Plots (a) and (b) are taken in two different weakly oriented phases, containing different concentrations of the bicelle-forming agents DMPC (dimyristoyl-phosphatidylcholine) and DHPC (dihexanoyl-phosphatidylcholine). Plot (c) is taken in isotropic solution. The splittings in (c) are equal to the ^{1}H–^{13}C *J*-couplings, and the splittings in (a) and (b) contain contributions from the dipole–dipole couplings. Most splittings increase when going from (a) to (c), but one decreases. This is because of the different relative angles of the ^{1}H–^{13}C internuclear vectors relative to the order axis. Adapted from M. Ottiger and A. Bax, *J. Biomol. NMR* **12**, 361–372 (1998), copyright, Springer Science and Business Media.

Similar studies are possible for other heteronuclear pairs of nuclei, such as ^{15}N and ^{1}H, and also homonuclear spin pairs, such as protons. The splittings for directly bonded ^{15}N–^{1}H pairs behave in the same way as for directly bonded ^{13}C–^{1}H pairs. The splitting becomes smaller in the oriented bicelle solution if the ^{15}N–^{1}H vector is parallel to the molecular long axis, and it becomes slightly larger in the oriented phase if the ^{15}N–^{1}H vector is perpendicular to the molecular long axis. This may be seen from Equations 16.22 and 16.23, using the fact that b_{IS} is positive for the ^{15}N–^{1}H interaction and that J_{IS} is negative for directly bonded ^{15}N–^{1}H pairs.

There are also many other media that may be used to induce a weak molecular orientation, giving rise to a similar dependence of the spectral splittings on the directions of the internuclear vectors. In some cases, the magnetic susceptibility of the biomolecules itself causes weak orientational effects, without assistance from agents such as bicelles (see *Further Reading*).

It might be expected that increasing the degree of orientation of the molecules would make these effects larger and, hence, improve the quality of the geometrical information. However, in most cases, increasing the molecular alignment sharply degrades the resolution, sensitivity, and simplicity of the spectra. This is because almost all realistic molecules contain many coupled spins. If the molecules are oriented too strongly, then all of the dipolar couplings in the system become finite. The spin system becomes strongly coupled, and the spectrum becomes intractable. The beauty of the bicelle work is that the molecules are oriented so slightly that the system remains weakly coupled. The largest dipolar couplings only act as weak perturbations of the J-couplings, and the huge number of additional dipolar couplings only give rise to a slight broadening.

Notes

1. The pulse sequence phases are consistent with the ‘sign-corrected’ version of the States procedure discussed in Section 5.9.4. The use of $\Phi = -\pi/4$ for the ‘sine’ signal derives from the fact that double-quantum coherences are twice as sensitive to r.f. phase shifts as single-quantum coherences (see Appendix A.11.3).

2. In strongly coupled systems, the signal induced by a coherence transfer pathway incurs an additional factor representing the coupling strength of the coherence to the receiver coil (see Appendix A.8). In the case of the weakly coupled systems discussed in the current chapter, the signal coupling strengths are the same for all observable (-1)-quantum coherences.

3. There are cases in which nuclei with large values of γ relax more *slowly* than nuclei with small values of γ. For example, consider an ensemble of isolated ^{13}C–^{1}H systems, and assume that the relaxation is caused predominantly by the intramolecular dipole–dipole interaction of the two spins, as discussed in Chapter 20. The mutual dipole–dipole interactions of the two spins are exactly equal: the ^{13}C spin experiences a strong local field generated by the strongly magnetic ^{1}H neighbour, but interacts weakly with that field since the γ-value of ^{13}C is relatively low. Similarly, the ^{1}H spin experiences a weak local field generated by the weakly magnetic ^{13}C neighbour, but interacts strongly with that field since the γ-value of ^{1}H is relatively high. Since the mutual dipole–dipole interactions are equal, one might expect that the spin–lattice relaxation time constants of the ^{1}H and ^{13}C spins should also be the same. However, there is another effect involved. As described in Chapter 20, the values of T_1 depend on the spectral density of the dipole–dipole fluctuations at the nuclear Larmor frequency. Since the ^{13}C spins have a lower Larmor frequency than ^{1}H spins in the same field, and since the spectral density function is peaked at zero frequency, the ^{13}C spins have *shorter* values of T_1 than ^{1}H spins in this particular case. This is actually observed experimentally in heavily deuterated biomolecules. More commonly, ^{1}H spins have more rapid longitudinal relaxation than ^{13}C spins, because each ^{1}H couples strongly to local fields generated by *other* protons.

4. The formula in Equation 16.15, which relates the signal-to-noise ratio to γ and B^0, is very rough and assumes comparable linewidths and probe performance.

5. The INEPT pulse sequence was invented by Gareth Morris (see G. A. Morris and R. Freeman, *J. Am. Chem. Soc.* **101**, 760 (1979)). Non-native English speakers may not be aware that INEPT is another ironical NMR acronym. The word means ‘clumsy’ or ‘incompetent’.

6. Estimating the spectral appearance in Figures 16.32 and 16.37 requires great care. Equation 16.18 indicates the presence of a non-transferred term proportional to $+\frac{1}{4}\mathbb{B}_S\hat{S}_y$ and a transferred term proportional to $+\frac{1}{4}\mathbb{B}_I 2\hat{I}_z\hat{S}_y$. Taking the non-transferred term first, one should remember that the thermal equilibrium density operator contains a term proportional to $+\frac{1}{4}\mathbb{B}_S\hat{S}_z$, which may be converted into a term proportional to $-\frac{1}{4}\mathbb{B}_S\hat{S}_y$ by a $(\pi/2)_x$ pulse. For the case $S = {}^{15}\mathrm{N}$, the Boltzmann factor $\mathbb{B}_S$ is negative (see Equation 16.17), and hence we should interpret a *positive* term proportional to $\hat{S}_y$ as representing a positive absorption signal. The non-transferred term in Equation 16.18, therefore, represents a negative in-phase signal, as shown in Figure 16.32. The transferred term, on the other hand, is proportional to $+\frac{1}{4}\mathbb{B}_I 2\hat{I}_z\hat{S}_y$, which should be interpreted as a *positive* antiphase signal, since $\mathbb{B}_I$ is positive for the case $I = {}^{1}\mathrm{H}$. Finally, the assignment of the spectral peaks to the coherences $\rho_{\boxed{\alpha-}}$ and $\rho_{\boxed{\beta-}}$ requires taking into account the negative values of γ_S and the one-bond ${}^{1}\mathrm{H}$–${}^{15}\mathrm{N}$ J-coupling (see Section 15.5). Experimental realizations of this experiment may not reproduce the expected peak pattern because of inconsistencies in the signs of r.f. phase shifts on many NMR spectrometers (see M. H. Levitt, *J. Magn. Reson.* **126**, 164 (1997) and M. H. Levitt and O. G. Johannessen, *J. Magn. Reson.* **142**, 190–194 (2000).

7. It is possible that lipids do not actually form disk-like bicelles under the conditions typically used for biochemical NMR. There is evidence that the lipid bilayers are organized in highly perforated sheet-like structures (the 'Swiss cheese model'), rather than disks. Nevertheless, the precise nature of the lipid phase does not have appreciable consequences for the NMR properties of the partially oriented molecules outside the bilayers.

Further Reading

- For a pedagogical explanation of the experiments in this chapter, use J. Keeler, *Understanding NMR Spectroscopy*, Wiley, Chichester, 2005.
- For a more detailed description of NMR experiments on coupled spin systems, including double-quantum-filtered COSY, see J. Cavanagh, W. J. Fairbrother, A. G. Palmer and N. J. Skelton, *Protein NMR Spectroscopy. Principles and Practice*, Academic Press, New York, 1996.
- For further discussion of INADEQUATE and INEPT, see R. Freeman, *Spin Choreography. Basic Steps in High Resolution NMR*, Spektrum, Oxford, 1997.
- For more on biomolecular NMR experiments in weakly oriented media, see E. de Alba and N. Tjandra, *Prog. NMR Spectrosc.* **40**, 175–197 (2002) and M. Blackledge, *Prog. NMR Spectrosc.* **46**, 23–61 (2005).

Exercises

16.1 This exercise investigates the important *heteronuclear multiple-quantum coherence* (HMQC) experiment, which generates two-dimensional spectra in which the chemical shifts of different spin species appear along the two axes. In this exercise, the HMQC experiment is examined for the simple case of two coupled spins-1/2 of different species I and S.

The pulse sequence for the 'cosine' experiment in the States procedure is shown below:

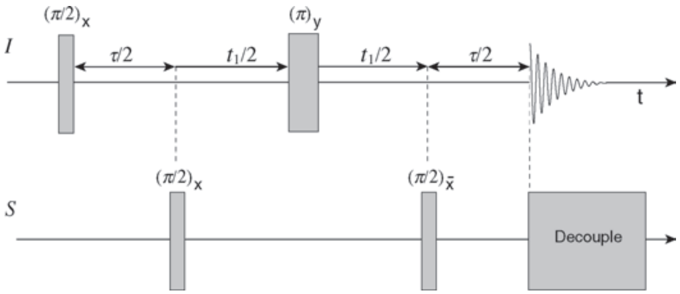

The delays τ are given by $\tau = (2J_{IS})^{-1}$, where J_{IS} is the J-coupling between the two spins. The interval t_1 is incremented in an arrayed fashion (the I-spin π pulse is always kept in the middle of the t_1 interval). The I-spin signal is observed at the end of each pulse sequence.

(i) If the spin density operator before the first pulse is given by $\hat{\rho}(0) = \hat{I}_z$, and relaxation is neglected, what is the spin density operator at the start of the detection period for an arbitrary value of t_1?
(ii) Sketch the form of the two-dimensional spectrum for a single IS spin system.
(iii) How should the pulse sequence be modified in order to provide the 'sine' component in the States procedure?

16.2 This exercise investigates the *double-quantum-filtered COSY* (2QF-COSY) experiment. The 'cosine' pulse sequence is as follows:

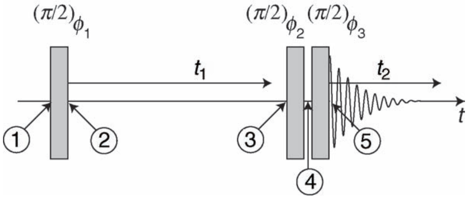

The phase table is as follows:

Cycle counter $\mathfrak{m}$	ϕ_1	ϕ_2	ϕ_3	ϕ_{rec}
0	$3\pi/2$	0	$\pi/2$	0
1	$3\pi/2$	0	π	$3\pi/2$
2	$3\pi/2$	0	$3\pi/2$	π
3	$3\pi/2$	0	0	$\pi/2$

Assume a homonuclear AX spin system. The short delay between the last two $\pi/2$ pulses may be ignored.

(i) Take the first step in the phase cycle procedure ($\mathfrak{m} = 0$). For simplicity, start with an initial spin density operator $\hat{\rho}_{①} \sim \hat{I}_{1z}$. What is the spin density operator at time point ④?
(ii) Convert the x- and z-operators at time point ④ into shift operators. Which coherence orders are excited at this point?
(iii) The phase cycle has the effect of suppressing all signal components that do not pass through (± 2)-quantum coherences at time point ④. Select the operators that have order ± 2 and apply the final $\pi/2$ pulse. What is the spin density operator at time point ⑤? To bring out the meaning

of the final expression, replace all products of trigonometric functions by single trigonometric functions.

(iv) Repeat the calculation for the ‘sine’ component of the States procedure, in which the first pulse has phase π instead of phase $3\pi/2$. Use the same initial density operator.

(v) Repeat the calculations using the full form of the initial spin density operator, $\hat{\rho}_{①} \sim \hat{I}_{1z} + \hat{I}_{2z}$. Sketch the form of the two-dimensional spectrum and remark on the shapes of the diagonal peaks and cross-peaks. What are the favourable properties of the double-quantum-filtered COSY spectrum? Are there any disadvantages of double-quantum-filtered COSY compared with ordinary COSY?

17

Many-Spin Systems

Most molecules contain many more than two coupled nuclear spins. In this chapter, I discuss how to write down the spin Hamiltonian for many-spin systems.

⚠Much of the discussion in this chapter is specific to the NMR of isotropic liquids, and is not generally applicable to solids and liquid crystals.

17.1 Molecular Spin System

In isotropic liquids, the only terms that survive the motional averaging are (i) the isotropic parts of the intramolecular interactions and (ii) the long-range dipole–dipole interactions. If the long-range dipole–dipole interactions are ignored (see Section 8.6.4), the spin Hamiltonian in an isotropic liquid is *purely intramolecular*.

All molecules of the same isotopomeric species, therefore, have the same motionally averaged spin Hamiltonian, given by

$$\widehat{\mathcal{H}} = \widehat{\mathcal{H}}^0 + \widehat{\mathcal{H}}_{\mathrm{RF}}$$

where $\widehat{\mathcal{H}}_{\mathrm{RF}}$ represents the interaction with the r.f. field, and $\widehat{\mathcal{H}}^0$ contains the interaction with the static field, plus the secular parts of the intramolecular chemical shift and J-coupling terms:

$$\boxed{\widehat{\mathcal{H}}^0 = \underbrace{\sum_j \omega_j^0 \hat{I}_{jz} + \sum_{j<k} 2\pi J_{jk} \hat{\mathbf{I}}_j \cdot \hat{\mathbf{I}}_k}_{\text{all spins in one molecule}} \qquad (17.1)}$$

The isotropic chemically shifted Larmor frequency ω_j^0 is defined in Equation 9.16.

The term *molecular spin system* refers to the coupled nuclear spins in a single molecule. Often, the term *spin system* is used to imply the molecular spin system.

If all the spins in the molecular spin system are of the same isotopic type, then the spin system is said to be *homonuclear*. If more than one isotope is present, then the spin system is said to be *heteronuclear*.

Suppose, for example, that each molecule contains four spins, of the same isotopic type. The molecular spin system has the following spin Hamiltonian:

Spin Dynamics: Basics of Nuclear Magnetic Resonance, Second Edition Malcolm H. Levitt

$$\begin{aligned}\widehat{\mathcal{H}}^0 &= \omega_1^0 \hat{I}_{1z} + \omega_2^0 \hat{I}_{2z} + \omega_3^0 \hat{I}_{3z} + \omega_4^0 \hat{I}_{4z} \\ &\quad + 2\pi J_{12} \hat{\mathbf{I}}_1 \cdot \hat{\mathbf{I}}_2 + 2\pi J_{13} \hat{\mathbf{I}}_1 \cdot \hat{\mathbf{I}}_3 + 2\pi J_{14} \hat{\mathbf{I}}_1 \cdot \hat{\mathbf{I}}_4 \\ &\quad + 2\pi J_{23} \hat{\mathbf{I}}_2 \cdot \hat{\mathbf{I}}_3 + 2\pi J_{24} \hat{\mathbf{I}}_2 \cdot \hat{\mathbf{I}}_4 + 2\pi J_{34} \hat{\mathbf{I}}_3 \cdot \hat{\mathbf{I}}_4 \end{aligned} \tag{17.2}$$

where the chemically shifted Larmor frequencies are given by

$$\omega_j^0 = -\gamma_j B^0 (1 + \delta_j)$$

These four chemically shifted spins, and the six couplings between them, may be depicted by the following icon:

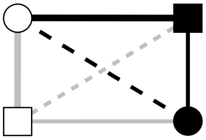

Figure 17.1
A four-spin system.

I have used different symbols to depict the four different chemical shifts and different line types to depict the six different J-couplings.

17.2 Spin Ensemble

The molecules of one isotopomer all have the same motionally averaged spin Hamiltonian. The collection of non-interacting, identical, spin systems is called the *spin system ensemble*:

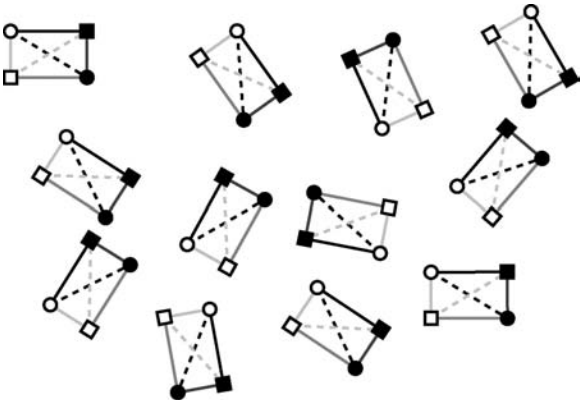

Figure 17.2
An ensemble of
four-spin systems.

In a given sample, there are usually several compounds, each with several isotopomers. All the molecules of one isotopomer constitute a single spin ensemble. If there are several isotopomers present, then there are several independent spin ensembles.

17.3 Motionally Suppressed J-Couplings

In some cases, J-couplings are not observed to certain spins, because of a rapid motional process that averages the J-coupling to zero. There are two common situations:

1. Chemical bonds are rapidly forming and reforming, so that a particular nucleus jumps between different molecules;

2. The relevant nuclear spin undergoes very rapid longitudinal relaxation.

In the first case, the rapid dynamics of the nuclear spin is *spatial* – the spin moves physically from molecule to molecule. In the second case, the nucleus remains fixed in a given molecule, but the *polarization* of the spin fluctuates rapidly.

The first case is called *fast chemical exchange*. It is discussed in Section 19.5. A typical case is that of the OH proton in ethanol (CH_3CH_2OH). Unless special precautions are taken, traces of acid or base catalyse the rapid chemical exchange of the hydroxyl proton between different ethanol molecules. As a result, the NMR signals from this proton are usually broad and J-couplings between this proton and the others are not observed.

The second case is typified by *quadrupolar* nuclei. As discussed in Section 8.2.1, most nuclei with spin $> 1/2$ couple strongly to electric field gradients in the molecule. As the molecules rotate, the electric field gradients rotate too, and this causes the magnetic moments of these nuclei to fluctuate relatively strongly. This is manifested in very short spin–lattice relaxation time constants T_1 for most quadrupolar nuclei in a liquid. The rapid spin–lattice relaxation of quadrupolar spins averages out their J-couplings to other spins in the same molecule.

As shown in Section 19.5.3, the J-coupling of a spin I_j to a rapidly relaxing spin I_k may be ignored if the second spin has a longitudinal relaxation time constant T_1^k fulfilling the condition

$$|2\pi J_{jk} T_1^k| << 1$$

The longitudinal relaxation time constants for many quadrupolar spins in solution are as short as microseconds, in which case this condition is easily fulfilled. For example, the ^1H spins in ethyl chloride CH_3CH_2Cl experience no noticeable J-couplings to the abundant Cl isotopes ^{35}Cl and ^{37}Cl, since both of these have large quadrupole moments and relax rapidly.

In many cases, the molecular spin Hamiltonian in an isotropic liquid may therefore be written as

$$\widehat{\mathcal{H}}^0 \cong \sum_j \omega_j^0 \hat{I}_{jz} + \underbrace{\sum_{j<k} 2\pi J_{jk} \hat{\mathbf{I}}_j \cdot \hat{\mathbf{I}}_k}_{\text{except spins with motionally suppressed } J\text{-couplings}} \tag{17.3}$$

There are some cases in which couplings to quadrupolar spins must be considered in solution NMR. In particular, the isotope ^2H has a relatively small quadrupole moment, and ^1H–^2H or ^2H–^{13}C couplings are sometimes observed. Even isotopes such as ^{14}N, which has a large quadrupole moment, relax slowly if they are in molecular sites with a very small electric field gradient, because of high local symmetry. This is the case, for example, in the tetrahedral ion $^{14}NH_4^+$.

17.4 Chemical Equivalence

Spins are said to be chemically equivalent if the following conditions are both satisfied:

1. The spins are of the same isotopic species.

2. There exists a molecular symmetry operation that exchanges the two spins.

Consider, for example, the molecule 1,1-difluoroethene, which contains two ^1H and two ^{19}F spins:

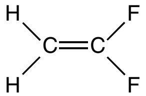

Figure 17.3
1,1-Difluoroethene.

There is clearly a reflection symmetry plane down the centre of the molecule (top to bottom in the diagram above). Reflection in the plane exchanges the two protons, indicating that they are chemically equivalent. The same reflection exchanges the two fluorine atoms, indicating that they are also chemically equivalent. The four-spin system of 1,1-difluoroethene may, therefore, be represented by the following icon:

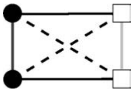

Figure 17.4
The four-spin system of 1,1-difluoroethene.

Chemically equivalent spins have been given the same symbol. Those J-couplings that are interchanged by reflection have been given the same style.

Other familiar examples of chemical equivalence are the six protons in benzene and the two protons in water:

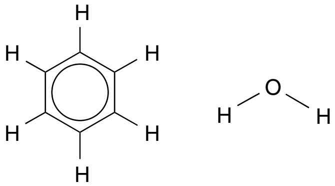

Figure 17.5
Benzene and water.

The corresponding spin systems may be depicted by the following icons:

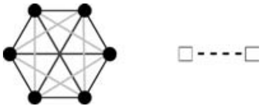

Figure 17.6
Proton spin systems in benzene and water.

Spins with identical chemical shifts are depicted by identical symbols; identical J-couplings are represented by lines of the same style.

Chemically equivalent spins have the same chemical shift. However, the inverse does not always hold. Two spins with the same chemical shift are not necessarily chemically equivalent. The coincidence of the shifts may be purely accidental, having nothing to do with molecular symmetry.

In molecules that have rapid internal mobility, the spin Hamiltonian is averaged over the accessible molecular conformations, weighted by their populations. This often creates additional opportunites for chemical equivalence. Consider, for example, the methyl protons in ethyl chloride (CH_3CH_2Cl). Looking down the C–C bond, we would see the following picture in one of the low-energy staggered conformations:

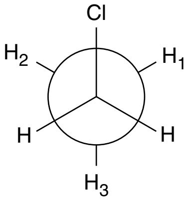

Figure 17.7
Newman projection of CH_3CH_2Cl.

The two CH_2 protons are clearly chemically equivalent, because of the plane of symmetry defined by Cl–C–C–H_3. The two CH_3 protons marked H_1 and H_2 are also chemically equivalent for the same reason. However, the proton H_3 cannot be exchanged with H_1 or H_2 by a symmetry operation, so it is not chemically equivalent to the other two, in this conformation.

However, the methyl group rapidly rotates around the C–C bond, allowing the molecule to explore the other two staggered conformations:

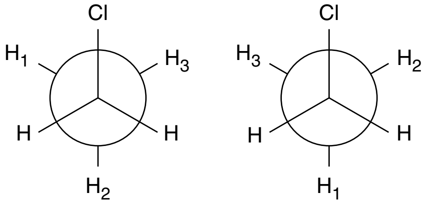

Figure 17.8
Two more staggered conformations of CH_3CH_2Cl.

The three staggered conformations have the same energy, so the molecule spends equal time in each of them. When averaged over all three conformations, each of the three CH_3 protons experiences the same environment, so all three CH_3 protons in ethyl chloride are chemically equivalent. The coupling diagram for the protons in ethyl chloride is as follows:

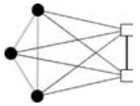

Figure 17.9
Coupling diagram for CH_3CH_2Cl.

There are some subtle traps in this type of system. Consider, for example, the two CH_2 protons in a molecule of the following type:

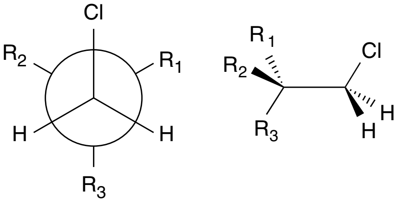

Figure 17.10
A molecule containing diastereotopic CH_2 protons.

where the groups R_1, R_2 and R_3 are all different. Assume, again, that the molecule has full rotational mobility about the C–C bond.

It is tempting to assume that high rotational mobility tends to average out the environments of the two CH_2 protons, leading to chemical equivalence. This is incorrect, as may be seen from the following representations of the three staggered conformations, looking down the C–C bond:

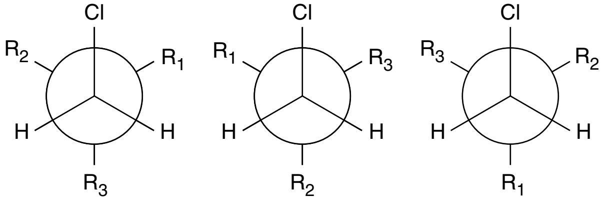

Figure 17.11
Three staggered conformations, all inequivalent.

None of these conformations has a plane of symmetry, so no pair of protons is chemically equivalent in any of the three conformations. Furthermore, no two conformations have the same energy. The three conformations have different populations in thermal equilibrium. The CH_2 protons in this type of system, therefore, are *not* chemically equivalent in general, whatever the degree of internal mobility. The two CH_2 protons have different chemical shifts.

The chemical equivalence of CH_2 protons is even broken by remote influences. Suppose that the groups R_2 and R_3 are identical, but the group R_1 is *chiral* (meaning that it cannot be superimposed on its own mirror image). In this case, the two CH_2 protons are still inequivalent. This situation is common in biological NMR, since most biologically active molecules are chiral.

Although chirality often leads to chemical inequivalence, inequivalent CH_2 protons may also occur in molecules that are not chiral. The case of citric acid is instructive:

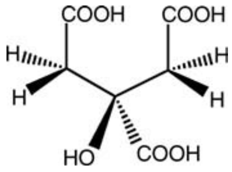

Figure 17.12
Molecular structure of citric acid.

The molecule as a whole has a plane of symmetry (perpendicular to the paper, through the central carbon atom) and is therefore not chiral. Nevertheless, there is no molecular symmetry operation that exchanges the two protons in the same CH_2 group with each other (the mirror reflection exchanges protons in different CH_2 groups). The two protons within each CH_2 group are chemically inequivalent. This remains true even if there is full rotational mobility around the carbon–carbon bonds.

Chemically inequivalent protons in CH_2 groups are called *diastereotopic* protons.

17.5 Magnetic Equivalence

Magnetic equivalence is a strong form of chemical equivalence. A set of spins is magnetically equivalent IF

- Condition 1: the spins have the same chemical shifts

  AND

- (Condition 2a: the spins have identical couplings to all *other* spins in the molecule

  OR

- Condition 2b: there are no other spins in the molecule.)

Consider, for example, the protons in the commonest isotopomer of benzene. The protons are chemically equivalent (Condition 1). Since there are no other spins in the molecule, they are also magnetically equivalent (Condition 2b). The same is true for the usual isotopomer of water. The two protons are chemically equivalent (Condition 1), and there are no other spins in the molecule (Condition 2b). The two protons of water are magnetically equivalent.

As a second example, reconsider the case of ethyl chloride, CH_3CH_2Cl. As discussed before, the two CH_2 protons are chemically equivalent (Condition 1). In addition, each of the two CH_2 protons has the same coupling with each of the three CH_3 protons (Condition 2a). Similarly, the three CH_3 protons are chemically equivalent (Condition 1) and have identical couplings with each of the two CH_2 protons (Condition 2a). The spin system in CH_3CH_2Cl contains one group of three magnetically equivalent protons and one group of two magnetically equivalent protons.

Magnetic equivalence is important because it allows the spin Hamiltonian to be simplified. One example of this was already encountered in Section 14.4, for the case of a spin-1/2 pair. It was shown that the J-coupling between the two spins has no effect on the NMR properties, providing that (i) there are only two spins and (ii) they have the same chemical shift. In this case, the J-coupling term may be omitted from the spin Hamiltonian, without changing any physical predictions.

In the special case of the two-spin system discussed in Section 14.4, chemical equivalence necessarily implies to magnetic equivalence, through Condition 2b above. In the general case of *more than two coupled spins*, chemical equivalence does *not* imply magnetic equivalence.

In Appendix A.9, it is shown that the NMR signal is independent of spin–spin coupling terms *within* magnetically equivalent groups. It is therefore convenient to omit these couplings from the spin Hamiltonian, which then reads

$$\boxed{\widehat{\mathcal{H}}^0 = \sum_j \omega_j^0 \hat{I}_{jz} + \underbrace{\sum_{j<k}{}' \, 2\pi J_{jk} \hat{\mathbf{I}}_j \cdot \hat{\mathbf{I}}_k}_{\text{except spins with motionally suppressed } J\text{-couplings}} \qquad (17.4)}$$

The ‘prime’ on the summation indicates the exclusion of couplings between magnetically equivalent spins.

For example, consider the spin system specified in Equation 17.2. If spin I_1 is magnetically equivalent to I_2, and I_3 is magnetically equivalent to I_4, then we have

$$\omega_1^0 = \omega_2^0 \qquad \omega_3^0 = \omega_4^0$$
$$J_{13} = J_{14} = J_{23} = J_{24}$$

as depicted in the following coupling diagram:

Figure 17.13
A four-spin system with two pairs of magnetically equivalent spins.

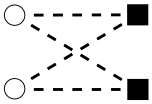

Since there are two groups of magnetically equivalent pairs of spins, the following simplified spin Hamiltonian may be used:

$$\widehat{\mathcal{H}}^0 = \omega_1^0(\hat{I}_{1z} + \hat{I}_{2z}) + \omega_3^0(\hat{I}_{3z} + \hat{I}_{4z}) + 2\pi J_{13}(\hat{\mathbf{I}}_1 + \hat{\mathbf{I}}_2) \cdot (\hat{\mathbf{I}}_3 + \hat{\mathbf{I}}_4) \qquad (17.5)$$

which may be represented by the following diagram:

Figure 17.14
The couplings between magnetically equivalent spins may be omitted.

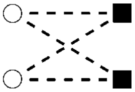

Another example is the spin system of CH_3CH_2Cl, which may be represented as follows:

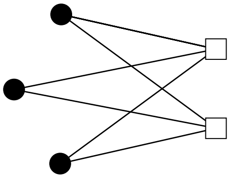

Figure 17.15
Coupling diagram for CH_3CH_2Cl, omitting couplings between magnetically equivalent spins.

Similarly, the spin systems of benzene and water may be depicted thus:

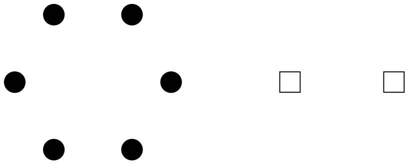

Figure 17.16
Proton spin systems in benzene and water, omitting couplings between magnetically equivalent spins.

indicating that, effectively, there are no active *J*-couplings between any of the spins in these last two molecules.

Reconsider now the 1,1-difluoroethene molecule. As discussed before, the two protons are chemically equivalent, as are the two fluorine spins. Are the two protons magnetically equivalent?

Rather surprisingly, the answer is negative. Each of the two protons has a different coupling with each of the two fluorine nuclei, since one coupling is between spins in trans geometry and the other coupling involves cis geometry:

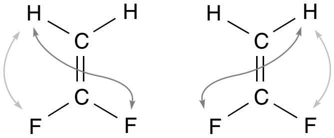

Figure 17.17
Spin-spin couplings in 1,1-Difluoroethene.

It follows that the two protons in this molecule are chemically equivalent, but *not* magnetically equivalent. The same holds for the two fluorine nuclei. The coupling diagram for 1,1-difluoroethene cannot be simplified, and is still as shown below:

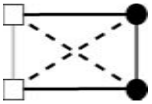

Figure 17.18
The four-spin system of 1,1-Difluoroethene.

It is instructive to contrast this case with the similar molecule 1,1-Difluoropropan-1,2-diene, which has the following molecular geometry:

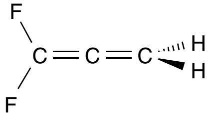

Figure 17.19
1,1-Difluoropropan-1,2-diene.

The two protons nuclei are clearly chemically equivalent, as are the two ^{19}F nuclei. In addition, the geometry of the molecule is such that all four ^{19}F–^{1}H couplings are equal:

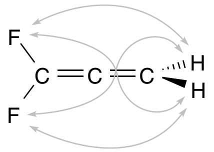

Figure 17.20
Spin-spin couplings in 1,1-difluoropropan-1,2-diene.

The two protons are therefore magnetically equivalent, as are the two ^{19}F nuclei. The spin system for this molecule, therefore, may be simplified:

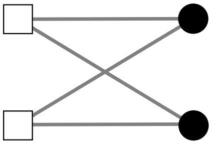

Figure 17.21
The four-spin system of 1,1-difluoropropan-1,2-diene.

The apparent disappearance of J-couplings between magnetically equivalent spins is quite surprising. A physical explanation runs as follows. For magnetically equivalent spins, the local magnetic fields, whatever their source, are exactly the same on the two spins. It follows that the motion of the two spin polarizations is identical. Whatever happens, the polarizations of the two spins are locked in the same relative orientation. There is, therefore, no need to incorporate a term in the spin Hamiltonian that takes into account the dependence of the energy on this relative spin orientation.

17.6 Weak Coupling

The weak-coupling approximation has already been encountered for the case of spin-1/2 pairs in Section 14.5.

The situation is a bit more complicated when more than two spins are involved. A system of many coupled spins is said to be *weakly coupled* if the following condition is satisfied for *all pairs of magnetically inequivalent spins*:

$$|\omega_j^0 - \omega_k^0| >> |\pi J_{jk}| \tag{17.6}$$

In other words, the frequency differences created by chemical shifts must be much larger than the J-couplings between magnetically inequivalent spins. If the weak-coupling approximation is valid, then the following simplified spin Hamiltonian may be used:[1]

$$\widehat{\mathcal{H}}^0_{\text{weak}} = \sum_j \omega_j^0 \hat{I}_{jz} + \underbrace{\sum_{j<k}{}' \, 2\pi J_{jk} \hat{I}_{jz} \hat{I}_{kz}}_{\text{except spins with motionally suppressed } J\text{-couplings}} \tag{17.7}$$

For example, suppose that the spin system in Equation 17.5 obeys the condition:

$$|\omega_1^0 - \omega_3^0| >> |\pi J_{13}|$$

The approximate spin Hamiltonian

$$\widehat{\mathcal{H}}^0_{\text{weak}} = \omega_1^0(\hat{I}_{1z} + \hat{I}_{2z}) + \omega_3^0(\hat{I}_{3z} + \hat{I}_{4z}) + 2\pi J_{13}(\hat{I}_{1z} + \hat{I}_{2z})(\hat{I}_{3z} + \hat{I}_{4z}) \tag{17.8}$$

may be used in this case.

Weak coupling is an example of the *secular approximation* discussed in Appendix A.6. It may be viewed as a form of motional averaging generated by the *differential precession* of the different spins. Since the coupled spins precess at different frequencies, the interactions between the transverse components of the spin polarizations average out to zero. The only coupling terms that are not averaged out involve the longitudinal components of spin polarization, which are unchanged by the spin precession.

Since chemical shift frequency differences are proportional to the applied field, weak coupling is especially common on instruments with large magnetic fields. The development of NMR instrumentation towards ever higher fields has extended the range of the weak coupling approximation. Much NMR methodology in isotropic liquids is based on the reasonable validity of weak coupling.

Spin systems that are not weakly coupled are said to be *strongly coupled*. In these cases, the full form of the spin Hamiltonian shown by Equation 17.4 must be used. Appendix A.8 explores the spectral consequences of strong coupling.

17.7 Heteronuclear Spin Systems

Heteronuclear spin systems contain at least two different isotopic species. The difference in Larmor frequencies between two different isotopes is almost always much larger than the spin–spin couplings. The couplings between spins of different species, therefore, are almost always 'weak', in the sense of the previous section.

Consider, for example, a molecule with four spins, two of species I, called I_1 and I_2, and two of species S, called S_3 and S_4. Suppose that the chemical shifts of all four spins are different. The following spin Hamiltonian may be used:

$$\begin{aligned}\widehat{\mathcal{H}}^0 = {} & \omega_1^0\hat{I}_{1z} + \omega_2^0\hat{I}_{2z} + \omega_3^0\hat{S}_{3z} + \omega_4^0\hat{S}_{4z} + 2\pi J_{12}\hat{\mathbf{I}}_1 \cdot \hat{\mathbf{I}}_2 + 2\pi J_{13}\hat{I}_{1z}\hat{S}_{3z} + 2\pi J_{14}\hat{I}_{1z}\hat{S}_{4z} \\ & + 2\pi J_{23}\hat{I}_{2z}\hat{S}_{3z} + 2\pi J_{24}\hat{I}_{2z}\hat{S}_{4z} + 2\pi J_{34}\hat{\mathbf{S}}_3 \cdot \hat{\mathbf{S}}_4\end{aligned} \tag{17.9}$$

where

$$\begin{aligned}\omega_1^0 &= -\gamma_I B^0(1+\delta_1) \qquad & \omega_3^0 &= -\gamma_S B^0(1+\delta_3) \\ \omega_2^0 &= -\gamma_I B^0(1+\delta_2) \qquad & \omega_4^0 &= -\gamma_S B^0(1+\delta_4)\end{aligned}$$

and γ_I and γ_S are the gyromagnetic ratios of the two isotopes.

Now suppose that the two I spins are chemically, but not magnetically, equivalent. Similarly, suppose that the two S spins are chemically, but not magnetically, equivalent (see Figures 17.17 and 17.18). The Larmor frequencies and couplings have the following symmetry:

$$\omega_1^0 = \omega_2^0 \qquad J_{13} = J_{24}$$
$$\omega_3^0 = \omega_4^0 \qquad J_{14} = J_{23}$$

In this case, the spin Hamiltonian may be written as follows:

$$\begin{aligned}\widehat{\mathcal{H}}^0 &= \omega_1^0(\hat{I}_{1z} + \hat{I}_{2z}) + \omega_3^0(\hat{S}_{3z} + \hat{S}_{4z}) + 2\pi J_{12}\hat{\mathbf{I}}_1 \cdot \hat{\mathbf{I}}_2 + 2\pi J_{13}(\hat{I}_{1z}\hat{S}_{3z} + \hat{I}_{2z}\hat{S}_{4z}) \\ &\quad + 2\pi J_{14}(\hat{I}_{1z}\hat{S}_{4z} + \hat{I}_{2z}\hat{S}_{3z}) + 2\pi J_{34}\hat{\mathbf{S}}_3 \cdot \hat{\mathbf{S}}_4 \end{aligned} \tag{17.10}$$

Suppose, now, that the two I spins are magnetically equivalent and the two S spins are also magnetically equivalent (see Figures 17.19 and 17.20). The J-couplings now have the symmetry

$$J_{13} = J_{14} = J_{23} = J_{24}$$

and the spin Hamiltonian may be simplified further:

$$\widehat{\mathcal{H}}^0 = \omega_1^0(\hat{I}_{1z} + \hat{I}_{2z}) + \omega_3^0(\hat{S}_{3z} + \hat{S}_{4z}) + 2\pi J_{13}(\hat{I}_{1z}\hat{S}_{3z} + \hat{I}_{2z}\hat{S}_{4z} + \hat{I}_{1z}\hat{S}_{4z} + \hat{I}_{2z}\hat{S}_{3z})$$

Now go back to the case in which the spins are chemically equivalent but not magnetically equivalent (Equation 17.10). Suppose that a strong r.f. decoupling field is applied continuously at the Larmor frequency of species I, in order to effectively remove the couplings to species S (see Section 3.9). In the presence of a heteronuclear decoupling field, all Hamiltonian terms involving the irradiated spins may usually be dropped from the effective spin Hamiltonian, providing caution is used.[2] In the presence of I-spin decoupling, the spin Hamiltonian may therefore be written as follows:

$$\widehat{\mathcal{H}}^0(\text{with } I\text{-spin decoupling}) = \omega_3^0(\hat{S}_{3z} + \hat{S}_{4z}) + 2\pi J_{34}\hat{\mathbf{S}}_3 \cdot \hat{\mathbf{S}}_4$$

The decoupling field effectively renders the S-spins magnetically equivalent, so the spin Hamiltonian may be simplified further:

$$\widehat{\mathcal{H}}^0(\text{with } I\text{-spin decoupling}) = \omega_3^0(\hat{S}_{3z} + \hat{S}_{4z})$$

For this system, the S-spins behave as isolated spins in the presence of I-spin decoupling.

17.8 Alphabet Notation

Molecular spin systems are often denoted using the letters of the alphabet. The idea is that spins with very different chemical shifts are denoted by letters that are remote in the alphabet. This usually implies weak coupling. Spins with similar chemical shifts are denoted by letters which are close in the alphabet. The notation AB implies strong coupling.

Magnetically equivalent groups are denoted by a numerical subscript. Spins that are chemically equivalent, but not magnetically equivalent, are denoted by primes.

For example, the six protons in benzene are magnetically equivalent, so the system is denoted A_6.

The five protons in ethyl chloride divide into two groups of magnetically equivalent spins, one containing three spins and the other containing two spins. Since the chemical shift difference is normally sufficient to ensure weak coupling, the spin system is denoted A_3X_2.

The heteronuclear spin system in 1,1-difluoroethene (Figure 17.3) displays chemical equivalence, but not magnetic equivalence. The ^{1}H– ^{19}F couplings are 'weak', since two different isotopes are involved, so the spin system is denoted AA′ XX′.

The heteronuclear spin system of 1,1-Difluoropropan-1,2-diene (Figure 17.19) displays magnetic equivalence. The appropriate notation for this system is therefore A_2X_2.

The diastereotopic CH_2 protons of amino acid side-chains in proteins are chemically inequivalent, and usually have similar chemical shifts. They often form strongly coupled AB spin systems.

The two pairs of diastereotopic CH_2 protons in citric acid (Figure 17.12) form a strongly coupled AA′BB′ spin system, neglecting the rapidly exchanging carboxyl and hydroxyl protons. Each CH_2 group in citric acid contains one A proton and one B proton.

17.9 Spin Coupling Topologies

The Hamiltonian terms in Equation 17.4 may be represented as a diagram, in which each spin is represented as a symbol and couplings between them are represented by lines. This chapter already contains many schematic diagrams of this kind. It is sometimes useful to classify spin systems according to the *topology* of this network. For example, consider the following coupling networks for four-spin-1/2 systems:

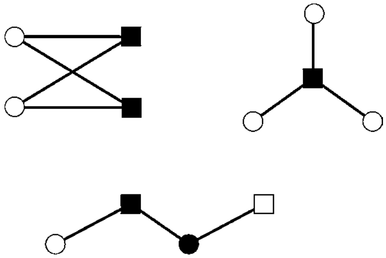

Figure 17.22
Coupling topologies in four-spin systems.

The top-left example represents an A_2X_2 spin system, with a spin Hamiltonian of the form given in Equation 17.5. The coupling network forms a ring.

The 'star-shaped' network at the top right represents an AX_3 spin system. The corresponding spin Hamiltonian for this system has the form

$$\widehat{\mathcal{H}}^0 = \omega_1^0 \hat{I}_{1z} + \omega_2^0(\hat{I}_{2z} + \hat{I}_{3z} + \hat{I}_{4z}) + 2\pi J(\hat{I}_{1z}\hat{I}_{2z} + \hat{I}_{1z}\hat{I}_{3z} + \hat{I}_{1z}\hat{I}_{4z})$$

This type of coupling toplogy is encountered, for example, between ^{13}C and ^{1}H spins in CH_3 groups.

The lower diagram represents a *linear* spin system, in which all J-couplings vanish except between immediate neighbours and no spin has more than two coupling partners. The spin Hamiltonian for an AMXY system of this kind is

$$\widehat{\mathcal{H}}^0 = \omega_1^0 \hat{I}_{1z} + \omega_2^0 \hat{I}_{2z} + \omega_3^0 \hat{I}_{3z} + \omega_4^0 \hat{I}_{4z} + \; 2\pi J_{12} \hat{I}_{1z} \hat{I}_{2z} + 2\pi J_{23} \hat{I}_{2z} \hat{I}_{3z} + 2\pi J_{34} \hat{I}_{3z} \hat{I}_{4z}$$

Linear spin systems are commonly encountered when the molecular structure has the form of a chain, e.g. in the side chains of some amino acids.

Notes

1. The validity of the weak coupling approximation depends on the r.f. pulse sequence. In particular, the weak coupling Hamiltonian is only valid if Equation 17.6 is satisfied and if the spin system is allowed to evolve in the absence of r.f. fields for an interval τ that is long enough to satisfy the condition

   $$|\omega_j^0 - \omega_k^0|\tau >> 1$$

   Sometimes, densely spaced pulse sequences are applied that deliberately violate this condition, causing a weakly coupled spin system to behave temporarily as if it were strongly coupled (see Section 18.14 and Appendix A.6).

2. It is not always safe to take decoupling into account by cleansing the spin Hamiltonian of those operators which involve the irradiated spins. Although this approach gives correct results for the evolution of the observed spins, it does not give correct results for the evolution of the irradiated spins. One can get away with this if the decoupling field is maintained for the rest of the pulse sequence, but misleading results are obtained if the decoupling field is switched on and off. For a description of the pitfalls, see M. H. Levitt, G. Bodenhausen, and R. R. Ernst, *J. Magn. Reson.*, **53**, 443 (1983).

Further Reading

- For a thorough text on the classification of spin systems, see P. L. Corio, *Structure of High-Resolution NMR Spectra*, Academic Press, New York, 1966. Unfortunately, this book is hard to obtain, and I am unaware of a good alternative.
- For an accessible discussion of heteronuclear spin decoupling, see R. Freeman, *Spin Choreography. Basic Steps in High Resolution NMR.*, Spektrum, Oxford, 1997.

Exercises

17.1 For each of the compounds given below, indicate whether the protons H_a and H_b are chemically equivalent, magnetically equivalent, or both.

i

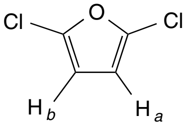

ii

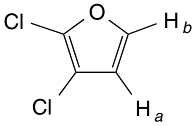

iii

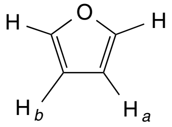

17.2 Give the alphabet notation for the proton spin systems in the following compounds:

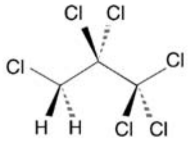
i

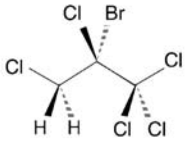
ii

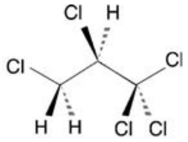
iii

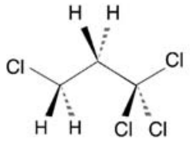
iv

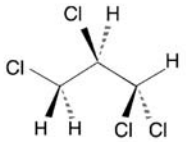
v

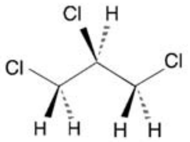
vi

In each case, assume free rotation around the C─C single bonds.

18 Many-Spin Dynamics

The dynamics of many-spin systems can be quite complicated. Nevertheless, matters may still be kept well under control, at least in favourable circumstances.[1]

For simplicity, this chapter deals only with weakly coupled spin-1/2 systems in isotropic liquids.

18.1 Spin Hamiltonian

In the absence of an r.f. field, the spin Hamiltonian for a set of weakly coupled spins in an isotropic liquid is given by Equation 17.7:

$$\widehat{\mathcal{H}}^0 \cong \sum_j \omega_j^0 \hat{I}_{jz} + \sum_{j<k}{}' \, 2\pi J_{jk} \hat{I}_{jz} \hat{I}_{kz} \tag{18.1}$$

The sum is taken over all magnetically inequivalent spins, ignoring spins undergoing rapid dynamics.

As a first example, consider the three-proton AMX system of 2,3-dibromopropanoic acid:

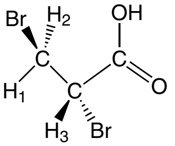

Figure 18.1
2,3-Dibromopropanoic acid

The OH proton is in fast intermolecular exchange and may be ignored. The quadrupolar Br nuclei may also be ignored. The two –CH_2Br protons are diastereotopic and have different chemical shifts (see Section 17.4). The chemical shifts of the three spins are $\delta_1 = 3.70\,\text{ppm}$, $\delta_2 = 3.92\,\text{ppm}$ and $\delta_3 = 4.50\,\text{ppm}$, and the three J-couplings are $J_{12} = -10.1\,\text{Hz}$, $J_{13} = +4.3\,\text{Hz}$ and $J_{23} = +11.3\,\text{Hz}$. In a reasonably high magnetic field, the weak coupling condition (Equation 17.6) is well satisfied for all spin pairs.

If the spectrometer reference frequency is set to $\delta_{\text{ref}} = 4.10\,\text{ppm}$ and the magnetic field is $B^0 = 11.74\,\text{T}$, then the rotating-frame spin Hamiltonian for the three non-exchangeable protons in 2,3-dibromopropanoic acid is given by

$$\widehat{\mathcal{H}}^0 \cong \Omega_1^0 \hat{I}_{1z} + \Omega_2^0 \hat{I}_{2z} + \Omega_3^0 \hat{I}_{3z} + 2\pi J_{12} \hat{I}_{1z} \hat{I}_{2z} + 2\pi J_{13} \hat{I}_{1z} \hat{I}_{3z} + 2\pi J_{23} \hat{I}_{2z} \hat{I}_{3z}$$

where the resonance offset frequencies of the three spins are $\Omega_1^0/2\pi = +200\,\text{Hz}$, $\Omega_2^0/2\pi = +90\,\text{Hz}$ and $\Omega_3^0/2\pi = -200\,\text{Hz}$.

Spin Dynamics: Basics of Nuclear Magnetic Resonance, Second Edition Malcolm H. Levitt

As a second example, consider the five-spin A_2X_3 system of the protons in ethanol CH_3CH_2OH (ignoring the rapidly exchanging hydroxyl proton). As described in Section 17.5, the magnetic equivalence of the CH_2 and CH_3 protons leads to the following coupling topology:

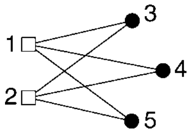

Figure 18.2
Coupling topology for the non-exchangeable protons in ethanol.

If the spectrometer reference frequency set to $\delta_{\text{ref}} = 2.425\,\text{ppm}$ and the magnetic field is $B^0 = 11.74\,\text{T}$, then the rotating-frame spin Hamiltonian for the five non-exchangeable protons in ethanol is given by

$$\widehat{\mathcal{H}}^0 \cong \Omega_1^0(\hat{I}_{1z} + \hat{I}_{2z}) + \Omega_3^0(\hat{I}_{3z} + \hat{I}_{4z} + \hat{I}_{5z}) + 2\pi J(\hat{I}_{1z}\hat{I}_{3z} + \hat{I}_{1z}\hat{I}_{4z} + \hat{I}_{1z}\hat{I}_{5z} + \hat{I}_{2z}\hat{I}_{3z} + \hat{I}_{2z}\hat{I}_{4z} + \hat{I}_{2z}\hat{I}_{5z}) \tag{18.2}$$

where the resonance offset frequencies and J-couplings are $\Omega_1^0/2\pi = -617.5\,\text{Hz}$, $\Omega_3^0/2\pi = +617.5\,\text{Hz}$ and $J = +6.9\,\text{Hz}$.

18.2 Energy Eigenstates

A weakly coupled system of N spins-1/2 has 2^N stationary states, given by the direct products of the Zeeman eigenstates of the individual spins. For example, the eight stationary states of the AMX system are

$$\begin{aligned}
|1\rangle &= |\alpha\alpha\alpha\rangle & |2\rangle &= |\alpha\alpha\beta\rangle \\
|3\rangle &= |\alpha\beta\alpha\rangle & |4\rangle &= |\alpha\beta\beta\rangle \\
|5\rangle &= |\beta\alpha\alpha\rangle & |6\rangle &= |\beta\alpha\beta\rangle \\
|7\rangle &= |\beta\beta\alpha\rangle & |8\rangle &= |\beta\beta\beta\rangle
\end{aligned} \tag{18.3}$$

These are all eigenstates of the z-angular momentum operators of the individual spins; for example:

$$\begin{aligned}
\hat{I}_{1z}|\alpha\alpha\alpha\rangle &= +\frac{1}{2}|\alpha\alpha\alpha\rangle & \hat{I}_{2z}|\alpha\beta\alpha\rangle &= -\frac{1}{2}|\alpha\beta\alpha\rangle \\
\hat{I}_{2z}|\alpha\alpha\alpha\rangle &= +\frac{1}{2}|\alpha\alpha\alpha\rangle & \hat{I}_{3z}|\alpha\alpha\beta\rangle &= -\frac{1}{2}|\alpha\alpha\beta\rangle
\end{aligned}$$

In general, these relationships may be denoted as

$$\hat{I}_{jz}|r\rangle = m_j^{(r)}|r\rangle$$

where $m_j^{(r)} = +1/2$ if the state $|r\rangle$ has an 'α' label in the jth place, and $m_j^{(r)} = -1/2$ if the state $|r\rangle$ has a 'β' label in the jth place. For example, the state $|2\rangle$ in Equation 18.3 has $m_2^{(2)} = +1/2$, $m_2^{(2)} = +1/2$ and $m_3^{(2)} = -1/2$.

It is also convenient to define the *total* z-angular momentum quantum numbers as

$$M_r = \sum_j m_j^{(r)}$$

For example, the state $|1\rangle = |\alpha\alpha\alpha\rangle$ has $M_1 = +3/2$, whereas the states $|6\rangle = |\beta\alpha\beta\rangle$ and $|7\rangle = |\beta\beta\alpha\rangle$ have $M_6 = M_7 = -1/2$.

The direct product Zeeman eigenstates are eigenstates of the weakly coupled spin Hamiltonian in Equation 18.1, according to

$$\widehat{\mathcal{H}}^0|r\rangle = \omega_r|r\rangle$$

The energies of the states are

$$\omega_r = \sum_j \omega_j^0 m_j^{(r)} + \sum_{j<k}{}' \, 2\pi J_{jk} m_j^{(r)} m_k^{(r)}$$

The diagram below shows these energy levels for systems of $N = 1, 2, 3, 4$ and 5 spins-1/2. The state energies fall into distinct groups, distinguished by the value of M_r:

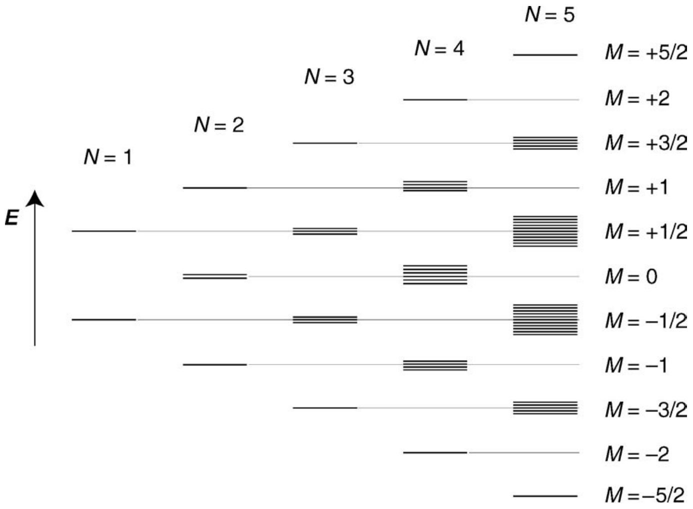

Figure 18.3
Energy levels for coupled spins-1/2.

This diagram greatly exaggerates the small differences in energy between levels in the same group, which are caused by chemical shift differences and J-couplings.

The number of levels in each group follows the binomial distribution. In general, for a system of N spins-1/2, the number of levels with a given value of M is equal to $N!/\{(N/2 - M)!\,(N/2 + M)!\}$.

18.3 Superposition States

In general, each coupled spin system is not in an energy eigenstate. The *superposition states* are defined in the usual way:

$$|\psi\rangle = \sum_{r=1}^{2^N} c_r |r\rangle$$

where the coefficients c_r are normalized complex numbers:

$$\sum_{r=1}^{2^N} |c_r|^2 = 1$$

For example, the state

$$|\psi\rangle = \frac{1}{\sqrt{2}}|\alpha\alpha\alpha\rangle + \frac{1}{2\sqrt{2}}|\alpha\alpha\beta\rangle + \frac{1}{2\sqrt{2}}|\beta\alpha\alpha\rangle + \frac{\mathrm{i}}{2}|\beta\beta\beta\rangle$$

is a valid superposition state for the AMX system.

18.4 Spin Density Operator

The quantum state of an ensemble of multiple-spin systems is described by the spin density operator, defined by

$$\hat{\rho} = \overline{|\psi\rangle\langle\psi|}$$

where $|\psi\rangle$ is the state of an individual spin system and the overbar indicates an ensemble average.

The spin density operator of an ensemble of N-spin-1/2 systems may be written as a $2^N \times 2^N$ density matrix. The 'box notation', described in Section 15.2, is very useful for specifying the density matrix elements. For example, the 8×8 density matrix of an ensemble of AMX spin systems may be written as follows:

$$\hat{\rho} = \begin{pmatrix}
\rho_{\boxed{\alpha\alpha\alpha}} & \rho_{\boxed{\alpha\alpha+}} & \rho_{\boxed{\alpha+\alpha}} & \rho_{\boxed{\alpha++}} & \rho_{\boxed{+\alpha\alpha}} & \rho_{\boxed{+\alpha+}} & \rho_{\boxed{++\alpha}} & \rho_{\boxed{+++}} \\
\rho_{\boxed{\alpha\alpha-}} & \rho_{\boxed{\alpha\alpha\beta}} & \rho_{\boxed{\alpha+-}} & \rho_{\boxed{\alpha+\beta}} & \rho_{\boxed{+\alpha-}} & \rho_{\boxed{+\alpha\beta}} & \rho_{\boxed{++-}} & \rho_{\boxed{++\beta}} \\
\rho_{\boxed{\alpha-\alpha}} & \rho_{\boxed{\alpha-+}} & \rho_{\boxed{\alpha\beta\alpha}} & \rho_{\boxed{\alpha\beta+}} & \rho_{\boxed{+-\alpha}} & \rho_{\boxed{+-+}} & \rho_{\boxed{+\beta\alpha}} & \rho_{\boxed{\alpha\beta+}} \\
\rho_{\boxed{\alpha--}} & \rho_{\boxed{\alpha-\beta}} & \rho_{\boxed{\alpha\beta-}} & \rho_{\boxed{\alpha\beta\beta}} & \rho_{\boxed{+--}} & \rho_{\boxed{+-\beta}} & \rho_{\boxed{+\beta-}} & \rho_{\boxed{+\beta\beta}} \\
\rho_{\boxed{-\alpha\alpha}} & \rho_{\boxed{-\alpha+}} & \rho_{\boxed{-+\alpha}} & \rho_{\boxed{-++}} & \rho_{\boxed{\beta\alpha\alpha}} & \rho_{\boxed{\beta\alpha+}} & \rho_{\boxed{\beta+\alpha}} & \rho_{\boxed{\beta++}} \\
\rho_{\boxed{-\alpha-}} & \rho_{\boxed{-\alpha\beta}} & \rho_{\boxed{-+-}} & \rho_{\boxed{-+\beta}} & \rho_{\boxed{\beta\alpha-}} & \rho_{\boxed{\beta\alpha\beta}} & \rho_{\boxed{\beta+-}} & \rho_{\boxed{\beta+\beta}} \\
\rho_{\boxed{--\alpha}} & \rho_{\boxed{--+}} & \rho_{\boxed{-\beta\alpha}} & \rho_{\boxed{-\beta+}} & \rho_{\boxed{\beta-\alpha}} & \rho_{\boxed{\beta-+}} & \rho_{\boxed{\beta\beta\alpha}} & \rho_{\boxed{\beta\beta+}} \\
\rho_{\boxed{---}} & \rho_{\boxed{--\beta}} & \rho_{\boxed{-\beta-}} & \rho_{\boxed{-\beta\beta}} & \rho_{\boxed{\beta--}} & \rho_{\boxed{\beta-\beta}} & \rho_{\boxed{\beta\beta-}} & \rho_{\boxed{\beta\beta\beta}}
\end{pmatrix}$$

The density matrix of an ensemble of AMX systems contains eight populations $\rho_{\boxed{\alpha\alpha\alpha}}$, $\rho_{\boxed{\alpha\alpha\beta}} \ldots \rho_{\boxed{\beta\beta\beta}}$ (on the top-left to bottom-right diagonal) and 56 coherences $\rho_{\boxed{\alpha\alpha+}}$, $\rho_{\boxed{\alpha+\alpha}} \ldots \rho_{\boxed{\beta\beta-}}$ (off the diagonal).

The procedure for obtaining the 'box notation' for a given element may be illustrated by the following example. Consider the density matrix element $\rho_{67} = \langle 6|\hat{\rho}|7\rangle = \langle\beta\alpha\beta|\hat{\rho}|\beta\beta\alpha\rangle$. This is a coherence between states $|\beta\beta\alpha\rangle$ and $\langle\beta\alpha\beta|$, and since the spin states should be read from *right to left*, the 'coherence arrow' points in this case from to $|\beta\beta\alpha\rangle \rightarrow |\beta\alpha\beta\rangle$.

The state labels for the three spins may now be compared between the two states $|\beta\beta\alpha\rangle$ and $|\beta\alpha\beta\rangle$. Spin I_1 is in state $|\beta\rangle$ for both states, which is indicated by a 'β' label inside the box. Spin I_2 is transformed from state $|\beta\rangle$ to state $|\alpha\rangle$ in making the transformation $|\beta\beta\alpha\rangle \rightarrow |\beta\alpha\beta\rangle$, which is indicated by a '+' label inside the box. Spin I_3 is transformed from state $|\alpha\rangle$ to state $|\beta\rangle$, which is indicated by a '−' label inside the box. The box notation for the element $\langle 6|\hat{\rho}|7\rangle$ is therefore $\rho_{\boxed{\beta+-}}$.

Similarly, the box notation for the element $\rho_{35} = \langle 3|\hat{\rho}|5\rangle = \langle\alpha\beta\alpha|\hat{\rho}|\beta\alpha\alpha\rangle$ is $\rho_{\boxed{+-\alpha}}$.

The box notation is easily extended to larger numbers of spins-1/2. For example, in the five-spin-1/2 system of ethanol, the density matrix element $\langle\beta\alpha\alpha\alpha\beta|\hat{\rho}|\alpha\alpha\beta\alpha\beta\rangle$ may be denoted $\rho_{\boxed{-\alpha+\alpha\beta}}$.

Spins with labels '+' or '−' inside the box are termed *active*. Spins with labels 'α' or 'β' inside the box are termed *passive*. For example, in the coherence $\rho_{\boxed{-\alpha+\alpha\beta}}$, spins I_1 and I_3 are active, while spins I_2, I_4 and I_5 are passive.

Table 18.1 Numbers of coherences for N-spin-1/2 systems. There are equal numbers of coherences with order $-p$ and $+p$.

Number of spins N	1	2	3	4	5	6	10	100	500
0-quantum	0	2	12	54	220	860	183 732	9.0×10^{58}	2.7×10^{299}
(+1)-quantum	1	4	15	56	210	792	167 960	8.9×10^{58}	2.7×10^{299}
(+2)-quantum	0	1	6	28	120	495	125 970	8.7×10^{58}	2.7×10^{299}
(+3)-quantum	0	0	1	8	45	220	77 520	8.3×10^{58}	2.7×10^{299}
(+4)-quantum	0	0	0	1	10	66	38 760	7.7×10^{58}	2.6×10^{299}
(+5)-quantum	0	0	0	0	1	12	15 504	7.1×10^{58}	2.6×10^{299}
(+6)-quantum	0	0	0	0	0	1	4845	6.3×10^{58}	2.5×10^{299}
1-spin-(+1)-quantum	1	4	12	32	80	192	5120	6.3×10^{31}	8.2×10^{152}
2-spin-(+2)-quantum	0	1	6	24	80	240	11 520	1.5×10^{33}	1.0×10^{155}
3-spin-(+3)-quantum	0	0	1	8	40	160	15 360	2.6×10^{34}	8.5×10^{156}
4-spin-(+4)-quantum	0	0	0	1	10	60	13 440	3.1×10^{35}	5.3×10^{158}
5-spin-(+5)-quantum	0	0	0	0	1	12	8064	3.0×10^{36}	2.6×10^{160}
6-spin-(+6)-quantum	0	0	0	0	0	1	3360	2.4×10^{37}	1.1×10^{162}

18.5 Populations and Coherences

18.5.1 Coherence orders

The box notation makes it very easy to deduce the *order* of a coherence. Each '+' symbol inside the box contributes +1 to the order, each '−' symbol inside the box contributes −1, and α or β symbols contribute zero. For example, $\rho_{\boxed{\alpha++}}$ is a (+2)-quantum coherence, and $\rho_{\boxed{-+-}}$ is a (−1)-quantum coherence.

The number of coherences of a given order increases very rapidly with the number of coupled spins. The top half of Table 18.1 shows the number of coherences of different order for systems of 1, 2, 3, 4, 5, 6, 10, 100 and 500 coupled spins-1/2.

For a single spin-1/2, there are no zero-quantum coherences, and only one coherence of order +1. For two spins-1/2, there are two zero-quantum coherences, four (+1)-quantum coherence, and one (+2)-quantum coherence. For three spins-1/2, there are 12 zero-quantum coherences, 15 (+1)-quantum coherences, six (+2)-quantum coherences, and one (+3)-quantum coherence.

For 10 coupled spins-1/2, there are 167 960 (+1)-quantum coherences. In a small protein, there are approximately 500 protons, and the number of (+1)-quantum coherences is given by the mind-boggling figure of $\sim 2.7 \times 10^{299}$.

18.5.2 Combination coherences and simple coherences

Consider the coherences $\rho_{\boxed{+-+}}$ and $\rho_{\boxed{\alpha\alpha-}}$ of an AMX spin ensemble. The order of coherence is −1 in both cases. However, the number of active spins is three in the first case and one in the second case. These different types of coherence are distinguished by denoting $\rho_{\boxed{+-+}}$ as a three-spin-(−1)-quantum coherence, while $\rho_{\boxed{\alpha\alpha-}}$ is a one-spin-(−1)-quantum coherence.

Coherences in which the number of active spins is greater than the coherence order are called *combination coherences*. Coherences that are not combination coherences are referred to in this book as *simple coherences*.[2] In the example above, $\rho_{\boxed{+-+}}$ is a combination coherence, whereas $\rho_{\boxed{\alpha\alpha-}}$ is a simple coherence.

The lower half of Table 18.1 shows the number of *simple* coherences in different spin systems. For these coherences, the number of active spins is equal to the coherence order. For example, in a three-spin-1/2 system, there are 15 (+1)-quantum coherences. Twelve of these are simple coherences, and three are combination coherences (these are $\rho_{\boxed{+-+}}$, $\rho_{\boxed{++-}}$ and $\rho_{\boxed{-++}}$). In a five-spin-1/2 system, there are 45 (+3)-quantum coherences, of which 40 are simple coherences and five are combination coherences.

The number of simple p-quantum coherences in an N-spin-1/2 ensemble is equal to $\{N! \times 2^{N-|p|}\}/\{|p|!\,(N-|p|)!\}$.

By definition, zero-quantum coherences are combination coherences.

18.5.3 Coherence frequencies

In the absence of r.f. fields, and if relaxation is ignored, all coherences evolve as described in Section 15.4. The equation of motion of an individual coherence between time points t_{a} and t_{b} is:

$$\boxed{\rho_{rs}(t_{\mathrm{b}}) = \rho_{rs}(t_{\mathrm{a}}) \exp\{(\mathrm{i}\Omega_{rs} - \lambda_{rs})(t_{\mathrm{b}} - t_{\mathrm{a}})\} \qquad (18.4)}$$

where Ω_{rs} is the coherence frequency (in the rotating frame) and λ_{rs} is the decay rate constant of the coherence.

The box notation makes it easy to determine the precession frequency Ω_{rs} of a given coherence. As an example, consider the coherence $\rho_{\boxed{+-\alpha}}$ in an AMX spin system. The frequency $\Omega_{\boxed{+-\alpha}}$ of this coherence may be determined as follows:

1. Draw out the coupling topology of the spin system and attach the coherence labels. Draw a lasso around the active spins:

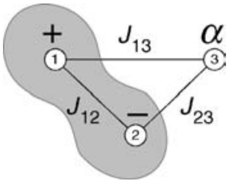

Figure 18.4
Diagram used for calculating the frequency $\Omega_{\boxed{+-\alpha}}$.

2. Calculate the chemical shift contribution to the frequency by assigning $+\Omega_j^0$ to active spins with a '−' label and $-\Omega_j^0$ to active spins with a '+' label. For the coherence $\rho_{\boxed{+-\alpha}}$, the chemical shift frequency contribution comes to

$$\text{chemical shift contribution} = -\Omega_1^0 + \Omega_2^0$$

3. Compute the J-coupling part of the coherence frequency by summing together contributions from all couplings between active spins and passive spins, i.e. from 'inside the lasso' to 'outside the lasso'. Ignore the couplings of active spins with each other, and of passive spins with each other. There are four possible cases:
   (i) The combination of a '−' and an 'α' label contributes $+\pi J_{jk}$.
   (ii) The combination of a '−' and a 'β' label contributes $-\pi J_{jk}$.
   (iii) The combination of a '+' and an 'α' label contributes $-\pi J_{jk}$.
   (iv) The combination of a '+' and a 'β' label contributes $+\pi J_{jk}$.
   In the case of $\rho_{\boxed{+-\alpha}}$, the J-coupling contribution is

$$J\text{-coupling contribution} = -\pi J_{13} + \pi J_{23}$$

The rotating-frame precession frequency of the coherence $\rho_{\boxed{+-\alpha}}$ is therefore

$$\Omega_{\boxed{+-\alpha}} = -\Omega_1^0 + \Omega_2^0 - \pi J_{13} + \pi J_{23}$$

As a more complicated example, consider the three-spin-(−1)-quantum coherence $\rho_{\boxed{-\alpha+\beta-}}$ in the five-spin-1/2 system of ethanol. The 'lasso' picture of this coherence is shown here:

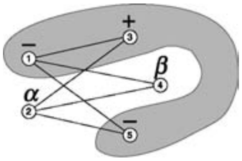

Figure 18.5
Diagram used for calculating the frequency $\Omega_{\boxed{-\alpha+\beta-}}$.

Applying the rules above, and using the magnetic equivalences defined in Equation 18.2, gives the following chemical shift frequency contribution:

$$\text{chemical shift contribution} = +\Omega_1^0 - \Omega_3^0 + \Omega_5^0 = +\Omega_1^0$$

For the J-coupling contribution one gets

$$J\text{-coupling contribution} = -\pi J_{14} - \pi J_{23} + \pi J_{25} = -\pi J$$

The overall precession frequency of this coherence is therefore

$$\Omega_{\boxed{-\alpha+\beta-}} = +\Omega_1^0 - \pi J$$

The frequency of any coherence in a weakly coupled system of spins-1/2 may be deduced in the same way.

18.5.4 Degenerate coherences

Coherences that have the same precession frequency are termed *degenerate*. Degeneracy occurs whenever there is magnetic equivalence, or whenever the J-couplings between any pair of spins is vanishingly small.

For example, in an AMX system, the coherences $\rho_{\boxed{-\alpha\alpha}}$ and $\rho_{\boxed{-\alpha\beta}}$ are degenerate if the coupling J_{13} vanishes, so that the spin system is *linear* (see Section 17.9).

In the A_2X_3 system of the protons in ethanol, the coherences $\rho_{\boxed{-\alpha\alpha\beta}}$, $\rho_{\boxed{-\alpha\beta\alpha}}$, $\rho_{\boxed{-\beta\alpha\alpha}}$, $\rho_{\boxed{\alpha-\alpha\alpha\beta}}$, $\rho_{\boxed{\alpha-\alpha\beta\alpha}}$, $\rho_{\boxed{\alpha-\beta\alpha\alpha}}$, $\rho_{\boxed{-\beta\alpha\alpha\beta}}$, $\rho_{\boxed{-\beta\alpha\beta\alpha}}$, $\rho_{\boxed{-\beta\beta\alpha\alpha}}$, $\rho_{\boxed{\beta-\alpha\alpha\beta}}$, $\rho_{\boxed{\beta-\alpha\beta\alpha}}$ and $\rho_{\boxed{\beta-\beta\alpha\alpha}}$ are all degenerate.

Most large systems of coupled spins-1/2 have a high degree of degeneracy, since it is unlikely that every spin has a finite J-coupling with every other spin.

Degeneracy has important practical consequences: although the number of *coherences* in a small protein molecule is astronomical (see Table 18.1), the number of non-degenerate coherence *frequencies* is relatively manageable. If this were not so, it would be essentially impossible to interpret the NMR spectrum for molecules of a reasonable size.

A very high degree of degeneracy is a characteristic property of weakly coupled spin systems in isotropic liquids. In liquid crystals, the degeneracy is relatively low, and the NMR spectra of molecules containing more than around 10 coupled spins are essentially intractable.[3]

18.5.5 Observable coherences

Only simple (−1)*-quantum coherences generate observable signals in a quadrature receiver.*

This may readily be seen by using the formula for the total spin magnetization along the x-axis:

$$M_x \sim \langle \hat{I}_x \rangle = \mathrm{Tr}\{\hat{\rho}\hat{I}_x\} = \mathrm{Tr}\{\hat{\rho}\hat{I}_{1x}\} + \mathrm{Tr}\{\hat{\rho}\hat{I}_{2x}\} + \ldots$$

In the case of a three-spin-1/2 system we get

$$M_x \sim \mathrm{Tr}\{\hat{\rho}\hat{I}_{1x}\} + \mathrm{Tr}\{\hat{\rho}\hat{I}_{2x}\} + \mathrm{Tr}\{\hat{\rho}\hat{I}_{3x}\}$$

Each individual term may be expanded as follows:

$$\begin{aligned}\mathrm{Tr}\{\hat{\rho}\hat{I}_{1x}\} &= \mathrm{Tr}\{\hat{\rho}\tfrac{1}{2}(\hat{I}_1^+ + \hat{I}_1^-)(\hat{I}_2^\alpha + \hat{I}_2^\beta)(\hat{I}_3^\alpha + \hat{I}_3^\beta)\}\\ &= \tfrac{1}{2}\,\mathrm{Tr}\{\hat{\rho}\hat{I}_1^+\hat{I}_2^\alpha\hat{I}_3^\alpha\} + \tfrac{1}{2}\,\mathrm{Tr}\{\hat{\rho}\hat{I}_1^+\hat{I}_2^\alpha\hat{I}_3^\beta\} + \ldots\end{aligned}$$

Operators such as $\hat{I}_1^+\hat{I}_2^\alpha\hat{I}_3^\beta$ may be written in the following 'ket-bra' form:

$$\hat{I}_1^+\hat{I}_2^\alpha\hat{I}_3^\beta = |\alpha\alpha\beta\rangle\langle\beta\alpha\beta|$$

The properties of the trace (see Section 7.7.4) may be exploited as follows:

$$\mathrm{Tr}\{\hat{\rho}\hat{I}_1^+\hat{I}_2^\alpha\hat{I}_3^\beta\} = \mathrm{Tr}\{\hat{\rho}|\alpha\alpha\beta\rangle\langle\beta\alpha\beta|\} = \langle\beta\alpha\beta|\hat{\rho}|\alpha\alpha\beta\rangle = \rho_{\boxed{-\alpha\beta}}$$

These arguments may be put together to obtain:

$$M_x \sim \langle \hat{I}_x \rangle = \frac{1}{2}\rho_{\boxed{-\alpha\alpha}} + \frac{1}{2}\rho_{\boxed{-\alpha\beta}} + \ldots + \frac{1}{2}\rho_{\boxed{+\alpha\alpha}} + \ldots$$

Only simple (±1)-quantum coherences appear in the sum.

Although the transverse magnetization M_x contains contributions from the simple (+1)-quantum coherences as well as the simple (−1)-quantum coherences, the quadrature-detected NMR signal is purely generated by the simple (−1)-quantum coherences, defined as usual in the rotating frame. The arguments given in Appendix A.5 may be used to derive the following formula for the quadrature NMR signal:

$$s(t) \sim 2\mathrm{i}(\rho_{\boxed{-\alpha\alpha}}(t) + \rho_{\boxed{-\alpha\beta}}(t) + \ldots)\exp\{-\mathrm{i}\phi_{\mathrm{rec}}\}$$

Here, ϕ_{rec} is the receiver phase, as specified in Section 4.5.4.

Although only simple (−1)-quantum coherences generate observable signals directly, the other coherences may be observed *indirectly* by using two-dimensional spectroscopy.

18.6 NMR Spectra

Each of the simple (-1)-quantum coherences is associated with a single spectral peak.

For example, the NMR spectrum of an AMX system has the following mathematical form:

$$S(\Omega) = a_{\boxed{-\alpha\alpha}}\mathcal{L}(\Omega;\Omega_{\boxed{-\alpha\alpha}},\lambda) + a_{\boxed{-\alpha\beta}}\mathcal{L}(\Omega;\Omega_{\boxed{-\alpha\alpha}},\lambda) + \ldots$$

There is one term for each of the 12 observable coherences, and the complex amplitudes have the form

$$\begin{aligned} a_{\boxed{-\alpha\alpha}} &= 2\mathrm{i}\rho_{\boxed{-\alpha\alpha}}(0)\exp\{-\mathrm{i}\phi_{\mathrm{rec}}\} \\ a_{\boxed{-\alpha\beta}} &= 2\mathrm{i}\rho_{\boxed{-\alpha\beta}}(0)\exp\{-\mathrm{i}\phi_{\mathrm{rec}}\} \end{aligned}$$

and so on. The time point $t = 0$ corresponds to the beginning of signal detection.

As described in Section 15.5, each peak contributes an absorption Lorentzian if the complex amplitude is a real number, but contributes a dispersion Lorentzian if the complex amplitude is an imaginary number.

If the amplitudes of the simple (-1)-quantum coherences are real and equal at time $t = 0$, then the spectrum of an AMX system has the following appearance:

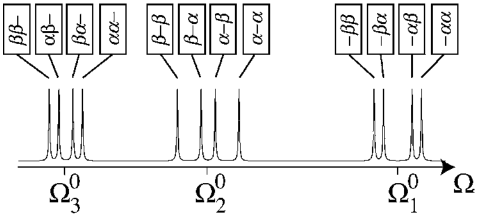

Figure 18.6
Assignment of AMX spectral peaks if all J-couplings and the gyromagnetic ratio are positive.

This spectrum corresponds to the case $\Omega_1^0/2\pi = 300\,\mathrm{Hz}$, $\Omega_2^0/2\pi = 100\,\mathrm{Hz}$, $\Omega_3^0/2\pi = -50\,\mathrm{Hz}$, $J_{12} = 40\,\mathrm{Hz}$, $J_{13} = 10\,\mathrm{Hz}$ and $J_{23} = 25\,\mathrm{Hz}$.

The signs of the J-couplings do not affect the appearance of the spectrum, but do influence the correct labelling of the peaks. For example, if $J_{23} = -25\,\mathrm{Hz}$, while all other parameters are unchanged, the spectrum should be labelled as follows:

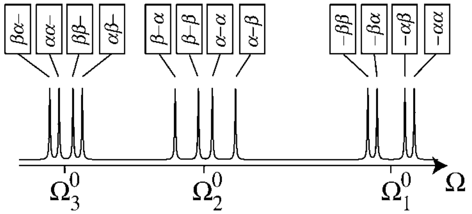

Figure 18.7
Assignment of AMX spectral peaks if J_{23} is negative.

Suppose, now, that the coupling J_{13} vanishes, so that the spin system is linear (see Section 17.9). Several pairs of coherences become degenerate, and the spectrum has the following form:

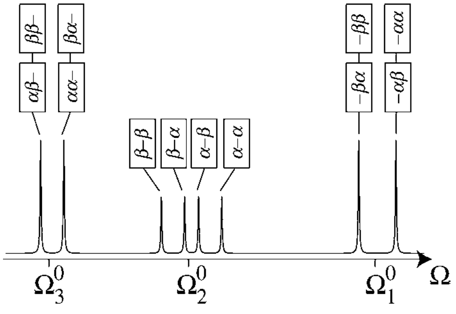

Figure 18.8
Assignment of AMX spectral peaks for a linear three-spin system, showing degeneracy.

This spectrum corresponds to the J-coupling parameters $J_{12} = 40\,\text{Hz}$, $J_{13} = 10\,\text{Hz}$ and $J_{23} = 0$.

If spins I_1 and I_3 are magnetically equivalent, then further degeneracy arises, since the chemical shift frequencies Ω_1^0 and Ω_3^0 are the same, and the J-couplings J_{12} and J_{23} are also identical. The spectrum has the following form in this case:

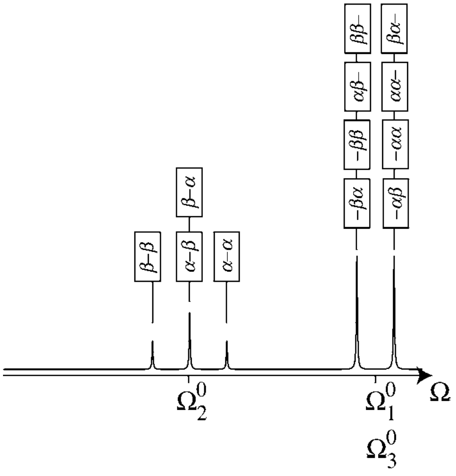

Figure 18.9
Assignment of spectral peaks for an AX$_2$ spin system.

This corresponds to an AX$_2$ spectrum with parameters $\Omega_1^0/2\pi = \Omega_3^0/2\pi = 300\,\text{Hz}, \Omega_2^0/2\pi = 100\,\text{Hz}$ and $J_{12} = J_{23} = 40\,\text{Hz}$.

This AX$_2$ spectrum reveals the J-coupled multiplet structure discussed in Section 3.8. The 'A' spin (I_2) is coupled to two magnetically equivalent 'X' spins (I_1 and I_3), providing a triplet multiplet structure, with amplitudes in the ratio 1:2:1. The 'X' spins (I_1 and I_3) are coupled to a single 'A' spin (I_2), so the 'X' spin peak is a doublet.

Note how the amplitude ratios of the multiplet components may be interpreted in terms of the degeneracies of the coherences. The central peak of the 'A' spin triplet is twice as intense as the two outer peaks, because it is generated by twice as many coherences.

The spectrum of the A$_2$X$_3$ ethanol spin system appears as follows (the J-coupling is exaggerated for clarity):

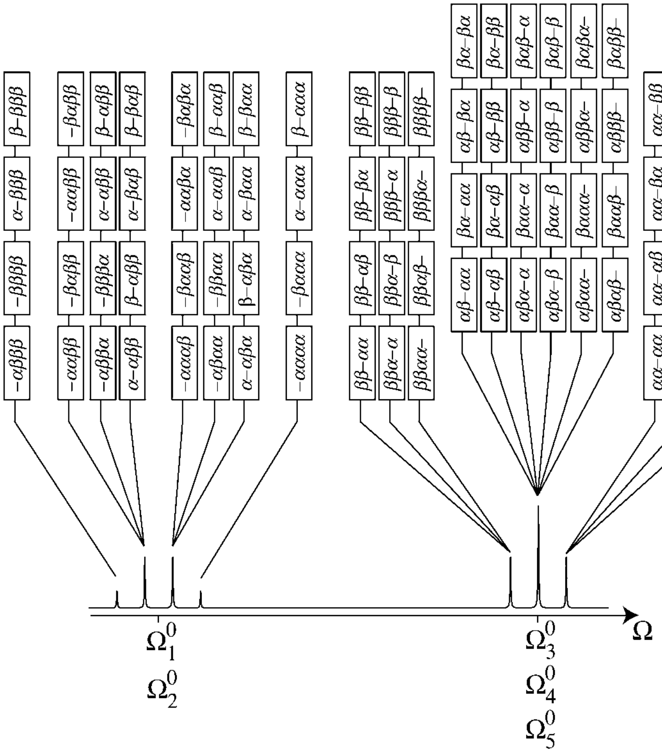

Figure 18.10
Assignment of spectral peaks for an A_2X_3 system.

The magnetic equivalence leads to a high degeneracy of the coherences. Even the smallest peaks in the spectrum contain contributions from four degenerate coherences, and the largest peak in the spectrum is 24-fold degenerate. The A-spin peak is a quartet, since each A spin is coupled to three X spins. The X-spin peak is a triplet, since each X spin is coupled to two A spins.

18.7 Many-Spin Product Operators

Spin dynamical calculations in weakly coupled spin-1/2 systems are greatly facilitated by the product operator formalism, introduced in Section 15.6. The formalism needs to be extended in order to handle systems of more than two coupled spins-1/2.

18.7.1 Construction of product operators

Product operators for an ensemble of N-spin-1/2 systems may be constructed through the following procedure:

$$\boxed{\begin{array}{l}\text{product}\\\text{operator}\end{array}} = 2^{(N-1)} \times \boxed{\begin{array}{l}\text{operator for}\\\text{spin } I_1\\\text{(4 choices)}\end{array}} \times \boxed{\begin{array}{l}\text{operator for}\\\text{spin } I_2\\\text{(4 choices)}\end{array}} \cdots \times \boxed{\begin{array}{l}\text{operator for}\\\text{spin } I_N\\\text{(4 choices)}\end{array}}$$

The choices for each operator are as follows:

$$\boxed{\begin{array}{l}\text{operator for}\\ \text{spin } I_j\\ \text{(4 choices)}\end{array}} = \begin{cases} \frac{1}{2}\widehat{1}_j \\ \hat{I}_{jx} \\ \hat{I}_{jy} \\ \hat{I}_{jz} \end{cases}$$

Products of unity operators may be eliminated; for example:

$$4 \times \frac{1}{2}\widehat{1}_1 \times \frac{1}{2}\widehat{1}_2 \times \frac{1}{2}\widehat{1}_3 = \frac{1}{2}\widehat{1}$$

$$4 \times \frac{1}{2}\widehat{1}_1 \times \hat{I}_{2z} \times \hat{I}_{3x} = 2\hat{I}_{2z}\hat{I}_{3x}$$

Some valid product operators in a three-spin-1/2 system are $\frac{1}{2}\widehat{1}$, $\hat{I}_{1z}$, $2\hat{I}_{2z}\hat{I}_{3x}$, $4\hat{I}_{1x}\hat{I}_{2z}\hat{I}_{3x}$. Some valid product operators in a five-spin-1/2 system are $\frac{1}{2}\widehat{1}$, $\hat{I}_{1z}$, $2\hat{I}_{2z}\hat{I}_{3x}$, $4\hat{I}_{1x}\hat{I}_{2z}\hat{I}_{3x}$, $8\hat{I}_{1x}\hat{I}_{2z}\hat{I}_{3x}\hat{I}_{4y}$, $16\hat{I}_{1z}\hat{I}_{2z}\hat{I}_{3z}\hat{I}_{4z}\hat{I}_{5z}$.

As usual, it is advisable to keep strict sequential order for the spin indices, and to keep the proper numerical prefactor together with the product operator.

18.7.2 Populations and coherences

In a system of N spins-1/2, each product operator term in the density operator consists of a superposition of 2^N coherences and populations. The use of product operators allows one to keep track of large groups of coherences and populations at the same time, permitting calculations in systems with large numbers of coupled spins.

Consider, for example, an AMX spin system. The product operator $\hat{I}_{1y}$ may be expanded as follows:

$$\begin{aligned}\hat{I}_{1y} &= 4 \times \hat{I}_{1y} \times \frac{1}{2}\widehat{1}_2 \times \frac{1}{2}\widehat{1}_3 \\ &= 4 \times \frac{1}{2\mathrm{i}}(\hat{I}_1^+ - \hat{I}_1^-) \times \frac{1}{2}(\hat{I}_2^\alpha + \hat{I}_2^\beta) \times \frac{1}{2}(\hat{I}_3^\alpha + \hat{I}_3^\beta) \\ &= \frac{1}{2\mathrm{i}}\left(\hat{I}_1^+\hat{I}_2^\alpha\hat{I}_3^\alpha - \hat{I}_1^-\hat{I}_2^\alpha\hat{I}_3^\alpha + \hat{I}_1^+\hat{I}_2^\alpha\hat{I}_3^\beta - \hat{I}_1^-\hat{I}_2^\alpha\hat{I}_3^\beta + \hat{I}_1^+\hat{I}_2^\beta\hat{I}_3^\alpha - \hat{I}_1^-\hat{I}_2^\beta\hat{I}_3^\alpha + \hat{I}_1^+\hat{I}_2^\beta\hat{I}_3^\beta - \hat{I}_1^-\hat{I}_2^\beta\hat{I}_3^\beta\right)\end{aligned}$$

If the density operator contains a term $\hat{I}_{1y}$, this implies the presence of coherences such as $\rho_{\boxed{+\alpha\alpha}}$, $\rho_{\boxed{+\alpha\beta}}$, and also observable (−1)-quantum coherences such as $\rho_{\boxed{-\alpha\alpha}}$ and $\rho_{\boxed{-\alpha\beta}}$.

Product operators such as $\hat{I}_y$, $2\hat{I}_{1y}\hat{I}_{2z}$, $2\hat{I}_{1y}\hat{I}_{3z}$ and $4\hat{I}_{1y}\hat{I}_{2z}\hat{I}_{3z}$ contain the same combinations of coherences, but with different relative phases. Consider again an AMX system, with all couplings resolved. If the AMX density operator contains a term proportional to $-\hat{I}_{1y}$ at the beginning of the detection interval, then the spectrum has the following appearance:

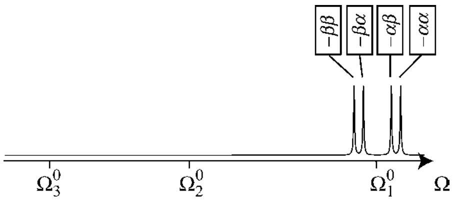

Figure 18.11
Spectrum associated with a product operator term $-\hat{I}_{1y}$, in an AMX system.

If the AMX density operator contains a term proportional to $-2\hat{I}_{1y}\hat{I}_{2z}$ at the beginning of the detection interval, then the spectrum has the following antiphase appearance:

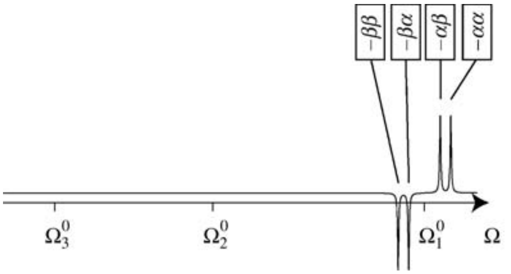

Figure 18.12
Spectrum associated with a product operator term $-2\hat{I}_{1y}\hat{I}_{2z}$, in an AMX system.

Note that peaks from coherences with different labels for spin I_2 have opposite sign.

A term proportional to $-2\hat{I}_{1y}\hat{I}_{3z}$ at the beginning of the detection interval generates a different sort of antiphase spectrum:

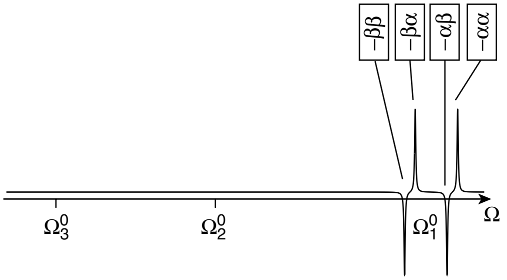

Figure 18.13
Spectrum associated with a product operator term $-2\hat{I}_{1y}\hat{I}_{3z}$, in an AMX system.

This time, the peaks from coherences with different labels for spin I_3 have opposite sign.

A term proportional to $-4\hat{I}_{1y}\hat{I}_{2z}\hat{I}_{3z}$ at the beginning of the detection interval generates a ‘doubly antiphase’ spectrum:

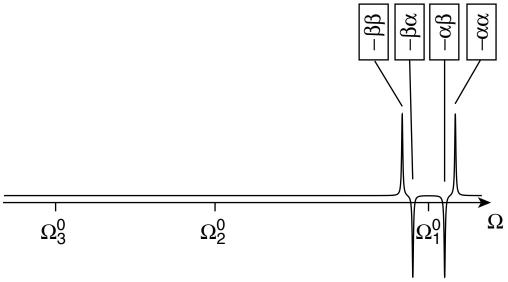

Figure 18.14
Spectrum associated with a product operator term $-4\hat{I}_{1y}\hat{I}_{2z}\hat{I}_{3z}$, in an AMX system.

The peak signs are inverted according to the labels of both spins I_2 and I_3.

In magnetically equivalent systems, the degenerate peaks may either reinforce or cancel each other. For example, consider an AX_2 system, in which I_1 and I_3 are magnetically equivalent. A product operator term $-\hat{I}_{1y}$ generates a spectrum with the following in-phase appearance:

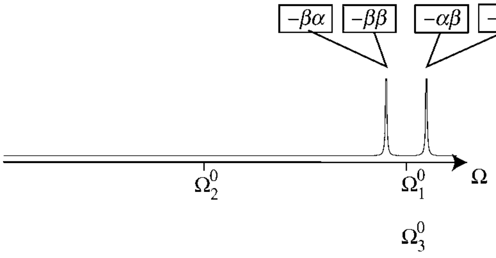

Figure 18.15
Spectrum associated with a product operator term $-\hat{I}_{1y}$, in an AX$_2$ system.

A product operator term $-2\hat{I}_{1y}\hat{I}_{2z}$ generates an antiphase spectrum:

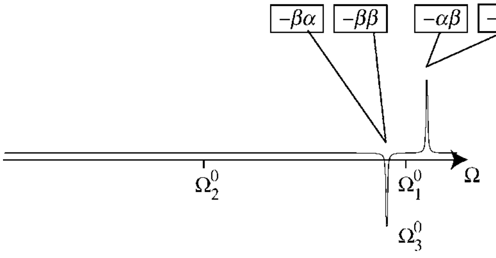

Figure 18.16
Spectrum associated with a product operator term $-2\hat{I}_{1y}\hat{I}_{2z}$, in an AX$_2$ system.

A product operator term $-2\hat{I}_{1y}\hat{I}_{3z}$, on the other hand, generates no signal at all, since the antiphase peaks from degenerate coherences such as $\rho_{\boxed{-\alpha\alpha}}$ and $\rho_{\boxed{-\alpha\beta}}$ have opposite sign and cancel exactly.[4]

Similarly, the central peak in the A-spin triplet of the AX$_2$ system vanishes for the antiphase spectrum generated by the term $-2\hat{I}_{1z}\hat{I}_{2y}$:

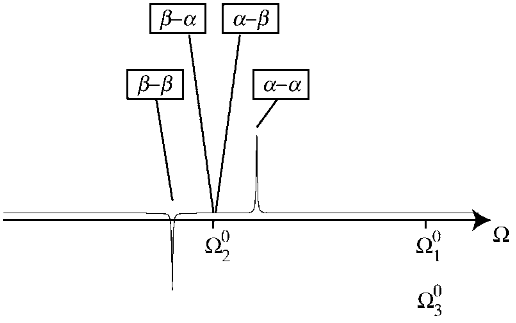

Figure 18.17
Spectrum associated with a product operator term $-2\hat{I}_{1z}\hat{I}_{2y}$, in an AX$_2$ system.

18.7.3 Physical interpretation of product operators

Product operators in systems of many coupled spins-1/2 have an analogous physical intepretation to that given in Section 15.6 for coupled spin pairs. Density operator terms such as $\hat{I}_{1x}$ indicate a partial alignment of spins I_1 with the x-axis. Density operator terms such as $2\hat{I}_{1x}\hat{I}_{2x}$ indicate that the x-components of the spin angular momenta for spins I_1 and I_2 are correlated.

Density operator terms such as $4\hat{I}_{1x}\hat{I}_{2x}\hat{I}_{3x}$ indicate three-way correlations. The presence of a term $4\hat{I}_{1x}\hat{I}_{2x}\hat{I}_{3x}$ in the density operator indicates that all three spins I_1, I_2 and I_3 tend to have the same polarization along the x-axis. This is depicted (in greatly exaggerated form) in the following diagram:

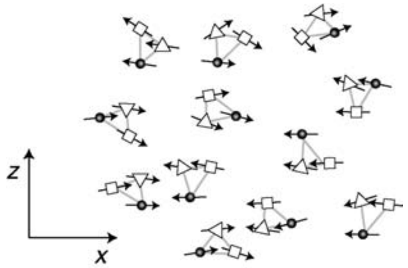

Figure 18.18
Physical interpretation of a density operator term $4\hat{I}_{1x}\hat{I}_{2x}\hat{I}_{3x}$.

18.8 Thermal Equilibrium

Thermal equilibrium in an ensemble of N-spin-1/2 systems corresponds to the usual Boltzmann distribution of populations (see Sections 11.3 and 15.7). In high magnetic field and at normal temperatures, the thermal equilibrium spin density operator of a homonuclear spin system may be approximated as follows:

$$\begin{aligned}\hat{\rho}^{\text{eq}} &\cong 2^{-N}\hat{1} + 2^{-N}\mathbb{B}\hat{I}_z \\ &= 2^{-N}\hat{1} + 2^{-N}\mathbb{B}\left(\hat{I}_{1z} + \hat{I}_{2z} + \ldots + \hat{I}_{Nz}\right)\end{aligned}$$

where $\mathbb{B}$ is the Boltzmann factor, $\mathbb{B} = \hbar\gamma B^0/k_B T$.

In many calculations, it is permissible to omit the unity operator and the numerical factors, and simply write

$$\hat{\rho}^{\text{eq}} \sim \hat{I}_z = \hat{I}_{1z} + \hat{I}_{2z} + \ldots + \hat{I}_{Nz}$$

In the case of heteronuclear spin systems, the Boltzmann factors are different for different spins. For example, the thermal equilibrium spin density operator for a heteronuclear I_2S system is written as

$$\hat{\rho}^{\text{eq}} \cong \frac{1}{8}\hat{1} + \frac{1}{8}\left(\mathbb{B}_I\hat{I}_{1z} + \mathbb{B}_I\hat{I}_{2z} + \mathbb{B}_S\hat{S}_{3z}\right)$$

where $\mathbb{B}_I = \hbar\gamma_I B^0/k_B T$ and $\mathbb{B}_S = \hbar\gamma_S B^0/k_B T$.

18.9 Radio Frequency Pulses

The transformation of a multiple-spin product operator by a strong r.f. pulse is easily calculated by rotating each of the individual operator terms. The technique is exactly the same as for two-spin product operators, as described in Section 15.8. The appropriate transformations for strong pulses with phases $\phi_\text{p} = 0$ and $\phi_\text{p} = \pi/2$ are summarized in Equations 15.6 and 15.7.

For example, a product operator term $4\hat{I}_{1z}\hat{I}_{2x}\hat{I}_{3y}$ is rotated by a non-selective $(\pi/2)_x$ pulse as follows:

$$4\hat{I}_{1z}\hat{I}_{2x}\hat{I}_{3y} \quad \xrightarrow{(\pi/2)_x} \quad 4(-\hat{I}_{1y})(\hat{I}_{2x})(\hat{I}_{3z}) = -4\hat{I}_{1y}\hat{I}_{2x}\hat{I}_{3z}$$

In heteronuclear spin systems, only the operators that belong to the resonant spin species are rotated; for example:

$$4\hat{I}_{1z}\hat{I}_{2x}\hat{S}_{3y} \quad \xrightarrow{(\pi/2)_x^I} \quad 4(-\hat{I}_{1y})(\hat{I}_{2x})(\hat{S}_{3y}) = -4\hat{I}_{1y}\hat{I}_{2x}\hat{S}_{3y}$$

$$4\hat{I}_{1z}\hat{I}_{2x}\hat{S}_{3y} \xrightarrow{(\pi/2)_x^S} 4\hat{I}_{1z}\hat{I}_{2x}\hat{S}_{3z}$$

18.10 Free Precession

If relaxation is ignored, the evolution of a multiple-spin product operator under an interval of free evolution may be deduced by extending the treatment in Section 15.9.

For weakly coupled systems, the calculation of product operator evolution may be split up into separate sub-calculations for the evolution under each chemical shift frequency, and under each J-coupling. These sub-calculations may be taken in any order, since the corresponding spin propagators commute.

For example, in an AMX system, the evolution of a particular product operator term over an interval τ may be calculated by the following sequence of transformations:

$$\xrightarrow{\Omega_1^0\tau} \quad \xrightarrow{\Omega_2^0\tau} \quad \xrightarrow{\Omega_3^0\tau} \quad \xrightarrow{\pi J_{12}\tau} \quad \xrightarrow{\pi J_{13}\tau} \quad \xrightarrow{\pi J_{23}\tau}$$

18.10.1 Chemical shift evolution

The evolution under a chemical shift term is readily calculated by rotating the appropriate spin operator I_j through the angle $\Omega_j^0\tau$ about the z-axis. The appropriate transformations are given in Equation 15.22.

The calculation is repeated for each spin operator in the product.

For example, the chemical shift evolution of the product operator term $4\hat{I}_{1z}\hat{I}_{2x}\hat{I}_{3y}$ in an AMX system is as follows:

$$\begin{tikzcd}
4\hat{I}_{1z}\hat{I}_{2x}\hat{I}_{3y} \arrow[d, "\Omega_1^0\tau"] \\
4\hat{I}_{1z}\hat{I}_{2x}\hat{I}_{3y} \arrow[d, "\Omega_2^0\tau"] \\
4\hat{I}_{1z}(\hat{I}_{2x}\cos\Omega_2^0\tau + \hat{I}_{2y}\sin\Omega_2^0\tau)\hat{I}_{3y} \arrow[d, "\Omega_3^0\tau"] \\
4\hat{I}_{1z}(\hat{I}_{2x}\cos\Omega_2^0\tau + \hat{I}_{2y}\sin\Omega_2^0\tau)(\hat{I}_{3y}\cos\Omega_3^0\tau - \hat{I}_{3x}\sin\Omega_3^0\tau)
\end{tikzcd}$$

or, to summarize:

$$\begin{tikzcd}
4\hat{I}_{1z}\hat{I}_{2x}\hat{I}_{3y} \arrow[d, "\Omega_1^0\tau"] \\
{} \arrow[d, "\Omega_2^0\tau"] \\
{} \arrow[d, "\Omega_3^0\tau"] \\
\begin{array}{c} 4\hat{I}_{1z}\hat{I}_{2x}\hat{I}_{3y}\cos\Omega_2^0\tau\,\cos\Omega_3^0\tau + 4\hat{I}_{1z}\hat{I}_{2y}\hat{I}_{3y}\sin\Omega_2^0\tau\,\cos\Omega_3^0\tau \\ -4\hat{I}_{1z}\hat{I}_{2x}\hat{I}_{3x}\cos\Omega_2^0\tau\,\sin\Omega_3^0\tau - 4\hat{I}_{1z}\hat{I}_{2y}\hat{I}_{3x}\sin\Omega_2^0\tau\,\sin\Omega_3^0\tau \end{array}
\end{tikzcd}$$

18.10.2 *J*-coupling evolution

The calculation of J-coupling evolution in multiple-spin product operators exploits the commutation relationships summarized in Equations 15.23 and 15.24.

Suppose that we wish to calculate the transformation under the J-coupling between spins I_j and I_k over the interval τ. The product operator does *not* evolve under the coupling J_{jk} in the following cases:

1. If both spins I_j and I_k are missing in the product operator.
2. If only one spin I_j or I_k is present, and that spin carries a z label.
3. If both spins I_j or I_k are present, but *both* spins carry a z label.
4. If both spins I_j or I_k are present, but *neither* spin carries a z label.

Some examples of these cases are as follows:

$$\begin{array}{rcll}
\hat{I}_{3y} & \xrightarrow{\pi J_{12}\tau} & \hat{I}_{3y} & \text{(case 1)} \\
\hat{I}_{2z} & \xrightarrow{\pi J_{12}\tau} & \hat{I}_{2z} & \text{(case 2)} \\
2\hat{I}_{1z}\hat{I}_{3y} & \xrightarrow{\pi J_{12}\tau} & 2\hat{I}_{1z}\hat{I}_{3y} & \text{(case 2)} \\
2\hat{I}_{1z}\hat{I}_{2z} & \xrightarrow{\pi J_{12}\tau} & 2\hat{I}_{1z}\hat{I}_{2z} & \text{(case 3)} \\
2\hat{I}_{2x}\hat{I}_{3x} & \xrightarrow{\pi J_{23}\tau} & 2\hat{I}_{2x}\hat{I}_{3x} & \text{(case 4)} \\
2\hat{I}_{1y}\hat{I}_{3x} & \xrightarrow{\pi J_{13}\tau} & 2\hat{I}_{1y}\hat{I}_{3x} & \text{(case 4)} \\
4\hat{I}_{1y}\hat{I}_{2x}\hat{I}_{3z} & \xrightarrow{\pi J_{12}\tau} & 4\hat{I}_{1y}\hat{I}_{2x}\hat{I}_{3z} & \text{(case 4)}
\end{array}$$

In all *other* cases, the product operator does evolve under the relevant J-coupling, and the appropriate transformation may be deduced using Equation 15.23.

For example, consider the transformation of $4\hat{I}_{1y}\hat{I}_{2x}\hat{I}_{3z}$ under the coupling J_{23}. The product operator may be written as

$$4\hat{I}_{1y}\hat{I}_{2x}\hat{I}_{3z} = 2\hat{I}_{1y}(2\hat{I}_{2x}\hat{I}_{3z})$$

The following diagram may be used to deduce the J-coupling evolution of the bracketed term:

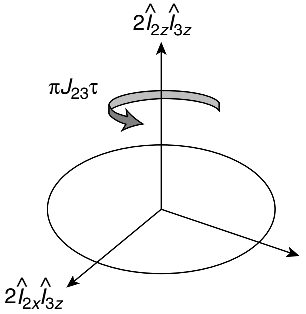

Figure 18.19 Cyclic commutation diagram used for calculating the evolution of $2\hat{I}_{2x}\hat{I}_{3z}$ under J_{23}.

This leads to

$$\begin{tikzcd}
2\hat{I}_{1y}(2\hat{I}_{2x}\hat{I}_{3z}) \arrow[d, "\pi J_{23}\tau"] \\
2\hat{I}_{1y}\left(2\hat{I}_{2x}\hat{I}_{3z}\cos\pi J_{23}\tau + \hat{I}_{2y}\sin\pi J_{23}\tau\right)
\end{tikzcd}$$

or to summarize:

$$\begin{tikzcd}
4\hat{I}_{1y}\hat{I}_{2x}\hat{I}_{3z} \arrow[d, "\pi J_{23}\tau"] \\
4\hat{I}_{1y}\hat{I}_{2x}\hat{I}_{3z}\cos\pi J_{23}\tau + 2\hat{I}_{1y}\hat{I}_{2y}\sin\pi J_{23}\tau
\end{tikzcd}$$

The evolution of the term $4\hat{I}_{1y}\hat{I}_{2x}\hat{I}_{3z}$ under all three J-couplings may be deduced by putting all of these arguments together:

$$\begin{tikzcd}
4\hat{I}_{1y}\hat{I}_{2x}\hat{I}_{3z} \arrow[d, "\pi J_{12}\tau"] \\
{}
\end{tikzcd}$$

$$\begin{tikzcd}
4\hat{I}_{1y}\hat{I}_{2x}\hat{I}_{3z} \arrow[d, "\pi J_{23}\tau"] \\
4\hat{I}_{1y}\hat{I}_{2x}\hat{I}_{3z}\cos\pi J_{23}\tau + 2\hat{I}_{1y}\hat{I}_{2y}\sin\pi J_{23}\tau \arrow[d, "\pi J_{13}\tau"] \\
\begin{array}{c} 4\hat{I}_{1y}\hat{I}_{2x}\hat{I}_{3z}\cos\pi J_{23}\tau\ \cos\pi J_{13}\tau - 2\hat{I}_{1x}\hat{I}_{2x}\cos\pi J_{23}\tau\ \sin\pi J_{13}\tau \\ +2\hat{I}_{1y}\hat{I}_{2y}\sin\pi J_{23}\tau\ \cos\pi J_{13}\tau - 4\hat{I}_{1x}\hat{I}_{2y}\hat{I}_{3z}\sin\pi J_{23}\tau\ \sin\pi J_{13}\tau \end{array}
\end{tikzcd}$$

18.10.3 Relaxation

In practice, the precession of the coherences is accompanied by decay. In simple cases, the coherence decay may be taken into account by multiplying each product operator term with an exponential decay factor. However, this procedure is invalid if the different coherences that make up a given product operator term have different decay time constants (see Section 20.8).

18.11 Spin Echo Sandwiches

Spin echo sandwiches may be used to simplify the evolution of product operator terms, as described in Section 15.10. Under suitable conditions (see Appendix A.10), chemical shift terms are suppressed, and the propagation may be calculated using a π rotation of all spin operators, followed by an interval of free evolution under the J-couplings alone.

For example, the evolution of the term $4\hat{I}_{1y}\hat{I}_{2x}\hat{I}_{3z}$ under a spin echo sandwich (SES) containing a central π_x pulse is as follows:

$$\begin{tikzcd}
4\hat{I}_{1y}\hat{I}_{2x}\hat{I}_{3z} \arrow[d, "\pi_x"] \\
4(-\hat{I}_{1y})\hat{I}_{2x}(-\hat{I}_{3z}) = 4\hat{I}_{1y}\hat{I}_{2x}\hat{I}_{3z} \arrow[d, "\pi J_{12}\tau"] \\
4\hat{I}_{1y}\hat{I}_{2x}\hat{I}_{3z}
\end{tikzcd}$$

$$\begin{tikzcd}
{} \arrow[d, "\pi J_{13}\tau"] \\
4\hat{I}_{1y}\hat{I}_{2x}\hat{I}_{3z}\cos\pi J_{13} - 2\hat{I}_{1x}\hat{I}_{2x}\sin\pi J_{13} \arrow[d, "\pi J_{23}\tau"] \\
\begin{array}{c} 4\hat{I}_{1y}\hat{I}_{2x}\hat{I}_{3z}\cos\pi J_{13}\tau\ \cos\pi J_{23}\tau + 2\hat{I}_{1y}\hat{I}_{2y}\cos\pi J_{13}\tau\ \sin\pi J_{23}\tau \\ -2\hat{I}_{1x}\hat{I}_{2x}\sin\pi J_{13}\tau\ \cos\pi J_{23}\tau - 4\hat{I}_{1x}\hat{I}_{2y}\hat{I}_{3z}\sin\pi J_{13}\tau\ \sin\pi J_{23}\tau \end{array}
\end{tikzcd}$$

or in summary:

$$\begin{tikzcd}
4\hat{I}_{1y}\hat{I}_{2x}\hat{I}_{3z} \arrow[d, "\text{SES}"] \\
\begin{array}{c} 4\hat{I}_{1y}\hat{I}_{2x}\hat{I}_{3z}\cos\pi J_{13}\tau\ \cos\pi J_{23}\tau + 2\hat{I}_{1y}\hat{I}_{2y}\cos\pi J_{13}\tau\ \sin\pi J_{23}\tau \\ -2\hat{I}_{1x}\hat{I}_{2x}\sin\pi J_{13}\tau\ \cos\pi J_{23}\tau - 4\hat{I}_{1x}\hat{I}_{2y}\hat{I}_{3z}\sin\pi J_{13}\tau\ \sin\pi J_{23}\tau \end{array}
\end{tikzcd}$$

In the case that all J-couplings between magnetically inequivalent spins have the same magnitude, a particularly simple effect is obtained when the spin echo sandwich has a duration $\tau = |(2J)^{-1}|$. Each product operator is transformed into only one term. Consider, for example, the product operator $4\hat{I}_{1z}\hat{I}_{2x}\hat{I}_{3y}$ in the A_2X_3 system of the protons in ethanol. As shown in Figure 18.20, this term propagates as follows:

$$\begin{tikzcd}
4\hat{I}_{1z}\hat{I}_{2x}\hat{I}_{3y} \arrow[d, "\text{SES}"] \\
8(-\hat{I}_{2x})(-\hat{I}_{3x})(+\hat{I}_{4z})(+\hat{I}_{5z}) = 8\hat{I}_{2x}\hat{I}_{3x}\hat{I}_{4z}\hat{I}_{5z}
\end{tikzcd}$$

Note that the final result of this propagation depends strongly on the topology of the coupling network.[5]

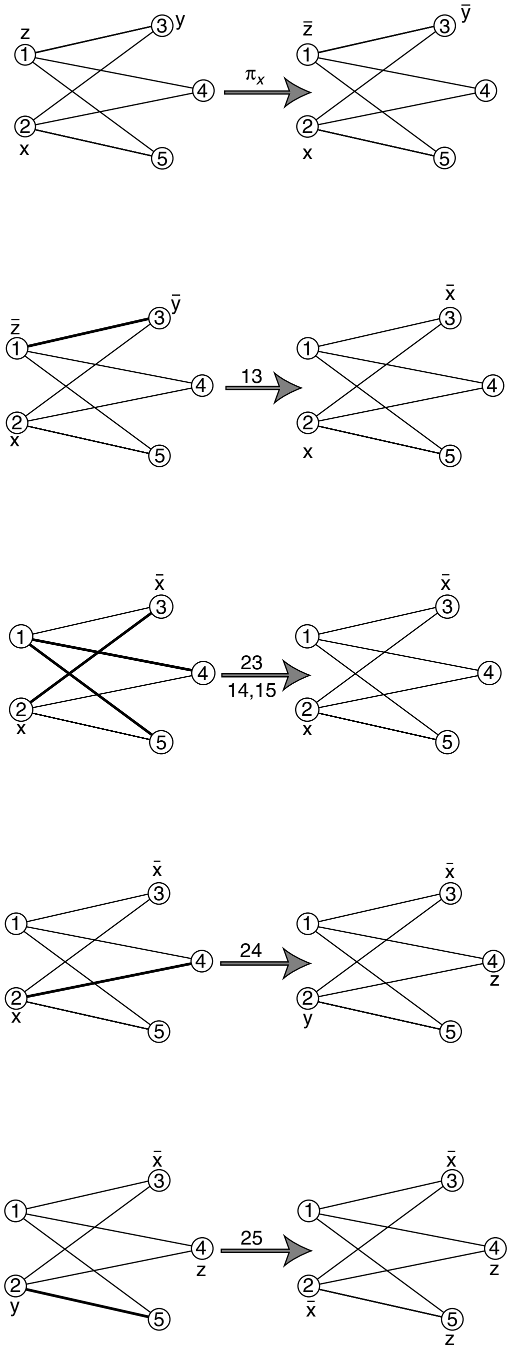

Figure 18.20
Propagation of a product operator in a A_2X_3, system, assuming positive *J*-couplings.

18.12 INEPT in an I_2S System

Consider the refocused INEPT pulse sequence (see Section 16.3):

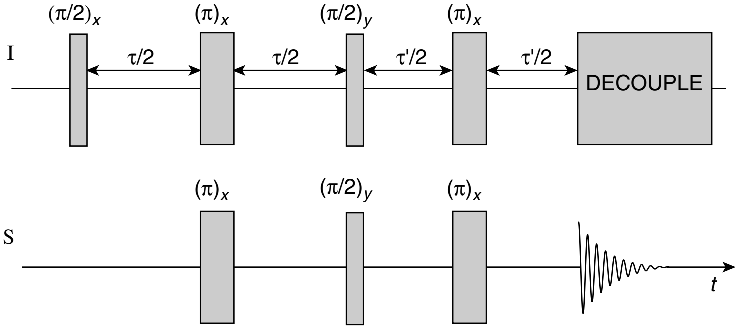

Figure 18.21 Refocused INEPT pulse sequence.

Assume that the two spin echo sandwiches have different durations, denoted τ and τ'. The first spin echo sandwich has duration $\tau = |(2J_{IS})^{-1}|$, and the second interval τ' may be chosen freely. The pulse sequence may be analysed using the following simplified form:

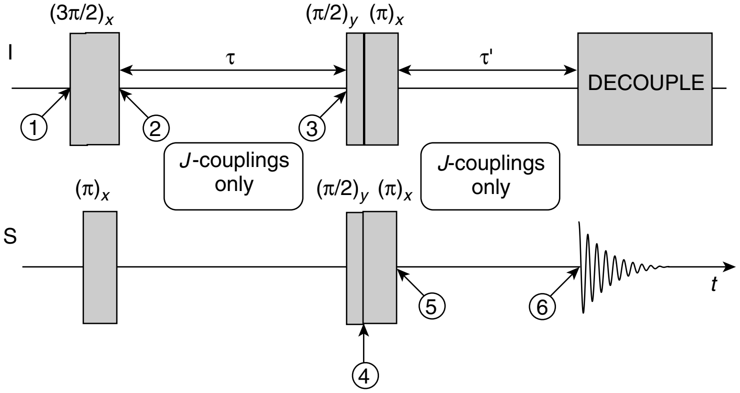

Figure 18.22 Simplification of the refocused INEPT pulse sequence.

Suppose that the pulse sequence is applied to an ensemble of I_2S spin systems, each consisting of three spins I_1, I_2 and S_3. For simplicity, assume that the two I-spins are magnetically equivalent.

The initial spin density operator of the I_2S system is

$$\hat{\rho}_{①} = \frac{1}{8}\hat{1} + \frac{1}{8}\mathbb{B}_I(\hat{I}_{1z} + \hat{I}_{2z}) + \frac{1}{8}\mathbb{B}_S\hat{S}_{3z} \tag{18.5}$$

The thermal equilibrium S-spin magnetization and the unity operator may be dropped for simplicity, leading to the simplified expression

$$\hat{\rho}_{①} = \frac{1}{8}\mathbb{B}_I(\hat{I}_{1z} + \hat{I}_{2z}) + \ldots$$

If relaxation is ignored, then the propagation of the spin density operator during the first half of the pulse sequence is as follows:

$$\begin{tikzcd}
\hat{\rho}_{\textcircled{1}} = \tfrac{1}{8}\mathbb{B}_I(\hat{I}_{1z} + \hat{I}_{2z}) + \ldots \arrow[d, "(3\pi/2)^I_x;\, \pi^S_x"] \\
\hat{\rho}_{\textcircled{2}} = \tfrac{1}{8}\mathbb{B}_I(\hat{I}_{1y} + \hat{I}_{2y}) + \ldots \arrow[d, "\tau"', "(J\text{-couplings only})"] \\
\hat{\rho}_{\textcircled{3}} = -\tfrac{1}{8}\mathbb{B}_I(2\hat{I}_{1x}\hat{S}_{3z} + 2\hat{I}_{2x}\hat{S}_{3z}) + \ldots \arrow[d, "(\pi/2)^I_y,\, (\pi/2)^S_y"] \\
\hat{\rho}_{\textcircled{4}} = \tfrac{1}{8}\mathbb{B}_I(2\hat{I}_{1z}\hat{S}_{3x} + 2\hat{I}_{2z}\hat{S}_{3x}) + \ldots
\end{tikzcd}$$

This shows that the thermal equilibrium I-spin magnetization is converted into antiphase transverse S-spin magnetization.

Each of the product operator terms in $\hat{\rho}_{\textcircled{4}}$ continues to propagate as follows:

$$\begin{tikzcd}
2\hat{I}_{1z}\hat{S}_{3x} \arrow[d, "\pi^I_x;\, \pi^S_x"] \\
-2\hat{I}_{1z}\hat{S}_{3x} \arrow[d, "\pi J_{13}\tau'"] \\
-2\hat{I}_{1z}\hat{S}_{3x}\cos\pi J_{13}\tau' - \hat{S}_{3y}\sin\pi J_{13}\tau' \arrow[d, "\pi J_{23}\tau'"] \\
\begin{array}{c} -2\hat{I}_{1z}\hat{S}_{3x}\cos\pi J_{13}\tau'\ \cos\pi J_{23}\tau' - 4\hat{I}_{1z}\hat{I}_{2z}\hat{S}_{3y}\cos\pi J_{13}\tau'\ \sin\pi J_{23}\tau' \\ -\hat{S}_{3y}\sin\pi J_{13}\tau'\ \cos\pi J_{23}\tau' + 2\hat{I}_{2z}\hat{S}_{3x}\sin\pi J_{13}\tau'\ \sin\pi J_{23}\tau' \end{array}
\end{tikzcd}$$

The propagation of the spin density operator through the entire sequence, therefore, may be written as

$$\hat{\rho}_{\textcircled{1}} = \tfrac{1}{8}\mathbb{B}_I(\hat{I}_{1z} + \hat{I}_{2z}) + \ldots$$

$$\Big\downarrow$$

$$\begin{aligned}\hat{\rho}_{\textcircled{6}} &= -\tfrac{1}{8}\mathbb{B}_I\hat{S}_{3y}(2\sin\pi J_{13}\tau' \ \cos\pi J_{23}\tau') + \ldots \\ &= -\tfrac{1}{8}\mathbb{B}_I\hat{S}_{3y}\sin(2\pi J_{13}\tau') + \ldots\end{aligned}$$

The other terms have been dropped from the density operator because they generate antiphase S-spin signals that cancel out when a decoupling field is applied to the I-spins.

The transferred signal is maximized by adjusting the duration of the second spin echo sandwich to the value $\tau' = |(4J_{IS})^{-1}|$. The final density operator is then

$$\hat{\rho}_{\textcircled{7}} = -\frac{1}{8}\mathbb{B}_I\hat{S}_{3y} + \ldots \tag{18.6}$$

This may be contrasted with the thermal equilibrium S-spin term in Equation 18.5, which has a factor $\frac{1}{8}\mathbb{B}_S$. When τ' is given by $\tau' = |(4J_{IS})^{-1}|$, the S-spin magnetization is enhanced by a factor γ_I/γ_S, compared with its thermal equilibrium value.

This shows that, in this idealized case, refocused INEPT leads to the same maximum enhancement of the S-spin signal for I_2S and IS spin systems, but that the optimal duration of the second spin echo is different in the two cases. The optimal duration τ' for an I_2S system is one-half of the optimal duration for an IS spin system (assuming equal coupling constants).

If the arguments are repeated for an idealized I_3S spin system, consisting of three chemically equivalent spins I_1, I_2, I_3 and a fourth spin S_4, we obtain a final spin density operator given by

$$\hat{\rho}_{\textcircled{7}} = -\frac{1}{8}\mathbb{B}_I\hat{S}_{4y} \times 3\sin(\pi J_{13}\tau')\cos^2(\pi J_{13}\tau') + \ldots$$

The enhancement reaches a maximum value of $2\gamma_I/\sqrt{3}\gamma_S = 1.155\gamma_I/\gamma_S$ for the pulse sequence interval $\tau' = \left\{\cos^{-1}\sqrt{2/3}\right\}/(\pi J_{IS})$. Therefore, it is possible to enhance the S-spin magnetization by slightly more than the ratio γ_I/γ_S, in the case of an ideal I_3S spin system.

The refocused INEPT enhancement factors for IS, I_2S and I_3S spin systems are sketched below as a function of the interval τ':

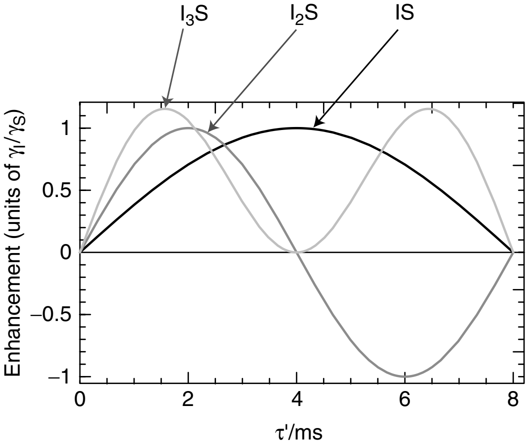

Figure 18.23
Enhancements of the S-spin magnetization by a refocused INEPT pulse sequence, for IS, I_2S and I_3S spin systems, with $J_{IS} = 125\,\text{Hz}$.

Note that the optimal value of τ' depends on the type of spin system.

In reality, most spin systems contain a distribution of J-couplings, and there are also relaxation effects. The optimum pulse sequence intervals and the enhancements achieved depend strongly on the practical spin system.

A variety of pulse sequences have been described which are less sensitive than INEPT to deviations of the J-couplings from the 'ideal' or expected values, and which are also less sensitive to the type of spin system (see *Further Reading*).

An interesting question is whether the enhancements achieved by refocused INEPT are the maximum possible, even in principle. Can one do better by using a different pulse sequence? For example, in an I_3S spin system, is it possible to transfer the sum magnetization of *all three* I-spins to the S-spin, leading to a very large enhancement? These deceptively simple questions lead into a lively field of research concerned with the *theoretical bounds on operator transformations*. See *Further Reading* for some references and the answer to the above question.

18.13 COSY in Multiple-Spin Systems

We now examine what happens when the COSY pulse sequence, described in Section 16.1, is applied to weakly coupled systems with more than two coupled spins-1/2. The product operator formalism is used to treat the two-dimensional spectrum.

The pulse sequence for COSY is given by:

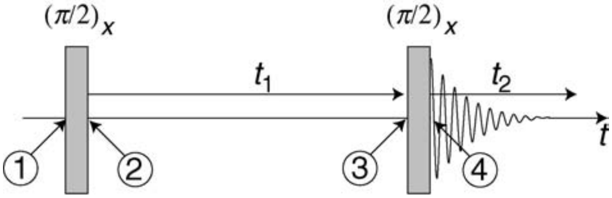

Figure 18.24
COSY pulse sequence.

This provides the 'cosine' signal in the States procedure (Section 5.9.4). The 'sine' signal is obtained by changing the phase of the first pulse to $\overline{y}$ (see Note 6).

18.13.1 AMX spectrum

Consider first an AMX spin system. The initial spin density operator is

$$\hat{\rho}_{\textcircled{1}} \sim \hat{I}_z = \hat{I}_{1z} + \hat{I}_{2z} + \hat{I}_{3z} \tag{18.7}$$

omitting the unity operator and numerical factors. Consider the fate of the first term, under the 'cosine' pulse sequence (phase x for the first pulse):

$$\hat{\rho}_{\textcircled{1}} = \hat{I}_{1z} + \ldots$$

$$\Bigg\downarrow (\pi/2)_x$$

$$\hat{\rho}^{\cos}_{\textcircled{2}} = -\hat{I}_{1y} + \ldots$$

$$\Bigg\downarrow t_1$$

$$\begin{aligned}
\hat{\rho}^{\cos}_{\textcircled{3}} = {} & -\hat{I}_{1y}\cos(\Omega_1^0 t_1)\cos(\pi J_{12} t_1)\cos(\pi J_{13} t_1) + \hat{I}_{1x}\sin(\Omega_1^0 t_1)\cos(\pi J_{12} t_1)\cos(\pi J_{13} t_1) \\
& + 2\hat{I}_{1x}\hat{I}_{2z}\cos(\Omega_1^0 t_1)\sin(\pi J_{12} t_1)\cos(\pi J_{13} t_1) + 2\hat{I}_{1y}\hat{I}_{2z}\sin(\Omega_1^0 t_1)\sin(\pi J_{12} t_1)\cos(\pi J_{13} t_1) \\
& + 2\hat{I}_{1x}\hat{I}_{3z}\cos(\Omega_1^0 t_1)\cos(\pi J_{12} t_1)\sin(\pi J_{13} t_1) + 2\hat{I}_{1y}\hat{I}_{3z}\sin(\Omega_1^0 t_1)\cos(\pi J_{12} t_1)\sin(\pi J_{13} t_1) \\
& + 4\hat{I}_{1y}\hat{I}_{2z}\hat{I}_{3z}\cos(\Omega_1^0 t_1)\sin(\pi J_{12} t_1)\sin(\pi J_{13} t_1) - 4\hat{I}_{1x}\hat{I}_{2z}\hat{I}_{3z}\sin(\Omega_1^0 t_1)\sin(\pi J_{12} t_1)\sin(\pi J_{13} t_1) + \ldots
\end{aligned} \tag{18.8}$$

The second $(\pi/2)_x$ pulse transforms the product operators as follows:

$$\hat{\rho}^{\cos}_{\textcircled{3}}$$

$$\Bigg\downarrow (\pi/2)_x$$

$$\begin{aligned}
\hat{\rho}^{\cos}_{\textcircled{4}} = {} & -\hat{I}_{1z}\cos(\Omega_1^0 t_1)\cos(\pi J_{12} t_1)\cos(\pi J_{13} t_1) + \hat{I}_{1x}\sin(\Omega_1^0 t_1)\cos(\pi J_{12} t_1)\cos(\pi J_{13} t_1) \\
& - 2\hat{I}_{1x}\hat{I}_{2y}\cos(\Omega_1^0 t_1)\sin(\pi J_{12} t_1)\cos(\pi J_{13} t_1) - 2\hat{I}_{1z}\hat{I}_{2y}\sin(\Omega_1^0 t_1)\sin(\pi J_{12} t_1)\cos(\pi J_{13} t_1) \\
& - 2\hat{I}_{1x}\hat{I}_{3y}\cos(\Omega_1^0 t_1)\cos(\pi J_{12} t_1)\sin(\pi J_{13} t_1) - 2\hat{I}_{1z}\hat{I}_{3y}\sin(\Omega_1^0 t_1)\cos(\pi J_{12} t_1)\sin(\pi J_{13} t_1) \\
& + 4\hat{I}_{1z}\hat{I}_{2y}\hat{I}_{3y}\cos(\Omega_1^0 t_1)\sin(\pi J_{12} t_1)\sin(\pi J_{13} t_1) - 4\hat{I}_{1x}\hat{I}_{2y}\hat{I}_{3y}\sin(\Omega_1^0 t_1)\sin(\pi J_{12} t_1)\sin(\pi J_{13} t_1) + \ldots
\end{aligned}$$

For simplicity, suppress all terms that do not contain observable (simple) (−1)-quantum coherences:

$$\begin{aligned}
\hat{\rho}^{\cos}_{\textcircled{4}} = {} & +\hat{I}_{1x}\sin(\Omega_1^0 t_1)\cos(\pi J_{12} t_1)\cos(\pi J_{13} t_1) \\
& - 2\hat{I}_{1z}\hat{I}_{2y}\sin(\Omega_1^0 t_1)\sin(\pi J_{12} t_1)\cos(\pi J_{13} t_1) \\
& - 2\hat{I}_{1z}\hat{I}_{3y}\sin(\Omega_1^0 t_1)\cos(\pi J_{12} t_1)\sin(\pi J_{13} t_1) + \ldots
\end{aligned} \tag{18.9}$$

These terms correspond to the following spectral features:

1. The *first* term in Equation 18.9 is proportional to $\hat{I}_{1x}$ and contains (-1)-quantum coherences of spin I_1. These coherences precess at frequencies close to Ω_1^0 during the detection interval t_2. Since this term is also modulated at frequencies close to Ω_1^0 during the evolution interval t_1, the first term generates a *diagonal peak* in the two-dimensional spectrum, with frequency coordinates around $(\Omega_1, \Omega_2) = (\Omega_1^0, \Omega_1^0)$.

2. The *second* term in Equation 18.9 is proportional to $-2\hat{I}_{1z}\hat{I}_{2y}$ and contains (-1)-quantum coherences of spin I_2. These coherences precess at frequencies close to Ω_2^0 during the detection interval t_2. Since this term is modulated at frequencies close to Ω_1^0 during the evolution interval t_1, the second term generates a *cross-peak* in the two-dimensional spectrum, with frequency coordinates around $(\Omega_1, \Omega_2) = (\Omega_1^0, \Omega_2^0)$.

3. The *third* term in Equation 18.9 is proportional to $-2\hat{I}_{1z}\hat{I}_{3y}$ and contains (-1)-quantum coherences of spin I_3. It resembles the second term and generates a *cross-peak* in the two-dimensional spectrum, with frequency coordinates around $(\Omega_1, \Omega_2) = (\Omega_1^0, \Omega_3^0)$.

The complete two-dimensional spectrum has the following schematic appearance:

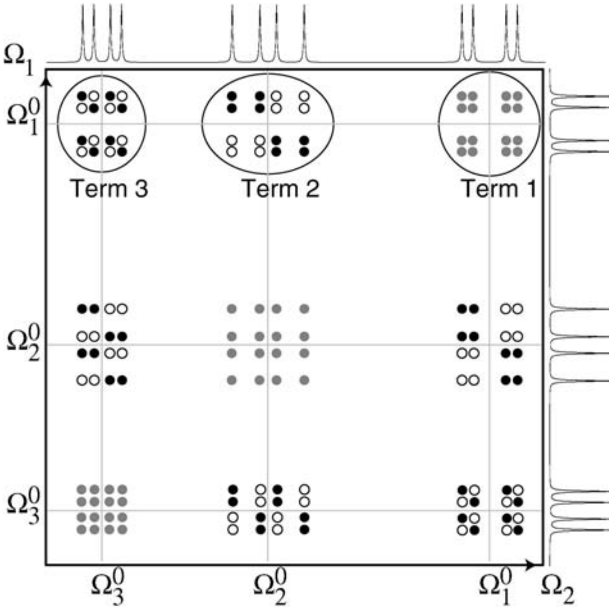

Figure 18.25
Form of the COSY spectrum for an AMX spin system.

This is shown for the case $\Omega_1^0/2\pi = 300\,\text{Hz}$, $\Omega_2^0/2\pi = 100\,\text{Hz}$, $\Omega_3^0/2\pi = -50\,\text{Hz}$, $J_{12} = 40\,\text{Hz}$, $J_{13} = 10\,\text{Hz}$ and $J_{23} = 25\,\text{Hz}$. Positive absorption peaks are indicated by black circles, negative absorption peaks are indicated by white circles, and dispersion peaks are indicated by grey circles. The multiplets generated by the three terms in Equation 18.9 are indicated by the ellipses. The remaining signals in the two-dimensional spectrum are generated by the $\hat{I}_{2z}$ and $\hat{I}_{3z}$ operators in Equation 18.7.

18.13.2 Active and passive spins

In Section 18.4, a definition of active and passive spins was given for *individual* coherences. For example, spin I_1 is active in coherence $\rho_{\boxed{-\alpha\alpha}}$, whereas spins I_2 and I_3 are passive in the same coherence.

The definition of active and passive spins will now be widened to encompass *coherence transfer processes*, i.e. the transfer of amplitude from one coherence into another. The expanded definition is as follows:

1. If a spin is active in *any* of the participating coherences, then that spin is said to be *active in the coherence transfer process.*

2. If a spin is passive in *both* of the participating coherences, then that spin is said to be *passive in the coherence transfer process*.

For example, spins I_1 and I_2 are active in the coherence transfer process $\rho_{\boxed{-\alpha\alpha}} \rightarrow \rho_{\boxed{\alpha-\alpha}}$, whereas spin I_3 is passive in the same process.

Consider now the second term in Equation 18.9, which is associated with the transformation of the density operator term $+2\hat{I}_{1y}\hat{I}_{2z}$ into $-2\hat{I}_{1z}\hat{I}_{2y}$ by the second $(\pi/2)_x$ pulse. Since spin I_1 is active in all coherences contained in $+2\hat{I}_{1y}\hat{I}_{2z}$, and spin I_2 is active in all terms contained in $-2\hat{I}_{1z}\hat{I}_{2y}$, one says that spins I_1 and I_2 are active in the transfer process $+2\hat{I}_{1y}\hat{I}_{2z} \rightarrow -2\hat{I}_{1z}\hat{I}_{2y}$. Since spin I_3 is passive for all coherences contained in both terms $+2\hat{I}_{1y}\hat{I}_{2z}$ and $-2\hat{I}_{1z}\hat{I}_{2y}$, one says that spin I_3 is passive in the same process $+2\hat{I}_{1y}\hat{I}_{2z} \rightarrow -2\hat{I}_{1z}\hat{I}_{2y}$.

The third term in Equation 18.9 is associated with the transformation of the density operator term $+2\hat{I}_{1y}\hat{I}_{3z}$ into $-2\hat{I}_{1z}\hat{I}_{3y}$ by the second $(\pi/2)_x$ pulse. In this case, spins I_1 and I_3 are active, while spin I_2 is passive.

18.13.3 Cross-peak multiplets

Examine the second term in Equation 18.9 more closely:

$$\hat{\rho}^{\cos}_{\textcircled{4}} = -2\hat{I}_{1z}\hat{I}_{2y}\sin(\Omega_1^0 t_1)\sin(\pi J_{12}t_1)\cos(\pi J_{13}t_1) + \ldots \qquad (18.10)$$

The form of this term (proportional to $-2\hat{I}_{1z}\hat{I}_{2y}$) indicates that the signal in the Ω_2 dimension corresponds to a spin I_2 multiplet, antiphase with respect to spin I_1. In the case $\Omega_1^0/2\pi = 300\,\text{Hz}$, $\Omega_2^0/2\pi = 100\,\text{Hz}$, $\Omega_3^0/2\pi = -50\,\text{Hz}$, $J_{12} = 40\,\text{Hz}$, $J_{13} = 10\,\text{Hz}$ and $J_{23} = 25\,\text{Hz}$, this multiplet has the following appearance *in the Ω_2 dimension*:

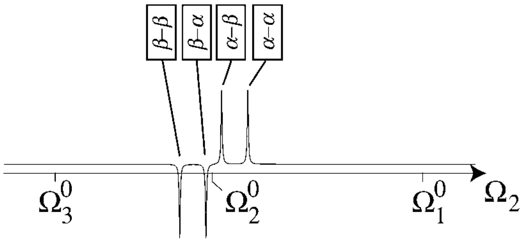

Figure 18.26
The Ω_2-multiplet generated by Equation 18.10.

Note that the sign of the peaks does not depend on the state label for the passive spin (I_3 in this case).

In order to understand the form of the two-dimensional multiplet, expand the trigonometric functions in Equation 18.10 as follows:

$$\begin{aligned}\hat{\rho}^{\cos}_{\textcircled{4}} = {} & -2\hat{I}_{1z}\hat{I}_{2y} \times \\ & \left\{\frac{1}{4}\cos((\Omega_1^0 - \pi J_{12} - \pi J_{13})t_1) - \frac{1}{4}\cos((\Omega_1^0 + \pi J_{12} - \pi J_{13})t_1)\right. \\ & \left. + \frac{1}{4}\cos((\Omega_1^0 - \pi J_{12} + \pi J_{13})t_1) - \frac{1}{4}\cos((\Omega_1^0 + \pi J_{12} + \pi J_{13})t_1)\right\}\ldots \qquad (18.11)\end{aligned}$$

If the calculation is repeated for the 'sine' pulse sequence (with the first pulse being $(\pi/2)_{\bar{y}}$ instead of $(\pi/2)_x$), we get

$$
\begin{aligned}
\hat{\rho}^{\sin}_{④} &= -2\hat{I}_{1z}\hat{I}_{2y} \times \\
&\quad \left\{ \frac{1}{4}\sin\left((\Omega_1^0 - \pi J_{12} - \pi J_{13})t_1\right) - \frac{1}{4}\sin\left((\Omega_1^0 + \pi J_{12} - \pi J_{13})t_1\right) \right. \\
&\quad \left. + \frac{1}{4}\sin\left((\Omega_1^0 - \pi J_{12} + \pi J_{13})t_1\right) - \frac{1}{4}\sin\left((\Omega_1^0 + \pi J_{12} + \pi J_{13})t_1\right) \right\} \ldots
\end{aligned}
\tag{18.12}
$$

The 'cosine' pulse sequence only gives rise to cosine modulation terms in t_1, whereas the 'sine' experiment only gives rise to sine modulation terms. As a result, the States procedure gives pure absorption lineshapes for all spectral components generated by Equation 18.10.

Equations 18.11 and 18.12 show that the modulation components have different signs. The components with frequency $\Omega_1^0 - \pi J_{12} \pm \pi J_{13}$ are positive and the components with frequency $\Omega_1^0 + \pi J_{12} \pm \pi J_{13}$ are negative. This implies the following appearance for the multiplet *in the* Ω_1 *dimension*:

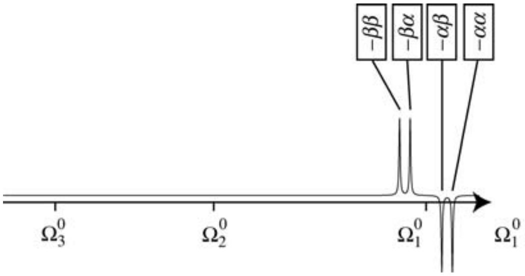

Figure 18.27
The Ω_1-multiplet generated by Equation 18.10.

The form of the multiplet in the Ω_1 dimension may be traced to its origin in the term proportional to $+2\hat{I}_{1y}\hat{I}_{2z}$ in Equation 18.8.

The two-dimensional cross-peak between spins I_1 and I_2, therefore, has the following appearance:

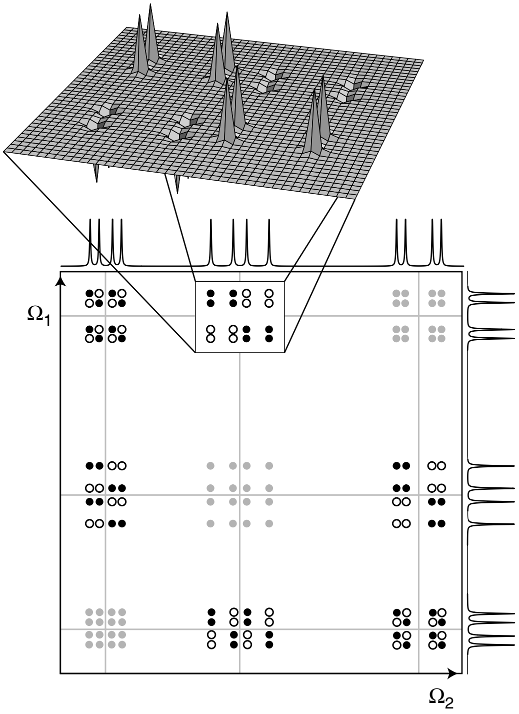

Figure 18.28
Form of the COSY multiplet between spins I_1 and I_2.

A similar calculation of the cross-peaks between spins I_1 and I_3 and between I_2 and I_3 shows that the multiplets have the following form:

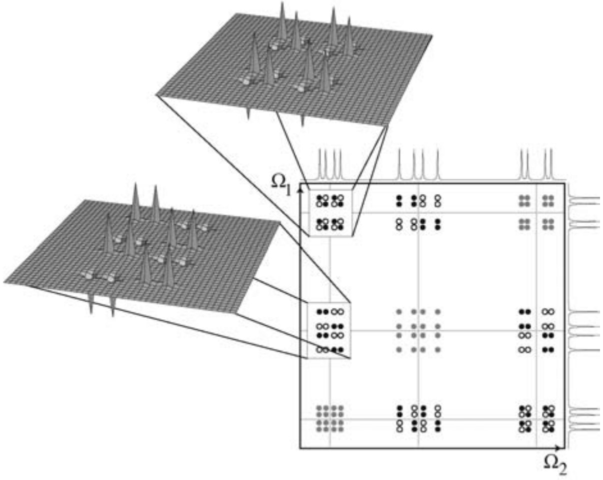

Figure 18.29 Form of the COSY multiplets between spins I_1 and I_3, and between spins I_2 and I_3.

In all cases, coherences with different state labels for the *active* spins have *opposite* sign, whereas coherences with different state labels for the *passive* spins have the *same* sign.

18.13.4 Diagonal peaks

The diagonal peaks in the COSY spectrum of an AMX system come out in pure dispersion when the data are acquired and processed according to the States scheme. If the calculation given in Section 16.1.4 is repeated for the AMX system, we get the following form for the diagonal peak multiplet of spin I_1:

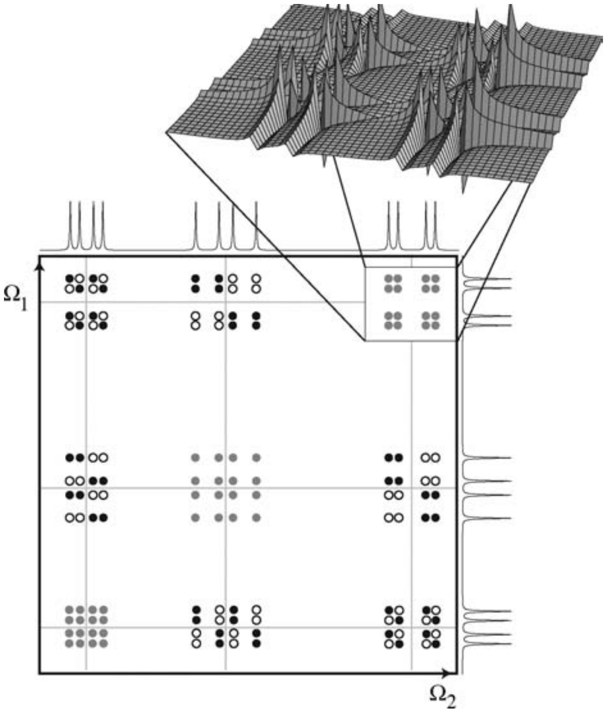

Figure 18.30 Form of the COSY diagonal peak multiplet for spin I_1.

The other diagonal peak multiplets have a similar appearance.

Such dispersion peakshapes are undesirable. The *double-quantum-filtered COSY* experiment is used to suppress the dispersion diagonal components (see *Further Reading* and Exercise 16.2).

18.13.5 Linear spin systems

If the coupling J_{13} vanishes, then the spin system is *linear* (see Section 17.9). In this case, the cross-peaks between spins I_1 and I_3 vanish, since the relevant antiphase terms $2\hat{I}_{1y}\hat{I}_{3z}$ and $2\hat{I}_{1z}\hat{I}_{3y}$ are never created during the evolution interval. In the frequency domain, we can imagine that the multiplet components with opposite sign have exactly the same frequency and cancel each other out. The two-dimensional COSY spectrum has the following form:

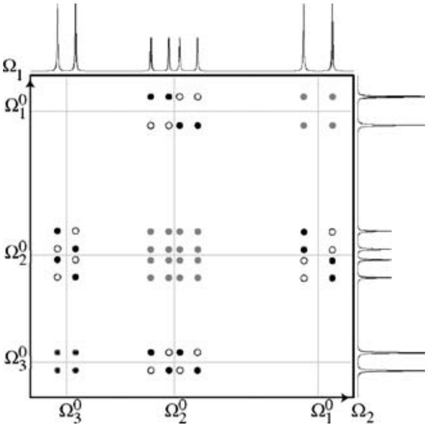

Figure 18.31
The COSY spectrum for a linear three-spin-1/2 system.

Note the two missing cross-peak multiplets.

This is a general property of COSY spectra. *The COSY cross-peak between two spins vanishes unless the two spins have a finite mutual J-coupling.*[4]

18.14 TOCSY

18.14.1 The ambiguity of COSY spectra

In many cases, one would like to identify two peaks as being generated by the same spin system, even if the corresponding spins do not have a finite J-coupling. For example, consider the case where the sample contains two independent linear three-spin systems A–M–X and A′–M′–X′. If all six chemical shifts are different, then the COSY spectrum has the following appearance (neglecting the multiplet structure):

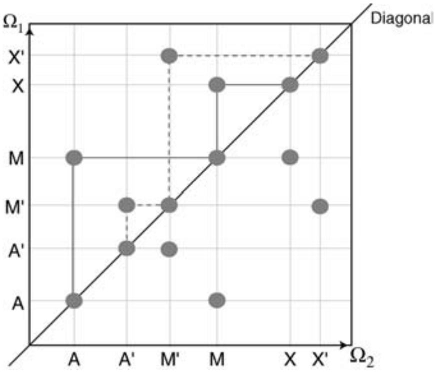

Figure 18.32
Form of the COSY spectrum for two linear AMX systems, with non-overlapping peaks.

If the spin systems are linear, then there are no cross-peaks between A and X spins, or between A′ and X′ spins. Nevertheless, it is possible to establish that the A and X spins belong to the spin system by following the connectivity through the M spin peak, as illustrated by the solid line. Similarly, the A′–M′–X′ connectivity may be established by following the dashed line through the M′ peak.

Now suppose that the chemical shifts of M and M′ are the same. The COSY spectrum has the following appearance:

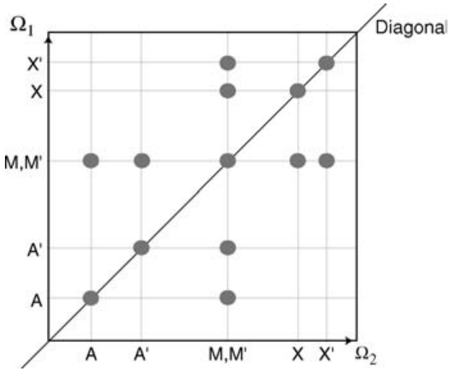

Figure 18.33
Form of the COSY spectrum for two linear AMX systems, in the case that the two M spins have the same chemical shifts.

The coincidence of the M and M′ resonances makes it impossible to disentangle the peaks from the two spin systems. The assignments become ambiguous, even though the A, A′, X and X′ peaks are all well resolved.

This simple example shows that the information content of COSY spectra is rapidly compromised when some peaks overlap, particularly in linear spin systems.

For this reason, NMR methods have been developed to allow the identification of resonances generated by the same spin system, even if they belong to spins that are not *directly* coupled with each other. One popular set of methods is called TOCSY (which stands for Total Correlation Spectroscopy).[7]

The basic aim of TOCSY is to produce cross-peaks between all spins that belong to the same spin system. An idealized TOCSY spectrum for a mixture of linear AMX and A′M′X′ spin systems, in which M and M′ have the same chemical shifts, appears as follows:

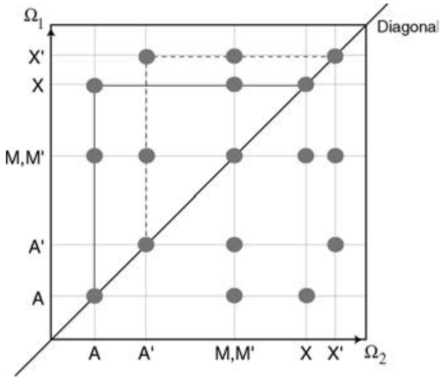

Figure 18.34
Form of the TOCSY spectrum for two linear AMX systems, in the case that the two M spins have the same chemical shifts.

This clearly establishes that the A and X peaks belong to one spin system, and that the A′ and X′ peaks belong to another.

18.14.2 TOCSY pulse sequence

There are many different variants of TOCSY pulse sequences. The simplest version (and the original one) is as follows:

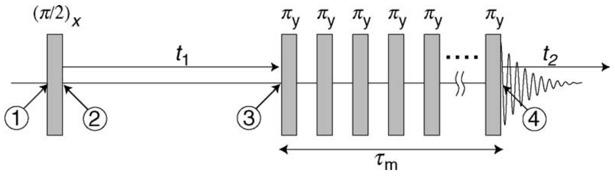

Figure 18.35
TOCSY pulse sequence.

This resembles the COSY pulse sequence, except that the second $(\pi/2)_x$ pulse is replaced by a train of many strong π pulses, spanning the *mixing interval* τ_m. In practice, the number of π pulses is large: I have only drawn six, for simplicity. If the interval between the pulses is denoted τ, and there are N equally spaced pulses, then the timings are related through

$$N\tau = \tau_\mathrm{m}.$$

I assume here that the π pulses are infinitely strong and short, so that their duration may be neglected.

This pulse sequence requires that the π pulses are closely separated in time, so that there is little spin precession between the pulses (in the rotating frame). In general, the interval τ *between* pulses should be short enough to satisfy the condition

$$|(\Omega_j^0 - \Omega_k^0)\tau| << 1 \tag{18.13}$$

for all pairs of coupled spins j and k, where Ω_j^0 and Ω_k^0 are the resonance offsets in the rotating frame. At the same time, the *total* duration of the sequence τ_m should be long compared with the inverse of the J-couplings.

In practice, for proton systems, the spread in chemical shifts is around 10 ppm. If the proton Larmor frequency is around 500 MHz, and the reference frequency is placed in the centre of the spectrum, the resonance offsets $\Omega_j^0/2\pi$ lie in the range ±2.5 kHz. The π pulses should, therefore, be separated by intervals of around 100 μs or less. At the same time, the total interval τ_m should be around 100 ms, to allow the J-couplings sufficient time to mix the coherences around. A typical TOCSY mixing sequence, therefore, consists of a train of several *hundred* π pulses.

This simple form of the TOCSY pulse sequence is quite sensitive to various sorts of experimental imperfections. A large number of alternative TOCSY pulse sequences have been developed which are more robust (see *Further Reading*). I only treat the simplest TOCSY sequence in this book.

18.14.3 Theory of TOCSY

The first part of the TOCSY pulse sequence is the same as for COSY. The initial spin density operator is

$$\hat{\rho}_{①} \sim \hat{I}_z = \hat{I}_{1z} + \hat{I}_{2z} + \hat{I}_{3z}$$

omitting the unity operator and numerical factors. The fate of the first term during the $(\pi/2)_x$ pulse and the t_1 interval is as follows:

$$\begin{aligned} \hat{\rho}_{\textcircled{1}} &= \hat{I}_{1z} + \dots \\ &\Big\downarrow (\pi/2)_x \\ &\Big\downarrow t_1 \\ \hat{\rho}_{\textcircled{3}} &= -\hat{I}_{1y}\cos(\Omega_1^0 t_1)\cos(\pi J_{12} t_1)\cos(\pi J_{13} t_1) + \dots \end{aligned} \tag{18.14}$$

There now follows the TOCSY mixing sequence of many closely spaced π pulses. Since the delay between the pulses satisfies Equation 18.13, the treatment given in Appendix A.10.1 is appropriate. The propagator for the mixing sequence is therefore

$$\widehat{U}_{\text{mix}} \cong \widehat{U}_J^{\text{strong}}(\tau_{\text{m}}) = \exp\{-\mathrm{i}\widehat{\mathcal{H}}_J^{\text{strong}}\tau_{\text{m}}\} \tag{18.15}$$

where $\widehat{\mathcal{H}}_J^{\text{strong}}$ is given by:

$$\widehat{\mathcal{H}}_J^{\text{strong}} = \sum_{j<k}{}' \, 2\pi J_{jk} \hat{\mathbf{I}}_j \cdot \hat{\mathbf{I}}_k$$

For a three-spin system, the TOCSY mixing Hamiltonian is:

$$\begin{aligned} \widehat{\mathcal{H}}_J^{\text{strong}} &= 2\pi J_{12}(\hat{I}_{1x}\hat{I}_{2x} + \hat{I}_{1y}\hat{I}_{2y} + \hat{I}_{1z}\hat{I}_{2z}) \\ &\quad + 2\pi J_{13}(\hat{I}_{1x}\hat{I}_{3x} + \hat{I}_{1y}\hat{I}_{3y} + \hat{I}_{1z}\hat{I}_{3z}) \\ &\quad + 2\pi J_{23}(\hat{I}_{2x}\hat{I}_{3x} + \hat{I}_{2y}\hat{I}_{3y} + \hat{I}_{2z}\hat{I}_{3z}) \end{aligned}$$

It is not easy to calculate the evolution of the spin density operator $\hat{\rho}_{\textcircled{3}}$ in Equation 18.14 under this Hamiltonian. The product operator evolution rules given in Section 18.10 do not apply because the system is strongly coupled in the presence of the dense sequence of π pulses.

Nevertheless, some general conclusions about the evolution are readily drawn. The strongly coupled J-coupling Hamiltonian $\widehat{\mathcal{H}}_J^{\text{strong}}$ commutes with the *total* angular momentum operators along all three axes:

$$\begin{aligned} \left[\widehat{\mathcal{H}}_J^{\text{strong}}, \hat{I}_x\right] &= 0 \\ \left[\widehat{\mathcal{H}}_J^{\text{strong}}, \hat{I}_y\right] &= 0 \\ \left[\widehat{\mathcal{H}}_J^{\text{strong}}, \hat{I}_z\right] &= 0 \end{aligned} \tag{18.16}$$

where

$$\hat{I}_x = \hat{I}_{1x} + \hat{I}_{2x} + \hat{I}_{3x}$$

and so on. As discussed in Section 7.5, these commutation properties imply that the total angular momentum along any axis is always preserved under the strongly coupled TOCSY evolution.

Consider, for example, the first term in Equation 18.14, representing angular momentum of spins I_1 along the $-y$-axis. During the mixing sequence, the angular momentum of spins I_1 along the $-y$-axis must decrease, since this term is converted into other terms. However, the commutation rules shown in

Equation 18.16 imply that this decrease must be accompanied by an increase in the polarization of spins I_2 and I_3 along the same axis. In other words, the total polarization along the $-y$-axis (or any other axis) may only be *transferred* between spins, never destroyed, as long as relaxation is neglected.

The idea of TOCSY mixing may be expressed in terms of magnetization vectors as follows:

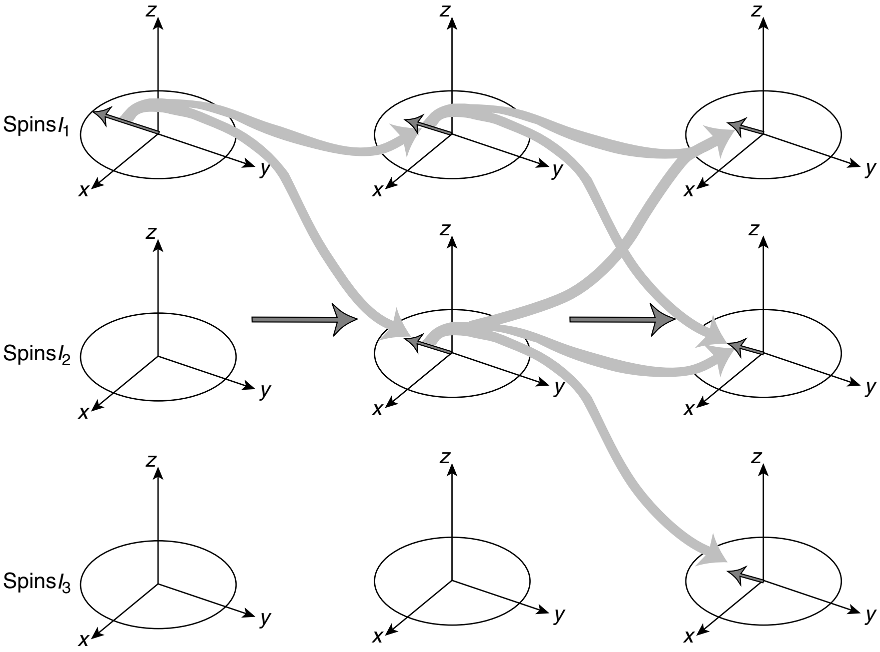

Figure 18.36

A qualitative picture of magnetization transfer between three spins under TOCSY.

The magnetization along a particular axis is transferred between the three spins through the network of J-couplings, keeping the total magnetization in any direction constant.

Note in particular that magnetization may be transferred from spins I_1 to spins I_3, even if the coupling constant J_{13} is vanishingly small. Given sufficient time, magnetization will get there, as long as the spins participate in the same coupling network.

Figure 18.37 shows accurate simulations of TOCSY dynamics in a linear four-spin system, with coupling constants $J_{12} = 10\,\text{Hz}$, $J_{23} = 5\,\text{Hz}$ and $J_{34} = -7\,\text{Hz}$: Magnetization starts on spin I_1 and oscillates rapidly between the two directly bonded spins I_1 and I_2. After a short delay, magnetization starts to develop on the next spin I_3, reaching a maximum on that spin after around 160 ms. Magnetization appears a little more slowly on the most distant spin I_4. Although the system never reaches a true equilibrium, the state at long times corresponds very roughly to an even distribution of magnetization throughout the whole spin system.

The calculation of a TOCSY spectrum for the AMX system may now be continued, based on the very rough assumption that the magnetization reaches an even distribution amongst the spins after a long TOCSY pulse sequence. With this assumption, we get[8] the following equation:

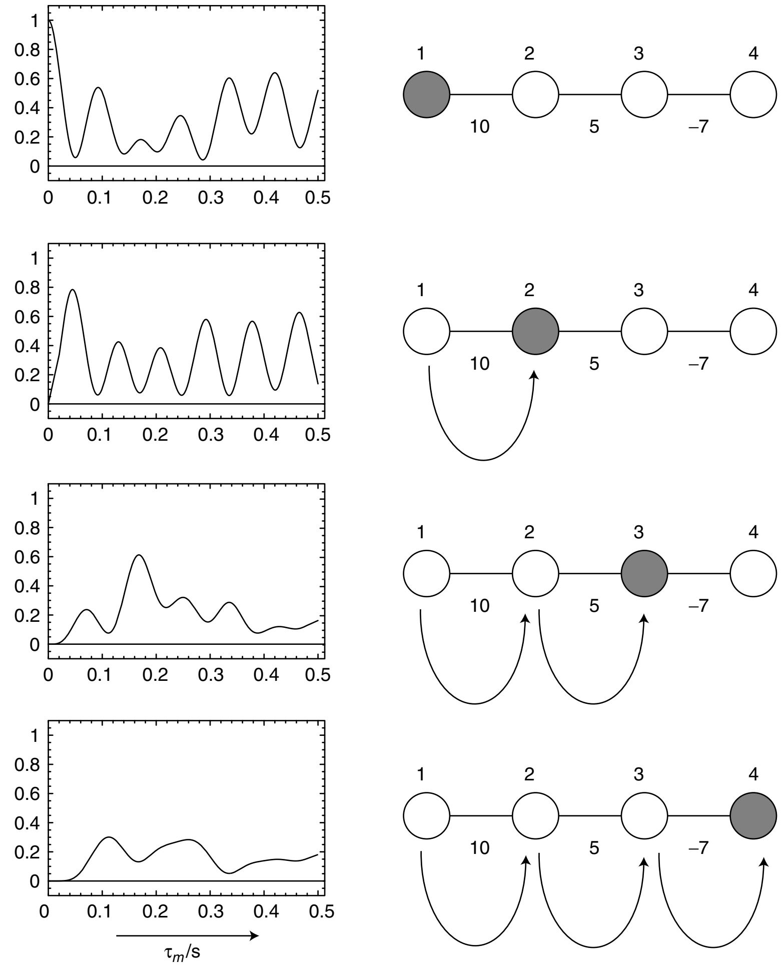

Figure 18.37
Accurate simulations of TOCSY spin dynamics, for a linear four-spin system, with the indicated J-couplings.

$$\hat{\rho}_{③} = -\hat{I}_{1y}\cos(\Omega_1^0 t_1)\cos(\pi J_{12}t_1)\cos(\pi J_{13}t_1) + \ldots$$

$$\Big\downarrow \text{TOCSY mixing}$$

$$\begin{aligned}\hat{\rho}_{④} \cong &-\tfrac{1}{3}\hat{I}_{1y}\cos(\Omega_1^0 t_1)\cos(\pi J_{12}t_1)\cos(\pi J_{13}t_1)\\ &-\tfrac{1}{3}\hat{I}_{2y}\cos(\Omega_1^0 t_1)\cos(\pi J_{12}t_1)\cos(\pi J_{13}t_1)\\ &-\tfrac{1}{3}\hat{I}_{3y}\cos(\Omega_1^0 t_1)\cos(\pi J_{12}t_1)\cos(\pi J_{13}t_1) + \ldots\end{aligned}$$

This corresponds to one diagonal peak and two cross-peaks, and it is readily shown that all multiplet components are in positive absorption after the States procedure.[8]

The idealized form of a TOCSY spectrum in an AMX system is therefore as follows:

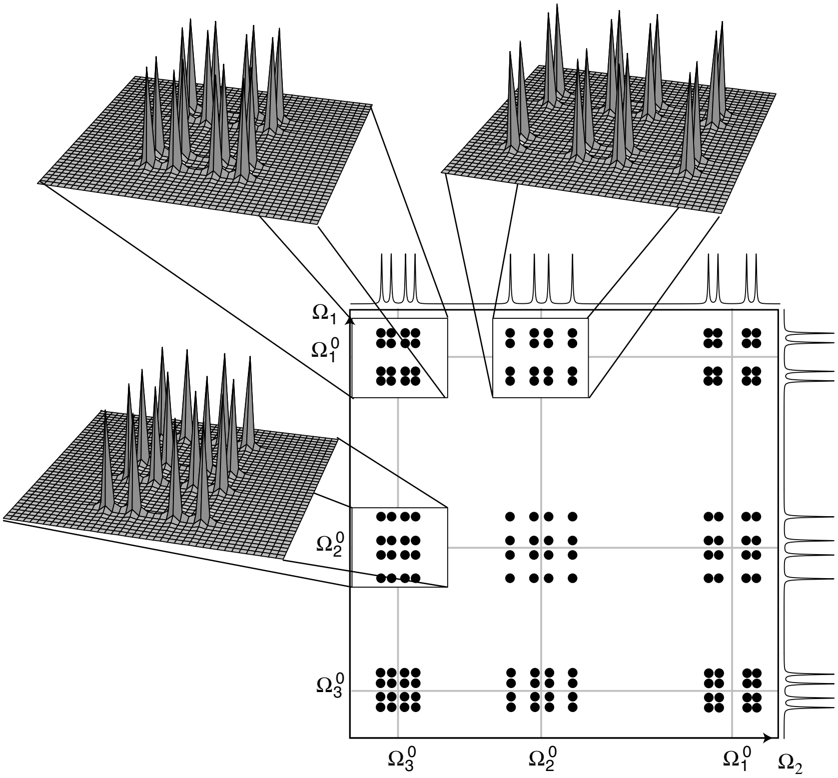

Figure 18.38
Ideal form of the TOCSY spectrum of an AMX spin system.

Notes

1. In favourable cases, many successive manipulations of coupled multiple-spin systems may be performed with great accuracy. It has been proposed to exploit such predictable spin manipulations as a way of performing certain algorithmic computations. In principle, the quantum-mechanical nature of the spin system allows certain computational tasks to be performed more rapidly than by using conventional sequential algorithms. Some primitive demonstrations of *NMR quantum computing* have actually been performed (see J. A. Jones, *Prog. NMR Spectrosc.* **38**, 325–360 (2001)). However, as of 2007, practical quantum computing by NMR appears to be a very long way off. For a critical view, see W. S. Warren *Science*, 277, 1688–1689 (1997).

2. The term *simple coherence* is new. There does seem to be a need for a term that is complementary to *combination coherence*.

3. An exception is when the liquid crystal phase is very weakly ordered, so that the secular dipole–dipole couplings are essentially finite only for neighbouring pairs of spins. This maintains a large degree of degeneracy, keeping such spectra interpretable (see Section 16.4).

4. The cancellation of opposite degenerate peaks is imperfect if the peaks have different widths. Typically, this occurs in the presence of cross-correlated relaxation mechanisms (see Section 20.8). For an example of unexpected coherence transfer caused by cross-correlated relaxation, see N. Müller, G. Bodenhausen, K. Wüthrich, R. R. Ernst, *J. Magn. Reson.*, **65**, 531 (1985).

5. This property has been used to design pulse sequences that select out signals generated by spin systems with a given coupling topology (see M. H. Levitt and R. R. Ernst, *J. Chem. Phys.*, **83**, 3297 (1985)).

6. The pulse sequence phases are consistent with the 'sign-corrected' version of the States procedure discussed in Section 5.9.4.

7. TOCSY is also known as *HOHAHA*, which stands for *Homonuclear Hartmann–Hahn*. This name comes from the close relationship between the TOCSY method and an older polarization transfer scheme originally invented for *heteronuclear* spin systems by Hartmann and Hahn. The Hartmann–Hahn method is best known in solid-state NMR, but the original paper does describe liquid-state applications as well (see S. R. Hartmann and E. L. Hahn, *Phys. Rev.* **128**, 2042 (1962)).

8. I have omitted the x-components of spin angular momentum in Equation 18.14, which are also preserved through the TOCSY mixing process and give rise to dispersion-mode peak components. In practice, these x-components tend to be destroyed by the accumulating effect of pulse imperfections (the phases of the π pulses are selected so as to rotate the magnetization components around the y-axis, so that all y-components are preserved, even if the pulses are imperfect). There are also many more sophisticated TOCSY pulse sequences in which the x-components are destroyed in a more exact way (see *Further Reading*).

Further Reading

- For a different angle on the material in this chapter, see J. Keeler, '*Understanding NMR Spectroscopy.*' Wiley, Chichester, 2005.
- For a detailed treatment of experiments on multiple-spin systems, including many applications, see J. Cavanagh, W. J. Fairbrother, A. G. Palmer and N. J. Skelton, *Protein NMR Spectroscopy. Principles and Practice*, Academic Press, New York, 1996.
- For deeper analysis of multiple spin-1/2 systems, see R. R. Ernst, G. Bodenhausen and A. Wokaun, *Principles of Nuclear Magnetic Resonance in One and Two Dimensions*, Clarendon Press, Oxford, 1987, and M. Goldman, *Quantum Description of High-Resolution NMR in Liquids*, Clarendon Press, Oxford, 1988.
- For reviews of polarization transfer pulse sequences, see O. W. Sørensen, *Prog. NMR Spectrosc.* 21, 503–569 (1989) and D. M. Doddrell, in the *Encyclopedia of Nuclear Magnetic Resonance*, vol. **6**, D. M. Grant and R. K. Harris (eds), Wiley, 1996, pp. 3645–3654.
- For the subject of polarization transfer bounds, e.g. see S. J. Glaser, T. Schulte-Herbrüggen, M. Sieveking, O. Schedletzky, N. C. Nielsen, O. W. Sørensen and C. Griesinger, *Science* ***280***, 421–424 (1998) and references therein.
- For a review of more advanced TOCSY pulse sequences, see J. Sleucher, J. Quant, S. J. Glaser and C. Griesinger, in the *Encyclopedia of Nuclear Magnetic Resonance*, vol. 6, D. M. Grant and R. K. Harris (eds), Wiley, 1996, p. 4789.

Exercises

18.1 This exercise investigates the DEPT pulse sequence for polarization transfer between different spin species (see D. M. Doddrell, D. T. Pegg, and M. R. Bendall *J. Magn. Reson.*, **48**, 323 (1982)). One version of the DEPT pulse sequence is as follows:

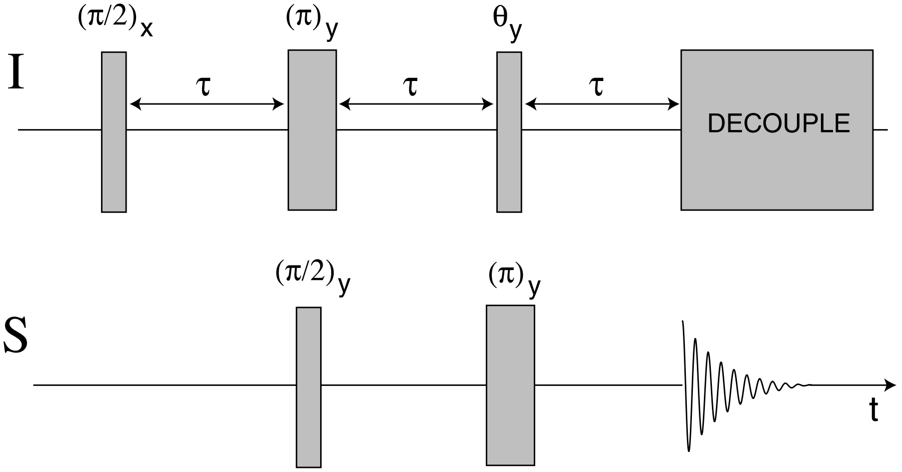

The flip angle θ of the last pulse on the I-spin channel is variable. Consider two spin species, I and S, with gyromagnetic ratios γ_I and γ_S. Assume that the delays are set to the value $\tau = (2J_{IS})^{-1}$, where J_{IS} is the J-coupling.

(i) Consider the case of an IS spin system. If the initial spin density operator is $\hat{\rho}_{①} \sim \hat{I}_z$, what is the spin density operator at the start of the signal detection period, for an arbitrary value of θ? What flip angle θ should be used to obtain the largest signal? By how much may the signal be enhanced compared with an experiment in which the signal is induced by a single $\pi/2$ pulse on the S-spin?

(ii) Repeat the calculation for an I_2S spin system. At the end of the calculation, only retain terms that give rise to observable signals. What flip angle θ should be used to obtain the largest signal? What is the maximum signal enhancement factor?

(iii) Repeat the calculation in (ii) for an I_3S spin system.

Part 7

Motion and Relaxation

19 Motion

One of the most important and useful features of NMR is its ability to probe molecular motion, over a wide range of time-scales, ranging from picoseconds (10^{-12} s) to tens of seconds, or even longer in favourable cases.

19.1 Motional Processes

Motional processes may be detected by NMR if they change the nuclear spin Hamiltonian. The nature of these motional effects depends on the type of motion and their time-scale.

19.1.1 Molecular vibrations

Molecules are not rigid objects. They are full of internal dynamics. In general, all nuclei oscillate rapidly around their mean positions. Such motions are called *vibrations*, and typically are on the time-scale of picoseconds (10^{-12} s) or shorter. In general, a vibrational motion is slow if there are many atoms involved, and if those atoms are relatively massive.

Light atoms, such as hydrogen, undergo particularly rapid local oscillations, with a relatively large amplitude. These highly local motions are called *librations*. For example, the typical motion of a C−H group may be depicted as follows:

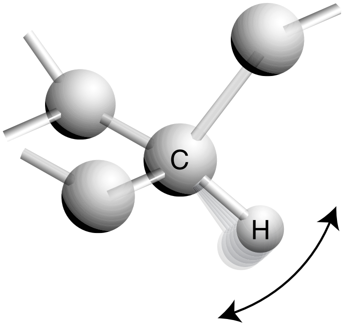

Figure 19.1
Librational motion of a hydrogen atom attached to a heavy atom.

Note that the main direction of the libration is *perpendicular* to the C−H bond direction. Typical libration amplitudes are about ±15°.

Spin Dynamics: Basics of Nuclear Magnetic Resonance, Second Edition Malcolm H. Levitt

19.1.2 Local rotations of molecular groups

Many symmetrical molecular groups rotate rapidly at normal temperatures. For example, methyl groups (CH_3) usually rotate very rapidly around their local threefold axes:

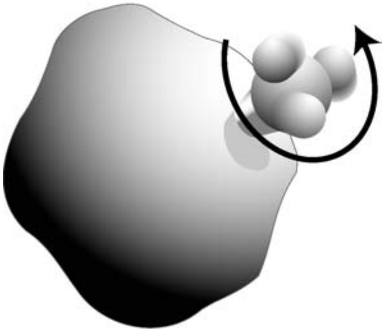

Figure 19.2
Rotational motion of a methyl group.

This motion is typically on the picosecond time-scale at room temperature, but may be as slow as microseconds or milliseconds if the motion is *hindered*, i.e. if the methyl group butts up against something else in the molecule, preventing it from turning around freely.

NH_3^+ groups in proteins and amino acids usually undergo a similar rotational motion about the local threefold axis.

19.1.3 Molecular flexibility

Large molecules, like proteins, have a large degree of internal flexibility, which in some cases is indispensible for their function. One of the most powerful features of NMR is its ability to make such flexibility visible. One example is given in Plate 2.

19.1.4 Chemical exchange

If the motional process involves the making and breaking of chemical bonds, then the molecular motion is called *chemical exchange*.

As a simple example of chemical exchange, consider the following internal cyclization reaction:

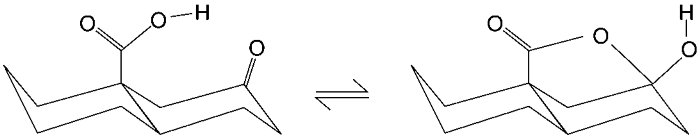

Figure 19.3
A chemical exchange process.

Since the electronic structure is different in the two forms, the chemical shifts and J-couplings change when the exchange process takes place. The formation and breaking of the internal ring, therefore, are detectable by NMR, provided that the process is on an appropriate time-scale.

The term chemical exchange is also used if the conformation of the molecule changes around a relatively rigid entity, such as a double bond or a similar conjugated system. The reaction may even lead to a product that is physically and chemically *identical* to the reactant. An example of this is the slow exchange of the N-methyl groups in N, N'-dimethylformamide:

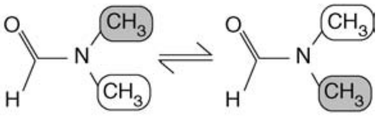

Figure 19.4
N, N'-dimethylformamide.

To make the process visible, the above sketch uses grey and white boxes to label the exchanging methyl groups.

Chemical exchange processes occur over a very wide range of time-scales, from nanoseconds (10^{-9} s) to many seconds or longer.

Many methods for detecting chemical reactions require that the concentrations of the two species change as a function of time. For example, if the optical absorption of one of the species is different from the other species, and if the reaction is initially far from equilibrium, then the optical absorption changes as the reaction proceeds, thus allowing the reaction to be followed.

One of the most powerful aspects of NMR is its ability to detect chemical exchange phenomena, *even when the system is in equilibrium*. This is because NMR detects the *molecular motion itself*, rather than the numbers of molecules in different states.

NMR is even capable of detecting the chemical exchange process in N, N'-dimethylformamide, in which the reactant and the product are indistinguishable.

NMR may detect this type of symmetrical reaction because it involves the individual nuclear spins, which are located at particular sites in the molecule and which act as 'internal spies' reporting on the molecular motion. The two sites are not chemically equivalent, so the chemical shift of a nuclear spin in the 'grey' box changes as the box is transported from one side of the molecule to the other. The change in the chemical shift leads to strong effects on the NMR spectrum, as discussed below. The fact that nuclear spins in the 'white' box experience an exactly symmetrical change in their chemical shifts does not matter.

19.1.5 Molecular rotations

In a *liquid*, the molecules undergo constant random rotations:

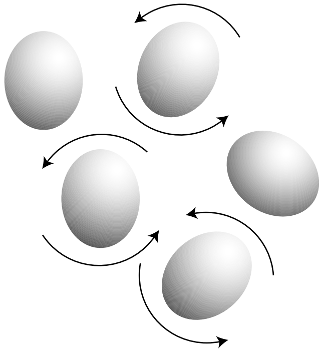

Figure 19.5
Random molecular rotations.

These random rotations are detectable by NMR because they change the anisotropic spin interactions, such as CSA and direct dipole–dipole couplings.

The time-scale of molecular rotations in a liquid depends on the molecular size, and also on other physical parameters such as the viscosity and the temperature. Typically, small molecules rotate in a liquid on the picosecond time-scale, whereas large molecules, such as proteins, rotate in a liquid on the nanosecond time-scale.

In biochemical NMR, a rough estimate of the molecular rotational time-scale (in units of nanoseconds) is obtained by taking the molecular mass (in units of kilodaltons) and dividing by two. For example, the rotational time-scale of a 30 kDa protein molecule in aqueous solution is typically around 15 ns.

The effect of molecular rotations on the motional averaging of nuclear spin interactions was discussed in Section 8.6.

19.1.6 Translational motion

In a liquid, molecules undergo *translations*, i.e. motion of the molecular mass centre through space. Translational motion that is random and uncoordinated is called *diffusion*. Translational motion that is concerted and directed is called *flow*:

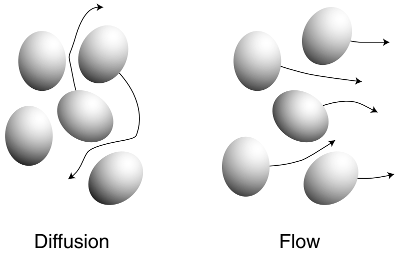

Figure 19.6
Diffusion and flow.

NMR is capable of detecting both kinds of motion, and of distinguishing them.

Molecular translations affect the NMR properties in two different ways:

1. Molecular diffusion on a *microscopic* scale averages out short-range intermolecular spin interactions, as discussed in Section 8.6.
2. Diffusion and flow transport the molecules from one region of space to another, on a *macroscopic* scale. This also affects the behaviour of the spins, if the external magnetic field is *inhomogeneous*.

Detection of *macroscopic* diffusion or flow by NMR is possible in an inhomogeneous magnetic field, because the spin Hamiltonian changes as the molecules move into a different region of space. The inhomogeneous magnetic field may be generated externally, using field gradient coils (see Section 4.7). The motion of the molecules in the direction of the gradient changes the Larmor frequency:

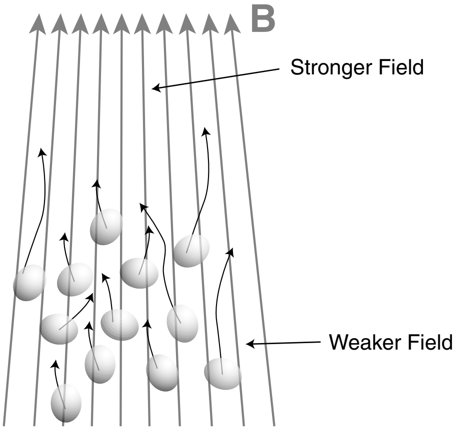

Figure 19.7
Molecules in a flowing liquid, and the application of a magnetic field gradient in the same direction as the flow.

A very important part of NMR is concerned with quantitating molecular diffusion and flow using magnetic field gradients.

In some cases, the inhomogeneous magnetic field is generated by the sample itself. This happens if the sample is grainy and contains particles with different magnetic susceptibility. For example, such effects are important when NMR is used to study the penetration of liquids (such as crude oil) into minerals. Another example is provided by the study of blood flow in the lungs and other body tissues.

Macroscopic diffusion and flow typically change the nuclear spin interactions on the time-scale of milliseconds to seconds.

19.1.7 Mechanical motion

In a *solid*, the thermal molecular rotations are strongly restricted, except in special cases where the molecules are very symmetrical (see the example of fullerene, discussed in Section 1.6.3). Nevertheless, even in a rigid solid, it is possible to influence the nuclear spins by *mechanical rotation of the whole sample* (see Section 19.6).

19.2 Motional Time-Scales

The range of motional time-scales typically encountered for the different motional mechanisms is summarized in the following figure:

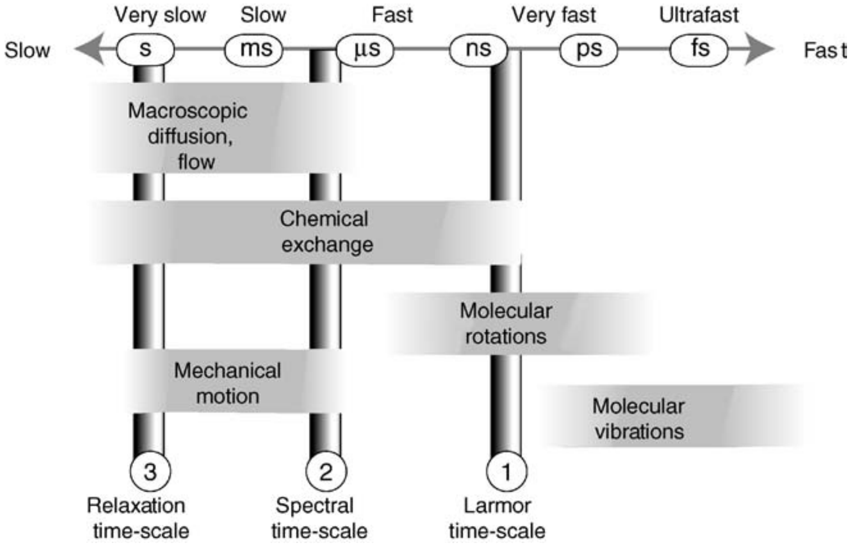

Figure 19.8
Typical motional time-scales for physical processes.

The relevant time-scales run from fractions of a picosecond (for librations), through nanoseconds (for molecular rotations), milliseconds (for many chemical exchange processes and fast mechanical motions), to many seconds (for macroscopic diffusion, flow, slow mechanical motions, and some chemical exchange processes).

The effects of these motional processes on the nuclear spins depend on their relationship to the three characteristic time-scales of the nuclear spin system, indicated by the vertical bars in Figure 19.8.

1. *Larmor time-scale*. Bar ① indicates roughly the time required for the spins to precess through 1 rad in the magnetic field. The characteristic time-scale for bar ① is given by τ^0, where

$$|\omega^0 \tau^0| \sim 1$$

For example, if the Larmor frequency of the spins is $\omega^0/2\pi = -500\,\mathrm{MHz}$, then the Larmor time-scale corresponds to $\tau^0 \sim 0.3\,\mathrm{ns}$.

2. *Spectral time-scale*. The characteristic time indicated by bar ② represents the inverse width of the NMR spectrum, measured in frequency units. For example, suppose that the spin system contains two spins, with chemical shift frequencies Ω_1^0 and Ω_2^0. If the chemical shift interactions are dominant, then the spectral time-scale τ_{spec} is given by:

$$|(\Omega_1^0 - \Omega_2^0)\tau_{\mathrm{spec}}| \sim 1$$

If the two spins are both ^{13}C, with a chemical shift difference of 100 ppm, then the time-scale τ_{spec} in a field of 11.74 T is ~13 μs. If the two spins are protons, with a chemical shift difference of 5 ppm, then the time-scale τ_{spec} ~64 μs in the same field.

3. *Relaxation time-scale*. Bar ③ indicates the value of the spin–lattice relaxation time constant T_1. Normally, this is of the order of seconds.

All of these characteristic time-scales depend on the sample, the spin isotope, and physical parameters, such as the magnetic field and the temperature.

19.3 Motional Effects

The effects of motion on the nuclear spin dynamics depend on their time-scale, as summarized by the following diagram:

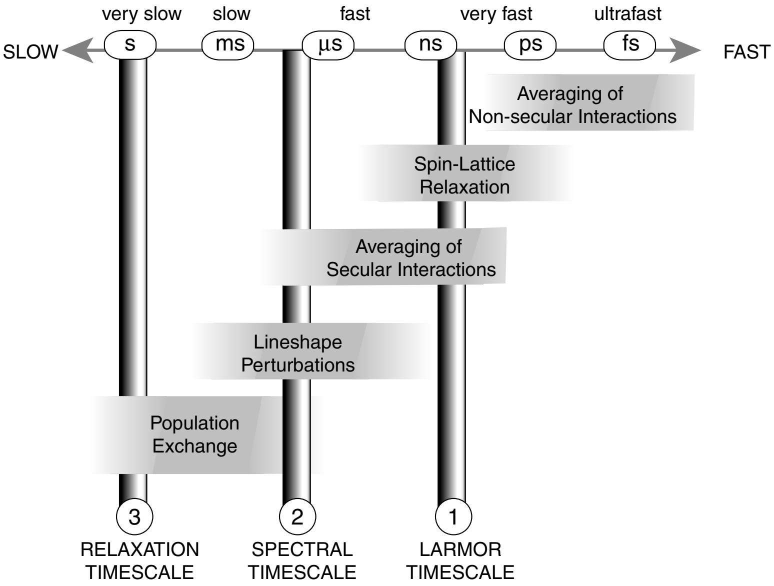

Figure 19.9
Motional time-scales associated with different phenomena.

1. *Averaging of non-secular spin interactions.* Processes that are *faster than the Larmor time-scale* (typically librations and vibrations) average the spin Hamiltonian terms *before* the secular approximation is made (see Section 8.5.2). This process is discussed in Section 19.4.

2. *Spin–lattice relaxation.* Processes that are *on the Larmor time-scale* are responsible for spin–lattice relaxation. Some processes of this type are discussed in Chapter 20.

3. *Averaging of secular spin interactions.* Processes that are *faster than the spectral time-scale but slower than the Larmor time-scale* average the spin Hamiltonian terms *after* the secular approximation is made. This process is also discussed in Section 19.4.

4. *Spectral lineshape perturbations.* Processes that are *on the spectral time-scale* affect the NMR lineshapes strongly. If the motional process is random (such as chemical exchange), such processes typically broaden the spectra, but more complex phenomena may also be observed. A simple case is analysed in Section 19.5. If the motional process is *periodic* (such as mechanical rotation), then the motion generally leads to *sideband* formation. This is discussed in Section 19.6.

5. *Population exchange.* Processes that are *slower than the spectral time-scale* do not significantly affect the NMR lineshapes or relaxation processes. Nevertheless, such slow processes may still be detected by NMR through their influence on the dynamics of spin populations, as long as their time-scale does not greatly exceed T_1 (see Note 1). An example is treated in Section 19.7.

19.4 Motional Averaging

If the motion is rapid (microseconds to femtoseconds), then the nuclear spins experience *motionally averaged* spin interactions, as described in Section 8.6.

An example is the removal of the direct dipole–dipole couplings by molecular rotation and diffusion in an isotropic liquid, as described in Section 9.3.2.

The correct treatment of motional averaging depends on the relative time-scale of the process compared with the Larmor time-scale. Motions that are faster than the Larmor time-scale (typically vibrations) average the spin Hamiltonian *before* the secular approximation is made. Motions that are slower than the Larmor time-scale (typically rotations) average the spin Hamiltonian *after* the secular approximation is made.

The distinction is important because relaxation is caused by *non-secular* Hamiltonian terms, whereas the form of the NMR spectrum is determined by *secular* Hamiltonian terms.

Spin–lattice relaxation is caused by spin interactions that are already averaged over motions that are faster than the Larmor time-scale, but not over slower motions. Typically, this implies that one should correct the values of the spin interaction parameters for rapid vibrational and librational motions, but that one should not correct for rotational or translational motions when treating the spin relaxation.

As an example, consider vibrational averaging of the through-space dipole–dipole coupling. The distance between a ^{13}C nucleus and a directly bonded ^{1}H in a typical C–H group has been determined by neutron diffraction to be 0.109 nm. This corresponds to a direct dipole–dipole coupling of $b_{jk}/2\pi = -23.3\,\text{kHz}$. In practice, the observed dipole–dipole coupling in a solid is only $b_{jk}/2\pi \sim -20.9\,\text{kHz}$. The discrepancy is due to the rapid librational motion of the protons. Note that the motion of the protons *perpendicular* to the bond direction is mainly responsible for this reduction in the direct dipole–dipole coupling.[2]

Since the librational motion of CH bonds is much faster than the Larmor time-scale, calculation of dipole–dipole relaxation should use a librationally corrected value for the dipole–dipole coupling constant, i.e. $b_{jk}/2\pi \sim -20.9\,\text{kHz}$.[3]

It would *not* be appropriate to correct the dipole–dipole coupling for the *rotational* motion of the molecules in a relaxation treatment, since this motion is typically on the Larmor time-scale, or slower.

In the case of calculations of the NMR *spectra* (rather than the relaxation behaviour), it is appropriate to average the spin interactions over all motions that are faster than the spectral time-scale, including both rotations and vibrations. This approach was taken in Chapter 9.

A rather formidable-looking flow chart for motional averaging of the spin Hamiltonian is given below:

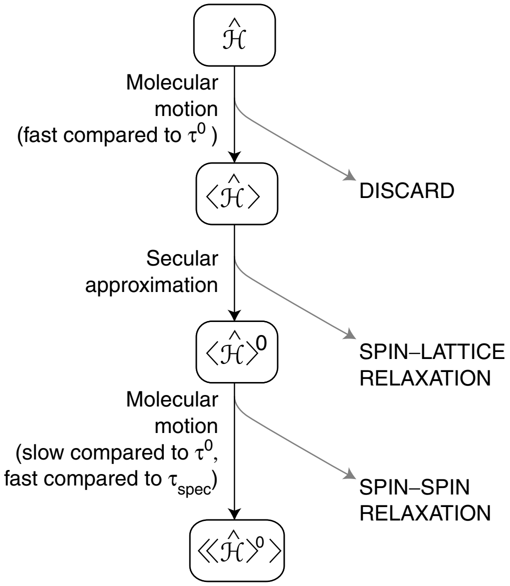

Figure 19.10
A flow diagram for motional averaging.

In the above diagram, angular brackets are used for motional averaging, and the superscript zero is used for the secular part of the spin Hamiltonian. The final result $\langle < \hat{\mathcal{H}} >^0 \rangle$ is the motionally averaged secular Hamiltonian, whose components are listed in Chapter 9. Such Hamiltonian terms have passed through two stages of motional averaging and one secular approximation.

19.5 Motional Lineshapes and Two-Site Exchange

Motion on the spectral time-scale τ_{spec} causes the NMR lineshapes to change. In this section, the effect of a simple random process is examined.

The example to be discussed now is called *symmetrical two-site exchange*, in which an isolated nuclear spin is transported between two different chemical environments, with different chemical shifts but identical free energies. The process may be depicted thus:

$$A \underset{k}{\overset{k}{\rightleftharpoons}} B$$

where the species A and B have equal probability. The exchange of the N-methyl groups in N, N'-dimethylformamide is a good example of this (see Figure 19.4).

The transition between A and B is considered to be extremely rapid, so that no intermediate states are involved. The *rate constants* for the reactions A → B and B → A are considered to be equal, and are denoted

k. This means that each molecule has a probability $k\tau$ of making a transition to the other state within a short interval τ. The rate constant k is also known as the *transition probability per unit time*.

The trajectories of five different molecules, all starting in the state A, have the following form:

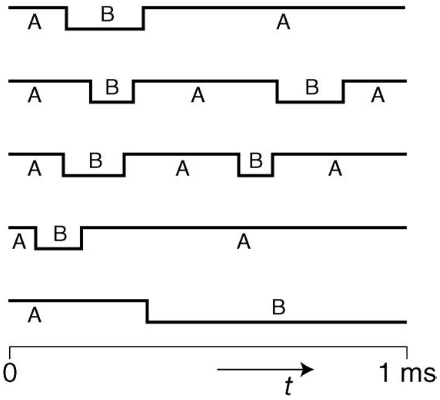

Figure 19.11
A set of trajectories for molecules undergoing two-site exchange.

These examples are consistent with the case $k = 3 \times 10^3\ \mathrm{s}^{-1}$.

The effect of the exchange process on the NMR spectrum depends on the difference in the chemical shift frequencies of the two sites, compared with the exchange rate. Denote the chemical shift frequencies in the two states by Ω_A^0 and Ω_B^0. Define the *chemical shift difference frequency* through:

$$\Omega_\Delta = \Omega_A^0 - \Omega_B^0 \tag{19.1}$$

If the exchange rate constant has roughly the same magnitude as Ω_Δ, then the system is said to be in the *intermediate exchange* regime. This is the regime in which the NMR lineshapes are particularly sensitive to the chemical exchange process.

In the following discussion, we distinguish between two different 'sub-regimes' of intermediate exchange:

1. If the exchange rate constant is smaller than half the magnitude of Ω_Δ (but still comparable in size to Ω_Δ), then the process is said to be in the *slow intermediate exchange* regime:

$$\boxed{k < |\Omega_\Delta/2| \qquad \text{(slow intermediate exchange)}} \tag{19.2}$$

2. If the exchange rate constant is larger than half the magnitude of Ω_Δ (but still comparable in size to Ω_Δ), then the process is said to be in the *fast intermediate exchange* regime:

$$\boxed{k > |\Omega_\Delta/2| \qquad \text{(fast intermediate exchange)}} \tag{19.3}$$

The case $k = |\Omega_\Delta/2|$ is known as the *crossover point*.[4]

These motional regimes may be located on the time-scale diagram as follows:

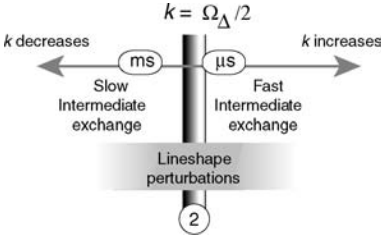

Figure 19.12
The two regimes of intermediate two-site exchange, located on the time-scale diagram.

For two-site exchange, the quantity $|2/\Omega_\Delta|$ corresponds to the 'spectral time-scale' τ_{spec}, mentioned above.

The effect of the chemical exchange on the spectrum is now explored in these two regimes.

19.5.1 Slow intermediate exchange and motional broadening

The term 'slow intermediate exchange' is rather misleading. In fact, the transitions between the two molecular states do not happen very often, but when a transition does occur, it is extremely fast. The term 'infrequent exchange' would be more accurate. For simplicity, I continue to use the common term 'slow intermediate exchange', despite its defects.

When the molecule makes a transition between the two states, the precession frequency of the nucleus changes suddenly. This is depicted for a single molecule in the following diagram:

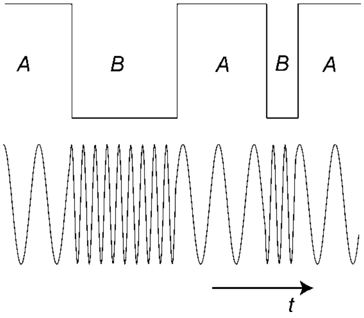

Figure 19.13
Change in the precession frequency on a molecular exchange process.

In the case shown, the precession frequency (relative to the spectrometer reference frequency) is higher for spins in molecules of type B than for molecules of type A (the simulation parameters are $\Omega_A^0/2\pi = 10\,\text{kHz}$, $\Omega_B^0/2\pi = 30\,\text{kHz}$ and $k = 3 \times 10^3\,\text{s}^{-1}$).

The unpredictable jumps in precession frequency cause enhanced dephasing of the transverse magnetization, as shown in the figure below. This shows a superposition of 20 different simulations of the precessing transverse magnetization of spins starting off in molecules of type A but which jump at random intervals between the states A and B:

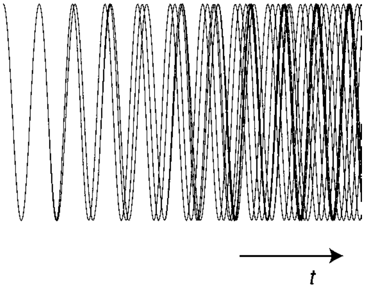

Figure 19.14
Superposition of transverse magnetization oscillations for 20 chemically exchanging molecules, all starting in the same state.

(In this case, the simulation parameters are $\Omega_A^0/2\pi = 10\,\text{kHz}$, $\Omega_B^0/2\pi = 11\,\text{kHz}$ and $k = 500\,\text{s}^{-1}$). The precessing magnetization starts off in phase, but gradually loses coordination as the molecules jump back and forth. This loss of coordination leads to enhanced decay of the total transverse magnetization. The simulation below shows the sum of many such simulations:

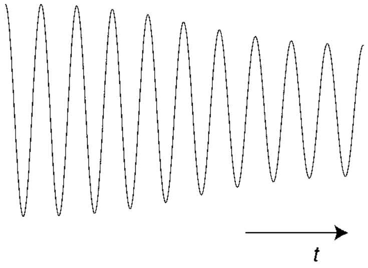

Figure 19.15
Total transverse magnetization for many chemically exchanging molecules, all starting in the same state.

The decay of the transverse magnetization is plain.

Figure 19.16 shows a superposition of precessing transverse magnetization components from many different molecules on the left and the behaviour of the total transverse magnetization on the right for a set of different k values:

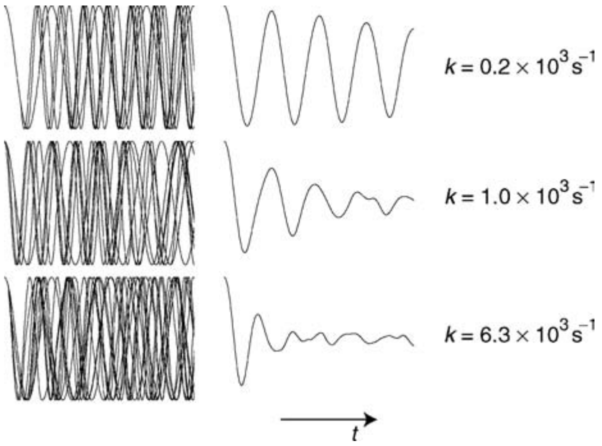

Figure 19.16
Simulations of the precessing transverse magnetization, for three different exchange rate constants in the slow intermediate exchange regime.

(The simulation parameters are $\Omega_A^0/2\pi = 2\,\text{kHz}$ and $\Omega_B^0/2\pi = 4\,\text{kHz}$; each plot spans 1 ms.) If the exchange is faster, then the decay is faster, leading to broader NMR peaks. This is called *motional broadening*.

A formal treatment of the symmetrical two-site exchange spectrum is given in Appendix A.14. In the slow intermediate exchange regime ($k < |\Omega_\Delta/2|$), the spectral lineshape is given by

$$\begin{aligned} S(\Omega) = {} & \frac{1}{2}\left(1 - \frac{\mathrm{i}k}{R}\right)\mathcal{L}(\Omega; \overline{\Omega} + R, \lambda + k) \\ & + \frac{1}{2}\left(1 + \frac{\mathrm{i}k}{R}\right)\mathcal{L}(\Omega; \overline{\Omega} - R, \lambda + k) \end{aligned} \tag{19.4}$$

where

$$\overline{\Omega} = \frac{1}{2}(\Omega_A^0 + \Omega_B^0)$$
$$R = \sqrt{|k^2 - (\Omega_\Delta/2)^2|} \tag{19.5}$$

Here, $\mathcal{L}$ is the complex Lorentzian lineshape specified in Section 5.8.2 and λ is the decay rate constant of the single-quantum coherences, in the absence of the chemical exchange process.

The following plots show how the spectral lineshapes change as the rate constant k increases:

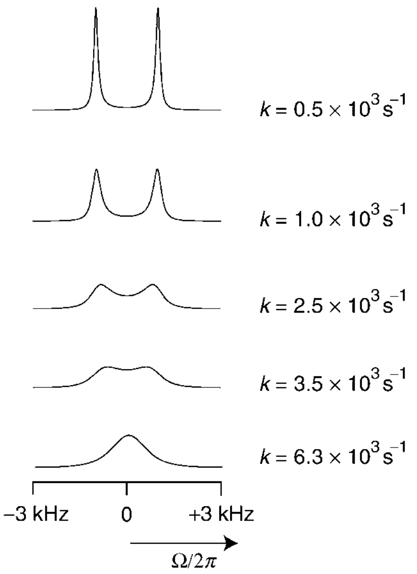

Figure 19.17
Simulated spectra for two-site exchange, in the slow intermediate exchange regime.

The simulation parameters are $\Omega_A^0/2\pi = -1\,\text{kHz}$, $\Omega_B^0/2\pi = +1\,\text{kHz}$, and $\lambda = 0$. Notice how the peaks broaden and come together as k increases. The last plot shows the spectrum at the *crossover point*[4] ($k = |\Omega_\Delta/2|$).

19.5.2 Fast intermediate exchange and motional narrowing

What happens as the exchange rate k increases beyond the crossover point, $k > |\Omega_\Delta/2|$?

Naively, it might be expected that the peaks continue to broaden as k increases, since the jumps in precession frequency occur more often. In fact, the opposite occurs. The left column in Figure 19.18 shows the precessing transverse magnetization components from many different molecules, for a set of different exchange rate constants, in the fast intermediate exchange regime. The right column shows the behaviour of the total transverse magnetization.

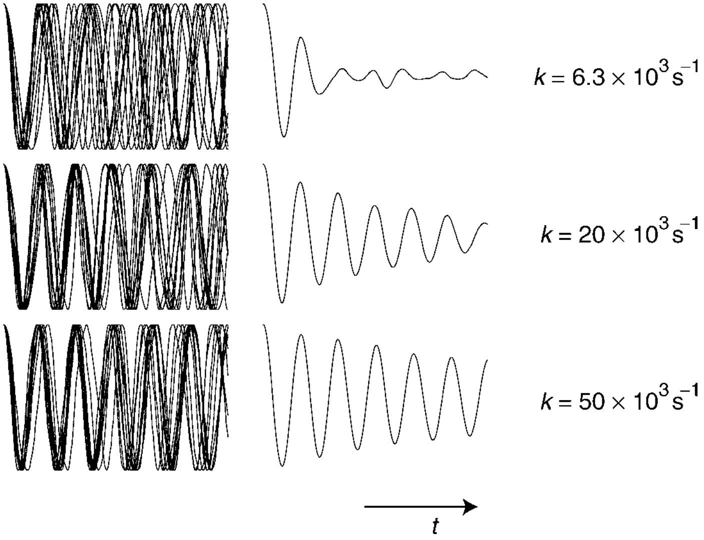

Figure 19.18
Simulations of the precessing transverse magnetization, for three different exchange rate constants in the fast intermediate exchange regime.

(The simulation parameters are $\Omega_A^0/2\pi = 2\,\mathrm{kHz}$ and $\Omega_B^0/2\pi = 4\,\mathrm{kHz}$; each plot spans 1 ms.) Remarkably, the decay of the total transverse magnetization gets *slower* as the exchange rate constant k increases. In the fast exchange regime, the NMR peakwidth is *reduced* by the rapid molecular jumps. This is called *motional narrowing*.

Motional narrowing occurs when the jumps are so frequent that spins in different chemical sites have no time to accumulate a significant phase difference between jumps. Significant precession takes place only after a time interval that corresponds to a large number of site jumps. Since roughly equal amounts of time are spent in the two sites, the *average* precession frequency is rather well defined, even when the precise timing of the individual frequency jumps is unpredictable. In the limit of very fast jumps, the spins experience the average precession frequency of the two sites.

In the fast intermediate exchange regime ($k > |\Omega_\Delta/2|$), the theoretical spectral lineshape is given by the following expression:

$$\begin{aligned} S(\Omega) &= \frac{1}{2}\left(1+\frac{k}{R}\right)\mathcal{L}(\Omega;\overline{\Omega},\lambda+k-R) \\ &\quad +\frac{1}{2}\left(1-\frac{k}{R}\right)\mathcal{L}(\Omega;\overline{\Omega},\lambda+k+R) \end{aligned} \tag{19.6}$$

where $\overline{\Omega}$ and R are defined as in Equation 19.5. Some calculated spectra are shown in Figure 19.19 for the case $\Omega_A^0/2\pi = -1\,\mathrm{kHz}$, $\Omega_B^0/2\pi = +1\,\mathrm{kHz}$, and $\lambda = 0$. Notice how the peak gets narrower as k increases beyond the crossover point.

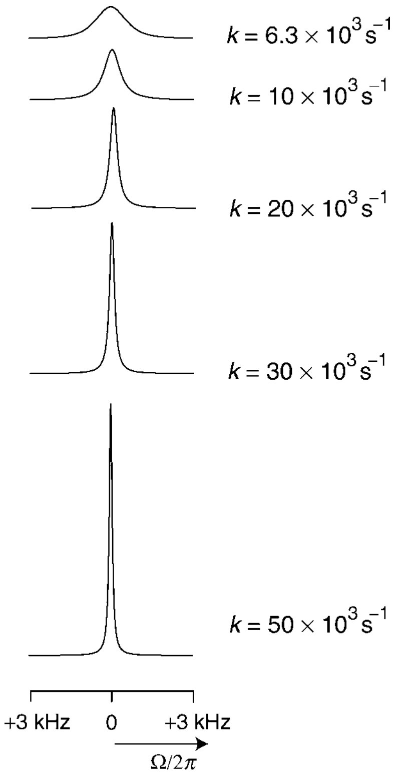

Figure 19.19
Simulated spectra for two-site exchange, in the fast intermediate exchange regime.

The spectral effects of motion may, therefore, be specified exactly for the case of symmetrical two-site exchange. In the slow intermediate exchange regime, the motion causes broadening. As the exchange rate is increased towards the crossover point, the peaks from the distinct chemical sites move together and finally merge. Further increase in the exchange rate causes narrowing of the coalesced peak. In the limit of very fast exchange, the spins only experience the average chemical shift, taken over the motion.

We may now place the case of two-site exchange firmly on the time-scale diagram:

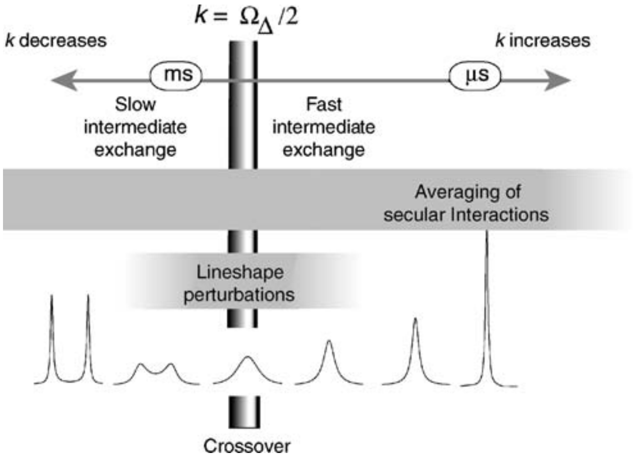

Figure 19.20
Intermediate two-site exchange located on the time-scale diagram.

In the intermediate exchange regime $k \cong |\Omega_\Delta/2|$, experimental spectra are very sensitive to the dynamics and may be used to obtain an accurate estimate of the exchange rate constant.

Some experimental ^{13}C spectra of ^{13}C-enriched N, N'-dimethylformamide, taken at a variety of temperatures in the gas phase, are shown in Figure 19.21. The rate constant k was determined at each temperature by fitting the experimental spectrum to the theoretical lineshape of Equations 19.4 and 19.6, and is shown on each plot.[5] In this case, the temperature-dependent rate constants $k(T)$ fit well to an *Arrhenius equation* of the form

$$k(T) = A \exp\{-E_{\mathrm{act}}/\mathbb{N}_{\mathrm{A}} k_B T\}$$

where $\mathbb{N}_{\mathrm{A}} = 6.022 \times 10^{23}$ mol^{-1} denotes the Avogadro constant (number of molecules in a mole of substance). The determined values of the Arrhenius activation energy and the pre-exponential factor are $E_{\mathrm{act}} = 90.1$ kJ mol^{-1} and $A = 1.16 \times 10^{14}$ s^{-1} respectively.

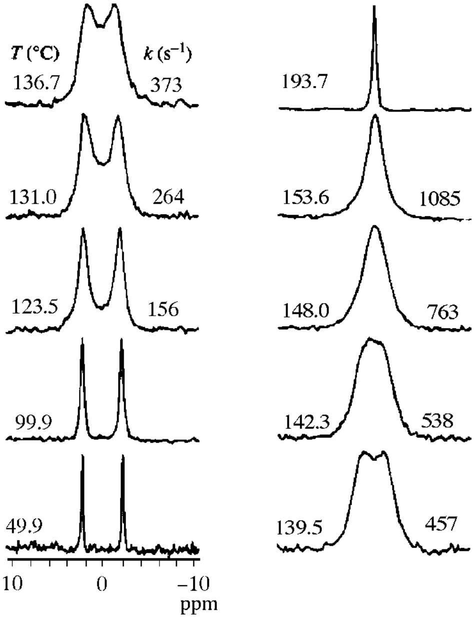

Figure 19.21
Experimental ^{13}C spectra of ^{13}C-enriched N, N'-dimethylformamide gas at a set of different temperatures in a field of 4.7 T. Taken from B. D. Ross and N. S. True, *J. Am. Chem. Soc.* **106**, 2451 (1984). (Reproduced by permission of the American Chemical Society.)

19.5.3 Averaging of J-splittings

Consider a heteronuclear two-spin-1/2 system, consisting of an I-spin coupled to an S-spin, with coupling constant J_{IS}. As described in Chapter 15, the S-spin spectrum consists of two peaks, separated in frequency by $2\pi J_{IS}$ (in radians per second). One of the peaks is associated with the $\rho_{\boxed{\alpha-}}$ (-1)-quantum coherence, and the other peak is associated with the $\rho_{\boxed{\beta-}}$ (-1)-quantum coherence.

Now suppose that the I-spin has a short spin–lattice relaxation time constant T_1. In Section 20.3.6 it is shown that the spin–lattice relaxation process may be modelled as a kinetic exchange of the I-spin states $|\alpha\rangle$ and $|\beta\rangle$ with rate constant $k = \frac{1}{2}T_1{}^{-1}$. The S-spin lineshapes correspond to the equations given above for two-site chemical exchange (Equations 19.4 and 19.6), if the following substitutions are made:

$$k \Rightarrow \frac{1}{2}T_1{}^{-1}$$

$$\Omega_\Delta \Rightarrow 2\pi J_{IS}$$

In the slow exchange limit ($T_1{}^{-1} << 2\pi|J_{IS}|$), the T_1 process broadens each doublet component by $\frac{1}{2}T_1{}^{-1}$ rad s^{-1}. In the fast exchange limit ($T_1{}^{-1} >> 2\pi|J_{IS}|$), the doublet splitting disappears and the S-spin spectrum has the form of a single peak at the Sspin chemical shift:

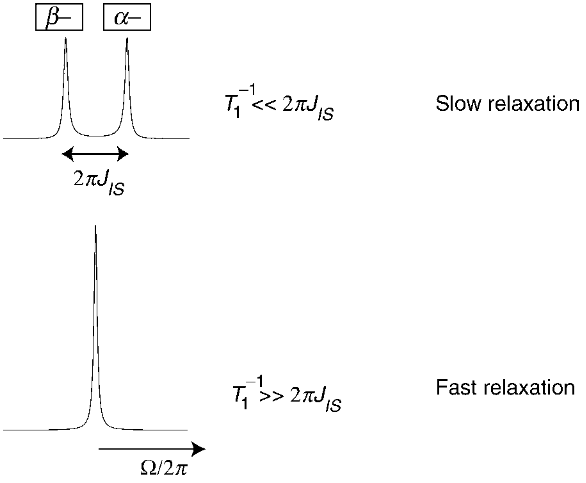

Figure 19.22 Averaging of a heteronuclear J-splitting by spin–lattice relaxation of the coupled spin.

Essentially the same conclusions apply if the rapidly relaxing I-spin has spin > 1/2. This is the most common case, since the quadrupole couplings of spins > 1/2 provide a powerful relaxation mechanism. The averaging of J-splittings by rapid longitudinal relaxation was exploited in Section 17.3.

19.5.4 Asymmetric two-site exchange

Consider again the case of chemical exchange between two molecular species, A and B. In general, the rate constant from A to B is different from the rate constant from B to A:

$$\underset{k'}{\overset{k}{A \rightleftharpoons B}}$$

For example, the exchange could represent a reversible reaction that favours one side. The reaction A → B runs faster than the reaction B → A, because of an asymmetric energy barrier:

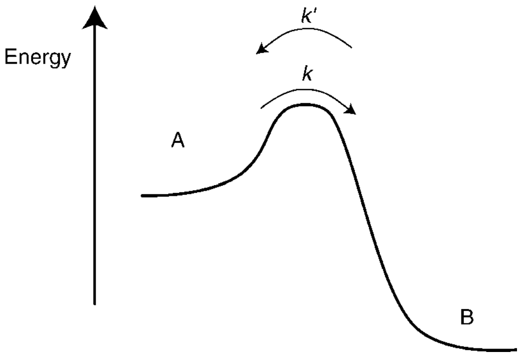

Figure 19.23 An asymmetric chemical reaction.

The ratio of rate constants $K = k/k'$ is called the *equilibrium constant* of the reaction; it is equal to the ratio of species concentrations $[\mathrm{B}]_{\mathrm{eq}} / [\mathrm{A}]_{\mathrm{eq}}$ when the reaction is in equilibrium.[6]

The full expressions for the lineshapes in the case of asymmetric two-site exchange will not be given here. The most important conclusion is that, in the fast exchange limit $k >> |\Omega_{\Delta}/2|$, the spectrum collapses to a single peak whose position is given by the mean of the two chemical shifts, *weighted by the equilibrium concentrations of the two species* (see Figure 19.24):[6]

$$\Omega_{\mathrm{peak}} = \frac{[A]_{\mathrm{eq}}\,\Omega_{\mathrm{A}}^{0} + [B]_{\mathrm{eq}}\,\Omega_{\mathrm{B}}^{0}}{[A]_{\mathrm{eq}} + [B]_{\mathrm{eq}}} = \frac{\Omega_{\mathrm{A}}^{0} + K\Omega_{\mathrm{B}}^{0}}{1 + K}$$

If the chemical shifts of the two species are known, then the position of the peak in the rapid-exchange spectrum may be used to derive the equilibrium constant of the reaction. This is a very useful property that is widely applied in many branches of chemistry.

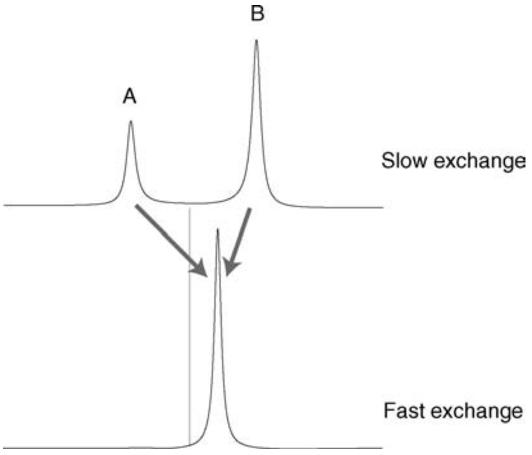

Figure 19.24
NMR spectrum for an asymmetric two-site exchange process.

Sometimes, the spectral frequency of an NMR peak is found to have a strong temperature dependence. Very often, this is because of a rapid asymmetric exchange process; since the equilibrium constant depends on temperature, so does the peak position.

19.5.5 Knight shift

An interesting example of rapid asymmetric exchange is encountered in the NMR of metals.

Nuclear spins in metals are coupled to unpaired conduction electrons, through a mechanism called the *hyperfine coupling* (this resembles the J-coupling, but has a much larger magnitude, often many megahertz). In practice, each nucleus is coupled to a large number of electrons, but, in order to simplify the discussion, let us consider only one electron. The NMR spectrum of the nucleus would be expected to display the usual doublet structure, since the electron has spin-1/2:

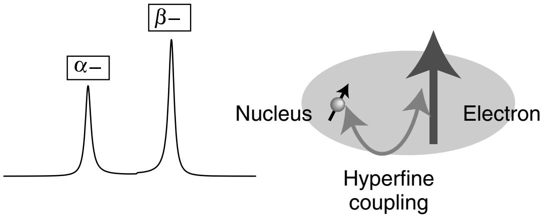

Figure 19.25
Hyperfine doublet of a nucleus coupled to an electron.

In this diagram, the $\rho_{\boxed{\beta-}}$ peak is shown as being more intense than the $\rho_{\boxed{\alpha-}}$ peak, since the Boltzmann distribution leads to a higher population in the electronic $|\beta\rangle$ states than in the electronic $|\alpha\rangle$ states, because of the Zeeman splitting of the electron in the magnetic field, and the fact that the electron has negative gyromagnetic ratio.

In the case of nuclear spins, this population difference is negligible, because the Zeeman energy is at least five orders of magnitude smaller than the available thermal energy, at room temperature. For electrons, on the other hand, the Zeeman splitting is three orders of magnitude larger, and the Boltzmann population differential may no longer be ignored.

As a result, the case of a nucleus coupled to an electron corresponds to the asymmetric two-site exchange problem. The asymmetry is caused by the different energies of the electronic $|\alpha\rangle$ and $|\beta\rangle$ states.

If the electrons have a very short T_1 (which is almost always the case), then the NMR spectrum collapses to a single peak, as described in Section 19.5.4. The position of the peak depends on the relative populations of the electronic states and is therefore shifted, since these states are not equally populated:

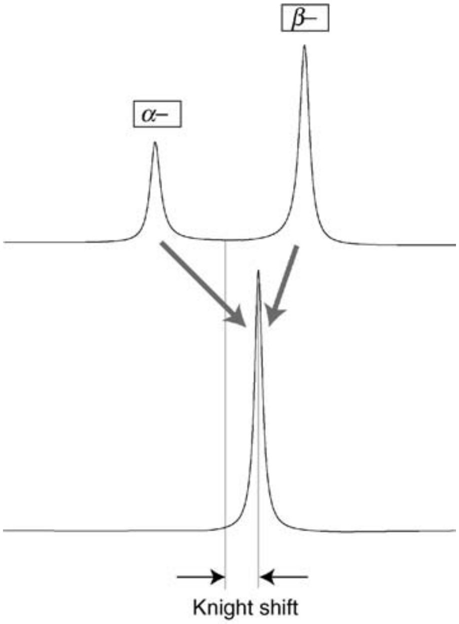

Figure 19.26
Origin of the Knight shift.

This is called the *Knight shift* (after its discoverer), and is widely used to probe the electronic structures of metals, semiconductors, and superconductors.[7]

The Knight shift depends linearly on the magnetic field and is inversely proportional to the absolute temperature, as may easily be deduced from the rough mechanistic sketch given above.

If a metal is cooled, the Knight shift increases, since the difference in Boltzmann populations between the electronic states increases. However, if the metal is cooled so much that it makes a transition into a superconductor, then the Knight shift suddenly becomes much smaller, since the electron spins pair up to form the spin-pair bosons, which are characteristic of the superconducting state.[7]

19.5.6 Paramagnetic shifts

The nuclear spin resonances of paramagnetic materials are shifted in frequency for exactly the same reason as for the Knight shift. Paramagnetic substances contain localized unpaired electrons, which couple to surrounding nuclei through the hyperfine interactions. Since the electron Zeeman states are unequally populated, and the electron relaxation is very fast, the overall effect is to shift the nuclear spin resonances.

For example, it is possible to add *paramagnetic shift reagents* to a solution in order to shift selectively the resonances of those nuclear spins that are relatively exposed to the solvent.

19.6 Sample Spinning

Mechanical sample rotation is typically on the spectral time-scale and influences the NMR spectra of solids strongly, since it modulates the anisotropic spin interactions (quadrupole couplings, chemical shift anisotropies and direct dipole–dipole couplings). In some circumstances, it is possible to use rapid sample spinning to average out anisotropic spin interactions completely. Typical rotation frequencies range from a few hundreds of hertz up to around 70 kHz. In favourable cases, fast sample spinning provides a solid-state NMR spectrum that resembles that of a liquid sample.

In *magic-angle spinning* (MAS), the solid sample is rotated rapidly around an axis which subtends the 'magic angle' ($\Theta_{\text{magic}} = \arctan\sqrt{2} = 54.74^\circ$; see Section 9.3) with respect to the static field:

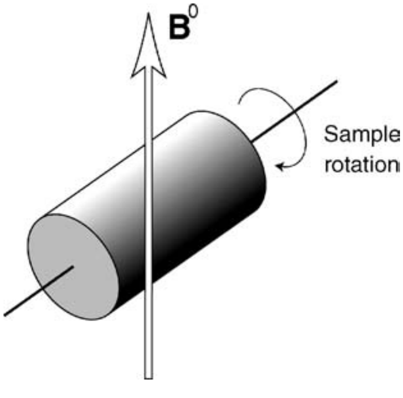

Figure 19.27
Magic-angle sample spinning.

This process averages out the secular parts of the CSA and dipolar interactions. If the spinning frequency is large enough, this leads to spin-1/2 spectra with peaks at the isotropic chemical shifts, and a resolution approaching that of a liquid sample (see Figure 19.28).

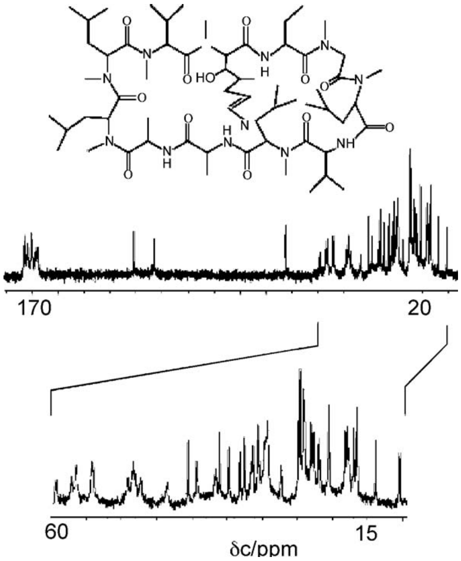

Figure 19.28
^{1}H-decoupled solid-state ^{13}C spectra of cyclosporin A (see inset), in a magnetic field of 11.74 T, at a magic-angle spinning frequency of $\omega_r/2\pi = 33.3\,\text{kHz}$. Adapted from D. D. Laws, H.-M. L. Bitter and A. Jerschow, *Angew. Chem. Int. Ed.* **41**, 3096–3129 (2002).

If the magic-angle-spinning frequency is not sufficiently large compared with shift anisotropies, the spectrum contains extra peaks called *spinning sidebands*. These appear at frequencies given by $\omega_j^{\text{iso}} + k\omega_r$, where ω_r is the spinning frequency and k is an integer. A set of experimental spectra displaying spinning sidebands is shown in Figure 19.29. A variety of methods exist for separating or suppressing spinning sidebands, even at low spinning frequencies (see *Further Reading*).

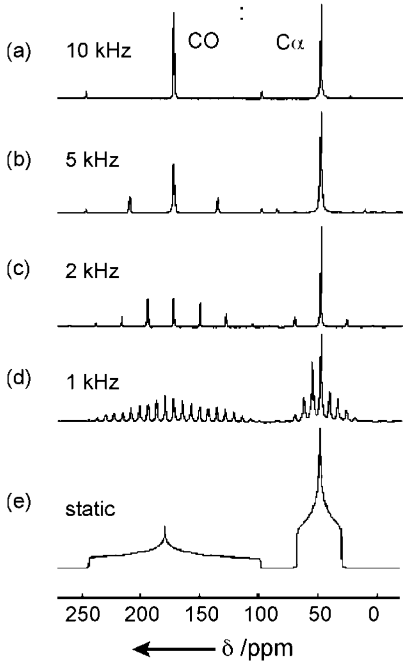

Figure 19.29
^{1}H-decoupled solid-state ^{13}C spectra of $^{13}C_2$-glycine powder, in a magnetic field of 11.74 T, at a variety of magic-angle spinning frequencies. Spectrum (e) is a simulated static spectrum. Adapted from D. D. Laws, H.-M. L. Bitter and A. Jerschow, *Angew. Chem. Int. Ed.* **41**, 3096–3129 (2002).

In most commercial magic-angle-spinning NMR probes, the r.f. coil is wound about the sample rotation axis ($\theta_{\text{RF}} = \Theta_{\text{magic}}$, see Figure 8.10). This leads to the simplest mechanical construction, but reduces the nutation frequency generated by a given r.f. field. The nutation frequency scaling factor for a coil at the magic angle is $\sin\theta_{\text{RF}} = \sin(\arctan\sqrt{2}) = \sqrt{2/3} = 0.816$.

The central transition peaks of half-integer quadrupolar nuclei are broadened by second-order quadrupolar interactions, which cannot be eliminated by magic-angle spinning alone. A variety of methods are available for eliminating second-order quadrupolar broadening, including rotation of the sample about two axes at the same time, and combinations of magic-angle spinning and r.f. pulses (see the *Further Reading* to Chapter 13).

19.7 Longitudinal Magnetization Exchange

Let us now return to the symmetrical two-site exchange process between species A and B:

$$A \underset{k}{\overset{k}{\rightleftharpoons}} B$$

Suppose now that the exchange process occurs infrequently, so that $k << |\Omega_\Delta/2|$. In this regime of *very slow exchange*, the effect on the NMR spectrum is minor. The exchange process merely broadens the NMR peaks slightly. According to Equation 19.4, the widths of the two peaks are given by $2(\lambda + k)$ rad s^{-1}, rather than 2λ rad s^{-1}, which would be the peak widths if there were no exchange. If the natural decay constant λ is larger than k, then the lineshapes are insensitive to the exchange process.

In this regime, it is very difficult to study the slow exchange process using the peak broadening, which is neither strong nor particularly specific. A different approach is therefore necessary for studying dynamic processes in the slow exchange regime.

19.7.1 Two-dimensional exchange spectroscopy

Slow exchange may be studied by using the *exchange of longitudinal magnetization* between the two chemical sites. This may be done by performing two-dimensional spectroscopy with a sequence of three $\pi/2$ pulses:

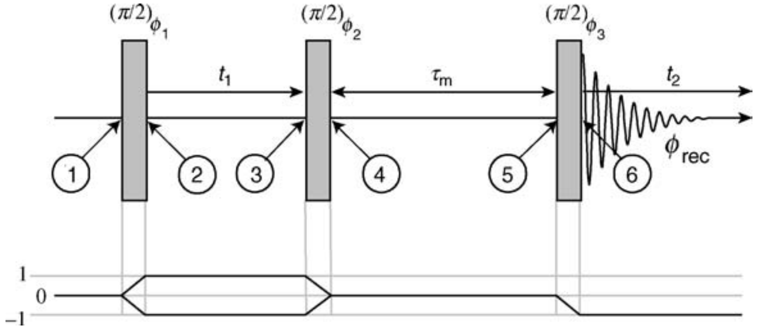

Figure 19.30
Pulse sequence for two-dimensional exchange spectroscopy.

Table 19.1 An eight-step phase cycle ($\mathfrak{n} = 8$) appropriate for the 2D-exchange experiment[8]. The phase Ψ is used in the States scheme for generating pure absorption 2D lineshapes, with discrimination of positive and negative Ω_1-frequencies (see Section 5.9.4). For the "cosine" data set, $\Psi = 0$. For the "sine" data set, $\Psi = -\pi/2$ (see Note 9).

Cycle counter $\mathfrak{m}$	ϕ_1	ϕ_2	ϕ_3	$\phi_{\rm rec}$
0	Ψ	π	0	0
1	$\Psi + \pi$	π	0	π
2	Ψ	π	$\pi/2$	$\pi/2$
3	$\Psi + \pi$	π	$\pi/2$	$3\pi/2$
4	Ψ	π	π	π
5	$\Psi + \pi$	π	π	0
6	Ψ	π	$3\pi/2$	$3\pi/2$
7	$\Psi + \pi$	π	$3\pi/2$	$\pi/2$

As usual, the single-headed arrow labelled t_1 implies arrayed signal acquisition with variation of this time delay. The double-headed arrow marked $\tau_{\rm m}$ implies that this interval is kept fixed during the acquisition of the two-dimensional data matrix $s(t_1, t_2)$.

The fixed interval $\tau_{\rm m}$ plays a central role in this experiment and is called the *mixing interval*.

The diagram shows the coherence transfer pathways for this pulse sequence: the desired signals pass through (± 1)-quantum coherence during the interval between the first $\pi/2$ pulses, have coherence order zero during the mixing interval $\tau_{\rm m}$, and are converted into observable (-1)-quantum coherences by the last $\pi/2$ pulse. An eight-step phase cycle for selecting this signal pathway is given in Table 19.1. This phase table also includes the implementation of the States scheme for generating pure absorption two-dimensional lineshapes (see Section 5.9.4). The phase cycle may be treated using the principles in Appendix A.11.

Consider the simplest possible case, in which each molecule contains a single, isolated, nuclear spin-1/2. The chemical exchange process changes the chemical shift of the spin. In the case of slow symmetrical two-site exchange, the two-dimensional spectrum has the following form:

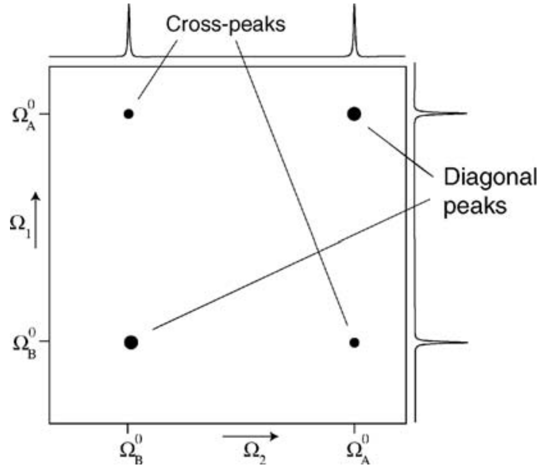

Figure 19.31
Schematic form of a two-dimensional exchange spectrum.

There are two *diagonal peaks*, at frequency coordinates $(\Omega_1, \Omega_2) = \left(\Omega_A^0, \Omega_A^0\right)$ and $(\Omega_1, \Omega_2) = \left(\Omega_B^0, \Omega_B^0\right)$, and two *cross-peaks*, at frequency coordinates $(\Omega_1, \Omega_2) = \left(\Omega_A^0, \Omega_B^0\right)$ and $(\Omega_1, \Omega_2) = \left(\Omega_B^0, \Omega_A^0\right)$. The existence of the cross-peaks is a signature of the dynamic exchange process between the two sites. The cross-peak amplitudes provide a quantitative estimate of the exchange rate constant.

At short mixing intervals $\tau_m < k^{-1}$, the cross-peaks are absent and the spectrum contains only diagonal peaks. As the mixing interval increases, the cross-peaks become more intense and the diagonal peaks weaker. If the mixing interval is longer than around $2k^{-1}$, the cross-peaks and diagonal peaks have approximately equal intensity. Further increase in τ_m causes both cross-peaks and diagonal peaks to decrease:

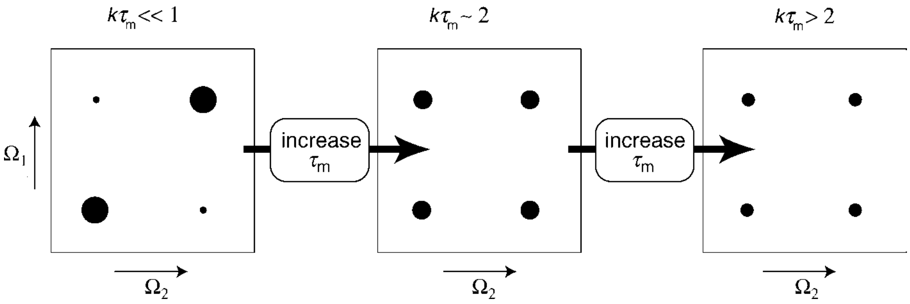

Figure 19.32 Change in the two-dimensional exchange spectrum as the mixing interval τ_m increases, for the case of symmetrical two-site exchange.

A derivation of the theoretical peak amplitudes is given in Appendix A.14.4. If the spin–lattice relaxation times of the two sites are the same ($T_1^A = T_1^B = T_1$), then the amplitudes of the diagonal and cross-peaks are given by

$$\boxed{\begin{aligned} a_{\text{diag}}(\tau_m) &= \cosh(k\tau_m)\exp\{-(k+T_1^{-1})\tau_m\} \\ a_{\text{cross}}(\tau_m) &= \sinh(k\tau_m)\exp\{-(k+T_1^{-1})\tau_m\} \end{aligned} \qquad (19.7)}$$

where the hyperbolic cosine and sine functions are defined as:

$$\cosh x = \frac{1}{2}(e^x + e^{-x})$$
$$\sinh x = \frac{1}{2}(e^x - e^{-x})$$

The peak amplitudes are shown below for the case $k = 10\,\text{s}^{-1}$ and $T_1^A = T_1^B = T_1 = 1\,\text{s}$:

Figure 19.33 Diagonal and cross-peak amplitudes as a function of τ_m.

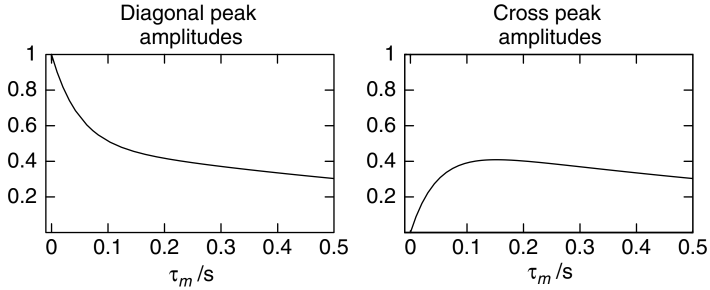

The *ratio* of the cross-peak and diagonal-peak amplitudes is independent of the spin–lattice relaxation time T_1, and is given by

$$\frac{a_{\mathrm{cross}}}{a_{\mathrm{diag}}}(\tau_{\mathrm{m}}) = \frac{\sinh(k\tau_{\mathrm{m}})}{\cosh(k\tau_{\mathrm{m}})} = \tanh k\tau_{\mathrm{m}} \tag{19.8}$$

where the hyperbolic tangent is defined as

$$\tanh x = \sinh x / \cosh x$$

The behaviour of the cross-peak/diagonal-peak ratio is shown below for the case $k = 10\,\mathrm{s}^{-1}$ and $T_1^{\mathrm{A}} = T_1^{\mathrm{B}} = T_1 = 1\,\mathrm{s}$:

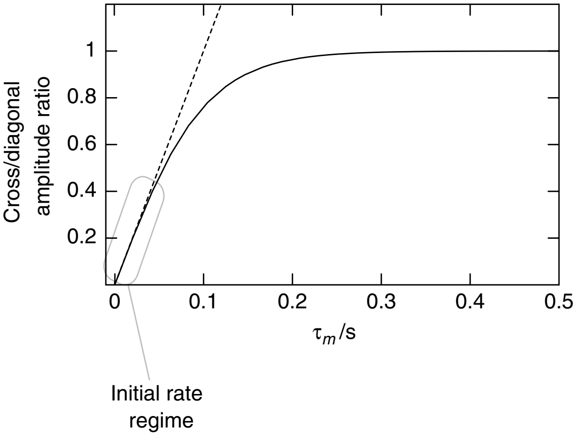

Figure 19.34
Ratio of the cross-peak amplitude to the diagonal-peak amplitude as a function of τ_{m}.

At short mixing intervals ($k\tau_{\mathrm{m}} < 1$), the cross-peak to diagonal-peak ratio is approximately linearly dependent on τ_{m}, according to

$$\frac{a_{\mathrm{cross}}}{a_{\mathrm{diag}}}(\tau_{\mathrm{m}}) \cong k\tau_{\mathrm{m}} \tag{19.9}$$

as shown by the dotted line in the plot. This is called the *initial rate regime*.

The rate constant k of the exchange process may be estimated by repeating the two-dimensional experiment with several values of the mixing interval τ_{m}, followed by fitting the experimental cross-peak/diagonal-peak ratios to Equation 19.8 (in the general case), or to Equation 19.9 (in the initial rate regime).

19.7.2 Theory

I now give a theoretical description of the two-dimensional exchange experiment using the density operator formalism. We must take into account the fact that the spins are transported between two different sorts of molecules, A and B, in a dynamic exchange process.

As discussed in Appendix A.14, it is possible to write the spin density operator as

$$\hat{\rho} = \frac{1}{2}\hat{\rho}^A + \frac{1}{2}\hat{\rho}^B$$

for the case of two-site exchange. The density operator of spins in molecules of type A is given by

$$\hat{\rho}^A = \overline{|\psi\rangle\langle\psi|}^A$$

where the overbar indicates averaging over all type-A molecules. Similarly, the density operator of spins in molecules B is given by

$$\hat{\rho}^B = \overline{|\psi\rangle\langle\psi|}^B$$

where the overbar indicates averaging over all type-B molecules.

The spin density operator components at the beginning of the pulse sequence are given by

$$\hat{\rho}^A_{\textcircled{1}} \sim I_z \,; \qquad \hat{\rho}^B_{\textcircled{1}} \sim I_z$$

ignoring the unity operator and the usual numerical factors. This describes a state in which the spins of both types of molecule are weakly polarized along the z-axis by the external magnetic field.

In the case of very slow exchange ($k << |\Omega_\Delta/2|$), the evolution of the spin density operator components up to time point ④ may be calculated independently, using the geometrical arguments developed in Chapters 11 and 12. For spins in molecules of type A, the first two $\pi/2$ pulses and the variable interval t_1 lead to the following transformation:

$$\begin{tikzcd}
\hat{\rho}^A_{\textcircled{1}} = I_z \arrow[d, "(\pi/2)_x"] \\
\hat{\rho}^A_{\textcircled{2}} = -I_y \arrow[d, "t_1"] \\
\hat{\rho}^A_{\textcircled{3}} = \left(-I_y \cos(\Omega^0_\mathrm{A} t_1) + I_x \sin(\Omega^0_\mathrm{A} t_1)\right) \ \exp\{-\lambda' t_1\} \arrow[d, "(\pi/2)_{\bar{x}}"] \\
\hat{\rho}^A_{\textcircled{4}} = \left(+I_z \cos(\Omega^0_\mathrm{A} t_1) + I_x \sin(\Omega^0_\mathrm{A} t_1)\right) \ \exp\{-\lambda' t_1\}
\end{tikzcd}$$

(The phases of the pulses correspond to the first row of Table 19.1, with $\Psi = 0$.) These transformations are depicted in the following diagrams:

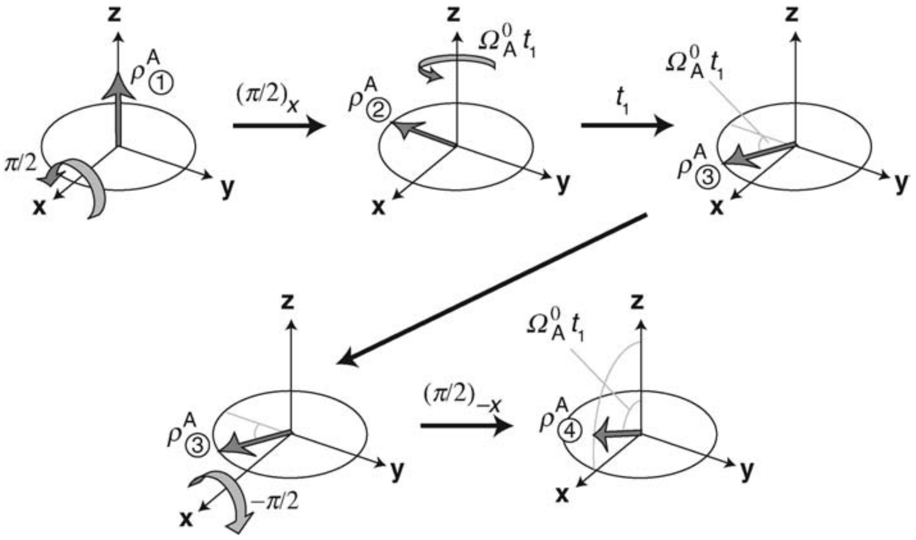

Figure 19.35 Transformations of the density operator of spins in type-A molecules, during the first part of a two-dimensional exchange pulse sequence.

Equation 19.10 includes a damping factor $\exp\{-\lambda' t_1\}$ for the decay of transverse relaxation during the evolution interval t_1. According to Equation 19.4, the decay rate constant is given by

$$\lambda' = \lambda + k$$

where the contribution k takes into account the peak broadening from the slow exchange process and λ takes into account any other coherence decay mechanisms. The overall transverse relaxation time is $T_2 = 1/\lambda'$.

Similarly, the density operator for spins in molecules of type B at time point ④ is given by

$$\hat{\rho}^{B}_{④} = \left(+I_z \cos(\Omega^0_{\rm B} t_1) + I_x \sin(\Omega^0_{\rm B} t_1)\right) \ \exp\{-\lambda' t_1\}$$

As shown in Appendix A.11, the phase cycle specified in Table 19.1 has the effect of suppressing all signal contributions that do not pass through longitudinal magnetization under the mixing interval. As a result, only the longitudinal spin density operator components at time point ④ need be taken into account. These are

$$\begin{aligned}\hat{\rho}^{A}_{④} &= I_z \cos(\Omega^0_{\rm A} t_1) \exp\{-\lambda' t_1\} + \ldots \\ \hat{\rho}^{B}_{④} &= I_z \cos(\Omega^0_{\rm B} t_1) \exp\{-\lambda' t_1\} + \ldots\end{aligned}$$

In the two-dimensional experiment, data are collected with a large number of values of the evolution interval t_1. As t_1 increases, the longitudinal magnetization of spins in molecules A oscillates at the frequency $\Omega^0_{\rm A}$. Similarly, the longitudinal magnetization of spins in molecules B oscillates at the frequency $\Omega^0_{\rm B}$. These characterisitic t_1 modulations provide *frequency labels* that reveal the origin of the longitudinal magnetization components at time point ④.

Consider now the evolution of the density operator in the mixing interval τ_{m}. The exchange process leads to a transport of longitudinal magnetization between the two components of the spin density operator, $\hat{\rho}^A$ and $\hat{\rho}^B$, at the same time as the magnetization components decay, due to spin–lattice relaxation. The fate of the A-type spin magnetization during the mixing interval is sketched below:

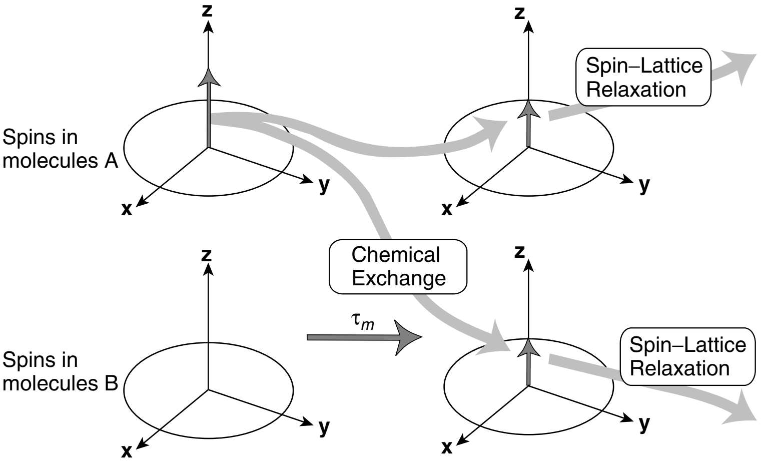

Figure 19.36
Physical processes during the mixing interval of a two-dimensional exchange experiment.

An accurate treatment of the magnetization dynamics is given in Appendix A.14.4. The spin density operator at time ⑤ is given by

$$\hat{\rho}^{\mathrm{A}}_{\textcircled{5}} = I_z \left\{ a_{\mathrm{A}\to\mathrm{A}}(\tau_{\mathrm{m}}) \cos(\Omega^0_{\mathrm{A}} t_1) + a_{\mathrm{B}\to\mathrm{A}}(\tau_{\mathrm{m}}) \cos(\Omega^0_{\mathrm{B}} t_1) \right\} \exp\{-\lambda' t_1\} + \ldots$$

$$\hat{\rho}^{\mathrm{B}}_{\textcircled{5}} = I_z \left\{ a_{\mathrm{B}\to\mathrm{B}}(\tau_{\mathrm{m}}) \cos(\Omega^0_{\mathrm{B}} t_1) + a_{\mathrm{A}\to\mathrm{B}}(\tau_{\mathrm{m}}) \cos(\Omega^0_{\mathrm{A}} t_1) \right\} \exp\{-\lambda' t_1\} + \ldots$$

where the diagonal- and cross-magnetization transfer amplitudes are given in Equation 19.7.

The final $\pi/2$ pulse performs the usual conversion of longitudinal magnetization into transverse magnetization:

$$\hat{\rho}^{\mathrm{A}}_{\textcircled{6}} = -I_y \left\{ a_{\mathrm{A}\to\mathrm{A}}(\tau_{\mathrm{m}}) \cos(\Omega^0_{\mathrm{A}} t_1) + a_{\mathrm{B}\to\mathrm{A}}(\tau_{\mathrm{m}}) \cos(\Omega^0_{\mathrm{B}} t_1) \right\} \exp\{-\lambda' t_1\} + \ldots$$

$$\hat{\rho}^{\mathrm{B}}_{\textcircled{6}} = -I_y \left\{ a_{\mathrm{B}\to\mathrm{B}}(\tau_{\mathrm{m}}) \cos(\Omega^0_{\mathrm{B}} t_1) + a_{\mathrm{A}\to\mathrm{B}}(\tau_{\mathrm{m}}) \cos(\Omega^0_{\mathrm{A}} t_1) \right\} \exp\{-\lambda' t_1\} + \ldots$$

The (-1)-quantum coherences at the beginning of the detection interval, therefore, are

$$\hat{\rho}^{\mathrm{A}}_{\boxed{-}}\textcircled{6} = \frac{1}{2\mathrm{i}} \left\{ a_{\mathrm{A}\to\mathrm{A}}(\tau_{\mathrm{m}}) \cos(\Omega^0_{\mathrm{A}} t_1) + a_{\mathrm{B}\to\mathrm{A}}(\tau_{\mathrm{m}}) \cos(\Omega^0_{\mathrm{B}} t_1) \right\} \exp\{-\lambda' t_1\}$$

$$\hat{\rho}^{\mathrm{B}}_{\boxed{-}}\textcircled{6} = \frac{1}{2\mathrm{i}} \left\{ a_{\mathrm{B}\to\mathrm{B}}(\tau_{\mathrm{m}}) \cos(\Omega^0_{\mathrm{B}} t_1) + a_{\mathrm{A}\to\mathrm{B}}(\tau_{\mathrm{m}}) \cos(\Omega^0_{\mathrm{A}} t_1) \right\} \exp\{-\lambda' t_1\}$$

The transverse magnetization precesses during the subsequent detection interval at the appropriate chemical shift frequency and induces a quadrature NMR signal in the usual way. For spins in molecules A during the detection interval, the signal is given by

$$s_A^{\cos}(t_1, t_2) = 2\mathrm{i}\hat{\rho}^{A}_{\boxed{-}}\textcircled{6}\ \exp\{(\mathrm{i}\Omega_A^0 - \lambda')t_2\}$$

(The superscript 'cos' indicates the 'cosine' data set in the States procedure, generated with phase $\Psi = 0$.) For spins in molecules B during the detection interval, the signal is given by

$$s_B^{\cos}(t_1, t_2) = 2\mathrm{i}\hat{\rho}^{B}_{\boxed{-}}\textcircled{6}\ \exp\{(\mathrm{i}\Omega_\mathrm{B}^0 - \lambda')t_2\}$$

These results may be combined to obtain the full two-dimensional signal for the 'cosine' data set ($\Psi = 0$):

$$s^{\cos}(t_1, t_2) = s^{\cos}_{\mathrm{A}\to\mathrm{A}}(t_1, t_2) + s^{\cos}_{\mathrm{A}\to\mathrm{B}}(t_1, t_2) + s^{\cos}_{\mathrm{B}\to\mathrm{A}}(t_1, t_2) + s^{\cos}_{\mathrm{B}\to\mathrm{B}}(t_1, t_2)$$

with

$$\begin{aligned}
s^{\cos}_{\mathrm{A}\to\mathrm{A}}(t_1, t_2) &= a_{\mathrm{A}\to\mathrm{A}}(\tau_\mathrm{m})\cos(\Omega^0_\mathrm{A}t_1)\exp\{-\lambda' t_1\}\exp\{(\mathrm{i}\Omega^0_\mathrm{A} - \lambda')t_2\}\\
s^{\cos}_{\mathrm{A}\to\mathrm{B}}(t_1, t_2) &= a_{A\to B}(\tau_\mathrm{m})\cos(\Omega^0_\mathrm{A}t_1)\exp\{-\lambda' t_1\}\exp\{(\mathrm{i}\Omega^0_\mathrm{B} - \lambda')t_2\}\\
s^{\cos}_{\mathrm{B}\to\mathrm{A}}(t_1, t_2) &= a_{\mathrm{B}\to\mathrm{A}}(\tau_\mathrm{m})\cos(\Omega^0_\mathrm{B}t_1)\exp\{-\lambda' t_1\}\exp\{(\mathrm{i}\Omega^0_\mathrm{A} - \lambda')t_2\}\\
s^{\cos}_{\mathrm{B}\to\mathrm{B}}(t_1, t_2) &= a_{\mathrm{B}\to\mathrm{B}}(\tau_\mathrm{m})\cos(\Omega^0_\mathrm{B}t_1)\exp\{-\lambda' t_1\}\exp\{(\mathrm{i}\Omega^0_\mathrm{B} - \lambda')t_2\}
\end{aligned}$$

The terms $s^{\cos}_{A\to A}$ and $s^{\cos}_{B\to B}$ generate the two diagonal peaks in the two-dimensional spectrum. The terms $s^{\cos}_{A\to B}$ and $s^{\cos}_{B\to A}$ generate the two cross-peaks.

Note that all four signals display cosine modulations with respect to t_1, as required for the 'cosine' data set in the States data acquisition scheme.

If the derivation is repeated for the 'sine' data set ($\Psi = -\pi/2$),[9] we get

$$s^{\sin}(t_1, t_2) = s^{\sin}_{\mathrm{A}\to\mathrm{A}}(t_1, t_2) + s^{\sin}_{A\to B}(t_1, t_2) + s^{\sin}_{\mathrm{B}\to\mathrm{A}}(t_1, t_2) + s^{\sin}_{B\to B}(t_1, t_2)$$

with

$$\begin{aligned}
s^{\sin}_{\mathrm{A}\to\mathrm{A}}(t_1, t_2) &= a_{\mathrm{A}\to\mathrm{A}}(\tau_\mathrm{m})\sin(\Omega^0_\mathrm{A}t_1)\exp\{-\lambda' t_1\}\exp\{(\mathrm{i}\Omega^0_\mathrm{A} - \lambda')t_2\}\\
s^{\sin}_{\mathrm{A}\to\mathrm{B}}(t_1, t_2) &= a_{\mathrm{A}\to\mathrm{B}}(\tau_\mathrm{m})\sin(\Omega^0_\mathrm{A}t_1)\exp\{-\lambda' t_1\}\exp\{(\mathrm{i}\Omega^0_\mathrm{B} - \lambda')t_2\}\\
s^{\sin}_{\mathrm{B}\to\mathrm{A}}(t_1, t_2) &= a_{\mathrm{B}\to\mathrm{A}}(\tau_\mathrm{m})\sin(\Omega^0_\mathrm{B}t_1)\exp\{-\lambda' t_1\}\exp\{(\mathrm{i}\Omega^0_\mathrm{A} - \lambda')t_2\}\\
s^{\sin}_{\mathrm{B}\to\mathrm{B}}(t_1, t_2) &= a_{\mathrm{B}\to\mathrm{B}}(\tau_\mathrm{m})\sin(\Omega^0_\mathrm{B}t_1)\exp\{-\lambda' t_1\}\exp\{(\mathrm{i}\Omega^0_\mathrm{B} - \lambda')t_2\}
\end{aligned}$$

All terms have sine modulations with respect to t_1, as required by the States scheme.

The data sets $s^{\cos}(t_1, t_2)$ and $s^{\sin}(t_1, t_2)$ are combined and processed as described in Section 5.9.4 to obtain the two-dimensional spectrum:

$$S(\Omega_1, \Omega_2) = S_{\mathrm{A}\to\mathrm{A}}(\Omega_1, \Omega_2) + S_{\mathrm{A}\to\mathrm{B}}(\Omega_1, \Omega_2) + S_{\mathrm{B}\to\mathrm{A}}(\Omega_1, \Omega_2) + S_{\mathrm{B}\to\mathrm{B}}(\Omega_1, \Omega_2)$$

where

$$\begin{aligned}
\mathrm{Re}\{S_{\mathrm{A}\to\mathrm{A}}(\Omega_1, \Omega_2)\} &= a_{\mathrm{diag}}(\tau_{\mathrm{m}})\, \mathcal{A}(\Omega_1, \Omega_2;\, \Omega^0_{\mathrm{A}}, \lambda', \Omega^0_{\mathrm{A}}, \lambda') \\
\mathrm{Re}\{S_{\mathrm{A}\to\mathrm{B}}(\Omega_1, \Omega_2)\} &= a_{\mathrm{cross}}(\tau_{\mathrm{m}})\, \mathcal{A}(\Omega_1, \Omega_2;\, \Omega^0_{\mathrm{A}}, \lambda', \Omega^0_{\mathrm{B}}, \lambda') \\
\mathrm{Re}\{S_{\mathrm{B}\to\mathrm{A}}(\Omega_1, \Omega_2)\} &= a_{\mathrm{cross}}(\tau_{\mathrm{m}})\, \mathcal{A}(\Omega_1, \Omega_2;\, \Omega^0_{\mathrm{B}}, \lambda', \Omega^0_{\mathrm{A}}, \lambda') \\
\mathrm{Re}\{S_{\mathrm{B}\to\mathrm{B}}(\Omega_1, \Omega_2)\} &= a_{\mathrm{diag}}(\tau_{\mathrm{m}})\, \mathcal{A}(\Omega_1, \Omega_2;\, \Omega^0_{\mathrm{B}}, \lambda', \Omega^0_{\mathrm{B}}, \lambda')
\end{aligned}$$

and

$$\begin{aligned}
a_{\mathrm{diag}} &= a_{A\to A} = a_{B\to B} \\
a_{\mathrm{cross}} &= a_{A\to B} = a_{B\to A}
\end{aligned}$$

The two-dimensional absorption lineshape $\mathcal{A}$ is defined in Equation 5.26.

The result is a two-dimensional spectrum containing two absorption diagonal peaks with amplitudes a_{diag} and two absorption cross-peaks with amplitudes a_{cross}:

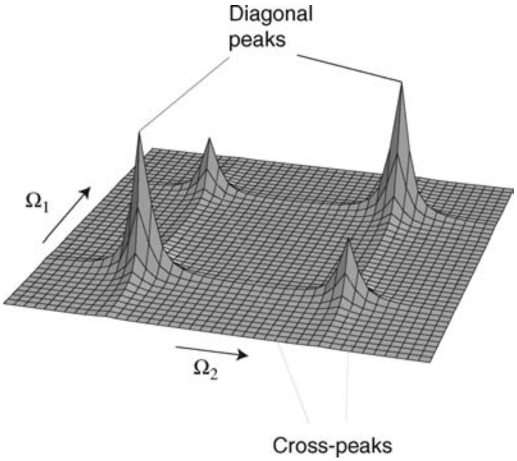

Figure 19.37
Form of the two-dimensional exchange spectrum.

An experimental application of two-dimensional exchange spectroscopy is shown in Figure 19.38.

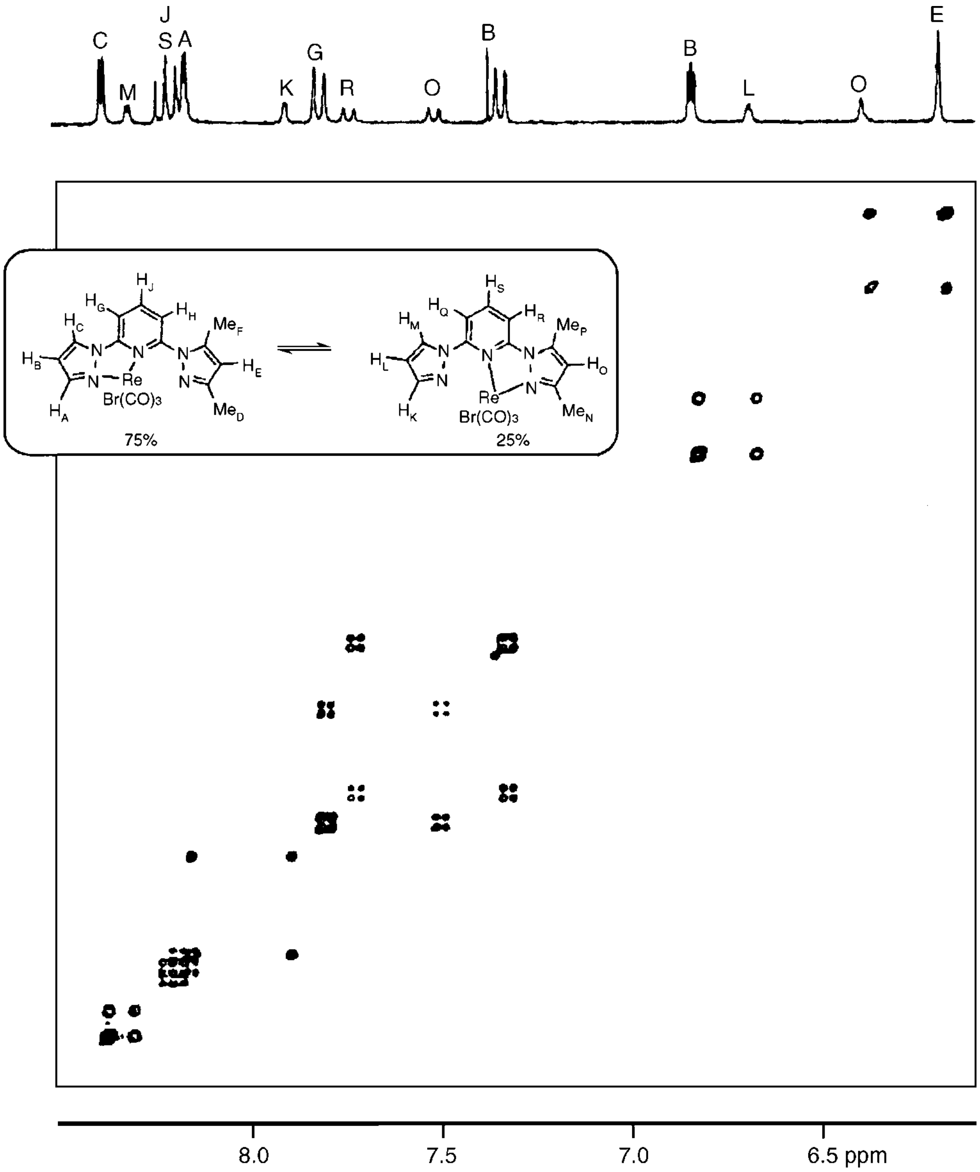

Figure 19.38 Proton two-dimensional exchange spectrum of the organometallic fluxional compound [ReBr(CO)$_3$(Me$_2$-bppy)], where bppy denotes 2,6-bis(pyrazol-1-yl)pyridine (see inset). The mixing interval was $\tau_m = 0.1$ s. The off-diagonal peaks may be interpreted in terms of an exchange of the metal atom between two pairs of nitrogen binding sites, as shown in the inset. Adapted from E. W. Abel, *et al.*, *J. Chem. Soc. Dalton Trans.*, 1079 (1994). (Copyright, the Royal Society of Chemistry.)

19.7.3 Motional regimes

Two-dimensional exchange spectroscopy allows chemical exchange processes to be identified and quantitated in the slow exchange regime $T_1{}^{-1} < k << |\Omega_\Delta/2|$:

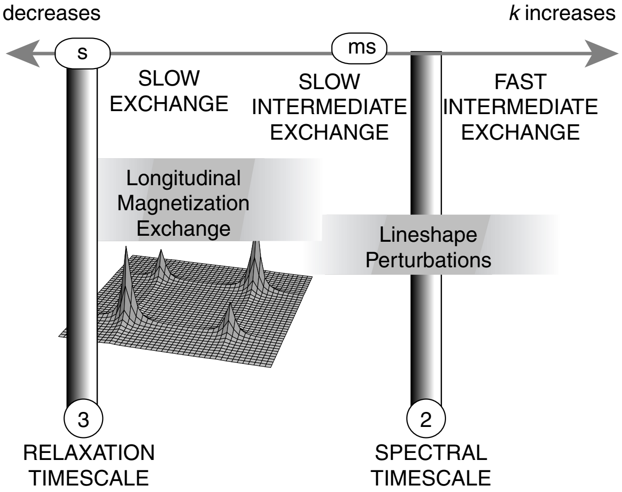

Figure 19.39
Two-dimensional magnetization exchange located on the time-scale diagram.

The two-dimensional exchange experiment does not work if the exchange is much slower than $T_1{}^{-1}$, since the spin populations equilibrate completely during the mixing interval, and the ‘frequency labelling’ of the longitudinal magnetization components is lost.

If the exchange is fast enough to approach the spectral time-scale, the intepretation of the two-dimensional exchange experiment is less straightforward, since the two-dimensional peaks are also broadened and distorted.

19.8 Diffusion

The study of molecular diffusion by NMR is a large and important subject. Only a few superficial remarks will be made here.

One of the basic pulse sequences used to study molecular diffusion is shown in Figure 5.9. This is a three-pulse *stimulated echo* sequence, with pulsed field gradients applied between the first two pulses and after the third one. This pulse sequence has a close relationship with the NOESY sequence in Figure 19.30, and it functions in a similar way. Instead of chemical shift evolution between the first two $\pi/2$ pulses, there is evolution of transverse magnetization in the presence of a field gradient. Instead of chemical exchange during the mixing interval τ_m, there is molecular diffusion. In both experiments, magnetization is stored in the longitudinal form during the relatively long mixing interval, to allow the exchange or motional process to take place.

Suppose that the gradient pulses are applied along the x-axis. It may be shown that the amplitude of the NMR signal after the stimulated echo sequence is proportional to

$$a(T) = a(0) \exp\{-D_x \kappa^2 T\} \tag{19.10}$$

where T is the effective time interval between the two gradient pulses (in general, this takes into account their finite duration), D_x is the diffusion coefficient of the molecules in the x-direction, and κ is a measure of the strength of the gradient pulses, given by

$$\kappa = \gamma\sigma_{\mathrm{G}}\mathrm{G}_{\max}\tau_{\mathrm{G}}$$

where $G_{\max}$ is the maximum gradient strength, τ_G is the gradient pulse duration, and the factor σ_G takes into account the rounded shape of the gradient pulse:

$$\sigma_{\mathrm{G}} = G_{\max}^{-1} \int_0^{\tau_{\mathrm{G}}} G(t)\,\mathrm{d}t$$

The signal, therefore, decays as a function of the interval between the gradient pulses, and the rate constant of this decay may be used to estimate the diffusion constant.

If the experiment is repeated with gradient pulses in the three different directions, it is possible to estimate the three diffusion constants $\{D_x, D_y, D_z\}$ individually. In an isotropic medium, all three diffusion constants are the same, but in an anisotropic medium, such as many body tissues, they are not. For example, the diffusion of water is easier along the length of a narrow channel rather than perpendicular to it:

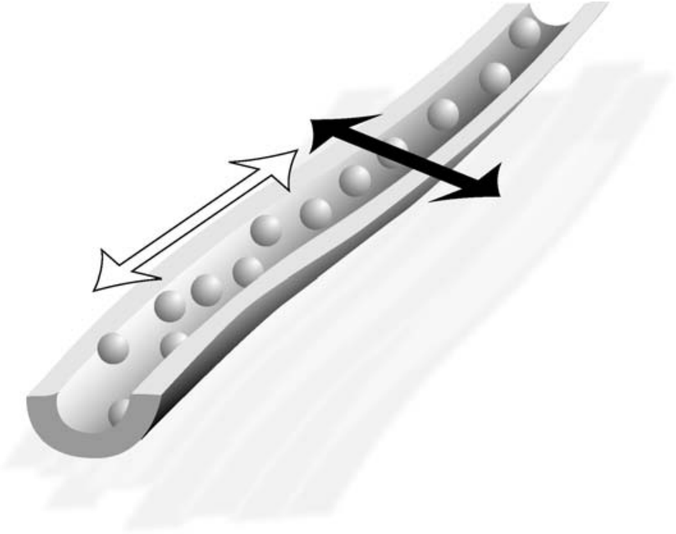

Figure 19.40
The diffusion of water in a fibrous or channel-like system is anisotropic: diffusion is faster along the channel (white) than diffusion perpendicular to the channel (black).

By studying the directions of fastest diffusion for neighbouring volume elements in an NMR image, it is possible to trace out the pathways of nerves and similar channel-like structures in the human body. This technique is called *diffusion tensor imaging*. An experimental result is shown in Plate 4.

Notes

1. In some cases, motional processes that are significantly slower than T_1 may be studied by exploiting *long-lived spin states*. For example, see S. Cavadini, J. Dittmer, S. Antonijevic and G. Bodenhausen, *J. Am. Chem. Soc.* **127**, 15 744–15 748 (2005).

2. The spin–spin *distance* also varies during vibrational or librational motion. However, the oscillation of the distance tends to *increase* the value of the dipole–dipole coupling constant. The observed *decrease* in the dipole–dipole coupling constants is due to the angular libration, which more than compensates the opposite effect of the bond length oscillations. To calculate the motionally averaged dipolar coupling, one must average the *full form* of the dipolar interaction (Equation 9.3).A motional average of the r^{-3} term alone gives incorrect results. The commonly encountered expression $b \sim \left\langle r^{-3} \right\rangle$, where the angular brackets denote motional averaging, is *incorrect* in general.

3. Relaxation calculations in liquids that do not employ librationally corrected dipole–dipole coupling constants may lead to an overestimate of the internal molecular mobility and flexibility.

4. The crossover point between the two exchange regimes is close, but not identical, to the *coalescence point*, at which the two peaks merge into one. Coalescence is defined by the point at which the second derivative of $\mathrm{Re}\{S(\Omega)\}$ with respect to Ω vanishes, at the mean frequency of the two peaks $\Omega = \overline{\Omega}$. If λ is ignored, coalescence occurs at the rate constant $k = \Omega_\Delta/(2\sqrt{2})$.

5. When performing such fits, one should be aware that the chemical shifts may be temperature dependent, as well as the exchange rate constant.

6. I neglect here the distinction between the concentration and the kinetic activity of a substance.

7. At first sight, it is surprising that NMR may be performed at all on superconductors, which are known to exclude the magnetic field (this is called the *Meissner effect*). NMR studies are possible because of the finite *penetration depth* of the magnetic field into the interior of a superconductor. If a superconducting sample is sufficiently finely divided, then NMR signals may be picked up from most of the sample volume.

8. The r.f. phases specified in Table 19.1 employ a π phase shift for the second pulse. This choice of phases leads to consistently positive diagonal peaks and cross-peaks in two-dimensional exchange spectra.

9. The pulse sequence phases are consistent with the 'sign-corrected' version of the States procedure discussed in Section 5.9.4.

Further Reading

- For a review of chemical exchange effects in NMR, see A. D. Bain, *Prog. NMR Spectrosc.* **43**, 63–103 (2003).
- For reviews of solid-state NMR, including magic-angle-spinning, see M. J. Duer, *Introduction to Solid-State NMR Spectroscopy*, Blackwell Science, 2004; K. Schmidt-Rohr, H. W. Spiess, *Multidimensional Solid-State NMR and Polymers*, Academic Press, London, 1994; M. Mehring, *High Resolution NMR in Solids*, 2nd edition, Springer, Berlin, 1982.
- For a review of sideband suppression and separation methods in magic-angle-spinning NMR, see O. N. Antzutkin, *Prog. NMR Spectrosc.* **35**, 203–266 (1999).
- For diffusion and flow measurements by NMR, see C. S. Johnson Jr, *Prog. NMR Spectrosc.* **34**, 203–256 (1999), and the articles in the *Encyclopedia of Nuclear Magnetic Resonance*, D. M. Grant and R. K. Harris (eds), Wiley, 1996, by K. J. Packer (vol. 3, pp. 1615–1626) and C. S. Johnson Jr, (vol. 3, pp. 1626–1644).
- See *Concepts in Magnetic Resonance, Part A*, **28** (2), (2006) for a series of explanatory articles on diffusion tensor imaging.

Exercises

19.1 Consider an idealized symmetrical two-site exchange process, with kinetics described by the Arrhenius equation over a wide range in temperature. The pre-exponential constant is $A = 10^{14}\,\mathrm{s}^{-1}$ and the activation energy is $E_{\mathrm{act}} = 57\,\mathrm{kJ\,mol}^{-1}$. The exchange process causes a change in the ^{13}C chemical shift at a certain molecular site to change by 50 ppm, while the ^{1}H chemical shift at a different molecular site changes by 5 ppm. All the parameters are assumed to be temperature independent.

(i) At what magnetic field is the crossover in the ^{13}C lineshapes observed if the sample temperature is $T = 300\,\mathrm{K}$?
(ii) At what magnetic field is the crossover in the ^{1}H lineshapes observed if the sample temperature is $T = 300\,\mathrm{K}$?
(iii) At what temperature is the crossover in the ^{1}H lineshapes observed if the proton Larmor frequency is $\omega^0/2\pi = -200\,\mathrm{MHz}$?
(iv) Over which range in temperatures does one expect two-dimensional exchange spectroscopy to be useful for studying the exchange process? Assume that T_1 is of the order of several seconds.
(v) Around which temperature does one expect the exchange process to become a mechanism for proton spin–lattice relaxation if the magnetic field is $B^0 = 11\,\mathrm{T}$?

20 Relaxation

20.1 Types of Relaxation

If the sample is allowed to be undisturbed for a long time in the magnetic field, it reaches a state of *thermal equilibrium*. As discussed in Section 11.3, this implies (i) that all coherences are absent and (ii) that the populations are given by the Boltzmann distribution, at the temperature of the molecular environment.

R.f. pulses disturb the equilibrium of the spin system. The populations after a pulse usually deviate from their thermal equilibrium values and, in many cases, coherences are created. For example, a π pulse inverts the population distribution, whereas a $\pi/2$ pulse equalizes spin state population and generates coherences.

Relaxation is the process by which equilibrium is regained, through interaction of the spin system with the thermal molecular environment.

Relaxation processes may be divided into two types. *Spin–lattice relaxation* is concerned with the movement of spin populations back to their Boltzmann distribution values. *Spin–spin relaxation* is concerned with the decay of coherences. Spin–lattice relaxation is also known as *longitudinal relaxation*; spin–spin relaxation is also known as *transverse relaxation*.

In an ensemble of isolated spins-1/2, there are only two time constants for the relaxation processes: these are the *spin–lattice relaxation time constant* T_1 for the equilibration of populations and the *transverse relaxation time constant* T_2 for the decay of single-quantum coherences.

In systems with coupled spins, relaxation is a more subtle and varied phenomenon, and one needs many more time constants to characterize it, as discussed below.

The study of nuclear spin relaxation is important for several reasons, including the following:

1. Many motional processes in molecules may be studied by nuclear spin relaxation.

2. Nuclear spin relaxation is sensitive to non-secular spin interactions (see Section 8.5.2). The study of relaxation can reveal these 'hidden' spin interactions, which have little effect on the ordinary NMR spectrum. A very important example is the through-space dipole–dipole coupling in isotropic liquids. As discussed in Section 9.3, the secular dipole–dipole couplings average to zero in isotropic liquids, and have almost no effect on the ordinary NMR spectrum. The study of spin relaxation reveals the non-secular parts of the dipole–dipole coupling, thus allowing these couplings to be used for the determination of molecular structure in biomolecules, through the so-called NOESY and ROESY experiments, as discussed below.

20.2 Relaxation Mechanisms

For spins-1/2, relaxation is caused by fluctuating magnetic fields at the sites of the nuclear spins, caused by thermal motion of the molecules.

Spin Dynamics: Basics of Nuclear Magnetic Resonance, Second Edition Malcolm H. Levitt

For example, consider the direct dipole–dipole coupling between two nuclear spins in the same molecule. As the molecule tumbles, the magnitude and direction of the magnetic field exerted by one spin on the other changes:

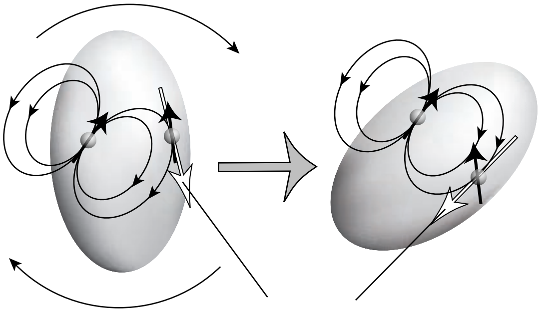

Figure 20.1
Modulation of the local dipolar field by molecular rotation.

Another source of local fields is the *CSA*. As discussed in Section 9.1, these fields are caused by molecular electron currents induced by the external magnetic field. As the molecules tumble in a liquid, the direction and magnitude of these local fields also change:

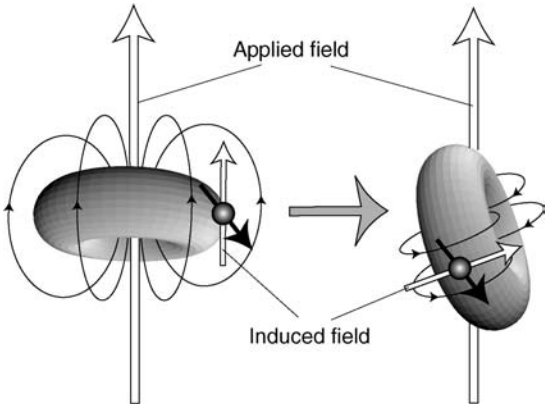

Figure 20.2
Modulation of the chemical shift interaction by molecular rotation.

If one adds these small local fields to the large static field from the magnet, one gets a total field that fluctuates slightly in direction and magnitude as the molecules rotate:

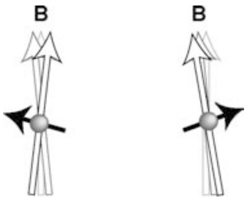

Figure 20.3
Wobbling of the total local field.

As discussed qualitatively in Section 2.6, this 'wobbling' of the local magnetic field is very slight, but is sufficient to cause spin–lattice relaxation.

For spins-1/2, the usual order of importance of relaxation mechanisms is as follows:

dipole–dipole > CSA > spin–rotation

The CSA becomes increasingly important at high magnetic fields, where it starts to compete effectively with the dipole–dipole mechanism. The spin–rotation mechanism is usually unimportant, except for small molecules in gases or non-viscous liquids.

For spins > 1/2, the usual order of importance of relaxation mechanisms is as follows:

quadrupole >> dipole–dipole > CSA > spin–rotation

In most cases, the electric quadrupole relaxation mechanism clearly dominates the relaxation of spins > 1/2.

In most experimental cases, a single relaxation mechanism dominates, but others may also be significant. When several mechanisms are present at the same time, there is the possibility of *cross-correlation* effects, as discussed in Section 20.8.

20.3 Random Field Relaxation

As an introduction to the subject of relaxation, consider a set of non-coupled spins-1/2 exposed to two fields: a large static field B^0 along the z-axis and a small magnetic field $B_x(t)$ along the x-axis. Suppose that each spin experiences the same longitudinal field B^0, but that the transverse fields $B_x(t)$ are different for each spin, and also fluctuate in time:

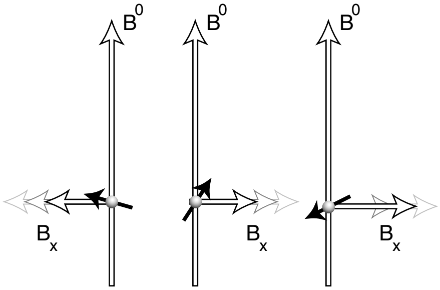

Figure 20.4
The sum of the external field and a fluctuating transverse field.

The value of the transverse field B_x for two different spins has the following appearance when plotted against time:

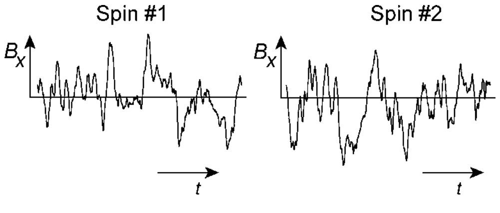

Figure 20.5
Fluctuations of the transverse field at two different spins.

The fluctuations of the fields at the two spins are unrelated to each other in detail, but they have the same general time-scale and the same general amplitude.

20.3.1 Autocorrelation functions and correlation times

In the simplest model, one assumes that the fluctuating transverse fields have the following properties:

1. The fluctuating fields have *zero average*:

$$\langle B_x(t) \rangle = 0$$

For each spin, the field switches between the negative and positive x-axis, so that the average field along the x-axis is zero. In this equation, the angular brackets imply either an average over a long time for a single spin, or an average over many spins at any particular moment; one assumes that these two types of average are the same (this is called the *ergodic hypothesis*).

2. One needs a way of defining the *magnitude* of the fluctuating fields. The average value of the field will not do, because it is zero for all spins, as indicated above. Instead, one uses the *mean square fluctuating field* defined by

$$\langle B_x^2(t) \rangle \neq 0$$

The square field B_x^2 is plotted below as a function of time for two spins:

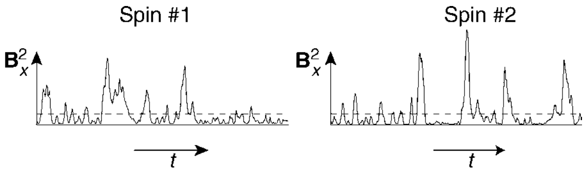

Figure 20.6 Fluctuations of the square transverse field at two different spins.

Since the square of the field is always positive, the mean square field is not zero, and is the same for all spins. The value of $\langle B_x^2(t) \rangle$ is indicated by a dashed line in the plots.

3. One also needs a way of defining *how rapidly* the field fluctuates. This is done by using the *autocorrelation function* of the field, which is defined as follows:

$$\boxed{\mathbb{G}(\tau) = \langle B_x(t) B_x(t+\tau) \rangle \neq 0 \qquad (20.1)}$$

Here, τ is a time interval, whose meaning is examined below. A rapidly fluctuating field has an autocorrelation function that decays quickly with respect to τ:

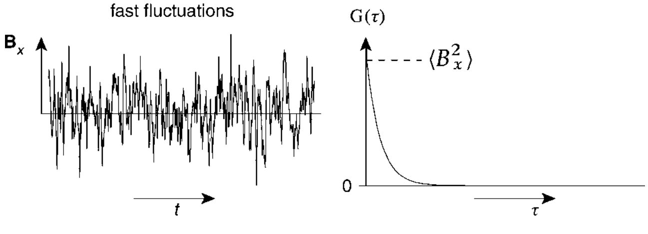

Figure 20.7 Autocorrelation function of a rapidly fluctuating field.

A slowly fluctuating field, on the other hand, has an autocorrelation function that decays slowly with respect to τ:

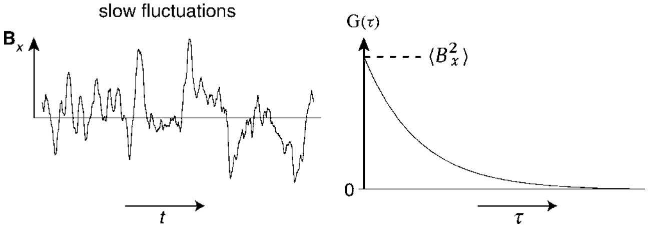

Figure 20.8 Autocorrelation function of a slowly fluctuating field.

By definition, the autocorrelation function at $\tau = 0$ is equal to the mean square field:

$$\mathbb{G}(0) = \left\langle B_x^2(t) \right\rangle$$

As discussed below, the decay rate and form of the autocorrelation function $\mathbb{G}(\tau)$ turns out to be very important for the spin relaxation.

4. The definition of the autocorrelation function, Equation 20.1, is independent of the time point t. This is called the *stationary* assumption.

5. The fluctuating fields are assumed to be *spin independent*. This means that the field experienced by a particular spin depends neither on the orientation of that spin, nor on the orientations of other spins in the vicinity. The fields are assumed to emanate from some source external to the spin system, which is itself ignorant of the states of the spins on which it acts. This is clearly an incorrect assumption for relaxation mechanisms such as the dipole–dipole coupling, in which the fields depend explicitly on the states of neighbouring spins. We must expect the treatment to be only qualitative in this case. In fact, the assumption of spin-independent random fields is not strictly valid for *any* true relaxation mechanism, as discussed in Section 20.3.6.

The physical meaning of the autocorrelation function is now examined in more detail. The general idea is to compare the field at any one time point t with its value at a later time point $t + \tau$.

If the interval τ is small compared with the time-scale of the fluctuations, then the values of the field at the two time points tend to be similar: if $B_x(t)$ is positive, then $B_x(t + \tau)$ also tends to be positive; while if $B_x(t)$ is negative, then $B_x(t + \tau)$ is usually also negative. In both cases, the product of $B_x(t)$ and $B_x(t + \tau)$ is positive, and is close to the value $\left\langle B_x^2(t) \right\rangle$. This is illustrated below for two choices of the initial time point t:

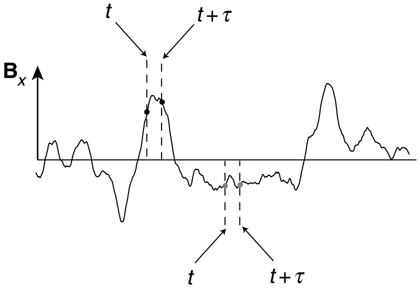

Figure 20.9 Comparison of the fields at close time intervals.

The values of B_x indicated by the black dots have the same sign. The same is true for the values of B_x indicated by the grey dots.

If the interval τ is long compared with the time-scale of the fluctuations, then the system loses its 'memory'. There is no longer any consistent relationship between the value of the function at times separated by τ.

This is illustrated below:

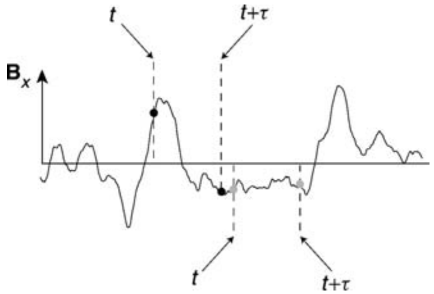

Figure 20.10 Comparison of the fields at long time intervals.

The values of B_x indicated by the black dots have opposite sign, whereas the values of B_x indicated by the grey dots have the same sign. When the product $B_x(t)B_x(t+\tau)$ is averaged over the ensemble, the result will be close to zero.

In general, the autocorrelation function $\mathbb{G}(\tau)$ tends to be large for small values of τ and tends to zero for large values of τ. Often, one *assumes* a simple exponential form for the autocorrelation function:

$$\mathbb{G}(\tau) = \left\langle B_x^2 \right\rangle \mathrm{e}^{-|\tau|/\tau_c} \tag{20.2}$$

This has the correct qualitative form, but it is difficult to justify on the basis of a deeper theory. The parameter τ_c is called the *correlation time* of the fluctuations. Rapid fluctuations have a small value of τ_c, whereas slow fluctuations have a large value of τ_c. For rotating molecules in a liquid, τ_c is in the range of tens of picoseconds to several nanoseconds.

Qualitatively, the correlation time indicates how long it takes before the random field changes sign.

In practice, the correlation time depends on the physical parameters of the system, such as the temperature. Generally, correlation times are *decreased* by *warming* the sample, since an increase in temperature corresponds to more rapid molecular motion. Conversely, correlation times are *increased* by *cooling* the sample.

20.3.2 Spectral density

An important role is played in relaxation theory by the *spectral density* $\mathbb{J}(\omega)$, which is defined as twice the Fourier transform of the autocorrelation function:[1]

$$\mathbb{J}(\omega) = 2\int_0^\infty \mathbb{G}(\tau)\exp\{-\mathrm{i}\omega\tau\}\,\mathrm{d}\tau \tag{20.3}$$

For a fluctuating field along the x-axis, with an exponentially decaying autocorrelation function given by Equation 20.2, the spectral density is given by

$$\mathbb{J}(\omega) = 2\left\langle B_x^2 \right\rangle \mathcal{A}(\omega; 0, \tau_c{}^{-1})$$

where $\mathcal{A}$ is the absorption Lorentzian, given in Equation 5.14. Explicitly, the spectral density may be written as follows:

$$\mathbb{J}(\omega) = 2\left\langle B_x^2 \right\rangle \frac{\tau_c}{1+\omega^2\tau_c^2} \tag{20.4}$$

If the transverse field fluctuates rapidly, then the correlation time is short and the spectral density function is broad:

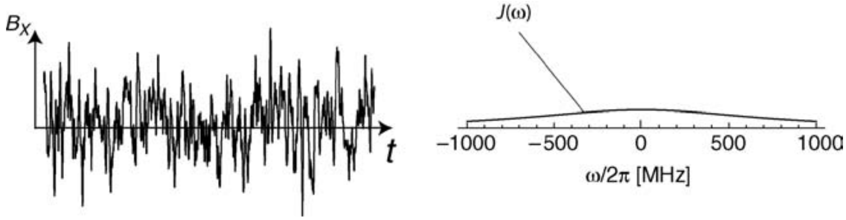

Figure 20.11
Spectral density function of a rapidly fluctuating field ($\tau_c = 0.2$ns).

If the transverse field fluctuates slowly, then the correlation time is long and the spectral density function is narrow:

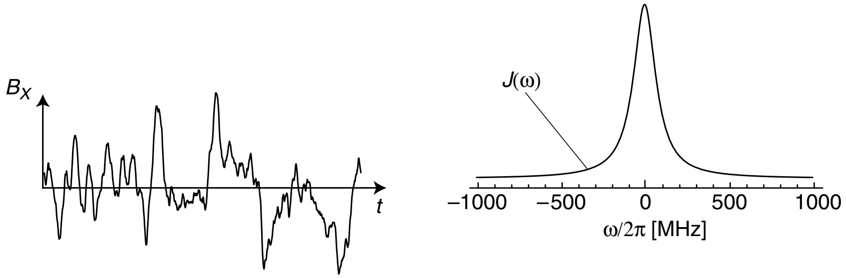

Figure 20.12
Spectral density function of a slowly fluctuating field ($\tau_c = 2.0$ns).

The area under the spectral density function is independent of τ_c, and is given in the present model by $2\langle B_x^2\rangle$, i.e. twice the mean square amplitude of the fluctuating field.

20.3.3 Normalized spectral density

It is common to work with a *normalized spectral density*, denoted here $\mathcal{J}(\omega)$, which is just the last part of Equation 20.4, i.e.

$$\boxed{\mathcal{J}(\omega) = \mathcal{A}(\omega; 0, {\tau_c}^{-1}) = \frac{\tau_c}{1 + \omega^2 \tau_c^2} \qquad (20.5)}$$

For a random field along the x-axis, the spectral density function is given by

$$\mathbb{J}(\omega) = 2\left\langle B_x^2 \right\rangle \mathcal{J}(\omega)$$

From now on, I will use the term 'spectral density' to imply 'normalized spectral density', which is common practice in the NMR literature.

20.3.4 Transition probabilities

The fluctuating transverse field induces *transitions* between the spin energy eigenstates $|\alpha\rangle$ and $|\beta\rangle$. Suppose that a spin is in the energy state $|\alpha\rangle$ at time t. At a later time $t+\tau$, the spin will be in a different state $|\alpha'\rangle$, because of the action of the fluctuating field. The new state $|\alpha'\rangle$ is generally a superposition of states $|\alpha\rangle$ and $|\beta\rangle$, which implies that a subsequent measurement may produce a result appropriate to the state $|\beta\rangle$. The *transition probability per unit time* from state $|\alpha\rangle$ to state $|\beta\rangle$ is defined for small values of τ through the following equation:

$$W_{\boxed{-}} = \tau^{-1}\overline{|\langle\beta|\alpha'\rangle|^2}$$

where the overbar defines an ensemble average. The notation $W_{\boxed{-}}$ indicates that the spin angular momentum along the z-axis *decreases* upon the transition $|\alpha\rangle \rightarrow |\beta\rangle$.

Similarly, the transition probability per unit time from state $|\beta\rangle$ to state $|\alpha\rangle$ is defined through the following equation:

$$W_{\boxed{+}} = \tau^{-1}\overline{|\langle\alpha|\beta'\rangle|^2}$$

where the overbar defines an ensemble average, and it is assumed that the system starts out in state $|\beta\rangle$ but assumes a new state $|\beta'\rangle$ after an interval τ. The notation $W_{\boxed{+}}$ indicates that the spin angular momentum along the z-axis increases upon the transition $|\beta\rangle \rightarrow |\alpha\rangle$.

The 'transition probability per unit time', denoted W, is often loosely referred to as the 'transition probability'.

In this book, the relaxation-induced transition probabilities between energy eigenstates are denoted on energy level diagrams using *dashed arrows*:

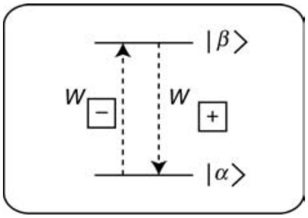

Figure 20.13
Transition probabilities in two directions.

This notation should not be confused with the solid grey arrows used for coherences; as described in Section 11.2, coherences do *not* imply transitions between energy eigenstates, whereas transition probability arrows do.

The subscripts $\boxed{+}$ and $\boxed{-}$ used in the notation for transition probabilities refer to the change in the angular momentum along the z-axis, not to the change in energy. For spins with positive γ, the transition arrow for $W_{\boxed{+}}$ points *down*.

It is possible to derive the transition probabilities for the random field model from first principles (see *Further Reading*). I will state the result without proof:

$$W_{\boxed{-}} = W_{\boxed{+}} = \frac{1}{2}\gamma^2 \left\langle B_x^2 \right\rangle \mathfrak{J}(\omega^0) \tag{20.6}$$

The transition probabilities in the two directions are predicted to be equal, and are proportional to the spectral density of the random field at the Larmor frequency ω^0:

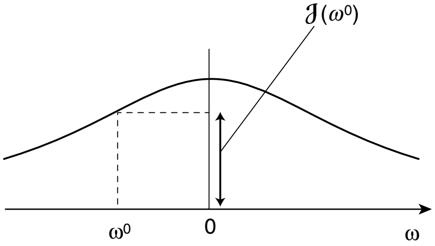

Figure 20.14
For a fluctuating random field, the transition probabilities are proportional to the spectral density at the Larmor frequency ω^0.

20.3.5 Thermally corrected transition probabilities

The equation for transition probabilities, Equation 20.6, is clearly incorrect in detail. Obviously, a simple model in which the fields fluctuate along a single axis is unrealistic. More realistic relaxation models must take into account the fluctuation of the fields in all three directions, and the dependence of the fields on the polarizations of other nuclear spins.

Furthermore, Equation 20.6 is fundamentally incorrect for a deeper reason. The equation predicts that spins have an equal probability of making a transition from a low energy state to a high energy state, as from a high energy state to a low energy state. If this were true, the spin system would eventually adopt an equilibrium position with equal numbers of spins in the two states. In practice, this does not happen: the equilibrium state of the spin ensemble corresponds to a Boltzmann distribution of populations, with the lower energy state more populated than the upper energy state (see Section 11.3).

Consider the case with $\gamma > 0$, so that $|\alpha\rangle$ is lower in energy than $|\beta\rangle$. The Boltzmann distribution is only stable if the probability $W_{\boxed{-}}$ for transitions from $|\alpha\rangle$ to $|\beta\rangle$ is smaller than the probability $W_{\boxed{+}}$ for transitions from $|\beta\rangle$ to $|\alpha\rangle$. In equilibrium, the flow of population in the two directions must be equal:

$$\rho_{\boxed{\alpha}}^{\mathrm{eq}} W_{\boxed{-}} = \rho_{\boxed{\beta}}^{\mathrm{eq}} W_{\boxed{+}}$$

Here, $\rho_{\boxed{\alpha}}^{\mathrm{eq}}$ and $\rho_{\boxed{\beta}}^{\mathrm{eq}}$ are the thermal equilibrium populations given in Section 11.3. Since $\rho_{\boxed{\alpha}}^{\mathrm{eq}} > \rho_{\boxed{\beta}}^{\mathrm{eq}}$ and $W_{\boxed{-}} < W_{\boxed{+}}$, the equilibrium spin system remains in dynamic balance:

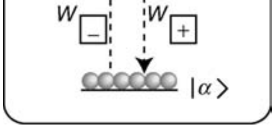

Figure 20.15
The dynamic balance at thermal equilibrium.

In practice, the difference in thermal equilibrium populations is very small (around 10^{-4} or less), so the difference in the two transition probabilities is also of this order of magnitude. Although this difference is small, the existence of thermal equilibrium spin magnetization depends upon it.

Equation 20.6 may be ‘fixed’ in order to take into account this small imbalance in the transition probabilities. A more accurate version of Equation 20.6 is given by

$$W_{\boxed{-}} = W(1 - \frac{1}{2}\mathbb{B})$$

$$W_{\boxed{+}} = W(1 + \frac{1}{2}\mathbb{B}) \tag{20.7}$$

where the mean transition probability W is

$$W = \frac{1}{2}\gamma^2 \left\langle B_x^2 \right\rangle \mathcal{J}(\omega^0)$$

and $\mathbb{B}$ is the usual Boltzmann factor:

$$\mathbb{B} = \frac{\hbar\gamma B^0}{k_B T}$$

Here, k_B is the Boltzmann constant and T is the temperature of the molecular environment. The ‘thermally corrected’ transition probabilities given in Equation 20.7 reproduce the correct equilibrium position.

Why does the random field model break down in such a fundamental way? The weak point in the model is the assumption of spin-independent random fields. This assumption sounds plausible, but it fails in a real molecular situation because the energies of the nuclear spins contribute to the total energy of each molecule. In order to raise the energy of the nuclear spin system, energy must be withdrawn from the other degrees of freedom in the molecule, and this has an entropic cost. As a result, processes that raise the energy of the nuclear spin system are slightly less likely than those that decrease the nuclear spin energy. Since the random fields have a molecular origin, they *must* be correlated with the nuclear spin states.

Basically, the motion of the molecules depends slightly on the nuclear spin states, and an accurate relaxation model must take these tiny correlations into account. In practice, this is done by ‘fudging’ the relaxation equations, on the lines of Equation 20.7. It is difficult to justify this procedure on fundamental grounds, but empirically it is found to give correct results.

The small imbalance in the transition probabilites corresponds to the ‘biased wandering motion’ of the spin polarizations, introduced in Section 2.6.

20.3.6 Spin–lattice relaxation

Now let us examine how the spin state populations move around under these transition processes.

The kinetic equation for the population of the $|\alpha\rangle$ state is

$$\frac{\mathrm{d}}{\mathrm{d}t}\rho_{\boxed{\alpha}} = -W_{\boxed{-}}\,\rho_{\boxed{\alpha}} + W_{\boxed{+}}\,\rho_{\boxed{\beta}}$$

The first term on the right-hand side describes the flow of population out of state $|\alpha\rangle$, through $|\alpha\rangle \rightarrow |\beta\rangle$ transitions, and the second term on the right-hand side describes the flow of population into the state $|\alpha\rangle$, through $|\beta\rangle \rightarrow |\alpha\rangle$ transitions.

Similarly, the kinetic equation for the population of the $|\beta\rangle$ state is

$$\frac{\mathrm{d}}{\mathrm{d}t}\rho_{\boxed{\beta}} = +W_{\boxed{-}}\,\rho_{\boxed{\alpha}} - W_{\boxed{+}}\,\rho_{\boxed{\beta}}$$

The z-component of the spin magnetization vector is proportional to the difference in the spin state populations, as described in Section 11.5:

$$M_z = 2\mathbb{B}^{-1}(\rho_{\boxed{\alpha}} - \rho_{\boxed{\beta}}) \tag{20.8}$$

It follows that the z-component of the normalized magnetization vector has the following equation of motion:

$$\begin{aligned}\frac{\mathrm{d}}{\mathrm{d}t}M_z &= 2\mathbb{B}^{-1}\left(\frac{\mathrm{d}}{\mathrm{d}t}\rho_{\boxed{\alpha}} - \frac{\mathrm{d}}{\mathrm{d}t}\rho_{\boxed{\beta}}\right)\\ &= 4\mathbb{B}^{-1}(-W_{\boxed{-}}\,\rho_{\boxed{\alpha}} + W_{\boxed{+}}\,\rho_{\boxed{\beta}})\\ &= -2W(M_z - 1)\end{aligned}$$

The last line follows by using $\rho_{\boxed{\alpha}} + \rho_{\boxed{\beta}} = 1$, and Equations 20.7 and 20.8.

The equation of motion may be integrated to get

$$M_z(\tau) = (M_z(0) - 1)\,\mathrm{e}^{-2W\tau} + 1$$

which is exactly the same as that given in Equation 11.45, provided the spin–lattice relaxation rate constant is set equal to

$$\boxed{T_1{}^{-1} = 2W \qquad (20.9)}$$

The spin–lattice relaxation rate constant is equal to twice the mean transition probability per unit time between the states.

For the model of a fluctuating random field along the x-axis, this implies the following expression for the spin–lattice relaxation rate constant:

$$T_1{}^{-1} = \gamma^2\left\langle B_x^2\right\rangle \mathfrak{J}(\omega^0) = \gamma^2\left\langle B_x^2\right\rangle \frac{\tau_c}{1+(\omega^0\tau_c)^2}$$

If we plot the spin–lattice relaxation time constant against the correlation time τ_c, we get the following curve:

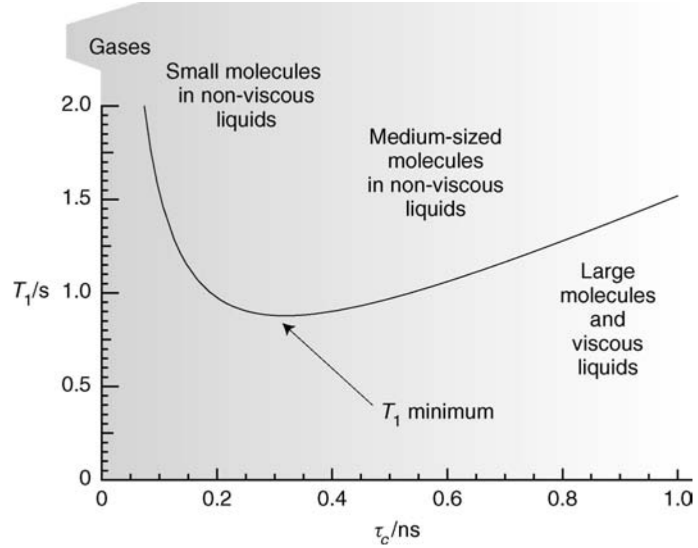

Figure 20.16
The spin–lattice relaxation time constant as a function of correlation time for random field fluctuations. Typical ranges of correlation time are shown.

(This curve is calculated for protons in a static field of 11.74 T, with a fluctuating random field of mean square amplitude $\left\langle B_x^2 \right\rangle = 10^{-8}\,\mathrm{T}^2$.) There is a certain correlation time τ_c for which relaxation is most efficient. In the example above, the T_1 minimum occurs at $\tau_c \cong 0.32\,\mathrm{ns}$.

Figure 20.16 shows typical ranges of correlation times around room temperature. Molecules in gases have the lowest correlation times, followed by small molecules in non-viscous liquids. Large molecules, or molecules in viscous liquids, have correlation times of several nanoseconds at room temperature.

It is a fortuitous circumstance that the most common experimental situation in solution NMR, namely medium-size molecules in non-viscous solutions near room temperature, falls close to the T_1 minimum. The small values of T_1 permit more rapid averaging of NMR signals, and hence a relatively high signal-to-noise ratio within a given experimental time (see Section 5.2).

The physical reason for the T_1 minimum may be seen from the spectral density plots. If we plot the spectral density against frequency for a set of correlation times τ_c, one sees that the spectral density at a certain frequency ω^0 first rises when τ_c is increased from a very small value. The following plots show the spectral density at the proton Larmor frequency $\omega^0/2\pi = -500\,\mathrm{MHz}$:

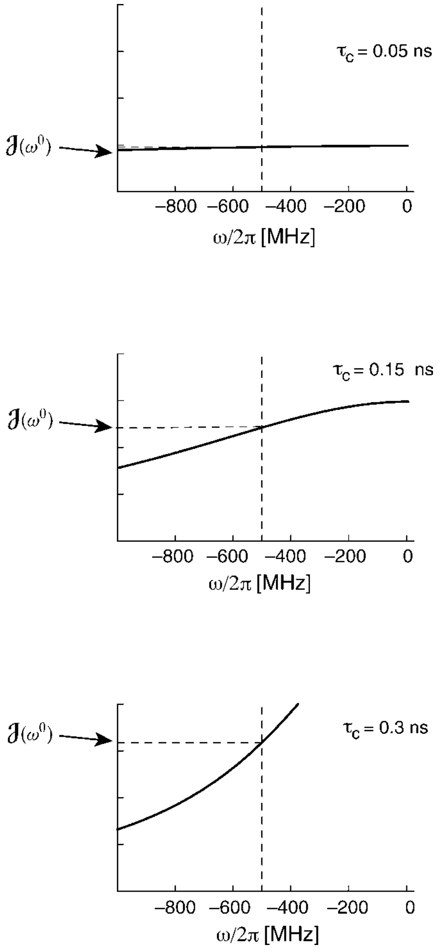

Figure 20.17
Spectral density as a function of correlation time, for fluctuations faster than the T_1 minimum.

The spectral density falls again as τ_c is increased beyond the optimum value, as shown below:

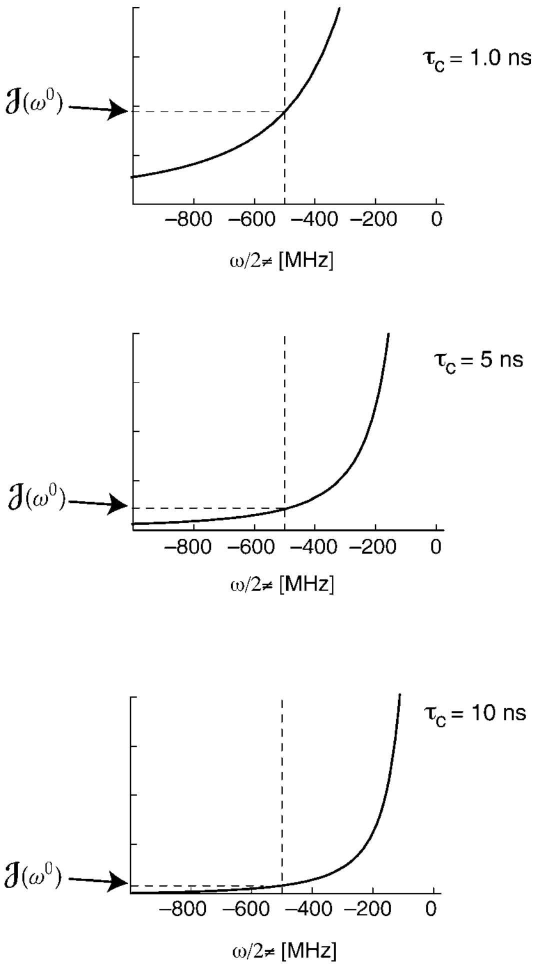

Figure 20.18
Spectral density as a function of correlation time, for fluctuations slower than the T_1 minimum.

At short correlation times τ_c, the spectrum of the fluctuations is very broad, so that the value of $\mathfrak{J}$ at any particular frequency is small. At long correlation times, the spectral density function is sharply peaked around $\omega = 0$, so the value of $\mathfrak{J}$ at any high frequency is again small. Relaxation is most efficient at an intermediate value of τ_c, where the spectral density function is neither too broad nor too narrow.

In practice, the spin–lattice relaxation time constant T_1 depends on temperature. This is because the random field fluctuations originate in the molecular environment, and the correlation time τ_c is temperature dependent. Warming the sample makes the fluctuations faster, reducing the correlation time, whereas cooling the sample slows down the fluctuations, lengthening the correlation time. The effect of temperature on T_1 depends on the location of τ_c with respect to the T_1 minimum. For systems with *long* correlation times (typically, viscous solutions or large molecules), warming the sample generally *reduces* the spin–lattice relaxation time constant T_1:

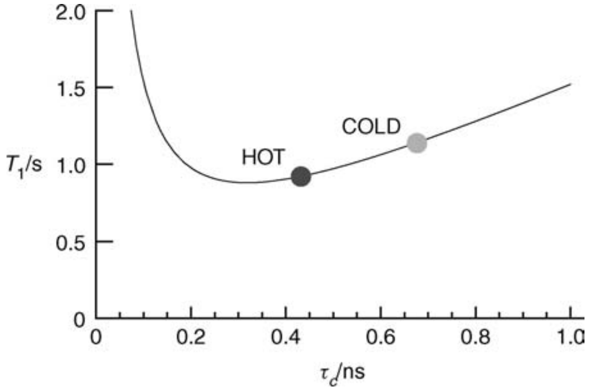

Figure 20.19
For systems with a long correlation time, warming the sample reduces T_1.

For systems with *short* correlation times (typically, small molecules in non-viscous solutions), warming the sample generally *increases* the spin–lattice relaxation time constant T_1:

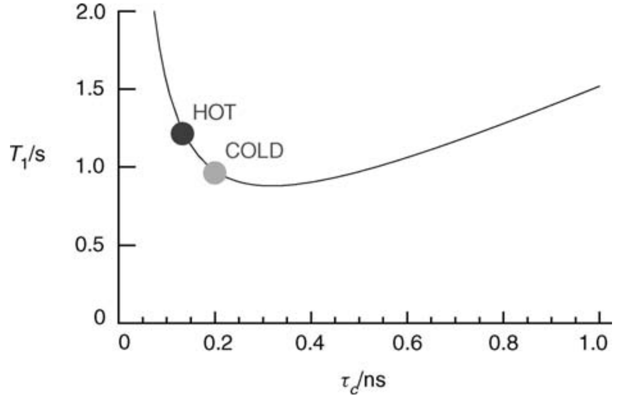

Figure 20.20
For systems with a long correlation time, warming the sample increases T_1.

The value of T_1 is also field-dependent, since the Larmor frequency ω^0 is proportional to the field B^0.

Although these results are quantitative only for a simplified model of relaxation, the general conclusions are qualitatively valid in realistic cases.

20.4 Dipole–Dipole Relaxation

For spins-1/2, the most important relaxation mechanism is usually the through-space dipolar coupling between the spins. The secular part of the coupling averages to zero in isotropic liquids, but the non-secular parts are still capable of causing relaxation.[2]

20.4.1 Rotational correlation time

In a liquid, the magnetic fields exerted by spins on each other are modulated by the random molecular tumbling. The correlation time of the random fields τ_c corresponds to the *rotational correlation time* of the molecules. The rotational correlation time is given (roughly) by the average time taken for the molecules to rotate by 1 rad.[3] Generally speaking, small molecules have short rotational correlation times, whereas large molecules have long rotational correlation times:

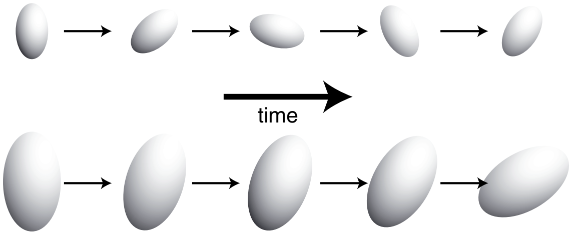

Figure 20.21
In the same time interval, a small molecule rotates more than a large molecule.

The rotational correlation time is also influenced by the viscosity of the liquid (increasing viscosity increases the rotational correlation time) and by temperature (increasing temperature reduces the rotational correlation time).

20.4.2 Transition probabilities

Consider an ensemble of weakly coupled homonuclear AX spin systems, each consisting of a spin I_1 coupled to a spin I_2. There are four energy eigenstates, and hence 12 different transition probabilities, in general. There are eight single-quantum transitions, each with different probabilities:

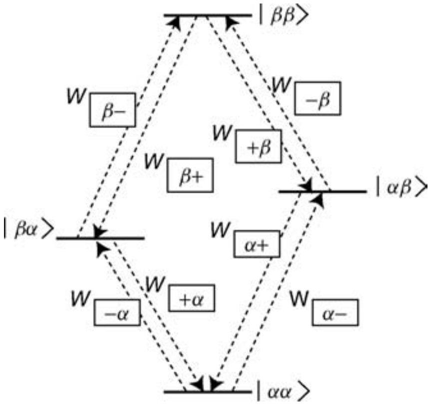

Figure 20.22
Single-quantum transition probabilities in a homonuclear AX system.

There are four double- and zero-quantum transitions, which also have different probabilities.

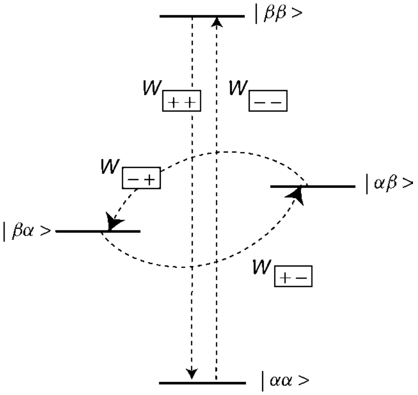

Figure 20.23
Double- and zero-quantum transition probabilities in a homonuclear AX system.

The notation resembles that used for coherences, but recall that coherences do *not* involve transitions between states, whereas spin–lattice relaxation processes do.

Suppose that each molecule only contains two spins of the same type and that the *only* relaxation mechanism is the intramolecular dipole–dipole interaction of these spins with each other. In this case, the following relationships exist between the transition probabilities (see *Further Reading*):

$$\begin{aligned}
W_{\boxed{+\alpha}} &= W_{\boxed{+\beta}} = W_{\boxed{\alpha+}} = W_{\boxed{\beta+}} = W_1(1+\tfrac{1}{2}\mathbb{B})\\
W_{\boxed{-\alpha}} &= W_{\boxed{-\beta}} = W_{\boxed{\alpha-}} = W_{\boxed{\beta-}} = W_1(1-\tfrac{1}{2}\mathbb{B})\\
W_{\boxed{++}} &= W_2(1+\mathbb{B})\\
W_{\boxed{--}} &= W_2(1-\mathbb{B})\\
W_{\boxed{+-}} &= W_{\boxed{-+}} = W_0
\end{aligned} \tag{20.10}$$

Here, W_1 is the *single-quantum transition probability*. Detailed calculation (see *Further Reading*) provides the following result:

$$\boxed{W_1 = \frac{3}{20} b^2 \mathfrak{J}(\omega^0)} \tag{20.11}$$

where the quantity $\mathfrak{J}(\omega^0)$ is the spectral density of the dipole–dipole couplings at the Larmor frequency ω^0:

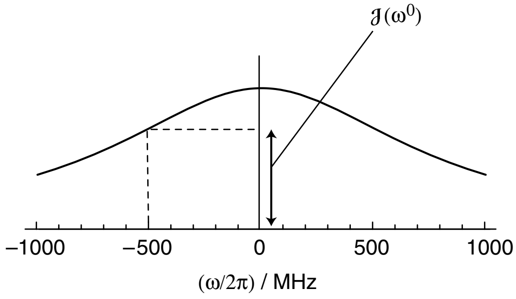

Figure 20.24
Dipole–dipole spectral density at the Larmor frequency $\omega = \omega^0$.

(This and the following plots are shown for protons in a field $B^0 = 11.74\,\mathrm{T}$ and a rotational correlation time $\tau_c = 0.2\,\mathrm{ns}$.) If vibrational motions are ignored, then the dipole–dipole coupling constant is given by

$$b = -\frac{\mu_0}{4\pi}\frac{\hbar\gamma^2}{r^3}$$

where the distance between the spins is denoted r. In practice, the value of the dipole–dipole coupling constant is somewhat smaller than this estimate, because of rapid vibrational and librational motions (see Section 19.4).

The *double-quantum transition probability* W_2 is given by

$$\boxed{W_2 = \frac{3}{5} b^2 \mathfrak{J}(2\omega^0)} \tag{20.12}$$

where $\mathfrak{J}(2\omega^0)$ is the spectral density at twice the Larmor frequency:

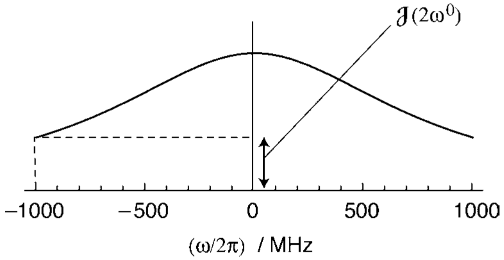

Figure 20.25
Dipole–dipole spectral density at twice the Larmor frequency $\omega = 2\omega^0$.

The *zero-quantum transition probability* W_0 is given by

$$W_0 = \frac{1}{10} b^2 \mathfrak{J}(0) \tag{20.13}$$

where $\mathfrak{J}(0)$ is the spectral density at zero frequency:

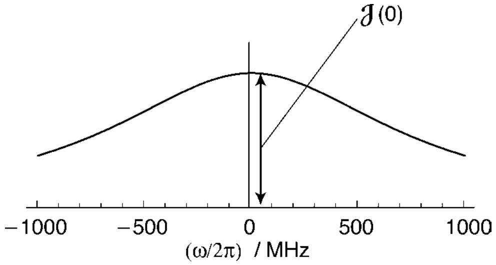

Figure 20.26
Dipole-dipole spectral density at zero frequency $\omega = 0$.

The factors $\mathbb{B}$ in Equation 20.10 provide thermal corrections of the transition probabilities, as in Section 20.3.5. These factors ensure the correct thermal equilibrium state of the AX ensemble, as described in Section 15.7.

All of the transition probabilities depend on the square of the dipole–dipole coupling, and hence on the *inverse sixth power of the internuclear distance*:

$$W \propto r^{-6} \tag{20.14}$$

This very important relationship summarizes the principle behind the determination of molecular structure by NMR in isotropic liquids.

These equations predict that, for *short* rotational correlation times (typically, small molecules in non-viscous solutions), the transition probabilities have the following relationship:

$$W_2 > W_1 > W_0 \qquad \text{(short } \tau_c\text{)}$$

For short τ_c, the spectral density function $\mathfrak{J}(\omega)$ is almost independent of ω, and the numerical factors in Equations 20.11–20.13 govern the relative magnitude of the transition probabilities.

For long rotational correlation times, on the other hand (typically, for large molecules or for viscous solutions), the transition probabilities have the following relationship:

$$W_0 > W_1 > W_2 \qquad \text{(long } \tau_c\text{)}$$

In this case, the peaked form of $\mathfrak{J}(\omega)$ around $\omega = 0$ governs the magnitude of the transition probabilities.

The importance of the spectral density at *twice* the Larmor frequency is striking and demands a physical explanation. What's going on?

The basic reason for the $2\omega^0$ terms is the geometry of the dipolar local field. To see this, consider a molecule containing two spins, I_1 and I_2. Suppose that the molecule is oriented so that the vector joining the two spins is in the plane of the paper, and suppose that the angular momentum of spin I_1 is also in the same plane. The angular momentum of spin I_2 is assumed to be perpendicular to the plane of the paper. We view the dipolar magnetic field emanating from spin I_1, and the local field experienced by spin I_2:

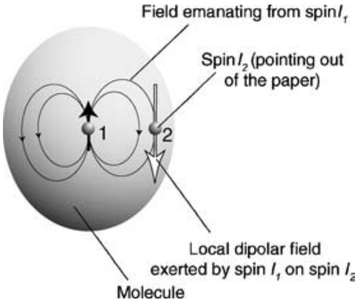

Figure 20.27
Local fields in a molecule.

Suppose, now, that the molecule rotates in the plane of the paper. Keep the polarization of spin I_1 fixed and follow carefully the motion of the local field at spin I_2 (indicated by the white arrow):

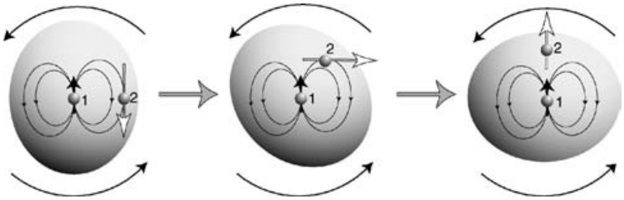

Figure 20.28
Rotation of the local field as the molecule rotates, keeping the spin polarization fixed.

Although the molecule rotates by $\pi/4$ between snapshots, the local dipolar field rotates by roughly $\pi/2$ each time. This implies that, to a good approximation, molecular rotation at the frequency ω modulates the dipolar field at the frequency 2ω. The fluctuation frequency of the dipole–dipole couplings is effectively doubled by this effect. *The* $\mathfrak{J}(2\omega^0)$ *term in the dipole–dipole spectral density is mainly produced by molecular rotations at the Larmor frequency* ω^0.

Now let's take into account the precession of the spins in the magnetic field. Assume that the static magnetic field is coming out of the plane of the paper, and allow spin I_1 to precess around the magnetic field (in the negative sense, assuming $\gamma > 0$). Initially, we keep the molecule fixed and then see what effect the precession of spin I_1 has on the local field at spin I_2:

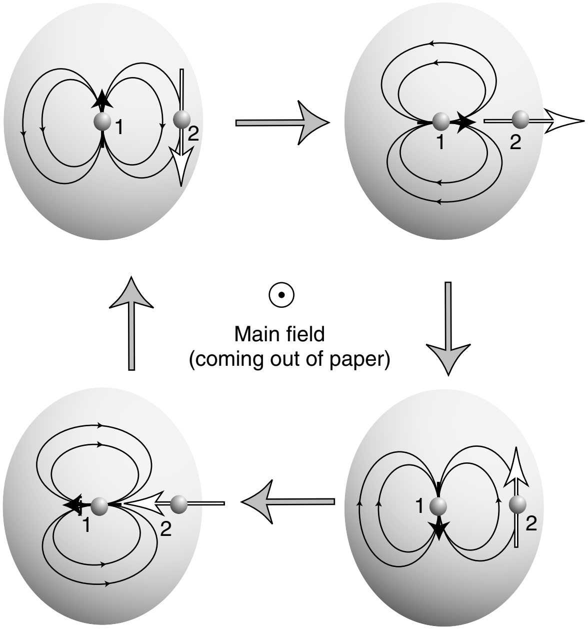

Figure 20.29
Rotation of the local field as spin I_1 precesses, keeping the molecule fixed.

(The snapshots are taken at intervals separated by one-quarter of a Larmor period.) Notice that although spin I_1 precesses in the *negative* sense around the main field, the local field at spin I_2 rotates in the *positive* sense, i.e. at the frequency $-\omega^0$. As discussed in Section 8.4.2, a field rotating in the opposite sense to the Larmor precession is ineffective in inducing spin transitions. Figure 20.29 implies that the precession of the spins in the field does not *by itself* induce transitions of neighbouring spins (at least in this molecular orientation). Molecular motion is necessary for spin–lattice relaxation through dipole–dipole couplings.

Now combine the modulation of the local fields by spin precession with the molecular motion at the Larmor frequency (which is associated with the $\mathfrak{J}(2\omega^0)$ term, as discussed above). If the above diagram is repeated, while allowing the molecule to rotate at the same time as the spin precesses, we get the picture shown in Figure 20.30. This shows that a combination of spin precession and molecular motion can generate a local field at spin I_2 that rotates at the Larmor frequency ω^0. This is the correct frequency, and the correct sense of rotation, for transitions of spin I_2 to be induced by the dipolar coupling to spin I_1.

Intramolecular dipole–dipole relaxation is therefore caused by a complicated combination of spin precession and molecular rotation.

In practice, the modulation by the dipolar couplings involves all possible orientations of the spins and the molecules. Detailed analysis gives rise to the numerical factors in Equations 20.11–20.13 that take into account all of these effects.

20.4.3 Solomon equations

The equation of motion of an individual state population may be derived by taking into account the transition probabilities to the other states. For example, the population of state $|\alpha\alpha\rangle$ is depleted by the transition into state $|\beta\alpha\rangle$ (probability per unit time = $W_{\boxed{-\alpha}}$), the transition into state $|\beta\beta\rangle$ (probability per unit time = $W_{\boxed{--}}$), and the transition into state $|\alpha\beta\rangle$ (probability per unit time = $W_{\boxed{\alpha-}}$). At the same time, the population of state $|\alpha\alpha\rangle$ is replenished by the transition from state $|\beta\alpha\rangle$ (probability per unit time = $W_{\boxed{+\alpha}}$), the transition

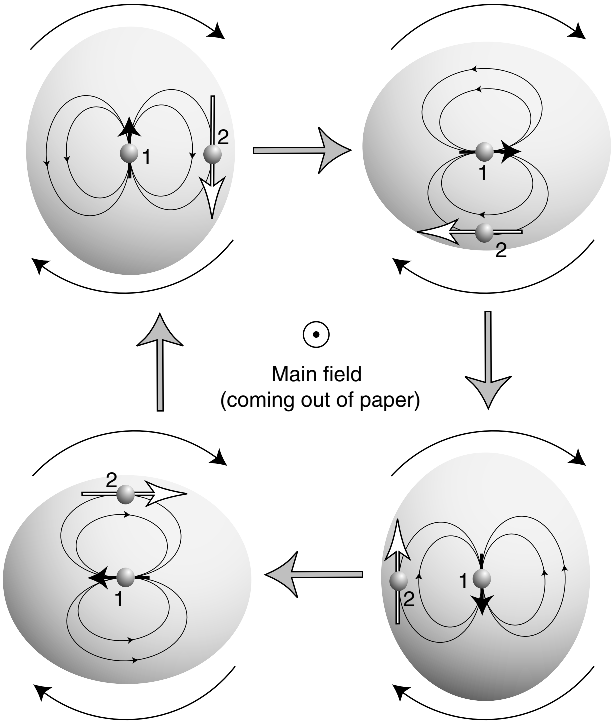

Figure 20.30
The combined effects of molecular rotation and spin precession.

from state $|\beta\beta\rangle$ (probability per unit time = $W_{\boxed{++}}$), and the transition from state $|\alpha\beta\rangle$ (probability per unit time = $W_{\boxed{\alpha+}}$). The kinetic equation for the population of state $|\alpha\alpha\rangle$ is therefore

$$\begin{aligned}\frac{\mathrm{d}}{\mathrm{d}t}\rho_{\boxed{\alpha\alpha}} = &-W_{\boxed{-\alpha}}\rho_{\boxed{\alpha\alpha}} - W_{\boxed{--}}\rho_{\boxed{\alpha\alpha}} - W_{\boxed{\alpha-}}\rho_{\boxed{\alpha\alpha}} \\ &+W_{\boxed{+\alpha}}\rho_{\boxed{\beta\alpha}} + W_{\boxed{++}}\rho_{\boxed{\beta\beta}} + W_{\boxed{\alpha+}}\rho_{\boxed{\alpha\beta}}\end{aligned}$$

The individual transition probabilities are given by Equation 20.10. Similar equations may be written down for the kinetic equations of the other three populations.

It is convenient to convert the kinetic equations for the populations into kinetic equations for the longitudinal magnetizations of the two types of spin. The longitudinal magnetizations of the two spins I_1 and I_2 are given by

$$\begin{aligned}\langle \hat{I}_{1z}\rangle &= \frac{1}{2}\rho_{\boxed{\alpha\alpha}} - \frac{1}{2}\rho_{\boxed{\beta\alpha}} + \frac{1}{2}\rho_{\boxed{\alpha\beta}} - \frac{1}{2}\rho_{\boxed{\beta\beta}} \\ \langle \hat{I}_{2z}\rangle &= \frac{1}{2}\rho_{\boxed{\alpha\alpha}} + \frac{1}{2}\rho_{\boxed{\beta\alpha}} - \frac{1}{2}\rho_{\boxed{\alpha\beta}} - \frac{1}{2}\rho_{\boxed{\beta\beta}}\end{aligned}$$

As shown in Appendix A.15, these equations may be rewritten in terms of the *Solomon equations* for the relaxation of the two-spin system:[4]

$$\boxed{\frac{\mathrm{d}}{\mathrm{d}t}\begin{pmatrix}\langle \hat{I}_{1z}\rangle \\ \langle \hat{I}_{2z}\rangle\end{pmatrix} = \begin{pmatrix}-R_{\mathrm{auto}} & R_{\mathrm{cross}} \\ R_{\mathrm{cross}} & -R_{\mathrm{auto}}\end{pmatrix}\begin{pmatrix}\langle \hat{I}_{1z}\rangle - \langle \hat{I}_{1z}\rangle^{\mathrm{eq}} \\ \langle \hat{I}_{2z}\rangle - \langle \hat{I}_{2z}\rangle^{\mathrm{eq}}\end{pmatrix} \qquad (20.15)}$$

The terms $\langle \hat{I}_{1z} \rangle^{\mathrm{eq}}$ and $\langle \hat{I}_{2z} \rangle^{\mathrm{eq}}$ in Equation 20.15 are the thermal equilibrium expectation values of the angular momentum operators, and are given by

$$\langle \hat{I}_{1z} \rangle^{\mathrm{eq}} = \langle \hat{I}_{2z} \rangle^{\mathrm{eq}} = \frac{1}{4}\mathbb{B}$$

as given in Section 15.7.

R_{auto} is called the *leakage rate constant* or *auto-relaxation rate constant*, and is given by

$$\boxed{R_{\mathrm{auto}} = W_0 + 2W_1 + W_2 \qquad (20.16)}$$

or in terms of the spectral densities as

$$R_{\mathrm{auto}} = \frac{1}{10} b^2 \left\{ \mathfrak{J}(0) + 3\mathfrak{J}(\omega^0) + 6\mathfrak{J}(2\omega^0) \right\}$$

The auto-relaxation rate constant has the following dependence on the rotational correlation time τ_c:

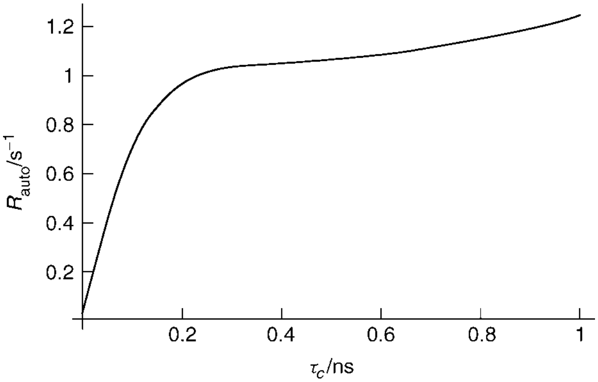

Figure 20.31 Variation of the auto-relaxation rate constant with correlation time.

(Calculated for two protons separated by 0.2 nm, in a field of 11.74 T.)

The term R_{cross} is called the *cross-relaxation rate constant*, and is given by[4]

$$\boxed{R_{\mathrm{cross}} = W_0 - W_2 \qquad (20.17)}$$

or in terms of the spectral densities as

$$R_{\mathrm{cross}} = \frac{1}{10} b^2 \left\{ \mathfrak{J}(0) - 6\mathfrak{J}(2\omega^0) \right\}$$

The cross-relaxation rate constant R_{cross} has a strong dependence on the rotational correlation time and changes sign as τ_c is increased:

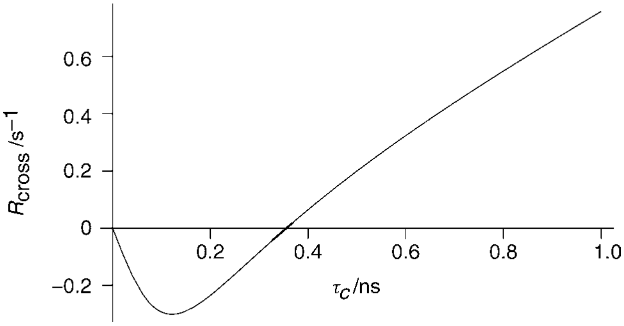

Figure 20.32 Variation of the cross-relaxation rate constant with correlation time.

(Calculated for two protons separated by 0.2 nm, in a field of 11.74 T.) The cross-relaxation rate constant R_{cross} is negative for short correlation times (small molecules in non-viscous solution), but is positive for long correlation times (large molecules, or for molecules in viscous solutions).

The cross-relaxation rate constant vanishes at the *critical correlation time*, given by

$$\boxed{\tau_{\text{c}}^{\text{crit}} = |\frac{\sqrt{5}}{2\omega^0}| \qquad (20.18)}$$

Many smallish and medium-sized molecules are often close to this condition. Large molecules, on the other hand, usually have $\tau_{\text{c}} >> \tau_{\text{c}}^{\text{crit}}$, and have large (positive) cross-relaxation rate constants R_{cross}.

Cross-relaxation is an essential component of the important NOESY experiment, as discussed in Section 20.6.

20.4.4 Longitudinal relaxation

Using the Solomon equations, one can figure out how the spin system relaxes, starting from an arbitrary configuration of spin state populations.

As a first example, let's calculate the relaxation of the *sum* z-angular momentum of the two spins, i.e. $\langle \hat{I}_z \rangle = \langle \hat{I}_{1z} \rangle + \langle \hat{I}_{2z} \rangle$. From the Solomon equations, the equation of motion of the sum z-angular momentum is given by

$$\begin{aligned}\frac{\text{d}}{\text{d}t}\langle \hat{I}_z \rangle &= \frac{\text{d}}{\text{d}t}\langle \hat{I}_{1z} \rangle + \frac{\text{d}}{\text{d}t}\langle \hat{I}_{2z} \rangle \\ &= -R_{\text{auto}}(\langle \hat{I}_{1z} \rangle - \frac{1}{4}\mathbb{B}) + R_{\text{cross}}(\langle \hat{I}_{2z} \rangle - \frac{1}{4}\mathbb{B}) \\ &\quad + R_{\text{cross}}(\langle \hat{I}_{1z} \rangle - \frac{1}{4}\mathbb{B}) - R_{\text{auto}}(\langle \hat{I}_{2z} \rangle - \frac{1}{4}\mathbb{B})\end{aligned}$$

If intramolecular dipole–dipole couplings are the only relaxation mechanism, then we get

$$\frac{\text{d}}{\text{d}t}\langle \hat{I}_z \rangle = -R_{\text{sum}}(\langle \hat{I}_z \rangle - \langle \hat{I}_z \rangle^{\text{eq}}) \qquad (20.19)$$

where the relaxation rate constant for the sum magnetization is

$$R_{\text{sum}} = R_{\text{auto}} - R_{\text{cross}} = 2W_1 + 2W_2 \qquad (20.20)$$

Equation 20.19 may be integrated to obtain the trajectory of the sum longitudinal magnetization. If two time points t_{a} and t_{b} are separated by an interval $\tau = t_{\text{b}} - t_{\text{a}}$ (in which no r.f. fields are applied), then the sum longitudinal magnetization at the later time point t_{b} is given by

$$\langle \hat{I}_z \rangle(t_{\text{b}}) = \left(\langle \hat{I}_z \rangle(t_{\text{a}}) - \langle \hat{I}_z \rangle^{\text{eq}}\right) \exp\{-R_{\text{sum}}\tau\} + \langle \hat{I}_z \rangle^{\text{eq}}$$

where R_{sum} is given by Equation 20.20. This describes the usual exponential recovery of the sum longitudinal magnetization, as described in Section 11.9.2. The spin–lattice relaxation rate constant for the two-spin system is therefore given by

$$T_1^{-1} = R_{\text{sum}} = 2W_1 + 2W_2$$

or in terms of spectral densities as

$$\boxed{T_1^{-1} = \frac{3}{10}b^2 \left\{\mathcal{J}(\omega^0) + 4\mathcal{J}(2\omega^0)\right\} \qquad (20.21)}$$

This simple exponential relaxation behaviour only applies to the relaxation of the *sum* of the longitudinal spin magnetizations. The motion of the *individual* z-magnetization components is more complicated, as described in Section 20.6.

The relaxation time constant T_1 displays the usual minimum as a function of the correlation time, as shown by the following plot (calculated for two protons separated by 0.2 nm, in a field of 11.74 T):

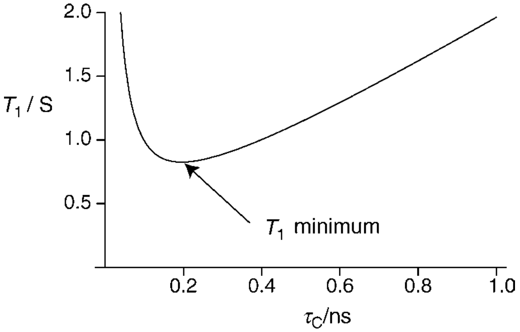

Figure 20.33
Variation of the spin–lattice relaxation time constant with correlation time, for intramolecular dipole–dipole relaxation.

It might appear that Equation 20.21 allows one to estimate the distance between the spins, through a measurement of the spin–lattice relaxation time constant T_1. However, this does not prove to be realistic. First, most molecules contain more than two spins, in which case the expression for T_1 consists of a superposition of many dipole–dipole couplings, and the contributions from individual spin pairs are difficult to disentangle. Second, there are many other relaxation mechanisms, and there is no simple way of distinguishing the dipole–dipole contribution from the others. In summary, the spin–lattice relaxation constant proves to be a poor source of information on molecular geometry, except in extremely simple cases.

20.4.5 Transverse relaxation

The transverse relaxation rate constant ${T_2}^{-1}$ takes the following value in the case of intramolecular dipole–dipole relaxation:

$$\boxed{{T_2}^{-1} = \frac{3}{20} b^2 \left\{ 3\mathcal{J}(0) + 5\mathcal{J}(\omega^0) + 2\mathcal{J}(2\omega^0) \right\} \qquad (20.22)}$$

The relaxation time constants T_1 and T_2 are compared in Figure 20.34:

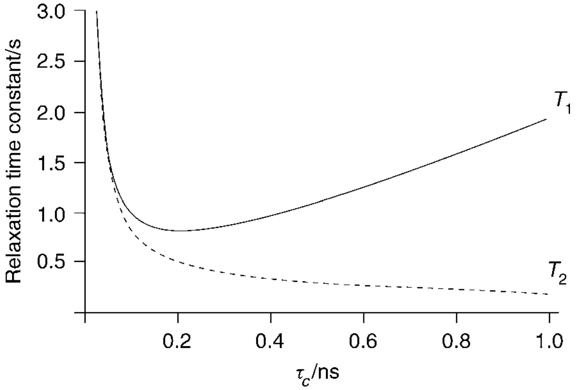

Figure 20.34
Variation of T_1 and T_2 with correlation time, for intramolecular dipole-dipole relaxation.

At very short rotational correlation times, the values of T_1 and T_2 are equal. This is called the *extreme narrowing limit*. As the correlation time is increased, T_1 passes through a minimum and then increases. The transverse relaxation time constant T_2, on the other hand, continues to decrease.

In practice, this means that the NMR peaks get progressively broader as the molecular mass is increased.

For many years, this behaviour was believed to set a fundamental limit on the size of molecule that may be studied by solution NMR. However, the development of the TROSY method (see Section 20.8.4) allows one to overcome the increase in linewidth at large rotational correlation times, at least in favourable cases.

20.5 Steady-State Nuclear Overhauser Effect

The Solomon equations predict a surprising effect: application of a weak r.f. field at the Larmor frequency of one of the spins, for a sufficiently long time, has a strong effect on the longitudinal magnetization of the non-irradiated spins, and, in some cases, even *enhances* the magnetization of those spins.

This is called the *steady-state nuclear Overhauser effect*, or *steady-state NOE* (the original Overhauser effect applied to electrons and nuclei).

In modern NMR, the steady-state NOE is mainly exploited in heteronuclear spin systems, where the enhancement of magnetization can be useful and dramatic. The INADEQUATE pulse sequence, described in Section 16.2, is an example. Therefore, we will treat this effect in the case of an ensemble of heteronuclear AX systems, with a spin species I of gyromagnetic ratio γ_I, coupled to a species S with gyromagnetic ratio γ_S, with $|\gamma_I| > |\gamma_S|$. For example, I could represent protons and S could represent ^{13}C nuclei.

A detailed treatment of dipole–dipole relaxation in the heteronuclear case leads to the following expressions for the transition probabilities:

$$\begin{aligned}
W_{\boxed{+\alpha}} &= W_{\boxed{+\beta}} = W_{1I}(1+\tfrac{1}{2}\mathbb{B}_I) & W_{\boxed{++}} &= W_2(1+\tfrac{1}{2}\mathbb{B}_I+\tfrac{1}{2}\mathbb{B}_S) \\
W_{\boxed{-\alpha}} &= W_{\boxed{-\beta}} = W_{1I}(1-\tfrac{1}{2}\mathbb{B}_I) & W_{\boxed{--}} &= W_2(1-\tfrac{1}{2}\mathbb{B}_I-\tfrac{1}{2}\mathbb{B}_S) \\
W_{\boxed{\alpha+}} &= W_{\boxed{\beta+}} = W_{1S}(1+\tfrac{1}{2}\mathbb{B}_S) & W_{\boxed{+-}} &= W_0(1+\tfrac{1}{2}\mathbb{B}_I-\tfrac{1}{2}\mathbb{B}_S) \\
W_{\boxed{\alpha-}} &= W_{\boxed{\beta-}} = W_{1S}(1-\tfrac{1}{2}\mathbb{B}_S) & W_{\boxed{-+}} &= W_0(1-\tfrac{1}{2}\mathbb{B}_I+\tfrac{1}{2}\mathbb{B}_S)
\end{aligned} \tag{20.23}$$

The Boltzmann factors $\mathbb{B}_I$ and $\mathbb{B}_S$ are required in order to reproduce the correct thermal equilibrium state (see Section 16.3):

$$\hat{\rho}^{\text{eq}} = \frac{1}{4}\widehat{1} + \frac{1}{4}\mathbb{B}_I\hat{I}_z + \frac{1}{4}\mathbb{B}_S\hat{S}_z \tag{20.24}$$

Since $\mathbb{B}_I/\mathbb{B}_S = \gamma_I/\gamma_S$, the thermal equilibrium polarization of the I-spins is larger than that of the S-spins, by a factor γ_I/γ_S.

The single-quantum transition probabilities are given by

$$W_{1I} = \frac{3}{20}b_{IS}^2\mathfrak{J}(\omega_I^0) \qquad W_{1S} = \frac{3}{20}b_{IS}^2\mathfrak{J}(\omega_S^0)$$

while the double- and zero-quantum transition probabilities are equal to

$$W_2 = \frac{3}{5}b_{IS}^2\mathfrak{J}(\omega_I^0+\omega_S^0) \qquad W_0 = \frac{1}{10}b_{IS}^2\mathfrak{J}(\omega_I^0-\omega_S^0)$$

where the dipole–dipole coupling constant is given in Equation 9.32.

In the heteronuclear case, the spectral density of the dipole–dipole coupling is sampled at four different frequencies:

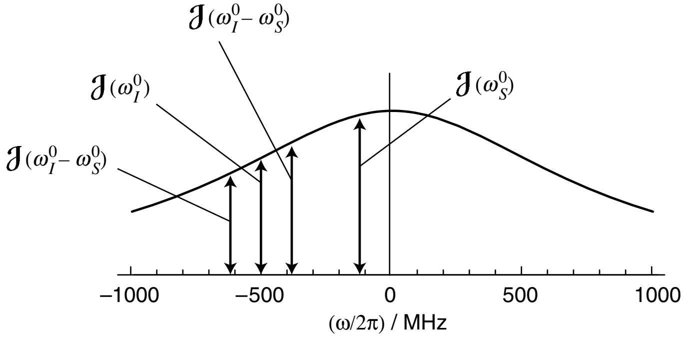

Figure 20.35
Spectral densities in a heteronuclear spin pair.

(This plot is shown for $I = {}^1\mathrm{H}$ and $S = {}^{13}\mathrm{C}$, in a field of $B^0 = 11.74\,\mathrm{T}$.)

Now assume that a continuous r.f. field is applied at the I-spin Larmor frequency, inducing transitions across two pairs of energy levels:

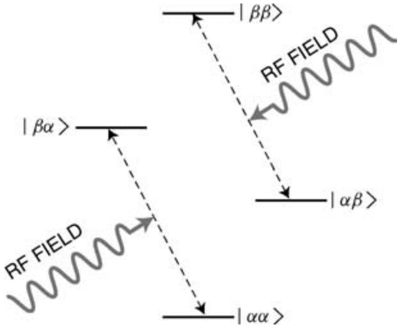

Figure 20.36
Irradiation of two pairs of transitions in a steady-state NOE experiment.

Assume that, after sufficient time, the r.f. field equalizes the populations across the irradiated transitions, so that one may write

$$\rho^{\mathrm{ss}}_{\boxed{\alpha\alpha}} = \rho^{\mathrm{ss}}_{\boxed{\beta\alpha}} = A$$

$$\rho^{\mathrm{ss}}_{\boxed{\alpha\beta}} = \rho^{\mathrm{ss}}_{\boxed{\beta\beta}} = B \tag{20.25}$$

where A and B are as yet unknown. The superscript 'ss' stands for 'steady state', implying that, after sufficiently long r.f. irradiation, the populations settle into steady-state values, which do not change any more, as long as the r.f. field is left on.

The fact that the populations equalize after a sufficiently long interval of resonant irradiation is called *saturation*. It is presented here as an assumption, but it may be justified theoretically, for sufficiently strong r.f. fields, by using a more sophisticated analysis of the combined effects of r.f. irradiation and relaxation.

Equation 20.25 allows us to deduce the steady-state populations A and B by simple kinetic arguments. In the steady state, the flux into the pair of populations $\rho_{\boxed{\alpha\alpha}}$ and $\rho_{\boxed{\beta\alpha}}$ is equal to the flux out. Similarly, the flux into the pair of populations $\rho_{\boxed{\alpha\beta}}$ and $\rho_{\boxed{\beta\beta}}$ is equal to the flux out.

The flux *into* the $\{\rho_{\boxed{\alpha\alpha}}, \rho_{\boxed{\beta\alpha}}\}$ pair is given by

$$\text{flux in} = (W_{\boxed{\beta+}} + W_{\boxed{++}} + W_{\boxed{-+}} + W_{\boxed{\alpha+}})B$$

as may be seen from the following diagram:

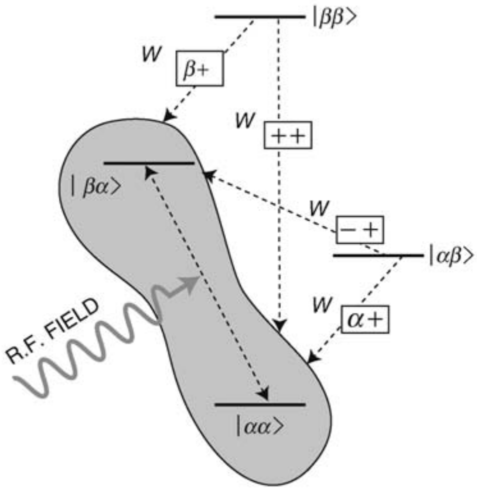

Figure 20.37
Population flux into one pair of states in a steady-state NOE experiment.

Similarly, the flux *out* of the $\{\rho_{\boxed{\alpha\alpha}}, \rho_{\boxed{\beta\alpha}}\}$ pair is given by

$$\text{flux out} = (W_{\boxed{\beta-}} + W_{\boxed{--}} + W_{\boxed{+-}} + W_{\boxed{\alpha-}})A$$

as shown below:

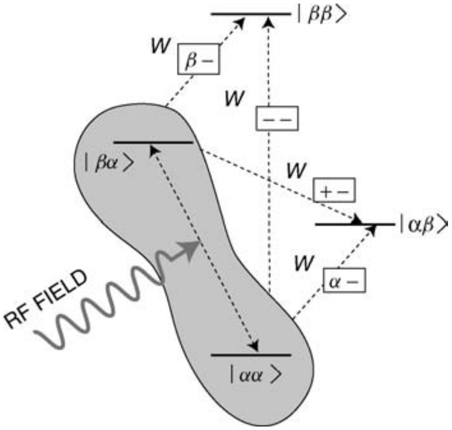

Figure 20.38
Population flux out of a pair of states in a steady-state NOE experiment.

At the steady state:

$$\text{flux in} = \text{flux out} \tag{20.26}$$

In addition, the sum of all populations is equal to one:

$$2A + 2B = 1 \tag{20.27}$$

Equations 20.26 and 20.27 may be solved and the transition probabilities in Equation 20.23 substituted in. By using the fact that $\mathbb{B}_I$ and $\mathbb{B}_S$ are very small, we get after some manipulations:

$$\rho^{\mathrm{ss}}_{\boxed{\alpha\alpha}} = \rho^{\mathrm{ss}}_{\boxed{\beta\alpha}} \cong \frac{1}{4}\left(1 + \epsilon_{\mathrm{NOE}}\frac{1}{2}\mathbb{B}_S\right)$$

$$\rho^{\mathrm{ss}}_{\boxed{\alpha\beta}} = \rho^{\mathrm{ss}}_{\boxed{\beta\beta}} \cong \frac{1}{4}\left(1 - \epsilon_{\mathrm{NOE}}\frac{1}{2}\mathbb{B}_S\right)$$

where the *NOE enhancement factor* ϵ_{NOE} is given by[5]

$$\boxed{\epsilon_{\mathrm{NOE}} = 1 + \frac{\gamma_I}{\gamma_S}\frac{W_2 - W_0}{W_0 + 2W_{1S} + W_2}} \tag{20.28}$$

The steady-state spin density operator is

$$\hat{\rho}^{\mathrm{ss}} = \frac{1}{4}\hat{1} + \epsilon_{\mathrm{NOE}}\frac{1}{4}\mathbb{B}_S\hat{S}_z$$

By comparing with Equation 20.24, one sees that the S-spin magnetization is enhanced by a factor ϵ_{NOE}, compared with its thermal equilibrium value.

The NOE enhancement factor depends on the correlation time, and hence the motion of the molecules. In the limit of very rapid molecular motion (small values of τ_c), the enhancement factor is given by

$$\epsilon_{\mathrm{NOE}}(\text{fast motion}) = 1 + \frac{\gamma_I}{2\gamma_S}$$

This factor is equal to 2.99 for the case $I = {}^{1}\mathrm{H}$ and $S = {}^{13}\mathrm{C}$, and -3.93 for the case $I = {}^{1}\mathrm{H}$ and $S = {}^{15}\mathrm{N}$, implying that the ^{15}N magnetization changes sign when the ^{1}H spins are saturated.

The enhancement factor is reduced if the molecular motion is slow. In the limit of slow molecular motion (very large values of τ_c), the enhancement factor is given by

$$\epsilon_{\mathrm{NOE}}(\text{very slow motion}) = \frac{(\gamma_I^2 - \gamma_S^2)(3\gamma_I^2 + 5\gamma_I\gamma_S - 10\gamma_S^2)}{3\gamma_I^4 + \gamma_I^2\gamma_S^2 - 10\gamma_I\gamma_S^3 + 10\gamma_S^4}$$

This factor is equal to 1.153 for the case $I = {}^{1}\mathrm{H}$ and $S = {}^{13}\mathrm{C}$, and 0.783 for the case $I = {}^{1}\mathrm{H}$ and $S = {}^{15}\mathrm{N}$. For very slow molecular motion, the ^{13}C magnetization is only slightly enhanced by ^{1}H irradiation, and for the case of ^{15}N the magnetization is reduced by ^{1}H irradiation. The following plot shows the variation of ϵ_{NOE} with τ_c, for $I = {}^{1}\mathrm{H}$ and $S = {}^{13}\mathrm{C}$ or ${}^{15}\mathrm{N}$ in a field of $B^0 = 11.74\,\mathrm{T}$:

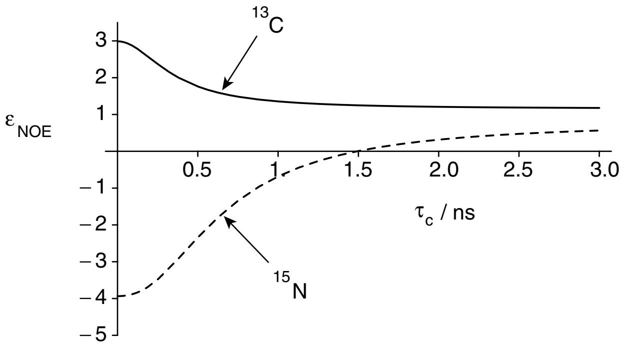

Figure 20.39
Variation of steady-state NOE as a function of correlation time, for ^{13}C–^{1}H and ^{15}N–^{1}H pairs.

Note that the sign of the steady-state ^{15}N magnetization changes sign as the molecular motion is slowed down.

In practice, the spin relaxation is not purely due to the heteronuclear dipole–dipole interaction. The presence of additional relaxation mechanisms further reduces the steady-state magnetization.

The steady-state NOE gives smaller theoretical enhancements than the INEPT method (see Section 16.3), and is sensitive to the details of the relaxation mechanisms and the molecular motion. Nevertheless, the technique is useful for positive-γ nuclei, such as ^{13}C, where it is more simple and reliable than the INEPT method, and has the advantage of not requiring a resolved J-coupling. For negative-γ nuclei, such as ^{15}N, on the other hand, saturation of the protons often destroys the ^{15}N magnetization rather than enhancing it.

20.6 NOESY

The cross-relaxation phenomenon is used in the NOESY experiment, which is one of the most widely used NMR methods for determining the structures of molecules in solution.

NOESY stands for *Nuclear Overhauser Effect Spectroscopy*.[6]

20.6.1 NOESY pulse sequence

The basic NOESY pulse sequence is precisely the same as that used in two-dimensional exchange spectroscopy, described in Section 19.7. The pulse sequence diagram is repeated here:

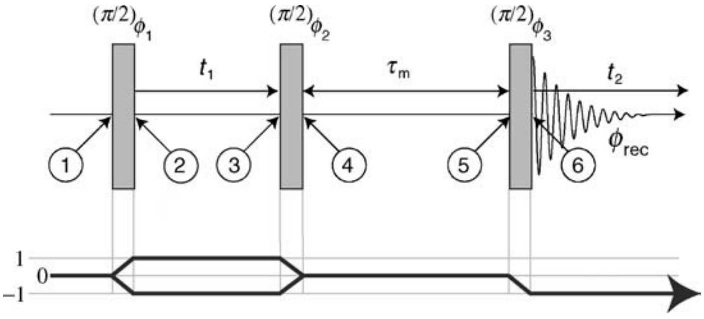

Figure 20.40
NOESY pulse sequence.

The phase cycle[7] is specified in Table 19.1.

20.6.2 NOESY signal

Consider an ensemble of homonuclear two-spin systems, in which the spins have chemical shift frequencies Ω_1^0 and Ω_2^0. The spins within each pair are assumed to be close in space, but have no J-coupling with each other.

The density operator may be calculated from time point ① to time point ④ as follows:

$$\begin{tikzcd}[row sep=large]
\hat{\rho}_{\textcircled{1}} = \hat{I}_{1z} + \hat{I}_{2z} \arrow[d, "(\pi/2)_x"] \\
\hat{\rho}_{\textcircled{2}} = -\hat{I}_{1y} - \hat{I}_{2y} \arrow[d, "t_1"] \\
\begin{array}{l} \hat{\rho}_{\textcircled{3}} = \left(-\hat{I}_{1y}\cos(\Omega_1^0 t_1) + \hat{I}_{1x}\sin(\Omega_1^0 t_1)\right)\ \exp\{-\lambda t_1\} \\ \qquad + \left(-\hat{I}_{2y}\cos(\Omega_2^0 t_1) + \hat{I}_{2x}\sin(\Omega_2^0 t_1)\right)\ \exp\{-\lambda t_1\} \end{array} \arrow[d, "(\pi/2)_{\bar{x}}"] \\
\begin{array}{l} \hat{\rho}_{\textcircled{4}} = \left(\hat{I}_{1z}\cos(\Omega_1^0 t_1) + \hat{I}_{1x}\sin(\Omega_1^0 t_1)\right)\ \exp\{-\lambda t_1\} \\ \qquad + \left(\hat{I}_{2z}\cos(\Omega_2^0 t_1) + \hat{I}_{2x}\sin(\Omega_2^0 t_1)\right)\ \exp\{-\lambda t_1\} \end{array}
\end{tikzcd} \tag{20.29}$$

(The phases of the pulses correspond to the first row of Table 19.1, with $\Psi = 0$.) The decay rate constant of the transverse magnetization is given by $\lambda = T_2{}^{-1}$.

The phase cycle has the effect of suppressing signals that do not originate in longitudinal magnetization between time points ④ and ⑤. The transverse terms in Equation 20.29 may therefore be ignored:

$$\hat{\rho}_{\textcircled{4}} = \left(\hat{I}_{1z}\cos(\Omega_1^0 t_1) + \hat{I}_{2z}\cos(\Omega_2^0 t_1)\right)\ \exp\{-\lambda t_1\} + \ldots$$

The magnetization components evolve in the mixing interval τ_m according to the following simplified form of the Solomon equations, in which the thermal equilibrium terms are dropped:

$$\frac{\mathrm{d}}{\mathrm{d}t}\begin{pmatrix} \langle \hat{I}_{1z}\rangle \\ \langle \hat{I}_{2z}\rangle \end{pmatrix} = \begin{pmatrix} -R_\mathrm{auto} & R_\mathrm{cross} \\ R_\mathrm{cross} & -R_\mathrm{auto} \end{pmatrix}\begin{pmatrix} \langle \hat{I}_{1z}\rangle \\ \langle \hat{I}_{2z}\rangle \end{pmatrix} \tag{20.30}$$

This step is justifiable, since the magnetization exchange takes place in the middle of a pulse sequence that involves phase cycling. The thermal equilibrium terms give rise to constant signals that are removed by the phase cycling procedure.[8]

The equation of motion of the magnetization components is solved in Appendix A.16. The density operator components are transformed as follows during the mixing interval τ_m of the NOESY pulse sequence:

$$\begin{aligned} \hat{I}_{1z} &\xrightarrow{\tau_\mathrm{m}} a_{1\to1}(\tau_\mathrm{m})\hat{I}_{1z} + a_{1\to2}(\tau_\mathrm{m})\hat{I}_{2z} \\ \hat{I}_{2z} &\xrightarrow{\phantom{\tau_\mathrm{m}}} a_{2\to1}(\tau_\mathrm{m})\hat{I}_{1z} + a_{2\to2}(\tau_\mathrm{m})\hat{I}_{2z} \end{aligned} \tag{20.31}$$

where the transfer amplitudes are given by Equation A.100:

$$\begin{aligned} a_{1\to1}(\tau_\mathrm{m}) = a_{2\to2}(\tau_\mathrm{m}) &= \cosh(R_\mathrm{cross}\tau_\mathrm{m})\exp\{-R_\mathrm{auto}\tau_\mathrm{m}\} \\ a_{1\to2}(\tau_\mathrm{m}) = a_{2\to1}(\tau_\mathrm{m}) &= \sinh(R_\mathrm{cross}\tau_\mathrm{m})\exp\{-R_\mathrm{auto}\tau_\mathrm{m}\} \end{aligned} \tag{20.32}$$

The longitudinal part of the density operator at time point ⑤ is therefore given by

$$
\begin{aligned}
\hat{\rho}_{⑤} = {} & \hat{I}_{1z}\, a_{1\to 1}(\tau_\mathrm{m}) \cos(\Omega_1^0 t_1) \exp\{-\lambda t_1\} \\
& + \hat{I}_{1z}\, a_{2\to 1}(\tau_\mathrm{m}) \cos(\Omega_2^0 t_1) \exp\{-\lambda t_1\} \\
& + \hat{I}_{2z}\, a_{2\to 2}(\tau_\mathrm{m}) \cos(\Omega_2^0 t_1) \exp\{-\lambda t_1\} \\
& + \hat{I}_{2z}\, a_{1\to 2}(\tau_\mathrm{m}) \cos(\Omega_1^0 t_1) \exp\{-\lambda t_1\} + \ldots
\end{aligned}
$$

The last $(\pi/2)_x$ pulse gives

$$
\begin{aligned}
\hat{\rho}_{⑥} = {} & -\hat{I}_{1y}\, a_{1\to 1}(\tau_\mathrm{m}) \cos(\Omega_1^0 t_1) \exp\{-\lambda t_1\} \\
& - \hat{I}_{1y}\, a_{2\to 1}(\tau_\mathrm{m}) \cos(\Omega_2^0 t_1) \exp\{-\lambda t_1\} \\
& - \hat{I}_{2y}\, a_{2\to 2}(\tau_\mathrm{m}) \cos(\Omega_2^0 t_1) \exp\{-\lambda t_1\} \\
& - \hat{I}_{2y}\, a_{1\to 2}(\tau_\mathrm{m}) \cos(\Omega_1^0 t_1) \exp\{-\lambda t_1\} + \ldots
\end{aligned}
$$

The two-dimensional signal is therefore

$$
\begin{aligned}
s^{\cos}(t_1, t_2) = {} & a_{1\to 1}(\tau_\mathrm{m}) \cos(\Omega_1^0 t_1) \exp\{\mathrm{i}\Omega_1^0 t_2 - \lambda(t_1 + t_2)\} \\
& + a_{2\to 1}(\tau_\mathrm{m}) \cos(\Omega_2^0 t_1) \exp\{\mathrm{i}\Omega_2^0 t_2 - \lambda(t_1 + t_2)\} \\
& + a_{1\to 2}(\tau_\mathrm{m}) \cos(\Omega_1^0 t_1) \exp\{\mathrm{i}\Omega_2^0 t_2 - \lambda(t_1 + t_2)\} \\
& + a_{2\to 2}(\tau_\mathrm{m}) \cos(\Omega_2^0 t_1) \exp\{\mathrm{i}\Omega_1^0 t_2 - \lambda(t_1 + t_2)\}
\end{aligned}
\tag{20.33}
$$

where the amplitudes of the diagonal- and cross-signals are

$$
\boxed{
\begin{aligned}
a_\mathrm{diag} = a_{1\to 1} = a_{2\to 2} &= \cosh(R_\mathrm{cross}\tau_\mathrm{m}) \exp\{-R_\mathrm{auto}\tau_\mathrm{m}\} \\
a_\mathrm{cross} = a_{1\to 2} = a_{2\to 1} &= \sinh(R_\mathrm{cross}\tau_\mathrm{m}) \exp\{-R_\mathrm{auto}\tau_\mathrm{m}\} \qquad (20.34)
\end{aligned}
}
$$

The superscript 'cos' in Equation 20.33 indicates the 'cosine' two-dimensional experiment in the States procedure ($\Psi = 0$ in Table 19.1).

Repetition of the calculation for the 'sine' component of the States two-dimensional signal ($\Psi = -\pi/2$ in Table 19.1) gives

$$
\begin{aligned}
s^{\sin}(t_1, t_2) = {} & a_{1\to 1}(\tau_\mathrm{m}) \sin(\Omega_1^0 t_1) \exp\{\mathrm{i}\Omega_1^0 t_2 - \lambda(t_1 + t_2)\} \\
& + a_{2\to 1}(\tau_\mathrm{m}) \sin(\Omega_2^0 t_1) \exp\{\mathrm{i}\Omega_2^0 t_2 - \lambda(t_1 + t_2)\} \\
& + a_{1\to 2}(\tau_\mathrm{m}) \sin(\Omega_1^0 t_1) \exp\{\mathrm{i}\Omega_2^0 t_2 - \lambda(t_1 + t_2)\} \\
& + a_{2\to 2}(\tau_\mathrm{m}) \sin(\Omega_2^0 t_1) \exp\{\mathrm{i}\Omega_1^0 t_2 - \lambda(t_1 + t_2)\}
\end{aligned}
\tag{20.35}
$$

All signal components have the correct cosine and sine modulations in the two States experiments, so the procedure in Section 5.9.4 may be followed to obtain a two-dimensional spectrum with pure absorption lineshapes for all components:

$$\begin{aligned} S(\Omega_1, \Omega_2) = {} & a_{\text{diag}}(\tau_{\text{m}})\mathcal{A}(\Omega_1, \Omega_2;\ \Omega_1^0, \lambda, \Omega_1^0, \lambda) \\ & + a_{\text{diag}}(\tau_{\text{m}})\mathcal{A}(\Omega_1, \Omega_2;\ \Omega_2^0, \lambda, \Omega_2^0, \lambda) \\ & + a_{\text{cross}}(\tau_{\text{m}})\mathcal{A}(\Omega_1, \Omega_2;\ \Omega_1^0, \lambda, \Omega_2^0, \lambda) \\ & + a_{\text{cross}}(\tau_{\text{m}})\mathcal{A}(\Omega_1, \Omega_2;\ \Omega_2^0, \lambda, \Omega_1^0, \lambda) \end{aligned} \tag{20.36}$$

The spectrum contains two diagonal peaks, with amplitudes given by a_{diag}, and two cross-peaks, with amplitudes given by a_{cross} (Equation 20.34).

One should note the origin of the spectral peaks in Equation 20.36. The diagonal peak at frequency coordinates $(\Omega_1, \Omega_2) = (\Omega_1^0, \Omega_1^0)$ and the cross-peak at frequency coordinates $(\Omega_1, \Omega_2) = (\Omega_1^0, \Omega_2^0)$ originate in the $\hat{I}_{1z}$ part of the initial density operator $\hat{\rho}_{①}$. These peaks, therefore, are totally independent of the state of the spins I_2 at the beginning of the pulse sequence. Similarly, the diagonal peak at frequency coordinates $(\Omega_1, \Omega_2) = (\Omega_2^0, \Omega_2^0)$ and the cross-peak at frequency coordinates $(\Omega_1, \Omega_2) = (\Omega_2^0, \Omega_1^0)$ are independent of the state of the spins I_1 at the beginning of the pulse sequence.

20.6.3 NOESY spectra

The relative signs of the cross-peaks in a NOESY spectrum depend on the rotational correlation time.

1. *Long rotational correlation time.* If the rotational correlation time of the molecules is long ($\tau_c > \tau_c^{\text{crit}}$), then the sense of the magnetization transfer during the mixing interval is *positive*. The process may be visualized as follows:

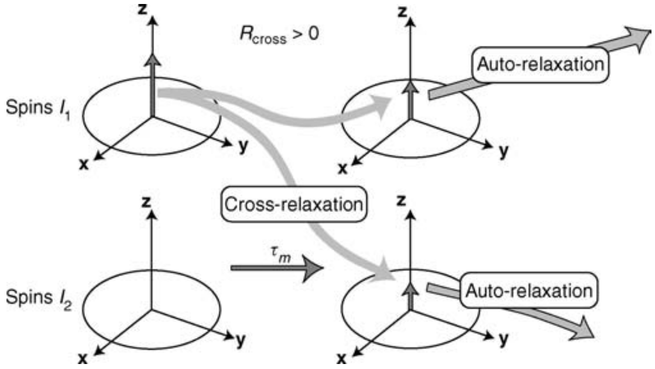

Figure 20.41
Visualization of the magnetization transfer process, for a long rotational correlation time.

The magnetization of spins I_1 is converted into magnetization of spins I_2, at the same time as it decays with rate constant R_{auto}. At long times, the two sets of spins reach a state of *internal equilibrium*, in which the magnetizations of the two species become equal and decay together.

This resembles the act of magnetizing a piece of iron by bringing it close to another piece of magnetic material.

In this regime, the diagonal- and cross-peak amplitudes vary as a function of τ_{m} as follows:

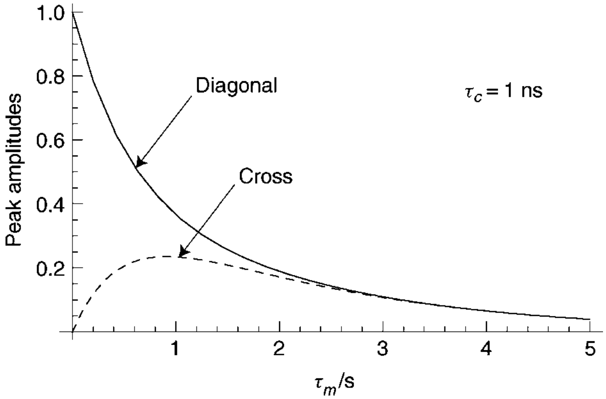

Figure 20.42
NOESY peak amplitudes for a long rotational correlation time.

These simulations are for an ensemble of proton pairs separated by 0.2 nm in a field of 11.74 T, with a rotational correlation time $\tau_c = 1$ ns.

The diagonal and cross-peaks in the two-dimensional spectrum have the *same* sign in the long correlation time regime:

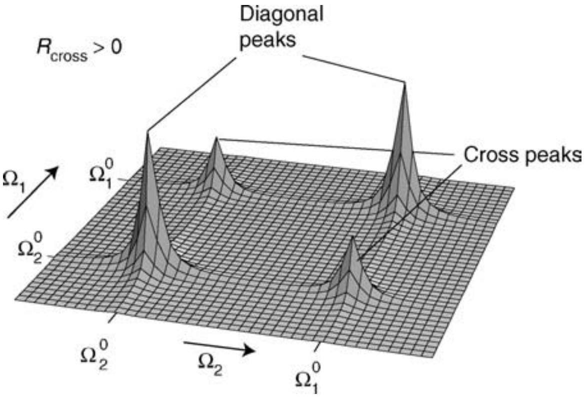

Figure 20.43
Form of the NOESY spectrum in the case of a long rotational correlation time.

2. *Short rotational correlation time*. If the rotational correlation time of the molecules is short ($\tau_c < \tau_c^{\text{crit}}$), then the sense of the magnetization transfer during the mixing interval is *negative*, which may be visualized as follows:

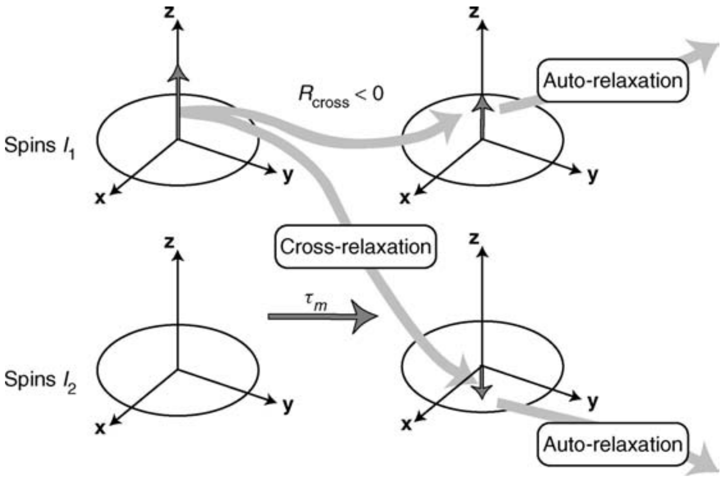

Figure 20.44
Visualization of the magnetization transfer process, for a short rotational correlation time.

The magnetization of spins I_1 is changed in sign on conversion into magnetization of spins I_2. In this regime, the diagonal- and cross-peak amplitudes vary as a function of τ_m as follows:

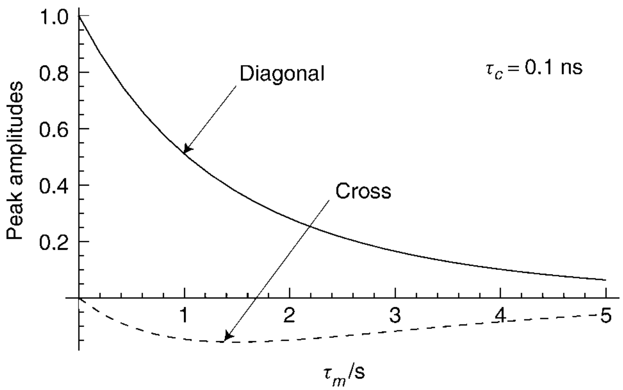

Figure 20.45
NOESY peak amplitudes for a short rotational correlation time.

These simulations are for an ensemble of proton pairs separated by 0.2 nm in a field of 11.74 T, with a rotational correlation time $\tau_c = 0.1$ ns.

The diagonal and cross-peaks in the two-dimensional spectrum have *opposite* sign in the short correlation time regime:

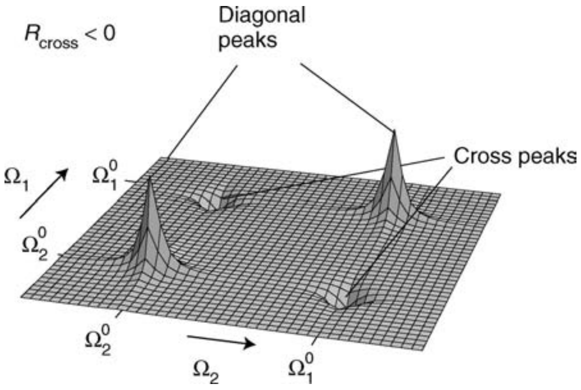

Figure 20.46
Form of the NOESY spectrum in the case of a short rotational correlation time.

3. *Critical rotational correlation time*. The cross-peaks disappear for the critical rotational correlation time τ_c^{crit} (Equation 20.18).

20.6.4 NOESY and chemical exchange

The NOESY and two-dimensional exchange experiments are identical. In general, this experiment does not distinguish between magnetization transfer through dipole–dipole spin interactions (cross-relaxation) and magnetization transfer due to chemical exchange processes (see Section 19.7). A partial distinction between these processes is obtained for small molecules, where cross-relaxation gives negative cross-peaks, whereas chemical exchange gives positive cross-peaks.

20.6.5 Molecular structure determination

At short values of mixing interval $\tau_{\rm m}$, the cross-peak amplitudes are given approximately by

$$a_{\rm cross}(\tau_{\rm m}) \cong R_{\rm cross}\tau_{\rm m}$$

The cross-relaxation rate constant is proportional to the square of the dipole–dipole interaction and, hence, to the inverse sixth power of the distance between the spins:

$$\boxed{a_{\rm cross}(\tau_{\rm m}) \sim r^{-6} \qquad (20.37)}$$

This equation accounts for the importance of NOESY in structural biology. By taking a NOESY spectrum of a biomolecule, and measuring the cross-peak amplitudes, one may estimate simultaneously a large number of internuclear distances and, hence, build up a picture of the molecular structure.

Kurt Wüthrich was awarded the Nobel Prize in 1992, in part for the development of NOESY into a powerful tool for the determination of biomolecular structures.

It is difficult to determine *absolute* internuclear distances by NOESY, since the proportionality constant in Equation 20.37 is difficult to determine. However, this does not matter too much in practice, since the distance scale may be calibrated using proton pairs separated by known distances in rigid parts of the molecule.

Figure 20.47 shows an experimental NOESY spectrum of a protein in isotropic solution. The spectrum displays a large number of cross-peaks, each of which may be analysed to obtain a single structural constraint – an estimated distance between one pair of nuclear sites. Usually, a computer is used to construct a molecular structural model in which all of the NOESY distance constaints are satisfied simultaneously, in the ideal case. An example of a solution-state biomolecular structure, solved with the assistance of NOESY, is shown in Plate 5.

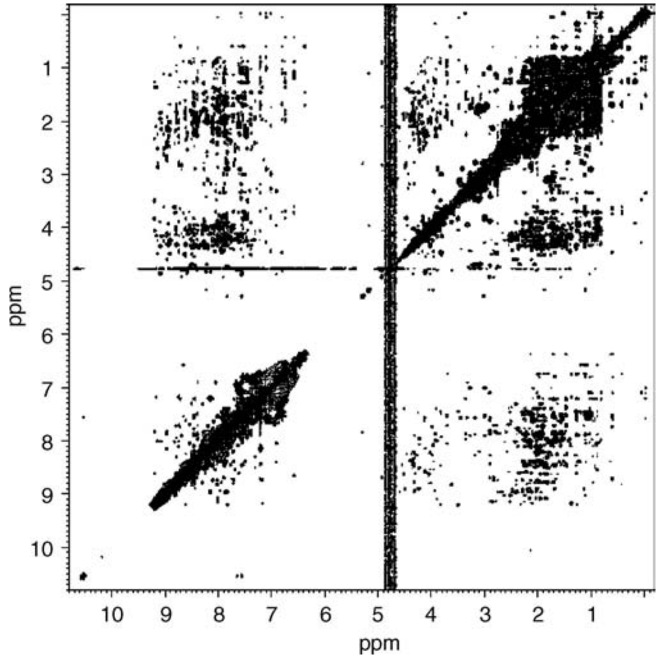

Figure 20.47
Experimental ^{1}H NOESY spectrum of a medium-sized biomolecule in solution (the C-terminal domain of rat ERp29 protein). The protein contains 120 amino acid residues. A special pulse technique was used to suppress the water proton resonance. For details, see G. Otting, E. Liepinsh and K. Wüthrich, *J. Am. Chem. Soc.* **114**, 7093–7095 (1992). Thanks to E. Liepinsh and G. Otting for providing this spectrum.

20.7 ROESY

20.7.1 Transverse cross-relaxation

Much has now been said about the through-space cross-relaxation of *longitudinal* magnetization components. What about *transverse* magnetization? Can transverse magnetization components also cross-relax?

The answer is yes, provided precautions are taken to arrest the mutual precession of spins at different chemical sites.

To see what this means, consider the precessing transverse magnetizations of two different sets of spins, I_1 and I_2. View the precession from a frame rotating at the average Larmor frequency of the spins I_1. From this frame, the transverse magnetization of spins I_1 appears to be static, whereas the transverse magnetization of spins I_2 precesses in the positive direction, if $\Omega_2^0 > \Omega_1^0$:

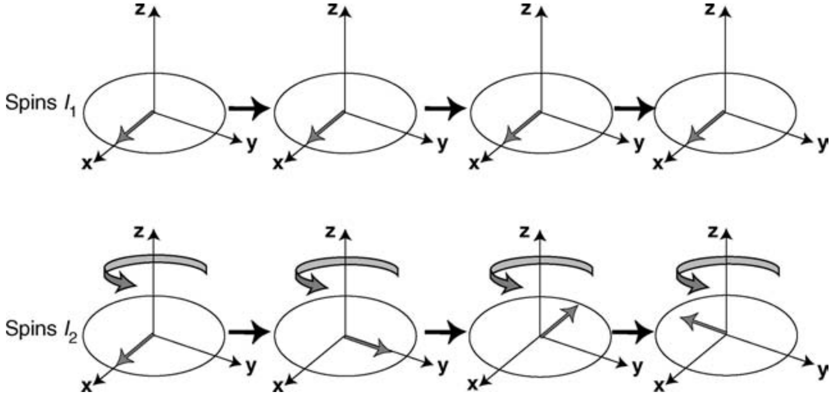

Figure 20.48 Transverse magnetization vectors in the rotating frame, for the case $\omega_{\text{ref}} = \omega_1^0$.

Now suppose that there is a *transverse cross-relaxation process* that allows the transverse magnetizations of the two species to communicate with each other. If the transverse cross-relaxation rate constant is positive, then the transferred magnetization has the same sign as the source magnetization.

Suppose that initially, spins I_1 have magnetization along the x-axis, whereas spins I_2 have no magnetization. The diagram below shows the course of events schematically:

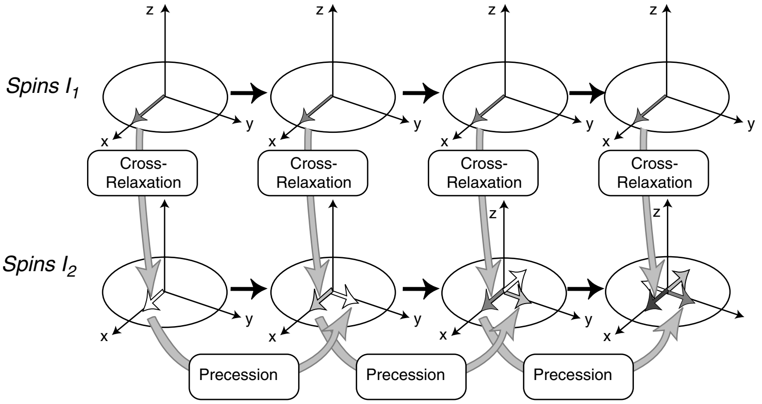

Figure 20.49 The cross-relaxation of transverse magnetization is suppressed by differential spin precession.

In the leftmost diagram, a small amount of magnetization is transferred from spins I_1 to I_2, appearing along the *x*-axis (short white arrow). In the next frame, some more magnetization is transferred along the *x*-axis (light grey arrow). However, in the preceding interval, the initially transferred magnetization (white arrow) has precessed, and is now oriented along the *y*-axis. The process is repeated in the next two frames: In the last frame, there are four transferred magnetization components, but they are all out of phase with each other and cancel exactly.

Because of the mutual precession, the transferred magnetization does not build up. Transverse cross-relaxation is effectively *decoupled* by the mutual spin precession.

It is only possible to observe transverse cross-relaxation without intervention if the participating spins have exactly the same precession frequency.

20.7.2 Spin locking

The mutual precession of spins with different chemical shifts may be suppressed by using *spin locking*, as described in Section 12.3. A strong, resonant r.f. field, applied with the same phase as the transverse magnetization, inhibits the differential precession:

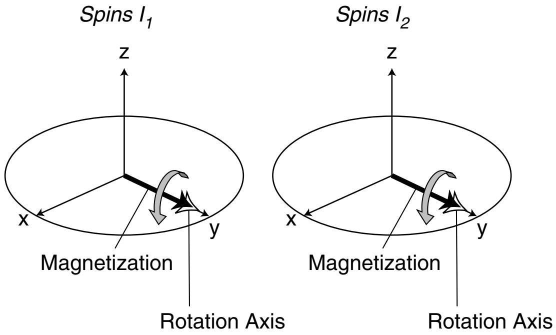

Figure 20.50
Suppression of the differential precession by the strong r.f. field.

The differential precession is suppressed effectively by the r.f. field, providing that the nutation frequency is strong compared to both chemical shift offset frequencies:

$$|\omega_{\text{nut}}| >> |\Omega_1^0|, |\Omega_2^0|$$

where the nutation frequency is as usual proportional to the r.f. field strength:

$$\omega_{\text{nut}} = \left| \frac{1}{2} \gamma B_{\text{RF}} \sin \theta_{\text{RF}} \right|$$

20.7.3 Transverse Solomon equations

The r.f. field inhibits the mutual precession of the spins and allows magnetization transfer to take place. The spin-locked magnetization components may then communicate through cross-relaxation processes. This process is described by the *transverse Solomon equations*, which are analogous to the simplified longitudinal Solomon equations given in Equation 20.30:

$$\frac{\mathrm{d}}{\mathrm{d}t}\begin{pmatrix}\langle \hat{I}_{1y}\rangle \\ \langle \hat{I}_{2y}\rangle\end{pmatrix} = \begin{pmatrix}-R^{\mathrm{T}}_{\mathrm{auto}} & R^{\mathrm{T}}_{\mathrm{cross}} \\ R^{\mathrm{T}}_{\mathrm{cross}} & -R^{\mathrm{T}}_{\mathrm{auto}}\end{pmatrix}\begin{pmatrix}\langle \hat{I}_{1y}\rangle \\ \langle \hat{I}_{2y}\rangle\end{pmatrix} \tag{20.38}$$

The superscript 'T' indicates 'transverse'.

The transverse relaxation rate constants are somewhat different from the longitudinal ones. For intramolecular dipole–dipole relaxation between two spins, the transverse auto-relaxation rate constant is given by

$$R^{\mathrm{T}}_{\mathrm{auto}} = \frac{1}{20}b^2\left\{5\mathfrak{J}(0) + 9\mathfrak{J}(\omega^0) + 6\mathfrak{J}(2\omega^0)\right\} \tag{20.39}$$

and the transverse cross-relaxation rate constant is given by[4]

$$R^{\mathrm{T}}_{\mathrm{cross}} = -\frac{1}{10}b^2\left\{2\mathfrak{J}(0) + 3\mathfrak{J}(\omega^0)\right\} \tag{20.40}$$

The longitudinal and transverse auto-relaxation rate constants are the same for fast molecular motion, but the transverse relaxation is faster if the molecular tumbling is slow (see Figure 20.51, which is calculated for two protons separated by 0.2 nm, in a field of 11.74 T.)

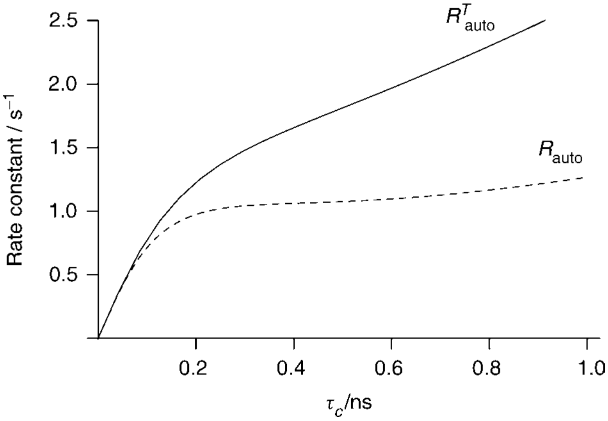

Figure 20.51
Transverse and longitudinal auto-relaxation rate constants, as a function of rotational correlation time.

The longitudinal and transverse cross-relaxation rate constants are also the same for rapid molecular tumbling, but behave quite differently as the rotational correlation time is increased. As discussed in Section 20.6, the longitudinal cross-relaxation rate constant changes sign as a function of τ_c. The transverse cross-relaxation rate constant, on the other hand, is always negative:[4]

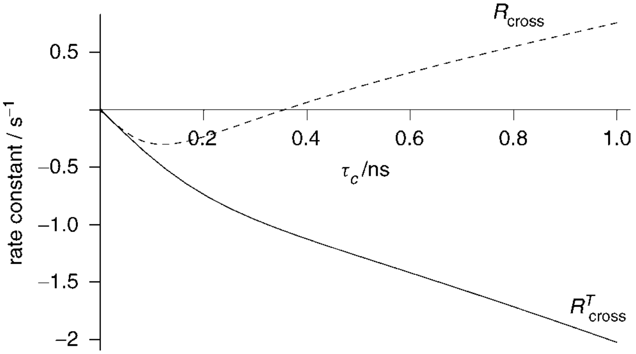

Figure 20.52 Transverse and longitudinal cross-relaxation rate constants, as a function of rotational correlation time.

Since there is no sign change in $R^{\mathrm{T}}_{\mathrm{cross}}$, it is easier to observe transverse cross-relaxation than longitudinal cross-relaxation, for the case of medium-sized molecules tumbling near the critical correlation time ($\tau_{\mathrm{c}} \sim \tau_{\mathrm{c}}^{\mathrm{crit}}$).

For *slowly* tumbling molecules ($\tau_{\mathrm{c}} >> \tau_{\mathrm{c}}^{\mathrm{crit}}$), on the other hand, transverse cross-relaxation is *less* easy to observe than longitudinal cross-relaxation, because of the large value of R^{T}_{auto}, which causes the transverse magnetization to decay quickly.

20.7.4 ROESY spectra

Transverse cross-relaxation is usually exploited by the two-dimensional experiment known as ROESY (which stands for *Rotating Frame Overhauser Effect Spectroscopy*[9]).

A basic ROESY pulse sequence is shown below:

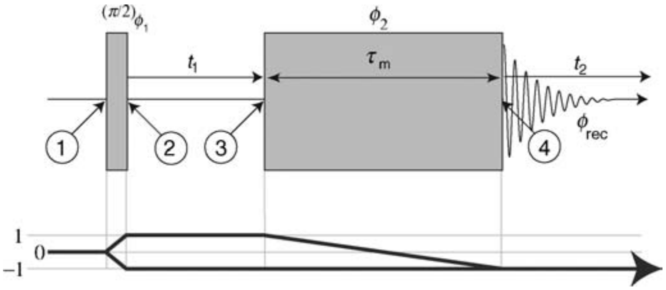

Figure 20.53 ROESY pulse sequence.

An initial $\pi/2$ pulse with phase ϕ_1 is followed by a variable evolution interval t_1 and a long mixing interval of continuous r.f. irradiation, of constant duration τ_{m} and phase ϕ_2. The signal is detected in the subsequent t_2 interval, using a receiver phase ϕ_{rec}.

A simple phase cycle for the ROESY experiment is given in Table 20.1. This includes a phase Ψ used in the States scheme for generating two-dimensional absorption lineshapes.

Table 20.1 A two-step phase cycle ($\mathfrak{n} = 2$) appropriate for the ROESY experiment. The phase Ψ is used in the States scheme for generating pure absorption two-dimensional lineshapes, with discrimination of positive and negative Ω_1-frequencies (see Section 5.9.4). For the 'cosine' data set, $\Psi = 0$. For the 'sine' data set, $\Psi = -\pi/2$.

Cycle counter $\mathfrak{m}$	ϕ_1	ϕ_2	ϕ_{rec}
0	Ψ	$\pi/2$	0
1	$\Psi + \pi$	$\pi/2$	π

Calculation of the spin-density operator for an ensemble of homonuclear spin pairs runs as follows up to time point ③, for the case $\Psi = 0$:

$$\begin{tikzcd}
\hat{\rho}_{\textcircled{1}} = \hat{I}_{1z} + \hat{I}_{2z} \arrow[d, "(\pi/2)_x"] \\
\hat{\rho}_{\textcircled{2}} = -\hat{I}_{1y} - \hat{I}_{2y} \arrow[d, "t_1"] \\
\hat{\rho}_{\textcircled{3}} = \left(-\hat{I}_{1y}\cos(\Omega_1^0 t_1) + \hat{I}_{1x}\sin(\Omega_1^0 t_1)\right)\ \exp\{-\lambda t_1\}
\end{tikzcd}$$

$$+\left(-\hat{I}_{2y}\cos(\Omega_2^0 t_1) + \hat{I}_{2x}\sin(\Omega_2^0 t_1)\right)\ \exp\{-\lambda t_1\} \tag{20.41}$$

The strong r.f. field is applied with phase $\phi_2 = \pi/2$, which spin-locks the y-components of the spin angular momenta. The x-components nutate rapidly around the spin-locking field, and are usually effectively destroyed by the inhomogeneity in the r.f. field. There are variants of the ROESY pulse sequence that destroy these components in a more sophisticated and exact way (see *Further Reading*).

The $\hat{I}_{1y}$ and $\hat{I}_{2y}$ components evolve according to the transverse Solomon equations, Equation 20.38. These equations may be solved using the technique described in Appendix A.16. The result is

$$\begin{aligned}
\hat{\rho}_{\textcircled{4}} = &-\hat{I}_{1y}\cos(\Omega_1^0 t_1)\cosh(R_{\text{cross}}^{\text{T}}\tau_{\text{m}})\exp\{-\lambda t_1 - R_{\text{auto}}^{\text{T}}\tau_{\text{m}}\} \\
&-\hat{I}_{1y}\cos(\Omega_2^0 t_1)\sinh(R_{\text{cross}}^{\text{T}}\tau_{\text{m}})\exp\{-\lambda t_1 - R_{\text{auto}}^{\text{T}}\tau_{\text{m}}\} \\
&-\hat{I}_{2y}\cos(\Omega_2^0 t_1)\cosh(R_{\text{cross}}^{\text{T}}\tau_{\text{m}})\exp\{-\lambda t_1 - R_{\text{auto}}^{\text{T}}\tau_{\text{m}}\} \\
&-\hat{I}_{2y}\cos(\Omega_2^0 t_1)\sinh(R_{\text{cross}}^{\text{T}}\tau_{\text{m}})\exp\{-\lambda t_1 - R_{\text{auto}}^{\text{T}}\tau_{\text{m}}\} + \ldots
\end{aligned}$$

The resulting two-dimensional signal, for the case of $\Psi = 0$, is given by

$$\begin{aligned}
s^{\cos}(t_1, t_2) = {} & a_{\text{diag}}(\tau_{\text{m}}) \cos(\Omega_1^0 t_1) \exp\{\text{i}\Omega_1^0 t_2 - \lambda(t_1 + t_2)\} \\
& + a_{\text{diag}}(\tau_{\text{m}}) \cos(\Omega_2^0 t_1) \exp\{\text{i}\Omega_2^0 t_2 - \lambda(t_1 + t_2)\} \\
& + a_{\text{cross}}(\tau_{\text{m}}) \cos(\Omega_1^0 t_1) \exp\{\text{i}\Omega_2^0 t_2 - \lambda(t_1 + t_2)\} \\
& + a_{\text{cross}}(\tau_{\text{m}}) \cos(\Omega_2^0 t_1) \exp\{\text{i}\Omega_1^0 t_2 - \lambda(t_1 + t_2)\}
\end{aligned}$$

where the amplitudes of the diagonal- and cross-signals are

$$\begin{aligned}
a_{\text{diag}}(\tau_{\text{m}}) &= \cosh(R^{\text{T}}_{\text{cross}}\tau_{\text{m}})\exp\{-R^{\text{T}}_{\text{auto}}\tau_{\text{m}}\} \\
a_{\text{cross}}(\tau_{\text{m}}) &= \sinh(R^{\text{T}}_{\text{cross}}\tau_{\text{m}})\exp\{-R^{\text{T}}_{\text{auto}}\tau_{\text{m}}\}
\end{aligned} \tag{20.42}$$

The peak amplitudes are exactly the same as in NOESY (Equation 20.34), but with the substitution of R_{cross} and R_{auto} by $R^{\text{T}}_{\text{cross}}$ and $R^{\text{T}}_{\text{auto}}$ respectively. Since $R^{\text{T}}_{\text{cross}}$ is negative, ROESY cross-peaks always have the opposite sign to the diagonal peaks:

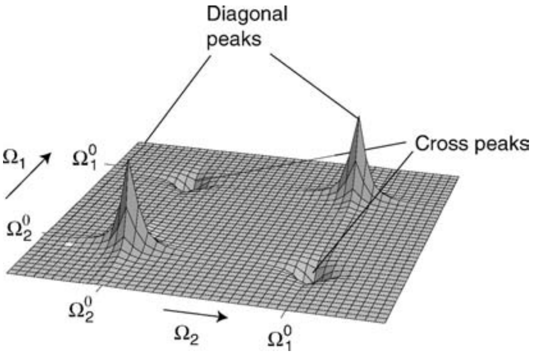

Figure 20.54
Form of the ROESY spectrum. The cross-peaks are always negative, independent of the correlation time.

Figure 20.55 shows simulations of NOESY and ROESY peak amplitudes, as a function of mixing interval τ_{m}, for a series of rotational correlation times τ_{c}. Note that the ROESY cross-peaks are always negative, and are larger than the NOESY cross-peaks for short values of τ_{c}. The NOESY cross-peaks vanish at the critical correlation time $\tau_{\text{c}}^{\text{crit}} = 0.36\,\text{ns}$. However, NOESY cross-peaks are larger when τ_{c} is long.

ROESY is widely used as a method for structure determination of small- to medium-sized molecules in solution (typically up to around 3000 atomic mass units).

20.7.5 ROESY and chemical exchange

ROESY enables a relatively clear distinction between cross-relaxation and chemical exchange. Cross-relaxation always gives rise to negative cross-peaks in a ROESY experiment, whereas chemical exchange

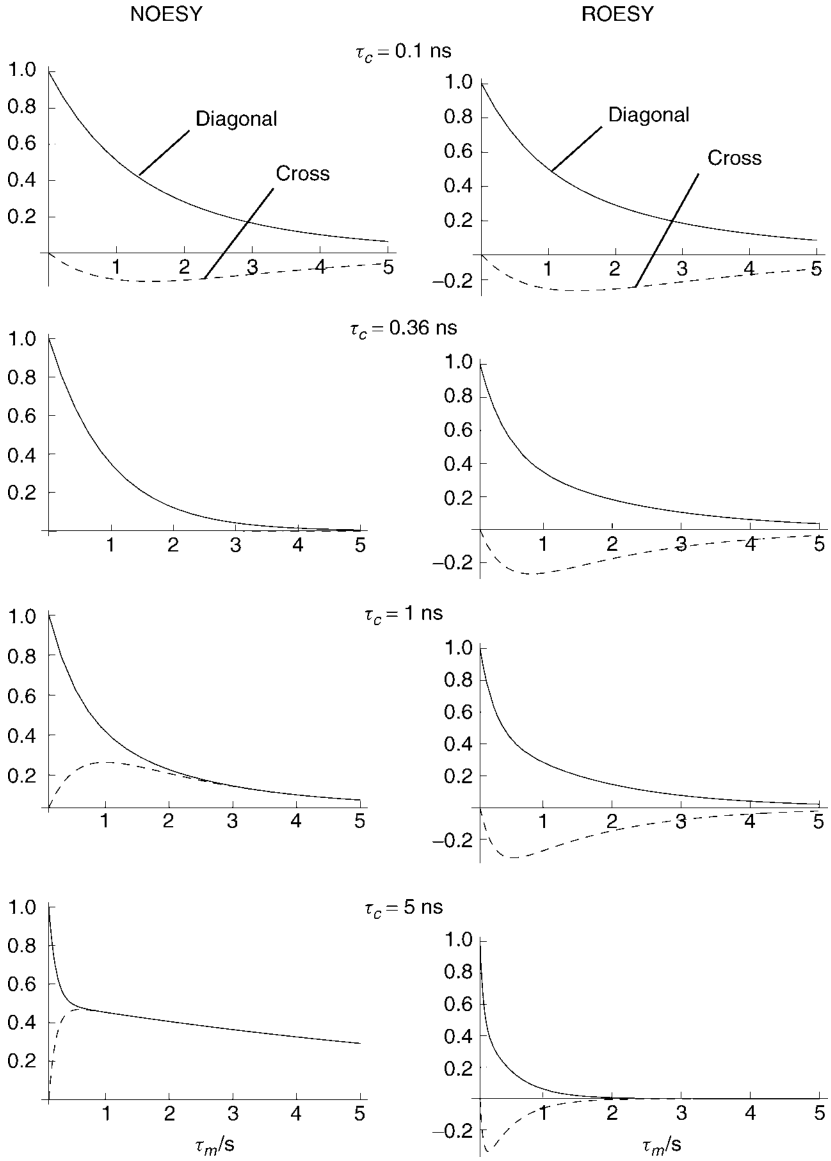

Figure 20.55
Comparison of diagonal-peak and cross-peak amplitudes for NOESY and ROESY for a set of rotational correlation times. All simulations are for the case of two protons separated by 0.2 nm in a field of 11.74 T.

always gives rise to positive cross-peaks in the same experiment. This distinction is not obtained so cleanly in the NOESY experiment (see Section 20.6.4).

20.7.6 ROESY and TOCSY

The ROESY pulse sequence is very similar to the TOCSY pulse sequence (see Section 18.14). Indeed, in general, TOCSY effects (magnetization transfer through J-couplings) are observed in the ROESY experiment, and ROESY effects (magnetization transfer through cross-relaxation) are observed in TOCSY experiments. A series of modified pulse sequences have been developed that give relatively 'clean' TOCSY and ROESY effects, compensated for pulse imperfections and off-resonance effects during the spin-locking pulse (see *Further Reading*).

20.8 Cross-Correlated Relaxation

20.8.1 Cross-correlation

Consider three random processes, A, B and C, that vary as a function of time. Suppose that they also have the same autocorrelation function. A plot of the three random processes against time might have the following appearance:

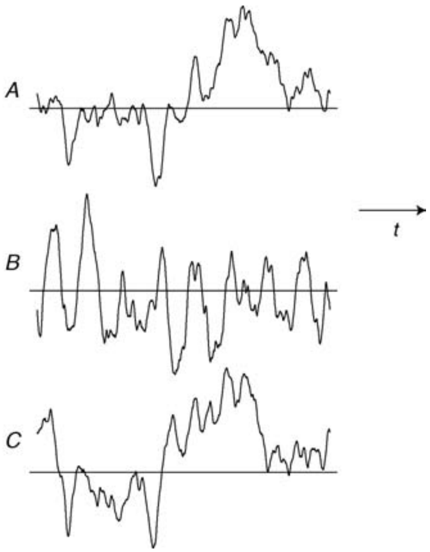

Figure 20.56 Three random processes.

In all cases, the value of the function at a particular time is unpredictable. Despite this, there is a relationship between two of the functions, as is seen clearly when they are superimposed:

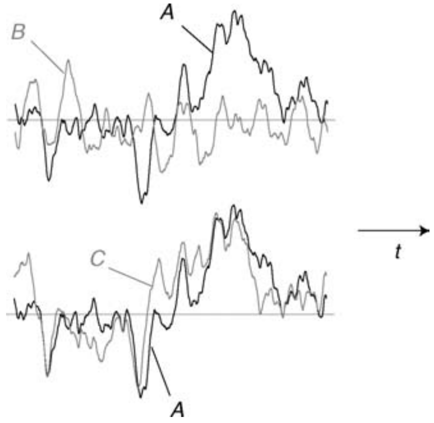

Figure 20.57 Overlay of the random processes, making the cross-correlation of A and C clear.

There is no particular relationship between A and B, whereas there is a distinct tendency for C and A to follow each other.

This tendency may be expressed mathematically in terms of the *cross-correlation* of the two processes, defined as

$$\boxed{\mathbb{K}_{AB}(\tau) = \left\langle A(t)B(t+\tau)\right\rangle \qquad (20.43)}$$

This is analogous to the autocorrelation function of a single process, defined in Equation 20.1.

In the examples shown above, the processes A and B are *uncorrelated* (meaning that the cross-correlation function is zero), whereas the processes A and C are *correlated* (meaning that the cross-correlation function is finite).

The existence of cross-correlation implies a common physical mechanism underlying both processes. Here is an example: the intensity of the northern lights (aurora borealis) fluctuates unpredictably. The same is true for the number of dark spots on the surface of the sun. Nevertheless, these two apparently unrelated processes are strongly correlated. This is because a common physical mechanism underlies both. Immense storms on the surface of the sun reduce locally the temperature of the surface (causing dark spots) and also eject particles into space, which generate the aurora as they impact the upper atmosphere of the Earth.

20.8.2 Cross-correlation of spin interactions

Typically, a nuclear spin experiences many different sources of local magnetic fields, which fluctuate as the molecule rotates in a liquid. Neighbouring nuclear spins generate magnetic fields – this comprises the dipole–dipole relaxation mechanism, described above. In addition, local magnetic fields are generated by induced electron currents, leading to spin relaxation through chemical shift anisotropy.

All of these local fields have a molecular origin. They are all modulated by the rotation of the molecule. There is, therefore, a common physical link between all molecular relaxation mechanisms, which implies a degree of correlation.

For example, consider a molecule containing three protons, arranged in a line. The central proton is relaxed by the dipole–dipole couplings to the two outer protons. If the molecule is rigid, all three dipole–dipole couplings change in synchrony when the molecule rotates, and are therefore strongly correlated:

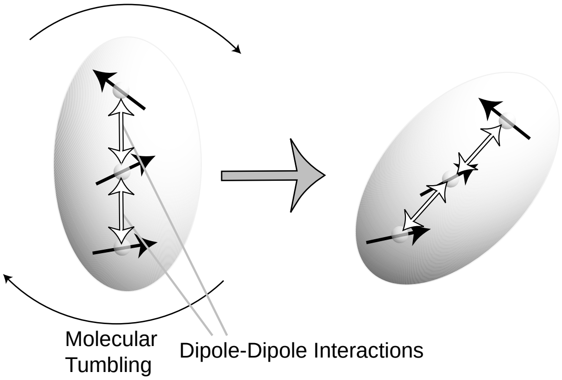

Figure 20.58
Cross-correlation of two dipole–dipole interactions.

Another example is when a nuclear spin experiences a local field from a different nuclear spin as well as a local field from the surrounding electrons. When the molecule rotates, both the nuclear spins and the electrons move at the same time. As a result, the fluctuations of dipole–dipole couplings and CSA also tend to be correlated.

Cross-correlation of different relaxation mechanisms is therefore a ubiquitous phenomenon in rigid molecules and is responsible for many interesting and useful effects. In general, cross-correlated relaxation breaks the symmetry of relaxation equations such as Equations 20.10 and 20.23. In the presence of cross-correlation, it is no longer true that transition probabilities such as $W_{\boxed{+\alpha}}$ and $W_{\boxed{+\beta}}$ are equal. Similarly, the transverse relaxation time constants of coherences such as $\rho_{\boxed{\alpha-}}$ and $\rho_{\boxed{\beta-}}$ are not, in general, equal in the presence of cross-correlated relaxation.

20.8.3 Dipole–dipole cross-correlation and angular estimations

In a rigid molecule, two different dipole–dipole interactions are, in general, cross-correlated, because there is a fixed geometrical relationship between them. For example, consider two different ^{13}C–^{1}H interactions in a $^{13}C_2$-labelled molecule, in which each labelled carbon atom is bonded to one proton. The two ^{13}C–^{1}H interactions are cross-correlated. The relevant cross-correlation function $\mathbb{K}_{\mathrm{CH,CH}}$ depends on the *angle* $\theta_{\mathrm{CH,CH}}$ between the two ^{13}C–^{1}H vectors, according to

$$\mathbb{K}_{\mathrm{CH,CH}} \sim \frac{1}{2}\left(3\cos^2\theta_{\mathrm{CH,CH}} - 1\right)$$

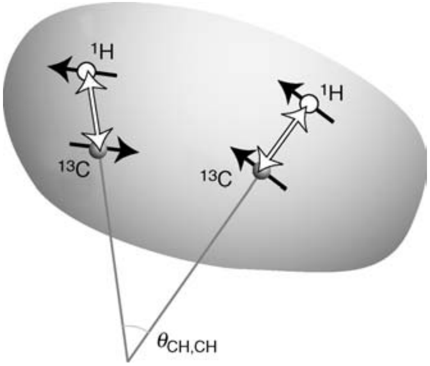

Figure 20.59
The angle between two ^{13}C–^{1}H vectors.

If the two vectors are *parallel or antiparallel* ($\theta_{\mathrm{CH,CH}} = 0$ or π), then the cross-correlation function is *positive*, since the two dipole–dipole couplings track each other exactly as the molecule rotates.

If the two vectors are *perpendicular* ($\theta_{\mathrm{CH,CH}} = \pi/2$), then the cross-correlation function is *negative*, implying that the two dipole–dipole couplings are *anticorrelated*. If the molecule is oriented so that one ^{13}C–^{1}H vector is parallel to the external field (leading to a positive secular dipolar coupling), then the second ^{13}C–^{1}H vector must be perpendicular to the field (leading to a negative secular dipolar coupling). In this geometry, the two secular dipolar couplings tend to have opposite signs as the molecule rotates.

This type of cross-correlation leads to a variety of effects on the spin dynamics, but perhaps the clearest effects are observed on the linewidths of the $^{13}C_2$ double-quantum coherences.

As an example, consider the two anomers of [1,2-$^{13}C_2$]-glucose, which have the following molecular structure:

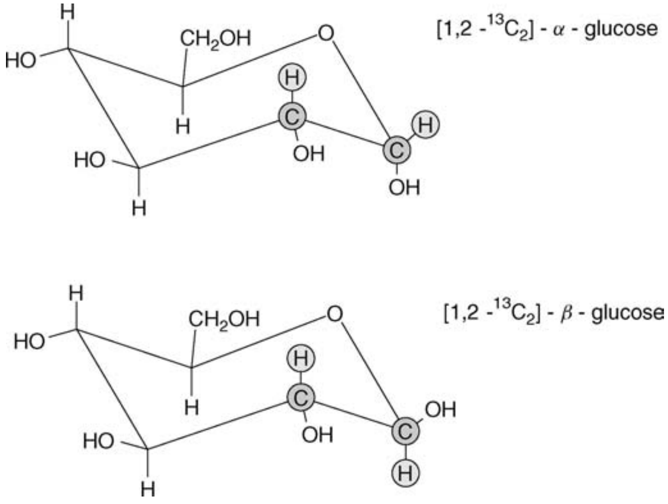

Figure 20.60
The two anomers of $[1,2\text{-}^{13}C_2]$-glucose, showing the HCCH four-spin moieties.

The two CH vectors are roughly perpendicular in the α-anomer, whereas they are approximately antiparallel in the β-anomer.

As discussed in Chapter 17, there are four (-2)-quantum $^{13}C_2$ coherences in this four-spin system, denoted $\rho_{\boxed{\alpha--\alpha}}$, $\rho_{\boxed{\alpha--\beta}}$, $\rho_{\boxed{\beta--\alpha}}$ and $\rho_{\boxed{\beta--\beta}}$ (the state labels are arranged as follows: ^{1}H–^{13}C–^{13}C–^{1}H). These coherences may be excited, for example, by using the INADEQUATE pulse sequence (see Section 16.2) and allowed to evolve in the absence of proton decoupling. Two-dimensional spectroscopy may be used to obtain a double-quantum ^{13}C spectrum, which contains four peaks, one for each (-2)-quantum $^{13}C_2$ coherence.

The frequencies of these coherences may be deduced using the arguments given in Section 18.5.3. They are as follows:

$$\Omega_{\boxed{\alpha--\alpha}} = \Omega_2^0 + \Omega_3^0 + \pi J_{12} + \pi J_{13} + \pi J_{24} + \pi J_{34}$$

$$\Omega_{\boxed{\alpha--\beta}} = \Omega_2^0 + \Omega_3^0 + \pi J_{12} + \pi J_{13} - \pi J_{24} - \pi J_{34}$$

$$\Omega_{\boxed{\beta--\alpha}} = \Omega_2^0 + \Omega_3^0 - \pi J_{12} - \pi J_{13} + \pi J_{24} + \pi J_{34}$$

$$\Omega_{\boxed{\beta--\beta}} = \Omega_2^0 + \Omega_3^0 - \pi J_{12} - \pi J_{13} - \pi J_{24} - \pi J_{34}$$

If proton decoupling is not used during the evolution interval, the $^{13}C_2$ double-quantum spectrum has the form of a four-peak multiplet, centred around the sum of the offset frequencies $\Omega_2^0 + \Omega_3^0$.

An experimental example for the β-anomer is shown in Figure 20.61. The different widths of the four peaks are clearly visible. The two central peaks, which are associated with the $\rho_{\boxed{\alpha--\beta}}$ and $\rho_{\boxed{\beta--\alpha}}$ coherences, are narrow, whereas the two outer peaks, which are associated with the coherences $\rho_{\boxed{\alpha--\alpha}}$ and $\rho_{\boxed{\beta--\beta}}$, are broad.

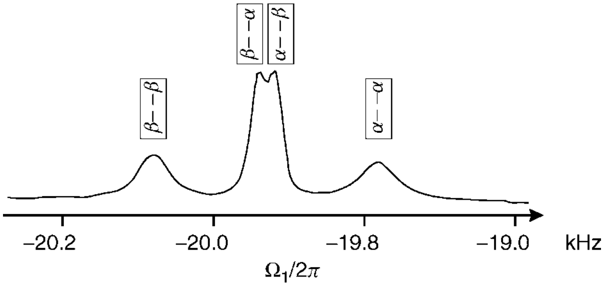

Figure 20.61 Experimental 2Q spectrum of [1,2-$^{13}C_2$]-β-glucose in viscous solution. The plot shows a one-dimensional slice through a two-dimensional 2Q spectrum. Adapted from S. Ravindranathan, X. Feng, T. Karlsson and M. H. Levitt, *J. Am. Chem. Soc.*, **122**, 1102–1115 (2000). (Copyright the American Chemical Society).

These peak width variations are due to the cross-correlation of the two ^{13}C–^{1}H dipolar interactions. The relaxation of the double-quantum $^{13}C_2$ coherences depends primarily on the *sum* of the local fields at the two ^{13}C sites. The sum of the local fields depends on the molecular geometry and also on the proton spin states.

Consider, for example, the coherence $\rho_{\boxed{\alpha--\beta}}$, which generates one of the central peaks in the 2Q multiplet. The local fields in the β-anomer, with the protons in states $|\alpha\rangle$ and $|\beta\rangle$, may be visualized as follows:

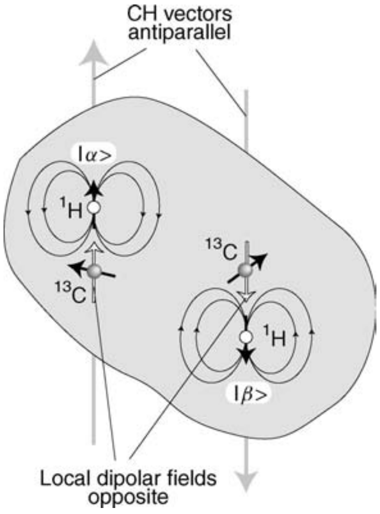

Figure 20.62
Local heteronuclear fields in the case that the two ^{13}C–^{1}H vectors are antiparallel, for opposite proton spin states.

Although each ^{13}C experiences a strong local field from its proton neighbour, the *sum* of the local fields, which is important for 2Q evolution, cancels out in this geometry. This remains true even when the molecule rotates.

The outer peaks, which belong to the $\rho_{\boxed{\alpha--\alpha}}$ and $\rho_{\boxed{\beta--\beta}}$ coherences, are broad because the heteronuclear local fields at the two carbon sites add up constructively, for these proton states, in this molecular geometry:

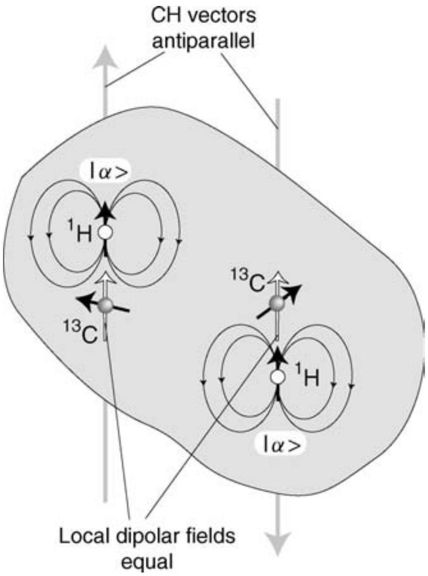

Figure 20.63 Local heteronuclear fields in the case that the two ^{13}C–^{1}H vectors are antiparallel, for equal proton spin states.

An experimental 2Q ^{13}C spectrum for the α-anomer is shown below. The outer peaks are narrower than the inner peaks, which are poorly resolved in this case:

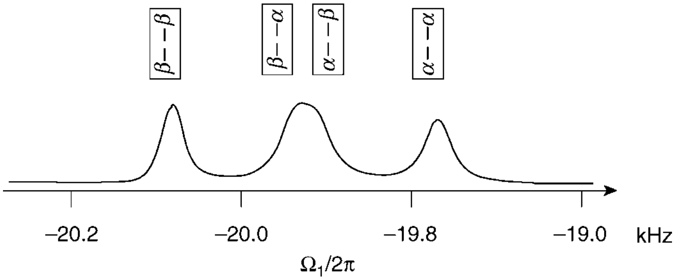

Figure 20.64 Experimental 2Q spectrum of [1,2-^{13}C$_2$]-α-glucose in viscous solution. The plot shows a one-dimensional slice through a two-dimensional 2Q spectrum. Adapted from S. Ravindranathan, X. Feng, T. Karlsson and M. H. Levitt, *J. Am. Chem. Soc.*, **122**, 1102–1115 (2000). (Copyright the American Chemical Society).

This peak width pattern is again easily rationalized by considering the molecular geometry. For the α-anomer, the two ^{13}C–^{1}H vectors are almost perpendicular. The local fields in the α-anomer, with the protons in states $|\alpha\rangle$ and $|\beta\rangle$, are depicted in Figure 20.65. In this case, the local fields at the two carbon sites build up constructively, leading to broad peaks for the coherences $\rho_{\boxed{\alpha--\beta}}$ and $\rho_{\boxed{\beta--\alpha}}$.

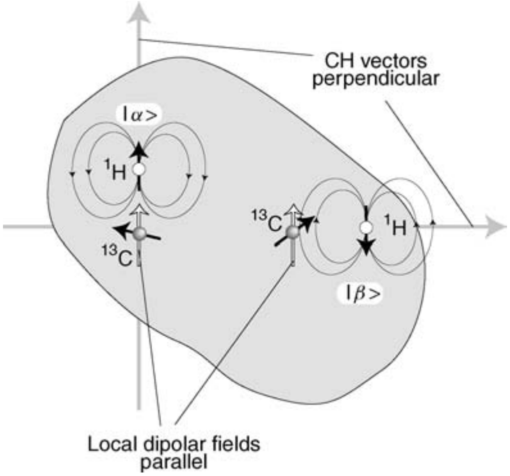

Figure 20.65
Local heteronuclear fields in the case that the two ^{13}C–^{1}H vectors are perpendicular, for opposite proton spin states.

A quantitative study of these linewidth effects allows one to determine the angle $\theta_{\mathrm{CH,CH}}$ between the two ^{13}C–^{1}H interactions.

Experiments of this type are exploited in solution NMR for obtaining *angular* information on the molecular structure (see *Further Reading*). A particularly important class of experiments uses cross-correlated relaxation to estimate the angles between ^{13}C–^{1}H and ^{15}N–^{1}H dipole–dipole interactions in labelled proteins, in order to constrain the secondary structure. This complements nicely the *distance* information available from NOESY and ROESY.

20.8.4 TROSY

One of the more remarkable aspects of cross-correlation is found in heteronuclear two-spin systems, e.g. the AX system of a ^{15}N coupled to a neighbouring ^{1}H. Typically, the ^{15}N nuclei are subjected to two sources of local fields, i.e. the magnetic field emanating from the neighbouring proton and the CSA interaction from the induced currents in the surrounding electron clouds. Both of these interactions are generated by sources within the molecule, and are therefore cross-correlated.

If proton decoupling is *not* employed, then the ^{15}N spectrum has two peaks, originating from the $\rho_{\boxed{\alpha-}}$ and $\rho_{\boxed{\beta-}}$ (-1)-quantum ^{15}N coherences. The rotating-frame frequencies of these coherences are

$$\Omega_{\boxed{\alpha-}} = \Omega_S^0 + \pi J_{IS} \qquad \Omega_{\boxed{\beta-}} = \Omega_S^0 - \pi J_{IS}$$

where the ^{15}N spin is denoted S and the ^{1}H spin is denoted I. The relative width of the two single-quantum peaks depends on the cross-correlation between the CSA and the heteronuclear dipole–dipole interaction.

Consider, for example, a ^{15}N–^{1}H moiety in a ^{15}N-labelled protein, such as may be found in the peptide bonds that make up the protein backbone. If the ^{15}N–^{1}H bond in a peptide is along the external magnetic field, then the induced currents in the electron clouds set up a local magnetic field at the ^{15}N nucleus that is *parallel* to the external field:[10]

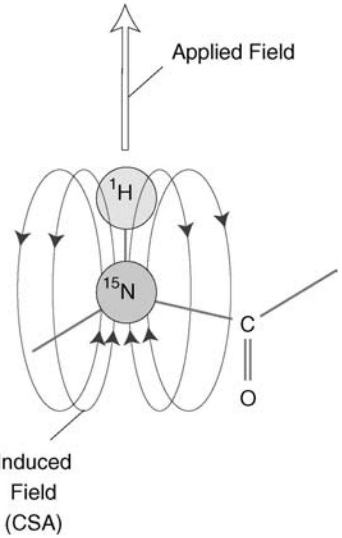

Figure 20.66
Induced field around the ^{15}N site in a ^{15}N-labelled peptide bond, when the NH vector is parallel to the external field.

If the ^{15}N–^{1}H bond is perpendicular to the external magnetic field, then the induced magnetic field at the ^{15}N nucleus tends to *oppose* the external field:

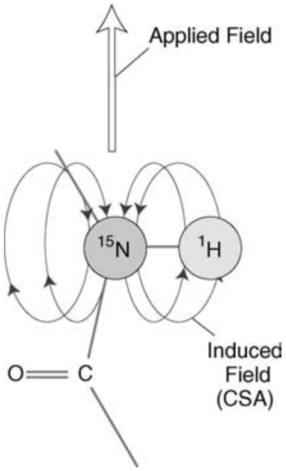

Figure 20.67
Induced field around the ^{15}N site in a ^{15}N-labelled peptide bond, when the NH vector is perpendicular to the external field.

As the molecule rotates, the induced fields at the ^{15}N nucleus are modulated, which leads to relaxation. This is the mechanism of relaxation through CSA.

The induced fields are proportional to the external magnetic field B^0, and the relaxation rate constants are proportional to the square of the local magnetic fields (Equation 20.6). As a result, the CSA relaxation mechanism is proportional to the square of the external magnetic field and becomes competitive with the dipole–dipole relaxation mechanism at the highest commercially-available magnetic field, which is currently around 22.3 T (in 2007).

Now consider what happens if we also take the local field from the ^{1}H into account. If the ^{1}H is in the $|\beta\rangle$ state and the NH vector is parallel to the field, then the local field from the ^{1}H at the site of the ^{15}N nucleus tends to *oppose* the external field:

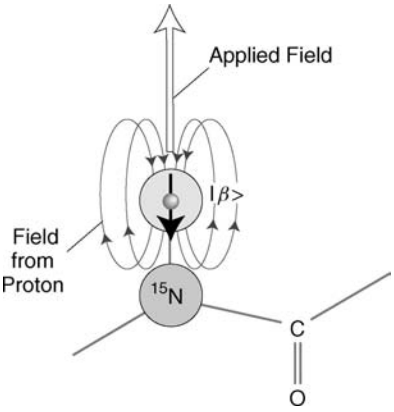

Figure 20.68
Local field generated by the proton in the $|\beta\rangle$ state, when the NH vector is parallel to the external field.

Similarly, if the ^{1}H is in the $|\beta\rangle$ state and the NH vector is perpendicular to the field, then the local field from the ^{1}H at the site of the ^{15}N nucleus tends to be *parallel* to the external field:

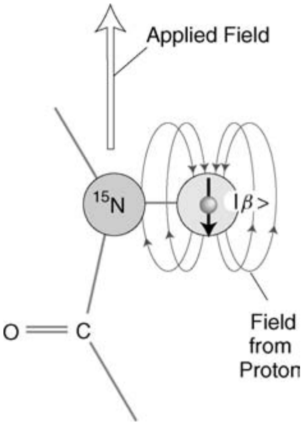

Figure 20.69
Local field generated by the proton in the $|\beta\rangle$ state, when the NH vector is perpendicular to the external field.

To summarize, the local field at the ^{15}N nucleus contains a contribution from the CSA and from the ^{1}H magnetic moment. When the ^{1}H is in the $|\beta\rangle$ state, these two contributions always have opposite sign, whatever the orientation of the molecule. The ^{15}N local field is *reduced* by the interference of the CSA and dipolar interactions, in the case of the $|\beta\rangle$ proton spin state.

Similarly, when the ^{1}H is in the $|\alpha\rangle$ state, these two contributions always have the same sign, whatever the orientation of the molecule. The ^{15}N local field is *increased* by the interference of the CSA and dipolar interactions, in the case of the $|\alpha\rangle$ proton spin state.

As a result, the peak due to the ^{15}N coherence $\rho_{\boxed{\beta-}}$ is *narrowed* by the CSA/dipole–dipole cross-correlation, whereas the peak due to the ^{15}N coherence $\rho_{\boxed{\alpha-}}$ is *broadened* by the CSA/dipole–dipole cross-correlation.

The CSA interaction is proportional to the external field. It is possible, therefore, to adjust the CSA interaction by changing the external field. At a certain value of the field, the CSA and dipole–dipole interactions exactly cancel each other out for the $|\beta\rangle$ proton spin state. The precise value of the optimum field depends on the magnitude and orientation of the chemical shift tensor and may differ from site to site in a biomolecule. For many ^{15}N–^{1}H spin pairs in proteins, the optimal narrowing effects are anticipated to occur in the range 20–25 T, and may now be exploited on the highest currently available magnetic fields.

Significant broadening/narrowing effects are observed even at moderate magnetic fields. The experimental example shown in Figure 20.70 was obtained for a ^{15}N-labelled protein–DNA complex in a field of 17.6 T. Note the assignment of the peaks: the absolute frequency axis for ^{15}N runs from right to left (see Section 3.5), and the one-bond ^{15}N–^{1}H J-coupling is negative, so the peak for $\rho_{\boxed{\alpha-}}$ is to the right of the peak for $\rho_{\boxed{\beta-}}$ (see Section 15.5).

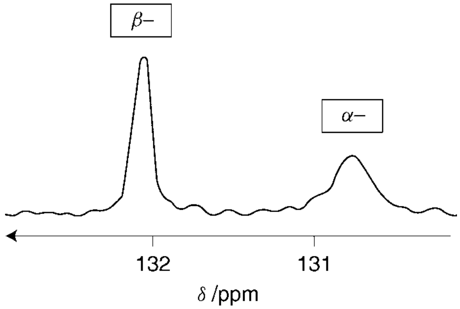

Figure 20.70
^{15}N doublet obtained from one protonated ^{15}N site in a 17 kDa protein–DNA complex without ^{1}H decoupling. Adapted from K. Pervushin, R. Riek, G. Wider and K. Wüthrich, *Proc. Natl. Acad. Sci. USA*, **94**, 12 366–12 371 (1997). Copyright National Academy of Sciences, U.S.A.

The narrowing of one multiplet component by CSA/dipole–dipole cross-correlation is only observed if the spectrum is acquired *without* proton decoupling. If the proton decoupler is turned on, then a single relatively broad peak is observed.

The term TROSY refers to a set of techniques that exploit these differential linewidth effects for enhancing the NMR of large biomolecules (the acronym stands for *Transverse Relaxation Optimized Spectroscopy*).[11] TROSY techniques exploit the following elements: (i) acquisition of the NMR signal without heteronuclear decoupling, in order to resolve the J-coupled multiplets; (ii) careful choice of the external magnetic field so as to achieve optimal line narrowing of some multiplet components through cross-correlation; (iii) careful pulse sequence design so as to make predominant use of the slowly decaying coherences, and to avoid passing the signal through coherences with short lifetimes; (iv) extensive deuteration of the biological molecules so as to reduce all sources of relaxation that are not amenable to cancellation by cross-correlation.

In suitable cases, TROSY allows narrow peaks to be obtained from large macromolecules in solution, under circumstances that would normally give hopelessly broad spectra.[11]

Notes

1. The factor of two in this equation is a consequence of the definition of the Fourier transform in this book, which employs an integral over time from 0 to $+\infty$. In the original relaxation theory, a 'two-sided' Fourier transform was used, in which the integral runs from $-\infty$ to $+\infty$.

2. All the transition probabilities derived in this section are roughly equal to $T_1{}^{-1}$ (give or take some numerical factors). Therefore, it is remarkable that, in the right circumstances, some types of spin order persist for orders of magnitude longer than T_1. See Chapter 14, Note 2.

3. The strict definition of the rotational correlation time τ_c is quite involved. Consider some vector fixed with respect to the molecule. The direction of this vector may be defined using two angles θ and ϕ. As the molecule rotates, the vector rotates with it, so the angles θ and ϕ change. It is possible to calculate some special functions, called *second-rank spherical harmonics*, which depend on θ and ϕ. There are five such functions, which resemble the d-orbitals used in atomic theory, and which are denoted

$Y_{2m}(\theta, \phi)$, where the index m takes values $m = -2, -1, 0, 1, 2$. Since θ and ϕ depend on time, the functions Y_{2m} also depend on time, and it is possible to define autocorrelation functions of the following form:

$$\mathbb{G}_m(\tau) = \left\langle Y_{2m}(0) Y_{2m}(\tau)^* \right\rangle$$

If the molecules tumble isotropically, then all five autocorrelation functions $\mathbb{G}_m$ are the same. In addition, it is usually assumed that the autocorrelation function decays exponentially with respect to τ. The rotational correlation time τ_c is defined as the time constant for this exponential decay.

4. For historical reasons, it is common to employ a Solomon cross-relaxation rate constant denoted σ that is equal to $-R_{\text{cross}}$. I have changed the sign of the cross-relaxation rate constant to bring the definition into line with that used in ordinary kinetics. I suspect that the historical definition of σ, and its curious choice of sign, was flavoured by early NMR experiments on small molecules, for which R_{cross} is negative. Readers who are used to the historical definition may substitute R_{cross} by $-\sigma$ in all expressions.

5. The NOE enhancement factor is often written as $\eta = \epsilon_{\text{NOE}} - 1$, where η is the last term in Equation 20.28. With this definition, $\eta = 0$ indicates no enhancement of the signal, and $\eta = 1$ indicates a doubling of the signal when the dipolar-coupled spin species is saturated.

6. Strictly speaking, the NOE refers to the steady-state enhancement of one spin species when the populations of a second spin species are saturated by a resonant r.f. field (Section 20.5). This is not obviously related to the NOESY experiment, which does not employ saturation. The name arose historically through the so-called *transient NOE* experiment, which was a precursor of NOESY. In this experiment, the populations of the spin states are perturbed by r.f. pulse sequences, and the cross-relaxation followed as a function of time.

7. The NOESY phase cycle specified in Table 19.1 includes a π phase shift for the second pulse and leads to consistently positive diagonal peaks. The cross-peaks are positive for NOESY experiments on slowly tumbling molecules ($R_{\text{cross}} > 0$), and negative for NOESY experiments on rapidly tumbling molecules ($R_{\text{cross}} < 0$). One should be aware that many standard NOESY pulse sequences do not include the π phase shift on the second pulse, and give rise to spectra in which *both* diagonal- and cross-peaks have an inverted sign.

8. For a justification of this, see R. R. Ernst, G. Bodenhausen and A. Wokaun, "*Principles of Nuclear Magnetic Resonance in One and Two Dimensions*", Clarendon Press, Oxford, 1987, p. 287–288.

9. It has become customary to name any experiment that employs an extended period of r.f. irradiation a 'rotating-frame experiment'. This is a curious and misleading practice, since essentially all NMR experiments are easiest to analyse in the rotating reference frame. The original name for the ROESY experiment is CAMELSPIN (which stands for Cross-Relaxation Appropriate for Minimolecules Emulated by Locked Spins), but this title is rarely used now.

10. The discussion of dipole–dipole CSA cross-correlation in a ^{15}N–^{1}H spin pair assumes a uniaxial ^{15}N CSA tensor with $\delta^j_{zz} < \delta^{\text{iso}}_j$, i.e. a negative CSA in deshielding units, and zero biaxiality. Experimentally determined ^{15}N CSA tensors in peptide bonds have approximately uniaxial CSA tensors with the sign and orientation assumed here.

11. K. Pervushin, R. Riek, G. Wider, and K. Wüthrich *Proc. Natl. Acad. Sci. USA*, **94**, 12 366–12 371 (1997) ; K. Wüthrich *Nature Struct. Biol.*, **5**, 492 (1998).

Further Reading

- The classic paper on relaxation in liquids is N. Bloembergen, E. M. Purcell and R. V. Pound, *Phys. Rev.* **73**, 679–712 (1948). It is still a fresh source of physical insights.
- For a thorough review of relaxation in liquids, including key results for many different mechanisms, see J. Kowalewski and L. Mäler, '*Nuclear Spin Relaxation in Liquids: Theory, Experiments and Applications*.' CRC Press, Boca Raton, Florida, 2006.
- For the formal relaxation theory, see A. Abragam, "The Principles of Nuclear Magnetism", Clarendon Press, Oxford, 1961; C. P. Slichter, "Principles of Magnetic Resonance", 3rd Edition Springer, Berlin, 1989 and R. R. Ernst, G. Bodenhausen, and A. Wokaun, "Principles of Nuclear Magnetic Resonance in One and Two Dimensions", Clarendon Press, Oxford, 1987.
- For a summary of theoretical relaxation time constants in liquids, treating a variety of motional models, see J. McConnell, "The Theory of NMR Spin Relaxation in Liquids", Cambridge University Press, Cambridge, 1987.
- For the application of NOESY to biomolecular structure determination, see K. Wüthrich, "NMR of Proteins and Nucleic Acids", Wiley, New York, 1986, and J. Cavanagh, W. J. Fairbrother, A. G. Palmer and N. J. Skelton, "Protein NMR Spectroscopy. Principles and Practice", Academic Press New York, 1996.
- For more detail on ROESY, see the articles in the "Encyclopedia of Nuclear Magnetic Resonance", Wiley, 1996, by A. Bax and S. Grzesiek, (vol. 7, p. 4157) and J. Sleucher, J. Quant, S. J. Glaser and C. Griesinger (vol. 6, p. 4789).
- For the applications of cross-correlated relaxation to biomolecules, see B. Reif, M. Hennig and C. Griesinger, *Science*, **276**, 1230 (1997), and B. Brutscher *Concepts Magn. Reson.*, **12**, 207–228 (2000).
- For parallels between cross-correlated double-quantum experiments in solids and liquids, see S. Ravindranathan, X. Feng, G. Widmalm, and M. H. Levitt, *J. Am. Chem. Soc.*, **122**, 1102–1115 (2000).
- For a comprehensive review of cross-correlation effects, see Anil Kumar, R. Christy Rani Grace and P. K. Madhu, *Prog. NMR Spectrosc.*, **37**, 191–319 (2000).

Exercises

20.1 Consider a molecule with rotational correlation time $\tau_c = 0.3\,\text{ns}$, containing a pair of protons separated by 2 nm. Assume that the relaxation is caused exclusively by intramolecular dipole–dipole couplings.
  (i) Plot the relaxation time constants T_1 and T_2 against field B^0, in the range $B^0 = 0$ to $B^0 = 20\,\text{T}$. Comment on the form of the plots.
  (ii) Plot the NOESY cross-relaxation rate constant R_{cross} and the ROESY cross-relaxation rate constant R^T_{cross} against the static field B^0, in the range $B^0 = 0$ to $B^0 = 20\,\text{T}$. Is NOESY or ROESY expected to be better at high magnetic field?

Part 8

Appendices

Appendix A: Supplementary Material

A.1 Euler Angles and Frame Transformations

The orientation of a rigid object in three-dimensional space may be specified using three angles. There are different systems for defining the three orientational angles, which have advantages in different circumstances. The *Euler angles* are particularly useful in many NMR contexts.

A.1.1 Definition of the Euler angles

In this book I use the *zyz-convention* for the Euler angles. In this system, a general rotation in three-dimensional space is expressed as the product of three rotations: a rotation by an angle γ about the z-axis, a rotation by an angle β about the y-axis, and a rotation by an angle α about the z-axis again:

$$\widehat{R}(\alpha, \beta, \gamma) = \widehat{R}_z(\alpha)\widehat{R}_y(\beta)\widehat{R}_z(\gamma) \tag{A.1}$$

Note the right-to-left chronological order of the rotations on the right-hand side.

In this appendix, the symbol Ω denotes a set of three Euler angles: $\Omega = \{\alpha, \beta, \gamma\}$. A modified font distinguishes Ω from the frequency symbol Ω.

A.1.2 Euler rotations: first scheme

To see how the Euler angles are used, consider the L-shaped object shown below, which has an arbitrary orientation with respect to a Cartesian reference frame:

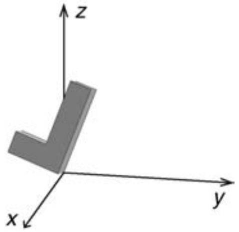

Figure A.1
An L-shaped object.

Spin Dynamics: Basics of Nuclear Magnetic Resonance, Second Edition Malcolm H. Levitt

The orientation of the object may be specified by providing the rotation $\widehat{R}(\alpha, \beta, \gamma)$ which turns the object so that its edges become parallel with the defined axis system. In the case above, the angles are $\alpha = \pi/5$, $\beta = \pi/8$, and $\gamma = \pi/3$. Figure A.2 shows how the object may be turned in three stages so that it becomes aligned with the reference frame:

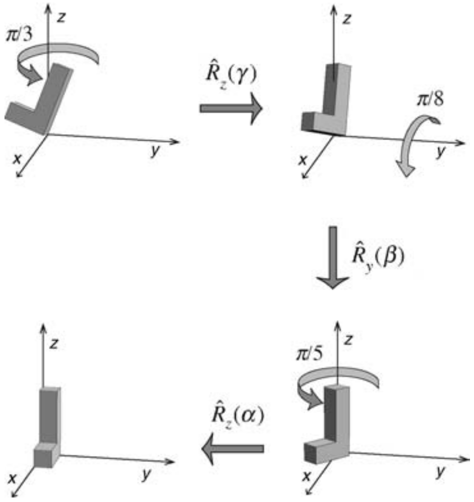

Figure A.2
Rotations around the reference frame axes.

Note the order of the rotations: since the rotation operator in Equation A.1 is applied from the *left*, the γ-rotation comes *first*.

A.1.3 Euler rotations: second scheme

The Euler rotations may also be formulated in a different way. Attach an axis system to the object, parallel to its edges:

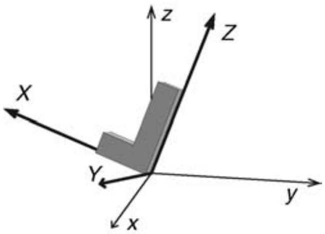

Figure A.3
An L-shaped object with a local axis system.

The attached axis system is shown in bold, and annotated by the upper-case letters $\{X, Y, Z\}$. Now execute the Euler rotations again, but this time (i) rotate *about the axes that are attached to the object itself* (instead of the reference-frame axes) and (ii) use the *opposite* order, i.e. first α, then β, then γ. The sequence of rotations is as follows:

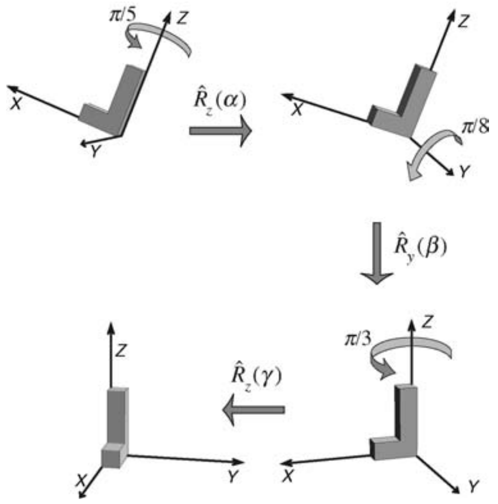

Figure A.4
Rotations around the local axes.

The final orientations in Figures A.2 and A.4 are identical, even though the intermediate positions are different! This equivalence may be expressed by the following equation:

$$\widehat{R}_z(\alpha)\widehat{R}_y(\beta)\widehat{R}_z(\gamma) = \widehat{R}_{Z''}(\gamma)\widehat{R}_{Y'}(\beta)\widehat{R}_Z(\alpha) \tag{A.2}$$

Here, $\widehat{R}_Z(\alpha)$ is a rotation around the Z-axis of the attached system, and $\widehat{R}_{Y'}(\beta)$ is a rotation around the Y-axis of the attached system, etc. The 'primed' notation $\widehat{R}_{Y'}(\beta)$ indicates that the central rotation occurs about a 'new' Y-axis that has *already* been transformed by the first $\widehat{R}_Z(\alpha)$ rotation. Similarly, the final $\widehat{R}_{Z''}(\gamma)$ rotation occurs about a 'new' Z-axis that has already been transformed by the first $\widehat{R}_Z(\alpha)$ rotation, and then by the second $\widehat{R}_{Y'}(\beta)$ rotation. As shown in Figure A.4, the rotation axes follow the object as it is rotated. The Euler angle β represents the angle between the initial and final z-axes.

Equation A.2 is a general result, independent of the values of the angles $\{\alpha, \beta, \gamma\}$.

The two different methods of performing the Euler rotations are equally valid, but the second way is often easier to visualize.

A.1.4 Euler rotation matrices

The Cartesian rotation matrix, written in terms of Euler angles, is as follows:

$$\mathcal{R}(\alpha,\beta,\gamma) = \begin{pmatrix} \cos\alpha\cos\beta\cos\gamma - \sin\alpha\sin\gamma & -\sin\alpha\cos\gamma - \cos\alpha\cos\beta\sin\gamma & \cos\alpha\sin\beta \\ \sin\alpha\cos\beta\cos\gamma + \cos\alpha\sin\gamma & \cos\alpha\cos\gamma - \sin\alpha\cos\beta\sin\gamma & \sin\alpha\sin\beta \\ -\sin\beta\cos\gamma & \sin\beta\sin\gamma & \cos\beta \end{pmatrix} \tag{A.3}$$

The inverse of $\mathcal{R}(\alpha,\beta,\gamma)$ is $\mathcal{R}(-\gamma,-\beta,-\alpha)$.

A.1.5 Reference-frame orientations

The Euler angles are particularly useful for defining the relative orientations of two different orthogonal axis systems. For example, consider two different orthogonal reference frames, A and B, defined by the sets of unit vectors $\{\mathbf{e}_x^{\mathrm{A}}, \mathbf{e}_y^{\mathrm{A}}, \mathbf{e}_z^{\mathrm{A}}\}$ and $\{\mathbf{e}_x^{\mathrm{B}}, \mathbf{e}_y^{\mathrm{B}}, \mathbf{e}_z^{\mathrm{B}}\}$. The set of Euler angles $\Omega^{\mathrm{BA}} = \{\alpha^{\mathrm{BA}}, \beta^{\mathrm{BA}}, \gamma^{\mathrm{BA}}\}$ may be used to specify the relative orientation of these two axis systems. The angles are defined in such a way that the matrix $\mathcal{R}(\Omega^{\mathrm{BA}}) = \mathcal{R}(\alpha^{\mathrm{BA}}, \beta^{\mathrm{BA}}, \gamma^{\mathrm{BA}})$ transforms each of the A-system vectors into the corresponding B-system vector:

$$\mathcal{R}(\Omega^{\mathrm{BA}}) \cdot \mathbf{e}_x^{\mathrm{A}} = \mathbf{e}_x^{\mathrm{B}}$$
$$\mathcal{R}(\Omega^{\mathrm{BA}}) \cdot \mathbf{e}_y^{\mathrm{A}} = \mathbf{e}_y^{\mathrm{B}}$$
$$\mathcal{R}(\Omega^{\mathrm{BA}}) \cdot \mathbf{e}_z^{\mathrm{A}} = \mathbf{e}_z^{\mathrm{B}}$$

where $\mathcal{R}$ is given in Equation A.3. For example, suppose that the 'B' axis system is the one in Figure A.1, and the 'A' axis system is the bold one in Figure A.3. In this case, the relative orientation of the two axis systems is described by the Euler angles $\Omega^{\mathrm{BA}} = \{\alpha^{\mathrm{BA}}, \beta^{\mathrm{BA}}, \gamma^{\mathrm{BA}}\} = \{\pi/5, \pi/8, \pi/3\}$. Figure A.2 and Figure A.4 show how the Euler rotations bring the two systems into coincidence.

The frame transformation may be performed the other way using:

$$\mathcal{R}(\Omega^{\mathrm{AB}}) \cdot \mathbf{e}_x^{\mathrm{B}} = \mathbf{e}_x^{\mathrm{A}}$$
$$\mathcal{R}(\Omega^{\mathrm{AB}}) \cdot \mathbf{e}_y^{\mathrm{B}} = \mathbf{e}_y^{\mathrm{A}}$$
$$\mathcal{R}(\Omega^{\mathrm{AB}}) \cdot \mathbf{e}_z^{\mathrm{B}} = \mathbf{e}_z^{\mathrm{A}}$$

which implies $\mathcal{R}(\Omega^{\mathrm{AB}}) = \mathcal{R}(\Omega^{\mathrm{BA}})^{-1}$ and hence $\alpha^{\mathrm{AB}} = -\gamma^{\mathrm{BA}}$, $\beta^{\mathrm{AB}} = -\beta^{\mathrm{BA}}$ and $\gamma^{\mathrm{AB}} = -\alpha^{\mathrm{BA}}$.

A.1.6 Consecutive reference-frame transformations

The Euler angles are particularly powerful for handling consecutive reference-frame rotations. For example, consider a third reference frame C, defined by the set of unit vectors $\{\mathbf{e}_x^{\mathrm{C}}, \mathbf{e}_y^{\mathrm{C}}, \mathbf{e}_z^{\mathrm{C}}\}$. If the relative orientation of C and B is specified by the Euler angles $\Omega^{\mathrm{CB}} = \{\alpha^{\mathrm{CB}}, \beta^{\mathrm{CB}}, \gamma^{\mathrm{CB}}\}$, and the relative orientation of B and A is specified by the Euler angles $\Omega^{\mathrm{BA}} = \{\alpha^{\mathrm{BA}}, \beta^{\mathrm{BA}}, \gamma^{\mathrm{BA}}\}$, then the relative orientation of C and A is specified by the Euler angles $\Omega^{\mathrm{CA}} = \{\alpha^{\mathrm{CA}}, \beta^{\mathrm{CA}}, \gamma^{\mathrm{CA}}\}$, where

$$\mathcal{R}(\Omega^{\mathrm{CA}}) = \mathcal{R}(\Omega^{\mathrm{CB}})\mathcal{R}(\Omega^{\mathrm{BA}})$$

Note the 'chain rule' for the frame superscripts, which may be continued as desired:

$$\mathcal{R}(\Omega^{\mathrm{DA}}) = \mathcal{R}(\Omega^{\mathrm{DC}})\mathcal{R}(\Omega^{\mathrm{CB}})\mathcal{R}(\Omega^{\mathrm{BA}})$$

A.1.7 Passive rotations

The discussion above concentrated on the *active* manipulation of objects (including reference frames) by a series of Euler rotations. In the theory of NMR, it is often relevant to consider the *representations* of objects (such as vectors, tensors, etc.) *as seen from* different reference frames, which are themselves related by Euler rotations. This *passive* perspective is indicated by a subtle change of notation. The frame indices are reversed, and superscripts are changed into subscripts, i.e. $\Omega_{\mathrm{AB}} = \Omega^{\mathrm{BA}}$, implying $\alpha_{\mathrm{AB}} = \alpha^{\mathrm{BA}}$, $\beta_{\mathrm{AB}} = \beta^{\mathrm{BA}}$ and $\gamma_{\mathrm{AB}} = \gamma^{\mathrm{BA}}$.

For example, the matrix representations of the same tensor $\mathbf{T}$ in two different reference systems are related by

$$[\mathbf{T}]^B = \mathcal{R}(\Omega_{\mathrm{BA}})\,[\mathbf{T}]^A\,\mathcal{R}(\Omega_{\mathrm{AB}})$$

where

$$\mathcal{R}(\Omega_{\mathrm{BA}}) = \mathcal{R}(\Omega_{\mathrm{AB}})^{\dagger}$$

The arrangement of the 'passive subscripts' allows use of the chain rule for consecutive transformations; for example:

$$[\mathbf{T}]^{C} = \mathcal{R}(\Omega_{\mathrm{CB}})\mathcal{R}(\Omega_{\mathrm{BA}})\,[\mathbf{T}]^{A}\,\mathcal{R}(\Omega_{\mathrm{AB}})\mathcal{R}(\Omega_{\mathrm{BC}}) \tag{A.4}$$

The chains of frame labels may readily be followed inwards, allowing the transformations to be written down by inspection. The convenience of this chain property is lost if active notation is used in this context.

Note that an 'active' angle such as α^{BA} has exactly the same meaning as the 'passive' angle $\alpha_{\mathrm{A}B}$ – the different notations are used purely for orthographic convenience, depending on whether the calculation involves the rotation of an object with respect to a fixed reference frame, or the appearance of a fixed object as seen from a rotated reference frame.

A.1.8 Tensor transformations

As one example of this technique, consider a chemical shift tensor $\boldsymbol{\delta}^{j}$ with principal components $\{\delta^{j}_{XX}, \delta^{j}_{YY}, \delta^{j}_{ZZ}\}$. When written in its principal axis frame, this tensor has a diagonal representation:

$$\left[\boldsymbol{\delta}^{j}\right]^{P} = \begin{pmatrix} \delta^{j}_{XX} & 0 & 0 \\ 0 & \delta^{j}_{YY} & 0 \\ 0 & 0 & \delta^{j}_{ZZ} \end{pmatrix}$$

Suppose, now, that a laboratory reference frame L is defined with the z-axis along the static magnetic field direction. The relative orientation of the principal axis frame of the chemical shift tensor at site I_j with respect to the laboratory frame L is specified using the Euler angle set $\Omega^{\mathrm{LP}}_{\mathrm{j}} = \{\alpha^{\mathrm{LP}}_{\mathrm{j}}, \beta^{\mathrm{LP}}_{\mathrm{j}}, \gamma^{\mathrm{LP}}_{\mathrm{j}}\}$ in active notation, or equivalently $\Omega^{\mathrm{j}}_{\mathrm{PL}} = \{\alpha^{\mathrm{j}}_{\mathrm{PL}}, \beta^{\mathrm{j}}_{\mathrm{PL}}, \gamma^{\mathrm{j}}_{\mathrm{PL}}\}$ in passive notation. The matrix representation of the tensor in the laboratory frame may be derived as follows:

$$\left[\boldsymbol{\delta}^{j}\right]^{L} = \mathcal{R}(\Omega^{j}_{\mathrm{LP}}) \cdot \left[\boldsymbol{\delta}^{j}\right]^{P} \cdot \mathcal{R}(\Omega^{\mathrm{j}}_{\mathrm{PL}}) \tag{A.5}$$

Note, again, the chaining of the frame labels in the passive convention.

Consider, now, the common situation in which the chemical shift tensor has a fixed orientation with respect to a molecule reference frame M, while the orientation of the molecule changes, relative to the external magnetic field. If the orientation of the chemical shift tensor principal axis system at site I_j with respect to the molecular reference frame is specified using the Euler angles $\Omega^{\mathrm{j}}_{\mathrm{PM}}$, and the orientation of the molecule with respect to the laboratory frame L is specified using the Euler angles Ω_{ML}, then the matrix $\mathcal{R}(\Omega^{\mathrm{j}}_{\mathrm{PL}})$ in Equation A.5 is given by

$$\mathcal{R}(\Omega^{\mathrm{j}}_{\mathrm{PL}}) = \mathcal{R}(\Omega^{\mathrm{j}}_{\mathrm{PM}})\mathcal{R}(\Omega_{\mathrm{ML}}) \tag{A.6}$$

The matrix $\mathcal{R}^{j}(\Theta)$ used in Section 9.1 should be identified with $\mathcal{R}(\Omega^{\mathrm{j}}_{\mathrm{PL}})$ in Equation A.6. The generic symbol Θ for the molecular orientation with respect to the static magnetic field, which is used throughout the book, should be identified with the Euler angle set Ω_{ML}.

For example, the term $R^{j}_{zX}(\Theta)$ in Equation 9.12 should be interpreted as follows:

$$\begin{aligned} R^{j}_{zX}(\Theta) &= R_{zx}(\Omega^{\mathrm{j}}_{\mathrm{PL}}) \\ &= R_{zx}(\Omega^{\mathrm{j}}_{\mathrm{PM}})R_{xx}(\Omega_{\mathrm{ML}}) + R_{zy}(\Omega^{\mathrm{j}}_{\mathrm{PM}})R_{yx}(\Omega_{\mathrm{ML}}) + R_{zz}(\Omega^{\mathrm{j}}_{\mathrm{PM}})R_{zx}(\Omega_{\mathrm{ML}}) \end{aligned}$$

where the rotation matrix elements are specified in terms of the Euler angles in Equation A.3.

A.1.9 Intermediate reference frames

The chain rule (Equation A.4) makes it straightforward to incorporate any number of intermediate reference frames between the principal axis system of a tensor and the laboratory frame. Multiple reference frames are often used in solid-state NMR. For example, in a rotating sample, it is often useful to define a reference frame R that is fixed to the sample holder and which rotates with respect to the laboratory frame. In this case, the transformation in Equation A.6 reads as follows:

$$\mathcal{R}(\Omega^{\mathrm{j}}_{\mathrm{PL}}(t)) = \mathcal{R}(\Omega^{\mathrm{j}}_{\mathrm{PM}})\mathcal{R}(\Omega_{\mathrm{MR}})\mathcal{R}(\Omega_{\mathrm{RL}}(t))$$

where $\Omega^{\mathrm{j}}_{\mathrm{PM}}$ defines the orientation of the CSA principal axis system with respect to the molecular reference frame, Ω_{MR} defines the orientation of the molecular reference frame with respect to the sample holder, and $\Omega_{\mathrm{RL}}(t)$ defines the orientation of the sample holder with respect to the magnetic field. In a rotating sample, the Euler angle α_{RL} is time dependent.

Any number of intermediate reference frames may be introduced this way, always chaining the frame labels to keep track of the successive rotations.

Further discussion is beyond the scope of this book, but the literature contains many examples of this technique. See, for example, A. Brinkmann and M. H. Levitt, *J. Chem. Phys.* **115**, 357–384 (2001).

A.2 Rotations and Cyclic Commutation

In this appendix, I prove that the cyclic commutation:

$$\left[\widehat{A}, \widehat{B}\right] = \mathrm{i}\widehat{C} \qquad \circlearrowright \tag{A.7}$$

implies the property

$$\boxed{\exp\{-\mathrm{i}\theta\widehat{A}\}\widehat{B}\exp\{+\mathrm{i}\theta\widehat{A}\} = \widehat{B}\cos\theta + \widehat{C}\sin\theta \tag{A.8}}$$

which may be interpreted as a rotation of operator $\widehat{B}$ towards the operator $\widehat{C}$, around the $\widehat{A}$ axis, as discussed in Section 6.6.2.

For clarity, the following proof is conducted in terms of the specific case $\widehat{A} = \hat{I}_z$, $\widehat{B} = \hat{I}_x$, $\widehat{C} = \hat{I}_y$, which corresponds to the identity

$$\widehat{R}_z(\theta)\hat{I}_x\widehat{R}_z(-\theta) = \hat{I}_x\cos\theta + \hat{I}_y\sin\theta \tag{A.9}$$

However, since only cyclic commutation is used, the result applies to any three operators satisfying Equation A.7.

A number of proofs of Equation A.9 exist.[1] My personal favourite runs as follows. Consider the operator $\hat{I}^-$, defined as usual:

$$\hat{I}^- = \hat{I}_x - \mathrm{i}\hat{I}_y$$

From the cyclic commutation relationships, the commutator of $\hat{I}_z$ and $\hat{I}^-$ is given by

$$\left[\hat{I}_z, \hat{I}^-\right] = \left[\hat{I}_z, \hat{I}_x\right] - \mathrm{i}\left[\hat{I}_z, \hat{I}_y\right] = \mathrm{i}\hat{I}_y - \mathrm{i}(-\mathrm{i}\hat{I}_x) = -\hat{I}^-$$

Hence, we have

$$\hat{I}_z\hat{I}^- - \hat{I}^-\hat{I}_z = -\hat{I}^-$$

or equivalently

$$\hat{I}_z\hat{I}^- = \hat{I}^-\hat{I}_z - \hat{I}^- = \hat{I}^-(\hat{I}_z - \widehat{1}) \tag{A.10}$$

Now multiply both sides of this equation on the left by $\hat{I}_z$. We get

$$\hat{I}_z^2 \hat{I}^- = \hat{I}_z \hat{I}^-(\hat{I}_z - \widehat{1})$$

If the identity shown in Equation A.10 is substituted in on the right-hand side, we get

$$\hat{I}_z^2 \hat{I}^- = \hat{I}^-(\hat{I}_z - \widehat{1})(\hat{I}_z - \widehat{1}) = \hat{I}^-(\hat{I}_z - \widehat{1})^2$$

This may be repeated any number of times to generate the relationship

$$\hat{I}_z^n \hat{I}^- = \hat{I}^-(\hat{I}_z - \widehat{1})^n$$

where n is a positive integer. The following result may, therefore, be established:

$$\begin{aligned}\exp\{-\mathrm{i}\theta \hat{I}_z\}\hat{I}^- &= \sum_{n=0}^{\infty} \frac{(-\mathrm{i}\theta)^n}{n!} \hat{I}_z^n \hat{I}^- \\ &= \hat{I}^- \sum_{n=0}^{\infty} \frac{(-\mathrm{i}\theta)^n}{n!} (\hat{I}_z - \widehat{1})^n \\ &= \hat{I}^- \exp\{-\mathrm{i}\theta(\hat{I}_z - \widehat{1})\}\end{aligned}$$

Since the unity operator commutes with all other operators, this may be written as

$$\exp\{-\mathrm{i}\theta \hat{I}_z\}\hat{I}^- = \hat{I}^- \exp\{-\mathrm{i}\theta \hat{I}_z\} \exp\{\mathrm{i}\theta \widehat{1}\}$$

Now, since $\widehat{1}^n = \widehat{1}$ for all n, we have

$$\exp\{\mathrm{i}\theta \widehat{1}\} = \mathrm{e}^{\mathrm{i}\theta} \widehat{1}$$

Therefore:

$$\exp\{-\mathrm{i}\theta \hat{I}_z\}\hat{I}^- = \mathrm{e}^{\mathrm{i}\theta} \hat{I}^- \exp\{-\mathrm{i}\theta \hat{I}_z\}$$

This equation may be multiplied from the right by $\exp\{+\mathrm{i}\theta \hat{I}_z\}$ to get

$$\exp\{-\mathrm{i}\theta \hat{I}_z\}\hat{I}^- \exp\{+\mathrm{i}\theta \hat{I}_z\} = \mathrm{e}^{\mathrm{i}\theta} \hat{I}^-$$

Similar arguments may be used to derive an analogous relationship for $\hat{I}^+$:

$$\exp\{-\mathrm{i}\theta \hat{I}_z\}\hat{I}^+ \exp\{+\mathrm{i}\theta \hat{I}_z\} = \mathrm{e}^{-\mathrm{i}\theta} \hat{I}^+$$

These two equations may be added together to generate the desired result:

$$\exp\{-\mathrm{i}\theta \hat{I}_z\}\hat{I}_x \exp\{+\mathrm{i}\theta \hat{I}_z\} = \frac{1}{2}\mathrm{e}^{\mathrm{i}\theta} \hat{I}^- + \frac{1}{2}\mathrm{e}^{-\mathrm{i}\theta} \hat{I}^+ = \hat{I}_x \cos\theta + \hat{I}_y \sin\theta$$

A.3 Rotation Sandwiches

In this appendix, I prove the rotation sandwich property:

$$\boxed{\widehat{R}_x(\theta)\widehat{R}_y(\beta)\widehat{R}_x(-\theta) = \exp\{-\mathrm{i}\beta\left(\hat{I}_y \cos\theta + \hat{I}_z \sin\theta\right)\} \quad \circlearrowleft \qquad \text{(A.11)}}$$

For clarity, the equations are written using spin angular momentum operators, but the properties are general for any set of three cyclically commuting operators.

The sandwich relationship for angular momentum operators (Equation A.8) may be used to write the right-hand side of Equation A.11 as

$$\exp\{-\mathrm{i}\beta\left(\hat{I}_y\cos\theta+\hat{I}_z\sin\theta\right)\}=\exp\{-\mathrm{i}\beta\widehat{R}_x(\theta)\hat{I}_y\widehat{R}_x(-\theta)\}$$

The exponential may be expanded as an infinite series:

$$\begin{aligned}\exp\{-\mathrm{i}\beta\widehat{R}_x(\theta)\hat{I}_y\widehat{R}_x(-\theta)\}&=\widehat{1}+(-\mathrm{i}\beta\widehat{R}_x(\theta)\hat{I}_y\widehat{R}_x(-\theta))\\&\quad+\frac{(-\mathrm{i}\beta)^2}{2!}[\widehat{R}_x(\theta)\hat{I}_y\widehat{R}_x(-\theta)]^2+\frac{(-\mathrm{i}\beta)^3}{3!}[\widehat{R}_x(\theta)\hat{I}_y\widehat{R}_x(-\theta)]^3+\ldots\end{aligned}$$

Consider the third term. We find

$$[\widehat{R}_x(\theta)\hat{I}_y\widehat{R}_x(-\theta)]^2=\widehat{R}_x(\theta)\hat{I}_y\widehat{R}_x(-\theta)\widehat{R}_x(\theta)\hat{I}_y\widehat{R}_x(-\theta)=\widehat{R}_x(\theta)\hat{I}_y\hat{I}_y\widehat{R}_x(-\theta)$$

since the opposite rotation operators in the middle of the expression annihilate. The same happens for all the other terms. Even the unity operator at the beginning of the series may be written as

$$\widehat{1}=\widehat{R}_x(\theta)\widehat{1}\widehat{R}_x(-\theta)$$

The whole expression is therefore

$$\begin{aligned}\exp\{-\mathrm{i}\beta\widehat{R}_x(\theta)\hat{I}_y\widehat{R}_x(-\theta)\}&=\widehat{R}_x(\theta)\left\{\widehat{1}+(-\mathrm{i}\beta\hat{I}_y)+\frac{(-\mathrm{i}\beta)^2}{2!}\hat{I}_y\hat{I}_y+\ldots\right\}\widehat{R}_x(-\theta)\\&=\widehat{R}_x(\theta)\exp\{-\mathrm{i}\beta\hat{I}_y\}\widehat{R}_x(-\theta)\\&=\widehat{R}_x(\theta)\widehat{R}_y(\beta)\widehat{R}_x(-\theta)\end{aligned}$$

which corresponds to the left-hand side of Equation A.11.

Numerous other rotation sandwich relationships may be generated by cyclically permuting the operators.

A.4 Spin-1/2 Rotation Operators

The operator for a rotation about the x-axis through the angle β is given by

$$\widehat{R}_x(\beta)=\exp\{-\mathrm{i}\beta\hat{I}_x\}$$

The matrix representation of this operator is not easy to calculate, since $\hat{I}_x$ is not diagonal. One way is to use the techniques in Section 6.5.8. An alternative method is given here.

The operator $\exp\{-\mathrm{i}\beta\hat{I}_x\}$ may be understood as the infinite series

$$\exp\{-\mathrm{i}\beta\hat{I}_x\}=\widehat{1}+(-\mathrm{i}\beta\hat{I}_x)+\frac{(-\mathrm{i}\beta)^2}{2!}\hat{I}_x\hat{I}_x+\frac{(-\mathrm{i}\beta)^3}{3!}\hat{I}_x\hat{I}_x\hat{I}_x+\ldots\tag{A.12}$$

The sum in Equation A.12 may be sorted into two 'sub-sums', one involving even powers and one involving odd powers of $2\hat{I}_x$ (we will see why we need the factor of two in a moment):

$$\begin{aligned}\exp\{-\mathrm{i}\beta\hat{I}_x\}&=\widehat{1}-\frac{1}{2!}\left(\frac{1}{2}\beta\right)^2(2\hat{I}_x)^2+\frac{1}{4!}\left(\frac{1}{2}\beta\right)^4(2\hat{I}_x)^4+\ldots\\&\quad-\mathrm{i}\left\{\left(\frac{1}{2}\beta\right)(2\hat{I}_x)-\frac{1}{3!}\left(\frac{1}{2}\beta\right)^3(2\hat{I}_x)^3+\frac{1}{5!}\left(\frac{1}{2}\beta\right)^5(2\hat{I}_x)^5+\ldots\right\}\end{aligned}$$

Now note the following property of the spin-1/2 matrix representation of $2\hat{I}_x$:

$$(2\hat{I}_x)^2 = \left\{2\frac{1}{2}\begin{pmatrix} 0 & 1 \\ 1 & 0 \end{pmatrix}\right\}^2 = \begin{pmatrix} 0 & 1 \\ 1 & 0 \end{pmatrix}\begin{pmatrix} 0 & 1 \\ 1 & 0 \end{pmatrix} = \begin{pmatrix} 1 & 0 \\ 0 & 1 \end{pmatrix} = \widehat{1}$$

This means that any *even* power of $2\hat{I}_x$ has the same spin-1/2 matrix representation as unity, and any *odd* power of $2\hat{I}_x$ has the same spin-1/2 matrix representation as $2\hat{I}_x$ itself. The series, therefore, may be written as

$$\begin{aligned}\exp\{-\mathrm{i}\beta\hat{I}_x\} = \widehat{1}&\left\{1 - \frac{1}{2!}\left(\frac{1}{2}\beta\right)^2 + \frac{1}{4!}\left(\frac{1}{2}\beta\right)^4 + \ldots\right\} \\ &-\mathrm{i}2\hat{I}_x\left\{\left(\frac{1}{2}\beta\right) - \frac{1}{3!}\left(\frac{1}{2}\beta\right)^3 + \frac{1}{5!}\left(\frac{1}{2}\beta\right)^5 + \ldots\right\}\end{aligned}$$

The individual series expansions may be identified as equal to the sine and cosine of half the angle; so, we can write

$$\widehat{R}_x(\beta) = \exp\{-\mathrm{i}\beta\hat{I}_x\} = \widehat{1}\cos\frac{1}{2}\beta - \mathrm{i}2\hat{I}_x\sin\frac{1}{2}\beta \qquad (\text{for } I = 1/2) \tag{A.13}$$

⚠This relationship applies only to the spin-1/2 matrix representations of $\widehat{R}_x(\beta)$ and $\hat{I}_x$, and not to the operators themselves.

The spin-1/2 matrix representation of the operator $\widehat{R}_x(\beta)$ is therefore

$$\widehat{R}_x(\beta) = \begin{pmatrix} \cos\frac{1}{2}\beta & -\mathrm{i}\sin\frac{1}{2}\beta \\ -\mathrm{i}\sin\frac{1}{2}\beta & \cos\frac{1}{2}\beta \end{pmatrix} \tag{A.14}$$

Similar arguments may be used to obtain the spin-1/2 matrix representation of the operator $\widehat{R}_y(\beta)$:

$$\widehat{R}_y(\beta) = \begin{pmatrix} \cos\frac{1}{2}\beta & -\sin\frac{1}{2}\beta \\ \sin\frac{1}{2}\beta & \cos\frac{1}{2}\beta \end{pmatrix} \tag{A.15}$$

The matrix representation of the operator $\widehat{R}_z(\beta)$ is obtained more easily, since $\hat{I}_z$ is diagonal in the Zeeman basis:

$$\widehat{R}_z(\beta) = \begin{pmatrix} \exp\{-\mathrm{i}\frac{1}{2}\beta\} & 0 \\ 0 & \exp\{+\mathrm{i}\frac{1}{2}\beta\} \end{pmatrix} \tag{A.16}$$

A.5 Quadrature Detection and Spin Coherences

The NMR signal is generated by electromagnetic induction of a current in the coil, produced by the precessing nuclear spin magnetization.

In this appendix, I use a notational distinction between the laboratory frame and the rotating-frame coherences. Rotating-frame coherences are denoted by a tilde.

Suppose that the coil is aligned along the x-axis of the laboratory frame. The nuclear spin magnetization along this axis is given by

$$M_x \sim \langle \hat{I}_x \rangle = \mathrm{Tr}\{\hat{\rho}\hat{I}_x\} \sim \rho_{\boxed{-}} + \rho_{\boxed{+}} \tag{A.17}$$

where $\rho_{\boxed{-}}$ and $\rho_{\boxed{+}}$ are laboratory-frame (±1)-quantum coherences. Both the ($+1$)- and (-1)-quantum coherences in the laboratory frame contribute to the transverse nuclear spin magnetization.

The voltage generated in the coil is proportional to the time derivative of the nuclear spin magnetization in the coil direction. Assuming that the FID is simply proportional to this voltage, and ignoring constant instrumental phase shifts, we obtain the following:

$$s_{\mathrm{FID}}(t) \sim \frac{\mathrm{d}}{\mathrm{d}t}\rho_{\boxed{-}}(t) + \frac{\mathrm{d}}{\mathrm{d}t}\rho_{\boxed{+}}(t)$$

The coherences are time dependent through the Schrödinger equation. Their equation of motion in the laboratory frame is

$$\begin{aligned}\rho_{\boxed{-}}(t) &= \rho_{\boxed{-}}(0)\exp\{(\mathrm{i}\omega^0 - \lambda)t\}\\ \rho_{\boxed{+}}(t) &= \rho_{\boxed{+}}(0)\exp\{(-\mathrm{i}\omega^0 - \lambda)t\}\end{aligned}$$

and hence the FID is given by

$$s_{\mathrm{FID}}(t) \sim \mathrm{i}\omega^0\rho_{\boxed{-}}(t) - \mathrm{i}\omega^0\rho_{\boxed{+}}(t)$$

since ω^0 is much larger than λ. The constant factor ω^0 is now omitted, after noting that the amplitude of the signal is proportional to the Larmor frequency (this is one of the reasons that high fields and large gyromagnetic ratios are favourable for NMR experiments; see Section 16.3.1).

We now assume that this signal is amplified and passed into the quadrature receiver without any substantial change.

A block diagram of a traditional quadrature receiver is shown below:

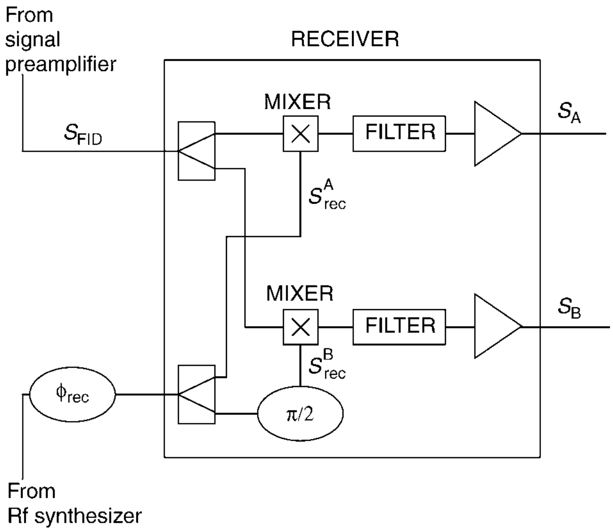

Figure A.5
Schematic of a quadrature receiver.

Modern equipment often uses a more sophisticated handling of the signal, but the basic principles are the same.

The NMR signal enters from the top left, whereas the receiver reference signal, given by

$$s_{\text{rec}}(t) \sim \cos(\omega_{\text{ref}} t + \phi^{\text{rf}}_{\text{rec}})$$

enters from the bottom left. The round symbol indicates the possibility of giving this reference signal an r.f. phase shift $\phi^{\text{rf}}_{\text{rec}}$.

The receiver reference signal is split into two paths. In the top path, the reference signal is unchanged:

$$s^{\text{A}}_{\text{rec}}(t) \sim \cos(\omega_{\text{ref}} t + \phi^{\text{rf}}_{\text{rec}})$$

In the lower path, the reference signal is given an additional phase shift of $\pi/2$:

$$s^{\text{B}}_{\text{rec}}(t) \sim \cos(\omega_{\text{ref}} t + \phi^{\text{rf}}_{\text{rec}} + \pi/2)$$

The NMR signal is also split into two paths. Consider the upper path first.

The NMR signal s_{FID} and the reference signal $s^{\text{A}}_{\text{rec}}$ both enter an electronic device called a *mixer*. This simply multiplies the two signals together. The signal exiting the upper mixer is therefore

$$s_{\text{FID}}(t) s^{\text{A}}_{\text{rec}}(t) \sim \text{i}\left(\rho_{\boxed{-}}(t) - \rho_{\boxed{+}}(t)\right) \cos(\omega_{\text{ref}} t + \phi^{\text{rf}}_{\text{rec}})$$

which evaluates to

$$\begin{aligned} s_{\text{FID}}(t) s^{\text{A}}_{\text{rec}}(t) \sim\ & \frac{1}{2}\text{i}\rho_{\boxed{-}}(0) \exp\{\text{i}[(\omega^0 + \omega_{\text{ref}})t + \phi^{\text{rf}}_{\text{rec}}]\}\, \text{e}^{-\lambda t} \\ & + \frac{1}{2}\text{i}\rho_{\boxed{-}}(0) \exp\{\text{i}[(\omega^0 - \omega_{\text{ref}})t - \phi^{\text{rf}}_{\text{rec}}]\}\, \text{e}^{-\lambda t} \\ & - \frac{1}{2}\text{i}\rho_{\boxed{+}}(0) \exp\{\text{i}[-(\omega^0 - \omega_{\text{ref}})t + \phi^{\text{rf}}_{\text{rec}}]\}\, \text{e}^{-\lambda t} \\ & - \frac{1}{2}\text{i}\rho_{\boxed{+}}(0) \exp\{\text{i}[-(\omega^0 + \omega_{\text{ref}})t - \phi^{\text{rf}}_{\text{rec}}]\}\, \text{e}^{-\lambda t} \end{aligned}$$

This signal now passes into a low-pass r.f. filter, which removes the high-frequency components. In the present case, the filter removes the components oscillating at $\omega^0 + \omega_{\text{ref}}$, and it retains those components oscillating at the low frequency $\Omega^0 = \omega^0 - \omega_{\mathrm{ref}}$. The signal s_{A} emerging from the filter is therefore

$$\begin{aligned} s_{\mathrm{A}}(t) \ \sim \ & \frac{1}{2}\mathrm{i}\rho_{\boxed{-}}(0)\,\exp\{\mathrm{i}(\Omega^0 t - \phi_{\mathrm{rec}}^{\mathrm{rf}})\}\,\mathrm{e}^{-\lambda t} \\ & -\frac{1}{2}\mathrm{i}\rho_{\boxed{+}}(0)\,\exp\{\mathrm{i}(-\Omega^0 t + \phi_{\mathrm{rec}}^{\mathrm{rf}})\}\,\mathrm{e}^{-\lambda t} \end{aligned}$$

From the relationship between laboratory frame and rotating-frame coherences (Equation 11.21), this equation may be written as

$$\begin{aligned} s_{\mathrm{A}}(t) \ \sim \ & \frac{1}{2}\mathrm{i}\tilde{\rho}_{\boxed{-}}(0)\,\exp\{\mathrm{i}(\Omega^0 t - \phi_{\mathrm{rec}}^{\mathrm{rf}} + \phi_{\mathrm{ref}})\}\,\mathrm{e}^{-\lambda t} \\ & -\frac{1}{2}\mathrm{i}\tilde{\rho}_{\boxed{+}}(0)\,\exp\{\mathrm{i}(-\Omega^0 t + \phi_{\mathrm{rec}}^{\mathrm{rf}} - \phi_{\mathrm{ref}})\}\,\mathrm{e}^{-\lambda t} \end{aligned} \tag{A.18}$$

The term ϕ_{ref} represents the angle of the rotating frame with respect to the laboratory frame at the time origin $t = 0$ (see Section 10.6).

The equation for the precession of the rotating-frame coherences (Equation 11.39) allows the above equation to be simplified:

$$s_{\mathrm{A}}(t) \sim \frac{1}{2}\mathrm{i}\tilde{\rho}_{\boxed{-}}(t)\,\exp\{-\mathrm{i}(\phi_{\mathrm{rec}}^{\mathrm{rf}} - \phi_{\mathrm{ref}})\} - \frac{1}{2}\mathrm{i}\tilde{\rho}_{\boxed{+}}(t)\,\exp\{\mathrm{i}(\phi_{\mathrm{rec}}^{\mathrm{rf}} - \phi_{\mathrm{ref}})\}$$

The same arguments may be repeated to obtain the filtered signal emerging from the second signal path in the receiver:

$$s_{\mathrm{B}}(t) \sim \frac{1}{2}\tilde{\rho}_{\boxed{-}}(t)\,\exp\{-\mathrm{i}(\phi_{\mathrm{rec}}^{\mathrm{rf}} - \phi_{\mathrm{ref}})\} + \frac{1}{2}\tilde{\rho}_{\boxed{+}}(t)\,\exp\{\mathrm{i}(\phi_{\mathrm{rec}}^{\mathrm{rf}} - \phi_{\mathrm{ref}})\}$$

These signals are treated as two components of one complex signal:

$$s(t) = s_{\mathrm{A}}(t) + \mathrm{i}s_{\mathrm{B}}(t)$$

This evaluates to

$$s(t) \sim \mathrm{i}\tilde{\rho}_{\boxed{-}}(t)\,\exp\{-\mathrm{i}(\phi_{\mathrm{rec}}^{\mathrm{rf}} - \phi_{\mathrm{ref}})\}$$

which only contains contributions from the rotating-frame (−1)-quantum coherence. The (+1)-quantum coherence contribution has disappeared.

In addition, a phase shift ϕ_{dig} is sometimes imposed after digitization of the signal. If this is included, we get

$$s(t) \sim \mathrm{i}\tilde{\rho}_{\boxed{-}}(t)\,\exp\{-\mathrm{i}(\phi_{\mathrm{rec}}^{\mathrm{rf}} + \phi_{\mathrm{dig}} - \phi_{\mathrm{ref}})\}$$

It is possible to ignore the constant phase ϕ_{ref}, since there are many other instrumental sources of a constant phase shift, and the spectral phase is adjusted anyway after FT using the phase correction parameter $\phi_{\mathrm{corr}}^{(0)}$ (see Section 5.8.5). If the frame phase shift ϕ_{ref} is removed, and numerical factors adjusted for convenience, then we get

$$s(t) \sim 2\mathrm{i}\tilde{\rho}_{\boxed{-}}(t)\,\exp\{-\mathrm{i}(\phi_{\mathrm{rec}}^{\mathrm{rf}} + \phi_{\mathrm{dig}})\}$$

The r.f. receiver reference phase and post-digitization phase shift may be combined to give an overall receiver phase:

$$\phi_{\mathrm{rec}} = \phi_{\mathrm{rec}}^{\mathrm{rf}} + \phi_{\mathrm{dig}}$$

This gives the following expression for the quadrature signal:

$$s(t) \sim 2\mathrm{i}\tilde{\rho}_{\boxed{-}}(t)\,\exp\{-\mathrm{i}\phi_{\mathrm{rec}}\}$$

which is used in the main text.

A.6 Secular Approximation

The secular approximation concerns the case where the Hamiltonian is the sum of two terms:

$$\widehat{\mathcal{H}} = \widehat{A} + \widehat{B}$$

where $\widehat{A}$ is a 'large' operator and $\widehat{B}$ is a 'small' operator. In the following discussion, both $\widehat{A}$ and $\widehat{B}$ are considered to be hermitian.

Since $\widehat{A}$ is hermitian, it is possible to form an orthogonal basis set from the eigenvectors $|n\rangle$ of $\widehat{A}$:

$$\widehat{A}|n\rangle = a_n|n\rangle$$

where a_n are the eigenvalues. Suppose that the eigenvalues of $\widehat{A}$ form the following pattern:

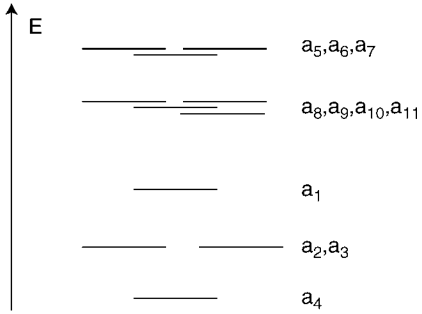

Figure A.6
Eigenvalues of the operator $\widehat{A}$.

The second and third eigenvalues are degenerate, the fifth, sixth and seventh eigenvalues form one near-degenerate group, and the eighth, ninth, tenth and eleventh eigenvalues form a second near-degenerate group.

If $\widehat{B}$ does not commute with $\widehat{A}$, then the matrix representation of $\widehat{B}$ in the eigenbasis of $\widehat{A}$ has finite elements everywhere, in general:

$$\begin{pmatrix}
\bullet & \bullet & \bullet & \bullet & \bullet & \bullet & \bullet & \bullet & \bullet & \bullet & \bullet & \cdots \\
\bullet & \bullet & \bullet & \bullet & \bullet & \bullet & \bullet & \bullet & \bullet & \bullet & \bullet & \cdots \\
\bullet & \bullet & \bullet & \bullet & \bullet & \bullet & \bullet & \bullet & \bullet & \bullet & \bullet & \cdots \\
\bullet & \bullet & \bullet & \bullet & \bullet & \bullet & \bullet & \bullet & \bullet & \bullet & \bullet & \cdots \\
\bullet & \bullet & \bullet & \bullet & \bullet & \bullet & \bullet & \bullet & \bullet & \bullet & \bullet & \cdots \\
\bullet & \bullet & \bullet & \bullet & \bullet & \bullet & \bullet & \bullet & \bullet & \bullet & \bullet & \cdots \\
\bullet & \bullet & \bullet & \bullet & \bullet & \bullet & \bullet & \bullet & \bullet & \bullet & \bullet & \cdots \\
\bullet & \bullet & \bullet & \bullet & \bullet & \bullet & \bullet & \bullet & \bullet & \bullet & \bullet & \cdots \\
\bullet & \bullet & \bullet & \bullet & \bullet & \bullet & \bullet & \bullet & \bullet & \bullet & \bullet & \cdots \\
\bullet & \bullet & \bullet & \bullet & \bullet & \bullet & \bullet & \bullet & \bullet & \bullet & \bullet & \cdots \\
\bullet & \bullet & \bullet & \bullet & \bullet & \bullet & \bullet & \bullet & \bullet & \bullet & \bullet & \cdots \\
\vdots & \vdots & \vdots & \vdots & \vdots & \vdots & \vdots & \vdots & \vdots & \vdots & \vdots & \ddots
\end{pmatrix}$$

The *secular approximation* for $\widehat{B}$ takes only the *block diagonal* form of this matrix:

$$\widehat{B}^0 = \begin{pmatrix} \bullet & 0 & 0 & 0 & 0 & 0 & 0 & 0 & 0 & 0 & 0 & \cdots \\ 0 & \bullet & \bullet & 0 & 0 & 0 & 0 & 0 & 0 & 0 & 0 & \cdots \\ 0 & \bullet & \bullet & 0 & 0 & 0 & 0 & 0 & 0 & 0 & 0 & \cdots \\ 0 & 0 & 0 & \bullet & 0 & 0 & 0 & 0 & 0 & 0 & 0 & \cdots \\ 0 & 0 & 0 & 0 & \bullet & \bullet & \bullet & 0 & 0 & 0 & 0 & \cdots \\ 0 & 0 & 0 & 0 & \bullet & \bullet & \bullet & 0 & 0 & 0 & 0 & \cdots \\ 0 & 0 & 0 & 0 & \bullet & \bullet & \bullet & 0 & 0 & 0 & 0 & \cdots \\ 0 & 0 & 0 & 0 & 0 & 0 & 0 & \bullet & \bullet & \bullet & \bullet & \cdots \\ 0 & 0 & 0 & 0 & 0 & 0 & 0 & \bullet & \bullet & \bullet & \bullet & \cdots \\ 0 & 0 & 0 & 0 & 0 & 0 & 0 & \bullet & \bullet & \bullet & \bullet & \cdots \\ 0 & 0 & 0 & 0 & 0 & 0 & 0 & \bullet & \bullet & \bullet & \bullet & \cdots \\ \vdots & \vdots & \vdots & \vdots & \vdots & \vdots & \vdots & \vdots & \vdots & \vdots & \vdots & \ddots \end{pmatrix} \tag{A.19}$$

where the blocks are formed by the pattern of degenerate or near-degenerate eigenvalues of $\widehat{A}$.

Another way of writing the secular approximation for $\widehat{B}$ is

$$\widehat{B}^0 = \sum_n b_{nn}|n\rangle\langle n| + \sum_{m \neq n}{}' b_{mn}|m\rangle\langle n| \tag{A.20}$$

where $|n\rangle$ are the eigenfunctions of $\widehat{A}$ and $b_{mn} = \langle m|\widehat{B}|n\rangle$ is a matrix element of $\widehat{B}$ in the eigenbase of $\widehat{A}$. The 'primed' summation only includes terms that 'connect' degenerate or near-degenerate eigenstates of $\widehat{A}$.

How 'near' does 'near-degenerate' have to be? Strictly, the summation in Equation A.20 omits terms for which the following inequality holds:

$$|b_{mn}| << |a_m - a_n| \tag{A.21}$$

A matrix element of $\widehat{B}$ may be dropped if its magnitude is small compared with the corresponding difference in the eigenvalues of $\widehat{A}$.

The secular Hamiltonian $\widehat{B}^0$ has the block-diagonal matrix representation given in Equation A.19. In general, $\widehat{B}^0$ does not commute with $\widehat{A}$, since the matrix representation in Equation A.19 may have off-diagonal elements connecting eigenstates of $\widehat{A}$ that are not *exactly* degenerate (contrast the discussion in Section 6.3.6).

The consequences of the secular approximation are best illustrated by specific examples.

Example 1. Chemical shift interaction of spin-1/2

Consider a single spin-1/2, with the following Hamiltonian terms:

$$\widehat{A} = \omega^0 \hat{I}_z$$

$$\widehat{B} = \omega_x \hat{I}_x + \omega_z \hat{I}_z$$

The term $\widehat{A}$ represents the interaction of the spin with a field along the z-axis, and $\widehat{B}$ represents the interaction of the spin with a small additional field, with a longitudinal component proportional to ω_z and a transverse component proportional to ω_x. The terms ω_x and ω_z are assumed to be much smaller than ω^0. This situation resembles the full form of the chemical shift interaction, given in Equation 9.11.

The eigenbasis of $\widehat{A}$ is defined by the two kets $|1\rangle = |+1/2\rangle$ and $|2\rangle = |-1/2\rangle$:

$$\widehat{A}|1\rangle = a_1|1\rangle \qquad \widehat{A}|2\rangle = a_2|2\rangle$$

with eigenvalues

$$a_1 = +\frac{1}{2}\omega^0 \qquad a_2 = -\frac{1}{2}\omega^0$$

The matrix representation of $\widehat{B}$ in this basis is

$$\widehat{B} = \frac{1}{2}\begin{pmatrix} \omega_z & \omega_x \\ \omega_x & -\omega_z \end{pmatrix}$$

The secular approximation for $\widehat{B}$, therefore, has a matrix representation given by

$$\widehat{B}^0 = \frac{1}{2}\begin{pmatrix} \omega_z & 0 \\ 0 & -\omega_z \end{pmatrix}$$

since the 'off-diagonal' elements ω_x connect eigenstates of $\widehat{A}$ with non-degenerate eigenvalues $\pm\frac{1}{2}\omega^0$. The secular approximation for $\widehat{B}$ is therefore

$$\widehat{B}^0 = \omega_z \hat{I}_z$$

which represents the interaction of the spin with only the longitudinal part of the additional field, as in Equation 9.13.

Example 2. Two spins-1/2

In a second example, consider the case of two spins-1/2 I_1 and I_2, with Larmor frequencies ω_1^0 and ω_2^0, a J-coupling J_{12}, and a secular dipole–dipole coupling d_{12}, as discussed in Chapter 14. The spin Hamiltonian may be written as $\widehat{\mathcal{H}} = \widehat{\mathcal{H}}_A^0 + \widehat{\mathcal{H}}_B^0$, where the matrix representations of the two parts of the Hamiltonian are given by Equations 14.7 and 14.8, in the Zeeman product basis.

The Hamiltonian $\widehat{\mathcal{H}}_B^0$ is off-diagonal in the Zeeman product basis. The secular approximation allows $\widehat{\mathcal{H}}_B^0$ to be omitted, providing that the off-diagonal elements of $\widehat{\mathcal{H}}_B^0$ are much smaller than the differences in the connected diagonal elements of $\widehat{\mathcal{H}}_A^0$.

Since the difference between the diagonal eigenvalues in rows 2 and 3 is equal to $\omega_1^0 - \omega_2^0$, and the off-diagonal elements are both equal to $\frac{1}{2}\omega_{12}^B = \pi J_{12} - \frac{1}{2}d_{12}$, the off-diagonal part of $\widehat{B}$ may be ignored if the condition

$$|\omega_1^0 - \omega_2^0| >> |\pi J_{12} - \frac{1}{2}d_{12}| \tag{A.22}$$

is satisfied. In an isotropic phase, this reduces to the condition in Equation 14.19.

Equation A.22 is always valid for the coupling between nuclei of different isotopic types, since the difference in Larmor frequency is very large in that case.

⚠The secular approximation shown in Equation A.20 is a result of *time-independent* perturbation theory. It must, therefore, be applied with caution to *time-dependent* situations, which are common in NMR. In general, the off-diagonal element b_{mn} may be ignored only if Equation A.21 is satisfied *and* if b_{mn} has a time dependence that is slow compared with the difference in eigenvalues $|a_m - a_n|$. For example, the homonuclear weak-coupling approximation breaks down if sufficiently rapid r.f. pulse sequences are applied (see Section 18.14 and Appendix A.10).

A.7 Quadrupolar Interaction

A.7.1 Full quadrupolar interaction

The spin Hamiltonian for the full electric quadrupolar interaction of spin I is given by (see *Further Reading*)

$$\widehat{\mathcal{H}}_Q^{\text{full}} = \frac{eQ}{2I(2I-1)\hbar}\hat{\mathbf{I}}.\mathbf{V}.\hat{\mathbf{I}} \tag{A.23}$$

where the tensor $\mathbf{V}$ represents the electric field gradient at the site of the nucleus:

$$\mathbf{V} = \begin{pmatrix} V_{xx} & V_{xy} & V_{xz} \\ V_{yx} & V_{yy} & V_{yz} \\ V_{zx} & V_{zy} & V_{zz} \end{pmatrix} \tag{A.24}$$

and Q is the nuclear electric quadrupole moment. The elements of $\mathbf{V}$ are given by the second derivatives of the electric potential V:

$$V_{xy} = \left.\frac{\partial^2 V}{\partial x \partial y}\right|_{\text{at nucleus}}$$

and similarly for the terms V_{zz}, V_{zx}, and so on. By definition, $\mathbf{V}$ is symmetric, i.e. $V_{xy} = V_{yx}$, etc. In addition, electromagnetic theory constrains $\mathbf{V}$ to be traceless, i.e. $V_{xx} + V_{yy} + V_{zz} = 0$.

The principal values of the electric field gradient tensor are

$$V_{XX} = -\frac{1}{2}eq(1-\eta_{\text{Q}})$$

$$V_{YY} = -\frac{1}{2}eq(1+\eta_{\text{Q}})$$

$$V_{XX} = eq$$

where η is the biaxiality. The representation of the electric field gradient tensor in the laboratory frame is given by

$$\mathbf{V} = \mathcal{R}(\Omega_{\text{LP}}^{\text{Q}}) \cdot \begin{pmatrix} V_{XX} & 0 & 0 \\ 0 & V_{YY} & 0 \\ 0 & 0 & V_{ZZ} \end{pmatrix} \cdot \mathcal{R}(\Omega_{\text{PL}}^{\text{Q}}) \tag{A.25}$$

Here, $\mathcal{R}(\Omega_{\text{PL}}^{\text{Q}})$ defines the relative orientation of the electric field gradient principal axis system and the laboratory frame:

$$\mathcal{R}(\Omega_{\text{PL}}^{\text{Q}}) = \mathcal{R}(\Omega_{\text{PM}}^{\text{Q}})\mathcal{R}(\Omega_{\text{ML}})$$

The Euler angle set $\Omega_{\text{PM}}^{\text{Q}}$ defines the orientation of the electric field gradient tensor in the molecular frame (compare with Equation A.6).

A.7.2 First-order quadrupolar interaction

The secular part of the quadrupolar Hamiltonian in Equation A.23 is given in the general case by

$$\widehat{\mathcal{H}}_Q^{(1)} = \omega_Q^{(1)} \times \frac{1}{6}\left(3\hat{I}_z^2 - I(I+1)\hat{1}\right) \tag{A.26}$$

where the first-order quadrupolar coupling is given by

$$\omega_{\mathrm{Q}}^{(1)} = \frac{3eQ}{2I(2I-1)\hbar} V_{zz} \tag{A.27}$$

Here, V_{zz} is a component of the electric field gradient tensor in the laboratory frame (Equation A.25).

In the case of a uniaxial electric field gradient tensor ($\eta_Q = 0$), this component is given by

$$V_{zz} = V_{ZZ}\frac{1}{2}(3\cos^2\theta_Q - 1)$$

where θ_{Q} is the angle between the unique principal axis of the electric field gradient tensor and the magnetic field (θ_{Q} corresponds to the Euler angle $\beta_{\mathrm{PL}}^{\mathrm{Q}}$). In the uniaxial case, Equation A.27 reduces to

$$\begin{aligned} \omega_Q^{(1)} &= \frac{3e^2Qq}{2I(2I-1)\hbar} \times \frac{1}{2}(3\cos^2\theta_Q - 1) \\ &= \frac{3\pi C_{\mathrm{Q}}}{I(2I-1)} \times \frac{1}{2}(3\cos^2\theta_Q - 1) \end{aligned} \tag{A.28}$$

as in Equation 9.30.

A.7.3 Higher-order quadrupolar interactions

The second-order quadrupolar interaction is best described using the technique of *irreducible spherical tensor operators* and is given explicitly elsewhere (e.g. see A. Jerschow, *Prog. NMR Spectrosc.* **46**, 63–78 (2005)).

For nuclei with spin $I \geq 2$, there are additional electric and magnetic interactions. For example, the $E_{\mathrm{elec}}^{(4)}$ term represents the interaction of the $\mathbb{C}^{(4)}$ part of the electric charge distribution (the 'electric hexadecapole moment') with the fourth derivative of the electric potential. There are also high-order magnetic interactions. In practice, all higher-order electromagnetic interactions are weak and unimportant.

A.8 Strong Coupling

A.8.1 Strongly-coupled Spin-1/2 pairs

Chapter 14 considers the dynamics of spin-1/2 pairs in two extreme cases: magnetic equivalence (no difference in chemical shifts) and weak coupling (a large difference in chemical shifts). This appendix considers the general case.

The rotating-frame spin Hamiltonian is given by

$$\widehat{\mathcal{H}}^0 = \Omega_1^0 \hat{I}_{1z} + \Omega_2^0 \hat{I}_{2z} + 2\pi J_{12}\hat{\mathbf{I}}_1 \cdot \hat{\mathbf{I}}_2 + d_{12}(3\hat{I}_{1z}\hat{I}_{2z} - \hat{\mathbf{I}}_1 \cdot \hat{\mathbf{I}}_2)$$

which has the following matrix representation in the Zeeman product basis:

$$\widehat{\mathcal{H}}^0 = \frac{1}{2}\begin{pmatrix} \Omega_\Sigma + \omega_{12}^{\mathrm{A}} & 0 & 0 & 0 \\ 0 & \Omega_\Delta - \omega_{12}^{\mathrm{A}} & \omega_{12}^{\mathrm{B}} & 0 \\ 0 & \omega_{12}^{\mathrm{B}} & -\Omega_\Delta - \omega_{12}^{\mathrm{A}} & 0 \\ 0 & 0 & 0 & -\Omega_\Sigma + \omega_{12}^{\mathrm{A}} \end{pmatrix} \tag{A.29}$$

where the A and B coupling terms are given by

$$\omega_{12}^{\mathrm{A}} = \pi J_{12} + d_{12}$$
$$\omega_{12}^{\mathrm{B}} = 2\pi J_{12} - d_{12}$$

and the sum and difference of the chemical shift frequencies are

$$\Omega_{\Sigma} = \Omega_1^0 + \Omega_2^0$$
$$\Omega_{\Delta} = \Omega_1^0 - \Omega_2^0$$

It is possible to solve for the eigenvalues and eigenvectors of the matrix in Equation A.29 using standard methods.[2] The eigenvectors are given by

$$|1\rangle = \begin{pmatrix} 1 \\ 0 \\ 0 \\ 0 \end{pmatrix} \qquad |2\rangle = \begin{pmatrix} 0 \\ \cos \frac{1}{2}\xi \\ \sin \frac{1}{2}\xi \\ 0 \end{pmatrix}$$

$$|3\rangle = \begin{pmatrix} 0 \\ -\sin \frac{1}{2}\xi \\ \cos \frac{1}{2}\xi \\ 0 \end{pmatrix} \qquad |4\rangle = \begin{pmatrix} 0 \\ 0 \\ 0 \\ 1 \end{pmatrix}$$

and the eigenvalues are given by

$$\Omega_1 = \frac{1}{2}(\Omega_{\Sigma} + \omega_{12}^{\mathrm{A}}) \qquad \Omega_2 = -\frac{1}{2}\omega_{12}^{\mathrm{A}} + \frac{1}{2}\sqrt{(\omega_{12}^{\mathrm{B}})^2 + \Omega_{\Delta}^2}$$
$$\Omega_3 = -\frac{1}{2}\omega_{12}^{\mathrm{A}} - \frac{1}{2}\sqrt{(\omega_{12}^{\mathrm{B}})^2 + \Omega_{\Delta}^2} \qquad \Omega_4 = \frac{1}{2}(-\Omega_{\Sigma} + \omega_{12}^{\mathrm{A}}) \tag{A.30}$$

where the angle ξ is defined by

$$\tan \xi = \frac{\omega_{12}^{\mathrm{B}}}{\Omega_{\Delta}} \tag{A.31}$$

If the angle ξ is small, then the system is weakly coupled. If the angle ξ approaches $\pi/2$, then the system is strongly coupled.

We can use these results to see what happens when an NMR signal is induced by a strong $\pi/2$ pulse.

Take the usual expression for the thermal equilibrium spin density operator:

$$\hat{\rho}_{①} = \hat{\rho}^{\mathrm{eq}} \sim \hat{I}_{1z} + \hat{I}_{2z}$$

omitting the unity operator and the Boltzmann factor. The thermal equilibrium density operator is independent of whether the spin system is weakly or strongly coupled, within the usual approximations of high temperature and high field.

The $(\pi/2)_x$ pulse rotates the spin density operator in the usual way, yielding

$$\hat{\rho}_{②} \sim -\hat{I}_{1y} - \hat{I}_{2y}$$

This transformation is also independent of the coupling state of the spin system.

Now suppose that the system evolves freely, in the absence of r.f. fields. The treatment in Section 15.9 does not apply if the system is strongly coupled. How does one proceed?

The first step is to express the spin density operator in terms of the coherences between the eigenstates of $\widehat{\mathcal{H}}$, defined in Equation A.30. This may be done using

$$\hat{\rho} = \sum_{r=1}^{4} \sum_{s=1}^{4} \rho_{rs} |r\rangle\langle s|$$

where ρ_{rs} is the coherence between eigenstate $|r\rangle$ and eigenstate $|s\rangle$. If the time point $t = 0$ corresponds to the end of the pulse, then the coherence ρ_{rs} at $t = 0$ is given by

$$\rho_{rs}(0) = \langle r|\hat{\rho}_{\textcircled{2}}|s\rangle = -\langle r|(\hat{I}_{1y} + \hat{I}_{2y})|s\rangle$$

The coherences may be evaluated by using the vector representations of $\langle r|$ and $|s\rangle$, and the matrix representation of $\hat{I}_{1y} + \hat{I}_{2y}$. For example, the (-1)-quantum coherence between states $|2\rangle$ and $|1\rangle$ is given by

$$\rho_{21}(0) = -\frac{1}{2\mathrm{i}} \begin{pmatrix} 0\,, & \cos\frac{1}{2}\xi\,, & \sin\frac{1}{2}\xi\,, & 0 \end{pmatrix} \cdot \begin{pmatrix} 0 & 1 & 1 & 0 \\ -1 & 0 & 0 & 1 \\ -1 & 0 & 0 & 1 \\ 0 & -1 & -1 & 0 \end{pmatrix} \cdot \begin{pmatrix} 1 \\ 0 \\ 0 \\ 0 \end{pmatrix}$$

$$= \frac{1}{2\mathrm{i}} \left(\cos\frac{1}{2}\xi + \sin\frac{1}{2}\xi \right)$$

If the calculation is repeated for the other three (-1)-quantum coherences, we get:

$$\rho_{31}(0) = \frac{1}{2\mathrm{i}}(\cos\frac{1}{2}\xi - \sin\frac{1}{2}\xi)$$

$$\rho_{42}(0) = \frac{1}{2\mathrm{i}}(\cos\frac{1}{2}\xi + \sin\frac{1}{2}\xi)$$

$$\rho_{43}(0) = \frac{1}{2\mathrm{i}}(\cos\frac{1}{2}\xi - \sin\frac{1}{2}\xi)$$

If the angle ξ is equal to zero, all four (-1)-quantum coherences have equal amplitude. This is the weak coupling case. If the angle ξ is equal to $\pi/2$, on the other hand, the coherences ρ_{31} and ρ_{43} are not excited by the pulse at all. This is the case of magnetic equivalence. In the general strong coupling case, all four (-1)-quantum coherences are excited, but with unequal amplitudes.

Now suppose that the system evolves for an interval t. The coherences oscillate as usual according to the difference in energies between the states involved (see Section 15.4). A given coherence, therefore, has the following value at time t:

$$\rho_{rs}(t) = \rho_{rs}(0) \exp\{[-\mathrm{i}(\Omega_r - \Omega_s) - \lambda]t\}$$

where a damping decay constant λ has been included to take into account transverse relaxation (assumed to be the same for all coherences, for the sake of simplicity). The rotating-frame eigenvalues Ω_r and Ω_s are specified in Equation A.30.

Each oscillating (-1)-quantum coherence induces an NMR signal, which therefore has the form

$$s(t) = \sum_{r=1}^{4} \sum_{s=1}^{4} a_{rs} \exp\{[\mathrm{i}\Omega_{rs} - \lambda]t\}$$

The terms a_{rs} are the complex amplitudes of the spectral peaks. The peak frequencies are given by differences in the Hamiltonian eigenvalues:

$$\Omega_{rs} = -\Omega_r + \Omega_s$$

In order to complete the calculation of the NMR signal, we require the signal amplitudes a_{rs}. Here, we must be careful, since in strongly coupled systems the different (-1)-quantum coherences couple to the observable magnetization with different efficiencies. This may be seen by repeating the arguments in Appendix A.5 for the strongly coupled system. For example, Equation A.17 becomes

$$M_x \sim \langle \hat{I}_x \rangle \quad = \mathrm{Tr}\{\hat{\rho}\hat{I}_x\} = \sum_{r=1}^{4}\sum_{s=1}^{4} \langle r|\hat{\rho}|s\rangle\langle s|\hat{I}_x|r\rangle = \sum_{r=1}^{4}\sum_{s=1}^{4} \rho_{rs}\langle s|\hat{I}_x|r\rangle$$

which shows that a coherence ρ_{rs} couples to the observable magnetization with a factor $\langle s|\hat{I}_x|r\rangle$. The signal coupling efficiencies for the four (-1)-quantum coherences in the AB system are readily calculated to be

$$\langle 1|\hat{I}_x|2\rangle = \frac{1}{2}(\cos\frac{1}{2}\xi + \sin\frac{1}{2}\xi) \qquad \langle 1|\hat{I}_x|3\rangle = \frac{1}{2}(\cos\frac{1}{2}\xi - \sin\frac{1}{2}\xi)$$

$$\langle 2|\hat{I}_x|4\rangle = \frac{1}{2}(\cos\frac{1}{2}\xi + \sin\frac{1}{2}\xi) \qquad \langle 3|\hat{I}_x|4\rangle = \frac{1}{2}(\cos\frac{1}{2}\xi - \sin\frac{1}{2}\xi)$$

In general, two of the four coherences provide stronger NMR signals than the other two. In the case of magnetic equivalence ($\xi = \pi/2$), two of the coherences do not induce NMR signals at all.

Taking this into account, we get the following general expression for the quadrature-detected signal amplitude generated by the coherence ρ_{rs}:

$$\boxed{a_{rs} = 2\mathrm{i}\rho_{rs}(0)\langle r|\hat{I}_x|s\rangle \exp\{-\mathrm{i}\phi_{\mathrm{rec}}\} \qquad \text{(A.32)}}$$

where ϕ_{rec} is the receiver phase. This equation applies to any (-1)-quantum coherence in an arbitrary coupled system.

The above expressions may be combined to obtain the NMR signal obtained by applying a single $\pi/2$ pulse to an ensemble of AB systems:

$$\begin{aligned} s(t) = a_{21}\exp\{[\mathrm{i}\Omega_{21} - \lambda]t\} + a_{31}\exp\{[\mathrm{i}\Omega_{31} - \lambda]t\} \\ + a_{42}\exp\{[\mathrm{i}\Omega_{42} - \lambda]t\} + a_{43}\exp\{[\mathrm{i}\Omega_{43} - \lambda]t\} \end{aligned}$$

The signal frequencies are given by

$$\begin{aligned} \Omega_{21} &= \frac{1}{2}\Omega_\Sigma + \omega_{12}^{\mathrm{A}} - \frac{1}{2}\sqrt{(\omega_{12}^{\mathrm{B}})^2 + \Omega_\Delta^2} \\ \Omega_{31} &= \frac{1}{2}\Omega_\Sigma + \omega_{12}^{\mathrm{A}} + \frac{1}{2}\sqrt{(\omega_{12}^{\mathrm{B}})^2 + \Omega_\Delta^2} \\ \Omega_{42} &= \frac{1}{2}\Omega_\Sigma - \omega_{12}^{\mathrm{A}} + \frac{1}{2}\sqrt{(\omega_{12}^{\mathrm{B}})^2 + \Omega_\Delta^2} \\ \Omega_{43} &= \frac{1}{2}\Omega_\Sigma - \omega_{12}^{\mathrm{A}} - \frac{1}{2}\sqrt{(\omega_{12}^{\mathrm{B}})^2 + \Omega_\Delta^2} \end{aligned}$$

and the signal amplitudes after a single $\pi/2$ pulse are

$$a_{21} = \frac{1}{2}\left(\cos\frac{1}{2}\xi + \sin\frac{1}{2}\xi\right)^2 = \frac{1}{2}(1+\sin\xi) \qquad a_{31} = \frac{1}{2}\left(\cos\frac{1}{2}\xi - \sin\frac{1}{2}\xi\right)^2 = \frac{1}{2}(1-\sin\xi)$$

$$a_{42} = \frac{1}{2}\left(\cos\frac{1}{2}\xi + \sin\frac{1}{2}\xi\right)^2 = \frac{1}{2}(1+\sin\xi) \qquad a_{43} = \frac{1}{2}\left(\cos\frac{1}{2}\xi - \sin\frac{1}{2}\xi\right)^2 = \frac{1}{2}(1-\sin\xi)$$

assuming $\phi_{\text{rec}} = 0$.

After FT, we get the following expression for the NMR spectrum:

$$S(\Omega) = a_{21}\mathcal{L}(\Omega; \Omega_{21}, \lambda) + a_{31}\mathcal{L}(\Omega; \Omega_{31}, \lambda) + a_{42}\mathcal{L}(\Omega; \Omega_{42}, \lambda) + a_{43}\mathcal{L}(\Omega; \Omega_{43}, \lambda)$$

displaying four peaks with different frequencies and amplitudes.

The simulations shown below illustrate the case with $\Omega_\Sigma = 0$, no dipole–dipole coupling ($d_{jk} = 0$), a J-coupling of $J_{jk} = 10\,\text{Hz}$, and different values for the chemical shift frequency difference Ω_Δ:

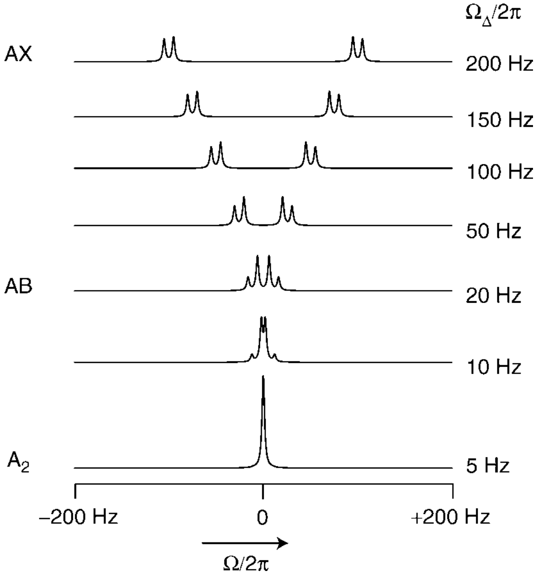

Figure A.7
Spectra of spin-1/2 pairs, in the case of $J_{jk} = 10\,\text{Hz}$ and zero dipole–dipole coupling.

In the limit of a large frequency difference Ω_Δ, the system is weakly coupled, and the spectrum displays the typical four-peak pattern of an AX spin system (although with small residual distortions in the relative peak amplitudes). As Ω_Δ is reduced, the outer peaks lose amplitude (these peaks correspond to the coherences ρ_{31} and ρ_{43}, which are weakly excited by the $\pi/2$ pulse and which also couple poorly to the observable signal). At the same time, the inner peaks gain amplitude. In the case of a very small chemical shift difference, the outer peaks disappear and the inner peaks coalesce. In the limit of a identical chemical shift frequencies, the system displays only a single spectral peak. This is the case of magnetic equivalence in the absence of J-coupling (see Figure 14.6a).

The simulation shown in Figure A.8 illustrates what happens if there is no J-coupling $J_{jk} = 0$, but there is a finite secular dipole–dipole coupling of $d_{jk}/2\pi = 10\,\text{Hz}$. The behaviour of the spin system is similar to the J-coupled case in the limit of large chemical shift difference: a four-peak AX pattern is observed, with a frequency splitting of $2d_{jk}/2\pi = 20\,\text{Hz}$ between the doublet components. However, when Ω_Δ is reduced, it is the central peaks that lose amplitude in the dipolar-coupled case. At very small values of Ω_Δ, the central peaks vanish altogether, leaving a doublet with splitting $3d_{jk}/2\pi = 30\,\text{Hz}$.

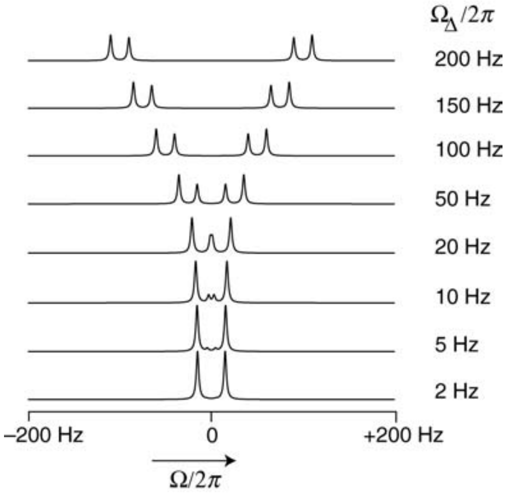

Figure A.8
Spectra of spin-1/2 pairs, in the case $d_{jk} = 10\,\text{Hz}$ and zero J-coupling.

Note carefully that the magnetic equivalence of the two spins in the case $\Omega_\Delta = 0$ does *not* remove the spin–spin splitting, in the case of a dipolar-coupled system (see Figure 14.6b).

The above expressions also apply when both J-couplings and secular dipolar couplings exist at the same time. The following simulation is for the case $\Omega_\Sigma = 0$ and $J_{jk} = d_{jk}/2\pi = 10\,\text{Hz}$:

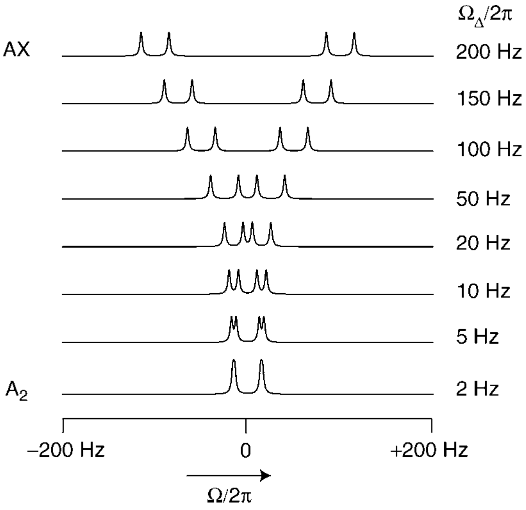

Figure A.9
Spectra of spin-1/2 pairs, in the case of $J_{jk} = d_{jk} = 10\,\text{Hz}$.

Remarkably, all four peak amplitudes remain the same, independent of the shift frequency difference Ω_Δ. Formally, this system is weakly coupled for all values of Ω_Δ ($\xi = 0$ in Equation A.31).

Strongly-coupled spectra are sometimes called “second-order spectra” in the literature, while weakly-coupled spectra are sometimes called "first-order". The meaning of these terms is unclear, and they should be avoided.

A.8.2 General strongly coupled systems

The situation is more complicated when there are more than two coupled spins, but the general principles are the same. The spectrum induced by a single strong $\pi/2$ pulse, applied to a thermal equilibrium spin ensemble in high magnetic field, may be calculated as follows:

1. Construct the rotating-frame Hamiltonian operator $\widehat{\mathcal{H}}$ for the spin system.

2. Calculate the matrix representation $\mathbf{H}$ of the Hamiltonian $\widehat{\mathcal{H}}$ in a suitable basis (for example the Zeeman product basis). If each spin system contains N coupled spins-1/2, the dimension of the matrix $\mathbf{H}$ is $2^N \times 2^N$.

3. Determine the matrix representation of the operator $\hat{I}^+$ in the same basis. Denote this $\mathbf{I}^+$.

4. Determine the eigenvalues and normalized eigenvectors of $\mathbf{H}$ (see Section 6.4). Each normalized eigenvector $\mathbf{x}_r$ corresponds to a rotating-frame Hamiltonian eigenvalue Ω_r, with the eigenvalue index r taking the values $\{1, 2 \ldots 2^N\}$:

   $$\mathbf{H} \cdot \mathbf{x}_r = \Omega_r \mathbf{x}_r$$

   In simple cases, the eigenvalues and eigenvectors may be determined analytically, as in Section A.8. In more complicated cases, numerical methods are available for diagonalizing the matrix.

5. In general, the NMR spectrum consists of 2^{2N} spectral peaks, each corresponding to a coherence between the eigenvectors. The coherence frequencies correspond to differences in Hamiltonian eigenvalues:

   $$\Omega_{rs} = -\Omega_r + \Omega_s$$

   The peak amplitudes correspond to the squares of the matrix elements of $\hat{I}^+$:

   $$a_{rs} = |\mathbf{x}_r{}^\dagger \cdot \mathbf{I}^+ \cdot \mathbf{x}_s|^2$$

6. The NMR spectrum is a sum of Lorentzians, one for each coherence:

   $$S(\Omega) = \sum_{r,s=1}^{2^N} a_{rs} \mathcal{L}(\Omega; \Omega_{rs}, \lambda) \tag{A.33}$$

   where $\lambda = T_2{}^{-1}$.

In practice, the sum in Equation A.33 may be restricted to (-1)-quantum coherences, since the amplitudes a_{rs} vanish in all other cases.

A.9 J-Couplings and Magnetic Equivalence

In this appendix, I prove that J-couplings between magnetically equivalent spins may be omitted from the spin Hamiltonian without changing the results of any calculations.

Consider first the following theorem. Suppose that the spin Hamiltonian contains two hermitian terms $\widehat{A}$ and $\widehat{B}$, which mutually commute:

$$\widehat{\mathcal{H}} = \widehat{A} + \widehat{B}$$
$$\left[\widehat{A}, \widehat{B}\right] = 0 \tag{A.34}$$

Suppose also that $\widehat{B}$ commutes with an operator $\widehat{Q}$:

$$\left[\widehat{B}, \widehat{Q}\right] = 0 \tag{A.35}$$

The theorem states that the expectation value of $\widehat{Q}$ may be calculated as a function of time without including the term $\widehat{B}$ in the Hamiltonian.

This may be shown as follows. The Schrödinger equation leads to the following equation of motion for a spin state $|\psi\rangle$:

$$|\psi\rangle(t) = \exp\{-\mathrm{i}\widehat{\mathcal{H}}t\}|\psi\rangle(0)$$

If the Hamiltonian contains two commuting terms, then the exponential operator may be written as

$$\exp\{-\mathrm{i}\widehat{\mathcal{H}}t\} = \exp\{-\mathrm{i}\widehat{B}t\}\exp\{-\mathrm{i}\widehat{A}t\}$$

The equation of motion for the ket and bra states is therefore

$$|\psi\rangle(t) = \exp\{-\mathrm{i}\widehat{B}t\}\exp\{-\mathrm{i}\widehat{A}t\}|\psi\rangle(0)$$
$$\langle\psi|(t) = \langle\psi|(0)\exp\{+\mathrm{i}\widehat{A}t\}\exp\{+\mathrm{i}\widehat{B}t\}$$

The expectation value of the operator $\widehat{Q}$ evolves as follows:

$$\begin{aligned}\langle\widehat{Q}\rangle(t) &= \langle\psi|(t)\;\widehat{Q}\;|\psi\rangle(t)\\ &= \langle\psi|(0)\exp\{+\mathrm{i}\widehat{A}t\}\exp\{+\mathrm{i}\widehat{B}t\}\widehat{Q}\exp\{-\mathrm{i}\widehat{B}t\}\exp\{-\mathrm{i}\widehat{A}t\}|\psi\rangle(0)\end{aligned}$$

Now if the operators $\widehat{Q}$ and $\widehat{B}$ commute, then

$$\exp\{+\mathrm{i}\widehat{B}t\}\widehat{Q}\exp\{-\mathrm{i}\widehat{B}t\} = \widehat{Q}$$

Hence

$$\langle\widehat{Q}\rangle(t) = \langle\psi|(0)\exp\{+\mathrm{i}\widehat{A}t\}\widehat{Q}\exp\{-\mathrm{i}\widehat{A}t\}|\psi\rangle(0)$$

which is independent of $\widehat{B}$.

This theorem may be applied to the problem of magnetic equivalence as follows. Consider a molecular spin system containing three spins I_1, I_2 and I_3, with the following relationships between the chemical shift frequencies and the J-couplings:

$$\begin{aligned}\omega_1^0 &= \omega' & \omega_2^0 &= \omega'\\ \omega_3^0 &= \omega'' & J_{12} &= J'\\ J_{13} &= J'' & J_{23} &= J''\end{aligned}$$

Spins I_1 and I_2 are magnetically equivalent according to the standard definition.

The spin Hamiltonian may be divided up as in Equation A.34, with

$$\begin{aligned}\widehat{A} &= \omega'(\hat{I}_{1z}+\hat{I}_{2z}) + \omega''\hat{I}_{3z} + 2\pi J''\left(\hat{\mathbf{I}}_1+\hat{\mathbf{I}}_2\right)\cdot\hat{\mathbf{I}}_3\\ \widehat{B} &= 2\pi J'\,\hat{\mathbf{I}}_1\cdot\hat{\mathbf{I}}_2\end{aligned}$$

The commutation of $\widehat{A}$ and $\widehat{B}$ may be demonstrated by repeating the following reasoning for all the relevant terms:

$$\left[\left(\hat{I}_{1x}+\hat{I}_{2x}\right)\hat{I}_{3x}\,,\;\hat{I}_{1z}\hat{I}_{2z}\right] = \left[\hat{I}_{1x}+\hat{I}_{2x},\,\hat{I}_{1z}\hat{I}_{2z}\right]\hat{I}_{3x} = 0 \tag{A.36}$$

Furthermore, all relevant observable operators also commute with $\widehat{B}$. This is because the observation process always involves a sum of contributions from all spins of the same isotopic type. For example, a typical observable operator corresponds to the sum of spin angular momentum along the x-axis:

$$\widehat{Q} = \hat{I}_{1x} + \hat{I}_{2x} + \hat{I}_{3x}$$

This operator also commutes with $\widehat{B}$. The theorem above indicates that the term $\widehat{B}$ may be dropped from the spin Hamiltonian without damage.

This reasoning may be extended to more complicated cases. Consider, for example, the case of four spins, in which the first three are magnetically equivalent:

$$\begin{aligned} \omega_1^0 &= \omega' & \omega_2^0 &= \omega' \\ \omega_3^0 &= \omega' & \omega_4^0 &= \omega'' \\ J_{12} &= J' & J_{13} &= J' \\ J_{14} &= J'' & J_{23} &= J' \\ J_{24} &= J'' & J_{34} &= J'' \end{aligned}$$

The Hamiltonian may be organized into two commuting terms as follows:

$$\begin{aligned} \widehat{A} &= \omega'(\hat{I}_{1z} + \hat{I}_{2z} + \hat{I}_{3z}) + \omega''\hat{I}_{4z} + 2\pi J''\left(\hat{\mathbf{I}}_1 + \hat{\mathbf{I}}_2 + \hat{\mathbf{I}}_3\right) \cdot \hat{\mathbf{I}}_4 \\ \widehat{B} &= 2\pi J'\left(\hat{\mathbf{I}}_1 \cdot \hat{\mathbf{I}}_2 + \hat{\mathbf{I}}_2 \cdot \hat{\mathbf{I}}_3 + \hat{\mathbf{I}}_3 \cdot \hat{\mathbf{I}}_4\right) \end{aligned} \tag{A.37}$$

If the observable operator has the form

$$\widehat{Q} = \hat{I}_{1x} + \hat{I}_{2x} + \hat{I}_{3x} + \hat{I}_{4x}$$

then the commutation properties shown in Equations A.34 and A.35 may be proved by repeating Equation A.36 for all relevant terms. The couplings within the group of magnetically equivalent spins may, therefore, be omitted from the spin Hamiltonian.

A.10 Spin Echo Sandwiches

In this appendix, I examine the properties of the spin echo sequence

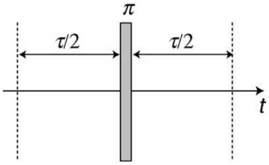

Figure A.10
Spin echo sandwich.

in coupled spin systems.

In the case of a general spin system in an isotropic liquid, the propagator for this pulse sequence element is given by

$$\widehat{U}_{\mathrm{SES}} = \widehat{U}(\tau/2)\widehat{R}_x(\pi)\widehat{U}(\tau/2) \tag{A.38}$$

where

$$\widehat{U}(\tau/2) = \exp\{-\mathrm{i}\widehat{\mathcal{H}}^0\tau/2\}$$

and the secular rotating-frame Hamiltonian has the form

$$\widehat{\mathcal{H}}^0 = \sum_j \Omega_j^0 \hat{I}_{jz} + \sum_{j<k}{}' \, 2\pi J_{jk}\hat{\mathbf{I}}_j \cdot \hat{\mathbf{I}}_k$$

This expression may be simplified, depending on the duration of the spin echo sequence and whether the spin system satisfies the weak-coupling conditions or not:

1. *The short-duration limit*. If the duration τ of the spin echo sequence satisfies

$$\boxed{|(\Omega_j^0 - \Omega_k^0)\tau| << 1} \tag{A.39}$$

for all pairs of coupled spins j and k, then the propagator for the spin echo sandwich may be written as

$$\boxed{\widehat{U}_{\text{SES}} \cong \widehat{U}_J^{\text{strong}}(\tau)\widehat{R}_x(\pi) \qquad \text{(short-duration limit)}} \tag{A.40}$$

where $\widehat{U}_J^{\text{strong}}$ is given by

$$\widehat{U}_J^{\text{strong}}(\tau) = \exp\{-\mathrm{i}\widehat{\mathcal{H}}_J^{\text{strong}}\tau\} \tag{A.41}$$

and

$$\widehat{\mathcal{H}}_J^{\text{strong}} = \sum_{j<k}{}' \, 2\pi J_{jk}\hat{\mathbf{I}}_j \cdot \hat{\mathbf{I}}_k \tag{A.42}$$

In the short-duration limit, the system is rotated by the π pulse, followed by evolution under the strongly coupled form of the J-couplings. Note that Equation A.40 always applies at short durations, even for systems that satisfy the usual weak-coupling condition.

2. *The long-duration limit*. If the spin system satisfies the weak-coupling condition

$$\boxed{|(\Omega_j^0 - \Omega_k^0)| >> |\pi J_{jk}|} \tag{A.43}$$

and the duration τ of the spin echo sequence is sufficiently long, i.e.

$$\boxed{|(\Omega_j^0 - \Omega_k^0)\tau| >> 1} \tag{A.44}$$

for all pairs of magnetically equivalent coupled spins j and k, then the propagator for the spin echo sandwich is given by

$$\boxed{\widehat{U}_{\text{SES}} \cong \widehat{U}_J^{\text{weak}}(\tau)\widehat{R}_x(\pi) \qquad \text{(long-duration limit)}} \tag{A.45}$$

where $\widehat{U}_J^{\text{weak}}$ is given by

$$\widehat{U}_J^{\text{weak}}(\tau) = \exp\{-\mathrm{i}\widehat{\mathcal{H}}_J^{\text{weak}}\tau\}$$

and

$$\widehat{\mathcal{H}}_J^{\text{weak}} = \sum_{j<k}{}' \, 2\pi J_{jk}\hat{I}_{jz}\hat{I}_{kz}$$

The expression for the propagator (Equation A.45) corresponds to Equation 15.25 in the case of an AX system. In the long-duration limit, the system is rotated by the π pulse, followed by evolution under the weakly coupled form of the J-couplings.

These properties are now proved.

A.10.1 Short-duration limit

In general, the propagator for the spin echo sandwich (Equation A.38) may be rewritten as follows:

$$\begin{aligned}\widehat{U}_{\mathrm{SES}} &= \widehat{U}(\tau/2)\widehat{R}_x(\pi)\widehat{U}(\tau/2)\\ &= \widehat{U}(\tau/2)\cdot\widehat{R}_x(\pi)\widehat{U}(\tau/2)\widehat{R}_x(-\pi)\cdot\widehat{R}_x(\pi)\\ &= \widehat{U}(\tau/2)\widehat{U}'(\tau/2)\widehat{R}_x(\pi)\end{aligned}$$

where

$$\widehat{U}'(\tau/2) = \widehat{R}_x(\pi)\widehat{U}(\tau/2)\widehat{R}_x(-\pi)$$

By the arguments of Appendix A.3, this may be rearranged as

$$\begin{aligned}\widehat{U}'(\tau/2) &= \widehat{R}_x(\pi)\exp\{-\mathrm{i}\widehat{\mathcal{H}}^0\tau/2\}\widehat{R}_x(-\pi)\\ &= \exp\{-\mathrm{i}\,\widehat{R}_x(\pi)\widehat{\mathcal{H}}^0\widehat{R}_x(-\pi)\,\tau/2\}\\ &= \exp\{-\mathrm{i}\,\widehat{\mathcal{H}}^{0\prime}\,\tau/2\}\end{aligned}$$

where

$$\widehat{\mathcal{H}}^{0\prime} = \widehat{R}_x(\pi)\widehat{\mathcal{H}}^0\widehat{R}_x(-\pi)$$

The bracketing π_x rotations have the effect of inverting the chemical shift terms, leaving the sign of the J-coupling terms unchanged:

$$\widehat{\mathcal{H}}^{0\prime} = -\sum_j \Omega_j^0\hat{I}_{jz} + {\sum_{j<k}}' 2\pi J_{jk}\hat{\mathbf{I}}_j\cdot\hat{\mathbf{I}}_k$$

The spin echo propagator is therefore given by

$$\widehat{U}_{\mathrm{SES}} = \exp\{-\mathrm{i}\widehat{\mathcal{H}}^0\tau/2\}\exp\{-\mathrm{i}\widehat{\mathcal{H}}^{0\prime}\tau/2\}\widehat{R}_x(\pi)$$

So far, this expression is general.

In general, $\widehat{\mathcal{H}}^0$ and $\widehat{\mathcal{H}}^{0\prime}$ do not commute. However, if the duration τ is sufficiently small, then Equation 6.35 applies, which leads to the following approximate result:

$$\widehat{U}_{\mathrm{SES}} \cong \exp\{-\mathrm{i}(\widehat{\mathcal{H}}^0+\widehat{\mathcal{H}}^{0\prime})\tau/2\}\widehat{R}_x(\pi)$$

and hence

$$\boxed{\widehat{U}_{\mathrm{SES}} \cong \widehat{U}_J^{\mathrm{strong}}(\tau)\widehat{R}_x(\pi) \qquad (\mathrm{A.46})}$$

as in Equation A.40.

A.10.2 Long-duration limit

The propagator for the spin echo sandwich

$$\widehat{U}_{\mathrm{SES}} = \exp\{-\mathrm{i}\widehat{\mathcal{H}}^0\tau/2\}\exp\{-\mathrm{i}\widehat{\mathcal{H}}^{0\prime}\tau/2\}\widehat{R}_x(\pi) \qquad (\mathrm{A.47})$$

cannot be simplified in general for large values of τ, since $\widehat{\mathcal{H}}^{0\prime}$ and $\widehat{\mathcal{H}}^{0}$ do not commute. However, if the system is weakly coupled, and the intervals $\tau/2$ are sufficiently long, then the secular approximation (Appendix A.6) may be applied locally within each precession interval. Under these conditions, the propagator may be approximated:

$$\widehat{U}_{\mathrm{SES}} \cong \exp\{-\mathrm{i}\widehat{\mathcal{H}}^{0}_{\mathrm{weak}}\tau/2\}\exp\{-\mathrm{i}\widehat{\mathcal{H}}^{0\prime}_{\mathrm{weak}}\tau/2\}\widehat{R}_x(\pi)$$

where $\widehat{\mathcal{H}}^{0}_{\mathrm{weak}}$ is the weakly coupled spin Hamiltonian in the rotating frame:

$$\widehat{\mathcal{H}}^{0}_{\mathrm{weak}} \cong \sum_{j}\Omega^0_j\hat{I}_{jz} + {\sum_{j<k}}' 2\pi J_{jk}\hat{I}_{jz}\hat{I}_{kz} \tag{A.48}$$

and

$$\begin{aligned}\widehat{\mathcal{H}}^{0\prime}_{\mathrm{weak}} &= \widehat{R}_x(-\pi)\widehat{\mathcal{H}}^{0}_{\mathrm{weak}}\widehat{R}_x(\pi)\\ &= -\sum_{j}\Omega^0_j\hat{I}_{jz} + {\sum_{j<k}}' 2\pi J_{jk}\hat{I}_{jz}\hat{I}_{kz}\end{aligned}$$

Since the Hamiltonians $\widehat{\mathcal{H}}^{0}_{\mathrm{weak}}$ and $\widehat{\mathcal{H}}^{0\prime}_{\mathrm{weak}}$ commute, Equation 6.32 may be used to write the product of the propagators in Equation A.47 as

$$\widehat{U}_{\mathrm{SES}} = \exp\{-\mathrm{i}(\widehat{\mathcal{H}}^{0\prime}_{\mathrm{weak}} + \widehat{\mathcal{H}}^{0}_{\mathrm{weak}})\tau/2\}\widehat{R}_x(\pi) \tag{A.49}$$

which evaluates to

$$\boxed{\widehat{U}_{\mathrm{SES}} = \widehat{U}^{\mathrm{weak}}_{J}(\tau)\widehat{R}_x(\pi) \qquad \text{(A.50)}}$$

as in Equation A.45.

The spin echo sandwich, therefore, has the same effect as a strong π pulse, followed by a period τ of evolution under the weak J-couplings. Since the operators commute, this sequence may also be applied the other way round.

The long-duration form of the spin echo sandwich is often used to manipulate spin systems under the weakly coupled J-couplings, without regard for the chemical shifts. This is the most common application of a spin echo sandwich, and is encountered in Sections 16.2, 16.3 and 18.12.

A.10.3 Two spin echo sequences

If two spin echo sequences follow each other immediately, as in the sequence

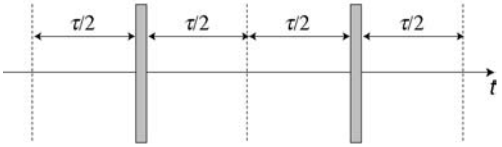

Figure A.11 Two spin-echo sandwiches.

then one may just multiply the propagators together, leading to

$$\widehat{U}_{\mathrm{SES}}\widehat{U}_{\mathrm{SES}} \cong \widehat{U}^{\mathrm{strong}}_{J}(\tau)\widehat{R}_x(\pi)\widehat{U}^{\mathrm{strong}}_{J}(\tau)\widehat{R}_x(\pi)$$

in the short-duration limit, and

$$\widehat{U}_{\text{SES}}\widehat{U}_{\text{SES}} \cong \widehat{U}_J^{\text{weak}}(\tau)\widehat{R}_x(\pi)\widehat{U}_J^{\text{weak}}(\tau)\widehat{R}_x(\pi)$$

in the long-duration limit.

In both cases, the π rotations commute with the spin coupling Hamiltonian, so the effective propagator under the double spin echo sequence is

$$\widehat{U}_{\text{SES}}\widehat{U}_{\text{SES}} \cong \widehat{U}_J^{\text{weak}}(2\tau)\widehat{R}_x(2\pi)$$

in the long-duration limit, and

$$\widehat{U}_{\text{SES}}\widehat{U}_{\text{SES}} \cong \widehat{U}_J^{\text{strong}}(2\tau)\widehat{R}_x(2\pi)$$

in the short-duration limit. The operator for a rotation by 2π may usually be omitted.[3]

In general, for n consecutive spin echo sequences, we get

$$\boxed{\widehat{U}_{\text{SES}}\widehat{U}_{\text{SES}} \ldots \widehat{U}_{\text{SES}} \cong \widehat{U}_J^{\text{weak}}(n\tau)\widehat{R}_x(2n\pi)} \tag{A.51}$$

in the long-duration limit, and

$$\boxed{\widehat{U}_{\text{SES}}\widehat{U}_{\text{SES}} \ldots \widehat{U}_{\text{SES}} \cong \widehat{U}_J^{\text{strong}}(n\tau)\widehat{R}_x(2n\pi)} \tag{A.52}$$

in the short-duration limit.

If n is even, then the operator $\widehat{R}_x(2n\pi)$ may be ignored,[3] so the application of a dense sequence of π pulses leads to evolution under the pure strongly coupled J-Hamiltonian. This property is used in the TOCSY pulse sequence (see Section 18.14).

A.10.4 Heteronuclear spin echo sequences

In heteronuclear systems, the Larmor frequency difference between spins of different type is very large. Both of the conditions in Equations A.43 and A.44 are always satisfied for the heteronuclear couplings. The heteronuclear part of the spin echo propagator always has the weakly coupled form.

In heteronuclear systems, the form of the spin echo propagator depends on whether the π pulse is applied to one or both of the spin species.

1. If a π pulse is applied to *both* spin species, then the following equivalence may be made:

   If the homonuclear couplings also satisfy the 'long limit' conditions, then the propagator for the heteronuclear spin echo sequence may be written as

   $$\widehat{U}_{\text{SES}} = \widehat{U}_J^{\text{weak}}(\tau)\widehat{R}_x^I(\pi)\widehat{R}_x^S(\pi)$$

   where $\widehat{R}_x^I(\pi)$ and $\widehat{R}_x^S(\pi)$ represent π rotations of the two spin species, and the weak coupling propagator is

   $$\widehat{U}_J^{\text{weak}}(\tau) = \exp\{-\mathrm{i}\widehat{\mathcal{H}}_J^{\text{weak}}\tau\}$$

   The weak-coupling Hamiltonian $\widehat{\mathcal{H}}_J^{\text{weak}}$ contains all the couplings in the system (both homonuclear and heteronuclear). All chemical shift interactions are suppressed. A heteronuclear spin echo sandwich with a π pulse applied to both spin species behaves in the same way as a homonuclear spin echo sandwich:

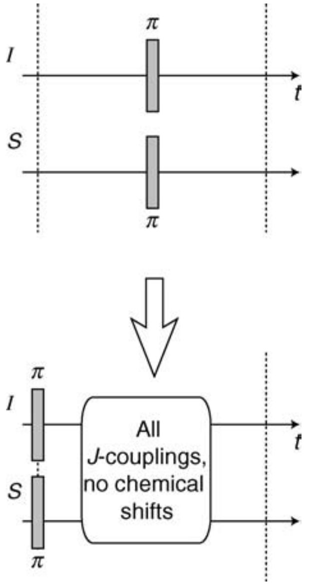

Figure A.12
Heteronuclear spin echo sequence, with π pulses on both channels.

2. If a π pulse is applied to *only one* spin species, on the other hand, the following equivalence applies:

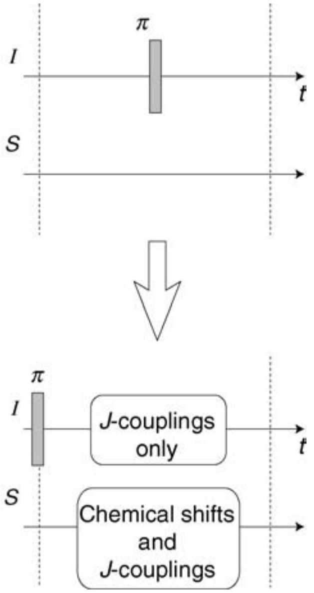

Figure A.13
Heteronuclear spin echo sequence, with a π pulse on the I-spin channel.

The spin echo sandwich suppresses chemical shifts for the irradiated species, but not for the non-irradiated species. Furthermore, the spin echo sandwich suppresses heteronuclear J-couplings, but retains homonuclear J-couplings. Formally, the propagator for this single-channel spin echo sandwich is

$$\widehat{U}_{\text{SES}} = \widehat{U}_{II}^{\text{weak}}(\tau)\widehat{U}_{S}^{\text{weak}}(\tau)\widehat{R}_{x}^{I}(\pi)$$

where the propagators are

$$\begin{aligned}\widehat{U}_{II}^{\text{weak}}(\tau) &= \exp\{-\mathrm{i}\widehat{\mathcal{H}}_{II}^{\text{weak}}\tau\}\\ \widehat{U}_{S}^{\text{weak}}(\tau) &= \exp\{-\mathrm{i}\widehat{\mathcal{H}}_{S}\tau\}\end{aligned}$$

and the Hamiltonians are

$$\begin{aligned}\widehat{\mathcal{H}}_{II}^{\text{weak}} &= \sum_{j<k}{}' \; 2\pi J_{jk}\hat{I}_{jz}\hat{I}_{kz}\\ \widehat{\mathcal{H}}_{S} &= \sum_{\ell}\Omega_{\ell}^{0}\hat{S}_{\ell z} + \sum_{\ell<m}{}' \; 2\pi J_{\ell m}\hat{S}_{\ell z}\hat{S}_{mz}\end{aligned}$$

assuming that the weak-coupling conditions are satisfied for the S-spins.

A.11 Phase Cycling

In this appendix, I discuss the principles of *phase cycling*, which is a powerful and commonly used procedure for selecting certain types of NMR signals and suppressing others.

The basic practice of phase cycling is presented in Section 5.3. The phases of r.f. pulses and the the receiver phase are varied from transient to transient in a cyclic fashion, and the NMR signals from these different experiments are added together.

In this appendix, I discuss (i) how to predict which NMR signals are selected by a given phase-cycling procedure and (ii) how to design a phase cycle for a particular experiment, using a systematic algorithm. The discussion given here is necessarily superficial. A more thorough discussion may be found in *Further Reading*.

A.11.1 Coherence transfer pathways

The first step in phase cycling theory is to draw the *coherence transfer pathway diagram* for an experiment. This represents the history of coherence orders leading to the desired NMR signals in a particular experiment.[4] Consider, for example, the COSY pulse sequence discussed in Section 16.1. The basic pulse sequence for this experiment, and its associated coherence transfer pathway diagram, is as follows:

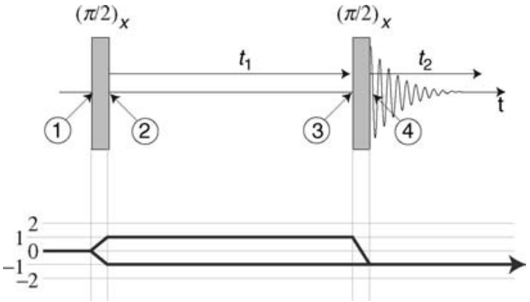

Figure A.14 COSY pulse sequence and its coherence transfer pathway.

This shows the ‘cosine’ pulse sequence in the States procedure. The ‘sine’ pulse sequence in the States procedure has the same coherence transfer pathway diagram.

In this book, thick black arrows indicate the desired histories of coherence orders leading to desirable NMR signals. In the case above, the desirable pathways are

$$0 \rightarrow +1 \rightarrow -1 \tag{A.53}$$

and

$$0 \rightarrow -1 \rightarrow -1 \tag{A.54}$$

All pathways start with order 0 (corresponding to spin populations) and terminate with order −1 (corresponding to observable (−1)-quantum coherences as detected in the quadrature receiver; see Appendix A.5).

The pathways given in Equations A.53 and A.54 indicate the conversion of spin populations into (±1)-quantum coherences by the first pulse, followed by conversion of these into observable (−1)-quantum coherences by the second pulse. The treatment given in Section 16.1 shows that *both* of these pathways are necessary to obtain pure absorption spectra using the States procedure. For example, the state $\hat{\rho}_{③}^{\cos}$ given in Equation 16.7 contains both (±1)-quantum coherences, and the States procedure would fail if any one of these pathways were suppressed. It is very important to maintain such essential dual pathways when designing phase-cycling procedures.

More complicated pulse sequences may have several coherence transfer steps, and a greater multiplicity of desirable signal pathways. For example, the INADEQUATE experiment (Section 16.2) has the following pulse sequence and coherence transfer pathway diagram:

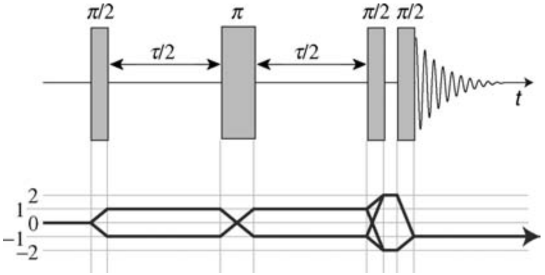

Figure A.15 INADEQUATE pulse sequence and its coherence transfer pathway.

There are four *desired coherence transfer pathways* in this case:

$$\begin{aligned} &0 \rightarrow +1 \rightarrow -1 \rightarrow +2 \rightarrow -1 \\ &0 \rightarrow +1 \rightarrow -1 \rightarrow -2 \rightarrow -1 \\ &0 \rightarrow -1 \rightarrow +1 \rightarrow +2 \rightarrow -1 \\ &0 \rightarrow -1 \rightarrow +1 \rightarrow -2 \rightarrow -1 \end{aligned} \tag{A.55}$$

In addition to these desirable signal pathways, it is also important to identify the *undesirable* signal pathways.

For example, in the COSY experiment, the signals passing through order 0 during the evolution interval t_1 may be relatively large, if the flip angle of the first pulse is not exactly $\pi/2$. These signals give rise to false two-dimensional peaks at the frequency coordinate $\Omega_1 = 0$ and must be suppressed to obtain a good result.

Similarly, in the INADEQUATE experiment, it is very important to suppress all signals that do not pass through (±2)-quantum coherences, in order to remove signals from isotopomers containing isolated ^{13}C spins.

A.11.2 Coherence transfer amplitudes

Phase cycling is based upon the transformation properties of the signals under phase shifts of the r.f. pulses.

Consider a general situation in which a pulse sequence element A, with phase ϕ, converts the coherence between two states $|r\rangle$ and $|s\rangle$ into a coherence between two different states $|u\rangle$ and $|v\rangle$:

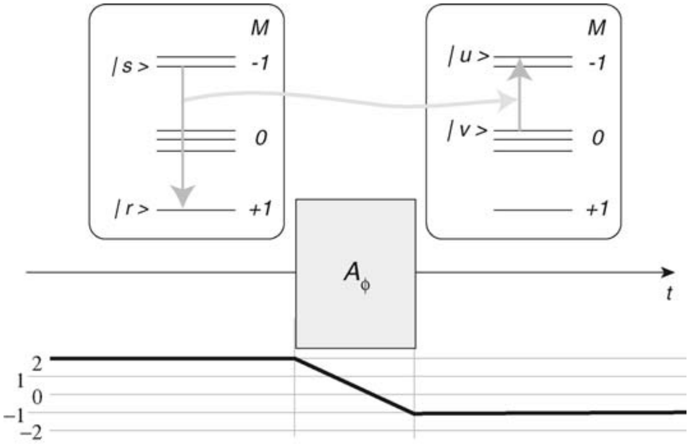

Figure A.16
A coherence transfer process.

In the example shown, the coherence between states $|r\rangle$ and $|s\rangle$ has order $p_{rs} = +2$, while the coherence between states $|u\rangle$ and $|v\rangle$ has order $p_{uv} = -1$. The change in coherence order is represented by the bold line on the coherence transfer pathway diagram.

This coherence transfer process may be represented mathematically as follows:

$$\widehat{A}_\phi |r\rangle\langle s| \widehat{A}_\phi{}^\dagger = \mathcal{Z}(\phi)|u\rangle\langle v| + \ldots \tag{A.56}$$

where $\widehat{A}_\phi$ is the propagator for the pulse sequence element A, with phase ϕ, and $\mathcal{Z}(\phi)$ is a complex number, called the *coherence transfer amplitude*.

The magnitude of $\mathcal{Z}$ indicates how efficiently the coherence $|r\rangle\langle s|$ is converted into the coherence $|u\rangle\langle v|$ by the pulse sequence element A.

The coherence transfer amplitude $\mathcal{Z}$ is easily evaluated by multiplying Equation A.56 on the left by $\langle u|$ and on the right by $|v\rangle$. By using the orthogonality of the spin eigenfunctions, we get

$$\mathcal{Z}(\phi) = \langle u|\widehat{A}_\phi|r\rangle\langle s|\widehat{A}_\phi{}^\dagger|v\rangle$$

This equation relates the coherence transfer amplitude to the product of two operator matrix elements.

A.11.3 Coherence orders and phase shifts

We now examine how the coherence transfer amplitude $\mathcal{Z}$ depends on the phase of the element A.

The propagator for the element A depends on the phase as follows:

$$\widehat{A}_\phi = \widehat{R}_z(\phi)\widehat{A}_0\widehat{R}_z(-\phi)$$

where $\widehat{R}_z(\phi)$ is the operator for a rotation by ϕ around the z-axis. It follows that the coherence transfer amplitude depends on the phase of A through

$$\mathcal{Z}(\phi) = \langle u|\widehat{R}_z(\phi)\widehat{A}_0\widehat{R}_z(-\phi)|r\rangle\ \langle s|\widehat{R}_z(\phi)\widehat{A}_0{}^\dagger\widehat{R}_z(-\phi)|v\rangle \tag{A.57}$$

In high magnetic field, all four spin states $|r\rangle$, $|s\rangle$, $|u\rangle$ and $|v\rangle$ are eigenstates of the total angular momentum along the z-axis:

$$\hat{I}_z|r\rangle = M_r|r\rangle \qquad \hat{I}_z|s\rangle = M_s|s\rangle$$

$$\hat{I}_z|u\rangle = M_u|u\rangle \qquad \hat{I}_z|v\rangle = M_v|v\rangle$$

where M_r, M_s, M_u and M_v are the Zeeman quantum numbers of the states.

Since the rotation operator $\widehat{R}_z(-\phi)$ is equal to $\exp\{+\mathrm{i}\phi\hat{I}_z\}$, the results in Section 6.5 may be used to give

$$\begin{aligned}\widehat{R}_z(-\phi)|r\rangle &= \exp\{+\mathrm{i}M_r\phi\}|r\rangle\\ \widehat{R}_z(-\phi)|v\rangle &= \exp\{+\mathrm{i}M_u\phi\}|v\rangle\end{aligned}$$

Similarly:

$$\begin{aligned}\langle s|\widehat{R}_z(\phi) &= \langle s|\exp\{-\mathrm{i}M_s\phi\}\\ \langle u|\widehat{R}_z(\phi) &= \langle u|\exp\{-\mathrm{i}M_u\phi\}\end{aligned}$$

These equations may be substituted into Equation A.57 to get

$$\mathcal{Z}(\phi) = \langle u|\widehat{A}_0|r\rangle\,\langle s|\widehat{A}_0{}^{\dagger}|v\rangle\,\exp\{\mathrm{i}(-M_u + M_r - M_s + M_v)\phi\}$$

which may be written as

$$\mathcal{Z}(\phi) = \mathcal{Z}(0)\exp\{-\mathrm{i}(p_{uv} - p_{rs})\phi\}$$

where $p_{uv} = M_u - M_v$ is the order of coherence $|u\rangle\langle v|$ and $p_{rs} = M_r - M_s$ is the order of coherence $|r\rangle\langle s|$.

The quantity $p_{uv} - p_{rs}$ corresponds to the *change in coherence order*. If the change in order is denoted Δp, we get the important equation

$$\boxed{\mathcal{Z}(\phi) = \mathcal{Z}(0)\exp\{-\mathrm{i}\phi\,\Delta p\} \qquad \text{(A.58)}}$$

This indicates that changing the phase of a pulse sequence element multiplies each coherence transfer amplitude by a complex exponential factor. The phase of the exponential factor is proportional to the phase of the pulse multiplied by the change in coherence order Δp.

In the example above, $p_{rs} = +2$ and $p_{uv} = -1$, so the change in coherence order is $\Delta p = -3$. If the phase of the pulse is changed by ϕ, the phase of the amplitude for the process $|r\rangle\langle s| \Rightarrow |u\rangle\langle v|$ changes by 3ϕ.

A.11.4 The pathway phase

Consider a particular signal pathway, such as the following example:

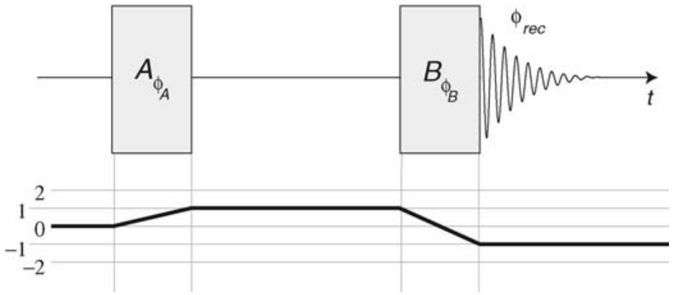

Figure A.17
An example of a coherence transfer pathway.

The first pulse sequence block A has phase ϕ_{A}, and the second block B has phase ϕ_{B}. The signal is detected and digitized using a receiver phase ϕ_{rec}.

The pathway is characterized by a shift in coherence order $\Delta p_{\mathrm{A}} = +1$ over the first block (the order increases from 0 to +1), and by a shift in coherence order $\Delta p_{\mathrm{B}} = -2$ over the second block (the order decreases from +1 to −1).

Suppose that an experiment is conducted with some value for the phases ϕ_A, ϕ_B and ϕ_{rec}. The NMR signal is the sum of contributions from many pathways, including the one shown. We may write this as

$$s(t; \phi_A, \phi_B, \phi_{rec}) = \sum_{\text{path}} s_{\text{path}}(t; \phi_A, \phi_B, \phi_{rec})$$

where the sum is taken over all possible signal pathways.

Now suppose that a 'reference' experiment is conducted, in which all phases ϕ_A, ϕ_B and ϕ_{rec} are equal to zero. The signal in the reference experiment is given by

$$s(t; 0, 0, 0) = \sum_{\text{path}} s_{\text{path}}(t; 0, 0, 0)$$

From Equation A.58, the signal contributions from each pathway have a simple relationship in the two experiments: They are related through

$$s_{\text{path}}(t; \phi_A, \phi_B, \phi_{rec}) = s_{\text{path}}(t; 0, 0, 0) \exp\{-i\Phi_{\text{path}}\}$$

where Φ_{path} is the *total pathway phase*, given by

$$\boxed{\Phi_{\text{path}} = \Delta p_A \phi_A + \Delta p_B \phi_B + \phi_{rec}} \tag{A.59}$$

In the example above, the changes in coherence order are $\Delta p_A = +1$ and $\Delta p_B = -2$, so the total pathway phase is

$$\Phi_{\text{path}} = +\phi_A - 2\phi_B + \phi_{rec}$$

A.11.5 A sum theorem

Before proceeding, we require the following result.

Consider the following sum of n terms:

$$S = 1 + x + x^2 + x^3 + \ldots + x^{(\mathfrak{n}-2)} + x^{(\mathfrak{n}-1)} \tag{A.60}$$

where

$$x = \exp\{i\frac{2\pi\mathfrak{p}}{\mathfrak{n}}\} \tag{A.61}$$

and $\mathfrak{p}$ and $\mathfrak{n}$ are integers.

This sum has the following property:

$$\boxed{S = \begin{cases} 0 \text{ if } \mathfrak{p} \neq \mathfrak{n} \times \text{integer} \\ \mathfrak{n} \text{ if } \mathfrak{p} = \mathfrak{n} \times \text{integer} \end{cases}} \tag{A.62}$$

The theorem Equation A.62 may be proved in the following way. Multiply Equation A.60 by x on both sides:

$$Sx = x + x^2 + x^3 + \ldots + x^{(\mathfrak{n}-1)} + x^{\mathfrak{n}} \tag{A.63}$$

Now from the definition of x (Equation A.61), we have

$$x^{\mathfrak{n}} = \exp\{i2\pi\mathfrak{p}\} = 1$$

since $\mathfrak{p}$ is an integer. Hence Equation A.63 becomes

$$\begin{aligned} Sx &= x + x^2 + x^3 + \ldots + x^{(\mathfrak{n}-1)} + 1 \\ &= 1 + x + x^2 + x^3 + \ldots + x^{(\mathfrak{n}-1)} \end{aligned} \tag{A.64}$$

The right-hand sides of Equations A.64 and A.60 are equal. Hence, we have

$$Sx = S$$

which may be written as

$$S(x-1) = 0$$

Take the case that x is not equal to 1, so that $x - 1 \neq 0$. In this case, the sum S must vanish in order to satisfy the equality. If, on the other hand, x is equal to 1, then the sum S need not vanish, and the definition in Equation A.60 leads to the value $S = \mathfrak{n}$. We have, therefore, derived the following property of the sum S:

$$S = \begin{cases} 0 \text{ if } x \neq 1 \\ \mathfrak{n} \text{ if } x = 1 \end{cases}$$

Now from Equation A.61, x is only equal to 1 if $\mathfrak{p}$ is equal to an integer multiple of $\mathfrak{n}$. This proves the theorem Equation A.62.

A.11.6 Pathway selection I

The above theorem may be used to design a simple phase cycle. Suppose that NMR signals are added together with the phases being cycled according to the following four-step table ($\mathfrak{n} = 4$).

Cycle counter $\mathfrak{m}$	ϕ_A	ϕ_B	ϕ_{rec}
0	0	0	0
1	$\pi/2$	0	0
2	π	0	0
3	$3\pi/2$	0	0

(A.65)

The total number of transients $\mathfrak{N}$ is a multiple of 4. The phase cycle counter $\mathfrak{m}$ is given by $\mathfrak{m} = \text{mod}(\mathfrak{M}, 4)$, where the transient counter is $\mathfrak{M} = 0, 1, 2 \ldots \mathfrak{N} - 1$. The phase table is read from top to bottom again and again, adding together the NMR signals, until all $\mathfrak{N}$ transients have been acquired. This simple phase cycle is generated by the formulae

$$\begin{aligned} \phi_A &= \frac{2\pi}{4}\mathfrak{m} \\ \phi_B &= 0 \\ \phi_{rec} &= 0 \end{aligned}$$

In this and the following formulae, all phases are taken modulo 2π. For example, the following phases are all equivalent: $\{\ldots - 3\pi/2, \pi/2, 5\pi/2, 9\pi/2 \ldots\}$. All of these equivalent phases are denoted as $\pi/2$ in the phase tables (sometimes, the computer software *requires* that phases are specified in the range 0 to 2π).

The signal component from a given coherence transfer pathway, at step $\mathfrak{m}$ in the phase cycle, is given by

$$s_{\text{path}}(t, \mathfrak{m}) = s_{\text{path}}(t, 0) \exp\{-i\Phi_{\text{path}}(\mathfrak{m})\}$$

where the pathway phase is equal to

$$\Phi_{\text{path}} = \Delta p_{\text{A}}\phi_{\text{A}} + \Delta p_{\text{B}}\phi_{\text{B}} + \phi_{\text{rec}}$$

In the present case, all phases are equal to zero except to ϕ_{A}. The pathway phase is therefore

$$\begin{aligned}\Phi_{\text{path}} &= \Delta p_{\text{A}}\phi_{\text{A}} \\ &= \frac{2\pi}{4}\Delta p_{\text{A}}\mathfrak{m}\end{aligned}$$

The *total* signal from a certain pathway, summed over all four steps in the phase cycle, is therefore

$$s^{\text{tot}}_{\text{path}}(t) = \sum_{\mathfrak{m}=0}^{3} s_{\text{path}}(t, \mathfrak{m}) = s_{\text{path}}(t, 0) \sum_{\mathfrak{m}=0}^{3} \exp\{-\text{i}\frac{2\pi\Delta p_{\text{A}}\mathfrak{m}}{4}\}$$

The sum on the right-hand side has the form of Equation A.62. The phase-cycled signal from a given pathway is therefore given by

$$s^{\text{tot}}_{\text{path}}(t) = \begin{cases} 0 & \text{if } \Delta p_{\text{A}} \neq 4 \times \text{integer} \\ 4s_{\text{path}}(t, 0) & \text{if } \Delta p_{\text{A}} = 4 \times \text{integer} \end{cases} \tag{A.66}$$

The phase-cycled pathway signal vanishes unless the change in order Δp_{A} *is an integer multiple of four (including zero).*

Since the coherence order before the first pulse is equal to zero, selection of the change in order Δp_{A} is the same as selecting the coherence order p after the first pulse sequence block A. The phase cycle in Equation A.65, therefore, allows signals passing through coherence orders $p = 0, \pm4, \pm8\ldots$ between the pulse sequence blocks. If one disregards coherences with orders $|p| > 4$, then the allowed signal pathways are as follows:

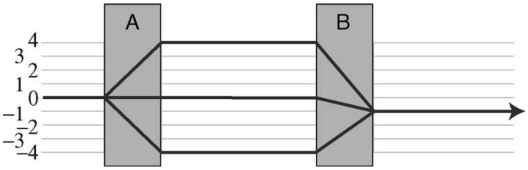

Figure A.18
Allowed signal pathways for Equation A.65.

Signals passing through all other pathways are suppressed:

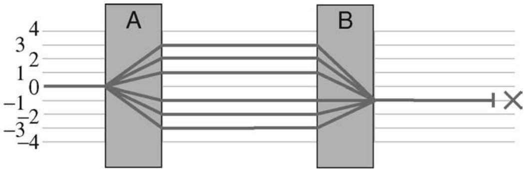

Figure A.19
Forbidden signal pathways for Equation A.65.

Note that the allowed pathways are separated in order by 4 units. This is a direct consequence of using four steps in the phase cycle.

A.11.7 Pathway selection II

Now suppose that one wants to detect signals passing through the following pathway:

$$0 \rightarrow +1 \rightarrow -1$$

while suppressing signals from neighbouring pathways.

Consider first the four-step phase cycle of Equation A.65. The table below shows the total phase Φ_{path} for the pathway $0 \to +1 \to -1$ at each step in the phase cycle, as specified from Equation A.59:

Cycle counter $\mathfrak{m}$	ϕ_A	ϕ_B	ϕ_{rec}	$\Phi_{\text{path}}(0 \to +1 \to -1)$
0	0	0	0	0
1	$\pi/2$	0	0	$\pi/2$
2	π	0	0	π
3	$3\pi/2$	0	0	$3\pi/2$

(A.67)

Since the total pathway phase varies from one step in the phase cycle to the next, the signals from the desired pathway $0 \to +1 \to -1$ cancel out exactly, under the phase cycle of Equation A.65, as predicted in Equation A.66.

Now suppose that the receiver phase ϕ_{rec} is changed in synchrony with the phase ϕ_A, in order to keep Φ_{path} constant for the desired pathway $0 \to +1 \to -1$. This may be done by setting the receiver phase equal to minus the last column in Equation A.67, providing

Cycle counter $\mathfrak{m}$	ϕ_A	ϕ_B	ϕ_{rec}	$\Phi_{\text{path}}(0 \to +1 \to -1)$
0	0	0	0	0
1	$\pi/2$	0	$-\pi/2$	0
2	π	0	$-\pi$	0
3	$3\pi/2$	0	$-3\pi/2$	0

The total pathway phase Φ_{path} is now equal to zero for all steps $\mathfrak{m}$, for the desired pathway $0 \to +1 \to -1$.

Phases may be converted into the interval 0 to 2π by the procedure $\phi \Rightarrow \text{mod}(\phi, 2\pi)$. We get the following table:

Cycle counter $\mathfrak{m}$	ϕ_A	ϕ_B	ϕ_{rec}
0	0	0	0
1	$\pi/2$	0	$3\pi/2$
2	π	0	π
3	$3\pi/2$	0	$\pi/2$

(A.68)

The phase cycle in Equation A.68 has $\Phi_{\text{path}} = 0$ for the pathway $0 \to +1 \to -1$, ensuring that signals passing through this pathway interfere constructively as the signals are accumulated.

Since ϕ_A is cycled in four steps, the phase cycle in Equation A.68 selects not only signals with Δp_A, but all signals obeying $\Delta p_A = +1 + 4 \times \text{integer}$, i.e. $\Delta p_A = \ldots -7, -3, +1, +5 \ldots$. If one disregards coherences with orders $|p| > 4$, then the allowed signal pathways are as follows:

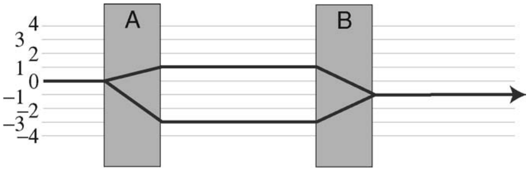

Figure A.20 Allowed signal pathways for Equation A.68.

Signals passing through all other pathways are suppressed:

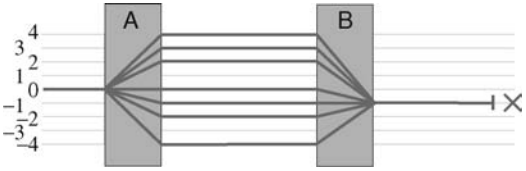

Figure A.21
Forbidden signal pathways for Equation A.68.

The four-step phase cycle in Equation A.68 again selects coherence orders in steps of four, but the motion of ϕ_{rec} in synchrony with ϕ_{A} shifts the centre position of the selection from order 0 to order +1.

It is often convenient to derive an explicit algorithm for calculating the phases. The total phase for the pathway $0 \rightarrow +1 \rightarrow -1$ is given by

$$\Phi_{\text{path}} = \Delta p_{\text{A}}\phi_{\text{A}} + \Delta p_{\text{B}}\phi_{\text{B}} + \phi_{\text{rec}} = +\phi_{\text{A}} - 2\phi_{\text{B}} + \phi_{\text{rec}} \tag{A.69}$$

since the pathway has $\Delta p_{\text{A}} = +1$ and $\Delta p_{\text{B}} = -2$. A constant pathway phase $\Phi_{\text{path}} = 0$ may, therefore, be imposed by using a receiver phase that satisfies the following equation:

$$\phi_{\text{rec}} = -\phi_{\text{A}} + 2\phi_{\text{B}} \tag{A.70}$$

The pulse phases in the phase cycle of Equation A.68 obey the following equations:

$$\begin{aligned} \phi_{\text{A}} &= \frac{2\pi}{4}\mathfrak{m} \\ \phi_{\text{B}} &= 0 \end{aligned} \tag{A.71}$$

This may be combined with Equation A.71 to give the following formula for the receiver phase:

$$\phi_{\text{rec}} = -\frac{2\pi}{4}\mathfrak{m} = -\frac{\pi}{2}\mathfrak{m}$$

This example illustrates a general principle for constructing phase cycles:

1. Identify the coherence transfer pathway of the *desirable* NMR signals.

2. Design the number of steps in the cycle according to the number of *neighbouring* signal pathways that must be suppressed.

3. Adjust the receiver phase on each step of the cycle to impose a constant total pathway phase Φ_{path} for the desired pathway.

A.11.8 Pathway selection III

A completely equivalent result may be obtained by cycling the phase ϕ_{B} of the second pulse sequence block B. If the phase cycle is constructed according to

$$\begin{aligned} \phi_{\text{A}}(\mathfrak{m}) &= 0 \\ \phi_{\text{B}}(\mathfrak{m}) &= \frac{2\pi\mathfrak{m}}{4} \end{aligned}$$

and the receiver phase is again adjusted to satisfy Equation A.70, then we get

$$\phi_{\text{rec}} = 2\frac{2\pi\mathfrak{m}}{4} = \pi\mathfrak{m}$$

This leads to the following $\mathfrak{n} = 4$ phase cycle:

Cycle counter $\mathfrak{m}$	ϕ_A	ϕ_B	ϕ_{rec}
0	0	0	0
1	0	$\pi/2$	π
2	0	π	0
3	0	$3\pi/2$	π

(A.72)

which has an identical effect to that in Equation A.68. Both cycles select the signal pathways in Figure A.20 and reject the signal pathways in Figure A.21.

A.11.9 Selection of a single pathway I

Suppose one is interested in selecting the *single* coherence transfer pathway $0 \to -3 \to -1$. The cycles given in Equations A.68 and A.72 do allow signals from this pathway, but they also allow signals from the pathway $0 \to +1 \to -1$.

In order to suppress signals from more coherence pathways, it is necessary to use more steps in the phase cycle. It is possible to select signals from the pathway $0 \to -3 \to -1$, at the same time as suppressing signals from all other pathways involving four-quantum coherences or lower, by using $\mathfrak{n} \geq 8$. A suitable phase cycle is

Cycle counter $\mathfrak{m}$	ϕ_A	ϕ_B	ϕ_{rec}
0	0	0	0
1	0	$\pi/4$	$3\pi/2$
2	0	$2\pi/4$	π
3	0	$3\pi/4$	$\pi/2$
4	0	$4\pi/4$	0
5	0	$5\pi/4$	$3\pi/2$
6	0	$6\pi/4$	π
7	0	$7\pi/4$	$\pi/2$

(A.73)

This eight-step cycle requires that the number of transients $\mathfrak{N}$ is a multiple of 8.

Since eight steps are used for ϕ_B, this cycle allows signal pathways with $\Delta p_A = -3 + 8 \times \text{integer}$. If one disregards coherences with order larger than 4, only a single signal pathway is selected:

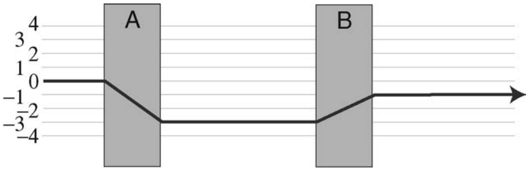

Figure A.22 Allowed signal pathway for Equation A.73.

All other signal pathways are suppressed:

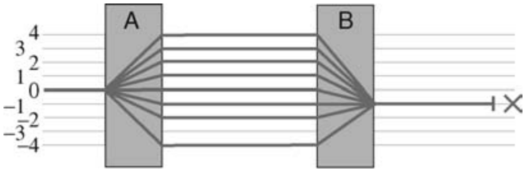

Figure A.23
Forbidden signal pathways for Equation A.73.

The phase cycle in Equation A.73 may be calculated in the systematic way developed above:

1. Identify $0 \to -3 \to -1$ as the desired signal pathway.
2. This pathway is characterized by $\Delta p_A = -3$ and $\Delta p_B = +2$. The pathway phase is therefore given by

$$\begin{aligned}\Phi_{\text{path}} &= \Delta p_A \phi_A + \Delta p_B \phi_B + \phi_{\text{rec}} \\ &= -3\phi_A + 2\phi_B + \phi_{\text{rec}}\end{aligned}$$

3. In order to suppress all other pathways with orders in the range $-5 < p < 5$, one requires at least eight phase cycle steps either for ϕ_A or ϕ_B (one can easily see this using Figure A.23: the seven orders $p = -2, -1 \ldots 3, 4$ must be suppressed between blocks A and B) . If one chooses to cycle ϕ_B, then the pulse phase definitions are

$$\begin{aligned}\phi_A &= 0 \\ \phi_B &= \frac{2\pi}{8}\mathfrak{m} = \frac{\pi}{4}\mathfrak{m}\end{aligned}$$

4. On each step of the phase cycle, adjust the receiver phase so as to hold the total pathway phase for $0 \to -3 \to -1$ equal to zero. This requires

$$\Phi_{\text{path}} = -3\phi_A + 2\phi_B + \phi_{\text{rec}} = 0$$

and hence

$$\phi_{\text{rec}} = 3\phi_A - 2\phi_B \tag{A.74}$$

leading to

$$\phi_{\text{rec}} = -2\frac{\pi}{4}\mathfrak{m} = -\frac{\pi}{2}\mathfrak{m}$$

This corresponds to the phase cycle given in Equation A.73 (after converting all phases into the range 0 to 2π).

A.11.10 Selection of a single pathway II

In the example above, suppose that we choose to cycle ϕ_A instead of ϕ_B. This time the definition of the pulse phases would be

$$\begin{aligned}\phi_A &= \frac{2\pi}{8}\mathfrak{m} = \frac{\pi}{4}\mathfrak{m} \\ \phi_B &= 0\end{aligned}$$

Equation A.74 then leads to

$$\phi_{\text{rec}} = \frac{3\pi}{4}\mathfrak{m}$$

The phase cycle is therefore

Cycle counter $\mathfrak{m}$	ϕ_A	ϕ_B	ϕ_{rec}
0	0	0	0
1	$\pi/4$	0	$3\pi/4$
2	$2\pi/4$	0	$3\pi/2$
3	$3\pi/4$	0	$\pi/4$
4	$4\pi/4$	0	π
5	$5\pi/4$	0	$7\pi/4$
6	$6\pi/4$	0	$\pi/2$
7	$7\pi/4$	0	$5\pi/4$

(A.75)

This cycle has the same effect as that in Equation A.73.

On older NMR instruments, it may be easier to implement Equation A.73 (which employs receiver phase-shifts in multiples of $\pi/2$) than Equation A.75 (which employs smaller receiver phase shift values). This example shows that, although some phase cycles are fully equivalent mathematically, certain cycles may be more difficult to implement than others, because of hardware limitations.

A.11.11 Dual pathway selection

Suppose that it is desired to select signals arising from *two* different pathways, e.g. $0 \rightarrow +1 \rightarrow -1$ and $0 \rightarrow -1 \rightarrow -1$:

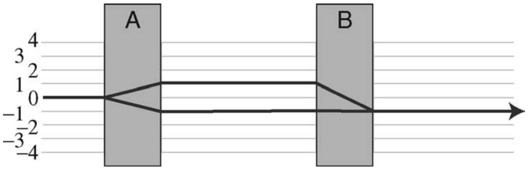

Figure A.24
Two coherence transfer pathways.

Such *dual pathway selection* is necessary for pure absorption two-dimensional spectroscopy using the States procedure (see Section 5.9.4). The two pathways given above are precisely those needed to obtain pure absorption COSY spectra (Section 16.1).

Selection of two pathways at the same time is accomplished by setting the number of steps in the cycle equal to the order separation between the two desired pathways. In the case above, this separation is equal to 2, so a two-step phase cycle is appropriate. The required phase cycle is a very simple one:

Cycle counter $\mathfrak{m}$	ϕ_A	ϕ_B	ϕ_{rec}
0	0	0	0
1	π	0	π

(A.76)

The phase cycle may be calculated formally by choosing one of the desired pathways (it doesn't matter which one), and following the systematic procedure given above. The pulse phase definitions are

$$\phi_A(\mathfrak{m}) = \frac{2\pi\mathfrak{m}}{2} = \pi\mathfrak{m}$$
$$\phi_B(\mathfrak{m}) = 0$$

The receiver phase may be worked out using the pathway 0 → −1 → −1 (which has $\Delta p_A = -1$ and $\Delta p_B = 0$) as follows:

$$\begin{aligned}\Phi_{\text{path}} &= \Delta p_A \phi_A + \Delta p_B \phi_B + \phi_{\text{rec}} \\ &= -\phi_A + \phi_{\text{rec}}\end{aligned}$$

Setting $\Phi_{\text{path}} = 0$ leads to the following relationship:

$$\phi_{\text{rec}} = \phi_A$$

and hence

$$\phi_{\text{rec}} = \pi\mathfrak{m}$$

as specified in Equation A.76.

As might be expected, this two-step phase cycle is not very selective. The following signal pathways are allowed:

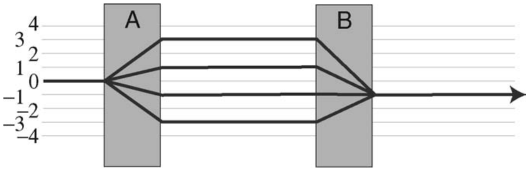

Figure A.25 Allowed signal pathways for Equation A.76.

while the following pathways are suppressed:

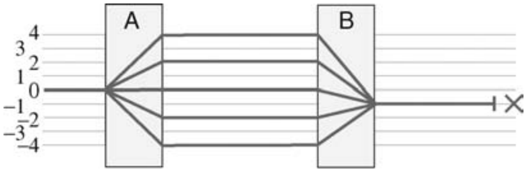

Figure A.26 Forbidden signal pathways for Equation A.76.

In particular, signals from the pathways 0 → ±3 → −1 are allowed as well as the desired signals from 0 → ±1 → −1.

It is not possible to select *only* the desired pair of pathways 0 → ±1 → −1 while suppressing all others, using this particular approach to phase cycling. If necessary, this selection task may be accomplished by more sophisticated data-processing procedures[5] or by employing field gradient selection (see Appendix A.12).

A.11.12 Internal phases I

In general, each pulse sequence block may itself consist of many r.f. pulses, possibly with different phases. Phase cycling works properly only if the *relative* pulse phases *within* each block are rigorously conserved throughout the phase cycle.

For example, consider the four-step phase cycle in Equation A.68, and suppose that block A consists of a $(\pi/2)_x$ pulse and a $(\pi/2)_y$ pulse separated by a delay, while block B consists of a $(\pi/2)_{\bar{y}}$ pulse. This may be visualized as follows:

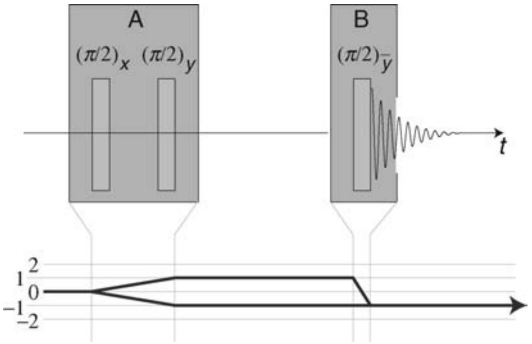

Figure A.27
Three pulses in two phase cycling blocks.

The phases of the pulses are related to those of the blocks as follows:

$$\phi_1 = \phi_A$$
$$\phi_2 = \phi_A + \pi/2$$
$$\phi_3 = \phi_A + 3\pi/2$$

These relationships must be rigorously followed if the phase cycle is to work properly.

For example, the phase cycle given in Equation A.76 takes the following form for this three-pulse sequence:

Cycle counter $\mathfrak{m}$	ϕ_1	ϕ_2	ϕ_3	ϕ_{rec}
0	0	$\pi/2$	$3\pi/2$	0
1	π	$3\pi/2$	$3\pi/2$	π

(A.77)

The phase cycle determines which types of signal are allowed and which are suppressed. *The phase cycle does not determine the magnitude or phase of the allowed signals*. Those parameters depend on the internal phases of the pulses within each block, and must be determined using the detailed reasoning given in this book.

Note that a pulse sequence block may contain a single phase-shifted pulse, as for the third pulse in Figure A.27.

A.11.13 Internal phases II

Consider the INADEQUATE pulse sequence, as discussed in Section 16.2. The pulse sequence and coherence transfer pathway diagram may be interpreted in terms of two blocks as follows:

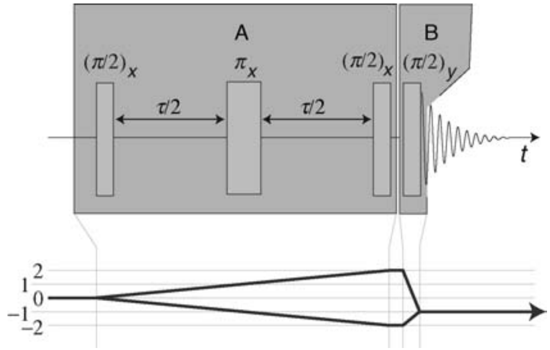

Figure A.28
INADEQUATE pulse sequence formulated as two blocks.

The first three pulses convert populations into (±2)-quantum coherences, and the last pulse converts the (±2)-quantum coherences into observable (−1)-quantum coherences.

The relationship between the four pulse phases and the two block phases is as follows:

$$\phi_1 = \phi_A \qquad \phi_2 = \phi_A$$
$$\phi_3 = \phi_A \qquad \phi_4 = \phi_B + \pi/2 \tag{A.78}$$

A four-step phase cycle for selecting the dual pathways $0 \to +2 \to -1$ and $0 \to -2 \to -1$ may be calculated using the arguments above:

Cycle counter $\mathfrak{m}$	ϕ_A	ϕ_B	ϕ_{rec}
0	0	0	0
1	0	$\pi/2$	$3\pi/2$
2	0	π	π
3	0	$3\pi/2$	$\pi/2$

(A.79)

An explicit phase cycle for this experiment is therefore

Cycle counter $\mathfrak{m}$	ϕ_1	ϕ_2	ϕ_3	ϕ_4	ϕ_{rec}
0	0	0	0	$\pi/2$	0
1	0	0	0	π	$3\pi/2$
2	0	0	0	$3\pi/2$	π
3	0	0	0	0	$\pi/2$

(A.80)

This phase cycle was used in Section 16.2.

Note that the phase of the last pulse starts at $\pi/2$. This has no bearing on the operation of the phase cycle, which only concerns *changes* in the relative phases of the pulse sequence blocks. The initial value of ϕ_4 is decided by external arguments. In the case of Equation A.80, the initial value $\phi_4 = \pi/2$ causes the spin-pair peaks to be in absorption mode, as discussed in Section 16.2.

A.11.14 Nested phase cycles I

Sometimes more than one stage of coherence transfer pathway selection is required in a pulse sequence. Consider, for example, the pulse sequence for double-quantum-filtered COSY, shown below:

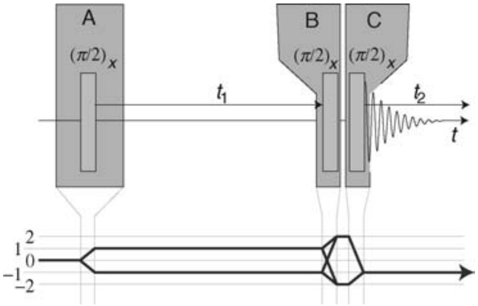

Figure A.29 Double-quantum-filtered COSY pulse sequence formulated as three blocks.

The indicated coherence transfer pathways may be selected by suppressing all signal paths that do not involve coherence order steps $\Delta p_A = \pm 1$ over the first block A, as well as those that do not involve coherence order steps $\Delta p_C = +1$ or -3 over the third block C.

The selection of coherence order steps $\Delta p_A = \pm 1$ implies that the block phase ϕ_A must be cycled in two steps. The selection of coherence order steps $\Delta p_C = +1$ or -3 implies that the block phase ϕ_C must be cycled in four steps. In order to select signal pathways with the desired values for both Δp_A and Δp_C, the phase cycles for blocks A and C are *nested*. This means that, for every step in the cycle of block A, a complete cycle of block C is performed. This leads to a full cycle consisting of 2 × 4 = 8 steps.

The mathematical function floor(x) proves to be useful for specifying nested phase cycles. The function floor(x) returns the largest integer that is not greater than x. It 'rounds down' the argument x to the next integer. Some examples are: floor(0.9) = 0; floor(1) = 1; floor(1.9) = 1; floor(−1.9) = −2.

A two-step phase cycle for ϕ_A, nested inside a four-step cycle for ϕ_C, may be specified as follows:

$$\phi_A = \frac{2\pi \mathfrak{m}}{2} = \pi \mathfrak{m}$$

$$\phi_B = 0$$

$$\phi_C = \frac{2\pi}{4}\text{floor}(\mathfrak{m}/2) = \frac{\pi}{2}\text{floor}(\mathfrak{m}/2)$$

The following table shows how the floor function generates the nested cycles:

Cycle counter $\mathfrak{m}$	floor($\mathfrak{m}/2$)	ϕ_A	ϕ_B	ϕ_C
0	0	0	0	0
1	0	π	0	0
2	1	0	0	$\pi/2$
3	1	π	0	$\pi/2$
4	2	0	0	π
5	2	π	0	π
6	3	0	0	$3\pi/2$
7	3	π	0	$3\pi/2$

The value of ϕ_{rec} may be calculated for each step of the phase cycle by keeping the total phase for one of the desired pathways constant (once again, it doesn't matter which of the desired pathways one selects). For example, the pathway $0 \rightarrow +1 \rightarrow +2 \rightarrow -1$ has the following changes in coherence order: $\Delta p_{\mathrm{A}} + 1$; $\Delta p_{\mathrm{B}} = +1$; $\Delta p_{\mathrm{C}} = -3$, which leads to the following condition:

$$\begin{aligned}\Phi_{\mathrm{path}} &= \Delta p_{\mathrm{A}}\phi_{\mathrm{A}} + \Delta p_{\mathrm{B}}\phi_{\mathrm{B}} + \Delta p_{\mathrm{C}}\phi_{\mathrm{C}} + \phi_{\mathrm{rec}} \\ &= +\pi\mathfrak{m} - \frac{3\pi}{2}\mathrm{floor}(\mathfrak{m}/2) + \phi_{\mathrm{rec}} \\ &= 0\end{aligned}$$

The receiver phase is therefore given by

$$\phi_{\mathrm{rec}} = -\pi\mathfrak{m} + \frac{3\pi}{2}\mathrm{floor}(\mathfrak{m}/2)$$

which leads to the following eight-step phase cycle:

Cycle counter $\mathfrak{m}$	ϕ_1	ϕ_2	ϕ_3	ϕ_{rec}
0	0	0	0	0
1	π	0	0	π
2	0	0	$\pi/2$	$3\pi/2$
3	π	0	$\pi/2$	$\pi/2$
4	0	0	π	π
5	π	0	π	0
6	0	0	$3\pi/2$	$\pi/2$
7	π	0	$3\pi/2$	$3\pi/2$

A.11.15 Nested phase cycles II

The nesting algorithm may be extended to any number of phase cycling steps. Suppose, for example, that a pulse sequence consists of four blocks, A, B, C and D, and that one wishes to select the steps in coherence order at blocks A, B and D. A nested phase cycle is constructed in which block A is cycled in $\mathfrak{n}_{\mathrm{A}}$ steps, block B is cycled in $\mathfrak{n}_{\mathrm{B}}$ steps, and block D is cycled in $\mathfrak{n}_D$ steps. The following algorithm does the trick:

$$\begin{aligned}\phi_{\mathrm{A}} &= \frac{2\pi}{\mathfrak{n}_{\mathrm{A}}}\mathfrak{m} \\ \phi_{\mathrm{B}} &= \frac{2\pi}{\mathfrak{n}_{\mathrm{B}}}\mathrm{floor}(\frac{\mathfrak{m}}{\mathfrak{n}_{\mathrm{A}}}) \\ \phi_{\mathrm{C}} &= 0 \\ \phi_{\mathrm{D}} &= \frac{2\pi}{\mathfrak{n}_{\mathrm{D}}}\mathrm{floor}(\frac{\mathfrak{m}}{\mathfrak{n}_{\mathrm{A}}\mathfrak{n}_{\mathrm{B}}})\end{aligned}$$

Note how the floor functions always act on the cycle counter $\mathfrak{m}$ divided by the total number of steps for all *previous* levels. For example, the specification for ϕ_{B} contains $\mathrm{floor}(\mathfrak{m}/\mathfrak{n}_{\mathrm{A}})$, while the specification for ϕ_{D} contains $\mathrm{floor}(\mathfrak{m}/\mathfrak{n}_{\mathrm{A}}\mathfrak{n}_{\mathrm{B}})$.

The total number of steps in such a nested phase cycle is $\mathfrak{n} = \mathfrak{n}_{\mathrm{A}}\mathfrak{n}_{\mathrm{B}}\mathfrak{n}_{\mathrm{D}}$.

The following table shows how the nesting works for the case $n_{\mathrm{A}} = 2$, $n_{\mathrm{B}} = 2$ and $n_{\mathrm{D}} = 4$:

Cycle counter m	floor($m/2$)	floor($m/4$)	ϕ_{A}	ϕ_{B}	ϕ_{C}	ϕ_{D}
0	0	0	0	0	0	0
1	0	0	π	0	0	0
2	1	0	0	π	0	0
3	1	0	π	π	0	0
4	0	1	0	0	0	$\pi/2$
5	0	1	π	0	0	$\pi/2$
6	1	1	0	π	0	$\pi/2$
7	1	1	π	π	0	$\pi/2$
8	0	2	0	0	0	π
9	0	2	π	0	0	π
10	1	2	0	π	0	π
11	1	2	π	π	0	π
12	0	3	0	0	0	$3\pi/2$
13	0	3	π	0	0	$3\pi/2$
14	1	3	0	π	0	$3\pi/2$
15	1	3	π	π	0	$3\pi/2$

At each step, the receiver phase ϕ_{rec} may be calculated so as to give a total phase of zero for any one of the desired signal pathways.

As an example, consider a more sophisticated version of the INADEQUATE phase cycle, in which the first two pulses are cycled independently, as well as the last pulse:

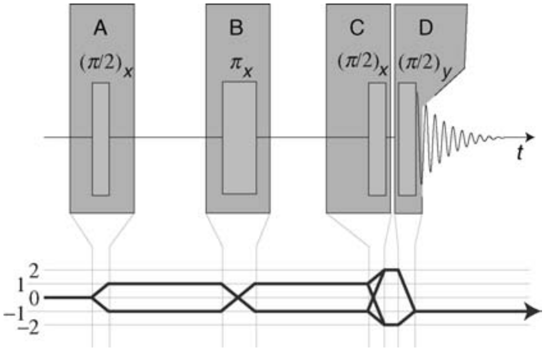

Figure A.30
INADEQUATE pulse sequence formulated as four blocks.

The pulse phases are related to the phases of the blocks through

$$\begin{aligned}\phi_1 &= \phi_A\\ \phi_2 &= \phi_B\\ \phi_3 &= \phi_C\\ \phi_4 &= \phi_D + \pi/2\end{aligned} \tag{A.81}$$

The phase of the first block ϕ_A is cycled in $\mathfrak{n}_A = 2$ steps (in order to select $\Delta p_A = \pm 1$); the phase of the second block ϕ_B is cycled in $\mathfrak{n}_B = 4$ steps (in order to select $\Delta p_B = \pm 2$); the phase of the fourth block ϕ_D is cycled in $\mathfrak{n}_D = 4$ steps (in order to select $\Delta p_D = +1$ and -3). The algorithm for the pulse phases is therefore

$$\begin{aligned}\phi_A(\mathfrak{m}) &= \frac{2\pi}{\mathfrak{n}_A}\mathfrak{m} = \pi\mathfrak{m}\\ \phi_B(\mathfrak{m}) &= \frac{2\pi}{\mathfrak{n}_B}\text{floor}(\frac{\mathfrak{m}}{\mathfrak{n}_A}) = \frac{\pi}{2}\text{floor}(\frac{\mathfrak{m}}{2})\\ \phi_C(\mathfrak{m}) &= 0\\ \phi_D(\mathfrak{m}) &= \frac{2\pi}{\mathfrak{n}_D}\text{floor}(\frac{\mathfrak{m}}{\mathfrak{n}_A\mathfrak{n}_B}) = \frac{\pi}{2}\text{floor}(\frac{\mathfrak{m}}{8})\end{aligned} \tag{A.82}$$

The total number of steps in this phase cycle is $\mathfrak{n} = \mathfrak{n}_A\mathfrak{n}_B\mathfrak{n}_D = 32$.

For each step in the phase cycle, the receiver phase may be calculated using the total phase equation for any one of desired pathways, e.g. $0 \rightarrow +1 \rightarrow -1 \rightarrow -2 \rightarrow -1$, which has $\Delta p_A = +1$, $\Delta p_B = -2$, $\Delta p_C = -1$, $\Delta p_D = +1$:

$$\begin{aligned}\Phi_{\text{path}} &= \Delta p_A\phi_A + \Delta p_B\phi_B + \Delta p_C\phi_C + \Delta p_D\phi_D + \phi_{\text{rec}}\\ &= +\pi\mathfrak{m} - \pi\text{floor}(\frac{\mathfrak{m}}{2}) + \frac{\pi}{2}\text{floor}(\frac{\mathfrak{m}}{8}) + \phi_{\text{rec}}\\ &= 0\end{aligned}$$

The algorithm for the receiver phase is therefore

$$\phi_{\text{rec}} = -\pi\mathfrak{m} + \pi\text{floor}(\frac{\mathfrak{m}}{2}) - \frac{\pi}{2}\text{floor}(\frac{\mathfrak{m}}{8}) \tag{A.83}$$

The explicit 32-step phase cycle is shown in Table A.1.

Whenever possible, it is best to allow the computer software to calculate the phases using an algorithm of the form given above, rather than by using laborious and error-prone phase tables. Unfortunately, pulse-programming software on commercial NMR instruments does not yet facilitate a rational approach.

Table A.1 A 32-step phase cycle for INADEQUATE.

Cycle counter $\mathfrak{m}$	ϕ_A	ϕ_B	ϕ_C	ϕ_D	ϕ_{rec}
0	0	0	0	$\pi/2$	0
1	π	0	0	$\pi/2$	π
2	0	$\pi/2$	0	$\pi/2$	π
3	π	$\pi/2$	0	$\pi/2$	0
4	0	π	0	$\pi/2$	0
5	π	π	0	$\pi/2$	π
6	0	$3\pi/2$	0	$\pi/2$	π
7	π	$3\pi/2$	0	$\pi/2$	0
8	0	0	0	π	$3\pi/2$
9	π	0	0	π	$\pi/2$
10	0	$\pi/2$	0	π	$\pi/2$
11	π	$\pi/2$	0	π	$3\pi/2$
12	0	π	0	π	$3\pi/2$
13	π	π	0	π	$\pi/2$
14	0	$3\pi/2$	0	π	$\pi/2$
15	π	$3\pi/2$	0	π	$3\pi/2$
16	0	0	0	$3\pi/2$	π
17	π	0	0	$3\pi/2$	0
18	0	$\pi/2$	0	$3\pi/2$	0
19	π	$\pi/2$	0	$3\pi/2$	π
20	0	π	0	$3\pi/2$	π
21	π	π	0	$3\pi/2$	0
22	0	$3\pi/2$	0	$3\pi/2$	0
23	π	$3\pi/2$	0	$3\pi/2$	π
24	0	0	0	0	$\pi/2$
25	π	0	0	0	$3\pi/2$
26	0	$\pi/2$	0	0	$3\pi/2$
27	π	$\pi/2$	0	0	$\pi/2$
28	0	π	0	0	$\pi/2$
29	π	π	0	0	$3\pi/2$
30	0	$3\pi/2$	0	0	$3\pi/2$
31	π	$3\pi/2$	0	0	$\pi/2$

A.11.16 Different ways of constructing phase cycles

Nested phase cycling may readily be extended to any number of coherence order selection steps. However, the number of required phase-cycle increments increases very rapidly with the number of selection steps. The nested approach usually becomes impractical for more than four or five selection steps. In certain cases, alternative strategies, such as *cogwheel phase cycling*, are far more economical with instrument time. The basic principle in cogwheel phase cycling is to advance all available phases at the same time in a concerted manner, like a set of interlocking cogs. In some cases, cogwheel phase cycling is orders of magnitude more efficient than nested phase cycling. More details are given in *Further Reading*.

The required number of phase-cycle steps may also be greatly reduced by combining phase cycling with field gradient selection (see below).

A.12 Coherence Selection by Pulsed Field Gradients

Phase cycling requires numerous repetitions of an entire pulse sequence, with a different set of r.f. phases. This is associated with several problems:

1. The repetition of near-identical experiments is very inefficient with respect to experimental time.
2. Phase cycling makes high demands on instrumental performance, since the degree of destructive interference between consecutive signal acquisitions depends on the instrumental stability.
3. Irreproducibility in the initial condition of the spin system, due to imperfect thermal equilibration between transients, or temperature fluctuations, also degrades the performance of phase cycling.

Pulsed field gradients may be used to accomplish many of the same pathway selection tasks as phase cycling, while avoiding many of these problems. In essence, the use of field gradient pulses allows the different phase cycle steps to be performed in parallel in different parts of the sample volume, with a great advantage of speed. In addition, undesired signals from unwanted coherence transfer pathways destructively interfere over the entire sample volume, i.e. during the signal induction process itself, and not in the post-processing stage in the computer. The demands of instrumental reproducibility are therefore greatly reduced.

Nevertheless, field gradient selection does have some restrictions and technical difficulties of its own.

A.12.1 Field gradient dephasing

Consider a time-dependent field gradient $G_z(t)$ along the z-axis, applied to a homonuclear spin system between time points t_a and t_b:

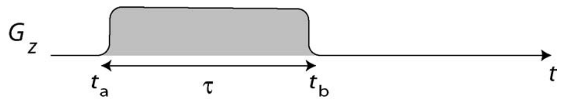

Figure A.31
A pulsed field gradient pulse.

During the pulse, the magnetic field is supplemented by a spatially dependent field $zG_z(t)$, where z is the spatial coordinate along the z-axis. The rotating-frame spin Hamiltonian during the field gradient pulse is given by

$$\widehat{\mathcal{H}}^0(\mathbf{r}, t) = \widehat{\mathcal{H}}_{\text{int}} + \widehat{\mathcal{H}}_G(\mathbf{r}, t) \tag{A.84}$$

where

$$\widehat{\mathcal{H}}_G(\mathbf{r}, t) = \omega_G(\mathbf{r}, t)\hat{I}_z$$

and the field-gradient-induced Larmor frequency shift is

$$\omega_{\text{G}}(\mathbf{r}, t) = -\gamma G_z(t) z$$

Crucially, the two terms in Equation A.84 commute, assuming the secular approximation for the internal spin Hamiltonian. This allows the spin system propagator to be factored into two commuting terms:

$$\widehat{U}(t_b, t_a) = \widehat{U}_{\text{int}}(t_b, t_a)\widehat{U}_G(t_b, t_a) \tag{A.85}$$

where the propagator under the field gradient pulse is

$$\widehat{U}_G(t_b, t_a) = \widehat{R}_z(\Phi_{\text{G}}(\mathbf{r})) \tag{A.86}$$

and the spatially dependent rotation angle is

$$\Phi_{\text{G}}(\mathbf{r}) = \int_{t_a}^{t_b} \omega_G(\mathbf{r}, t)\mathrm{d}t \tag{A.87}$$

Since the two terms in Equation A.85 commute, they may be considered independently. The propagator $\widehat{U}_{\text{int}}$ under the internal Hamiltonian may, therefore, be ignored for the moment, since it acts in just the same way as it does in the absence of the field gradient. One should simply remember that the internal spin interactions continue to act during the entire interval τ.

As shown in Equation A.86, the field gradient pulse induces a spatially dependent rotation around the z-axis, through the angle Φ_{G}. The effect on a Hamiltonian eigenstate is as follows:

$$\widehat{R}_z(\Phi_{\text{G}}(\mathbf{r}))|r\rangle = \exp\{\mathrm{i}M_r\Phi_{\text{G}}(\mathbf{r})\}|r\rangle$$

where M_r is the total Zeeman quantum number of the state

$$\hat{I}_z|r\rangle = M_r|r\rangle$$

The effect of the field gradient pulse on a spin coherence ρ_{rs} is therefore

$$\rho_{rs}(t_b) = \rho_{rs}(t_a)\exp\{\mathrm{i}p_{rs}\Phi_{\text{G}}(\mathbf{r})\}$$

where p_{rs} is the coherence order. This shows that the phase of a coherence p_{rs} is rotated by the field-gradient pulse, through the angle $p_{rs}\Phi_{\text{G}}(\mathbf{r})$. The phase rotation angle of the coherence is therefore proportional to

1. the coherence order p_{rs};
2. the amplitude of the gradient G_z, integrated over time (see Equation A.87);
3. the spatial coordinate z;
4. the gyromagnetic ratio γ.

After the field gradient pulse the phase of the coherence is given by

$$\phi_{rs}(\mathbf{r}) = \frac{2\pi z}{\Lambda_{rs}}$$

where Λ_{rs} is given by

$$\Lambda_{rs} = -2\pi \Big/ \left(p_{rs}\int_{t_a}^{t_b} \gamma B_z(t)\mathrm{d}t\right)$$

The phase of the coherence after the pulse, therefore, forms a helix with respect to the spatial coordinate z. The wavelength of the helix is given by Λ_{rs}:

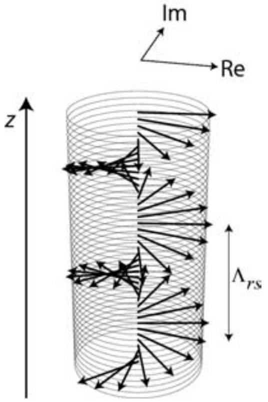

Figure A.32
Helix of phases for a coherence ρ_{rs} after a field gradient pulse.

The higher the coherence order p_{rs}, and the more powerful the gradient pulse, the shorter the wavelength Λ_{rs}.

If the wavelength Λ_{rs} is small compared with the length of the sample along the z-axis, the coherence ρ_{rs} dephases completely under the field gradient pulse. Any NMR signal that derives from this coherence vanishes, when integrated over the sample volume.

A.12.2 Pathway phase

Consider, now, a pulse sequence segment in which two field gradient pulses of different lengths and strengths bracket a pulse sequence block A. We follow a coherence transfer pathway involving order p_1 before the pulse and p_2 after the pulse:

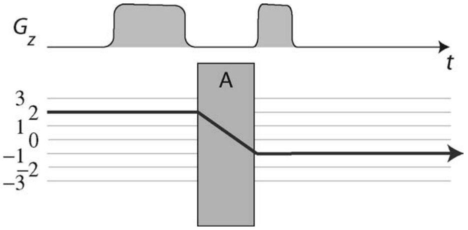

Figure A.33
Two pulsed field gradient pulses and a pulse sequence block.

The phase for the pathway $p_1 \to p_2$ is the equal to the accumulated phase for the two coherence orders:

$$\Phi_{p_1 \to p_2}(\mathbf{r}) = \frac{2\pi z}{\Lambda_{p_1 \to p_2}}$$

where the helix wavelength is given by

$$\Lambda_{p_1 \to p_2} = -2\pi \Big/ \left(p_1 \int_{t_{a1}}^{t_{b1}} \gamma B_z(t)\mathrm{d}t + p_2 \int_{t_{a2}}^{t_{b2}} \gamma B_z(t)\mathrm{d}t \right)$$

Here $\{t_{a1}, t_{b1}\}$ and $\{t_{a2}, t_{b2}\}$ are the start and end time points of the two field gradient pulses.

As before, if the helix wavelength $\Lambda_{p_1 \to p_2}$ is small compared with the sample length, all signals deriving from the pathway $p_1 \to p_2$ vanish when integrated over the sample volume.

A.12.3 Coherence transfer echoes

The wavelength of the phase helix for any coherence transfer pathway may be adjusted by varying the field gradient strengths or time profiles. If the wavelength $\Lambda_{p_1 \to p_2}$ becomes larger than the sample dimensions, then the defocusing effect is reversed and a *coherence transfer echo* is formed.

For example, suppose that the two field gradient pulses have an equal integral over time:

$$\int_{t_{a1}}^{t_{b1}} B_z(t)\mathrm{d}t = \int_{t_{a2}}^{t_{b2}} B_z(t)\,\mathrm{d}t$$

In this case, a coherence transfer echo is formed for pathways with the relationship

$$p_1 = -p_2$$

This condition includes the ordinary Hahn echo ((+1) → (−1)).

Consider the case where the field gradient pulses are instead adjusted so that the first one has twice the integral of the second one:

$$\int_{t_{a1}}^{t_{b1}} B_z(t)\mathrm{d}t = 2\int_{t_{a2}}^{t_{b2}} B_z(t)\,\mathrm{d}t$$

The coherence transfer echo is formed under the following condition:

$$p_2 = -2p_1$$

The echo pathways now involve double-quantum coherences, e.g. (+1) → (−2) and (−1) → (+2).

A.12.4 Pathway selection

Signals from individual coherence transfer pathways may therefore be selected by adjusting the strengths and time profiles of the field gradient pulses so as to form a coherence transfer echo for the desired pathway, while winding tight phase helices for the undesired pathways. If the helix winding is sufficiently tight, then the signals from all unwanted pathways average to zero over the sample volume, leaving only the echo signal from the desired pathway. All of this may be achieved in a single transient.

It is often difficult to engineer the selection of more than one coherence transfer pathway at the same time using pulsed field gradients. Since at least two pathways are often required in, for example, pure-absorption two-dimensional experiments, it is common to combine field gradient selection with a short phase cycle.

If two or more pathways are required to generate the NMR signal, then the experiment must often be repeated with a different field gradient scheme in order to acquire the signals from complementary pathways independently. In such cases, field gradients lead to a loss in signal-to-noise, since some desirable signal is inevitably destroyed in each experiment.

A.12.5 Heteronuclear coherence transfer echoes

When pulsed field gradients are used for coherence transfer pathway selection in *heteronuclear* systems, one must take into account the different gyromagnetic ratios for the two species. Consider, for example, the case where an echo is formed by transferring coherences of order p_I of a spin species I to coherences of order p_S of a different spin species S. The condition for the formation of the echo in this case is as follows:

$$\gamma_I p_I \int_{t_{a1}}^{t_{b1}} B_z(t)\,\mathrm{d}t + \gamma_S p_S \int_{t_{a2}}^{t_{b2}} B_z(t)\,\mathrm{d}t = 0$$

For example, a (−1)-quantum coherence ^{1}H coherence forms an echo with a (+1)-quantum coherence ^{13}C coherence if the gradient pulse under which the ^{13}C coherence evolves has roughly four times the integral of the ^{1}H gradient pulse.

A.13 Bloch Equations

The isolated spins-1/2 ensemble may be treated using the magnetization vector, as described in Section 11.5. The motion of the magnetization vector during short strong r.f. pulses is described in Section 11.6, and the motion of the magnetization vector during intervals between pulses is described in Section 11.9. Relaxation and the resonance offset are taken into account between pulses, but not during the pulses.

If a pulse is weak or long then these results are not applicable, since off-resonance effects and relaxation are significant in this case. The *Bloch equations* provide a general framework for treating the simultaneous effects of relaxation, r.f. fields, and resonance offset for the isolated spin-1/2 ensemble.

The Bloch equations are a set of three coupled differential equations for the components of the magnetization vector. They may be written as follows:

$$\frac{\mathrm{d}}{\mathrm{d}t}\begin{pmatrix} M_x \\ M_y \\ M_z \end{pmatrix} = \begin{pmatrix} 0 & -\Omega^0 & \omega_{\mathrm{nut}}\sin\phi \\ \Omega^0 & 0 & -\omega_{\mathrm{nut}}\cos\phi \\ -\omega_{\mathrm{nut}}\sin\phi & \omega_{\mathrm{nut}}\cos\phi & 0 \end{pmatrix}\begin{pmatrix} M_x \\ M_y \\ M_z \end{pmatrix} - \begin{pmatrix} T_2{}^{-1}M_x \\ T_2{}^{-1}M_y \\ T_1{}^{-1}(M_z-1) \end{pmatrix} \tag{A.88}$$

where Ω^0 is the resonance offset, ω_{nut} is the nutation frequency of the pulse, and ϕ is the phase of the r.f. field. Equation A.88 employs the definition of the magnetization vector given in Section 11.5, so that the thermal equilibrium value of the z-magnetization is $M_z = 1$.

It is readily shown that Equation A.88 leads to the behaviour described in Section 11.6, if the resonance offset Ω^0 and the relaxation rate constants $T_1{}^{-1}$ and $T_2{}^{-1}$ are all set to zero. Equation A.88 also leads to the behaviour described in Section 11.9, if the nutation frequency ω_{nut} is set to zero.

The Bloch equations are also capable of treating the complicated dynamics of spins that experience r.f. fields and relaxation at the same time. For example, suppose that an on-resonance r.f. field is applied for a very long time. What is the final value of the transverse magnetization?

The problem is complicated, because there are conflicting forces that create and destroy transverse magnetization. Transverse relaxation continually destroys transverse magnetization; so, at long times, one may expect that the transverse magnetization should be zero. However, at the same time, spin–lattice relaxation continously generates longitudinal magnetization, which is rotated into the transverse plane by the r.f. field. At a sufficiently long time, the system settles down into a *steady state*, under which these two tendencies are balanced.

The Bloch equations allow the steady-state value of the transverse magnetization to be predicted easily. If the phase ϕ and resonance offset Ω^0 are both equal to zero, then the equations for the time derivatives of the magnetization components M_y and M_z are

$$\frac{\mathrm{d}}{\mathrm{d}t}M_y = -T_2{}^{-1}M_y - \omega_{\mathrm{nut}}M_z$$

$$\frac{\mathrm{d}}{\mathrm{d}t}M_z = \omega_{\mathrm{nut}}M_y - T_1{}^{-1}(M_z - 1)$$

In the steady state, both time derivatives vanish, which allows one to solve for the two magnetization components:

$$\begin{aligned} M_y(\text{steady state}) &= -\frac{T_2\omega_{\text{nut}}}{1+T_1T_2\omega_{\text{nut}}^2} \\ M_z(\text{steady state}) &= \frac{1}{1+T_1T_2\omega_{\text{nut}}^2} \end{aligned} \tag{A.89}$$

This shows that steady-state magnetization can exist, as long as T_2 is not too short and the nutation frequency ω_{nut} is not too large. However, if the nutation frequency ω_{nut} is strong compared with the relaxation rate constants, then the spin magnetization is destroyed in the steady state. This is called *saturation*.

Before 1966, most chemical applications of NMR were performed using *continuous-wave* spectrometers, which relied on the detection of the steady-state transverse magnetization, as a function of the static magnetic field. The Bloch equations lost their central place in NMR theory when the continuous-wave method was displaced by the Fourier transform technique, which is much more versatile and sensitive.

A.14 Chemical Exchange

In this appendix, I discuss the theory of spin dynamics in the presence of symmetrical two-site exchange, as used for the calculation of lineshapes in Section 19.5 and for the calculation of the two-dimensional exchange spectrum in Section 19.7.

Consider a symmetrical two-site exchange of the form:

$$A \underset{k}{\overset{k}{\rightleftharpoons}} B$$

where the species A and B have equal probability. The rate constants k are equal to the transition probability per unit time between the two species, and are the same for the forward and backward reaction.

The definition of the spin density operator, as given in Section 11.1, is

$$\hat{\rho} = \overline{|\psi\rangle\langle\psi|}$$

where the overbar indicates the average over all spin systems in the sample. If the sample contains $\mathbb{N}_{\text{A}}$ molecules of type A and $\mathbb{N}_{\text{B}}$ molecules of type B, then the density operator may be written as

$$\hat{\rho} = \frac{\mathbb{N}_{\text{A}}}{\mathbb{N}}\hat{\rho}^A + \frac{\mathbb{N}_{\text{B}}}{\mathbb{N}}\hat{\rho}^B$$

where the total number of molecules is $\mathbb{N} = \mathbb{N}_{\text{A}} + \mathbb{N}_{\text{B}}$. The density operator of spins in molecules A is given by

$$\hat{\rho}^A = \overline{|\psi\rangle\langle\psi|}^A$$

where the overbar indicates averaging over all molecules of type A. Similarly, the density operator of spins in molecules B is given by

$$\hat{\rho}^B = \overline{|\psi\rangle\langle\psi|}^B$$

where the overbar indicates averaging over all molecules of type B.

In the case of isolated spins-1/2, each density operator term may be written in terms of two populations and two coherences, which are defined in the usual way:

$$\begin{aligned} \rho^{\text{A}}_{\boxed{\alpha}} &= \overline{\langle\alpha|\psi\rangle\langle\psi|\alpha\rangle}^A \\ \rho^{\text{A}}_{\boxed{+}} &= \overline{\langle\alpha|\psi\rangle\langle\psi|\beta\rangle}^A \end{aligned}$$

$$\rho^{\mathrm{B}}_{\boxed{-}} = \overline{\langle\beta|\psi\rangle\langle\psi|\alpha\rangle}^{B}$$

and so on.

We need to develop a dynamic equation for the four populations and four coherences, under the influence of the spin Hamiltonian, as well as the chemical exchange process. The behaviour of the spins under the spin Hamiltonian is called *coherent dynamics*, since the spin Hamiltonian is the same for all molecules of a certain type. The exchange behaviour is termed *incoherent dynamics*, since the precise instant at which each molecule changes state is unpredictable.

A.14.1 The incoherent dynamics

Consider first *only* the exchange process, omitting the magnetic fields and other interactions. Consider the term $\rho^{\mathrm{A}}_{\boxed{\alpha}}$, which represents the population of state $|\alpha\rangle$, averaging over the $\mathbb{N}_{\mathrm{A}}$ molecules that are in state A. Imagine the fate of this population during a small interval of time $\mathrm{d}t$.

On average, $k\mathbb{N}_{\mathrm{A}}\mathrm{d}t$ molecules change state from A to B in an interval $\mathrm{d}t$, carrying their spins with them. The contribution to $\rho^{\mathrm{A}}_{\boxed{\alpha}}$ from these spins will therefore be lost. However, at the same time, the population $\rho^{\mathrm{A}}_{\boxed{\alpha}}$ receives an influx from the $k\mathbb{N}_{\mathrm{B}}\mathrm{d}t$ spins that change their state in the opposite direction, from B to A. These spins carry their population $\rho^{\mathrm{B}}_{\boxed{\alpha}}$ with them.

If one assumes that the spin states do not change under the exchange process (which is a good approximation if the jumps are very fast), then the equation of motion for the population $\rho^{\mathrm{A}}_{\boxed{\alpha}}$, taking into account only the exchange process, is

$$\frac{\mathrm{d}}{\mathrm{d}t}\rho^{\mathrm{A}}_{\boxed{\alpha}} = -k\rho^{\mathrm{A}}_{\boxed{\alpha}} + k\rho^{\mathrm{B}}_{\boxed{\alpha}} \qquad \text{(exchange only)}$$

Similarly, the equation of motion for $\rho^{\mathrm{B}}_{\boxed{\alpha}}$, taking into account only the exchange process, is

$$\frac{\mathrm{d}}{\mathrm{d}t}\rho^{\mathrm{B}}_{\boxed{\alpha}} = -k\rho^{\mathrm{B}}_{\boxed{\alpha}} + k\rho^{\mathrm{A}}_{\boxed{\alpha}} \qquad \text{(exchange only)}$$

These equations may be combined to obtain

$$\frac{\mathrm{d}}{\mathrm{d}t}\begin{pmatrix}\rho^{\mathrm{A}}_{\boxed{\alpha}} \\ \rho^{\mathrm{B}}_{\boxed{\alpha}}\end{pmatrix} = \begin{pmatrix}-k & +k \\ +k & -k\end{pmatrix}\begin{pmatrix}\rho^{\mathrm{A}}_{\boxed{\alpha}} \\ \rho^{\mathrm{B}}_{\boxed{\alpha}}\end{pmatrix} \qquad \text{(exchange only)}$$

An equivalent equation is obtained for each component of the density operator. For example, for the (−1)-quantum coherences we get

$$\frac{\mathrm{d}}{\mathrm{d}t}\begin{pmatrix}\rho^{\mathrm{A}}_{\boxed{-}} \\ \rho^{\mathrm{B}}_{\boxed{-}}\end{pmatrix} = \begin{pmatrix}-k & +k \\ +k & -k\end{pmatrix}\begin{pmatrix}\rho^{\mathrm{A}}_{\boxed{-}} \\ \rho^{\mathrm{B}}_{\boxed{-}}\end{pmatrix} \qquad \text{(exchange only)} \qquad \text{(A.90)}$$

These equations assume that the chemical exchange is a *Markow process*, implying that the probability of a jump during a small interval $\mathrm{d}t$ is independent of the previous history of the molecule. In practice, this is a good approximation for chemical reactions.

A.14.2 The coherent dynamics

The spins also evolve under their spin interactions. For example, if exchange were absent, then the rotating-frame (−1)-quantum coherences of spins in molecules of type A evolve according to

$$\rho^{\mathrm{A}}_{\boxed{-}}(t_b) = \rho^{\mathrm{A}}_{\boxed{-}}(t_a)\exp\{(\mathrm{i}\Omega^0_A - \lambda)\tau\} \qquad \text{(no exchange)}$$

where τ is the interval between time points t_a and t_b, and λ is the natural decay rate constant. This equation may be differentiated to obtain

$$\frac{\mathrm{d}}{\mathrm{d}t}\rho^{\mathrm{A}}_{\boxminus} = (\mathrm{i}\Omega^0_A - \lambda)\rho^{\mathrm{A}}_{\boxminus} \qquad \text{(no exchange)}$$

The analogous equation for the (-1)-quantum coherences of spins in molecules of type B is

$$\frac{\mathrm{d}}{\mathrm{d}t}\rho^{\mathrm{B}}_{\boxminus} = (\mathrm{i}\Omega^0_B - \lambda)\rho^{\mathrm{B}}_{\boxminus} \qquad \text{(no exchange)}$$

These equations may be combined to give

$$\frac{\mathrm{d}}{\mathrm{d}t}\begin{pmatrix}\rho^{\mathrm{A}}_{\boxminus} \\ \rho^{\mathrm{B}}_{\boxminus}\end{pmatrix} = \begin{pmatrix}\mathrm{i}\Omega^0_A - \lambda & 0 \\ 0 & \mathrm{i}\Omega^0_B - \lambda\end{pmatrix}\begin{pmatrix}\rho^{\mathrm{A}}_{\boxminus} \\ \rho^{\mathrm{B}}_{\boxminus}\end{pmatrix} \qquad \text{(no exchange)} \tag{A.91}$$

A.14.3 The spectrum

In practice, exchange and coherent evolution takes place at the same time. This may be taken into account by simply adding Equations A.90 and A.91 together. We get

$$\frac{\mathrm{d}}{\mathrm{d}t}\begin{pmatrix}\rho^{\mathrm{A}}_{\boxminus} \\ \rho^{\mathrm{B}}_{\boxminus}\end{pmatrix} = \mathbf{L}_{\boxminus}\begin{pmatrix}\rho^{\mathrm{A}}_{\boxminus} \\ \rho^{\mathrm{B}}_{\boxminus}\end{pmatrix} \tag{A.92}$$

where the matrix $\mathbf{L}_{\boxminus}$ is equal to

$$\mathbf{L}_{\boxminus} = \begin{pmatrix}\mathrm{i}\Omega^0_A - \lambda - k & +k \\ +k & \mathrm{i}\Omega^0_B - \lambda - k\end{pmatrix}$$

In order to calculate the NMR spectrum, we need to figure out how the (-1)-quantum coherences evolve in time. This is easily done by integrating Equation A.92:

$$\begin{pmatrix}\rho^{\mathrm{A}}_{\boxminus}(t) \\ \rho^{\mathrm{B}}_{\boxminus}(t)\end{pmatrix} = \mathbf{V}_{\boxminus}(t)\begin{pmatrix}\rho^{\mathrm{A}}_{\boxminus}(0) \\ \rho^{\mathrm{B}}_{\boxminus}(0)\end{pmatrix}$$

where the propagator $\mathbf{V}_{\boxminus}$ is given by

$$\mathbf{V}_{\boxminus}(t) = \exp\{\mathbf{L}_{\boxminus}t\}$$

As shown in Section 6.5.8[2] the exponential may be written as follows:

$$\exp\{\mathbf{L}_{\boxminus}t\} = \mathbf{X}_{\boxminus}\exp\{\mathbf{D}_{\boxminus}t\}\mathbf{X}_{\boxminus}^{-1}$$

where $\mathbf{X}_{\boxminus}$ is a matrix whose columns are given by the eigenvectors of $\mathbf{L}_{\boxminus}$, $\mathbf{X}_{\boxminus}^{-1}$ is the inverse of $\mathbf{X}_{\boxminus}$, and $\mathbf{D}_{\boxminus}$ is a diagonal matrix with diagonal elements equal to the eigenvalues of $\mathbf{L}_{\boxminus}$. Evaluation of the eigenvalues and eigenvectors gives the following formulae:

$$\mathbf{D}_{\boxminus} = \begin{pmatrix}d_1 & 0 \\ 0 & d_2\end{pmatrix}$$

$$\mathbf{X}_{\boxminus} = \begin{pmatrix} -\mathrm{i}(2\mathbb{R} + \Omega_\Delta) & \mathrm{i}(2\mathbb{R} - \Omega_\Delta) \\ 2k & 2k \end{pmatrix}$$

$$\mathbf{X}_{\boxminus}{}^{-1} = \frac{1}{8Rk} \begin{pmatrix} 2\mathrm{i}k & 2\mathbb{R} - \Omega_\Delta \\ -2\mathrm{i}k & 2\mathbb{R} + \Omega_\Delta \end{pmatrix}$$

where

$$\begin{aligned} \Omega_\Delta &= \Omega_A^0 - \Omega_B^0 \\ \mathbb{R} &= \sqrt{(\Omega_\Delta/2)^2 - k^2} \end{aligned}$$

and the two eigenvalues are

$$\begin{aligned} d_1 &= \overline{\Omega} - \mathrm{i}\mathbb{R} - k - \lambda \\ d_2 &= \overline{\Omega} + \mathrm{i}\mathbb{R} - k - \lambda \end{aligned}$$

Here, $\overline{\Omega}$ is defined in Equation 19.5 as

$$\overline{\Omega} = \frac{1}{2}(\Omega_A^0 + \Omega_B^0)$$

The complex quantity $\mathbb{R}$ is related to the real quantity R defined in Equation 19.5 as follows:

$$\begin{aligned} \mathbb{R} &= R \qquad \text{if } k < \Omega_\Delta/2 \\ \mathbb{R} &= \mathrm{i}R \qquad \text{if } k \geq \Omega_\Delta/2 \end{aligned}$$

Since $\mathbf{D}_{\boxminus}$ is diagonal, the exponential is given by (see Section 6.5)

$$\exp\{\mathbf{D}_{\boxminus} t\} = \begin{pmatrix} \exp\{d_1 t\} & 0 \\ 0 & \exp\{d_2 t\} \end{pmatrix}$$

If the (-1)-quantum coherences are excited by a $(\pi/2)_x$ pulse, then the initial coherences are

$$\begin{pmatrix} \rho_{\boxminus}^{\mathrm{A}}(0) \\ \rho_{\boxminus}^{\mathrm{B}}(0) \end{pmatrix} = \frac{1}{4\mathrm{i}} \begin{pmatrix} 1 \\ 1 \end{pmatrix}$$

The (-1)-quantum part of the spin density operator at time t is therefore

$$\begin{pmatrix} \rho_{\boxminus}^{\mathrm{A}}(t) \\ \rho_{\boxminus}^{\mathrm{B}}(t) \end{pmatrix} = \frac{1}{4\mathrm{i}} \mathbf{X}_{\boxminus} \exp\{\mathbf{D}_{\boxminus} t\} \mathbf{X}_{\boxminus}{}^{-1} \cdot \begin{pmatrix} 1 \\ 1 \end{pmatrix}$$

The quadrature NMR signal is proportional to the amplitude of the (-1)-quantum coherences, multiplied by 2i (ignoring the receiver and digitizer phase). The time-domain signal may therefore be written as

$$\begin{aligned} s(t) &= (\,2\mathrm{i}\,, \quad 2\mathrm{i}\,) \cdot \begin{pmatrix} \rho_{\boxminus}^{\mathrm{A}}(t) \\ \rho_{\boxminus}^{\mathrm{B}}(t) \end{pmatrix} \\ &= \frac{1}{2}(\,1\,, \quad 1\,) \cdot \mathbf{X}_{\boxminus} \exp\{\mathbf{D}_{\boxminus} t\} \mathbf{X}_{\boxminus}{}^{-1} \cdot \begin{pmatrix} 1 \\ 1 \end{pmatrix} \end{aligned}$$

Since $\mathbf{D}_{\boxed{-}}$ has two eigenvalues, the signal is given by the sum of two exponential decays, and has the form

$$s(t) = \frac{1}{2}(1 + \frac{\mathrm{i}k}{\mathbb{R}}) \exp\{d_1 t\} + \frac{1}{2}(1 - \frac{\mathrm{i}k}{\mathbb{R}}) \exp\{d_2 t\}$$

FT of the signal gives two Lorentzians, as in Equations 19.4 and 19.6.

A.14.4 Longitudinal magnetization exchange

The calculation of longitudinal magnetization exchange must take into account the transitions between state $|\alpha\rangle$ and state $|\beta\rangle$ through spin–lattice relaxation processes, as well as the chemical exchange of molecules.

For example, the population $\rho^{\mathrm{A}}_{\boxed{\alpha}}$ is converted into $\rho^{\mathrm{A}}_{\boxed{\beta}}$ according to the spin–lattice transition probability W (see Section 20.3.6), and is also converted into $\rho^{\mathrm{B}}_{\boxed{\alpha}}$ by the chemical exchange. A suitable dynamic equation for the two pairs of populations is therefore

$$\frac{\mathrm{d}}{\mathrm{d}t}\begin{pmatrix} \rho^{\mathrm{A}}_{\boxed{\alpha}} \\ \rho^{\mathrm{A}}_{\boxed{\beta}} \\ \rho^{\mathrm{B}}_{\boxed{\alpha}} \\ \rho^{\mathrm{B}}_{\boxed{\beta}} \end{pmatrix} = \mathbf{L}_{\mathrm{pop}} \begin{pmatrix} \rho^{\mathrm{A}}_{\boxed{\alpha}} \\ \rho^{\mathrm{A}}_{\boxed{\beta}} \\ \rho^{\mathrm{B}}_{\boxed{\alpha}} \\ \rho^{\mathrm{B}}_{\boxed{\beta}} \end{pmatrix}$$

where

$$\mathbf{L}_{\mathrm{pop}} = \begin{pmatrix} -W-k & W & k & 0 \\ W & -W-k & 0 & k \\ k & 0 & -W-k & W \\ 0 & k & W & -W-k \end{pmatrix}$$

This equation neglects the asymmetry in the upwards and downwards transition probabilities (see Section 20.3.6), and assumes that the spin–lattice relaxation rate constants are the same in the two types of molecule. Since this equation neglects the difference in the upwards and downwards transition probabilities, it does not lead to the correct thermal equilibrium magnetization, but this defect is of no account when applied to the mixing interval of a two-dimensional exchange experiment. The phase cycling anyway removes the signal contribution from the magnetization that has been thermally equilibrated during τ_m.

The z-magnetization components are proportional to the difference in the populations of the $|\alpha\rangle$ and $|\beta\rangle$ states:

$$\begin{aligned} \langle \hat{I}_z \rangle^{\mathrm{A}} &\sim \rho^{\mathrm{A}}_{\boxed{\alpha}} - \rho^{\mathrm{A}}_{\boxed{\beta}} \\ \langle \hat{I}_z \rangle^{\mathrm{B}} &\sim \rho^{\mathrm{B}}_{\boxed{\alpha}} - \rho^{\mathrm{B}}_{\boxed{\beta}} \end{aligned}$$

The differential equation for the Zeeman components is therefore

$$\frac{\mathrm{d}}{\mathrm{d}t}\begin{pmatrix} \langle \hat{I}_z \rangle^{\mathrm{A}} \\ \langle \hat{I}_z \rangle^{\mathrm{B}} \end{pmatrix} = \mathbf{L}_z \begin{pmatrix} \langle \hat{I}_z \rangle^{\mathrm{A}} \\ \langle \hat{I}_z \rangle^{\mathrm{B}} \end{pmatrix} \tag{A.93}$$

where

$$\mathbf{L}_z = \begin{pmatrix} -2W-k & k \\ k & -2W-k \end{pmatrix}$$

The relevant eigenvalue and eigenvector matrices in this case are

$$\mathbf{D}_z = \begin{pmatrix} d_1 & 0 \\ 0 & d_2 \end{pmatrix}$$

$$\mathbf{X}_z = \begin{pmatrix} -1 & 1 \\ 1 & 1 \end{pmatrix}$$

$$\mathbf{X}_z{}^{-1} = \frac{1}{2}\begin{pmatrix} -1 & 1 \\ 1 & 1 \end{pmatrix}$$

where the two eigenvalues are

$$d_1 = -2k - 2W = -2k - T_1{}^{-1}$$
$$d_2 = -2W = -T_1{}^{-1}$$

The amplitude for Zeeman magnetization transfer from molecules A to molecules B is therefore given by

$$a_{\mathrm{A}\to\mathrm{B}}(\tau_m) = (\,0\,, \quad 1\,)\cdot \mathbf{X}_z \exp\{\mathbf{D}_z\tau_m\}\mathbf{X}_z{}^{-1}\cdot \begin{pmatrix} 1 \\ 0 \end{pmatrix}$$

which evaluates to

$$a_{\mathrm{A}\to\mathrm{B}}(\tau_m) = \sinh(k\tau_m)\exp\{-(k+T_1{}^{-1})\tau_m\}$$

Similarly, the amplitude for Zeeman magnetization to remain on the molecules A is

$$a_{\mathrm{A}\to\mathrm{A}}(\tau_m) = (\,1\,, \quad 0\,)\cdot \mathbf{X}_z \exp\{\mathbf{D}_z\tau_m\}\mathbf{X}_z{}^{-1}\cdot \begin{pmatrix} 1 \\ 0 \end{pmatrix}$$

which evaluates to

$$a_{\mathrm{A}\to\mathrm{A}}(\tau_m) = \cosh(k\tau_m)\exp\{-(k+T_1{}^{-1})\tau_m\}$$

The amplitudes of the diagonal peaks in a two-site two-dimensional exchange spectrum are therefore

$$a_{\mathrm{diag}} = a_{\mathrm{A}\to\mathrm{A}} = a_{\mathrm{B}\to\mathrm{B}} = \cosh(k\tau_m)\exp\{-(k+T_1{}^{-1})\tau_m\} \tag{A.94}$$

The amplitudes of the cross-peaks are

$$a_{\mathrm{cross}} = a_{\mathrm{A}\to\mathrm{B}} = a_{\mathrm{B}\to\mathrm{A}} = \sinh(k\tau_m)\exp\{-(k+T_1{}^{-1})\tau_m\} \tag{A.95}$$

as in Equation 19.7.

A.15 Solomon Equations

The relaxation equations for the populations in an ensemble of homonuclear two-spin systems may be cast in the following form:

$$\frac{\mathrm{d}}{\mathrm{d}t}\mathbb{P} = \mathbb{W}_{\mathrm{P}}\mathbb{P}$$

where the population vector is

$$\mathbb{P} = \begin{pmatrix} \rho_{\boxed{\alpha\alpha}} \\ \rho_{\boxed{\alpha\beta}} \\ \rho_{\boxed{\beta\alpha}} \\ \rho_{\boxed{\beta\beta}} \end{pmatrix}$$

and the kinetic matrix for the populations is

$$\mathbb{W}_{\mathrm{P}} = \begin{pmatrix} (-W_{\boxed{\alpha-}} - W_{\boxed{-\alpha}} - W_{\boxed{--}}) & W_{\boxed{\alpha+}} & W_{\boxed{+\alpha}} & W_{\boxed{++}} \\ W_{\boxed{\alpha-}} & (-W_{\boxed{\alpha+}} - W_{\boxed{-+}} - W_{\boxed{-\beta}}) & W_{\boxed{+-}} & W_{\boxed{+\beta}} \\ W_{\boxed{-\alpha}} & W_{\boxed{-+}} & (-W_{\boxed{+\alpha}} - W_{\boxed{+-}} - W_{\boxed{\beta-}}) & W_{\boxed{\beta+}} \\ W_{\boxed{--}} & W_{\boxed{-\beta}} & W_{\boxed{\beta-}} & (-W_{\boxed{++}} - W_{\boxed{+\beta}} - W_{\boxed{\beta+}}) \end{pmatrix}$$

The diagonal elements ensure that the sum of all populations remains constant. The transition probabilities $W_{\boxed{\alpha-}}$, $W_{\boxed{-\alpha}}$ . . . are given in Equation 20.10.

In order to define the state of the ensemble in terms of product operators, introduce the *Zeeman order vector*:

$$\mathbb{Z} = \begin{pmatrix} \langle\widehat{1}\rangle \\ \langle\hat{I}_{1z}\rangle \\ \langle\hat{I}_{2z}\rangle \\ \langle 2\hat{I}_{1z}\hat{I}_{2z}\rangle \end{pmatrix}$$

The vector of populations may be transformed into the Zeeman order vector as follows:

$$\mathbb{Z} = \mathbb{T}_{\mathrm{ZP}}\mathbb{P}$$

where the transformation matrix is

$$\mathbb{T}_{\mathrm{ZP}} = \frac{1}{2}\begin{pmatrix} 1 & 1 & 1 & 1 \\ 1 & 1 & -1 & -1 \\ 1 & -1 & 1 & -1 \\ 1 & -1 & -1 & 1 \end{pmatrix}$$

The kinetic matrix may be transformed between the two bases using

$$\mathbb{W}_{\mathrm{Z}} = \mathbb{T}_{\mathrm{ZP}} \mathbb{W}_{\mathrm{P}} \mathbb{T}_{\mathrm{PZ}}$$

where

$$\mathbb{T}_{\mathrm{PZ}} = \mathbb{T}_{\mathrm{ZP}}{}^{-1} = \mathbb{T}_{\mathrm{ZP}}$$

The result is

$$\mathbb{W}_{\mathrm{Z}} = \begin{pmatrix} 0 & 0 & 0 & 0 \\ \mathbb{B}(W_1 + W_2) & -(W_0 + 2W_1 + W_2) & W_0 - W_2 & \mathbb{B}W_2 \\ \mathbb{B}(W_1 + W_2) & W_0 - W_2 & -(W_0 + 2W_1 + W_2) & \mathbb{B}W_2 \\ 0 & \mathbb{B}W_1 & \mathbb{B}W_1 & -4W_1 \end{pmatrix} \tag{A.96}$$

The equation of motion of the Zeeman order vector $\mathbb{Z}$ is therefore

$$\frac{\mathrm{d}}{\mathrm{d}t}\mathbb{Z} = \mathbb{W}_{\mathrm{Z}}\mathbb{Z} \tag{A.97}$$

The thermal equilibrium value of the Zeeman order vector is defined by

$$\frac{\mathrm{d}}{\mathrm{d}t}\mathbb{Z}_{\mathrm{eq}} = \mathbb{W}_{\mathrm{Z}}\mathbb{Z}_{\mathrm{eq}} = 0$$

and is given by

$$\mathbb{Z}_{\mathrm{eq}} \cong \begin{pmatrix} 1 \\ \frac{1}{2}\mathbb{B} \\ \frac{1}{2}\mathbb{B} \\ 0 \end{pmatrix} \tag{A.98}$$

to first order in the Boltzmann factor $\mathbb{B}$, which is very small. Hence, Equation A.97 may be written as:

$$\frac{\mathrm{d}}{\mathrm{d}t}(\mathbb{Z} - \mathbb{Z}_{\mathrm{eq}}) = \mathbb{W}_{\mathrm{Z}}(\mathbb{Z} - \mathbb{Z}_{\mathrm{eq}}) \tag{A.99}$$

Since the difference vector $\mathbb{Z} - \mathbb{Z}_{\mathrm{eq}}$ has elements that are only of the order of the Boltzmann factor $\mathbb{B}$, it is possible to drop elements of the order $\mathbb{B}$ in the kinetic matrix $\mathbb{W}_{\mathrm{Z}}$, in order to obtain results that are accurate to first order in the Boltzmann factor. The expression Equation A.96, therefore, may be replaced by

$$\mathbb{W}_{\mathrm{Z}} \cong \begin{pmatrix} 0 & 0 & 0 & 0 \\ 0 & -(W_0 + 2W_1 + W_2) & W_0 - W_2 & 0 \\ 0 & W_0 - W_2 & -(W_0 + 2W_1 + W_2) & 0 \\ 0 & 0 & 0 & -4W_1 \end{pmatrix}$$

providing the matrix $\mathbb{W}_Z$ is used in the context of Equation A.99. The block-diagonal form of this matrix allows the central two rows and columns to be extracted, giving

$$\frac{\mathrm{d}}{\mathrm{d}t}\begin{pmatrix}\langle \hat{I}_{1z}\rangle \\ \langle \hat{I}_{2z}\rangle\end{pmatrix} = \begin{pmatrix}-R_{\mathrm{auto}} & R_{\mathrm{cross}} \\ R_{\mathrm{cross}} & -R_{\mathrm{auto}}\end{pmatrix}\begin{pmatrix}\langle \hat{I}_{1z}\rangle - \langle \hat{I}_{1z}\rangle^{\mathrm{eq}} \\ \langle \hat{I}_{2z}\rangle - \langle \hat{I}_{2z}\rangle^{\mathrm{eq}}\end{pmatrix}$$

which are the Solomon equations, with

$$\begin{aligned}R_{\mathrm{auto}} &= W_0 + 2W_1 + W_2 \\ R_{\mathrm{cross}} &= W_0 - W_2\end{aligned}$$

as used in the text.

The treatment given here is readily generalized by allowing pairs of transition probabilities such as $W_{\boxed{-\alpha}}$ and $W_{\boxed{-\beta}}$ to be different, in order to take into account cross-correlation effects (see Section 20.8). This leads to the *generalized Solomon equations*, in which the two-spin order $\langle 2\hat{I}_{1z}\hat{I}_{2z}\rangle$ participates in the dynamic equations together with the one-spin orders $\langle \hat{I}_{1z}\rangle$ and $\langle \hat{I}_{2z}\rangle$ (see *Further Reading*).

A.16 Cross-Relaxation Dynamics

The equation of motion for the magnetization exchange between spins I_1 and I_2 under the mixing interval of a NOESY experiment is given by the simplified Solomon equations (Equation 20.30), in which the thermal equilibrium terms are dropped:

$$\frac{\mathrm{d}}{\mathrm{d}t}\begin{pmatrix}\langle \hat{I}_{1z}\rangle \\ \langle \hat{I}_{2z}\rangle\end{pmatrix} = \mathbf{L}_{\mathrm{Solomon}}\begin{pmatrix}\langle \hat{I}_{1z}\rangle \\ \langle \hat{I}_{2z}\rangle\end{pmatrix}$$

where

$$\mathbf{L}_{\mathrm{Solomon}} = \begin{pmatrix}-R_{\mathrm{auto}} & R_{\mathrm{cross}} \\ R_{\mathrm{cross}} & -R_{\mathrm{auto}}\end{pmatrix}$$

and the auto- and cross-relaxation rate constants are given in Equations 20.16 and 20.17. The situation is precisely analogous to that holding under two-site chemical exchange (Equation A.93), if one makes the following substitutions:

$$\begin{aligned}\langle \hat{I}_z\rangle^{\mathrm{A}} &\Rightarrow \langle \hat{I}_{1z}\rangle & \langle \hat{I}_z\rangle^{\mathrm{B}} &\Rightarrow \langle \hat{I}_{2z}\rangle \\ 2W = T_1{}^{-1} &\Rightarrow R_{\mathrm{auto}} - R_{\mathrm{cross}} & k &\Rightarrow R_{\mathrm{cross}}\end{aligned}$$

The amplitudes for the magnetization transfer processes may therefore be obtained by making the appropriate substitutions in Equations A.94 and A.95:

$$\begin{aligned}a_{1\to 1}(\tau_{\mathrm{m}}) = a_{2\to 2}(\tau_{\mathrm{m}}) &= \cosh(R_{\mathrm{cross}}\tau_{\mathrm{m}})\exp\{-R_{\mathrm{auto}}\tau_{\mathrm{m}}\} \\ a_{1\to 2}(\tau_{\mathrm{m}}) = a_{2\to 1}(\tau_{\mathrm{m}}) &= \sinh(R_{\mathrm{cross}}\tau_{\mathrm{m}})\exp\{-R_{\mathrm{auto}}\tau_{\mathrm{m}}\} \qquad \text{(A.100)}\end{aligned}$$

This result is used in Equations 20.34 and 20.42.

Notes

1. For a different proof of Equation A.9, see C. P. Slichter *Principles of Magnetic Resonance*, 3rd edition, Springer, Berlin, 1989.

2. See, for example, G. Strang, *Linear Algebra and its Applications*, 3rd edition, Harcourt Brace Jovanovich, San Diego, 1988.

3. For a system of N spins-1/2, the operator for a rotation through the angle 2π is given by

   $$\widehat{R}_x(2\pi) = (-1)^N \widehat{1}$$

   The factor of $(-1)^N$ is usually irrelevant, since propagators always act on the spin density operator in pairs (e.g. see Equation 11.27). The product of two $\widehat{R}_x(2\pi)$ propagators is always equal to unity.

4. The coherence transfer pathway technique was described almost simultaneously by A. D. Bain, *J. Magn. Reson.* **56**, 418–427 (1984) and G. Bodenhausen, H. Kogler and R. R. Ernst, *J. Magn. Reson.* **58**, 370–388 (1984).

5. See N. Ivchenko, C. E. Hughes and M. H. Levitt, *J. Magn. Reson.* **160**, 52–58 (2003).

Further Reading

- For a full discussion of the quadrupolar Hamiltonian, see A. Jerschow, *Prog. NMR Spectrosc.* **46**, 63–78 (2005).
- For more on the selection of coherence transfer pathways by phase cycling and pulsed field gradients, see J. Keeler, *Understanding NMR Spectroscopy*, Wiley, Chichester, 2005.
- For cogwheel phase cycling, see: M. H. Levitt, P. K. Madhu and C. E. Hughes, *J. Magn. Reson.* **155**, 300–306 (2002); A. Jerschow and R. Kumar, *J. Magn. Reson.* **160**, 59–64 (2003) and N. Ivchenko, C. E. Hughes and M. H. Levitt, *J. Magn. Reson.* **164**, 286–293 (2003); G. Zuckerstätter and N. Müller, *Concepts in Magn. Reson.*, **30A**, 81–99 (2007).
- For the selection of coherence transfer pathways by pulsed field gradients, see R. E. Hurd, in *Encyclopedia of Nuclear Magnetic Resonance*, D. M. Grant and R. K. Harris (eds) Wiley, 1996, vol. 3, p. 1990, and A. Jerschow and N. Müller, *J. Magn. Reson.*, **134**, 17–29 (1998).
- For the generalized Solomon equations, including cross-correlated relaxation, see C. Dalvit and G. Bodenhausen, *Adv. Magn. Reson.*, **14**, 1 (1990).
- For more theory of NMR in chemically exchanging systems, see A. D. Bain, *Prog. NMR Spectrosc.* **43**, 63–103 (2003).

Appendix B: Symbols and Abbreviations

$\widehat{0}$	null operator
$\widehat{1}$	unity operator
$\widehat{1}_j, \widehat{1}_k$	unity operators for spins I_j and I_k
$\widehat{1}_1, \widehat{1}_2 \ldots$	unity operators for spins $I_1, I_2 \ldots$
①, ②, ③ . . .	time points in a pulse sequence
$\lvert 1\rangle, \lvert 2\rangle \ldots$	energy eigenstates in a coupled spin system
a	complex amplitude
a_ℓ	complex amplitude of signal component s_ℓ
a_j	peak amplitudes for spins j
a_{cross}	amplitude of a cross-peak
a_{diag}	amplitude of a diagonal peak
$a_{1\to 1}, a_{1\to 2} \cdots$	amplitudes for auto-relaxation and cross-relaxation processes in NOESY
$a_{\text{A}\to\text{A}}, a_{\text{A}\to\text{B}} \cdots$	amplitudes for magnetization transfer processes in two-site exchange
$a_{\boxed{-\alpha}}, a_{\boxed{-\beta}} \cdots$	amplitudes of (-1)-quantum coherence signals, in an ensemble of spin-1/2 pairs
$\alpha_{\boxed{-\alpha\alpha}}, \alpha_{\boxed{-\alpha\beta}} \cdots$	amplitudes of signals from coherences $\rho_{\boxed{-\alpha\alpha}}, \rho_{\boxed{-\alpha\beta}} \ldots$ in an ensemble of three-spin-1/2 systems
$a_{\boxed{pq}}$	amplitudes of signal from a coherence of quantum order p and satellite order q in an ensemble of quadrupolar nuclei
a_{rs}	amplitudes of signal from coherence ρ_{rs}
$a^{[\mathfrak{m}]}$	signal amplitude for the pulse sequence corresponding to phase cycle index $\mathfrak{m}$
$a^{[\mathfrak{m}]}_{\boxed{-\beta}}$	signal amplitude from coherence $\rho_{\boxed{-\beta}}$, for phase cycle index $\mathfrak{m}$
$a^{\text{av}}_{\boxed{-\beta}}$	phase-cycled signal amplitude from coherence $\rho_{\boxed{-\beta}}$
a_n	eigenvalues of the operator $\widehat{A}$
α	an Euler angle
α^{BA}	last Euler angle used when transforming the reference axes of frame A into those of frame B
α_{AB}	passive notation for α^{BA}
$\lvert\alpha\rangle$	state of spin-1/2 with angular momentum of $+1/2$ along the z-axis
$\lvert\alpha\alpha\rangle, \lvert\alpha\beta\rangle \ldots$	states of a spin-1/2 pair
$\lvert\alpha\alpha\alpha\rangle, \lvert\alpha\alpha\beta\rangle \ldots$	spin states in an ensemble of three-spin-1/2 systems

---

Spin Dynamics: Basics of Nuclear Magnetic Resonance, Second Edition Malcolm H. Levitt

A	pre-exponential factor in Arrhenius equation
AB	strongly coupled two-spin-1/2 system
AX	weakly coupled two-spin-1/2 system
$\widehat{A}$	arbitrary operator
$\widehat{A}^{\dagger}$	adjoint of operator $\widehat{A}$
$\widehat{A}^{-1}$	inverse of operator $\widehat{A}$
$\widehat{A}^{N}$	Nth power of operator $\widehat{A}$
$\widehat{A}_{\phi}$	propagator for a pulse sequence element A with phase ϕ
$\mathbf{A}$	an arbitrary matrix
$\mathcal{A}$	absorption Lorentzian function
b_{jk}	dipole–dipole coupling constant between spins I_j and I_k
b_{IS}	dipole–dipole coupling constant between spins I and S
B	rotational constant
B^0	magnitude of static (main) magnetic field
B_x, B_y, B_z	Cartesian components of the magnetic field
B^{RF}	magnitude of r.f. magnetic field
B_{RF}	peak value of the r.f. magnetic field
$B_{j,x}^{\mathrm{induced}}$, $B_{j,y}^{\mathrm{induced}}$, $B_{j,z}^{\mathrm{induced}}$	Cartesian components of the induced magnetic field at the site of spin I_j
$\mathbf{B}$	magnetic field
$\mathbf{B}^0$	static field vector
$\mathbf{B}^{\mathrm{tot}}$	total magnetic field
$\mathbf{B}_j^{\mathrm{induced}}$	induced magnetic field at the site of spin I_j
$\mathbf{B}_j^{\mathrm{loc}}$	local magnetic field at the site of spin I_j
$\mathbf{B}_{\mathrm{RF}}$	r.f. field vector
$\mathbf{B}_{\mathrm{non\,res}}^{\mathrm{RF}}$	non-resonant component of the r.f. field vector
$\mathbf{B}_{\mathrm{res}}^{\mathrm{RF}}$	resonant component of the r.f. field vector
$\mathbf{B}_x^{\mathrm{grad}}$	gradient field, corresponding to a variation of field along the z-axis with respect to the x-coordinate
$\mathbf{B}_y^{\mathrm{grad}}$	gradient field, corresponding to a variation of field along the z-axis with respect to the y-coordinate
$\mathbf{B}_z^{\mathrm{grad}}$	gradient field, corresponding to a variation of field along the z-axis with respect to the z-coordinate
$\widehat{B}$	arbitrary operator
$\widehat{B}^0$	secular part of the operator $\widehat{B}$
$\mathbb{B}$	Boltzmann factor
$\mathbb{B}_I$, $\mathbb{B}_S$	Boltzmann factors for spin species I and S
β	an Euler angle
β^{BA}	second Euler angle used when transforming the reference axes of frame A into those of frame B
β_{AB}	passive notation for β^{BA}
β_{p}	flip angle of r.f. pulse
$\beta_{\mathrm{p}}^{\mathrm{C}}$	central transition flip angle
$(\beta_{\mathrm{p}})_{\phi_p}$	r.f. pulse with flip angle β_{p} and phase ϕ_{p}
$(\beta_{\mathrm{p}})_{x}$	r.f. pulse with flip angle β_{p} and phase $\phi_{\mathrm{p}} = 0$
$(\beta_{\mathrm{p}})_{\overline{x}}$	r.f. pulse with flip angle β_{p} and phase $\phi_{\mathrm{p}} = \pi$
$(\beta_{\mathrm{p}})_{y}$	r.f. pulse with flip angle β_{p} and phase $\phi_{\mathrm{p}} = \pi/2$
$(\beta_{\mathrm{p}})_{\overline{y}}$	r.f. pulse with flip angle β_{p} and phase $\phi_{\mathrm{p}} = 3\pi/2$

$\lvert\beta\rangle$	state of spin-1/2 with angular momentum of $-1/2$ along the z-axis
cosh	hyperbolic cosine $\cosh x = \frac{1}{2}(\mathrm{e}^{x} + \mathrm{e}^{-x})$
COSY	COrrelation SpectroscopY, a simple form of two-dimensional spectroscopy useful for mapping coherence transfer processes and assigning peaks
c_r	superposition coefficient of state $\lvert r\rangle$
c_α, c_β	superposition coefficients for one spin-1/2
$c_{\alpha\alpha}, c_{\alpha\beta} \ldots$	superposition coefficients for a spin-1/2 pair
C_{M}	value of matching capacitor
C_{T}	value of tuning capacitor
C_{Q}	quadrupolar coupling
$\widehat{C}$	arbitrary operator
$\mathbb{C}$	electric charge density
$\mathbb{C}^{(0)}, \mathbb{C}^{(1)} \ldots$	multipole components of the nuclear electric charge density
Da	Dalton, a unit of molecular mass; the mass of one ^{12}C atom is 12 Da
d_{IS}	secular dipole–dipole coupling between spins I and S
d_{jk}	secular dipole–dipole coupling between spins I_j and I_k
D_x	diffusion coefficient in the x-direction
$\widehat{D}_x$	operator for the first derivative with respect to x
$\widehat{D}_x^2$	operator for the second derivative with respect to x
$\mathfrak{D}$	dispersion Lorentzian function
$\mathbf{D}$	a diagonal matrix
$\mathbf{D}_{\boxminus}$	diagonal matrix with elements given by the eigenvalues of $\mathbf{L}_{\boxminus}$
$\mathbf{D}_z$	diagonal matrix with elements given by the eigenvalues of $\mathbf{L}_z$
δ_{mn}	Kronecker delta: $\delta_{mn} = 0$ for $m \neq n$; $\delta_{mn} = 1$ for $m = n$
δ	chemical shift (dimensionless)
$\delta_1, \delta_2 \ldots$	isotropic chemical shifts of spins $I_1, I_2 \ldots$
δ_j^{iso}	isotropic chemical shift of spin I_j
$\delta_j^{\mathrm{aniso}}$	chemical shift anisotropy of spin I_j
δ_{ref}	equivalent chemical shift of the spectrometer reference frequency
$\delta_{xx}^j, \delta_{xy}^j \ldots$	components of the chemical shift tensor of spin I_j
$\delta_{XX}^j, \delta_{YY}^j, \delta_{ZZ}^j$	principal values of the chemical shift tensor of spin I_j
δ^j	chemical shift tensor of spin I_j
e	electric charge of the proton; $e = 1.602 \times 10^{-19}$ C
eq	largest principal value of the electric field gradient tensor
e	Euler's number, $\mathrm{e} = 2.71828\ldots$
$\exp\{\widehat{A}\}$	exponential of operator $\widehat{A}$
E_J	energy of a rotational state with quantum number J
E_n	energy level (=Hamiltonian eigenvalue)
E_{act}	activation energy in Arrhenius equation
E_{elec}	electric interaction energy
$E_{\mathrm{elec}}^{(0)}, E_{\mathrm{elec}}^{(1)} \ldots$	multipole components of the electric interaction energy
$\mathbf{e}_x, \mathbf{e}_y, \mathbf{e}_z$	unit vectors along three orthogonal axes
$\mathbf{e}'_x, \mathbf{e}'_y, \mathbf{e}'_z$	rotating frame axes
$\mathbf{e}_x^{\mathrm{A}}, \mathbf{e}_y^{\mathrm{A}}, \mathbf{e}_z^{\mathrm{A}}$	orthogonal axis system of reference frame A
$\mathbf{e}_x^{\mathrm{B}}, \mathbf{e}_y^{\mathrm{B}}, \mathbf{e}_z^{\mathrm{B}}$	orthogonal axis system of reference frame B
$\mathbf{e}_{jk}$	unit vector parallel to the vector between spins I_j and I_k
$\mathbf{E}$	electric field

ϵ_{NOE}	nuclear Overhauser enhancement factor, defined as the ratio between the enhanced and the non-enhanced magnetization
FID	free induction decay = NMR signal
floor	floor function; floor(x) returns the largest integer that is not greater than x
$\mathbf{f}$	vector representation of function $f(x)$
$f_1, f_2 \ldots$	coefficients of the expansion of $f(x)$ in the basis of functions $\psi_n(x)$
$\vert f\rangle$	Dirac notation for the function $f(x)$
ϕ	r.f. phase
ϕ_{p}	phase of an r.f. pulse
$\phi_1, \phi_2 \ldots$	phases of r.f. pulses
$\phi_{\mathrm{A}}, \phi_{\mathrm{B}} \ldots$	phases of pulse sequence blocks A,B…
ϕ_{rec}	combined phase shift of NMR signal, including receiver phase shift and post-digitization phase shift
ϕ_{dig}	phase shift of digitized NMR signal
ϕ_{ℓ}	phase of signal component s_{ℓ}
ϕ_{ref}	angle of the rotating frame at time $t = 0$
$\phi_{\boxed{-}}$	phase of the coherence $\rho_{\boxed{-}}$
$\phi^{(1)}$	first-order part of the frequency dependence of the peak phase
$\phi^{(0)}$	zero-order part of the frequency dependence of the peak phase
$\phi^{(1)}_{\mathrm{corr}}$	first-order phase correction parameter
$\phi^{(0)}_{\mathrm{corr}}$	zero-order phase correction parameter
Φ	rotation angle of rotating frame
Φ_{G}	rotation angle induced by gradient pulse
Φ_{path}	total pathway phase
G	gauss, an old unit of magnetic field (non-SI); $1\,\mathrm{G} = 10^{-4}\,\mathrm{T}$
G_x	magnitude of the gradient in the z-component of the field with respect to the x-axis
G_y	magnitude of the gradient in the z-component of the field with respect to the y-axis
G_z	magnitude of the gradient in the z-component of the field with respect to the z-axis
G_{max}	maximum gradient strength
$\mathbb{G}(\tau)$	autocorrelation function of a random process
$\mathbb{G}_m(\tau)$	autocorrelation function of a second-rank spherical harmonic
γ	gyromagnetic ratio; also, an Euler angle
$\gamma_j, \gamma_k \ldots$	gyromagnetic ratios of nuclei I_j, $I_k \ldots$
γ_I, γ_S	gyromagnetic ratios of two different isotopes
γ^{BA}	first Euler angle used when transforming the reference axes of frame A into those of frame B
γ_{AB}	passive notation for γ^{BA}
h	Planck's constant; $h = 6.626 \times 10^{-34}\,\mathrm{J\,s}$
$\hbar$	Planck's constant divided by 2π; $\hbar = 1.055 \times 10^{-34}\,\mathrm{J\,s}$
Hz	hertz, cycles per second (unit of frequency)
$\widehat{\mathrm{H}}$	Hamiltonian operator, in SI units
$\mathbf{H}$	matrix representation of a Hamiltonian
$\widehat{\mathcal{H}}$	Hamiltonian operator (in natural units)
$\widehat{\mathcal{H}}^0$	secular spin Hamiltonian
$\widehat{\mathcal{H}}^{\mathrm{DD}}$	secular dipole–dipole interaction (for all spin pairs)

$\widehat{\mathcal{H}}^{\mathrm{DD,full}}$	full form of the dipole–dipole interaction (for all spin pairs)
$\widehat{\mathcal{H}}_{\mathrm{ext}}$	external spin Hamiltonian
$\widehat{\mathcal{H}}_{\mathrm{full}}$	complete Hamiltonian operator of the sample
$\widehat{\mathcal{H}}_{\mathrm{grad}}$	Hamiltonian for the interaction with the gradient field
$\widehat{\mathcal{H}}_{\mathrm{int}}$	internal spin Hamiltonian
$\widehat{\mathcal{H}}_{\mathrm{int}}^{\mathrm{iso}}$	isotropic part of a secular spin interaction $\widehat{\mathcal{H}}_{\mathrm{int}}^{0}$
$\widehat{\mathcal{H}}_{\mathrm{int}}^{0}$	secular part of internal spin Hamiltonian $\widehat{\mathcal{H}}_{\mathrm{int}}$
$\overline{\widehat{\mathcal{H}}}_{\mathrm{int}}^{0}$	motionally averaged secular Hamiltonian
$\widehat{\mathcal{H}}_{j}^{\mathrm{CS}}$	chemical shift interaction of spin I_j
$\widehat{\mathcal{H}}_{j}^{\mathrm{CS,iso}}$	isotropic chemical shift interaction of spin I_j
$\widehat{\mathcal{H}}_{j}^{\mathrm{elec}}$	electric part of the Hamiltonian for spin I_j
$\widehat{\mathcal{H}}_{jk}^{\mathrm{DD}}$	secular dipole–dipole interaction between spins I_j and I_k
$\widehat{\mathcal{H}}_{jk}^{\mathrm{DD,full}}$	full form of the dipole–dipole interaction between spins I_j and I_k
$\widehat{\mathcal{H}}_{jk}^{\mathrm{iso}}$	isotropic J-coupling interaction between spins I_j and I_k
$\widehat{\mathcal{H}}_{jk}^{\mathrm{J}}$	secular J-coupling interaction between spins I_j and I_k
$\widehat{\mathcal{H}}_{jk}^{\mathrm{J,full}}$	full form of the J-coupling interaction between spins I_j and I_k
$\widehat{\mathcal{H}}_{j}^{\mathrm{mag}}$	magnetic part of the Hamiltonian for spin I_j
$\widehat{\mathcal{H}}_{\mathrm{j}}^{\mathrm{Q}}$	electric quadrupole interaction of nucleus I_j
$\widehat{\mathcal{H}}_{j}^{\mathrm{RF}}$	r.f. spin Hamiltonian for nucleus I_j
$\widehat{\mathcal{H}}_{J}^{\mathrm{strong}}$	J-coupling Hamiltonian in the strongly coupled limit
$\widehat{\mathcal{H}}_{J}^{\mathrm{weak}}$	J-coupling Hamiltonian in the weakly coupled limit
$\widehat{\mathcal{H}}_{\mathrm{RF}}$	r.f. part of external spin Hamiltonian
$\widehat{\mathcal{H}}_{\mathrm{Q}}^{(1)}$	first-order quadrupolar Hamiltonian
$\widehat{\mathcal{H}}_{\mathrm{Q}}^{(2)}$	second-order quadrupolar Hamiltonian
$\widehat{\mathcal{H}}_{\mathrm{static}}$	static part of external spin Hamiltonian
$\widehat{\mathcal{H}}_{12}^{0}$	secular Hamiltonian for the coupling between spins I_1 and I_2
$\widehat{\mathcal{H}}^{0\prime}$	secular spin Hamiltonian with the opposite sign of the chemical shift terms
$\hat{\widehat{\mathcal{H}}}^{0}$	secular spin Hamiltonian, in the rotating frame
$\widehat{\mathcal{H}}_{\mathrm{weak}}^{0}$	weakly coupled form of the secular spin Hamiltonian
$\widehat{\mathcal{H}}_{\mathrm{weak}}^{0\prime}$	weakly coupled form of the secular spin Hamiltonian, with the opposite sign of the chemical shift terms
$\widehat{\mathcal{H}}_{1}^{0}, \widehat{\mathcal{H}}_{2}^{0} \ldots$	secular Hamiltonians for spins $I_1, I_2 \ldots$
η	old definition of the NOE enhancement factor. $\eta = 1$ indicates a doubling of the signal (see ϵ_{NOE})
η_j	biaxiality (asymmetry parameter) of chemical shift tensor of spin I_j
η_{Q}	biaxiality (asymmetry parameter) of electric field gradient tensor
i	square root of -1
Im	imaginary part of a complex number

INADEQUATE	Incredible Natural Abundance DoublE QUAnTum Experiment, a pulse sequence that selects peaks passing through double-quantum coherences, suppressing isolated spin signals
INEPT	Insensitive Nuclei Enhanced by Polarization Transfer, a pulse sequence that implements magnetization transfer from one spin species to another, using the J-couplings
I	nuclear spin quantum number; in addition, a nuclear spin species
$\hat{I}_x, \hat{I}_y, \hat{I}_z$	operators for the three components of nuclear spin angular momentum
$\hat{I}^+, \hat{I}^-$	nuclear spin shift operators
$\hat{I}^\alpha$	projection operator onto state $\lvert\alpha\rangle$ for a single spin-1/2
$\hat{I}^\beta$	projection operator onto state $\lvert\beta\rangle$ for a single spin-1/2
$\hat{I}_{1x}, \hat{I}_{1y}, \hat{I}_{1z}$	angular momentum operators for spin I_1
$\hat{I}_{2x}, \hat{I}_{2y}, \hat{I}_{2z}$	angular momentum operators for spin I_2
$\hat{I}_{jx}, \hat{I}_{jy}, \hat{I}_{jz}$	spin angular momentum operators of nucleus I_j
$\hat{I}_1^\alpha, \hat{I}_2^\alpha \ldots$	projection operators onto state $\lvert\alpha\rangle$ for spins $I_1, I_2 \ldots$
$\hat{I}_1^\beta, \hat{I}_2^\beta \ldots$	projection operators onto state $\lvert\beta\rangle$ for spins $I_1, I_2 \ldots$
$\hat{\mathbf{I}}_j$	vector operator for the spin angular momentum of nucleus I_j, $\hat{\mathbf{I}}_j = \hat{I}_{jx}\mathbf{e}_x + \hat{I}_{jy}\mathbf{e}_y + \hat{I}_{jz}\mathbf{e}_z$
$\hat{\mathbf{I}}_j \cdot \hat{\mathbf{I}}_k$	scalar product of angular momentum operators, equal to $\hat{I}_{jx}\hat{I}_{kx} + \hat{I}_{jy}\hat{I}_{ky} + \hat{I}_{jz}\hat{I}_{kz}$
$\lvert I, M\rangle$	state of spin-I nucleus with azimuthal quantum number M
$\mathbf{I}^+$	matrix representation of the operator $\hat{I}^+$
j	a spin index
J	J-coupling (in hertz); in addition, angular momentum quantum number
J', J''	J-couplings
J_1, J_2, J_3	total angular momentum quantum numbers
J_{CH}	J-coupling between ^{13}C and ^{1}H (units of hertz)
J_{jk}	isotropic J-coupling between spins I_j and I_k
$J_{12}, J_{13} \ldots$	J-couplings between spins I_1 and I_2, etc.
J_{IS}	heteronuclear J-coupling constant (in hertz)
^1J	one-bond J-coupling
^2J	two-bond J-coupling
^3J	three-bond J-coupling
$\mathbf{J}_{jk}$	J-coupling tensor between spins I_j and I_k
$J_{xx}^{jk}, J_{xy}^{jk} \ldots$	components of the J-coupling tensor between spins I_j and I_k
$\mathbb{J}(\omega)$	spectral density
$\mathfrak{J}(\omega)$	normalized spectral density
k	a spin index; in addition, a kinetic rate constant
k'	a kinetic rate constant
k_{B}	Boltzmann constant = $1.381 \times 10^{-23}\,\mathrm{J\,K^{-1}}$
K	equilibrium constant of an exchange process
$\widehat{\mathrm{K}}$	kinetic energy operator
$\mathbb{K}_{\mathrm{AB}}$	cross-correlation function of two random processes
$\mathbb{K}_{\mathrm{CH,CH}}$	cross-correlation of the dipole–dipole interactions within two ^{13}C–^{1}H pairs
κ	strength of a gradient pulse
ℓ	an index for signal components and for spectral peaks;in addition, orbital angular momentum quantum number
$\hat{l}_x, \hat{l}_y, \hat{l}_z$	angular momentum operators (in natural units)
$\hat{l}^2$	operator for the total square angular momentum (in natural units)

$\hat{l}^+, \hat{l}^-$	angular momentum shift operators
$\|\ell, m\rangle$	angular momentum eigenstate with total square angular momentum $l(l+1)\hbar$ and z-angular momentum $m\hbar$
L	inductance of coil
L_{tot}	total angular momentum
$\mathfrak{L}$	complex Lorentzian function
$\mathbf{L}_{\boxed{-}}$	dynamic matrix for the evolution of (-1)-quantum coherences in a two-site exchange problem
$\mathbf{L}_{\text{pop}}$	dynamic matrix for the evolution of populations in a two-site exchange problem
$\mathbf{L}_{\text{Solomon}}$	Solomon matrix for relaxation in a two-spin-1/2 system
$\mathbf{L}_z$	dynamic matrix for the evolution of Zeeman magnetizations in a two-site exchange problem
λ	decay rate constant of a coherence (or transverse magnetization); $\lambda = {T_2}^{-1}$; peakwidth at half-height = 2λ in units of radians per second
λ'	coherence decay rate constant in slow two-site exchange; sum of the natural decay rate constant λ and the exchange rate constant k
λ_j	linewidth parameter for spins j
λ_ℓ	decay rate constant of signal component s_ℓ
$\lambda_\ell^{(1)}$	width parameter of a two-dimensional peak in the Ω_1 dimension
$\lambda_\ell^{(2)}$	width parameter of a two-dimensional peak in the Ω_2 dimension
λ_{rs}	decay rate constant of coherence ρ_{rs}
Λ_{rs}	spatial wavelength of phase helix induced by gradient pulse, for coherence ρ_{rs}
mod	modulo function; mod(a, b) takes the remainder when a is divided by b
ms	millisecond, 10^{-3} s
m	an integer; in addition, mass of a particle
$m_j^{(r)}$	azimuthal quantum number of spin I_j in the state $\|r\rangle$
M_J	azimuthal quantum number for a rotating object; $M_J = -J, -J+1 \ldots + J$
M_r	angular momentum of state $\|r\rangle$ along z-axis
M_s	angular momentum of state $\|s\rangle$ along z-axis
M_S	azimuthal quantum number for a spin; $M_S = -S, -S+1 \ldots + S$
M_x, M_y, M_z	components of the magnetization vector
M_x^{nuc}, M_y^{nuc}, M_z^{nuc}	components of nuclear magnetization
$M_{\text{eq}}^{\text{nuc}}$	equilibrium value of nuclear magnetization along z-axis
$\mathbf{M}$	magnetization vector
$\mathbf{M}^{\text{eq}}$	equilibrium nuclear magnetization vector
$\mathfrak{m}$	phase cycle counter, $\mathfrak{m} = 0, 1 \ldots \mathfrak{n} - 1$
$\mathfrak{M}$	transient counter, $\mathfrak{M} = 0, 1 \ldots \mathfrak{N} - 1$
μ_0	magnetic constant; $\mu_0 = 4\pi \times 10^{-7}\,\text{H}\,\text{m}^{-1}$. Often required for electromagnetic equations in SI units
$\boldsymbol{\mu}$	magnetic moment
μ_{induced}	induced magnetic moment
$\hat{\boldsymbol{\mu}}$	operator for the magnetic moment vector
NOE	nuclear Overhauser effect, the change in the magnetization of one nuclear spin species when a second spin species is saturated. The original Overhauser effect involved nuclei and electrons in metals
NOESY	Nuclear Overhauser SpectroscopY, a form of two-dimensional spectroscopy in which the cross-peaks are generated by dipole–dipole cross-relaxation.

nm	nanometre, 10^{-9} m
ns	nanosecond, 10^{-9} s
n	an integer
n_{sample}	number of signal sampling points
N	number of spins in a spin system; in addition, number of pulses; in addition, an integer
N	normalization constant
$\mathfrak{n}$	total number of steps in a phase cycle
$\mathfrak{n}_{\mathrm{A}}, \mathfrak{n}_{\mathrm{B}} \ldots$	number of steps in the phase cycles for individual pulse sequence blocks A, B...
$\mathfrak{N}$	number of acquired transients
$\mathbb{N}$	number of members of the spin ensemble
$\mathbb{N}_{\mathrm{A}}, \mathbb{N}_{\mathrm{B}}$	number of molecules of types A and B
$\mathbb{N}_{\mathrm{A}}$	Avogadro's number, i.e. number of molecules in a mole of substance = 6.022×10^{23}
ppm	parts per million, 10^{-6}
p	coherence order
p_{rs}	order of the coherence ρ_{rs}
Δp	change in coherence order
$\Delta p_{\mathrm{A}}, \Delta p_{\mathrm{B}} \ldots$	changes in coherence order over pulse sequence blocks A, B...
P	probability
$\mathsf{P}_{\mathrm{I}}, \mathsf{P}_{\mathrm{II}} \ldots$	probabilities of isotopomers
$\mathsf{P}(q_n)$	probability of observing the result q_n
$\mathsf{P}_{\alpha \rightarrow \beta}$	probability of a spin-1/2 making a transition $\lvert\alpha\rangle \rightarrow \lvert\beta\rangle$
p	probability density function
$\mathsf{p}(\Theta) \quad \mathrm{d}\Theta$	probability of a molecule having an orientation in the range Θ to $\Theta + \mathrm{d}\Theta$
$\mathfrak{p}$	an integer
$\mathbb{P}$	vector of populations in a two-spin-1/2 system
π	mathematical constant, $\pi = 3.1415\ldots$
$(\pi/2)_x$	pulse of flip angle $\pi/2$ and phase $\phi_{\mathrm{p}} = 0$
$(\pi/2)_y$	pulse of flip angle $\pi/2$ and phase $\phi_{\mathrm{p}} = \pi/2$
$(\pi/2)_{\bar{x}}$	pulse of flip angle $\pi/2$ and phase $\phi_{\mathrm{p}} = \pi$
$(\pi/2)_{\bar{y}}$	pulse of flip angle $\pi/2$ and phase $\phi_{\mathrm{p}} = 3\pi/2$
π_x	pulse of flip angle π and phase $\phi_{\mathrm{p}} = 0$
π_y	pulse of flip angle π and phase $\phi_{\mathrm{p}} = \pi/2$
$\pi_{\bar{x}}$	pulse of flip angle π and phase $\phi_{\mathrm{p}} = \pi$
$\pi_{\bar{y}}$	pulse of flip angle π and phase $\phi_{\mathrm{p}} = 3\pi/2$
$(\pi/2)_x^I$	$\pi/2$ pulse applied to spin species I
$(\pi/2)_x^S$	$\pi/2$ pulse applied to spin species S
q	largest principal value of the electric field gradient tensor, divided by e; also satellite order
q_n	an eigenvalue of the operator $\widehat{Q}$
q_{rs}	satellite order of the coherence ρ_{rs}
Q	electric quadrupole moment
Q_{macro}	result of a macroscopic observation of the operator $\widehat{Q}$
$Q_{\alpha\alpha}, Q_{\alpha\beta} \ldots$	matrix elements of a spin-1/2 operator $\widehat{Q}$
$\widehat{Q}$	arbitrary operator
$\langle\widehat{Q}\rangle$	expectation value of the operator $\widehat{Q}$
$\langle\widehat{Q}\rangle^{\mathrm{eq}}$	expectation value of the operator $\widehat{Q}$ in thermal equilibrium

θ_1, θ_2	tilt angles of rotation axes for spins I_1 and I_2
$\theta_{\mathrm{CH,CH}}$	angle between two ^{13}C–^{1}H internuclear vectors
θ_{IS}	angle subtended by the molecular long axis and the vector between spins I and S
θ_{Q}	angle between the unique axis of an uniaxial electric field gradient tensor and the static magnetic field
θ_{RF}	angle between the r.f. and static magnetic fields
Θ	molecular orientation
Θ_{magic}	the magic angle, $\Theta_{\mathrm{magic}} = \arctan\sqrt{2} = 54.7356^\circ$
Θ_{IS}	angle subtended by the external field and the vector between spins I and S
Θ_{jk}	angle between the vector $\mathbf{e}_{jk}$ and the magnetic field
r.f.	radio-frequency
Re	real part of a complex number
ROESY	Rotating-frame nuclear Overhauser SpectroscopY, a form of two-dimensional spectroscopy in which the cross-peaks are generated by transverse cross-relaxation in the presence of an r.f. field
$\mathbf{r}$	spatial position, written as a three-dimensional vector
r_{jk}	distance between spins I_j and I_k
$R, \mathbb{R}$	expressions appearing in the theory of two-site exchange
$\mathcal{R}(\alpha, \beta, \gamma)$	three-dimensional rotation matrix, written using Euler angles
$\mathcal{R}^j$	rotation matrix describing the orientation of the principal axis system of the chemical shift tensor for spin I_j with respect to the static field
$\mathcal{R}_{\mathrm{Q}}$	rotation matrix describing the orientation of the principal axis system of the electric field gradient tensor with respect to the static field
$R^j_{xX}, R^j_{xY} \ldots$	elements of the matrix $\mathcal{R}^j$
R_{auto}	auto-relaxation rate constant in Solomon equations
$R^{\mathrm{T}}_{\mathrm{auto}}$	transverse auto-relaxation rate constant
R_{cross}	cross-relaxation rate constant in Solomon equations (with sign corrected)
$R^{\mathrm{T}}_{\mathrm{cross}}$	transverse cross-relaxation rate constant (with sign corrected)
R_{sum}	relaxation rate constant for the sum magnetization
$\widehat{R}_x(\beta)$	operator for the rotation through the angle β about the rotating-frame x-axis
$\widehat{R}_y(\beta)$	operator for the rotation through the angle β about the rotating-frame y-axis
$\widehat{R}_z(\beta)$	operator for the rotation through the angle β about the z-axis
$\widehat{R}_{\phi_{\mathrm{p}}}(\beta_{\mathrm{p}})$	operator for a rotation of one or more spins through the angle β_{p} about the axis $\mathbf{e}'_x \cos\phi_{\mathrm{p}} + \mathbf{e}'_y \sin\phi_{\mathrm{p}}$
$\widehat{R}_{1x}(\beta)$	operator for the rotation of spin I_1 through the angle β about the rotating-frame x-axis
$\widehat{R}_{2z}(\beta)$	operator for the rotation of spin I_2 through the angle β about the z-axis
$\widehat{R}_{1,\phi_{\mathrm{p}}}(\beta_{\mathrm{p}}), \widehat{R}_{2,\phi_{\mathrm{p}}}(\beta_{\mathrm{p}}) \ldots$	operators for rotations of individual spins $I_1, I_2 \ldots$ through the angle β_{p} about the axis $\mathbf{e}'_x \cos\phi_{\mathrm{p}} + \mathbf{e}'_y \sin\phi_{\mathrm{p}}$
ρ_{rr}	population of state $\lvert r\rangle$
ρ_{rs}	coherence between states $\lvert r\rangle$ and $\lvert s\rangle$
ρ^{eq}_{rr}	thermal equilibrium value of the population ρ_{rr}
ρ^{eq}_{rs}	thermal equilibrium value of the coherence ρ_{rs}
$\rho_{\boxed{\alpha}}, \rho_{\boxed{\beta}}$	populations of states $\lvert\alpha\rangle$ and $\lvert\beta\rangle$, in a spin-1/2 ensemble
$\rho_{\boxed{+}}, \rho_{\boxed{-}}$	coherences in a spin-1/2 ensemble

$\rho^{\mathrm{eq}}_{\boxed{\alpha}}$, $\rho^{\mathrm{eq}}_{\boxed{\beta}}$	thermal equilibrium populations of states $\lvert\alpha\rangle$ and $\lvert\beta\rangle$, in a spin-1/2 ensemble
$\rho_{\lvert+1\rangle}$	population of state $\lvert 1, +1\rangle$ in a spin-1 ensemble
$\rho_{\lvert 0\rangle}$	population of state $\lvert 1, 0\rangle$ in a spin-1 ensemble
$\rho_{\lvert-1\rangle}$	population of state $\lvert 1, -1\rangle$ in a spin-1 ensemble
$\rho_{\lvert+3/2\rangle}$	population of state $\lvert I, +3/2\rangle$ in an ensemble of half-integer spins $I \geq 3/2$
$\rho_{\lvert+1/2\rangle}$	population of state $\lvert I, +1/2\rangle$ in an ensemble of half-integer spins $I \geq 3/2$
$\rho_{\lvert-1/2\rangle}$	population of state $\lvert I, -1/2\rangle$ in an ensemble of half-integer spins $I \geq 3/2$
$\rho_{\lvert-3/2\rangle}$	population of state $\lvert I, -3/2\rangle$ in an ensemble of half-integer spins $I \geq 3/2$
$\rho_{\boxed{p_q}}$	coherence in an ensemble of quadrupolar nuclei, with coherence order p and satellite order q
$\rho_{\boxed{-1_0}}$	central transition (-1)-quantum coherence in an ensemble of half-integer spins $I \geq 3/2$
$\rho_{\boxed{\alpha\alpha}}$, $\rho_{\boxed{\alpha+}} \cdots$	populations and coherences for an ensemble of spin-1/2 pairs
$\rho^{\mathrm{eq}}_{\boxed{\alpha\alpha}}$, $\rho^{\mathrm{eq}}_{\boxed{\alpha\beta}} \cdots$	thermal equilibrium populations in an ensemble of spin-1/2 pairs
$\rho_{\boxed{\alpha\alpha\alpha}}$, $\rho_{\boxed{\alpha\alpha+}} \cdots$	populations and coherences in an ensemble of three-spin-1/2 systems
$\rho_{\boxed{\alpha--\alpha}}$, $\rho_{\boxed{\alpha--\beta}} \cdots$	(-2)-quantum coherences in an ensemble of four-spin systems
$\rho_{\boxed{-\alpha+\alpha\beta}} \cdots$	coherences in an ensemble of five-spin-1/2 systems
$\rho^{\mathrm{A}}_{\boxed{\alpha}}$, $\rho^{\mathrm{A}}_{\boxed{+}} \cdots$	populations and coherences for molecules of type A
$\rho^{\mathrm{B}}_{\boxed{\alpha}}$, $\rho^{\mathrm{B}}_{\boxed{+}} \cdots$	populations and coherences for molecules of type B
$\rho^{[\mathfrak{m}]}_{\boxed{-\beta}\textcircled{5}}$	coherence $\rho_{\boxed{-\beta}}$ at time point ⑤, for the pulse sequence corresponding to phase cycle index $\mathfrak{m}$
$\hat{\rho}$	spin density operator
$\hat{\rho}^{\mathrm{eq}}$	thermal equilibrium spin density operator
$\hat{\rho}^{\mathrm{A}}$, $\hat{\rho}^{\mathrm{B}}$	components of the spin density operator in a two-site exchange problem
$\hat{\rho}_{\textcircled{1}}$, $\hat{\rho}_{\textcircled{2}} \cdots$	spin density operator at time points ①, ② ...
$\hat{\rho}^{\cos}_{\textcircled{1}}$, $\hat{\rho}^{\cos}_{\textcircled{2}} \cdots$	spin density operator at time points ①, ② ... during the 'cosine' pulse sequence of a States data-acquisition scheme
$\hat{\rho}^{\sin}_{\textcircled{1}}$, $\hat{\rho}^{\sin}_{\textcircled{2}} \cdots$	spin density operator at time points ①, ② ... during the 'sine' pulse sequence of a States data-acquisition scheme
$\hat{\rho}^{[\mathfrak{m}]}_{\textcircled{5}}$	density operator at time point ⑤, for the pulse sequence corresponding to phase cycle index $\mathfrak{m}$
$\hat{\tilde{\rho}}$	rotating-frame spin density operator
$\tilde{\rho}_{\boxed{\alpha}}$, $\tilde{\rho}_{\boxed{\beta}}$	spin-1/2 populations in the rotating frame
$\tilde{\rho}_{\boxed{-}}$, $\tilde{\rho}_{\boxed{+}}$	spin-1/2 coherences in the rotating frame
s	second (unit of time)
sinh	hyperbolic sine, $\sinh x = \frac{1}{2}(\mathrm{e}^{x} - \mathrm{e}^{-x})$
$s(t)$	complex NMR signal emerging from the digitizer
$s(\tau, t)$	signal matrix of an arrayed experiment with variation of the interval τ
$s(t_1, t_2)$	two-dimensional signal surface
$s(t_1, t_2, t_3)$	three-dimensional signal surface
$s^{\cos}(t_1, t_2)$	cosine signal surface in the two-dimensional States procedure
$s^{\sin}(t_1, t_2)$	sine signal surface in the two-dimensional States procedure
$s_{\ell}(t)$	signal component corresponding to one spectral peak in a one-dimensional spectrum
$s_{\ell}(t_1, t_2)$	signal component corresponding to one spectral peak in a two-dimensional spectrum

s_{FID}	r.f. NMR signal emerging from the probe
$s_{\mathrm{A}}, s_{\mathrm{B}}$	output signals of quadrature receiver
s_{NMR}	component of the digitized signal $s(t)$ due to the nuclear spins
s_{noise}	component of the digitized signal $s(t)$ due to noise
s_{guess}	guessed form of NMR signal
s_{synth}	r.f. output signal of the synthesizer
s_{path}	signal component with a certain history of coherence orders
$s_{\mathrm{path}}^{\mathrm{tot}}$	signal component with a certain history of coherence orders, summed over all steps in a phase cycle
$s_{\mathrm{rec}}^{\mathrm{A}}, s_{\mathrm{rec}}^{\mathrm{B}}$	r.f. reference signals for the quadrature receiver
$s_{\mathrm{A}\to\mathrm{A}}^{\cos}, s_{\mathrm{A}\to\mathrm{B}}^{\cos}\ldots$	components of the cosine signal surface in a two-dimensional exchange experiment
$s_{\mathrm{A}\to\mathrm{A}}^{\sin}, s_{\mathrm{A}\to\mathrm{B}}^{\sin}\ldots$	components of the sine signal surface in a two-dimensional exchange experiment
$s_{\boxed{-\alpha}\to\boxed{\alpha-}}$	two-dimensional signal component for one coherence transfer process in a COSY experiment
S	a nuclear spin species
$S(\Omega)$	one-dimensional NMR spectrum
$S(\tau, \Omega)$	NMR spectrum as a function of the variable interval τ
$S(\Omega_1, \Omega_2)$	two-dimensional NMR spectrum
$S_{\mathrm{States}}(\Omega_1, \Omega_2)$	States two-dimensional spectrum
$S(\Omega_1, \Omega_2, \Omega_3)$	three-dimensional NMR spectrum
$S_{\ell}(\Omega)$	one peak in a one-dimensional NMR spectrum
$S_{\ell}(\Omega_1, \Omega_2)$	one peak in a two-dimensional NMR spectrum
$S_{\mathrm{A}\to\mathrm{A}}, S_{\mathrm{A}\to\mathrm{B}}\ldots$	components of a two-dimensional exchange spectrum
$\hat{S}_x, \hat{S}_y\ldots$	operators for the spin angular momentum components of spin S
$\hat{S}_{1x}, \hat{S}_{1y}\ldots$	operators for the spin angular momentum components of spin S_1
$\hat{\mathbf{S}}$	vector operator for the spin angular momentum, $\hat{\mathbf{S}} = \hat{S}_x\mathbf{e}_x + \hat{S}_y\mathbf{e}_y + \hat{S}_z\mathbf{e}_z$
$\lvert S_0\rangle$	singlet state
σ	old definition of the cross-relaxation rate constant in the Solomon equations (see R_{cross}); in addition, chemical shielding factor (opposite in sign to the chemical shift δ). Both meanings of σ are avoided in this book
$\hat{\sigma}$	alternative notation for spin density operator $\hat{\rho}$ (not used in this book)
σ_{G}	shape factor for gradient pulse
σ_{noise}	mean-square noise
$\sum'_{j<k}$	sum over spin pairs, excluding those that are magnetically equivalent
tanh	hyperbolic tangent, where $\tanh x = \sinh x/\cosh x$
t	a time point, and a time coordinate
$t_{\mathrm{a}}, t_{\mathrm{b}}$	two time points
t_1	incremented time interval in a two-dimensional experiment
t_2	signal acquisition interval in a two-dimensional experiment
$t_{\mathrm{on}}, t_{\mathrm{off}}$	time points at which a field is turned on and off
T	tesla, unit of magnetic field
Tr	trace of a matrix representation (sum of diagonal elements)
TOCSY	TOtal Correlation SpectroscopY, a form of two-dimensional spectroscopy generating cross-peaks for all spins belonging to the same spin system
TMS	tetramethylsilane, $\mathrm{Si(CH_3)_4}$
T	absolute temperature in units of Kelvin

T_1	longitudinal relaxation time constant = spin–lattice relaxation time constant
T_1^j	spin–lattice relaxation time of spins I_j
T_1^k	spin–lattice relaxation time constant of spins I_k
$T_1^{\mathrm{A}}, T_1^{\mathrm{B}}$	spin–lattice relaxation time constants of spins in chemical species A and B
$T_{1\rho}$	spin–lattice relaxation time constant in the rotating frame = transverse relaxation time constant in the presence of a spin-locking field
T_2	transverse relaxation time constant = spin–spin relaxation time constant
$T_2{}^*$	fictitious transverse relaxation time constant corresponding to the inhomogeneously broadened linewidth
$\lvert T_{+1}\rangle, \lvert T_0\rangle, \lvert T_{-1}\rangle$	triplet states
$\mathbb{T}_{\mathrm{PZ}}$	matrix for the transformation of Zeeman orders into populations
$\mathbb{T}_{\mathrm{ZP}}$	matrix for the transformation of populations into Zeeman orders
$\mathbf{T}$	a spin interaction tensor
$[\mathbf{T}]^{\mathrm{A}}$	matrix representation of a spin interaction tensor, in reference frame A
τ	an interval between two time points
τ_{m}	mixing interval in TOCSY, NOESY and ROESY pulse sequences
τ_{p}	r.f. pulse duration
τ_{G}	gradient pulse duration
τ^0	Larmor time-scale
τ_{c}	correlation time of a random process
$\tau_{\mathrm{c}}^{\mathrm{crit}}$	critical rotational correlation time (at which cross-relaxation disappears)
τ_{acq}	signal detection interval
τ_{spec}	spectral time-scale
τ_{sample}	interval between signal sampling points
$\widehat{U}(\tau)$	free precession propagator over an interval τ
$\widehat{U}_1, \widehat{U}_2 \ldots$	free precession propagators under the Hamiltonians $\widehat{\mathcal{H}}_1^0, \widehat{\mathcal{H}}_2^0 \ldots$
$\widehat{U}_{12}$	free precession propagator under the Hamiltonian $\widehat{\mathcal{H}}_{12}^0$
$\widehat{U}_{\mathrm{G}}$	propagator under a field gradient pulse
$\widehat{U}_J^{\mathrm{strong}}$	propagator under the strongly coupled J-coupling Hamiltonian $\widehat{\mathcal{H}}_J^{\mathrm{strong}}$
$\widehat{U}_J^{\mathrm{weak}}$	propagator under the weakly coupled J-coupling Hamiltonian $\widehat{\mathcal{H}}_J^{\mathrm{weak}}$
$\widehat{U}_{\mathrm{mix}}$	propagator for the mixing interval of a pulse sequence
$\widehat{U}_{\mathrm{SES}}$	propagator for a spin echo sandwich
V	volume; in addition, electric potential
$\widehat{\mathrm{V}}$	potential energy operator
$\mathbf{V}$	electric field gradient tensor
$V^{(0)}, V^{(1)} \ldots$	multipole components of the electric potential
$V_{xx}, V_{xy} \ldots$	Cartesian components of the electric field gradient at spin I_j
V_{XX}, V_{YY}, V_{ZZ}	principal values of the electric field gradient tensor at spin I_j
$\mathbf{V}_{\boxed{-}}$	propagator for (-1)-quantum coherences in a two-site exchange problem
W	mean transition probability per unit time in a spin-1/2 ensemble
W_0	mean zero-quantum transition probability per unit time in a homonuclear spin pair ensemble
W_2	mean double-quantum transition probability per unit time in a homonuclear spin pair ensemble
W_1	mean single-quantum transition probability per unit time in a homonuclear spin pair ensemble

W_{1I}, W_{1S}	mean single-quantum transition probabilities per unit time for species I and S
$W_{\boxed{+}}$, $W_{\boxed{-}}$	transition probabilities per unit time in a spin-1/2 ensemble
$W_{\boxed{-\alpha}}$, $W_{\boxed{-\beta}}\ldots$	transition probabilities per unit time in a 2-spin-1/2 ensemble
$\mathbb{W}_{\mathrm{P}}$	kinetic matrix for the evolution of populations in a 2-spin-1/2 system
ω	frequency in units of radians per second
$\omega/2\pi$	frequency in units of hertz
ω^0	signed) precession frequency (=Larmor frequency) in units of radians per second
$\omega^0/2\pi$	signed) precession frequency (=Larmor frequency) in units of hertz
ω_j^0, $\omega_k^0\ldots$	chemically shifted Larmor frequencies of spins I_j, $I_k\ldots$
ω_1^0, $\omega_2^0\ldots$	chemically shifted Larmor frequencies of spins I_1, $I_2\ldots$
ω_{12}^{A}, ω_{12}^{B}	components of the spin–spin coupling between spins I_1 and I_2
ω_{IS}	heteronuclear spin–spin coupling in anisotropic phase
ω_{G}	field-gradient-induced Larmor frequency shift
$\omega_{\mathrm{Q}}^{(1)}$	first-order quadrupole coupling
$\omega_{Q}^{(2)}$	second-order quadrupole coupling
ω_n	eigenvalue of the Hamiltonian $\widehat{\mathcal{H}}$ = energy level (in units of $\hbar$)
ω_{nut}^j	nutation frequency of spin I_j
$\omega_{\mathrm{nut}}^{\mathrm{C}}$	central transition nutation frequency
ω_{osc}	oscillation frequency of tuned circuit in probe
ω_{ref}	signed) spectrometer reference frequency in units of radians per second
ω_I^0	resonance offset frequency of spins I
ω_S^0	resonance offset frequency of spins S
ω_{TMS}^0	Larmor frequency of spins in $\mathrm{Si(CH_3)_4}$ in units of radians per second
ω', ω''	chemical shift frequencies
$\omega_{\alpha\alpha}$, $\omega_{\alpha\beta}\ldots$	energy eigenvalues for a weakly coupled spin-1/2 pair
ω_x, ω_y, ω_z	Cartesian components of the magnetic field, expressed as frequencies (e.g. $\omega_x = -\gamma B_x$)
Ω	signed) frequency relative to spectrometer reference (=resonance offset frequency) in units of radians per second
$\Omega/2\pi$	signed) frequency relative to spectrometer reference (=frequency coordinate in spectrum) in units of hertz
Ω^0	Larmor frequency relative to spectrometer reference (=resonance offset frequency) in units of radians per second
$\Omega^0/2\pi$	Larmor frequency relative to spectrometer reference (=resonance offset frequency = frequency coordinate of spectral peak) in units of hertz
Ω_1	frequency coordinate of a two-dimensional spectrum (in the indirectly detected dimension)
Ω_2	frequency coordinate of a two-dimensional spectrum (in the directly detected dimension)
Ω_Δ	difference in chemical shift frequencies
Ω_Σ	sum of chemical shift frequencies
Ω_ℓ	rotating-frame frequency of a spectral peak
$\Omega_\ell^{(1)}$	frequency coordinate of a two-dimensional peak in the Ω_1 dimension
$\Omega_\ell^{(2)}$	frequency coordinate of a two-dimensional peak in the Ω_2 dimension
Ω_{guess}	guessed frequency of NMR signal
Ω_1^0, $\Omega_2^0\ldots$	resonance offset frequencies of spins I_1, $I_2\ldots$

$\Omega^0_j, \Omega^0_k \ldots$	resonance offset frequencies of spins $I_j, I_k \ldots$
$\Omega^0(1)$	resonance offset frequency in the t_1 interval
$\Omega^0(2)$	resonance offset frequency in the t_2 interval
$\Omega^0_{\mathrm{A}}, \Omega^0_{\mathrm{B}}$	resonance offset frequency of a spin in two different chemical species, A and B
$\overline{\Omega}$	mean resonance offset frequency of a spin in a chemically exchanging molecule
$\Omega_{\alpha\alpha}, \Omega_{\alpha\beta} \ldots$	eigenvalues of the rotating-frame Hamiltonian, for a weakly coupled spin-1/2 pair
Ω_{rs}	rotating-frame frequency of coherence ρ_{rs}
$\Omega_{\boxed{-\alpha}}, \Omega_{\boxed{-\beta}} \ldots$	rotating-frame precession frequencies of coherences in an ensemble of spin-1/2 pairs
$\Omega_{\boxed{+-\alpha}}$	frequency of a coherence $\rho_{\boxed{+-\alpha}}$ in an ensemble of three-spin-1/2 systems
$\Omega_{\boxed{-\alpha+\beta-}}$	frequency of a coherence $\rho_{\boxed{-\alpha+\beta-}}$ in an ensemble of five-spin-1/2 systems
$\Omega_{\boxed{\alpha--\alpha}}, \Omega_{\boxed{\alpha--\beta}} \ldots$	frequencies of (-2)-quantum coherences in an ensemble of four-spin systems
Ω^{BA}	set of Euler angles $\{\alpha^{\mathrm{BA}}, \beta^{\mathrm{BA}}, \gamma^{\mathrm{BA}}\}$ that may be used to transform the reference axes of frame A into those of frame B
Ω_{AB}	passive notation for the Euler angle set Ω^{BA}
x	spatial coordinate; in addition, used to indicate an r.f. phase $\phi = 0$
$\overline{x}$	indicates an r.f. phase $\phi = \pi$
x_{Ω}	position in space corresponding to a resonance offset Ω, in the presence of a field gradient G_x
x_{Ω_1}	position in space corresponding to a resonance offset Ω_1, in the presence of a field gradient G_x
$\hat{x}$	operator for multiplication by the coordinate x
$\lvert +x\rangle$	spin-1/2 state with angular momentum $+1/2$ along the x-axis
$\lvert -x\rangle$	spin-1/2 state with angular momentum $-1/2$ along the x-axis
$\mathbf{X}$	matrix with columns given by the eigenvectors of $\mathbf{A}$
$\mathbf{X}_z$	matrix with columns given by the eigenvectors of $\mathbf{L}_z$
$\mathbf{X}_{\boxed{-}}$	matrix with columns given by the eigenvectors of $\mathbf{L}_{\boxed{-}}$
χ	magnetic susceptibility
χ_{nuc}	nuclear contribution to the magnetic susceptibility
ξ	angle appearing in the theory of the AB system
y	spatial coordinate; in addition, used to indicate an r.f. phase $\phi = \pi/2$
$\overline{y}$	indicates an r.f. phase $\phi = 3\pi/2$
$\lvert +y\rangle$	spin-1/2 state with angular momentum $+1/2$ along the y-axis
$\lvert -y\rangle$	spin-1/2 state with angular momentum $-1/2$ along the y-axis
$Y_{2m}(\theta, \phi)$	second-rank spherical harmonic
$\psi(x, t)$	one-dimensional particle wavefunction
$\psi_n(x)$	one of a set of continuous orthonormal functions of x
$\lvert\psi\rangle$	Dirac notation ('ket-psi') for an arbitrary spin state, or the spatial wavefunction $\psi(x, t)$
$\langle\psi\rvert$	Dirac notation ('bra-psi') for the adjoint of $\lvert\psi\rangle$
$\lvert\psi\rangle_{①}, \lvert\psi\rangle_{②} \ldots$	spin states at time points ①, ② ...
$\lvert\psi_{\mathrm{full}}\rangle$	complete wavefunction of the sample
$\lvert\psi_{\mathrm{spin}}\rangle$	quantum state of the nuclear spins
Ψ	additional r.f. phase shift in States procedure
z	spatial coordinate, usually in the direction of the main magnetic field

z_{Ω_2}	position in space corresponding to a resonance offset Ω_2, in the presence of a field gradient G_z
Z	atomic number = nuclear charge/e
$\mathfrak{Z}$	coherence transfer amplitude
$\mathbb{Z}$	vector of Zeeman orders in a two-spin-1/2 system
$\mathbb{Z}_{\mathrm{eq}}$	vector of thermal equilibrium Zeeman orders in a two-spin-1/2 system
$\otimes$	direct product
$\langle m \vert n \rangle$	Dirac bracket of $\langle m \vert$ and $\vert n \rangle$
$\left[\widehat{A}, \widehat{B}\right]$	commutator $\widehat{A}\widehat{B} - \widehat{B}\widehat{A}$
$\xrightarrow{(\pi/2)_x}$	propagation under a $(\pi/2)_x$ pulse
$\xrightarrow{\pi J_{12}\tau}$	propagation under the J-coupling between spins I_1 and I_2 over an interval τ
$\xrightarrow{\pi_x}$	propagation under a π_x pulse
$\xrightarrow{\Omega_1^0\tau}$	propagation under the chemical shift of spin I_1 over an interval τ
$\xrightarrow{\Omega_2^0\tau}$	propagation under the chemical shift of spin I_2 over an interval τ
$\xrightarrow{\text{SES}}$	propagation under a spin echo sandwich
$[\mathrm{A}]_{\mathrm{eq}}$	equilibrium concentration of chemical species A
$\langle \widehat{Q} \rangle$	expectation value of the operator $\widehat{Q}$
$\circlearrowleft$	cyclic commutation

Answers to the Exercises

Chapter 1

1.1 (i) Might possibly be correct. The total number of nucleons is odd, so the ground-state spin is a half-integer. More cannot be said using the simple rules for spin. In fact, the ground-state spin is $I = 1/2$, so the statement is correct.

(ii) Cannot be correct. The numbers of protons and neutrons are both even, so the ground-state spin must be $I = 0$.

(iii) Might possibly be correct. The total number of nucleons is odd, so the ground-state spin must be a half-integer. In fact, the ground-state spin is $I = 5/2$.

(iv) Must be correct. The numbers of protons and neutrons are both even, so the ground-state spin is $I = 0$.

(v) Cannot be correct. The numbers of protons and neutrons are both odd, so the ground-state spin must be an integer larger than zero. In fact, $I = 5$.

1.2 1, 2, 3 or 4.

Chapter 2

2.1 The field and magnetization trajectories are as follows:

Spin Dynamics: Basics of Nuclear Magnetic Resonance, Second Edition Malcolm H. Levitt

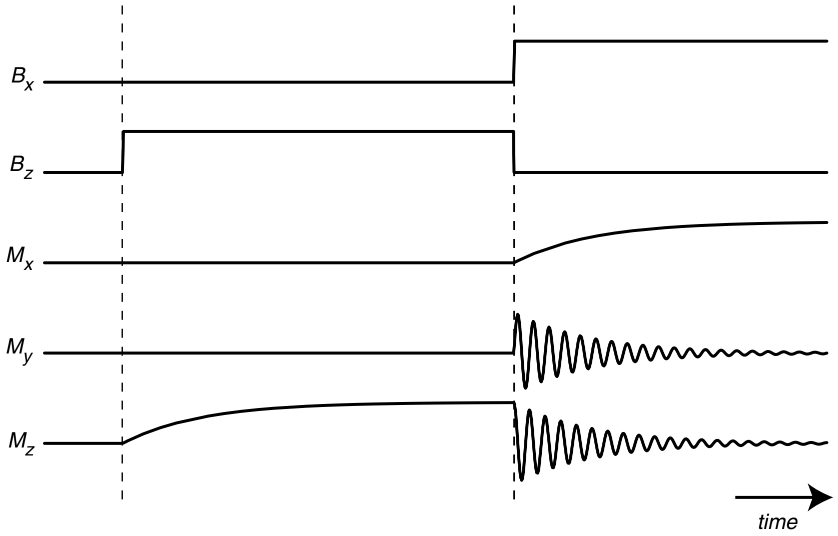

Chapter 3

3.1 (i) The ^{1}H spectrum contains a doublet with a splitting of around 7 Hz on the right-hand side of the spectrum (low δ) and a quartet with a splitting of around 7 Hz on the left-hand side of the spectrum (high δ). The integrated intensity of the doublet is three times more than that of the quartet.

(ii) The ^{13}C spectrum contains a doublet with a splitting of around 135 Hz on the left-hand side of the spectrum (high δ) and a quartet with a splitting of around 135 Hz on the right-hand side of the spectrum (low δ). The quartet and the doublet have approximately the same integrated intensity. When viewed with high resolution, each component of the doublet displays a quartet fine structure, and each peak of the quartet displays a doublet fine structure.

(iii) In the presence of proton decoupling, the ^{13}C spectrum takes the form of two narrow peaks. A close inspection should reveal two very small 'satellites' on each side of both peaks, due to the rare isotopomers with two ^{13}C nuclei in each molecule.

3.2 The isotopomers, their relative proportions, and their ^{1}H-decoupled ^{13}C spectra are as follows:

(i) Isotopomer I: $(^{12}CH_3)_2{}^{12}CO$. Abundance = 21.6%. No ^{13}C spectrum.

(ii) Isotopomer II: $^{13}CH_3{}^{12}CH_3{}^{12}CO$. Abundance = 28.8%. A single peak at low δ (right-hand side of the spectrum).

(iii) Isotopomer III: $(^{12}CH_3)_2{}^{13}CO$. Abundance = 14.4%. A single peak at high δ (left-hand side of the spectrum).

(iv) Isotopomer IV: $^{13}CH_3{}^{12}CH_3{}^{13}CO$. Abundance = 19.2%. A doublet at high δ, and another doublet at low δ.

(v) Isotopomer V: $(^{13}CH_3)_2{}^{12}CO$. Abundance = 9.6%. A single peak at low δ.

(vi) Isotopomer VI: $(^{13}CH_3)_2{}^{13}CO$. Abundance = 6.4%. A triplet at high δ, and a doublet with twice the integrated intensity at low δ.

The ^{1}H-decoupled ^{13}C spectrum, and the assignments of the peaks to the isotopomers, are as follows:

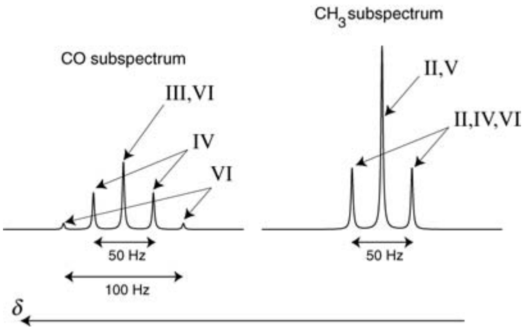

3.3 (i) $B^0 = 13.341\,\text{T}$.

(ii) $\delta_{\text{ref}} = 72.0\,\text{ppm}$.

Chapter 5

5.1 The horizontal axes show frequency $\Omega/2\pi$ in units of hertz:

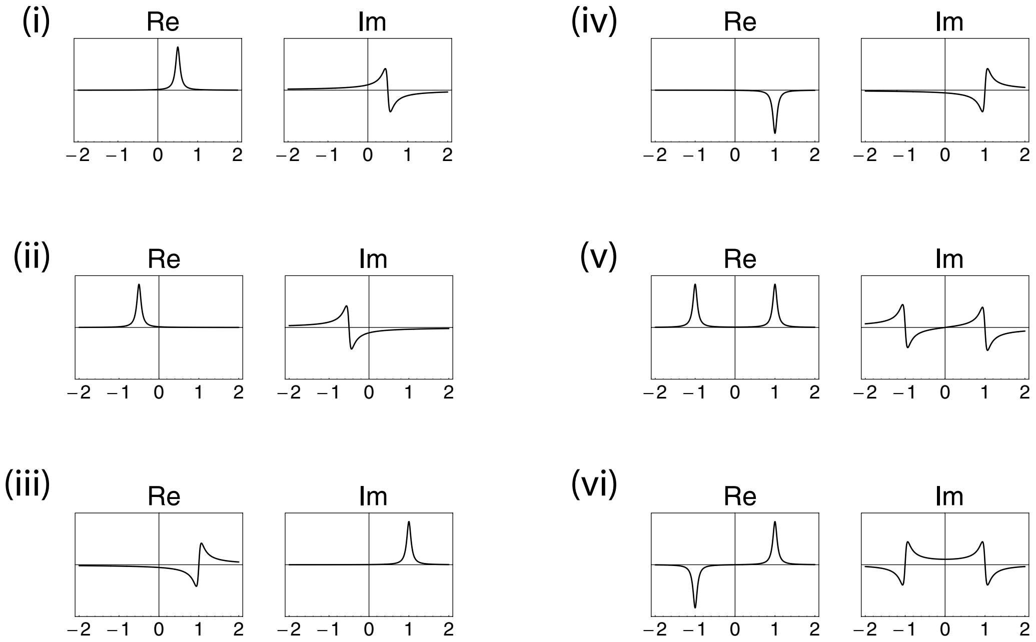

5.2 Running for 2 h at 40 °C with a delay of 5 s between transients gives a signal-to-noise ratio that is a factor of $\sqrt{4/3}$ better than running for 3 h at 20 °C with a delay of 10 s between transients.

Chapter 6

6.1 (iii) $N = 4 \times 5^{-1/2}$.

6.3 $\left[\hat{x}, \widehat{D}_x^2\right] = -2\widehat{D}_x$

6.6 (i) Suppose that the operator $\widehat{A}$ is hermitian, and that $|a\rangle$ is an eigenvector of $\widehat{A}$ with eigenvalue a, i.e.

$$\widehat{A}|a\rangle = a|a\rangle \tag{1}$$

The adjoint of both sides gives

$$\langle a|\widehat{A}^\dagger = a^*\langle a|$$

Since $\widehat{A}$ is hermitian, we can write $\widehat{A}^\dagger = \widehat{A}$, and multiplying with $|a\rangle$ from the right gives

$$\langle a|\widehat{A}|a\rangle = a^*\langle a|a\rangle$$

Similarly, multiplying Equation (1) from the left with $\langle a|$ gives

$$\langle a|\widehat{A}|a\rangle = a\langle a|a\rangle$$

The two last equations may be subtracted from each other to give

$$(a - a^*)\langle a|a\rangle = 0$$

It follows that the eigenvalue a is real, except in the pathological (and trivial) case where $|a\rangle$ is a vector of zeros, so that $\langle a|a\rangle = 0$.

(ii) Suppose that $|1\rangle$ and $|2\rangle$ are eigenvectors of the hermitian operator $\widehat{A}$ with eigenvalues a_1 and a_2 respectively, i.e.

$$\begin{aligned}\widehat{A}|1\rangle &= a_1|1\rangle \\ \widehat{A}|2\rangle &= a_2|2\rangle\end{aligned} \tag{2}$$

The adjoint of the second equation in Equation (2) gives

$$\langle 2|\widehat{A}^\dagger = a_2{}^*\langle 2|$$

and hence

$$\langle 2|\widehat{A} = a_2\langle 2|$$

using the hermiticity of $\widehat{A}$ and the fact that α_2 is real. Multiplying with $|1\rangle$ from the right gives

$$\langle 2|\widehat{A}|1\rangle = a_2\langle 2|1\rangle$$

Similarly, multiplying the first equation in Equation (2) with $\langle 2|$ from the left gives

$$\langle 2|\widehat{A}|1\rangle = a_1\langle 2|1\rangle$$

Subtracting the last two equations from each other gives

$$(a_2 - a_1)\langle 2|1\rangle = 0 \tag{3}$$

If the eigenvalues a_1 and a_2 are different (non-degenerate case), then the bracketed term is non-zero. In this case, Equation (3) may only be satisfied if $\langle 2|1\rangle = 0$, which proves the orthogonality of $|1\rangle$ and $|2\rangle$. If, on the other hand, the eigenvalues a_1 and a_2 are the same (degenerate case), then (Equation (3)) is satisfied even if $\langle 2|1\rangle$ is non-zero. The eigenvectors may be non-orthogonal in this case.

Chapter 7

7.1 (i)

$$\begin{aligned}\left[2\hat{I}_{1x}\hat{I}_{2y}, 2\hat{I}_{1x}\hat{I}_{2z}\right] &= \mathrm{i}\hat{I}_{2x}\\ \left[\hat{I}_{2x}, 2\hat{I}_{1x}\hat{I}_{2y}\right] &= \mathrm{i}2\hat{I}_{1x}\hat{I}_{2z}\\ \left[2\hat{I}_{1x}\hat{I}_{2z}, \hat{I}_{2x}\right] &= \mathrm{i}2\hat{I}_{1x}\hat{I}_{2y}\end{aligned}$$

(ii)

$$\exp\{-\mathrm{i}\theta 2\hat{I}_{1x}\hat{I}_{2y}\}2\hat{I}_{1x}\hat{I}_{2z}\exp\{+\mathrm{i}\theta 2\hat{I}_{1x}\hat{I}_{2y}\} = 2\hat{I}_{1x}\hat{I}_{2z}\cos\theta + \hat{I}_{2x}\sin\theta$$

(iii)

$$\exp\{-\mathrm{i}\theta 2\hat{I}_{1x}\hat{I}_{2y}\}\hat{I}_{2x}\exp\{+\mathrm{i}\theta 2\hat{I}_{1x}\hat{I}_{2y}\} = \hat{I}_{2x}\cos\theta - 2\hat{I}_{1x}\hat{I}_{2z}\sin\theta$$

7.2 (i) The state $\psi_1(x)$ in Equation 6.1 is an eigenstate of $\widehat{D}_x^2$ with eigenvalue $-\pi^2$ (see Equation 6.24). The probability of obtaining the value $-\pi^2$, therefore, is given by

$$\mathtt{P}(-\pi^2) = |\langle 1|f\rangle|^2$$

This evaluates to

$$|\langle 1|f\rangle|^2 = \left(\frac{5}{3}\sqrt{\frac{2}{7}}\right)^2 = \frac{50}{63} = 0.794$$

using the expansion coefficient given in Equation 6.8.

(ii) The state $\psi_3(x)$ in Equation 6.1 is an eigenstate of $\widehat{D}_x^2$ with eigenvalue $-9\pi^2$ (see Equation 6.24). The probability of obtaining the value $-9\pi^2$, therefore, is given by

$$\mathtt{P}(-9\pi^2) = |\langle 3|f\rangle|^2 = \frac{25}{126} = 0.198$$

(iii) The probability of obtaining the value 2 is exactly zero, since 2.0 is not an eigenvalue of $\widehat{D}_x^2$.

(iv) The average of many observations tends to the expectation value of $\widehat{D}_x^2$ for particles in state $|f\rangle$, which is given by

$$\langle f|\widehat{D}_x^2|f\rangle = \int_0^1 \mathrm{d}x f(x)^* \widehat{D}_x^2 f(x) = -\frac{25}{9}\pi^2$$

7.3 One way to prove this is as follows (the dots are only intended to clarify the working, and have no meaning):

$$\begin{aligned}\widehat{R}_x(\pi/2)\widehat{R}_y(\pi)\widehat{R}_x(\pi/2) &= \widehat{R}_x(\pi/2)\widehat{R}_y(\pi)\widehat{R}_x(\pi/2)\cdot\widehat{1}\\ &= \widehat{R}_x(\pi/2)\widehat{R}_y(\pi)\widehat{R}_x(\pi/2)\cdot\widehat{R}_y(-\pi)\widehat{R}_y(\pi)\\ &= \widehat{R}_x(\pi/2)\cdot\widehat{R}_y(\pi)\widehat{R}_x(\pi/2)\widehat{R}_y(-\pi)\cdot\widehat{R}_y(\pi)\\ &= \widehat{R}_x(\pi/2)\cdot\widehat{R}_x(-\pi/2)\cdot\widehat{R}_y(\pi)\\ &= \widehat{1}\cdot\widehat{R}_y(\pi)\\ &= \widehat{R}_y(\pi)\end{aligned}$$

The crucial step in the proof uses the sandwich relationship in Equation 7.15.

7.4 The matrix representations for spin-5/2 operators, in the basis $|I, M\rangle = \{|5/2, +5/2\rangle, |5/2, +3/2\rangle, |5/2, +1/2\rangle, |5/2, -1/2\rangle, |5/2, -3/2\rangle, |5/2, -5/2\rangle\}$ are as follows:

$$\hat{I}^{+} = \begin{pmatrix} 0 & \sqrt{5} & 0 & 0 & 0 & 0 \\ 0 & 0 & 2\sqrt{2} & 0 & 0 & 0 \\ 0 & 0 & 0 & 3 & 0 & 0 \\ 0 & 0 & 0 & 0 & 2\sqrt{2} & 0 \\ 0 & 0 & 0 & 0 & 0 & \sqrt{5} \\ 0 & 0 & 0 & 0 & 0 & 0 \end{pmatrix}$$

$$\hat{I}^{-} = \begin{pmatrix} 0 & 0 & 0 & 0 & 0 & 0 \\ \sqrt{5} & 0 & 0 & 0 & 0 & 0 \\ 0 & 2\sqrt{2} & 0 & 0 & 0 & 0 \\ 0 & 0 & 3 & 0 & 0 & 0 \\ 0 & 0 & 0 & 2\sqrt{2} & 0 & 0 \\ 0 & 0 & 0 & 0 & \sqrt{5} & 0 \end{pmatrix}$$

$$\hat{I}_y = \frac{1}{2\mathrm{i}} \begin{pmatrix} 0 & \sqrt{5} & 0 & 0 & 0 & 0 \\ -\sqrt{5} & 0 & 2\sqrt{2} & 0 & 0 & 0 \\ 0 & -2\sqrt{2} & 0 & 3 & 0 & 0 \\ 0 & 0 & -3 & 0 & 2\sqrt{2} & 0 \\ 0 & 0 & 0 & -2\sqrt{2} & 0 & \sqrt{5} \\ 0 & 0 & 0 & 0 & -\sqrt{5} & 0 \end{pmatrix}$$

$$\hat{I}_z = \begin{pmatrix} \frac{5}{2} & 0 & 0 & 0 & 0 & 0 \\ 0 & \frac{3}{2} & 0 & 0 & 0 & 0 \\ 0 & 0 & \frac{1}{2} & 0 & 0 & 0 \\ 0 & 0 & 0 & -\frac{1}{2} & 0 & 0 \\ 0 & 0 & 0 & 0 & -\frac{3}{2} & 0 \\ 0 & 0 & 0 & 0 & 0 & -\frac{5}{2} \end{pmatrix}$$

Chapter 8

8.1 (i) $B^0 = 1.174\,\mathrm{T}$; (ii) $\omega_{\mathrm{nut}}/2\pi = 21.29\,\mathrm{kHz}$; (iii) $\omega_{\mathrm{nut}}/2\pi = 17.38\,\mathrm{kHz}$; (iv) $B^0 = 11.593\,\mathrm{T}$; (v) $\omega_{\mathrm{nut}}/2\pi = 2.15\,\mathrm{kHz}$; (vi) $\omega_{\mathrm{nut}}/2\pi = 1.76\,\mathrm{kHz}$.

Chapter 9

9.1 (i) $b_{12}/2\pi = -15.012\,\mathrm{kHz}$; (ii) $b_{13}/2\pi = -15.012\,\mathrm{kHz}$; (iii) $d_{12}/2\pi = +7.506\,\mathrm{kHz}$; (iv) $d_{12}/2\pi = -9.382\,\mathrm{kHz}$; (v) $d_{12}/2\pi = -3.753\,\mathrm{kHz}$; $d_{13}/2\pi = -13.504\,\mathrm{kHz}$; $d_{23}/2\pi = +5.997\,\mathrm{kHz}$.

9.2 (ii) $d_{jk} = \int_0^\pi \mathrm{d}\Theta_{jk}\, \mathrm{p}(\Theta_{jk})\, b_{jk} \frac{1}{2}(3\cos^2\Theta_{jk} - 1)\, \sin\Theta_{jk} = 2b_{jk}/155$. If $r = 0.3\,\mathrm{nm}$, then $d_{jk}/2\pi = -57.4\,\mathrm{Hz}$.

Chapter 10

10.1 (i) The eigenvalue is $+\frac{1}{2}$. (ii) The state may be represented as an arrow in the zy plane subtending an angle θ with the z-axis. (iii) The required pulse has flip angle $(\pi/2 - \theta)$ and phase π.

10.2 (i) $\omega_{\mathrm{nut}}/2\pi = 10\,\mathrm{kHz}$. (ii) $25\,\mu\mathrm{s}$; (iii) π.

10.3 (i) $|\beta\rangle$.

(ii) $-1/2$.

10.4 (i) $\frac{1}{2}\begin{pmatrix} 1+\mathrm{i} \\ -1+\mathrm{i} \end{pmatrix}$.

(ii) $+1/2$.

10.5 $\tau_{\mathrm{p}} = 35.35\,\mu\mathrm{s}$.

Chapter 11

11.1 (i) $14.68\,\mathrm{T}$; (ii) $-625.1\,\mathrm{MHz}$; (iii) 12.6×10^{-6}.

11.2 (i) π; $-\mathbf{e}_z$.

(ii) $-0.309\mathbf{e}_y - 0.951\mathbf{e}_z$; 18°.

(iii) $-\mathbf{e}_z$.

(iv) $0.048\mathbf{e}_x - 0.008\mathbf{e}_y - 0.999\mathbf{e}_z$; 2.8°.

(v) See R. Freeman, *Spin Choreography. Basic Steps in High Resolution NMR*, Spektrum, Oxford, 1997.

Chapter 12

12.1 Peak 1: $T_1 \cong 2\,\mathrm{s}$; peak 2: $T_1 \cong 5\,\mathrm{s}$.

12.2 The signal phases are as follows:

(i) zero (the spin echo sequence refocuses the phase).

(ii) $-\gamma \Delta B x_0 / v$

(iii) $\gamma \Delta B \tau + \gamma \Delta B x_0 / v$

(iv) zero (the spin echo sequence refocuses the phase).

Chapter 13

13.1 A spin I has $2I+1$ energy levels, with M running from $-I$ to $+I$ in integer steps. There are, therefore, $I+\frac{1}{2}$ levels with positive M running from $+1/2$ to $+I$ in integer steps. The mean value of M for all positive-M levels, therefore, is $\frac{1}{2}(I+\frac{1}{2})$. This should be compared with the value of 1/2 when no saturation is applied. The central-transition enhancement factor on satellite saturation, therefore, is $I+\frac{1}{2}$.

13.2 From Equation 7.30 the matrix element of $\hat{I}^{+}$ across the central transition is $\sqrt{I(I+1)-(\frac{1}{2})(-\frac{1}{2})} = I+\frac{1}{2}$. The central transition nutation enhancement on selective excitation, therefore, is $I+\frac{1}{2}$ (again!).

13.3 The matrix representation of a $(\pi/2)_x$ pulse is given in Section 7.9.1, and is equal to

$$\widehat{R}_x(\pi/2) = \frac{1}{2}\begin{pmatrix} 1 & -\mathrm{i}\sqrt{2} & -1 \\ -\mathrm{i}\sqrt{2} & 0 & -\mathrm{i}\sqrt{2} \\ -1 & -\mathrm{i}\sqrt{2} & 1 \end{pmatrix}$$

Matrix multiplications as in Equation 13.27 give

$$\widehat{R}_x(\pi/2)\begin{pmatrix} 0 & 0 & 0 \\ 1 & 0 & -1 \\ 0 & 0 & 0 \end{pmatrix}\widehat{R}_x(\pi/2)^{\dagger} = \mathrm{i}\sqrt{2}\begin{pmatrix} 1 & 0 & -1 \\ 0 & 0 & 0 \\ 1 & 0 & -1 \end{pmatrix}$$

$$\widehat{R}_x(\pi/2)\begin{pmatrix} 0 & -1 & 0 \\ 0 & 0 & 0 \\ 0 & 1 & 0 \end{pmatrix}\widehat{R}_x(\pi/2)^{\dagger} = \mathrm{i}\sqrt{2}\begin{pmatrix} 1 & 0 & 1 \\ 0 & 0 & 0 \\ -1 & 0 & -1 \end{pmatrix} \tag{4}$$

It follows that double-quantum coherences are excited, with amplitudes proportional to $2\mathrm{i}(\,\exp\{\mathrm{i}\frac{1}{4}\omega_{\mathrm{Q}}^{(1)}\tau\} - \exp\{-\mathrm{i}\frac{1}{4}\omega_{\mathrm{Q}}^{(1)}\tau\}) = \sin\frac{1}{4}\omega_{\mathrm{Q}}^{(1)}\tau$.

13.4 A nine-peak multiplet with intensities in the ratio 9:16:21:24:25:24:21:16:9.

Chapter 14

14.1 (i) 10.8 G corresponds to 1.08×10^{-3} T. This may be multiplied by the proton gyromagnetic ratio of $267.5 \times 10^{6}\,\mathrm{rad\,s^{-1}\,T^{-1}}$ to obtain $288 \times 10^{3}\,\mathrm{rad\,s^{-1}} = 45.98\,\mathrm{kHz}$.

(ii) The splitting between the strong 'perpendicular' peaks in the Pake doublet is $|3b/2|$, where b is the dipole–dipole coupling constant. Hence $|b/2\pi| = \frac{2}{3} \times 45.98\,\text{kHz} = 30.66\,\text{kHz}$. Solution of $|b| = (\mu_0/4\pi)\gamma^2\hbar r^{-3} = 2\pi \times 30.66 \times 10^3\,\text{rad s}^{-1}$ gives $r = 158\,\text{pm}$.

Chapter 15

15.1 (i)

$$\hat{\rho} = \frac{1}{4}\begin{pmatrix} 1 & 1 & 1 & 1 \\ 1 & 1 & 1 & 1 \\ 1 & 1 & 1 & 1 \\ 1 & 1 & 1 & 1 \end{pmatrix}$$

(ii)

$$\hat{\rho} = \begin{pmatrix} C^4 & C^3S & C^3S & C^2S^2 \\ C^3S & C^2S^2 & C^2S^2 & C^3S \\ C^3S & C^2S^2 & C^2S^2 & C^3S \\ C^2S^2 & CS^3 & CS^3 & S^4 \end{pmatrix}$$

where $C = \cos(\beta/2)$ and $S = \sin(\beta/2)$.

(iii)

$$\hat{\rho} = \begin{pmatrix} 1 - \frac{1}{2}\beta^2 & \frac{1}{2}\beta & \frac{1}{2}\beta & \frac{1}{4}\beta^2 \\ \frac{1}{2}\beta & \frac{1}{4}\beta^2 & \frac{1}{4}\beta^2 & 0 \\ \frac{1}{2}\beta & \frac{1}{4}\beta^2 & \frac{1}{4}\beta^2 & 0 \\ \frac{1}{4}\beta^2 & 0 & 0 & 0 \end{pmatrix}$$

Single-quantum coherences that share a state with the original population are excited to first order in β. Multiple-quantum coherences are excited to second order in β.

Chapter 16

16.1 (i) $\hat{\rho} = -\hat{I}_y \cos\Omega_S^0 t_1 - \left(2\hat{I}_x\hat{S}_x \cos\Omega_S^0\tau + 2\hat{I}_x\hat{S}_y \sin\Omega_S^0\tau\right)\sin\Omega_S^0 t_1$;
(iii) change the phase of the first pulse to $-y$.

16.2 (i)

$$\begin{aligned}\hat{\rho}_{④} &= -\hat{I}_{1x}\cos\Omega_1^0 t_1 \cos\pi J t_1 + 2\hat{I}_{1z}\hat{I}_{2y}\cos\Omega_1^0 t_1 \sin\pi J t_1 \\ &\quad -\hat{I}_{1z}\sin\Omega_1^0 t_1 \cos\pi J t_1 - 2\hat{I}_{1x}\hat{I}_{2y}\sin\Omega_1^0 t_1 \sin\pi J t_1\end{aligned}$$

(ii) For a general value of t_1, all coherence orders $-2, -1, 0, 1$ and 2 are excited at time point ④.

(iii)

$$\begin{aligned}\hat{\rho}^{\cos}_{⑤} &= -2\hat{I}_{1y}\hat{I}_{2z}\,\frac{1}{4}\left(\cos(\Omega_1^0+\pi J)t_1 - \cos(\Omega_1^0-\pi J)t_1\right)\\ &\quad -2\hat{I}_{1z}\hat{I}_{2y}\,\frac{1}{4}\left(\cos(\Omega_1^0+\pi J)t_1 - \cos(\Omega_1^0-\pi J)t_1\right)\end{aligned}$$

(iv)

$$\begin{aligned}\hat{\rho}^{\sin}_{⑤} &= -2\hat{I}_{1y}\hat{I}_{2z}\,\frac{1}{4}\left(\sin(\Omega_1^0+\pi J)t_1 - \sin(\Omega_1^0-\pi J)t_1\right)\\ &\quad -2\hat{I}_{1z}\hat{I}_{2y}\,\frac{1}{4}\left(\sin(\Omega_1^0+\pi J)t_1 - \sin(\Omega_1^0-\pi J)t_1\right)\end{aligned}$$

(v) Both the diagonal-peak multiplets and the cross-peak multiplets are in antiphase absorption. Another advantage of 2QF-COSY is that signals from non-coupled spins-1/2 are suppressed, as in the INADEQUATE experiment. One drawback of 2QF-COSY is that one half of the signal amplitude is lost, compared with ordinary COSY.

Chapter 17

17.1 (i) Chemically and magnetically equivalent; (ii) chemically and magnetically inequivalent; (iii) chemically equivalent but magnetically inequivalent.

17.2 (i) A_2; (ii) AB; (iii) ABX; (iv) AA′BB′; (v) ABMX; (vi) AA′BB′X.

Chapter 18

18.1 (i) The final spin density operator is $\hat{\rho}_{⑤} \sim -\hat{S}_y \sin\theta + \ldots$. The optimal flip angle is $\theta = \pi/2$. The maximum signal enhancement is γ_I/γ_S.

(ii) The final spin density operator is $\hat{\rho}_{⑤} \sim -\hat{S}_y \sin 2\theta + \ldots$. The optimal flip angle is $\theta = \pi/4$. The maximum signal enhancement is γ_I/γ_S.

(iii) The final spin density operator is $\hat{\rho}_{⑤} \sim -3\hat{S}_y \cos^2\theta \sin\theta + \ldots$. The optimal flip angle is $\theta = \arccos\sqrt{2/3}$. The maximum signal enhancement is $1.15\gamma_I/\gamma_S$. Note that these results resemble those obtained for INEPT, but with the dependence on the pulse sequence delay τ replaced by a dependence on the flip angle θ.

Chapter 19

19.1 (i) $B^0 = 7.08\,\mathrm{T}$.

(ii) $B^0 = 17.8\,\mathrm{T}$.

(iii) $T = 283.5\,\mathrm{K}$.

(iv) Between around $T = 210\,\mathrm{K}$ and $280\,\mathrm{K}$.

(v) Around $T = 660\,\mathrm{K}$.

Chapter 20

20.1 (i) The plots of T_1 and T_2 against field are as follows:

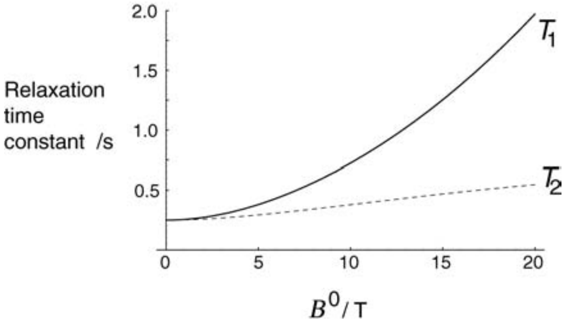

T_1 increases with field, since spin–lattice relaxation requires spectral density at the Larmor frequency ω^0 (and also twice the Larmor frequency). Spin–lattice relaxation is less effective at high field since the spectral density function decays with respect to frequency, and the Larmor frequency is higher at high field. Transverse relaxation, on the other hand, involves spectral densities at a selection of frequencies, including zero. The zero-frequency contribution to the transverse relaxation is field independent. As a result, the transverse relaxation time constant is relatively insensitive to field. (This applies to the case of homonuclear dipole–dipole relaxation, but not necessarily to other relaxation mechanisms, such as those involving the CSA).

(ii) The plots of R_{cross} and $R^{\mathrm{T}}_{\mathrm{cross}}$ against field are as follows:

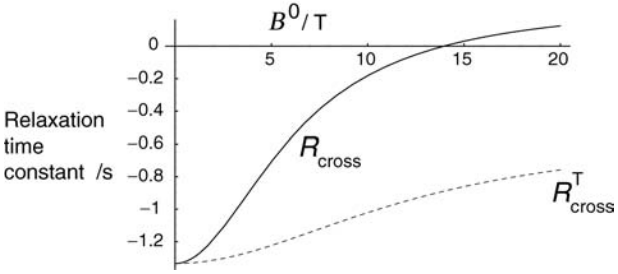

The ROESY experiment is expected to be superior at high field, since the transverse cross-relaxation rate constant remains large (and negative). The longitudinal cross-relaxation rate constant, involved in the NOESY experiment, becomes small (and positive) at high field.

Index

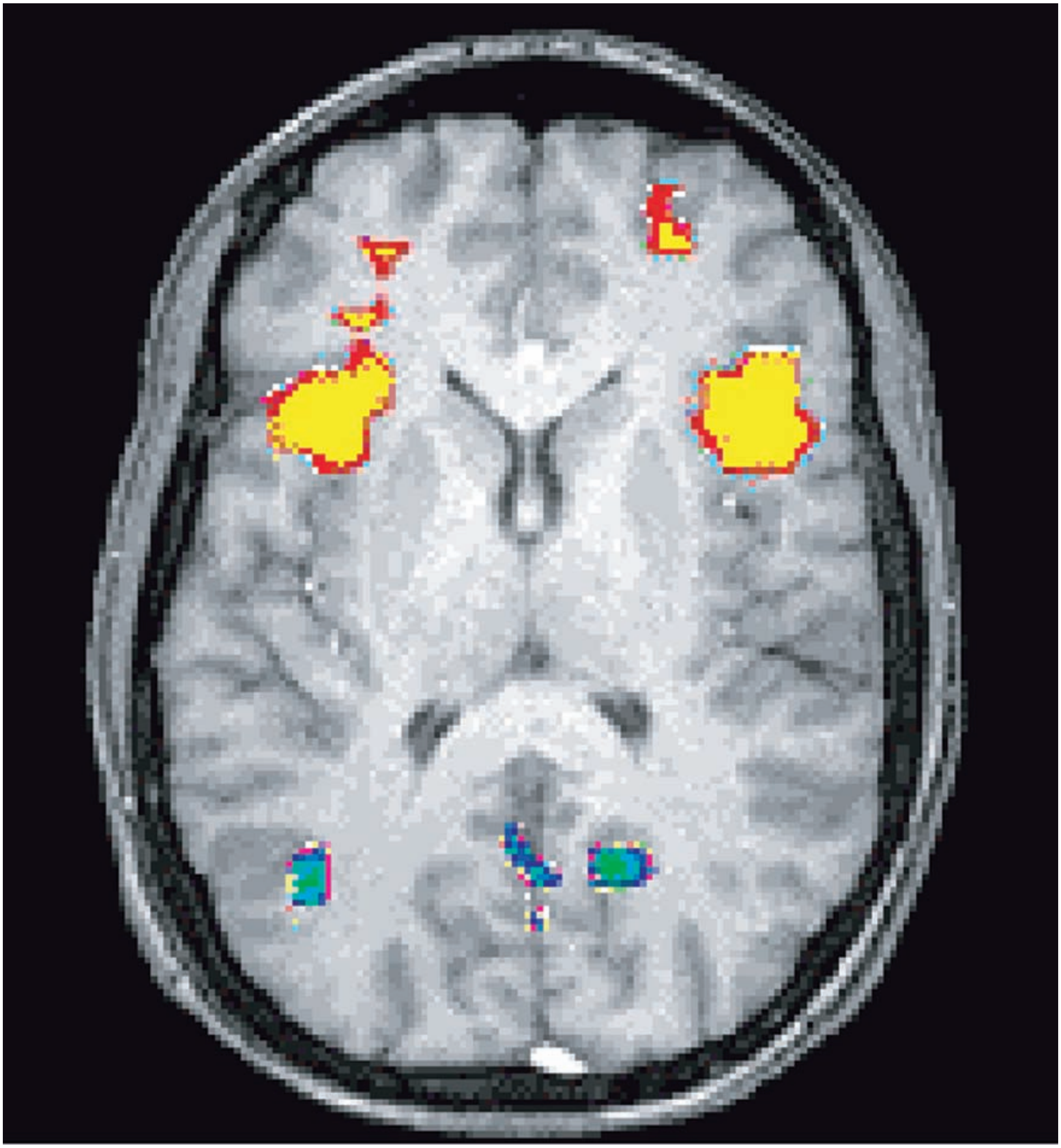

Plate 1 A functional NMR image. The grey image is a cross-section through the head of a person (the person may be thought of as lying down on their back, feet towards you). The grey-scale image shows the lobes of the brain. The yellow and red patches show activation of the prefrontal cortex after a face is removed from view, detected as small differences in the NMR signals. The blue patches denote diminished activation of these regions of the brain, under the same task. (From S. M. Courtney, L. G. Underleider, K. Keil and J. V. Haxby, *Nature* **386**, 608–611 (1997). Copyright, Macmillan Publishers Ltd.)

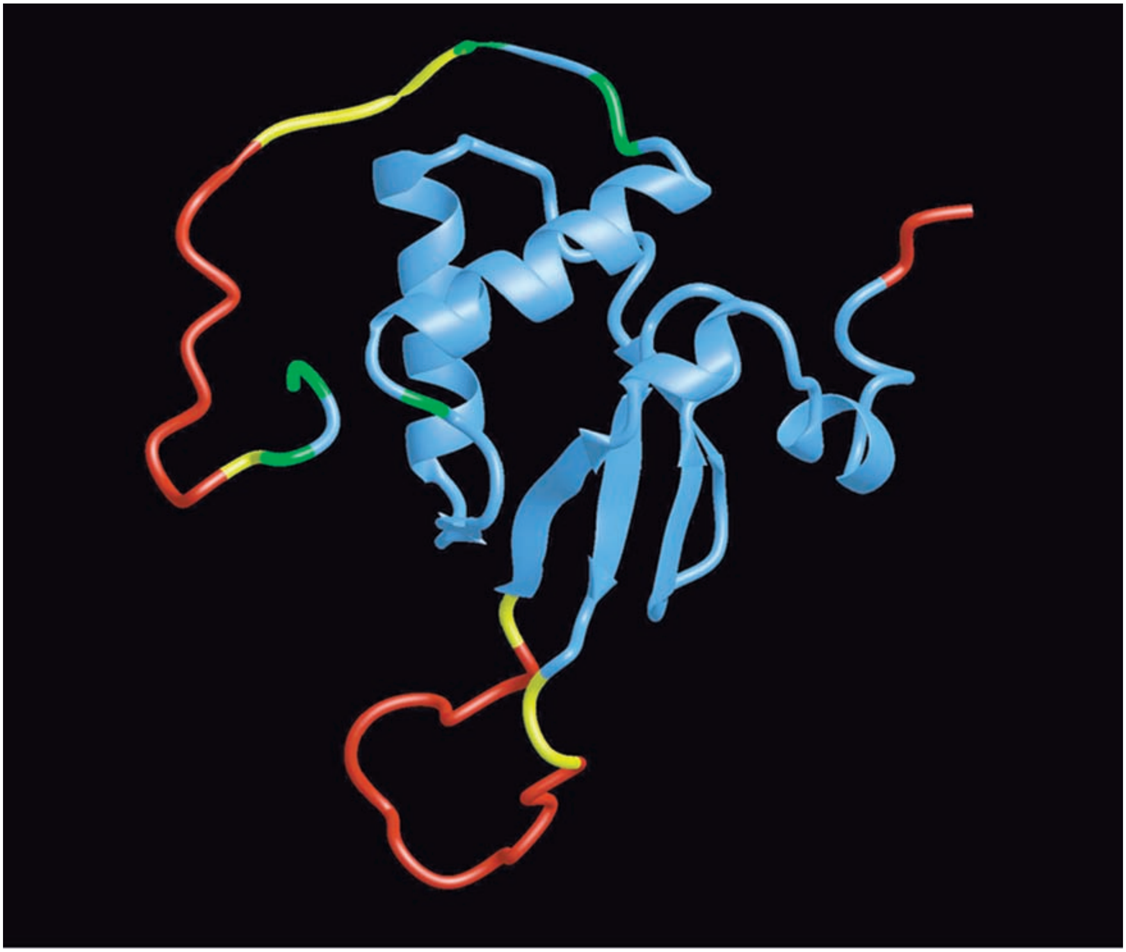

Plate 2 Backbone structure of a protein molecule in solution (residues 55–206 of the HIV-1 Nef protein), as determined by NMR. The structure is colour encoded to display the mobilities of different parts of the molecule, as revealed by ^{1}H–^{15}N NOE values (see Chapter 20). Blue: least mobile; red: most mobile. The N-terminal tail that anchors the protein to the membrane is disordered and not shown. (For details, see S. Grzesiek, A. Bax, J. Hu, J. Kaufman, I. Palmer, S. J. Stahl, N. Tjandra, and P. T. Wingfield, *Protein Science*, **6**, 1248–1263 (1997)). Thanks to Ad Bax for supplying this figure.

Plate 3 Three-dimensional NMR image of a human head, with layers of tissue computationally peeled off so that the brain is partially visible. The yellow spot shows the approximate location of neuronal activity in response to a sound. This spot was not obtained by functional NMR imaging, but by magnetoencephalography (analysis of the weak magnetic fields generated by electrical currents in the brain). The illustration was prepared by Mr Eero Salli. Thanks to Professor Hannu Aronen, Department of Radiology, and Dr Risto Ilmoniemi, BioMag Laboratory, Helsinki University Central Hospital, Finland, for permission to use this image.

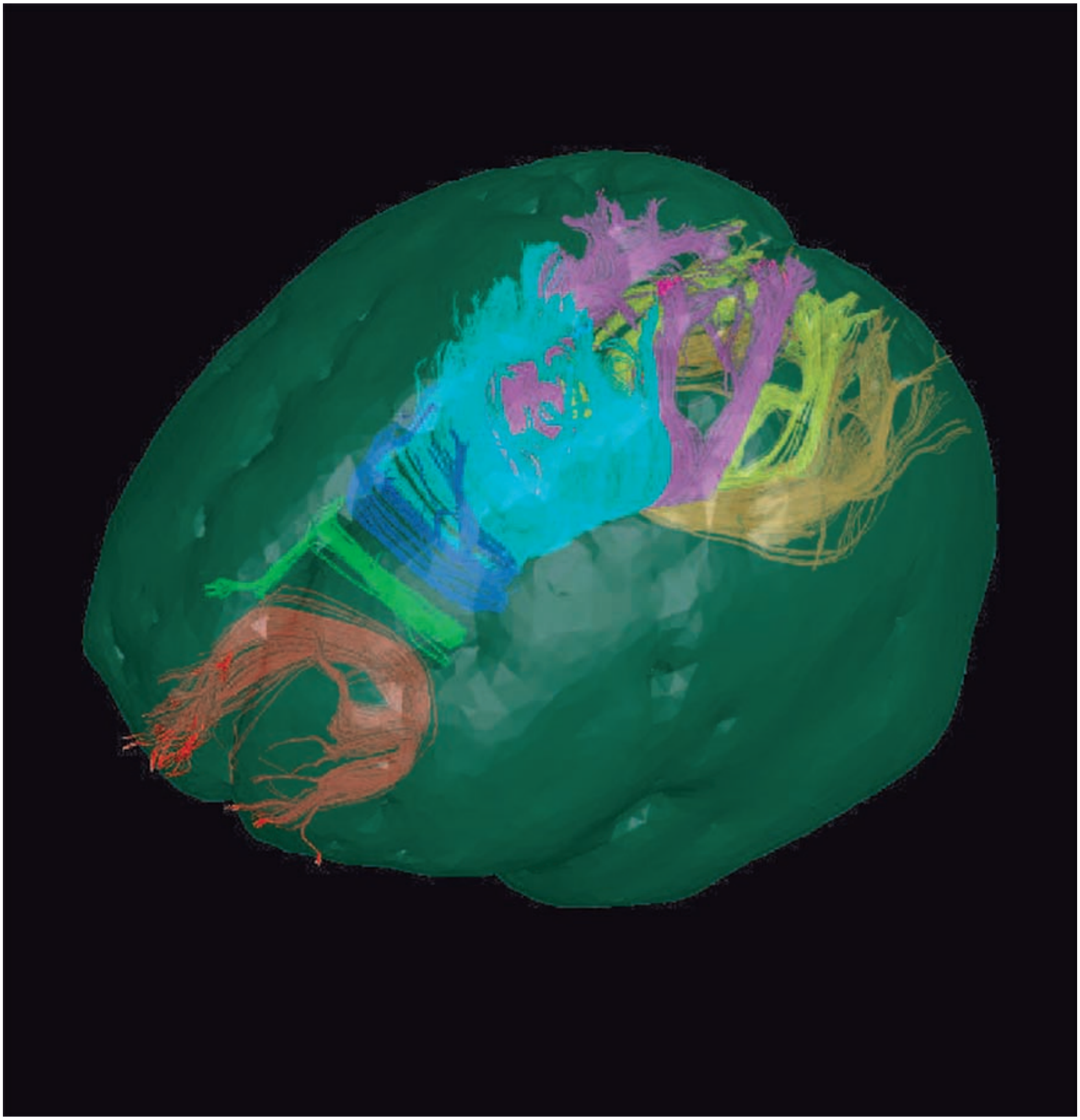

Plate 4 A three-dimensional rendering of the neural pathways connecting the two hemispheres of the human brain. These pathways were delineated using diffusion tensor MRI. The different colours indicate tracks connecting distinct brain regions. This figure was supplied by Roland Henry and SungWon Chung, Department of Radiology, University of California, San Francisco, USA.

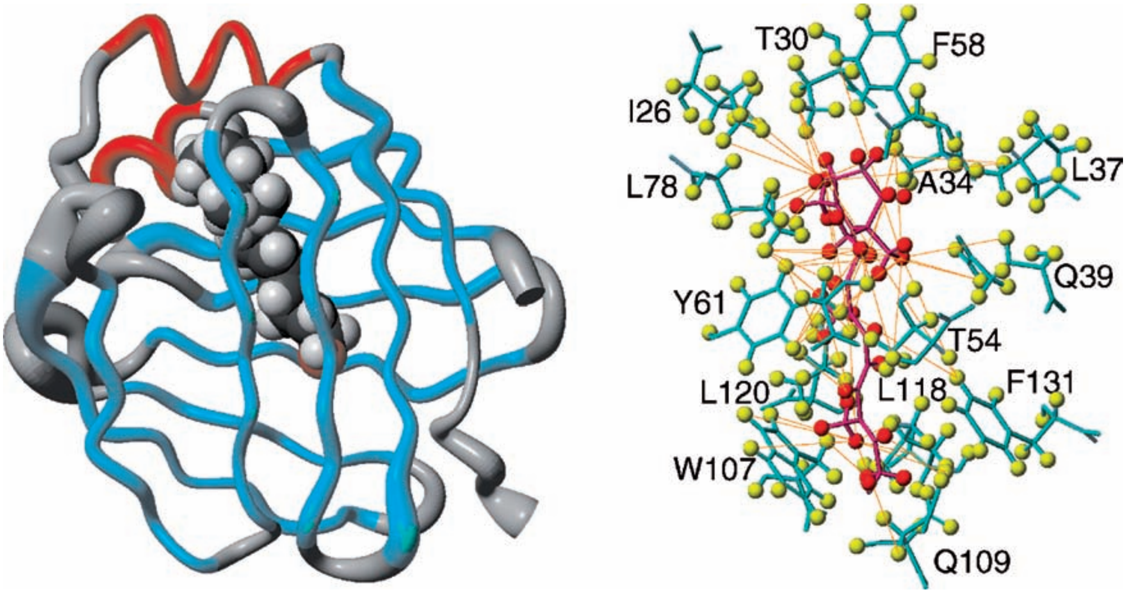

Plate 5 Experimental solution-state structure of a protein, solved by using NOESY distance constraints. The molecule is a 15 kDa protein called cellular retinol binding protein II. The structure was solved using a combination of double-quantum-filtered COSY, NOESY and TOCSY experiments, including three-dimensional combinations of these techniques. The final structure was derived employing 3980 NOESY distance constraints and displays a 10-stranded β-barrel motif. **(a)** The protein backbone, depicted as a sausage, enclosing the retinol ligand (space-filling model). **(b)** The retinol binding site and the retinol ligand (red). The NOESY distance constraints involving the protein protons (yellow) and the ligand protons are shown by lines. For full details, see J. Lu, C.-L. Lin, C. Tang, J. W. Ponder, J. L. F. Kao, D. P. Cistola; and E. Li, *J. Mol. Biol.*, **286**, 1179–1195 (1999) and the same authors in *J. Mol. Biol.*, **300**, 619–632 (2000). Thanks to J. Lu for preparing this figure.

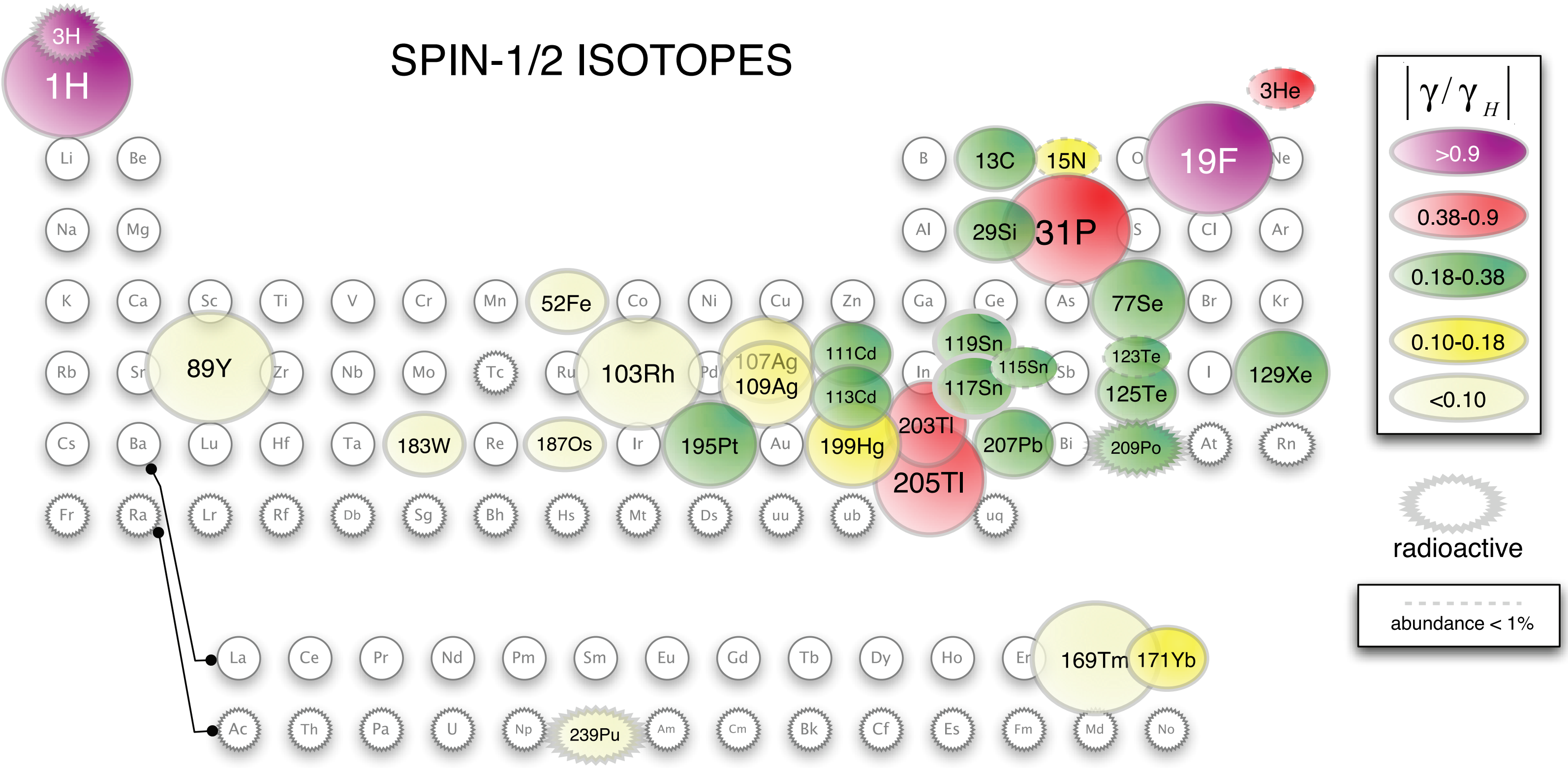

Plate A Distribution of spins-1/2 in the periodic table. In this and the following plates, the colours indicate the magnitude of the gyromagnetic ratio γ, relative to that of ^{1}H (see inset). The sizes of the symbols are related to the natural abundance of the isotopes, with a dotted border indicating a natural abundance of less than 1%.

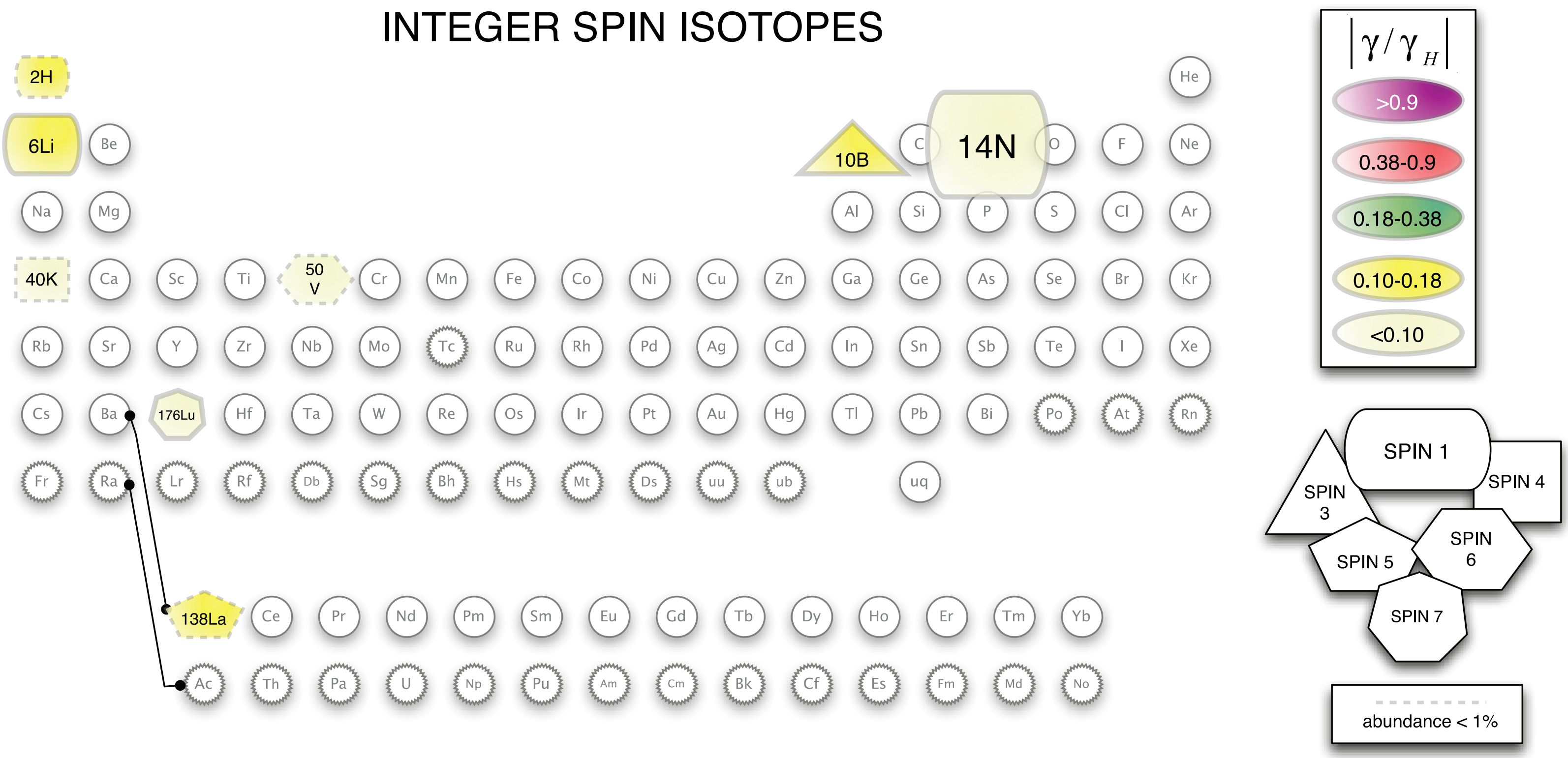

Plate B Distribution of integer spins in the periodic table. The symbol shape indicates the spin quantum number (see inset).

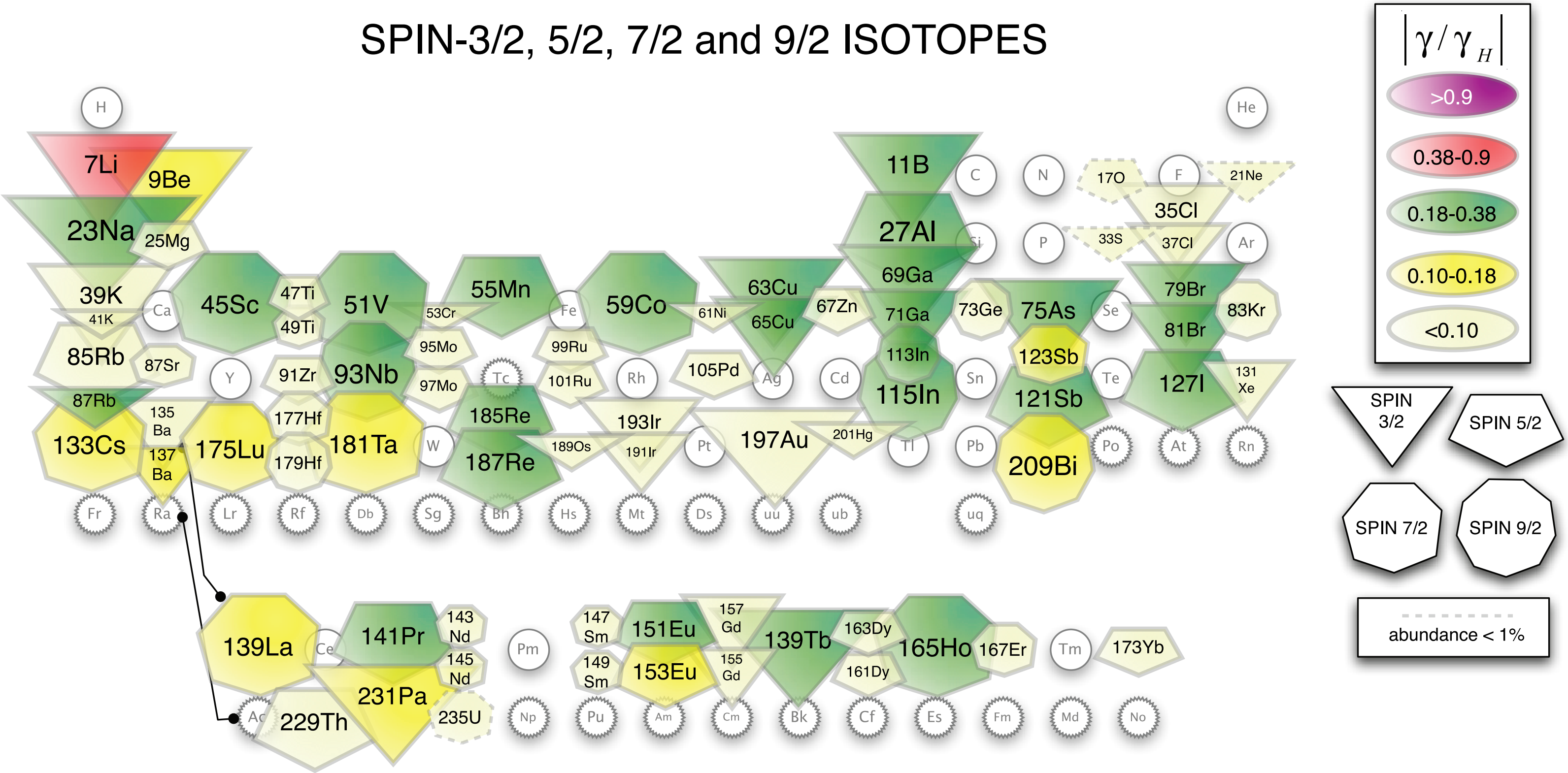

Plate C Distribution of half-integer spins with $I > 1$. The symbol shape indicates the spin quantum number (see inset).